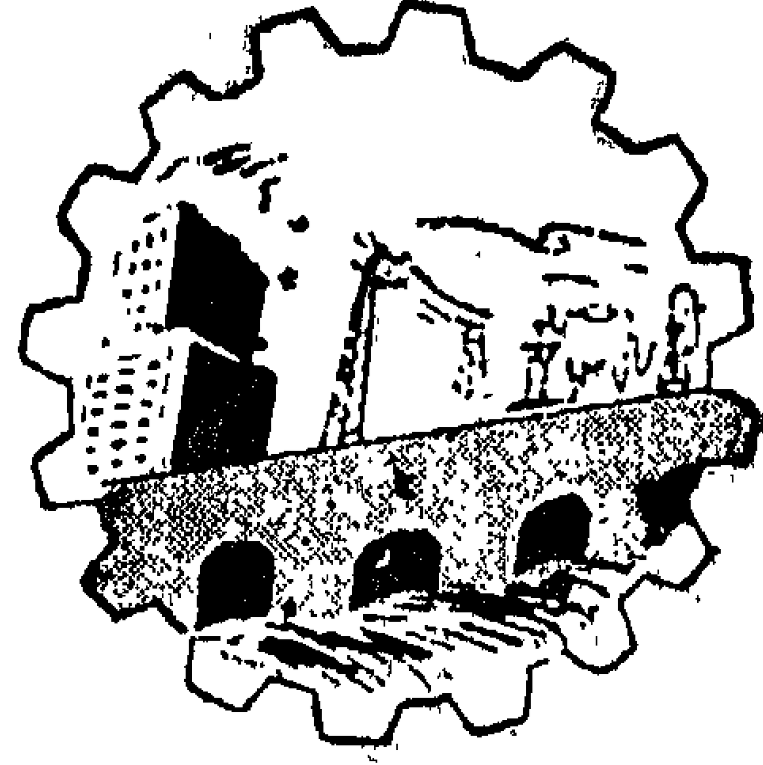
ESEN-CPS-BK-0000001054-ESE

00471207



مجلة

جمعية المهندسين المصرية

العـــدد الأول | المجلد العاشر | يناير – فبراير – مارس ١٩٧١

رقم الإيداع بدار الكتب المصرية ١٩٧١/٢٩٨

المطبعة العالمية ١٦ و١٧ ش ضريح سعد بالقاهرة

مجلة

جمعية المهندسين المصرية

مجلة علمية هندسية – تصدرها كل ثلاث شهور

جمعية المهندسين المصرية بالقاهرة

السنة العاشرة | العدد الأول | يناير – فبراير – مارس ١٩٧١

محتويات هذا العدد

القسم العربى

صفحة

فن العمارة والخرسانة المسلحة ... ... للدكتور المهندس على رأفت ٧

القسم الأفرنجى

التسليح غير المعدنى للأجزاء الخرسانية للمنشآت – الجزء الأول (البامبو) – للدكتور المهندس أحمد على العريان والدكتور المهندس محمد محسن توفيق والمهندس محمود على رضا يوسف ٧

استقبال الموجات الطويلة جداً ... ... للدكتور المهندس أحمد لطفى السيد ٢٩

دراسة مقاومة الوصلات الأنبوبية المشكلة على البارد ... ... للدكتور المهندس مجدى شنوده ٣٤

السريان السريع المتغير فوق المنشآت الهيدروليكية ... ... – للدكتور المهندس محمود سعيد عبد الله والدكتور المهندس محمد مخلص أبو سعده والدكتور المهندس محمد أحمد سليمان ٤٦

أكسدة كبريتيت الصوديوم فوق الأقراص المثقوبة ... ... للدكتور المهندس فكرى شلبى ٦١

تطبيق لنظرية التحكم الأمثل فى تصميم أجهزة التحكم فى الطائرات ... ... – للدكتور المهندس أسامة الخولى والمهندس ممدوح عونى ٧١

السلوك الحرارى للأسقف من الخرسانة المسلحة فى الأجواء الحارة الجافة وأثر ذلك على الإحساس بالحرارة داخل المبانى الاقتصادية ... ... – للدكتور المهندس على صالح ٩٢

بيانات

مقر المجلة

جمعية المهندسين المصرية

٢٨ شارع رمسيس بالقاهرة

تليفون : ٥٢١٠٦

- جميع أعضاء جمعية المهندسين مشتركون فى المجلة بحكم عضويتهم
- الإشتراك السنوى لغير الأعضاء : ٦٠ جـ للمهندس ، ١٠٠ جـ للهيئات
- ترسل البحوث والموضوعات والتعليقات إلى أمانة التحرير بمقر جمعية المهندسين
- المصرية بالقاهرة
- ترحب المجلة بما يرسل إليها من بحوث وموضوعات هندسية وأى تعليقات علمية للمناقشة
- المجلة غير مسئولة عن الآراء التى تنشر بها وتعبر عن رأى كاتبها فقط .

لجنة التحرير

رئيس التحرير الأستاذ الدكتور احمد على العريان

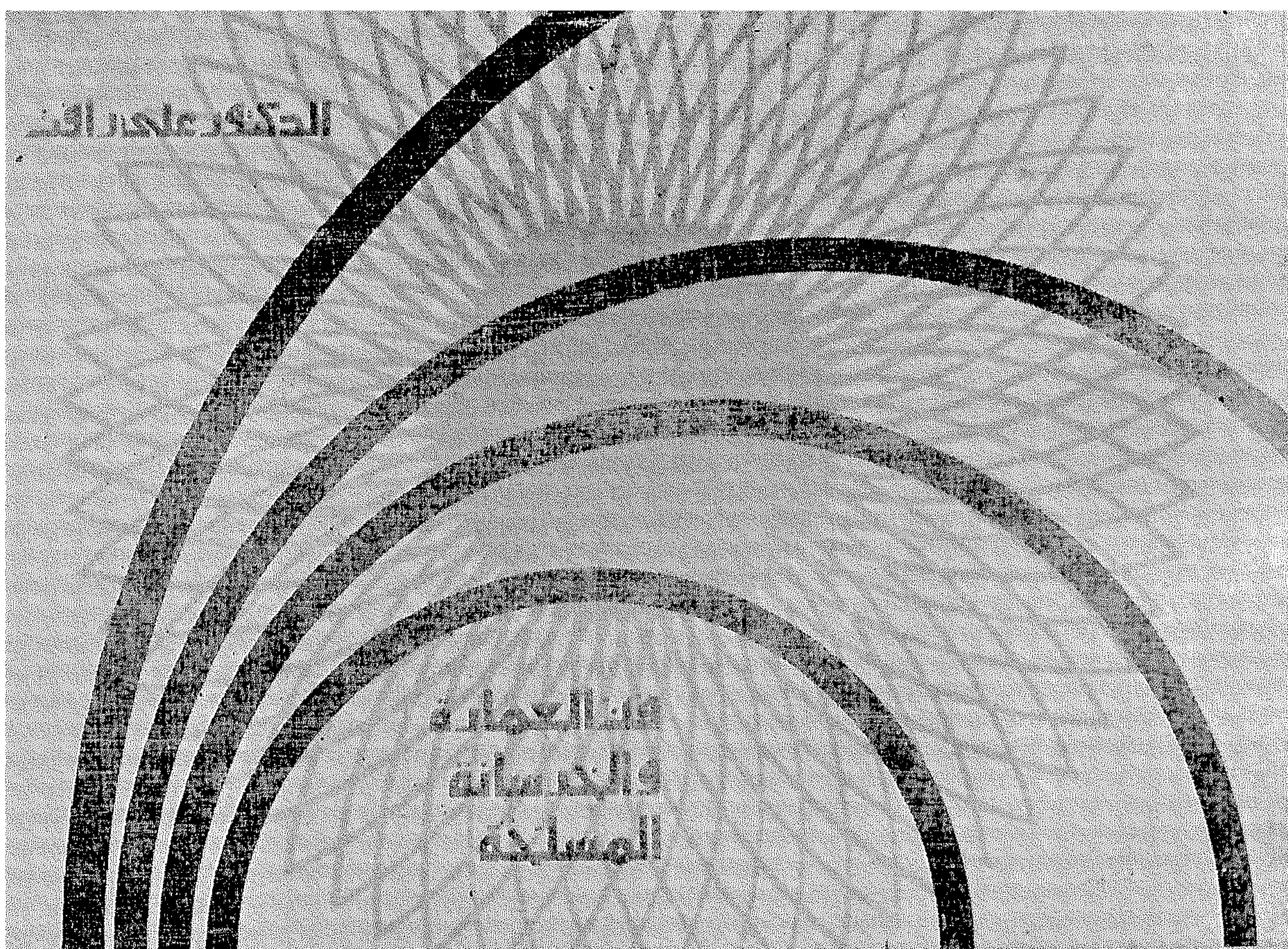
أمناء التحرير:
- المهندس عز الدين فرج
- الأستاذ الدكتور محمد فهيم صقر
- المهندس مدحت العلايلى
- الأستاذ الدكتور يحيى العجماوى

أمين الصندوق المهندس عبد الحميد وهبة الزنفلى

فن العمارة والخرسانة المسلحة

للدكتور المهندس على رأفت

أستاذ قسم العمارة — جامعة القاهرة



كتاب فن العمارة والخرسانة المسلحة — الدكتور المهندس على رأفت

مؤسسة الحلبي القاهرة ١٩٧١ (٥٠٠ صفحة ؛ ٠٠ شكل وصورة)

مقـــدمـــة : اليوم ونحن نجتاز الربع الأول من القرن الثانى من حياة الخرسانة المسلحة ، نجد أنه من الضرورى النظر فيما حققته المادة من النواحى الإنشائية والمعمارية محاولين بذلك استكشاف الخطوط السليمة للتطور المستقبل لعمارة الخرسانة المسلحة .

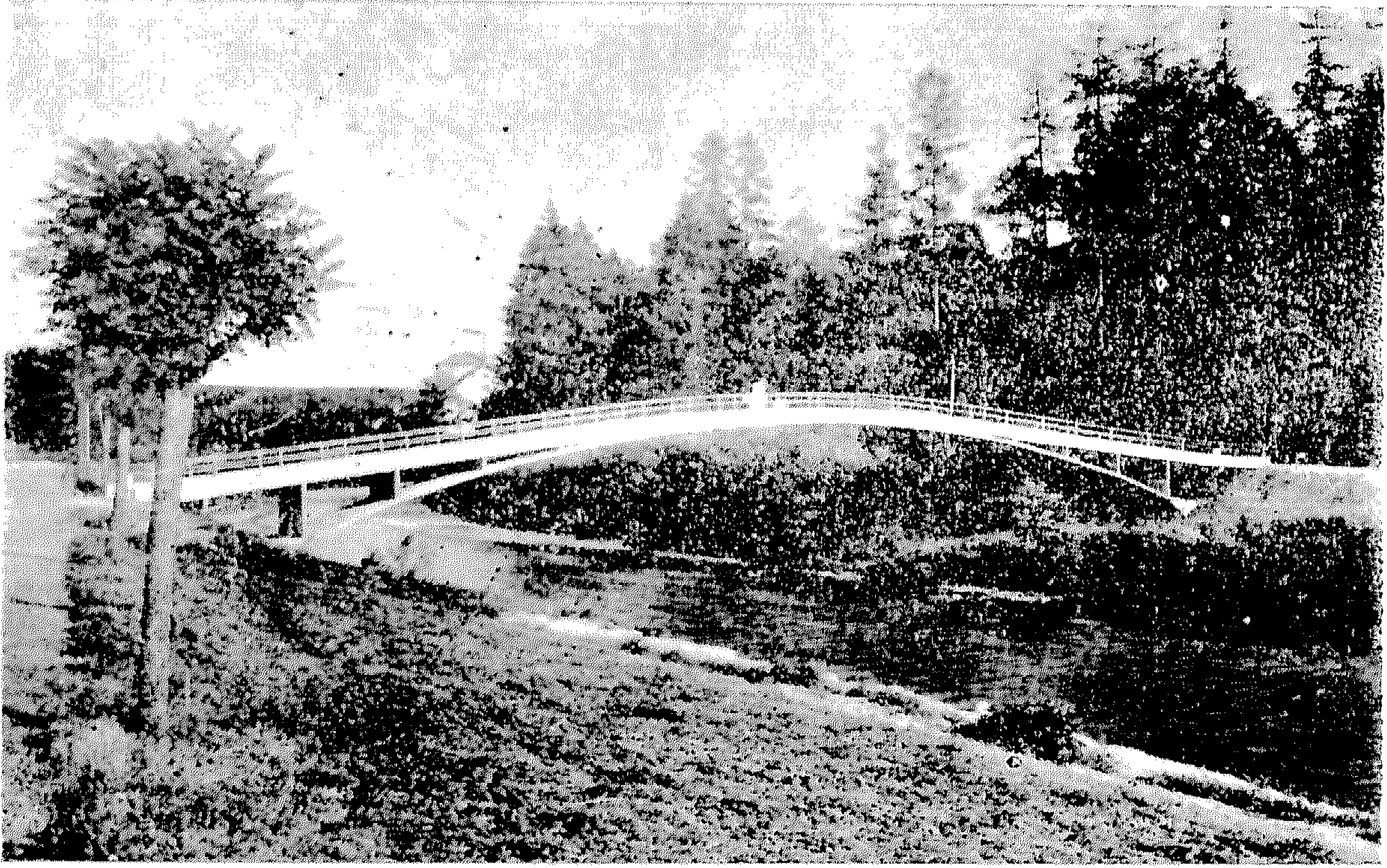


شكل (١) المركز القومى للبحوث الاجتماعية والجنائية — القاهرة ١٩٦٠
المهندس المعمارى دكتور على رأفت

الفن المعمارى كفن انتفاعى يتأثر بجانب عدة عوامل أخرى تأثراً كبيراً بالمادة الفنية التى يتحقق عن طريقها ، فطبيعة المادة تفرض على المعمارى تشكيلاتها الإنشائية ولغتها التعبيرية . والتشكيلات الإنشائية الجديدة عندما تستتب ، تخلق طرزاً معمارية خاصة . فالحجارة تفرض تجميعات على بلوكات متراصة رأسياً فى أعمدة أو حوائط تحمل أسقفاً من بلوكات حجرية على شكل أعتاب أو عقود أو كمرات وجمالونات خشبية . والتكوين الإنشائى يرتبط ببعضه البعض عن طريق الجاذبية الأرضية Gravity Construction بدون أى استمرار مادى أو هندسى بين الجزء والكل . والمنشأ هنا يتعرض لقوى أفقية نتيجة للرياح ، ومقاومته هنا تتأتى من كتلته فى حالة الأعمدة الحجرية ، ومن إمكانيته لمقاومة الانحناء فى حالة الخشب والحديد . والكمرات الرئيسية فى هذه الحالة معرضة لعزوم انحناء كبيرة وخاصة بالنسبة للبحور الواسعة مما يتطلب استعمال أعماق كبيرة للكمرات . ولا يوجد هنا أى تعاون بين وحدات المنشأ بل على العكس تضيف كل وحدة إنشائية حملها إلى الحمل الذى تنقله إلى الوحدة المجاورة . ويمكن تشبيه كفاءة مثل هذا الإنشاء بكفاءة ثلاثة حمالين يحمل كل منهم الآخر ويحمل الآخير البيانو أو الثلاجة . ونتيجة لذلك تميز الإنشاء المصرى بالحجارة بضخامة أعمدته المتقاربة وأعماق كمراته الحجرية الكبيرة . والإنشاء الخشبى والحديدى يضيف إلى الإنشاء السابق قوة أكبر لمقاومة الانضغاط والشد فتقل قطاعات الأعمدة وتزداد إمكانيات البحور المغطاة بأسقف قليلة العمق .

الخرسانة المسلحة ، بإمكانياتها الكامنة فى التشكيل فى قطاعات على رغبة المصمم وبطبيعتها [illegible]ة متماسكة مستمرة مادياً باستمرار حديد التسليح من قطاع لآخر ، أدخلت إمكانيات جديدة للمنشأ المغلف للفراغ المعمارى . هذه الإمكانيات أحدثت ثورة حقيقية فى مجال الإنشاء المعمارى ، وبالتالى فى مجال التشكيل المعمارى فلأول مرة تمكن الإنشاء من تحقيق التعاون بين كافة أجزاء المنشأ على المستوى الخطى فى المنشآت الهيكلية وعلى المستوى السطحى فى المنشآت الفراغية . وفى المنشآت الهيكلية توفر الخرسانة المسلحة وصلة ثابتة بين العمود والكمرة أى توفر استمراراً مادياً بينهما . وفى الهيكل المتماسك يتعرض العمود والكمرة للانحناء وتتولد فيهما عزوم انحناء ، وهنا يكون للكمرة نهايتان ثابتتان وتتعرض لعزوم انحناء أقل . أما الأعمدة فتتعرض إلى إجهادات ضغط كبيرة وانحناء . والهيكل أقوى من الإنشاء بالعمود والكمرة فى مقاومة القوى الأفقية كالرياح مثلا . والعقود الهيكلية ترتفع كفاءتها إذا ما كان ضلعها العلوى مثلثاً أو متعدد الأضلاع حيث تنتقل الأحمال بمجموعة من إجهادات الانضغاط والانحناء فى جميع أضلاع الهيكل . وبزيادة عدد الأضلاع يتحول الهيكل إلى عقد وكلما انطبق على مضلع القوى تعرض العقد كله إلى إجهادات انضغاط وقلت إجهادات الانحناء . من هذه العقود أمكن تحقيق القباب الكروية أو النصف الكروية من أضلاع خطية كقباب شويدلر أو القباب الجيوديسية أو القبوات الحلقية .

إلى هنا والخرسانة المسلحة ما زالت تستعمل فى اتجاهات خطية أى بنفس استعمالات الحديد والخشب . وقد اكتشف المهندس السويسرى روبرت مايار والامريكى تيرنر منفردان ولكن فى نفس الوقت ، عام ١٩٠٨ ، إمكانيات الخرسانة فى التشكيل فى بلاطات مستوية تنقل



شكل (٢) كوبرى للمشاة بسويسرا — المهندس روبرت مايار

الأحمال فى اتجاهين إلى الأعمدة دون الاستعانة بكمرات أو عقود . وقد استخدم مايار البلاطة الإنشائية مستوية أو مقوسة كما جمع بين الإثنين فى هياكل صندوقية فى تصميمات لكبارى منذ عام ١٨٩٩ (شكل٢) وفى مبانى متعددة الطوابق محملة على أعمدة مشرومية . وقد كان ذلك الاكتشاف الهام مقدمة لتطور حديث نحو الإنشاء الخرسانى القشرى فى البلاطات ذات الانحناء المفرد أو المزدوج وذات السمك الصغير بالنسبة للمسطح والمصنوعة من مادة كالخرسانة المسلحة تتحمل الانضغاط والشد . وهنا سار الإنشاء الخرسانى على طريق تحقيق الكفاءة الإنشائية الكاملة حين يندمج الحامل والمحمول فى وحدة واحدة مرتبطة متكاملة وتتحول الإجهادات الداخلية إلى إجهادات أغلبها محورية بالضغط والشد وتنخفض عزوم الانحناء أو تقل لتتركز فى أضيق الحدود حول الفتحات ونقط الارتكاز . هذا التطور حقق نسباً وتشكيلات معمارية جديدة مفردة ومزدوجة الانحناء برقائق من الخرسانة المسلحة ذات أشكال تحقق أكبر قوة مع أقل وزن للمادة . فبين صالة معبد الكرنك بالحجارة وبها ١٣٤ عموداً بأقطار وصلت إلى أربعة أمتار وبين صالة معرض تورينو بالخرسانة المسلحة والخالية تماماً من الأعمدة يتجسم لنا الفرق بين الإنشاء بالبلوكات الحجرية Block Gravity Construction والإنشاء

المستمر هندسياً ومادياً . وبمقارنة قبتى روما الشهيرتين ، قبة البارثنون وقبة قصر الرياضة ، والاثنان يفرقهما ألفا عام من التطور الإنشائى ، نجد أن الأول غطت فراغاً دائرياً قطره أربعة وأربعون متراً بسمك مصمت من ١,٢٠ م إلى ٥,٣م من الخرسانة والطوب ، والثانية غطت فراغاً داخلياً دائرياً قطره ستون متراً بسمك ١٠ سنتيمترات وأعصاب سمكها أربعون سنتيمتراً . وبين التحفتين المعماريتين يظهر تأثير إمكانيات الخرسانة المسلحة فى الاستمرار المادى الفراغى بمادة ذات إمكانيات مناسبة فى الضغط والشد سهلة التشكيل فى أوضاع مناسبة لسهولة انتقال الأحمال الحية والميتة إلى الأرض . ولأول مرة حققت الخرسانة المسلحة بپلاستيكيتها للعمارة إمكانيات التشكيل فى أوضاع تحقق القوة الناتجة عن الشكل بدلا من القوة الناتجة عن الكتلة .

مرحـــلة النمـــو : لقد مضى قرن من الزمان على اكتشاف الخرسانة المسلحة لكى تبدأ على الطريق السليم نحو تحقيق إمكانياتها الخاصة معمارياً وإنشائياً وقد مرت المادة خلال هذا القرن فى مرحلة الاكتشافات الأولى فى انجلترا بتسجيل ولكنصن عام ١٨٥٤ لتسليح بلاطات خرسانية بكابلات مجدولة ، وفى فرنسا عن طريق تسجيلات فرانسوا كونييه لبلاطات خرسانية بأسياخ متقاطعة على شكل قطع الشطرنج عام ١٨٥٦ ، وبراءة اختراع مونيه عام ١٨٦٧ لأحواض نباتية من الأسمنت المقوى بسلك شبكى . وفى أمريكا قام هايات بتجارب على كمرات وبلاطات خرسانية ذات تسليح متباين منذ عام ١٨٥٥ والتى نشرت فى كتابه سنة ١٨٦٦ ، كما بنى وارد مسكنه بالخرسانة المسلحة بقرب بورتشستر بولاية نيويورك بين عامى ١٨٧٣ ، ١٨٧٦ . ثم انتقلت الخرسانة المسلحة إلى مرحلة التطور عن طريق مهندسين ومقاولين من أمثال وايس فى ألمانيا وهنبيك فى فرنسا وبيلى ورانسوم فى أمريكا . وفى بداية القرن العشرين نرى الخرسانة المسلحة وقد اكتسبت القبول الشعبى والهندسى ، وانتقلت من مرحلة المحاولات الاستكشافية إلى مرحلة الاستعمال الثابت فى المجال الإنشائى .

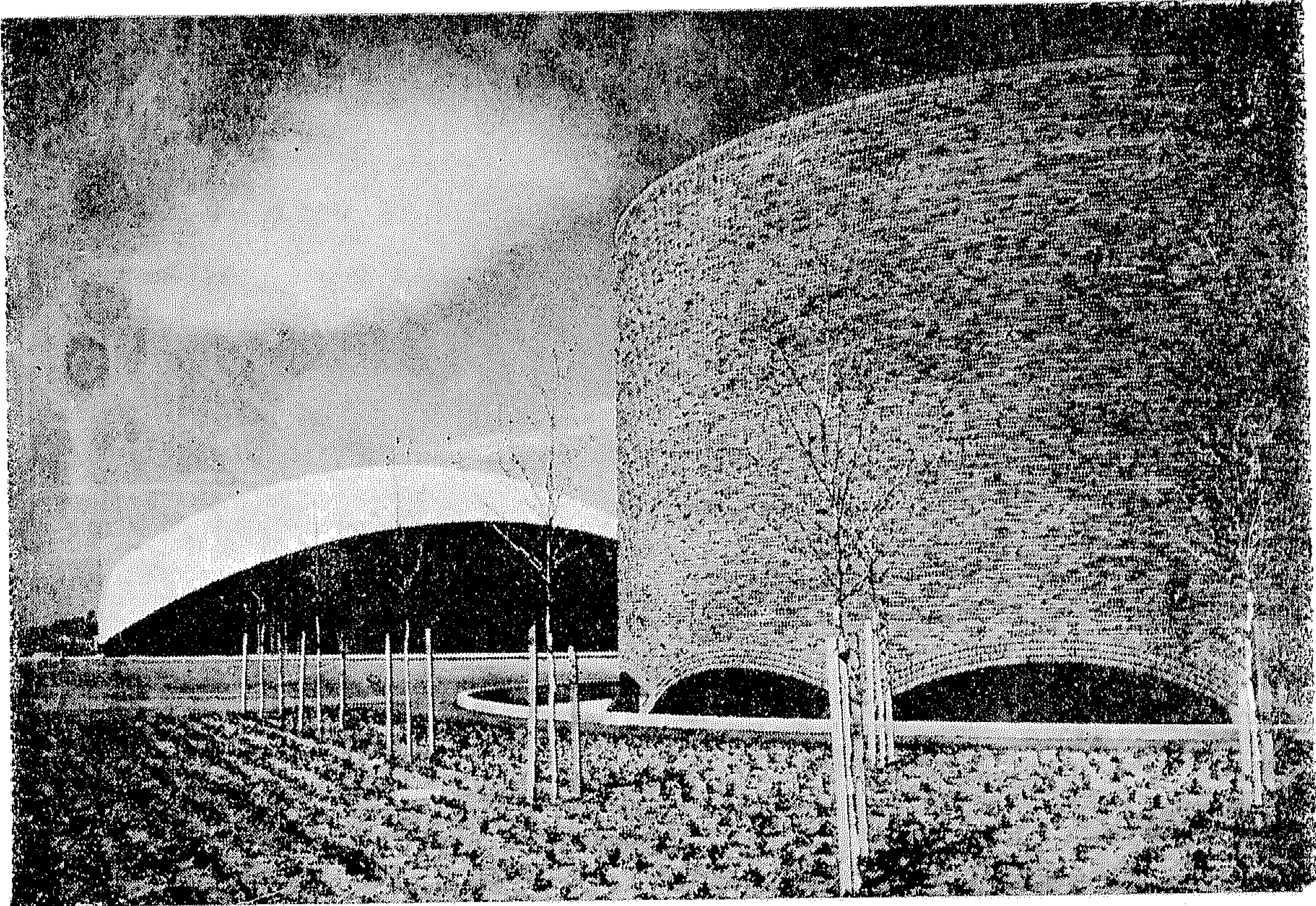
حتى هذه المرحلة كانت النظرة الإنشائية للخرسانة المسلحة امتداداً للنظرة الإنشائية للخشب بالكمرات الرئيسية والثانوية . وبالتدريج ازداد الوعى الإنشائى بالمادة وخرج للوجود اكتشاف إنشائى أحدث ثورة فى مجال الإنشاء المعمارى وهو اكتشاف مايار وتيرنر السابق الإشارة إليه للبلاطات الخرسانية الفعالة الذى فتح المجال للانشاء القشرى وللوصول بالتالى إلى ذروة الكفاءة الإنشائية .

لقد فتحت هذه الاكتشافات مجالات واسعة أمام الإنشاء الخرسانى ، مما شجع على تطويره علمياً وتكنولوجياً ، فحدثت فى السنين الأخيرة تطورات غير محدودة فى مواد الخرسانة فى أنواع الركام والأسمنتات وطرق الصناعة وبالتالى إمكانيات الخرسانة الناتجة . هذه التطورات ضاعفت عشرات المرات فى قوة الخرسانة وقوة تحملها للبيئة المحيطة بها . وفى متناول الصناعة الآن أنواع متباينة من الأسمنتات ، وما زالت أنواع أخرى فى مجال التطوير المعملى . كما تطورت

إمكانيات حديد التسليح نحو القوة العالية فى الشد مع تماسك أكبر بالخرسانة المحيطة بها . حدثت تطورات هائلة نحو حل أكبر مشاكل الإنشاء الخرسانى فى الشدات المؤقتة والصب تحت العوامل الجوية المختلفة والزمن الضائع فى انتظار عملية الشك . وقد اتجهت هذه التطورات نحو تعدد استعمال الشدات عن طريق تحريكها رأسياً أو أفقياً أو دائرياً ، كما حدثت تطورات طفيفة ومتوقعة نحو سبق تجهيز الهياكل المتكررة وذات البحور الواسعه والحوائط الخرسانية الحاملة وذلك رغم معارضات كبيرة من الهيئات التى تفضل استمرار الأوضاع القائمة لأسباب اقتصادية أو اجتماعية . ومن أبرز تطورات سبق التجهيز التوصل إلى وحدات سابقة التجهيز يتم تجميعها على موقعها وتتخذ شكلها النهائى بواسطة خرسانة مصبوبة على الموقع تكون جزءاً هاماً من القطاع الإنشائى ، وبذلك يتحقق للانشاء الجاهز مزايا خفة الوزن والاستمرار المادى بين أجزائه المختلفة .

ماذا كان موقف العمارة من هذه الثورة الإنشائية ؟ فى البداية بعدت عنها وعن حق محاولة تفهمها . العمارة فى القرن التاسع عشر تسير فى خطوط رومانتيكية إكليكتيكية . المعمارى يصمم المبنى على طراز معين والمقاول ينفذه بما يحلو له من مادة . فى هذه الفترة رأينا مبانى خرسانية على طرز كلاسيكية وغوطية وإسلامية وغيرها من الطرز المعمارية المختلفة . ومن الطبيعى أن هذه الحالة لم ترض جيلا من المعماريين الشبان من تلاميذ ڤيوليه لى دوك المؤمن بضرورة تقيد العمارة بالمنطق الإنشائى السليم . ثار هؤلاء من أمثال بوديه وبيريه وجارنيه فى فرنسا على الأوضاع الأكليكتيكية محاولين إيجاد لغة معمارية خاصة بالخرسانة المسلحة ، إلا أن طريقهم إلى هذه اللغة ولو أنه تحرر من القيود الأكليكتيكية إلا أنه سار على طريق الإنشاء الخشبى والمعدنى ، فى حين أن البلاطات الإنشائية والصدفات القشرية كانت من الحلول الشائعة لدى الإنشائيين . بالتدريج ابتدأت العمارة فى التجاوب ببطء وتردد ناتج عن عدم دراية كافية بالأسس الإنشائية المستحدثة وبآثارها وإمكانياتها المعمارية . وقد أصبح لازماً على المعمارى إذا قدر له أن يحتل مكانه الطبيعى فى تطور عمارة الخرسانة المسلحة أن يتخطى الهوة الموجودة بين الحقيقة الإنشائية والخلق الفنى . أصبح لزاماً عليه أن يتتبع الإمكانيات الإنشائية بالخرسانة المسلحة مبتدأ من أبسط تكويناتها بالعمود والعتب إلى نهايتها نحو التكامل فى الاستمرار المادى والهندسى متتبعاً العلاقة التسلسلية بين جميع التكوينات الإنشائية على مقياس الكفاءة الإنشائية .

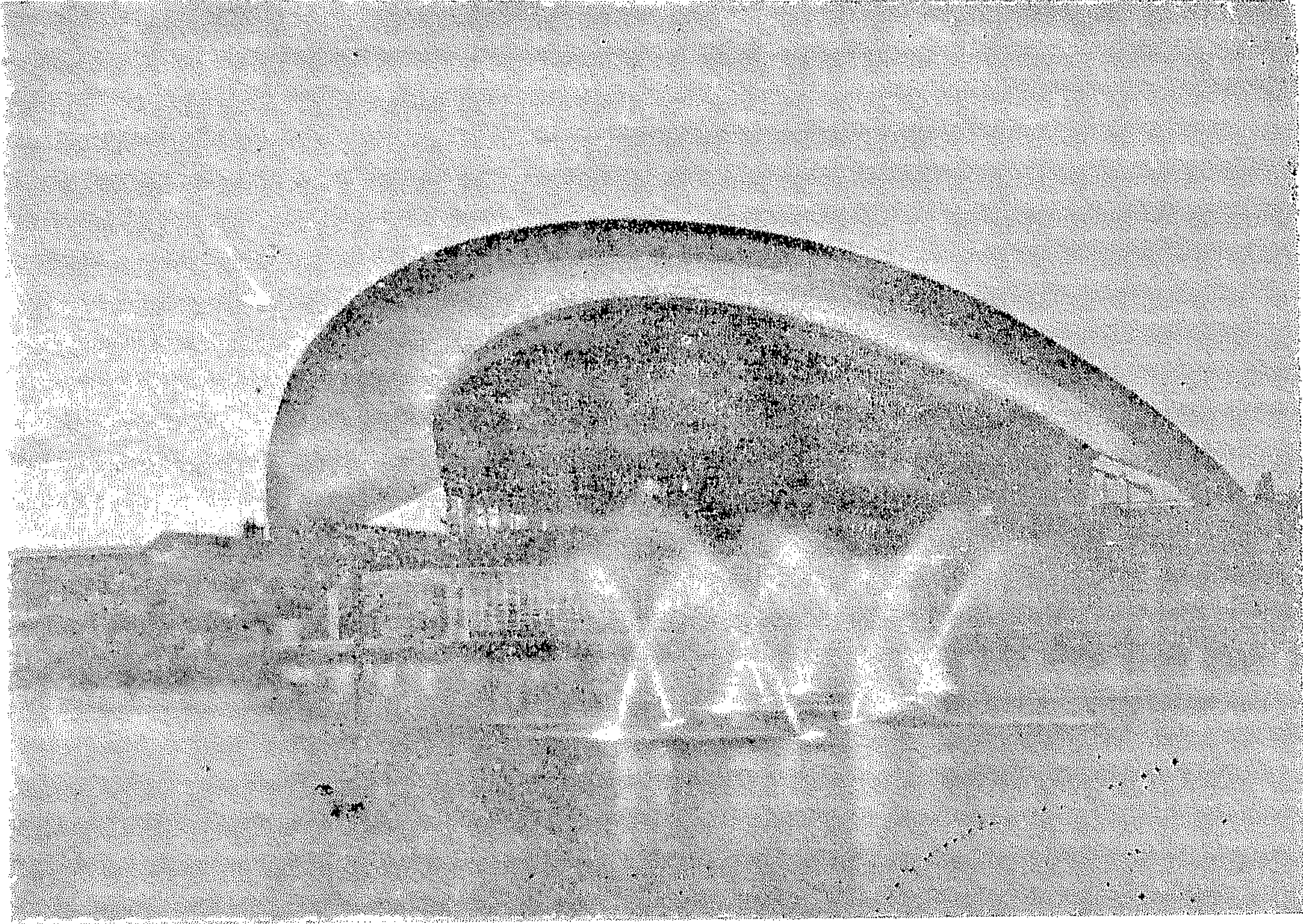
الفراغات المعمارية والخرسانة المسلحة : هذه الحرية اللانهائية فى التشكيل على أسس إنشائية منطقية تقابلها معمارياً احتمالات عديدة وصعوبات جمة . أصبح على المعمارى أن يدرس هذه الاحتمالات والصعوبات وأن يدرك أن هذه التشكيلات ليست هدفاً فى ذاتها بحيث يسعى إليها طلباً للتجديد أو الطرافة بل هى وسيلة لتحقيق إمكانيات انتفاعية لفراغات معمارية اجتماعية مختلفة . على المعمارى أن يختار لفراغه



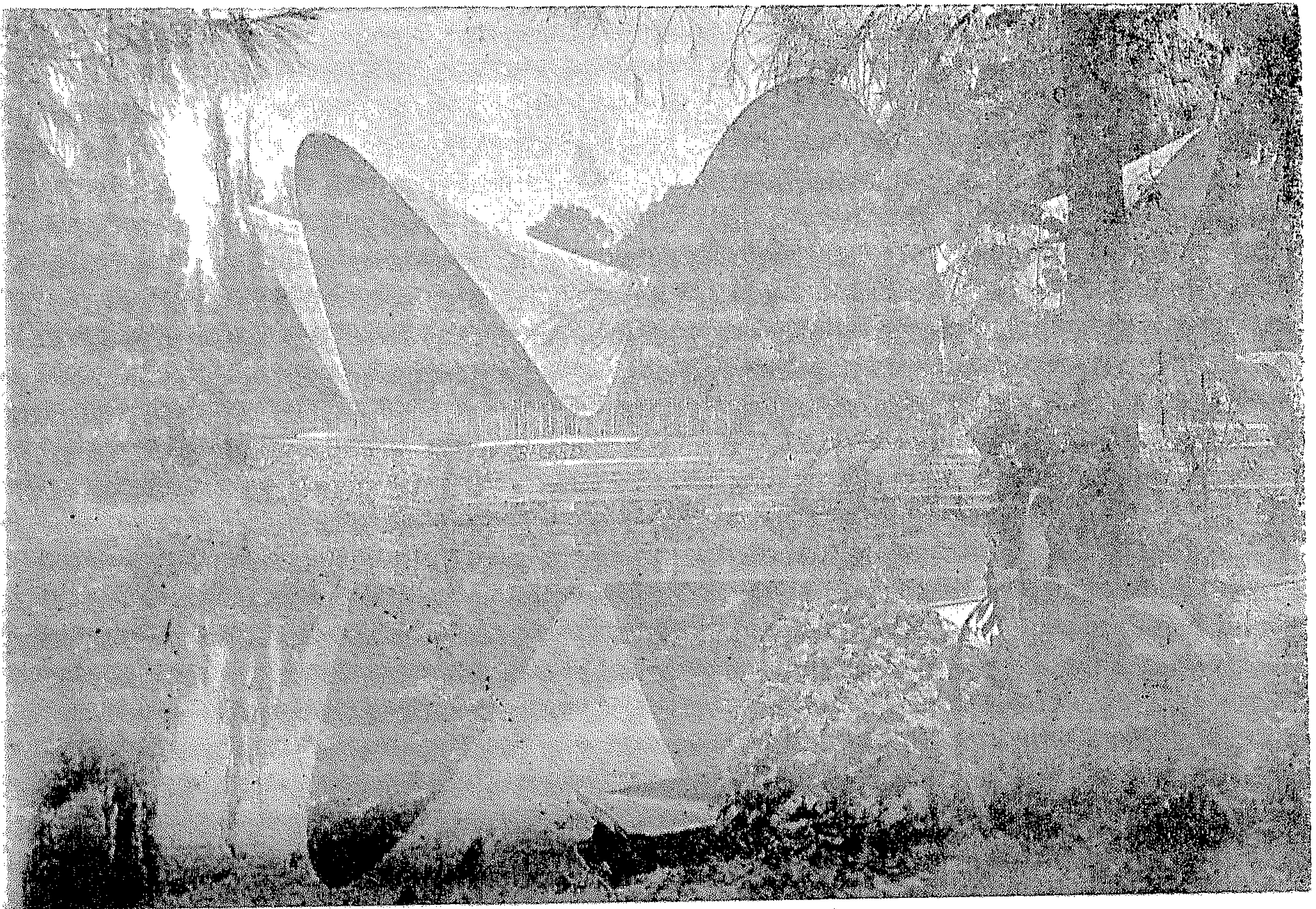
شكل (٢) صالة الاجتماعات بمعهد ماساتشوستس التكنولوجيا — أمريكا

الإنشاء المناسب ثم عليه أن يدرس التفصيلات المعمارية المختلفة التى تتطلبها هذه التشكيلات الجديدة من مداخل وفتحات الاضاءة والتهوية وحوائط وسلالم ومعالجات للحرارة الصوت والإضاءة والتكسيات الداخلية والخارجية وغيرها من المشاكل التى هى الآن محل بحوث ومؤتمرات متعددة . هذا بخلاف دراسته لإمكانيات التنفيذ مع توفير احتمالات التغيير بالإضافة والحذف ، وهى الاحتمالات المتوفرة فى الإنشاء الهيكلى .

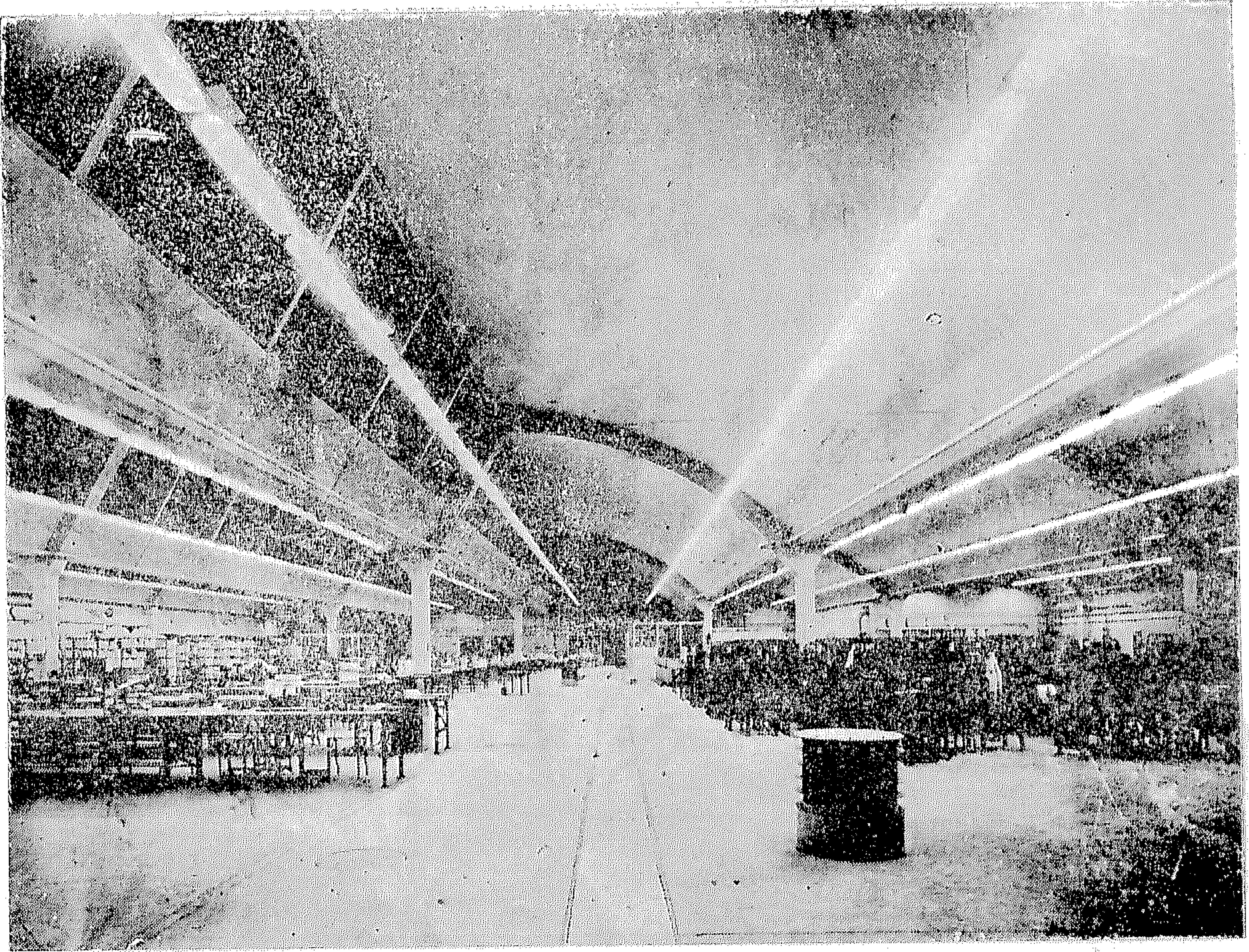
هذه الظروف للفراغات المعمارية المختلفة هى التى تتطلب الوقوف عند درجات مختلفة من الاستمرار المادى والهندسى مبتدءاً من قمة الإنشاء الكروى المتكامل إلى انعدامه فى الإنشاء بالعمود والعتب . وبينما القمة الإنشائية مقفلة ومحدودة الإمكانيات المعمارية ، نجد الإنشاء ذو الإنحناءين بنفس الإشارة فى القباب وخلافها يكون صعوبات معمارية عند صلته بالأرض كما يخلق صعوبات وفى الإضاءة مما قد يتطلب فى حالات معمارية رفع القبة على أعمدة ، أو قطعها بمستويات (شكل ٣) . كما نجد أن الاحتمالات المعمارية لأحد صور الإنشاء ذو الإنحناءين المختلفى الإشارة ، وهو القطاع الزائدى المكافىء واسعة سواء مفرداً (شكل ٤) ، أو مجمعاً فى مجموعات متلاصقة أو متباعدة (شكل ٥) ، مرتكزاً على الأرض أو مرفوعاً على أعمدة . أما



(شكل ٤) صالة اجتماعات الـكونجرس — برلين الغربية

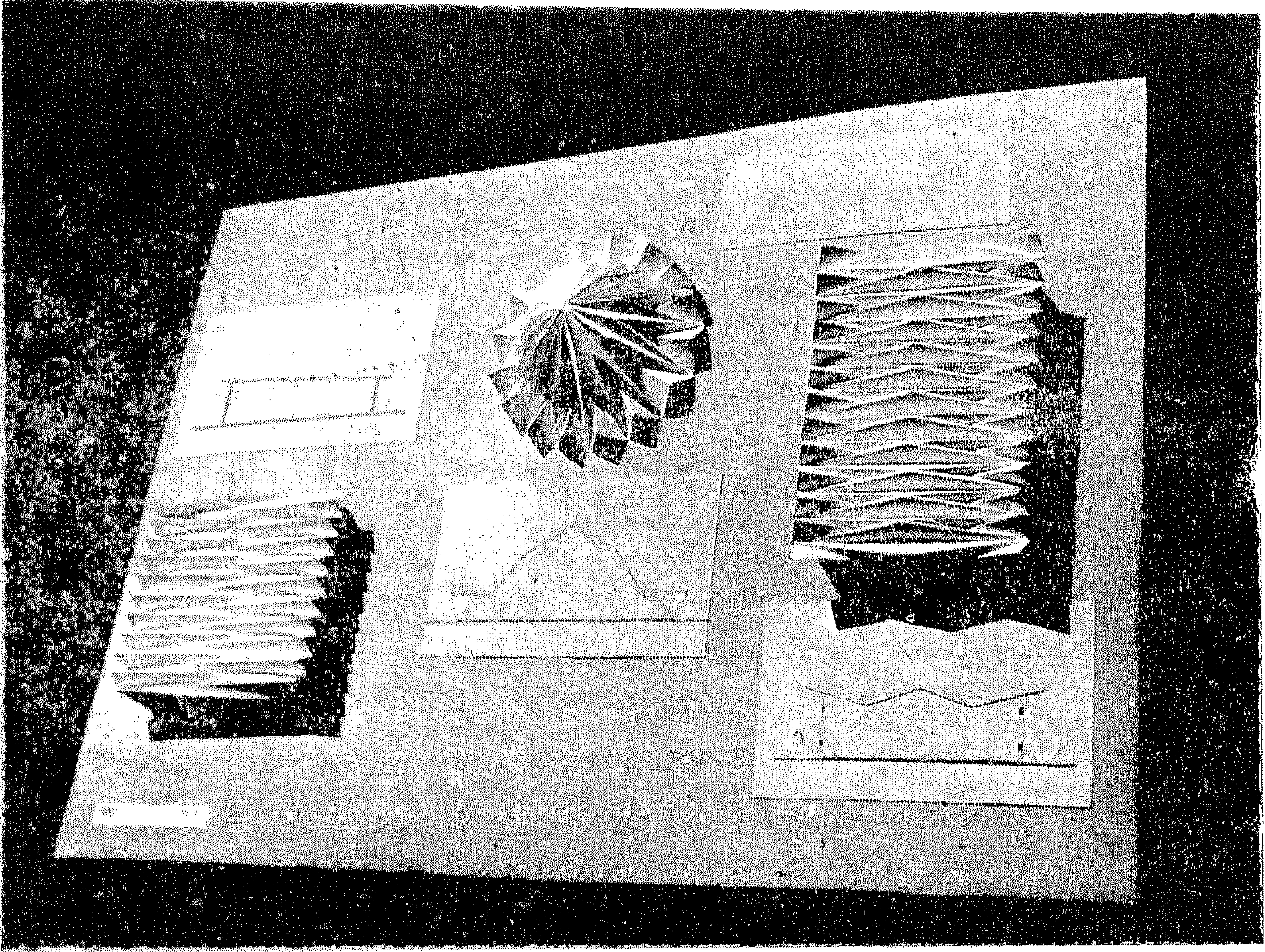


(شكل ٥) صالة مطعم لوس ، ماننتيالس ، بالمكسيك



(شكل ٦) مصنع دونارلويد — سوانسى بانجلترا

الأسقف المفردة الإنحناء (شكل ٦) أو المسطحة أو المنطبقة (شكل٧) فإنها تحقق استمراراً مادياً وهندسياً فى اتجاه واستمراراً مادياً فقط فى اتجاه آخر ، وهى بذلك تتيح حرية فى الفتحات المعمارية فى الجانبين . هذه التشكيلات قد تستعمل مجمعة أو منفردة على الأرض مباشرة أو على بلاطات أو أعمدة ، وبذلك تتحقق إمكانيات المسقط المفتوح على مستوى الأرض . وقد تتطلب الاحتياجات المعمارية للفراغات المتكررة رأسياً مع توافر إمكانيات المسقط المفتوح واحتمالات التغيير على المستوى الأفقى ، الاستمرار فى استعمال الإنشاء الخطى الهيكلى والزوايا المتعامدة بالخرسانة المسلحة رغم قصورها فى الكفاءة الإنشائيــة . كما قد تتطلب عملية سبق التجهيز الكامل بالمصنع لأعمدة وكمرات ، الارتباط بالإنشاء بالعمود والعتب محتفظة بإمكانياته فى التغيير والحذف والنقل من مكان لآخر رغم ما فيه من انعدام فى الكفاءة الإنشائية .



شكل (٧) نماذج من تجارب طلبة السنة الثانية عمارة بالأسقف المنطبقة — جامعة القاهرة

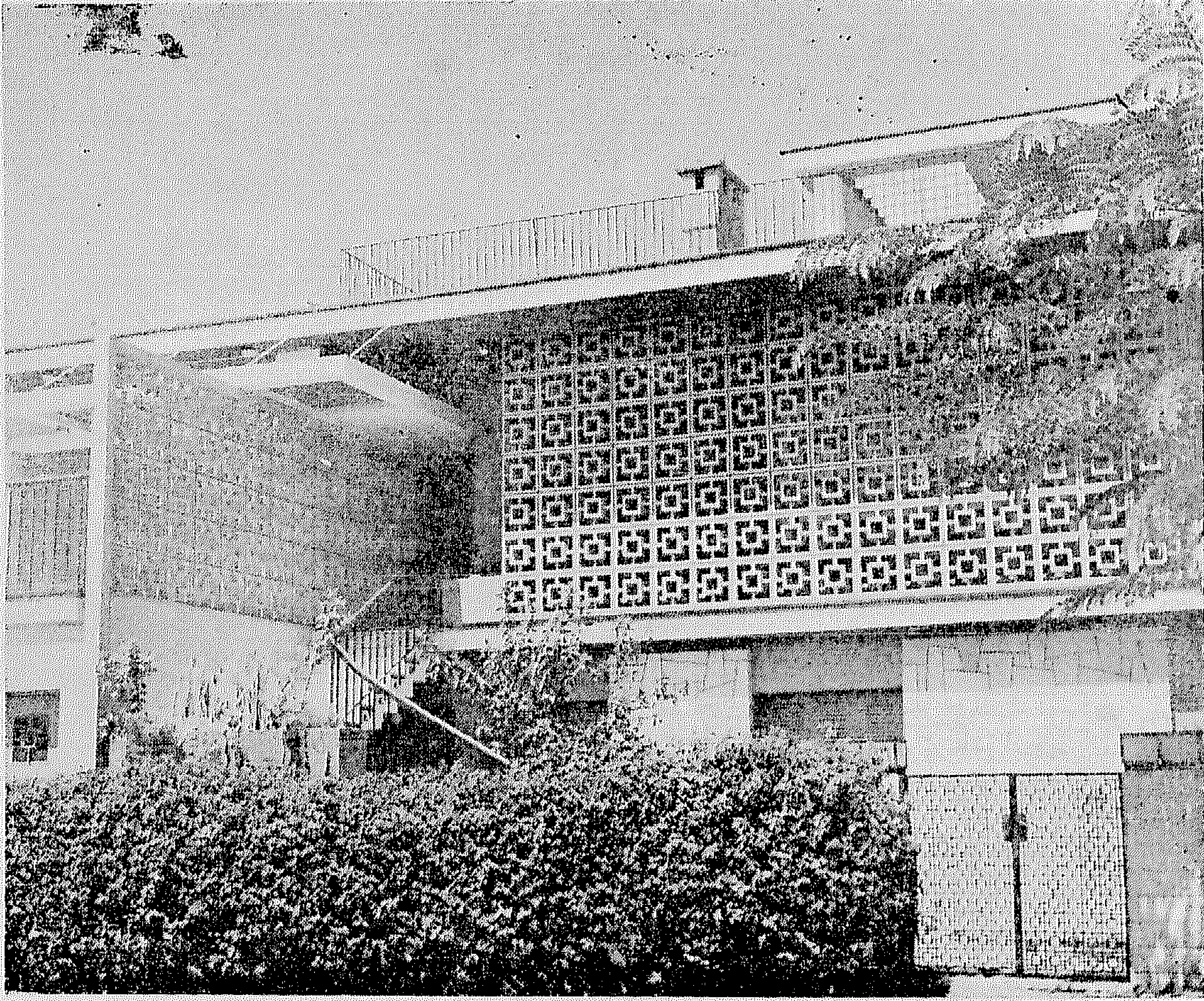
الجمـــال المعمـــارى والخرسانة المسلحة :

ومن الناحية الجمالية نجد أن الخرسانة المسلحة قد فتحت مجالات جديدة للسطح والشكل والتعبير المعمارى . وعلى المعمارى أن يجعل من الحرية التى أتاحتها له الخرسانة نعمة لا نقمة على خلقه الفنى ، وذلك ببناء كل تصرفاته على أساس منطق سليم مبنى على دراسة لطبيعة المـادة وإمكانياتها ، مع دراسة للانسان ومدى تأثره بصرياً وفكرياً ونفسياً بالمؤثرات المعمارية المختلفة على المستوى السطحى والشكلى والتعبيرى .

السطح الخرســـانى :

الخرسانة مادة ذات إمكانيات ممتازة فى المعالجة المعمارية للأسطح . والخرسانة المكشوفة يجب معالجتها بمهارة الإخصائى وعناية الفنان لإنتاج أسطح قوية دائمة على درجات مختلفة من الظل والنور . فهى تنتج لنا الأسطح الناعمة المصقولة بشدات من الصاج أو الخشب الممسوح . وقد يتعمد المعمارى إظهار انطباعات الشدات للتقليل من تأثيرها على انتظام السطح وليعبر عن طريقة الصناعة . ومن الأسطح الخرسانية ما يتعمد فيها المعمارى إظهار مكونات الخرسانة من ركام منتق من أحجام وألوان مختلفة وذو كثافة معينة قرب السطح الخارجى ، وذلك بالطرق

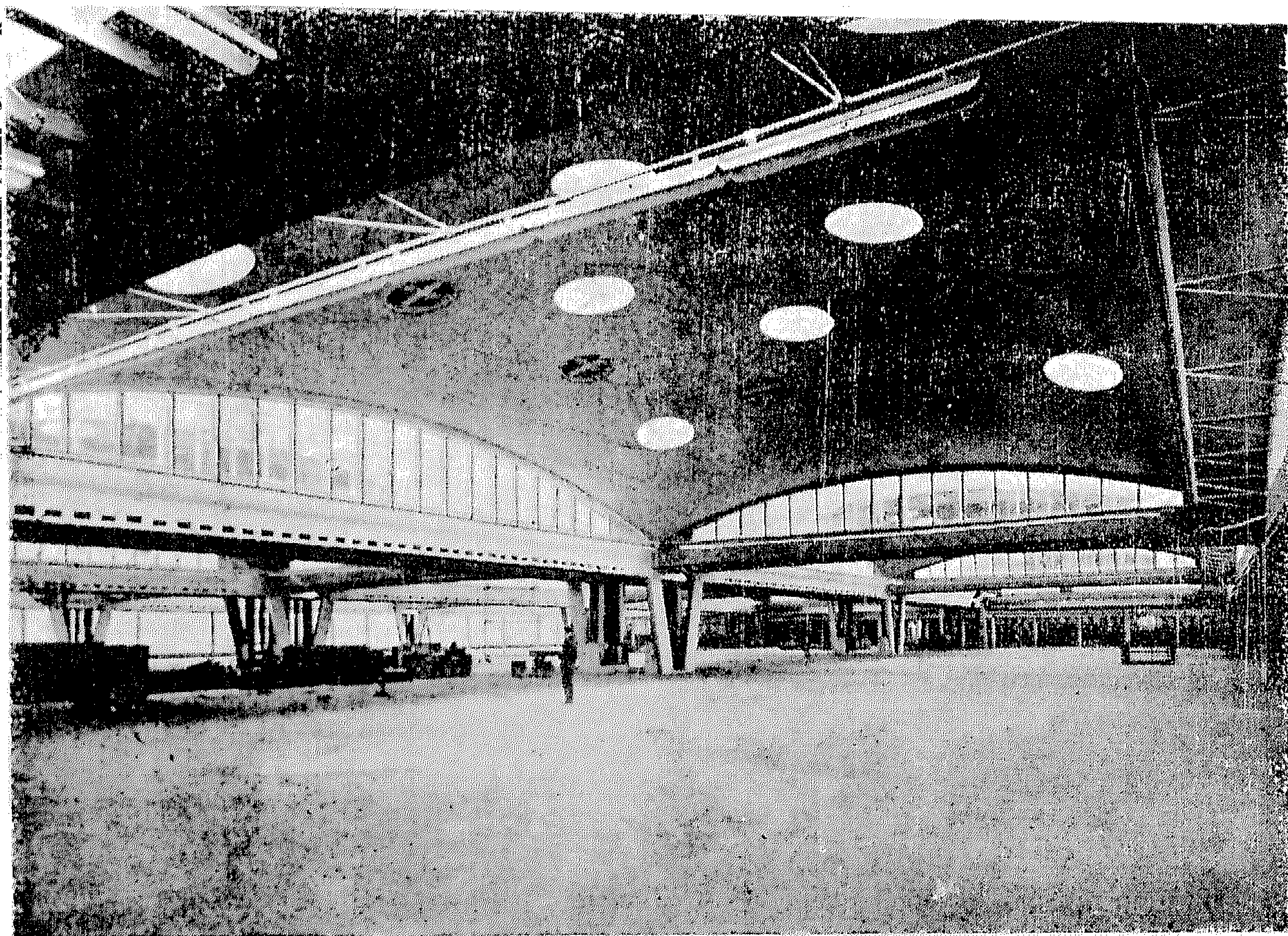
أو الكشط والتسوية أو بمسدس الرمل ، أو المسح بفرشاة سلك . وقد تستغل إمكانيات إنطباعات الشدات البارزة أو الغاطسة للحصول على أسطح خرسانية ذات تشكيلات فنية هندسية أو تعبيرية . وقد تستغل فى هـذا إمكانيات البلوكات سابقة التجهيز المفرغة أو المصمتة (شكل ٨) .



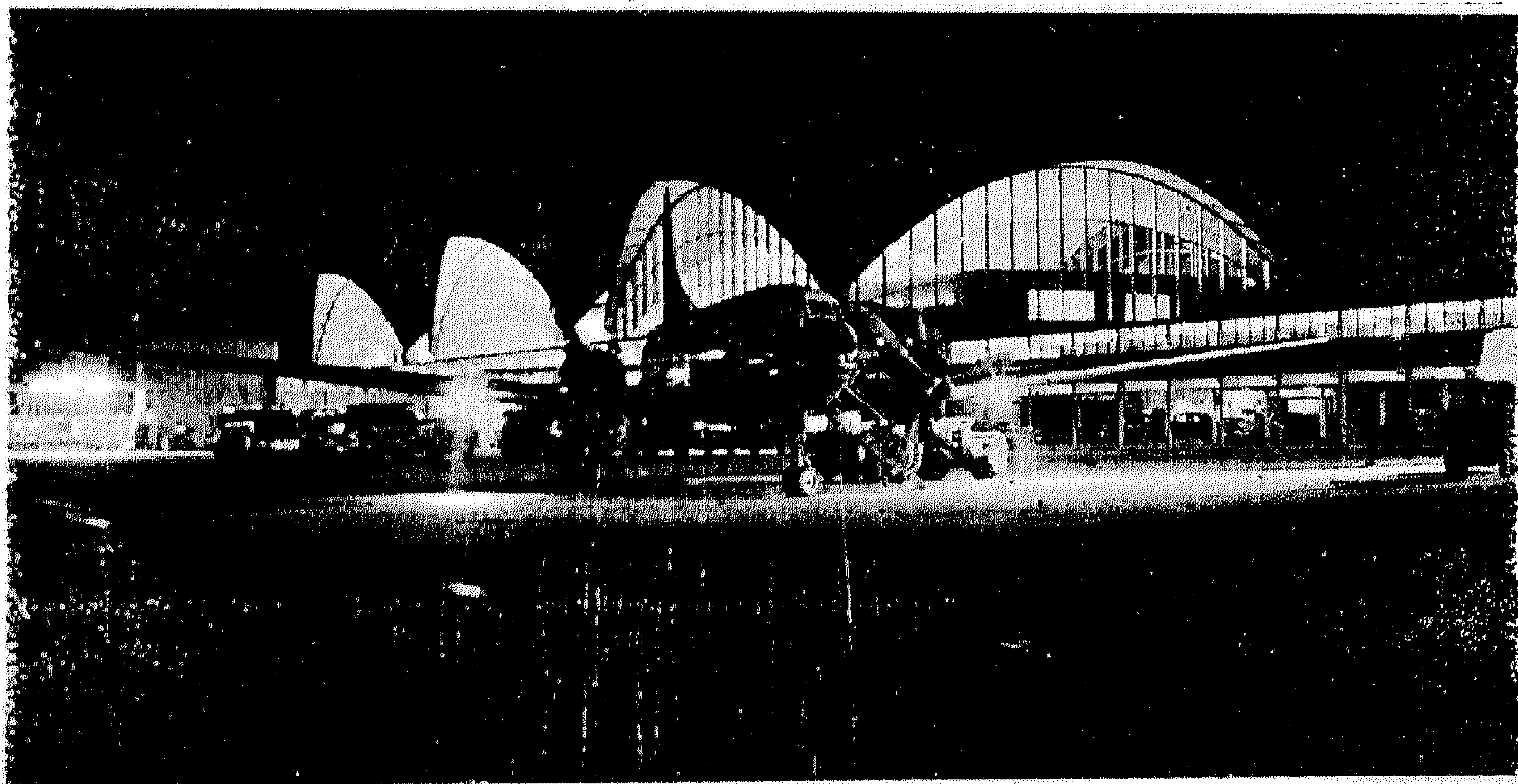
(شكل ٨) فيلا المهندس فؤاد شلبى والمهندس المعمارى دكتور على رأفت

ومن ناحية التمتع باللون الخارجى نجد أن الخرسانة بلونها الطبيعى الرمادى المخضر ذات لون محايد بارد ثابت على مر الزمن قليل التأثر بالعوامل الجوية .

وهنا يجب إضافة ألوان أخرى معه . وهنا يهدف المصمم إلى تكوينات ناجحة باللون تلعب فيها المسطحات الخرسانية دور اللون المحايد المتغلب وتلعب فيها ألوان مركزة أخرى فى الفتحات والأسوار والمزروعات دور الألوان المتناقضة Accent وقد يتعمد المصمم تغيير اللون الرمادى للخرسانة عن طريق كشف ركام ملون طبيعياً كان أم صناعياً .

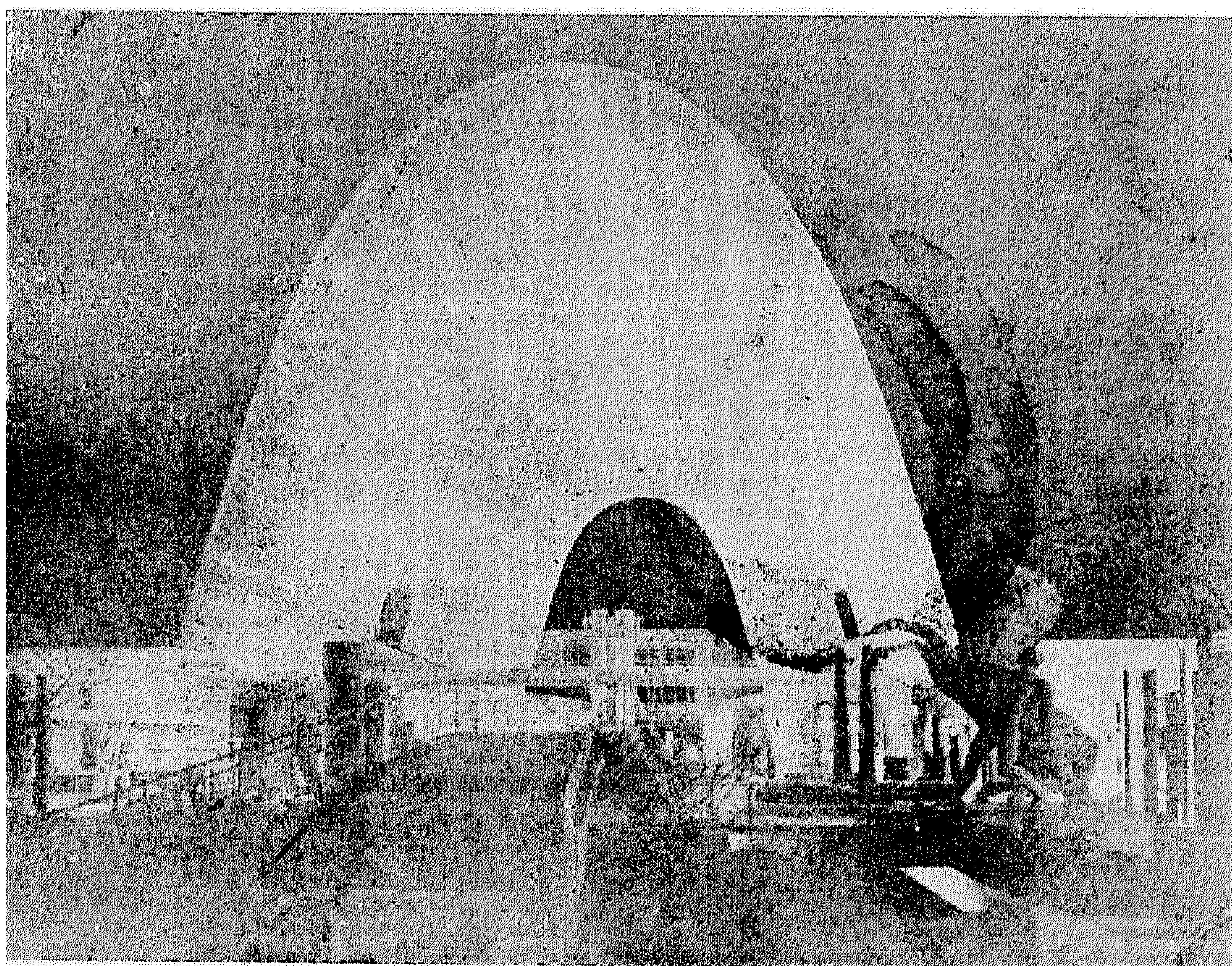


(شكل ٩) مصانع برنتادر للمطاط — انفيلد — انجلترا



(شكل ١٠) مطار لويسى — أمريكا

الشكل الخرسـانى : على مستوى الشكل نجد أن الخرسانة المسلحة قد أنتجت أشكالا جديدة مغايرة تماماً لما تعودت عليه العين البشرية على مر العصور . لا تتكون هذه الأشكال من مستويات رأسية وأفقية متعامدة وموازية للأرض، كما أنها لاتحتوى على الفتحات الرأسية أو الأفقية ذات الأعتاب الأفقية أو المعقودة ، بل هى أشكال بلاستيكية ترتكز على الأرض أو على أعمدة ، هى فى تشكيلات هندسية بسيطة سهلة الاستيعاب والإدراك ذات بروفيل إنسيابى يريح العين . هذه التشكيلات يتوقف نجاحها على ملاءمتها للاحتياجات المعمارية للفراغ ومدى ملاءمتها للكفاءة الإنشائية . وعلى المعمارى أن يدرس طرق الإدراك البصرى لشكلها ومقياسها داخلياً وخارجياً عن طريق الرواسم على سطحها ، وهذه تنتج عن طريق الفتحات (شكل ٩) أو التقاطعات (شكل ١٠) أو التموجات أو الأعصاب.



(شكل ١١) جناح صناعة الأسمنت السويسرية — زيورخ ١٩٣٩
المهندس روبرت مايار

والادراك البصرى للشكل يلزم توفير طرق التعرف على مقياسه ، وهذه تتواجد عن طريق توفير وحدات انتفاعية مألوفة كعنصر المقارنة مثل السلالم والأبواب والأرائك ، والتماثيل والأسوار وسقيفات المداخل (شكل ١١) وقد تتوافر بتكرار وحدة إنشائية معينة كوحدات الجمالونات ، أو الكمرات الرئيسية والثانوية أو الفتحات المتكررة بالأسقف ، أو الحوائط ، أو الوحدات الزخرفية السابقة التجهيز كسطح خارجى أو داخلى للحوائط .

التعبير الخرســــانى :

ولا تتكامل المتعة الفنية بالشكل المعمارى إلا بتكامل الإدراك الفكرى له الأمر الذى يتأتى عن طريق التعبير المباشر والمؤكد عن المادة ، وطرق صناعتها ، وطرق تجميعها وتشكيلها . وعن طرق تأكيد هذا التعبير يتضح الاستيعاب الفكرى والمنطق للحقيقة الإنشائية الأمر الذى تتكامل معه المتعة الفنية . والخرسانة المسلحة كمادة بلاستيكية متماسكة تبرزها التكوينات الأقرب إلى الإنشاء المثالى كما تؤكدها المنشآت ذات الأسقف الكابولية بأنواعها المختلفة . كما تعبر عن هـــذه الخاصة البلاستيكية كافة التصميمات التى تستغل الإمكانيات البلاستيكية للخرسانة فى الصب فى قوالب زخرفية للوصول لتكوينات فنية حرة أو متكررة ، وتعتبر كافة الاتجاهات نحو تأكيد وإظهار تأثير الشدات على الشكل المعمارى النهائى للخرسانة أو تأثير سبق التجهيز هى فى نفس الوقت تعبير عن طرق الصناعة . كما أنه من الواجب تأكيد وتوضيح طريقة التجميع الإنشائى سواء أكان ذلك الإنشاء خطياً بالهيا كل الخرسانية المفردة أو المتكررة أفقياً ورأسياً ، أو الإنشاء بالأسطح الفعالة . وهنا تتحتم التفرقة فى التعبير بين الأسطح الحاملة والأسطح غير الحاملة من ناحية القوة والضعف ، كما يلزم تأكيد السمك الرقيق للأسطح الفعالة بالخرسانة المسلحة (شكل ٩) .

عمارة الخرسانة المسلحة على أبواب ثورة هائلة ، هذه الثورة ولو أنها حلقة فى سلسلة التطور المعمارى إلا أنها جديدة فى كل مكوناتها وهى تحمل فى ذاتها بذور إمكانياتها وتقدمها . هذه الإمكانيات متوفرة فى أغلب بلاد العالم مما يعطيها صفة الدولية ، وهى للبلاد النامية خير فرصة لإشباع الاحتياجات الماسة للفراغات المعمارية الانتفاعية الجميلة .

والخرسانة المسلحة كما تكمن فيها بذور نضجها وتقدمها ، فإن فيها احتمالات تدهورها واضمحلالها ، فقد تتعدد الأسطح أو تزدحم بالزخارف أو تكبر التشكيلات وتتعقد لتصبح جبالا رمادية رابضة على الأرض يتضاءل أمامها الإنسان وتتضاءل أعماله السابقة . والفرق بين النتيجتين ، هو الفرق بين التفكير المنطقى السليم ، وبين مجرد استغلال الطاقات للفت الأنظار ، أو لكسر الأرقام والإحصاءات . ولتوجيه التطور نحو الهدف الأول كان الهدف من إصدار الكتاب .

ملخص الموضوعات بالقسم الافرنجى

استقبال الموجات الطويلة

للدكتور المهندس أحمد لطفى السيد

يشتمل هذا البحث على نتائج مقارنة أمام التردد القومى (المعهد القومى للقياس والمعايرة) مع أئمة التردد فى الدول الأخرى . وقد دامت هذه المقارنة سنتين كان يستقبل خلالهما محطق GBR, W W V L ونورد نتائج السنة الأولى باختصار إذ أنها كانت موضوع بحث سابق . وتوضح كذلك الأجهزة المستعملة .

ويناقش البحث التغير اليومى فى السطور ويلاحظ أنه هناك تأثير موسمى كبير . ويتضح من البحث أن الإمام القومى للتردد لا يختلف عن المتوسط الدولى للتردد بأكثر من بضع أجزاء من $١٠^{١٢}$.

* * *

REFERENCES

1. Ali Saleh "Gundsätze Für die wärmetechnisch und wirtschaftlich günstige Ausbildung von Gebäude Wänden un Dächern in warmen Ländern." Dr. Dissertation, T.H. Hannover, 1962.

2. Olgyay and Olgyay. "Solar control and shading devices." Princeton University Press, New Jersey 1957.

3. E. Eckert. "Einfühung in den Wärme- und Stoffaustausch." Springer-Verlag. Berlin. 1959.

4. Mackay and Watson. "Summer weather data and Sol-air temperature." ASHVE Journal. 1944.

5. M. Jakob. "Heat transfer. Volume 1." John Wiley Inc. New York. 1958.

6. Gröber-Erk-Grigul, "Grundgesetz der Wärmeübertragung". Springer Verlag 1961.

7. Hiller, F. "Wärmehaushalt und Klimafaktoren des Gewächshauses." Heizung-Lüftung-Haustechnik, Bd. 8 (1957).



In Khartoum however, a feeling of excessive heat prevails during the complete daily cycle.

The above results refer to normal summer weather conditions usually prevailing between April and September. They illustrate the short duration of the periods of comfort inside of buildings erected according to low cost construction methods in developing countries.

The temperature of the free air decreases gradually during afternoon hours. The heat that has been gained at the outer surface of the slab by radiation and partly stored within the slab during the overheated periods of the day is then dissipated during the following afternoons by convection losses to the cooler outside and inside air. The room air temperature also decreases, but at a lower rate. This explains why open air areas are preferred at that period of the day. The process of heat loss by convection continues until the next sunrise. The late hours before sunrise are the coolest periods inside of buildings. Just after sunrise, the outer surface of the slab warms up. A certain time-lag elapses however before the heat reaches the inner side of the slab. During that period, the indoor temperatures stay within the comfortable limitts. The feeling of excessive heat is felt afterwards. It covers the working hours of the mornings and continues until the late periods of the night. The duration of comfort decreases however for southern latitudes.

The explained time-variation of comfort conditions during a complete daily cycle coincides with the actual situation prevailing during summer periods in hot dry climates. The exact periods and duration of comfort changes slightly according to the building materials and methods of constructions applied for each case. The boundary conditions chosen in this study have therefore offered results that normally occur in low-cost dwellings in subtropical countries.

9. CONCLUSION

With the increasing demand on low-cost dwelleings in developing countries, bare reinforced concrete roof slabs are generally used instead of multi-layer roof constructions. This construction method is mainly introduced to cut erection costs. Due to the absence of air-conditioning, the low thermal capacity of thin slabs, and the wide diurnal variations of outdoor weather conditions, the comfort requirements inside of buildings are clearly disturbed.

In hot dry localities represented in this study by Cairo, Halfa and Khartoum and under normal summer weather conditions prevailing between April and September, it was found that a time-lag of two hours is created when bare 0.33 ft.- thick reinforcement concrete roof slabs are applied. The maximum and minimum indoor temperatures occur therefore two hours behind the outside extreme temperatures.

The maximum temperature values developing the highest feeling of discomfort are higher than the peak temperatures of the free air by a considerable temperature difference which equals to 35 (ft). This is due to the direct exposure of the unprotected slab to the rays of the sun.

In comparison to the outside temperature fluctuations, the indoor temperature ranges are doubled. Under the specified set of conditions, they reach an average value of 50 (F). The duration of comfortable temperatures is therefore considerably shorter than that in the free air. A feeling of comfortable indoor temperatures prevails only for 6 1/2 (h) in Cairo and 2 1/2 (h) in Halfa. In Khartoum, however a feeling of excessive heat remains during the whole daily cycle.

Despite the wide distance between the investigated localities which covers 14 degrees latitude, the results show interesting similarities. Fluctuations of indoor temperatures produce analogous trends. The time-lag of temperature waves and the range of temperature oscillations are almost equal.

7. PERIODIC TEMPERATURE FLUCTUATIONS

The reduced indoor air temperature values Θ_r for a complete daily cycle in Cairo, Halfa and Kartoum are plotted in Diagram 3. Considering the values of $t_{a,ma}$ and $t_{a,min}$ for each latitude separately, the actual indoor air temperature variations t_r are obtained by substitution in Equation 1. They are then plotted in Diagram 4. The shade dry-bulb temperatures in the free air t_a are taken from Table 1. Diagram 5 is prepared accordingly.

8. DISCUSSION AND RESULTS

8—1. Outdoor Temperature Variations :

$t_{a,min}$ occurs for the three localities at $05^{\circ\circ}$h (Diagram 5). This happens just before sunrise, after the greatest part of the heat stored within the slab during sunshine hours of the preceding day is lost by convection to the environment.

The maximum temperature $t_{a,ma}$ occurs at $15^{\circ\circ}$ h. This follows three hours behind the maximum intensity of solar radiation I_{ma} .

8—2. Time-lags Of Temperature Waves.

The temperature-time variations of indoor air take similar paths for different latitudes. They reach their lowest positions $t_{r,min}$ at $07^{\circ\circ}$ h, lagging 2 (h) behind $t_{a,min}$ of the free air. They rise afterwards placing their peaks at $17^{\circ\circ}$ h. This also occurs 2 (h) after $t_{a,ma}$. An equal time-lag that amounts to 2 (h) is therefore taking place at the three latitudes.

The time interval between the minimum and maximum temperature values is 10 (h). This is true at both sides of the slab (Diagrams 4 and 5).

8—3. Ranges of Temperature Fluctuations.

The range of indoor temperature fluctuations shows small differences for the different localities (Table 4). ($t_{r,ma}$ — $t_{r,min}$) in average, is equal to 51 (F). ($t_{a,ma}$ — $t_{a,min}$) of the free air oscillates between 21.5 (F) and 27.2 (F), with an average value of 24 (F).

In the three localities the range of indoor temperature fluctuations is therefore increased to double its value in the free air. This is mainly influenced by solar radiation, directly received at the bare surface of the slab.

8—4. Extreme Temperature Values.

Table 5 is prepared by comparing the extreme temperature values shown in Diagrams 4 and 5. The mentioned values could also be obtained from Table 4. ($t_{r,ma}$ — $t_{a,ma}$) maintains almost the same value, which equals to 35 (F) for different latitudes. ($t_{r,min}$ — $t_{a,min}$) oscillates however, within a smaller range of about 7 (F).

8—5 Indoor Comfort Conditions.

In hot dry climates, the main index affecting human comfort inside of buildings is the indoor air temperature. The lower limit of comfort in Cairo is at 71.5 (°F). In Halfa and Khartoum, it is raised to 72.4 (°F) and 73.6 (°F) respectively. The highest limit of comfort remains at 82 (°F) for the three latitudes (Reference 2). Beyond that limit, a feeling of excessive heat provails. The zones of comfort are enclosed in Diagrams 4 and 5 by the limits mentioned above. Table 6 is accordingingly prepared.

In outdoor shaded areas in Cairo, a feeling of comfort prevails during early morning hours. This takes place between 07^{30} and 10^{30} h, and also between $19^{\circ\circ}$ h and 00^{00} h. The total duration of comfort is equal to $8\frac{1}{2}$(h).

Considering the boundary conditions introduced in this study, the duration of comfort inside of buildings in Cairo decreases to 6 1/2 (h) when bare reinforced concrete roofs are applied. A feeling of comfort occurs between 03^{50} h and $10^{\circ\circ}$ h.

In Halfa comfort is felt only for 2 1/2 (h), and occurs during the early hours of the morning, between $06^{\circ\circ}$ and 08^{30} h.

Table 4_ AVERAGE INDOOR AND OUTDOOR TEMPERATURE RANGES DURING NORMAL SUMMER PERIODS.

Locality	Degree	Indoor temperatures					Outdoor temperatures					Increase in temp. range
		Max	Time	Min.	Time	Range	Max.	Time	Min.	Time	Range	
CAIRO	F	124.0	17^{00}	74.5	07^{00}	49.5	89.5	15^{00}	68.0	05^{00}	21.5	28.0
	C	51.0		23.5		27.5	32.0		20.0		12.0	15.5
HALFA	F	134.5	17^{00}	81.0	07^{00}	53.5	100.0	15^{00}	73.0	05^{00}	27.2	26.3
	C	57.0		27.0		30.0	38.0		23.0		15.0	15.0
KHARTOUM	F	135.5	17^{00}	84.0	07^{00}	51.5	100.0	15^{00}	77.6	05^{00}	22.4	29.1
	C	57.5		29.0		28.5	38.0		25.5		12.5	16.0

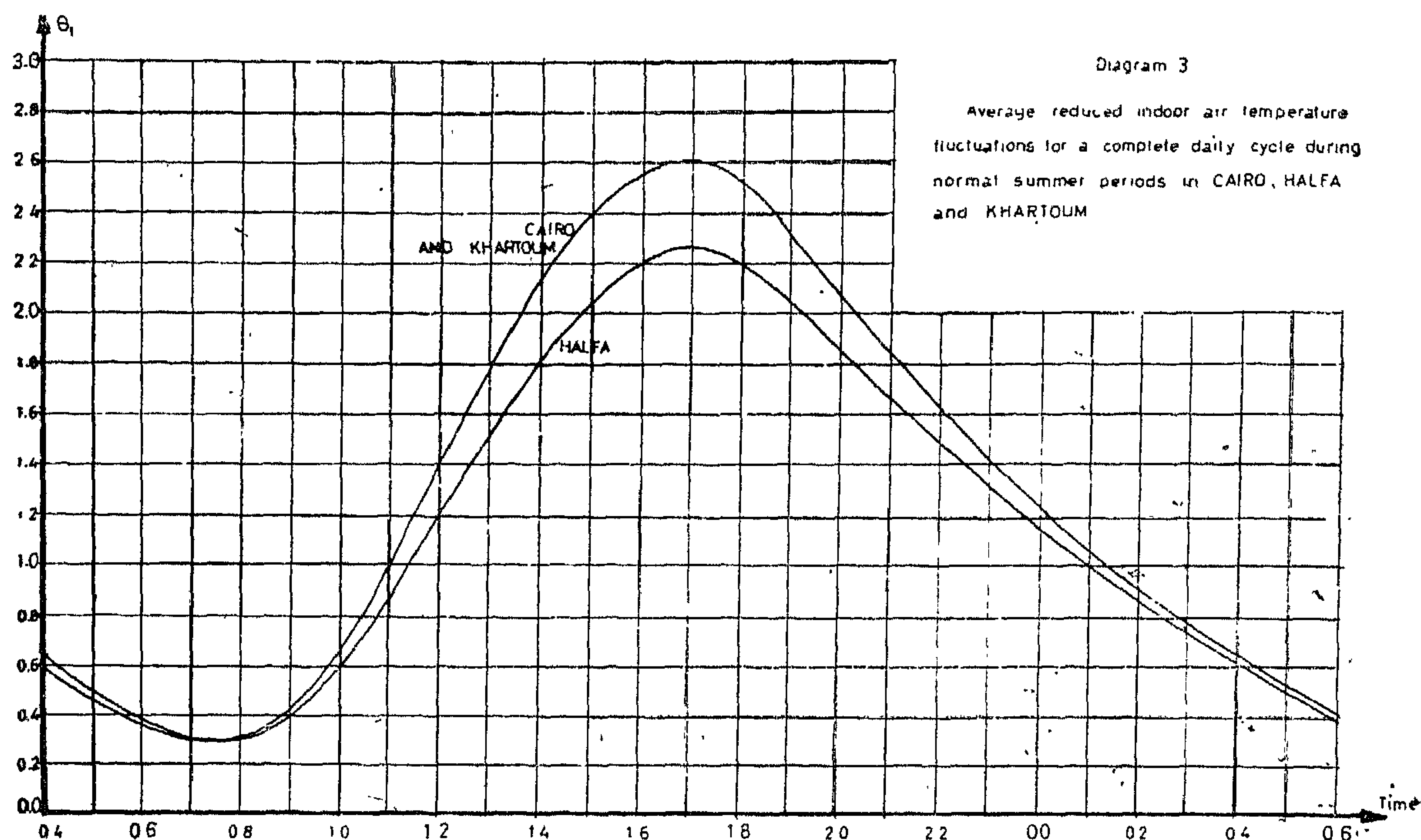
Table 5_ COMPARISON OF THE EXTREME TEMPERATURE VALUES AT BOTH SIDES OF THE ROOF SLAB.

Locality	$t_{r,max}$ $t_{a,max.}$	$t_{r,min}$ $t_{a,min.}$
CAIRO	34.5 (F)	6.5
HALFA	34.5	8.0
KHARTOUM	35.5	6.4

Table 6_ AVERAGE INDOOR AND OUTDOOR COMFORT CONDITIONS DURING NORMAL SUMMER PERIODS.

Locality	Indoor comfort conditions		Outdoor comfort conditions	
	Periods	Duration in hours	Periods	Duration in hours
CAIRO	03^{30} — 10^{00}	6 ½	07^{30} — 10^{30} 19^{00} — 00^{00} *)	3 5 ½ 8 ½
HALFA	06^{00} — 08^{30}	2 ½	22^{30} — 08^{30}	10
KHARTOUM	———	———	23^{30} — 07^{30}	8

*) In CAIRO, fresh outdoor air temperatures that are slightly lower than the comfortable limits are prevailing for 7 hours between 00^{30} and 7^{30} h.



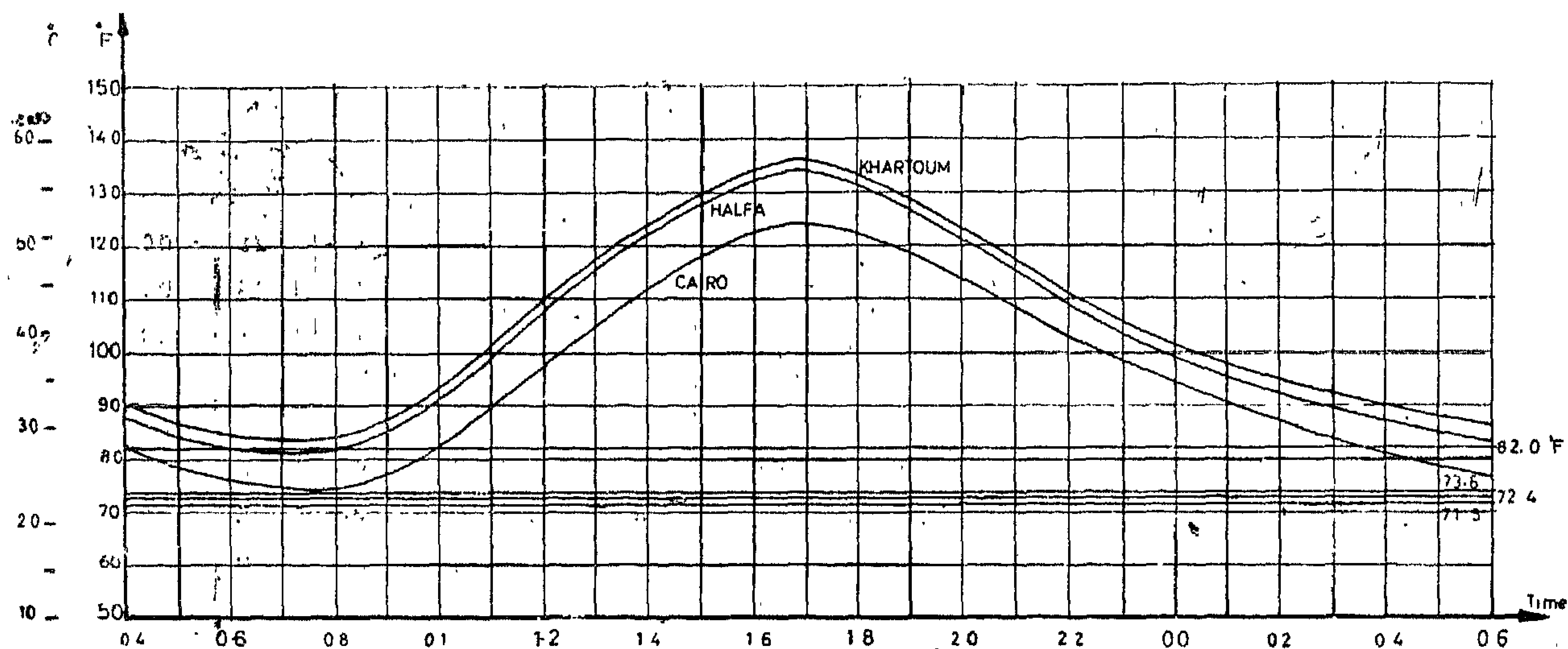


Diagram 4 : Average actual indoor air temperature fluctuations for a complete daily cycle during normal summer periods in CAIRO, HALFA and KHARTOUM.

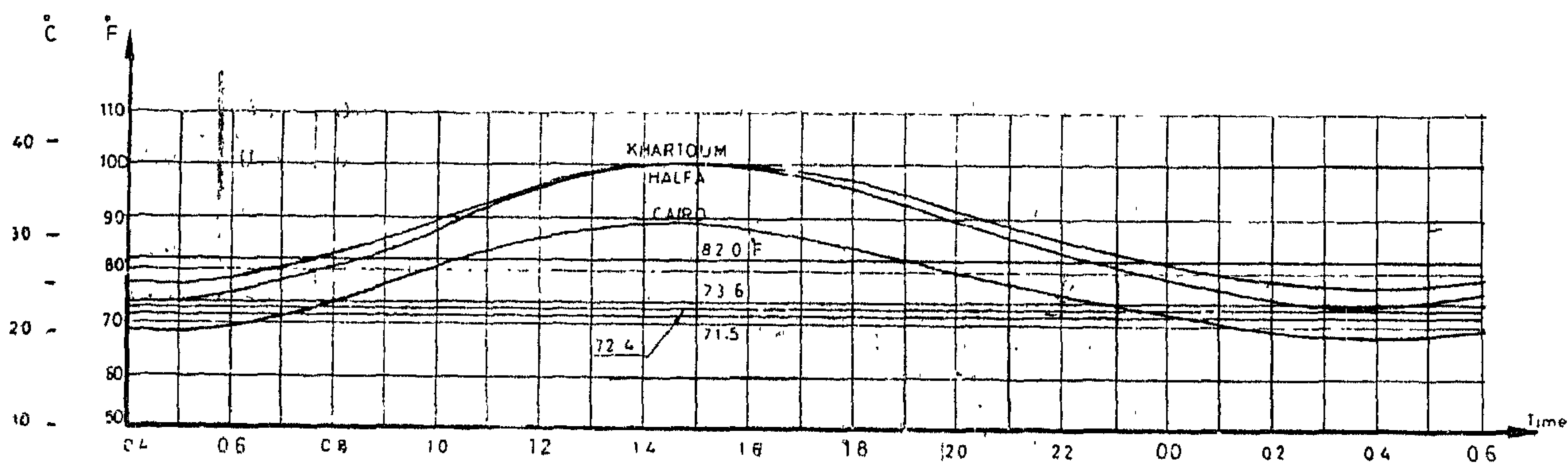


Diagram 5 : Average actual outdoor air temperature fluctuations for a complete daily cycle during normal summer periods in CAIRO, HALFA and KHARTOUM.

Table 3 _ NUMERICAL CALCULATIONS

	Time	θ_a	θ_o	θ_w	θ_i	θ_r	$\frac{I_\tau}{I_{max.}}$
First Cycle	05	0 00	0 06	0.12	0.15	0.15	0.00
		00	06	11	14	15	02
		01	08	11	13	14	03
	06	02	10	11	12	13	05
		04	14	11	12	12	11
Second Cycle	05	00	21	39	46	49	00
		00	20	35	42	46	02
		01	21	33	39	42	03
	06	02	21	31	36	39	05
		04	23	29	34	36	11
		06	32	28	31	34	18
	07	08	42	29	30	31	24
		12	52	32	29	30	31
		16	65	36	30	29	39
	08	20	80	41	32	30	46
		28	95	48	36	32	53
		35	1.12	57	41	36	61
	09	43	1.31	67	48	41	69
		48	1.51	78	56	48	74
		53	1.67	91	65	56	79
	10	58	1.83	1.04	76	65	85
		62	2.00	1.17	87	76	89
		66	2.15	1.30	99	87	92
	11	70	2.28	1.44	1.12	99	96
		74	2.42	1.57	1.25	1.12	97
		79	2.52	1.70	1.38	1.25	99
	12	83	2.64	1.82	1.51	1.83	1.00
		86	2.74	1.95	1.63	1.51	99
		89	2.81	2.07	1.76	1.63	97
	13	92	2.86	2.18	1.88	1.76	96
		94	2.91	2.28	2.00	1.88	92
		97	2.92	2.37	2.11	2.00	89
	14	99	2.94	2.44	2.21	2.11	85
		99	2.93	2.51	2.30	2.21	79
		99	2.88	2.56	2.38	2.30	74
	15	1.00	2.84	2.60	2.45	2.38	69
		99	2.79	2.62	2.51	2.45	67
		99	2.77	2.64	2.55	2.51	53
	16	99	2.59	2.65	2.58	2.55	46
		98	2.49	2.62	2.61	2.58	39
		97	2.38	2.58	2.61	2.61	31

Time	θ_a	θ_o	θ_w	θ_i	θ_r	$\frac{I_\tau}{I_{max.}}$
17	0.96	2.24	2.54	2.60	2.61	0 24
	93	2.11	2.48	2.57	2.60	18
	91	1.98	2.41	2.53	2.57	11
18	0.88	1.74	2.33	2.48	2.53	05
	84	1.73	2.22	2.42	2.48	03
	79	1.60	2.15	2.33	2.42	02
19	75	1.52	2.06	2.26	2.33	00
	69	1.43	1.98	2.18	2.26	00
	64	1.36	1.89	2.09	2.18	00
20	58	1.29	1.81	2.01	2.09	00
	54	1.22	1.73	1.93	2.01	00
	51	1.16	1.65	1.85	1.93	00
21	47	1.10	1.58	1.77	1.85	00
	44	1.04	1.51	1.69	1.77	00
	40	0.99	1.44	1.62	1.69	00
22	37	0.94	1.37	1.55	1.62	00
	34	0.89	1.31	1.48	1.55	00
	37	0.84	1.25	1.41	1.48	00
23	28	0.82	1.19	1.35	1.41	00
	25	0.75	1.14	1.28	1.35	00
	23	0.71	1.08	1.23	1.28	00
00	20	67	1.02	1.17	1.23	00
	18	62	0.97	1.11	1.17	00
	15	59	92	1.05	1.11	00
01	13	55	87	1.00	1 05	00
	12	51	82	0.95	1.00	00
	10	48	78	0.90	0.95	00
02	09	45	74	85	0.90	00
	08	42	70	81	0.85	00
	06	40	66	76	81	00
03	05	37	62	72	76	00
	04	34	58	68	72	00
	03	32	54	64	68	00
04	02	29	51	60	64	00
	01	27	48	56	60	00
	00	25	45	53	56	00
05	00	23	42	50	53	00

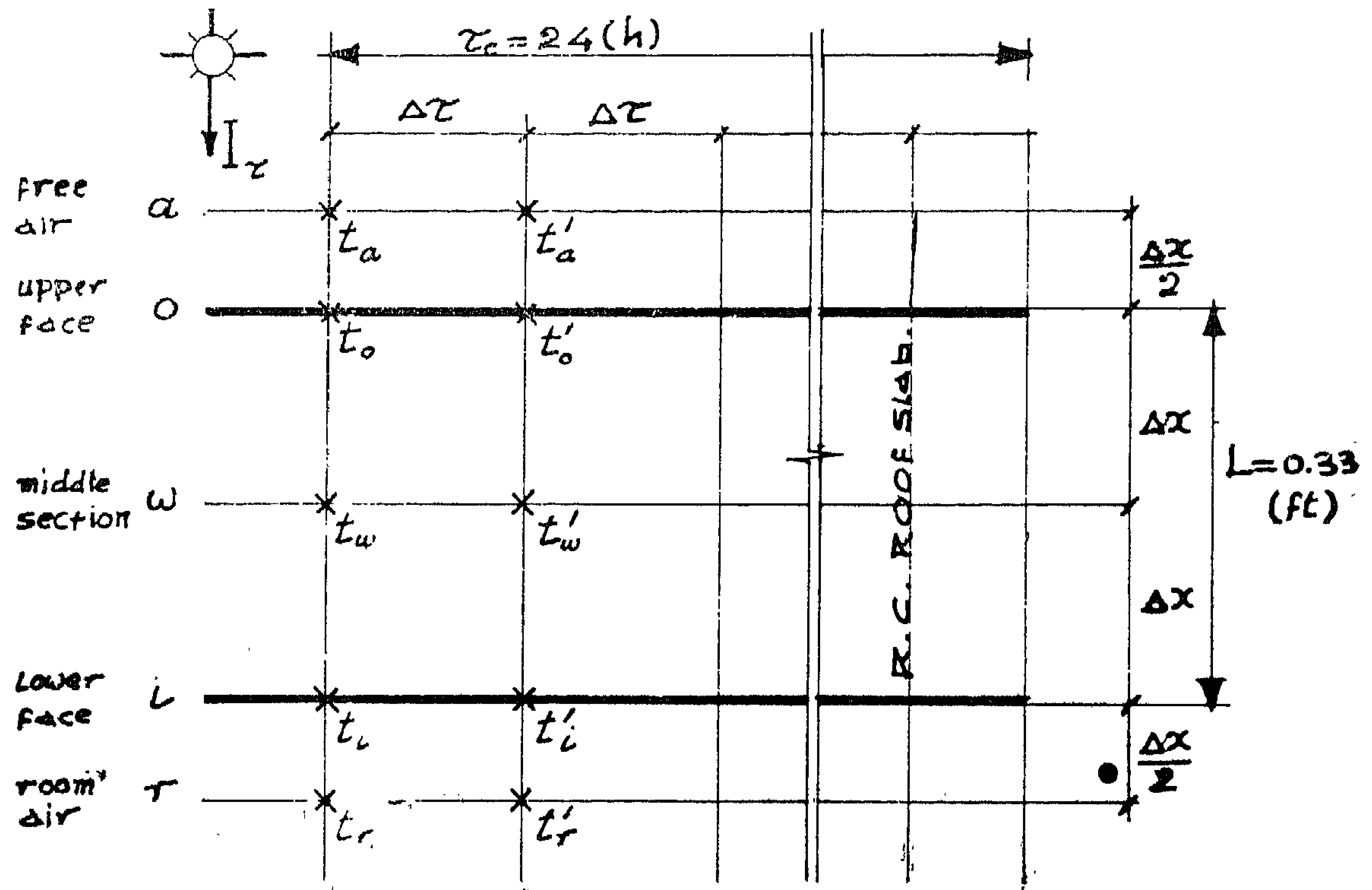
Table 2 – AVERAGE TOTAL SOLAR RADIATION INTENSITY ON HORIZONTAL SURFACES I_γ IN $[B.h^{-1}.ft^{-2}]$ AND THEIR REDUCED VALUES I_γ / I_{max}.

	CAIRO Apr. → Sep.		HALFA Apr → Sep.		KHARTOUM Apr. → Sep.	
Time	I_γ	I_γ/I_{max}	I_γ	I_γ/I_{max}	I_γ	I_γ/I_{max}
05	0.0	0.00	0.0	0.00	0.0	0.00
06	14.8	0.05	12.9	0.04	16.0	0.05
07	78.9	0.25	72.6	0.23	81.7	0.25
08	150.0	0.49	150.4	0.47	174.6	0.54
09	219.7	0.71	205.0	0.64	230.3	0.72
10	265.5	0.86	272.9	0.84	281.0	0.87
11	297.1	0.96	307.9	0.96	314.6	0.97
12	309.3	1.00	321.43	1.00	321.4	1.00
13	297.1	0.96	307.9	0.96	314.6	0.97
14	265.5	0.86	272.9	0.84	281.0	0.87
15	219.7	0.71	205.0	0.64	230.3	0.72
16	150.0	0.49	150.4	0.47	174.6	0.54
17	78.9	0.25	72.6	0.23	81.7	0.25
18	14.8	0.05	12.9	0.04	16.0	0.05
19	0.0	0.00	0.0	0.00	0.0	0.00

Table 1_ AVERAGE SHADE DRY—BULB TEMPERATURE t_o (°F) AND THEIR REDUCED VALUES θ_a

	CAIRO (ALMAZA) Apr → Sep. 1958		HALFA, SUDAN Apr → Sep. 1946 → 1956		KHARTOUM Apr. → Sep. 1945 → 1955	
Time	$t_{a,\tau}$	$\theta_{a,\tau}$	$t_{a,\tau}$	$\theta_{a,\tau}$	$t_{a,\tau}$	$\theta_{a,\tau}$
10	71.5	0.16	78.6	0.21	83.0	0.24
02	70.2	0.10	77.1	0.15	81.5	0.17
03	69.4	0.06	76.0	0.11	80.5	0.12
04	68.7	0.03	74.2	0.04	79.2	0.06
05	68.0	0.00	73.0	0.00	78.3	0.02
06	68.4	0.02	73.1	0.01	77.8	0.00
07	70.5	0.11	75.8	0.14	79.9	0.10
08	73.9	0.27	81.5	0.31	83.0	0.24
09	78.6	0.48	87.8	0.54	88.0	0.46
10	80.6	0.57	91.0	0.63	92.0	0.65
11	83.9	0.71	94.5	0.79	94.5	0.76
12	86.2	0.83	96.8	0.88	96.9	0.87
13	88.1	0.91	99.0	0.96	98.5	0.94
14	89.9	0.99	100.0	0.99	99.4	0.98
15	90.2	1.00	100.2	1.00	99.8	1.00
16	90.0	0.99	100.1	0.99	99.7	0.99
17	89.0	0.95	99.2	0.96	98.7	0.95
18	86.9	0.86	96.9	0.88	96.2	0.84
19	83.5	0.70	93.0	0.77	93.2	0.70
20	80.5	0.57	90.3	0.60	91.0	0.60
21	77.9	0.44	87.3	0.52	89.0	0.51
22	75.5	0.34	85.0	0.46	87.2	0.43
23	74.1	0.28	83.9	0.40	85.8	0.36
00	72.6	0.21	80.7	0.28	84.2	0.30
$t_{a,max} - t_{a,min}$	22.2 F		27.2 F		22.0 F	

Diagram 2
TEMPERATURE — TIME DISTRIBUTION



$$L = 0.33 \text{ (ft)} = 0.10 \text{ (m)}$$

$$\Delta x = \frac{L}{2} = 0.165 \text{ (ft)}$$

$$\tau_c = 24 \text{ (h)}$$

$$\Delta\tau = \frac{\tau_c}{72} = \frac{1}{3} \text{ (h)}$$

Fig. No. 2

The first cytcle of calculations, which is partly given in Table 3, show unsatisfactory closing effect, Comparing Θ—values at the beginning and at the end of the second cycle, it could be extracted that the highest error is that of Θ_r which amounts to 0.04 × 22.2 put here the foot not of page 14 of my original text. .) (F.) This is equal to 0.89 (F) which is a negligible error. Therefore the Θ—value contained in the last cycle of Table 3 represent the reduced temperature variations for the specified case when steady periodic conditions are prevailing. The solutions are intended to be illustrative and the results are therefore comparative in relation to the boundary conditions encountered in the report.

The same procedure is then repeated for Halfa and Khartoum.

Diagram 1
COMPOSITE ROOF CONSTRUCTION

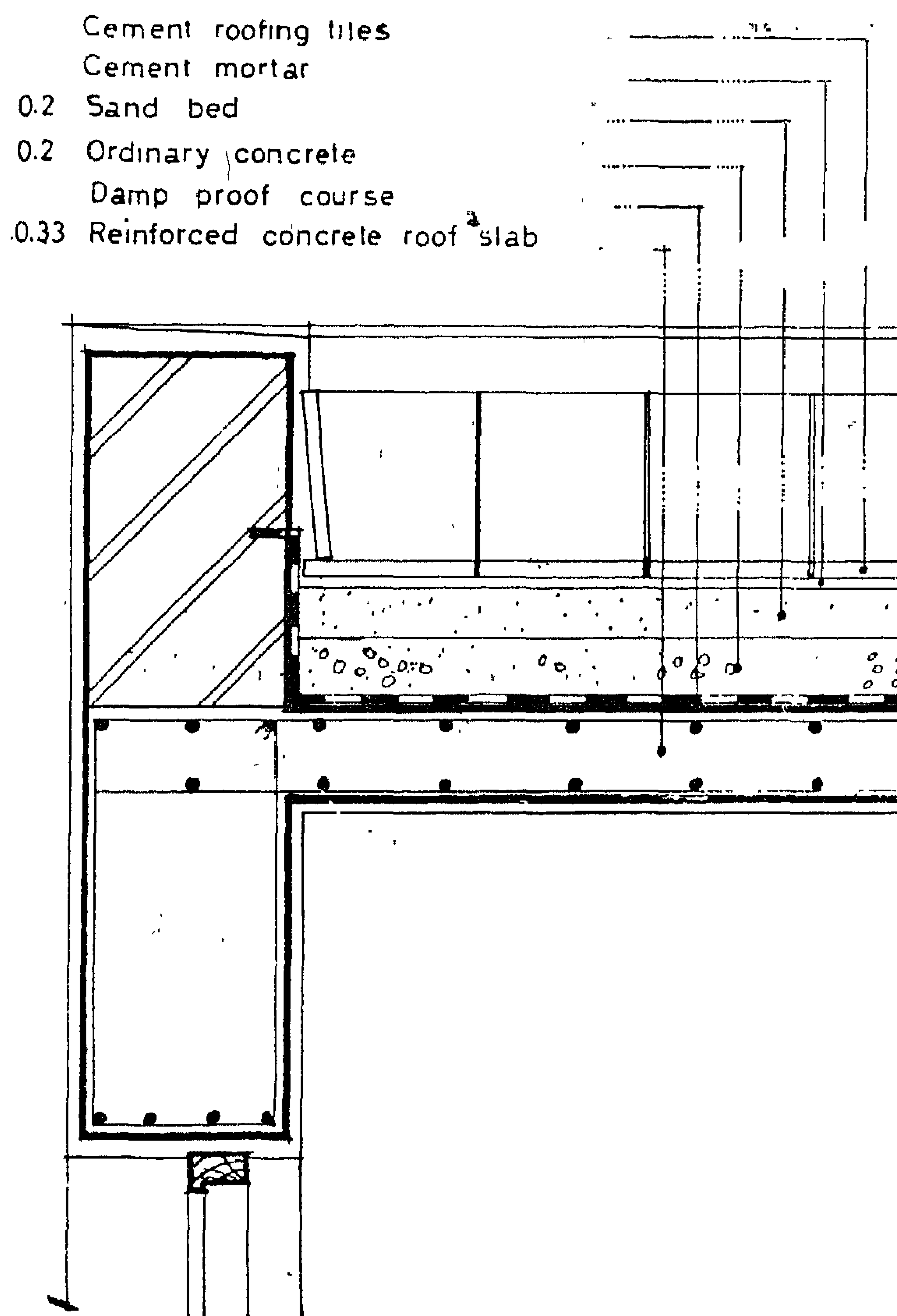


Fig. No. 1

.) The average value of ($t_{a,max}$ —$t_{a,min}$) in Cairo is equal to 22,2 (F). This could be extracted from Table 1.

area is exchanging heat with a column of air with an effective depth ...) of 40 (ft.).

5—4. Depth and Time Intervals at which the Calculations are carried out.

Refering to Diagram 2 and Equations 9 and 10,

$L = 0.33$ (ft) , $\triangle x = 0.165$ (ft) , hence

$$\triangle X = \frac{\triangle x}{L} = \frac{1}{2} \text{ (dimensionless).}$$

$\tau_0 = 24$ (h) , $\triangle \tau = 1/3$ (h) , hence

$$\triangle T = \frac{\triangle \tau}{\tau_c} = \frac{1}{72} \text{ (dimensionless).}$$

5—5. Dimensionless Groups.

Substituting the foregoing values in Equations 5, 6, 16, 19 and 12, the dimensionless groups take the following values :

$$M = \frac{(\triangle x)^2}{\alpha \,.\, (\triangle \tau)} = \frac{L^2 \, (\triangle X)^2}{\alpha \,.\, \tau_0 \, (\triangle T)} = 4.00 \quad \ldots\ldots \text{ Equ. 21.}$$

$$N_0 = \frac{h_0 \, (\triangle x)}{k} = \frac{h_0 \, L \, (\triangle X)}{k} = 0.94 \quad \ldots\ldots \text{ Equ. 22.}$$

$$N_r = \frac{h_r \, (\triangle x)}{k} = \frac{h_r \, L \, (\triangle X)}{k} = 0.47 \quad \ldots\ldots \text{ Equ. 23.}$$

$$R = \frac{m_a'' \,.\, C_{p,a} \,.\, L \, (\triangle x)}{k \,.\, \tau_c \, (\triangle T)} = 0.47 \quad \ldots\ldots \text{ Equ. 24.}$$

$$F = \frac{2 \, \varepsilon \, \alpha \, \tau_c \, (\triangle T)}{L \, k \, (\triangle X)} \,.\, \frac{I_{max}}{(t_{a,max} - t_{a,min})} \,.\, \frac{I_\tau}{I_{ma}} \quad \ldots\ldots \text{ Equ. 25.}$$

which equals to 1.36 I_τ/I_{ma} for Cairo
1.11 I_τ/I_{ma} for Halfa
and 1.35 I_τ/I_{ma} for Khartoum.

5—6. Heat Balance Equations.

The heat balance Equations 11, 14, 17 and 20 are therefore reduced to the following final forms :

$$\Theta_0' = 0.47 \, \Theta_a + 0.03 \, \Theta_0 + 0.50 \, \Theta_w + F \quad \ldots\ldots \text{ Equ. 26.}$$

$$\Theta_w' = 0.25 \, \Theta_0 + 0.50 \, \Theta_w + 0.25 \, \Theta_i \quad \ldots\ldots \text{ Equ. 27.}$$

$$\Theta_i' = 0.50 \, \Theta_w + 0.26 \, \Theta_i + 0.24 \, \Theta_r \quad \ldots\ldots \text{ Equ. 28.}$$

$$\Theta_r' = 1.00 \, \Theta_i \quad \ldots\ldots \text{ Equ. 29.}$$

The radiation factor F however, is obtained from Equation 25.

6. PROCEDURE OF CALCULATIONS

An initial temperature distribution for Θ_0 , Θ_w , Θ_i and Θ_r is assumed at 05^{00} (h) (Table 3). This is the time interval at which an outdoor minimum temperature occurs. Θ_a and I_τ/I_{max} are however, known functions of time. Equations 26, 27, 28 and 29 are then engaged to obtain Θ_0' , Θ_w' , Θ_i' and Θ_r' occuring at the following time interval 05^{20} h. The same procedure is repeated till the end of the cycle at 05^{00} (h) of the next day.

...) Further investigations, «Effect of Ceiling Heights and Poom Widths of the on the Indoor Air Temperature Fluctuations and Human Thermal Sensations» by A. Saleh, Building Research Center, Cairo, 1969, has illustrated that the indoor air temperature fluctuations are hardly influenced by small changes of the inside film coefficient of heat transfer. This was proved by comparing the thermal performance of a homogenious 0.33 ft. thick reinforced concrete roof slab and the resulting indoor air temperature fluctuations under conditions similar to those occuring in this report when

and

a) $h_r = 2$ ($B.h^{-1}. ft^{-2}. F^{-1}$) and $V_a = 40$ (ft)
b) $h_r = 1.2$ and $V_a = 18.6$

4—4. Thermal Behaviour of the Room-Air.

The heat lost by convection at the lower side of the slab is equalized by the heat gained by the room-air.

$$h_r\ (t_i - t_r) = m_a'' . C_{p,a} . \frac{\partial t}{\partial \tau} \quad \ldots\ldots \text{ Equ. 18}$$

If m_a'' (lb . ft^{-2}) is the mass of air which is exchanging heat with each square foot of the slab area, $C_{p,a}$ ($B.lb^{-1}. F^{-1}$) is the specific heat of air, then the heat capacity of the room air is equal m_a'' . $C_{p,a}$ ($B.\ ft^{-2}.\ F^{-1}$)

Introducing $$R = \frac{m_a'' . C_{p,a} . L}{k\ .\ \tau_o} . \frac{(\triangle X)}{(\triangle T)} \quad \ldots\ldots \text{ Equ. 19.}$$

and proceeding with the same mathematical treatment, Equation 18 takes the following dimensionless form :

$$\Theta_r' = \frac{N_r}{R}\ \Theta_i + (1 - \frac{N_r}{R})\ \Theta_r \quad \ldots\ldots \text{ Equ. 20.}$$

Under steady periodic conditions, the thermal behaviour of the roof slab is governed by the dimentionless heat balance Eauations 11, 14, 17 and 20.

5. PROPERTY VALUES AND BOUNDARY CONDITIONS

The numerical treatment of the problem underhand considers the following property values :

5—1. Physical Properties Of Reinforced Concrete.

Thermal conductivity

$k = 0.7$ ($B.h^{-1}.\ ft^{-1}.\ F^{-1}$).

Density $\rho = 140$ ($lb.\ ft^{-3}$).

Specific Heat

$c = 0.24$ ($B.\ lb^{-1}.\ F^{-1}$).

hence, thermal diffusivity

$$\alpha = \frac{k}{\rho c} = 0.021\ (ft^2.\ h^{-1}).$$

5—2. Main Weather Conditions.

The average fluctuations of Θ_a and I_τ / I_{ma} which could be applied for the three localities under study are discussed in Chapter 2 and given in Table 3. The value of t_{max}, t_{min} and I_{max} are given in tables 1 and 2.

Considering normal wind velocity, h_o is equal to 4 ($B.h^{-1}.\ ft^{-2}.\ F^{-1}$)

$\varepsilon = 0.8$ (compare with eqution 3).

5—3. Indoor. Conditions.

h_r for steady movement of indoor air reaches a value of 2 ($B.h^{-1}.\ ft^{-2}.\ F^{-1}$) .).

The heat capacity of the inside air m_a''. $C_{p,a}$ = 0.71 ($B.\ ft^{-2}.\ F^{-1}$) ..) is calculated by assuming that each square foot of the slab

.) $m_a'' = 0.074 \times 40 = 2.960$ ($lb.\ ft^{-2}$)
density of air $= 0.074$ ($lb.\ ft^{-3}$)
Cp,a $= 0.24$ ($B.\ lb^{-1}.\ F^{-1}$)

..) V_a The quantity of indoor air exchanging heat with each square foot of the slab area is dependent on several factors. To cover different possibilities, 40 (ft^3) were considered in the calculations.

ed from the temperature distribution at an earlier time interval τ

The slab thickness L (ft) as shown in Diagram 2 is divided into equal segments $\triangle$ x (ft).

$$\text{Thus} \quad \triangle x = \frac{(\triangle x)}{L} \qquad \ldots\ldots \text{ Equ. 9.}$$

This is a reduced depth representing the ratio of the thickness of each subdivision ($\triangle$ x) (ft) to the slab thickness L(ft).

The daily cyclic period τ_c which equals to 24 (h), is divided into equal time intervals $\triangle\tau$ (h).

$$\text{Thus} \quad \triangle T = \frac{(\triangle \tau)}{\tau_c} \qquad \ldots\ldots \text{ Equ. 10.}$$

This is the dimensionless value of the time intervals at which the calculations are to be carried out.

Introducing the dimensionless abbreviations $\triangle$ T and $\triangle$ x and divinding by the daily temperature range ($t_{a,max} - t_{a,min}$) which is formely applied in Equation 1,

Equation 8 could be put in the following dimensionless form :

$$\Theta'_o = \frac{2\ N_o}{M}\ \Theta_a + \frac{M - 2\ N_o - 2}{M}\ \Theta_o + \frac{2}{M}\ \Theta_w + F \qquad \ldots\ldots \text{ Equ. 11.}$$

fis however equal to

$$\frac{2\ \varepsilon\ \alpha\ \tau_o}{L.k} \cdot \frac{\triangle T}{\triangle X} \cdot \frac{I_{max}}{(t_{a,max} - t_{a,min})} \cdot \frac{I_\tau}{I_{max}} \qquad \ldots\ldots \text{ Equ. 12.}$$

The value $\dfrac{I_\tau}{(t_{a,max} - t_{a,min})}$ is replaced by the ratio $\dfrac{I_{max}}{(t_{a,max} - t_{a,min})}$ which has a certain average value for each locality, multiplied by the dimenionless time-function $\dfrac{I_\tau}{I_{max}}$

which was found to be applicable for the three localities, as formerly explained in Chapter 2.

4—2. Heat Conduction Through The Slab.

The heat flow through the thickness of the slab is governed by the Fourier general heat conduction equation which reads :

$$\frac{\partial t}{\partial \tau} = \alpha \cdot \frac{\partial^2 t}{\partial x^2} \qquad \ldots\ldots \text{ Equ. 13.}$$

Replacing the partial differentials by finite differences, introducing M from Equation 5 and then dividing by the daily temperature range, the following dimensionless form is obtained :

$$\Theta'_w = \frac{1}{M}\ \Theta_o + \frac{M - 2}{M}\ \Theta_w + \frac{1}{M}\ \Theta_i \qquad \ldots\ldots \text{ Equ. 14.}$$

4—3. Heat Exchange Conditions at the Lower Surface of the Slab.

The quantity of heat conducted to the lower surface of the slab is compensated by :

a) the heat stored within a lower element of the slab thikness.

b) the heat dissipated to the room-air.

$$-k \frac{\partial t}{\partial x} = \rho\, c\, \frac{\partial t}{\partial \tau}\, dx + h_r\ (t_i - t_r) \qquad \ldots\ldots \text{ Equ. 15.}$$

Introducing

$$N_r = \frac{h_r \cdot (\triangle x)}{k} = \frac{h_r \cdot L}{k}\ (\triangle x) \qquad \ldots\ldots \text{ Equ. 16.}$$

where h_r ($B.h^{-1}.\ ft^{-2}.\ F^{-1}$) is the film coefficient of heat transfer at the lower surface of the slab, the following relation is obtained :

$$\Theta_i' = \frac{2}{M}\ \Theta_w + \frac{M - 2\ N_r - 2}{M}\ \Theta_i + \frac{2\ N_r}{M}\ \Theta_r \qquad \ldots\ldots \text{ Equ. 17.}$$

of the general heat conduction equation is applied by replacing its partial differentials by finite differences ..). Hence put here the *foot* note remarked by ..) from page 7 in my originl text.

As shown in Diagram 2, the thickness of the slab L (ft) is divided into equal segments, the thickness of each is $\triangle\chi$ (ft). The daily cyclic period τ_0 (h) is also divided into smaller time-increments, the duration of each is equal to $\triangle\tau$ (h).

Under conditions of unidirectional heat flow, the temperature-time variation is extracted as follows :

4—1. Heat Exchange Conditions At the Upper Surface Of the Slab.

If the intensity of solar radiation on horizontal surfaces at a certain time-interval τ is equal to I_τ ($B.h^{-1}\ ft^{-2}$), the quantity of heat gain at the upper side of the roof slab $\varepsilon . I_\tau$ is balanced by the sum of :

a) ho (to — ta) which is the heat quantity rejected by convection to the free air.

b) $\rho . c \dfrac{\partial t}{\partial \tau} . dx$ representing the portion of the heat stored within an outer element of the slab, the thickness of that element is considered to be $\dfrac{\triangle\chi}{2}$

c) $k \dfrac{\partial t}{\partial \chi}$ which is the heat conducted through the slab.

The heat balance equation at the upper side of the slab reads :

$$\varepsilon . I_\tau = h_o\ (t_o - t_a) + \rho\ c\ \frac{\partial t}{\partial \tau}\ dx - k \frac{\partial t}{\partial x} \qquad \text{..... Equ 3.}$$

Replacing the partial differentials by finite differences, Equation 3 takes the following form :

$$\varepsilon . I_\tau = h_o\ (t_o - t_a) + \rho\ c\ \frac{t_o' - t_o}{\triangle\tau} . \frac{\triangle x}{2} + \frac{k}{\triangle x}(t_o - t_w) \qquad \text{...... Equ. 4}$$

The above equations include the following values :

ε is the sum of absorptivity and transmissivity values of the weather-side surface of the slab to solar radiation.

ρ ($lb.ft^{-3}$) and c ($B.lb^{-1} . F^{-1}$) are the bulk density and specific heat of reinforced concrete

ho and k are as formerly introduced in Equation 2.

The back radiation lost to the atmosphere by the weather-side surface of the slab is neglected in Equation 3. Its value in comparison to the intensity of solar radiation is negligible (Reference 7).

Multiplying Equation 4 by $\dfrac{\triangle x}{k}$ and introducing the following mathematical abbreviations :

$$M = \frac{(\triangle x)^2}{\alpha . (\triangle \tau)} = \frac{\rho . c. (\triangle x)^2}{k . (\triangle \tau)} \qquad \text{...... Equ. 5.}$$

$$N_o = \frac{h_o\ (\triangle x)}{k} \qquad \text{...... Equ. 6.}$$

where α ($ft^2. h^{-1}$) is the thermal diffusivity of reinforced concrete and equals to $k / \rho.c$, the following equation is obtained :

$$\frac{\varepsilon . I_\tau . (\triangle x)}{k} = N_o\ (t_o - t_a) + \frac{M}{2}(t_o' - t_o) + t_o - t_w \qquad \text{...... Equ. 7.}$$

$$t_o' = \frac{2\ N_o}{M} t_a + \frac{M - 2\ N_o - 2}{M} t_o + \frac{2}{M} t_w + \frac{2\ \varepsilon\ I_\tau\ (\triangle x)}{M\,k} \qquad \text{...... Equ. 8.}$$

Applying Equation 8, the temperature value to' of the upper surface of the slab at a certain time interval ($\tau + \triangle \tau$) is then obtain-

The numercial solution Reference 1 is dependant on the graphical solution developed by E. Schimidt (Reference 6).

ed in Reference 1, simplifies the substitution of the main weather conditions in the dimensionless heat balance equations governing the exchange of heat at both surfaces of the roof slab. The mathematical procedure is explained in Chapter 4.

3. HEAT RESISTANCE OF DIFFERENT REINFORCED CONCRETE ROOF CONSTRUCTIONS UNDER STEADY STATE CONDITIONS

According to Reference 3, the overall resistance to heat transmissin through a composite section section

$$R = \frac{1}{h_o} + \frac{1}{h_r} + \Sigma \frac{d}{k} \qquad \text{...... Equ. 2}$$

ho and hr ($B.h^{-1} . ft^{-2} F^{-1}$) represent the film coefficients of heat transfer at the weather-side and the room-side surfaces of the roof construction.

k ($B.h^{-1} , ft^{-1} . F^{-1}$) and d (ft) are the thermal conductivity and thickness of each layer respectively.

It follows that the average resistance of a simple reinforced Concrete roof slab with a thickness of 0.33 ft (0.10 m), plastered at its lower side by a layer of 0.07 ft (0.02 m) gypsum plaster is equal to 1.35 (B^{-1} h. ft^{-2}. F).

Considering the multi-layer roof construction shown in Diagram 1, the resistance to heat transmission under steady state conditions increase to 2.70 (B^{-1}. h. ft^{-2}. F). This is equal to the resistance of a simple roof slab with a thickness of 1.32 ft (0.40 m).

If a layer of an insulating foam concrete with a thickness of 0.23 ft (0.07 m) is added to the multi-layer roof construction, its resistance increases to about 5.40 (B^{-1}. h. ft^{-2}, F). This is equivalent to the resistance of a simple reinforced concrete slab with a thickness of 3.2 ft (0.98 m).

The above calculations demonstrate to which extent the resistance to heat transmission is lowered when thick composite roof sections are replaced by simple reinforced concrete slabs. Despite these facts, simple slabs are still extensively applied in low-cost housing projects in developing countries.

The above results are obtained by applying Equation 2 which calculates the resistance of a building component by considering the thermal conductivitiees of its different layers. This is only applicable if steady state conditions prevail.

Steady flow of heat however, only occurs if the air temperatures at both sides of a building component do not change with time.

Concerning the case under study, both outdoor and indoor enviroments are not controlled. The air temperature in contact with the two surfaces of the roof slab changes with time. The influence of the heat storage capacity of the slab under steady periodic conditions must then be considered.

4. THERMAL PERFORMANCE OF BARE REINFORCED CONCRETE ROOF SLABS UNDER STEADY PERIODIC CONDITIONS

If both effects of air temperatures and Solar radiation intensities at the exterior surface of the slab are super imposed, it could be easily extracted that the resulting effect .) Hence put here the *foot note* remarked by .) from page 7 in my original text does not follow a sine-function with a fixed frequency.

The air in contact with the room-side surface of the slab also varies with time. The slab does not behave therefore as an infinctely thick plate (Reference 5) and a direct application of the general heat conduction equation is thus disturbed.

To obtain the temperature-time variation at different positions of the homogenious roof slab under study, a numerical approximation

.) The concept of the «sol-air-temp». as explained in Reference 4 could also be con sulted in this respect.

of simple reinforced concrete roof slabs accelerates the rate of exchange of heat between outdoors and indoors. The insides of buildings are therefore readily affected by the wide ranged fluctuations of outdoor air temperatures and solar radiation intensities prevailing during summer periods. Indoor comfort conditions are then considerably disturbed.

To investigate the effect of applying unprotected reinforced concrete roof slabs on the indoor temperature fluctuations and state of comfort, average summer weather conditions at Cairo, Halfa and Khartoum, known for their hot dry climates are gathered and set into reduced forms. The physical properties of reinforced concrete and the mentioned reduced values of weather conditions are then substitutted in the heat balance euqations, governing the exchange of heat at the weather-side and room-side surfaces of the slab. The temperature-time variation of the room air is then extracted. The mentioned heat balance equations are developed in dimensionless forms (Reference 1) to overcome mathematical complications and to simplify obtainning the results in any system of units.

Throughout the calculations, heat is considered to be flowing only perpendicular to a 0.33 ft-thick (10 cms) roof slab. The course of indoor temperatures, amplitudes, time-Lags and the resulting state of comfort under natural periodic heat exchange conditions are discussed and compared for Cairo, Halfa and Khartoum.

2. WEATHER INVESTIGATIONS

In hot dry climates, the main index affecting human comfort inside of buildings is the indoor air temperatures. This is mainly influenced by the wide diurnal variations of outdoor air temperatures and solar radiation intensities.

2—1. Shade Dry Bulb Temperature :

The average hourly dry-bulb temperature ta (°F) during summer periods at Cairo, Halfa and Khartom .) are contained in Table 1. :

Their temperature-time variation during a complete daily cycle are taking similar paths. They reach their lowest positions ta,min (°F) at about 05°°h, just before sunrise. They take afterwards higher values placing their peaks ta, max (°F) at about 15°°h.

If the hourly rise of air temperature ta over ta, min is divided by the daily temperature range (ta,max — ta, min), it could be seen, as shown from table 1 that the average reduced temperature values

$$\Theta_a = \frac{t_a - t_{a,min}}{t_{a,max} - t_{a,min}} \quad \ldots\ldots \text{ Equ. 1}$$

are also maintaining similar paths for the three different localities. Slight deviations are however noticed before sunrise.

An average reduced temperature course Θ_a, applicable for Cairo, Halfa and Khartoum is therefore extracted and then listed in Table 3.

2—2. Solar Radiation :

The average hourly total solar radiation intensity on horizontal surfaces I_τ ($B.h^{-1}\ ft^{-2}$) is given in Table 2, (Reference 2).

If Imax. ($B.h^{-1}.\ ft^{-2}$) is the maximum value that occurs during a complete daily cycle, I_τ/Imax. is then a chosen reduced form of the solar radiation intensity values (Table 2).

The average variations of I_τ/Imax that could be applied for the different latitudes under study are given in the last column of Table 3.

The concept of the reduced outdoor air temperature Θ_a and the reduced total solar radiation intensity I_τ/Imax, formerly develop-

) Cairo, latitude	30°	08′	N.- longitude	31°	34′	E.
Halfa,	22°		N.-	31°	20′	E.
Khartoum,	16°		N.-	33°		E.

THERMAL PERFORMANCE OF REINFORCED CONCRETE ROOF SLABS IN HOT DRY CLIMATES AND THE RESULTING STATE OF COMFORT INSIDE LOW COST BUILDINGS

By

ALI SALEH

The wide developments of reinforced concrete applications carried out during the last years in warm countries are clearly accompanied by deficiences in indoor comfort conditions.

In developing countries the use of insulating materials and air-conditioning is only limited to luxury buildings. The majority of contemporary low cost buildings are however, only roofed by bare reinforced concrete slabs. Due to the small thickness and high thermal conductivity of such slabs, indoor temperatures are clearly affected by wide-ranged fluctuations of air temperatures and solar radiation intensities prevailing in hot dry climates.

The influence of such low cost construction methods on the indoor comfort conditions are not yet thoroughly investigated.

In this study, the course of temperatures and state of comfort inside low cost dwellings in hot dry climates, sheltered only by bare reinforced concrete roof slabs are investigated. The weather conditions in Cairo, Halfa and Khartoun serve as examples of hot dry climates.

1. INTRODUCTION

In building materials technology, great advances have been achieved during the last century. The resulting applications in contemporary construction methods have widely introduced reinforced concrete skeleton structures. New buildings in developing countries are therefore mostly roofed by thin reinforced concrete slabs.

In common practice, the roof slab is protected, as shown in Diagram 1, by a damp proof course, a layer of ordinary concrete, a sand bed and finally, mortar and cement roofing tiles. The mentioned layers are normally enclosed within a brick parapet. In luxury buildings, a layer of an insulating material, usually a foam light-weight concrete with a low thermal conductivity value, is added to retard the exchange of heat between outdoors and indoors. In the case of air-conditioned buildings, the heat load is also minimized.

If low-cost housing projects in developing countries are to be designed, budget requirements exclude the application of insulating materials and air-conditioning. The other layers shown in Diagram 1 are also neglected to reduce the building erection costs. The inhabitants of such dwellings, representing the majority of the urban population in developing countries are therefore only sheltered by a bare reinforced concrete roof slab.

Cooling and warming up of structures are dependent on the heat storage capacity of their external components. Thick multi-layer roof constructions therefore act as a barrier against extreme weather conditions. Even in the absence of air-conditioning, they are capable of maintaining a cool comfortable indoor atmosphere during the overheated periods of the day. On the other hand, the smaller heat capacity and higher thermal conductivity

(suitable) forms of time varying factors. They could be taken as linear time functions.

(e) The values of the weighting factors may be changed to reveal the sensitivity of the system to such variation.

(f) The attacking course may be also changed and the effect on control system configuration detected.

ACKNOWLEDGEMENT

This work was carried out under the supervision and with the help and encouragement of Prof. Dr. Osama El-Kholy, Professor of Aernautical Mechanics, University of Cairo.

REFERENCES

(1) Merriam, C.W. III, "Optimization theory and the design of feedback control system", McGraw Hill 1964.

(2) Ellert, F.J., and Merriam, C.W. III, "Synthesis of feedback controls using optimization theory — An Example", Trans. on Aut. Control, IEEE, vol. AC—8, No. 2, 1965.

(3) Bellman, R., "Dynamic Programming", Princeton, New Jersey, 1957.

(4) Bellman, R., "Adaptive Control Processes, a guide tour", Princeton, New Jersey, 1961.

(5) Bellman, R., and Dreyfus, S.E., "Applied Dynamic Programming", Princeton, New Jersey, 1962.

(6) Blaklock, J. H., "Automatic Control of Aircrafts and Missiles", John Wiley, 1965.

(7) Seckel, Edward, "Stability and Control of Airplanes an Helicopters", Academic Press, 1964.

(8) Locke, Arthur S., et al., "Guidance", Princeton, New Jersey, 1960.

(9) Awny, M.M., "A linear optimum control system design for an aircraft in an attacking mode", M.Sc. Thesis submitted to Cairo University, May 1969.



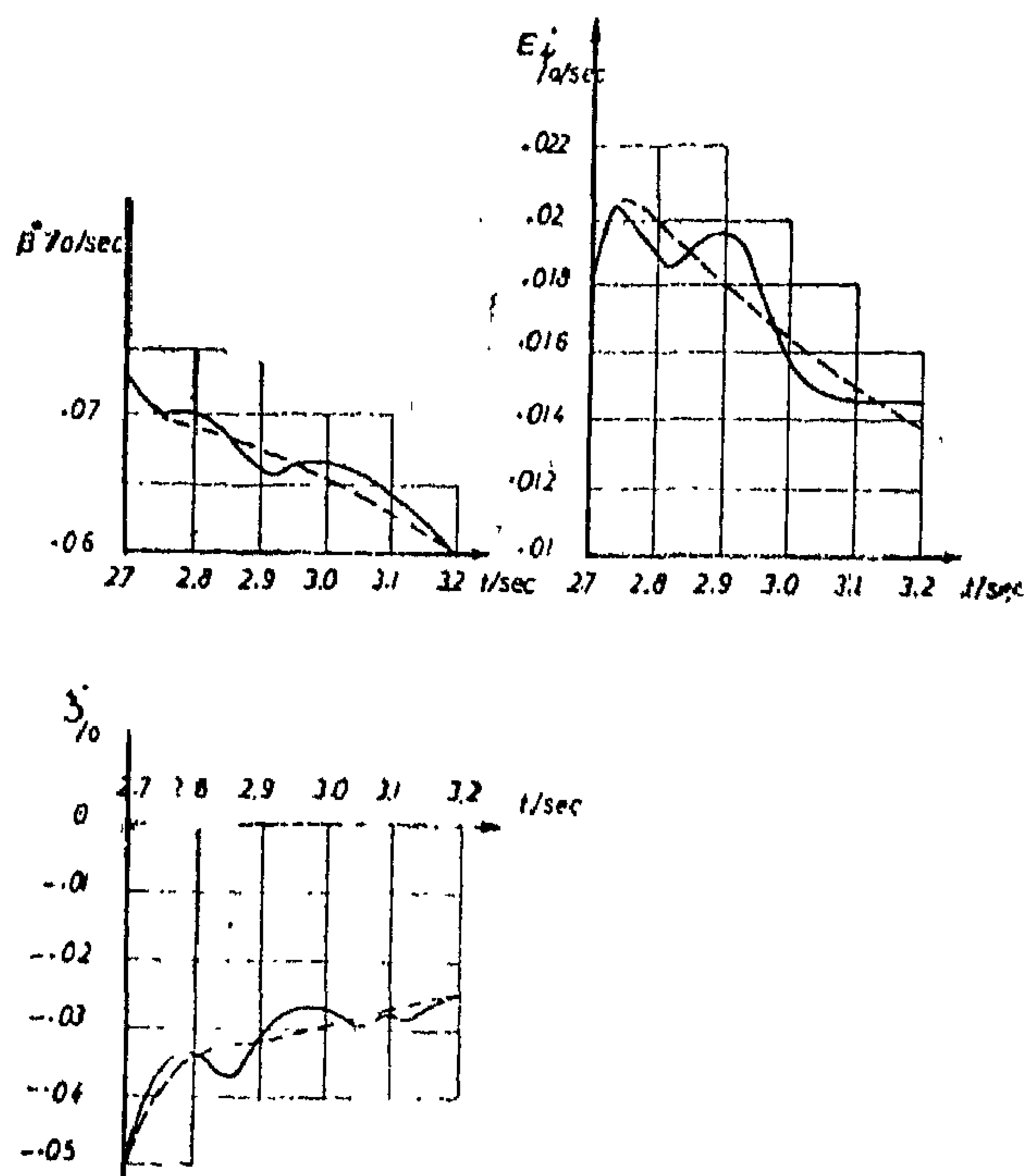


Fig. 15. — Sensitivity of the response to the smoothness of the K-functions.

(a) K-functions as linear segments of al period.

(b) K-functions as linear part in the period from 2-7 10 32 seconds.

LIST OF SYMBOLS

B	: State transformation matrix
E	: Minimum error function
$\vec{M}$	: Required control signal
$\vec{Q}$	: Required response signal
r	: Distance between target and aircraft
V_b	: Speed of bullet relative to aircraft
$\vec{x}$	: System state vector
ψ	: Yaw deflection
ζ	: Rudder deflection
χ	: Angle of relative vector "r" to the reference direction
Φ_i	: Response error weighting function
C	: Control transformation matrix
K_{ij}	: Optimum control parameter
$\vec{m}$	: Controller vector signal
$\vec{q}$	: System response vector
V_a	: Speed of attacking aircraft
V_T	: Speed of the target
β	: Side slip angle
ϕ	: Roll deflection
ξ	: Aileron deflection
δ	: Lead angle
ψ_i	: Control error weighting function
$\Phi_{ii}T$	: Area factor of the impulse weighting function

SUGGESTIONS FOR FURTHER STUDIES

The previous work opens new vistas for many interesting studies. Some of these are discussed below.

(a) We have seen that the maximum yaw deflection error is small while that of the side slip is relatively large. This result could serve as a guide in changing the weighting factors of both, decreasing the first and increasing the latter.

(b) To bring the response errors closer to zero at the end of the attack we may increase the values of the impulse weighting factors concerned.

(c) It is seen that the roll angle reaches large values along the path. This is not desirable because it changes the lateral plane of motion significantly from the horizontal and may render the linearization of the equation of motion invalid. Therefore, this error is to be weighted in the performance index. Yet a relatively small factor is to be used.

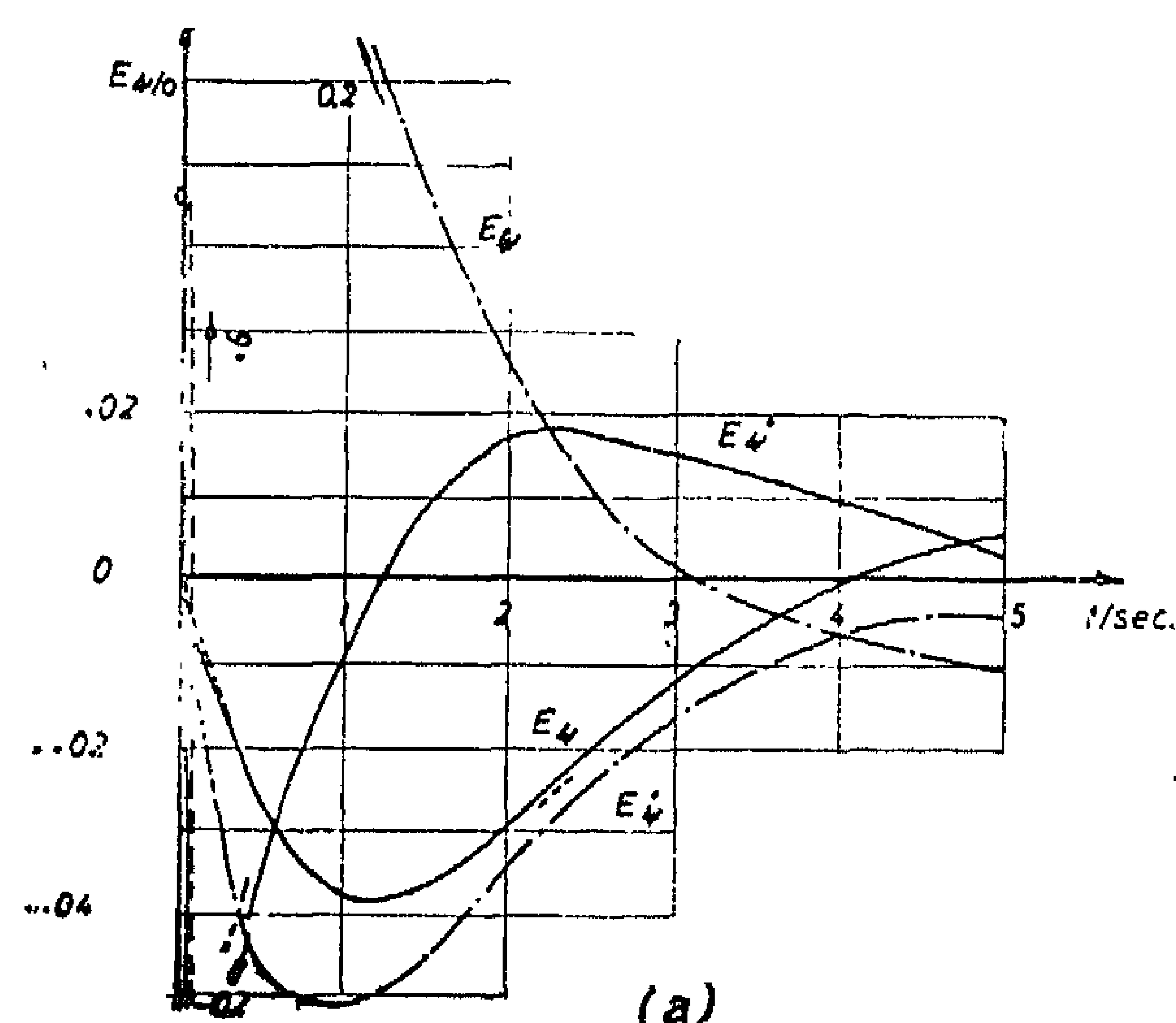
(d) The maximum allowable errors of each response changes as the distance between aircraft and target decreases. Therefore, our choice of costant weightings of the response response errors could be modified by more

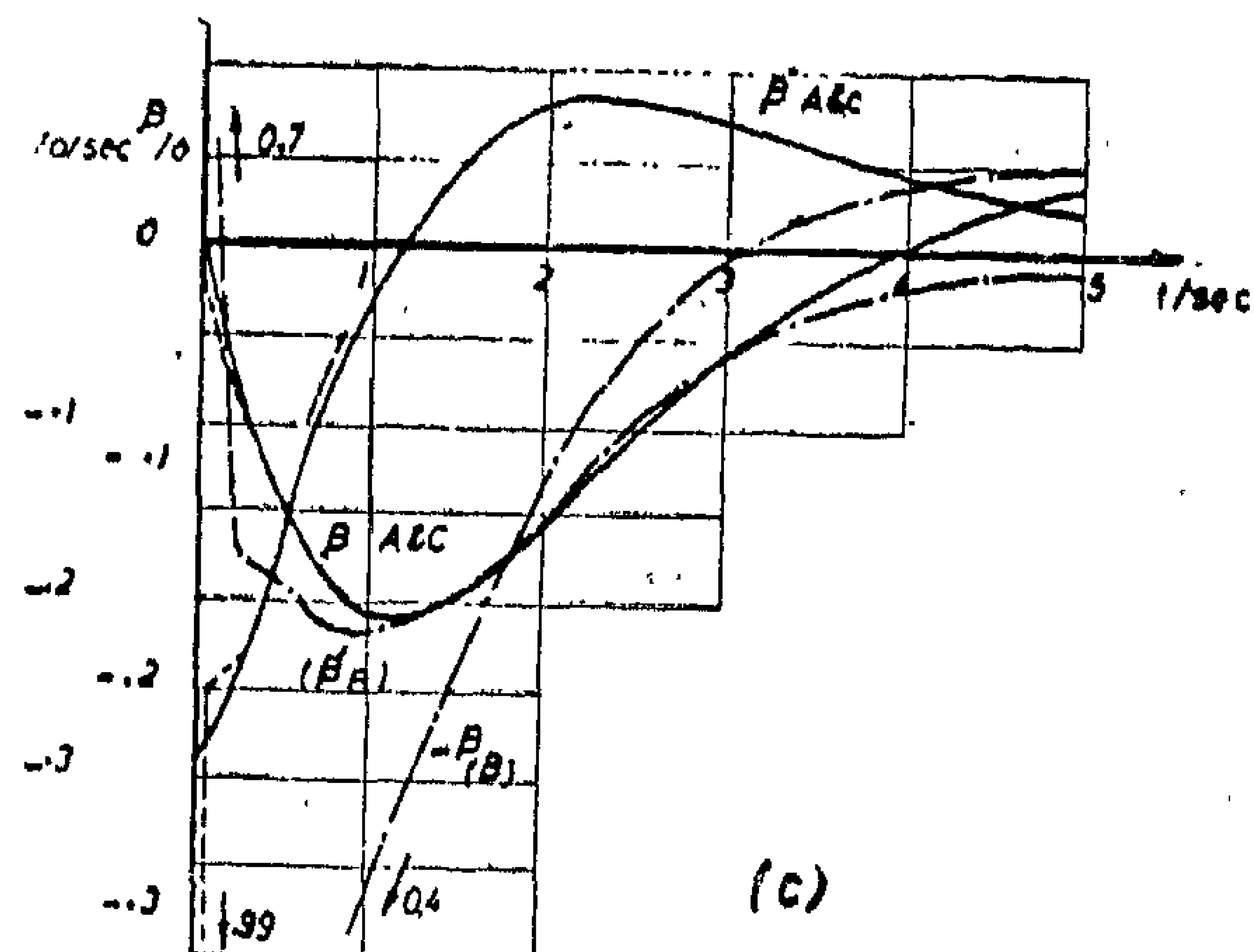
(b) The initial roll, and yaw rate errors have a slight effect on the total response. The effect almost vanishes after 0.3 seconds.

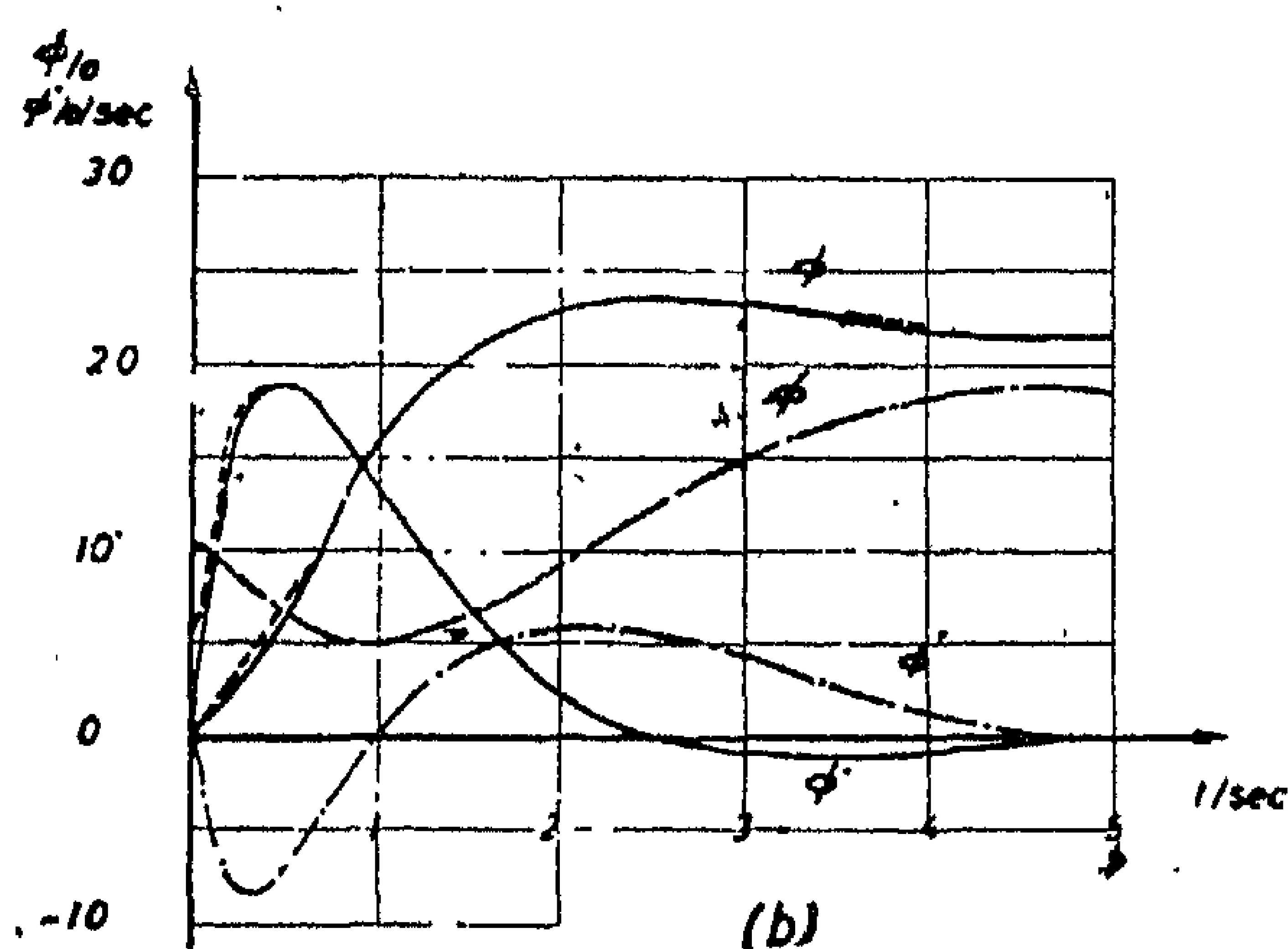
(c) Positive intial roll angle decreases the aircraft response errors. This is reasonable since the vehicle has to bank with positive roll angle, while turning to follow the required path.

(d) Positive initial side slip causes less response error during the course. This, too, is due to the dynamics of the vehicle along the path.

(e) With the initial yaw error, the performance differs significantly. This shows that the initial angular misalignment of the aircraft is of great importance.







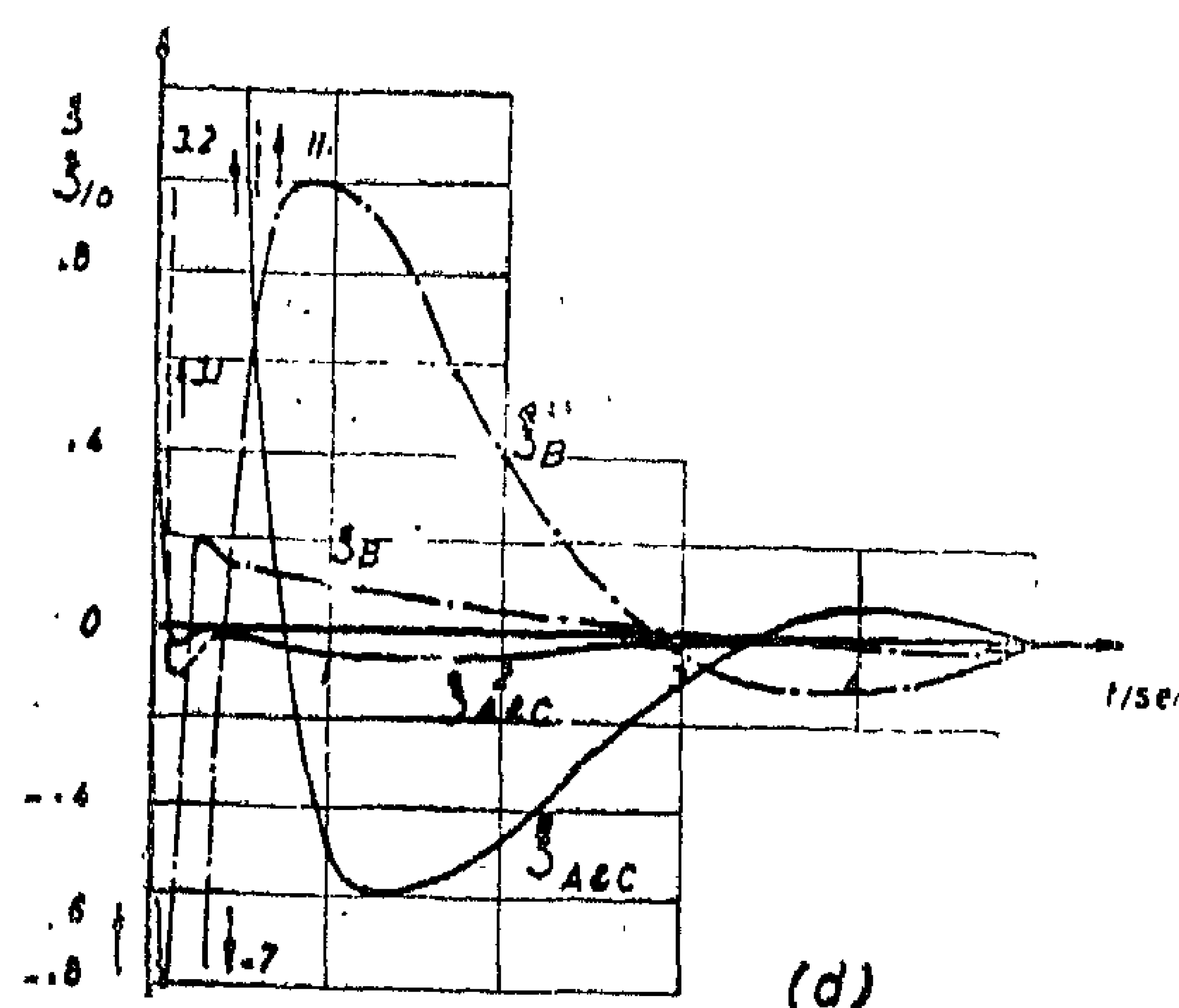


Fig. 14

GENERATION OF THE K-FUNCTIONS

It was noticed that there are unsteady oscillations appearing in some of the responses. namely; the yaw rate, side slip rate, and rudder deflection. These oscillations were found to be due to the unsmoothness of the K-functions and the variation in their rates of change. The introduction of the K-functions as polynomials, instead of linear segments versus time, will diminish these oscillations (Fig. 15).

We conclude that when generating the feedback and feedforward gains, satisfactorily smoothed functions must be available. The introduction of noise to the generation of these functions should be carefully filtered. Otherwise, some sort of oscillation in the response may occur.

The following remarks concern the response signals (Fig. 13) :

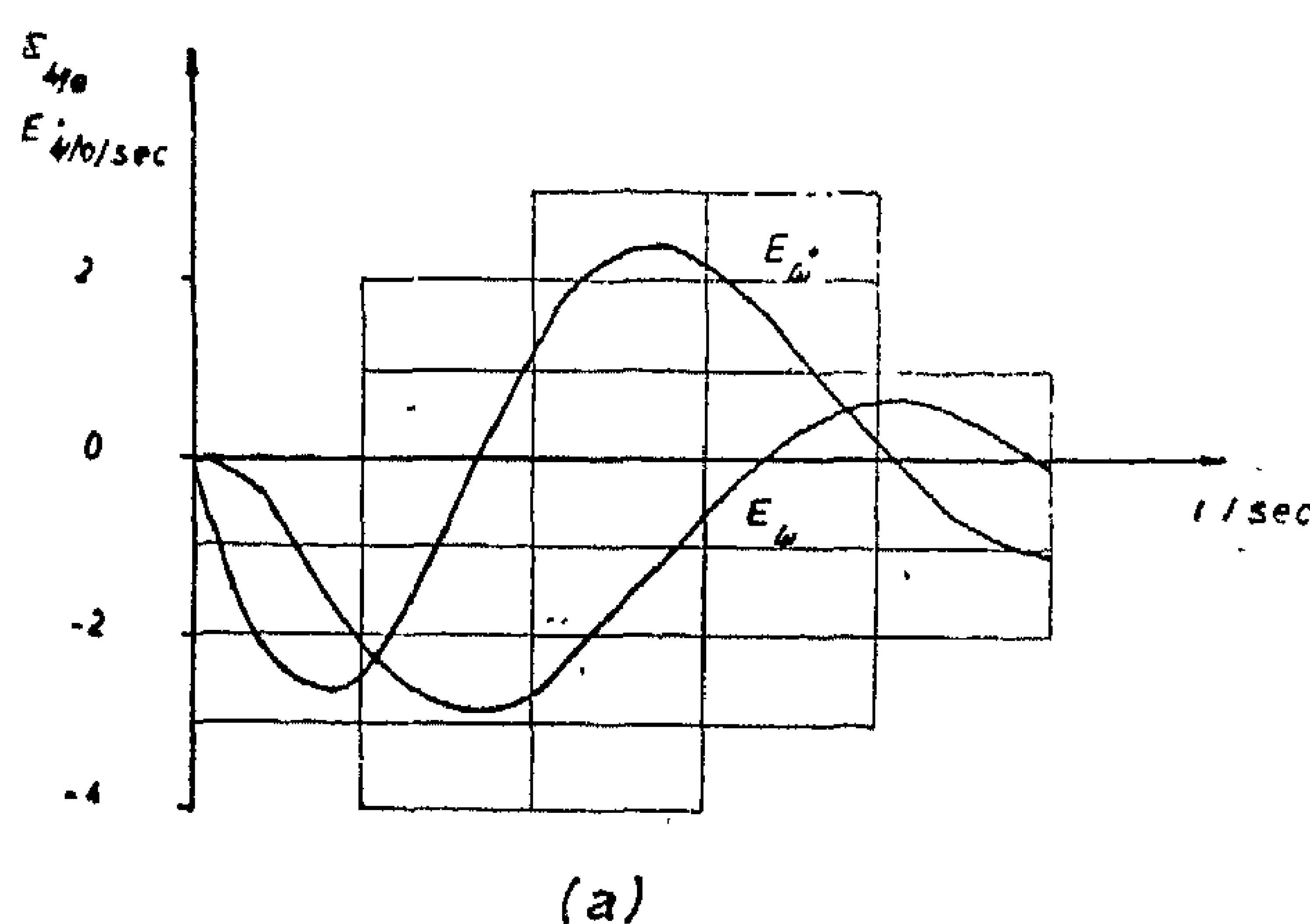
(a) The response errors during the course exceed those allowable. This is expected since no weightings from these errors were considered.

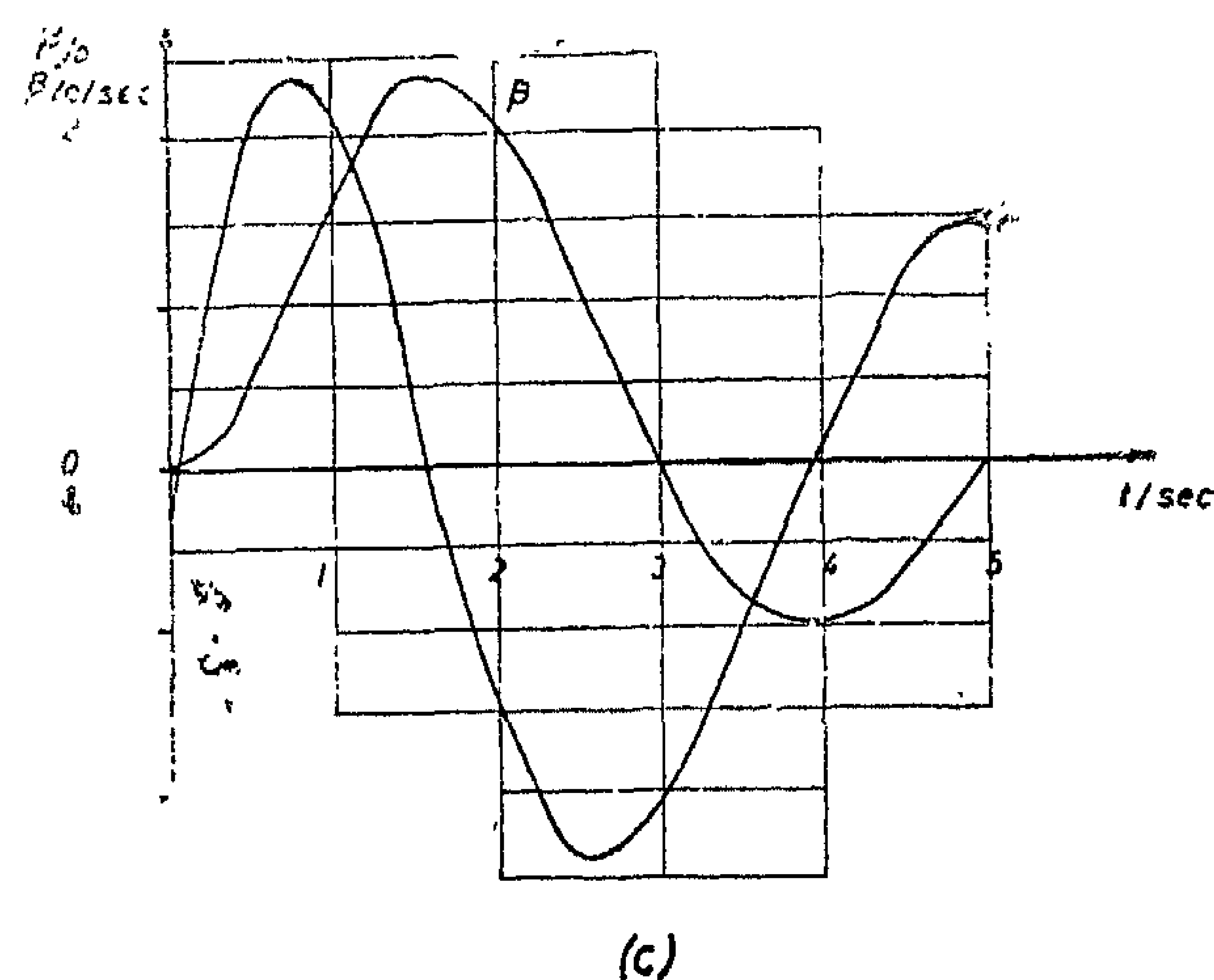
(b) As a direct effect of impulse weighting at the end of the period, the side slip and yaw deflection errors begins to decrease before the end and reach very small values.

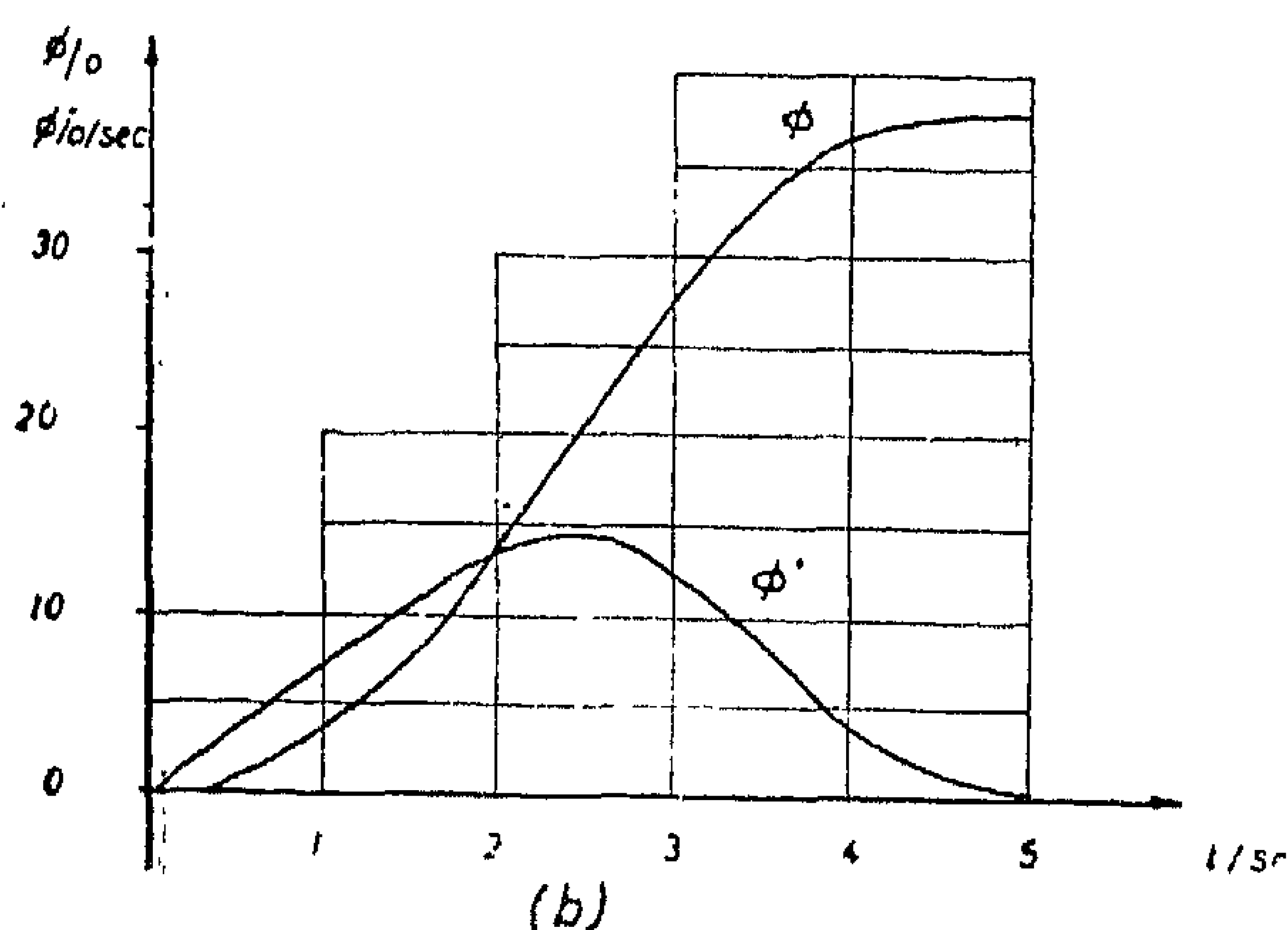
(c) Although the roll rate error is not weighted in the performance index, it decreases to small values. Thus, we conclude that this error is indirectly controlled by weighting the yaw and side slip errors.

(d) The control deflections attain relatively large valaues at the beginning of the attack due to the effect of initial conditions discussed before.

(e) Before break away of the attack, control deflections increase to account for the impulse weightings.







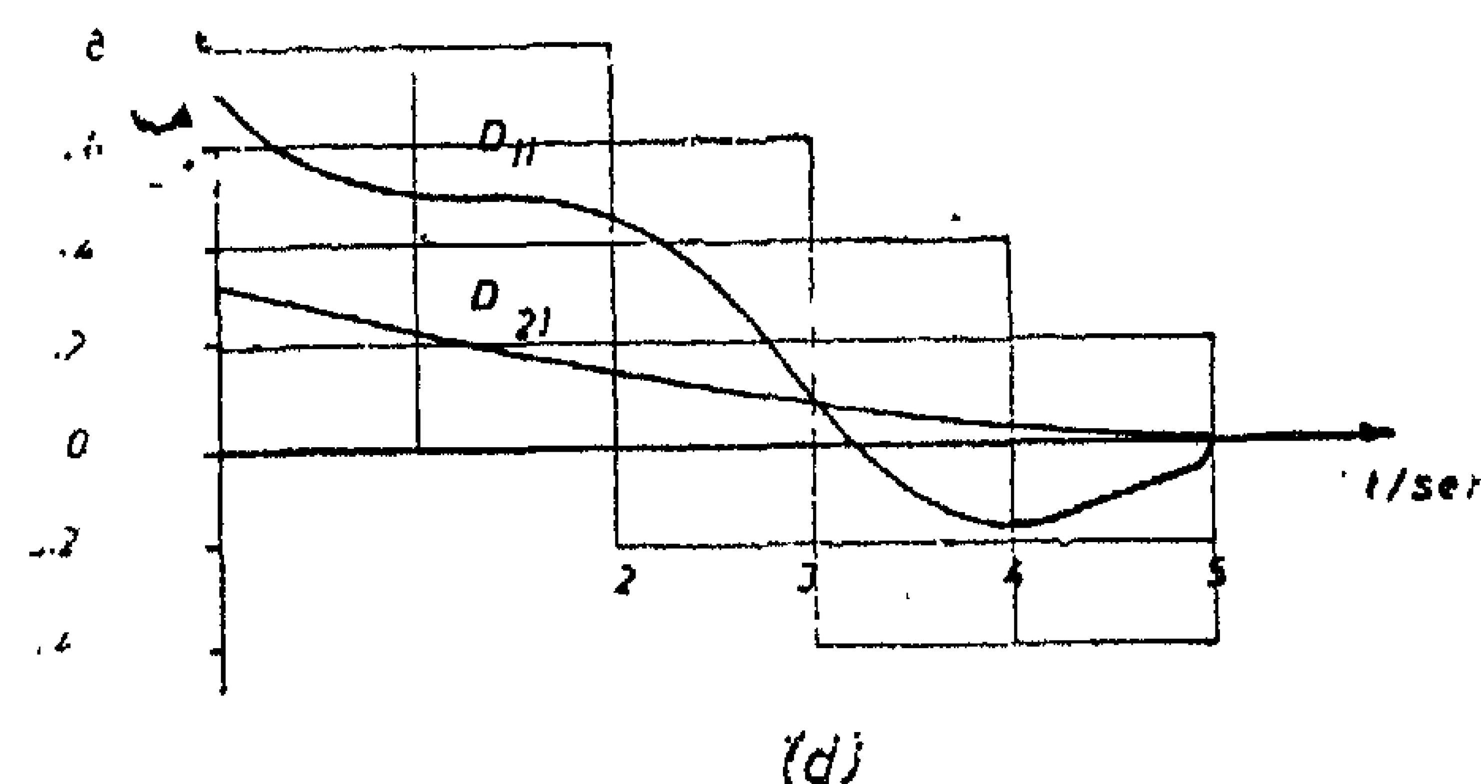


Fig. 13

EFFECT OF INITIAL STATE VECTOR

To deduce the effect of different initial state vectors on the response errors of the aircraft, we evaluate the performance equations with one specific control system configuration (case 1), for the following successive cases of deviated initial conditions seperately, namely; the error in side slip, roll rate, yaw rate, and yaw angle. The following features were noted (Fig. 14) :

(a) All initial response errors decrease as time goes on.

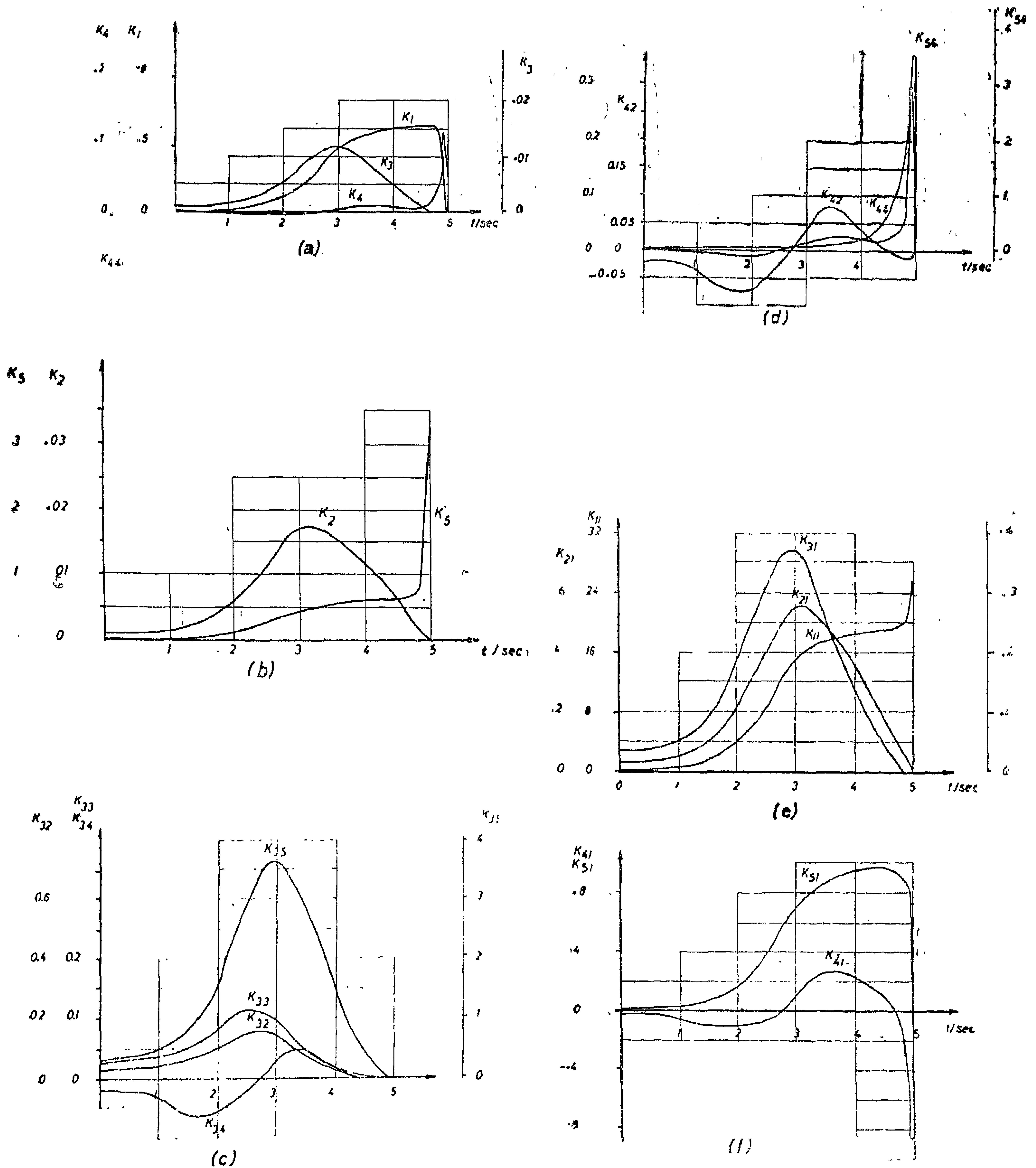


Fig. 12

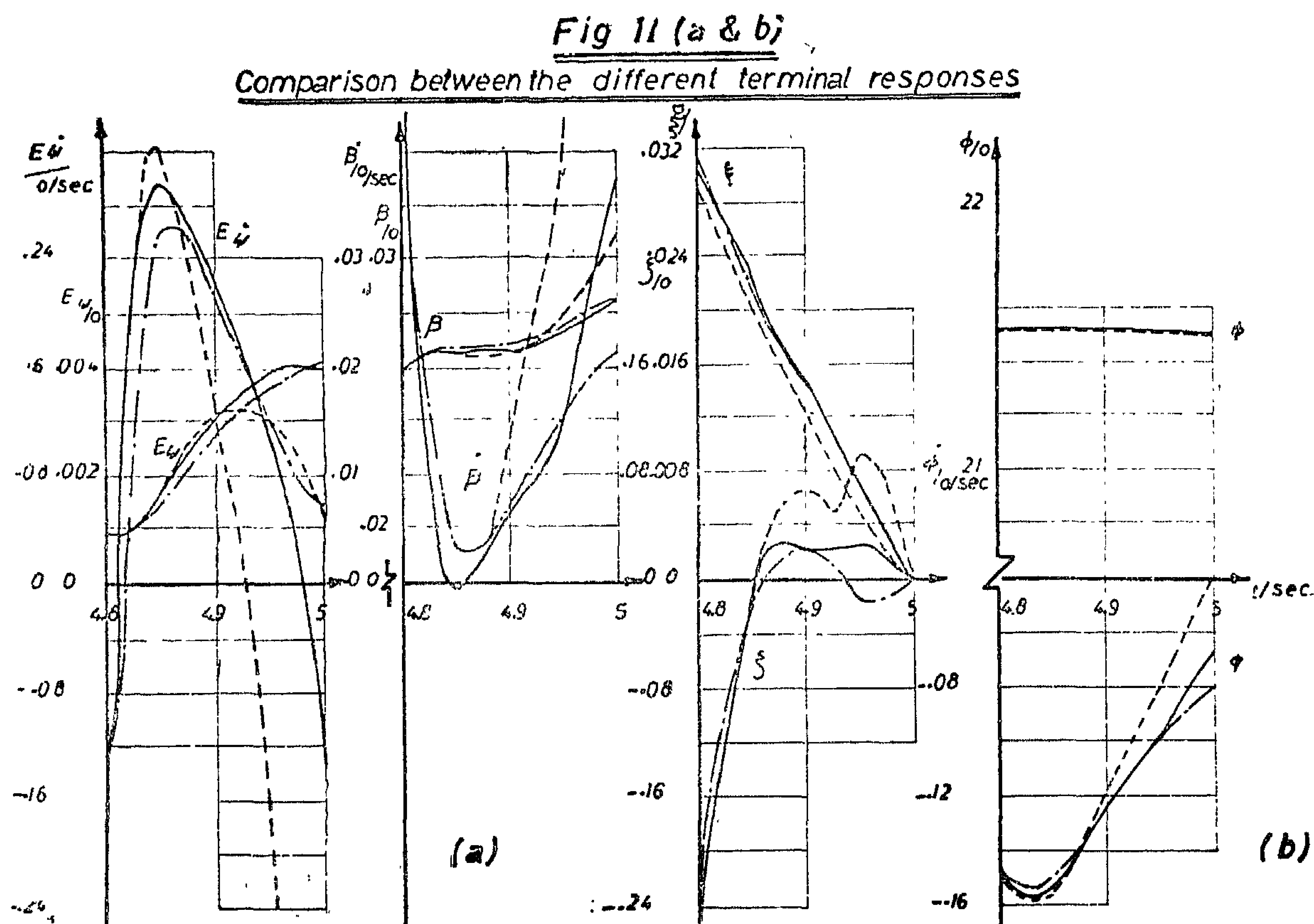


Fig 11 (a & b)

Comparison between the different terminal responses

II Pure Terminal Control :

This case differs from previous cases in that no consideration is taken of the system errors during the entire path, with the exception of the control effort.

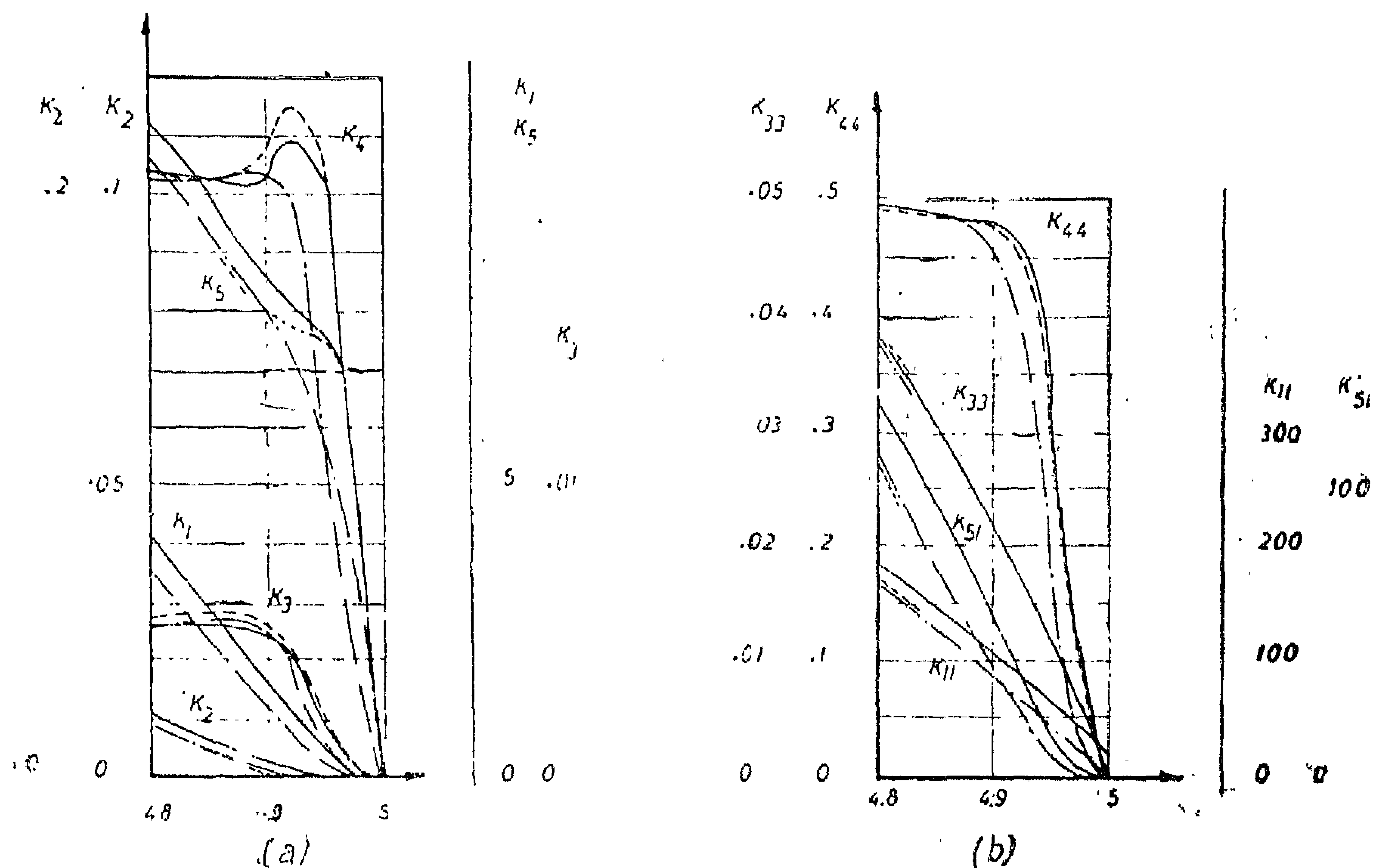
The control configuration has the following features : (Fig. 12) :

(a) The input signals have very small values during most of the time. This is due to the fact that no consideration is taken for the aircraft response during the attacking period and consequently no input is required.

(b) Before the end of the period, however, the input signals that are responsible for the yaw and yaw rate, rise to appreciable values so that the control system may receive signals strong enough to cause the aircraft to to aquire the required response at the end. This rise begins at about 0.2 second from the end.

(c) The feedback gains are almost zero during most of the attacking course. This renders the overal system almost similar to an open loop system. However, before the end of the course, the feedback gains increase at high rates to cause sufficient powerful signals proportional to the response errors to be transmitted to the controls for achieving the aircraft terminal posiation required.

Figures 10 and 11 show comparison between the different control system configurations and the consequent terminal responses of the overall systems.



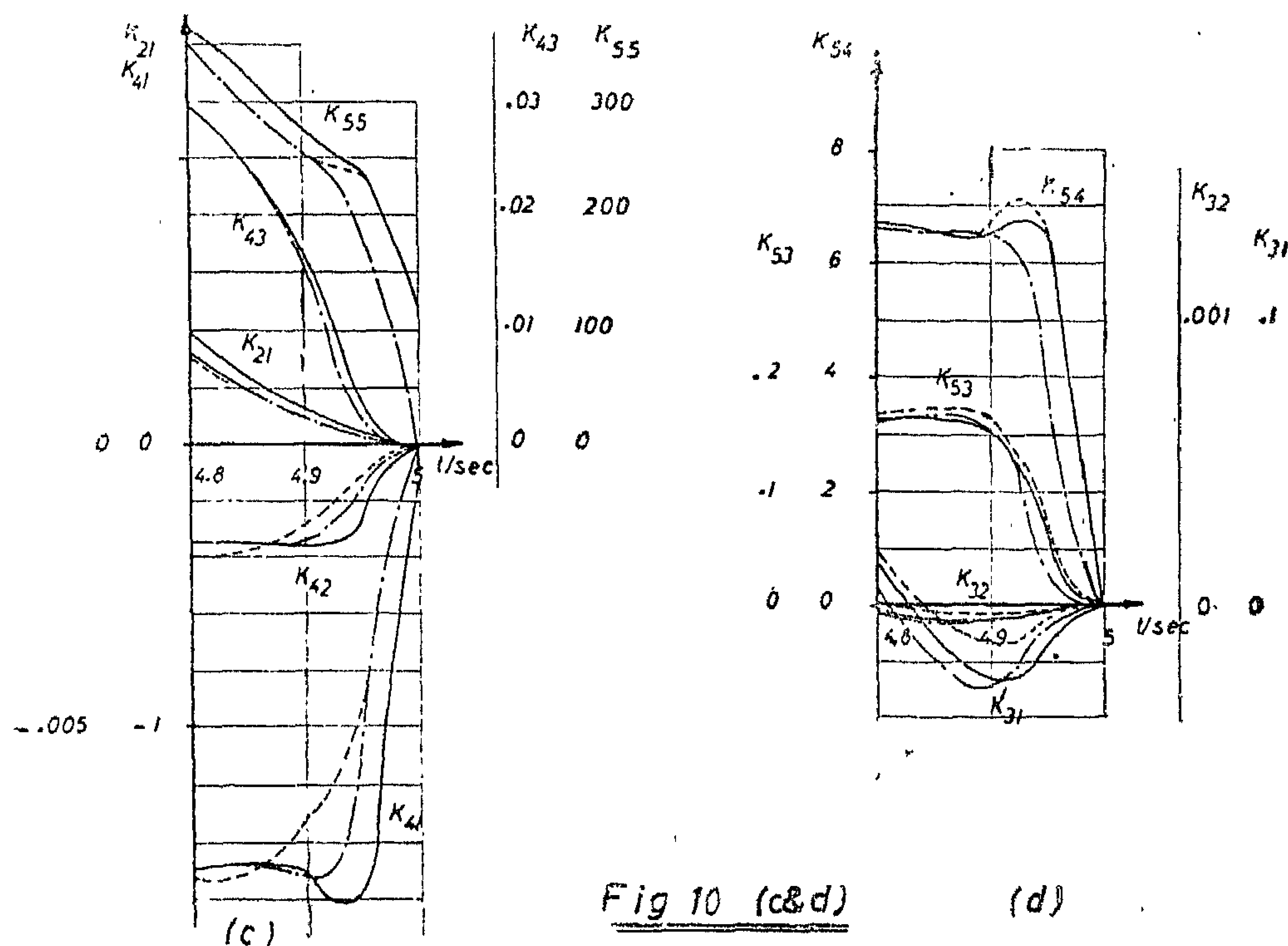


Fig. 10. — Comparison between the different control system configurations.

(b) The response errors; initially set to zero, change with time as a result of the compound dynamics of the aircraft and controls but still fall under the restriction of minimizing the error index specified for each case.

(c) All the response errords and control deflections converge to small values with the exception of the roll angle which is not directly weighted in the performance index.

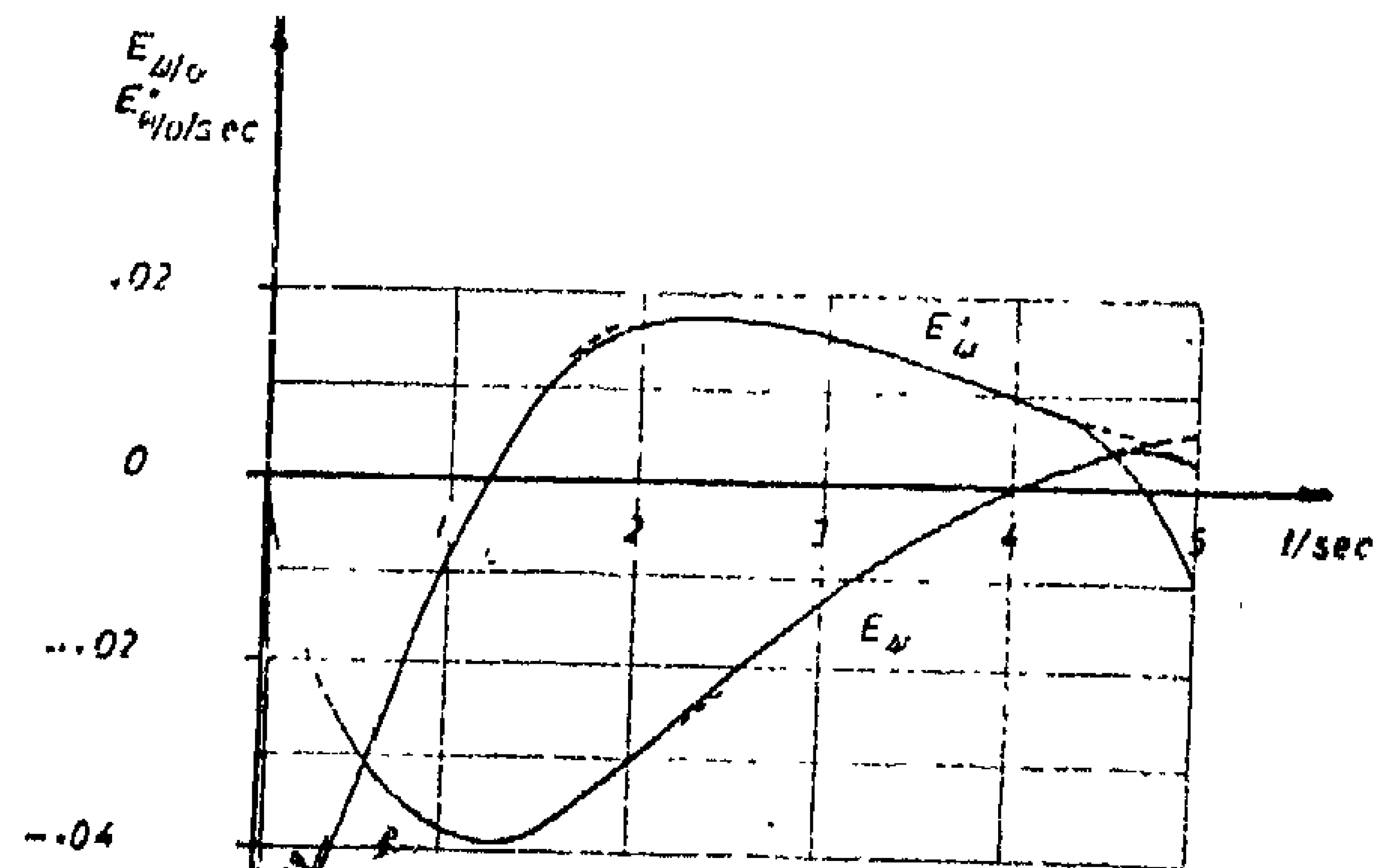
(d) The yaw deflection rate and the rudder deflection have similar profiles, as might be expected from the aircraft dynamic relations.

(e) The aircraft performance, considering the three systems of control configurations, is almost similar during about the first 4.8 seconds of the course. This is clear since the control system configurations do not change significantly throughout this period.

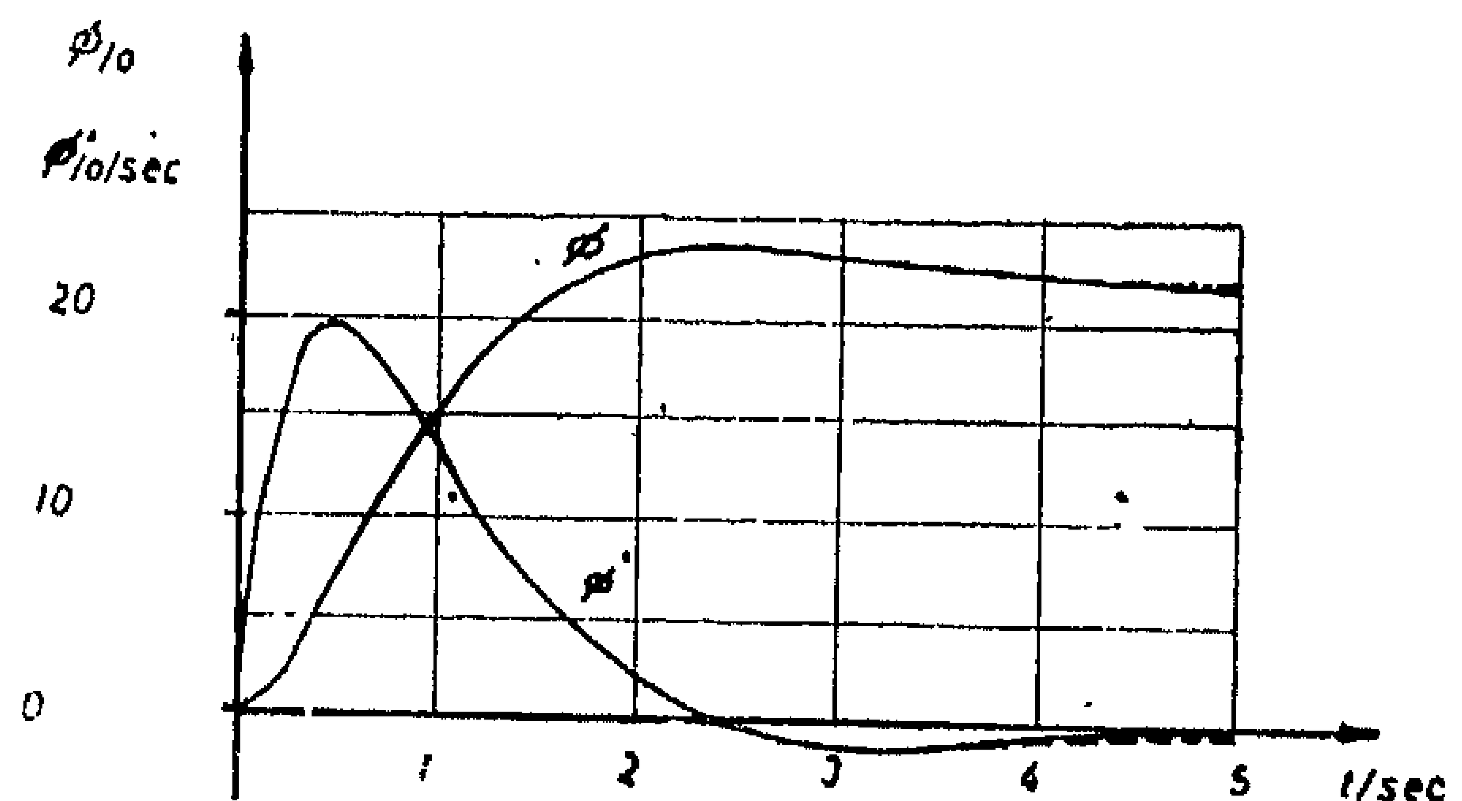
(f) In comparison with the case of no terminal restrictions the following deviations were detected :

(i) When yaw terminal restriction is imposed (case 2), the yaw error, response drops more rapidly to a lower value at the end of the attack. As a penalty, the side slip angle and the rudder deflection increase slightly. This increase could be directly deduced from the features of the K-functions which rise near the end to account for the terminal restriction.

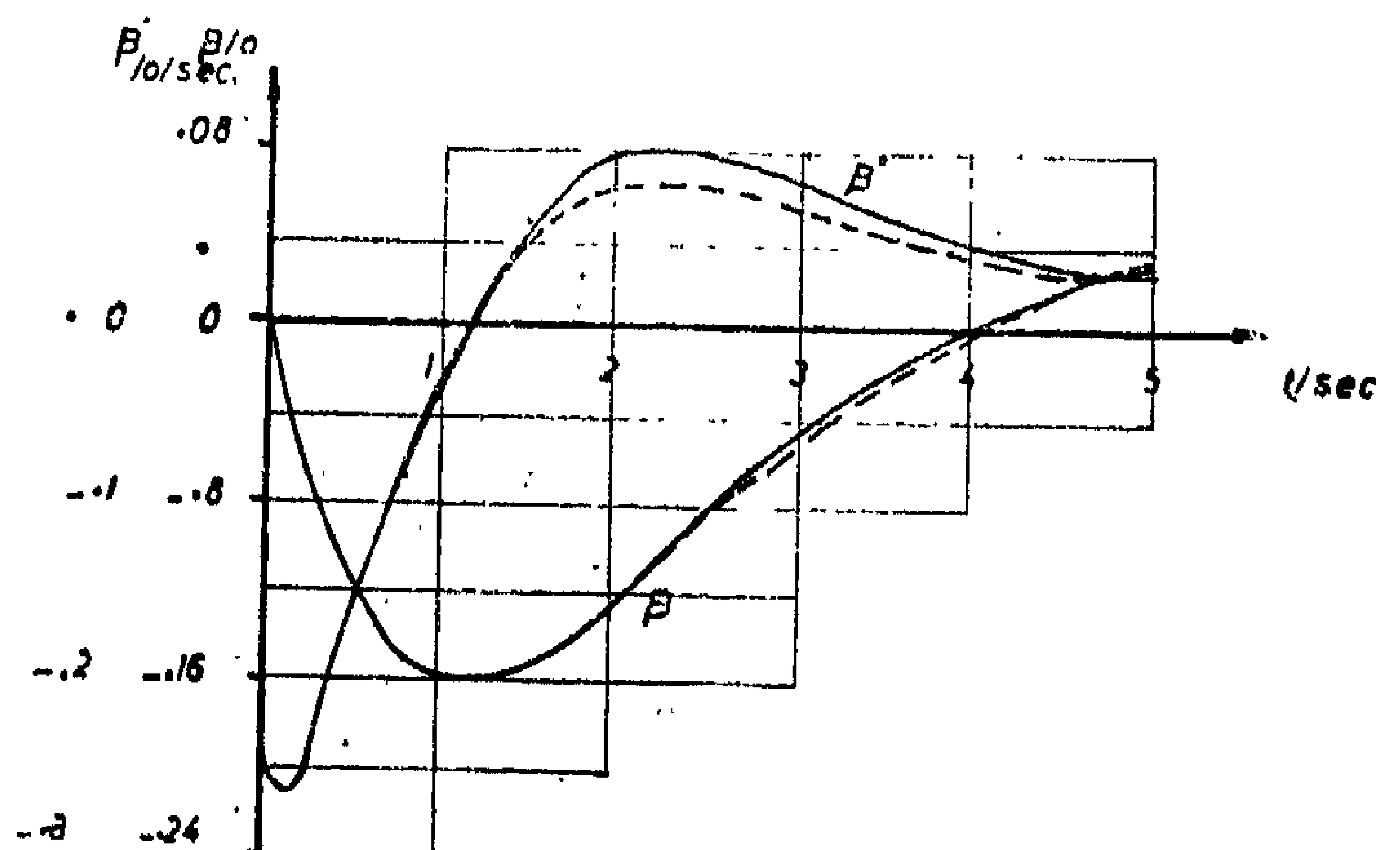
(ii) When both yaw and side slip terminal restrictions are considered (case 3), we notice that the terminal yaw deflection error is higher than case 2. This is expected since the new additional requirement takes part of the control effort required. Moreover, the rudder deflection is seen to increase to a lower which is accompanied, on the other hand, by relatively higher values of aileron deflection. This happens because the side slip angle is affected indirectly by the aileron deflection, through a term including the roll deflection that has a relatively large coefficient*, while the yaw deflection is affected by the aileron through the roll rate term which has a relatively negligible effect**. The preceeding discussion stresses the fact that controlling the yaw deflection is affected mainly by the rudders, while the side slip angle is controlled by both rudder and aileron deflections, although not with the same effectiveness.



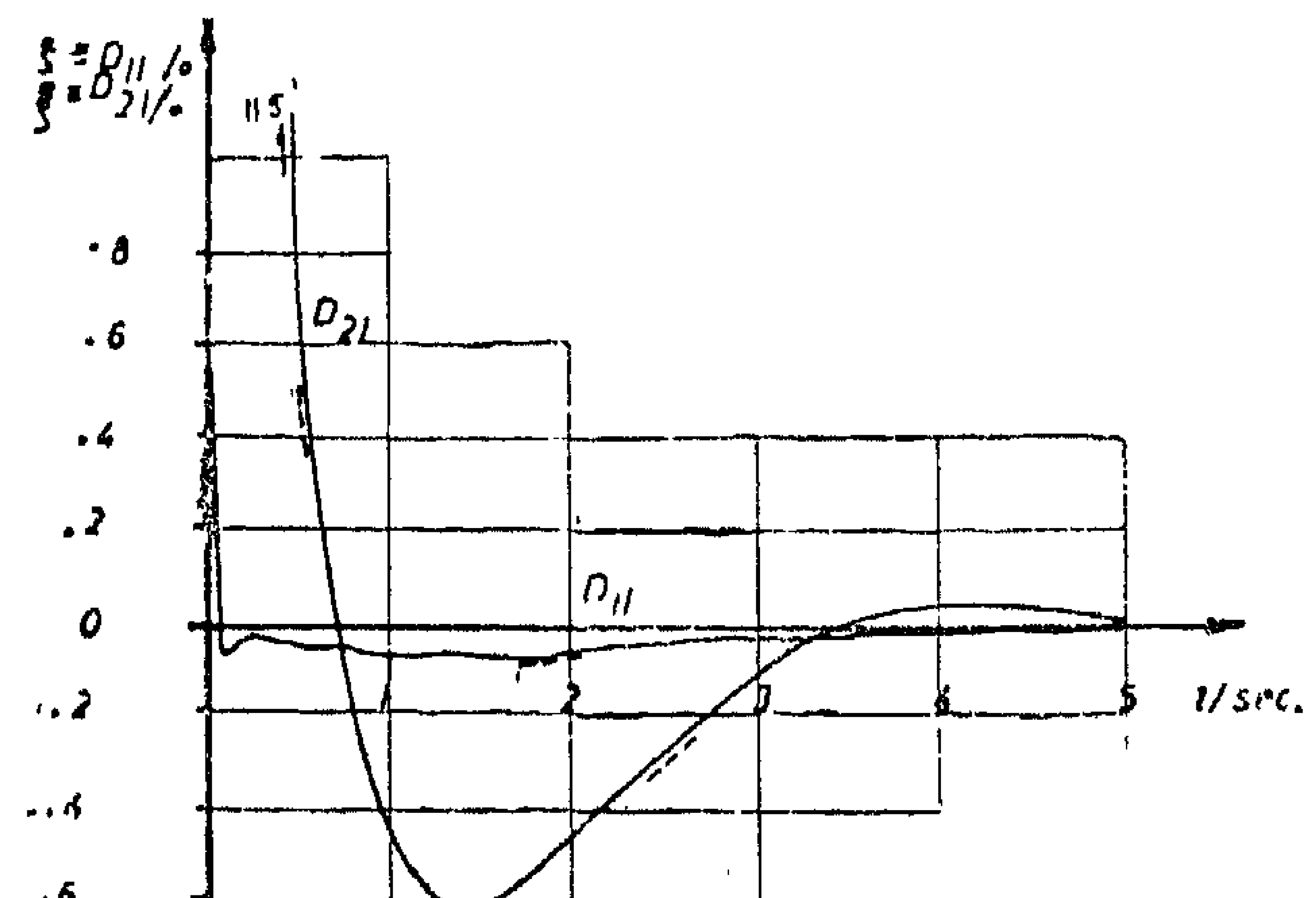
(a)



(b)

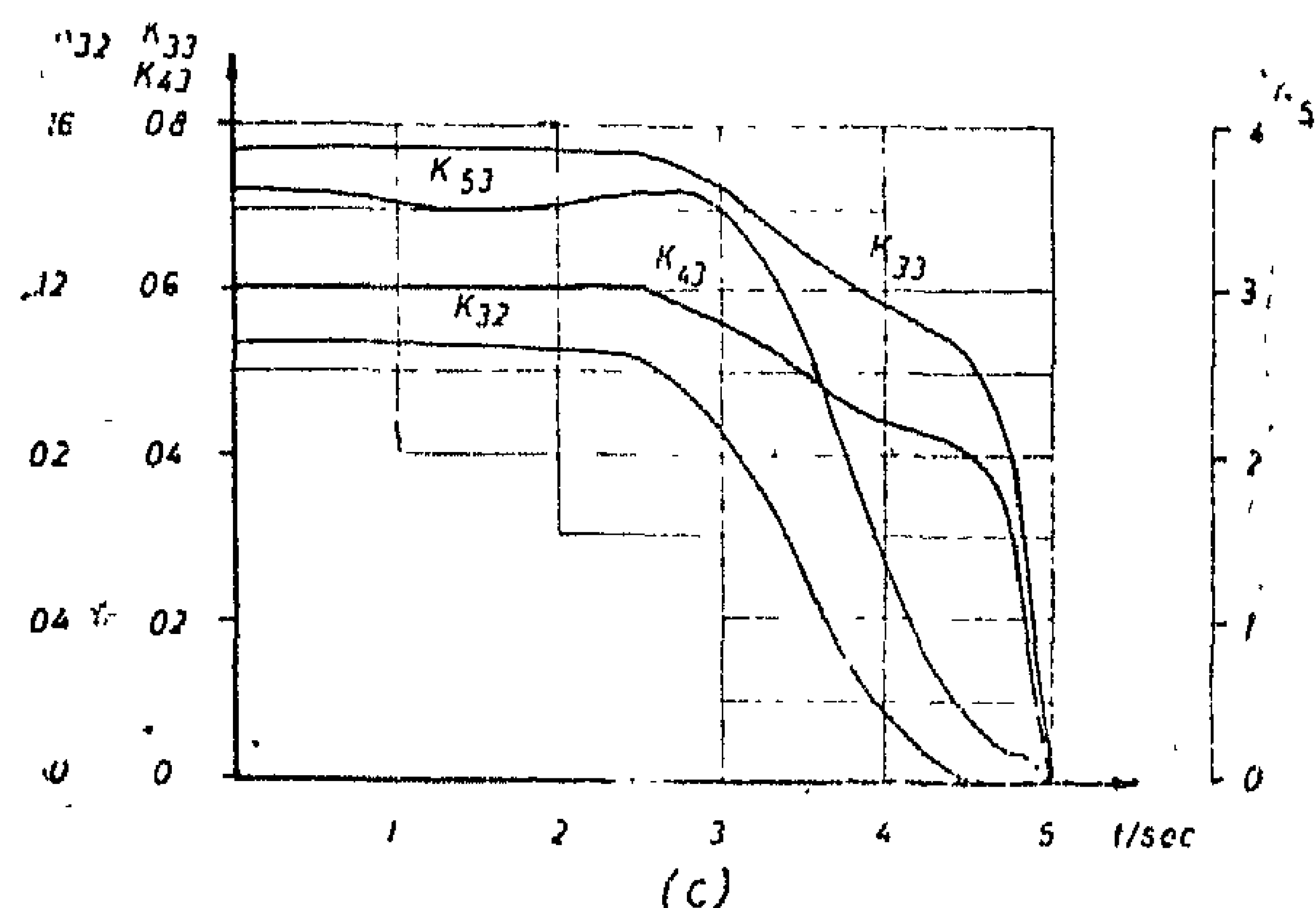


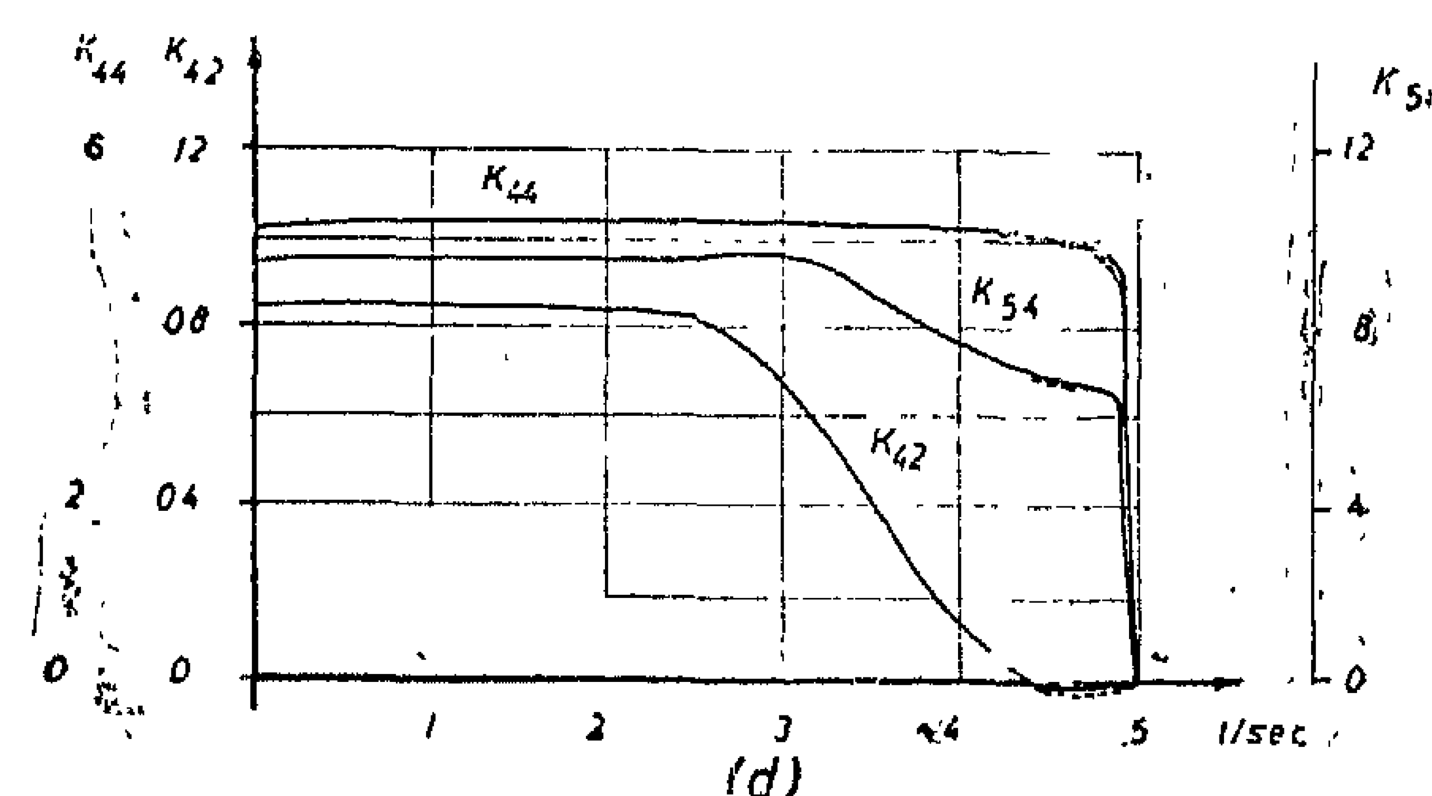
(c)

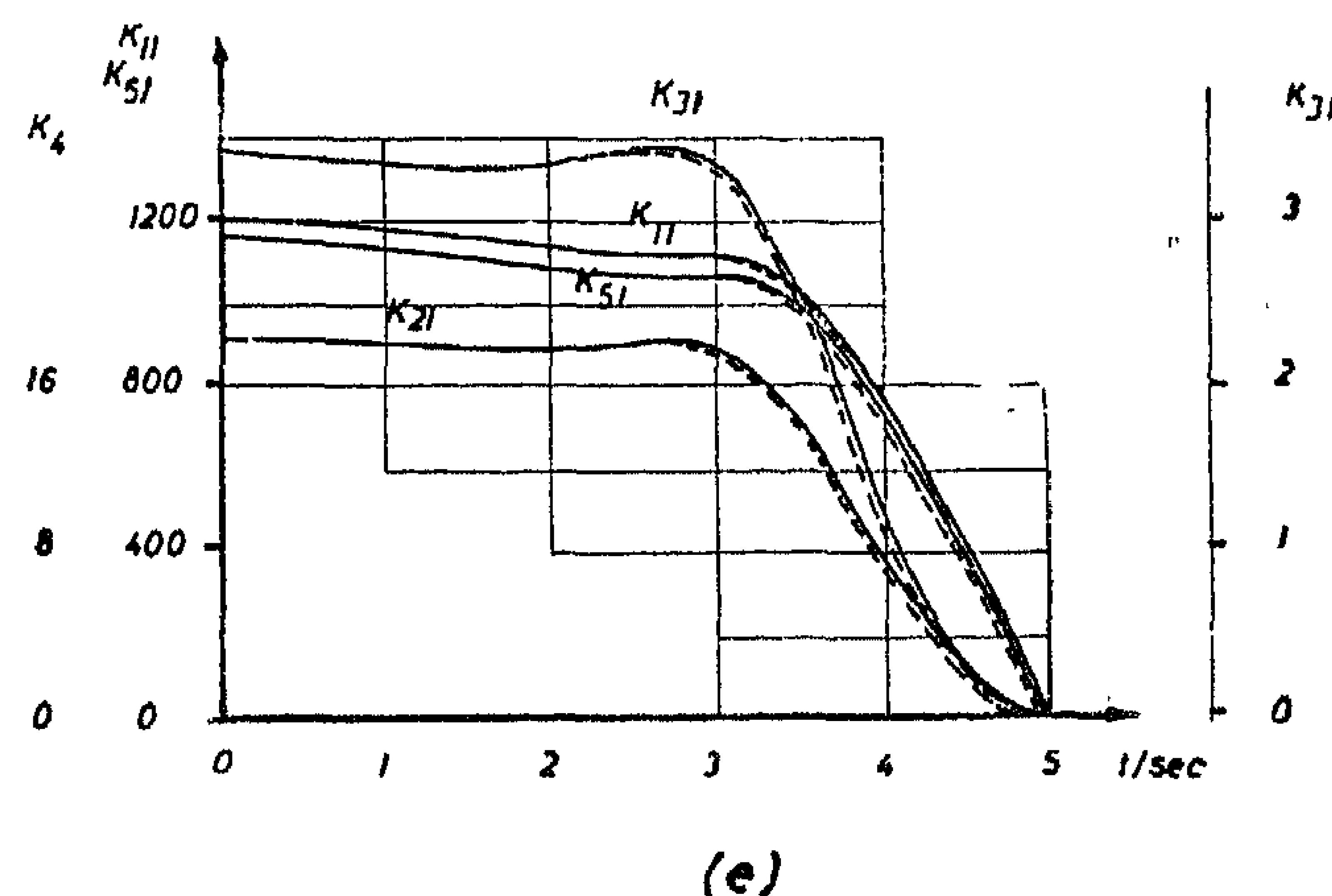


(d)

* The coefficient mentioned is b of equation 1.


(c)


(d)


(e)

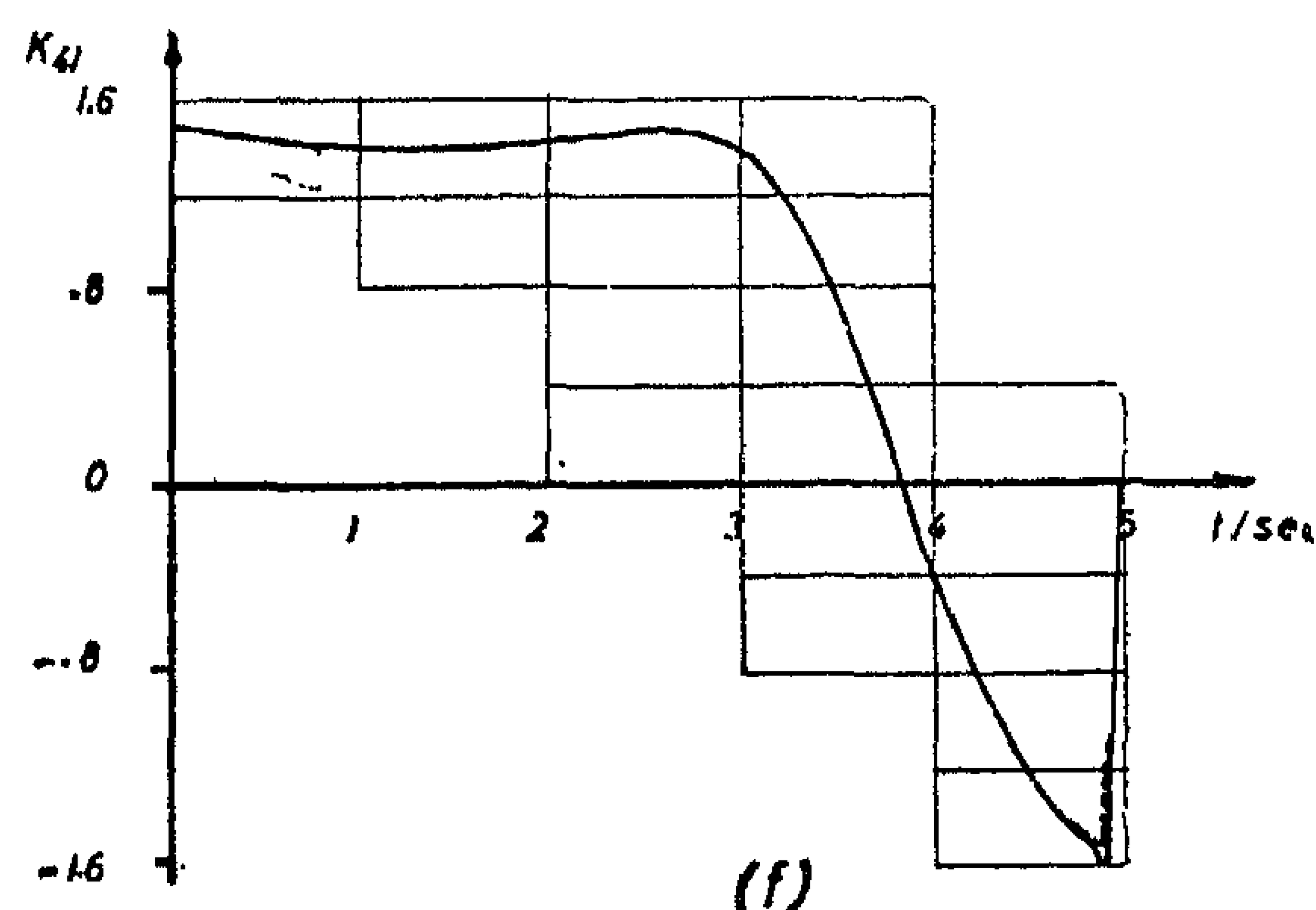

(f)

Fig. 8

By the addition of the terminal restrictions, the resulting K-functions are very close to the normal case up to about the last 0.2 second. This is reasonable, since the weighting functions are the same during that period. During the last 0.2 second, some of the functions, that are concerned mainly with the response signal under terminal restriction, deviate clearly. This deviation accounts for the supplementary requirement of fixed terminal condition appearing in the form of non-zero boundary conditions for the K-functions concerned.

(2) *Feedback gains:* These are described by the double subscripted K-parameters (Fig. 8, c-d). They are almost constant for about two thirds of the attacking course. This corresponds to the constant weightings of the response errors. It also confirms the independency of this period of the boundary conditions as discussed before.

In cases of additional terminal restrictions, deviations are observed from the normal case, during the last 0.2 second. These deviations are in forms of impulse near the end of the attack. This is understandable since we need heavy weighting of the concerned errors at the end of the attack so as to bring them down to the descried values.

It is noted that some of the feedback gains are negative over a certain period. This shows that positive feedback could occur without affecting the system overall stability.

The roll angle, although not weighted in the performance index, is seen to be fed back into the control system. This is a result of the coupling between the different elements of the state vector in the dynamics of the aircraft.

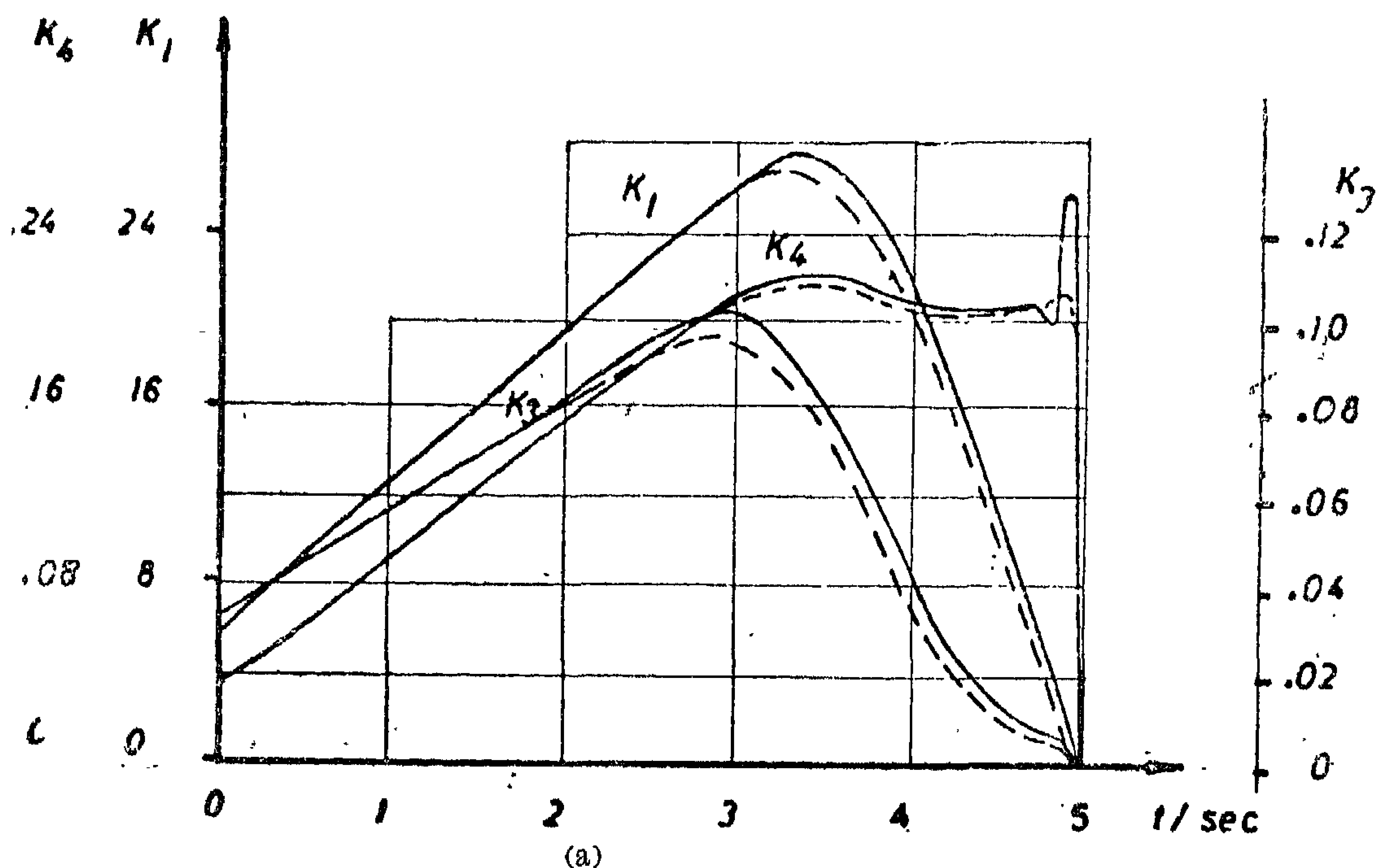
(3) *Evaluation of aircraft performance:* The aircraft performance using the optimum control system designed is evaluated and the following general remarks could be made (Fig. 9) :

(a) At the instant of control application, the control deflections attain high values although the response errors may be zero. This is due to the fact that the initial conditions do not correspond to the equilibrium situation.

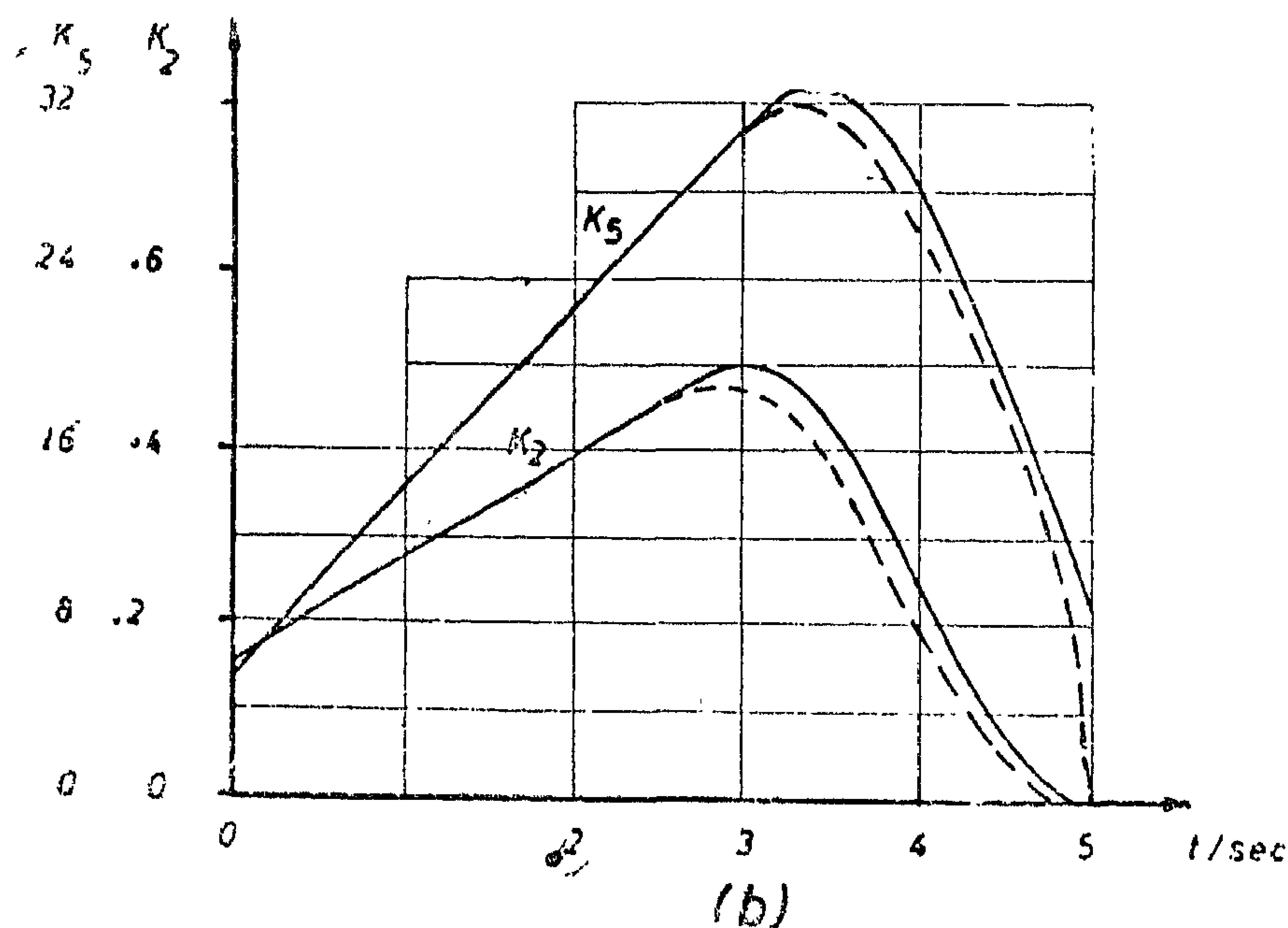
(1) *Feedforward gains.* These are described by the single subscripted k-parameters. (Fig. 8 a-b). They increase monotonically with time during the first 3 seconds. This corresponds to the behaviour of the required yaw and yaw rate deflection functions.

In this period, the terminal conditions have almost no effect on the system configuration. The additional restrictions on the terminal values of either the yaw deflection and/or the side slip angle, do not seem to violate this fact.

In the last two seconds of the controlled phase, these functions begin to decrease slightly, going to zero in accordance with the boundary conditions of the K-functions.



(a)



(b)

Fig. 8

CASE III

Constant weightings of the response and control errors with impulse weighting of both yaw and side slip errors.

In this case we emphasize the importance of the end response of both yaw and side slip angles. Hence, the performance index is :

$$e(t) = 25\,\beta^2(5) + 100\,[\chi(5) - \Psi(5)]^2 + \int_t^5 \{ 1000\,\beta^2(\mu) + .256\,\dot{\Phi}^2(\mu) + .71\,[\dot{\chi}(\mu) - \dot{\Psi}(\mu)]^2 + 4000\,[\chi(\mu) - \Psi(\mu)]^2 + \zeta^2(\mu) + 1.78\,\xi^2(\mu) \}\, d\mu$$

The boundary conditions for the K-functions at $t=T=5$, are all zeros except :
$K_5(5) = 3.204$, $K_{11}(5) = 25$, $K_{35}(5) = 100$

CASE IV

Impulse weightings of side slip and yaw errors at the instant of break away of the attack.

This is a pure terminal control problem with respect to the side slip and yaw deflection errors. The error index will take the form :

$$e(t) = 25\,\beta^2(5) + 100\,[\chi(5) - \Psi(5)]^2 + \int_t^5 \{ \zeta^2(\mu) + 1.78\,\xi^2(\mu) \}\, d\mu$$

The boundary values for the K-functions will be :

$K_5(5) = 3.204$, $K_{35}(5) = 100$, $K_{11}(5) = 25$
All the K-functions other than the above are zeros at $t=5$.

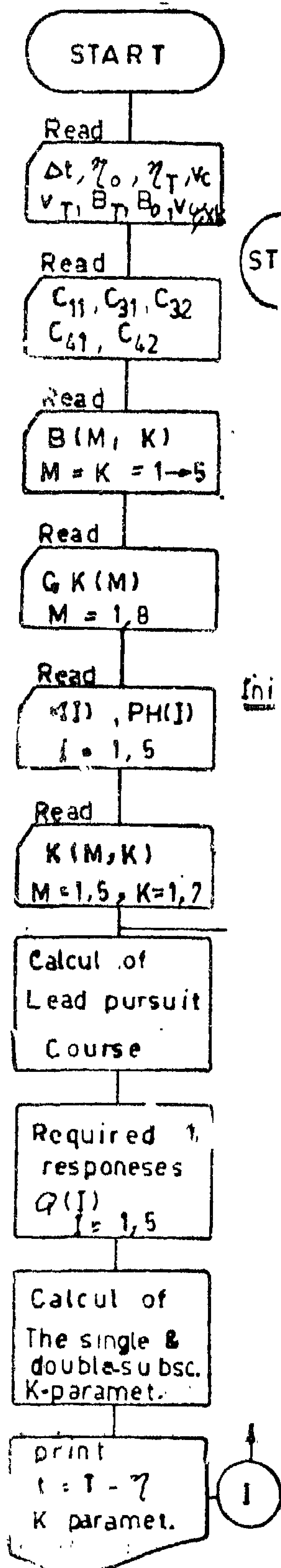
GENERAL REMARKS AND CONCLUSIONS

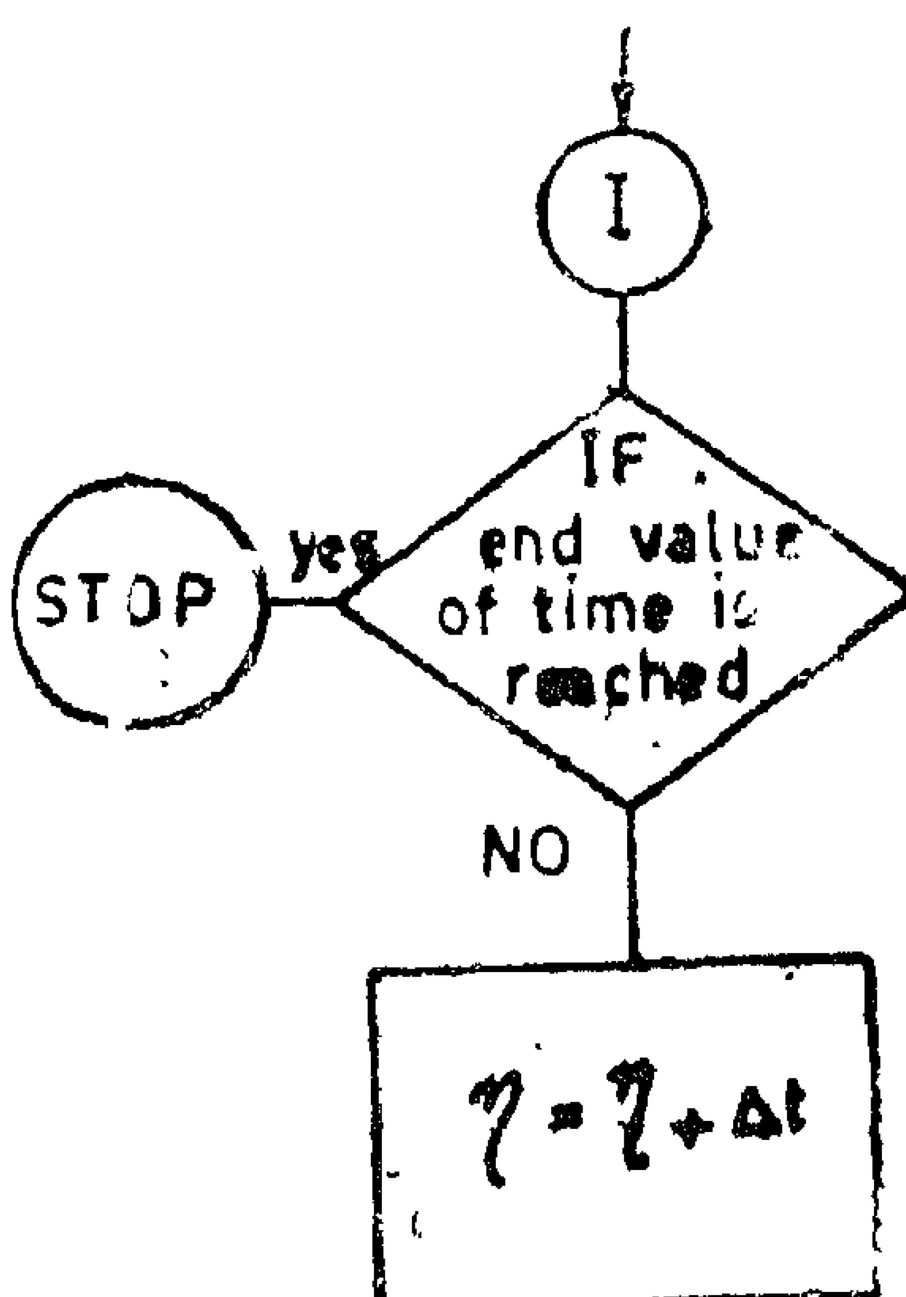
The dynamics of the aircraft as a complex system, together with the desired response signals affect the configuration of the optimum control system, as specified by the k-functions, in a complex manner. Hence it would be rather diffiult to rationalize the detailed behaviour of each parameter. Yet some general of these parameters could be discussed and explained.

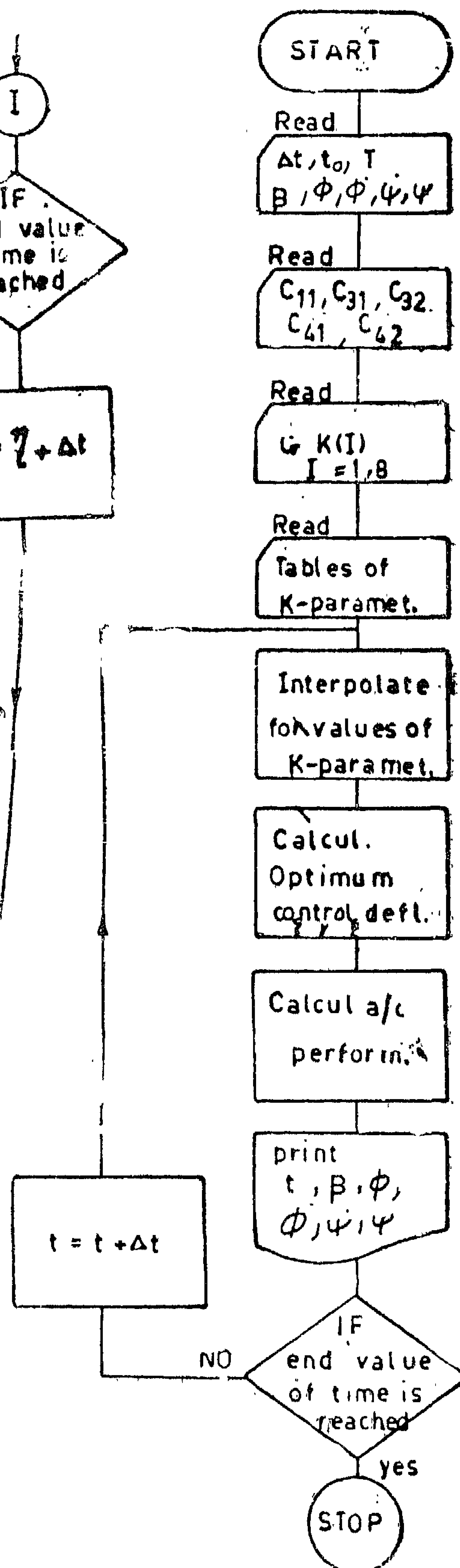
In the following divided the pervious cases into two groups. One described the systems that control, continuously, the output responses (cases 1,2 and 3). The other group contains case 4 which describes the pure terminal control system. Moreover, case 2 and 3 are, in fact, combinations of the two, although in the first group.

I. Continuously Controlled Systems :

The following remarks can be made, concerning both system configuration and response.


PART I
START
Read
Read
C_{11}, C_{31}, C_{32}
C_{41}, C_{42}
Read
B (M, K)
M = K = 1→5
Read
G K (M)
M = 1, 8
Read
, PH(I)
I = 1, 5
Read
K (M, K)
M = 1, 5, K = 1, 7
Calcul of
Lead pursuit
Course
Required
responeses
Q (I)
I = 1, 5
Calcul of
The single &
double-subsc.
K-paramet.
print
t = T - η
K paramet.
I


I
IF
end value
of time is
reached
STOP
yes
NO
η = η + Δt
Initial conditions


PART II
START
Read
Δt, t_0, T
Read
C_{11}, C_{31}, C_{32}
C_{41}, C_{42}
Read
G K(I)
I = 1, 8
Read
Tables of
K-paramet.
Interpolate
for values of
K-paramet.
Calcul.
Optimum
control defl.
Calcul a/c
perform.
print
t = t + Δt
IF
end value
of time is
reached
NO
yes
STOP

OPTIMUM CONTROL SYSTEM CONFIGURATION RESPONSE

We discuss here the design of four types of optimum control systems. They differ according to the formulation of the performance index which reflects directly the performance requirements.

The optimization problem is solved in two steps (Fig. 6, 7) First, we design the control system that is "optimum" for any set of initial conditions. This is done through obtaining the K-parameters described by the set of ordinary differential equations (equ. 1), having the initial conditions specified by the formulation of the performance index*. The second step is to evaluate the aircraft performance when acted upon by the designed control system. In this latter step, the differential equations describing the aircraft dynamics have to be solved.

The desired response signals are obtained from the solution of the equations describing the kinematics of the lead pursuit course (equ. 2).

The following cases are classified according to the form of the performance index chosen for each.

CASE I

Constant weighting of errors in the side slip, roll rate, yaw and yaw rate, rudder and aileron deflections.

The error index is given by :

$$e(t) = \int_t^5 \{ 1000\, \beta^2(\mu) + .256\, \dot{\Phi}^2(\mu) + .71\, [\dot{\chi}(\mu) - \dot{\Psi}(\mu)]^2 + 4000\, [\chi(\mu) - \Psi(\mu)]^2 + \zeta^2(\mu) + 1.78\, \xi^2(\mu) \}\, d\mu$$

with initial conditions

$K_i(T) = K_{ij}(T) = o$, $i = 1,2,\ldots,5$; $j = 1,2,\ldots,5$

CASE II

Constant weighting of the response and control errors with impulse weighting of the yaw error at t=T.

This is almost the same as the previous case, although it emphasizes the importance of terminal yaw angle response. The error index has the form :

$$e(t) = 100\,[\chi(5) - \psi(5)]^2 + \int_t \{ 1000\, \beta^2(\mu) + .256\, \dot{\phi}^2(\mu) + .71\,[\dot{\chi}(\mu) - \dot{\psi}(\mu)]^2 + 4000\,[\chi(\mu) - \psi(\mu)]^2 + \zeta^2(\mu) + 1.78\, \xi^2(\mu) \}\, d\mu$$

The boundary conditions for the K-functions, at t=T=5, are all zeros except :

$K_5(5) = 3.204$, $K_{55}(5) = 100$

* These are given at the final time T, and the solution is thus carried out backwards, i.e. from T up to time t_0.

The following properties of the control system can be deduced :

(1) The optimum control system is linear with respect to the state signal and, consequently, the overall optimum system is linear.

(2) The feedback portion is independent of the desired response and desired control signals (Q's & M's). It depends, only, on the fixed system characteristics.

(3) The feedforward portion is a linear function of the desired signals.

Therefore, once the desired response, and/or control signal, change; only the feedforward gains are to be re-adjusted. This reveals the adaptability of the method to changes in the desired signals. This also resembles exactly the situation of the simple conventional feedback control systems.

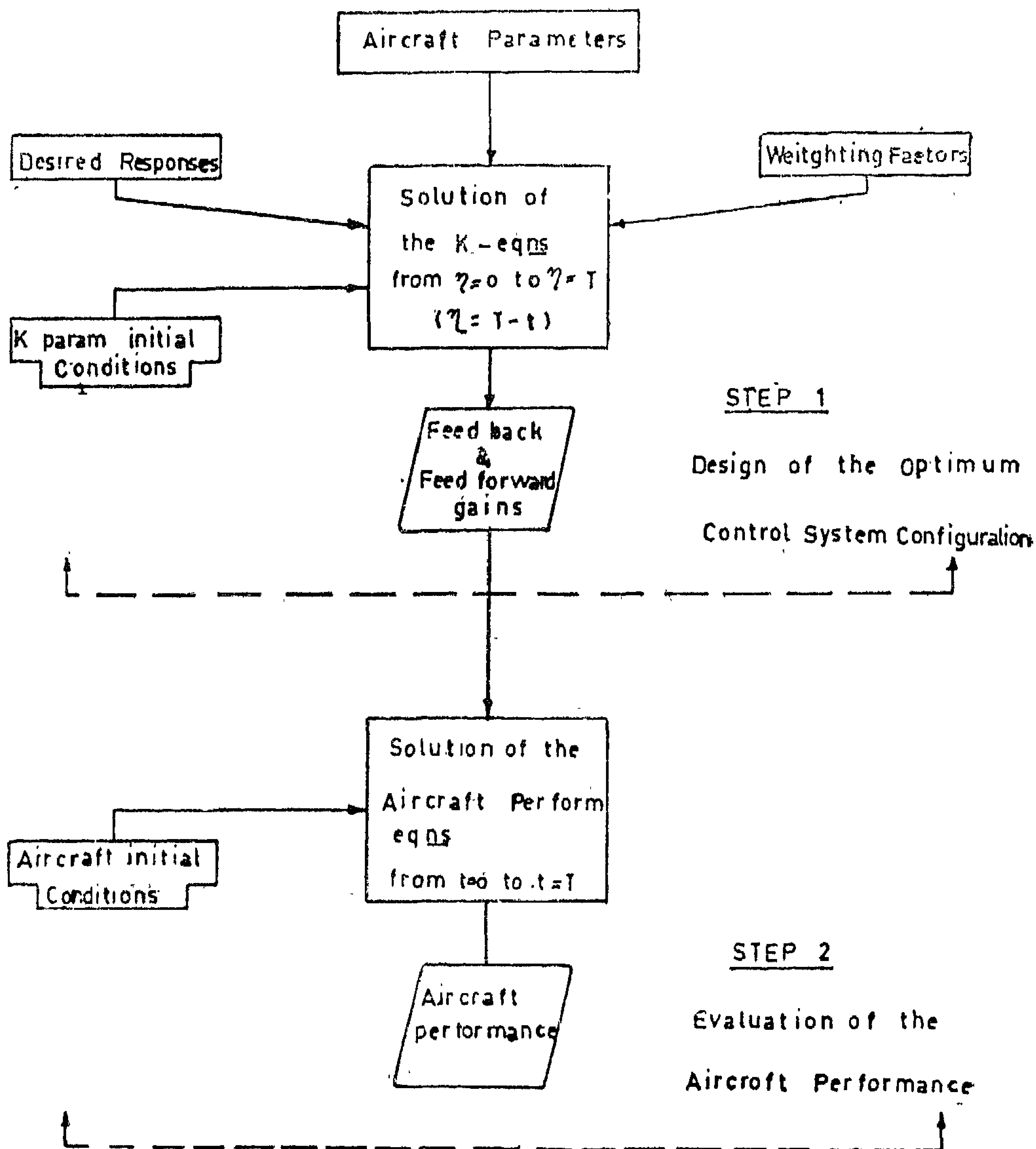


Fig. 6. — Steps of solving the optimization problem.

The boundary conditions for these equations are to be obtained by evaluating the minimum error function at the final time T.

The optimum control signal is (Fig. 5) :

$$m_i^*(t) = M_i(t) + 1/\psi_i(t) \sum_{m=1}^{N} c_{mi}(t) \Big[K_m(t) - \sum_{k=1}^{N} K_{mk}(t)\, x_k(t) \Big] \qquad i = 1, 2, \ldots, M$$

The feed forward gains (reference signals) are* :

$$R_i(t) = M_i(t) + 1/\psi_i \sum_{m=1}^{N} c_{mi}(t)\, K_m(t)$$

and the feedback gains are** :

$$B_{ik}(t) = 1/\psi_i(t) \sum_{m=1}^{N} c_{mi}(t)\, K_{mk}(t) \qquad i = 1, 2, \ldots, M; \; k = 1, 2, \ldots, N$$

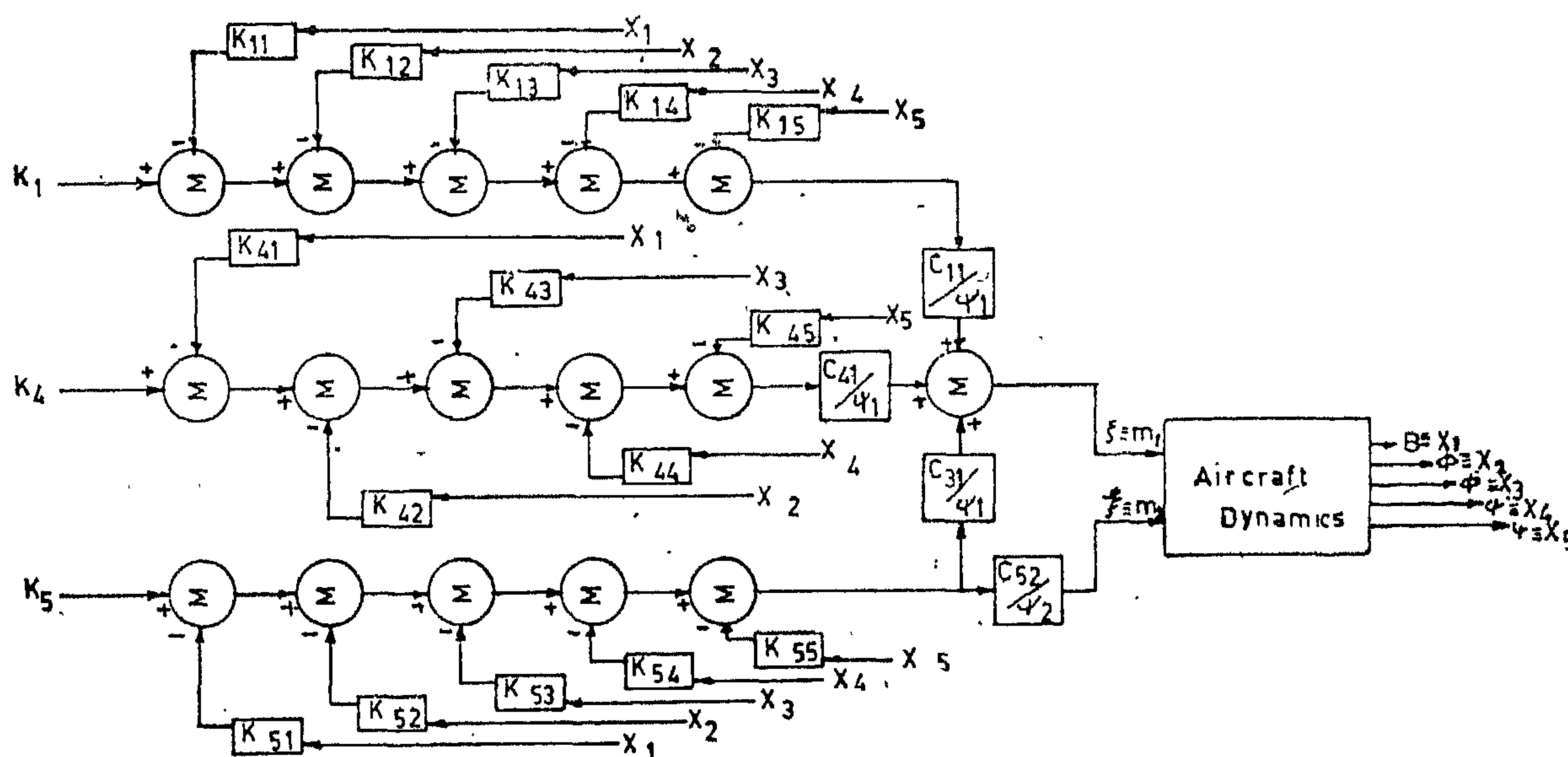


FIG. 5

Input Signals and Feedback Gains of the Optimum Control System

This optimum control equation holds for any initial condition of the state vector. Thus the dynamic programming approach gives the solution for all possible states of the dynamic process. In other words we bypass by this approach the difficulty of specifying the initial conditions of the state vector which results in the two-point-boundary value problem associated with the classical calculus of variation.

** In our case N = Q = 5, M = 2 and T = 5 seconds.

Now, a substitution in equation 3 using equation 4 will lead to :

$$K' - 2\sum_{m=1}^{N} K'_m x_m + \sum_{m=1}^{N}\sum_{k=1}^{N} K_{mk} x_k + \sum_{n=1}^{N} \emptyset_n Q_n^2 - 2\sum_{n=1}^{N} \emptyset_n x_n + \sum_{n=1}^{N} \emptyset_n x_n^2 + \sum_{n=1}^{M} \psi_n \Big\{ M_n^2 - 2M_n \Big(M_n + 1/\psi_n \sum_{k=1}^{N} c_{kn} K_k - 1/\psi_n \sum_{k=1}^{N}\sum_{m=1}^{N} K_{mk} x_m\Big) + \Big(M_n + 1/\psi_n \sum_{k=1}^{N} c_{kn} K_k - 1/\psi_n \sum_{k=1}^{N}\sum_{m=1}^{N} K_{mk} x_m\Big)^2 \Big\} + \sum_{n=1}^{N}\Big[\sum_{i=1}^{N} b_{ni} x_i + \sum_{i=1}^{M} c_{ni} \Big(M_i + 1/\psi_i \sum_{k=1}^{N} c_{ki} K_k - 1/\psi_i \sum_{k=1}^{N}\sum_{m=1}^{N} K_{mk} x_n\Big)\Big] = 0 \quad \text{------(5)}$$

where: $K' = dK/d\mu$

Collecting terms together, the above equation can be put in the form :

$$(K' + F) - 2\sum_{m=1}^{N}(K'_m + F_m)\, x_m + \sum_{m=1}^{N}(K'_{mm} + F_{mm})\, x_m^2 + 2\sum_{m=1}^{N}\sum_{k=1}^{m-1}(K'_{mk} + \tfrac{1}{2} F_{mk} + \tfrac{1}{2} F_{km})\, x_m x_k = 0 \quad \text{--------(6)}$$

where : F's are functions of the fixed element characteristics a,b, c-coefficients, the weighting functions of the errors, the desired response signals, but do not depend upon the components of the state vector.

Now, since the conditions for minimum error, as expressed by equation 6, must hold for all possible value of the state vector components, therefore, each bracketed term appearing in the equation must vanish independently. Equating each assigned term to zero and substituting the F-function, we obtain the set of ordinary differential equations defining the K-parameters as*:

$$-K'(\mu) = \sum_{n=1}^{Q}(\emptyset_n Q_n^2) - \sum_{n=1}^{M}\Big[2M_n \sum_{i=1}^{N} c_{in} K_i + \sum_{i=1}^{N}\sum_{j=1}^{N}(c_{jn}\, c_{in}/\psi_n\, K_i K_j)\Big]$$

$$-K'_m(\mu) = \emptyset_m Q_m + \sum_{n=1}^{M}(b_{nm} K_n) - \sum_{n=1}^{M}\Big\{M_n \sum_{i=1}^{N}(c_{ni} K_{im}) + \sum_{i=1}^{N}\sum_{j=1}^{N}(c_{jn}\, c_{in}/\psi_n\, K_i K_{jm})\Big]$$

$$-K'_{mk}(\mu) = f + \sum_{n=1}^{N}(b_{nm} K_{nk} + b_{nk} K_{nm}) - \sum_{n=1}^{M}\Big[\sum_{i=1}^{N}\sum_{j=1}^{N}(c_{jn}\, c_{in}/\psi_n\, K_{im} K_{jk})\Big] \quad \text{-----(7)}$$

$k = 1,2,\ldots,M \;;\; M = 1,2,\ldots,N$

where:

$$f = \begin{cases} 0 & \text{for } m \neq k \\ \emptyset_m & \text{for } m = k \end{cases}$$

* These equations differ slightly from that derived by Merriam (1). Certain mistakes occur in his work and comparison of our derived equations and his reveals these mistakes.

The performance index is therefore, the integration of the performance measure during the time-to-go period, i.e. from the present time "t" to the final time "T", or :

$$e(t) = \int_{t}^{t} em(\mu)\, d\mu$$

DYNAMIC PROGRAMMING AND THE PARAMETRIC EXPANSION METHOD

Applying the dynamic programming technique to the case of minimizing the error index of the N-order dynamic process described above, we arrive, finally, to the dynamic programming condition[1] as :

$$\partial E[\vec{x}(\mu), \mu]/\partial\mu + \sum_{n=1}^{N}[\phi_n(\mu) - q_n(\mu)]^2 + \sum_{n=1}\psi_n[M_n(\mu) - m_n^*(\mu)]^2 + \sum_{n=1}^{N}\sum_{m=1}^{N}(b_{nm}x_m + c_{nm}m_n^*(\mu))\,\partial E\,\vec{x}(\mu)/\partial x_n(\mu) = 0 \qquad \text{------(3)}$$

where: $E[\vec{x}(t), t] = \min_{m(\mu)} \int_{t}^{T} e_m[\vec{x}(\mu), \vec{u}(\mu), \mu]\, d\mu$

and $m^*(\mu)$ is the optimum control signal:

$$m_i^*(\mu) = M_i(\mu) - \tfrac{1}{2}\psi_i(\mu)\sum_{n=1}^{N}c_{ni}(\mu)\,\partial E[\vec{x}(\mu), \mu]/\partial x_n(\mu)$$

To solve the above equation (3) for the optimum control signals, m_i^*, Merriam introduced the parametric expansion method. The procedure includes four main steps :

(a) The mathematical form of the solution of the minimum error function, E, is assumed.

(b) This postulated solution is substituted in equation 3.

(c) The assumed solution is shown to be, in fact, the solution under certain mathematical conditions.

(d) These mathematical conditions uniquely specify the optimum control equation.

Merriam showed that for a linear dynamic process and quadratic error measure, the minimum error function is quadratic with respact to the state variables, or,*

$$E[\vec{x}, \mu] = K - 2\sum_{m=1}^{N} K_m x_m + \sum_{m=1}^{N}\sum_{k=1}^{N} K_{mk} x_m x_k \qquad (4)$$

where :

$K_{mk} = K_{km}$, for all values of m and k.

Hence, for an N-order dynamic process we have $(1 + 2N + N!/2!\,(N-2)!)$ distinct K-parameters.

* Each letter in the following equations represents a function of time, e.g. K represents K (t).

The weighting functions will thus be in the form ;

$$\phi_1(\mu) = \phi_{11} + \phi_{1,T} \cdot U_0(T-\mu) \;, \quad \phi_2 = 0.0$$

$$\phi_3(\mu) = \phi_{33} \;, \quad \phi_4 = \phi_{44}$$

$$\phi_5(\mu) = \phi_{55} + \phi_{5,T} \cdot U_0(T-\mu) \;, \quad \psi_1 = \psi_{11}$$

$$\psi_2(\mu) = \psi_{22}$$

where: $U_0(T-\mu)$ is an impulse unit area occuring at $\mu = T$.

Since there must be some reasonable maximum allowable response error for each system variable (Fig. 2, 3, 4), and assuming that the maximum allowable response error at any instant of time contributes equally to the error measure, the following values for the weighting functions are obtained[9] as :

$$\psi_1 = 1.0 \;, \quad \psi_2 = 1.73$$

$$\phi_1 = 1000 + 25 \; U_0(T-\mu) \;, \quad \phi_4 = 0.\text{[illegible]}$$

$$\phi_2 = 0.0 \;, \quad \phi_3 = 0.256$$

$$\phi_5 = 4000 + 100 \; U_0(T-\mu)$$

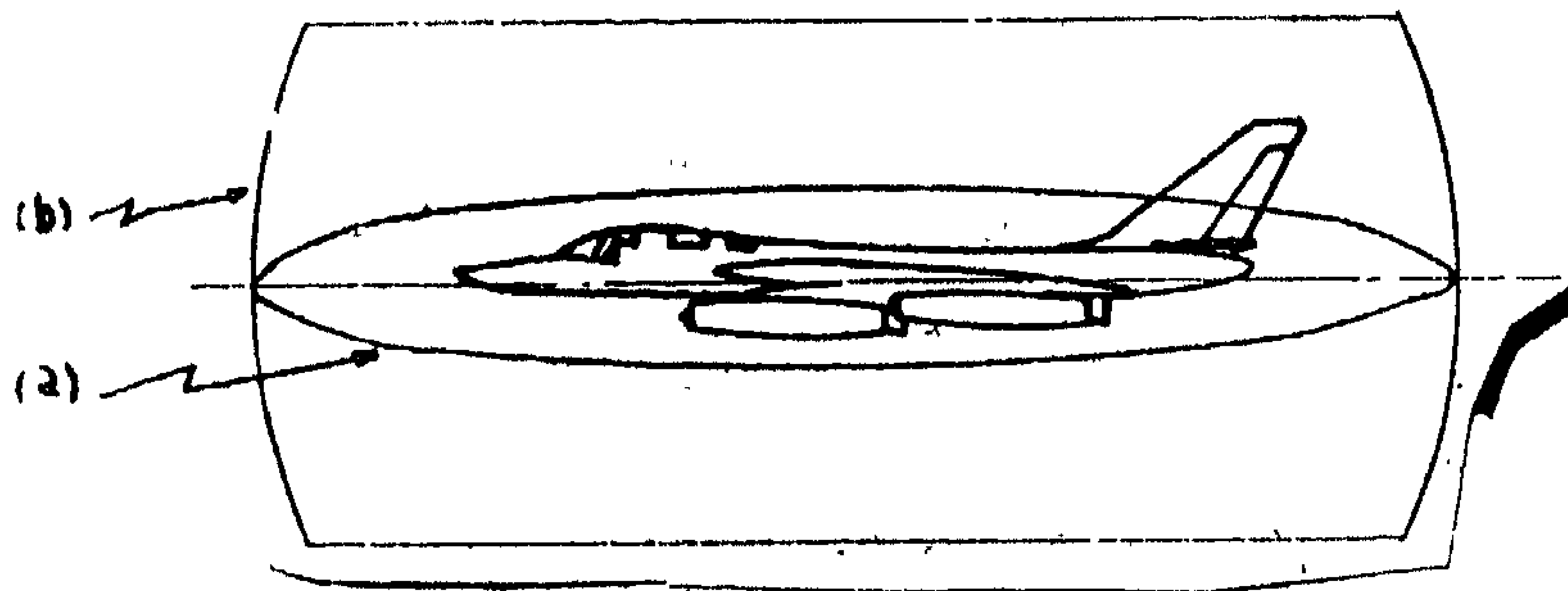


Fig. 2

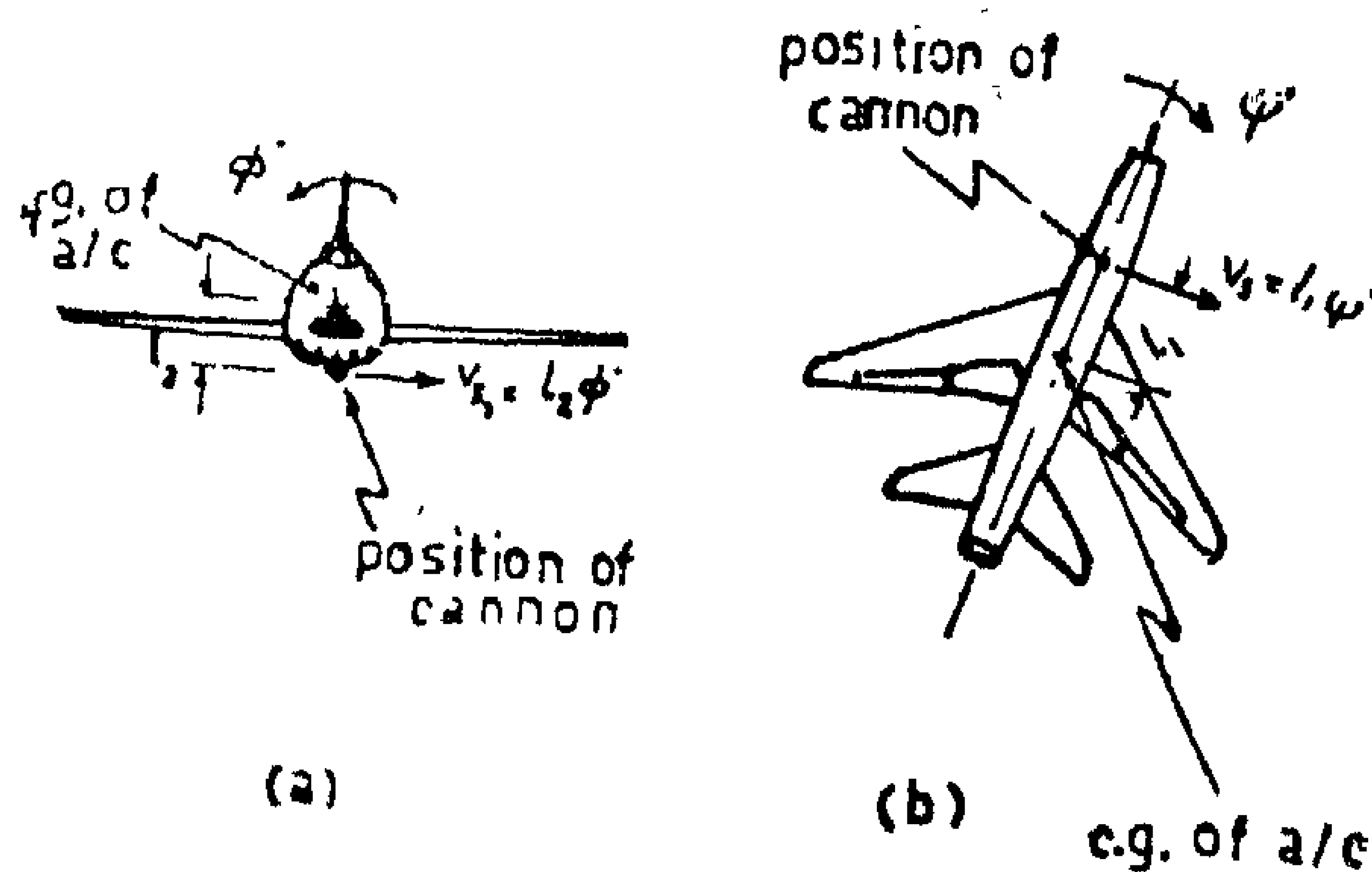


Fig. 3

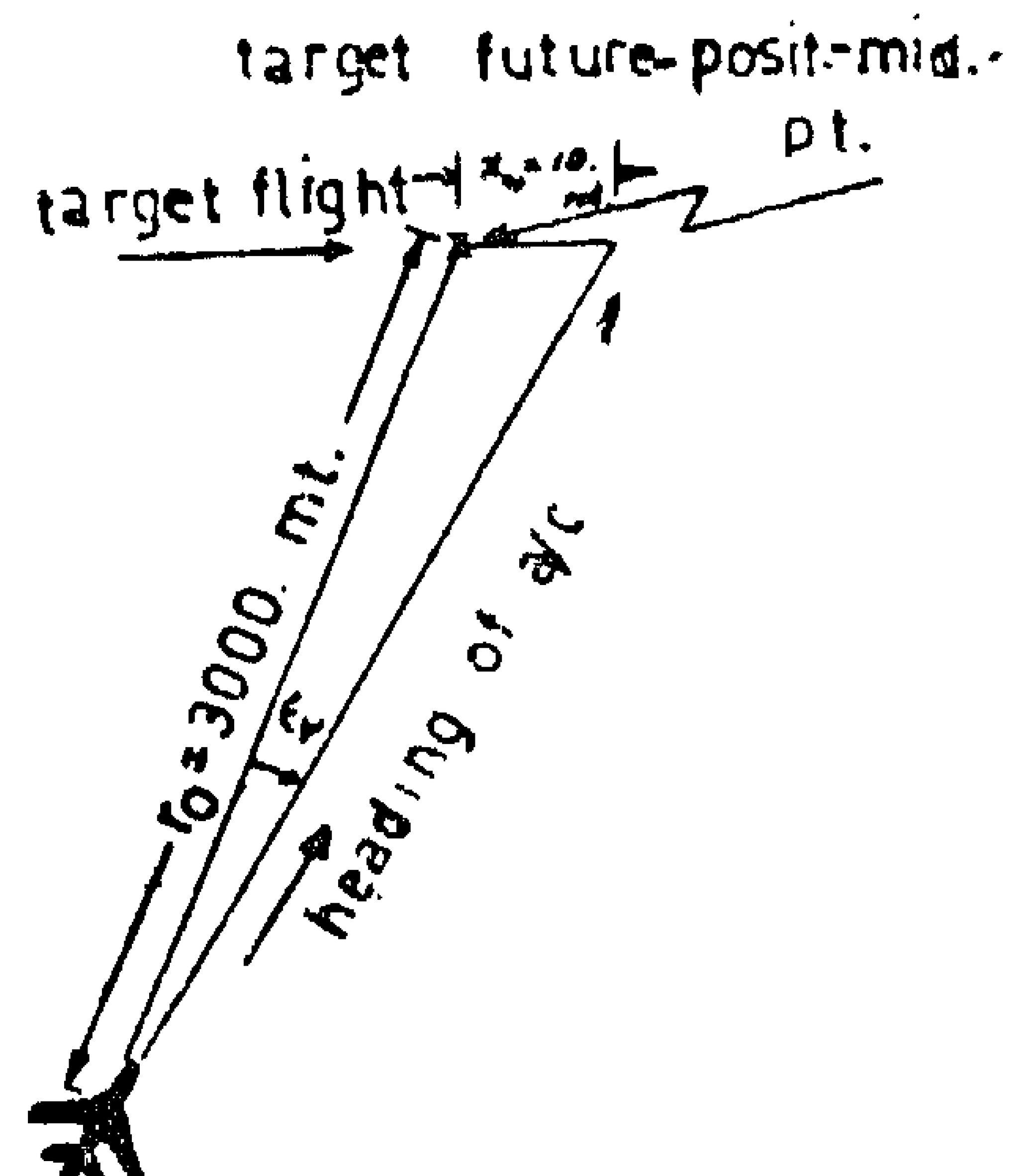


Fig. 4

The portion of this course to be studied begins when the attacking aircraft is at a distance of about 3 kmts. from the target. The automatic control system breaks off at a distance of 2 kmts. This occupies about 5 seconds of the flight.

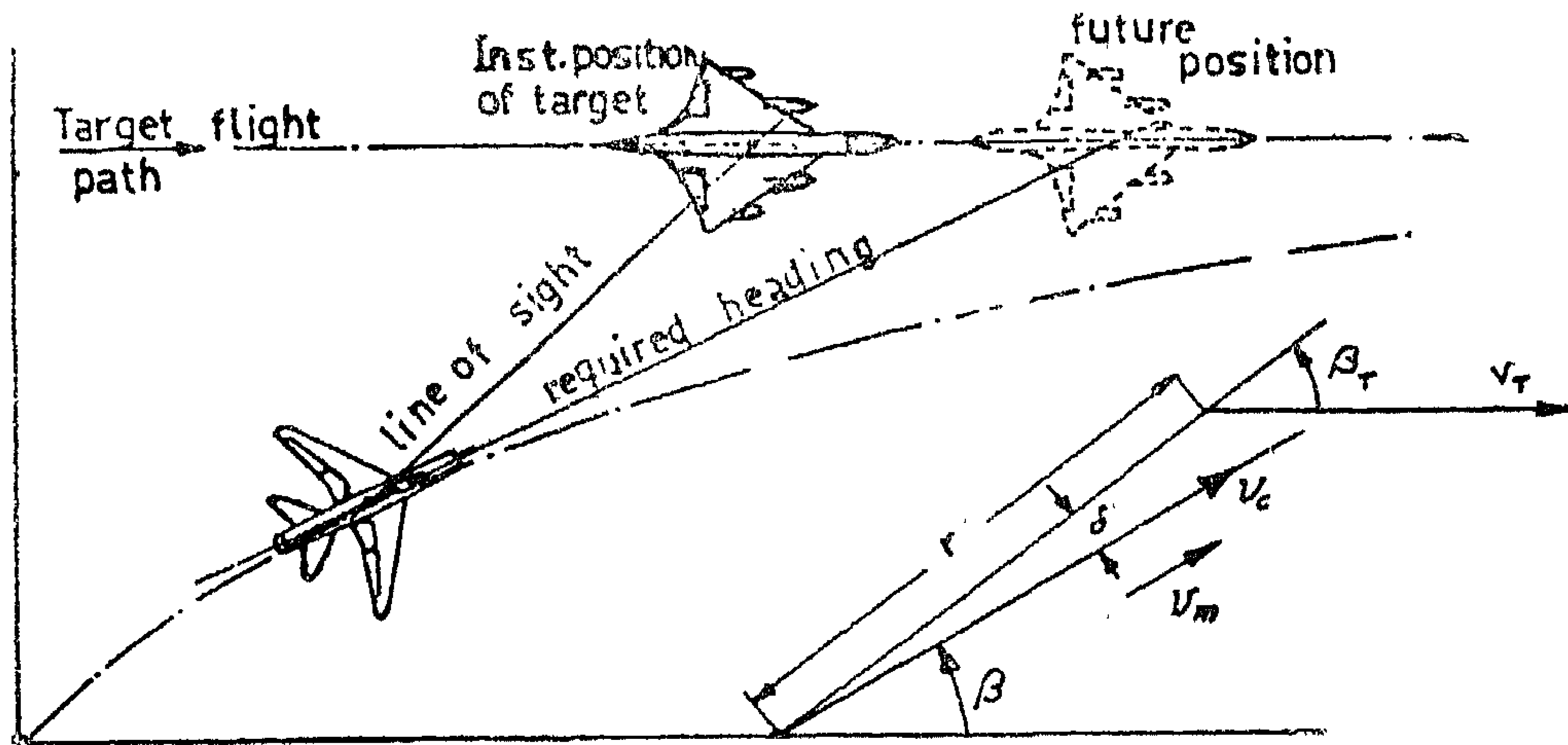


Fig. 1. — Lead-pursuit course configuration.

FORMULATION OF THE PERFORMANCE INDEX

A quadratic error measure is used wherein the primarily important state responses are considered using different weighting functions depending on their relative importance. This error measure is in the form :

$$e_m(t) = \sum_{n=1}^{5} \Phi_n(t)\,[Q(t) - q(t)]^2 + \sum_{n=1}^{2} \Psi_n(t)\,[M(t) - (t)]^2$$

The form of the weighting functions are to be derived directly from the performance requirements. The roll rate and yaw rate deflections are required to be zero throughout the whole flight path. Therefore, their weighting functions are simply taken as constant values. That applies also for the control signals $m_1(t)$, and $m_2(t)$, as well as the yaw and side slip deflections errors. In addition, a more accurate heading and side slip deflections are required at the end of the attacking course. This is similar to the case described by an end boundary condition problem and is accomplished in our problem by adding an impulse weighting function at the end of the path, for each deflection error mentioned. No restriction is made on the roll angle, although it will be indirectly controlled through its time rate. The required (input) signals (Q's and M's) are as follows :

$$Q_1(\mu) = Q_2(\mu) = Q_3(\mu) = \quad (\mu) = M_2(\mu) = 0.0$$

$$Q_4(\mu) = \dot{x}(\mu) \quad \text{and} \quad Q_5(\mu) = x(\mu)$$

where: $x(\mu)$ is the solution of the path kinematics (equ. 2)

FORMULATION OF THE PROBLEM

The linearized equations of motion of an aircraft in the lateral mode under zero disturbances can be explained in the form of a linear state vector equation as follows[6] :

$$dx(t)/dt = B.x(t) + C.m(t) \qquad \text{———(1)}$$

where :

$$x(t) = \begin{bmatrix} \beta \\ \phi' \\ \phi \\ \psi' \\ \psi \end{bmatrix} \qquad , \quad m(t) = \begin{bmatrix} \zeta \\ \xi \end{bmatrix}$$

We will assume that the attacking aircraft has special characteristics that will lead to* :

$$B = \begin{vmatrix} -0.05115 & 0.01942 & 0.0 & -1.0 & 0.0 \\ 0.0 & 0.0 & 1.0 & 0.0 & 0.0 \\ 3.759 & 0.0 & -.6481 & .1587 & 0.0 \\ 3.569 & 0.0 & .01465 & -.1601 & 0.0 \\ 0.0 & 0.0 & 0.0 & 1.0 & 0.0 \end{vmatrix} \quad \& \; C = \begin{vmatrix} .00271 & 0.0 \\ 0.0 & 0.0 \\ 6.7662 & 10.4314 \\ -8.6541 & 0.0 \\ 0.0 & 0.0 \end{vmatrix}$$

and we assume that $q = I.x$, where I is a unit matrix.

The state signals, then will appear, ultimately, as measured variables in the feedback portion of the optimum control system. The yaw and roll angles can be measured by gyros, while rate gyos can be used to measure their time rates.

The optimization problem is to find the optimum control system configuration in the sense of minimizing a performance index during the flight course of a prechosen path.

The control signals generated must lie, of course, within the allowable limits, which correspond to the mechanical limits of the control surfaces.

DESCRIPTION OF THE PATH

Let us choose the lead pursuit course for the attacking aircraft (Fig. 1). The kinematic equations of this path for the case of an outgoing target are[8] :

$$\left.\begin{aligned} dr/dt &= V_t \cos\chi - V_c \cos\delta \\ r.d\chi/dt &= -V_t \sin\chi + V_c \sin\delta \end{aligned}\right\} \quad \ldots\ldots \quad (2)$$

assuming the parameters of the path has the values :

$V_t = 300$ mts/sec , $V_c = 500$ mts/sec

$V_b = 500$ mts/sec , $r_0 = 15$ kmts

$\chi_0 = 30°$

* The model of aircraft specified here is close to the F—100 D jet fighter flying at Mach No. 1-7, at an altitude of 20 kmts [7].

AN APPLICATION OF DYNAMIC PROGRAMMING TO THE DESIGN OF AN AIRCRAFT AUTOMATIC CONTROL SYSTEM

By

M.M. AWNY* and O.A. EL-KHOLY**
B.Sc., M.Sc. *B. Eng. (Hons.), D.I.C., Ph.D.*

ABSTRACT

Parametric expansion concept is introduced to the dynamic programming technique for the design of a programmed autopilot system for an aircraft to accomplish an air-to-air attacking mode. The work follows the procedure suggested by Merriam III[1,2]. The K-equations specifying the control system configuration are derived anew and a digital computer is used to solve them numerically.

A comparison is made between control system configurations for different design concepts as dictated by different formulations for the performance index. Moreover, some conclusions are derived from the results and suggestions for further studies are made.

INTRODUCTION

The importance of optimization is increasing steadily nowadays, and will remain for some time in the future— a field of growing interest to engineers and scientists.

Amongst the various optimization techniques that have been developed in the last decade; the dynamic programming approach has shown great promise, especially when numerical results are to be obtained.

In it, the two point boundary value problem, associated with many other techniques, is bypassed by a flooding technique and the problem is reduced to two one-point boundary value problems.[3,4,5]

When the functional equations, developed applying Bellman's concept of optimality, are obtained in the case of systems described by continuous functions, a set of partial differential equations is ultimately obtained, which —when solved— leads to the optimal control system (optimum decision variables). These equations are, generally speaking, difficult to solve, especially when complex systems are considered. In addition, many difficulties may arise and instability of the solution may occur.

Merriam introduced the method of parametric expansion of the partial differential equations, another set of ordinary differential equations, which could be solved by classical methods.

---

* Development engineer, Egyptian General Aero Organization.

** Professor of Aeronautical Mechanics, University of Cairo.

REFERENCES

1. Fumitake Yoshida, Akio I keda, Shuhei Imakawa, and Yoshiharee Muira, Ind. and Eng. chem., Vol. 52 No. 5, 435, (1960).
2. Schultz, J.S., Gaden, E.L., Jr. Ibid., 48,-2209 (1956).
3. Phillips, D. H., Johnson, M. J., Ind. Eng. Chem. 51,83 (1959).
4. Fumitake Yoshida and kiyomi A Kita, A.I. ch. E. Journal, Vol. 11, No. 1, 9, (1965).
5. Cooper, C. M., Fernstrom, G. A., Miller, S.A., Ibid., 36, 504 (1944).
6. W.J. Braulick, J.R. Fair, and B.J. Lerner, A.I. ch. E. Journal, Vol. 11, No. 1, 73, (1965).
7. American Institute of chemical Engineers, "Tray Efficiencies in Distillation Columus." Fourth Annual Progress Report, pp. 9 and 45, New York (June 30, 1956).

ACKNOWLEDGEMENT

The author having no Dept. of Chem. Eng. at Assiut University is most grateful to Professor M.Z. Hathoot, Head of Mining Eng. Dept; for allowing this work to be carried out in his Dept., and for providing all the necessary facilities.



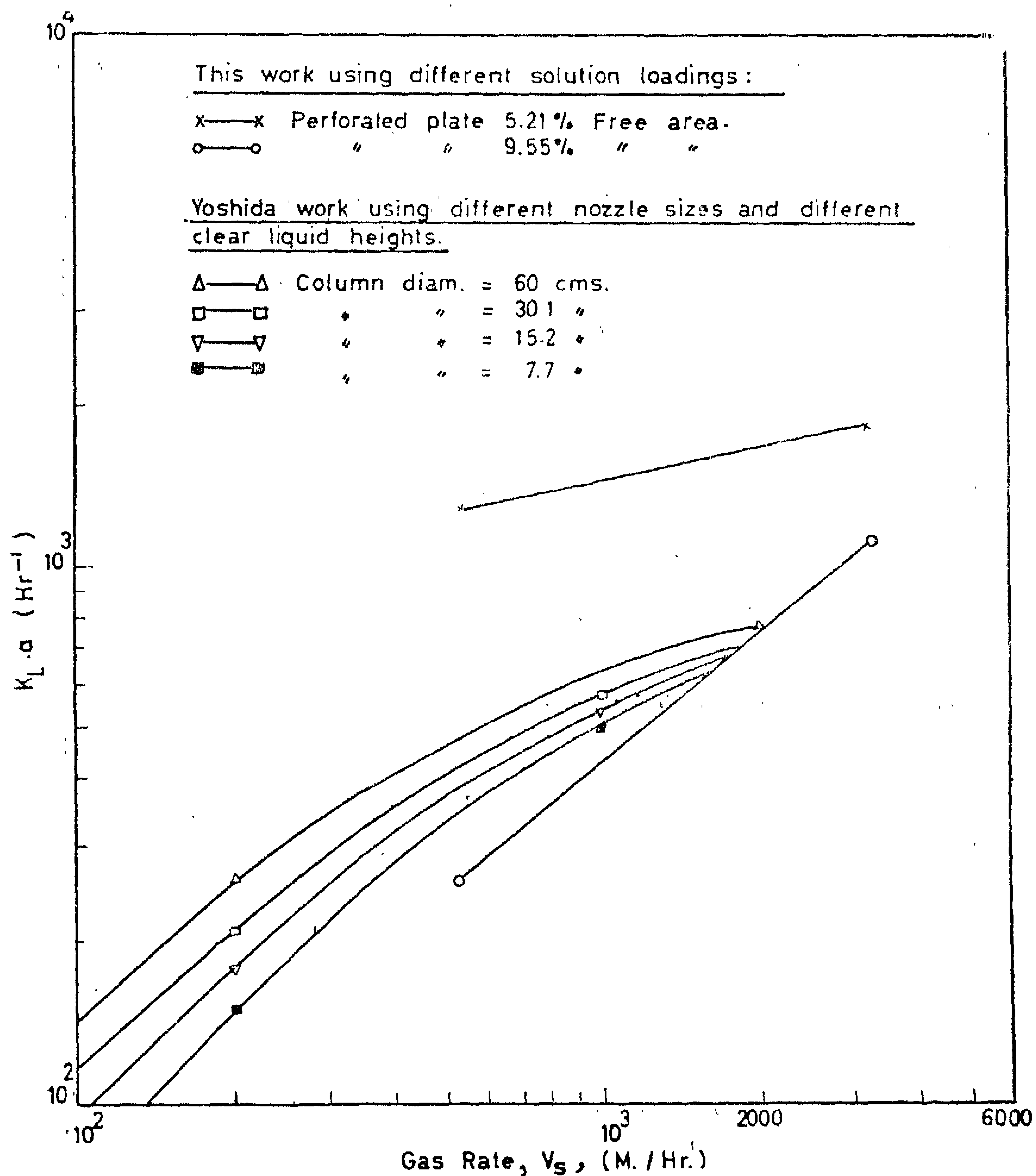


Fig. 8 – Comparison of Mass Transfer at Perforated and Bubble Column.

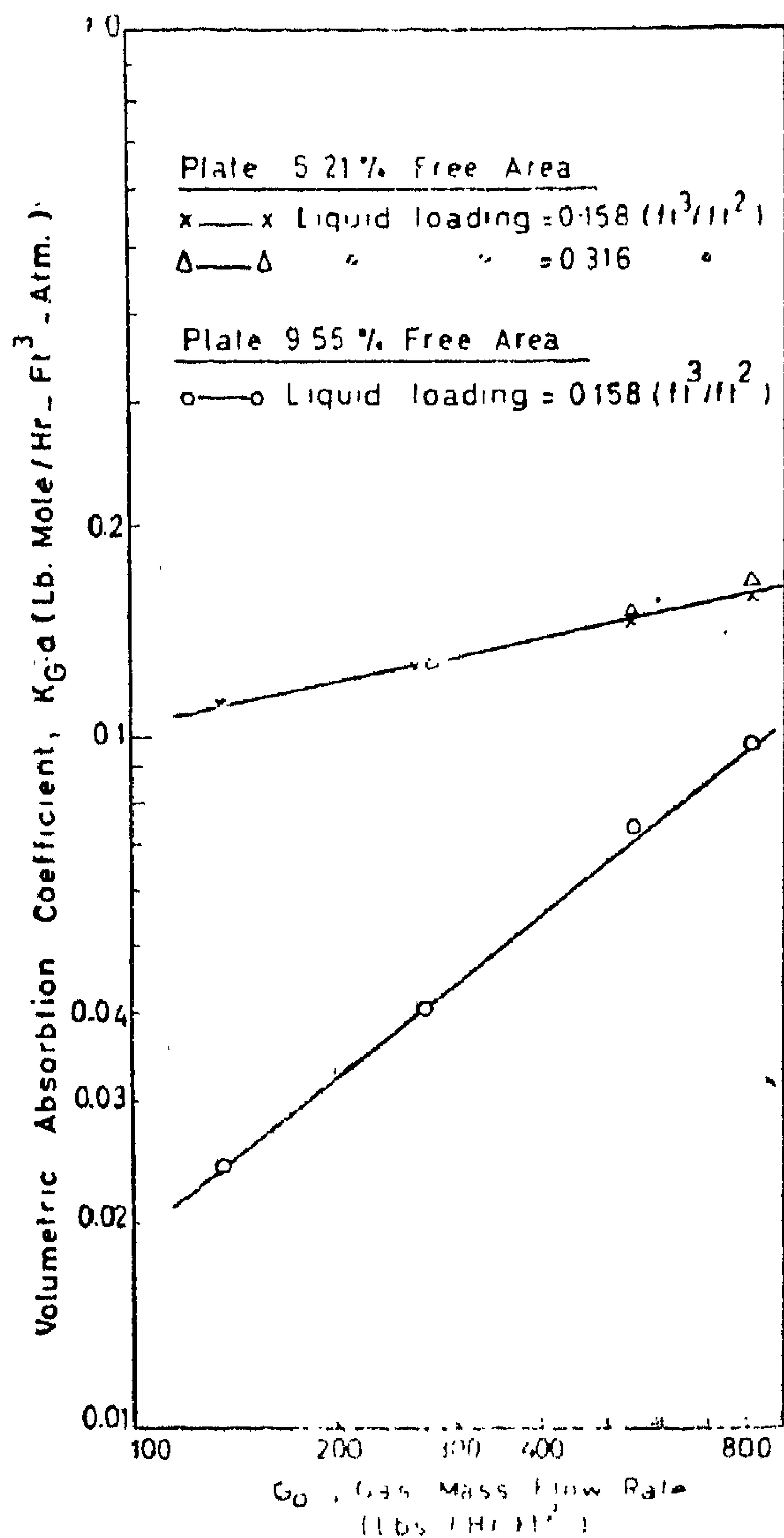


Fig 6 K_G a vs Gas Rate

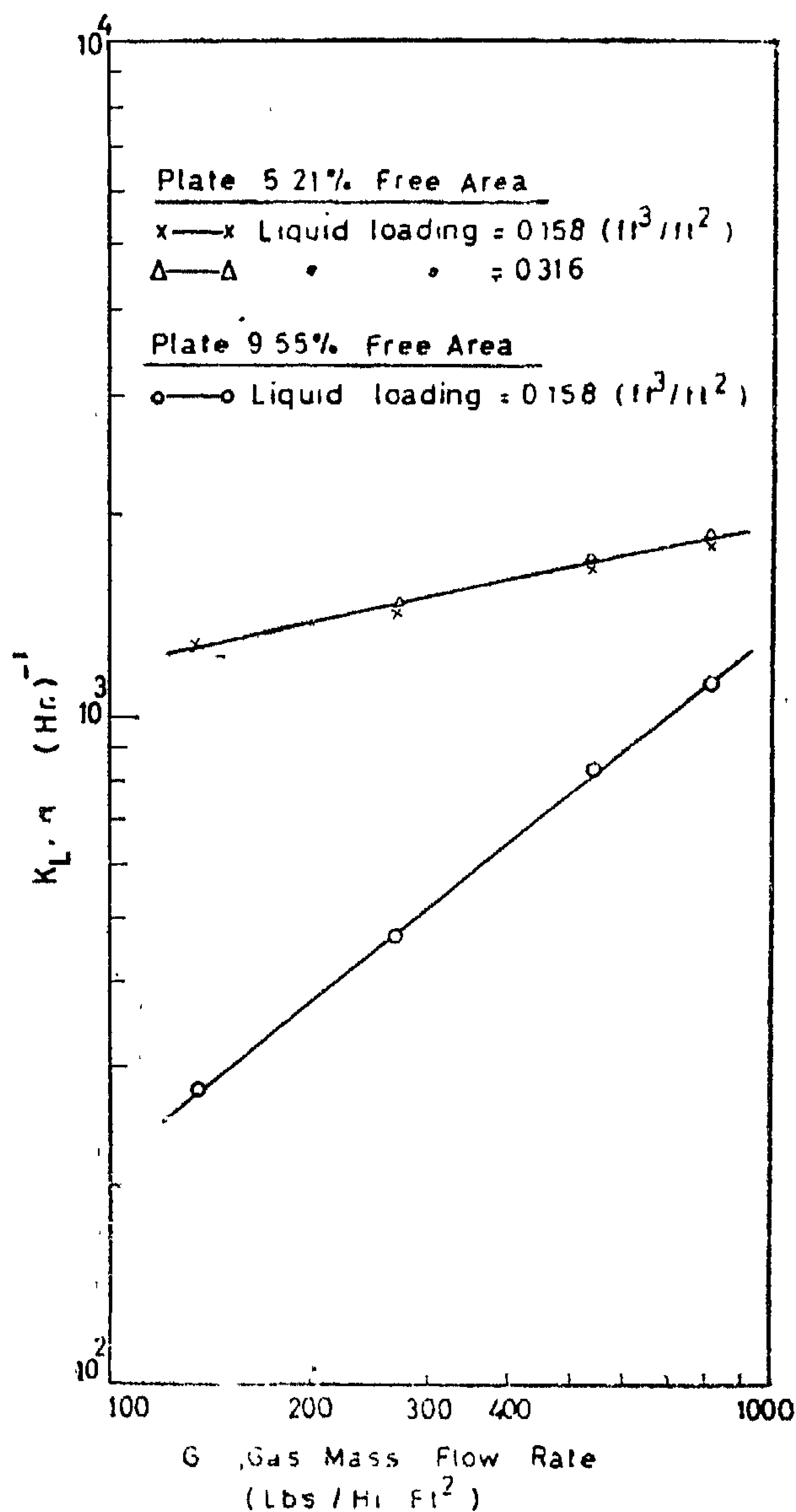


Fig 7. K_L a vs Gas Rate

SYMBOLS USED

Go = superficial gas mass velocity, lb./hr. ft².

H = Henry's law constant atm./mole fraction.

$k_L a$ = Volumetric liquid phase mass transfer coefficient, (Hr^{-1}).

$K_G a$ = Volumetric overall mass transfer coefficient based on gas phase, lb. moles/hr.ft³. atm.

Vs = Superficial gas velocity, (length/ time.)

Θ = Time of gas flow, minutes.

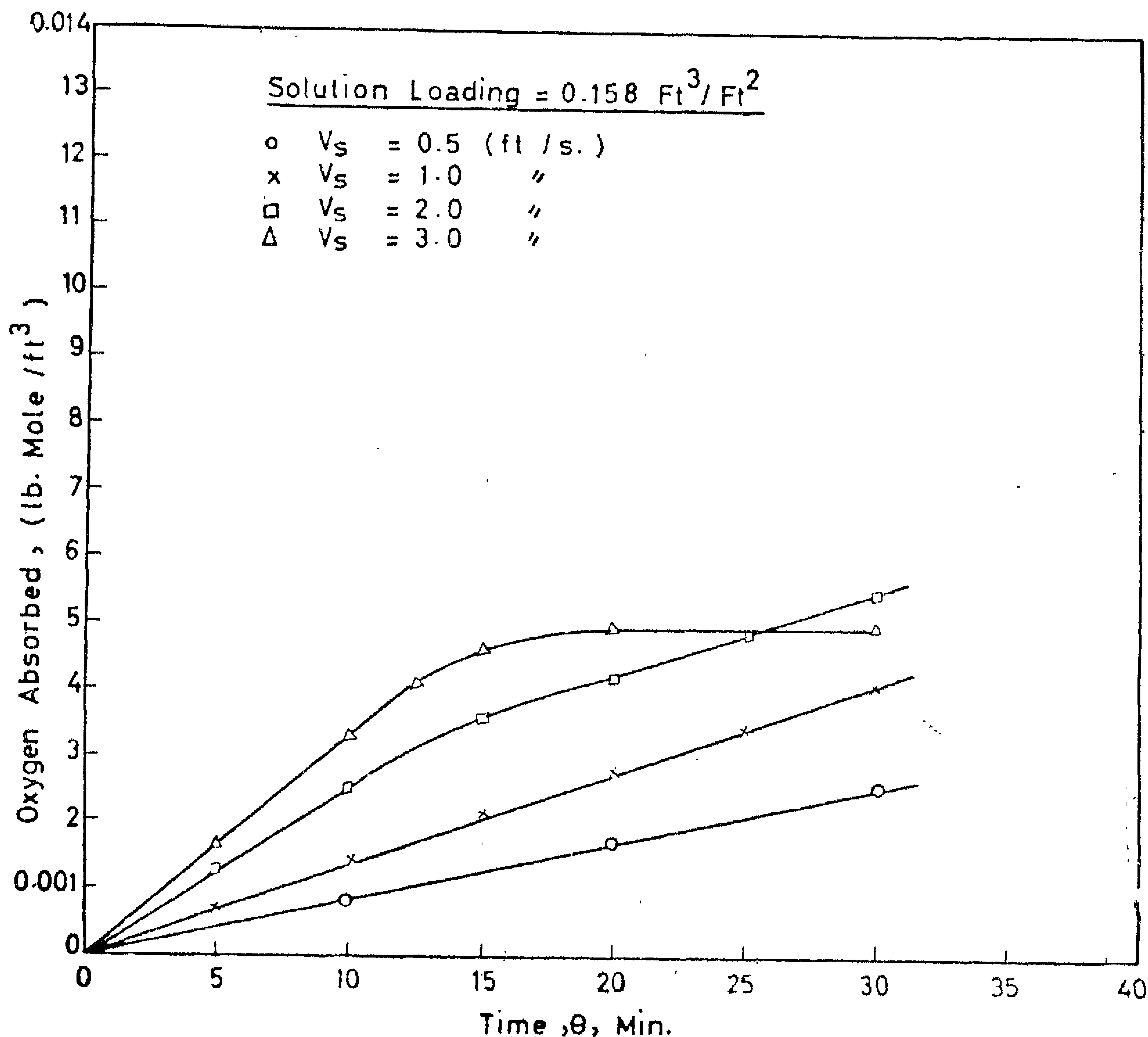
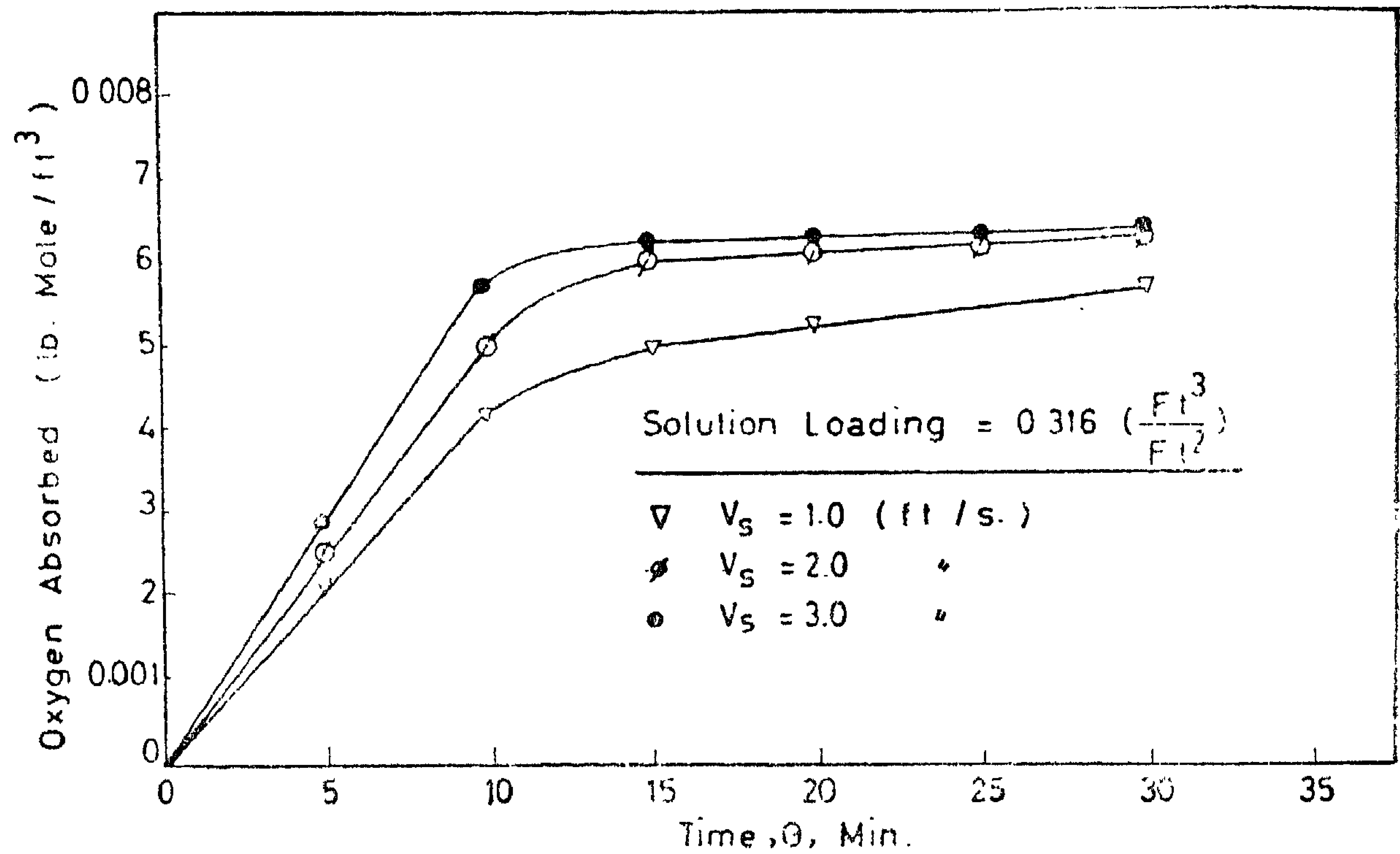


Fig. 5 – Oxygen Absorbed vs Time Plots for Sulfite Oxidation – Plate Having 9 55 % Free Area.

CONCLUSION

Perforated plates having free area of about 5% give higher absorption coefficients than those obtained with other gas-liquid bubble columns operated at the same superficial gas rates. Plates with higher free area can also give higher coefficients if they are operated at gas rates exceeding the critical gas rates required to prevent liquid weeping through the perforations. However, perforated plates with smaller free area give higher coefficient than others of higher free area at the same superficial gas flow rates. The absorption coefficients increase with increasing gas rate at both perforated plates and gas bubble columns and are not affected by the liquid loading or clear liquid height on the plate.



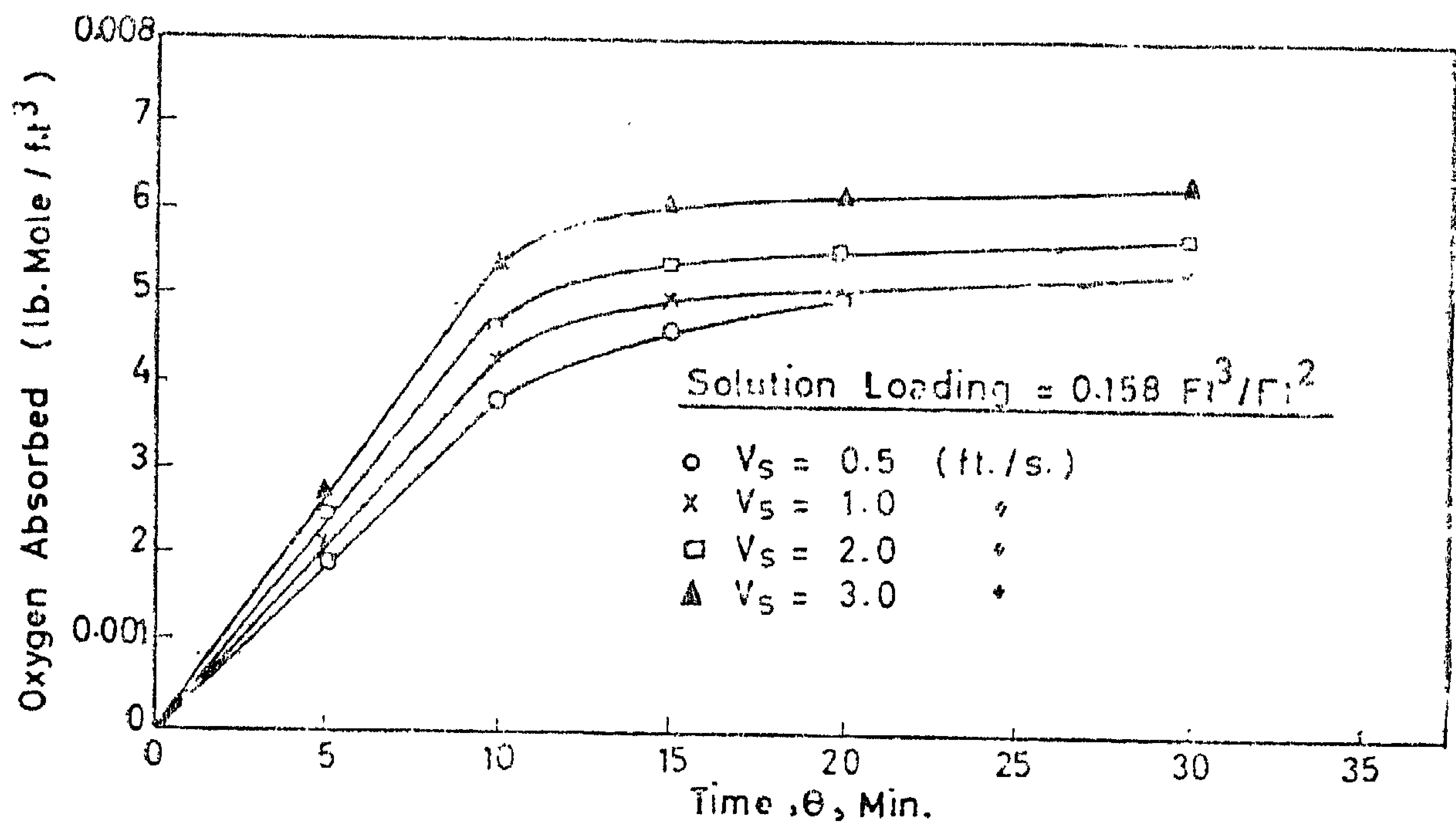


Fig. 4 – Oxygen Absorbed vs. Time Plots for Sulfite Oxidation – Plate 5.21 % Free Area.

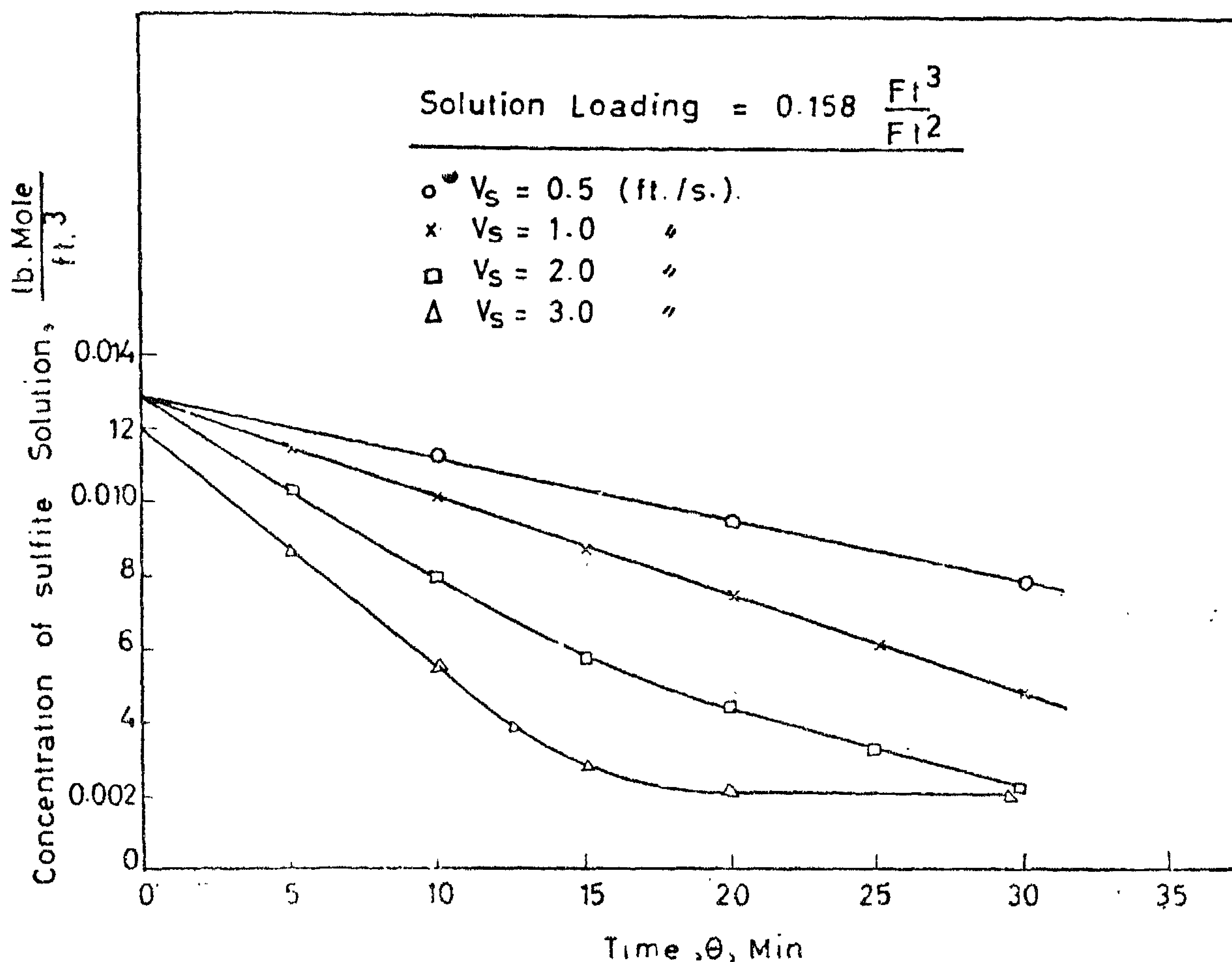


Fig 3_ Concentration vs Time Plots for Sulfite Oxidation (Plate having 9.55 % Free Area)

this figure that the more stable plate gives higher values of $k_L.a$ whereas the other plate having 9.55% free area gives lower values which tend to increase as the gas rate is increased due to the decrease in the weeping rate. Equation (4) represents the relation between $k_L.a.$ and the mass flow rate at the stable perforated plate for solution loadings ranging from 0.158 to 0.316 ft^3/ft^2.

$$k_La = 477.\ Go^{0.198} \qquad (4)$$

Figure (8) compares value of k_La at different gas rates using two different gas liquid contacting devices. It is observed that the coefficient is highest at stable perforated plates. However, plates having high free area of about 10% give higher coefficient of mass transfer than that obtained in gas bubble columns at superficial gas velocites exceeding 2000 meters per hour. (1.83 feet per second). This is explained as result of the liquid weeping from such plates at lower gas rates which tends to decrease and deminish as the gas rate is increased. Figure (8) also illustrates the findings of Yoshida et al (4) that the absorption coefficient is not affected by the clear liquid height which is quite in good agreement with this work.

per and lower curves of Figure (3) shows a slight increase in the amount of oxygen absorbed per unit volume for higher solution loading at superfrial gas velocites of 2 and 3 Ft./S.

Mass transfer rates at the earlier stages of oxidation were then converted into values of an overall volumetric transfer coefficient, $K_G a$, based on an overall driving force over the column. Oxygen back pressure from the solution was assumed to be zero. Figure (6) shows the variation of $K_G.a$ with gas rate at the two different perforated plates. It is seen from these plots that higher absorption coefficients are obtained with the plate having smaller free area. This is explained as a result of weeping of the solution through the perforations at the plate having higher free area whereas the other plate was stable even at the lowest applied gas rate. The weeping causes the uneven distribution of the gas in the liquid phase, and a fraction of the solution which existed over the weeping perforations was by-passed by the flowing gas phase. This resulted in a reduction in the volumetric absorption coefficient especially at lower gas rates at which the amount of weeping was excessive. It is also seen from Figure (6) that the dublication of liquid loading on the plate resulted only in a very small increase in the mass transfer coefficient at higher gas rates exceeding 270 Ibs/hr-ft². Equation (1) represents the relation between the volumetric absorption coefficient and gas mass flow rate for solution loadings ranging from 0.58 to 0.316 ft³/ft² at the stable perforated plate having 5.21% free area.

$$K_G.a = 0.0408\ G_o^{0.198} \qquad (1)$$

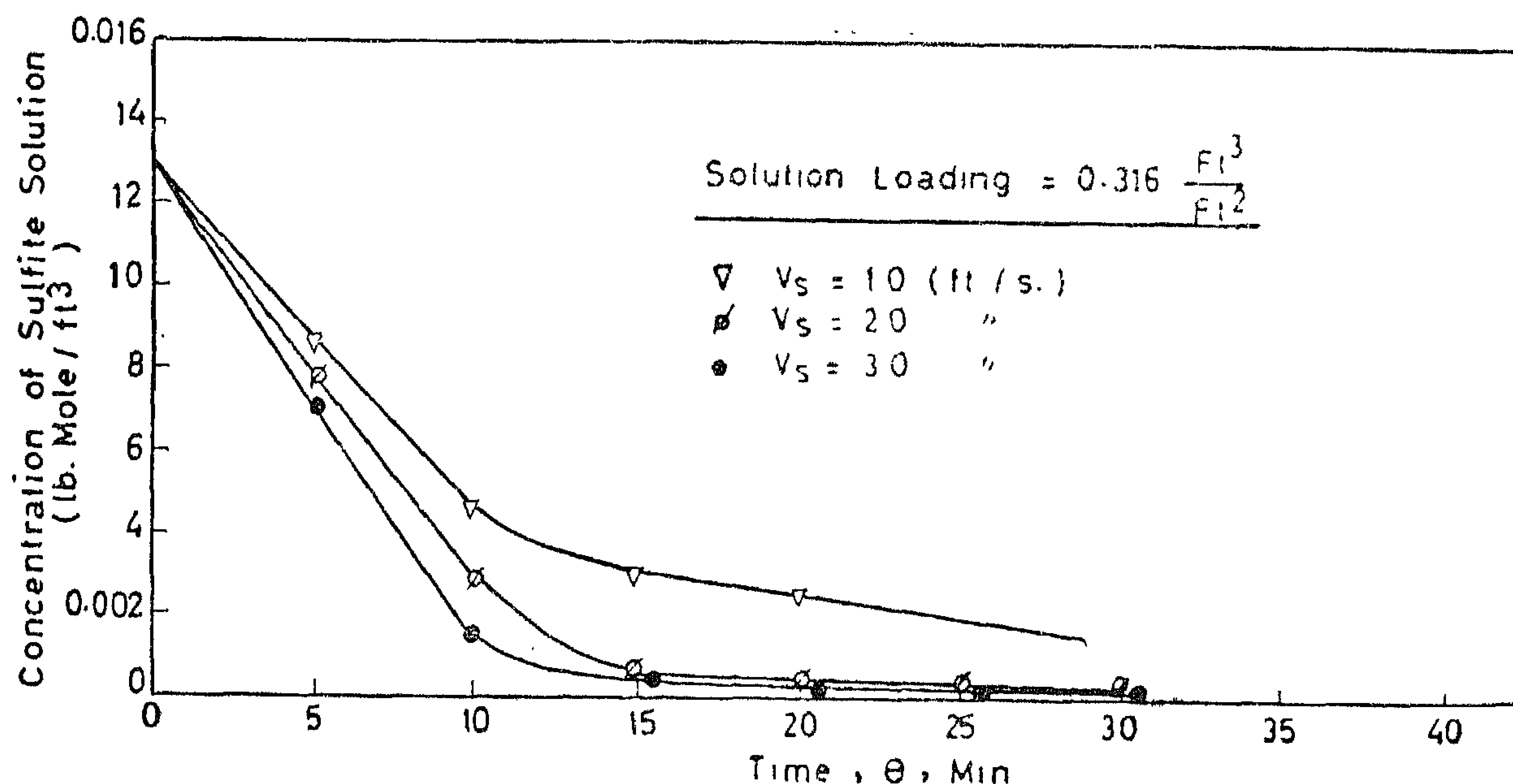
As the solubility of the gas follows Henry's law, the relationship between over-all and mass transfer coefficients is :

$$\frac{1}{K_G\ a} = \frac{1}{k_G\ a} + \frac{H}{k_L.a} \qquad (2)$$

$\frac{1}{k_G a}$ equals zero where the gas film resistance is negligible and we get

$$\frac{1}{K_G a} = \frac{H}{K_L.a} \text{ or } k_L a = H.\ K_G.a \qquad (3)$$

The mass transfer coefficient of liquid phase, $k_L a$, was calculated from equation (3) by subtituting the value of Henry's law constant, H, as 4.01×10^4 atm./mole fraction and values of $K_G.a$ being in Lb-Mole/hr.-lb. Mole.-atm. — Figure (7) shows the relation between $k_L.a$ and gas mass flow rate. It is observed from



contained holes of same diameter at 3/8 in. triangular pitch. The operation was conducted batch by batch with respect to liquid; a measured volume of solution was introduced inside the column in each run. At the end of each run the solution on the plate was collected and analysed by standard iodometric titration methods for the determination of sulfite concentration. The sodium sulfite solution was of an initial concentration of approximately 0.4 N and contained roughly 10^{-3} g-moles of cupric sulfate per liter. Air was fed to the column bottom after being metered by an orifice. The solution weeping through the perforations of the plate having 9.55% free area was returned inside the column during operation.

RESULTS AND DISCUSSION

The quantity directly measured in sulfite oxidation experiments is the decline of sulfite concentration as a function of the time of oxidation. At the earlier stages of air flow, the decline in sulfite concentration was steeper giving higher rates of oxygen obsorption than at later stages. Figure (2) shows plots for two different solution loadings at the plate having 5.21% free area; the solution loading being expressed, in ft^3 of solution per square foot of bubbling area.

It is evident from these plots that the decline in sulfite concentration is more rapid with higher gas flow rates and greater solution loading. Figure (3) represent corresponding plots at the plate having 9.55% free area and indicates the same phenomena of rapid rate of oxidation with increasing gas rate. The decline in sulfite concentration was converted into the amount of oxygen absorbed per unit volume of solution. Figures 4 and 5 illustrate the variation of the amount of oxygen absorbed with time of oxidation at the two different plates. It its clear from these plots that the amount of oxygen absorbed increases with the increase of the gas rate. Comparing the up-

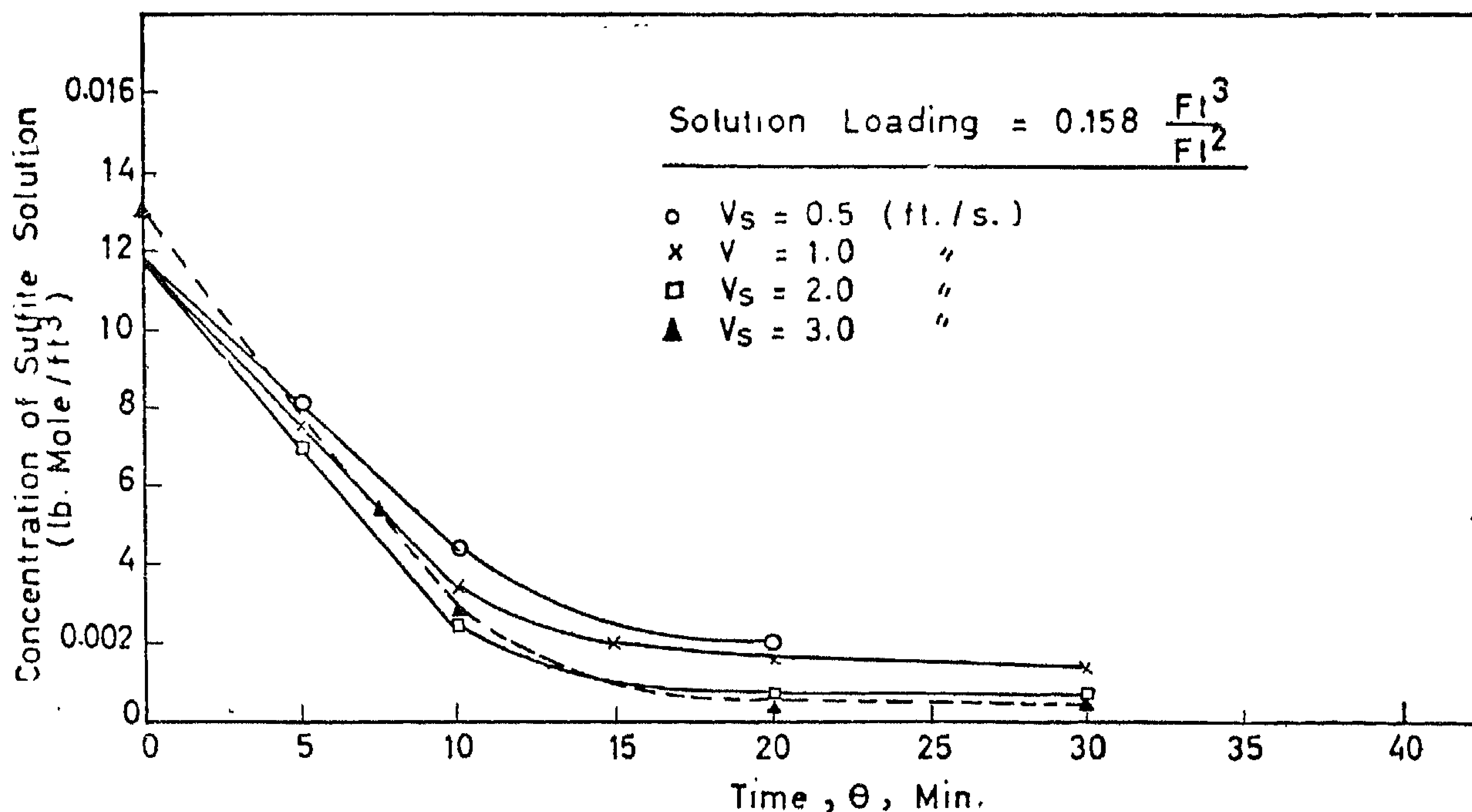


Fig. 2 – Concentration vs. Time Plots for Sulfite Oxidation (Plate Having 5.21 % Free Area).

on partial pressure differences, K_G. a, for air and pure oxygen which indicates that the gas film resistance is negligible. Braulick et al (6) studied mass transfer rates in a sparged contactor applying the air oxidation of aqueous sodium sulfite solutions, they found that mass transfer rates increase with gas rate and with submergence/diameter ratio. They compared the volumetric absorption coefficients obtained in their work with those given by the American Institute of Chemical Engineers (7) using bubble cap dispersers for oxygen desorption. The comparison showed mass transfer charachteristics of the gas sparged bubble column equivalent to those of stirred vessels.

It is intended by this work to study mass transfer rates using aqueous sulfite solutions at perforated plates and compare the performance of such plates with other gas-liquid contacting devices.

EXPERIMENTAL

The absorption studies were conducted in a 3-in. diameter copper pipe section, 1.5 ft. high. A perforated plate was fitted at the bottom of the column and the top was provided during operation with an entrainment shield. Figure (1) shows a schematic diagram of the apparatus. Two perforated plates were used having free areas of 5.21% and 9.55%. The first contained 1/8 in diameter holes at 4/8 in. triangular pitch, whereas the second

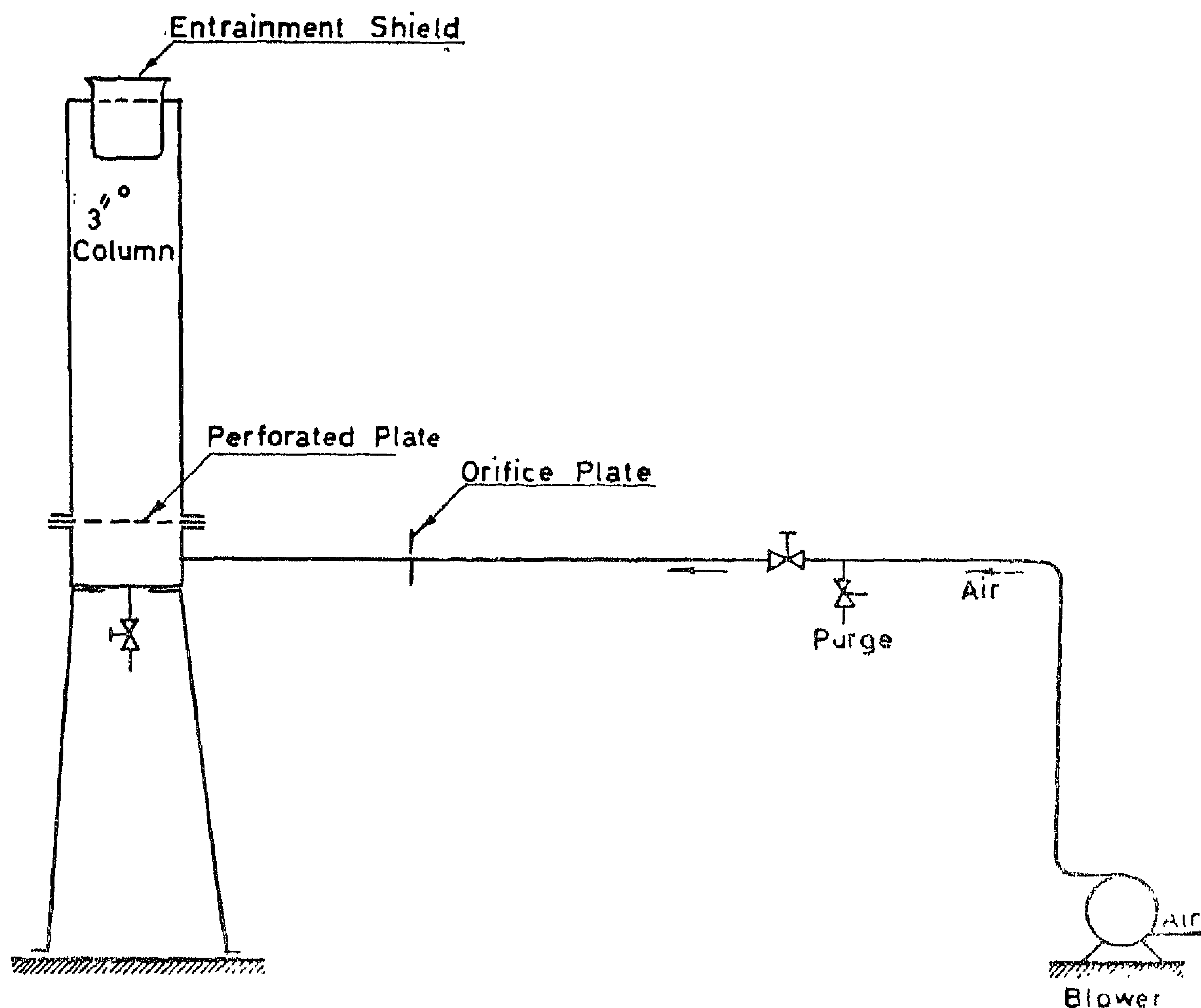


Fig 1_ Schematic Diagram of The Apparatus

OXIDATION OF SODIUM SULFITE AT PERFORATED PLATES

By

Dr. CHALABI, M.F., Ph.D.*
Chemical Engineering

ABSTRACT

Mass transfer rates and coefficients were determined experimentally at perforated plates of different free area in a 3 inches diameter column. Aqueous solutions of sodium sulfite were used as the liquid phase and air was used to provide oxygen for the oxidation. The operation was conducted batch by batch with respect to solution, the loading of solution varied from 0.158 to 0.316 ft^3 per ft^2 of bubbling area. Superficial gas rates varied from 135 to 810 Lbs/hr—ft^2. The rate of oxygen absorption was found to increase with the increase of the gas rate, increase of solution loading, and decrease of the plate free area. Mass transfer coefficients are presented to illustrate the effect of the different variables.

INTRODUCTION

Many investigations concerning the study of the rate of oxygen absorption by the sulfite oxidation method had been reported in literature. Yoshida et al (1) tested the rate of oxygen absorption in stirred gas — liquid contactors which are used for both submerged aerobic fermentation and chemical reactions. They reported higher values of K_La in case of sulfite solutions than in case of pure water for the same agitator speed and attributed this to the reduction in the size of bubbles in the electrolytic solution. At high agitator speeds, much smaller bubbles were formed in sulfite solutions than in pure water and this was explained by the electrostatic potential of the resultant ions at the liquid surface. They reported that in case of bubbling without mechanical agitation for water and solutions of both sodium sulfite and sulfate bubble sizes were the same and K_La values were nearly identical at the same gas rates. Schultz et al (2) showed that the value of K_L for sulfite oxidation decreases slighthy with increasing agitator speed, where as Phillips et al (3) reported that the rate of oxidation is independent of agitator speed and proportional to the 1.5 power of the partial oxygen pressure. Yoshida (1) explained the above mentioned disagreement as due to the differences in experimental equipment and mechanical agitation.

Yoshida et al (4) studied the effect of catalyst concentrations ranging from 10^{-5} to 10^{-3} g-moles cupric sulfate per liter of sulfite solution. Their results show that K_La values are neither affected by the catalyst concentration nor by nozzle diameter; where as the coefficient was found to increase with the increase of the gas rate, increase of the solution temperature, and increase in column diameter. Cooper et al (5) reported that oxidation rate is independent of sulfite concentration from 0.35 to I N.

Yoshida et al (1) reported same values of the over-all mass transfer coefficient based

* Dr. Mohamed Fikri Abdel-Aziz Chalabi, Assistant Professor, Chemical Engineering Dept., Cairo University.

plane. The stem is then rotated until the pressure manometer connected to the holes indicate the same reading. In this position, the velocity vector component V lies in the vertical plane that passes through the midway of the two holes. To find the magnitude of the velocity vector component V, the stem is to be rotated through an angle 50°.

In this second position the velocity vector is directly opposite to one of the two holes. Fig. 16. The manometric head of this hole would give the velocity head $\frac{V^2}{2g}$ and the velocity can be obtained from the reading of the manometer hm (s.g. — 1.00).

Scope of application

The previous mentioned analysis can be used for the following ;

1. It gives accurate hydraulic calculations to get the discharge over the different shapes of tail escapes used.
2. In new reclamed lands, small regulating structures, which feed small arable plots from secondary canals are used. In this case the curved weir structures provide the most suitable type for accurate water distribution for the following reasons ;
   a) They take into consideration the effect of the angle of entry of water, thus changing this angle will change the discharge entering without varying the design head.
   b) They provide sufficient crest length which suite the site conditions.

It is hoped that the derived equations together with the curves obtained for design purposes can be used in the field work to have more points and to check the validity of the work for full size structures.

REFERENCES

dallah, M. S., Abou-Seida, M. M., and liman, M.A., "Three-dimensional curvilear flow over curved escapes". Bulletin of the faculty of Engineering, Cairo University, 1970.

2. Fred W. Blausdell. "Equation of free faling nappe". Proc., A.S.C.E., Vol. 80, Aug. 1954.
3. Khafagi, A., and Hammad, S.Z., "The curvilinear flow in open channels"., Bulletin of the faculty of engineering, Cairo University, 1956.

hafagi, A. and Abdallah, M.S., "The use f scale models for short water structures with free surface". Bulletin of the faculty of engineering, Cairo University, 1960.

5. Khafagi, A., Abdallah, M.S., and Soliman, M.A. "Flow over curved escapes". Bulletin of the faculty of engineering, Cairo University, 1967.
6. Khafagi, A., Abdallah, M.S. and Lucman, A.M., "Curvilinear flow in some water structures". Bulletin of the faculty of Eng., Cairo Univ., 1968.
7. Wagner, W.R. "Determination of pressure controlled Profiles". Trans. A.S.C.E., Vol. 121, 1956.

end of the gauge and at an angle 122° at a distance 30.50 cm. The whole length of the bar was covered by a plastic tube for isolation except for the end which was left uncovered. The other negative end of the gauge was removed and replaced by a loose weir as shown in Fig. 15.

2. Measurement of velocities and directions of stream planes :

As it is required to measure the horizontal component of the velocity vector V, a pitot cylinder was used as shown in Fig. 16. The pitot cylinder has two brass tubes a and b enclosed in a casing stem. A Each tube has a small brass tapping at the top end to permit a rubber tubing connection with a pressure U — tube manometer. At the other end of the cylinder, the two tubes terminate in certain holes in the sheel of the cylinder which thus contains two holes. The two holes lie on a horizontal circle including a central angle of of 100°. A circular disks B and C are mounted on the stem A. The disk B is graduated in degrees and disk C is fixed to the stem A and contains a pointer showing the angular position of the zero line midway between the two holes. The stem A passes through a hole in in disk B so that when the disk is fixed in a certain position and the stem is rotated, the angle of deviation in degrees can be readily obtained. A special manometric fluid of specific gravity 1.25 was used in the manometer. An air pump connected to the top end of the pressure manometer is used to get out the air from the manometer tubes. To get the direction of the velocity vector, the instrument is to be held with its axis parallel to the x—z plane, this makes the two holes in a horizontal

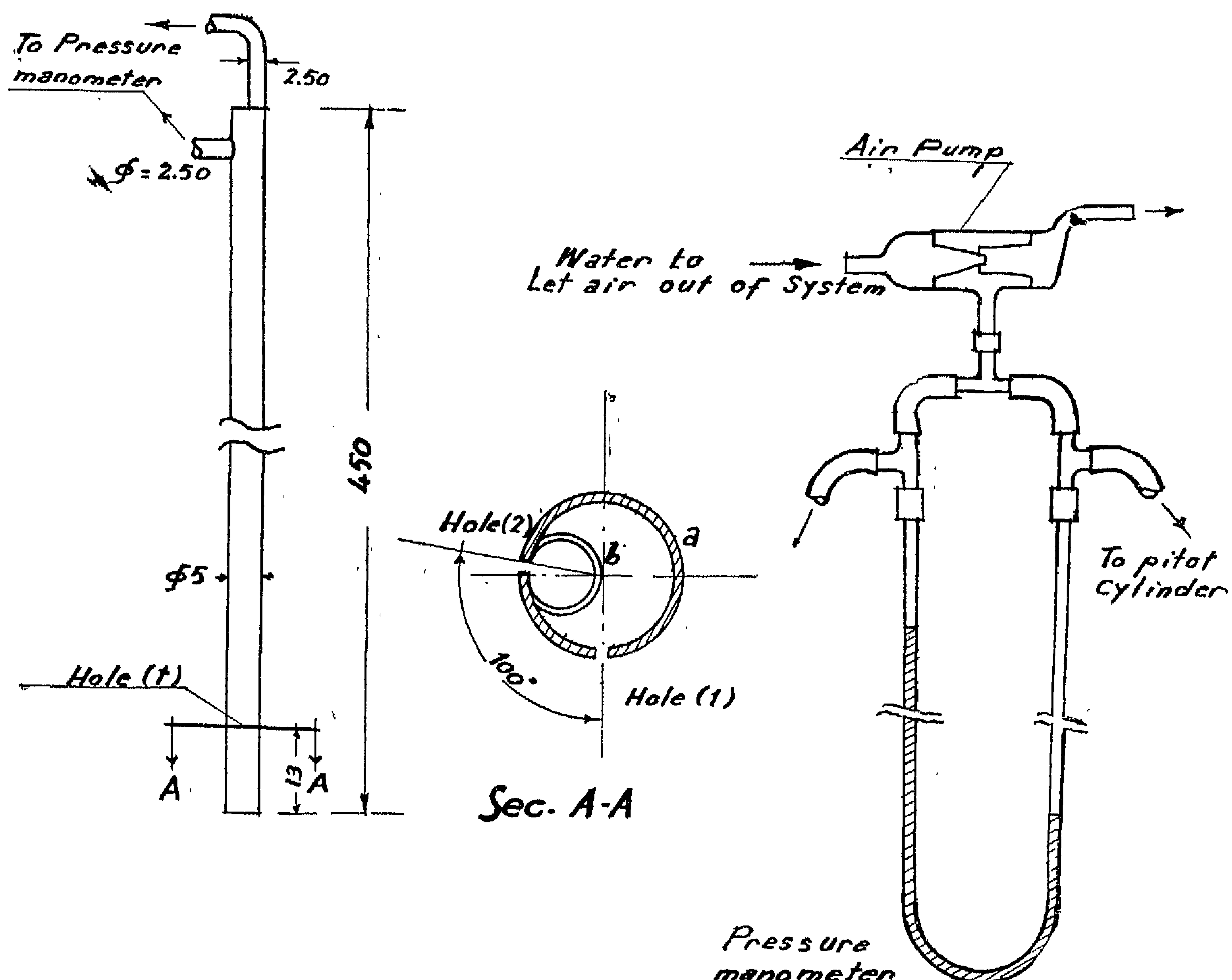


Fig. 16. — Pitat cylinder and the pressure gauge.

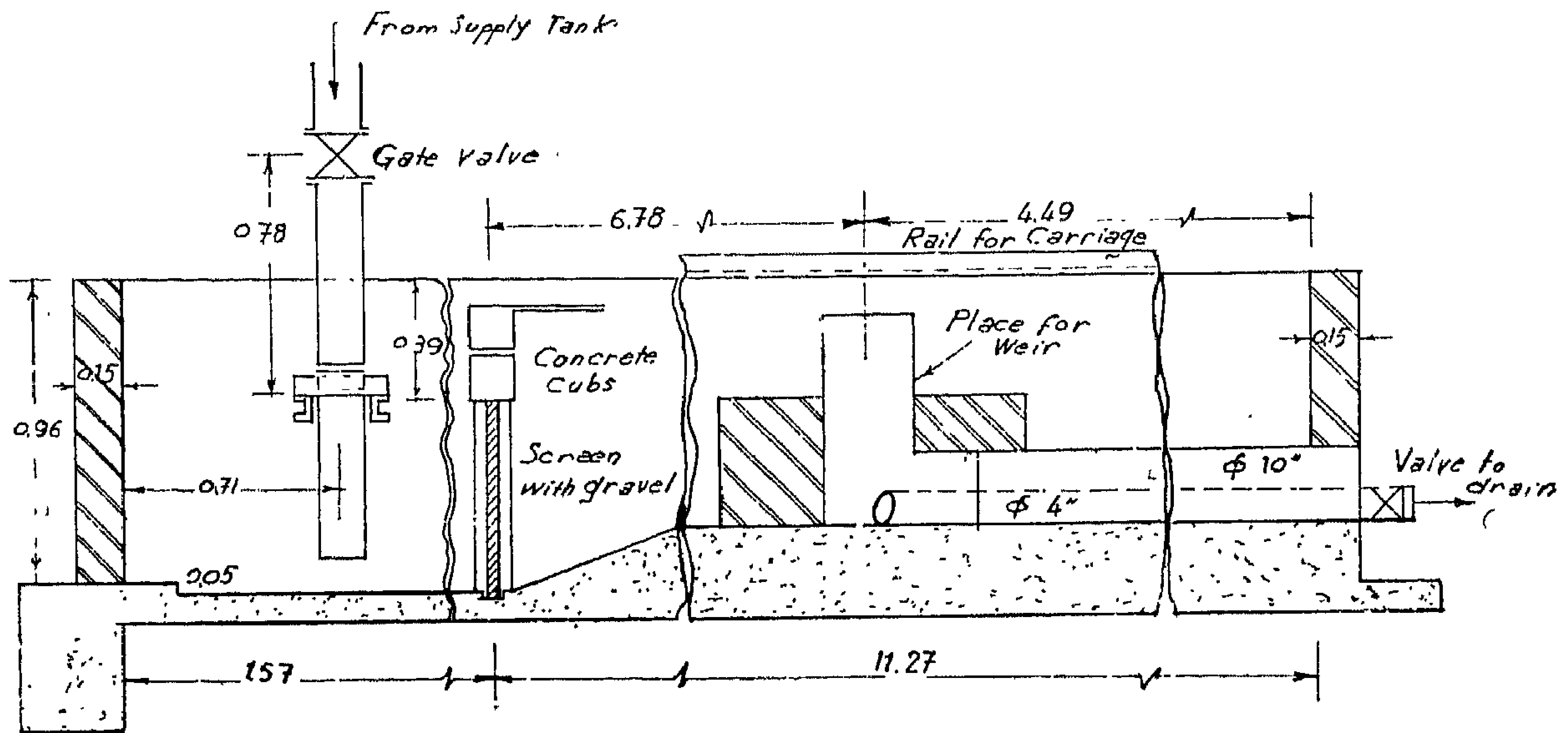


FIGURE (14) Channel Used

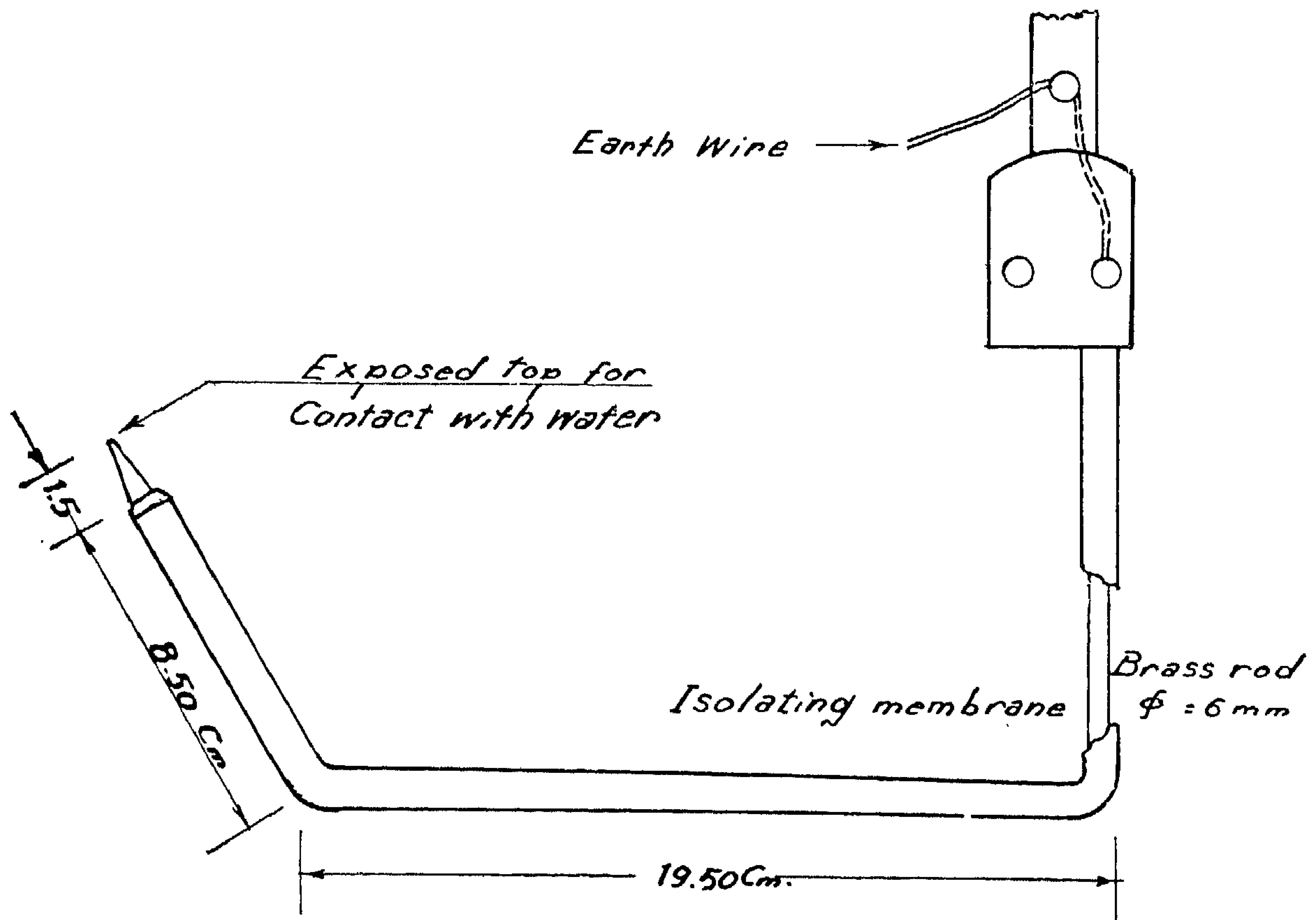
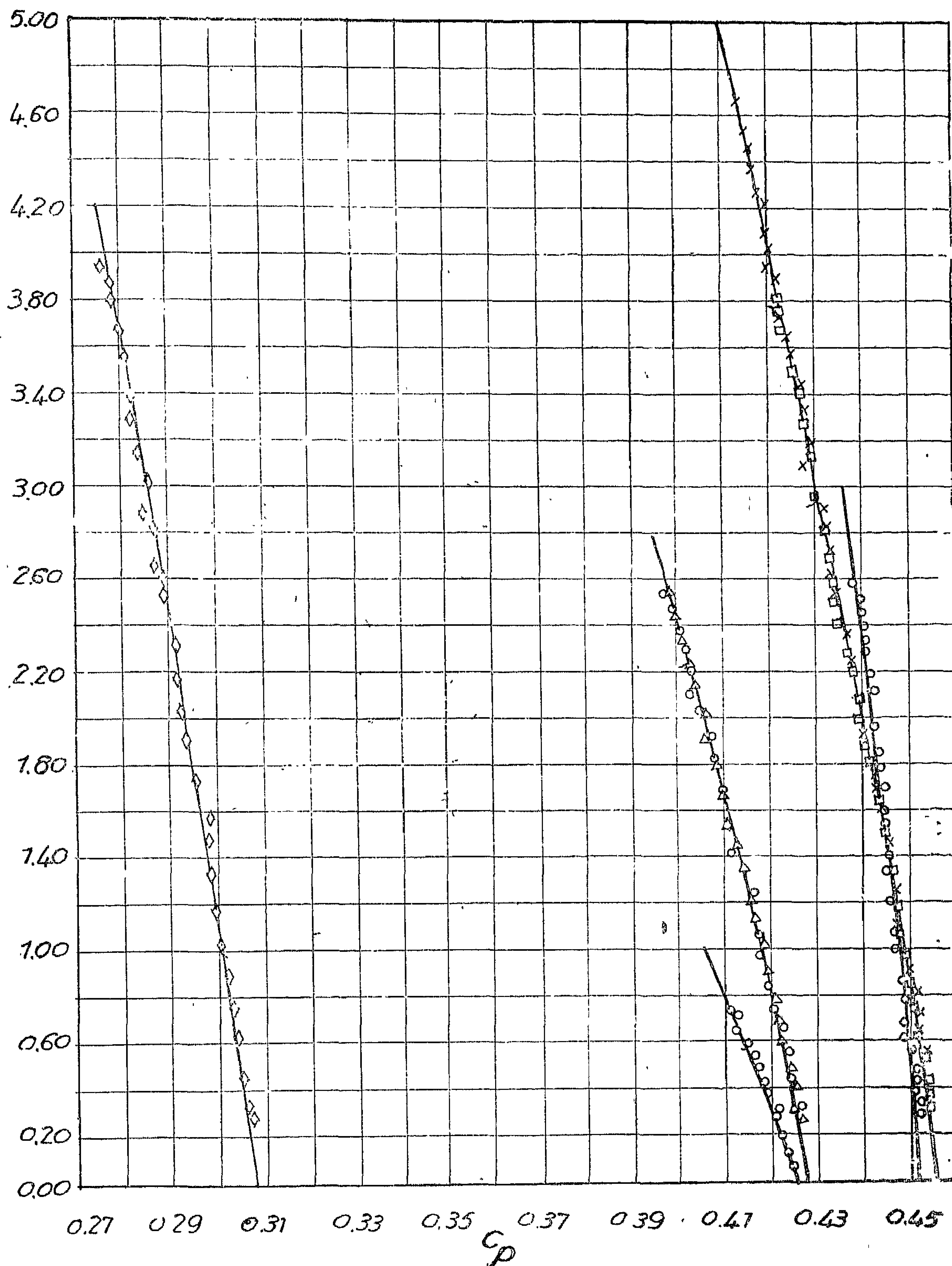


Fig. 15



○ MODEL	(9),	$\theta_e = 26^\circ 34'$	$\beta_e = 52^\circ 53'$	a = 18 cm.	A = −0.991
△ "	(10)	" $56^\circ 19'$	" $30^\circ 00'$	" 6 "	" 0.467
○ "	(11)	" $56^\circ 19'$	" $82^\circ 38'$	" 6 "	" −0.467
□ "	(12)	" $63^\circ 26'$	" $63^\circ 26'$	" 4 "	" 0.000
◇ "	(13)	" $63^\circ 26'$	" $00^\circ 00'$	" 4 "	" 1.000
× "	(14)	" $63^\circ 26'$	" $53^\circ 26'$	" 3 "	" 0.000
○ "	(15)	" $71^\circ 34'$	" $90^\circ 00'$	" 4 "	" −0.258

Transitional Curves according to equation.(80)

where $$I_1 = \int_{\Theta = 0}^{\Theta = \Theta_e} \frac{\cos (A. \Theta)}{\cos^3 \Theta .} d \Theta$$

and $$I_2 = \int_{\Theta = 0}^{\Theta = \Theta_e} (\cos \Theta)^{0.30} \cos (A. \Theta) \, d \Theta$$

The values of I_1 and I_2 can be computed graphically for different values of the angle Θ.

Again, the discharge over the parabolic curve can be expressed as follows ;

$$Q = C_p \, L \, \sqrt{2g} \, H^{3/2}$$

where $$C_p = \frac{4 a}{L} [0.457 \, I_1 - 0.024 \, (\frac{H}{a})^{1.10} I_2] \quad \ldots\ldots \quad (28)$$

The value of L the total length of the parabolic curve can be put in terms of the angle Θ as follows

$$\frac{dy}{dx} = \tan \Theta = \frac{y}{2 a}$$

and $\frac{dy}{d\Theta} = 2 a \sec^2 \Theta$ or $dy = 2 a \sec^2 \Theta \, d \Theta$

therefore $d_1 = \sqrt{1 + \tan^2 \Theta} \times 2 a \sec^2 \Theta \, d \Theta$
$= \sqrt{\sec^2 \Theta} \, . \, 2 a \sec^2 \Theta \, d \Theta = 2 a \sec^3 \Theta \, d \Theta$

$$\therefore \; I = \frac{L}{2} = \int_{\Theta = 0}^{\Theta = \Theta_e} 2 a \sec^3 \Theta \, d \Theta$$

putting this value of L in equation (28) we get;

$$C_p = \frac{0.914 \, I_1 - 0.048 \, (\frac{H}{a})^{1.10} I_2}{\sec \Theta_e \tan \Theta_e + \log_e (\mathrm{Sec} \, \Theta_e + \tan \Theta_e)} \quad \ldots\ldots \quad (29)$$

Equation (29) was represented graphically in Fig. (13) with the experimental points which showed a very good agreement between the theory and the experiments.

Equation (29) involves 4 variables : C_p, A, Θ_e and $\frac{H}{a}$. These variables were introduced in curves as shown in Fig. 13. These curves are calculated for different values of the variables as follows :

a. The value of β_e between 0.00° and 90°.

b. Practical values of Θ_e are between 5° and 89°.

c. Within the limit of the above mentioned ranges, certain maximum and minimum values of A were obtained and the value of C_p can be calculated.

EXPERIMENTAL VENIFICATION

The venification of the above mentioned equations were carried out using a channel of rectangular section 117 cm. breadth and 80 cm height. The length of the approach channel is about 8.0 m. The inlet of the channel was provided by a double screen of height 42 cm. and the space between the two faces of the screen was filled with gravel to dissipate the energy comming from the inlet pipe to the channel. The discharge entering the channel ranges between 60 and 25 lit./sec. and it was measured by an 8 inches orifice meter which was installed in the main feeding pipe. Dischanges lower than 25 lit./sec. were measured by a 90° V—notch installed at the end of the downstream channel. Water is pumped from the sump to a supply tank feeding the supplying pipe to the channel Fig. (14).

MEASURINGS DEVICES

Different types of devices for measuring the characteristics of this flow were developed and used as will be shown in the following.

1. *Measurement of the upper and lower nappe profile :*

The upper nappe profiles were determined using a standard point gauge which closes a low voltage electrical circuit whose needle end touches the water surface. The lower nappe was determined by using a modified standard gauge. The positive needle was removed and replaced by a brass bar 6 mms diameter, bent at right angle at a distance 11 cm. from bottom

This means that the coefficient of discharge over any two circular weirs will be the same for the same values of δ_0 and $\frac{H}{R_w}$. This means virtual dynamic similarity will occur despite the lack of geometrical similarity. Equation 24 was drawn with the experimental points for different values of $\frac{H}{R_w}$ and δ_e in fig. 12. It can be seen that equation 24 represents the coefficient of discharge over a sharp edged circular arc with a very good agreement with the experimental points.

b. Sharp edged parabolic weirs

To get the coefficient of discharge over a sharp edged parabolic weir the same procedure presented for a circular arc will be followed, see Fig. 11a.

assume the equation of the parabola $y^2 = 4\,a\,x$ Therefore the raduis of curvature ρ_N is given by ;

$$\rho_N = [1 + (\frac{dx}{dy})^2]^{3/2} \Big/ \frac{d^2x}{dy^2}$$

$$= 2\,a\,[1 + \frac{y^2}{4\,a^2}]^{3/2} \qquad \ldots\ldots(25)$$

The differential length $d_1 = \sqrt{(dx)^2 + (dy)^2}$

$$= dy\sqrt{1 + (\frac{dy}{dx})^2} = dy\sqrt{1 + \frac{y^2}{4\,a^2}}$$

$$\text{and } \cos\Theta = \frac{dy}{d_1} = \frac{1}{(1 + \frac{y^2}{4\,a^2})^{0.50}} \qquad \ldots \quad (26)$$

Where Θ is the angle which the normal makes with the x-axis. The raduis of curvature can be written as

$$\rho_N = \frac{2\,a}{\cos^3\Theta}$$

Using equation (22) and integrate to get the total Q.

$$Q = 4\,a\,\sqrt{2g}\,H^{3/2}\,[0.457\,I_1 - 0.024\,(\frac{H}{a})^{1.10}\,I_2] \qquad \ldots\ldots \quad (27)$$

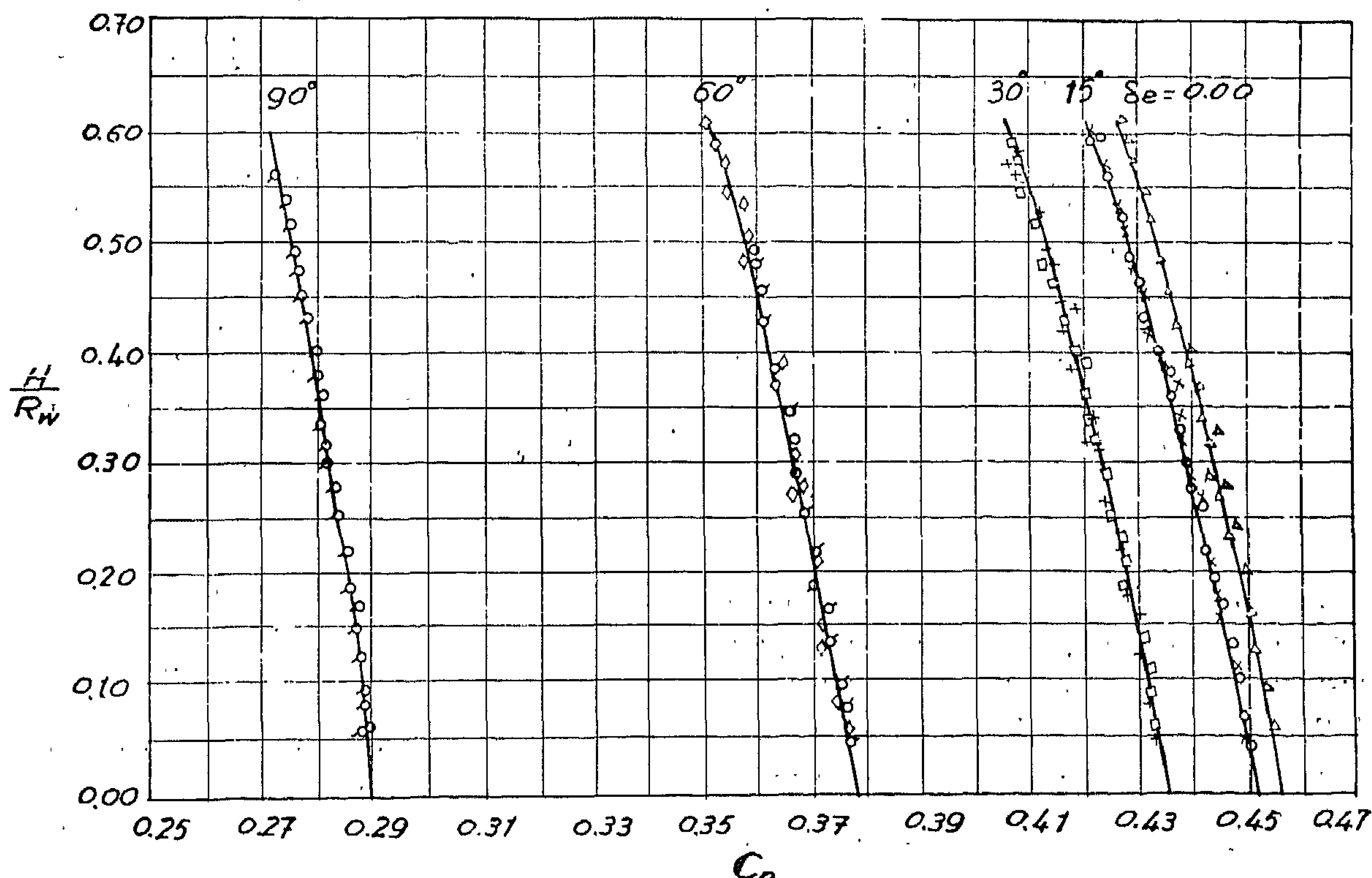


Fig. 12. — Circular weirs.

$= V_m \cos \delta \, (\alpha H) \, d_1 = C_R \sqrt{2g} \, H^{3/2} \, d_1$

therefore $C_R = \dfrac{V_m \cos \delta \, . \, \alpha}{\sqrt{2g \, H}}$

But since for radial flow $C_{R_1} = 0.457 - 0.0513 \left(\dfrac{H}{R_w}\right)^{1.10}$

therefore, $C_R = C_{R_1} \cos \delta$

$$= \left[0.457 - 0.513 \left(\frac{H}{R_w}\right)^{1.10} \right] \cos \delta$$

Now, consider the general case in which the curve of the weir follows an equation f (x, y) = 0. The curve can be regarded as composed of an infinite number of successive element arcs of circles, each of raduis equal to the raduis of curvature of that element.

therefore

$$dq = \left[0.457 - 0.0513 \left(\frac{H}{\rho_n}\right)^{1.10}\right] \cos \delta \sqrt{2g} \, H^{3/2} \, d_1 \quad \ldots\ldots \quad (21)$$

but

$$\rho_N = \frac{d_1}{d\Psi} \quad \text{where } \Psi = \frac{\pi}{2} - \Theta, \; d\Psi = - d\Theta$$

and

$$\delta = \Theta - \beta = \Theta - \Theta \frac{\beta_e}{\Theta_e}$$

$$= \Theta \left(1 - \frac{\beta_e}{\Theta_e}\right) = A \, \Theta$$

Substituting these values of δ and ρ_N in equation (21)

$$dq = \left[0.457 - 0.0513 \left(\frac{H}{p_N}\right)^{1.10}\right] \cos (A \, \Theta) \sqrt{2g} \, H^{3/2} \, \rho_N \, d\Theta \quad \ldots\ldots \quad (22)$$

Equation (22) is the differential equation for the discharge over any curved escape which follows a continuous curve in plane.

Two specific cases will be considered below namely the case of the sharp edged circular weirs and the sharp edged parabolic weirs.

a. Sharp edged circular weirs

In the case of circular weirs; $\rho_N = R_w$ the raduis of the circular arc.

The total discharge over the whole circular curve from $\Theta = 0$ to $\Theta = \Theta_e$ as shown in Fig. (11a) is given by ;

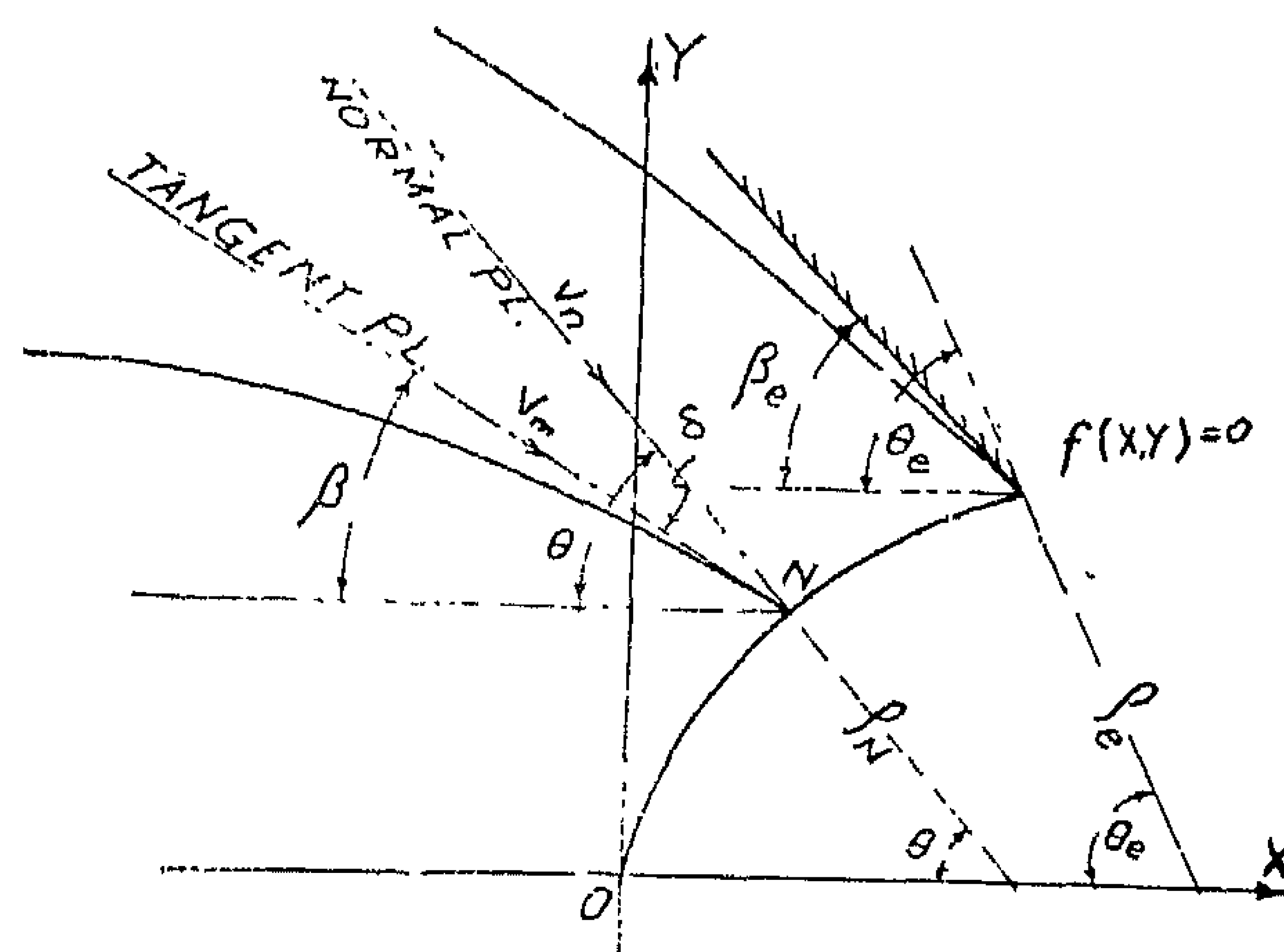


Fig. 11 (a)

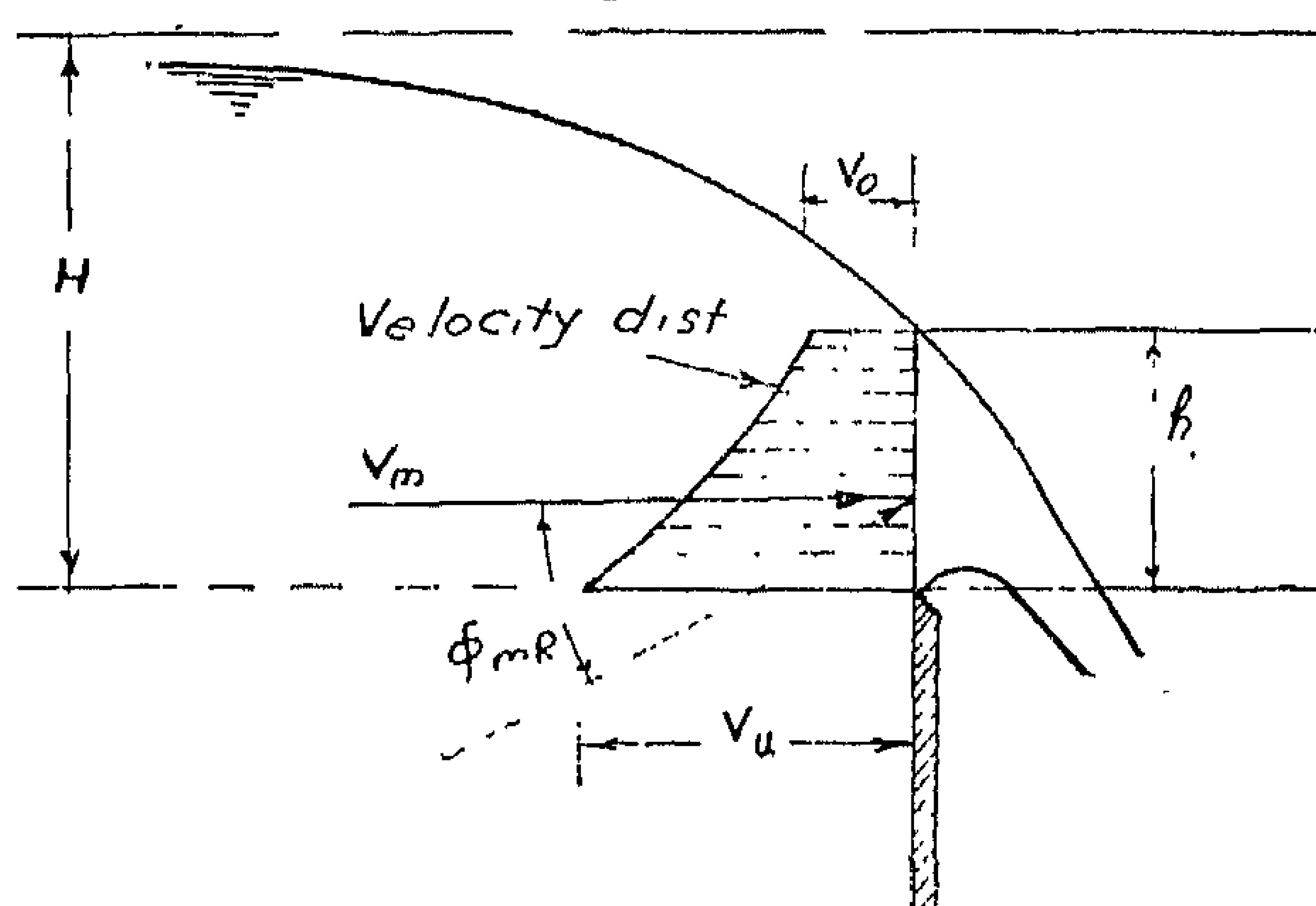


Fig. 11 (b)

$$Q = 2 \int_{\Theta=0}^{\Theta=\Theta_e} \left[0.457 - 0.0513 \left(\frac{H}{R_w}\right)^{1.10}\right] \cos (A . \Theta) \sqrt{2g} \, H^{3/2} \, R_w \, d\Theta$$

$$= \frac{2 \, R_w}{A} \sqrt{2g} \, H^{3/2} \left[0.457 - 0.0513 \left(\frac{H}{R_w}\right)^{1.10}\right] \sin (A \, \Theta_e)$$

But $A = 1 - \dfrac{B_e}{\Theta_e}$, $2 \, R_w \, \Theta_e = L$ and

$\delta_e = \Theta_e - B_e$

$$\text{therefore } Q = \frac{\sin \delta_e}{\delta_e} \left[0.457 - 0.0513 \left(\frac{H}{R_r}\right)^{1.10}\right] L \sqrt{2g} \, H^{3/2} \quad \ldots\ldots \quad (23)$$

If the equation is put in the form

$Q = C_r \, L \sqrt{2g} \, H^{3/2}$ the value of C_r can be given as

$$C_r = \frac{\sin \delta_e}{\delta_e} \left[0.457 - 0.0513 \left(\frac{H}{R_w}\right)^{1.10}\right] \quad \ldots\ldots \quad (24)$$

If this equation is put in the form $Q = C_p\ n\ L_s\ \sqrt{2g}\ H^{3/2}$ a general expression for C_p can be obtained as ;

$$C_p = 0.457 - \frac{0.914}{H/L_p} - \frac{4.373}{n} \left(\frac{H}{L_s}\right) \quad (20)$$

Equation (20) was calculated for three polygonal weirs namely an equilateral triangle, a square and a hexagon and shown in Fig. (8).

Experiments were carried out to investigate the effect of the geometrical shape

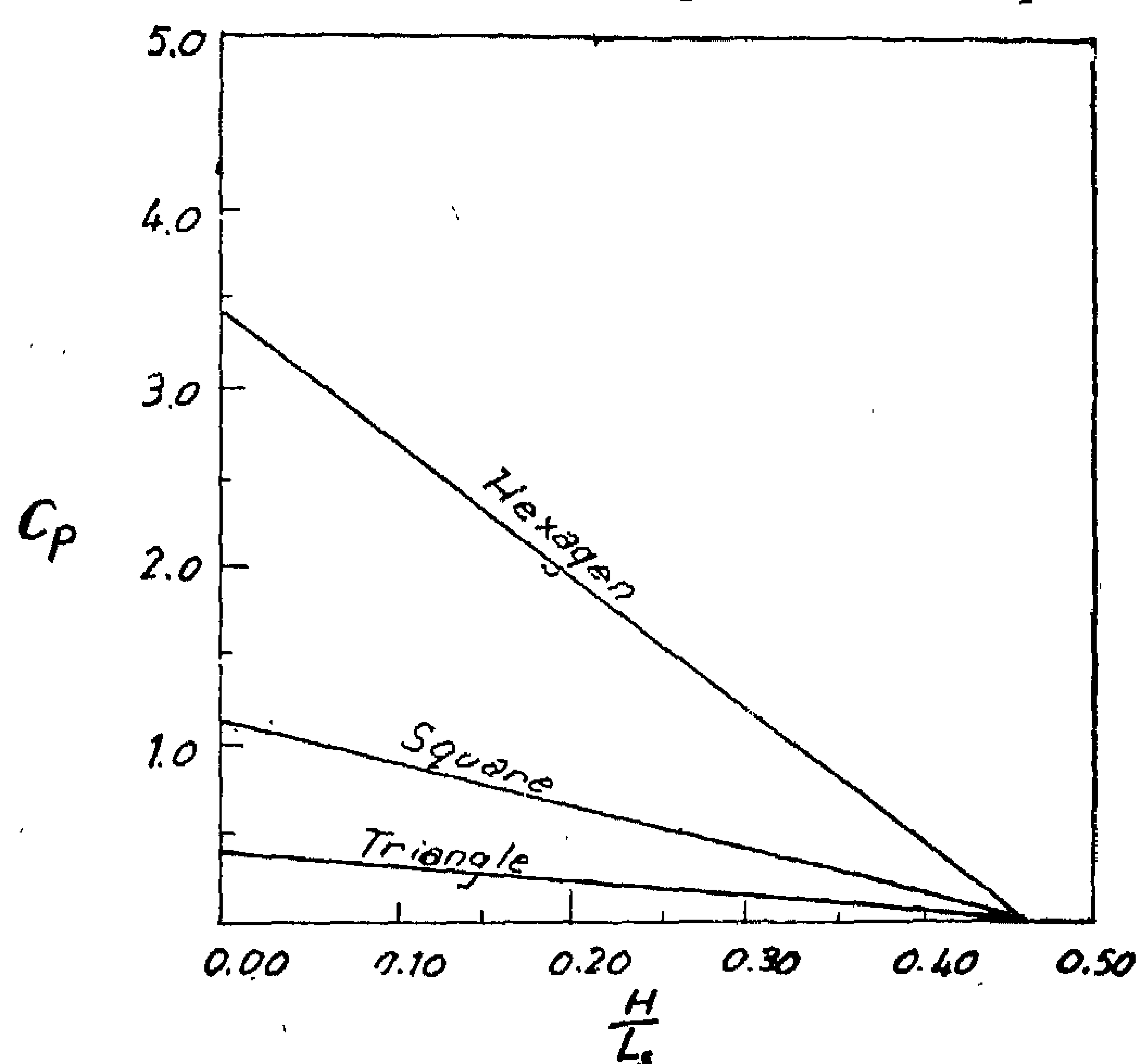


Fig. 8

of the polygonal weir on the flow and to find the coefficient of discharge for each shape.

Nine weirs were used in three groups. Each group composed of three models for each of equilateral triangle, square and hexagon weirs, whose total length of sides are 60 cms, 120 cms and 200 cms respectively. The discharge used varies between a minimum value of 1.09 lit/sec to a maximum 57.40 lit./sec. Fig. (9) shows the measured value of the discharge against the head H for the nine models used. Fig. (10) shows the velationship between the coefficient of discharge over polygonal weir and the ratio between the total head and the length of the side L_s. More experiments are needed for this part of study in

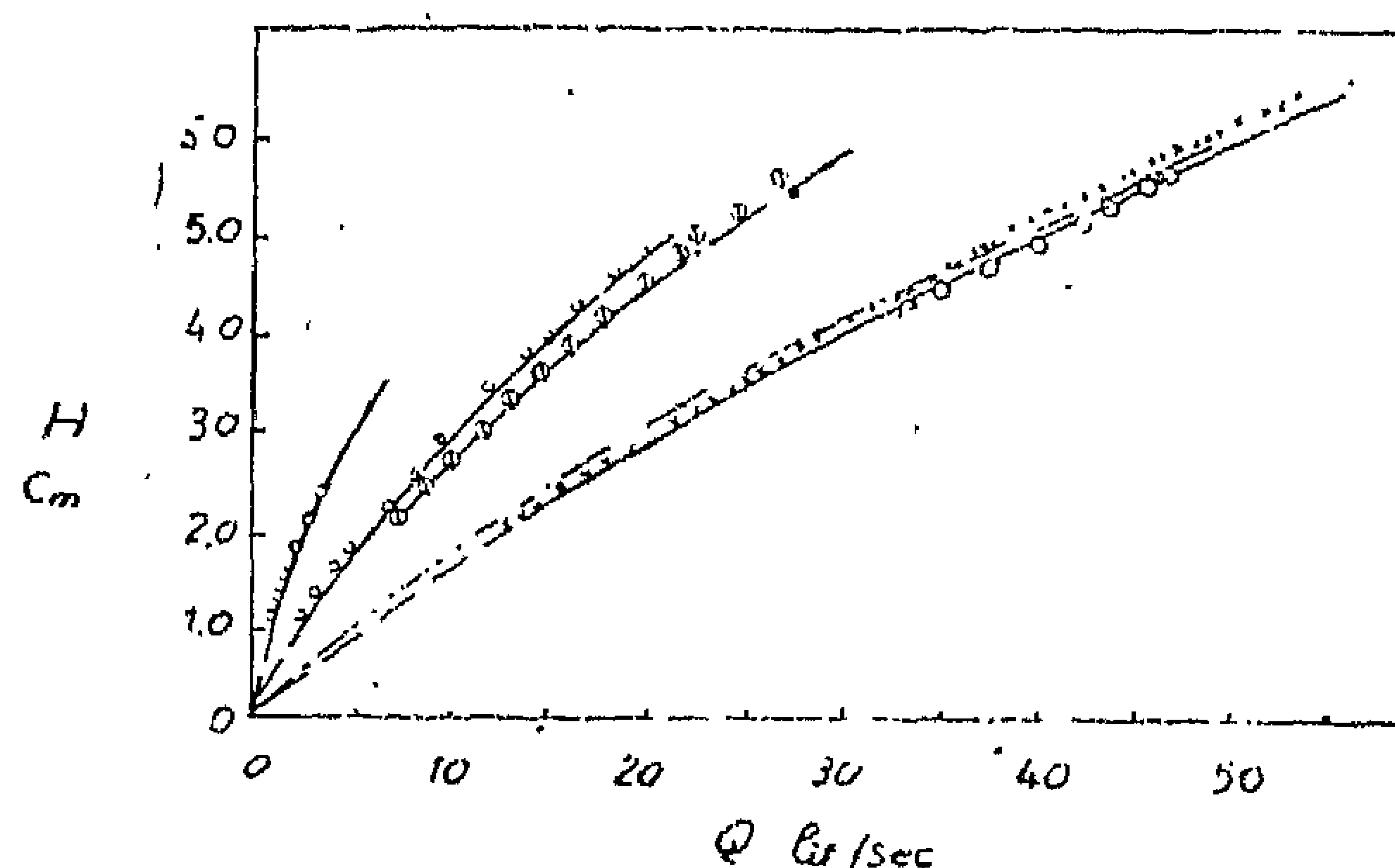


Fig. 9. — Discharge curve for the three shapes used.

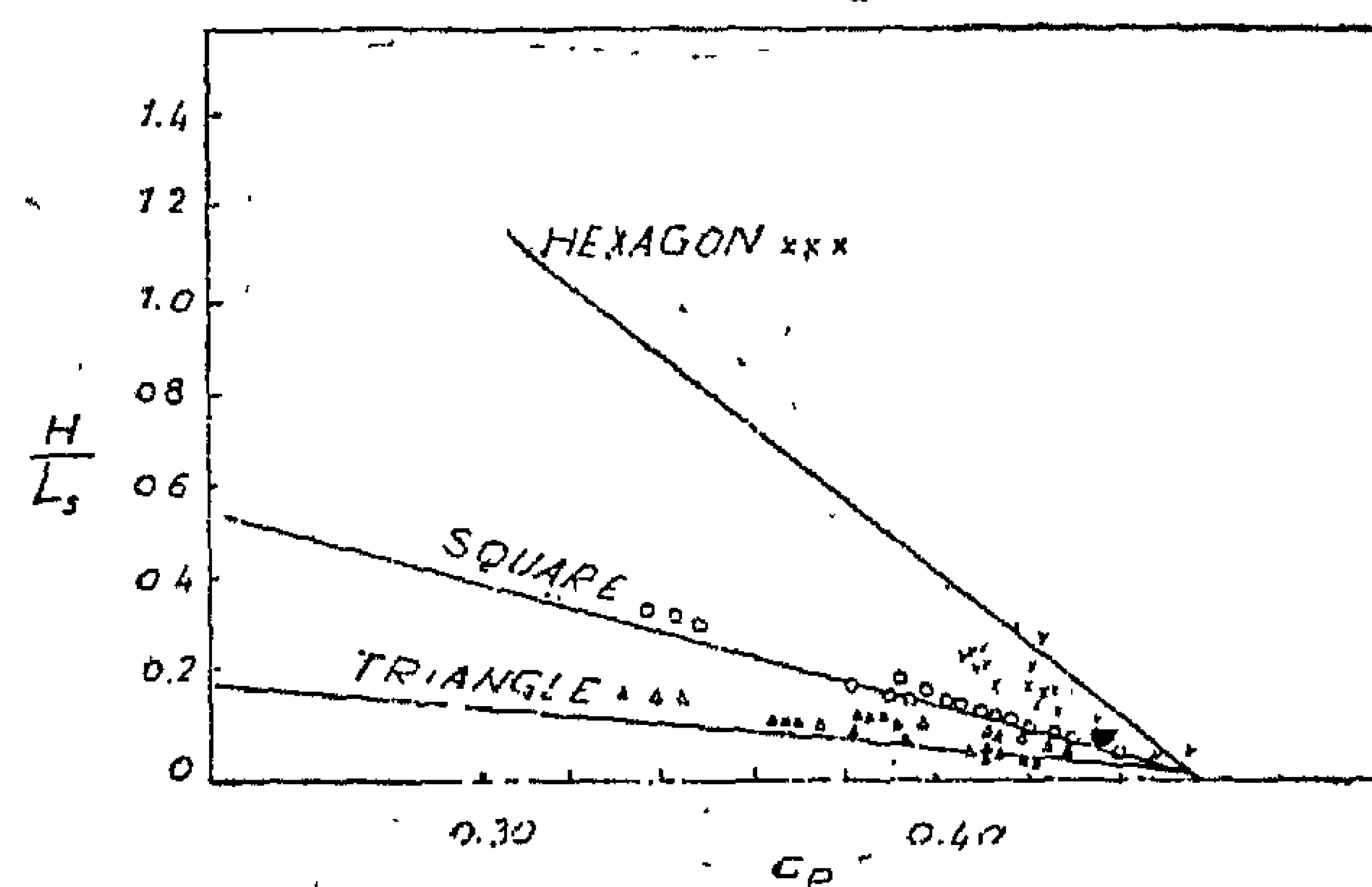


Fig. 10

order to get a clear idea about the effect of the presence of the sharp corners on the velocity distribution over the sharp edge, and on the shape of the nappe profile passing over these types of weirs.

C. Flow over circular arcs and parabolic curves

The extension of the study to include the general case of the flow over sharp edged weirs in which the crest (in plan) follow the shape of a circular arcs and a parabolic curve was essential. These two shapes represent spillway section of arch dams and can be used as tail escapes on irrigation canals. The parabolic curve gives more length as a tail escape than the circular curve and can take its place as a spillway section of an arch dam.

From Figs. (11a, 11b) the discharge can be calculated as ;

$$dq = V_m \cos \delta\ .\ h.\ d_l$$

tion of the mean velocity vector at the sharp section, it varied from 17.5° for straight weir as found before to 27° at $\frac{H}{R_w} = 0.50$.

B. *Polygonal Weirs*

Polygonal weirs are those structures composed of straight sides (in plan) like triangle, square and hexagon. The purpose of this part is to find an equation for getting the discharge over this type of structure. The flow over the closed polygon which is composed of n number of sides and whose internal angles are less than 180° can be treated as the summation of the flow over a group of separate straight weirs. The effect of the sharp corners will change the conditions of the flow in this vicinity. Therefore, the flow over this type can be treated as an approximation as the flow over a system of straight stretches connected by circular arcs at the corners.

a. *Discharge formulae*

The flow over a weir with a number of straight sides is considered as a summation of two flows; that part of a straight weir and that part of flow over a curved weir as shown in Fig. (7).

Let n the number of sides of a polygon, Θ interior corner angle, α the ratio of the straight part to the total length of sides of the polygon.

$$L_p = \frac{L_s\,(1 - \alpha)}{2} \quad \ldots\ldots \quad (17)$$

R_w is the raduis of the incribed circle in the polygon $= L_p \tan \Theta/2$.

Therefore if q_R is the discharge through a circular weir with a cirumference equal to L and q_{st} is the discharge through a straight weir with a total length equal to L. From equation (15) and (16)

$$\frac{q_R}{q_{st}} =$$

$$\frac{0.457 - 0.0513 \left(\dfrac{H}{L_p \tan \Theta/2}\right)^{1.10} L \sqrt{2g}\, H^{3/2}}{0.457 \times L \times \sqrt{2g}\, H^{3/2}}$$

$$= 1.00 - 0.116 \left(\frac{H}{L_p \tan \Theta/2}\right)^{1.167}$$

From which

$$\frac{H}{L_p} = 0.614 \tan \Theta/2 =$$

$$0.614 \tan \left[\frac{n-2}{2n} \times 180°\right] \quad \ldots\ldots \quad (18)$$

From equation (17)

$$\alpha = 1.00 - \frac{1}{0.307 \tan \Theta/2} \left(\frac{H}{L_s}\right) \quad \ldots\ldots \quad (19)$$

From the above statments we can deduce the equation of the discharge over any regular polygon by considering it as a summation of discharge of a straight weir of total length αL_s and a curved weir of raduis $R_o = \left(\frac{L_s - \alpha L_s}{2}\right) \tan \Theta/2$

or $Q = 0.457\, n\, \alpha\, L_s \sqrt{2g}\, H^{3/2} + [0.457 - 0.513 \left(\frac{H}{R_o}\right)^{1.10}] \times 2 \pi R_o \sqrt{2g}\, H^{3/2}$

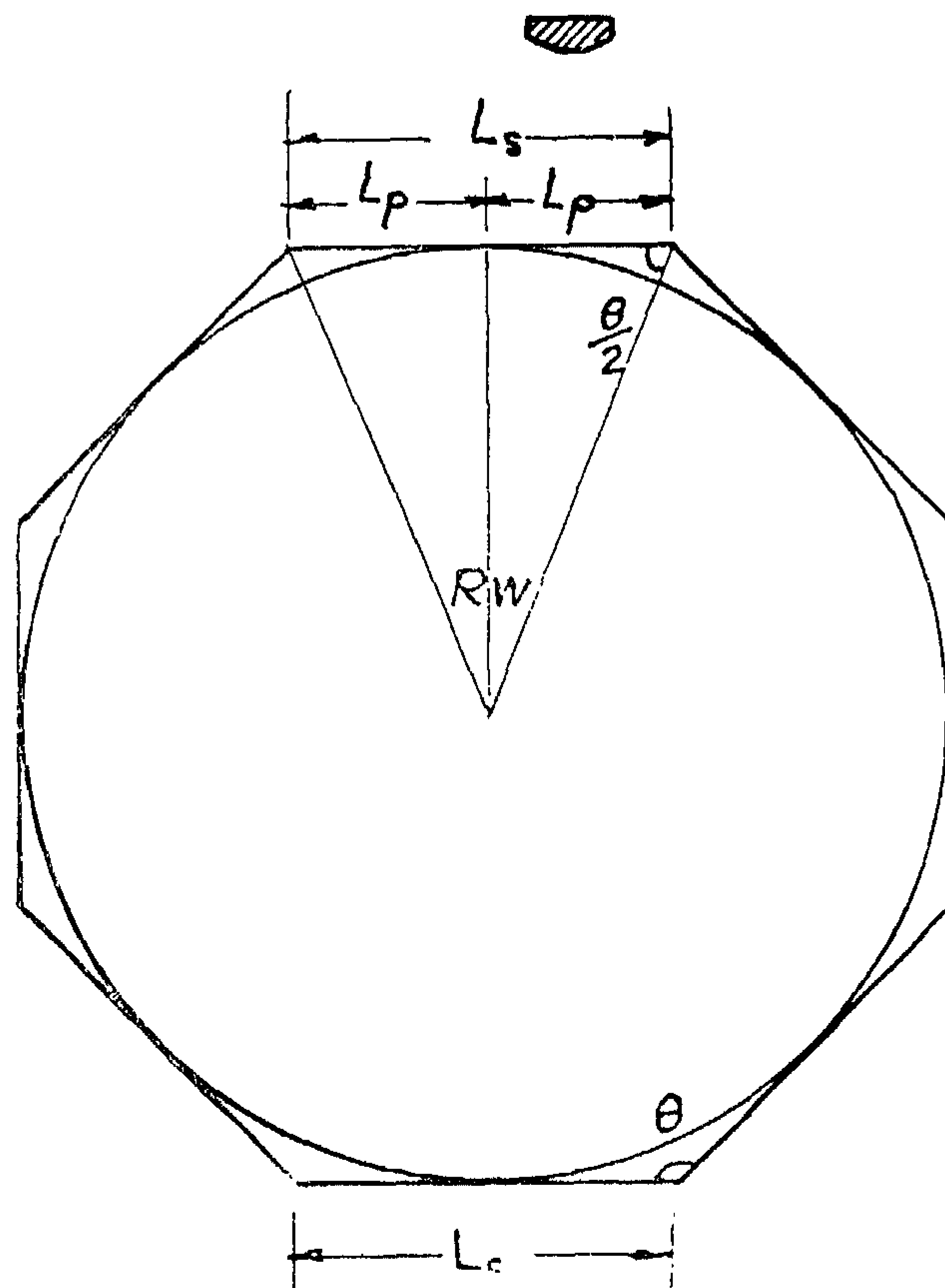


Fig. 7

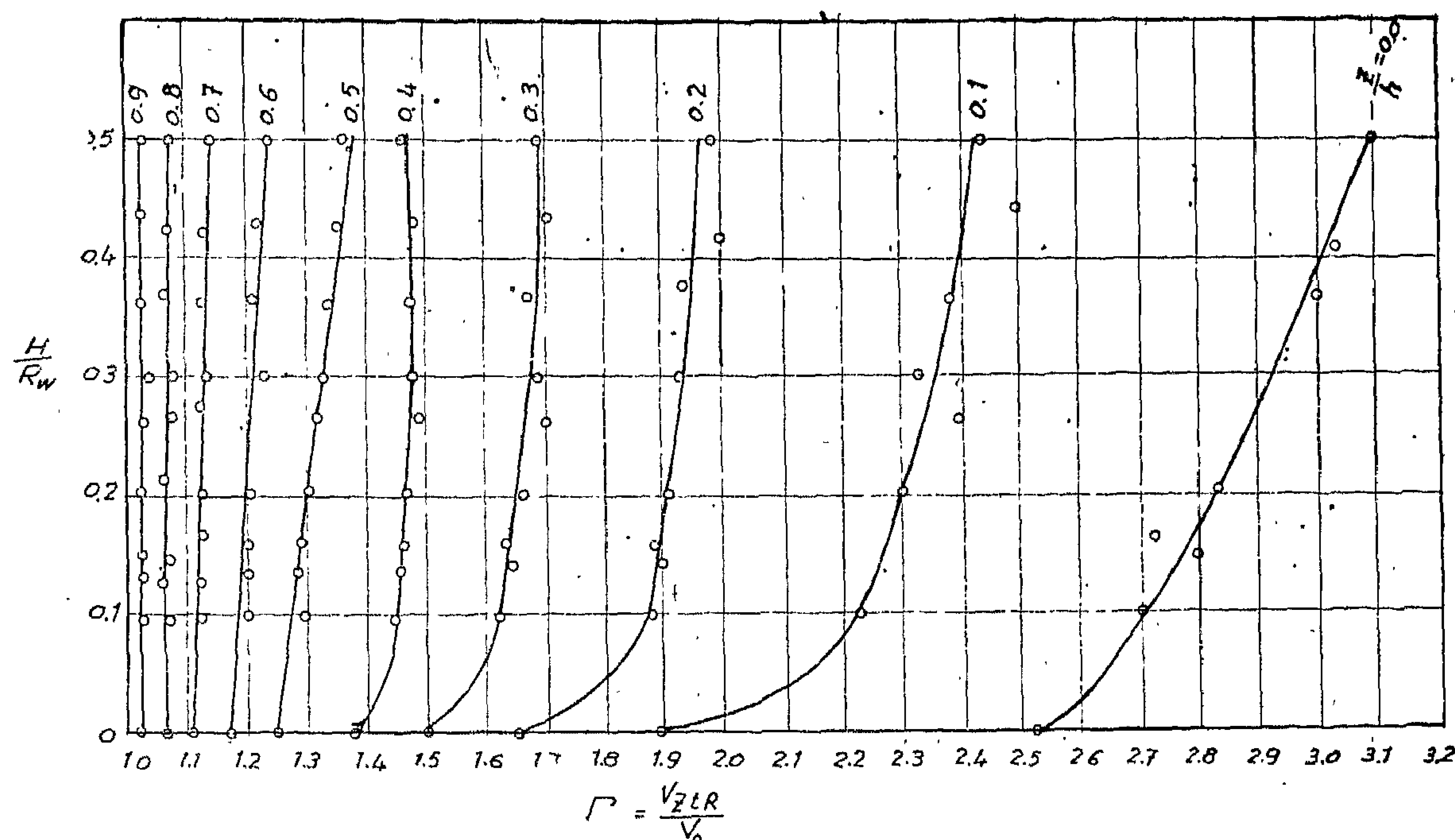


Fig. 5

$\Gamma_{mR} = \frac{VmR}{V_0}$ = is the area of the Γ — diagram devided by the vertical side which is equal to unity. Fig. 5 shows the relationship between Γ and $\frac{H}{R_w}$ with different values of $\frac{Z}{h}$ (From 0 to 1).

Comparision between flow over circular weirs and straight weirs per unit length

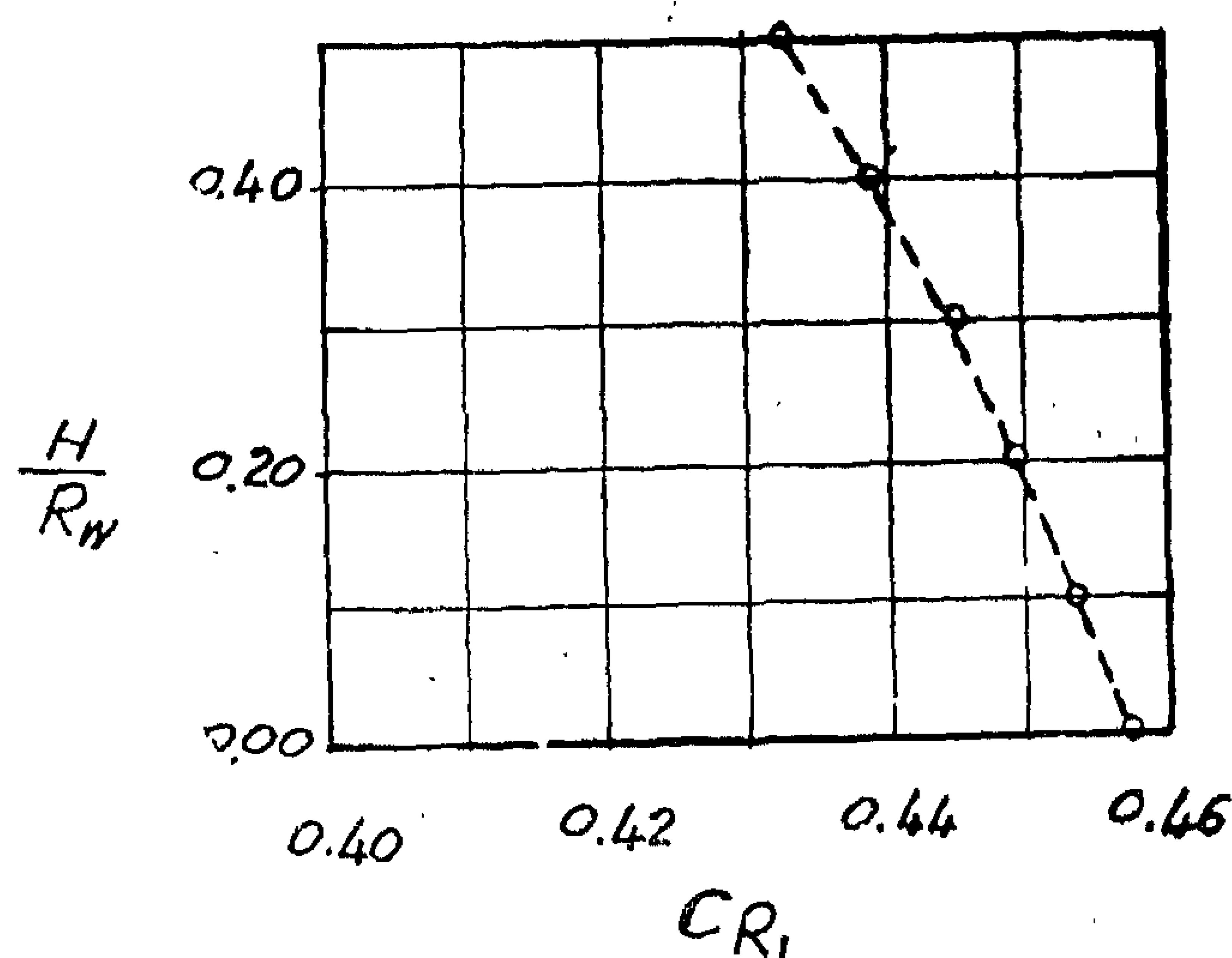


Fig. 6

was found to depend mainly on the ratio $\frac{H}{R_w}$ as given by the following equation

$$\frac{q_r}{q_{st}} = 1.00 - 0.116 \left(\frac{H}{R_w}\right)^{1.167} \qquad (15)$$

The discharge coefficient C_{R_1} for a sharp edged weir was plotted in Fig. 6 against the ration $\left(\frac{H}{R_w}\right)$ and this relation can be put in the form.

$$C_{R_1} = 0.457 - 0.0513 \left(\frac{H}{R_w}\right)^{1.10} \qquad (16)$$

It was concluded from the above study that the nappe of water flowing over a circular weir differs from that flowing over a straight one, this was the effect of circularity of the crest which causes a heading up of water in the vicinity of the crest. This means that the ratio $\frac{h}{H}$ for circular weir is greater than that of a straight weir. It was also shown that the coefficient of discharge in the circular case must depend on the ratio $\frac{H}{R_w}$. As for the direc-

assume $\cos \Phi_{mR} = \chi$

and $\sqrt{\frac{H}{h} 1} = \eta$

Therefore $\frac{Q_R}{2 \pi R_{uw}} =$

$$\frac{Q_R}{L} = q_R = \chi \Gamma_{mR} \sqrt{2g}\, h^{2/3} \quad \ldots\ldots \quad (8)$$

or $q_R = C_R \sqrt{2g}\ h^{2/3}$

where $C_R = \chi . \Gamma_{mR} . \eta$

If the total head H is introduced instead of h, equation (8) can be put as :

$$q_R = \chi\ \Gamma_{mR}\ \beta \sqrt{2g}\ H^{3/2} \quad \ldots\ldots \quad (9)$$

where $\beta = \sqrt{\alpha^2 - \alpha^3}$ and $\alpha = \frac{h}{H}$

or $q_R = C_{R1} \sqrt{2g}\ H^{3/2} \quad \ldots\ldots \quad (10)$

Experimental work as will be described afterward gives the values of ;

$$\chi = \cos \Phi_{mR} = 17.5 + 19.0 \left(\frac{H}{R_w}\right) \quad (11)$$

$$\Gamma_{mR} = 1.40 + 0.219 \left(\frac{H}{R_w}\right)^{0.508} \quad (12)$$

$$\eta = 0.436 - 0.065 \left(\frac{R_w}{H}\right)^{0.468} \quad (13)$$

and $$\beta = 0.336 - 0.035 \left(\frac{H}{R_w}\right)^{0.584} \quad (14)$$

These equations are represented in Fig. (3)

b. Velocity distribution

By measuring the nappe profile for 3 weirs and 10 different discharges as shown in Fig. (4) for weir number (1) the following data are known; the approach head h_s, depth of water at the sharp edged section h, the radius of curvature of water surface R_s, raduis of curvature of the lower nappe surface R_u, the outer radius of weir R_w and the height of crest above the channel bed p.

The value of the velocity ratio $\Gamma = \frac{V_{ztR}}{V_o}$ can be calculated using equation (6_1) then

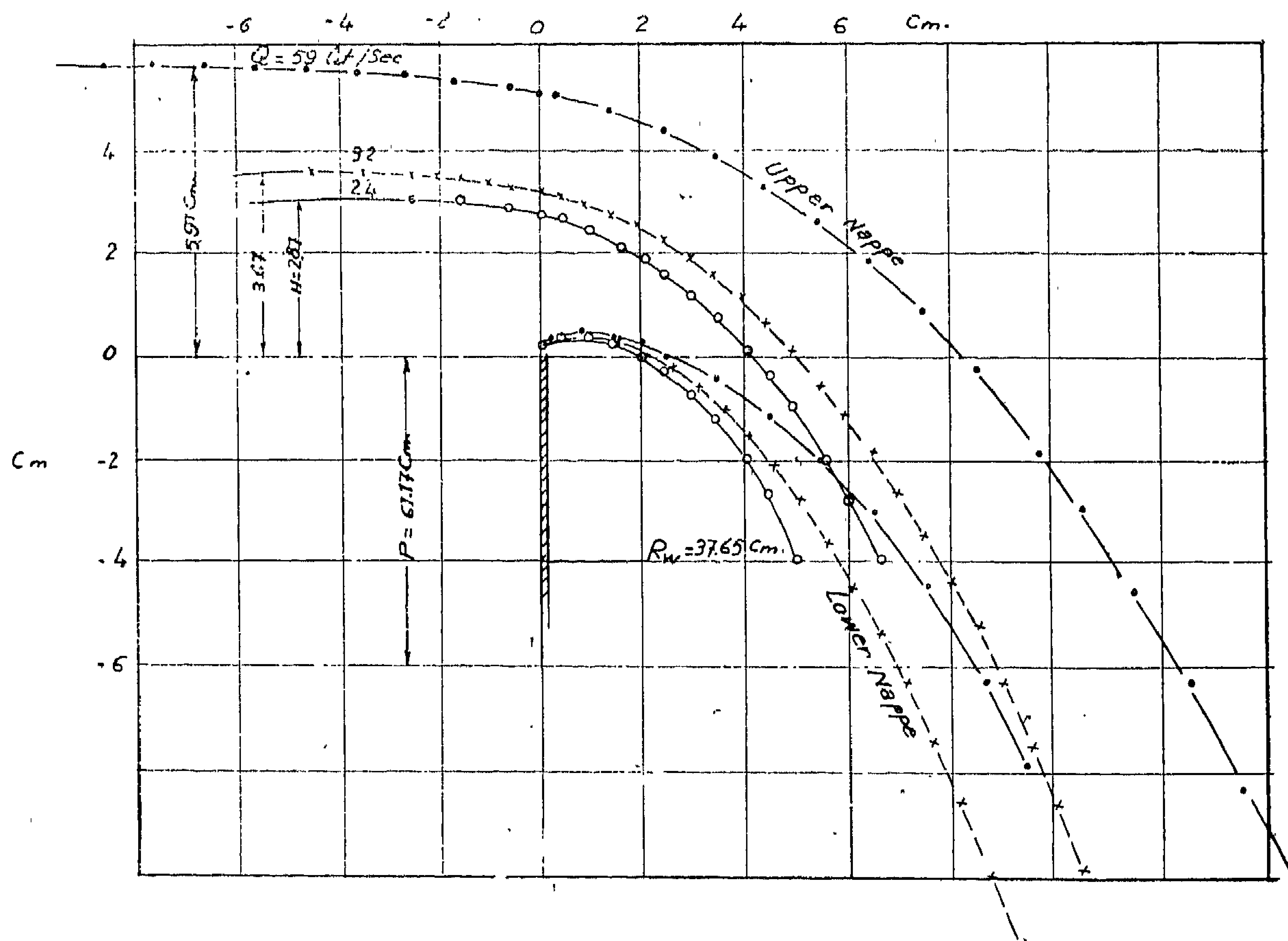
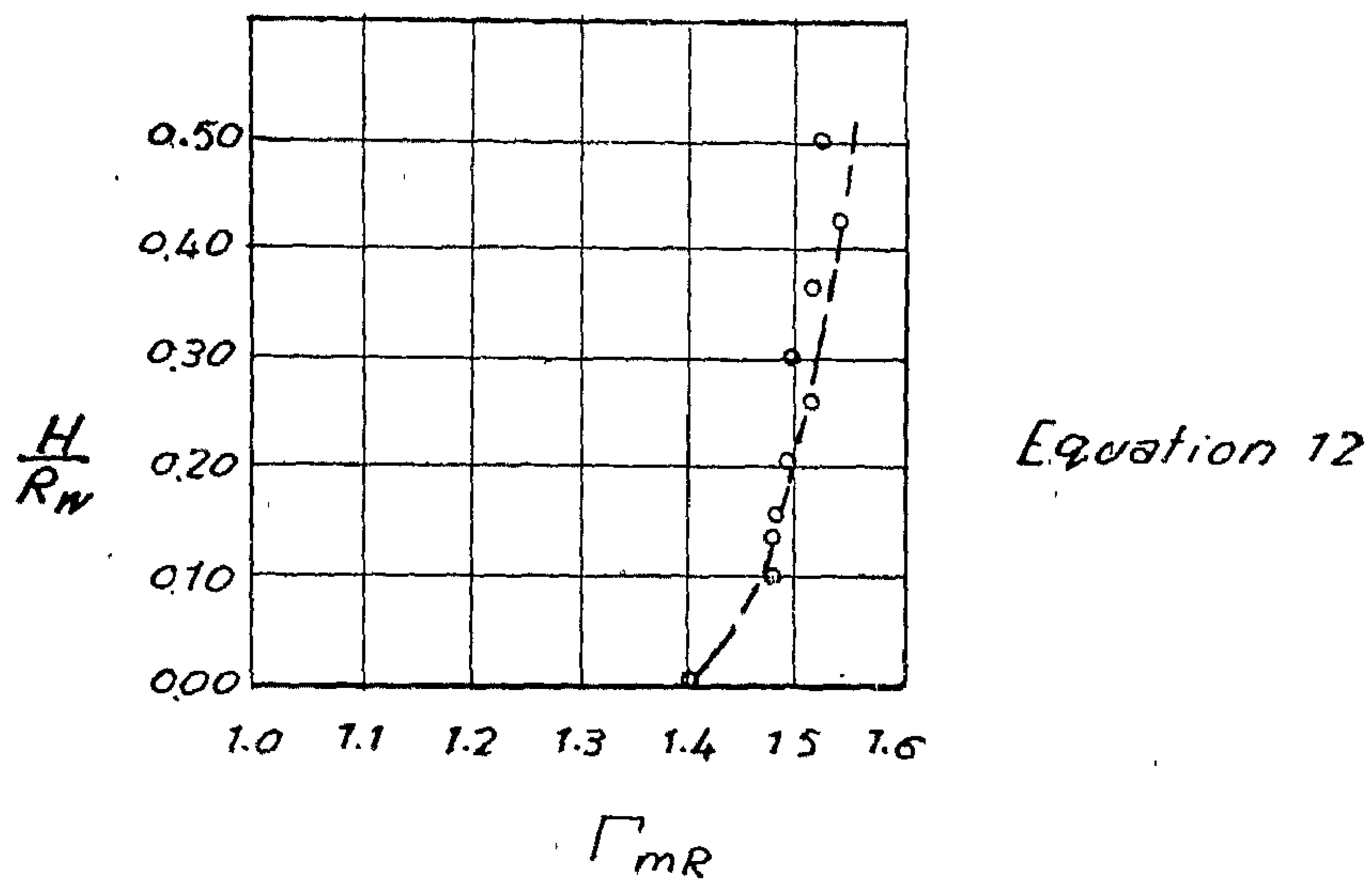
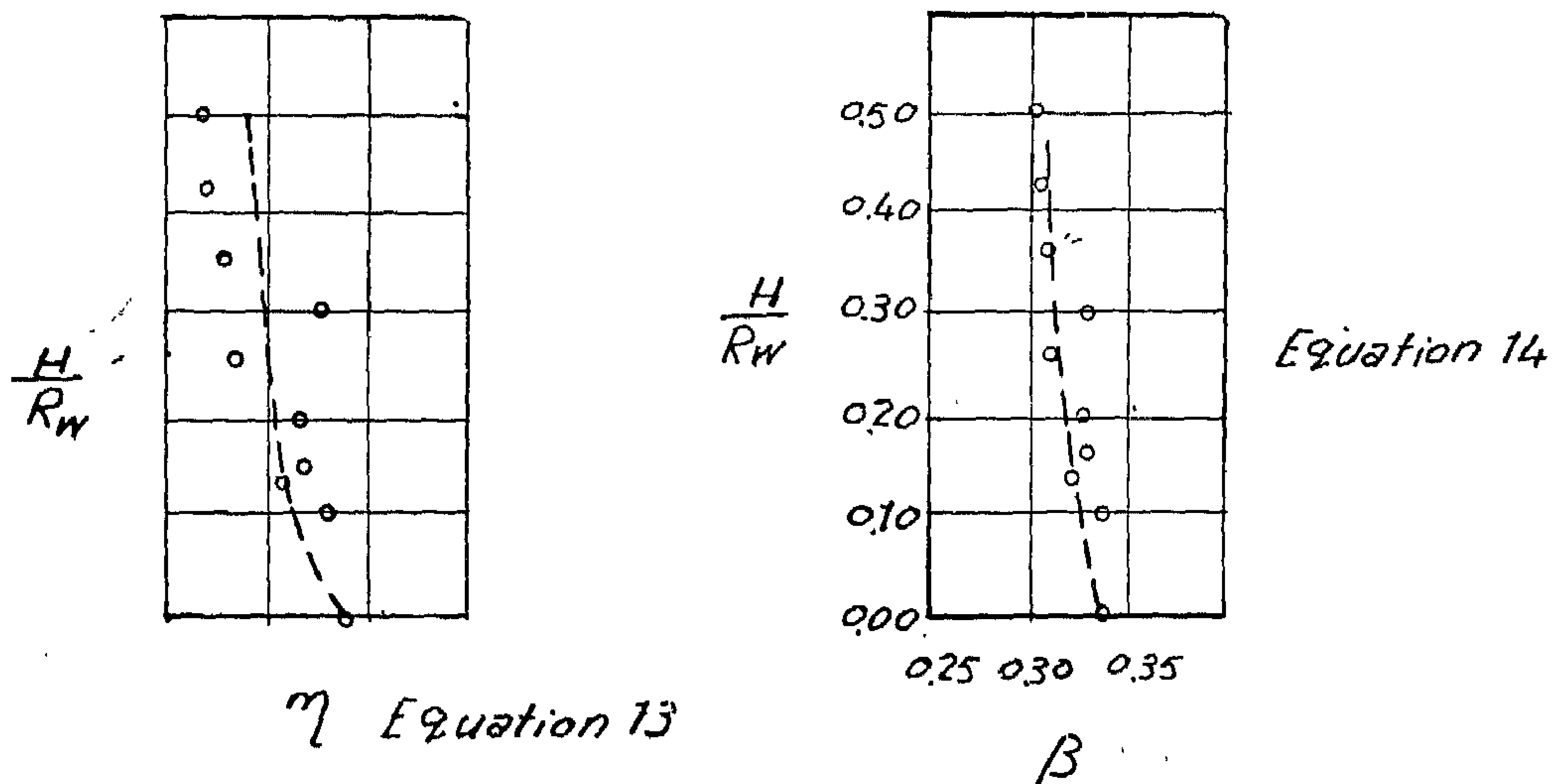


Fig. 4


0.50
0.40
0.30
H/Rw
0.20
0.10
0.00
1.0 1.1 1.2 1.3 1.4 1.5 1.6
ΓmR
Equation 12


H/Rw
η Equation 13
0.50
0.40
H/Rw
0.30
0.20
0.10
0.00
0.25 0.30 0.35
β
Equation 14

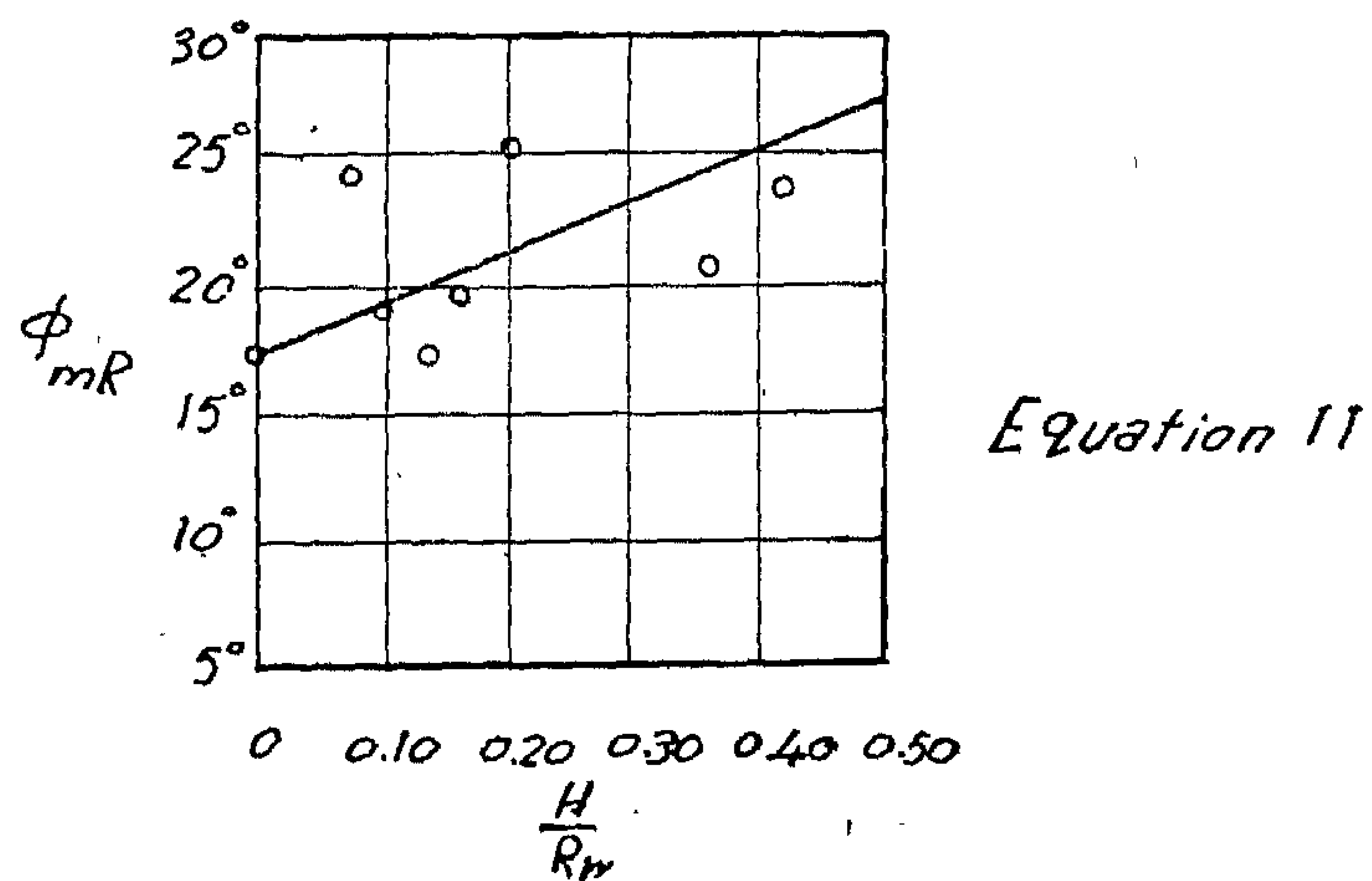

30°
25°
20°
φmR
15°
10°
5°
0 0.10 0.20 0.30 0.40 0.50
H/Rw
Equation 11

Fig. 3

h = depth of water at the section
V_o = the surface velocity.
and $\triangle P$ = the change in pressure.

The discharge over a shap edged straight weir was then studied for the case of rapidly varied flow and it was found that; the ratio $\frac{V_o}{V_u}$ was always constant = 0.40 and the horizontal component of velocity v_m was found to equal $v_m = V_m \cos \Phi_m$ Figs. (2a) and (2b).

where Φ_m = inclination of the tangent to the streamline passing through V_m which was found to be a constant = 17.5° and therefore an expression was obtained for the discharge over the weir as $Q = 0.95\ h\ V_m$.

A. Flow over circular weirs

The flow of water over a circular weir can be represented by an infinite number of radial (sheets) converging towards the centerline of the weir. Each of these sheets can be considered as case of two-dimensional form of flow with an infinitismal width instead of the finite width considered in the two dimensional case.

This case can be treated as two-dimensional problem, if the circular crest of the weir stretched in a straight line of length L providing that form of the sheet will contain the effect of circularity besides that of curvature and inclination.

The general equation for the velocity distribution in vertical sections laying in vertical planes which contain the centerline of the circular weir (radial planes) can be written as ;

$$V_{zt\ R} = V_{zc\ R} + V_{zi\ R} \qquad \ldots\ldots \quad (5)$$

Where R denots the effect of circularity of the crest. Equation (5) is similar to equation (3), the first term represents the total velocity, the second term is the effect of curvature and the third term gives the effect of the inclination of tangent.

The variables affecting the value of the velocity can be written as ; curvature as represented by the radius of curvature ρ_z of the streamline passing through the point at a distance Z above the crest, inclination Φ_z of the tangent to the streamline at distance Z, H the total head, the height of point Z above the crest, g the gravitational acceleration, the density ρ and R_w the raduis of the circular weir.

Therefore $V_{zt\ R} = F\ (\rho_z, \Phi_z, R_w, H, Z, g, \rho)$
By dimensional analysis we can get ;

$$V_{ZRt} = \sqrt{g\,H}\ F\left(\frac{H}{\rho_z}, \frac{1}{\Phi_z}, \frac{H}{R_w}, \frac{H}{Z}\right) \qquad \ldots\ldots \quad (6)$$

$$\text{or} \quad \frac{V_{ZRT}}{\sqrt{gH}} = F_r = F\left(\frac{H}{\rho_z}, \frac{1}{\Phi_z}, \frac{H}{R_w}, \frac{H}{Z}\right)$$

where F_r = Froude number.

But as V_o = constant $\sqrt{g\,H}$

$$\text{Therefore} \quad \frac{V_{ZTR}}{V_o} = \Phi\left(\frac{H}{\rho_z}, \frac{1}{\Phi_z}, \frac{H}{R_w}, \frac{H}{Z}\right) = F_r$$

$$\text{and} \quad \frac{V_{ZTR}}{V_o} = \frac{V_{ZCR}}{V_o} \pm \frac{V_{ZIR}}{V_o} \qquad (6')$$

a. Discharge Formula

The discharge over the circular weir can be put in the form ;

$$Q_R = V_{m\ R}.\cos \Phi_{mR}\ .\ h.\ 2\ \pi\ R_w$$

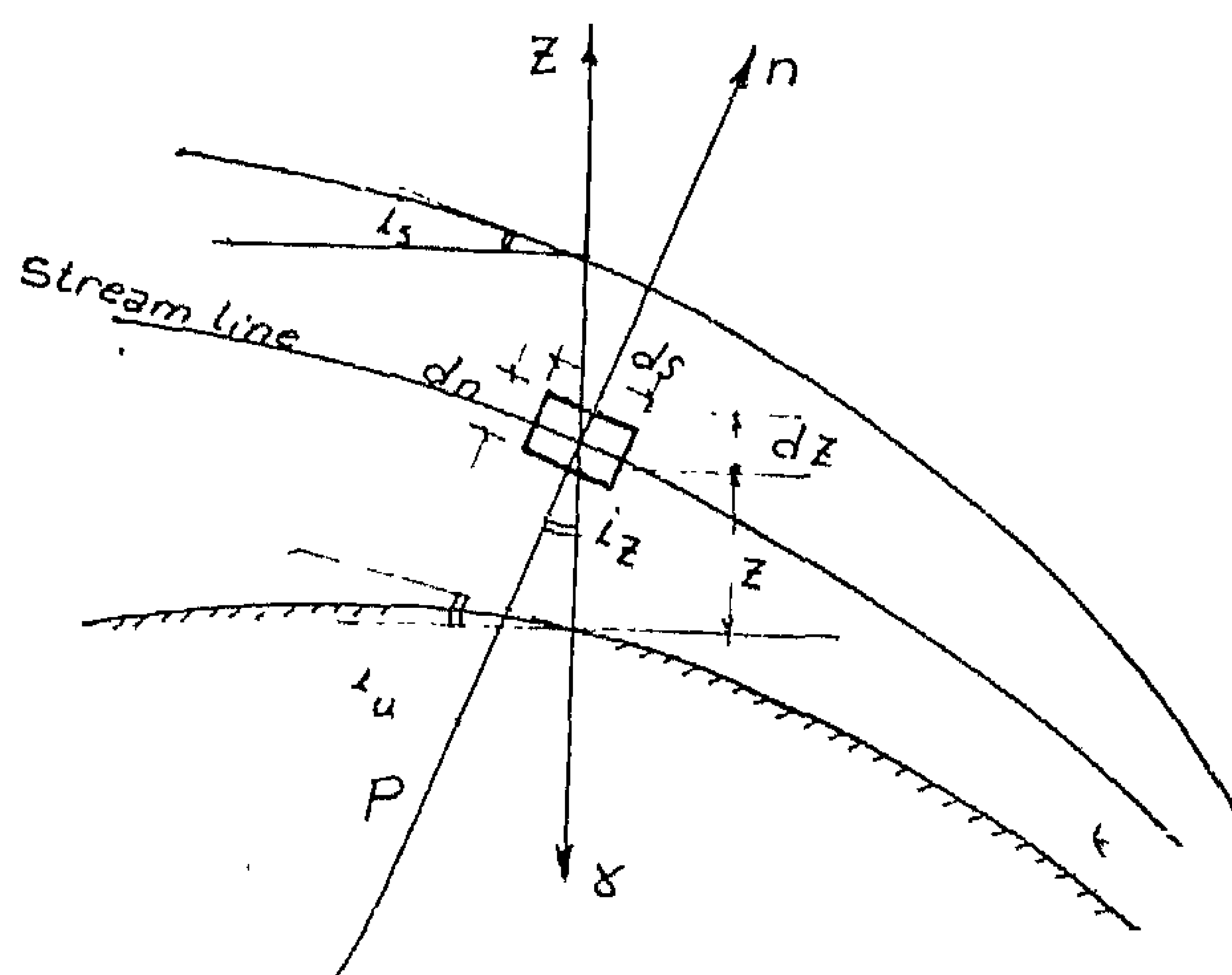
where V_{mR} = mean velocity in the direction of flow
Φ_{mR} = the direction of V_{mR} with respect to the horizontal
h = depth of water at the sharp edge section
R_w = outer radius of the circular weir.

$$\text{or} \quad Q_R = \frac{V_{mR}}{V_o} V_o \cos \Phi_{mR}\ h.\ (2\ \pi\ R_w) \quad (7)$$

$$\frac{V_{mR}}{V_o} = \frac{\text{mean velocity}}{\text{surface velocity}} = \text{velocity ratio} = \Gamma$$

But as $V_o = \sqrt{2g\ (H - h)} =$

$$\sqrt{2g\ h\ \left(\frac{H}{h} - 1\right)}$$



It was found further that the inclination of the streamline should be introduced in the analysis of the problem together with the curvature.

For the element dn x ds, the radius of the streamline passing through its center = ρ, the value of the change in pressure with the vertical direction can be written as :

$$\frac{dp}{dz} = [- \gamma + \frac{\gamma}{g} \frac{v^2}{g} \cos i_z] - [\frac{\gamma}{g} \frac{dv_s}{dt} \sin i_z]$$

The first term includes the effect of curvature while the second represents the effect of inclination.

i_z is the inclination of any streamline passing through a point at a height z from the bed at a verticall section.

$$i_z = i_u + (i_s - i_u) \frac{z}{h} \qquad \ldots\ldots \quad (2)$$

i_u is the bed inclination

i_s is the water surface inclination

$\frac{dp}{dz}$ is the pressure change with the distance z and γ is the specific weight.

Various cases of bed inclination were considered beside the inclination of water surface. It can be concluded that ;

$$V_{zt} = V_{zc} \pm V_{zi} \qquad \ldots\ldots \quad (3)$$

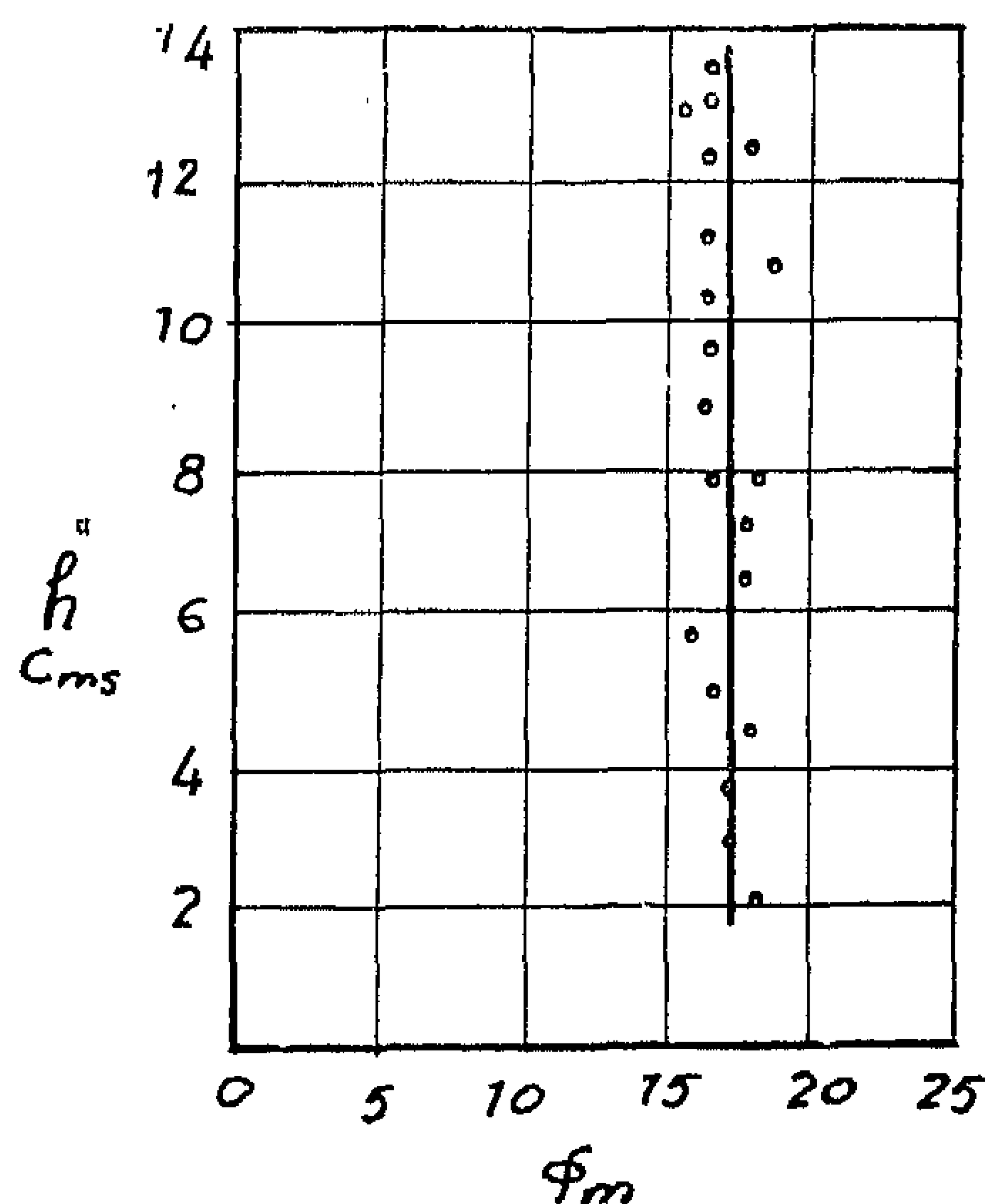
where V_{zt} is the total velocity at any point, V_{zc} is the velocity at the point for pure curvature which was given by $V_{zc} = V_u e^{-B}$ where :

$$B = Z [\frac{1}{R_u} + (\frac{1}{R_s} - \frac{1}{R_u}) \frac{Z^n}{h^n (n+1)}] \qquad (4)$$

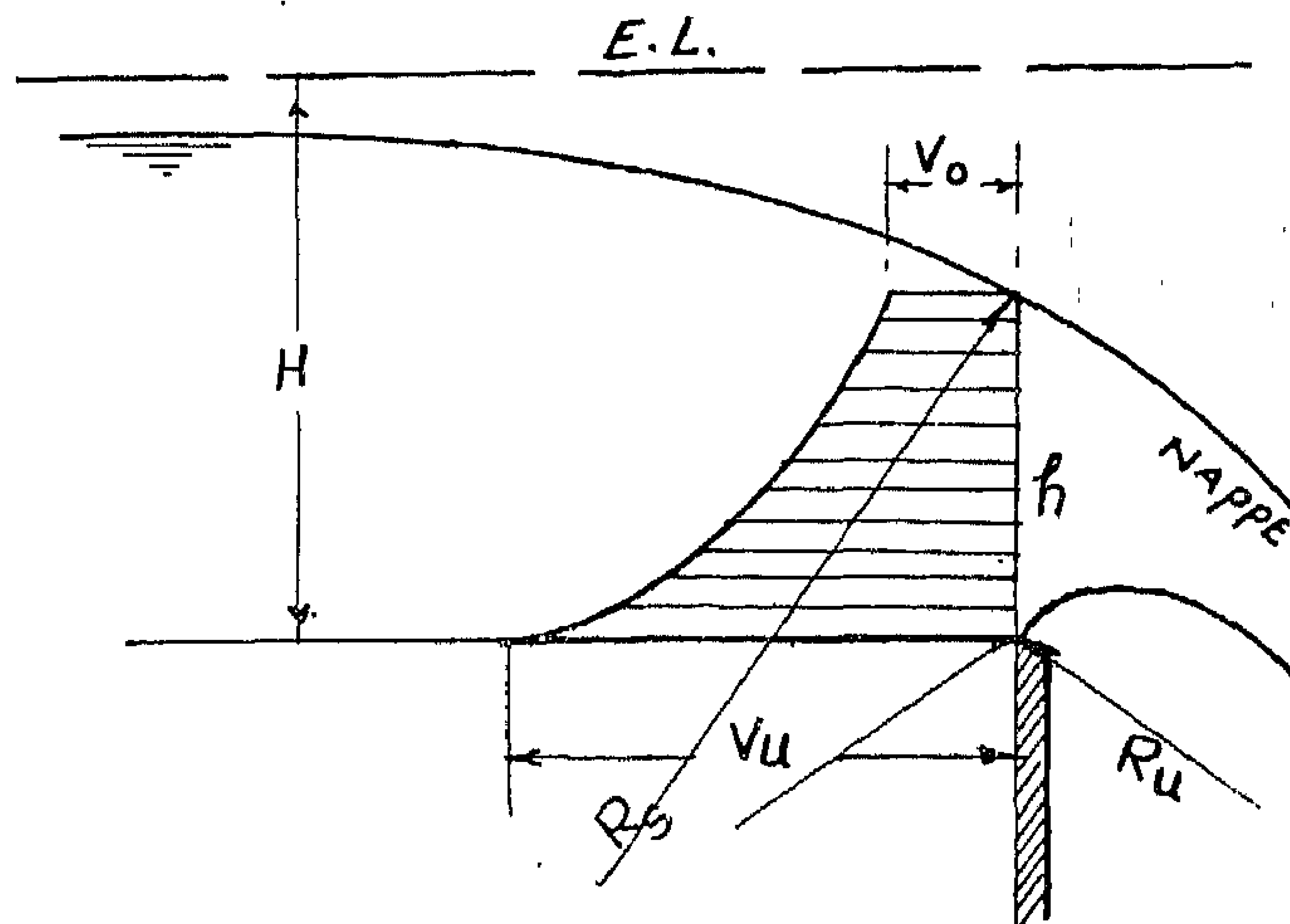
and V_{zi} is the velocity at the point due to the effect of inclination of the tangents at that point, this velocity is given by :

$$V_{zi} = \sqrt{V_o^2 + 2 g (\frac{\Delta P}{\gamma})_{zi}}$$

where R_u = raduis of curvature of the bed
R_s = raduis of curvature of the water surface



(a)



(b)

RAPIDLY VARIED FLOW OVER HYDRAULIC STRUCTURES

By

Dr. M.S. ABDALLAH, M.Sc., Ph.D., M.A.S.C.E.
Dr. M.M. ABOU-SEIDA, M.Sc., Ph.D., A.M.A.S.C.E.
Dr. M.A. SOLIMAN, M.Sc., Ph.D.

INTRODUCTION

The importance of the study the hydrodynamic behaviour of rapidly varied flow over spillways for storage and detention dams and over tail escapes for canals and drains can not be over-emphasized; many failure of dams have been caused by improperly designed spillways or by spillways of insufficient capacity. This paper attempts to introduce the work done at the hydraulic laboratory of Cairo University pretaining to the phenomenon of curvilinear flow over straight and curved water structures. An analytical and experimental study is introduced to provide the designer of all tools for complete understanding of this type of flow. The program of the study covers the phenomena of curvilinear flow over hydraulic structures of circular shapes (in plan) and polygonal types as sharp edged equilateral triangle, square, and hexagon weirs. The work was extended further to cover the case of three dimensional curvilinear flow over sharp edged weirs in which the crest (in plan), follow the shape of circular arcs, or parabolic arcs.

For all the types mentioned ; an attempt was tried to explain the behaviour of the flow in each case in order to provide the designer with design curves which enable him to get the best results from his structure.

GENERAL CONSIDERATIONS

Rapidly varied flow has very pronounced curvature of stream lines. In this case the pressure distribution cannot be assumed to be hydrostatic. The stream lines may be concave or convex and the centrifugal forces caused by the curvature of streamlines will act either in direction of gravity in concave flow, or opposite to it in convex flow. The resulting pressure will be more in the concave flow and less in the convex flow. Since the total energy is constant for each profile of flow, a decrease in pressure head means an increase in velocity head and vice versa.

Many theories and methods of analysis for rapidly varied flow were developed. Despite such developments, a satisfactory general solution of this type of problem has not yet obtained.

Therefore, the various phenomena of rapidly varied flow were regarded as a number of isolated cases.

In the following, typical problems of this flow will be introduced and the physical aspects of the flow will be interpreted according to the principles of energy, momentum, geometry and also by dimensional analysis.

A. *Velocity and pressure distribution in a curved streamline flow :*

Some authors gave theoretical relations between curvature of the streamlines and the velocity distribution in vertical sections. The velocity v in the direction of flow at any point on a vertical section can be written as :

$$v = v_0 \, e \int \frac{dn}{\rho} \qquad (1)$$

where v_0 = velocity of flow at the surface at the same section, ρ = raduis of curvature of the streamline passing through the center of the element dn (Fig. 1).

ACKNOWLEDGEMENT

This post-doctoral research work was conducted at the Department of Civil and Structural Engineering, Sheffield University, Sheffield, England and the author wishes to thank Professor W. Eastwood head of that department for his encouragement and constant interest.

REFERENCES

1. Eastwood W. Wood A.A. Welded Joints in tubular structures involving rectangular sections. Proceedings of the conference on joint in structures, University of Sheffield. July 1970.
2. Shinouda M.R., Stiffened tubular joints. Thesis submitted to the University of Sheffield, June 1967. Communicated privately to C.I.D.E.C.T.



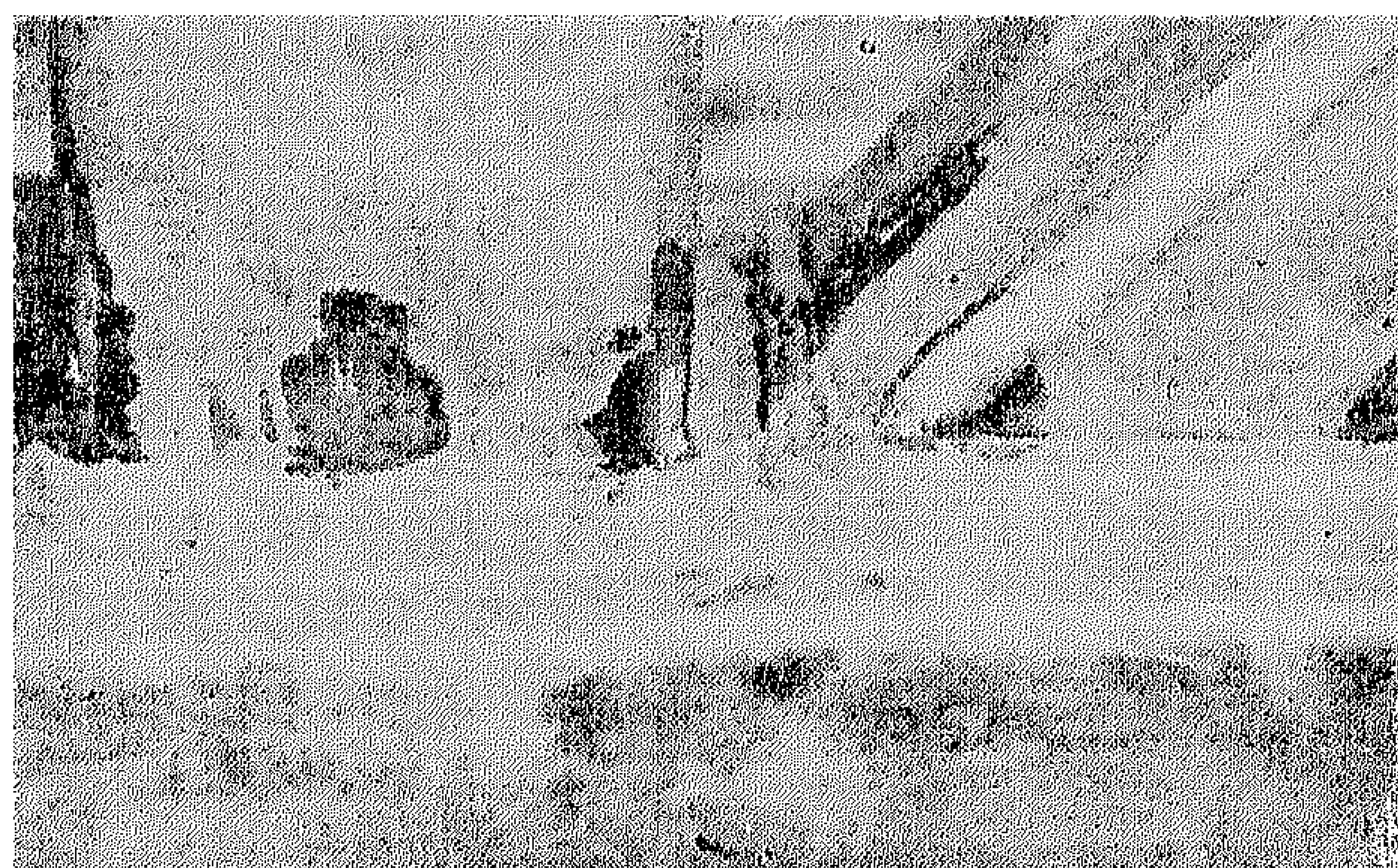


Fig. No. 1

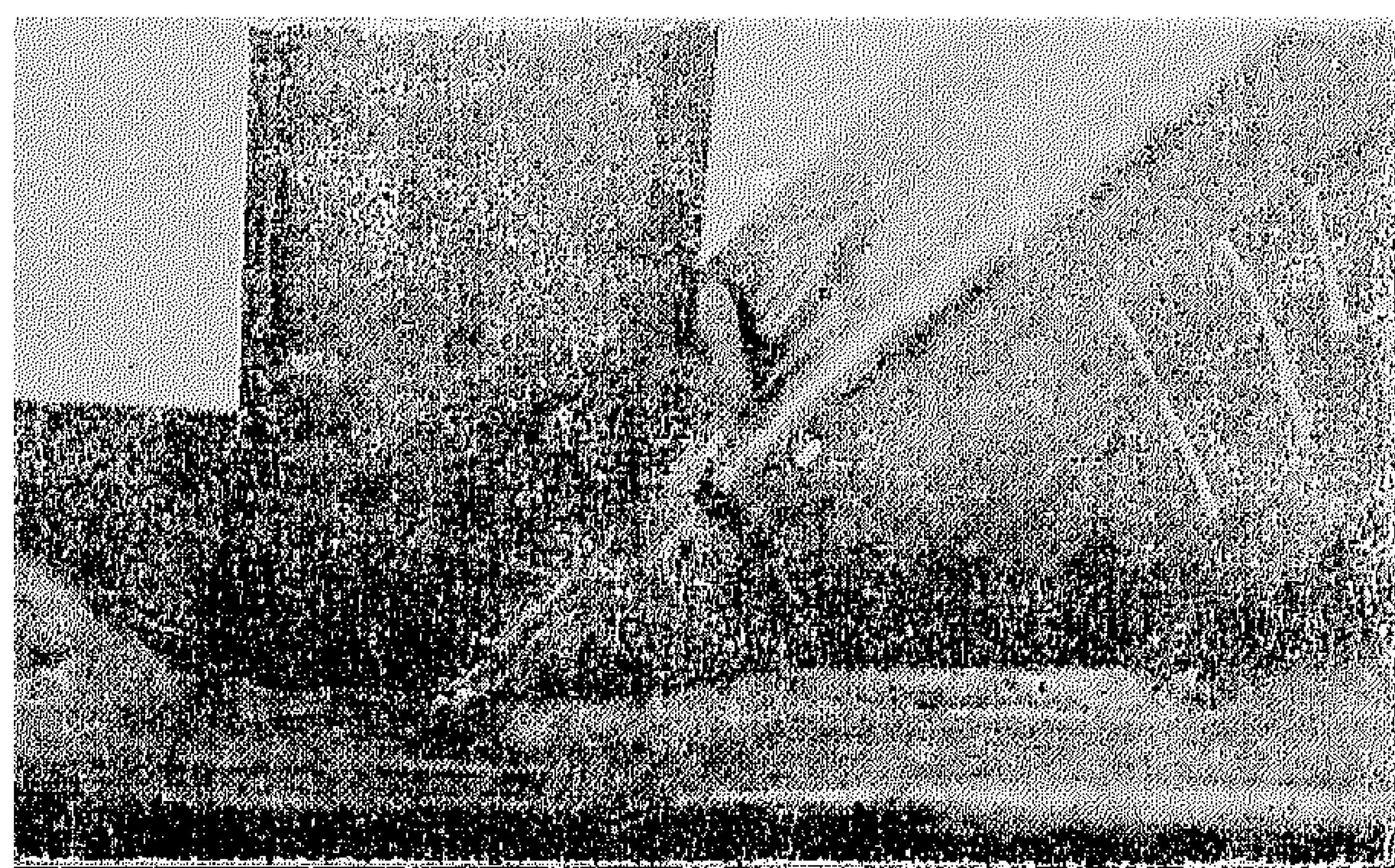


Fig. No. 2

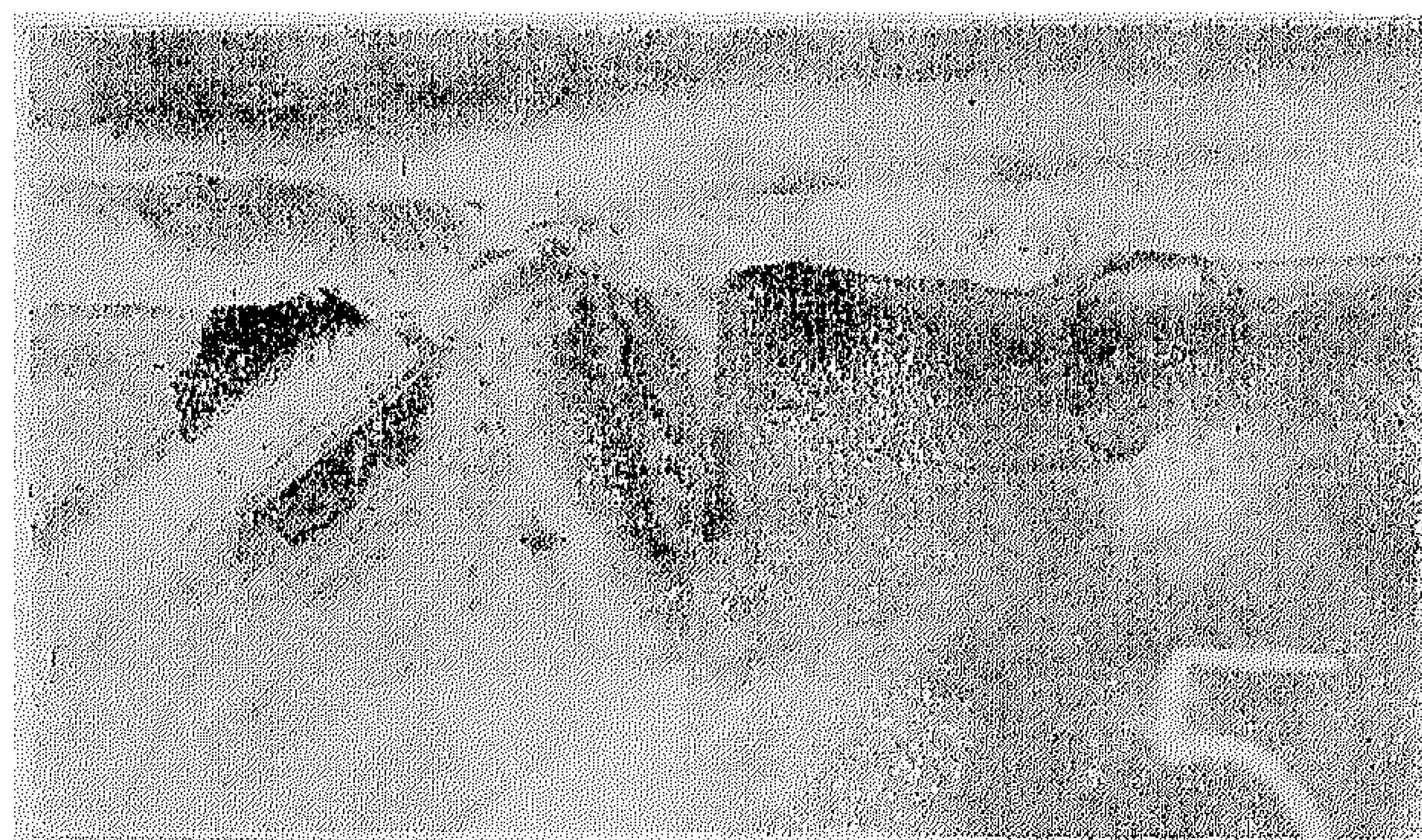


Fig. No. 5

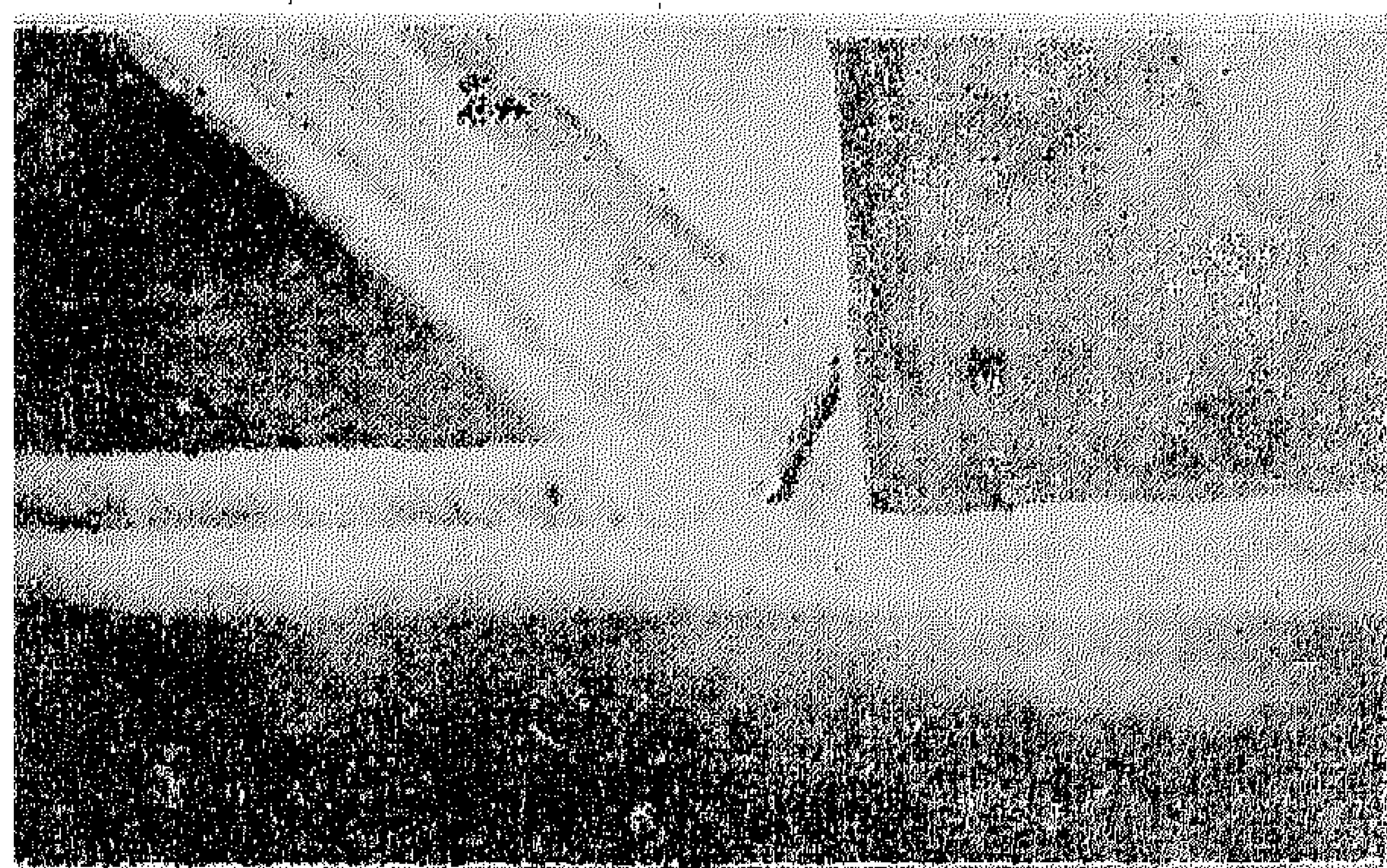


Fig. No. 3

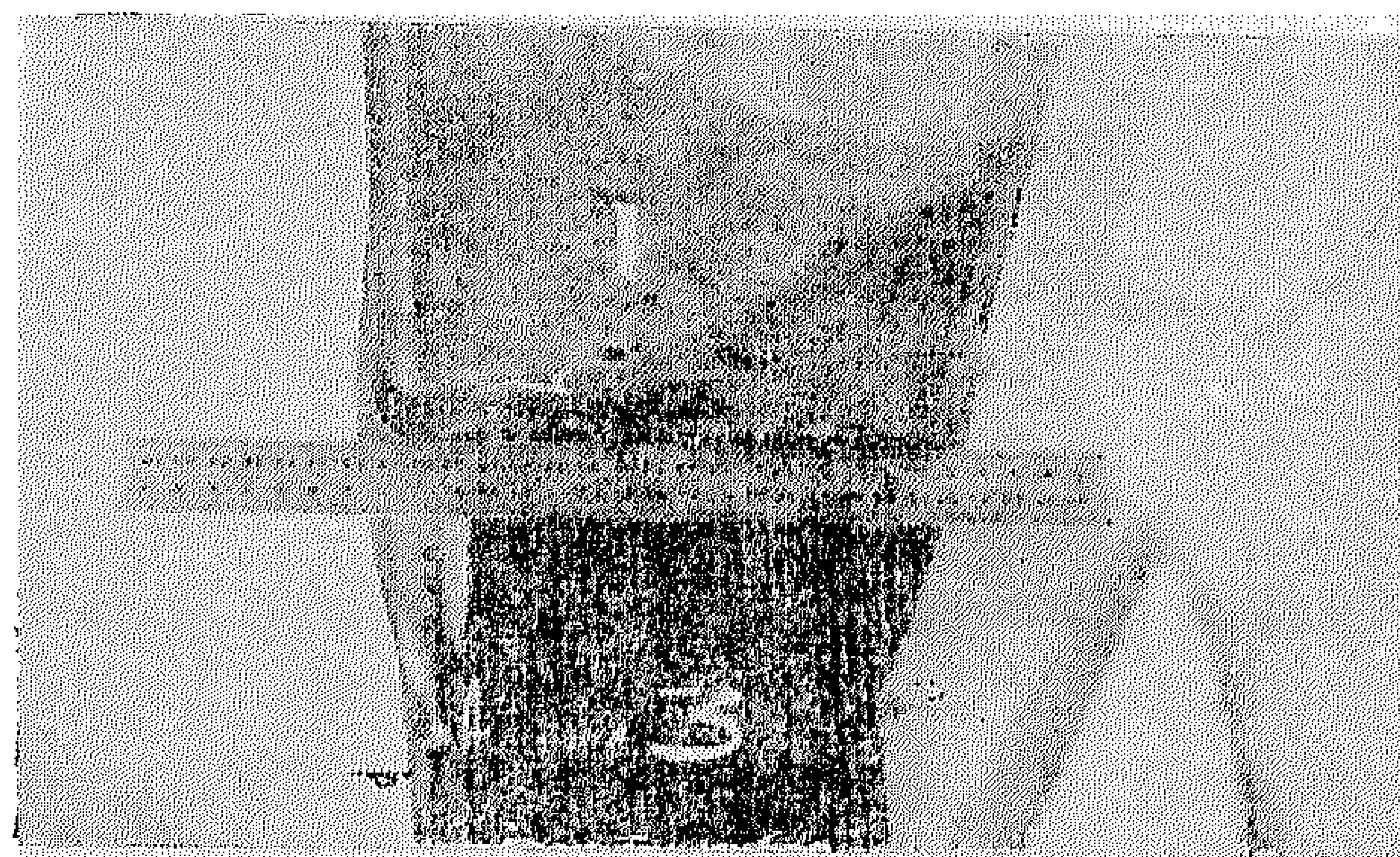


Fig. No. 6

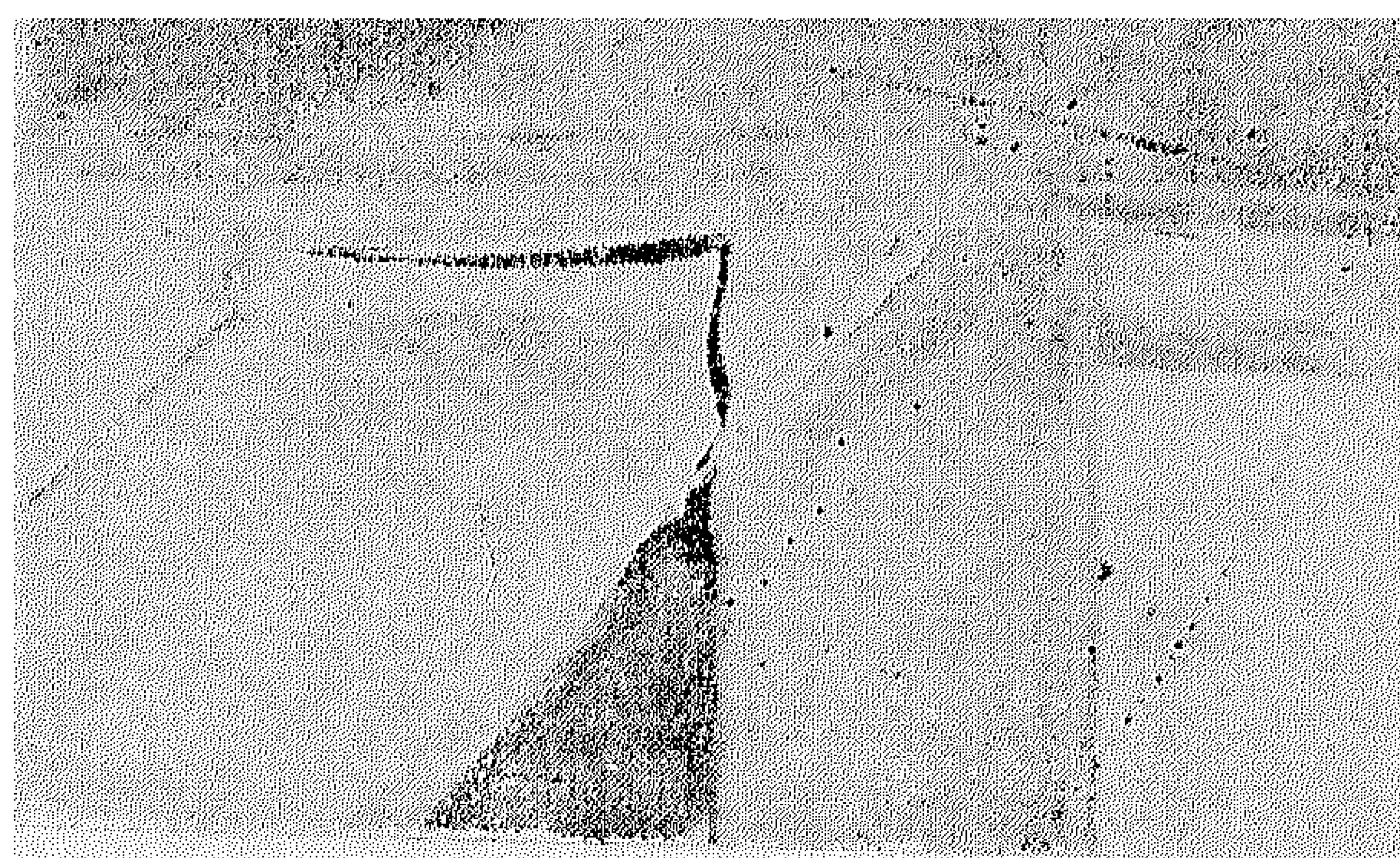


Fig. No. 4

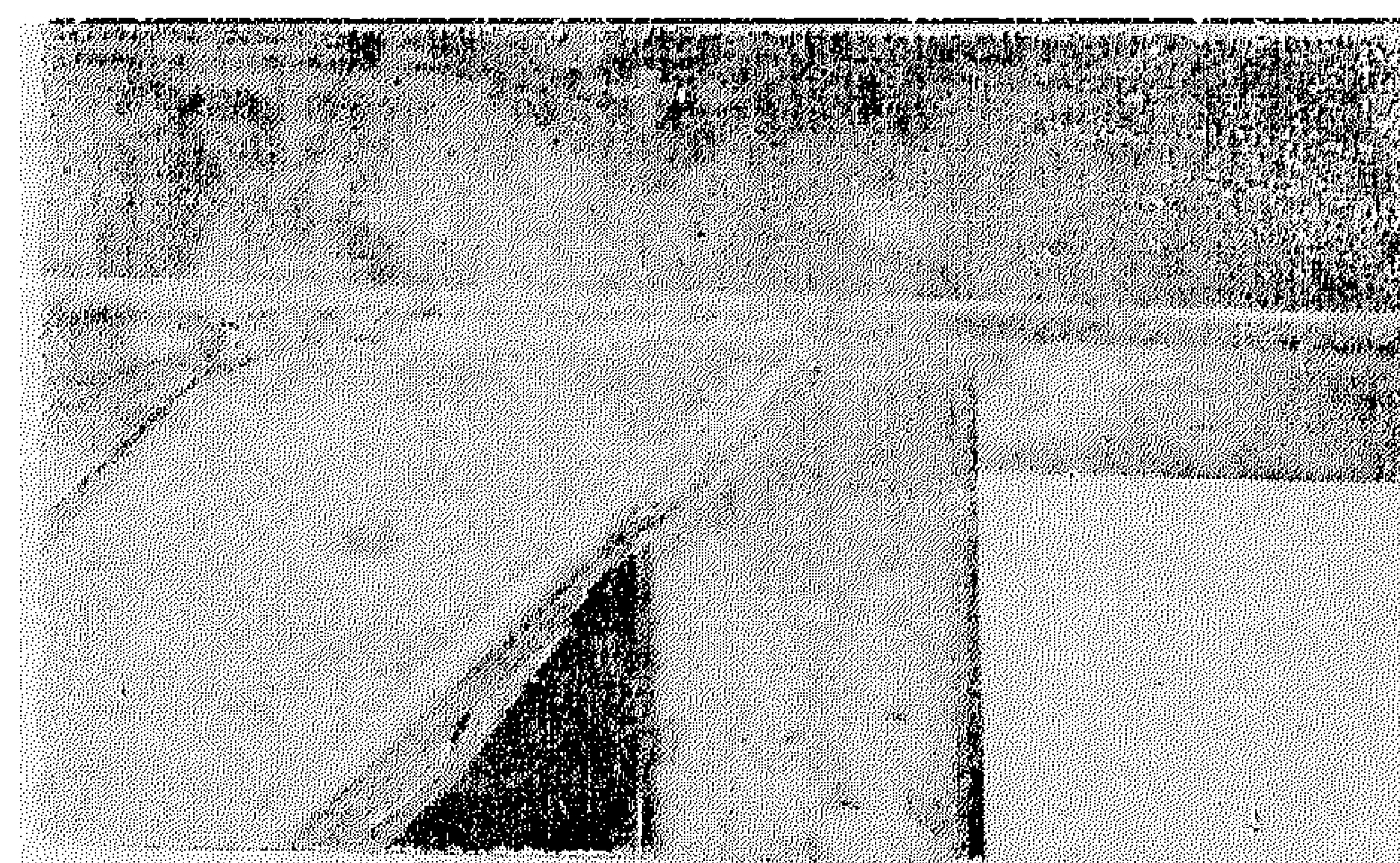


Fig. No. 7

critical positions were always at the middle of the two walls facing each other in the inner angle between the branch members. The compression member trying to push the chord wall inwards under its load is automatically pulling the toe of the tension member causing severe tensile stresses at this location endangering the welds.

The ratio between the strains at these particular locations and the average strains in the members is shown for various specimens in Table 3 recorded at working load. In the same table the loads at which yield occurred in tension and compression member are also indicated.

It will be seen that in general these yields were reached at well below the nominal working load of the member concerned. Fig. 6 shows a typical set of curves for strains in one specimen, namely 8 G, as an example. Negligible strains or even strains of opposite sense occurred in the branch members at their external aides.

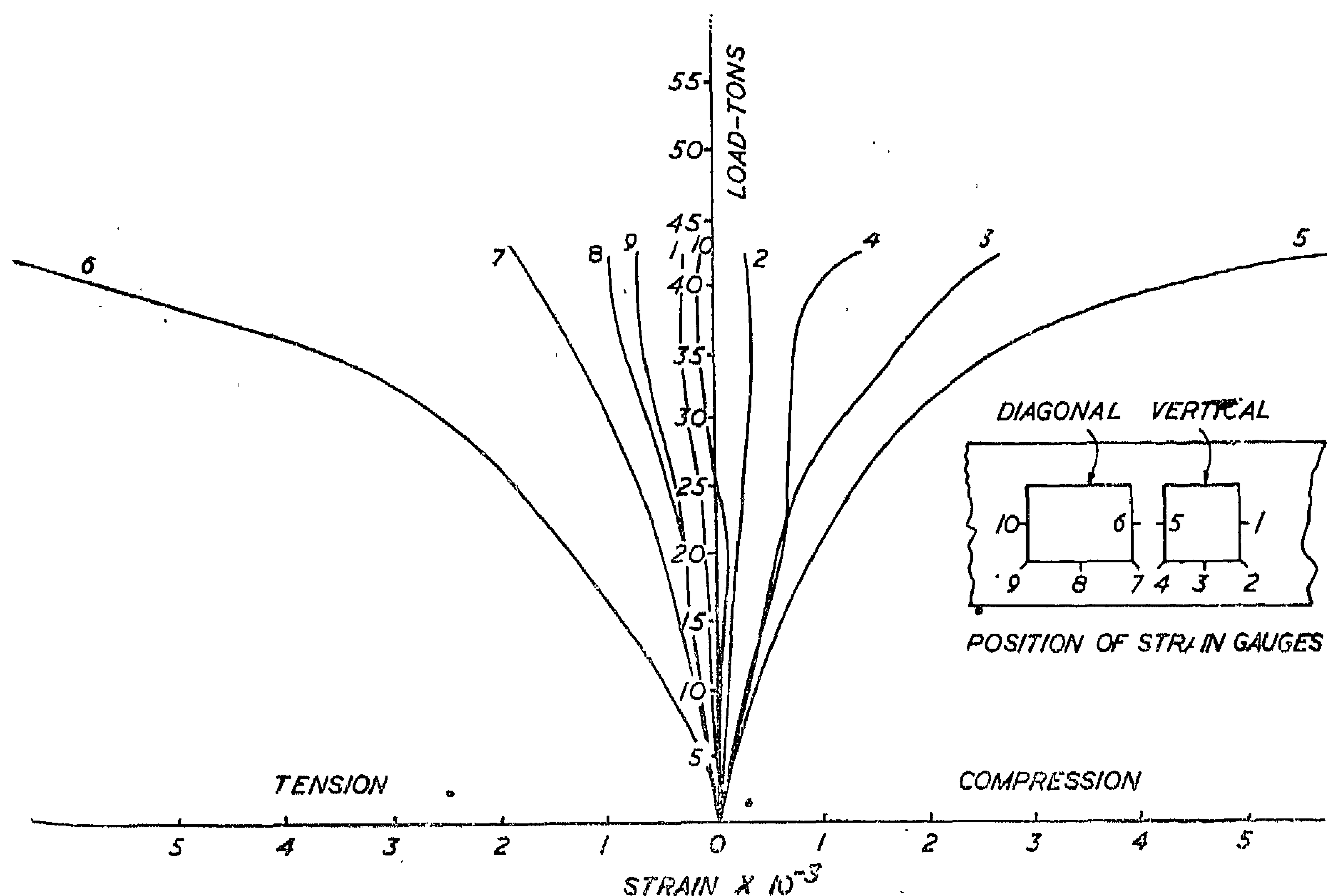


FIG. 6 LOAD-STRAIN CURVES FOR SPECIMEN 8G

CONCLUSIONS

It is clear, from the results of this investigation, that the gap joints can be dangerous specially with low ratios of branch to chord widths. It is recommended that, to obtain better behaviour of joints, web members have to be overlapping. If the overlapping is not desirable because of the eccentricity which it can produce or the more difficult cutting and welding specially where round members are used, then the joint has to be reinforced artificially as has been used before in hot formed joints[2].

The relatively low ductility of cold formed tubes compared to hot formed ones may be the cause of cracking in the welds in almost all the tested specimens. since strem concentrations are not relieved by plastic flow.

More test programmes are needed to investigate more parameters and to help in putting design rules for this sort of contruction.

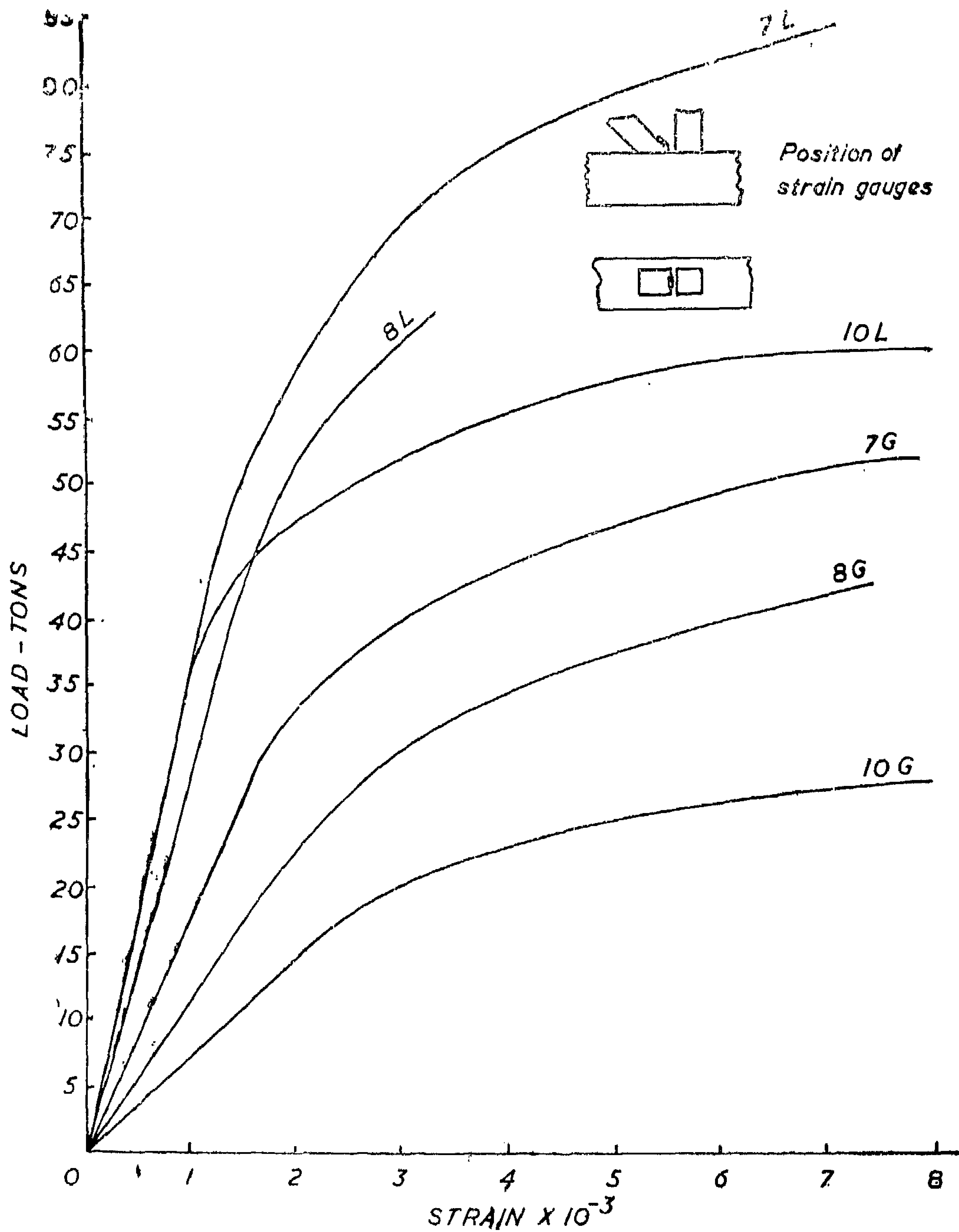


FIG. STRAINS IN THE TENSION WEB MEMBER

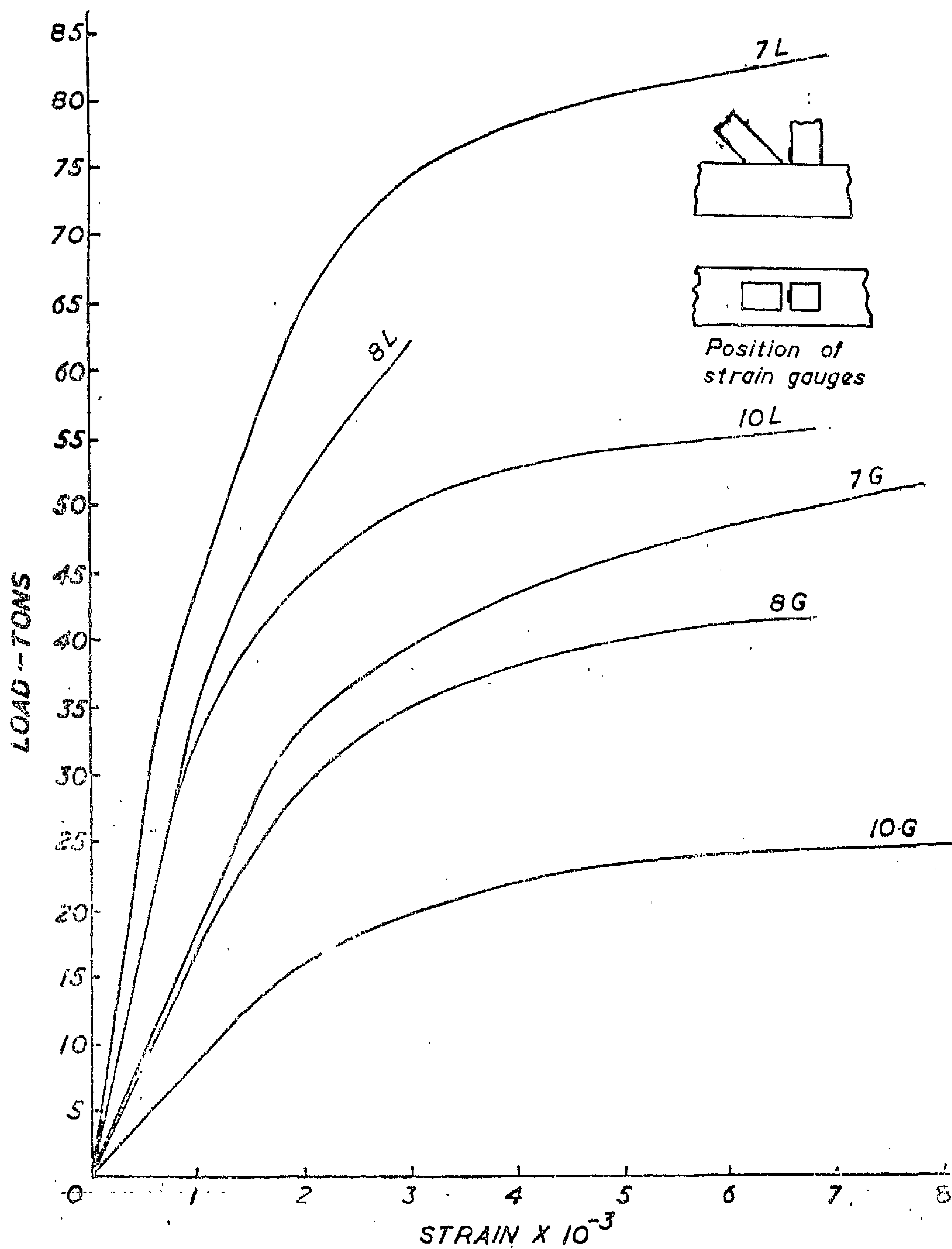


FIG. 4. STRAINS IN THE COMPRESSION WEB MEMBER

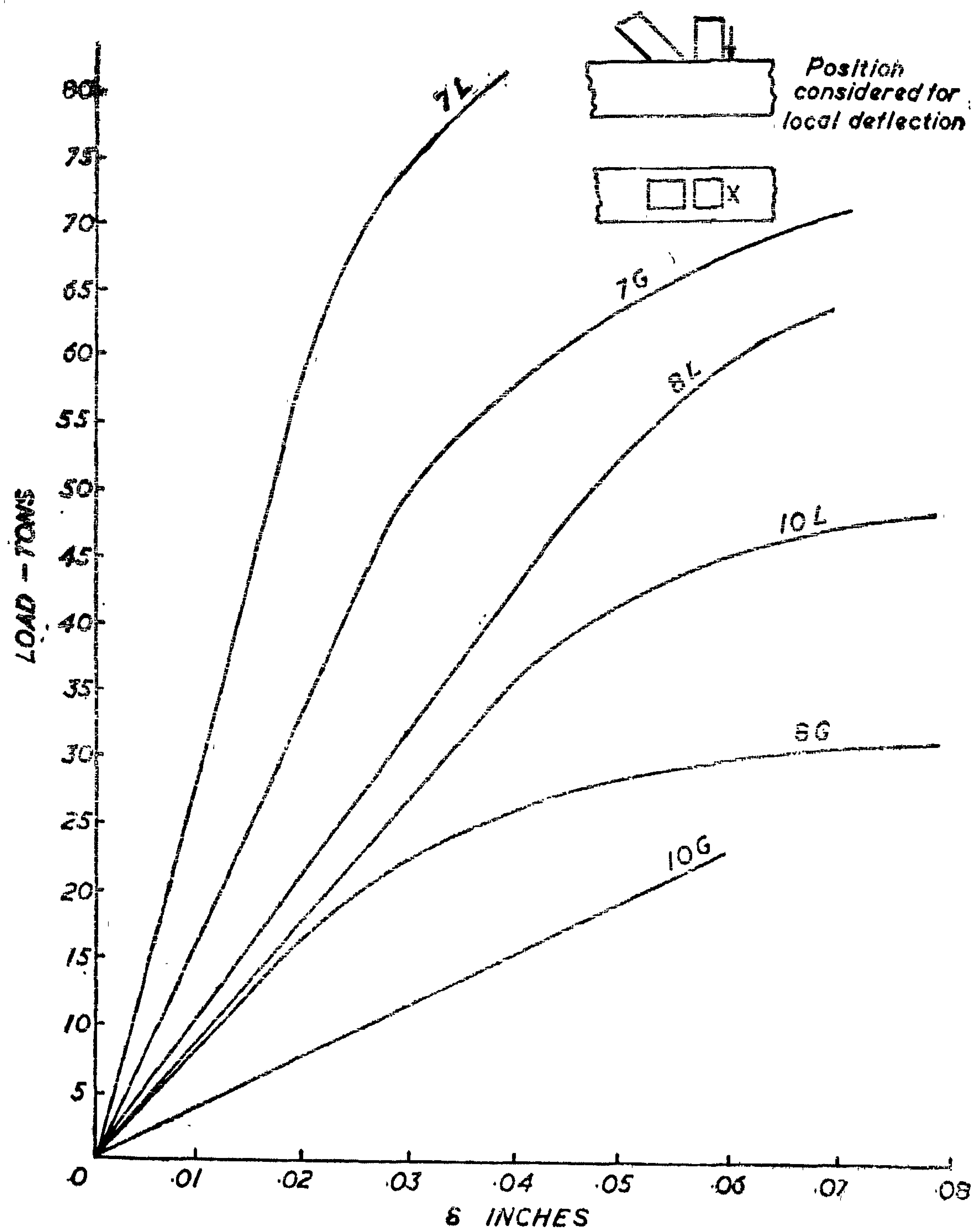


FIG. 3 LOCAL DEFLECTIONS δ

ed across the width of the chord member at the toe of the diagonal member.

In lap joints the initial crack extended to walls of the diagonal member themselves and some sort of tearing of the diagonal member occurred. Photo. 1-7 inclusive illustrate the form of cracking and the modes of failure for various specimens : local deformations can also be seen for the gap joints as in Photo. 6 for the specimen involving 7″ wide chord member.

3. *Deflections :*

Fig. 2 shows the overall deflection curves for various specimens. This deflection indicates the degree of flexibility of the joint as a whole and when the curves deviate from linearity it is an indication that some part of the joint has started yielding. It can be seen that when the ratio of branch to chord widths increased higher limits of proportionality were observed. Table 2 indicates the proportional limit in absolute value and also in a non-dimensional value related to the working load of the branch member. Specimen 7 L showed linear behaviour up to a load exceeding its working load.

Local deflections (δ) were quite visible for specimens with low ratios of branch to boom widths at working load:

The gap joints showed apparent wall flexibility. The 10 G specimen had already failed at working load but for the 8 G the local deflections were too excessive and for the specimen 7 G the local deflection was nearly 0.5% of the chord width. Fig. 3 shows the curves of local deflections and in Table 2 their values at working loads are indicated.

Table 2
Deflections of Specimens

Specimen	Prop. limit		Local deflection at W. Ld. /h
	Absol.	*Relative*	
10 G	20T	0.370	Already failed
10 L	48	0.889	0.110 $\frac{1}{90}$
8 G	36	0.667	Excessive
8 L	52	0.963	0.053 $\frac{1}{150}$
7 G	52	0.963	0.036 $\frac{1}{195}$
7 L	72	1.333	0.017 $\frac{1}{412}$

Strains :

Load strain curves are shown in Fig. 4 and Fig. 5 for the critical positions in tension and compression members respectively. These

Table 3
Critical Strains in Branch Members

Specimen	Strain factor at W. Ld.		Load at yield of vert.		Load at yield of diag.	
	Vert.	*Diag.*	*Absol.*	*Relative*	*Absol.*	*Relative*
10 G	already failed		13T	0.241	11T	0.204
10 L	5.5	8.5	40	0.741	44	0.815
8 G	excessive		24	0.444	17	0.315
8 L	2.2	2.1	45	0.833	42	0.778
7 G	exec-sive	8.5	27	0.500	27	0.500
7 L	1.5	1.75	56	1.037	50	0.926

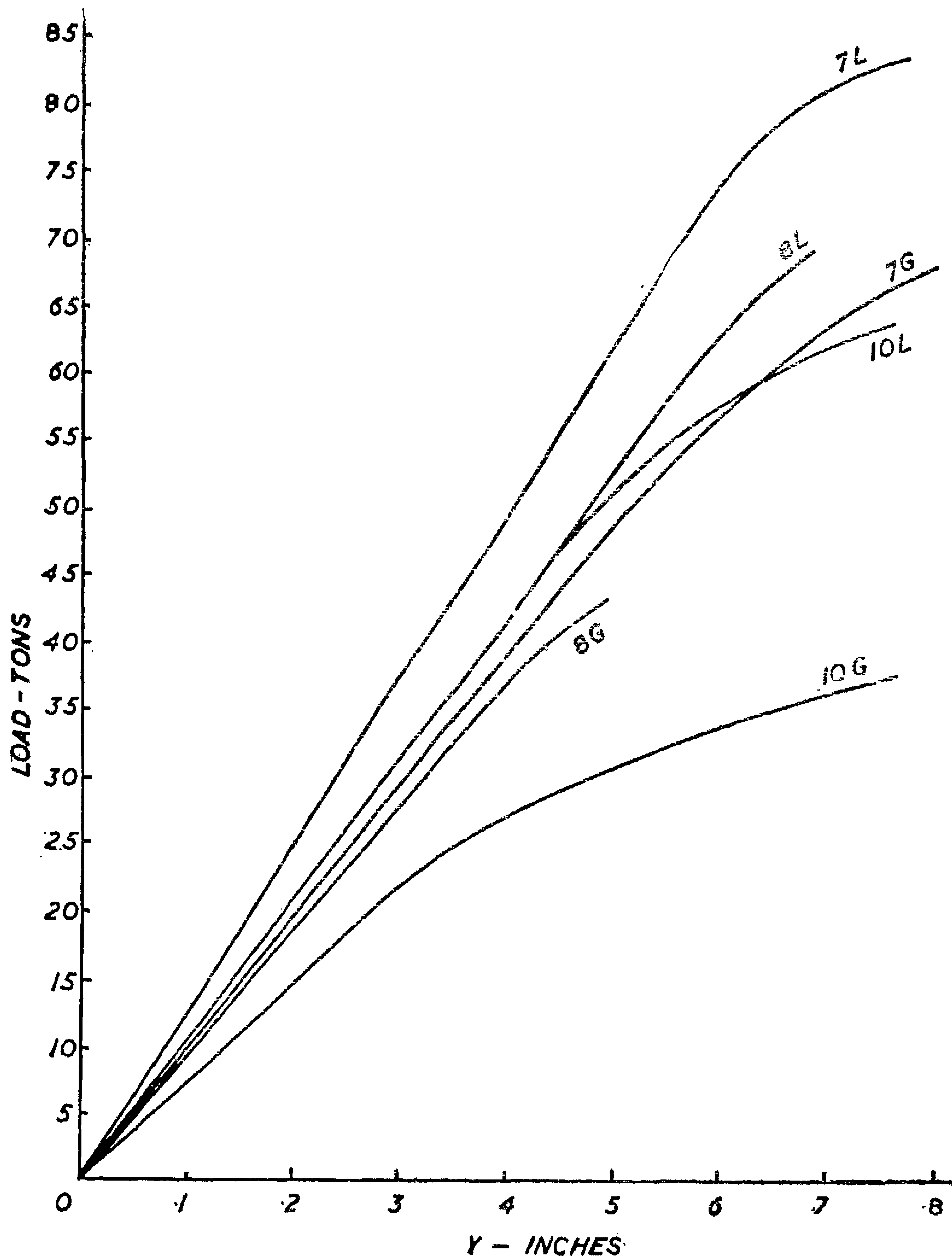


FIG. 2, OVERALL DEFLECTION Y

5. Investigated Parameters :

It was found from previous work that there are two significant parameters which control the strength of the joint and represent its geometry. These parameters are the rates of the chord wall thickness to its width $\frac{t_t}{h}$, and the ratio of the mean branch diameter to the chord width $\frac{d_1 + d_2}{2h}$. In this work it was not intended to study the effect of the first parameter. The second parameter which is investigated had the values of .786, .687 and .550 for the 7″, 8″ and 10″ boom widths respectively. It has already been mentioned that the comparison between the behaviour of gap and lap joints is also a main object of this work and is considered as an impotant parameter in the joint.

TEST RESULTS

1. Ultimate Load :

Table 1 shows a summary of the results. The sizes of members, the values of parameters, the failure load and the mode of failure are indicated. The load factor which appears in this table is the ratio between the load in the diagonal member at failure and its working load. The diagonal member was chosen for this purpose because in each case the failure was associated with this member and secondly, the working load in it is not a function of the effecttive length and is therefore less arbitrary. It is noted that the specimen with the 7″ × 7″ boom member and overlapping web memers did not fail at the limit capacity of the testing machine. At this limit the load factor of the joint was quite satisfactory and the shape of the specimen (photo. 7) did not show excessive distortion.

It is seen from table 1 that the load factor was considerably better for the lap joints, in each case, compared with those with weld gaps. This is because the loads in the case of lap joints are transferred from one web member to the other without affecting the chord wall.

The better performance of the joints with a high ratio of web width to chord member width is very remarkable. This is also typical of the results which were obtained on hot formed joints. This is because of the extra support afforded to the side walls of the web members by the side faces of the chord. Considering the first joints involving the 10″ wide chord member, it will be seen that in the gap joint failure occurred by fracture of the tension welds at a load only approximately three quarters of the working load of the member. This form of joint must clearly be regarded as highly dangerous. With the same member sizes the lap joint gave a load factor of 1.302 which can still be considered unacceptable for design purposes.

With the 8″ wide chord members the load factors were rather better but still unacceptable for the gap. joint.

With the 7″ wide chord members the results can be considered satisfactory specially with the lap joint when a reasonable factor of safety is required.

It is clear that the thickness of the chord wall has a major and a decisive effect on the load factor but, in the present range of test specimens this effect has not been investigated as was mentioned before.

2. Modes of Failure :

It can be seen that in every case final failure occurred by cracking or tearing at either the welds or a combination of the welds and the diagonal tension member wall. In gap joints specially with wider chord members, a considerable amount of local deformation occurred and in all specimens the crack extend-

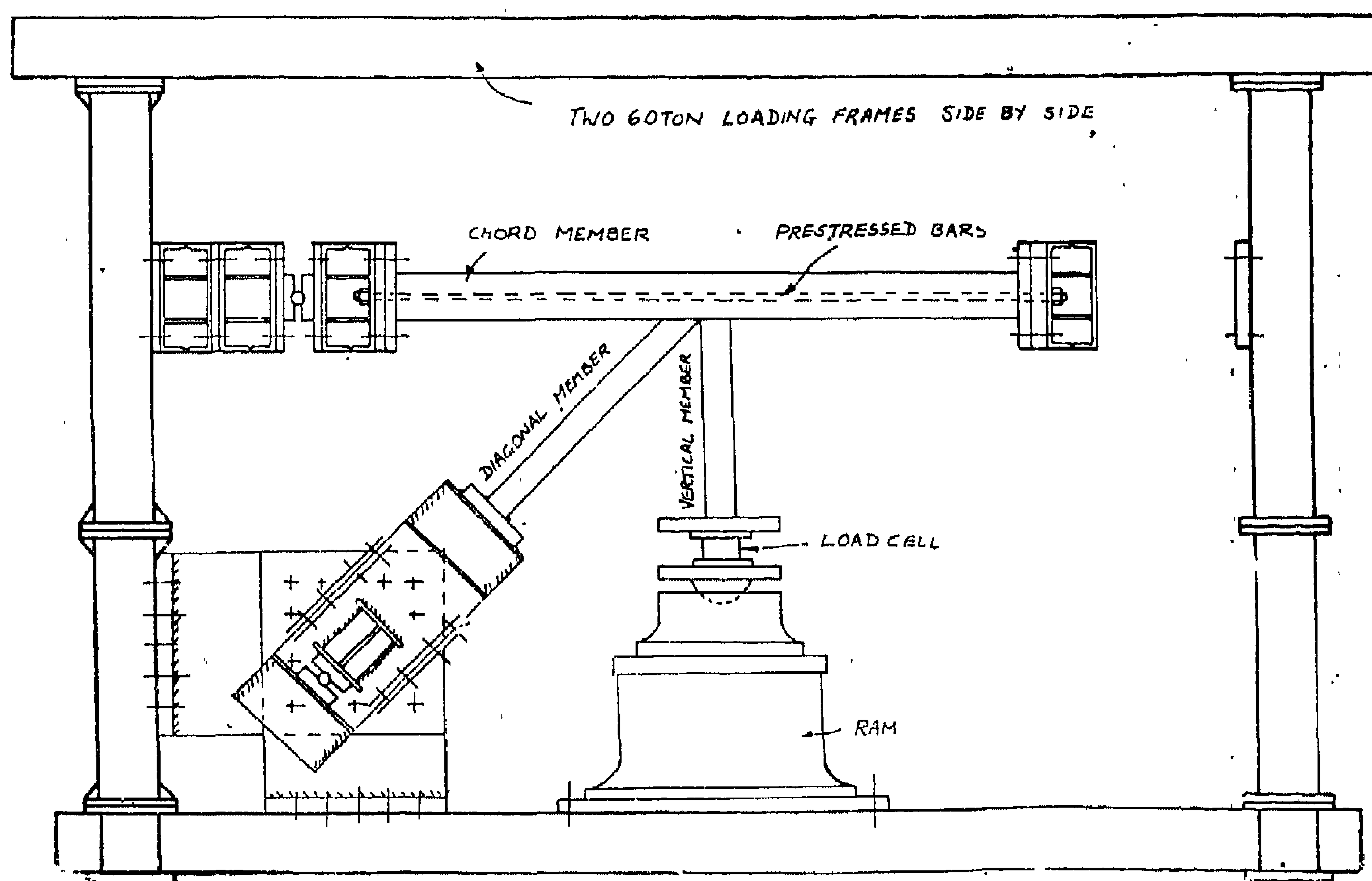
Table 1 Summary of Test Results

Joint	*Size and Working Load*			$\frac{d_1 + d_2}{2\,h}$	*Prestr. Force (Tons)*	*Ult. Load (Tons)*	*Load Factor*	*Made of Failure*
	Chord	*Vertical*	*Diagonal*					
10 G 10 × 10 × .25 120T	5 × 5 × 25 61T	6 × 6 × .39 76T		0.55	58.6T	41	0.674	Excessive deformations in the chord wall followed finally by crack between the welds and diagonal branch wall.
10 L	ditto	ditto	ditto	ditto	ditto	70	1.302	The welds cracked at the two corners of web members intersection and the crack propagated in the two side walls of the diagonal.
8 G 8 × 8 × .312 123T	ditto	ditto	ditto	0.69	62T	60	1.116	Deformations in the chord wall followed by a crack between the welds and the chord wall across its width.
8 L	ditto	ditto	ditto	ditto	ditto	84	1.563	Crack in the weld at one corner of web members intersection followed by tearing of the diagonal member wall across its width.
7 G 7 × 7 × .312	ditto	ditto	ditto	0.79	46T	77	1.43	Crack between the welds and the chord wall across the width of the chord.
7 L	ditto	ditto	ditto	ditto	ditto	over 95	over 1.767	The joint was so strong that it did not fail at the maximum capacity of the loading rig (95T). Littlel deformation.

All the joints were fabricated by 'full strength' welds which were intended to develop the full carrying capacity of the web members.

3. Loading Frame and Test Procedure :

The specimens were tested in a loading frame shown in Fig. 1. The ends of the diagonal member and of the chord member nearer to it were pin jointed to the frame, while the other and of the chord member was left free. The effect of leaving this end free rathei than supporting it was found from other tests[2] insignificant but it helped to remove beam action from developing in the boom. As it is a practical and economical design to get the working stress simultaneously in the chord and web members, it was necessary to prestress the chord member with a load the value of which is equal to the difference between its working load and the working load of the vertical member. This meant that when the load applied from the testing machine to the



vertical member was equal to its working load, the force existing in the part of the chord member nearer to the diagonal member was also equal to its working load. The working loads of the compression members were based on the assumption of 6 ft. effective length.

4. Instrumentation :

The specimens were instrumented with strain gauges, the number of which was about 12 gauges on each specimen. More gauges were put on the gap joints than in the lap ones because of the expected larger deformations. The strain gauges were of the type — PL 10—11 Tokyo Sokki Kenkyofo Co. Ltd. and were put on the tube walls as near to the welds as possible. As the load was applied to the vertical member, the movement of its end was recorded and it is called the overall deflection. Also two dial gauges were used to measure the local deformation in the chord wall adjacent to the joint, one at the middle and the other one at the edge of the face, both of them located at one transverse section. A calibrated load cell was used to read the applied to the vertical member.

AN INVESTIGATION OF THE STRENGTH OF COLD FORMED TUBULAR JOINTS

By

Dr. MAGDY R. SHINOUDA
Lecturer, Faculty of Engineering,
Alexandria University,
Alexandria, U.A.R.

SYNOPSIS

This paper presents an investigation of the strength and behaviour of joints in tubular plane frameworks in which the members are made from cold formed rectangular sections. The joints are of the N shape in which the chord and vertical members are under compression and the diagonal member at 45 degrees is under tension.

Six large size specimens were tested mainly to study the difference in behaviour between the joints with weld gap between the web members and the joints with overlapping web members. The effect of varying the ratio between the widths of branch and boom members is also investigated.

INTRODUCTION

1. *Scope of Work :*

Members of hollow section have now been increasingly used in structures and specially in plane frameworks. The behaviour of joints in these tubular frameworks is completely different from that in ordinary steelwork involving rolled sections. Some investigations(1) have been made into the strength and behaviour of these tubular joints when the members are of hot formed tubes but there is an evident lack of information about similar joints with cold formed members. It is the aim of this research to study the behaviour of such joints and their ultimate strength. For this purpose the same geometrical parameters which proved to be significant in the behaviour of hot formed tubular joints will be used in this investigation.

2. *Sizes and Manufacture of Specimen :*

Three pairs of specimens were tested and in every case the diagonal and vertical members were 6 × 6 × ¼″ respectively. The chord member consisted of 10 × 10 × ¼″ for the first pair, 8 × 8 × 9/32″ for the second pair and 7 × 7 × 9/32″ for the third pair of specimens.

In each pair of specimens one joint was constructed with a gap between the web members sufficient to enable adequate independent welds to be made with the chord face. In the other specimen of the pair there was a 50% overlap of the two web members that is the toe of the diagonal lying at the intersection of the vertical member axis with the chord member face.

The length of the members were such that their ends coincide with the mid panel points of a truss with 6 ft. panel length and height. These ends had hinged connections to the loading frame, except one end of the boom, to resemble the points of contraflexure in the actual truss. This assumption, although it is not always correct, is thought to have no significant effect on the test results.

It seems that further investigation of the reliability of the local use of WWVL is needed. This can be carried out by simultaneous reception of WWVL and GBR, and with the help of the reference phase established.

It is actually planned to continue the reception of GBR, to resume the reception of WWVL. and to investigate the possibilities of using Loran—C chain if it will be synchronized in the near future. That will improve the comparison accuracy of frequency standards as well as investigations of propagation, and increase the reliability of data.

REFERENCES

1. Barbar, N.F., Narrow band filter using modulation, Wireless Engineer, Vol. 24, May 1947.
2. Blackband, W.T., Editor, Propagation of radio waves at frequencies below 300 Kc/s, Pergamon Press, 1964.
3. Blair, B., J. Jespersen, G. Kamas, VLF precision timekeeping potential, Commission I, XVI General Assembly of URSI, Canada, 1969.
4. Bureau International de l'Heure, Annual reports, 1967 and 1968.
5. Loutfy el Sayed, A., Comparison of WWVL and the local standard, Proc. of the Math. and Phys. Society, UAR, 1969.
6. National Physical Laboratory, Standard frequency and time signal transmissions, MSF — Rugby.
7. NBS, Frequency and time broadcast services, Special publication 236, 1969 edition.
8. Pierce, J.A., Omega, IEEE Trans. on Aerospace and electronic systems, Vol. AES-1, No. 3, Dec. 1965.
9. Shapiro, L. Dennis, Time synchronization from Loran—C, IEEE Spectrum, Aug. 1968.
10. Thompson, A.M., R.W. Archer, I.K. Harvey, Some observations on VLF standard frequency transmissions as received at Sydney, Special Intern. issue IEEE, Vol. 51, No. 11, 1963.
11. Watt. A.D., VLF radio engineering, Pergamon Press, 1967.

At 16 KHz the spacing of the waveguide walls will be about four wavelengths [Blackband]. For this reason, the waveguide will support not only the first-order mode but a number of other modes of higher order. Because the rate of attenuation of these higher modes is greater than that for the first mode at long distances from the transmitter their amplitude will be negligible compared with that of the first mode. The effective limiting distance for the propagation of the higher mode is not easy to define, but an approximate value of 3800 Km for 16 KHz is given by Blackband.

Some typical diurnal variation curves of GBR's received phase is given in figure 2. All of them are taken in the second half of the month. The path (Rugby — Cairo) is 3612 Km long and the direction of propagation is almost South-East.

It is noted that the day to night change is season-dependent. It is 9, 12 and 25 microseconds in autumn, summer and mid-winter respectively. Two peaks start to appear clearly in October, and are very pronounced in November at sunrise and sunset. These two phenomenas could be due to a seasonal change in the phase of the ionispheric reflection coefficient. Watt noted that the change in the day to night phase velocity caused by height change is partially cancelled out by a change in the phase of the ionospheric reflection coefficient [Watt].

6. CONCLUSIONS :

Three different long-term average deviations, in parts in 10^{12}, of the local standard are given :

1. Nov. 67 — Nov. 1968 : —0.8 Loutfy.
2. Dec. 67 — Dec. 1968 : 4 (table 1).
3. Jan. — Dec. 1969 : —1.2 (table 2).

The first is the deviation of the local from WWVL, and not from A3. correcting that figure for the very small differences between WWVL and A3 will not improve it. This figure does not agree with the second one, but it is very near the third. There is no clear explanation for that.

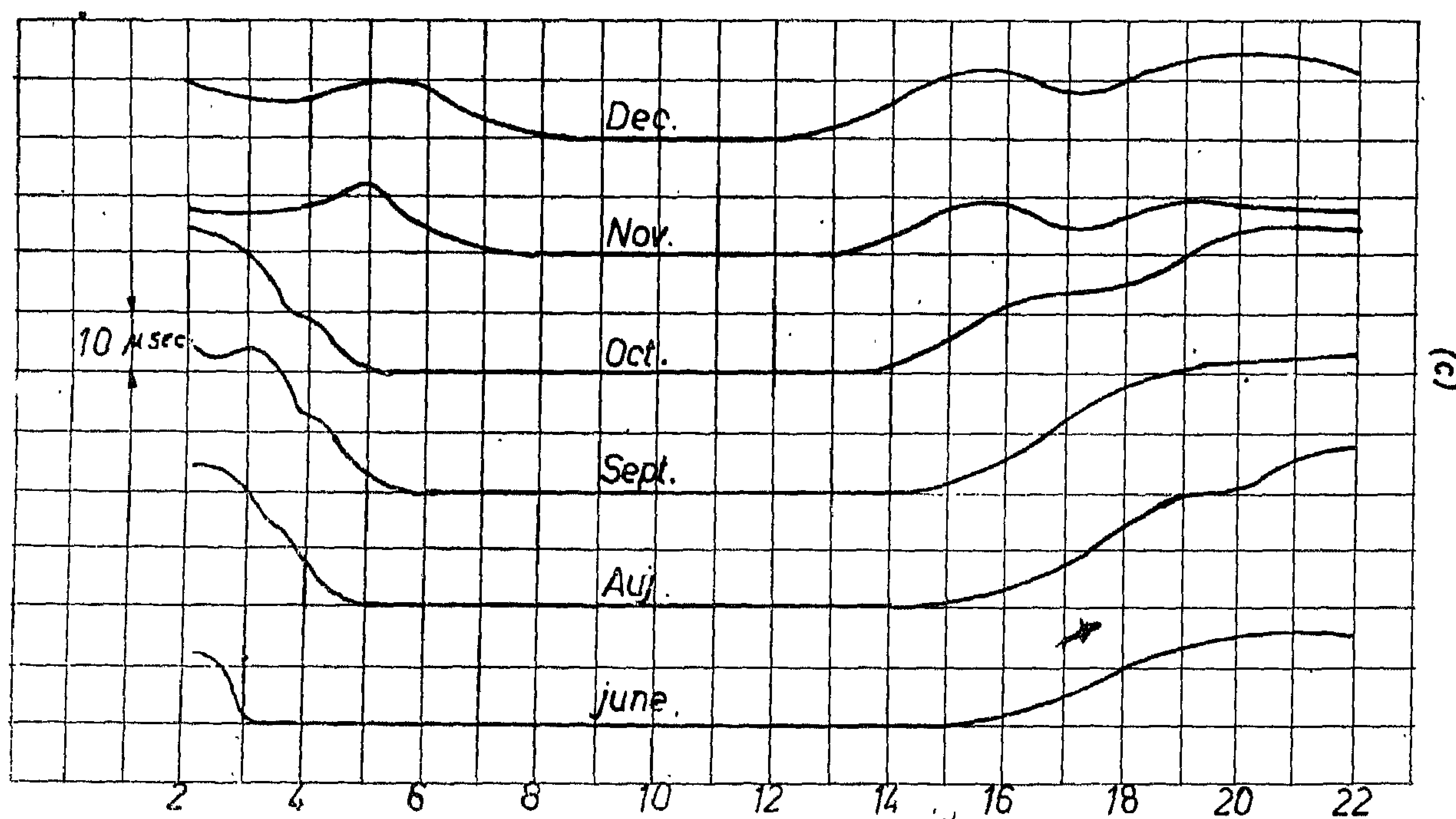


Fig. 2: Typical Diurnal Phase Variation Rugby — Cairo (16 KHZ)

The 16 kHz synthesizer, which is in continuous operation, was introduced lately because of the following. When a phase jump is recorded on the recorders of the two receivers, and not on that of the phase comparison with the quartz oscillator, then it is probably a phase jump in the received signal. But when it is one of the two receivers' recorders only, then it is caused by one of the receivers, and in that cases, the reference phase helps to determine the faulty receiver; Further, the reference phase eliminates the phase changes in the receiving system, especially those originating in the antenna.

4. MEASUREMENTS :

The total period of comparison reported is divided into two :

1. Dec. 67 — Dec. 1968 : During that period, WWVL (20 KHz) was received with a single receiver. The deviation A3-NIS standard is given by the Annual Reports of BIH and is shown in table 1, in parts in 10^{12}. The average deviation being about 4×10^{-12}.
2. Jan. — Dec. 1969 : During that period, GBR 16 KHz was received.

The A3 values are not yet available for the second period, and the deviation is calculated, temporarily, by establishing an approximate average from reports by other laboratories, receiving GBR also, together with our measurements (five values).

Table 2 gives the recorded monthly delay of GBR in microseconds and the deviation of the local standard from the average. During June 1969, the receivers were disturbed by long periods of power break, which resulted into a number of phase jumps. That month was excluded from the comparison.

The average value (of table 2) is about 3 microseconds advance, or in other words, the local standard is higher in frequency by about 1.2 parts in 10^{12}.

5. DIURNAL VARIATION :

Many aspects of the propagation of VLF waves to great distances can be explained conveniently in terms of the waveguide theory of propagation. This considers the space between the earth and the lower part of the ionosphere as a large waveguide in which the waves can propagate. During the night the ionospheric layer which reflects the waves has a height of about 85 — 90 Km, but at sunrise the action of the sunlight sets up an ionized layer below this at a height of about 67 — 72 Km. Thus, the phase velocity is greater by day than by night.

TABLE 1

Month	12	1	2	3	4	5	6	7	8	9	10	11	12
A3—NIS pp 109^{12}	4	4	— 1	6	3	2	6	2	2	4	4	8	— 9

TABLE 2

Month 1969	1	2	3	4	5	6	7	8	9	10	11	12
GBR—NIS sec.	— 8	— 7	7	15	12	—	—15	12	— 2	10	19	—13
Av. NIS sec.	— 3	0	— 5	— 4	— 2	—	— 3	— 4	— 2	1	1	— 1

At the National Institute for Standards (NIS), VLF standard frequency transmissions are received continuously since late 1967, and compared with the local cesium beam frequency standard, which is the national frequency standard.

Monthly reports of the comparison are sent to the Bureau International de l'Heure, in Paris, which receives similar reports from other national laboratories and computes the mean A3. The NIS receives similar reports.

Up to the end of 1968, WWVL was received continuously [Loutfy]. WWVL being one of the radio stations of the National Bureau of Standards NBS.

Since January 1969, reception of GBR was started. Because the path is much shorter, the reception is much better and the diurnal phase variation is less in total value and less composite in form. Further, many national laboratories are receiving GBR, and by comparing the reports we receive with our data, we can determine to a fairly good accuracy, our standards' deviation from A3 inspite of any phase jumps or deviations in GBR itself.

3. RECEIVERS :

The complete setup used for the reception of the VLF transmissions is shown schematically in figure 1. The cesium beam frequency standard feeds 100 KHz to both receivers, to a frequency synthesizer, and to a phase comparator. It also feeds a clock with the same frequency. A 2.5 MHz quartz oscillator is included, and its phase is continuously compared with that of the cesium standard.

Receiver I is of the phase tracking type, whereas receiver II is a Barbar filter type [Barbar], built at The Laboratory after a design developed at CSIRO, Australia [Thompson]. The phase and amplitude outputs of receiver one are continuously recorded on chart recorders, the outputs of receiver two are recorded part of the time. The two receivers are receiving the same transmission, GBR, NPL.

Three antennas of three different types are used :

1. Tuned air core shielded loop.
2. Tuned ferrite core shielded loop.
3. Simple horizontal wire.

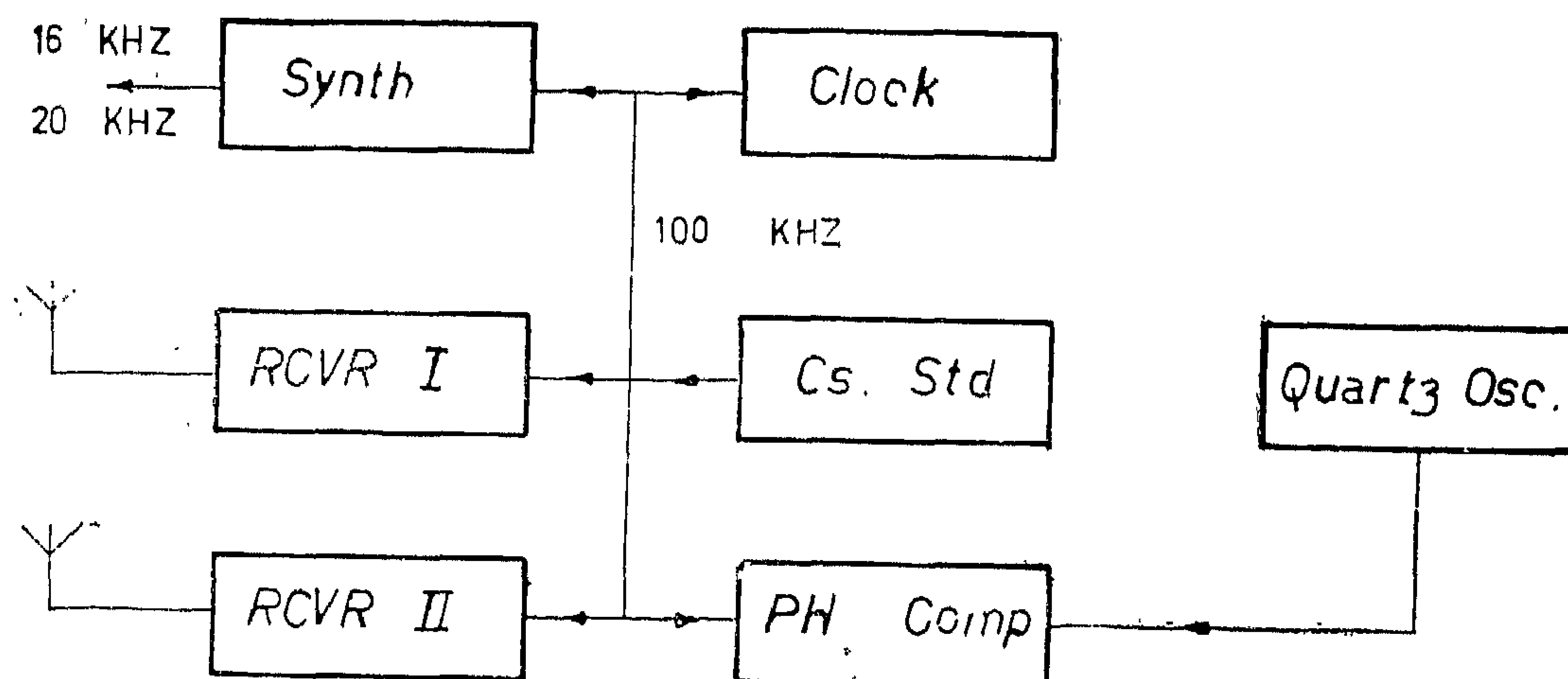


Fig.1 . Complete Set-up

RECEPTION OF VLF TRANSMISSION

By

A. LOUTFY EL SAYED°

1. SUMMARY :

Continuous comparison between the NIS standard frequency and other frequency standards abroad is carried out. An account of this comparison is given for a period of two years, during which WWVL and GBR were received. The first year is discussed very briefly, as it was the subject of a previous paper. A description of the equipment used is also given.

A short discussion of typical diurnal phase variations of the received GBR is given, and it is noted that there is strong seasonal effects.

The results show that the frequency standard of the NIS is within few parts in 10^{12} of the average over long periods.

2. INTRODUCTION :

During its general assembly of 1967 the IAU requested the BIH to maintain the International scale of atomic time (A3). In 1968, as during the previous years, A3 was established from the phase measurements of standard frequency transmissions on very low frequency (VLF) and low frequency (LF). Measurements are transmitted to the BIH under three forms :

1. Daily relative frequency differences between the local standard and the received standard frequency transmissions. The monthly mean was used by the BIH.
2. Most laboratories published the daily phase values, expressed in microseconds from an arbitrary origin. In such cases, the BIH computed the monthly mean of the relative frequency differences from the phase values for the last days of every month. A greater weight was given to these data.
3. Toward the end of 1968, a few laboratories began receiving regularly the pulses of the Loran—C navigation system, through ground wave transmissions. The measurements were used as explained under 2, but with a greater weight. For laboratories linked through Loran—C, the VLF transmissions had practically no value [BIH].

Thus, A3 is a mean standard of frequency.

Loran—C navigation transmissions, at a frequency of 100 KHz, can be used to provide; via ground wave, clock synchronization over long distances to accuracies within one microsecond [Shapiro]. Loran—C (Long Range Navigation) chains made it possible to establish a permanent link between laboratories with a far better accuracy than the VLF transmissions and without the danger of losing the phase.

Other proposed systems of precise timekeeping through VLF and cycle identification, namely the Omega system [Pierce] and dual carrier systems [Blair] show possibilities of microsecond timing.

Thus, at the time being, for areas not covered with synchronized Loran—C chains, the best method of comparing frequency standards over long distances is still through VLF transmissions.

---

* National Institute for Standards.

3. BROWN, WILLIAM H. and FISCHER, ARTHUR F. — Book "Philippine Bamboos". 1918.

4. CHOW, H.K. — "Bamboo for Reinforced Concrete". A thesis prepared by Mr. Chow at Massachusetts Institute of Technology. 1914.

5. "Concrete Road Construction in China" — The Surveyor and Municipal and Country Engineer, vol. 86 Sept. 7, 1934.

6. DE SIMONE, D. — "Possibilita di Impiego del Conglomerato Armato con Canne di Bambu". Annali dei Lavori Pubblici, June 1939.

7. ESPINOZA, J.C. — "Testing Bending and Compressive Strength of the Common Philippine Bamboo". Philippine Journal of Science, vol. 41 February 1930.

8. GLENN, H.E. — "Bamboo Reinforcement in Portland Cement Concrete". Engineering Experiment Station, Clemson, South Carolina. Bulletin No. 4, May 1950.

9. GLENN, H.E. — "Seasoning, Preservative and Water-repellent Treatment and Physical Property Studies of Bamboo". Engineering Experiment Station, Clemson, South Carolina. Bulletin No. 8, July 1956.

10. HOLME, A.S. — "Substitutes for Steel Reinforcement — Trials of Bamboo and Asbestos-Cement". Concrete and Constructional Engineering, vol. 36, March 1941.

11. "Materials of Construction in China. Uses of Bamboo". The Engineer 167, February 17, 1939.

12. MEHRA, S. R. and UPPAL, H. L. — "Some Preliminary Investigations in the Use of Bamboo for Reinforced Concrete". Indian Concrete Journal, vol. 25 January 1951.

13. NARAYANA, S.K. — "Bamboo-Concrete Composite Construction". Instn. Engrs. (India) — Journal, vol. 42 May 1962.

14. RYVES, R.A. — "Ligno Concrete". Civil Eng. (London), vol 39 Oct. 1944. Summary of paper by G.O. Case before Soc. of Engrs. 1912 and by G.H. Duff before joint meeting of Instn. of Civil Engrs. and Eng. Soc. of China, March 17, 1941.

15. "Utilization of Indian Bamboo". Chemical Age (London), July 30, 1932.

16. Youssef, M.A. Reda — "Non-metallic Reinforcement for Concrete Structural Elements". M.Sc. Thesis, Cairo University, Jan. 1969.

swelling cracks and giving the higher values for bond strength between concrete and reinforcement, together with preventing the formation of wet rot of bamboo.

10. In placing the reinforcing bamboo strips in concrete members, care should be taken to ensure having a clear spacing of not less than 2.5 to 3.0 centimeters between the individual strips and between the successive layers of reinforcement. Care should be also taken to avoid having the top row of reinforcement being too close to the neutral axis of the concrete section, otherwise there may be insufficient concrete to resist horizontal shear stresses.

11. High quality concrete with high cement content is recommended for concrete members reinforced with bamboo. It is also recommended to use High Early Strength cement in the concrete mixes, since it has some merit in preventing swelling cracks of the concrete member.

12. For the diagonal tension reinforcement, it is recommended to use vertical bamboo splints covering the whole length of the beam, with more closer spacings at the parts of high shear stresses, together with bending up the upper rows of longitudinal bamboo reinforcement from the lower part of the beam to the top.

13. The same procedure, as that used for the design of concrete members reinforced with conventional steel and subjected to flexure, is recommended for the design of concrete members reinforced with bamboo, provided using the given values for the modulus of elasticity in tension of bamboo together with the above recommended design values of allowable tensile and bond stresses.

14. In order to delay the appearance of cracks in bamboo reinforced concrete members subjected to flexure, it may be recommended to use either some kind of prestressing of the reinforcement or a small percentage of longitudinal steel reinforcement.

15. The factor of safety against bond failure, for bamboo reinforced concrete members, may be increased by using those bamboo strips having the greater number of nodes along their lengths.

16. The use of inverted concrete T—section, with the concrete flange being to the tension side, is recommended to provide for better distribution of reinforcement in the tensile zone of the beam. This will lower the neutral axis of the concrete section with the result of utilising more concrete in the compression zone.

17. It is highly recommended to increase the land areas cultivated with bamboo taking an advantage of the reclaimed areas in the New Valley and Al-Tahrir Province. Besides, the banks of Nasser Lake, at Aswan, are the ideal spot for the propagation of bamboos. Bamboo can be also cultivated on banks of canals and drains and along the sides of rural roads.

18. Further research work is needed to obtain :
    a) data on the behaviour of bamboo reinforced concrete members under sustained loads.
    b) data on the use of splices or lapped strips of bamboo.
    c) more exact data on concrete columns reinforced with bamboo.
    d) water-repellent agents other than those used in this research work for treating bamboo reinforcement.

SELECTED REFERENCES

1. BAUMANN, RICHARD — "Versuche uber die elastizitat und festigkeit von bambus". 1913.

2. BOSE, I.N. — "Use of bamboo as reinforcement in cement concrete". Assn. of Engrs. — J. vol. 26 Apr. — June 1950.

CONCLUSIONS AND RECOMMENDATIONS

The principal conclusions and recommendations indicated from the results of tests carried out in this investigation on native bamboo may be summarized in the following major findings :

1. The use of bamboo culms as reinforcement does not prevent the cracking of a concrete beam at loads materially in excess of those at ultimate failure of a similar concrete beam without any reinforcement. However, using higher percentages of reinforcement does slightly delay the discovery of the first crack formed under loading. On the other hand, bamboo reinforcement does increase the ultimate load capacity of the concrete beam to about four or five times that of an unreinforced concrete beam.

2. The ultimate load capacity of a concrete beam increases remarkably with the increase in percentage of longitudinal reinforcement of bamboo up to a value from 4 to 5 per cent of the cross sectional area of the beam. Moreover, the use of higher percentages of reinforcement does increase the ultimate failure load but with comparatively smaller amounts.

3. Design values not in excess of 350 to 400 kg/cm^2, for the allowable tensile stresses in the bamboo reinforcement, must be used if the maximum deflection of the concrete beam is to be kept under 1/360 of the span length. When these low design values are used, a high factor of safety of more than 2.5 usually results against ultimate failure of the member.

4. Design values not in excess of 3 to 5 kg/cm^2, for the allowable bond stresses between concrete and bamboo reinforcement, are recommended.

5. From a purely theoretical viewpoint, the cross sectional area of longitudinal bamboo reinforcement for a certain concrete beam must be about ten to eleven times the area required for steel reinforcement. However, ultimate load capacities, slightly exceeding those given by steel reinforced concrete beams, were attained for concrete beams reinforced with bamboo when the cross sectional area of longitudinal reinforcement was only about eight times that of steel.

6. Concrete columns reinforced with bamboo give ultimate load capacities nearly of the same order as those given by steel reinforced concrete columns, provided that the cross sectional area of bamboo reinforcement is from ten to eleven times that of steel. Accordingly, it may be recommended to take the safe working loads half the values at elastic limit, although no general conclusions for the design principles of columns could be really drawn out from the attained limited test results.

7. Bamboo is more economical than steel when used as reinforcement for concrete structural members. Culms of native bamboo can be obtained nearly free, except the cost of transportation, from many localities in U.A.R. No manufacturing process is required beyond splitting the bamboo culms into strips of required dimensions and treating them with a suitable water-repellent agent. Besides, bamboo gives lighter weight for concrete members in general, (specific gravity of bamboo culms is 0.80).

8. The use of green unseasoned bamboo culms as reinforcement in concrete members is not recommended. Instead, bamboo culms should be cut and allowed to dry and season for at least four to six weeks before being used.

9. The use of two brush coatings of the blown bitumen paint used in this investigation, followed by dusting with sand, is highly recommended as a water-repellent treatment for bamboo reinforcement. This treating agent has proved to be very successful in completely eliminating the

of "Primer" then dusted with sand. The bamboo reinforcement was distributed along the sides of the column such that a clear spacing of 2.0 cm resulted between the individual strips. The column was tied by steel hoops in the same way used in the steel reinforced concrete column.

The concrete columns were casted vertically in layers of small depths and compacted mechanically using two external form vibrators together with an internal one. The columns were cured using wet burlap and sand until tested at age of 14 days.

Deformation readings were measured, at the middle of the column height from the four sides, using four strain gages each with a 25—cm gage length. The test results of both columns are given in *Table (7)*, while the load-deformation diagrams are shown in *Fig. (17)*.

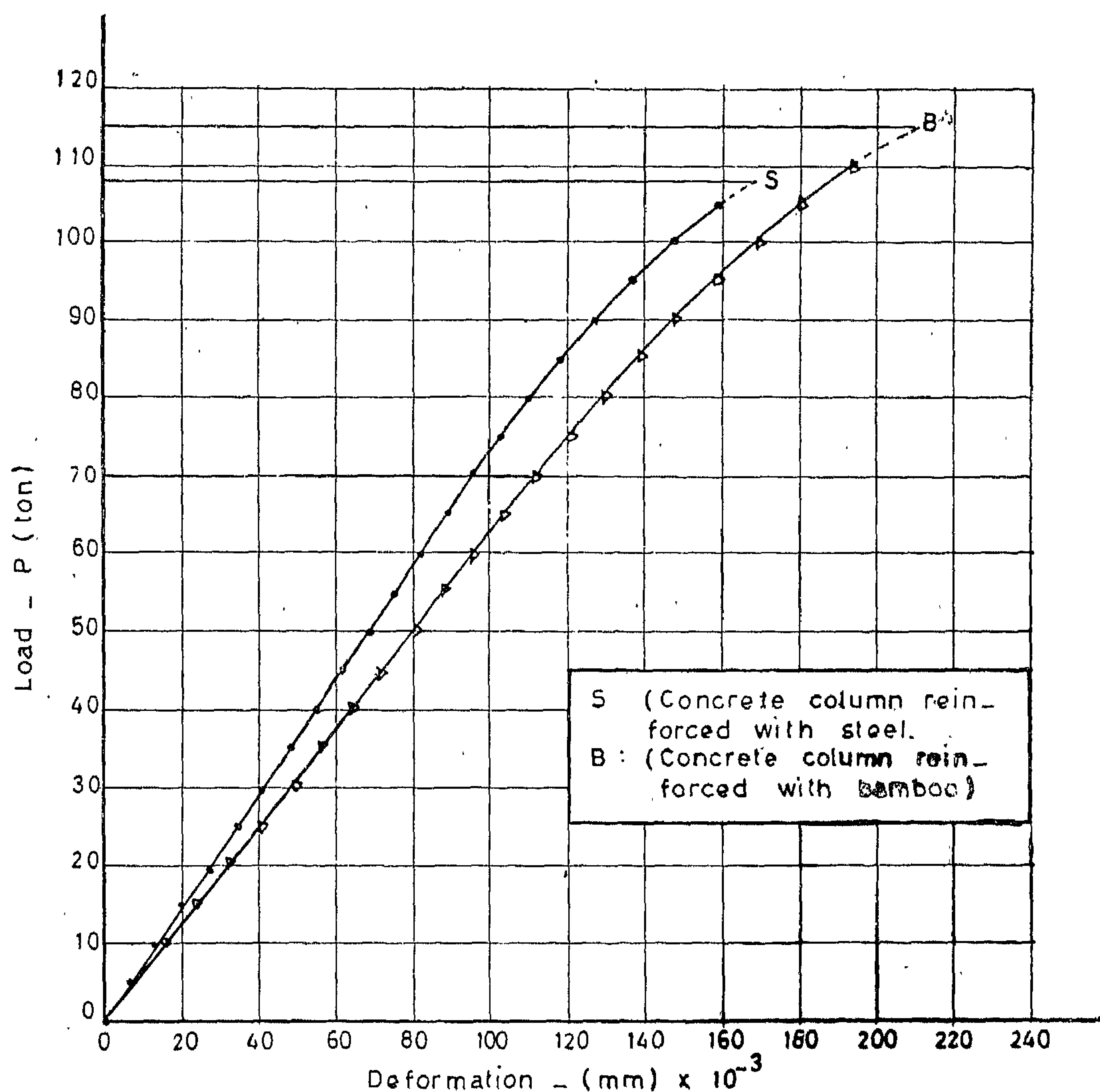


Fig. 17 _ LOAD_ DEFORMATION DIAGRAMS OF COMPRESSION TESTS ON CONCRETE COLUMNS REINFORCED WITH STEEL AND BAMBOO.

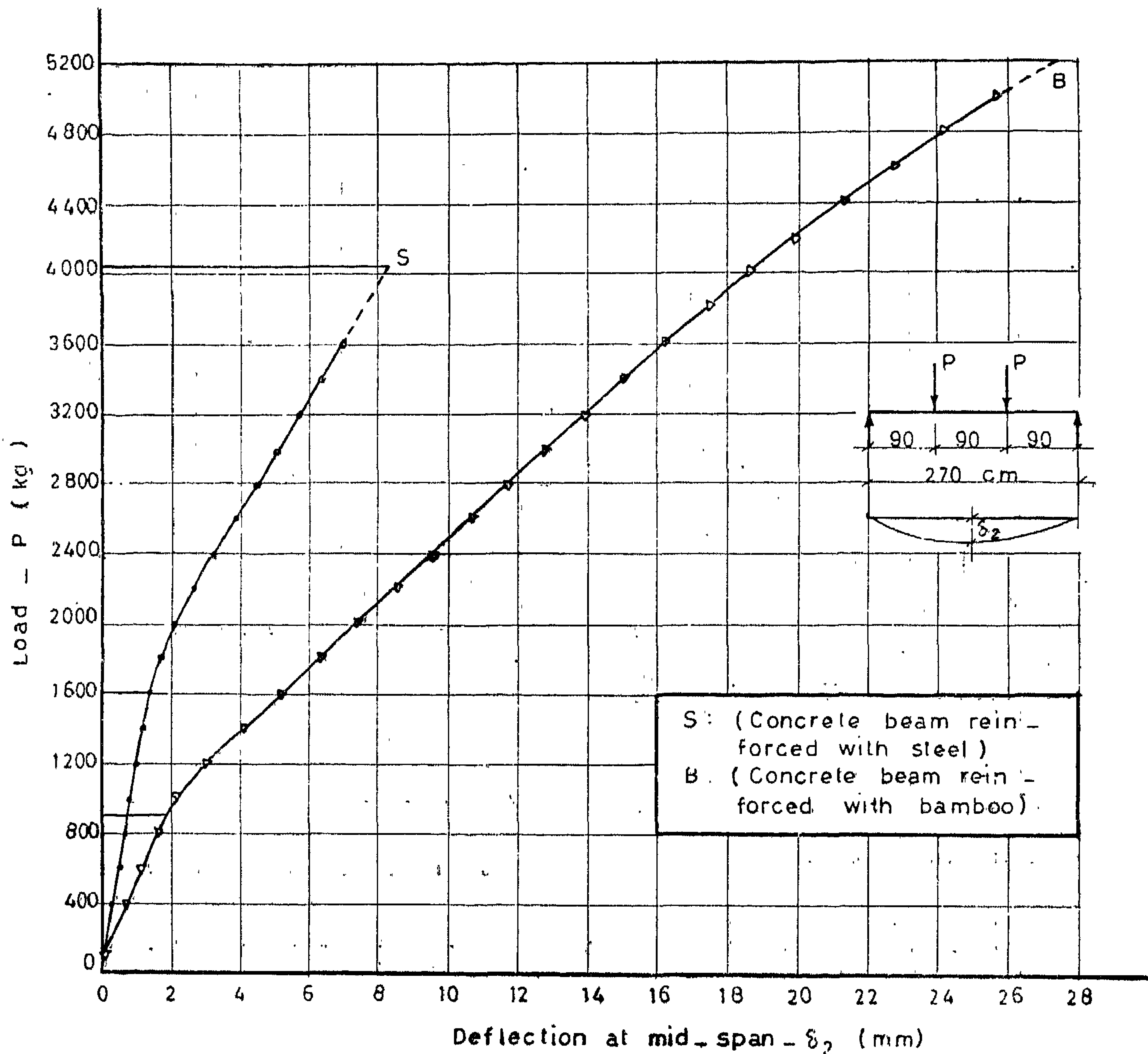


Fig 16— LOAD — DEFLECTION CURVES OF FLEXURE TESTS ON CONCRETE BEAMS (22.5 x 30 x 300 cm) REINFORCED WITH STEEL AND BAMBOO.

c) Tests on Columns (20 × 20 × 200 cm):

Two concrete columns were prepared, one reinforced with bamboo and the other with conventional mild steel, and both were of square cross section of 20 × 20 cm and a total height of 200 cm. They were fabricated using a concrete mix with a cement content of 400 kg/m³ of High Early Strength cement and the mix proportions by weight were 1 : 1.65 : 3.06 with (W/C) ratio of 0.44.

The steel reinforced concrete column was provided with four steel bars of 3/8 in. diameter placed in the four corners as main reinforcement. The column was tied by steel hoops of 3/16 in. diameter placed every 10 cm in the middle, and every 5 cm over a length of 35 cm at both ends.

The bamboo reinforced concrete column was provided with 16 vertical bamboo strips, having a total cross sectional area of about 30.0 cm², and treated with two brush coatings

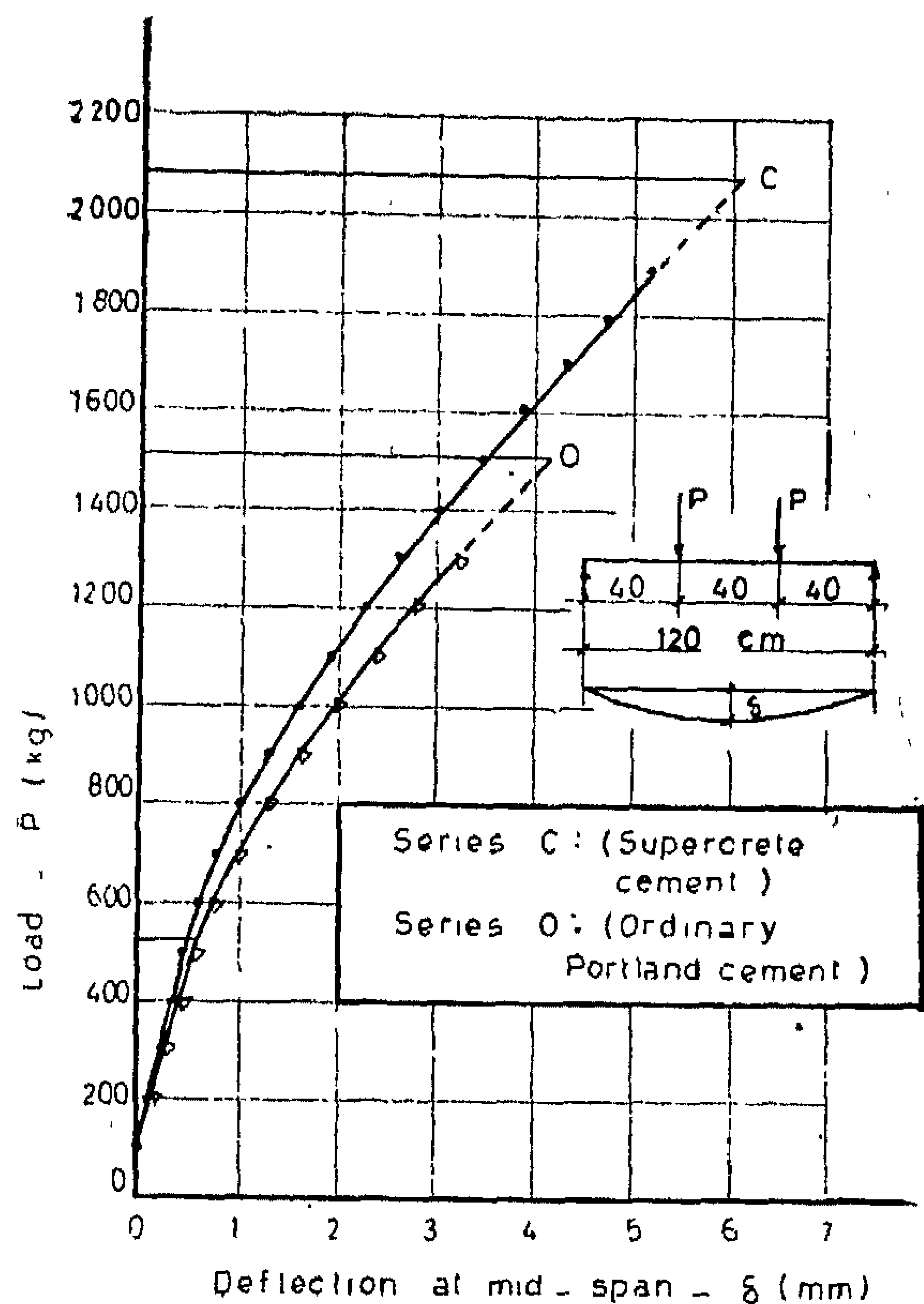


Fig. 14. EFFECT OF TYPE OF CEMENT ON LOAD-DEFLECTION CURVES OF CONCRETE BEAMS REINFORCED WITH BAMBOO

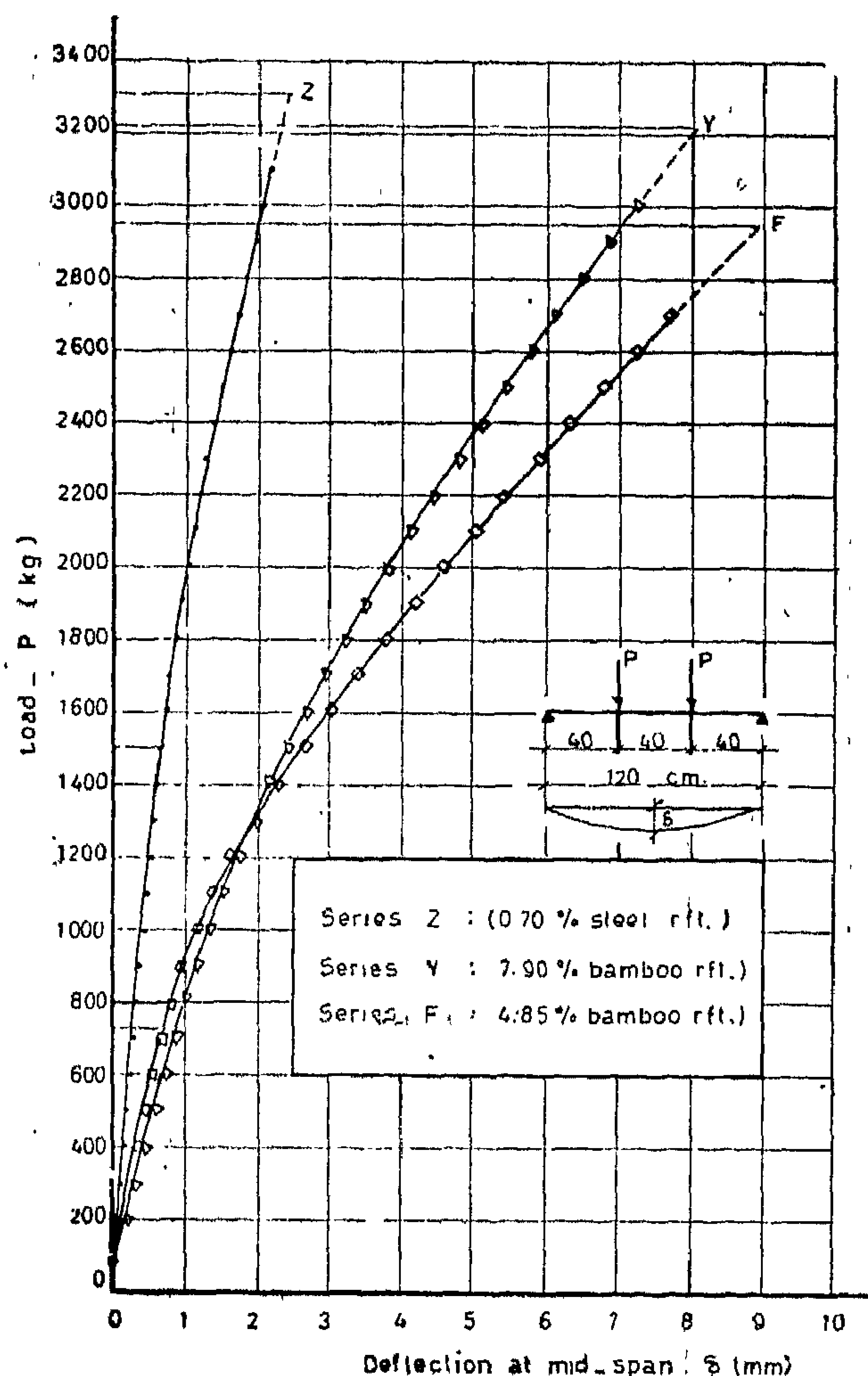


FIG. 15. LOAD-DEFLECTION CURVES OF CONCRETE BEAMS REINFORCED WITH STEEL AND WITH BAMBOO

Table (7) — Results of Compression Tests on Concrete Columns (20 × 20 × 200 cm) Reinforced with Steel and Bamboo.

(both columns were cured using wet burlap and sand until tested at age of 14 days.)

Mark on column	*Control cubes C (kg/cm²)*	*Load at elastic limit P (ton)*	*Strain at elastic limit (mm/mm)*	*Load at failure P (ton)*	*Strain at failure (mm/mm)*	*Type of failure*
S	385	70.00	3.82×10^{-4}	108.00	6.80×10^{-4}	Crushing of concrete at the ends of column
B	390	70.00	4.50×10^{-4}	115.00	8.52×10^{-4}	» » »

* C = Compressive strength of control cubes at age of 14 days.
* Elastic limit was considered as the point at the end of the straight line part of the load-deformation diagram.
* All strains were measured on G.L. = 25.0 cm.
* No swelling cracks were recorded for the concrete column (B) reinforced with bamboo.

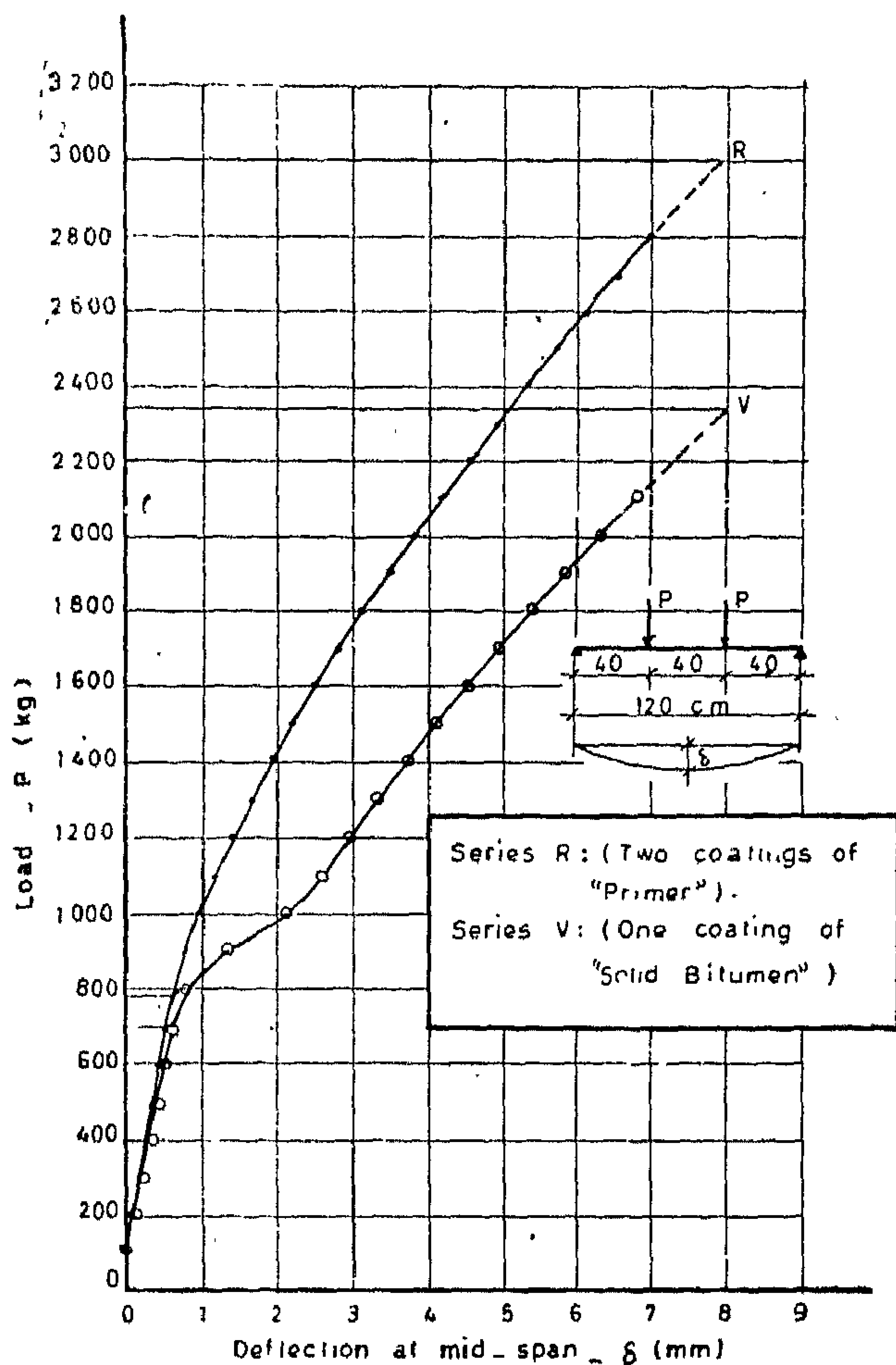


Fig 12. EFFECT OF TYPE OF TREATMENT OF REINFORCEMENT ON LOAD_DEFLECTION CURVES OF CONCRETE BEAMS REINFORCED WITH BAMBOO.

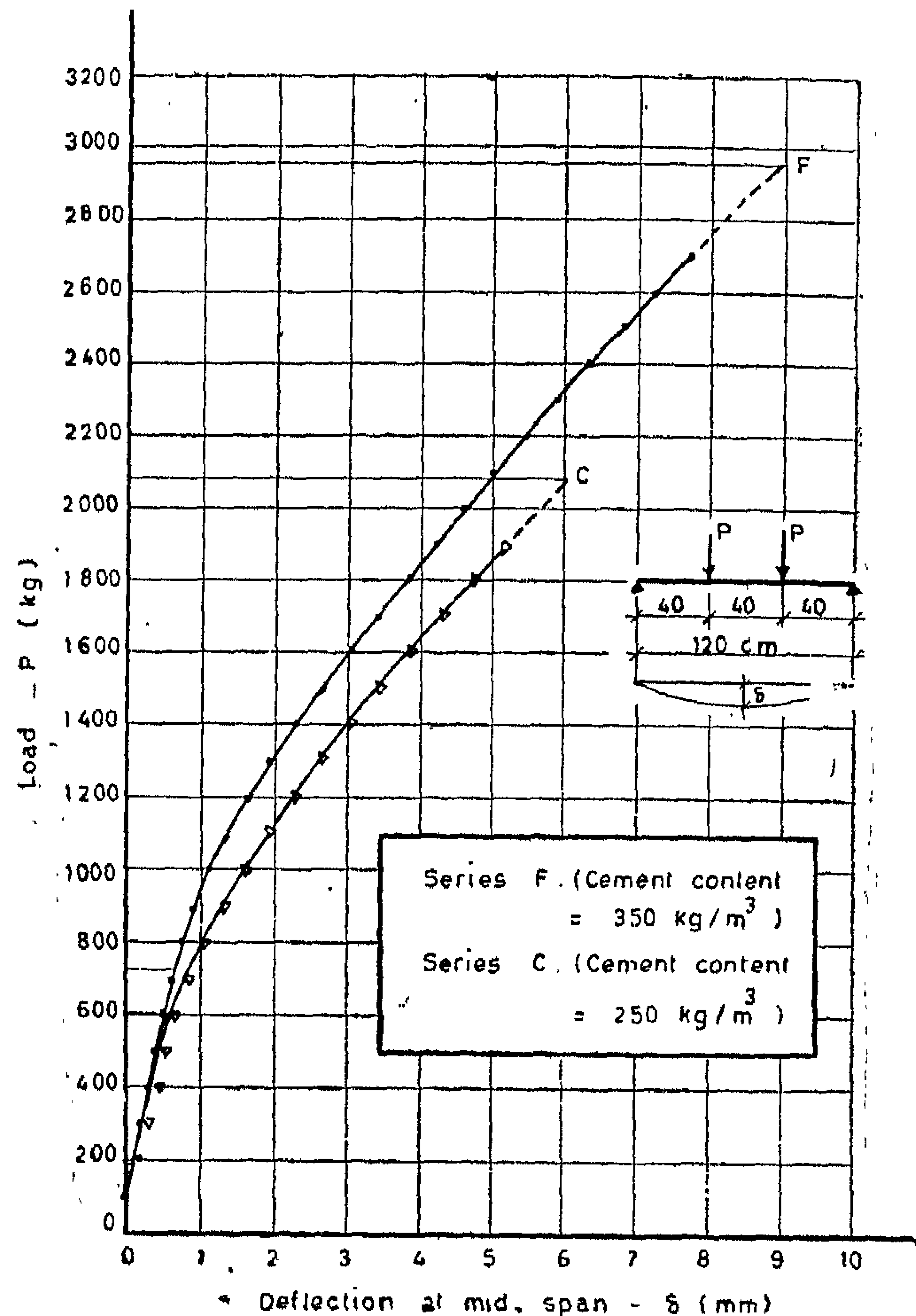


Fig. 13. EFFECT OF CEMENT CONTENT ON LOAD_DEFLECTION CURVES OF CONCRETE BEAMS REINFORCED WITH BAMBOO.

Table (6) — Maximum Tensile Stresses in Reinforcement for Different Values of Load P applied on Concrete Beam (22.5 × 30 × 300 cm) Reinforced with Bamboo. (average modulus of elasticity of bamboo was taken 200 t/cm²)

Applied load P (kg)	*Maximum tensile strain in reinforcement (mm/mm)*		*Maximum tensile stress in reinforcement (kg/cm²)*	
	Measured on G.L. = 25.0 cm	*Measured on G.L. = 2.0 cm*	*Calculated from strains measured on G.L. = 25.0 cm*	*Calculated from strains measured on G.L. = 2.0 cm*
800	0.30×10^{-3}	0.72×10^{-3}	60	144
1600	1.20×10^{-3}	2.70×10^{-3}	240	540
2400	2.30×10^{-3}	4.60×10^{-3}	460	920
3200	3.40×10^{-3}	6.45×10^{-3}	680	1290
4000	4.65×10^{-3}	8.40×10^{-3}	930	1680
5000	6.25×10^{-3}	10.80×10^{-3}	1250	2160

* P = Load applied at third points of the span ; equals half the total load on beam.

* For G.L. = 25.0 cm. strains were measured at the middle of the span on the concrete cover at the same level as the lower row of reinforcement.

* For G.L. = 2.0 cm. strains were measured directly on the lower row of reinfor cement by removing the concrete cover at the middle of the span.

Table (4) — Average Results of Flexure Tests on Rectangular Concrete Beams (15 × 20 × 130 cm) Reinforced with Bamboo.
(for all series, results are the average of two beams.)

Series number	*Control cubes C (kg/cm²)*	*Percentage of rft. μ (%)*	*Load at first crack P (kg)*	*Deflection at first crack δ (mm)*	*Load at failure P (kg)*	*Deflection at failure δ (mm)*
A	178	2.65	575	0.81	1625	5.25
B	170	4.00	525	0.61	1435	3.50
C	194	5.05	600	0.63	2083	6.33
D	185	2.40	700	0.85	2065	7.15
E	255	3.85	750	0.69	2845	9.00
F	240	4.85	725	0.80	2955	9.10
Y	250	7.90	800	1.18	3220	8.25
G	196	4.47	600	0.55	2165	6.20
H	185	4.10	600	0.48	1925	4.65
I	179	4.20	650	0.64	1750	4.50
J	248	4.00	700	0.66	2790	7.30
O	168	5.20	525	0.60	1510	4.35
P	233	4.80	625	0.70	2680	7.85
K	195	4.95	600	0.44	2165	5.90
L	159	5.35	575	0.50	2195	6.20
M	154	5.20	525	0.52	1715	5.20
N	210	4.80	600	0.51	2575	6.85
R	240	4.90	775	0.70	2990	8.15
V	245	5.20	700	0.71	2335	8.15

Table (5) — Average Results of Flexure Tests on Plain and Steel Reinforced Concrete Beams (15 × 20 × 130 cm).
(for all series, results are the average of two beams.)

Series number	*Control cubes C (kg/cm²)*	*Percentage of rft. μ (%)*	*Load at first crack P (kg)*	*Deflection at first crack δ (mm)*	*Load at failure P (kg)*	*Deflection at failure δ (mm)*
Q	173	0.70	1100	0.76	2940	3.05
U	195	0.70	1300	0.75	3110	2.88
Z	253	0.70	1500	0.70	3310	2.60
S	165	—	—	—	480	0.50
T	180	—	—	—	550	0.70
W	253	—	—	—	700	0.79

* C = Compressive strength of control cubes at age of 28 days.

* μ = Area of reinforcement divided by total cross sectional area of the concrete beam.

* P = Load applied at third points of the span ; equals half the total load on beam.

* δ = Deflection at mid-span.

the depth of each beam, mechanical strain gages each with a 25—cm gage length were fixed at mid-span at different levels across the beam depth. For measuring the maximum strains in the bamboo reinforcement, a Huggenberger extensometer was fixed directly on the lower row of bamboo strips on a gage length of 2.0 cm. The ultimate load and the type of failure were recorded at the end of the test as well as the compressive strength of the control cubes. The steel reinforced concrete beam failed by tension due to yield of steel at an ultimate total load of 8100 kg, while the bamboo reinforced concrete beam had an ultimate failure caused by diagonal tension followed by compression failure at a total load of 10400 kg.

The measured strains and the corresponding stresses of bamboo reinforcement are given in *Table (6)* for the different stages of loading, while *Fig. (16)* shows the load-deflection curves of the two concrete beams recorded for the central deflection.

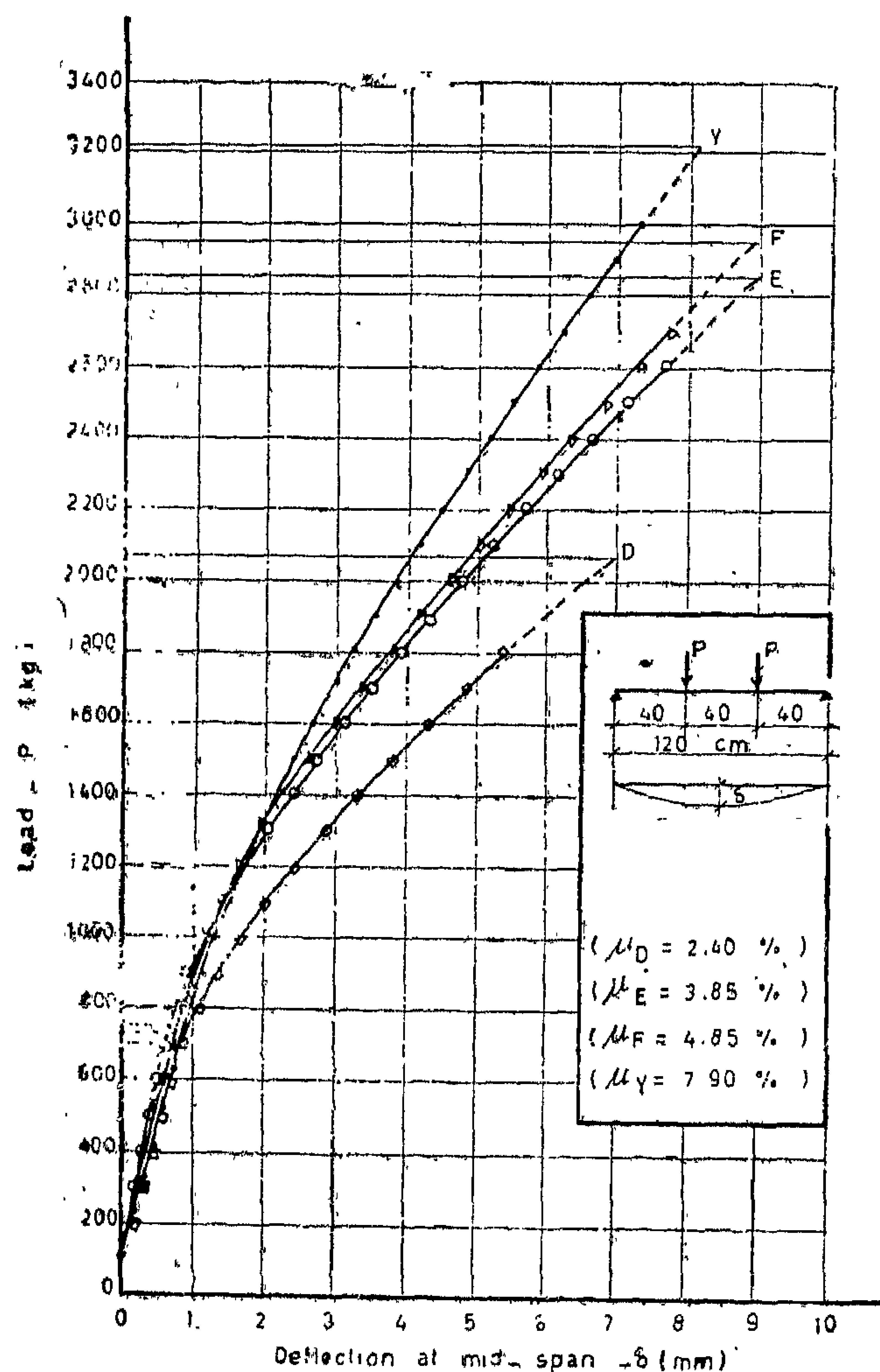


Fig 10. EFFECT OF PERCENTAGE OF LONGITUDINAL REINFORCEMENT ON LOAD-DEFLECTION CURVES OF CONCRETE BEAMS REINFORCED WITH BAMBOO

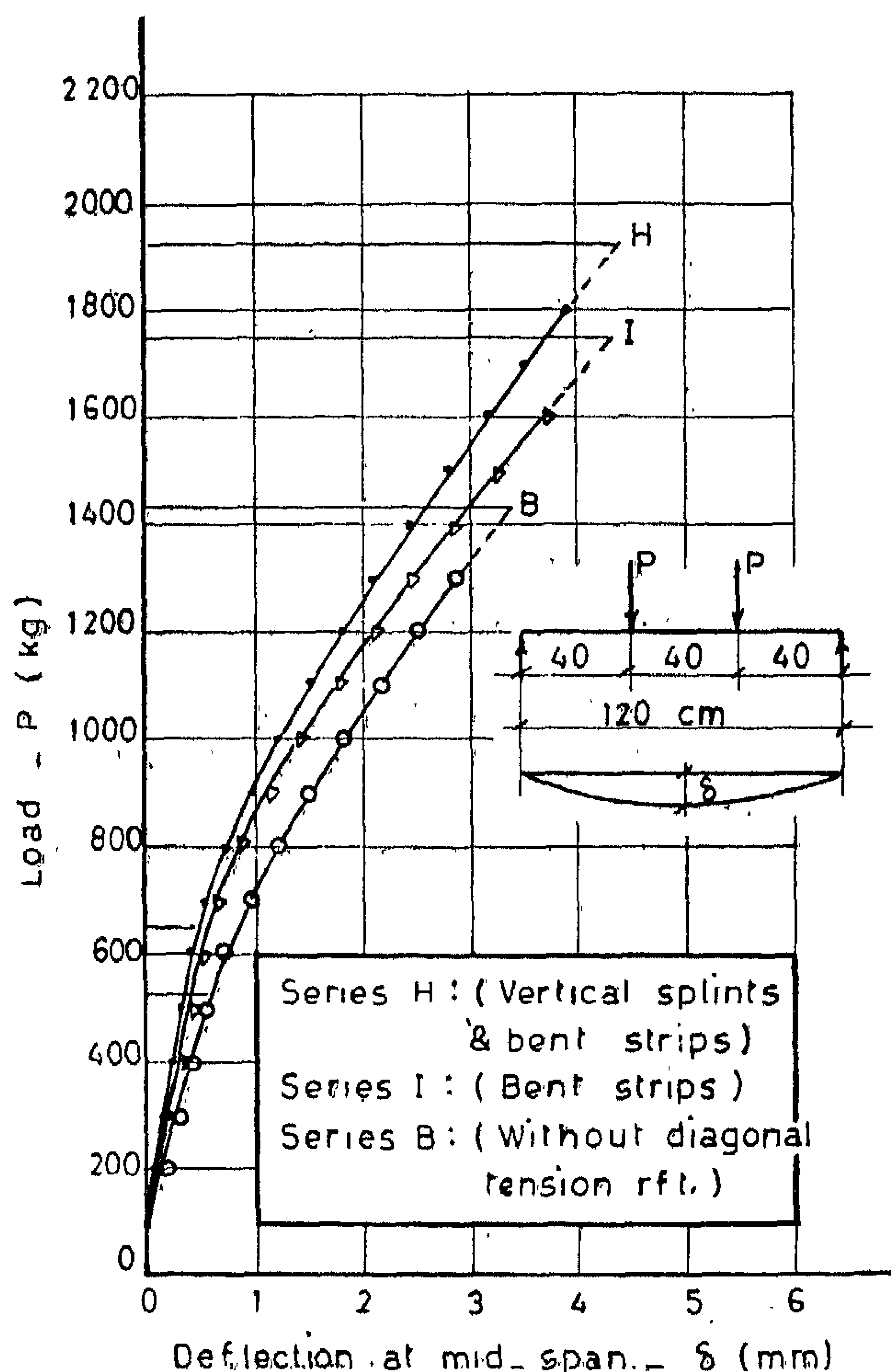


Fig. 11. EFFECT OF DIAGONAL TENSION REINFORCEMENT ON LOAD-DEFLECTION CURVES OF CONCRETE BEAMS REINFORCED WITH BAMBOO.

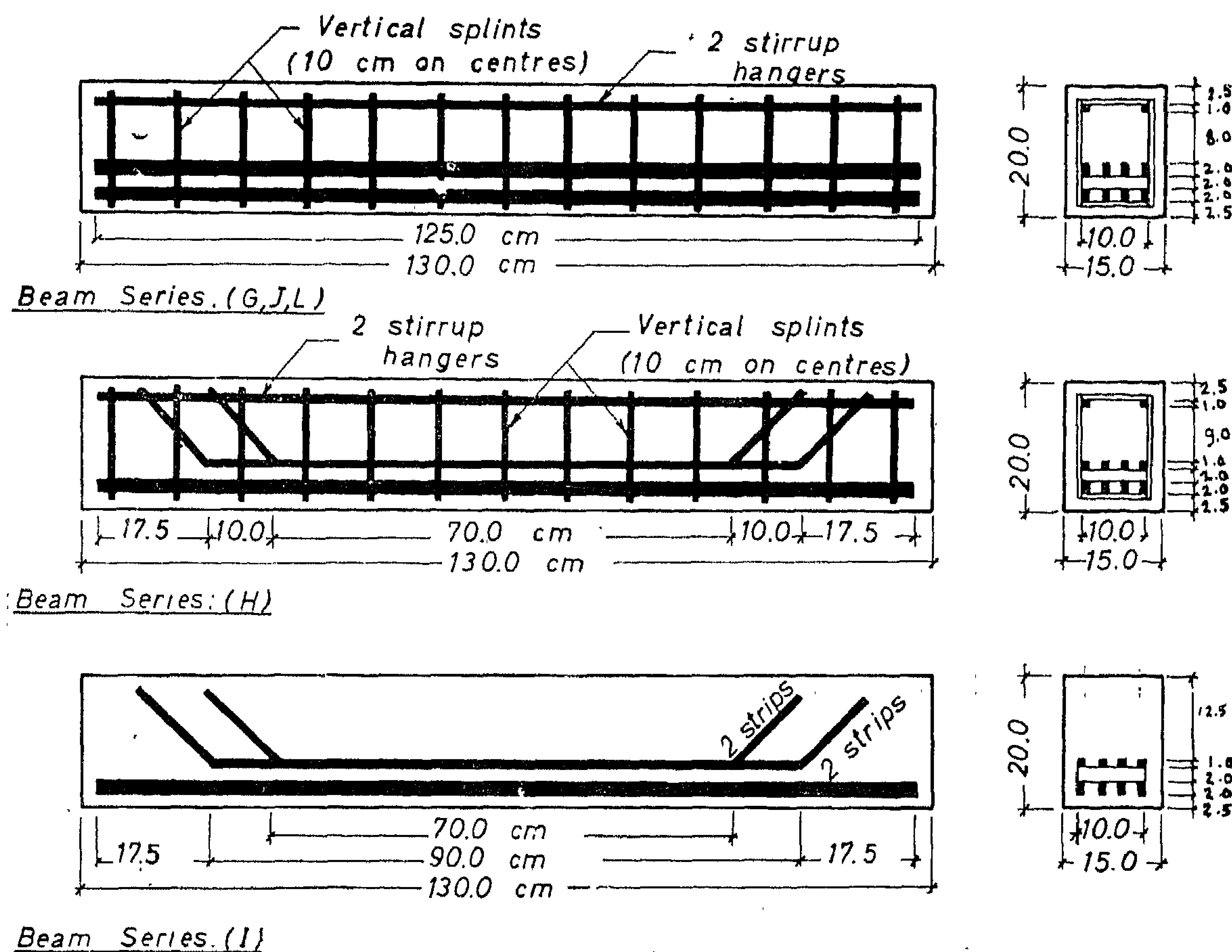


Fig. 9. — Rectangular Concrete Beams (15 × 20 × 130 cm) Reinforced with Bamboo.

of 22.5 cm, a total depth of 30 cm and a total length of 300 cm. They were fabricated using the same concrete mix designed before with cement content 350 kg/m³ of High Early Strength cement.

The steel reinforced concrete beam was provided with six steel bars of 3/8 in. diameter placed at bottom in one row as longitudinal reinforcement, together with vertical stirrups of box section having 3/16 in. diameter and placed 10 cm on centres.

The bamboo reinforced concrete beam was provided with 18 bamboo strips as longitudinal reinforcement placed in four rows with a clear spacing, between the individual strips and between the successive layers of strips, of slightly more than 2.0 cm. The total cross sectional area of longitudinal bamboo reinforcement was about 36.0 cm². The diagonal tension reinforcement consisted of vertical bamboo splints placed 10 cm on centres at both sides of the beam, with every two opposite vertical splints being connected with two horizontal bamboo splints forming a box section. The whole longitudinal and diagonal tension bamboo reinforcement were treated with two brush coatings of "Shell Pipe Primer" then dusted with sand and left to dry in air.

The two beams were cured using wet burlap and sand until tested at age of 14 days. Each beam was supported on a 270-cm span and loaded to failure with two concentrated loads applied at third points of the span. The beams were tested in a reversed position, the same as the small beam test specimens.

Deflection measurements were made at both the third-points and the middle of the span. For determining the strain distribution across

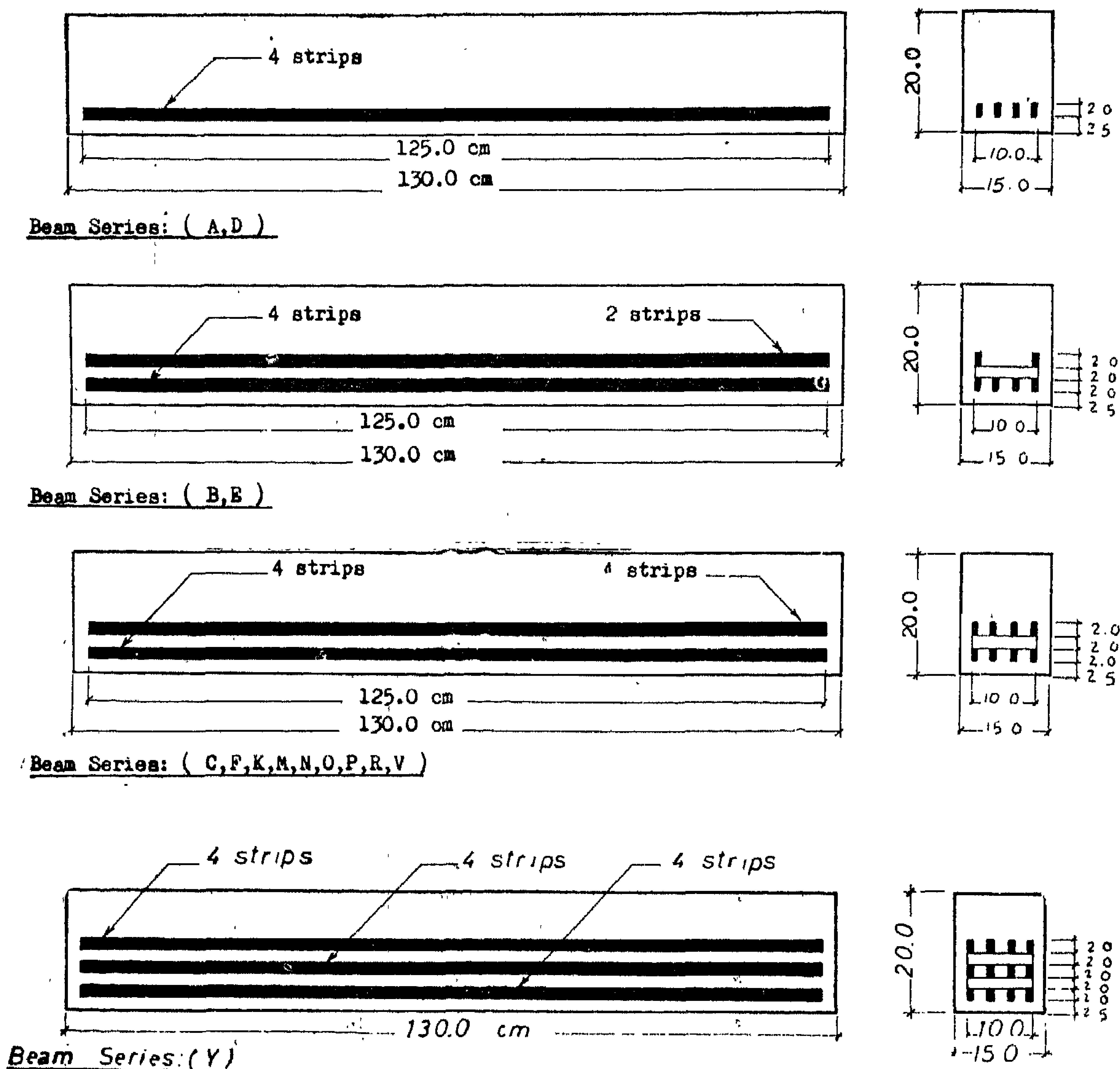


Fig. 8. — Rectangular Concrete Beams (15 × 20 × 130 cm) Reinforced with Bamboo.

the initial swelling cracks if any, and the compressive strength of control cubes casted from the same concrete mix of the beam.

The average test results of concrete beam series reinforced with bamboo are shown in *Table (4)*, while those of plain and steel reinforced concrete beams are given in *Table (5)*.

The load-deflection curves for the different beam series were plotted into groups showing the effect of the different factors previously mentioned. *Figures (10 to 15)* show some selected groups of curves.

b) Tests on Beams (22.5 × 30 × 300 cm):

Regarding the test results obtained for the relatively small concrete beams reinforced with bamboo, tests were carried out on bigger size concrete beams to secure further information required for establishing reliable design principles for concrete members reinforced with bamboo.

Two concrete beams were prepared, one reinforced with bamboo and the other with conventional mild steel, each having a width

Table (3 — List of Rectangular Concrete Beams Reinforced with Bamboo.
(all beams are 15 × 20 × 130 cm.)

Beam number	Type of cement	Cement content (kg/m^3)	Type of treatment of rft.	Arrangement of bamboo reinforcement	Area of rft. (cm^2)	Percentage of rft. μ (%)	Diagonal tension reinforcement
A—1	High Early Strength (Supercrete)	250	Untreated	4 strips, one row	7.6	2.53	None
A—2	»	250	»	» »	8.3	2.77	»
B—1	»	250	»	4 strips, 1st row 2 strips, 2nd row	11.8	3.93	»
B—2	»	250	»	» »	12.2	4.06	»
C—1	»	250	»	8 strips, 2 rows	14.7	4.90	»
C—2	»	250	»	» »	15.6	5.20	»
D—1	»	350	»	4 strips, one row	7.0	2.33	»
D—2	»	350	»	» »	7.4	2.47	»
E—1	»	350	»	4 strips, 1st row 2 strips, 2nd row	11.4	3.80	»
E—2	»	350	»	» »	11.7	3.90	»
F—1	»	350	»	8 strips, 2 rows	14.4	4.80	»
F—2		350	»	» »	14.7	4.90	»
Y—1	»	350	»	12 strips, 3 rows	23.4	7.80	»
Y—2	»	350	»	» »	24.0	8.00	»
G—1	»	250	Untreated	8 strips, 2 rows	13.4	4.47	Vertical splints 10 cm on centres
G—2	»	250	»	» »	13.4	4.47	»
H—1	»	250	»	4 strips, 1st row 4 bent strips, 2nd row	12.0	4.00	Vertical splints 10 cm on centres
H—2	»	250	»	» »	12.5	4.17	»
I—1	»	250	»	» »	12.3	4.10	None
I—2	»	250	»	» »	12.9	4.30	»
J—1	»	350	»	8 strips, 2 rows	11.7	3.90	Vertical splints 10 cm on centres
J—2	»	350	»	» »	12.3	4.10	»
O—1	Ordinary Portland Cement	250	»	» »	15.6	5.20	None
O—2	»	250	»	» »	15.6	5.20	»
P—1	»	350	»	» »	14.1	4.70	»
P—2	»	350	»	» »	14.7	4.90	»
K—1	High Early Strength (Supercrete)	250	Two coatings of « Varnish »	8 strips, 2 rows	14.7	4.90	»
K—2	»	250	»	» »	15.0	5.00	»
L—1	Ordinary Portland Cement	250	»	» »	15.9	5.30	Vertical splints 10 cm on centres
L—2	»	250	»	» »	16.2	5.40	»
M—1	»	250	»	» »	15.3	5.10	None
M—2	»	250	»	» »	16.0	5.33	»
N—1	»	350	»	» »	14.1	4.70	»
N—2	»	350	»	» »	14.7	4.90	»
R—1	High Early Strength (Supercrete)	350	Two coatings of « Primer »	» »	14.6	4.87	»
R—2	»	350	»	» »	14.7	4.90	»
V—1	»	350	One coating of «Solid Bitumen»	» »	15.5	5.17	»
V—2	»	350	»	» »	15.6	5.20	»

* Cement content in kilograms per cubic meter of finished concrete.
* μ = Area of reinforcement divided by total cross sectional area of the concrete beam.

As a result, the two water-repellent agents were mainly used in the further experiments conducted on concrete beams reinforced with bamboo.

CONCRETE STRUCTURAL MEMBERS REINFORCED WITH BAMBOO

An experimental investigation was carried out on concrete beams and columns reinforced with bamboo in an effort to obtain an evaluation of the effectiveness of the material as a substitute for steel reinforcement.

The carried out tests were classified into the following three groups :

a) Tests on beams (15 × 20 × 130 cm).
b) Tests on beams (22.5 × 30 × 300 cm).
c) Tests on columns (20 × 20 × 200 cm).

a) Tests on Beams (15 × 20 × 130 cm):

All beams used in this group of tests were rectangular in section with a width of 15 cm, a total depth of 20 cm, and a total length of 130 cm. They were reinforced with different percentages of bamboo reinforcement, treated with various types of water-repellent agents, provided with several types of diagonal tension reinforcement, and fabricated using two types of cement with two cement contents.

They were made, to be tested in flexure, in order to determine :

1. Effect of percentage of longitudinal bamboo reinforcement.
2. Effect of diagonal tension bamboo reinforcement.
3. Effect of type of water-repellent treatment of reinforcement.
4. Effect of type of cement and cement content used in the concrete mixes.
5. Comparative study between the behaviour of steel and bamboo reinforced concrete beams under loads.

In fabricating these concrete beams, two cement contents of 250 and 350 kg/m^3 were used together with two types of cement; namely Ordinary Portland cement and High Early Strength cement. The designed mix proportions by weight were just the same as those used in fabricating the concrete bond cylinders.

A full description of the bamboo reinforced concrete beams used in this research work is recorded in *Table (3)*, and the arrangements of bamboo reinforcement for the various beam series are shown in *Figures (8,9)*.

To obtain the data required for comparison, control beam series of plain concrete and steel reinforced concrete were prepared using the same mix proportions previously mentioned. The steel reinforced concrete beams of the different series were prepared, each having 3 Φ 3/8 in. mild steel bars as main reinforcement and provided with stirrups of diam. 3/16 in. placed 10 cm on centres. For a cement content of 250 kg/m^3, Beam Series (Q, S) were fabricated using Ordinary Portland cement while Series (U, T) were made using High Early Strength cement. For a cement content of 350 kg/m^3, Series (Z, W) were made using High Early Strength cement.

All beams were cured using wet burlap and sand until tested at age of 28 days. Each beam was supported on a 120—cm span and loaded to failure with two concentrated loads applied at third points of the span. The beams had to be tested in a reversed position since the piston loads acting at third points of the span were applied upwards.

For each beam, after test, a complete record was made for the ultimate failure load, the type of failure, the load-deflection readings, the cracking loads and crack pattern,

Table (2) — Average Results of Tests on Bond between Concrete and Seasoned Bamboo. (in all series, concrete cylinders 15 × 15 cm were cured using wet burlap and sand until tested at age of 28 days.)

Series number	*Type of cement*	*Cement content (kg/m³)*	*Type of treatment*	*Existing node at middle of embedded length*	*Control cubes C (kg/cm²)*	*Average bond strength (kg/cm²)*
A	Ordinary Portland Cement	250	Untreated	None	155	5.7
B	»	250	Two coatings of « Varnish »	»	160	11.3
C	»	350	Untreated	»	230	6.9
D	»	350	Two coatings of « Varnish »	»	225	12.9
E	High Early Strength (Supercrete)	250	Untreated	None	180	8.9
F	»	250	Untreated	One node	190	12.0
G	»	250	One coating of « Solid Bitumen »	None	190	0.9
H	»	250	Two coatings of « P.F. 4 »	»	180	9.4
I	»	250	Two coatings of « Primer »	»	195	13.2
J	»	250	Two coatings of « Varnish »	»	200	13.0
K	High Early Strength (Supercrete)	350	Untreated	None	260	10.3
L	»	350	Untreated	One node	260	13.5
M	»	350	One coating of « Solid Bitumen »	None	250	1.5
N	»	350	Two coatings of « P.F. 4 »	»	265	10.6
O	»	350	Two coatings of « Primer »	»	260	14.8
P	»	350	Two coatings of « Varnish »	»	265	14.3

* Cement content in kilograms per cubic meter of finished concrete.

* C = Compressive strength of control cubes at age of 28 days.

* Bond strength = Load at first slip, of free end of test specimen divided by surface area in contact with concrete.

* All test results are the average of 3 test specimens.

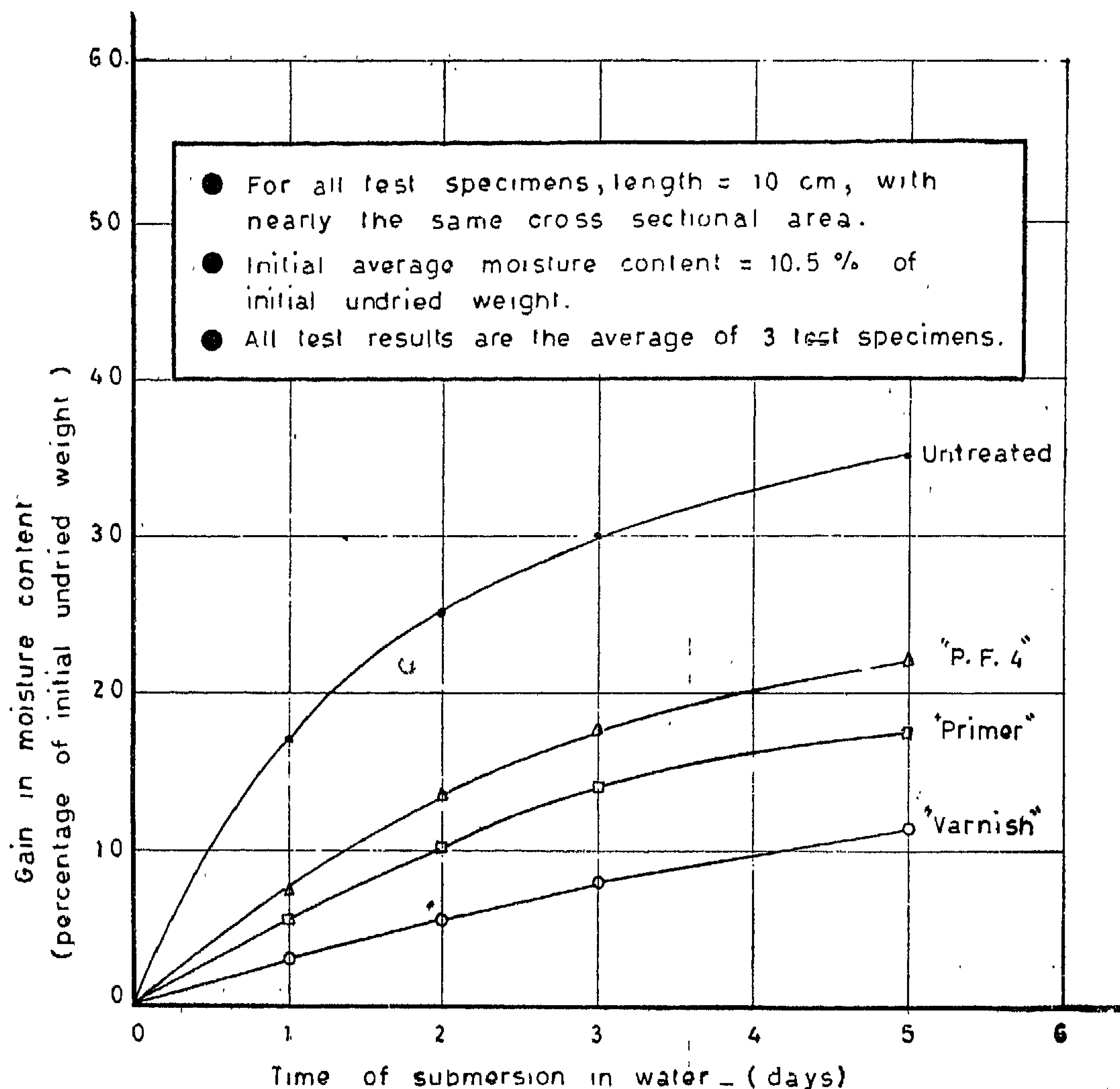


Fig. 7_ EFFECT OF TYPE OF TREATMENT ON WATER ABSORPTION OF BAMBOO.
(All types of treatment were applied in two coatings)

seems to be superior than the others. However, since all absorption tests were carried out using fresh drinking water, there would be a possibility for a chemical reaction with cement in the concrete mix. This was detected in further tests carried out on concrete beams reinforced with bamboo treated by "Varnish".

3. Although the "Primer" treatment gave comparatively higher values for water absorption than "Varnish" after the five days period, it would be convenient to use "Primer" treatment since it gave values of water absorption over the first day close to those given by "Varnish".

4. Concerning the price and cost, it was found that "Flatting Varnish" costs seven times as much as "Primer" treatment. In spite of the coverage area of "Varnish" coating which is 12 m^2/kg, approximately double as much as that of "Primer" treatment, "Varnish" is still much more expensive.

moved periodically from water and weighed to determine the amount of absorbed moisture. It was believed that testing the bamboo test pieces for only five days would be reasonable, since it is only the absorption values over the first few hours during setting and initial drying of concrete that are significant.

From the results of water absorption tests, curves of the gain in moisture content with time were plotted for the different water-repellent agents either applied in single or double coatings. These curves are shown in *Figures (6,7)*.

An evaluation of test results obtained from both the bond and absorption tests, concerning the choice of the most suitable water-repellent treatment for bamboo, gave the following conclusions :

1. Concerning the bond strength, it seems that "Varnish" and "Primer" treatments are the most suitable agents to give the higher values for bond, provided that they are to be applied in double coatings.
2. Regarding the ability of water-repellency, treatment by "Varnish"

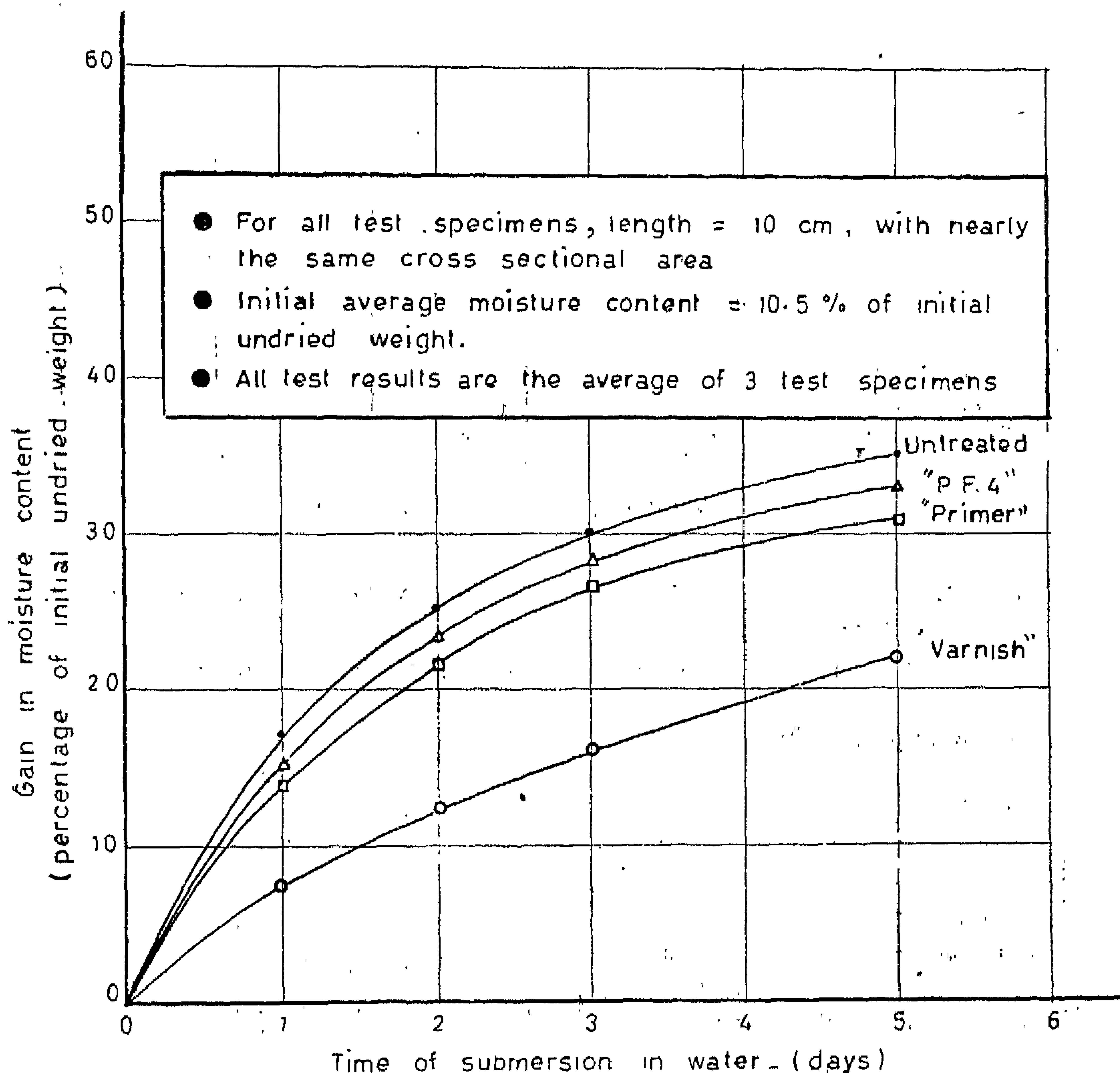


FIG 6 EFFECT OF TYPE OF TREATMENT ON WATER ABSORPTION OF BAMBOO.

(All types of treatment were applied in one coating)

Composition: 35% blown bitumen R 115/15.
65% solvent (mineral turpentine + toluene).

- *"P.F. 4"* :

A commercial name for a special bituminous paint locally produced by Misr Petrol Company.

Composition: 46% hard bitumen H 80/90
54% solvent (Naphta).

- *"Solid Bitumen"* :

A hard grade bitumen locally produced and used for road surfacing as a hot molten mix at a temperature of about 200°C.

All of the above water-repellent agents were applied in brush coatings on the surface of the material to be treated.

In order to select the most suitable treatment for inhibiting water absorption by bamboo, two groups of tests were devised. The first group was made to ascertain the bond strength developed between concrete and bamboo treated by the various types of water-repellent agents. Tests from this group were also made to compare between the values of bond strength for the treated and untreated bamboo test specimens. The second, was carried out to evaluate the ability of each treating agent to prevent water absorption by the treated bamboo test specimens.

a) Bond Tests :

Concrete cylinders 15 cm in diameter and 15 cm high were prepared, each provided with a central reinforcing strip of seasoned bamboo and tested using the pull-out test procedure. Preliminary bond tests were made using green unseasoned test specimens of bamboo without treatment. The test results showed complete failure in bond due to the drying and shrinkage of bamboo while encased in concrete. Considering these test results, the use of green unseasoned bamboo was dropped at an early stage and all the tests were only made on bamboo culms seasoned by air drying in shade for 45 days.

In fabricating the concrete bond cylinders, four concrete mixes, having the same combined aggregate grading, were made using two cement contents of 250 and 350 kg/m^3 for two types of cement; namely Ordinary Portland cement and High Early Strength cement. For concrete mixes of cement content 250 kg/m^3, the cement — sand — gravel mix proportions by weight were 1 : 2.77 : 5.15 with a water-cement ratio (W/C) of 0.60. Those for concrete mixes of cement content 350 kg/m^3 were 1 : 1.88 : 3.50 with (W/C) ratio of 0.44.

The central reinforcing strips of bamboo were all having nearly the same width of 2.0 cm, but actually with different wall thicknesses. In treating these bamboo strips, care was taken to add sand to the external layer of treatment in the proper amount and at the proper time so as to make it stick effectively to the treated surface.

The average test results of bond strength between bamboo and concrete are recorded in *Table (2)*.

b) Absorption Tests :

Small seasoned test pieces of bamboo were prepared, then devided into groups each containing three test pieces having the same length of 10 cm and all with their cross sections as much alike as possible. For each water-repellent agent two groups of test pieces were made, the first treated with one brush coating and the other with two brush coatings. One control untreated group of 3 test pieces was also prepared for comparison.

It was decided not to test the "Solid Bitumen" treatment for water absorption, on the basis of the obtained bond test results indicating complete failure in bond strength due to the high lubricating effect of the treating material.

After being weighed, the treated and untreated control test pieces were completely immersed in fresh water at room temperature. For five days, the test pieces were re-

in *Figures (4,5)*. When calculating the average values of strength and stiffness, some values of test results were excluded in order to have the maximum deviation within ± 10% of the average value.

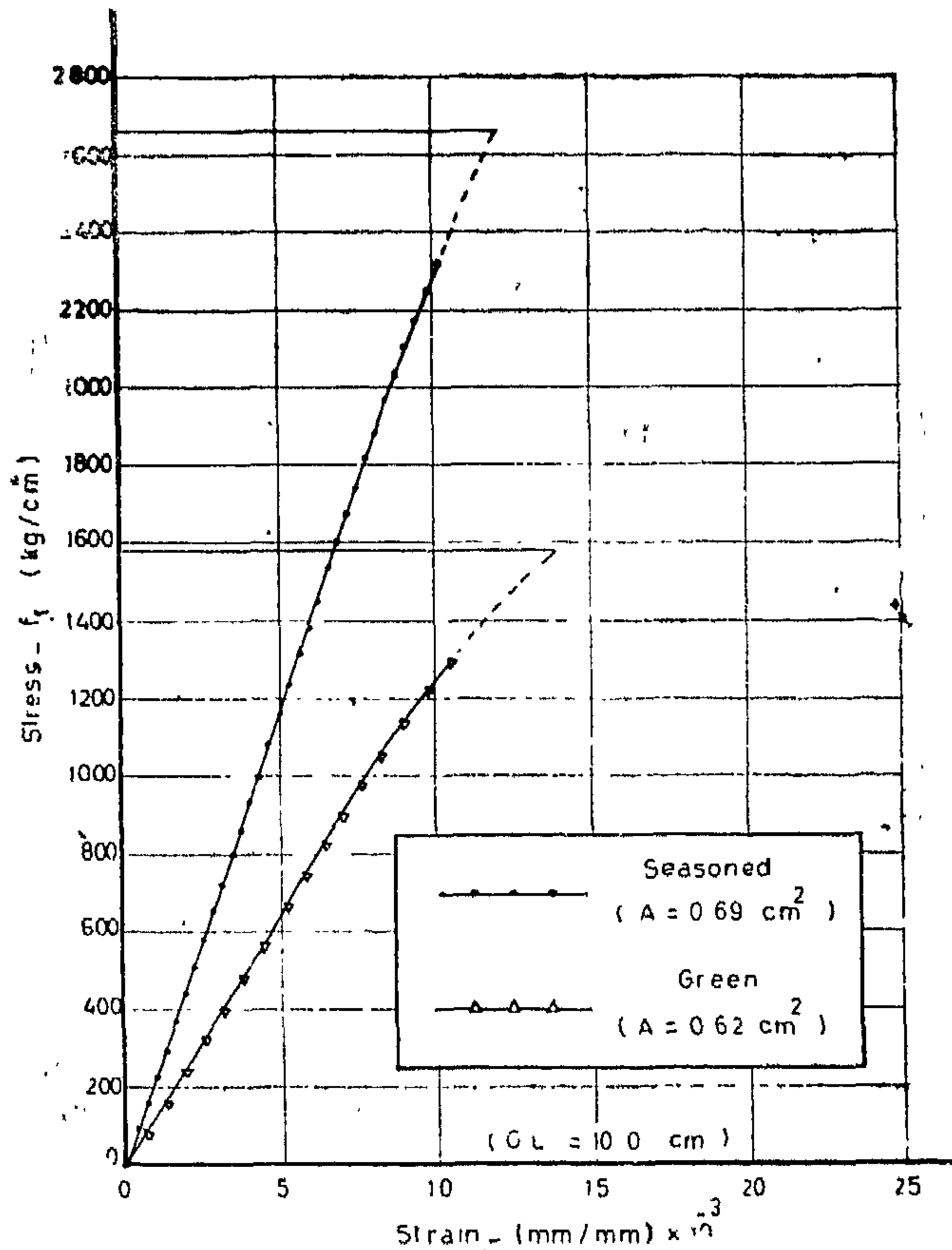


Fig 4. TYPICAL STRESS-STRAIN DIAGRAMS FOR GREEN AND SEASONED BAMBOO SPLINTS IN TENSION.

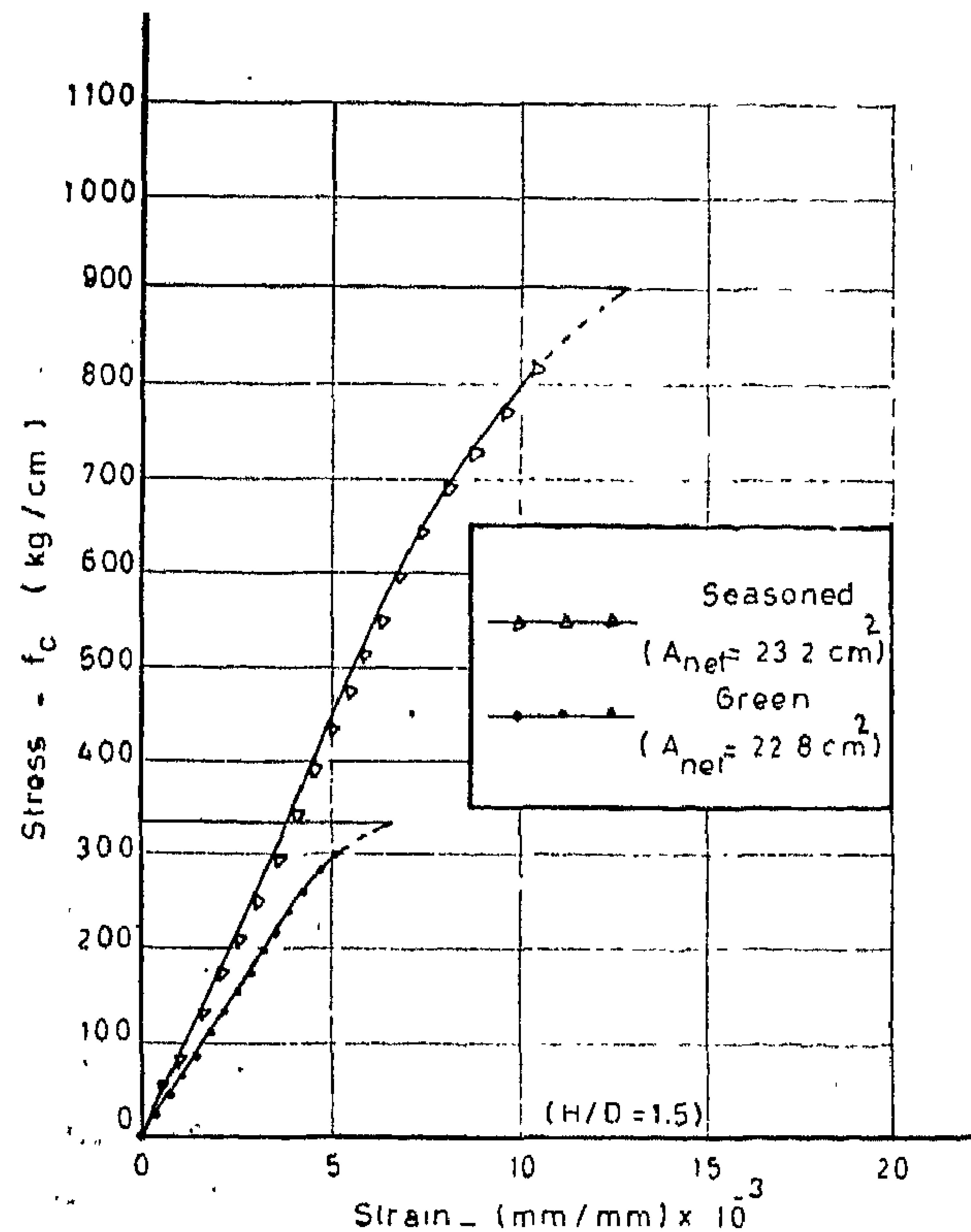


Fig 5. TYPICAL STRESS-STRAIN DIAGRAMS FOR GREEN AND SEASONED BAMBOO CULMS IN COMPRESSION

WATER-REPELLENT TREATMENT FOR BAMBOO REINFORCEMENT

Bamboo culms, being used as reinforcement in concrete members, would be subjected to high percentages of moisture existing in the concrete mass during the first few hours after casting. It was found, therefore, that using a suitable water-repellent treatment would be essential to ensure volume constancy of the reinforcing material while encased in concrete, hence eliminating the swelling cracks destroying the concrete member.

It was believed that the most suitable water-repellent treatment would be that which gives the higher values of bond strength between concrete and reinforcement and the lower values of water absorption, together with the reasonable economical cost.

The water-repellent agents selected in this investigation for treating the bamboo reinforcement were those commercially available and economical in price. The chosen agents are as follows :

- *"Flatting Varnish 601"* :

  A commercial name for a locally produced varnish used for painting different types of woody surfaces, including furniture and flooring, to give a hard shiny transparent cover.

- *"Shell Pipe Primer"* :

  A commercial name for a blown bitumen paint locally produced by Misr Petrol Company.

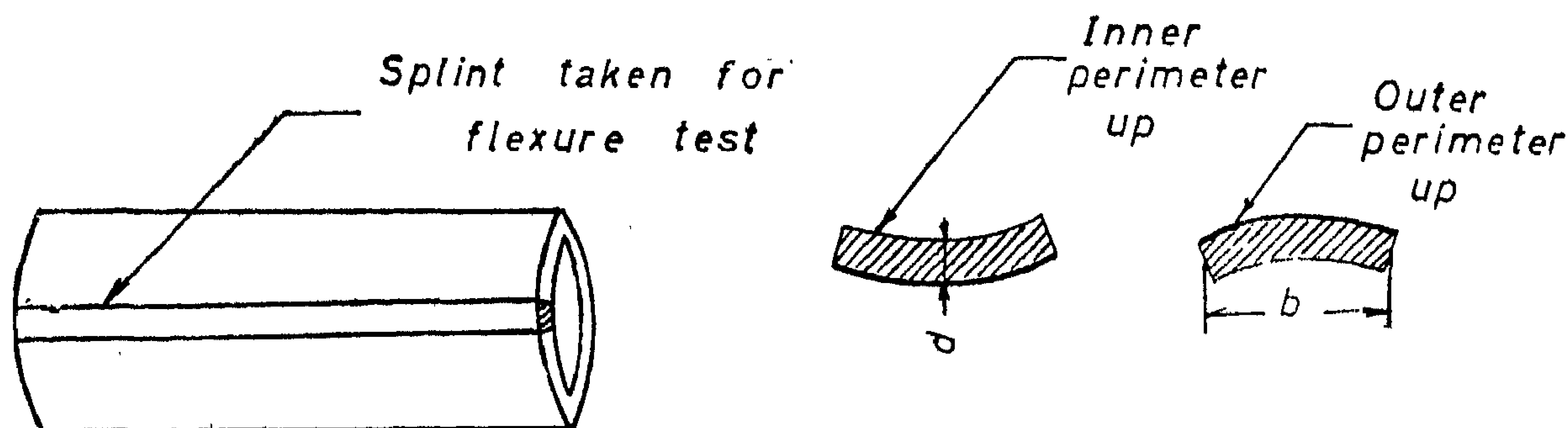


Fig. 3_ Position of Outer Perimeter of Bamboo Splints in Flexure

b) Test Results :

The determination of tensile strength presented some difficulty owing to the low strength in shear of the bamboo fibers. In a few number of cases the full tensile strength was not developed since the test specimens failed partly by shear and partly by tension. However, the tests gave a good indication of the order of the tensile strength to be expected.

For all compression test specimens, there was no sign of cracking before ultimate failure occurred. In most cases the ultimate failure occurred by splitting of wall fibers of the culm longitudinally. In the case of more thick-walled test specimens, failure generally occurred by crushing of both ends.

In flexure tests, putting the outer perimeter of the tested specimen to the tension side gave a sign of cracking in the outer layer of fibers fairly before ultimate failure occurred. However, putting the outer perimeter of the specimen to the compression side caused the sudden occurrence of ultimate failure.

The average values of test results for the mechanical characteristics of bamboo in tension, compression and flexure are recorded in *Table (1)*, while typical stress-strain diagrams for tension and compression tests are shown

Table (1) — Summary of the Average Values of Mechanical Characteristics of Bamboo.

Mechanical Characteristics	*Green Bamboo*		*Seasoned Bamboo*	
	with node	*without node*	*with node*	*without node*
Ultimate tensile strength (kg/cm²)	1170	1645	1920	2610
Ultimate compressive strength (kg/cm²)	296	323	890	934
Modulus of rupture in flexure* (kg/cm²)	602	683	1600	2100
Modulus of elasticity in tension (kg/cm²)	114,800	126,300	189,800	226,600
Modulus of elasticity in compression (kg/cm²)	46,900	59,020	68,500	97,800
Modulus of elasticity in flexure* (kg/cm²)	66,100	82,300	153,500	190,000

* Recorded for test specimens having the outer perimeter down, i.e. to the tension side.

its outer perimeter down indicates that the outer perimeter will be subject to tensile stresses while the inner perimeter to compressive stresses.

For the preparation of compression test specimens, each whole section was sized to have the height being equal to 1.5 times the outside diameter. For the sections containing nodes, care was taken to ensure having the node spaced equidistant from both ends.

The tension, compression and flexure test specimens of bamboo are shown in *Figures (1, 2, 3)*.

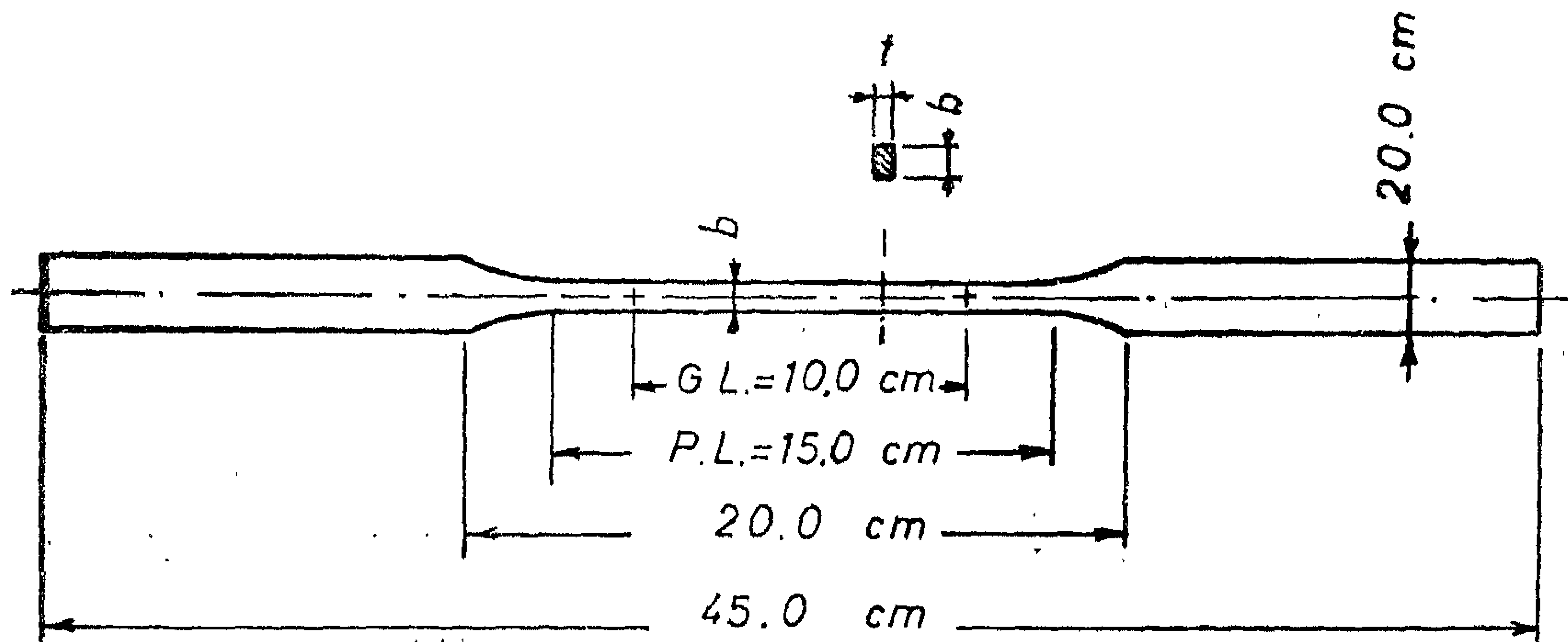


Fig. 1 – Tensile Test Specimen of Bamboo

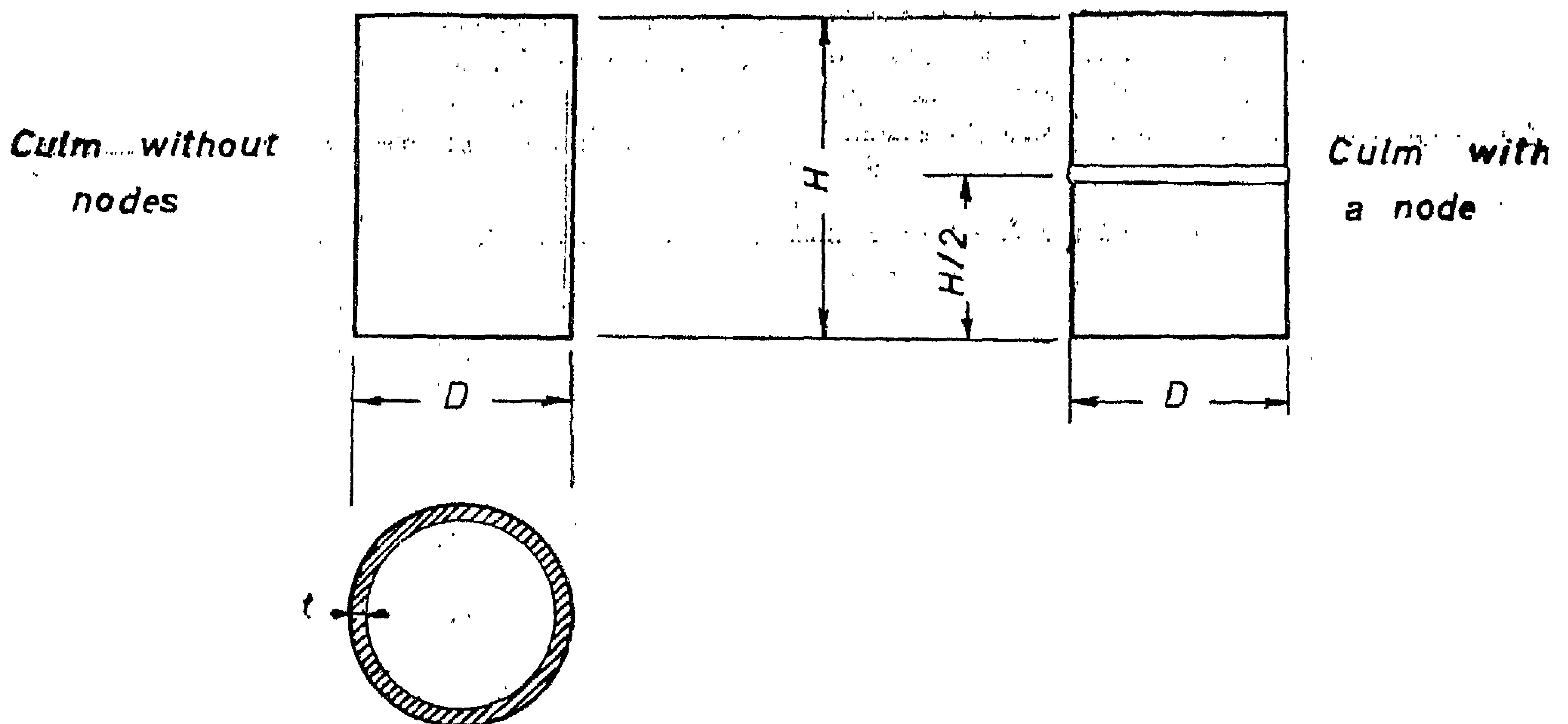


Fig. 2 – Compression Test Specimens of Bamboo

chosen to be judged as a substitute for steel reinforcement in concrete structural members. This choice was made regarding the promising results of bamboo given in previous investigations in many other countries.

Many earlier research workers have suggested the use of other non-metallic materials, such as fiber-glass and asbestos-cement bars, as substitutes for steel reinforcement. However, these materials were abandoned in carrying out this investigation since they are expensive and are produced using imported raw materials which disagreed with our self-sufficiency policy.

In carrying out this investigation, certain definite aims and objectives were set forth before work was begun.

The primary objectives for the work done were :

1. To establish the mechanical characteristics of bamboo which would be needed in the design of bamboo reinforced concrete members.
2. To find a suitable water-repellent treatment for bamboo reinforcement to ensure its volume constancy and prevent it from being rotten while encased in concrete.
3. To evaluate the effectiveness of bamboo as a substitute for steel reinforcement in concrete structural members.
4. To establish and recommend practical construction procedures and reliable design principles for load-carrying concrete members reinforced with bamboo.

All the bamboo specimens used in the various tests of this research work were obtained mainly from Orman Botanical Garden at Giza, and taken from one species indentified to be most probably "Arundinaria gigntea".

MECHANICAL CHARACTERISTICS OF BAMBOO

It was believed that the most comprehensive measure of the mechanical charaoteristics of the material could economically and significantly be determined by testing the bamboo culms in tension, compression and flexure. In determining these properties, tests were devised to find out the effect of both the degree of seasoning and the existance of nodes in bamboo specimens.

Regarding the results given in previous research work, it was concluded that bamboo attains its strength after being nearly three years old. Accordingly, in order to be on the safe side in our investigation on bamboo, it was decided that all tests would be conducted on four years old or older culms.

a) Test Specimens :

For each of the tension, compression and flexure tests, the tested species of bamboo was represented by at least three culms in the green unseasoned stage and three extra culms seasoned by air drying in shade for 45 days. From each bamboo culm, two sections were selected; one free of nodes and the other with a node spaced equidistant from both ends. For preparing the tensile and flexural test specimens, each bamboo section was ripped longitudinally into thin strips of not more than 2.0 cm in width. Each tensile test specimen was then devided into three equal parts; the end parts for the gripping and the central part to be prepared for a reduction in size to facilitate tensile breaking. There was no need for a reduction operation within the central part of the flexural test specimens. On the other hand, it was desired to investigate the effect of the position of outer perimeter on both the modulus of rupture and the modulus of elasticity in flexure. Hence, two groups of test specimens were prepared to be tested either with the outer perimeter up or down. It is to be noted that testing the specimen in flexure with

NON-METALLIC REINFORCEMENT FOR CONCRETE STRUCTURAL ELEMENTS*

By

Prof. Dr. AHMED A. EL-ERIAN
Head of Materials Testing Department
Cairo University

Prof. Dr. MOHAMED M. TEWFIK
Structural Engineering Department
Cairo University

MAHMOUD A. REDA YOUSSEF
B.Sc., M.Sc. (Structural Eng.)
Cairo University

PART 1 — BAMBOO

SYNOPSIS

The paper described herein is a part of an investigation studying the possibilities of using cheap and plentiful non-metallic materials as reinforcement in concrete members for suitable structural applications. This part reports an ex perimental investigation carried out on native bamboo to establish its mechanical character istics, to find a suitable water-repellent treatment for the bamboo reinforcement, and to evaluate its effectiveness as a substitute for steel reinforcement in concrete beams and columns. An attempt has been also made to establish and recommend practical construction procedures and reliable de sign principles for bamboo reinforced concrete structural members. A second part dealing with date-palm mid-ribs will be published later.

On the basis of the results obtained through this research, it was concluded that there are certain cases in construction where it would be safe and much more economical to recommend utilising bamboo as a substitute for steel reinforcement. Bamboo is recommended to be used as reinforcement in concrete structural elements of small units as in many of the rural housing projects, especially the one-storey buildings. The material is also highly recommended to be used as reinforcement for the various concrete structural precast units.

A special recommendation is given to the authorities to increase the land areas cultivated with bamboos taking an advantage of the re claimed areas in the New Valley and Al-Tahrir Province as well as Nasser Lake, at Aswan, whose banks are the ideal spot for the propagation of bamboo plant.

INTRODUCTION

This investigation was made under the immediate incentive of saving iron ore and steel to cover the demands of the national economic development plan in various sectors, to serve for the national defence requirements, and to meet the increasing local consumption of steel in the field of construction.

From among the locally available and cheap non-metallic materials, bamboo was

* This paper is based on an M. Sc. Thesis by the third author.

INFORMATION

- The editors welcome for publication engineering researches and articles as well as discussions on any material appearing in this periodical.
- This periodical does not hold itself responsible for the opinions expressed in it.
- Any material intended for publication must be sent to the Secretariat at the address of the Engineering Society at Cairo.

SUBSCRIPTIONS

All members of the Engineering Society at Cairo are ipso facto subscribers of this periodical.

Subscription for engineers P.T. 60 per annum.

Subscription for others P.T. 200 per annum.

HEAD OFFICE

Egyptian Society of Engineers,

28, Ramses Avenue, Cairo. Tel. 52106

ADVERTISEMENTS

JOURNAL OF
THE EGYPTIAN SOCIETY OF ENGINEERS
U.A.R.

QUARTERLY SCIENTIFIC PROCEEDINGS

ISSUED BY

THE EGYPTIAN SOCIETY OF ENGINEERS—U.A.R., CAIRO

Vol. X — No. 1 January-February-March 1971

CONTENTS

ENGLISH SECTION

Page

Mon-Metallic reinforcement for Concrete Structural Elements.
Dr. AHMED A. EL-ERIAN, Dr. MOHAMED M. TEWFIK, MAHMOUD A. REDA YOUSSEF. 7

Reception of Vef transmissions.
Dr. A. LOUTFY EL-SAYED. 29

An investigation of the strength of cold formed tubular joints.
Dr. MAGDY R. SHINOUDA. 34

Rapidly varied flow over hydraulic structures.
Dr. M.S. ABDALLAH, Dr. M.M. ABOU-SEIDA, Dr. M.A. SOLIMAN. 46

Oxidation of sodium sulfite at Perforated Plates.
Dr. M. FIKRI CHALABI 61

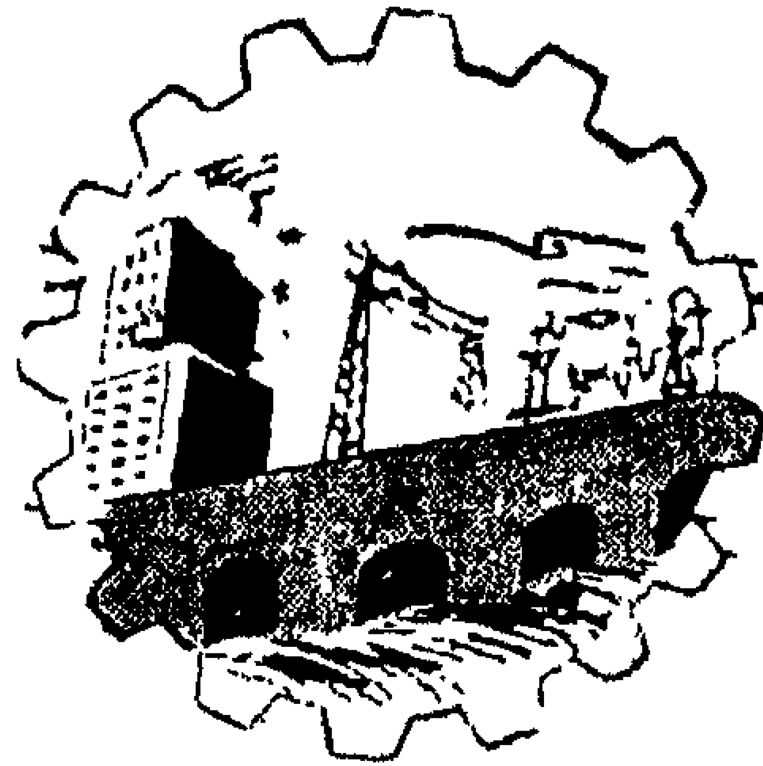
An Application of dynamic programming to the design of an aircraft control system.
Dr. O.A. EL-KHOLI, M.M. AWNY 71

Thermal performance of reinforced concrete roof slabs in hot dry climates and the resulting state of comfort inside low cost Buildings.
Dr. ALI SALEH. 82

ARABIC SECTION

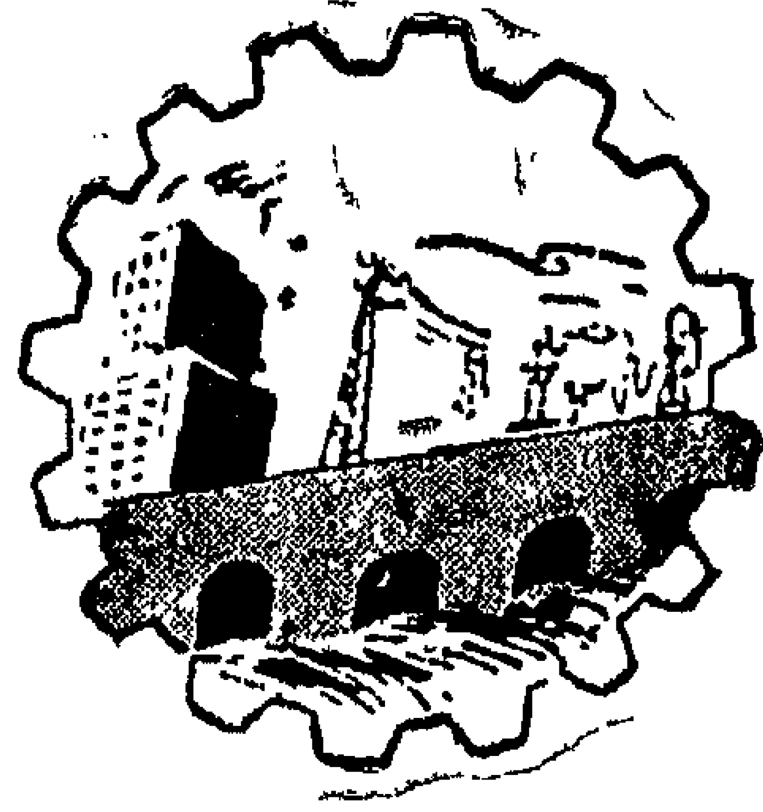
Reinforced Concrete in Architecture.
Dr. ALY RAAFAT. 7

«Mondiale» Press—Cairo



JOURNAL OF THE EGYPTIAN SOCIETY OF ENGINEERS U. A. R.

January-February-March 1971
Vol. X
No. 1



مجلة

جمعية المهندسين المصرية

أبريل – مايو – يونية ١٩٧١ | المجلد العاشر | العدد الثانى

المطبعة العالمية ١٦ ، ١٧ شارع ضريح سعد بالقاهرة

مجلة

جمعية المهندسين المصرية

مجلة علمية هندسية - تصدرها كل ثلاث شهور

جمعية المهندسين المصرية بالقاهرة

السنة العاشرة — العــدد الثانى — أبريل — مايو — يونيو ١٩٧١

محتويات هذا العدد

القسم العربى

		صفحة
دور التقييس فى توليد وتوزيع الطاقة الكهربائية	للدكتور المهندس فؤاد طاهر	٧

القسم الأفرنجى

التسليح غير المعدنى للأجزاء الخرسانية للمنشآت - الجزء الثانى (البامبو)	للدكتور المهندس أحمد على العريان والدكتور المهندس محمد محسن توفيق والمهندس محمود على رضا يوسف	٧
العزوم الحانية فى الصهاريج الخرسانية مستطيلة المقطع	للدكتور المهندس ميشيل باخوم والدكتور المهندس محمد محسن توفيق والدكتور المهندس محمد حمدى الكاتب	٢٩
تصميم الستائر غير المنفذة فى السدود الترابية مع الإشارة الخاصة إلى السد العالى بأسوان	للدكتور المهندس عبد الرحمن الرملى والمهندس حسن عبدون	٤٦
طرق اكتشاف منابع الأشعة تحت الحمراء وتتبعها	للدكتور المهندس عوض مختار هلوده	٥٥
بعض دراسات هيدروجيوكيميائية المياه الجوفية لحقل البترول برأس غارب واحتمالات استغلالها صناعياً	للدكتور المهندس نصرى زكى بشاى	٧٠
تصميم التسهيلات الحديثة لشحن البترول الخام	للدكتور المهندس ابراهيم محمود الاسيوطى	٨٥

بيانات

مقر المجلة

جمعية المهندسين المصرية

٢٨ شارع رمسيس بالقاهرة

تليفون : ٥٢١٠٦

- جميع أعضاء جمعية المهندسين مشتركون فى المجلة بحكم عضويتهم
- الإشتراك السنوى لغير الأعضاء : ٦٠ مليم للمهندس ، ١٠٠ مليم للهيئات
- ترسل البحوث والموضوعات والتعليقات إلى أمانة التحرير بمقر جمعية المهندسين
- المصرية بالقاهرة
- ترحب المجلة بما يرسل إليها من بحوث وموضوعات هندسية وأى تعليقات علمية للمناقشة
- المجلة غير مسئولة عن الآراء التى تنشر بها وتعبر عن رأى كاتبها فقط .

لجنة التحرير

دور التقييس
فى توليد وتوزيع الطاقة الكهربائية

للدكتور المهندس فؤاد طاهر

كما هو الحال فى جميع الدول ، فإن استهلاك الطاقة الكهربائية فى الدول العربية قد تزايد وسيستمر فى التزايد. ومع ذلك ، فإن الاستهلاك فى بعض هذه الدول قد تزايد بخطى واسعة جداً ، أوسع بكثير منها فى الدول الأوروبية. ومع هذا الازدياد ، ولقد طورت أيضاً منشآت توليد القدرة وأنظمة التوزيع لمقابلة احتياجات الاستهلاك ، ولتلبية الاحتياجات المستقبلة المتزايدة باستمرار ، فان السعة (الاستطاعة) المركبة لمحطات التوليد ستزداد ، فى حين ستنمو وتتسع شبكات النقل والتوزيع لتغطى كل المناطق المأهولة .

وسيؤدى هذا فى النهاية إلى ارتباط أنظمة القدرة فى الدول العربية المتجاورة ويلزم وجود مواصفات قياسية للمقننات والتصميم ليتحقق مثل هذا الارتباط .

ومنذ نهاية الحرب العالمية الثانية ، لجأت بعض الدول العربية إلى تغطية جزء من احتياجاتها الكهرتقنية عن طريق التصنيع المحلى للمعدات الكهربائية ، وسوف تتاح السلع الكهرتقنية للتبادل بين الدول العربية ، ويوضح مثل هذا التبادل الحاجة إلى التقييس فى مجال الصناعات الكهربائية .

استهلاك الطاقة الكهربائية وتطوره :

تزايد استهلاك الطاقة الكهربائية بخطى واسعة جداً فى الدول العربية . وطبقاً لإحصائيات الأمم المتحدة ، فلقد تطور استهلاك الطاقة الكهربائية من حوالى ٣,٧ مليار (ألف مليون) ك. و. س. فى عام ١٩٥٣ إلى حوالى ١٧,٥ مليار (ألف مليون) ك. و. س. فى عام ١٩٦٨ ، ويبين الجدول (١) تفاصيل هذا التطور . ولقد تراوح النمو السنوى لاستهلاك الطاقة بين حدود عالية ومنخفضة ، ولكن الاتجاه العام بلغ فى المتوسط ١١٪ سنوياً .

ويتوقف تطور استهلاك الطاقة الكهربائية فى المستقبل على عدة عوامل تشمل التطور الماضى للاستهلاك والمستويات المتوقعة للمعيشة، ومخططات التنمية الاقتصادية . مع ذلك فحيث أن تلك العوامل ليست موضوع هذا البحث ، لذلك فإن التكهن بالاحتياجات المستقبلة سيبنى على العوامل العامة . وهذه

جدول رقم (١)

إنتاج الطاقة الكهربائية

الدولة	١٩٥٣	١٩٦٠	١٩٦٥	١٩٦٨
الجزائر	٧٧١	١٣٢٥	١١١٤	١٣٠٥
البحرين	١٠	٤٩	١٣٤	٢١٦
العراق	٣٤٣	٨٥٢	١٢٠٧	—
الأردن	—	—	١٥٦	١٥٦
الكويت	—	٢٤٩	٨٠٢	١٦٥٩
لبنان	١٨٠	٤٢٢	٧٦٥	١٠٣٦
ليبيا	٥٠	١٠٥	١٥٢	٢٧٤
المغرب	٧٤٨	١٠١٢	١٣٦٢	١٥٣٨
المملكة العربية السعودية	—	٤٤	٢٦٨	—
اليمن الديمقراطية	١٦	١٤٤	٢٢٧	١٧٨
السودان	٣٢	٧٤	١٧٤	٣٣٤
سوريا	٢٠٥	٣٦٨	٦١٦	٧٧٣
ج.ع.م.	١٢٠٠	٢٦٣٩	٥٤٧٣	٦٧٣٥

ملحوظة : تتعلق البيانات المعطاة بإنتاج مراكز التوليد ، ولذلك فإنها تتضمن استعمال المحطات وفواقد النقل .

الدول لا تمر بمرحلة التنمية فحسب ، بل هي تمثل أحد المراكز الرئيسية لإنتاج البترول وهي حقيقة تفسر ارتفاع مستوى المعيشة ومن ثم معدل النمو في استهلاك الطاقة الكهربائية .

وإذا أخذنا هذه العوامل في الاعتبار . يمكننا أن نتوقع أن يكون معدل نمو الاستهلاك كما كان في العقد الماضي على الأقل . أي ١١٪ سنوياً . ومع ذلك . فيمكن أخذ هذا المعدل بمتوسط أقل خلال العقود التالية . ويمكن التنبؤ بالاستهلاك كما يلي :

١٩٧٠	٢٠٠٠٠	مليون	ك.و.س.
١٩٨٠	٥٥٠٠٠	مليون	ك.و.س.
١٩٩٠	١٢٥٠٠٠	مليون	ك.و.س.
٢٠٠٠	٣٠٠٠٠٠	مليون	ك.و.س.

وعامل الحمل لاستهلاك الطاقة في الدول النامية له قيمة

منخفضة بصفة عامة . ومع قيام الصناعات الثقيلة والصناعات الكهروكيميائية التى تستهلك مقادير كبيرة من الطاقة ، فإن عامل الحمل يتزايد تدريجياً . ومع ذلك ، فإن عامل الحمل يميل إلى التناقص ثانية فى مرحلة تالية للتنمية . عندما يمثل استهلاك المرافق العامة والاستهلاك المنزلى نسبة عالية من الاستهلاك الإجمالى .

وإذا بنينا توقعاتنا على ذلك ، فيمكن أن نفترض عامل حمل يبدأ بحوالى ٥٥٪ ويصل إلى حوالى ٧٠٪ خلال الفترة الجارى دراستها . وسيؤدى هذا إلى التنبؤ بحمل ذروى كالآتى :

٥٠٠٠	م٠و٠	فى ١٩٧٠
١٢٠٠٠	م٠و٠	فى ١٩٨٠
٢٥٠٠٠	م٠و٠	فى ١٩٩٠
٥٥٠٠٠	م٠و٠	فى ٢٠٠٠

ويجب ألا يغيب عن الذهن أن هذه الأرقام لا تمثل حملا ذرويا لنظام ما ، ولكنها تمثل مجموع الأحمال الذروية للشبكات الفردية فى الدول المختلفة بالمنطقة أو الشبكات الفردية لمجموعات الدول التى قد تترابط فى المستقبل .

الاحتياجات المستقلة من معدات أنظمة القدرة :

طبقاً لاحصائيات الأمم المتحدة ، فإن إجمالى السعة المركبة فى محطات التوليد بالدول العربية يبلغ حوالى ٦٠٠٠م٠و فى ١٩٦٨ . ولما كان هذا يحمل مجموع الأحمال الذروية حوالى ٥٠٠٠م٠و٠ للدول العربية المختلفة . لذلك نشعر بأنه أقل من اللازم بكثير . والشبكات الصغيرة المنعزلة ذات مقننِ الوحدات التوربينية الذى يمثل نسبة مئوية عالية من الحمل الذروى ، لا بد أن تتطلب حوالى ٣٠٪ من السعة الاحتياطية . أو سعة مركبة لا تقل عن ٦٥٠٠م٠و٠ ومع ذلك فمع ازدياد أنظمة القدرة وترابطها ، فإن السعة الاحتياطية كنسبة مئوية من الحمل الذروى ستكون أقل . وتتوقف السعة الاحتياطية اللازمة لنظام قدرة ما على عدة عوامل ، لا تدخل دراسة تفاصيلها ضمن نطاق هذا البحث . ولتقدير السعة المستقلة لمحطات التوليد اللازمة لتغذية الأحمال المذكورة بالسعة الاحتياطية المثلى ، سنفترض أن مجموع السعات المركبة فى الدول المختلفة يبلغ ١٢٥ فى المائة من مجموع الأحمال الذروية عند بداية فترة الدراسة ، وسيصل إلى ١٢٠ فى المائة فى نهاية فترة الدراسة . وهذا الافتراض يؤدى إلى التقديرات التالية للسعة المركبة الإجمالية .

٦٥٠٠	م٠و٠	فى ١٩٧٠
١٥٠٠٠	م٠و٠	فى ١٩٨٠
٣٠٠٠٠	م٠و٠	فى ١٩٩
٦٦٠٠٠	م٠و٠	فى ٢٠٠٠

وهذا يعنى ضرورة إنشاء وحدات توربينات — مولدات جديدة إضافية ، بخارية أو هيدرولية ، بمتوسط سنوى ٢٠٠٠م٠و٠ لمقابلة تطور الأحمال الكهربائية للدول العربية . وفى بداية فترة الدراسة ستكون الاحتياجات السنوية أقل من هذا المتوسط ، ولكن مع نهاية فترة الدراسة (أى فى التسعينات) قد تصل الاحتياجات السنوية إلى ٣٠٠٠م٠و٠ وباعتبار أن الحجم المتوسط للوحدة فى هذه المرحلة ٢٠٠ — ٣٠٠ م٠و٠ ، فسيلزم من ١٠ إلى ١٥ وحدة سنويا ، وهو عدد قد يثبت أنه اقتصادى لصناعة إقليمية .

ومع ازدياد استهلاك الكهرباء وتوسيع شبكات القدرة لتصل إلى جميع المستهلكين ، يجب نقل الطاقة الكهربائية على جهد عال ، وخاصة فى الحالات حيث يكون التوليد بعيداً عن مراكز الاستخدام . وقد يلزم رفع الجهد عند طرف التوليد ، وخفضه على عدة خطوات ليلائم احتياجات التوزيع والاستخدام . وللتقدير التقريبى لسعة المحولات ، اللازمة لشبكات النقل والتوزيع الجديدة ، سنفترض أنه ستكون هناك مرحلة رفع واحدة وثلاث مراحل خفض . ومع وجود

جدول رقم (٢)

السعة المركبة

الدولة	١٩٥٣	١٩٦٠	١٩٦٥	١٩٦٨
الجزائر	٤٩٦	٤٣٩	٥٠٠	٦٢٩
البحرين	٣,٨	٢٦,٣	٤٢,٢	٦٦,١٤
الكويت	—	٧٣	—	—
لبنان	٥٢	١٢٦	٣٧٤	٣٧٤
ليبيا	١٧,٩	٣٣,٤	٥٧,٨	١٦٨,٥
المغرب	٢٣٧	٣٣٦	٣٩٢	—
المملكة العربية السعودية	—	٢٨,٦	٩٤,٠	—
السودان	١٤,٢	٤٣,٥	٧٦,١	٩٧,٤
سوريا	٥٤	١١٩	٢٢٣	٢١٦
تونس	٨٤	١٢٩	٢١٣	٢٦٢
ج.ع.م.	٥٨٦	١١٦٧	١٤٦٦	٢٧٢٥

ملحوظة : البيانات المعطاة تمثل كل سنة نهاية العام الاعتبارية لجميع المولدات المتاحة للتشغيل الآلى فى المحطات الكهرهيدروليكية والحرارية الكهربائية .

سعة احتياطية فى محطات المحولات تتراوح بين ٢٥ فى المائة و ١٠٠ فى المائة ، فإن هذا يعطى سعة تحويل إجمالية تبلغ حوالى ٦,٥ أمثال الحمل الذروى .

وعلى ذلك ، فمع تطور الحمل الذروى السابق افتراضه يمكننا أن نتوقع إنشاء سعة تحويل تبلغ حوالى ١٠ مليون ك. ف. ا. سنوياً لتغطية جميع مستويات الجهد .

وتوضح البيانات التى قدمت فى مؤتمر المهندسين العرب الذى عقد فى ١٩٦٩ ، أن الاستهلاك السنوى للدول العربية من معدات القدرة الكهربائية فى ١٩٦٥ كان كالآتى :

كبلات وأسلاك معزولة	٤٨٠٠٠ طن
معدات قدرة كهربائية	٢٩٠٠٠ طن
مجموعات مفاتيح كهربائية	٢٠٠٠٠ طن

وبافتراض أن الأسلاك السنوى الإجمالى لمثل هذه المواد والمعدات يتناسب تناسباً مباشراً مع ازدياد الحمل ، فيمكننا أن نقدر الاستهلاك السنوى من تلك البنود كالآتى :

	١٩٨٠ — ١٩٩٠	١٩٩٠ — ٢٠٠٠
كبلات وأسلاك معزولة	١٥٠٠٠	٣٠٠٠٠
معدات قدرة كهربائية	٩٠٠٠٠	١٨٠٠٠٠
مجموعات مفاتيح كهربائية	٦٠٠٠٠	١٢٠٠٠٠

جدول رقم (٣)

تعـداد السكان

الدولة	تقديرات منتصف عام		الكثافة
	١٩٦٣	١٩٦٨	١٩٦٨
الجزائر	١١٢٠٥	١١٩٤٣	٥
البحرين	١٧٠	٢٠٠	٣٣٤
العراق	٧٦٦٠	٨٦٨٤	٢٠
الأردن	١٧٩٣	٢١٠٣	٢٢
الكويت	٣٨٨	٥٤٠	٣٤
ليبيـا	١٥٠٤	١٨٠٣	١
لبنان	٢٢٨٥	٢٥٨٠	٢٤٨
المغرب	١٢٦٠٥	١٤٥٨٠	٣٣
المملكة العربية السعودية	٦٥٣٠	٧١٠٠	٣
اليمن الديمقراطية	١٠٧٣	١١٩٥	٤
السودان	١٢٨٣١	١٤٧٧٠	٦
سوريا	٤٩٦٩	٥٧٠١	٣١
تونس	٤١٧٠	٧٦٦٠	٢٨
ج.ع.م.	٢٧٩٤٧	٣١٦٩٣	٣٢
مسقط وعمان	٥٦٥	٥٦٥	٣

ملحوظة الكثافة : تعداد السكان فى الكيلومتر المربع من المساحة

وبالإضافة إلى التقديرات السابق ذكرها ، فإن التوسعات المستقبلة فى أنظمة القدرة بالدول العربية ستستلزم إنشاء خطوط نقل وتوزيع تتطلب أبراجاً ، وأعمدة ، وعوازل ، وملحقات ، إلخ .

وستلزم مقادير هائلة من أنواع المعدات الكهربائية الأخرى للصناعات المختلفة ، وأغراض الجر ، والأجهزة المنزلية ، والتركيبات فى المبانى ، والاستخدامات الأخرى .

* * *

دور التقييس :

غنى عن البيان أن تناقش مزايا ترابط أنظمة القدرة فإنها معروفة تماما المسئولين فى جميع الهيئات والمؤسسات الكهربائية وتترابط شركات القدرة فى الولايات المتحدة الأمريكية عبر قارة أمريكا الشمالية ، كما تترابط معظم أنظمة المقدرة فى غرب أوروبا، وكذلك أنظمة القدرة فى الكتلة الشرقية الأوروبية. وسرعان ما سيأتى الوقت الذى نجد فيه أنه من الضرورى أن تترابط أنظمة القدرة للدول العربية . والواقع فإن تونس مترابطة حالياً مع الجزائر بخط ٩٠ ك. ف. ثم تشغيله فى الخمسينات فى حين يربط خط ٢٢ ف. ك. بين الجزائر والمغرب. وتجرى حالياً دراسات لربط الكويت والعراق ، وربط سوريا ولبنان. وسيتوالى سريعاً ترابط الدول العربية المتجاورة ، ولن نكون بعيدين عن الصواب إذا قلنا إن الترابط الكامل للدول العربية سيتحقق خلال العقود الثلاثة القادمة التالية . ومع الارتباط التام كهدف نهائى ، فان المهندسين الكهربائيين بالدول العربية يجب أن ينتبهوا إلى المشاكل التى ستنشأ وكيفية حلها . وأحد المسائل الرئيسية التى يجب أن تؤخذ فى الاعتبار هى جهد نظام الارتباط . وقد تنشأ فى وقت قريب شبكة فائقة Supergrid لتربط بين الدول العربية ، ويبدو أنه من المهم جداً الاتفاق من الآن على جهد هذه الشبكة الفائقة . ومن الطبيعى أن جميع المهندسين العرب يدركون ما كان عليه التقييس الدولى من عدم اتفاق فى الماضى فيما يتعلق بالجهود فائقة العلو . فمن بضع سنين تبنت اللجنة الدولية الكهرتقنية IEC نظام ٤٠٠ — ٤٢٠ ك. ف . كخطوة الجهد التالية فوق ٣٣٠ ك، ف. ولم تكن الولايات المتحدة الأمريكية فى ذلك الوقت معنية كثيراً بتقييس الـ IEC وبدأت بدلا من ذلك فى تطوير نظام ٣٤٥ — ٣٦٢ ك. ف وفى النهاية وافقت الـ IEC على تقييس الولايات المتحدة الأمريكية ولكنه كان إلى جانب نظام ٤٠٠ — ٤٢٠ ك. ف. المعمول به فى أوروبا .

وبالإضافة إلى مستويات الجهد المتقاربة هذه ، فلقد ووفق على نظام ٥٠٠ — ٥٢٥ ك. ف. كجهد قياسى ، وهو معمول به فى الولايات المتحدة الأمريكية والاتحاد السوفييتى وكثير من الدول الأخرى . ويوضح هذا أهمية تقييس جهد النقل والحاجة الملحة إليه ، لا فى مستويات الجهد بالغة العلو فحسب ، بل وفى مستويات الجهد المتوسطة والعالية ، حيث قد تترابط أنظمة التوزيع للدول المتجاورة لضمان إمكانية الاعتماد على التغذية لبعض الأحمال الهامة .

ومنذ نهاية الحرب العالمية الثانية ، تزايد استهلاك الطاقة الكهربائية بالدول العربية بسرعة عظيمة ، وبالتالى تزايدت احتياجاتها من المعدات الكهربائية . ولكى تتمكن الدول الصناعية من توسيع أسواقها العالمية ، فانها كانت تحاول أن تؤثر على تلك الدول الصغيرة لتختار مواصفاتها القياسية .

ولقد اتضح الشعور بأهمية توحيد المواصفات القياسية منذ بعض الوقت على النطاق الدولى . فاللجنة الدولية الكهرتقنية هى وليدة قرار اتخذه مندوبو الحكومات فى مؤتمر سان لويس الكهربائى الدولى الذى عقد عام ١٩٠٤. وتكونت هذه اللجنة فى ١٩٠٦ واجتمع مندوبو ١٤ دولة لأول مرة فى ١٩٠٨ .

وكانت المهمة الأصلية IEC هى النظر فى مسائل المصطلحات الفنية ومقننات الأجهزة والآلات الكهربائية . ثم تطورت مهمتها تدريجياً ، وهى ترعى حالياً أكثر من ٦٠ لجنة تقنية ويعاونها عدد من اللجان الفرعية . ومن المعتقد أن أعمالها التقنية تتزايد بمعدل ٢٠ فى المائة سنوياً .

ولقد اتخذت خطوة تالية نحو التقييس الدولى بقيام المنظمة الدولية للتقييس (ISO) فى ١٩٤٦ . وفى العام التالى انضمت الـ IEC إلى الأيزو بمثابة فرعها الكهربائى وكلاهما له وضع استشارى فى الأمم المتحدة .

وبالنسبة للتقييس الإقليمى ، فإن المجلس الاقتصادى لجامعة الدول العربية قد وافق على قرار ١٩٦٥ بإنشاء المنظمة العربية للمواصفات والمقاييس (ASMO) . ومن أهم الأهداف التى أنشئت من أجلها المنظمة :

١ — المعاونة فى إنشاء مؤسسات أو أجهزة خاصة للمقاييس والمواصفات فى الدول العربية .

٢ — تنسيق وتوحيد المواصفات القياسية بين الدول العربية كلما كان ذلك ممكناً .

وليس من شك فى أن تكون منظمة إقليمية مفيد ومهم جداً من عدة وجوه . ومع ذلك فإن التنسيق بين المنظمات الإقليمية والدولية أمر بالغ الأهمية . وفى المجال الكهرتقنى ، يسود الاعتقاد بضرورة قيام نوع من التنسيق بين اللجان الوطنية لـ (IEC) ، والمنظمة العربية للمواصفات والقاييس (ASMO) ، والمنظمة الدولية للتقييس (ISO) .

الخلاصة :

١ — من المتوقع لمواجهة الطلب المتزايد تزايداً سريعاً من الطاقة الكهربائية أن تركب الدول العربية سنوياً فى شبكاتها حوالى ٢٠٠٠ م و. من وحدات التوليد ، وحوالى ١٠ مليون ك . ف . ا . من السعة التحويلية ، وحوالى ١٠٠٠٠٠ طن من مجموعات المفاتيح الكهربائية والأنواع العديدة الأخرى من المعدات الكهرتقنية .

٢ — يجب لتنسيق تطور الصناعة العربية للمعدات الكهرتقنية أن تطبق نفس المواصفات القياسية لهذه المعدات فى جميع الدول العربية .

٣ — يلزم كذلك تطبيق نفس المواصفات القياسية فى جميع الدول العربية ، وذلك ليتم الارتباط الصحيح بين الشبكات الكهربية فى الدول العربية المتجاورة .

٤ — يلزم أن ينشأ شكل من أشكال التنسيق بين الهيئات المختلفة المسئولة عن التنسيق ، ونعنى بها المنظمة الدولية للتقييس ، والمنظمة العربية للمواصفات والمقاييس واللجان الوطنية للجنة الدولية الكهرتقنية فى الدول العربية .

* * *

ملخص الموضوعات بالقسم الافرنكى

طرق اكتشاف منابع الأشعة تحت الحمراء وتتبعها

للدكتور المهندس عوض مختار هلودا

لقد أصبحت الاستفادة من إمكان استغلال الأشعة تحت الحمراء أساسية في الاستخدامات سلمية كانت أو حربية فلقد مكنت نظارات الرؤية الليلية التحركات والمناورات ، وكان لتقدم نظم جمع الإشعاعات وزيادة حساسية المكتشفات أثر بالغ فى إمكان اكتشاف الأهداف وخاصة الحربية منها والتى تمثل منابع إشعاعات كبيرة وعلى رأسها الطائرات وقد قسمت أجهزة تتبع الأشعة تحت الحمراء فى المقالة من ناحية الاستخدام كما ذكرت علاقة إشعاعات الأهداف بالإشعاعات الطبيعية للخلفية التى تتواجد بها وكذا علاقة حجم الهدف بحجم الأجزاء المشعة من الخلفية وذكرت أمثلة للانواع المختلفة للاستخدامات .

بعض دراسات هيدروجيوكيميائية للمياه الجوفية لحقل البترول رأس غارب واحتمالات استغلالها صناعيا

للدكتور المهندس نصري زكي لبشاي

الدراسات الهيدروجيوكيميائية لحقل البترول رأس غارب تشمل التكوينات الجيولوجية الحاملة للزيت الخام والمياه . وهذه التكوينات تشمل : الحجر الرملي النوبي (المجموعات «د» و « ج » ، « ا ») ، الكريتاوى الأعلى ، الميوسين المتوسط ، والبليوسين (حاملة المياه فقط) . أثبتت التحاليل الكيميائية للمياه أنها ذات ملوحة عالية (من ٧٠ إلى ١٧١ جرام باللتر) . هذه الملوحة تزيد بزيادة العمق وبزيادة عمر التكوينات الجيولوجية . لقد ثبت كذلك أن هذه المياه تحتوى على تركيزات عالية من البروم والبورون . اليود يوجد ببعض تركيزات عالية . تركيز هذه العناصر يزيد بزيادة العمق وعمر التكوينات الجيولوجية ، تتميز هذه المياه كذلك بتركيزات منخفضة من الكبريتات والكربونات وعدم وجود النترات والنيتريتات : أما الغازات المصاحبة للبترول الخام والمياه فهى تتكون أساساً من غاز الميثين والغازات الهيدروكربونية والثقيلة الأخرى .

أثبت التمثيل الكيميائى أن نوعية هذه المياه هى كلوريد الصوديوم . وقد أثبتت دراسات المعاملات الهيدروجيوكيميائية (كل / بر / ، / ى ، ص / كل .. الخ) أن أصل هذه المياه الغنية بالبروم والبورون واليود والكالسيوم هى مياه البحر القديمة (ومياه البحيرات فى الميوسين المتوسط) التى تعرضت لبعض التحولات الكيميائية . وجود الأمونيوم يشير إلى وجود درجات عالية من الظروف المختزلة .

لكى تكون المياه الجوفية صالحة للاستغلال صناعياً ، هناك بعض المواصفات اللازمة لصلاحيتها لاستخراج عناصر البروم والبورون واليود . لقد ثبت أن شروط هذه المواصفات تنطبق على المياه الجوفية لرأس غارب وأنه يمكن استخراج أكثر من ألف طن من البروم هذا بجانب البورون واليود . كذلك وجدت تركيزات عالية من هذه العناصر فى حقلى البترول الغردقة ورأس بكر ولذلك فإنه يجب أن تنشأ هذه الصناعة فى الجمهورية العربية المتحدة فى حقول البترول المختلفة التى تقع على جانبى خليج السويس .

مجلة
جمعية المهندسين المصرية

مجلة علمية هندسية — تصدرها كل ثلاثة شهور

جمعية المهندسين المصرية بالقاهرة

الاشتراك السنوى لغير الأعضاء :

المهندس	قرش ٦٠
للهيئات	قرش ٢٠٠

A recent design of crude oil loading facilities is made in Libya. It is a single point mooring for tankers up to 300 000 WDT. The type of structures evolved is shown in figure 5. This consists of heavy steel base resting on the sea bottom in 40 metres of water and attached to the sea bottom with piles. A single vertical leg extends from the base by a universal joint permitting the buoy on the surface to move in any direction on the surface of the sea. Crude oil is carried to the base of the structure in a 120 cm diameter pipeline on the sea bottom. The oil is carried through the base and then through two hoses to the vertical leg which at this point is a 120 cm. diameter steel pipe. Oil flows through to a fluid swivel which is about 15 metres under water. From this fluid swivel a single 60 cm. diameter hose carries the crude oil to the ship's side. The first 60 metres of this hose is under water but sloping towards the surface, the remainder floates on the surface of the sea to the ship's side. A ship moors in this structure by heading into the wind towards the structure. Mooring lines are attached from the ship's bow to the mooring buoy. The end of the 60 cm. hose floating on the surface is towed to the tanker's side where it is picked up by the ship and connected to the ship's manifold.

CONCLUSION

A general background information on the type of mooring and loading structure for crude oil tankers in use in the world has been given. This information may assist the civil engineer in developing the scope of his problem if he is confronted with the design of tankers mooring and loading facilities. From what is presented it can be concluded that the type of berthing to be used at a certain location depends on the conditions that exist in that area.

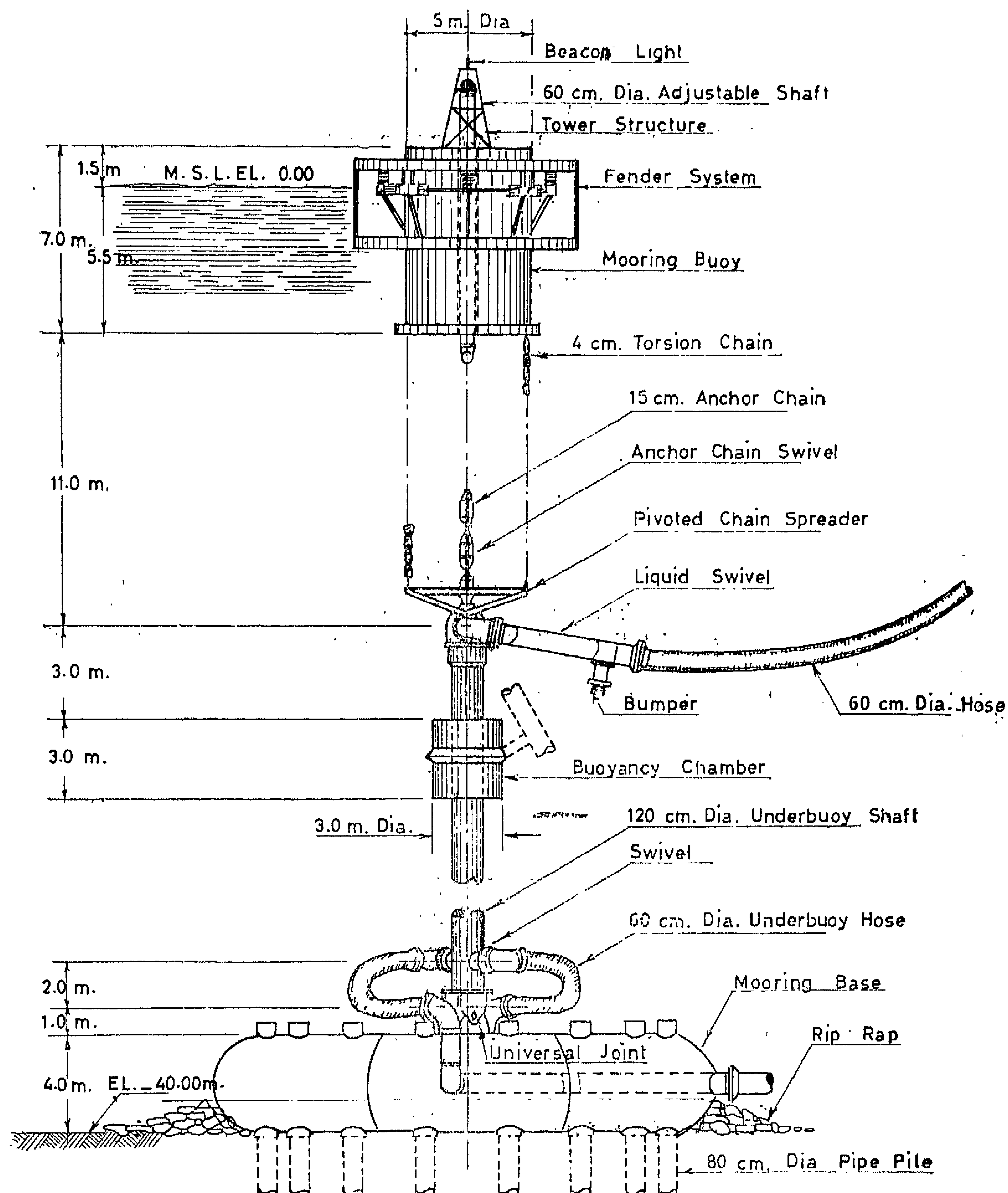


FIG. 5_ A MODERN DESIGN OF CRUDE OIL FACILITIES AT BREGA, LIBYA FOR TANKERS UP TO 300.000 DWT.

wind than when a head on wind. Nearly every location is subject to what is termed a prevailing wind or a wind blowing from one direction a majority of the time. Both the wind velocity, which can be converted to a force, and the wind direction must be considered in the design of any type of loading facility.

Waves, generally caused by winds, are another major force to be considered. Wave forces cause a ship to roll, pitch, heave and yaw, all of these movements must be dampened and restrained by the mooring system holding the ship. The forces cause by waves are a function of the wave height, the distance from the trough (low point) to the screst (high point). With knowledge of wave heights and direction in a berthing area the force on the ship and mooring device can be calculated and used in the design of the mooring structure.

Current is another force against the ship and mooring structure which must be conconsidered. Current is caused by the mass movement of water from one location to another and can be found at any water depth. Current velocity must be measured by special instruments and then converted into a force on whatever portion of the system it acts.

Tide is the periodic rise and fall of the sea water produced by the attraction of the moon and sun. Fortunately the Mediterranean Sea has less than one metre of tide and its effect on structures in our north coast is small. However other parts of the world have tides that range up to 10 metres which can play a major role in the selection of mooring type and design of the mooring.

The following would be a typical set of design conditions for a single point mooring at our Mediterranean coast :

Tide ;	Highest high water	+ 1.0 m.
	Lowest low water	0.3 m.
	Mean tide range	0.3 m.

Wind ; wave and current ;

tanker in berth

60 km/hr wind

3 metre wave height

2 km/hr cross current

No tanker on berth.

110 hm/hr wind

12 metre wave height

4 km/hr cross current.

C — Water depth :

To properly locate and design a mooring and loading facility a complete survey of the water depths must be available. In locating a proposed structure particular attention must be given to the following factors related to water depth :

a — Mancuvering room required by tankers to enter and leave berth.

b — Water depth required under the ship's bottom and now this is affected by the waves expected during operating periods, both in the manoeuering and loading area.

c — Ease of construction of underwater pipe line.

D — Soil Information :

The last design consideration to be reviewed is the properties of soil below sea bottom. These need to be known for several reasons. If pile driving is included in any of the possible types of structures the pile needs to be designed to resist the estimated loads. If anchors are to be part of the structure their holding power needs to be determined.

Obviously a steel anchor laying on bare rock has much less holding power than one burried in sand. If under water pipe line is part of the scheme selected, it must be designed to withstand the forces acting on it, and this design depends on the characteristics of the sea bottom.

DESIGN CONSIDERATION

A — Tanker Size :

A major consideration in the design of crude oil berthing facility is the size of the tanker to be handled. Figure 4 is a plot of dead weight tonnage of crude tankers versus the most important tanker dimensions. Dead weight tonnage (DWT) is defined as the carrying capacity of a tanker in tons and as such is the weight of the cargo, fuel, and stores which, a ship carries. Figure 4 shows the great growth in tanker size in the last 30 years. In 1940 the supertanker was 16,000 DWT with a draft (loaded depth in water) of 8 metres, a length of 150 metres, and a beam (width) of 20 metres. In 1950 the large tanker size was up to about 35,000 DWT and by 1960 was up to around 105 000 DWT. This has increased rapidly and in 1968 the first 312 000 DWT tanker was launched having a draft of about 22 metres, a length of about 360 metres and a beam of 60 metres. The draft, length, and beam of the tankers that will use a port will have a direct bearing on the design of the approach channel, on the selection of type of mooring and loading facility and on the locatiotn of the loading facility.

B — Wind, Waves, Current and Tides :

The next major consideration is the Physical environment in which the ship must moor and load crude oil, i.e., those nature forces to act on the tanker that must be resisted while the ship is moored. These are wind, waves, current and tide.

Wind causes forces on the ship's bull and superstructure. These forces are a function of the area of the ship exposed to the wind and thus total much greater with a broad side

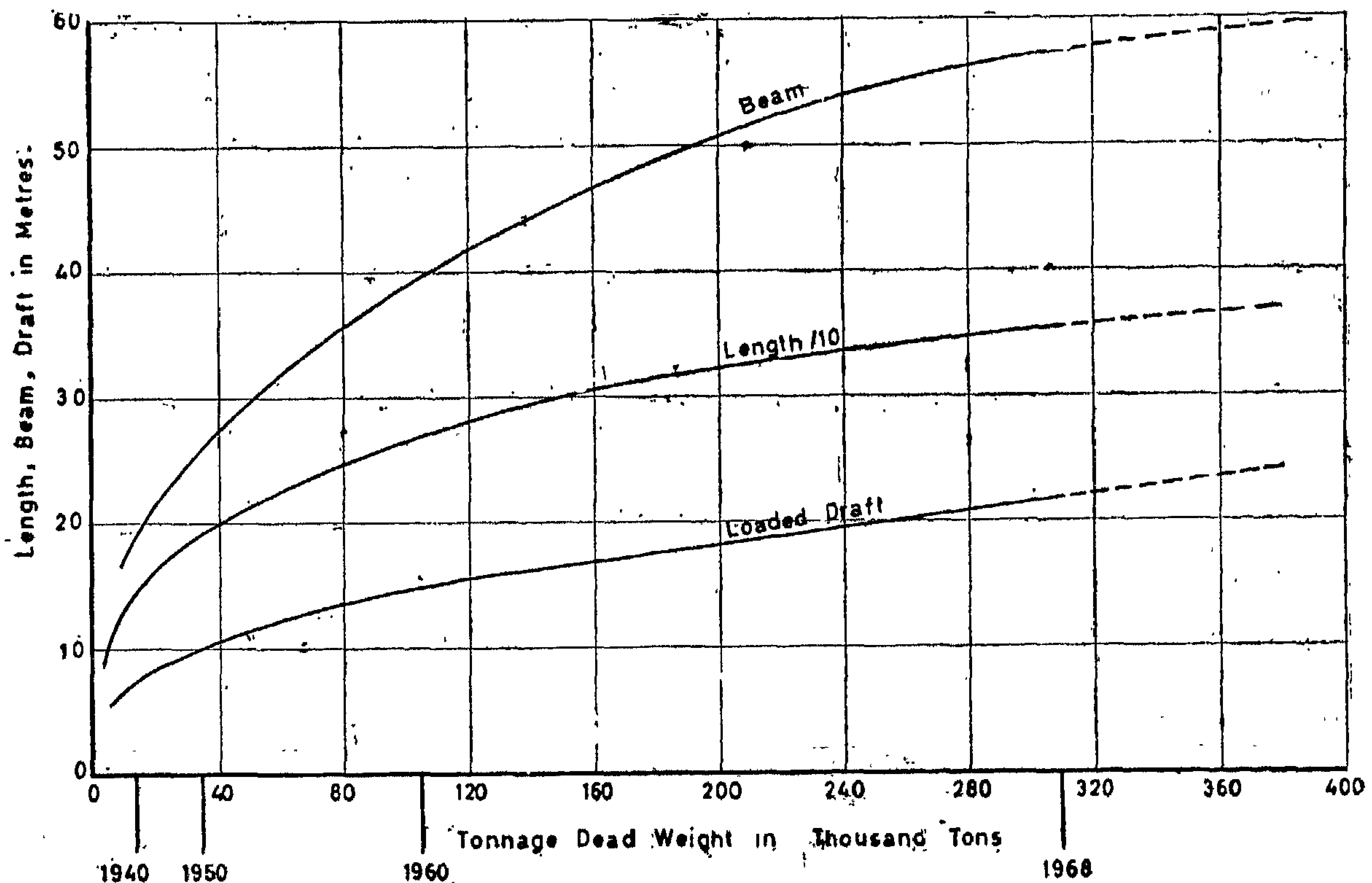


FIG 4. TANKER DIMENSIONS VERSUS DEAD WEIGHT TONNAGE.
(According to Delft Hydrauuc Laboratories.)

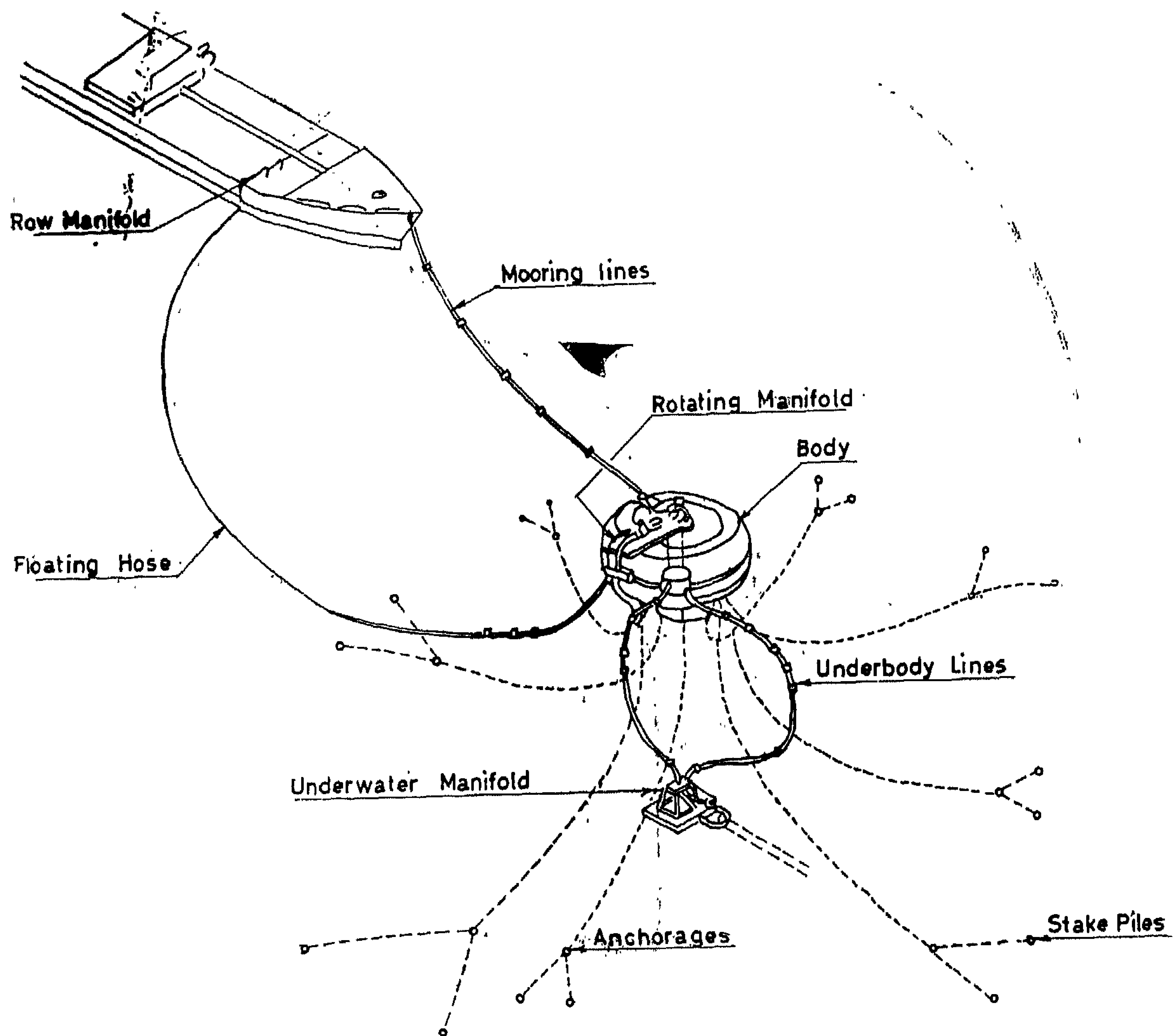


FIG. 3 _ GENERAL SKETCH OF A SINGLE POINT MOORING.

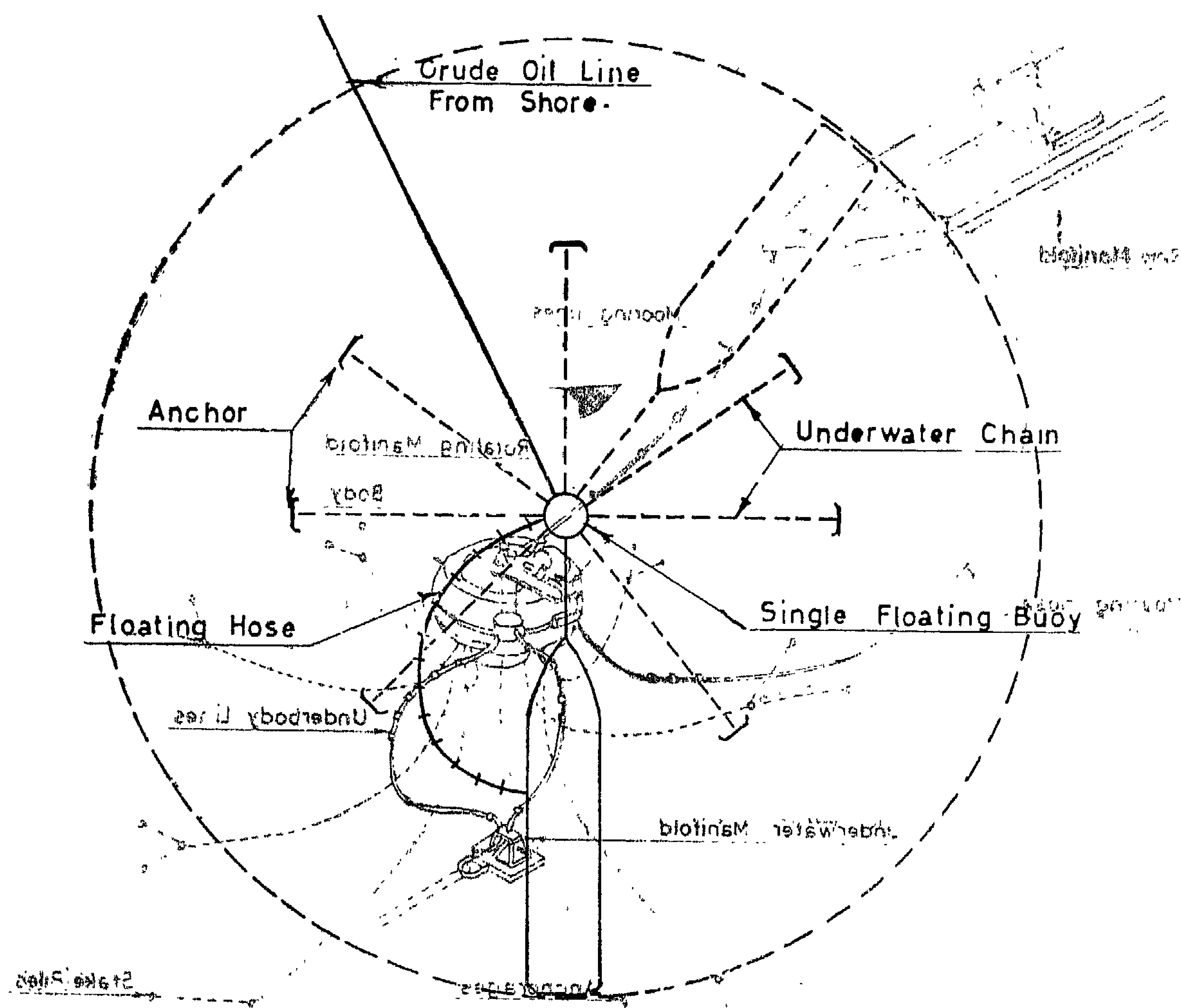


FIG. 2 – SINGLE POINT MOORING

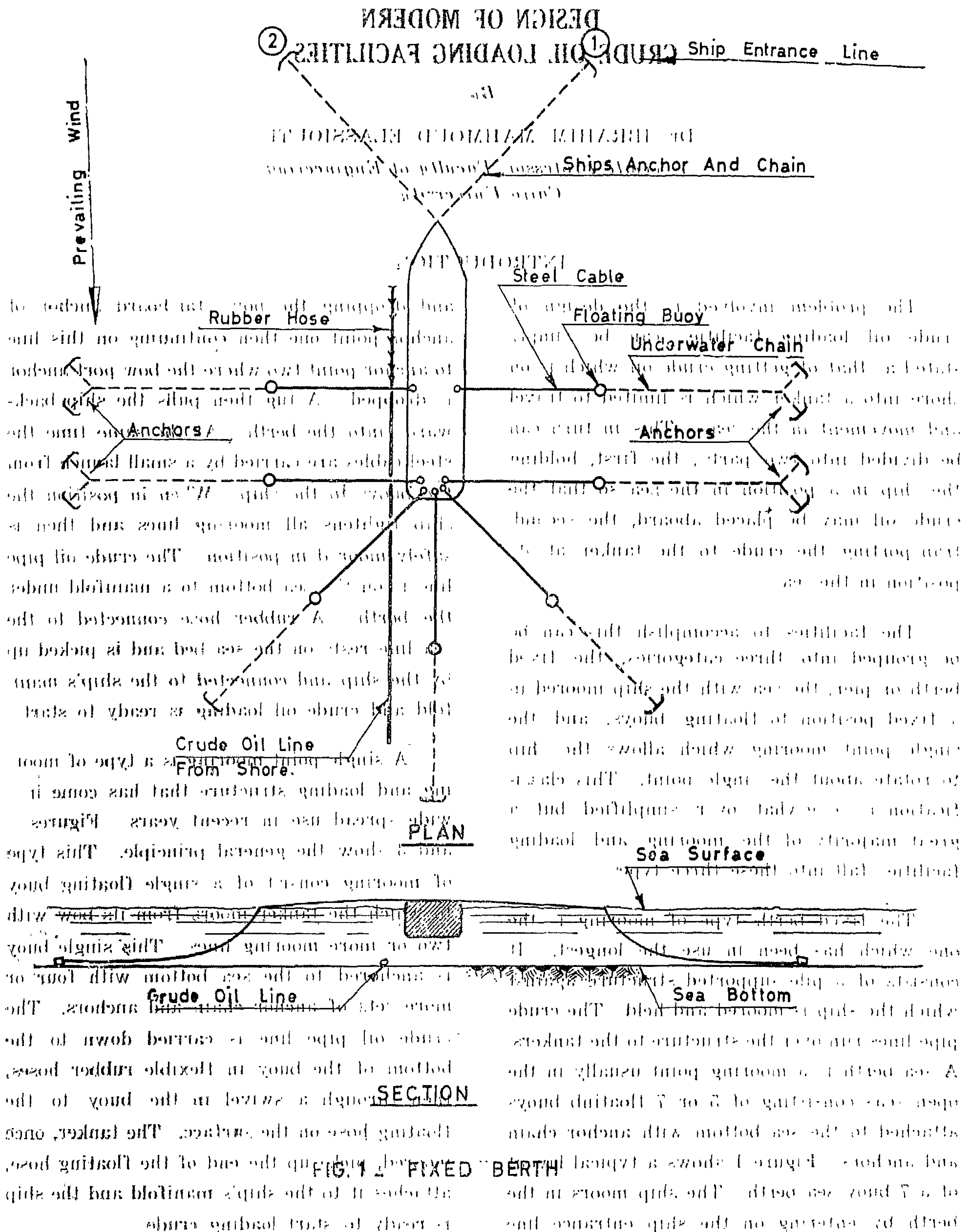


FIG. 1 FIXED BERTH

DESIGN OF MODERN CRUDE OIL LOADING FACILITIES

By

Dr. IBRAHIM MAHMOUD ELASSIOUTI
Associate Professor, Faculty of Engineering
Cairo University

INTRODUCTION

The problem involved in the design of vrude oil loading facilities can be simply stated as that of getting crude oil which is on shore into a tanker which is limited to travel and movement in the seas. This in turn can be divided into two parts; the first, holding the ship in a position in the sea so that the crude oil may be placed aboard, the second, transporting the crude to the tanker at its position in the sea.

The facilities to accomplish this can be be grouped into three categories, the fixed berth or pier, the sea with the ship moored in a fixed position to floating buoys, and the single point mooring which allows the ship to rotate about the single point. This classification is somewhat over simplified but a great majority of the mooring and loading facilities fall into these three types.

The fixed berth type of mooring is the one which has been in use the longest. It consists of a pile supported structure against which the ship is moored and held. The crude pipe lines run over the structure to the tankers. A sea berth is a mooring point usually in the open seas consisting of 5 or 7 floatinb buoys attached to the sea bottom with anchor chain and anchors. Figure 1 shows a typical layout of a 7 buoy sea berth. The ship moors in the berth by entering on the ship entrance line and dropping the bow star-board anchor of anchor point one then continuing on this line to anchor point two where the bow port anchor is dropped. A tug then pulls the ship backwards into the berth. At the same time the steel cables are carried by a small launch from the buoys to the ship. When in position the ship tightens all mooring lines and then is safely moored in position. The crude oil pipe line is on the sea bottom to a manifold under the berth. A rubber hose connected to the sea line rests on the sea bed and is picked up by the ship and connected to the ship's manifold and crude oil loading is ready to start.

A single point mooring is a type of mooring and loading structure that has come into wide spread use in recent years. Figures 2 and 3 show the general principle. This type of mooring consist of a single floating buoy to which the tanker moors from its bow with two or more mooring lines. This single buoy is anchored to the sea bottom with four or more sets of anchor chain and anchors. The crude oil pipe line is carried down to the bottom of the buoy in flexible rubber hoses, then through a swivel in the buoy to the floating hose on the surface. The tanker, once moored, picks up the end of the floating hose, attaches it to the ship's manifold and the ship is ready to start loading crude.

5. Ghorab M.A., 1961 : Abnormal stratig-phic features in Ras Gharib oil-field. Third Arab. Petroleum Congress.

6. Gurivich V.I., 1961 : On the distribution of bromine in chloride water, "Procpecting and Protection of Weath" No. 1 (In Russian).

7. Karsev A.A., 1963 : Hydrogeology of Oil and gas-fields. State technical Publishing house (In Russian).

8. Khattab H.A. and Hadidy T.A. 1961 : A comparative study of Bakr, Kareem, and Ras-Gharib Oil-fields. Third Arab Petroleum Congress.

9. Krotova V.A., 1956 : On chlorine bromine coefficients of underground water. Work all union Scientific geological procpecting institute. Geological collection, New series, issue 95. (In Russian).

10. Plotnikov N.A. 1959 : Iodine-bromine water and its fields, work of Moscow geological and procpecting Institute, P. XXXV. (In Russian).

11. Said R. 1962 : The geology of Egypt. Elsvier Publi. Co., Amesterdam — New York.

12. Sulin V.A., 1948 : Conditions of formation. Basis of classification and composition of natural water, P. 1 issue Academy of Science U.S.S.R. (In Russian).

13. Vinogradov A.P., 1944 : On chlorine bromine coefficients of underground water "Lecture of Academy of Science U.S.S.R.", P. XIV No. 2 (In Russian).

14. Vinogradov A.P., 1948 : Dispresed chemical elements in underground water of different orgin (on the meaning of proportional coefficients) In Russian.

15. Zaecev I.K., 1959 : Some regularities of distribution and formation of underground brines for U.S.S.R. territory (In Russian).

dustrial brines become more clear if more geological, hydrogeological, hydrogeochemical and palaeohydrogeological should be further studied for the area of the Gulf of Suez with special attention to oil-fields situated on both sides of the Gulf.

VII — Potentials for industrial use of underground water.

For determination that water can be used for industrial purposes, limited specifications are given by N.A. Plotnikov (1959). The minimum concentrations for different elements iodine, bromine and boron for establishment such industry are given in table 5. The minumum concentrations of iodine and bromine given in that table must be considered temporary. By the progress of technological processes of extraction of these elements from underground water and changing general economic conditions, the limitations of concentrations of these elements will be changed.

For establishment of iodine-bromine industry in one Oil-field, the product of iodine not less than 40-50 ton in a year and 500 tons of bromine. The quality of iodine-bromine water depends on its general salinity, chemical composition and the presence of harmful mixture (Naphthenic acids, hydrogen sulpide, ammonium salts and different organic substances). Concentration of oil more than 40 mg/1 is harmful for extraction of iodine and bromine. Temperature of brines is also important in extraction of iodine and bromine.

Underground water containing boron in amounts more than 500 mg/1 B_2O_3 represents special practical interest in chemical industry, less amount boron till 200 mg/1 B_2O_3 can be extracted from water and used for preparation of boron concentrations and as fertilizers.

However, seperate oil-fields where it is worthy to use oil-water, can be considered as an industrial field for water. PH underground water must not exceed 7.5. Content of naphthenic acids are not high and varies from 0.6 to 1.04 gm-equivalent per liter. Ammonium and hydrogen sulphides content are low.

From the above mentioned specifications it could be decided, that underground water of Ras-Gharib is suitable for use in extraction of iodine, bromine and boron if we take in consideration that the amount of water extracted with oil is very high and reaches more than 5000 m³/day. Consequently, from Ras-Gharib can be extracted more than 1000 tons/year of bromine only besides iodine. It is observed also such high concentrations in Ras-Bakr (10 km. north west Ras-Gharib) and Hurghada (Red sea coast) oil fields in bromine, iodine and boron (Bishay N.Z. 1965) in which such industry can be established. Such industry can, also be established in Oil-fields located on the eastern coast of the Gulf of Suez (El-Kiki F. 1965).

ACKNOWLEDGEMENT

The author wishes to thank geologists, chemists and engineers of the Egyptian Petroleum Organization, and to the workers in Ras-Gharib Oil-field for their help and facilities offered to him in the field.

REFERENCES

1. Beder B.A., 1948 : On bromine iodine ratio as a probable indicator in researching for oil Lecture of Academy of Science Az.S.S.R. No. 12 (In Russian).
2. Bishay N.Z., 1965 : Industrial underground water of the Gulf of Suez. J. Geo. and Procpecting No. 2 (In Russian).
3. Bishay N.Z., 1968 : Age determination of oil by He/Ar ratio in gases in the Gulf of Suez. J. of the Egyptian Society of Engineers U.A.R. Vol. VII, No. 4.
4. El Kiki F., 1965 : Hydrogeological conditions of the artezian basin of the Gulf of Suez. Ph.D. Thesis (In Russian).

Table (4) Concentrations of bromine and organic matter in Cores of Ras-Gharib

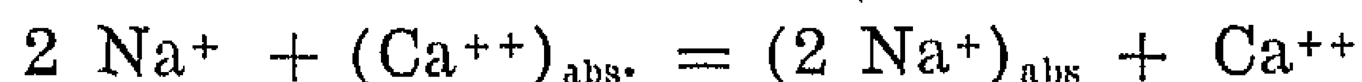
No. of well	Depth interval of core sample in M.	Geologic age	Lithology	Bromine in mg/kg	Organic matter Bitumens + Carbon in per cent
5	487.6 — 491.9	Middle miocene	Limestone	13.0	1.5 + 0.45
15	485.8 — 492.5	Basal miocene	"	15.0	1.5 + 1.04
39	742.7	Upper cretaceous	Shales	20.0	0.01 + 0.22
49	690.4 — 693.4	Nubian «A» series	Calc. S. S.	13.0	0.1 + 0.29
14	672.9 — 675.9	«B» series	Black shales	30.0	2.0 + 2.93
14	701.0 — 707.1	«B» series	"	40.0	0.02 + 0.75
14	803.0	«D» series	Sandstone	undetected	0.000n + 0.08

Table (5) Specifications for iodine bromine industry. (After Plotnikov N.A.)

Element Extracted	Iodine not less than in mg/1	Bromine not less than mg/1	Naphthenic acids not more than in mg/1	Oil not more than in mg/1	Boron not less than in mg/1
Extraction of I and Br	10	200	600	40	
Extraction of bromine		250	600	40	
Extraction of iodine	18		600	40	
Extraction of I and B	10		600	40	500 — 200*

* For different industrial purposes.

As a result of penetration of such water in surrounding rocks, the exchange of soluble sodium by adsorbed calcium (partly magnesium) in rocks is of great importance, resulting in formation of water enriched in calcium. This process takes place as follows :



$$2\ Na^{+} + (Ca^{++})_{abs.} = (2\ Na^{+})_{abs} + Ca^{++}$$

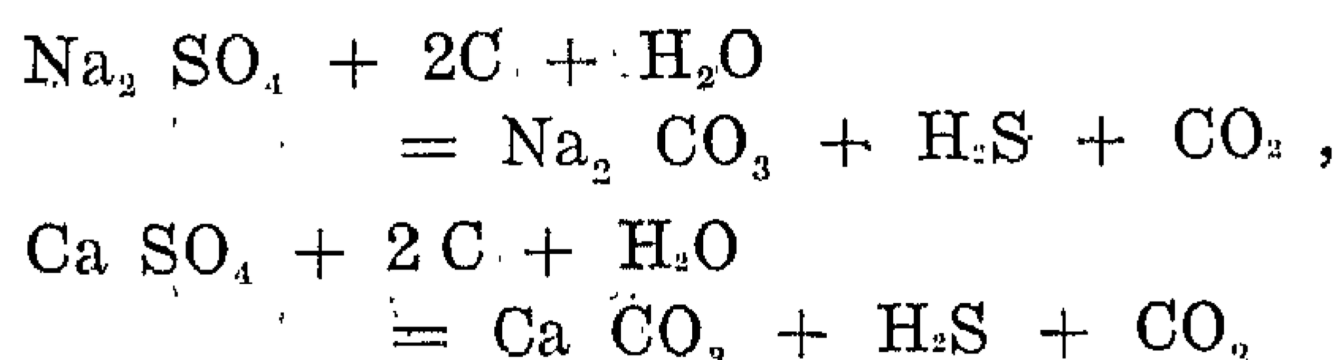
This leads to the decrease of rNa/rcl and increase of $\frac{rcl - rNa}{rMg}$ (coefficients of metamorphization) to 0.68 and 2.35 respectively. Such a decrease of rNa/rcl and increase of $\frac{rcl - rNa}{rMg}$ and increase of bromine content depends on the increase of calcium chloride in water. (V.A. Krotova, 1956). This increase of calcium in water is responsible for the increase of rca/rMg and rca/rSr coefficients in underground water than that for sea water especially by the increase with depth and for older geologic formations. Pliocene water are less metamophozed than that of cretaceous and nubian water as indicated by relative high values of rNa/rcl, low value of rca/rMg and low value of $\frac{rcl - rNa}{rMg}$ i.e. metamorphization and reducing conditions are more favourable for the deposits more than that of pliocene formations.

Also of great importance is the concentration of organic matter in rocks (see table 4) and microorganisms in connection with oxidiation-reduction processes e.g. for sulphates and nitrates. The reduction of sulphates takes place by such general formula, as follows ;



$$R\ SO_4 + 2\ C = RC + 2\ CO_2$$

in this process water becomes enriched by sulphides and other reduced forms of sulphur and CO_2. The chemical formula are as follows :



$$Na_2\ SO_4 + 2C + H_2O = Na_2\ CO_3 + H_2S + CO_2\ ,$$

$$Ca\ SO_4 + 2\ C + H_2O = Ca\ CO_3 + H_2S + CO_2$$

Reduction of sulphates can also take place by the presence of special microorganisms in some biochemical processes. The most widely distributed forms of bacterial reducing sulphates are these of Vibro desulfurcans and Vibro thermodesulfuricans. Such a decrease of $\frac{rSO_4}{rcl}$ 100 from 10.3 for sea water to 0.02 for oil-water of cretaceous and nubian water are an indication of intensive reduction of sulphates, which is less for pliocene water.

The conditions of accumulation of ammonium (NH_4^{+}) in Oil-water have a great meaning. Undoubtely, the appearance of NH_4^{+} represents a stage of organic matter decomposition in anaerobic conditions. The results of denitrification of NO_3^{-} in anaerobic conditions, also can be easily changed to NH_4^{+}.

Enrichment of underground water with iodine is different from that of bromine. Content of iodine in sea water (0.05 mg/1) is very low, and its accumulation must be as a result of additional enrichment. The great role in iodine accumulation in water is the organic matter dispersed in rocks. Table 4, shows high concentrations of bitumens and carbon of organic origin in cores especially for shales of the "B" — series of the nubian sandstones. Oil can also be a source for concentration of iodine in water. By the influence of different life activities of bacteria, oil decomposes and forms easily soluble materials which in its composition iodine is found. The Br/I ratio of water (55.3) is highly decreased from that of sea water (1300), which indicates proportional high increase of iodine accumulation relative to that of bromine.

Decomposition of organic matter and oil, also results in appearance of naphthenic acids in water.

In this short account, given above for the discussion of genesis and conditions of formation of brines of Ras-Gharib, is only an approach to solve such complicated problem. Conditions of formation of iodine bromine in-

VI — Genesis and conditions of formation of industrial water :

The formation of iodine-bromine brines (70-171.0 gm/1) of Ras-Gharib is a very complicated problem. Different factors took place in its formation, such as geologic, hydrogeologic, hydrodynamic, biochemical procosses and other factors. The effects of these processes on the chemical composition of water is not equal. In author's idea, the the most important factor is that of the geologic conditions. In the geologic history of the Gulf of Suez, deposition of different lithological facies took place under marine and lagoonal conditions (in middle miocene). The chemical composition of normal sea water represented by Kurlov's formula is as follows :

$$M_{35} \frac{cl_{90}\ SO^{4}_{10}}{Na_{78}\ Mg_{18}\ Ca_{4}}$$

; and that of the Gulf of Suez is as follows

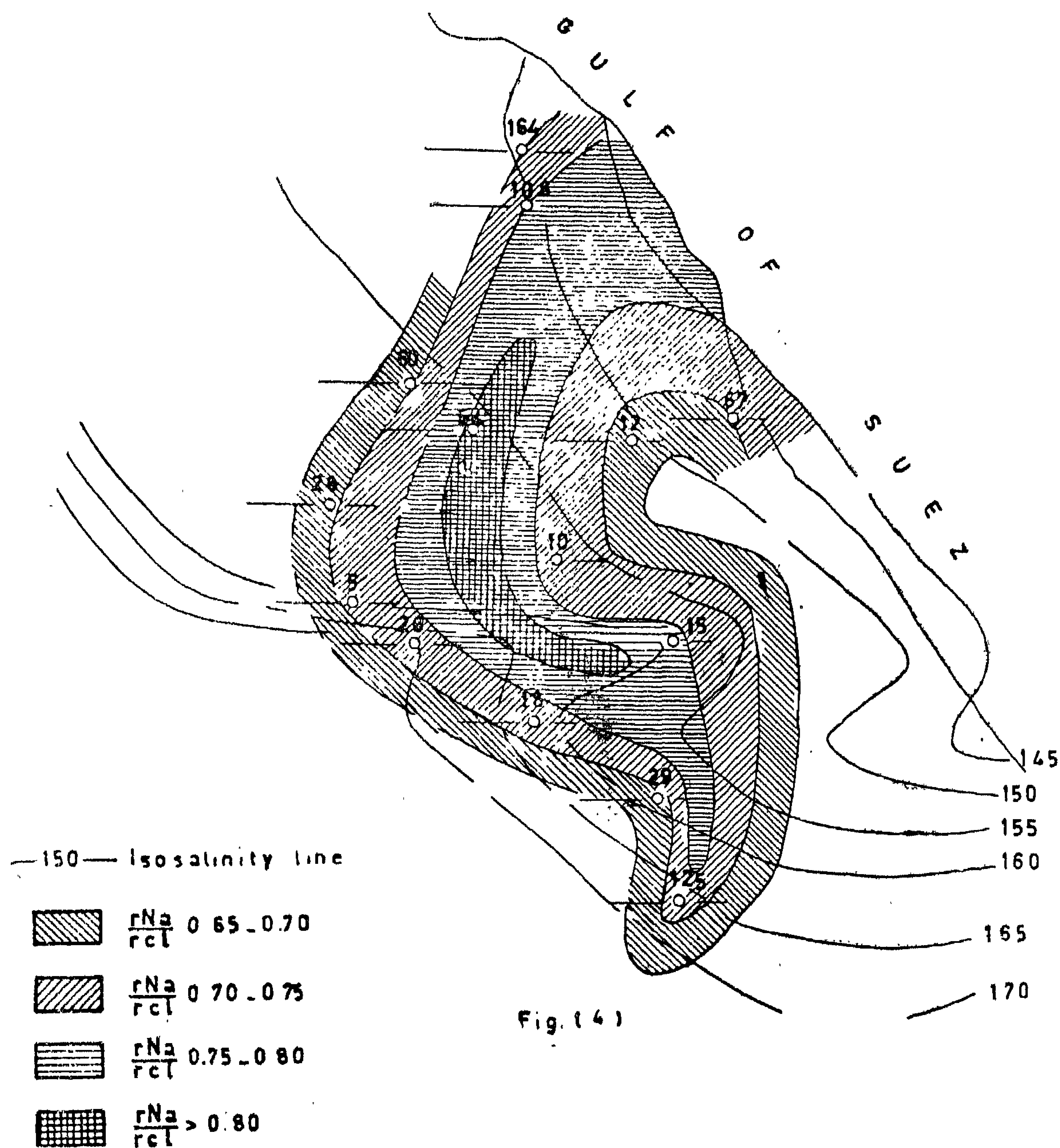
$$M_{43\cdot 6} \frac{cl_{90}\ SO^{4}_{10}}{(Na+k)_{80}\ Mg_{15\cdot 5}\ Ca_{3\cdot 5}}$$

According to Kurlov's formula both water are of sodium chloride type. The study of hydrochemistry and hydrogeochemical coefficients of underground water threw some light on the elucidation of processes taking places in its formation. The hydrogecochmical coefficients of Ras-Gharib underground water coincides with that of sea water, with its further change. Infilteration water (bicarbonate water of rain fall) are not mixed with sodium chloride sea water, such mixing is not reflected in values of different coefficients, thus it can be considered that they did not take a part in its formation.

Prevailing of lagoonal conditions in middle miocene resulting in deposition of anhydrites, gypsum and some rock salt causing the increase in salinity of sea water (lagoon) which also becomes concentrated in bromine. Such increase can be explained as follows : In sea water, bromine concentration is about 65.0 mg/1, under evaporation in arid climatic conditions salinity of water increases to high values also bromine concentration increases to 1000-10000." cl/Br—ratio at the begining is unchanged (about 300) and then after deposition of halites, it begins to decrease. This decrease in cl/Br cofficient is accompanied by a further increase (but in slower extent) in salinity of water and that shows, that accumulation of bromine takes place faster than the accumulation of chlorine. After deposition of potassium salts and accumulation of chlorine, the value cl/Br can be reduced down to 35-40. Thus, if deposits consists of layers of gypsum and anhydrites, this indicates that this layers were deposited in higher salinities but with normal ratio of cl/Br. The appearance of rock salt indicates that, this ratio begins to decrease under continuous increase in salinity. Further decrease takes place with deposition of potassinum salts. The high concentration of bromine in water can also be the result of leaching of rocks containing bromine in high values. In table 4, the chemical analysis is given for bromine in cores of Ras-Gharib. From table it is clear, that high concentrations of bromine in cores are observed especially for shales. Sandstones and limestones contain bromine but of lower concentration. In brines, high concentration of boron are observed from 5 to 25 times that of sea water (4 mg/1), which is an indication of continental salinization (Zaeceb I.K., 1959), thus increasing B/cl ratio to 1.8 10^{-3} for Ras-Gharib water.

Such brines, rich in calcium chloride, bromine, boron and biochemical gases (methane, heavier hydrocarbons, H_2S) and other components are a good indications that the corresponding part of the geologic section is characterized by prevailing reducing conditions and weakly washed deposits.

After closing the structure with such thick deposits, the mother brines (initial brines) under thickening of deposits migrate in surrounding rocks. Such highly concentrated water in such closed structure, can be represented as "Stagnant water", i.e. of very slow mobility. Further metamorphization of this stagnant water takes place i.e. enrichment in calcium, reducing of sulphates, nitrates and enrichment with iodine.



Geological and hydrogeochemical section of Ras-Gharib oil-field.

to 160. It decreases in older formation with depth and with increase in salinity. For sea water this ratio is about 300. This ratio reflects quantitavely the degree of exchange : in more washed deposits it has a great value, in less washed has a less value (V.A. Krotova, 1956). The cl/Br-ratio is of interesting genetic characterstic for natural water. It is easy to differentiate brines resulting from dissolving salt deposits (1000 — 1200, cl/Br value) and brines of another origin.

For Br/I — ratio, the relation do not increase more than 137,1 and decreases till 55.3, but for most of the samples this ratio does not increase 100. High values are observed for middle miocene water, for upper cretaceous and nubian sandstone are less than 100. The behaviour of Br/I coefficient is similar to that of cl/Br. For sea water the value of this ratio is about 1300. Uhis coefficient is not well studied.

rNa/rcl — ratio for all samples are < 1. The values of this ratio varies from 0,67 to 0.84, but most of samples are more or less of 0.7. This ratio decreases from pliocene to nubian sandstone formations. This decrease is accompanied by increase in salinity (see Fig. 2). In Fig. 4, it is shown for the nubian sandstone) that for the decrease of rNa/rcl to south and south west direction, salinity increases. For sea water this coefficient is about 0.85. rNa/rcl-ratio is considered as an indication for metamorphization of water (V.A. Šulin, 1948). He used rNa/rcl for belonging water to different geneitic groups, for example, water with coefficient rNa/rcl < 1 belongs to magnesium chloride "or" calsium-chloride "types and water with coefficients rNa/rcl > 1 belongs to" sodium bicarbonate "or" sodium sulphate" types.

The relation between rNa/rcl and cl/Br are represented by an empircal formula (V. Gurivich, 1961) as follows :

$$Cl/Br = m \frac{1 + \frac{rNa}{rcl}}{1 - \frac{rNa}{rcl}};$$

where m — coefficient of mean value equals 34.

B/cl-ratio for Ras-Gharib ranges from, $1,0 \cdot 10^{-3}$ to $2.2 : 10^{-4}$. This ratio shows some increase for older geologic formation. For sea water this ratio is about $2.4 \cdot 10^{-4}$. This value is for water at the surface and also for water at great depths (in oceans and seas).

The ratio rca/rSr ranges between 26.9 and 55.2 (mean is about 43). This ratio increases with depth and in older geologic formations, and also with increase in salinity. rca/rSr — for sea water is about 30.

rca/rMg — ratio varies from 0.17 to 1.81 (mean value is about one), which increases in older formations, with depth and with salinity. For sea water the value of this ratio is about 0.22.

Metamorphization coefficient $\frac{rcl - rNa}{rMg}$

for this water is always more than one except in two cases, where it is somewhat less than one. Its mean value especially for that of nubian sandstones is more than two. The more this values, the more its indicates metamorphization. In these two cases, where the ratio is < 1 only magnesium chloride and sodium chloride salts are present in water composition. This ratio increases in older geologic formations and with salinity. The increase in this coefficient is accompanied by a decrease in rNa/rcl-ratio (see Fig. 2).

For $\frac{rSO_4}{rcl} \cdot 100$, its value changes from 6,6

in pliocene water to 0,02 for nubian sandstone and cretaceous water. It is observed that the decrease of sulphate takes place with depth and also with salinity. For sea water this coefficient is about 10,3.

Fig. 2 shows some of these ratios and its change with depth geologic section and salinity of water.

ent, with depth and for other older formations increases to form up to 16.0% equivalent. Magnesium concentration shows a small decrease in concentration from pliocene to nubian sandstones. Nitrates and nitrites are undetected in water of Ras-Gharib.

Concentrations of lithium (table 2) represents from 1,8 to 7.6 mg/1. Its distribution does not show a special trend. . Ammonium (NH_4^+) content changes from 108.0 to 462.6 mg/1 (mean is of 250.0 mg/1). Naphethenic acids varies from 0.6 to 1.04 mg. equivalent/1.

Microelements (Br, I and B) concentrations are high especially that for bromine and boron, but to less extent for iodine (see table 2). Bromine content varies from 373.0 to 759.2 mg/1. Its mean concentration is more than 600.0 mg/1. Its increase is observed by increase in salinity and with depth in older formations. Iodine concentrations is of 3.4 — 14.2 mg/1. Also high concentrations are observed for nubian sandstones. Its behaviour is similar to that of bromine (see Fig. 2). Boron content in Ras-Gharib Oil-field is high. Its concentrations ranges from 21.0 to 101.7 mg/1, (mean is 80.0 mg/1).

Chemical composition of free gases accompaning oil and water are mainly of methane, and forms from 35.4 to 71.6 (in volume percent), heavier hydrocarbons forms the rest. N_2 and CO content are low but sometimes increases to 10.1%. CO_2 and H_2S are also low but the increase of its concentration reaches 7.2%. O_2 , H_2 , Ar and He are very low. He/Ar ratio was used for age determination of oil in the oilfields in the Gulf of Suez (Bishay N.Z., 1968).

Fig. 1, shows the chemical composition of water and gases represented by the circle method.

Fig. 3, shows the chemical representation of Ras-Gharib underground water by Ovchunnikov's A.M. graph. The analysis are represented in reducing conditions with gases of CH_4, other hydrocarbons and H_2S characterizing oil-water. Genetically the water is of sodium chloride type.

V — Hydrogeochemical coefficients :

To understand the genesis of underground water, it is represented by values of physicochemical properties of elements which are closely related for example Ca/Sr; Sr/Ba, Nb/Ta, Cl/Br, Br/I ... etc. (Vinogradov A.P. 1948). Other coefficients as Na/rcl,

$$\frac{rcl - rNa}{rMg} \text{ and } \frac{rSO_4}{rcl} . 100$$

are of special meanings for elucidation conditions of formation of underground water.

Hydrogeochemical coefficients of underground water for Ras-Gharib are given in table 3.

For Cl/Br — ratio, it ranges between 124.0 and 248, 9 which are for the nubian sandstones. Most of samples varies from 124

Hydrogeochemical Representation Of Underground Water Of Ras-Gharib

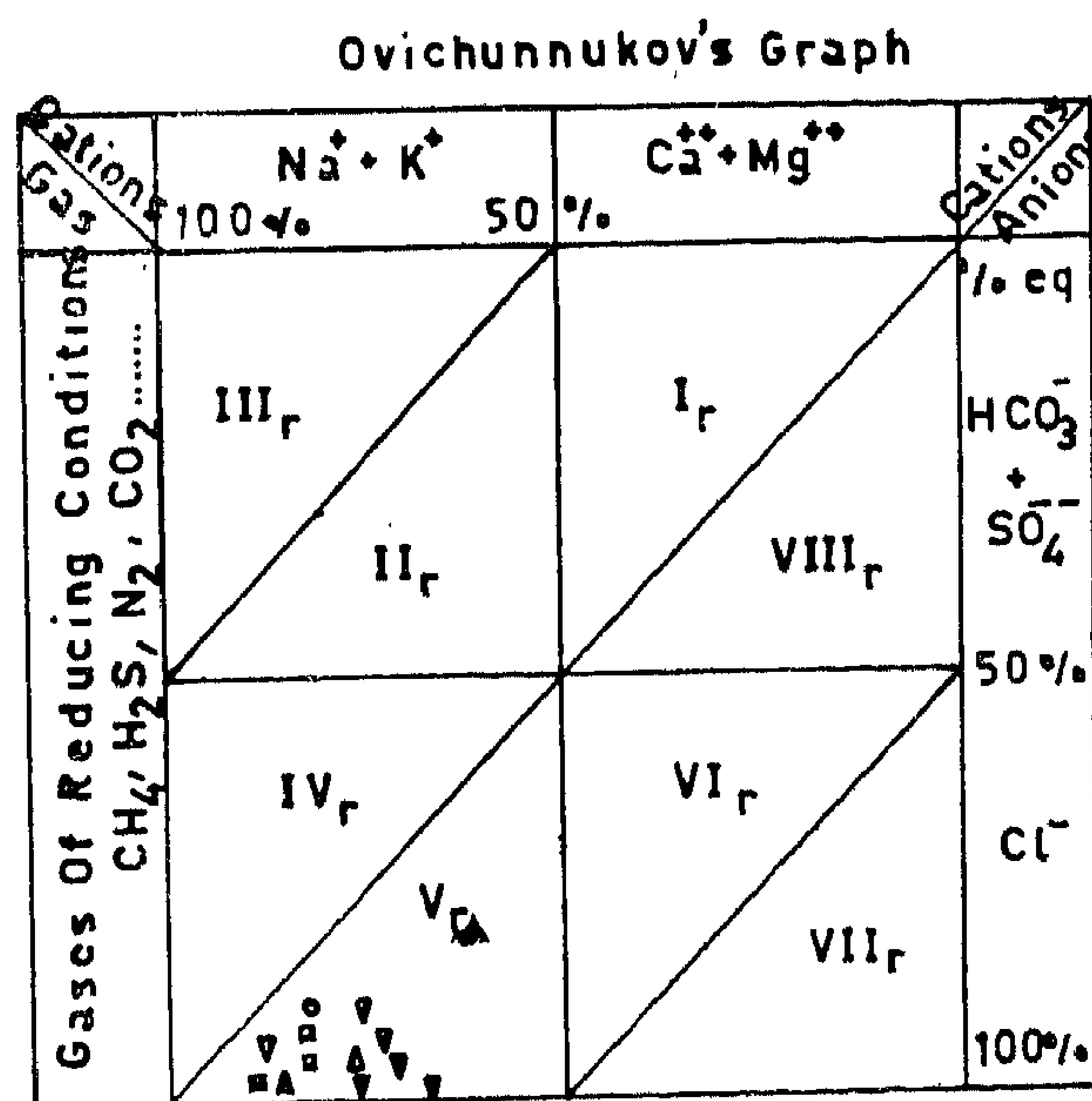


Fig (3)

- o Pliocene Water
- ■ Middle-Miocene Water
- ▲ Upper Cretaceous Water
- ▼ Nubian Sandstone Water.

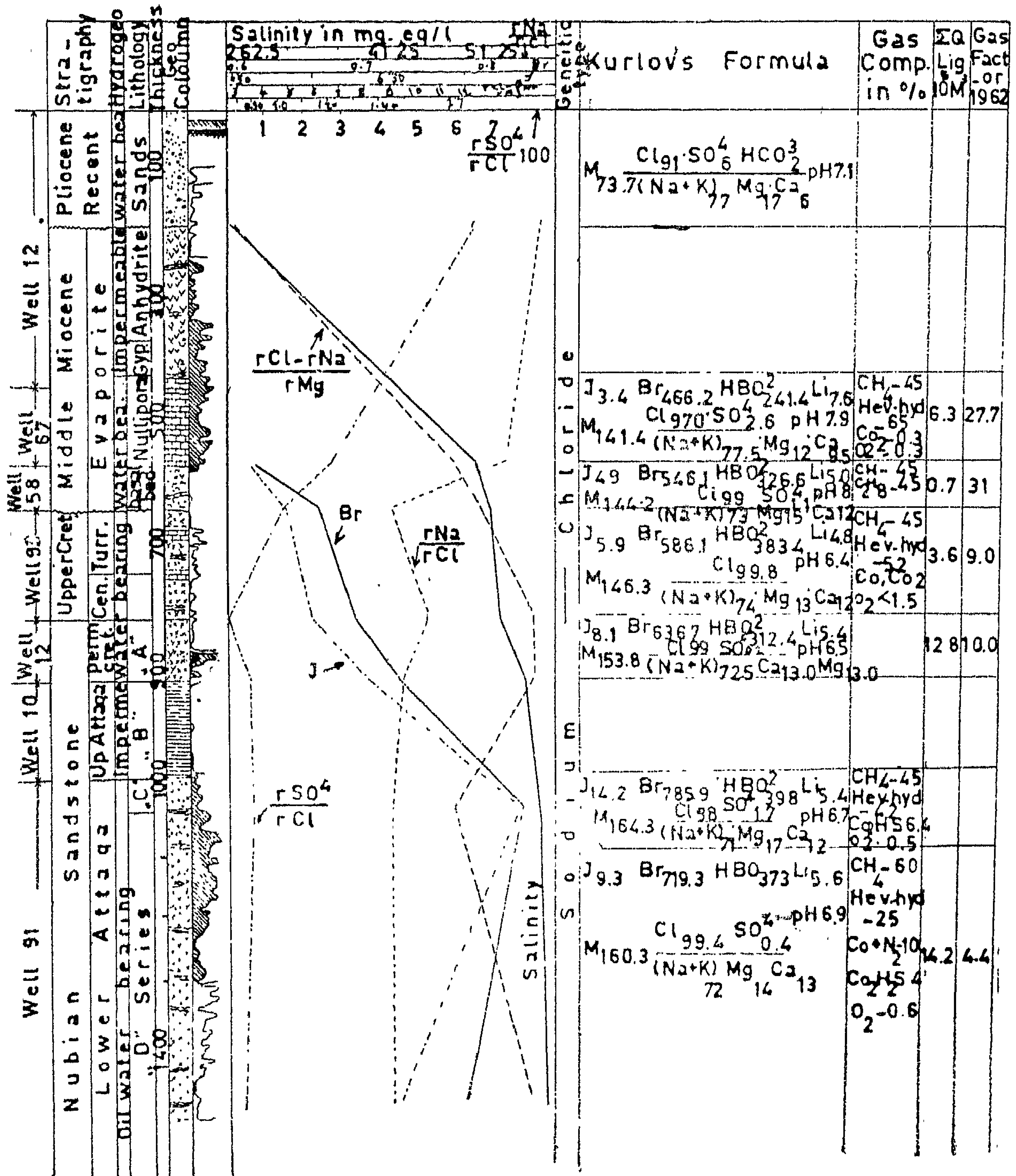

Stratigraphy
Hydrogeo
Lithology
Thickness
Geo Column
Salinity in mg. eq/l
Kurlov's Formula
Gas Comp. in %
Gas Factor 1962
Pliocene Recent
Well 12
Miocene
Middle Evaporite
Well 67
Well 58
Upper Cret.
Cen. Turr.
Well 91
Well 12
Well 10
Nubian Sandstone
Up Attaqa
Lower Attaqa
Well 91
Sands
Anhydrite
Gyp
Nullipore
Oil water bearing
"D" Series
Chloride
Sodium
rCl-rNa / rMg
Br
rNa / rCl
J
rSO4 / rCl
Salinity
CH4-45
CH4-60

Fig. (2)

Table (2) Concentrations of Li^+, NH_4^+, Naphthenic acids, Br, I and B

No. of well	*Geologic age*	*Li^+ in mg/1*	*NH_4^+ in mg/1*	*Naphthenic acids in mg. eq/1*	*Br^- in mg/1*	*I^- in mg/1*	*B in in mg/1*	*Salinity in mg/1*
83	Nullipore	7.6	108.0	0.6	466.2	3.4	59.66	141.6
157	Basal Miocene	5.0	204.8	0.8	546.1	4.9	80.71	142.0
85	Cretaceous	4.8	234.0	—	586.1	5.9	94.75	141.6
54	Nubian S.S.	1.8	288.0	1.04	373.0	—	21.06	157.7
60	» »	5.2	291.6	0.90	759.2	10.4	101.76	157.3
12	» »	5.2	273.6	0.90	732.6	11.0	87.73	150.0
164	» »	5.1	259.2	0.68	652.7	10.2	87.73	148.0
67	» »	4.6	208.8	0.50	666.0	8.9	87.73	148.8
29	» »	5.4	462.4	0.60	585.9	14.2	98.19	159.2
28	» »	5.6	255.6	0.70	719.3	9.3	92.23	151.4

Table (3) Hypdrogeochemical Coefficients of Underground Water of Ras-Gharib Oil-field

No. of well	*Geologic age*	*Cl/Br*	*Br/I*	*rNa/rCl*	*rCa/rSr*	*rCa/rMg*	*B/Cl*	*(rCl-rNa)/rMg*	*rSO_4/rCl .100*	*Salinity in gm/1*
59	Pliocene	—	—	0.84	..	0.35	— 10	0.82	6.6	73.0
83	Mid. miocene	182.6	137.1	0.753	33.9	0.5	6.1 10^{-4}	1.45	2.24	141.6
157	» »	158.4	111.5	0.724	38.2	0.8	9.3 10^{-4}	1.80	1.28	142.2
114	» »	—	—	0.84	—	1.25	—	1.90	3.20	140.7
168	Up. Cret.	—	—	0.76	—	0.71	—	1.85	0.10	146.0
93	» »	—	—	0.75	—	1.81	—	2.26	0.05	152.0
85	» »	149.3	99.3	0.717	55.2	0.93	1.8 10^{-3}	2.00	0.02	141.4
54	Nubian S.S.	248.9	—	0.812	55.2	0.25	2.2 10^{-4}	1.12	4.29	157.7
60	» »	127.5	73.0	0.697	49.2	1.07	1.1 10^{-3}	2.14	0.47	157.0
12	» »	126.9	66.6	0.686	37.9	1.07	9.4 10^{-4}	2.21	0.04	150.0
164	» »	155.7	64.0	0.707	54.1	1.08	9.5 10^{-4}	2.23	0.03	148.1
67	» »	138.0	74.6	0.707	40.0	1.15	9.5 10^{-4}	2.23	0.02	148.8
29	» »	124.0	55.3	0.676	42.2	1.07	1.0 10^{-3}	2.13	0.59	159.2
28	» »	129.0	77.3	0.696	26.9	1.00	9.9 10^{-4}	2.14	0.60	151.0
106	» »	—	—	0.750	—	1.27	—	2.27	0.02	157.0
125	» »	—	—	0.720	—	1.15	—	2.11	0.40	166.0
5	» »	—	—	0.71	—	1.07	—	2.20	0.34	161.5
10	» »	—	—	0.72	—	1.00	—	2.00	0.04	155.7
15	» »	—	—	0.76	—	1.40	—	2.35	0.33	159.4
18	» »	—	—	0.72	—	0.87	—	1.73	1.32	162.0
20	» »	—	—	0.73	—	0.17	—	0.96	0.46	171.0

beds, nullipore and gypsum. The basal beds are lithologically completely different and are composed of gravels, sanstones, conglomerates and sometimes contain boulders of chalk of upper cretaceous. Nullipore consists of reefy limestone, in its upper part of shalles and anhydrites. Nullipore reaches a thickness of 230.0 m. Both the basal beds and nullipore limestone are productive only in the western side of the field. Above nullipore rocks lies gypsum with a thickness of 50 to 150.0 m. The upper part of the evaporite group consists mainly of alternations of anhydrites, gypsum and shales, sometimes contains rock salt. i.e. lagoonal deposits. The maximum thickness of this part reaches 500.0 m. From the hydrogeological point of view this impermeable layer acts as a cap rock closing the structure and preventing any recharge from surface water to older rocks. This closure of structure is necessary for reducing conditions to previal, thus keeping Oil from decompostion.

Pliocene — Recent : water-bearing formations consists of, sands, gravels which contain tar impregnations. The base of these deposits are not well determined, but the appearance of anhydrites of the ovaporite group of middle miocene age is considered as its lower boundery. Also there are no sharp lines between pliocene and recent. The thickness of these formations ranges from 88.0 to 245.0 m. For pliocene-recent, it is somewhat more open structure and to some extent its water can exchange, freely, with surface water (mainly sea water; rainfall is of little importance). Also penetration of atmospheric oxygen takes place causing decomposition of oil which can be formed, i.e. changing conditions from highly reducing to somewhat oxidizing conditions which are not favourable for Oil-formation.

Structurally; Ras-Gharib is represented as submerged horst of pre-miocene age, the eastern side is gently sloping but the western is abruptly sloping. The area is divided by 16 faults into 15 blocks of different sizes. These faults are mainly of pre-miocene age. The fieeld is bounded by two major faults of miocene age in the west and south. To the west and south. To the west and south of these faults the wells are only producing water.

IV — Hydrochemistry :

Chemical analysis for water (see table 1) were of the ordinary types analysis (cations : 'Na+k'+, Ca^{++} and Mg^{++} and anions : HCO_3^-, Cl^- and SO_4^{--}), special analysis for iodine, bromine, boron and lithium (see table 2) were carried out. Organic matter and bromine contents for cores are also determined (see table 4). Also complete chemical analysis for gases accompaning oil specially for helium and argon gases were carried out.

From the table of chemical analysis of water, it is observed that underground water from all formations are brines (more than 50.0 mg/1). Salinity ranges from 73.7 gm/1 for pliocene deposits to 170.6 gm 1 in water of the nubian sandstones (see Fig. 2). Only for pliocene water salinity is relatively low respective to that of other formations. Normal salinity for other formations is not less than 140.0 gm/1. PH-values for water varies from 5.9 to 8.8 (its mean is 6.8.). In table 1, the chemical composition of water is represented by Kurlov's formula, anions and cations are given in percent equivalent. For all samples, the underground water from different formations are of sodium chloride type. Sodium represents from 67.0% to 79.5% equivalent. Chlorine represents from 91.0% to 99.9% equivalent. The least amount of chlorine is present only in pliocene water, for other formations is more than 96.0% equivalent. Sulphate (SO_4^{--}) anions are more represented in pliocene water which consists 6.0% equivalent. For other older formations and also with increase in depth sulphate concentration decreases and forms only one or two percent equivalent and sometimes are low that they nearly completely decrease to traces (19.0 mg/1). Bicarbonate (HCO_3^{--}) anions are only represented by two percent and for other older formation, also decrease to traces (31.0 mg/1) i.e. similar to that of sulphate anions. The less content of calcium is observed for pliocene water which represents 6.0% equival-

4*	496,2–513,5	»	7.3	157697	2283,9	5350	50638,9	390,4	5338	92827,9	$M_{157'7} \frac{Cl_{96}}{(Na + k)_{79'5}\ Mg_{16}\ Ca_{14}}$
0*	519.7–573,6	»	6.0	157253	8303,0	4718.1	44775,1	134,2	614,8	96820	$M_{157'3} \frac{Cl_{99}}{(Na + k)_{70}\ Ca_{15}\ Mg_{14}}$
2*	607,8–645,3	»	6.8	150282,6	7948,7	4523,5	42783,4	122,0	52,7	93015,1	$M_{150} \frac{Cl_{99}}{(Na + k)_{69'9}\ Ca_{15}\ Mg_{14}}$
4*	690.0–730,9	6	6.1	148120,7	7461,3	4183,0	43118,8	48,8	38,7	91662,7	$M_{148'1} \frac{Cl_{99}}{(Na + k)_{71'5}\ Ca_{14'5}\ Mg_{13'3}}$
7*	660.5–701,0	»	6,0	148837,4	7802,8	4037,1	43234,0	122,0	24,7	91955,0	$M_{148'8} \frac{Cl_{99}}{(Na + k)_{71'5}\ Ca_{15}\ Mg_{13}}$
25	665,6–707,1	Nubian S. «C» series	5.9	165642	9360	4990	51103	101	500	98588	$M_{165'6} \frac{Cl_{98}}{(Na + k)_{72}\ Ca_{15}\ Mg_{13}}$
18	554,4–579,4	»	7.3	162011	8128	5797	50478	192	1674	95742	$M_{162} \frac{Cl_{95}\ SO_4{}^4}{(Na + k)_{71}\ Mg_{15}\ Ca_{13}}$
20	463,2–475,4	»	6.9	170650	1920	6389	36970	91	6100	95742	$M_{170'6} \frac{Cl_{99}}{(Na + k)_{72}\ Mg_{24}\ Ca_{4}}$
29*	681.5–728,4	»	6.6	159258,1	8830,0	5204,5	43972,7	158,6	771,2	98196,5	$M_{159'2} \frac{Cl_{99'6}}{(Na + k)_{67}\ Ca_{16}\ Mg_{15}}$
5	563,6–708,7	Nubian S. «D» series	6.5	161517	8816	4845	51156	110	493	69097	$M_{161'5} \frac{Cl_{99}}{(Na + k)_{71}\ Ca_{14}\ Mg_{31}}$
28*	707.7–733,3	»	7.2	151373,4	7556,3	4669.4	4328[illegible],1	183	716,0	93021,2	$M_{151'4} \frac{Cl_{99'5}}{(Na + k)_{70'3}\ Ca_{14}\ Mg_{14}}$
	701 – 731,4	»	6.9	168119	6651	5370	55715	82	533	99850	$M_{168'1} \frac{Cl_{99'5}}{(Na + k)_{76}\ Mg_{14}\ Ca_{10}}$

* After author.

M Salinity in gm/1.

Table (1) Chemical Analysis of Ground Water From Ras-Gharib Oil-field

Well No.	Depth Inter-val in M.	Geologic age	PH	T.D.S. mg/1	Ca in mg/1	Mg in mg/1	Na + K in mg/1	HCO_3 in mg/1	SO_4 mg/1	Cl in mg/1	Kurlov's formula
59	243.8	Pliocene	7.1	73749	1404	2694	22275	1831	3870	40775	$M_{73'7} \frac{Cl_{91}\ SO_6^4\ HCO^2}{(Na + k)_{7-}\ Mg_{17}\ Ca_6}$
14	421.5 637,0	Nulli-pore	8.8	140719	5290	2622	49682	349	3611	79165	$M_{140'7} \frac{Cl_{97}\ SO^3_4}{(Na + k)_{..}\ Ca_{10}\ Mg_8}$
3*	346,8-365,5	»	7.5	141656	4115,5	4912,6	93035,2	264,1	2576	85152	$M_{141'6} \frac{Cl_{97}\ SO^2_4}{(Na + k)_{74'7}\ Mg_{16'4}\ Ca_{8'5}}$
7	679,3-698,9	Basal Miocene	7.5	146179	6320	4524	47902	211	1409	85813	$M_{146'1} \frac{Cl_{99}\ SO_1^4}{(Na + k)_{75}\ Mg_{14}\ Ca_{11}}$
7*	679.3-698,9	»	7.6	142360	5923,0	4426,2	42647,9	189,5	1500,0	86505,4	$M_{142} \frac{Cl_{98}\ SO_{1'3}^4}{(Na + k)_{72'6}\ Mg_{14'7}\ Ca_{12}}$
8	735,1-750,3	Up. Cret.	6.2	146000	5712	4398	48117	48	139	87586	$M_{146} \frac{Cl_{99'8}}{(Na + k)_{76}\ Mg_{13}\ Ca_{10}}$
3	647,7-678,1	Up. Cret.	6.2	151500	7680	3868	49114	31	30	90777	$M_{151'5} \frac{Cl_{99'9}}{(Na + k)_{75}\ Ca_{13}\ Mg_{11}}$
5*	632,6-691,8	Up. Cret.	6.7	141594	6661,9	4085,8	41553,2	158,6	28	87528,6	$M_{141'6} \frac{Cl_{99}}{(Na + k)_{72}\ Mg_{14}\ Ca_{13}}$
	664,4-720,8	Nubian SS «A» series	5.9	156922	8256	4019	51320	48	19	93260	$M_{157} \frac{Cl_{99'9}}{(Na + k)_{75}\ Ca_{14}\ Mg_{11}}$
)	450,1-469,9	Nubian S. «A» series	6.0	155682	8300	5070	49310	50	47	92905	$M_{155'7} \frac{Cl_{99'9}}{(Na + k)_{-2}\ Ca_{14}\ Mg_{14}}$
,	520,9-591.2	Nubian S. «A» series	7.1	159431	8720	3932	54125	134	324	92196	$M_{159'4} \frac{Cl_{99'5}}{(Na + k)_{75}\ Ca_{14}\ Mg_{10}}$

recent formations which contain oil but not of economic value. The consequence of hydro-stratigraphical units of Ras-Gharib are shown in Fig. 1 as follows :

Nubian Sandstones : The Oil-water bearing formations lying above the basement rocks up to the cenomanian consist of sandstones of nubian type. These sandstones are intercalated with shales. In Ras-Gharib these sanstones are divided into four series. "D" series reaches a thickness of 490.0 m., shales compose its upper part seperating it from the overlying "C" series with maximum thickness of 160.0 m. Overlying "C" — series is a thick layer consisting of black shales, rich in organic matter with a thickness of 120 m. the "B" — series, which are not Oil-water bearing formation. For "D" and "C" series are given carboniferous age of "lower" "Attaqa". For "B" series is given also carboniferous of "upper Attaqa". Overlies "B" series, the "A" series with a maximum thickness of 90.0 m. For this series is given permian age. The "D", "C", and "A" series are oil-water bearing formations.

Cretaceous : The Oil-water bearing deposits of creataceous of Ras-Gharib are represented by its upper part belonging to turronian-@ santonian and cenomanian. Cenomanian lies over "A" series of the nubian sandstone and consists of limestone, marls, shales and some thin layers of sands, its thickness reaches 70.0 m. Turronian-santonian consists of dolomitic limestones and its thickness reaches 100.0 m. These deposits are covered with shales intercalated by thin limestone layers.

Miocene : Only the middle miocene rocks are represented in Ras-Gharib, which is represented by the evaporite group. The lower part of the oveporite group is divided to basal

Hydrogeological Section In Ras-Gharib Oil-Field

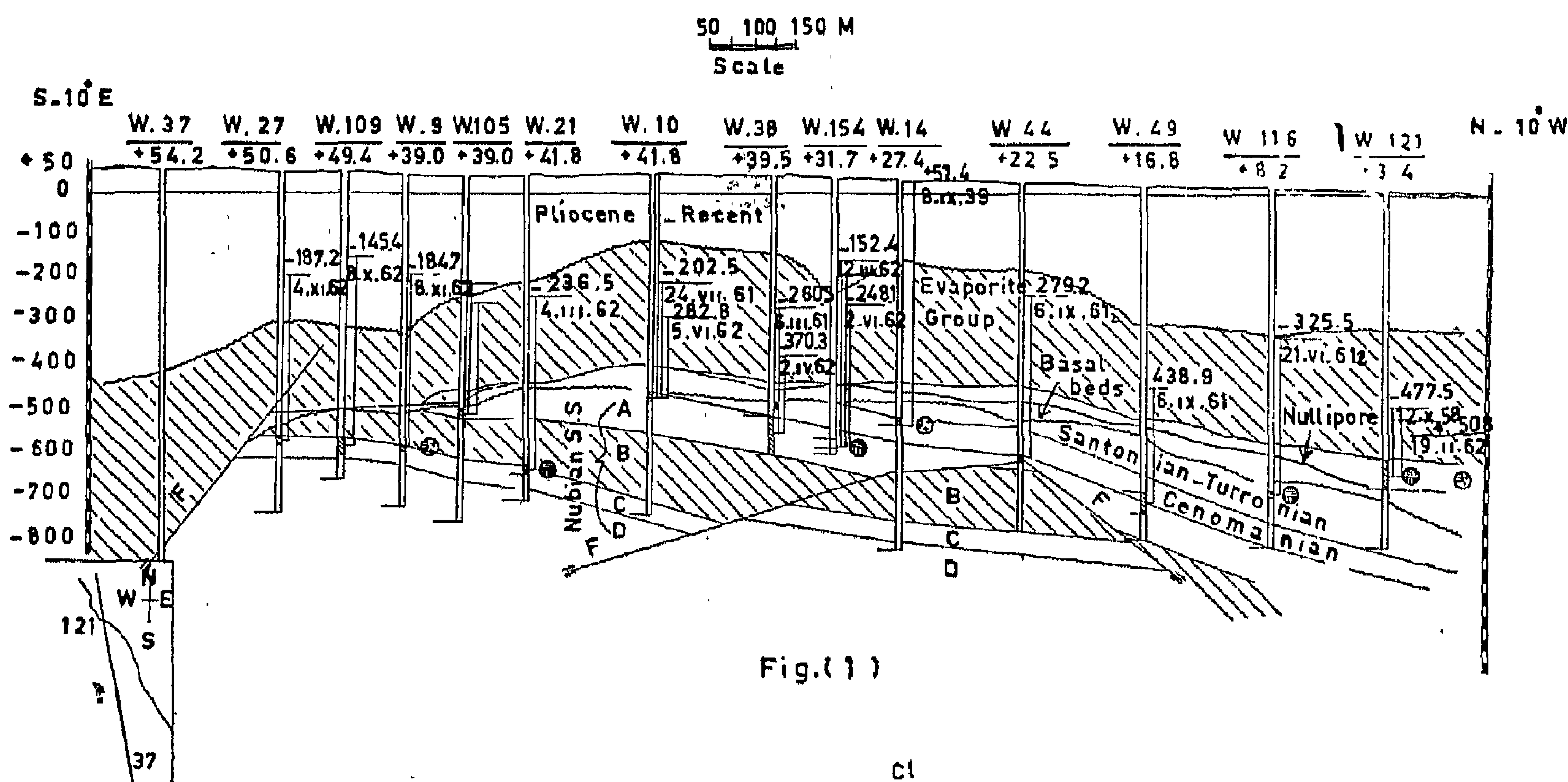
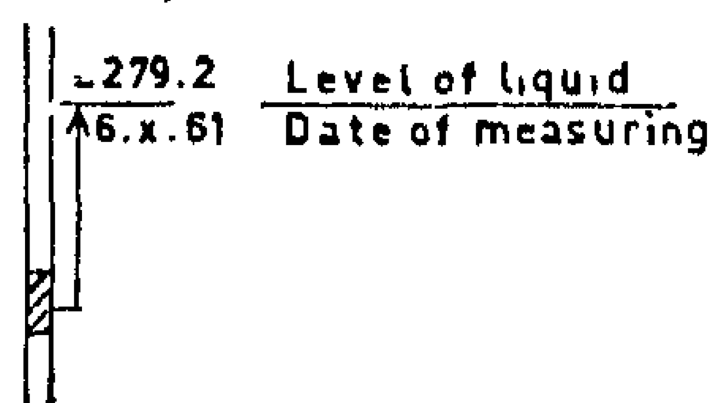
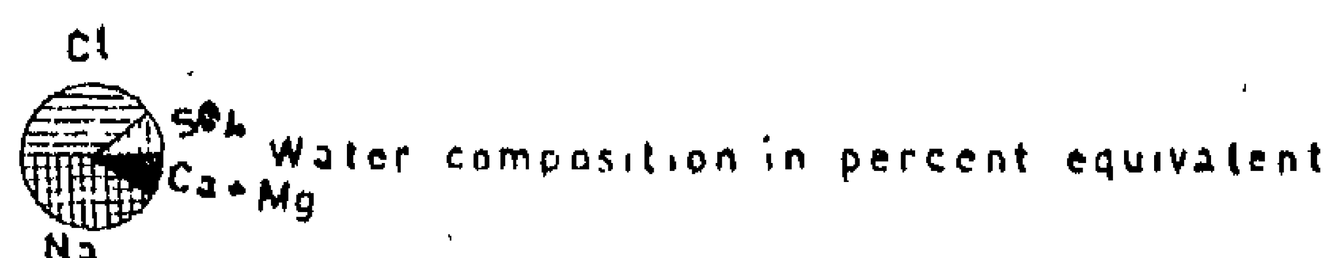
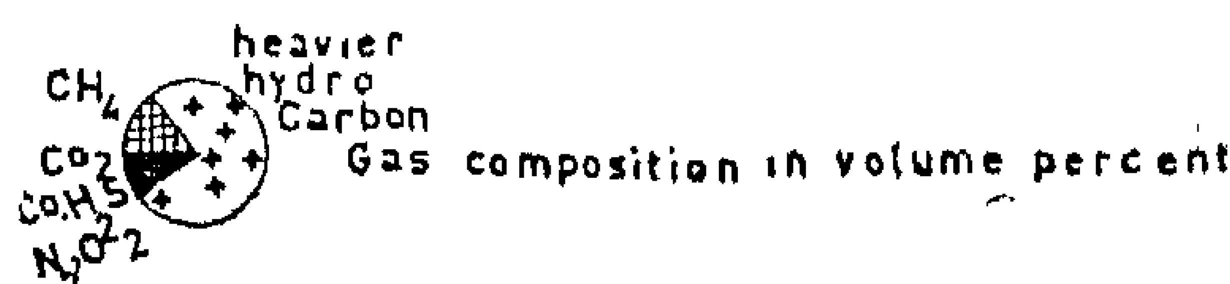


Fig.(1)





Impermeable layer



SOME HYDROGEOCHEMICAL STUDIES OF UNDERGROUND WATER OF RAS-GHARIB OIL-FIELD AND ITS POTENTIALS FOR INDUSTRY

By

NASRY ZAKY BISHAY

Abstract :

Hydrogeochemical studies for Ras-Gharib Oil-field are for oil-water bearing formations, which belong to : nubian sandstones (D, C and Aseries); upper cretaceous ; middle miocene (basal beds and nullipore) and pliocene (water bearing only). Water of these formations are brines and of very high salinitics (70-171 gm/1) which increases with depth and for older geologic formations. Water contain high concentrations of bromine and boron. Iodine is somewhat high. These elements increase with increase in salinity, depth and for older rock formations. Water of these deposits are characterised by low concentrations of sulphates, carbonates, absence of nitrates, and nitrites. Free gases are mainly of methane and other heavier hydrocarbons.

Hydrogeochemical representation shows, that this water are genetically of sodium chloride type. Study of hydrogeochemical coefficients cl/Br, Br/I , r Na/rcl and other coefficients shows, that the origin of such water i.e. enriched in bromine, boron, iodine, calcium is of ancient sea water (lagoonal conditions in middle niocene) which suffered further metamorphization. The presence of NH_4^+, decrease in sulphates, carbonates and absence of nitrates indicates the prevailance of highly intensive reducing conditions and weakly washed deposits.

From specifications needed for water to be utilized in industry (extraction of bromine, boron and partly iodine); it could be decided, that Ras-Gharib brines are suitable and can be extracted more than 1000 tons of bromine in a year, besides boron and iodine. High concentration of these elements are also observed for Hurghada and Ras-Bakr Oil-fields. This industry can be established in Oil-field located on both sides of the Gulf of Suez.

I — Introduction :

Underground water are considered in many countries (U.S.S.R, U.S.R. and in others) as an important source of bromine, iodine and other elements used in industry. In U.A.R. not much attention has been given so far to utilize the industrial water. It is therefore thought necessary to study the hydrogeochemical characterstics of industrial underground water of Oil-fields along the Gulf of Suez.

The aim of the present work is to study the hydrogeochemical characterstics of Ras-Gharib Oil-field and for special interest for the analysis of the industrial underground water, their chemical composition, genesis and their potentials for their use in extraction of bromine, iodine, boron and other elements (k, Li).

II — Location :

Ras-Gharib Oil-field is situated on the western coast of the Gulf of Suez, some 225 km. south of the town of Suez.

III — Hydrostratigraphy :

Since 1938, when the field of Ras-Gharib was discovered an amount of 175 wells were drilled, some of which reached the basement rocks. In Ras-Gharib, triassic, jurrassic, paleocene, eocene and oligocene formations are not represented.

Underground water which will be studied is that accompaning Oil, only for pliocene-

REFERENCES

1 — AROYAN George F., "The Technique of Spatial Fitlering". Proceedings IRE Vol. 47 No. 9. Sep. 1959 PP. 1561 ÷ 1568.

2 — CADE C. M. "IR Radar, Surveillance and Communication." British Communication and Electronics, June 1960 PP. 414 ÷ 418.

3 — DAY Josef N., "Spectrometric Analysis of Missile Flights." Electronics May 20, 1960 PP. 86 ÷ 88.

4 — FISCHER K., Godesberg B. "Missiles For Defence against Tanks and Low-Flying Aircraft". Interavia 12/1965 PP. 1923 ÷ 1929.

5 — HALLOUDA A. M., "Basis of IR Techniques and Their Use in Guidance." Journal of The Egyptian Society of Engineers U.A.R., Vol. No. 4. 1967 PP. 17 ÷ 34.

6 — JAMIESON H. McFee, N. Plass, H. Grube, G. Richards "IR Physics and Engineering" McGraw Hill 1963, Chapters 5 and 14.

7 — KRUSE, McGlauchlin, McQuistan., "Elements of IR Technology". John Wiley 1962 Chapters 2 and 9.

8 — McFEE R.H. "IR Search Systems Design Consideration." Proceeding IRE, Sep. 1959 PP. 1550 ÷ 1552.

9 — MUNDIE L.G., and Others., "An Airborn Spectroradiometer". JOSA Vol. 50 No. 12 1960, PP. 1187 ÷ 1192.

10 — PATTERSO C. L. "Application of the Lateral Photoeffect to a Tracking System". IR Physics, 1962, Vol. 2. PP. 75 ÷ 85.

11 — POVEJSIL D.J., S. Raven, P. Waterman., "Airborn Radar". D. Van Nostrand Company, Chapter 6.

12 — POWELL R.W., "Criteria for Performance of IR Systems". JOSA Vol. 56 No. 7 1960.

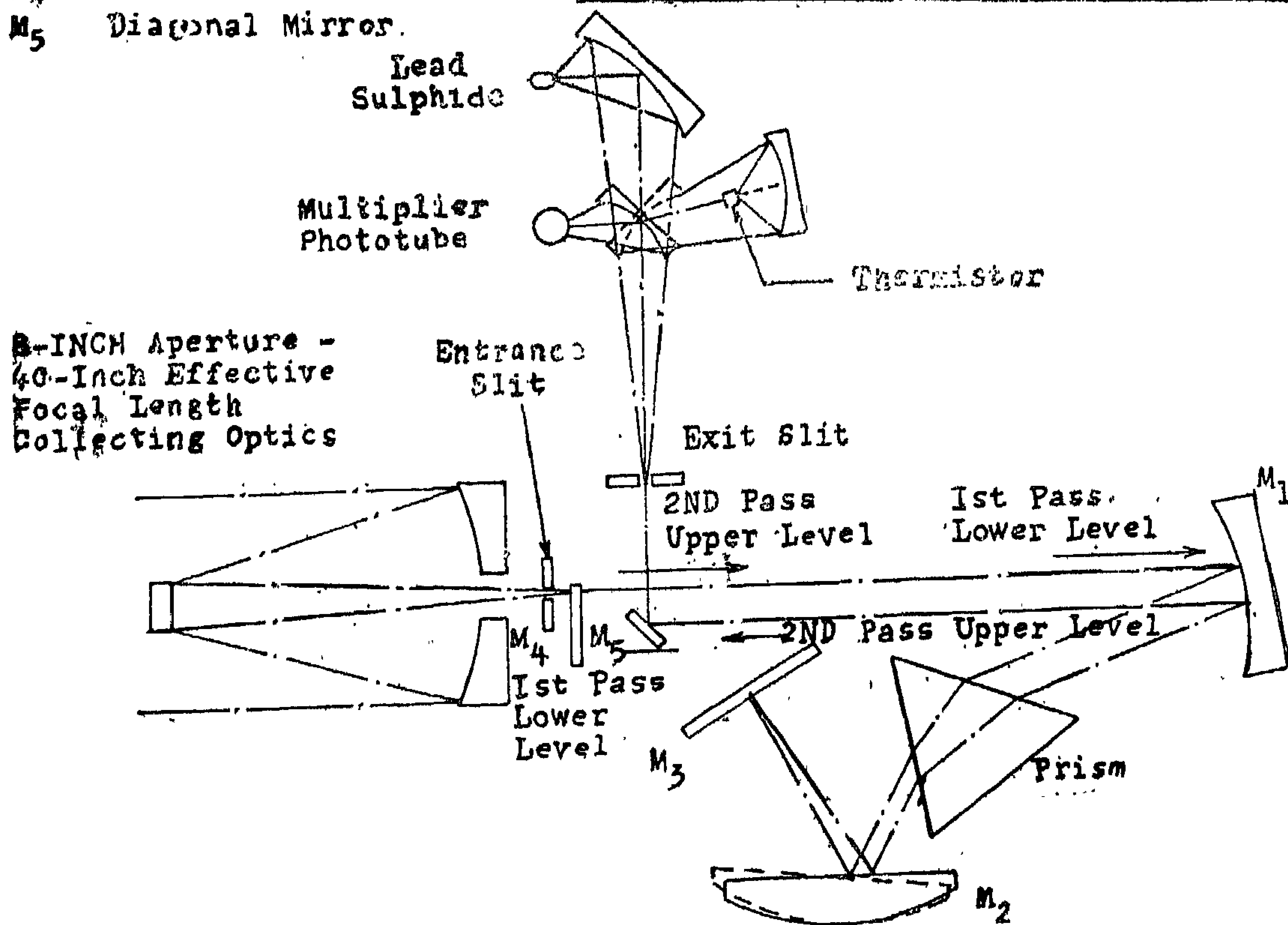
13 — SWIFT I.H. "Performance of BG Limited Systems For Space Use." IR Physics 1962 Vol. 2, PP. 19 ÷ 30.

14 — WEIHE W.K., "Classification and Analysis of Image-Forming Systems." Proceedings IRE Sep. 1959 PP. 1593 ÷ 1596.

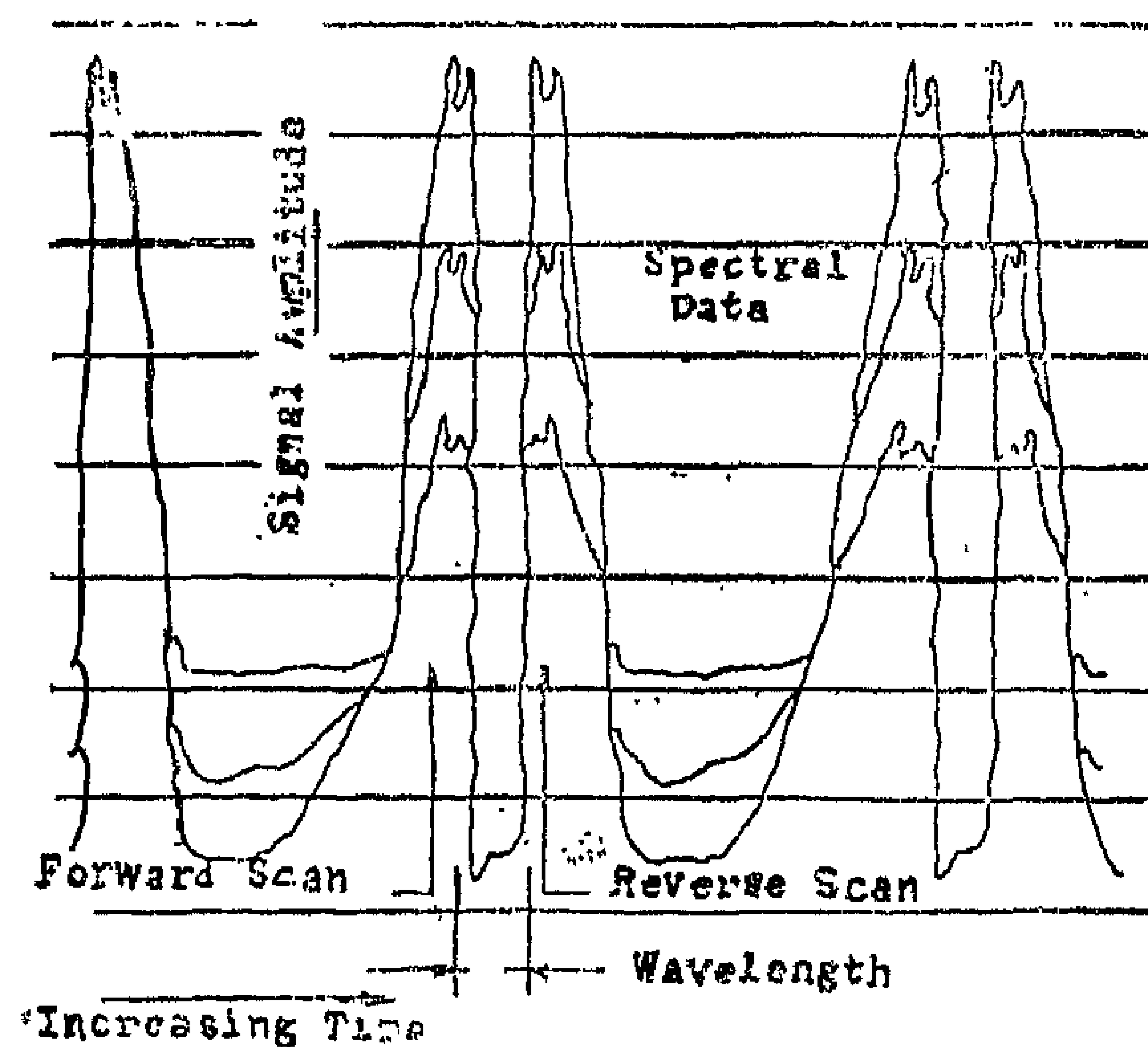
15 — WIESMAN R. S., M. W. Klein. "IR Viewing Systems." Proceedings IRE, Sep., 1959, PP. 1617 ÷ 1619.

16 — WILLIAM — Rayman "IR Emission Spectrum of the Atmosphere." JOSA, June 1955 P. 455.





a — Scheme



b — Record

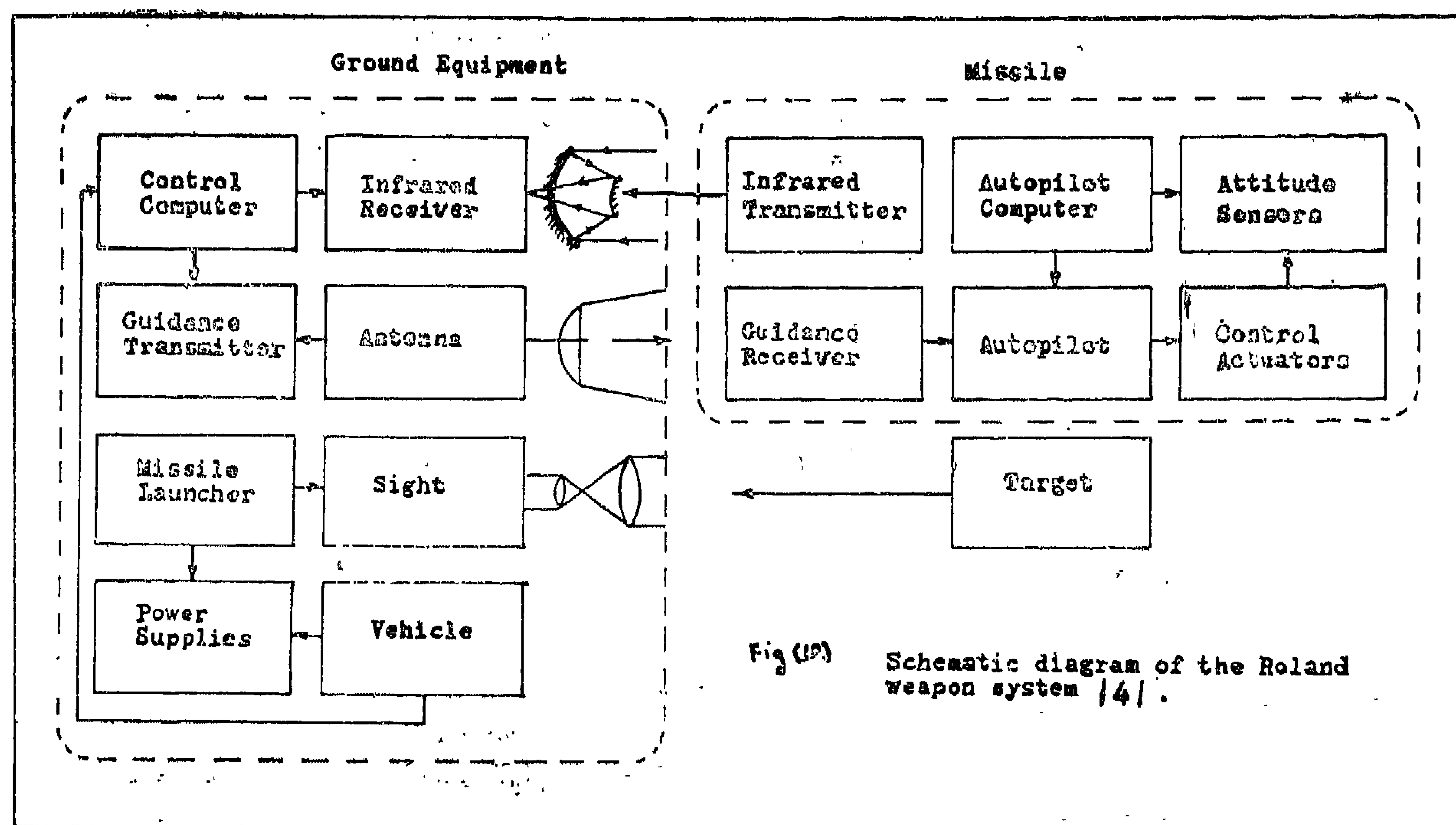


Fig (19) Schematic diagram of the Roland weapon system |4|.

C — Target Idendification :

It would be available only in big trackers, where the spectrum analysis is achieved simultaneously. The continuous comparsion of the spectrum with a standard one helps the identification. Originally such systems were designed for measurements and investigations of combustion during power plant development Fig. (19), but now it is thought of its utilization for identification. Special chemical addition or IR sources could help making this task simpler instead of depending on the inherent flame or exhaust spectrum.

D — Passive Homing :

This is the direct application and most widely used. It makes use mostly of simple reticle concentric with one detector. The reflecting optical system together with the reticle rotates in a gyroscopic fashion to make precession smooth. Firestreak uses pulse duration modulation. American Sidewinder uses a simple nonlinear reticle. All of these rockets apply proportional navigation in hunting their targets.

VI — CONCLUSION

This short account of IR systems in general and important design details for tracking systems shows the severe, precise and statistical measurements and analysis needed before achieving a proper design of these light, precise and cheep equipments.

(iii) Mosaic detector (multi-elemental)

In a mosaic system positional data is obtained without scanning. It needs, however complicated electronics to obtain the information. In presence of spatial filteration reticle, the responding detector or segment give the indication of the position. Without a reticle either the pulse necessary to show the presence of a target is predetermined or a continuous comparison is necessary replacing space filteration. The presence of a filtering reticle reduces the electronic complexity. The multielemental are different types of mosaic detectors either photon or thermal bolometer arrays Fig. (16).

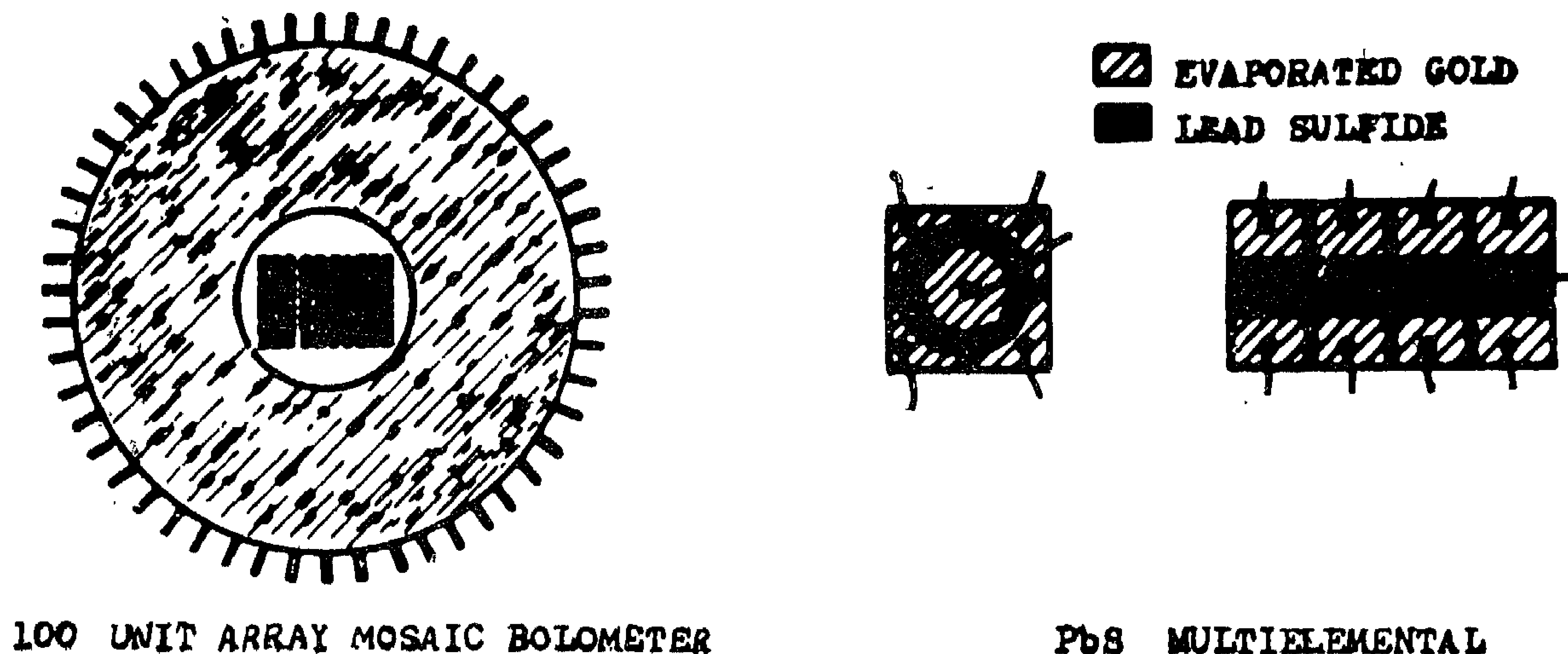


FIG. (16) MOSAIC DETECTORS.

III — PRACTICAL APPLICATIONS :

The replacement of Radar is one of the most important application specially at low altitudes. Besides we have the passive homing and the possibility of identification of missiles.

A — Passive Ground Trackers and Range Finders :

The IR tracking system replaced radar, but with no range measurement, at low altitude for follow up of boosting vehicles. It is found that the tracking was so accurate such that cameras on tracker photographing the take off had the missile continuously in the center of the field of view. The Radar systems would take over at a certain height. A tracker using photolateral effect, is discussed in /11/. IR fire control replaced radar in night fighters. It seems that a conventional range finding technique is achevied with two passive IR systems. A design of single detector system and eccentric reticle could be possible.

B — Missile Tracking Co-operative System For Command Guidance :

In anti-tank and low altitude Anti-aircraft missile systems, command guidance is almost alway in use. The tracking of target is optical or by Radar system. As for the missile the IR tracking proved to be effective, small, light, simple and precise. The block scheme of such systems is seen in Fig. (17) where an IR source is placed at the rear of missile to make easier the proper spectral filteration and hence effective detection and tracking of missile. The French-German Milan, Hot and Rolan use this system/4/.

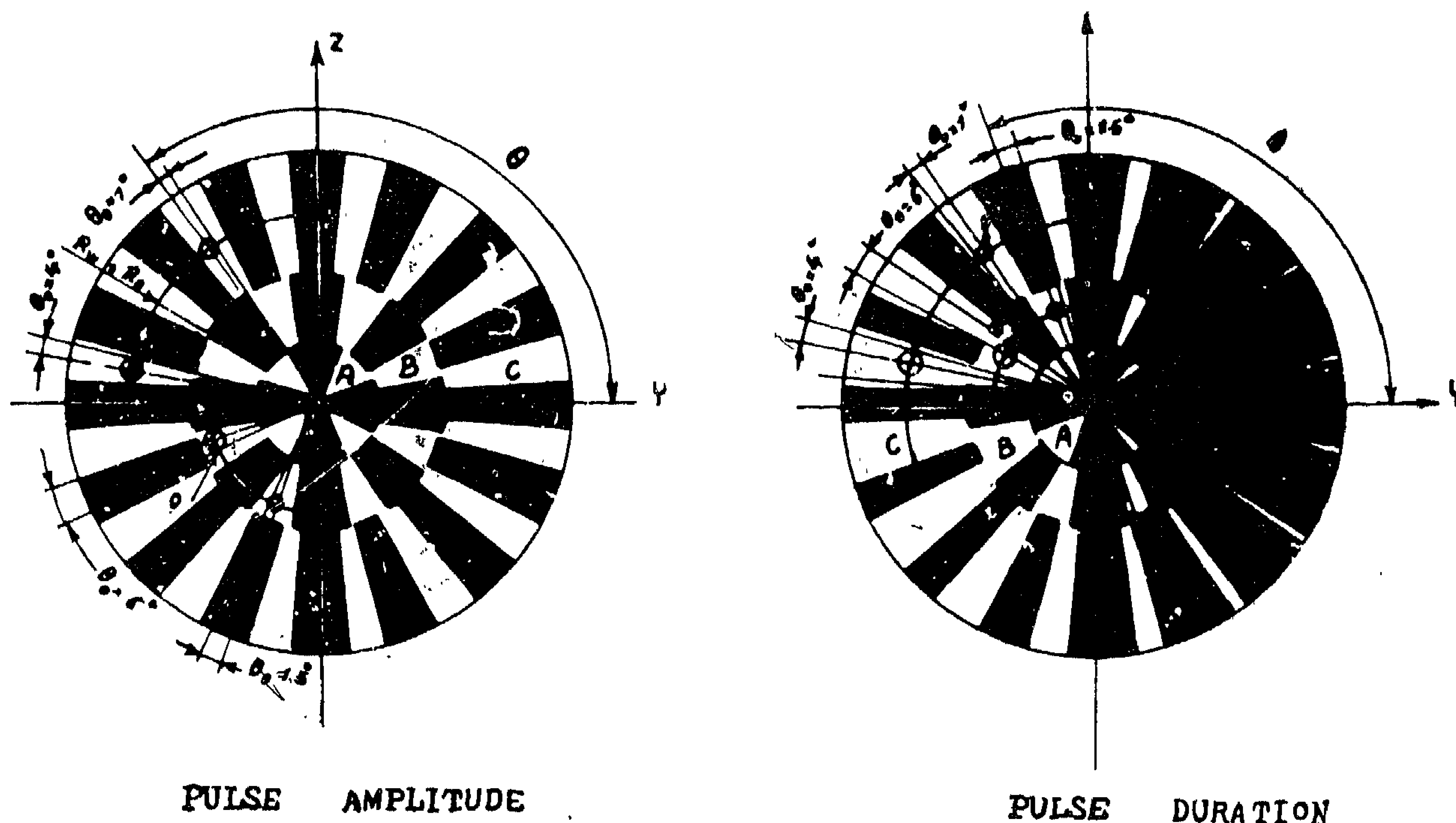
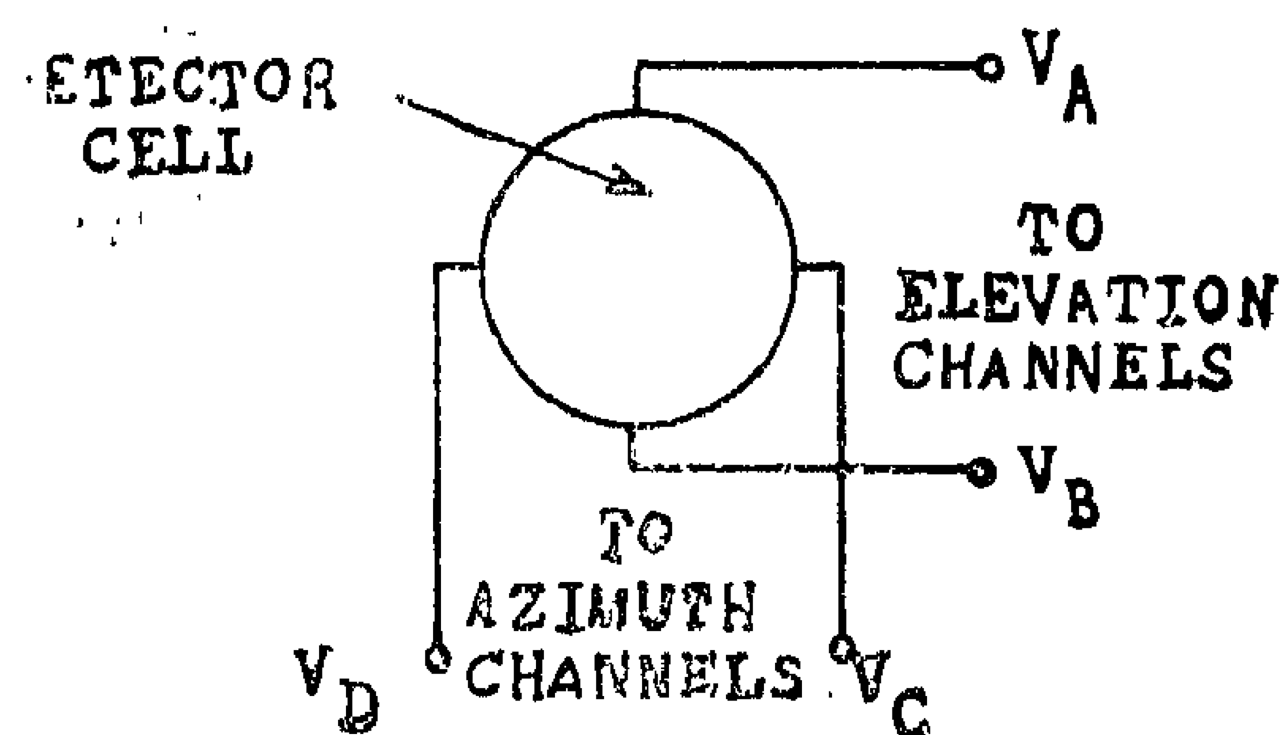


Fig. 14 — CONCENTRIC RETICLES

be achieved by superposition of a kind of modulation over the pattern for space filteration and carrier generation. Amplitude, frequency and pulse duration modulation Fig. (14) are all in use. Frequency change of carrier is used for increasing carrier generation efficiency and determination of target. (R_w) in the image plan.

(b) Photo lateral effect

Apart from the photovoltic effect across the the junction /7/, there is a voltage that appear in a uniform senstive junction when radiation concentration deviate from the senstivity center, parallel with the junction /10/. This photolateral voltage changes from positive to negative as a spot of radiation travel from one side to the other. The use of this phenomena to obtain positional data with respect to a reference was found possible by sampling the output of one opposit pair while short circuiting the other (being as reference). The results of tests on such circuit showed it suitable for practical use Fig. (15) /10/.



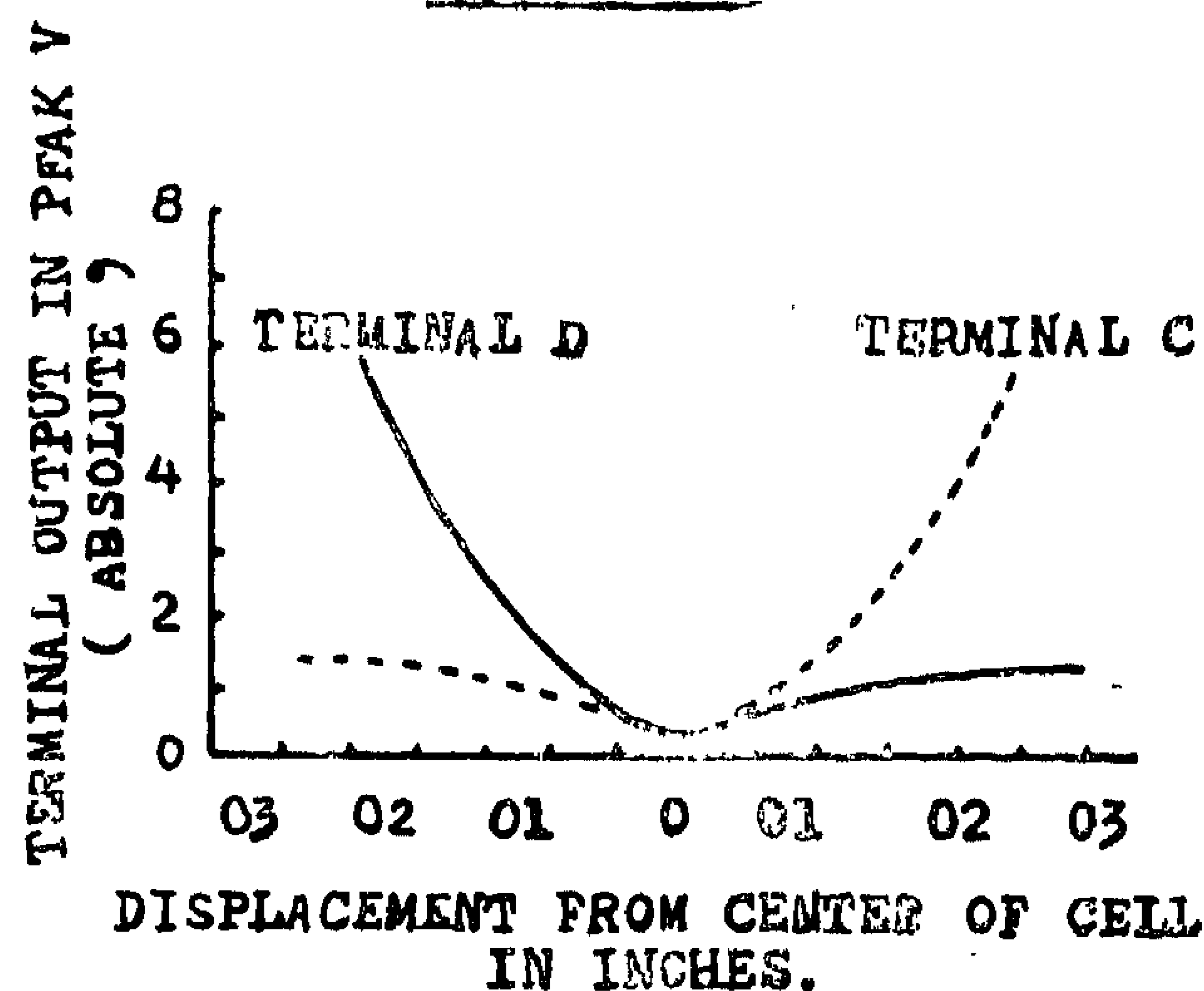


Fig. 15 — UTILIZATION OF PHOTO-LATERAL EFFECT.

Where,

T ... is time for complete scan

γ ... $\frac{1}{2}$ total scanned field angle

σ ... instantaneous field

τ ... dector time constant

For practical purposes a comprise is needed. This type actually is more used in IR Horizon sensor for local vertical, roll and pitch control, but for follow up of aircrafts and rockets it gave way to the image plan scanning.

(ii) Image plane scanning

In this type it is either making an interpretable pattern superimposed on the space filtering reticle or making use of the photo-lateral effect.

(a) Reticle types and interpretable patterns

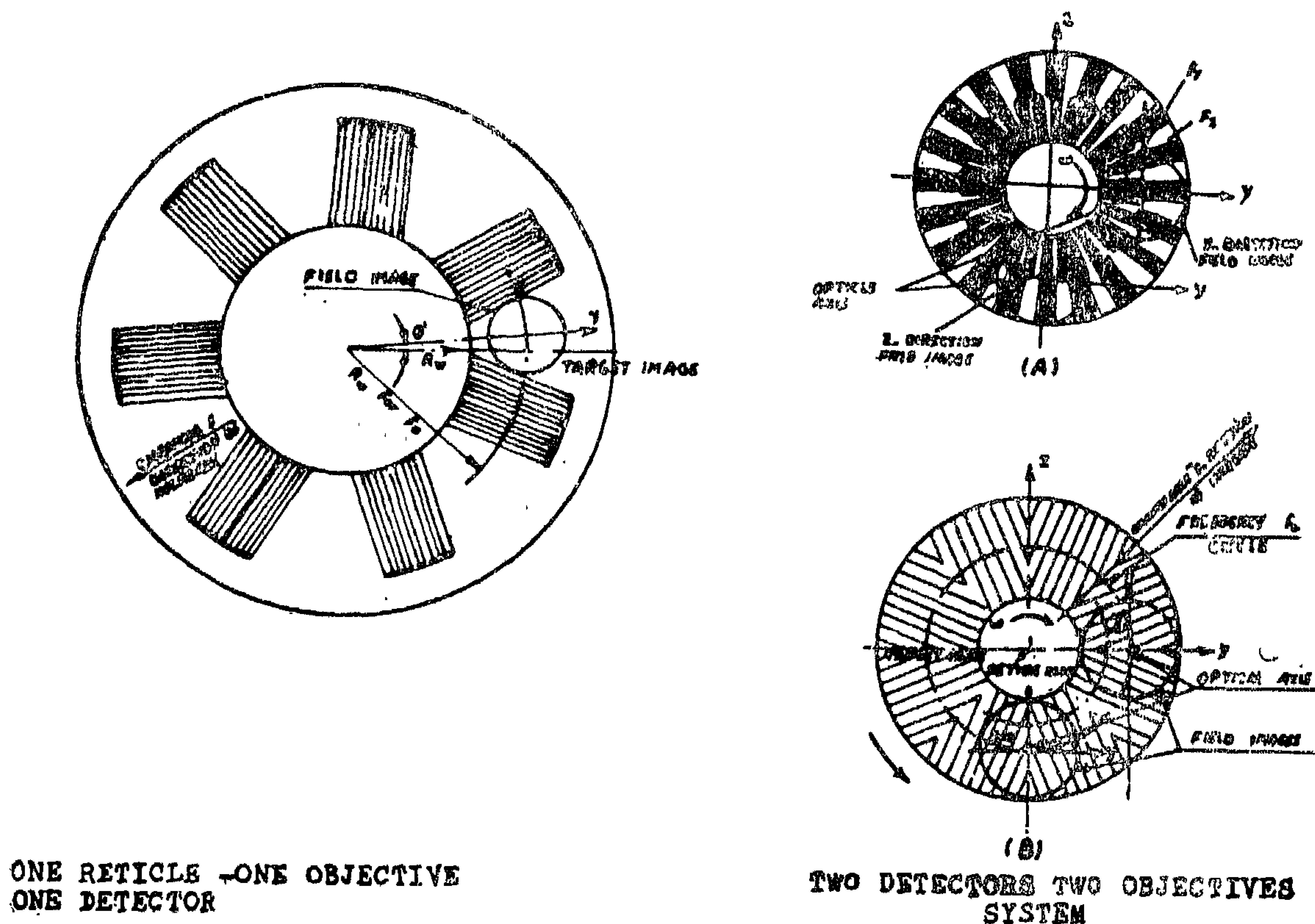
There are concentric and eccentric reticles. — eccentric reticle; Fig. (13).

The axis, of reticle rotation is not along the optical axis. In two objective, two detector, one reticle system, each set is responsible for one coordinate. In Fig. (13) we have a scheme of these reticle showing the Y and X direction field image. A is for a linear system and B shows a non linear one. The system of one reticle-one detector, one object is shown in Fig. (13—c) where the phase of the pulse give the angle from the center of the eccentric reticle and the frequency change give the radius of the radiation concentration.

In eccentric reticle type carrier generation efficiency and space filteration is nearly constant and are chosen at will but it needs more room than the concentric reticle to be discussed.

— Concentric Reticles :

The axis of reticle rotation is coincident with optical axis. Here the interpretation could



ONE RETICLE -ONE OBJECTIVE ONE DETECTOR

TWO DETECTORS TWO OBJECTIVES SYSTEM

FIG. (13) ECCENTRIC RETICLES

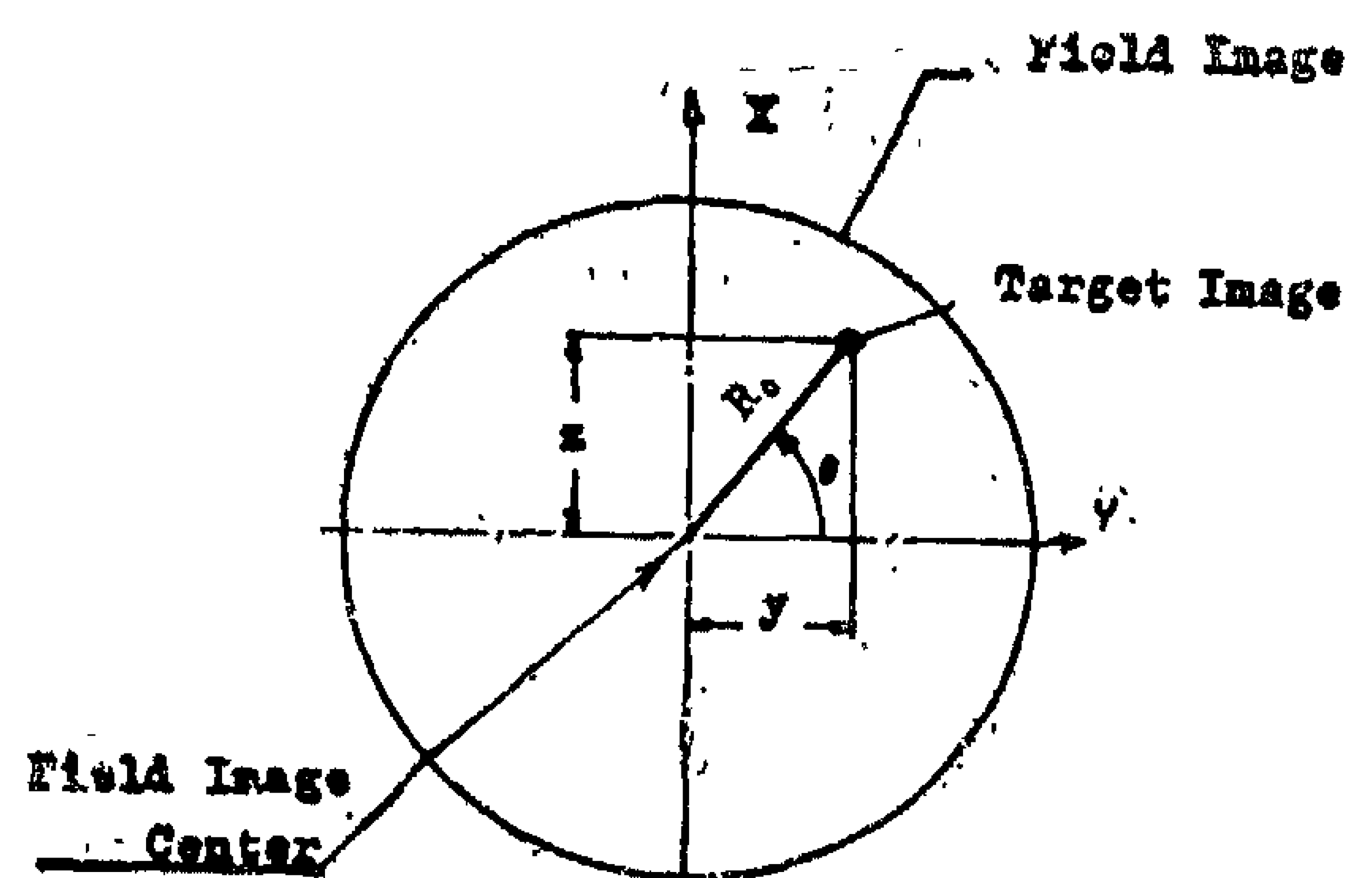


Fig. 11 — POSITIONAL DATA.

The means of determing position data are in broad sense :—

- By object plane scanning (spot scanning)
- By image plane scanning by interpretable modulation or by photolateral effect.
- Mosaic detectors

(i) Object plane scanning

The object plan is scanned with a small instantaneous field of view in a uniform manner and by referencing the target signal, which is a pulse higher than that of BG, it is possible to determine its position in the scanned field. The scanning is achieved by simple rotation of a single or a pair of optical elements. The main parameters of design are the instantaneous field of view, the scanned field of view, the scan pattern Fig. (12) and the detector time constant. The overall field and instantaneous field determines the kind of pattern suitable for a given detector. For a given pattern the detector constant can be determined from simple geometrical relations.

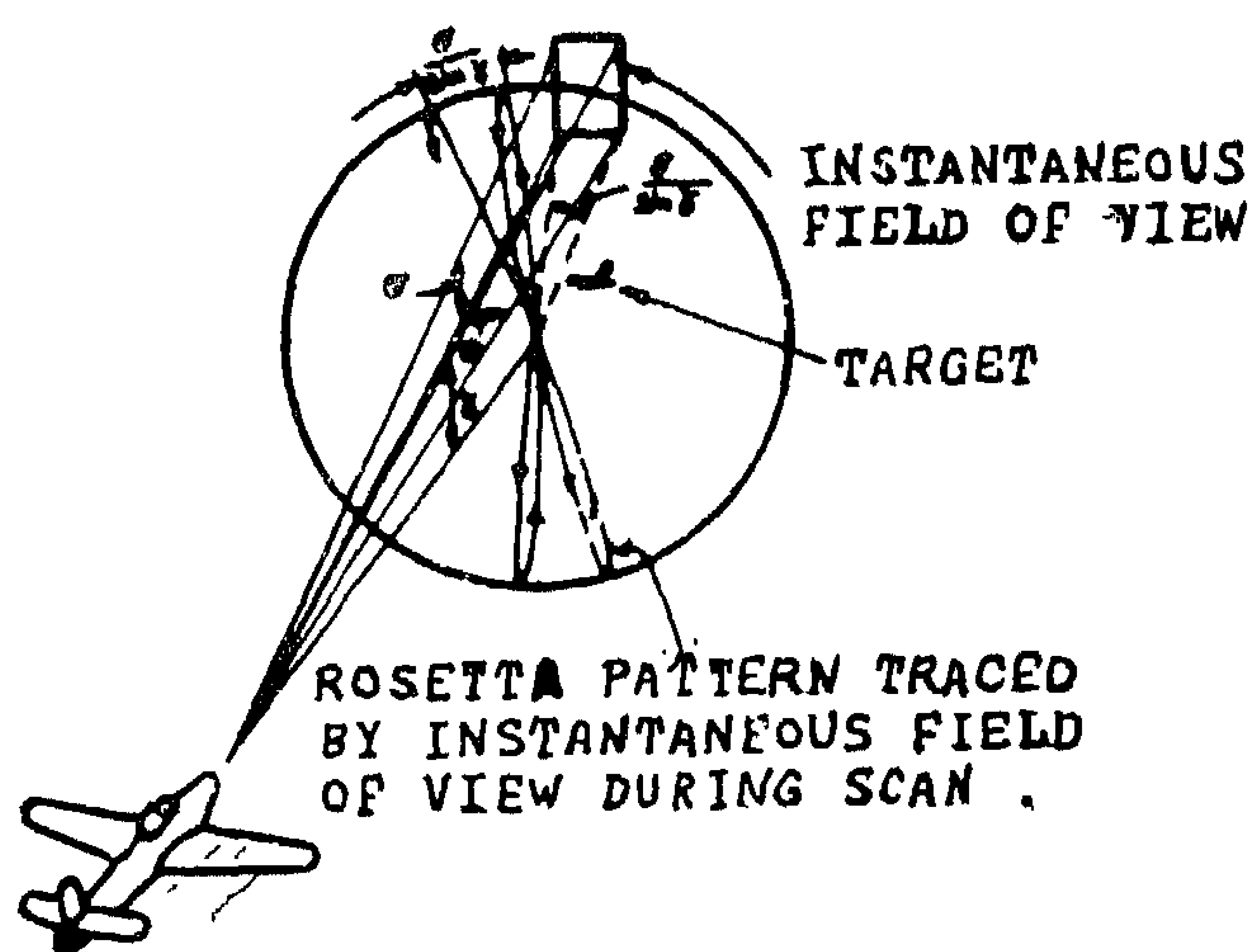
For rosetta pattern, we can write,

N°, of Spokes $= 2\pi / (\delta/\sin\gamma)$ spokes

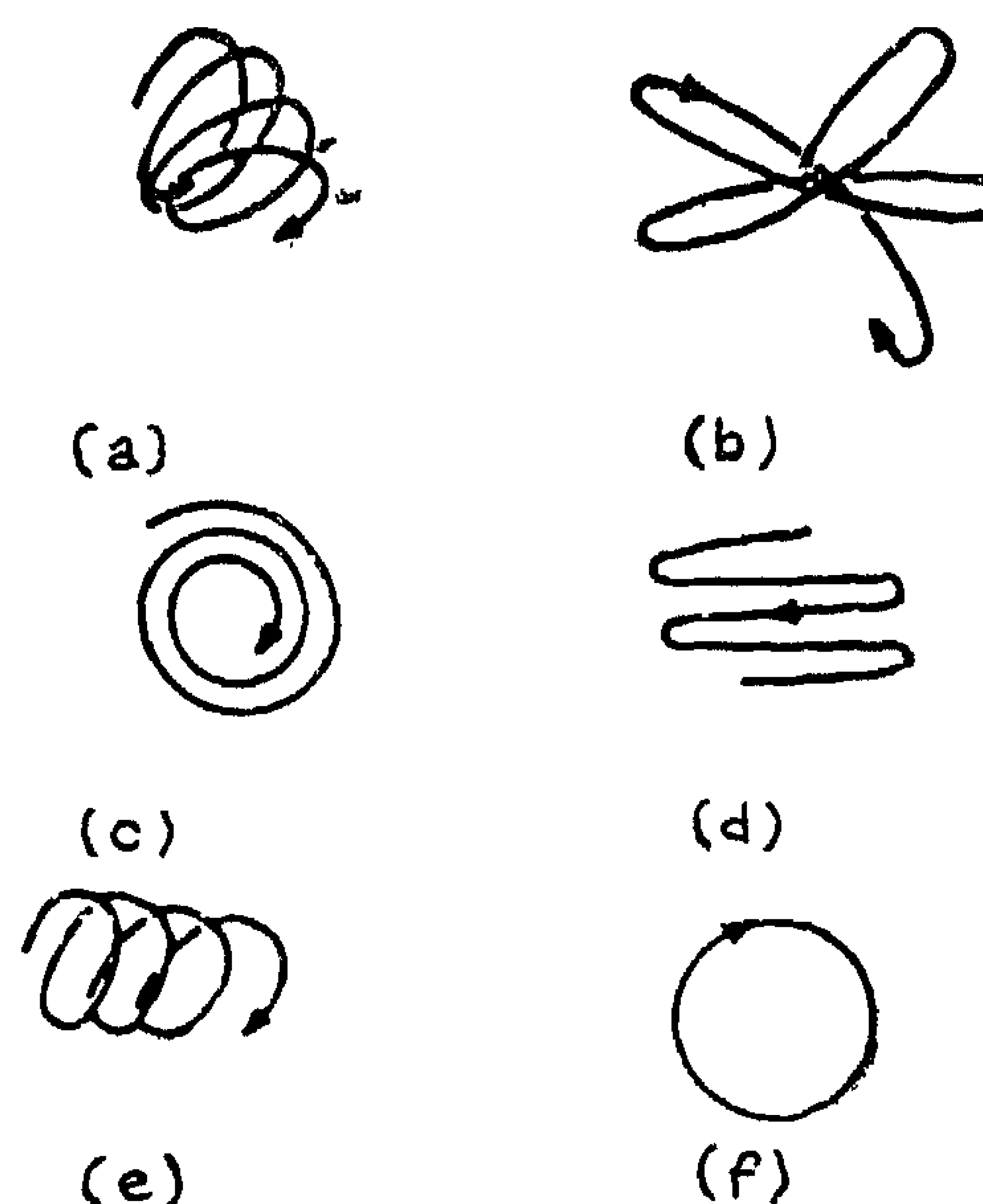
$$\text{Time for a spoke} = \frac{\text{Total time for scan}}{\text{N}^\circ\text{. of spokes}}$$

and after manipulation, the total time "T" for a complete scan is given by /11/

$$T = \frac{4\pi\gamma\sin\gamma\cdot\tau}{\sigma 2} \qquad (8)$$



(B) DETAIL OF ROSETTA PATTERN.



(A) DIFFERENT SCAN PATTERNS.

FIG. (12) SCAN PATTERNS

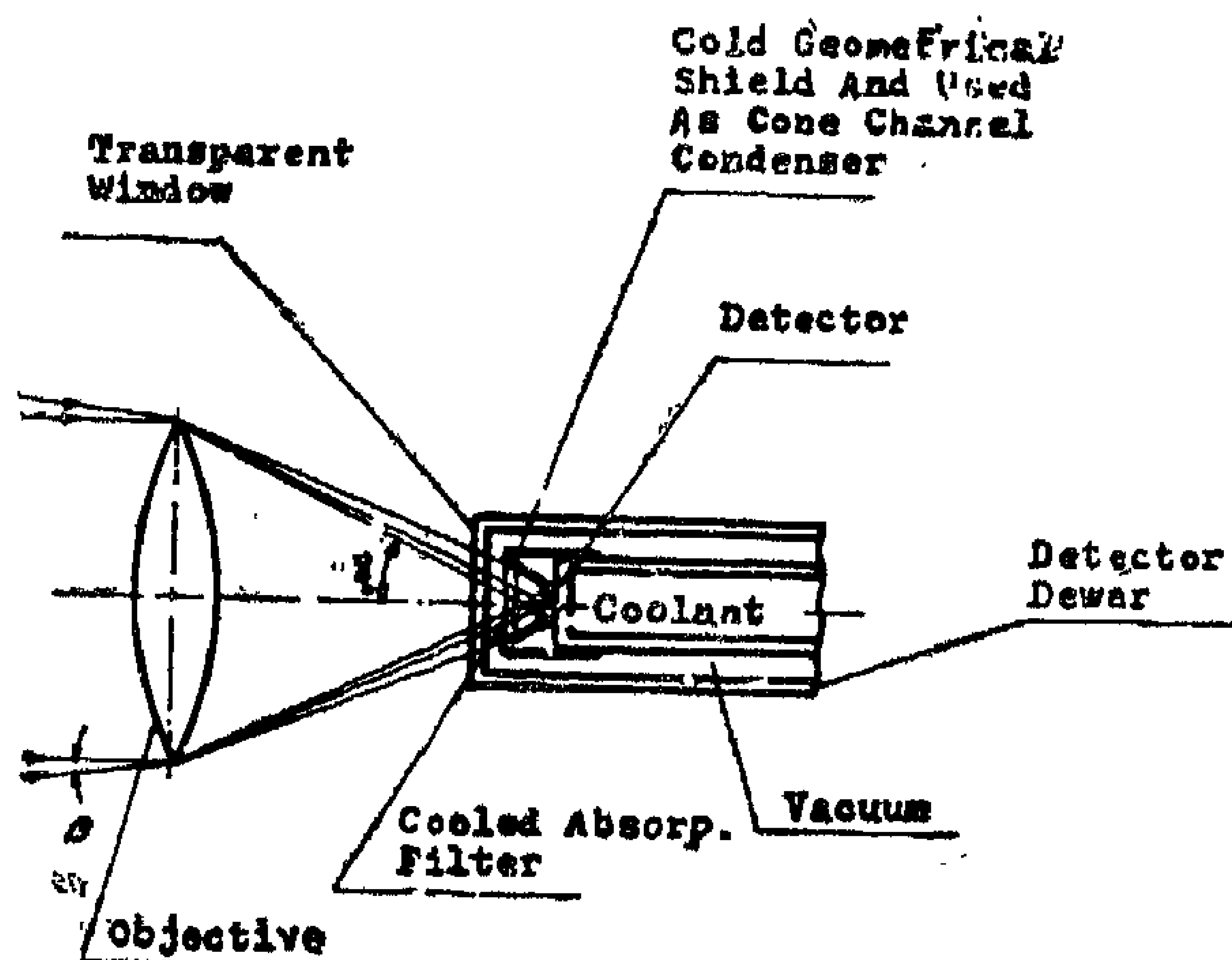


Fig. 7 — GEOMETRICAL SHIELDING

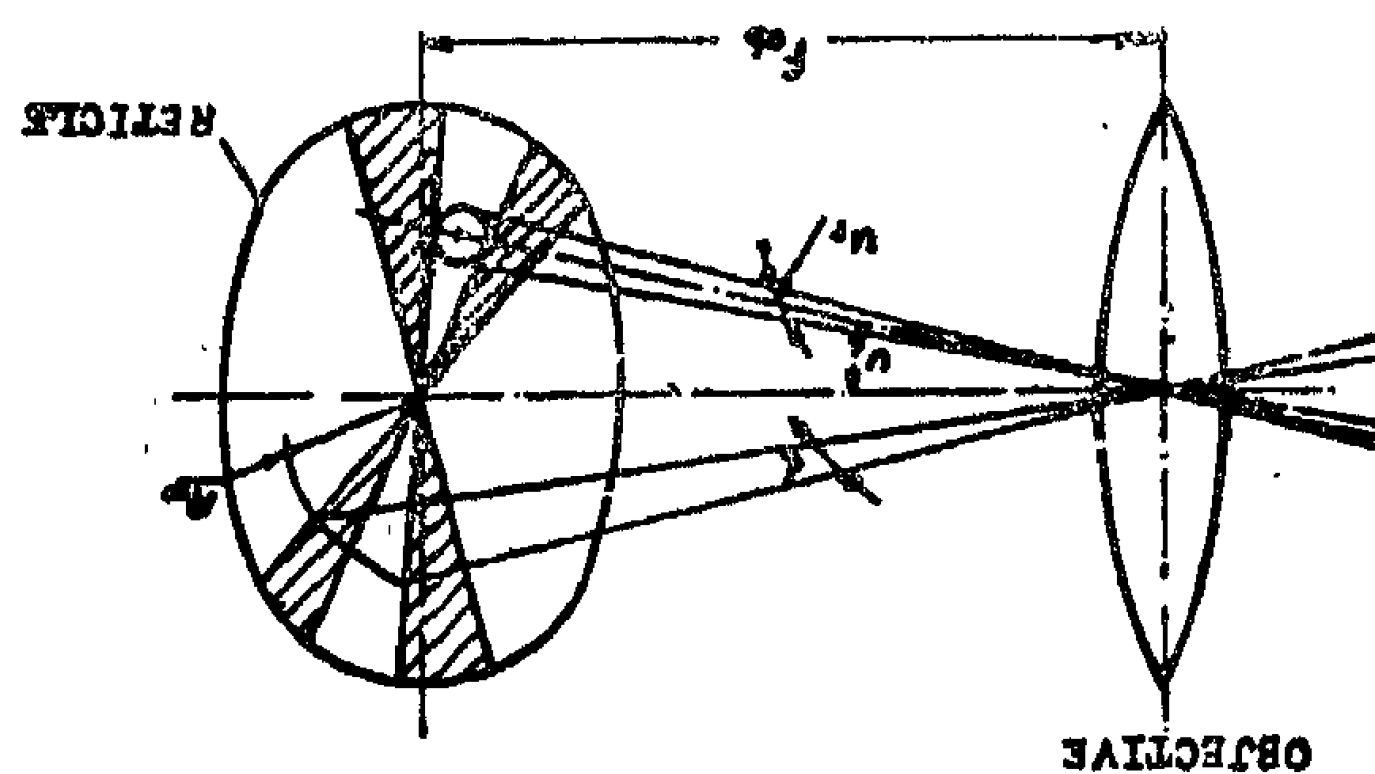


Fig. 8 — WAVES/RAD IN SPOKE RETICLE

$$C_1/S^2 \doteq -1{,}92 \log_{10} Zm + 1{,}067 \ldots$$

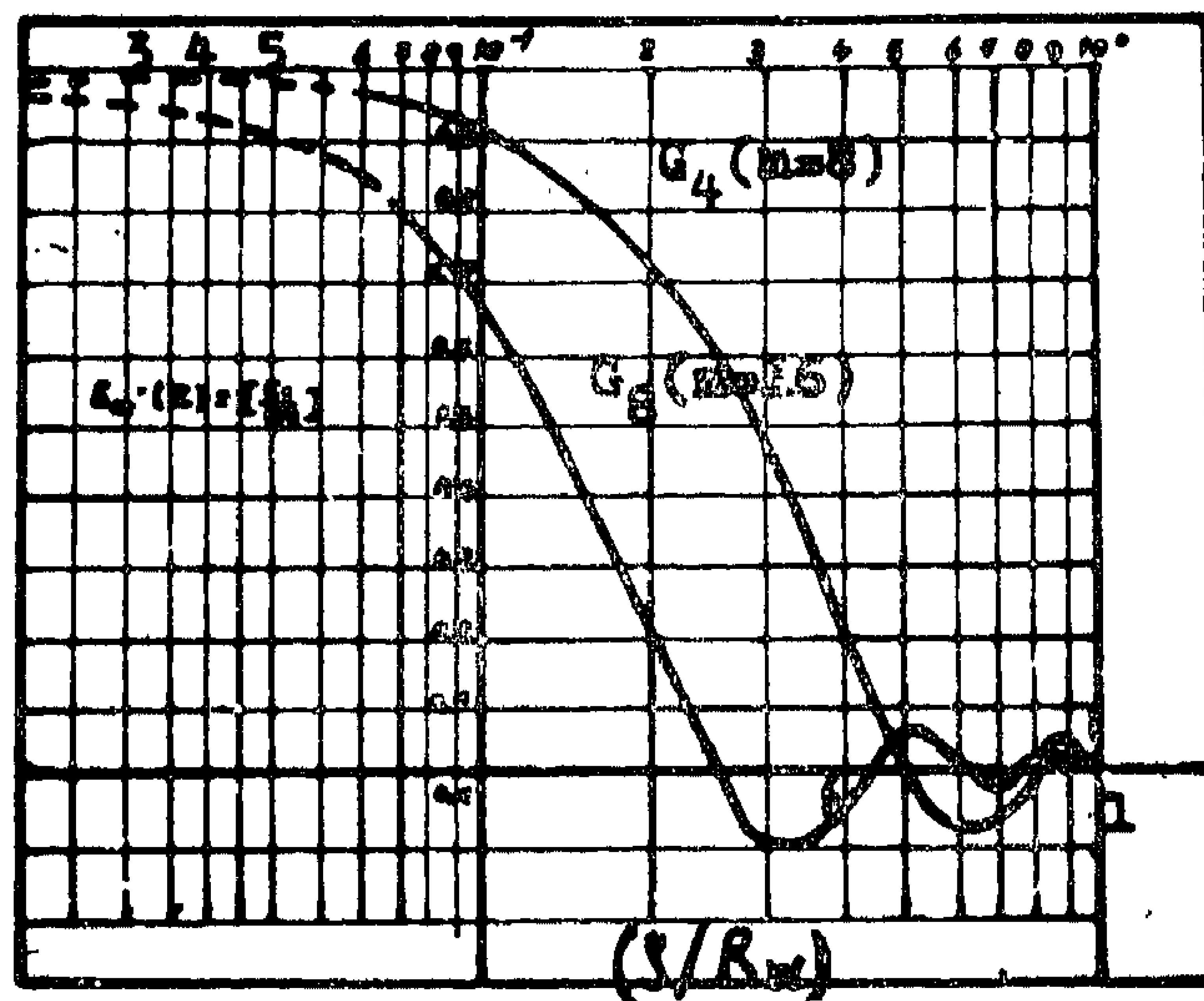
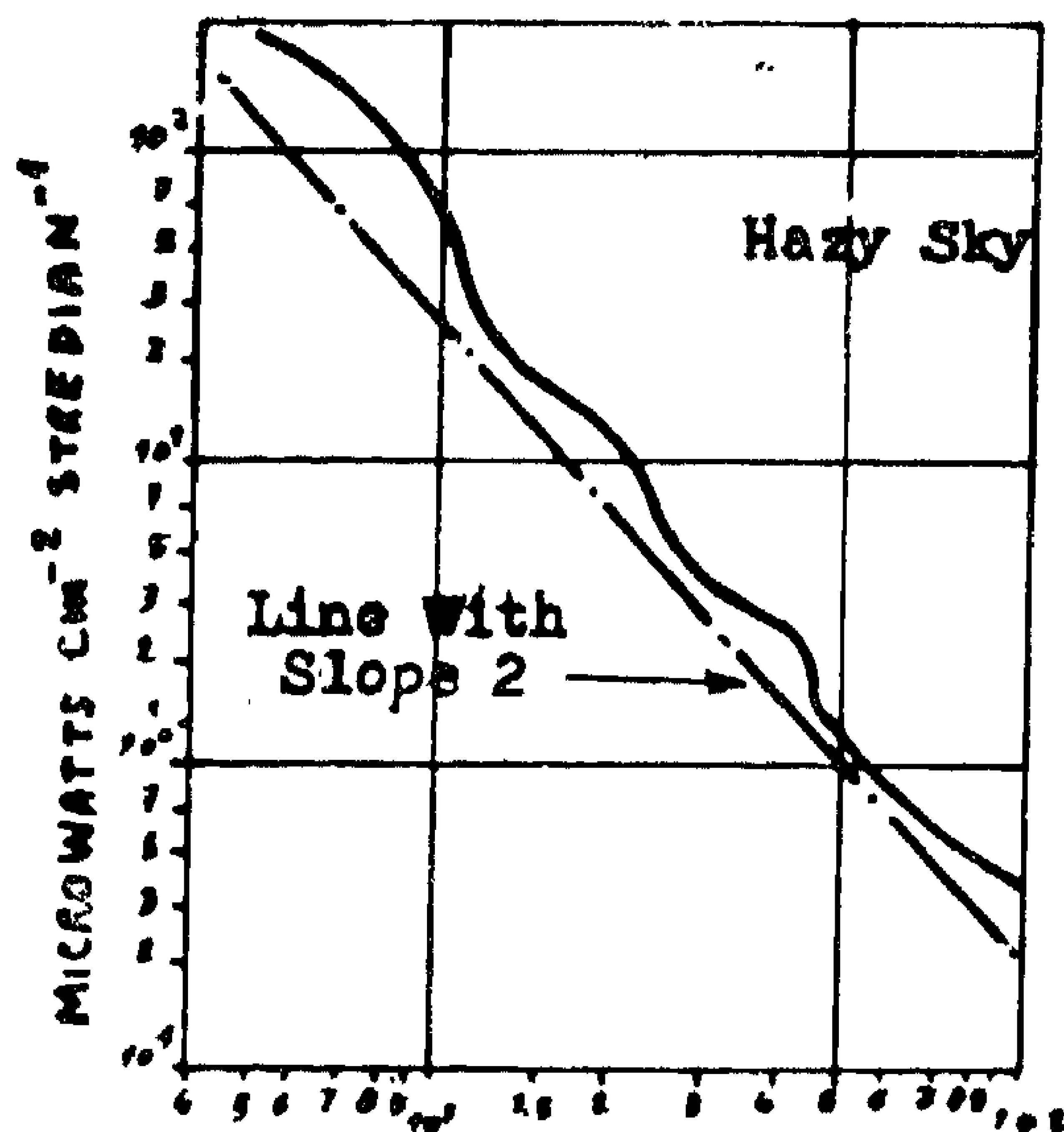


FIG.(9) First Harmonic Amplitude

P.S. WAVELENGTH BELOW 2,8 μ



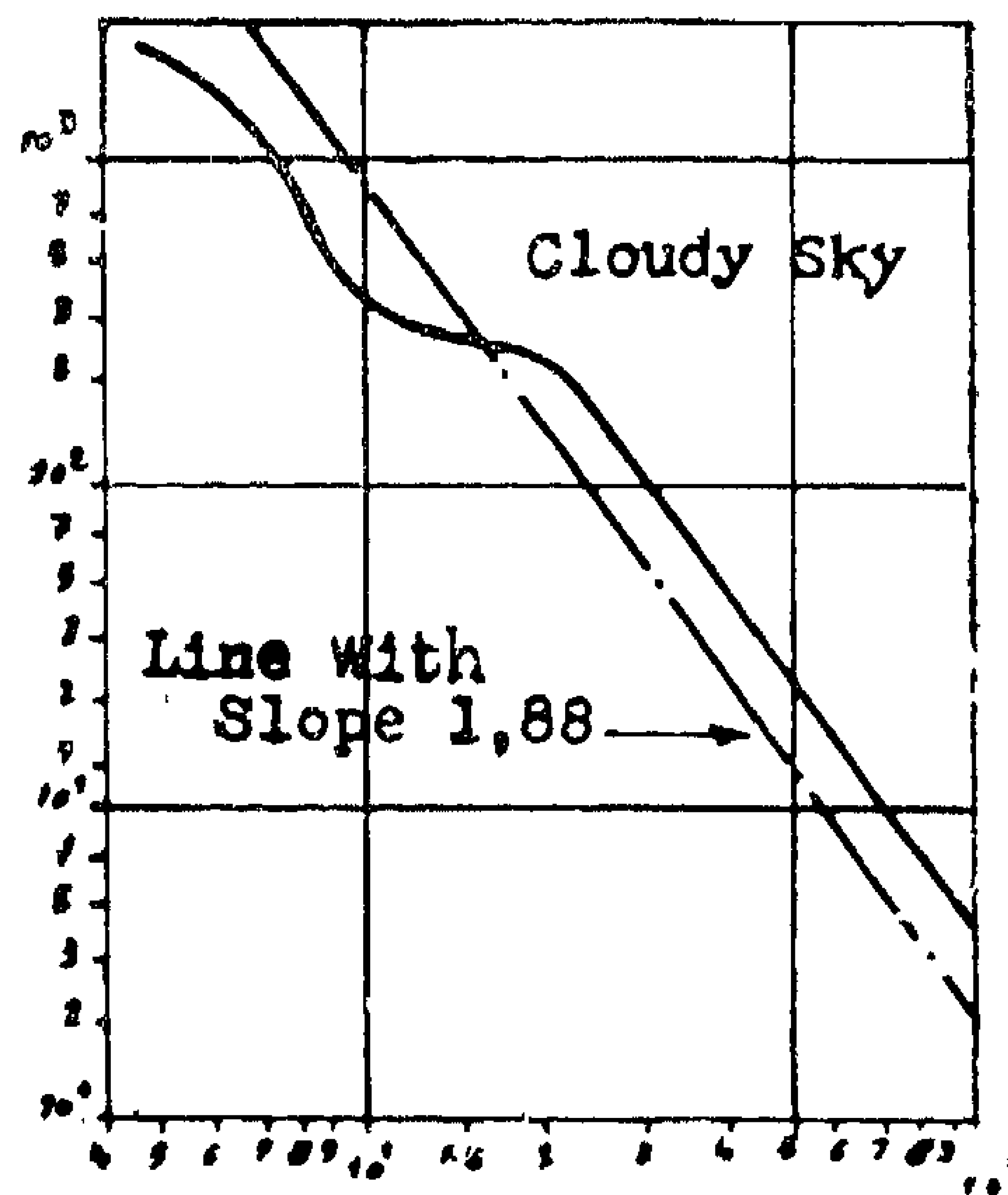
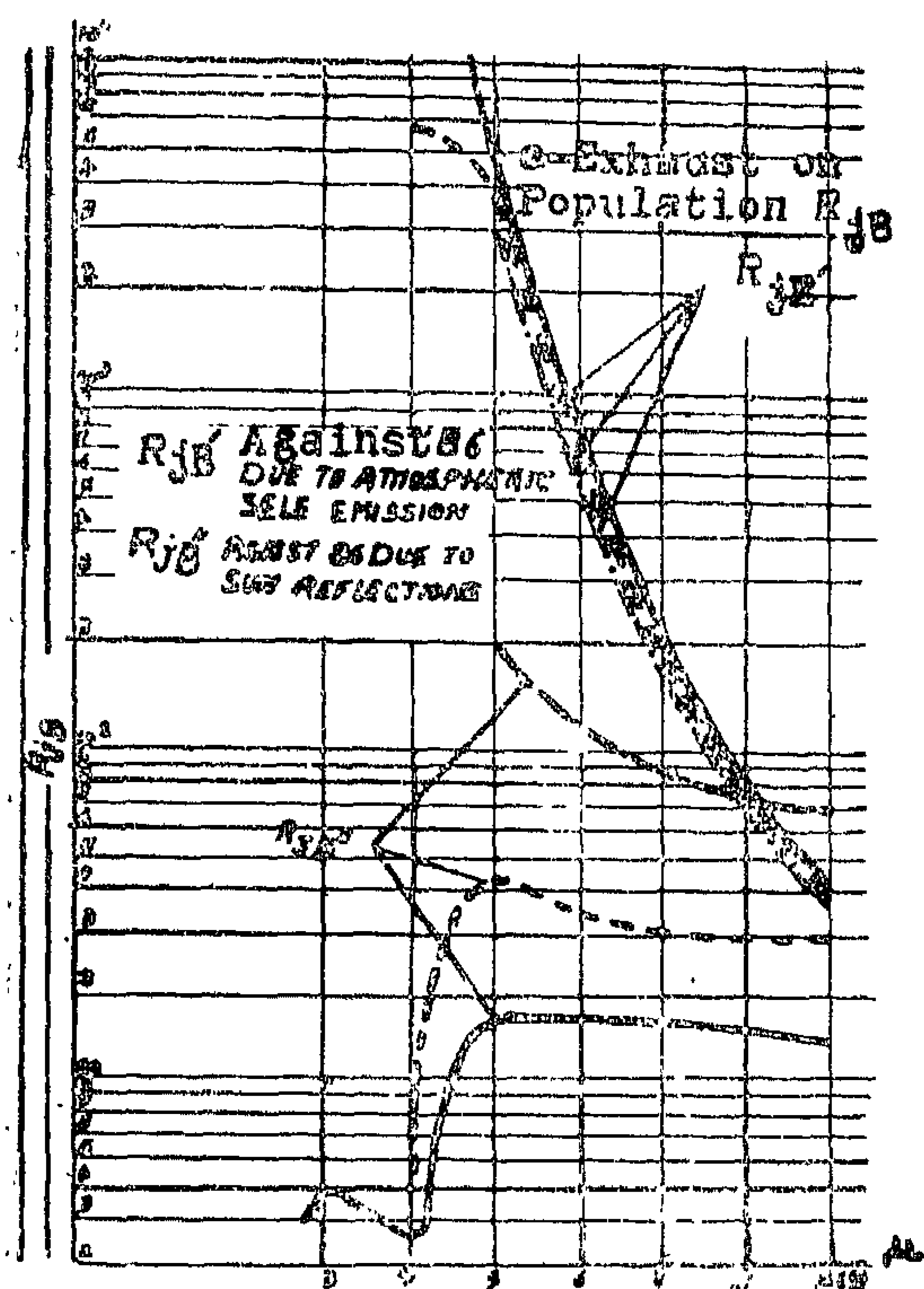
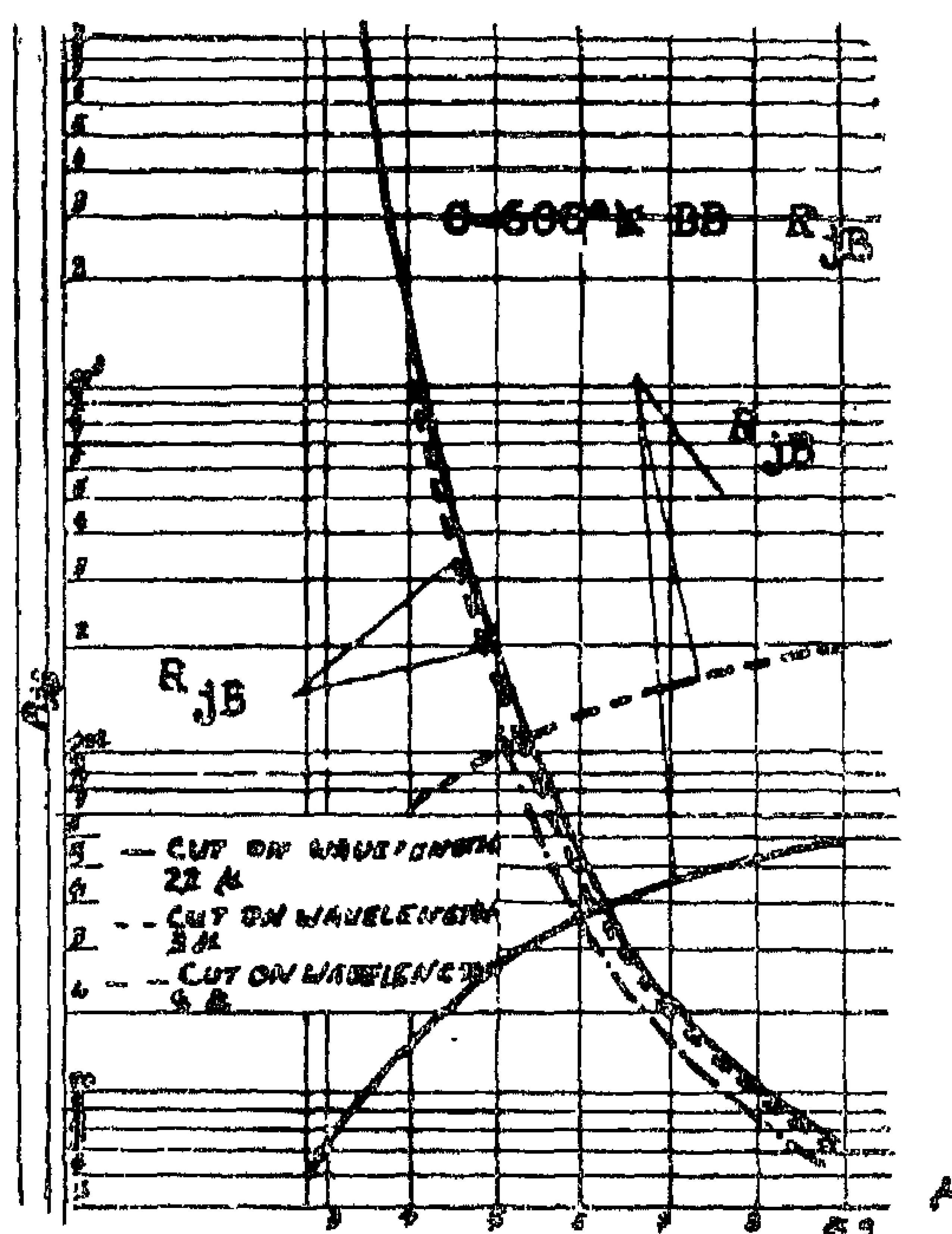
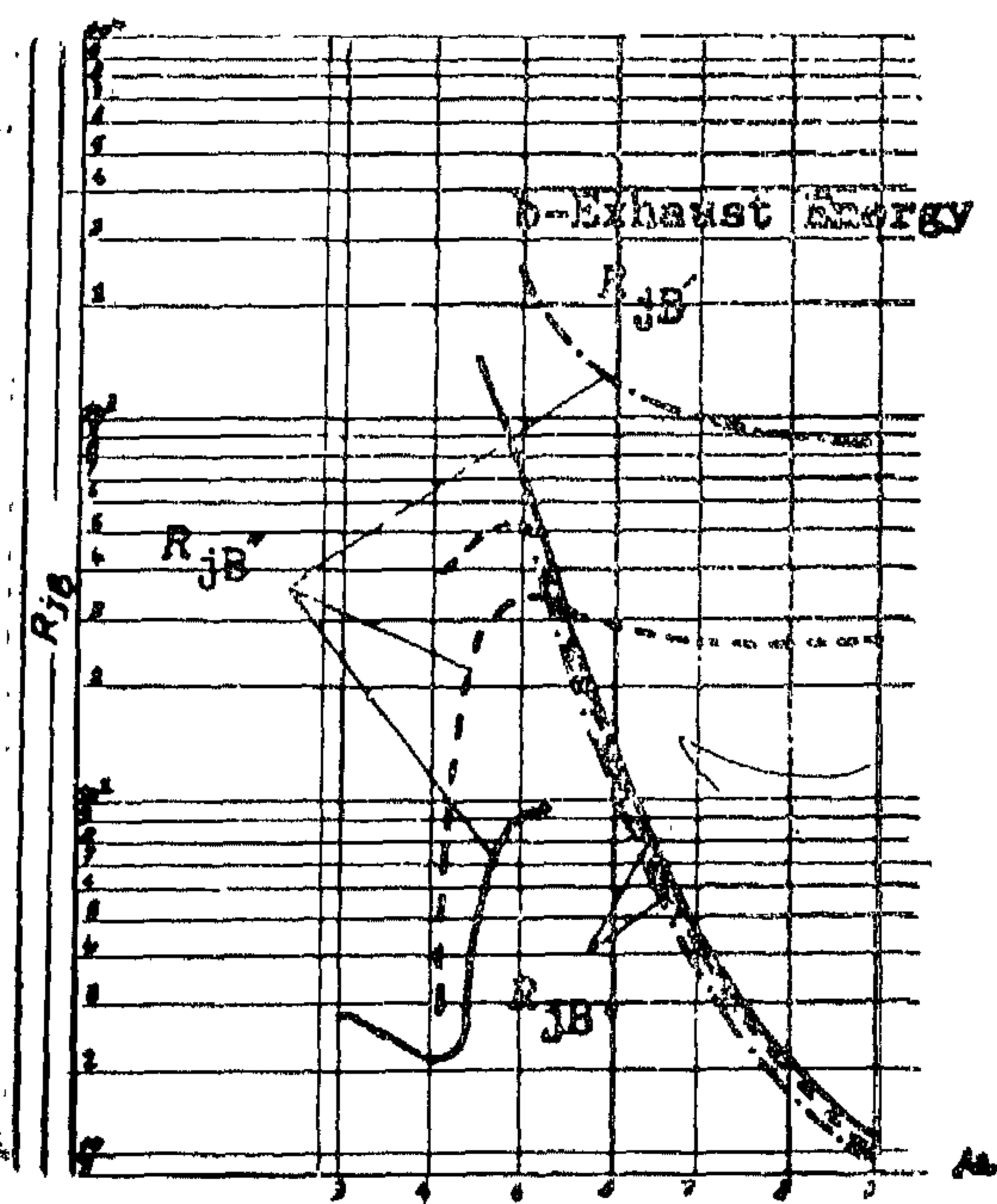


FIG (10) AVERAGE POWER DENSITY FOR SKY BG /11/.







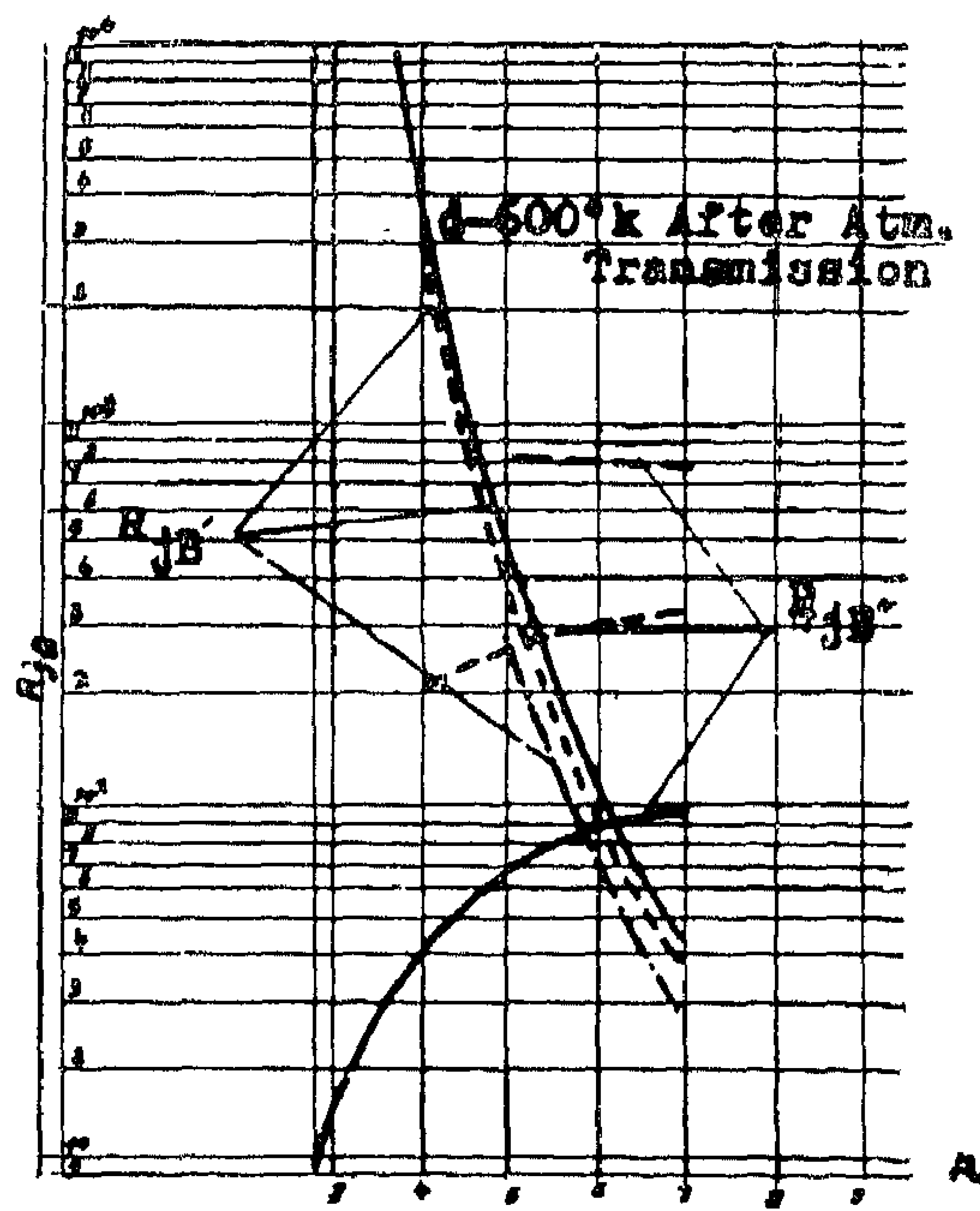


Fig. 6 — EXHAUST BG, 600°K BB — BG REJECTION RATIOS

The main two BG radiation to be rejected are the atmospheric self-emission and the coulds' and dust particles' reflections during the day time (assuming no direct viewing of the sun). The self emission of the atmosphere is possible to take ultimately as a BB at 300°K /17/. The sunreflection spectrum is taken as BB at 5600°K but reduced thousands of time /7/.

Rejection ration for different filters with cut on frequency 2, 2; 3; 4 μ wavelength are shown against BG due to atmospheric self emission and BG due to sun reflections with 600°K. BB and exhaust spectra as targets Fig. (6) from which the proper filter can be chosen (notice the smoothness of the BB target curve and that of exhaust).

(b) Geometrical shielding

The effect of geometrical shielding is reducing the BG radiation received by the detector to that only due to E.C.S. This is achieved by cooling the surroundings. The use of a cone condenser gives a simple and efficient construction Fig. (7) /13/.

(c) Space filteration

Objective of this filteration is to filter the dimensional features of the target against that of BG. In scanning spot pulse duration could be a measure and means of discrimination between target and BG. In reticle, it is a mean of carrier generation and space filteration. The useful signal is affected during this process. The efficiency of modulation in increasing signal to noise ratio is dependent on the space frequency measured in waves / radians Fig. (8).

$$\text{wav / rad} = 1/i \qquad (5\text{—a})$$

Where,

i ... is the angle subtending a black and transparent sector pair at objective center

$$i = \frac{2\,R_w}{m\,f_{ob}} \qquad (5\text{—b})$$

R_w ... distance from reticle axis to image center.

m ... is the number of black and transparent sector pairs.

The image size and distant from reticle center affects directly carrier generation efficiency. On the base of uniform circular radiation image,

IF

$\mathcal{S}$ ... is the image radius

$Z = \mathcal{S}/R_w$

The amplitude of the first harmonic for a given case is

$$C_1 = \mathcal{S}^2\ F\ (Z\ ,\ m) \qquad (6)$$

Calculation shows that :

— *for a very small image*

$C_1 = \mathcal{S}^2$ ... (given by pulse modulation equation)

— for $2\,\mathcal{S} = \pi\, R_w/m$

$C_1 = \pi\,\mathcal{S}^2/4$

The exact shape of the curves for different sector pair by numerical calculation is as shown in Fig. (9) from which an apprixmation for design purposes can be given by

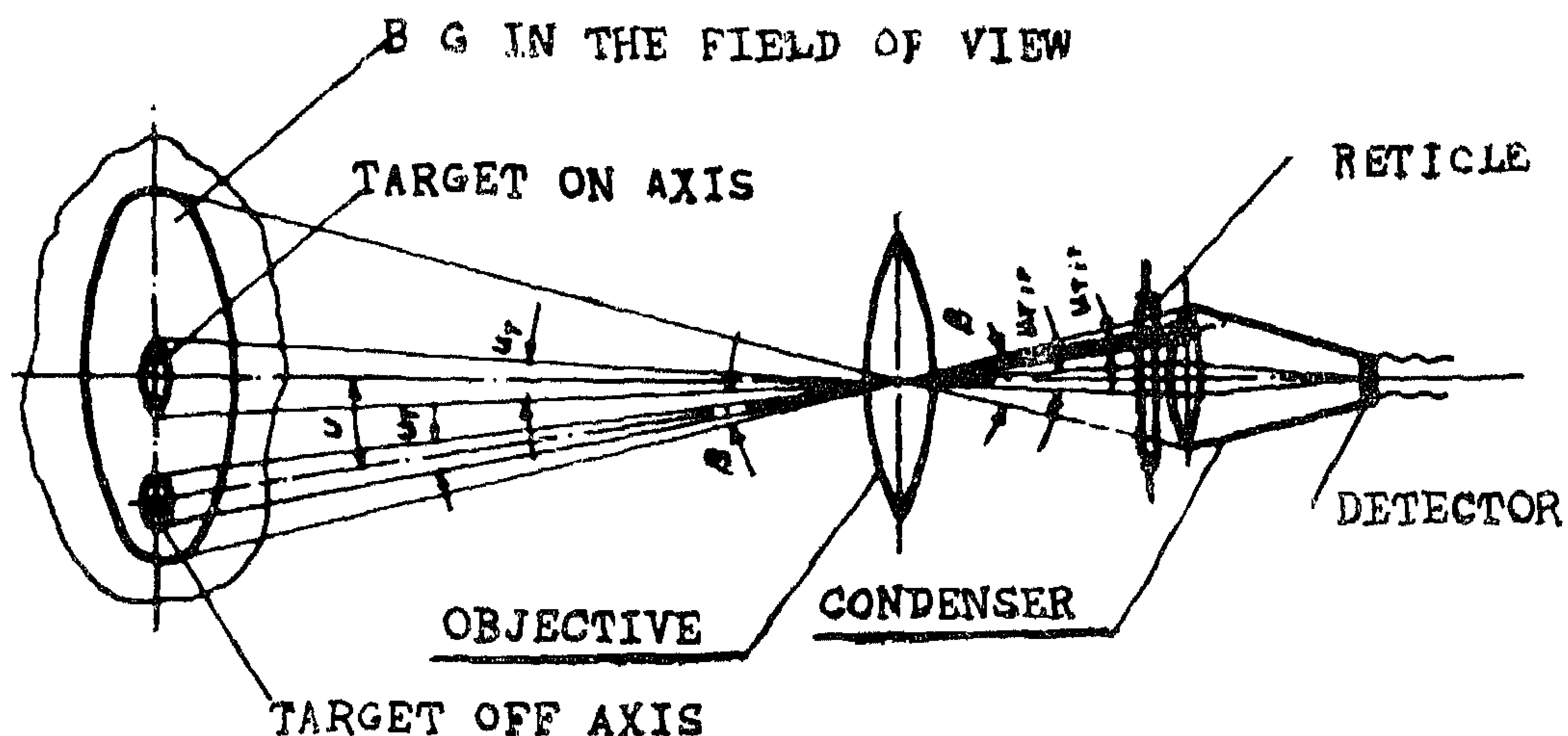
$$C_1/\mathcal{S}^2 = -1{,}92\ \log_{10}\ z\,m + 1{,}067 \qquad (7)$$

From which m/R_w is to be kept constant for a given efficiency or waves/radians.

In practice, after design measurements of BG space filteration is carried out. Fig. (10) shows results carried out in U.S.A. /1/. Optimum design needs a set of these measurements for different seasons, and wavelength pass bands at all hours of the day.

B — Positional Data

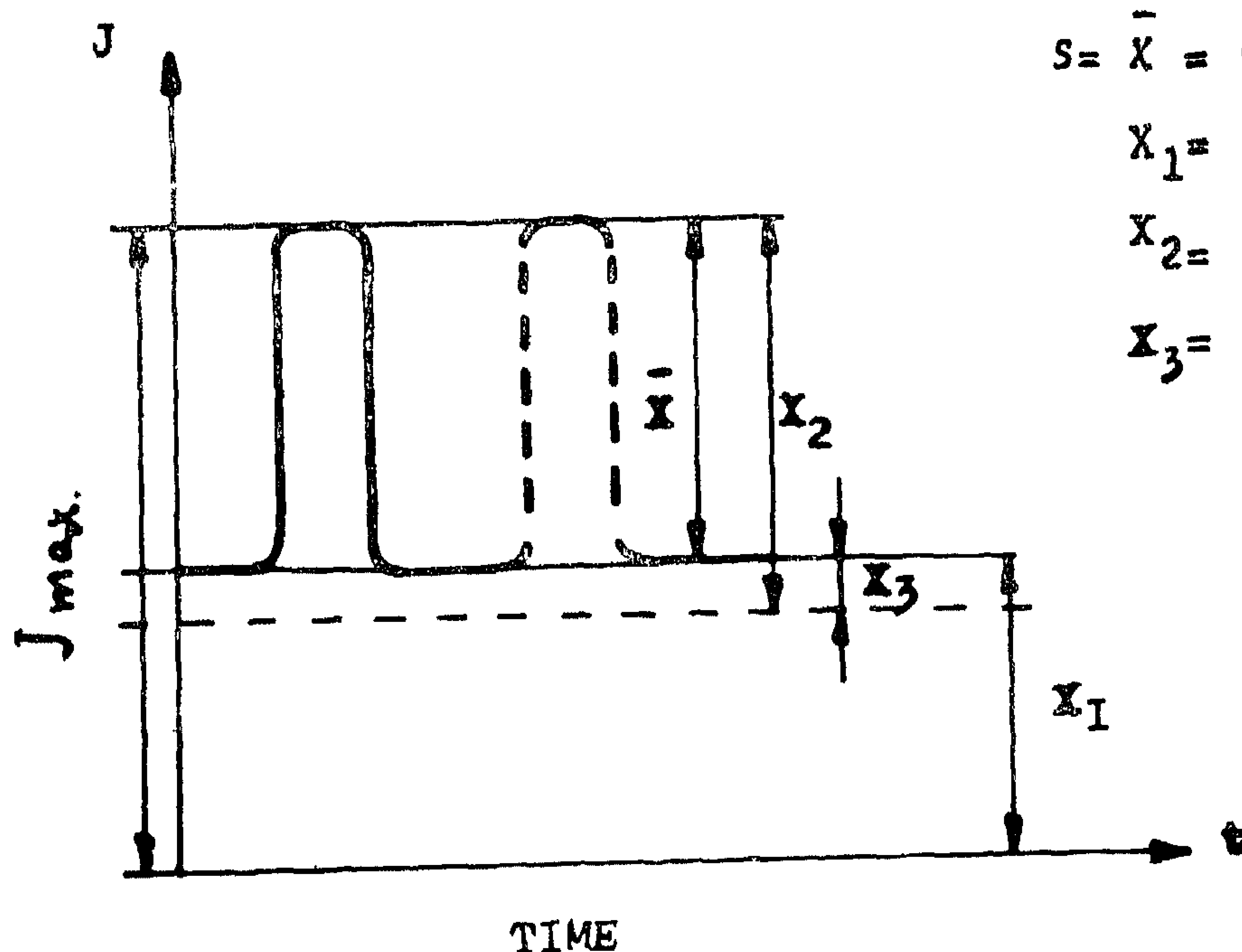
The required two values for search or tracking system are X, Y or R, Θ Fig. (11) in the image plane field of view regardless of target range in tracking system, however the ratio X/Y or Θ suffices for a nonlinear system.



J_{rBG}.... TOTAL BG RADIATION INCIDENT ON DETECTOR CONTINUOUSLY

J_T...... TOTAL TARGET RADIATION REACHING DETECTOR

ΔJ_{rBG} .. BG RADIATION FROM AN AREA SUBTENding the same solid ANGLE AS THE TARGET .



$S = \bar{X} = (J_T - \Delta J_{rB.G})$

$X_1 = J_{rB.G}$

$X_2 = J_T$

$X_3 = \Delta J_{rB.G}$

FIG (5) TARGET SIGNAL IN PRESENCE OF BG

A — BG Discrimation :

As the most important factor is to detect targets at long ranges, it is necessary to make use of contrast between target and BG to increase system response to target signal with respect to that of BG. In this it was made use of difference in size, and in radiation spectral characteristics beside the reduction of BG noise level. The effects of BG will be discussed and the different discrimination techniques explained.

(i) BG Effects

(a) On signal level Fig. (5) :

Signal to be felt on a detector is the difference in radiation levels incident on it in absence and presence of the target (the radiating source) and can be given by,

$$S = \triangle J = \frac{A_T \ A_o}{\pi \ r^2} \int_0^\infty \{ W\lambda_T \tau_a (\lambda) \ \tau_o (\lambda) \ Q (\lambda) - W\lambda_{BG} \ \tau_o (\lambda) \ Q (\lambda) \} \ d\lambda \ \ldots\ldots \quad (1)$$

Where,

$\triangle J$ ... is the signal, i.e., change of radiations incident on detector due to presence of target.

A_o ... objective area.

$Q(\lambda)$ ... relative spectrum radiation responsivity of detector.

$\tau_a(\lambda)$ ... transparency of the atmosphere for a give wavelength.

$\tau_o(\lambda)$ ... transparency of the energy collecting system for a given wavelength.

$W\lambda_{T,BG}$ ... spectral radiance of target and BG.

r ... target distance from IR system.

(b) BG Radiation and noise :

BG radiations fall on detector partly through the energy collecting system ECS and partly directly. These radiations fluctuations are the source of BG noise which is governed by Eistein-Bose relation

$$n^2 = n_{BG} \frac{\exp \ (h_\nu / k \ T_{BG})}{\{ \exp \ (h_\nu / k \ T_{BG}) - 1 \}} \quad \ldots\ldots \quad (2)$$

and to a good approximation

$$n = \sqrt{n_{BG}} \qquad \text{in photon (number)}$$

$$\text{OR} \quad P_n = \sqrt{J_{rBJ}} \qquad \text{in power (watts)} \qquad (3)$$

Where,

n is the mean noise photon number

p_n is the mean noise power

J_{rBG} is the BG power radiation

h Plank's constant

k Boltzman constant

So if the system is in BLIP (Background Limited Infrared Photoconductor) condition the reduction of total radiation is of effect.

(c) False signal from natural radiators

In the field of view are natural radiator which are fortunately of different sizes such as clouds' edges and celestial bodies, other than targets of interest.

(ii) BG Discrimination techniques

(a) Spectral filteration

Spectral filteration decreases noise in BLIP condition but increases signal in all cases. Here in for best filter the physical possible filters are chequed after preliminary analysis for their rejection ratios. A compromise could be made for one pass band for all hours of the day and different seasons or 2 or more filters are to be used and the proper one used for a given BG. condition. The Rejection ratio : is taken as a measure of filter efficiency /12/.

$$R_j = T_T \ / \ T_{BG} \qquad (4)$$

Where,

R_j ... is the rejection ration.

T_T ... is the transmission with respect to target radiation.

B_{BG} ... is the transmission with respect to BG radiation.

from other sources (such as the moon and surrounding bodies). These systems most important classification is according to the simultaneity with which information can be read out /14/. We scan to get a piture in sequential read out (thermograph) /15/ and a picture is directly obtained in a simultaneous read-out (evaporograph).

D — Communication :

Privacy is the chief advantage. It is the normal out come due to narrow beam and lack of side lobes. These systems are free from interference, simple, low in cost and small in size. The region in actual use is 1,8 ÷ 3,5 μ, where Tungesten lamp showed to be a good match with the lead sulphide detector. Radiations are amplitude modulated. Fig. (4) is a scheme of such systems.

E — Range Finding and IR Radar :

It is known that IR passive systems suffer from the basic defect of supplying no range information. It is possible, however to obtain range data by using more than one receiver and the conventional range finding techniques (measurement of the subtended angle at the target between two receivers optical line of sight a known distant apart). Recently the application of radar principles of range measurement seems feasable. Devices have been described which can produce intense accurately defined light pulses of the order of 0,01 ÷ 1 μ sec in length and at variable high rates (multi-spark light, sources). Detectors with very low time constant are also available so that all element for IR radar exists /2/.

F — Hyprid Systems :

Hyprid systems combine 2 or more of the a/m systems such as spectro-radiameter, search-track systems.

II — SEARCH AND TRACK SYSTEMS SPECIFIC PROBLEMS :

The 5 main units in search and track system are :

— Source of radiant energy
— Absorbing medium
— E C S
— Detector
— Data Display

Most interesting are the techniques used for B.G. discrimination and positional data.

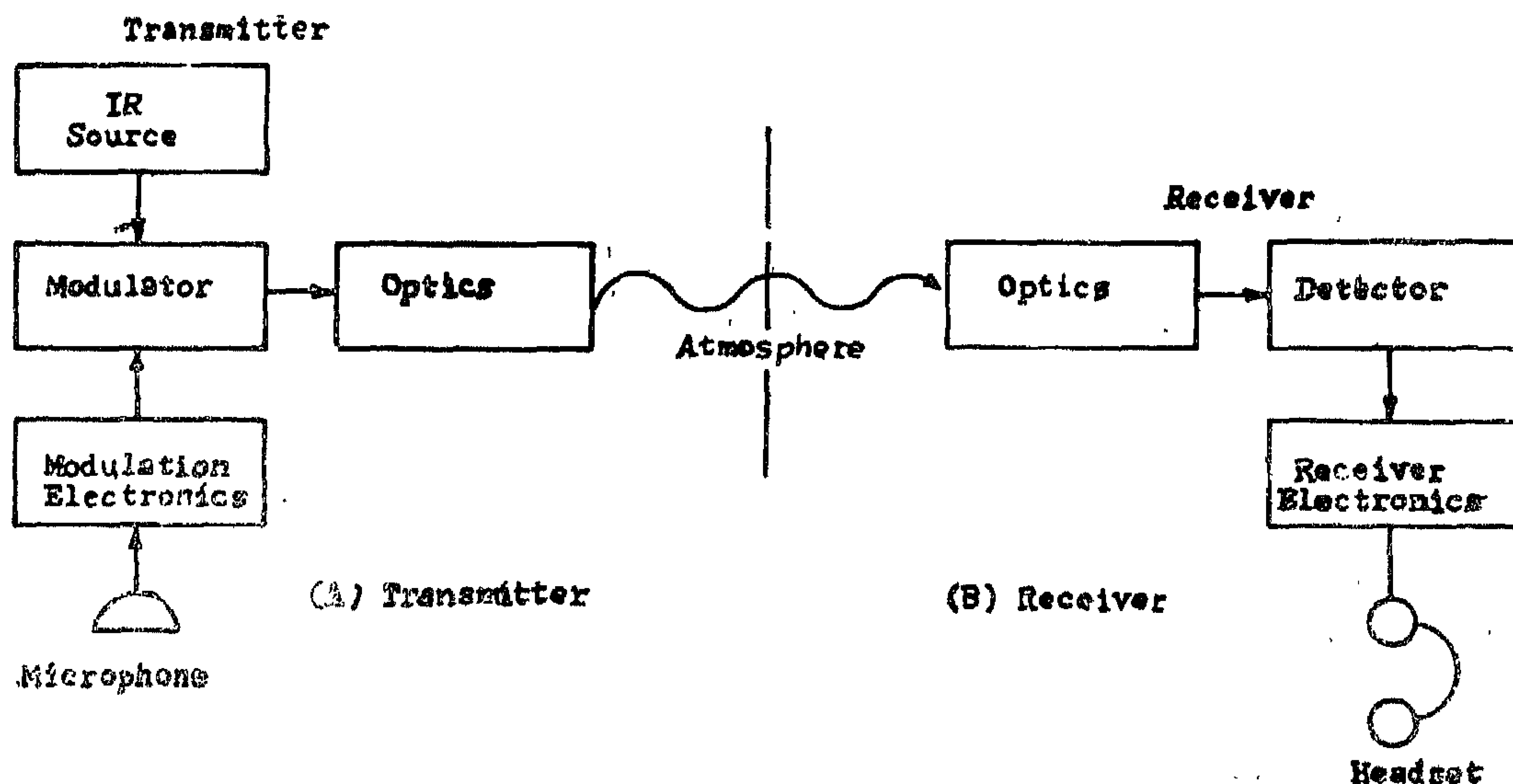


Fig. 4 — IR COMMUNICATION SYSTEM.

radiation or its quality). The new designs include airborne radio—spectrometers for measurement of target and B.G. radiations at different altitudes, time and atmospheric conditions Fig. (1) /9/, Rapid-scan spectrometer for inflight plume analysis is in the developmental stage /3/.

B — Search and Tracking Systems :

The distinction between search and tracking is not sharp. Broadly speaking both have to detect the target and define its position. Tracking systems has to follow accurately and automatically moving targets. The difference is similar to that between search radar and fire control radar. "A tracker is a specialized form of search equipment" /6/. When the system is following a target that carries a beacon to aid its detection, we have a co-operative system Fig. (2). Otherwise we have non-cooperative systems namely active, semi-active and passive /5/.

Detection of object utilizes contrast between object and its background (BG) by proper means of BG discrimination. The contrast could be in the intensity and/or nature of self emission, or the difference in reflectivity for given kind of radiation.

Positional data is obtained in principle by image plane scanning (modulating reticle) or by object plane scanning, mosaic detector /8/, or by means of photo — lateral effect phenomena in detector /10/.

C — Image Forming Systems :

The night viewing devices or image forming systems made possible blackout maneuver and operations..

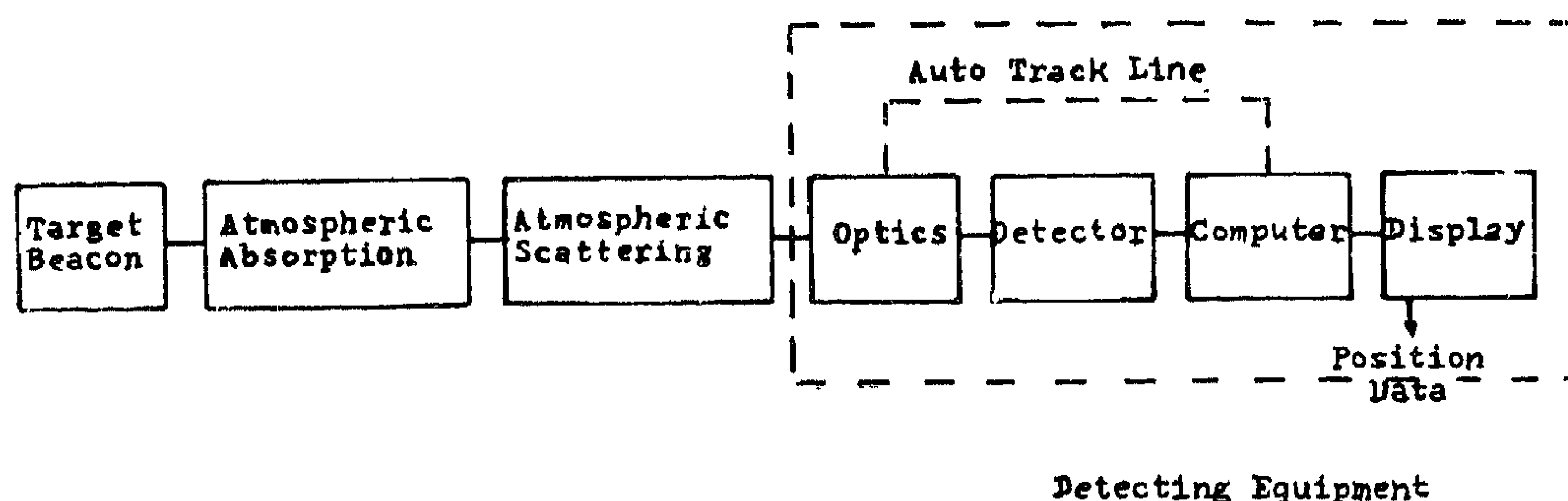


Fig. 2 — CO-OPERATIVE SYSTEM

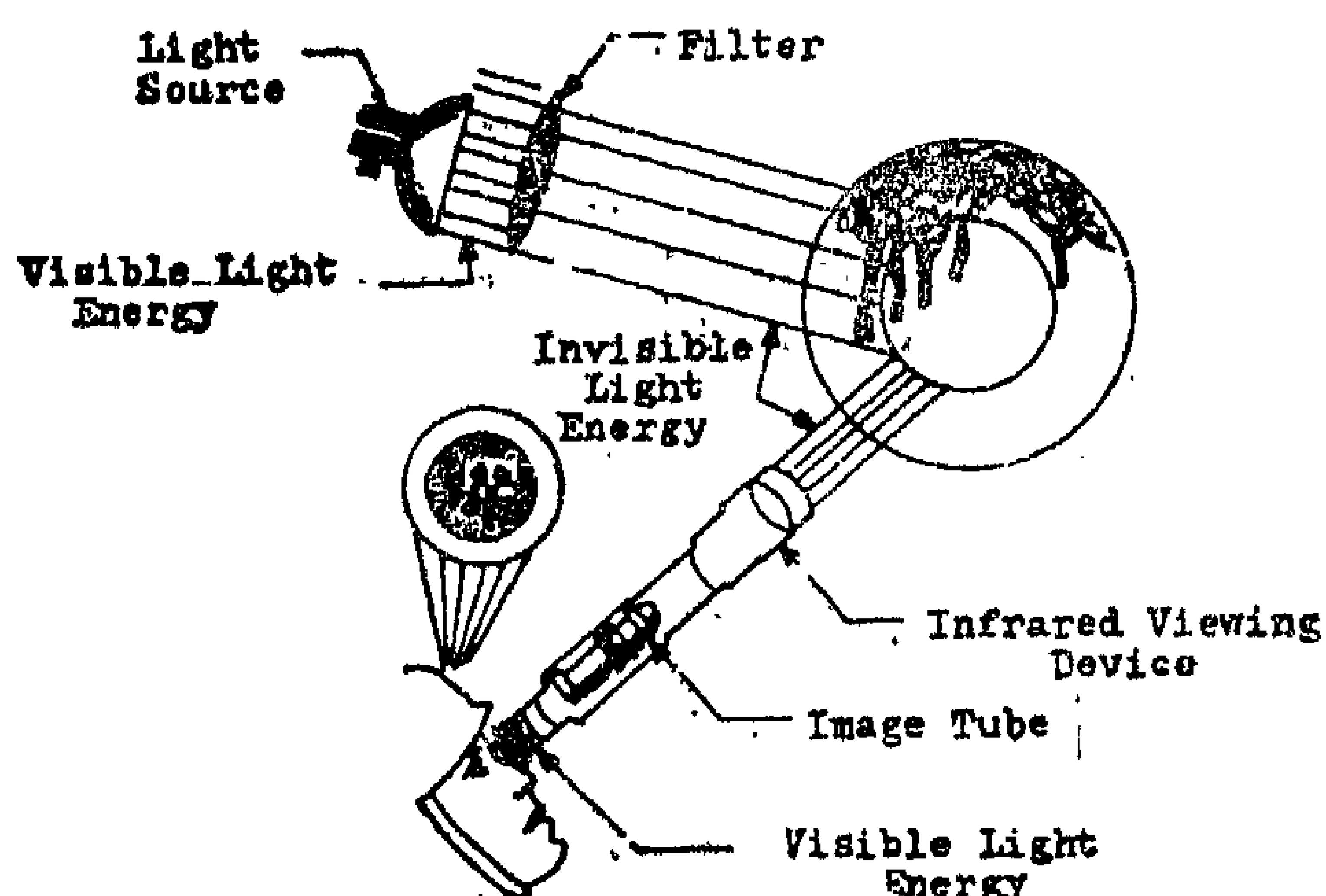


Fig. 3 — OPERATING PRINCIPLES OF NEAR IR VIEWING SYSTEMS.

The spectral region (0,8) ÷ 1,4 μ) are utilized in near IR viewing system. Tungesten or carbon arc are used as flood light with filter to take care of visible light elemination. The image formed on the photo emissive cathod (Cesium — silver oxide) is converteted into electrons refocused (electrostatically and electromagnetically) on a phospher screen giving a visible picture, Fig. (3) /15/. Here as in visible photographic systems contrast is established due to reflectivity differences and differences in the direction of illumination of individual elements (shadow).

Far IR (1,5 to beyound 14 μ) image devices are able to respond to elements self-emission, depending on their emissivitites, temperatures and also reflected radiations

IR SOURCES DETECTING AND TRACKING SYSTEMS

By

Dr. Eng. A.M. HALLOUDA

The infra red technique use is new, yet now basic. These techniques proved their worth in research and industry and are indespensible in military applications. IR image forming systems made possible blackout maneuvers and operations. The serious consideration of these systems in detection and tracking stemmed from 4 facts /11/ :

— Modern targets are better sources of IR radiation than their predecessors and in many cases poorer radar targets.

— Many important targets are encountered at high altitudes where attenuation and absorption of IR energy are minimized.

— The art of IR counter measures is not so advanced.

— IR technology has made significant advances, the greatest of which are the more senstive detectors and very fast energy collecting systems.

The object of this paper, is to give a short account about IR systems from the functional point of view, deal with the basis of detecting and tracking systems in specific, then end by representing samples of existing types.

I — IR SYSTEMS :

The IR systems can be functionally classified to the following categories :

— Radiometers (Rdm.) and Spectrometers
— Search and Track
— Image forming
— Communication
— Range measurement
— Hyprid

A — Radiometers and Spectometers :

These are systems that passively receive energy from relatively stationary objects for measurement purpose (either the quantity of

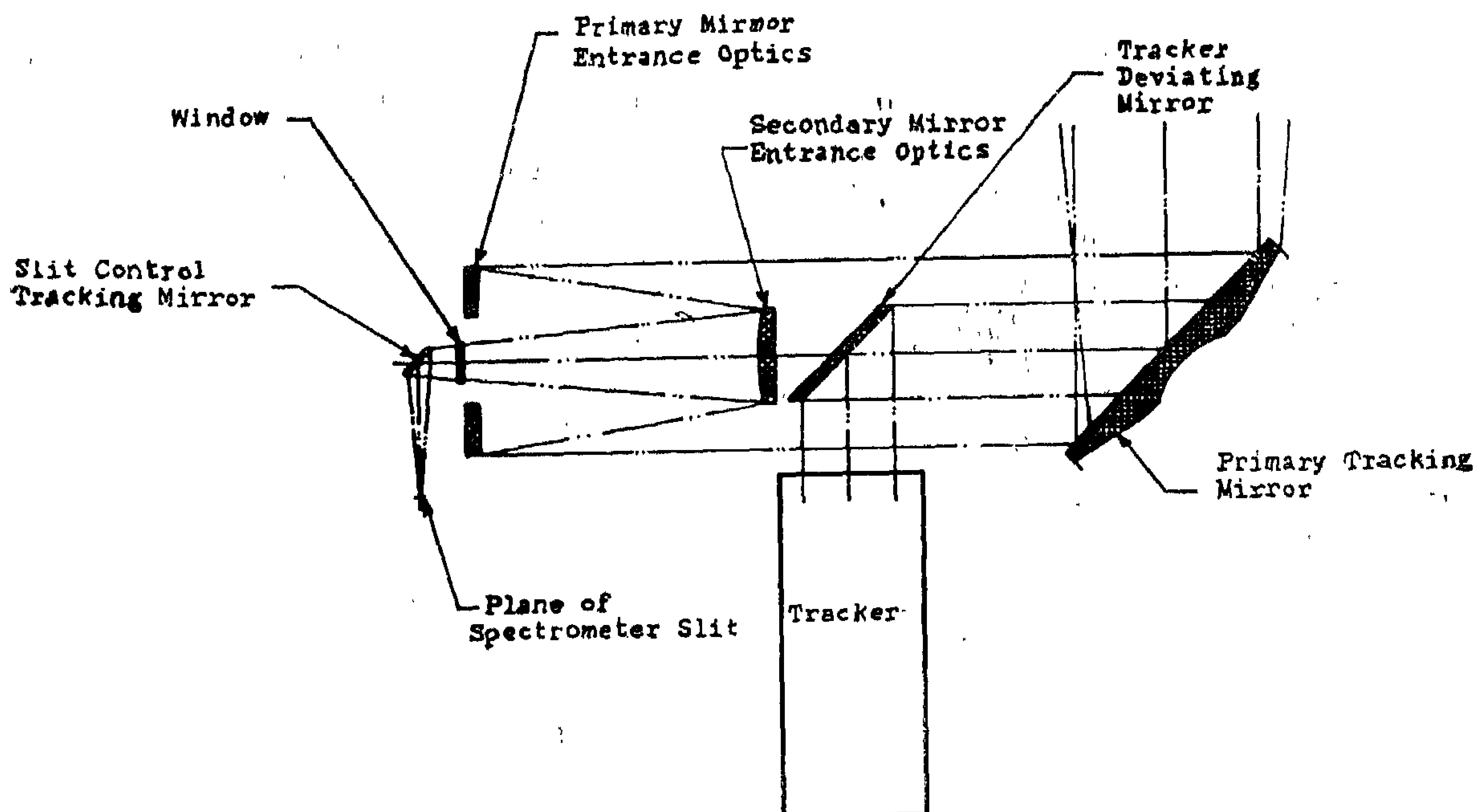


Fig. 1 — ENTRANCE OPTICS OF AIR BORNE SPECTRORADIOMETERS

on clay" show in table to a very small value corresponding to water content of sand equal to zero as shown on the vertical axis of the figure.

2. The angle of shearing resistance Φ does not follow the same path as c.
3. The contactant values of c and Φ decrease with increasing value of the initial placement water content of the sand.
4. There is a definite lack of pattern in the relationships given in figure 7 but there exists a visible trend to a reduction in the contact resistance that continous with increasing water content of sand up to 15% whereby the strength becomes more or less constant if expressed in terms of Φ only since cohesion values are really small at such conditions.

The above test results represent only specific soil conditions, yet they how clearly the necessity of investigation the contact strength of different materials are placed on each other.

If the contact strength is not sufficient to secure the required safety against sliding of the blanket along its underside the design has to be modified according to one of the following suggestions :

a. Replacing the sand at the contact face with a coarser material, preferably gravel or broken stones whose gradation is to be investigated expermentally.
b. Placing the blanket on the upstream slope if climatic conditions favour this approach. In the Mission Dam, (Terzaghi 1964) a plastic membrane is used to cover the blanket placed on upstream face.
c. By adopting a zigzag shape for the blanket. e.g. the High Dam, Aswan. By this means the blanket shall be properly keyed in the surrounding material of the upstream side of the dam. The probable surface of sliding in this case is not a plane but most conveniently a curved surface cutting intermittently parts of the zigzag and avoiding contact surfaces.

BIBLIOGRAPHY

Bishop A.W. 1952 : "Stability of Earth Dams" Ph.D. Thesis, University of London.

E.U.R. 1961 : "The Mission Dam".

Hafiz 1951 : "Shear strength of sands" Ph.D. Thesis University of London.

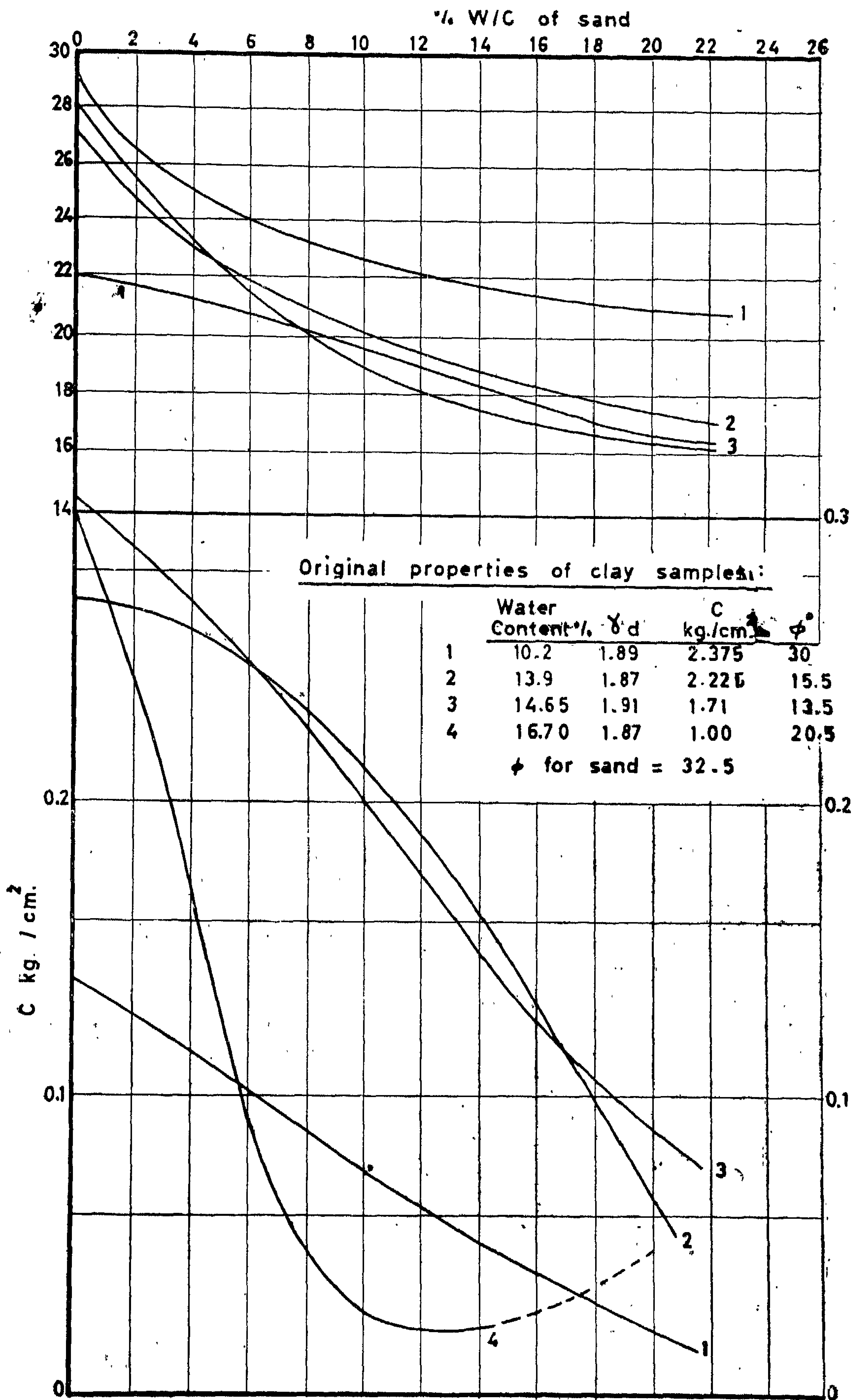
Knappen 1945 : Referred torn Davies : Hand book of Applied Hydraulics : John wiley and sons.

Leonards, G.A. 1963 : "Foundation Engineering" McGraw-Hill.

Skempton A.W. 1954 : "The Pore Pressure coefficient, A and B" : Geotechnique, March 1954.

Terzagh, K and Leroux ; "The Mission Dam" Geotechnique, March 1964.





% W/C of sand
0 2 4 6 8 10 12 14 16 18 20 22 24 26
30 28 26 24 22 20 18 16 14
ϕ
0.3
0.2
0.1
0
C kg. / cm.²
1
2
3
3
2
1
4
Original properties of clay samples :
Water Content % γ d C kg./cm.² ϕ°
1 10.2 1.89 2.375 30
2 13.9 1.87 2.225 15.5
3 14.65 1.91 1.71 13.5
4 16.70 1.87 1.00 20.5
ϕ for sand = 32.5

$(\sigma_1 - \sigma_3)$

$(\sigma_1 - \sigma_3)_f$

$(\sigma_1 - \sigma_3)_{f.b.}$

axial strain

$+\Delta u$

$B.\Delta\sigma_3$

$(\Delta u)_{f.b.}$

$(\Delta u)_f$

axial strain

$-\Delta u$

Fig. 5

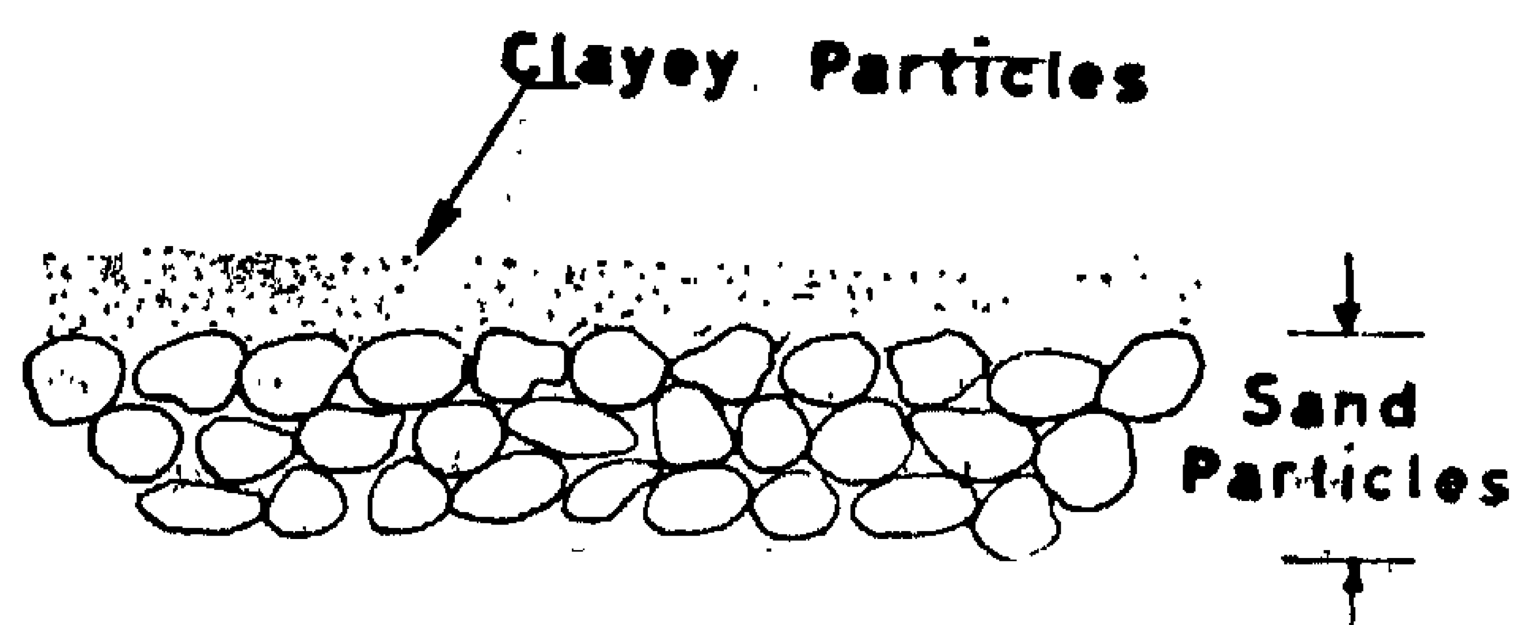


Fig. 6

with respect to its available strength τ_f i.e. only a fraction of τ_f is operating. The point is this : whether to consider in determing τ_f according to equation (6) the value of $(\triangle u)_f$ or $(\triangle u)_{fb}$. In other words to use for A the value at failure or the value corresponding to the required factor of safety implied in the design. In the writers opinion, one should not use A at failure since it is lower than A at a lower stress condition. The lower value of A is seen to overestimate the value of the available strength τ_f with a corresponding increase in the value of the factor of safety F_b. To obtain the proper value of A it becomes necessary to make few trials. A trial value is chosen according to a conveniently chosen factor of safety F_{b1}. This trial value is applied in equation (6) and the corresponding value of the factor of safety according to equation (1) is determined which ought to be equala to F_{b1}. If not another trial is made and so on.

B. Failure due to Strength Deficiency at contact Face between Blanket and underying soil.

When two different soil materials come into contact, the shearing resistance along the contact surface is essentially different from the strength of either materials. Experimental evidence illustrating the range of the contact strength is rather scanty and is mainly devoted to retaining wall, friction piles or caissoms problems. Hafiz (1951) showed that the contact strength between gravel and rock corresponded to an angle $\Phi' = 22°$, i.e. 14° smaller than the angle of internal friction of the gravel in its loosest state. The "Block" stability analysis for embankets. containing sands or gravels on rock should be carried out in terms of this reduced value of Φ at contact faces with rock.

Clayey blankets resting on sand layers, will, when touch storage water, exhibit a reduced strength at contact face with sand. The mechanics of this reduction are different from those of sands and gravels resting on rock. In this case the material of the embankment which is dumped in lumps and compacted (even if lumps are very small) will arch on the projecting surface of the sand particles. A large number of clay particles at contact plane will thus be acted upon by a small overburden pressure. The number of clay particles involved in this operation depends on the stastistical average of the projections of the sand particles at contact surface and is therefore governed by the gradation characteristics of the sand. When water rises to contact face the clay particles will soften due to :

1) Lack of overburden pressure.
2) softening caused by swelling effects of compacted material at locations with low overburen pressures a case that is particulary noticable for silty materials, and a soft film will be produced which will reduce the strength at contact face considerably.

The senior author while working with the High Dam othority at Aswan was able to study contact strength characteristics between dune sand and compacted Aswan clay in connection with the design of the blanket of the dam. Original design stipulated a horizontal blanket made of compacted Nile silt. Earlier design versions suggested a horizontal "clay concrete" blanket where stones are to be bedded in the silty material of the Nile alluvium by means of vibrators. This procedure was debated and ultimately both designs were abondened. Finally the Nile silt was replaced by Aswan claye; a silty deposit belonging to upper cretaceous age and is quarried from the Nubiam sandstone formations (liquid limit 34, plastic limit 20, shrinkage, limit 18).

Consolidated Quick shear box tests were performed in a circular shear box at the contact face between the compacted aswan clay and the dune sand. Both sand and clay were placed at different placement conditions (water content and density). The results are summarised in Fig. 6. The contact strength is conveniently expressed in terms of c and Φ too. From this figure and its accompanying table we note :

1. The "apparent cohesion" c drops steeply from a high value corresponding to "clay

Fig. 3

Fig. 4

The above values of principal stress increments are to be reduced by $\triangle u$, the pore water pressure, to obtain the corresponding effective stresses.

$$\triangle u = B \triangle \sigma_3 + A (\triangle \sigma_1 - \triangle \sigma_3) \quad (3)$$

Where A and B are the pore pressure coefficients (Skempton 1954) and are determined from undrained traxial shear tests with pore pressure measurements. For saturated or nearly saturated soils the upper limit for A and B is unity except for very loose fine sands and extra sensitive clays. (Leonards (1963).

The coefficient A depends primarily on the volumetric strains during undrained shear and secondly on the degree of saturation, while the coefficient B is can entire function of the degree of saturation being equal to unity for fully saturated soils. The results of undrained triaxial shear tests when expressed in terms of effective stresses will furnish values of c' and Φ'. The conditions of this test correspond approxmotely to actual conditions of the dam. At failure, the value of τ in Fig. 3 shall be replaced by τ_f as in (Fig. 4) whereby the (c' , Φ') straight envelope shall touch the corresponding mohr's circle platted for effective stresses.

from equations (2) and (3) and putting τ_f instead of τ :

$$\triangle u = B P_o + \frac{B K P_o}{2} + (2 A\text{-}B) \sqrt{P_o^2 \left(\frac{1-K}{2}\right)^2 + \tau_f^2} \quad (4)$$

from (Fig. 4) :

$$\tau_f = (K P_o - \triangle u + c' \cot \Phi') \tan \Phi'$$

or $\triangle u = K P_o + c' \cot \Phi' - \tau_f \cot \Phi' \quad (5)$

from (4) and (5) :

$$\tau_f \cot \Phi' = P_o \left(\frac{2K-B (2-K)}{2}\right) + c' \cot \Phi' - (2 A-B \sqrt{P_o^2 \left(\frac{1-K}{2}\right) + \tau_f^2} \quad (6)$$

equation (6) gives the value of the available shear strength τ_f along the horizontal plane of probable failure through the blanket which may be taken at its mid thickness. This developed value of τ_f is to be compared with the value of τ along the length L of the blacket as already described (item IV).

For simple homogeneous sections an average valaue of τ_f may be obtained for P_o determined at the centre of the length L. For non homogenious sections (with berams or varying slopes and materials) the length L may be subdivided into a convenient number of slices and for each slice τ_f is determined and an average (arithmetic) value can be readily obtained that will sufficiently represent the strength conditions along length L.

For an analysis of the case of steady seepage the coefficient B is to be taken as the ratio of the pore water pressure obtained from the seepage flow net to the total vertical weight at any point on the potential sliding surface.

Variation in the coefficient A during shear :

In the case of soils where the pore water pressure and hence the coefficient A does not change sharply during shear, the value of this coefficient can be taken as that corresponding to failure and the factor of safety f_b is obtained according to equation

(1). Failure may be taken as according to one of the following criteria :

(1) at peak ($\sigma_1 - \sigma_3$)

(2) at resedual ($\sigma_1 - \sigma_3$)

(3) at maximum prencipal stress ratio.

Dilatent soils show sharp variations in the value of A during shear as in (Fig. 5). In this figure we note that while the pore water pressure at failure (peak for example) is equal to $(\triangle u)_f$, its value at a certain fraction of the peak strength $(\triangle u)_{fb}$ which is higher than $(\triangle u)_f$. In the design, the soil of the blanket is subjected to a state of stress corresponding to a certain margin of safety

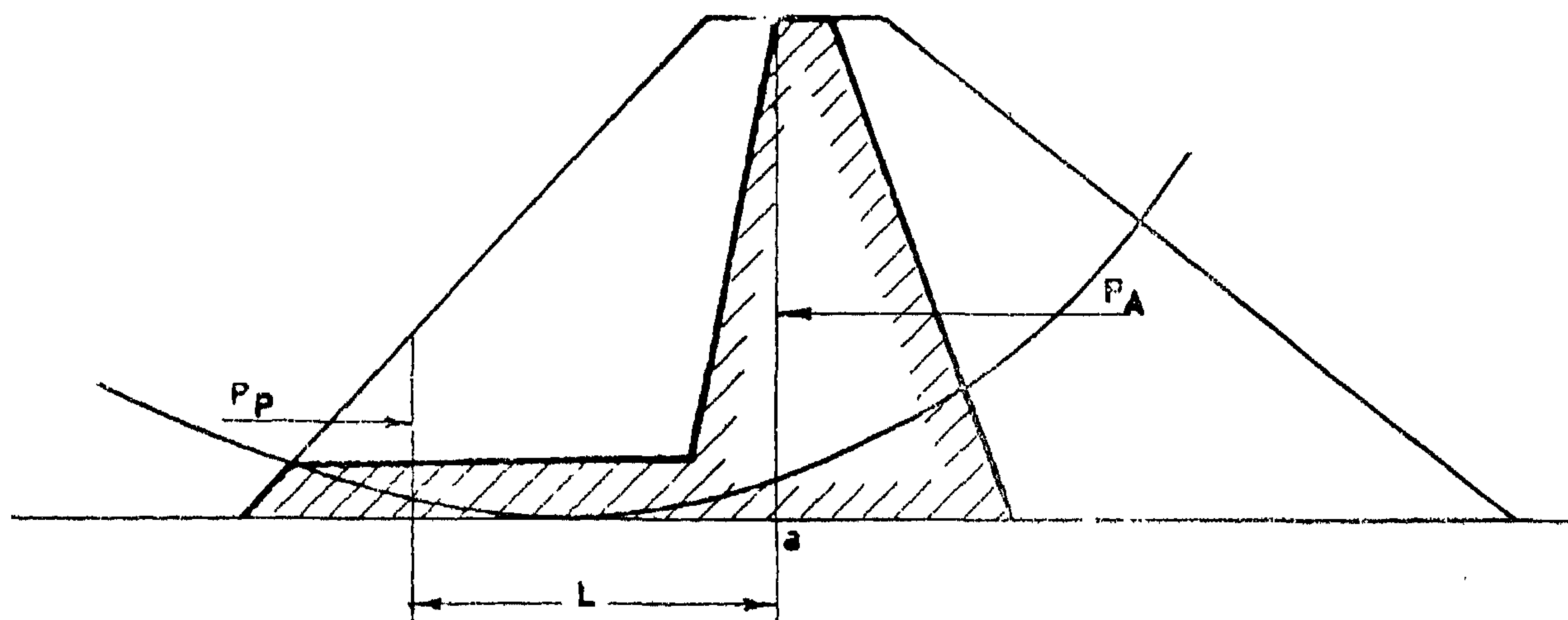


Fig. 2

V. Effect of Soil Properties :

Usually the blanket is formed of a compacted material. If this material is clayey and if the construction schedule allows storage before completion of the dam, water will touch the blanket and its material may approach full saturation whereby the analysis after construction can satisfactorily be made by considering the available strength τ_f as equal to one half the unconfined strength. Consolidation due to progressive increase in the weight of overlying fill will be considered in evaluating τ_f. Such consolidation may be partial or relatively complete according to construction rate.

If water does not contact blanket, it will still be a partly saturated material just after construction whose strength is to be determined in terms of the apparent shear strength parameters (c and Φ). The available shear strength τ_f along the length L (Fig. 2) is to be calculated by considering the weight of soil above blanket level. Thus the analysis has to be more appropriately carried out in terms of effective stresses.

VI. Mode of Failure :

The stability of a horizontal blanket based on plane horizontal surface of sliding necessitates that the location of this surface must be defined. If the blanket is of sufficient thickness probable failure may occur within its body unless the contact shear strength between its material and supporting soil is lower than that of the blanket proper. In the latter case, the probable failure surface will be located at bottom of blanket.

A. Failure surface within the blanket :

The total vertical stress increment acting on an element of the blanket is essentially equal to the weight of the material above it after completion and is equal to P_o. The corresponding horizontal stress is K P_o where K is the coefficient of earth pressure at rest while the corresponding shear stress component is τ. Assuming plane strain conditions, the geometry of the Mohrs diagram in (Fig. 3) gives for the total principal stress increments :

$$\begin{matrix}\Delta\sigma_1\\ \Delta\sigma_3\end{matrix} = P_o + \frac{K P_o}{2} \pm \sqrt{P_o^2 \left(\frac{1-K}{2}\right)^2 + \tau^2} \qquad (2)$$

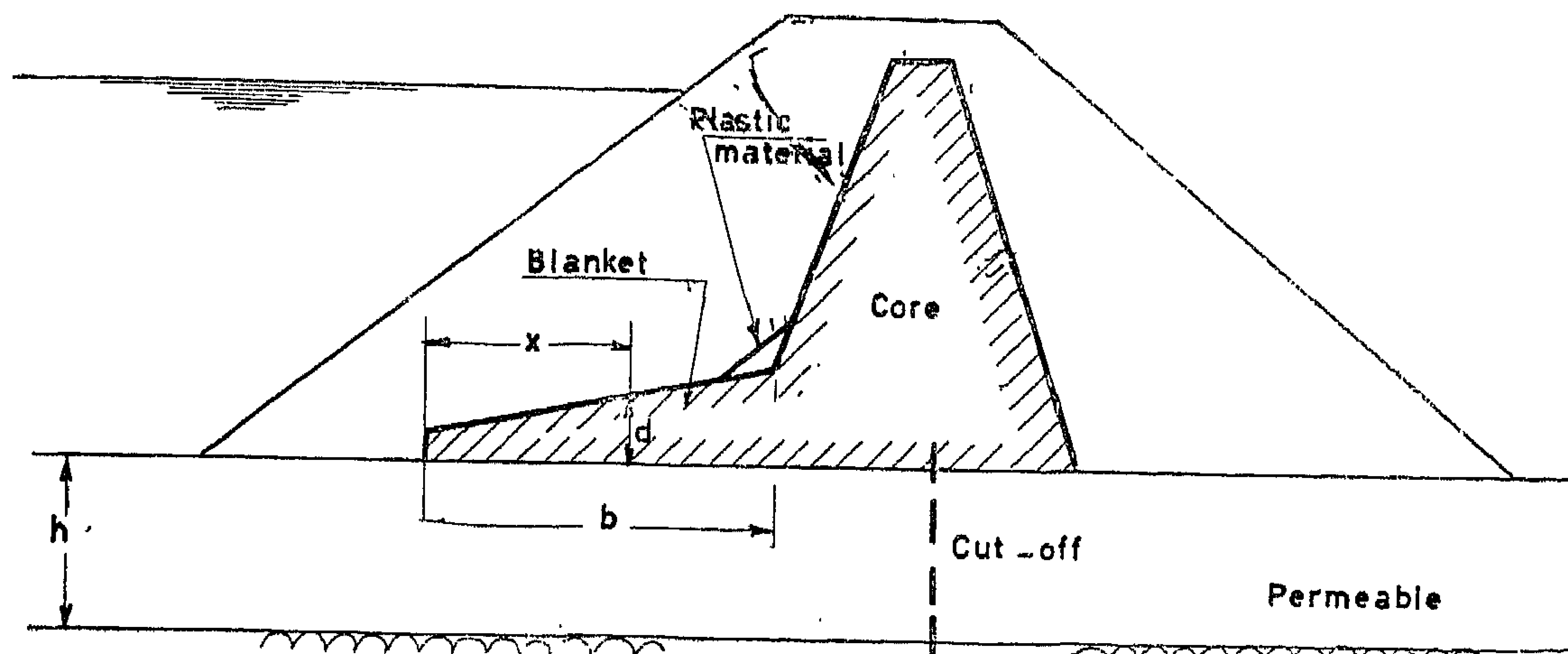


Fig. 1

III. Joint between Blanket and Core :

If the material supporting the blanket and the core is compressible, the joint between core and blanket should be provided with a more plastic material to safeguard against effects of differential moments which tend to produce separation at the joint. Usually, one uses the same material of blanket and core but placed at a higher water content. (Fig. 1). e.g. the High Dam Aswan.

IV. Method of Analysis :

A. Generally the blanket is relatively thin and its material is weaker than the soils alone and below it. Under this condition simple shear in a horizontal direction (along blanket) will govern the state of stress within the blanket. Limiting equilibrium will be reached when the available shear strength τ_f of the blanket material is just sufficient to balance the difference between the active and passive pressures (P_A — P_P) along a certain length L (Fig. 2), where L is the length of the blanket at the end of which P_P is determined. Its value is determined by trial to give the maximum value of $\tau = \frac{P_A - P_P}{L}$ τ is the existing shearing resistance of the soil and the corresponding factor of safety is F_b ; $F_b = \frac{\tau_f}{\tau}$ (1)

Generally the active pressure P_A is calculated on the vertical line a — a of the core according to the relevant soil data of the core material. For thin cores such as puddle clay cores or reinforced concrete cores of sufficient flexibility, P_A is calculated from the data of the soil material forming the shoulders. (Fig. 2).

B. Where the blanket material is not as week as in A, a circular arc analysis (base failure) will provide a more rigorous solution. However, if the plane failure surface is adopted here, the difference in the obtained factor of safty will not be too large and does not warrant the elaborate circular arc analysis for cases of horizontal blankets.

In all cases the analysis is made for the cases of loading corresponding to "end of construction" i.e. before operation and for the cases of "steady seepage" or operation condition.

A STUDY ON THE DESIGN OF IMPERVIOUS BLANKETS IN EARTHEN DAMS WITH PARTICULAR REFERENCE TO THE HIGH DAM AT ASWAN

By

Dr. A.H. EL-RAMLI, D.I.C., M.Sc., Ph.D.
Professor of Soil Mechanics, Cairo University.

and

Dr HASSAN ABDOUN M.Sc., Ph.D.
Lecture of Soil Mechanics, Cairo University.

The seepage characteristics of earth and rockfill dams, the character of the foundation soil and the permeability of available soil materials make it necessary under certain conditions to incorporate an impervious blanket into the upstream body of the dam. This will act as an anti-filtration element safeguarding principally against excessive seepage forces in the downstream side for dams built on pervious foundations and will also help reducing seepage losses.

The overall stability of the dam and its supporting soil may not depend on the strength of the blanket. However, since the blanket is essentially constructed of a relatively plastic material, the "local" stability of the part of the dam over-lying it, should also be studied. Blankets placed directly on the upstream face of the dam will affect the overall stability of the dam in the case of rapid draw-downs of the reservoir water e.g. The Mission Dam (E.N.R. 1961 "Geotechnique March 1964").

In this paper the case of horizontal blankets is considered. An expression for the available strength of the blanket materials in terms of existing state of stress is developed. The contact strength between the blanket and the supporting soil material is found to have a great role, under certain circumstances, in the stability of upstream face and may lead to readjustments in the design.

I. Thickness of Blanket :

The thickness of the blanket d at any distance x (Fig. 1) is given by :

$$d = \frac{Kb}{Ks} \cdot \frac{b}{h} \cdot x \text{ (knappen 1945)}$$

where Kb = coefficient of permeability of blanket

Ks = coefficient of permeability of underlying soil (average permeability in case of stratification).

b = length of blanket.

h = thickness of permeable layers below blanket and for a constant thickness, practically :

$$d = 0.6 + \frac{b}{100} \text{ in meters.}$$

II. Length of blanket

The length of the blanket is determind according to the filtration characteristies, of the cross section of the dam and its foundation. Generally an analysis is made by means of a flow not diagram and the length of blanket for a particular thickness is determined which will give the required margin of safety against seepage forces in the downstream exist of the dam.

APPENDIX II. — NOTATION

The following symbols are used in this paper:

A_i , B_i = Fourier cosine coefficients ;

a , b , c = depth, length and width of the tank, respectively ;

C_m = Fourier sine coefficients ;

D = flectural rigidity of the slab ;

E = Young s modulus ;

E_m, F_n, K_n = undetermined constants ;

h_1 = thickness of the longitudinal walls ;

h_2 = thickness of the transverse walls ;

h_f = floor thickness ;

M_x , M_y = bending moments per unit length perpendicular to the x and y axes, respectively ;

q_o = maximum intensity of hypdrostatic pressure = γ a .

q = intensity of uniformly distributed loading acting on the floor ;

w = plate deflection

W = resultant deflection

x_1 , y_1 = Cartesian coorrdinates of the longitudinal wall ;

x_2 , y_2 = Cartesian coorrdinates of the transverse wall ;

x_3 , y_3 = Cartesian coorrdinates of the floor ;

γ = unit weight of liquid ;

$\alpha_m = m \pi b / 2a$;

$\beta_i = i \pi a / 2b$;

$\gamma_m = m \pi c / 2a$;

μ = Poisson's ratio ;

$\delta_i = i \pi c / 2b$;

$\Theta_i = i \pi a / 2c$; and

$\Phi_i = i \pi b / 2c$.



CONCLUSIONS

An analytical procedure has been presented for determining bending moments in rectangular concrete tanks with constant wall thickness. The structural behaviour is based on considering the tank as composed of five slabs simply supported at the top edges and continuous along its vertical and bottom sides.

The analysis is provided according to the elastic theory of rectangular plates and the solution is obtained in the form of rapidly converging trigonometric series. Eqs. 46, 47 and 48 establish the basic relationships. They represent a set of simultaneous equations. In the numerical solution, four terms of each series are generally sufficient to give accurate results. All the redundant constants E_m, F_n and K_n and their coefficients converge very rapidly. Accordingly, in the case of a tank rectangular in plan, it is required to solve twelve simultaneous equations deduced from Eqs. 46, 47 and 48. However, when the tank is square in plan, the number of equations is reduced to eight because of symmetry. The solution of these eight equations is obtained by the method of successive approximations. It is noticed that accurate values are obtained from the second approximation. For illustration, the analysis is applied to an example of a cubic tank considering $\mu = 0.16$ for reinforced concrete.

If a digital computer is used, the computations will be greatly facilitated. In this case, design data can be prepared in the form of tables having moment coefficients for the design of rectangular concrete tanks.

APPENDIX I. — REFERENCES

1. Davies, J.D., "Bending Moments in Edge Supported Square Concrete Tanks, "The Structural Engineer, Vol. 40, May, 1962, p. 161.
2. El-kateb, Mohamed H., "Stress Distribution in Rectangular Concrete Tanks, M. Sc. thesis, Cairo Univ., Giza, Egypt, U.A.R., 1958.
3. Flatt, and Perks, "The Design of Reinforced Concrete Reservoirs and Tanks to Comply with the I.C.E. Code of Practice," Water and Water Engineering, November, 1952.
4. Ghali, Amin, "The Structural Analysis of Circular and Rectangular Concrete Tanks," Ph.D. thesis, Univ. of Leeds, 1957.
5. Gray, W.S., and Manning, G.P., "Reinforced Concrete Reservoirs and Tanks," Concrete Publications Limited, London, England, 1960.
6. Lightfoot, E., and Ghali, A., "The Analysis of Rectangular Concrete Tanks," Proceedings, 50th Anniversary Conference, Institution of Structural Engineers, London, England, 1958, p. 196.
7. "Mathematical Tables," British Association for the Advancement of Science Cambridge University Press, 3rd Edition, Vol. 1, England, 1951.
8. "Rectangular Concrete Tanks," Bulletin S.T. 63, Structural Bureau, Portland Cement Association, Chicago, 1947.
9. Timoshenko, S., and Woinowski-krieger, S., "Theory of Plates and Shells," McGraw-Hill Book Co., Inc. New York, N.Y., 1959.
10. Young, Dana, "Bending Moments in the Walls of Rectangular Tanks," Proceedings, ASCE, Vol. 67, Nov. 1941, pp. 1683-1696.

Table 1. — Moment coefficients for a cubic tank

x (—) b	z (—)	y = 0 M_x	y = 0 M_y	y = b/2 M_y	
1/2	1/4	0.00542	0.00769	—0.01712	$q_o\ b^2$
1/2	1/2	0.01034	0.01108	—0.02780	
1/2	3/4	0.00569	0.00575	—0.01676	
1/2	1	—0.04266	0	0	
0	1	0.02381	0.02381	—0.04266	$q_o\ b^2$
1/4	1	0.01329	0.01466	—0.02871	
1/2	1	—0.04266	0	0	

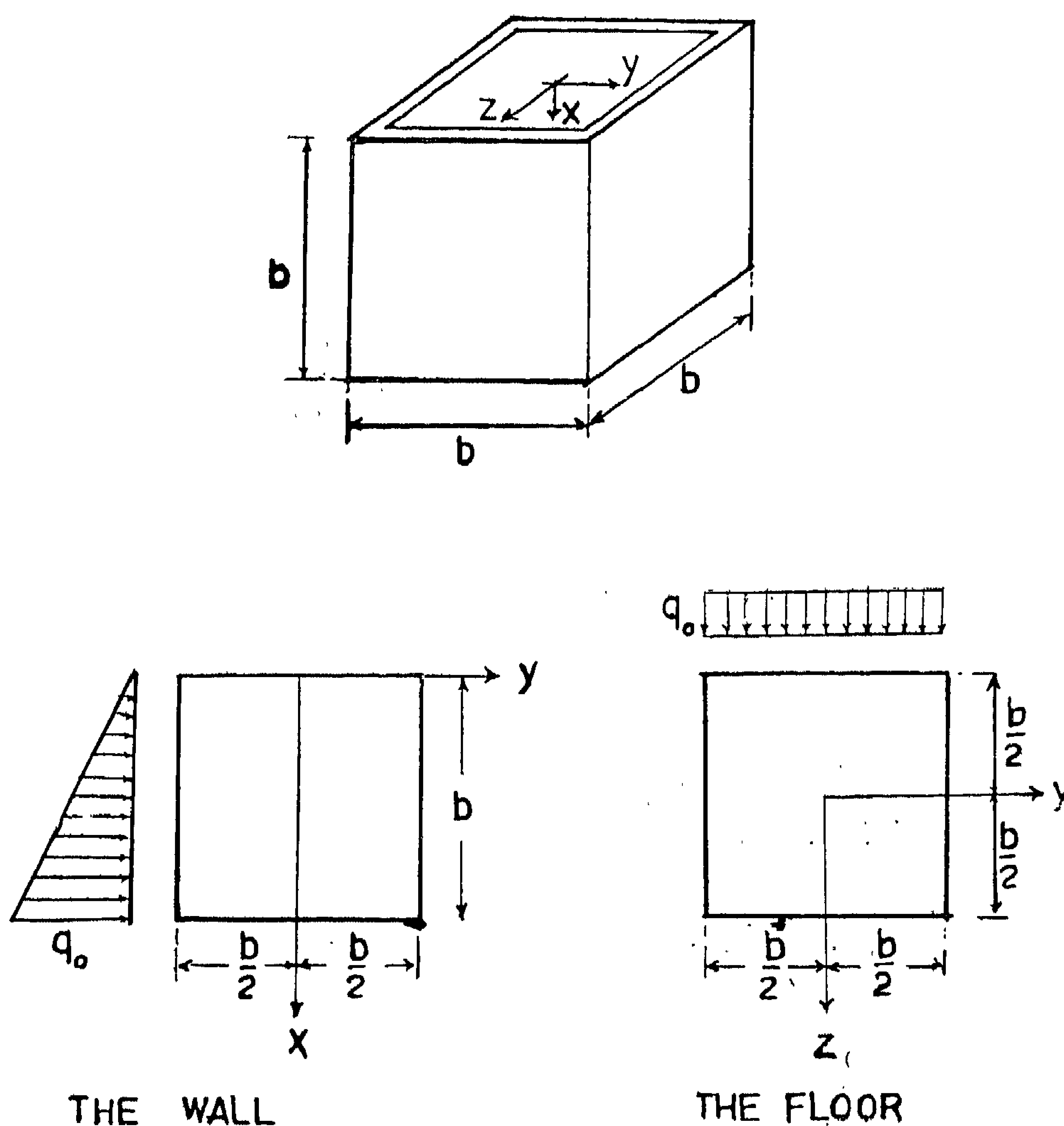


Fig. 6. — Cubic-shaped tank subjected to hydrostatic pressure

EXAMPLE

To illustrate the method developed above, a cubic tank is considered. Since the tank is square in plan, the distribution of the redundant bending moments along any side of the floor is the same. It follows that $F_n = K_n$. The following parameters are used : $a = b = c$; $h_1 = h_2$; $(D_1/D_f) = (D_2/D_f) = 0.5$; $q_o = q$; $\mu = 6.16$; and $\pi = 3.14157$. The first four terms in each series are considered for sufficient accuracy as it converges very rapidly.

By substituting the above values into Eqs. 46, 47 and 48, using tables of hyperbolic functions (7), one obtains the following set of simultaneous equations :

$$
\begin{aligned}
E_1 &= +\,1.14453\,C - 0.27285\,F_1 - 0.03274\,F_3 - 0.00807\,F_5 - 0.00305\,F_7 \\
E_2 &= -\,0.23850\,C + 0.19979\,F_1 + 0.08866\,F_3 + 0.02973\,F_5 + 0.01244\,F_7 \\
E_3 &= +\,0.07388\,C - 0.11444\,F_1 - 0.10599\,F_3 - 0.04943\,F_5 - 0.02379\,F_7 \\
E_4 &= -\,0.03128\,C + 0.07048\,F_1 + 0.09776\,F_3 + 0.06048\,F_5 + 0.03384\,F_7
\end{aligned}
\qquad (49)
$$

and

$$
\begin{aligned}
-\,0.82810\,F_1 + 0.00612\,F_3 + 0.00385\,F_5 + 0.00196\,F_7 &= -\,1.04843\,C \\
+\,0.01836\,F_1 - 0.76921\,F_3 - 0.01011\,F_5 - 0.00488\,F_7 &= +\,0.08417\,C \\
+\,0.01924\,F_1 - 0.01694\,F_3 - 0.77053\,F_5 - 0.01476\,F_7 &= +\,0.06195\,C \\
+\,0.01371\,F_1 - 0.01134\,F_3 - 0.02055\,F_5 - 0.76878\,F_7 &= +\,0.03889\,C
\end{aligned}
\qquad (50)
$$

in which $C = -\,q_o\,b^2/\pi^3$.

The solution of the system of equations given by Eqs. 50 is made by the method of successive approximations. After the second approximation, Eqs. 50 yields $F_1 = 1.26521\,C$, $F_3 = -\,0.07844\,C$, $F_5 = -\,0.04659\,C$, and $F_7 = -\,0.02561\,C$. Substituting these values into Eqs. 49 yields : $E_1 = +\,0.80235\,C$; $E_2 = +\,0.00562\,C$; $E_3 = -\,0.05969\,C$; and $E_4 = 0.04653\,C$.

Bending Moments. — The bending moments are calculated from the well-known equations

$$M_x = -\,D\,\left(\frac{\partial^2 w}{\partial x^2} + \mu\,\frac{\partial^2 w}{\partial y^2}\right)$$

and

$$M_y = -\,D\,\left(\frac{\partial^2 w}{\partial y^2} + \mu\,\frac{\partial^2 w}{\partial x^2}\right) \qquad (52)$$

in which W stands for the resultant deflection of any panel and D is the flectural rigidity of the same panel. Differentiating Eqs. 11, 15, 19, 36, 39 and 42 twice and substituting into Eqs. 51 and 52, bending moments at any point can be obtained. Regarding the sign convention of bending moments, it is negative when producing tension on the loaded side of the panel. Referring to Figs. 6, values of bending moments at some points are obtained and listed as shown in Table 1.

$$+ \frac{E_m}{2m} [\tanh \gamma_m (\gamma_m \tanh \gamma_m - 1) - \gamma_m] + \frac{2am (-1)^m}{\pi c} \sum_{n=1,3,\ldots}^{\infty} \frac{K_n}{n^3 (\frac{a^2}{c^2} + \frac{m^2}{n^2})^2} \Big\} = 0 \quad \ldots\ldots (46)$$

which represents an infinite number of linear equations containing E_m, F_n and K_n as redundants.

2. A similar system of equations is obtained from substituting Eqs. 14, 18, 20, 38, 40 and 44 into Eq. 8 which represents the condition of continuity along the edge $x_1 = a$ or $x_3 = - c/2$. At any point along the edge A'B', having a distance from the middle point of that edge

$$y_1 = - y_3$$

Thus

$$\cos \frac{i \pi y_1}{b} = \cos (- \frac{i \pi y_3}{b}) = \cos \frac{i \pi y_3}{b}$$

As a result, grouping together the terms that contain $\cos \frac{i \pi y_1}{b}$ or $\cos \frac{i \pi y_3}{b}$ as a factor, the result is

$$- \frac{8 q_o b^3}{a \pi^4} \sum_{m=1}^{\infty} \frac{1}{m^4 (\frac{b^2}{a^2} + \frac{i^2}{m^2})^2} + \frac{4 bi^2}{\pi a} \sum_{m=1}^{\infty} \frac{(-1)^m E_m}{m^3 (\frac{b^2}{a^2} + \frac{i^2}{m^2})^2} + \frac{F_i}{4}$$

$$(\beta_i \tanh^2 + \beta_i \coth^2 \beta_i - \tanh \beta_i - \coth \beta_i - 2 \beta_i) + \frac{D_1}{D_f} \Big\{ \frac{2 q b^2}{\pi^3 i^3} (\frac{\delta_i}{\cosh^2 \delta_i}$$

$$- \tanh \delta_i) - \frac{F_i}{2} (\frac{\delta_i}{\cosh^2 \delta_i} + \tanh \delta_i) \frac{4 bi^2}{\pi c} \sum_{n=1,3,\ldots}^{\infty} \frac{K_n}{n^3 (\frac{b^2}{c^2} + \frac{i^2}{n^2})^2} \Big\} = 0 \quad \ldots\ldots (47)$$

3. In a similar manner, substituting Eqs 28, 31, 33, 37, 41 and 43 into Eq. 9, leads to

$$- \frac{8 q_o c^3}{a \pi^4} \sum_{m=1}^{\infty} \frac{1}{m^4 (\frac{c^2}{a^2} + \frac{i^2}{m^2})^2} + \frac{4 ci^2}{\pi a} \sum_{m=1}^{\infty} \frac{(-1)^m E_m}{m^3 (\frac{c^2}{a^2} + \frac{i^2}{m^2})^2} + \frac{K_i}{4}$$

$$(\Theta_i \tanh^2 \Theta_i + \Theta_i \coth^2 \Theta_i - \tanh \Theta_i - \coth \Theta_i - 2 \Theta_i) + \frac{D_2}{D_f} \Big\{ \frac{2 qc^2}{\pi^3 i^3} (\frac{\Phi_i}{\cosh^2 \Phi_i}$$

$$- \tanh \Phi_i) - \frac{K_i}{2} (\frac{\Phi_i}{\cosh^2 \Phi_i} + \tanh \Phi_i) - \frac{4 ci^2}{\pi b} \sum_{n=1,3,\ldots}^{\infty} \frac{F_n}{n^3 (\frac{c^2}{b^2} + \frac{i^2}{n^2})^2} \Big\} \quad \ldots\ldots (48)$$

in which $\alpha_m = m \pi b/2a$, $\beta = i \pi a/2b$, $\gamma_m = m \pi c/2a$, $\Theta_i = i \pi a/2c$, $\Phi = i \pi b/2c$ and $\delta_i = i \pi c/2b$.

Eqs. 46, 47 and 48 establish the basic relationships which represent a system of simultaneous equations.

and

$$\left(\frac{\partial w_2''}{\partial y_3}\right)_{y_3 = -b/2} = \frac{4c^2}{\pi^2 b D_f} \sum_{n=1,3,\ldots}^{\infty} \frac{F_n}{n^3} \sum_{i=1,3,\ldots}^{\infty} \frac{i\,(-1)^{\frac{i-1}{2}}}{\left(\frac{c^2}{b^2} + \frac{i^2}{n^2}\right)^2} \cos \frac{i \pi x_3}{c} \quad \ldots\ldots\ldots (41)$$

3. In a similar manner, expressions for the deflection and slope equations can be obtained for the case shown in Fig. 5(c). They are

$$w_3'' = -\frac{c^2}{2\pi^2 D_f} \sum_{n=1,3,\ldots}^{\infty} \frac{(-1)^{\frac{n-1}{2}} K_n}{n^4 \cosh \Phi_n} \left(\frac{n\pi y_3}{c} \sinh \frac{n \pi y_3}{c} - \Phi_n \tanh \Phi_n \cosh \frac{n\pi y_3}{c}\right) \cos \frac{n \pi x_3}{c} \quad \ldots\ldots (42)$$

$$\left(\frac{\partial w_3''}{\partial y_3}\right)_{y_3 = -b/2} = \frac{c}{2\pi D_f} \sum_{n=1,3,\ldots}^{\infty} \frac{(-1)^{\frac{n-1}{2}} K_n}{n} \left(\tanh \Phi_n + \frac{\Phi_n}{\cosh^2 \Phi_n}\right) \cos \frac{n\pi x_3}{c} \quad (43)$$

and

$$\left(\frac{\partial w_3''}{\partial x_3}\right)_{x_3 = -c/2} = \frac{4\, b^2}{\pi^2 c D_f} \sum_{n=1,3,\ldots}^{\infty} \frac{K_n}{n^3} \sum_{n=1,3,\ldots}^{\infty} \frac{i\,(-1)^{\frac{i-1}{2}}}{\left(\frac{b^2}{c^2} + \frac{i^2}{n^2}\right)^2} \cos \frac{i\pi y_3}{c} \quad \ldots\ldots (44)$$

FORMULATION OF GOVERNING EQUATIONS

The fundamental relations for the determination of the constants E_m, F_m and K_n are found as follows :

1. Eq. 7 represents the condition of continuity along vertical edge $y_1 = + b/2$ or $y_2 = - c/2$. By the method of superposition, it can be written as

$$\left(\frac{\partial w_1}{\partial y_1} + \frac{\partial w_2}{\partial y_1} + \frac{\partial w_3}{\partial y_1}\right)_{y_1 = b/2} = \left(\frac{\partial w_1'}{\partial y_2} + \frac{\partial w_2'}{\partial y_2} + \frac{\partial w_3'}{\partial y_2}\right)_{y_2 = -c/2} \quad \ldots\ldots (45)$$

Substituting Eqs. 12, 16, 24, 27, 30 and 34 into Eq. 45 and grouping together the terms that contain the value $\sin \frac{m\pi x_1}{a}$ or $\sin \frac{m \pi x_2}{a}$ as a factor ($x_1 = x_2$), the result reduces to

$$\frac{q_o a^2}{\pi^3} \frac{(-1)^{m+1}}{m^4} [\alpha_m - \tanh \alpha_m (1 + \alpha_m \tanh \alpha_m)] + \frac{E_m}{2m} [\tanh \alpha_m (\alpha_m \tanh \alpha_m - 1) - \alpha_m]$$
$$+ \frac{2am\,(-1)^m}{\pi b} \sum_{n=1,3,\ldots}^{\infty} \frac{F_n}{n^3 \left(\frac{a^2}{b^2} + \frac{m^2}{n^2}\right)^2} + \left(\frac{D_2}{D_1}\right) \left\{ \frac{q_o a^2 (-1)^{m+1}}{\pi^3 m^4} [\gamma_m - \tanh \gamma_m (1 + \tanh \gamma_m)] \right.$$

the own weight of the floor per unit area. Let w_1'', w_2'' and w_3'' represent the deflections of the three cases shown in Figs. 5(a), 5(b) and 5(c), respectively. The resultant deflection of the floor W_f becomes

$$W_f = w_1'' + w_2'' + w_3'' \tag{35}$$

The deflection and slope equations of the three cases shown in Fig. 5 can be obtained as follows :

1. In Fig. 5(a), the floor is considered as a simply-supported rectangular plate uniformly loaded with intensity q. The deflection surface is given by (9)

$$w_1'' = \frac{4\,qc^4}{\pi^5 D_f} \sum_{n=1,3,\ldots}^{\infty} \frac{(-1)^{\frac{n-1}{2}}}{n^5} \left(1 - \frac{\Phi_n \tanh \Phi_n + 2}{2 \cosh \Phi_n} \cosh \frac{n\pi y_3}{c} + \frac{1}{2\cosh \Phi_n} \frac{n\pi y_3}{c} \sinh \frac{n\pi y_3}{c}\right) \cos \frac{n\pi x_3}{c} \quad \ldots\ldots \tag{36}$$

in which $\Phi_n = n\pi b/2c$, $D_f = E h_f^3 / 12(1-\mu^2)$, and h_f is the thickness of the floor.

Differentiating Eq. 36 leads to

$$\left(\frac{\partial w_1''}{\partial y_3}\right)_{y_3 = -b/2} = -\frac{2\,qc^3}{\pi^4 D_f} \sum_{n=1,3,\ldots}^{\infty} \frac{(-1)^{\frac{n-1}{2}}}{n^4} \left(\frac{\Phi_n}{\cosh^2 \Phi_n} - \tanh \Phi_n\right) \cos \frac{n\pi x_3}{c} \tag{37}$$

The rotation along the side $x_3 = -c/2$ can be computed in a form similar to that of Eq. 37, due to symmetry. It will be

$$\left(\frac{\partial w_1''}{\partial x_3}\right)_{x_3 = -c/2} = -\frac{2q\,b^3}{\pi^4 D_f} \sum_{n=1,3,\ldots}^{\infty} \frac{(-1)^{\frac{n-1}{2}}}{n^4} \left(\frac{\delta_n}{\cosh^2 \delta_n} - \tanh \delta_n\right) \cos \frac{n\pi y_3}{b} \tag{38}$$

in which $\delta_n = n\pi c / 2b$.

2. For the case shown in Fig. 5(b), the floor is considered as a simply-supported rectangular plate bent by moments distributed along the edges $x_3 = \pm c/2$. The deflection surface is (9)

$$w_2'' = -\frac{b^2}{2\pi^2 D_f} \sum_{n=1,3,\ldots}^{\infty} \frac{(-1)^{\frac{n-1}{2}} F_n}{n^2 \cosh \delta_n} \left(\frac{n\pi x_3}{b} \sinh \frac{n\pi x_3}{b} - \delta_n \tanh \delta_n \cosh \frac{n\pi x_3}{b}\right) \cos \frac{n\pi y_3}{b} \quad \ldots\ldots \tag{39}$$

from which the edge slopes are

$$\left(\frac{\partial w_2''}{\partial x_3}\right)_{x_3 = -c/2} = \frac{b}{2\pi D_f} \sum_{n=1,3,\ldots}^{\infty} \frac{(-1)^{\frac{n-1}{2}} F_n}{n} \left(\tanh \delta_n + \frac{\delta_n}{\cosh^2 \delta_n}\right) \cos \frac{n\pi y_3}{b} \tag{40}$$

3. For the case, shown in Fig. 4(c), the deflection surface is given by

$$w_3' = \frac{c^2}{4\pi^2 D_2} \sum_{n=1,3,\ldots}^{\infty} \frac{K_n (-1)^{\frac{n-1}{2}}}{n^2} \Big\{ \frac{1}{\cosh \Theta_n} \Big[\Theta_n \tanh \Theta_n \cosh \frac{n\pi(x_2 - a/2)}{c} - \frac{n\pi(x_2 - a/2)}{c} \sinh \frac{n\pi(x_2 - a/2)}{c} \Big] + \frac{1}{\sinh \Theta_n} \Big[\Theta_n \coth \Theta_n \sinh \frac{n\pi(x_2 - a/2)}{c} - \frac{n\pi(x_2 - a/2)}{c} \cosh \frac{n\pi(x_2 - a/2)}{c} \Big] \Big\} \cos \frac{n\pi y_2}{c} \quad \ldots\ldots (32)$$

in which $\Theta_n = n\pi a/2c$.

Differentiating Eq. 32 yields

$$\left(\frac{\partial w_3'}{\partial x_2}\right)_{x_2 = a} = \frac{c}{4\pi D_2} \sum_{n=1,3,\ldots}^{\infty} \frac{K_n (-1)^{\frac{n-1}{2}}}{n} (\Theta_n \tanh^2 \Theta_n + \Theta_n \coth^2 \Theta_n - \tanh \Theta_n - \coth \Theta_n - 2\Theta_n) \cos \frac{n\pi y_2}{c} \quad \ldots\ldots (33)$$

and

$$\left(\frac{\partial w_3'}{\partial y_2}\right)_{y_2 = -c/2} = -\frac{2a^2}{c\pi^2 D_2} \sum_{n=1,3,\ldots}^{\infty} \frac{K_n}{n^3} \sum_{m=1}^{\infty} \frac{m(-1)^m}{\left(\frac{a^2}{c^2} + \frac{m^2}{n^2}\right)^2} \sin \frac{m\pi x_2}{a} \quad \ldots\ldots\ldots (34)$$

Deflection and Slope Equations of the Floor A'B'C'D' (Fig. 5). — The floor is uniformly loaded with intensity q which is the summation of the weight of the liquid q_o plus

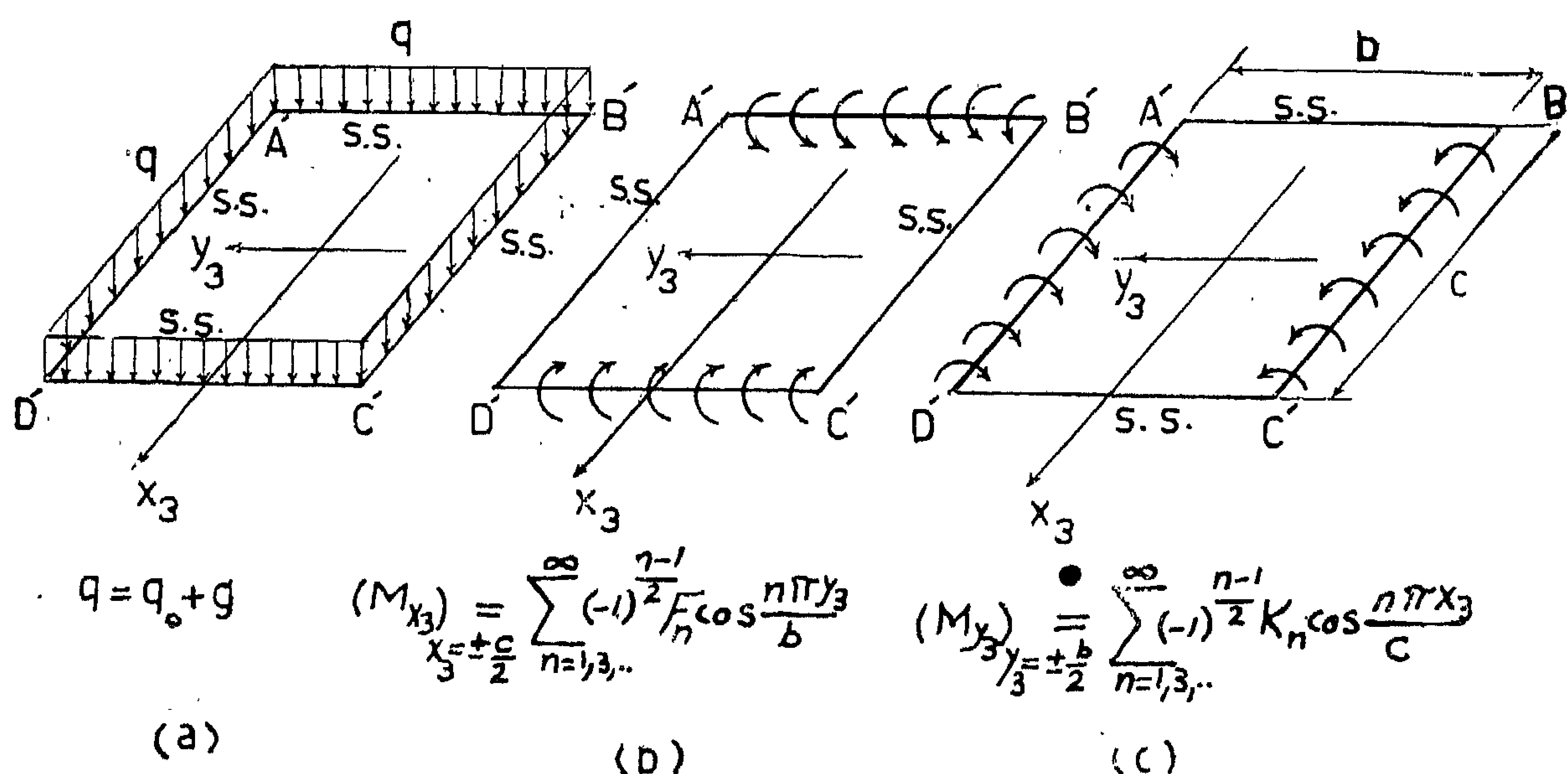


Fig. 5. — Forces acting on the floor A' B' C' D'

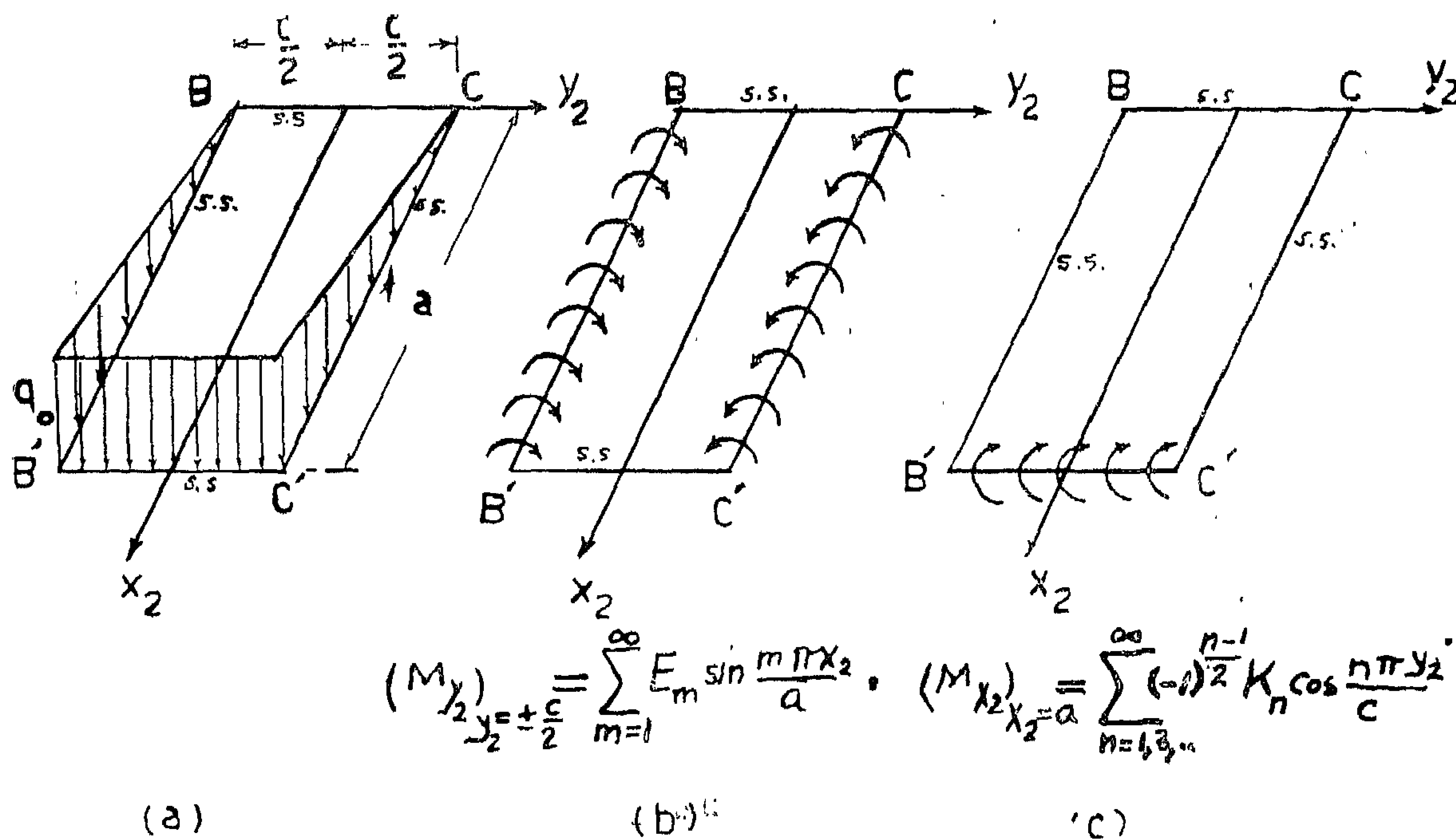


Fig. 4. — Forces acting on the wall B C C′ B′

in which $\gamma_m = m\,\pi\,c/2a$, $D_2 = Eh_2^3 / 12(1 - \mu^2)$
and h_2 is the thickness of the wall B C C′B′.

Differentiating Eq. 26 yields the edge rotations

$$\left(\frac{\partial w_1'}{\partial y_2}\right)_{y_2 = -c/2} = -\frac{q_o a^3}{\pi^4 D_2}\sum_{m=1}^{\infty}\frac{(-1)^{m+1}}{m^4}\left[\gamma_m - \tanh\gamma_m (1 + \gamma_m \tanh\gamma_m)\right]\sin\frac{m\pi x_2}{a} \qquad \text{...... (27)}$$

and

$$\left(\frac{\partial w_1'}{\partial x_2}\right)_{x_2 = a} = -\frac{8 q_o c^4}{a\pi^5 D_2}\sum_{m=1}^{\infty}\frac{1}{m^4}\sum_{i=1,3,\dots}^{\infty}\frac{(-1)^{\frac{i-1}{2}}}{i\left(\frac{c^2}{a^2}+\frac{i^2}{m^2}\right)^2}\cos\frac{i\pi y_2}{c} \qquad \text{...... (28)}$$

2. For the case, shown in Fig. 4(b), the deflection surface is given by

$$w_2 = \frac{a^4}{2\pi^{2}D_2}\sum_{m=1}^{\infty}\frac{E_m}{m^2\cosh\gamma_m}\left(\gamma_m \tanh\gamma_m \cosh\frac{m\pi y_2}{a} - \frac{m\pi y_2}{a}\sinh\frac{m\pi y_2}{a}\right)\sin\frac{m\pi x_2}{a} \qquad (29)$$

and the edge rotations are

$$\left(\frac{\partial w_2'}{\partial y_2}\right)_{y_2 = -c/2} = -\frac{a}{2\pi D_2}\sum_{m=1}^{\infty}\frac{E_m}{m}\left[\tanh\gamma_m(\gamma_m \tanh\gamma_m - 1) - \gamma_m\right]\sin\frac{m\pi x_2}{a} \qquad (30)$$

and

$$\left(\frac{\partial w_2'}{\partial x_2}\right)_{x_2 = a} = \frac{4c^2}{a\pi^2 D_2}\sum_{m=1}^{\infty}\frac{(-1)^m E_m}{m^3}\sum_{i=1,3,\dots}^{\infty}\frac{i\,(-1)^{\frac{i-1}{2}}}{\left(\frac{c^2}{a^2}+\frac{i^2}{m^2}\right)^2}\cos\frac{i\pi y_2}{c} \qquad \text{...... (31)}$$

and

$$\left(\frac{\partial w_3}{\partial y_1}\right)_{y_1 = b/2} = -\frac{b}{4\pi D_1} \sum_{n=1,3,\ldots}^{\infty} \frac{F_n}{n} \left\{ \frac{1}{\cosh \beta_n} \left[\beta_n \tanh \beta_n \cosh \frac{n\pi (x_1 - a/2)}{b} - \frac{n\pi (x_1 - a/2)}{b} \sinh \frac{n\pi (x_1 - a/2)}{b} \right] + \frac{1}{\sinh \beta_n} \left[\beta_n \coth \beta_n \sinh \frac{n\pi (x_1 - a/2)}{b} - \frac{n\pi (x_1 - a/2)}{b} \cosh \frac{n\pi (x_1 - a/2)}{b} \right] \right\} \quad \ldots\ldots\ldots (21)$$

Let $f_2(x_1)$ represent the expression between the brackets in Eq. 21. It vanishes at $x_1 = 0$ and $x_1 = a$. It can be expanded in a Fourier sine series

$$f_2(x_1) = \sum_{m=1}^{\infty} C_m \sin \frac{m\pi x_1}{a} dx_1 \quad (22)$$

in which

$$C_m = \frac{1}{a} \int_{-a}^{+a} [f_2(x_1)] \sin \frac{m\pi x_1}{a} dx_1$$

which results in

$$C_m = \frac{8 a^2}{b^2 \pi n^2} \sum_{m=1}^{\infty} \frac{m (-1)^{m+1}}{\left(\frac{a^2}{b^2} + \frac{m^2}{n^2}\right)^2} \sin \frac{m\pi x_1}{a} \quad \ldots\ldots (23)$$

Substituting Eqs. 22 and 23 into Eq. 21 gives

$$\left(\frac{\partial w_3}{\partial y_1}\right)_{y_1 = b/2} = \frac{2 a^2}{b \pi^2 D_1} \sum_{n=1,3,\ldots}^{\infty} \frac{F_n}{n} \sum_{m=1}^{\infty} \frac{m (-1)^m}{\left(\frac{a^2}{b^2} + \frac{m^2}{n^2}\right)^2} \sin \frac{m\pi x_1}{a} \quad \ldots\ldots (24)$$

Deflection and Slope Equations of the Wall B C C′B′ (Fig. 4). — In a similar manner from the previous results obtained for the wall A B B′A′, the deflection and slope equaions can be easily written for the adjacent wall BCC′B′.

Let w_1', w_2' and w_3' represent the deflections corresponding to the three cases of loading shown in Figs. 4(a), 4(b) and 4(c), respectively. Thus

$$W_2 = w_1' + w_2' + w_3' \quad \ldots\ldots (25)$$

in which W_2 is the resultant deflection of the wall B C C′B′. The deflection and slope equations are obtained as follows :

1. For the case, shown in Fig. 4(a), the deflection surface is given by

$$w_1' = \frac{q_0 a^4}{\pi^5 D_2} \sum_{m=1}^{\infty} \frac{(-1)^{m+1}}{m^5} \left(2 - \frac{2 + \gamma_m \tanh \gamma_m}{\cosh \gamma_m} \cosh \frac{m\pi y_2}{a} + \frac{1}{\cosh \gamma_m} \frac{m\pi y_2}{a} \sinh \frac{m\pi y_2}{a}\right) \sin \frac{m\pi x_2}{a} \quad \ldots (26)$$

In a similar manner, the expression in parentheses in Eq. 17 can be expressed in a Fourier cosine series. Let

$$f_1(y_1) = \left(\alpha_m \tanh \alpha_m \cosh \frac{m\pi y_1}{a} - \frac{m\pi y_1}{a} \sinh \frac{m\pi y_1}{a}\right)$$

Thus

$$f_1(y_1) = \sum_{i=1,3,\ldots}^{\infty} B_i \cos \frac{i\pi y_1}{b}$$

in which

$$B_i = \frac{2}{b} \int_{-b/2}^{+b/2} [f_1(y_1)] \cos \frac{i\pi y_1}{b}\, dy_1$$

which finally gives

$$\therefore B_i = \frac{8\, b^2\, i\, (-1)^{\frac{i-1}{2}} \cosh \alpha_m}{a^2 \pi m^2 \left(\frac{b^2}{a^2} + \frac{i^2}{m^2}\right)^2}$$

On substitution, Eq. 17 becomes

$$\left(\frac{\partial w_2}{\partial x_1}\right)_{x_1 = a} = \frac{4\, b^2}{a \pi^2 D_1} \sum_{m=1}^{\infty} \frac{(-1)^m E_m}{m^3} \sum_{i=1,3,\ldots}^{\infty} \frac{i\,(-1)^{\frac{i-1}{2}}}{\left(\frac{b^2}{a^2} + \frac{i^2}{m^2}\right)^2} \cos \frac{i\pi y_1}{b} \qquad \ldots\ldots (18)$$

3. In Fig. 3(c) the wall is considered as a simply-supported rectangular plate bent by the restraining moments distributed along the side $x_1 = a$. The corresponding deflection surface is given by (9)

$$w_3 = \frac{b^2}{4\pi^2 D_1} \sum_{n=1,3,\ldots}^{\infty} \frac{F_n (-1)^{\frac{n-1}{2}}}{n^2} \left\{ \frac{1}{\cosh \beta_n} \left[\beta_n \tanh \beta_n \cosh \frac{n\pi (x_1 - a/2)}{b} - \frac{n\pi (x_1 - a/2)}{b} \sinh \frac{n\pi (x_1 - a/2)}{b}\right] + \frac{1}{\sinh \beta_n} \left[\beta_n \coth \beta_n \sinh \frac{n\pi (x_1 - a/2)}{b} - \frac{n\pi (x_1 - a/2)}{b} \cosh \frac{n\pi (x_1 - a/2)}{b}\right] \right\} \cos \frac{n\pi y_1}{b} \qquad \ldots\ldots\ldots (19)$$

in which $\beta_n = n\pi a/2b$.

Differentiating Eq. 19 gives the edge rotations

$$\left(\frac{\partial w_3}{\partial x_1}\right)_{x_1 = a} = \frac{b}{4\pi D_1} \sum_{n=1,3,\ldots}^{\infty} \frac{F_n (-1)^{\frac{n-1}{2}}}{n} \left(\beta_n \tanh^2 \beta_n + \beta_n \coth^2 \beta_n - \tanh \beta_n - \coth \beta_n - 2\beta_n\right) \cos \frac{n\pi y_1}{b} \qquad \ldots\ldots (20)$$

and

$$\left(\frac{\partial w_1}{\partial x_1}\right)_{x_1 = a} = -\frac{q_o a^3}{\pi^4 D_1} \sum_{m=1}^{\infty} \frac{1}{m^4} \left(2 - \frac{2 + \alpha_m \tanh \alpha_m}{\cosh \alpha_m} \cosh \frac{m \pi y_1}{a} + \frac{1}{\cosh \alpha_m} \frac{m \pi y_1}{a} \sinh \frac{m \pi y_1}{a}\right) \quad \ldots\ldots \quad (13)$$

The expression in parentheses in Eq. 13 is an even function $f(y_1)$ which vanishes at $y_1 = \pm b/2$. Such an expression can be expanded in the Fourier series

$$f(y_1) = \sum_{i=1,3,\ldots}^{\infty} A_i \cos \frac{i \pi y_1}{b}$$

in which the coefficients A_i are found by

$$A_i = \frac{2}{b} \int_{-b/2}^{+b/2} \left(2 - \frac{2 + \alpha_m \tanh \alpha_m}{\cosh \alpha_m} \cosh \frac{m \pi y_1}{a} + \frac{1}{\cosh \alpha_m} \frac{m \pi y_1}{a} \sinh \frac{m \pi y_1}{a}\right) \cos \frac{i \pi y_1}{b} \, dy_1$$

which finally yields

$$A_i = \frac{8 (-1)^{\frac{i-1}{2}} b^4}{i \pi a^4 \left(\frac{b^2}{a^2} + \frac{i^2}{m^2}\right)^2}$$

Eq. 13 can then be rewritten in the form

$$\left(\frac{\partial w_1}{\partial x_1}\right)_{x_1 = a} = -\frac{8 q_o b^4}{a \pi^5 D_1} \sum_{m=1}^{\infty} \frac{1}{m^4} \sum_{i=1,3,\ldots}^{\infty} \frac{(-1)^{\frac{i-1}{2}}}{i \left(\frac{b^2}{a^2} + \frac{i^2}{m^2}\right)^2} \cos \frac{i \pi y_1}{b} \qquad (14)$$

2. Fig. 3(b) represents a rectangular plate simply supported at the sides, and bent by the restraining moment at $y_1 = \pm b/2$. The corresponding deflection is (9)

$$w_2 = \frac{a^2}{2 \pi^2 D_1} \sum_{m=1}^{\infty} \frac{E_m}{m^2 \cosh \alpha_m} \left(\alpha_m \tanh \alpha_m \cosh \frac{m \pi y_1}{a} - \frac{m \pi y_1}{a} \sinh \frac{m \pi y_1}{a}\right) \sin \frac{m \pi x_1}{a} \qquad (15)$$

Differentiating Eq. 15 gives the edge rotations

$$\left(\frac{\partial w_2}{\partial y_1}\right)_{y_1 = b/2} = \frac{a}{2 \pi D_1} \sum_{m=1}^{\infty} \frac{E_m}{m} [\tanh \alpha_m (\alpha_m \tanh \alpha_m - 1) - \alpha_m] \sin \frac{m \pi x_1}{a} \quad \ldots\ldots\ldots \quad (16)$$

and

$$\left(\frac{\partial w_2}{\partial x_1}\right)_{x_1 = a} = \frac{a}{2 \pi D_1} \sum_{m=1}^{\infty} \frac{(-1)^m E_m}{m \cosh \alpha_m} \left(\alpha_m \tanh \alpha_\pi \cosh \frac{m \pi y_1}{a} - \frac{m \pi y_1}{a} \sinh \frac{m \pi y_1}{a}\right) \quad \ldots\ldots \quad (17)$$

DEFLECTION AND SLOPE EQUATIONS

Deflection and Slope Equations of the Wall A B B′A′ (Fig. 3). — The wall A B B′A′, shown in Fig. 3, is considered as a simply-supported rectangular plate subjected to the following loads :

1. The hydrostatic pressure with maximum value q_o ;
2. the restraining moments distributed along the sides $y_1 = \pm b/2$; and
3. the restraining moments distributed along the edge $x_1 = a$. Let w_1 , w_2 and w_3 denote the deflections of the cases of loading shown in Figs. 3(a), 3(b) and 3(c), respectively. According to the principle of superposition, the resultant deflection W_1 of the wall A B B′A′ is equal to

$$W_1 = w_1 + w_2 + w_3 \qquad (10)$$

The deflection and slope equations of the three cases shown in Fig. 3 are found as follows :

(1) In Fig. 3(a), the wall is a simply-supported rectangular plate of constant thickness h_1 and is under hydrostatic pressure. The corresponding deflection surface is given as (9)

$$w_1 = \frac{q_o a^4}{\pi^5 D_1} \sum_{m=1}^{\infty} \frac{(-1)^{m+1}}{m^5} \left(2 - \frac{2 + \alpha_m \tanh \alpha_m}{\cosh \alpha_m} \cosh \frac{m \pi y_1}{a} + \frac{1}{\cosh \alpha_m} \frac{m \pi y_1}{a} \sinh \frac{m \pi y_1}{a}\right) \sin \frac{m \pi x_1}{a} \qquad (11)$$

in which $D_1 = Eh_1^3/12\ (1 - \mu^2)$, and $\alpha_m = m\,\pi\, b/2a$.

Differentiating Eq. 11 yields the edge rotations

$$\left(\frac{\partial w_1}{\partial y_1}\right) y_1 = b/2 = \frac{q_o a^3}{\pi^4 D_1} \sum_{m=1}^{\infty} \frac{(-1)^{m+1}}{m^4} \left[\alpha_m - \tanh \alpha_m \ (1 + \alpha_m \tanh \alpha_m)\right] \sin \frac{m \pi x_1}{a} \quad \ldots\ldots \quad (12)$$

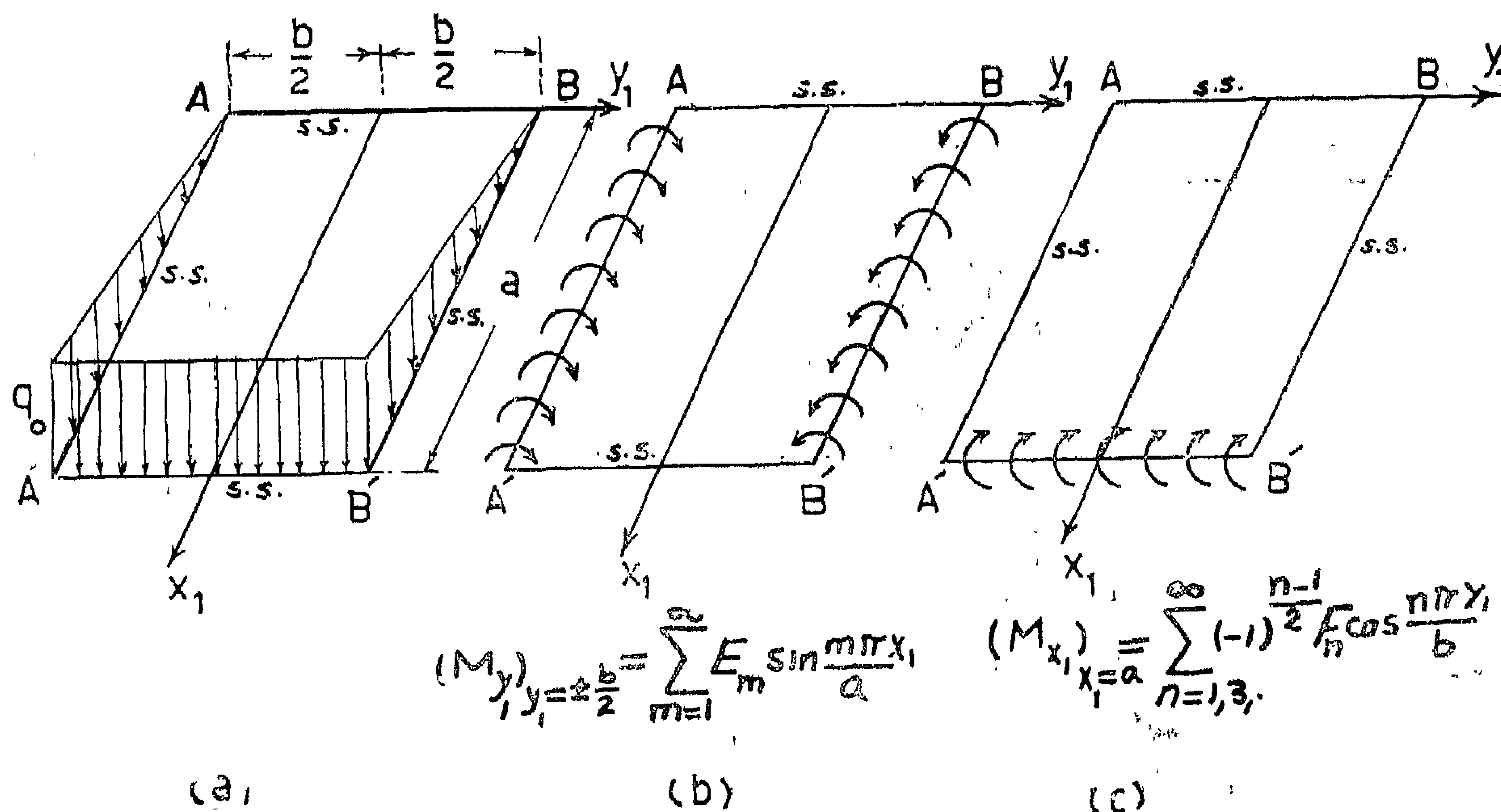


Fig. 3. — Forces acting on the wall A B B′ A′

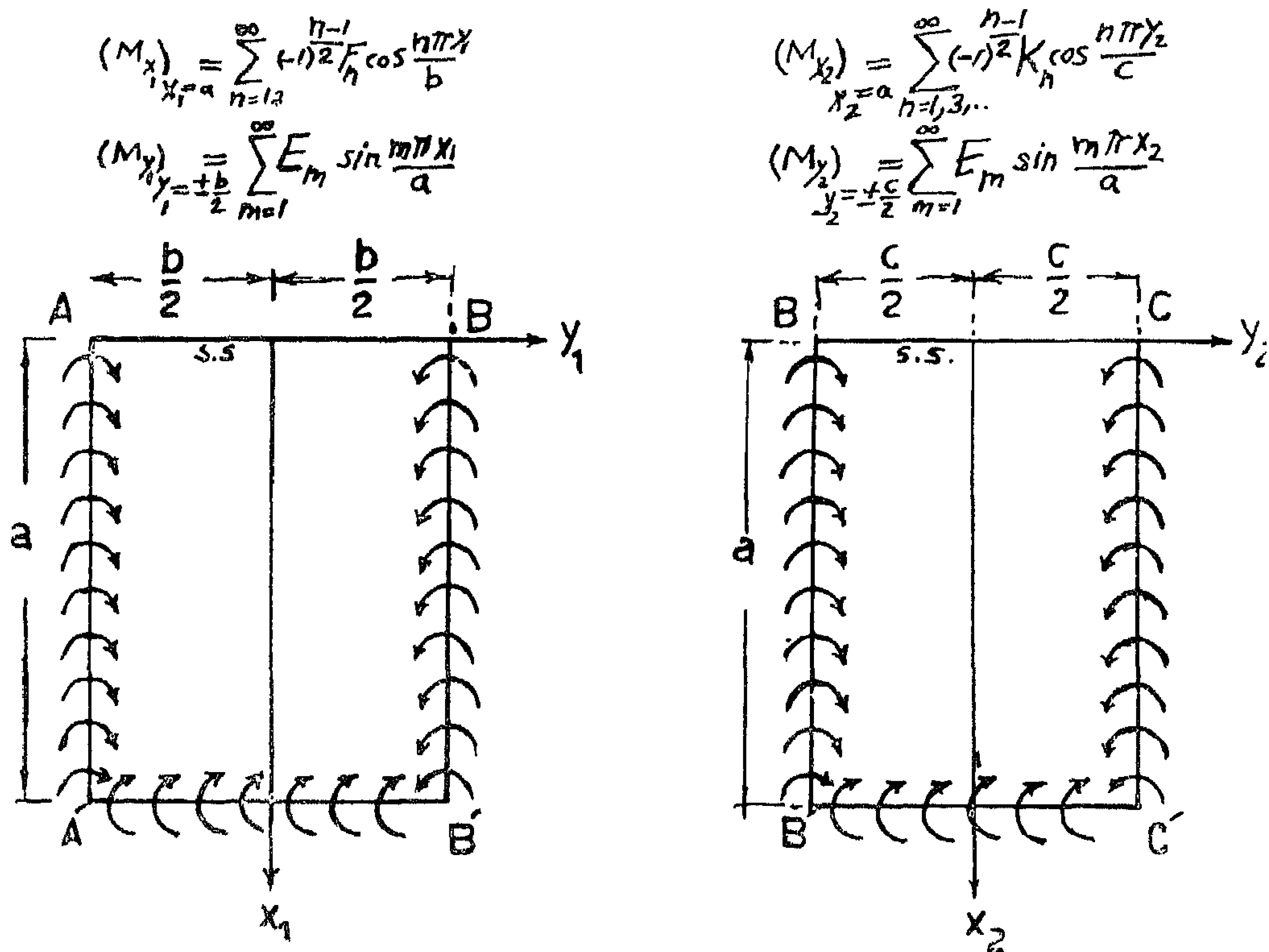


Fig. 2. — Redundant bending moments at the edges of a rectangular tank.

and K_n is an undetermined constant.

Boundary Conditions. — Let W_1, W_2 and W_f represent the resultant lateral deflections of the walls A B B′ A′, B C C′ B′ and the floor A′ B′ C′ D′, respectively. The constants E_m, F_n and K_n can be determined from the following boundary conditions :

1. $W_1 = W_2 = W_3 = 0$ at the edges of the tank ;

2. $\left(\frac{\partial^2 W_1}{\partial x_1^2}\right)_{x_1 = 0} = 0$ and $\left(\frac{\partial^2 W_2}{\partial x_2^2}\right)_{x_2 = 0} = 0$;

3. $\left(\frac{\partial W_1}{\partial x_1}\right)_{y_1 = b/2} = \left(\frac{\partial W_2}{\partial y_2}\right)_{y_2 = -c/2}$ along BB′ ; (7)

4. $\left(\frac{\partial W_1}{\partial x_1}\right)_{x_1 = a} = \left(\frac{\partial W_f}{\partial x_3}\right)_{x_2 = -c/2}$ along A′B′ ; and (8)

5. $\left(\frac{\partial W_2}{\partial x_2}\right)_{x_2 = a} = \left(\frac{\partial W_f}{\partial y_3}\right)_{y_3 = -b/2}$ along B′C′ (9)

The deflection is considered positive in the direction of the load. The edge slopes are angles made with the positive directions of the axes.

These series have redundant constants which can be determined from the boundary conditions at the continuous edges. Hence, moments at any point on the surface of the tank can be found from the well known formulas of the plate theory (9) using the superposition method.

Fig. 1 shows a rectangular tank with lateral dimensions a, b and c. Since the tank is assumed to have no deflections at the sides, it forms continuous slabs at the edges AA′, BB′, CC′, DD′, A′B′, B′C′, C′D′, and D′A′. The walls are simply supported at the top edges AB, BC, CD and DA. Each wall is a continuous slab round three sides, while the floor is continuous round all its sides. The continuous edges are subjected to redundant bending moments. Consider the individual panels shown in Fig. 2. The distribution of the restraining moments is the same along each of the vertical sides AA′, BB′, CC′ and DD′.

The redundant bending moments along the vertical sides of the adjacent walls A B B′A′ and B C C′B′ can be represented by the sine series :

$$(M_{y_1})_{y_1} = \pm\, b/2 = \sum_{m=1}^{\infty} E_m \sin \frac{m\pi x_1}{a} \qquad (1a)$$

or

$$(M_{y_2})_{y_2} = \pm\, c/2 = \sum_{m=1}^{\infty} E_m \sin \frac{m\pi x_2}{a} \qquad (1b)$$

in which

$$(M_{y_1})_{y_1} = b/2 = (M_{y_2})_{y_2} = -\, c/2 \qquad (2)$$

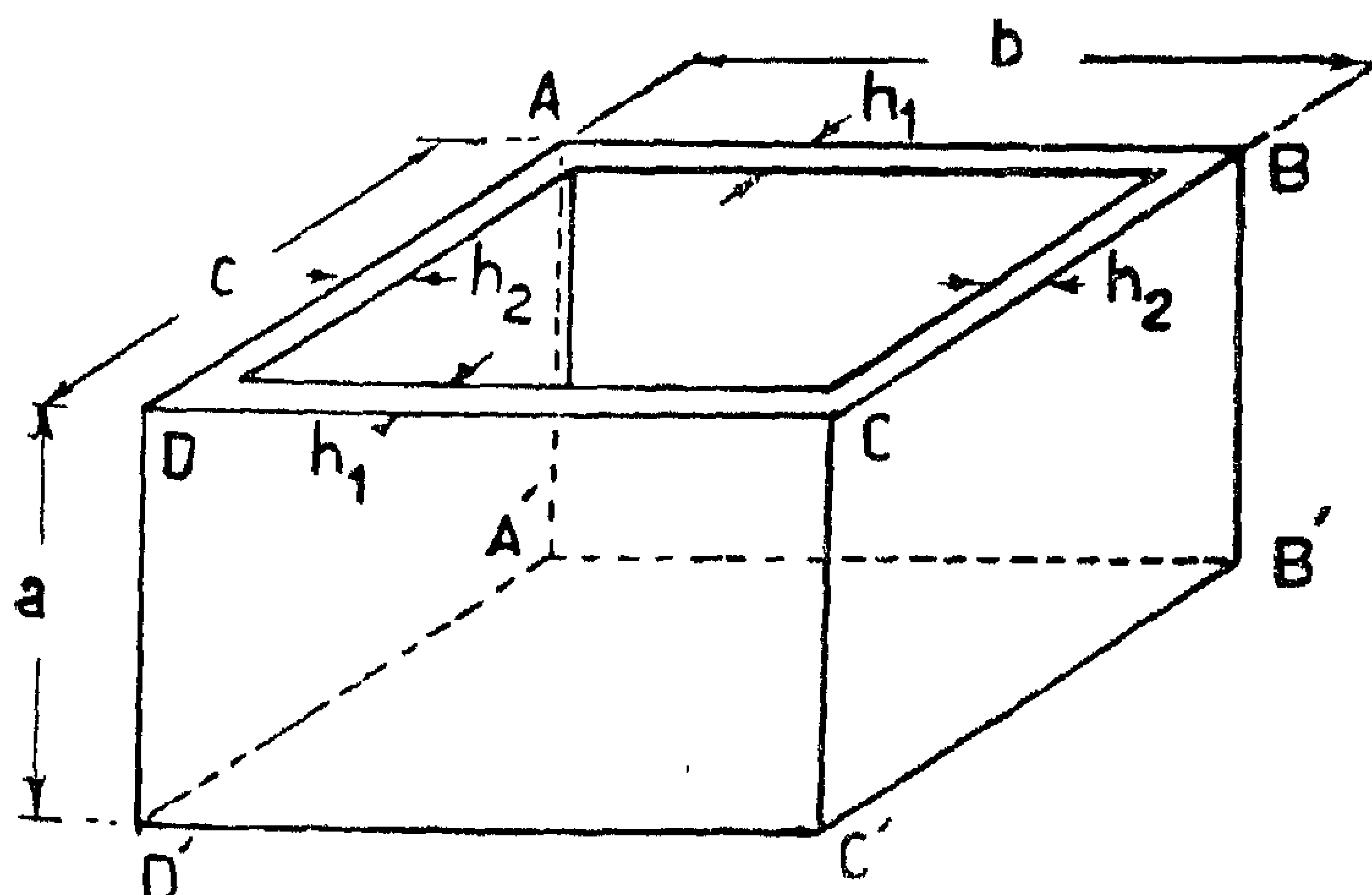


Fig. 1. — Perspective view of a rectangular tank.

where m is an integer with values as indicated on the summation signs, E_m is an undetermined constant, and M_y is the bending moment per unit length about the x-axis.

Regarding the floor, the distribution of the restraining moments along each two opposite sides is the same because of symmetry. Thus, the moments along the sides A′B′ and C′D′ are represented in the form

$$(M_{x_1})_{x_1} = a = \sum_{n=1,3,\ldots}^{\infty} (-1)^{\frac{n-1}{2}} F_n \cos \frac{n\pi y_1}{b} \qquad (3a)$$

or

$$(M_{x_3})_{x_3} = \pm\, c/2 = \sum_{n=1,3,\ldots}^{\infty} (-1)^{\frac{n-1}{2}} F_n \cos \frac{n\pi y_3}{b} \qquad (3b)$$

in which

$$(M_{x_1})_{x_1} = a = (M_{x_3})_{x_3} = -\, c/2 \qquad (4)$$

where n is an integer as indicated on the summation signs, F_n is an undetermined constant, and M_x is the bending moment per unit length about the y-axis.

In a similar manner, moments along A′D′ and B′C′ are expressed as :

$$(M_{x_2})_{x_2} = a = \sum_{n=1,3,\ldots}^{\infty} (-1)^{\frac{n-1}{2}} K_n \cos \frac{n\pi y_2}{c} \qquad (5a)$$

or

$$(M_{y_3})_{y_3} = \pm\, b/2 = \sum_{n=1,3,\ldots}^{\infty} (-1)^{\frac{n-1}{2}} K_n \cos \frac{n\pi x_3}{c} \qquad (5b)$$

in which

$$(M_{x_2})_{x_2} = a = (M_{y_3})_{y_3} = -\, b/2 \qquad (6)$$

tion was made by adjusting the moments at some points along the wall sides and in all cases the floor was not taken into consideration.

Lightfoot and Ghali (4,6) presented two methods for the analysis of rectangular concrete tanks. The first was the finite-differences method. The second was the analogous circular tanks method. In their study, the walls were considered free at the top, fixed to the floor and continuous round the vertical sides.

Davies (1) described a method of analysis of square tanks. He considered the wall to floor interaction on a quantitative basis in a similar manner to the method of moment distribution. From symmetry of square tanks, the analysis is simplified because the walls bcome fixed along the vertical sides, and the floor slab is always a square plate.

The study reported herein is conducted according to the elastic theory of plates for the analysis of rectangular concrete tanks. The structural treatment is based on considering continuity between all the walls and the floor while the top edges are simply supported.

METHOD OF ANALYSIS

An attempt (2) is made for an exact analysis of the rectangular tank based on the mathematical theory of elasticity of plates.

Description of The Tank. — The tank studied herein is rectangular in plan and supported on four similar columns at the corners of the floor. The walls are supported at the top on a ridge beam. Each panel has a constant thickness. Walls opposite to each other have the same thickness, while the floor thickness may be different from that of the walls.

Loads. — The walls are subjected to a hydrostatic pressure with zero value at the top and maximum value at the bottom. The floor is uniformly loaded by the total weight of the liquid plus its own weight. The hydrostatic pressure has a known value, while the dead weight of floor slab must be assumed approximately according to its thickness.

Assumptions. — The principal assumptions necessary for the analysis are :

1 The material of the tank is homogeneous, elastic and isotropic, its modulus of elasticity is E and Poisson's ratio is μ.
2. The walls are simply supported at the top.
3. The displacements at the edges are so small that they can be neglected.
4. The connections between the panels along the edges are rigid to ensure full continuity. Thus the slope angle of a panel at any point of its edge equals the slope angle of the adjacent panel in the same section.
5. The maximum deflection in any panel is small in comparison to its thickness, so that the effect of tensile stresses is neglected in computing the deflection equation; moreover, the thickness of each panel is so small with respect to its lateral dimensions that the effect of shearing stresses on deflection is neglected.
6. The effect of the direct tensile stresses, due to adjacent panels, on deflection is neglected.

Forms of the Redundant Bending Moments at the Edges. — The rectangular tank is considered to be simply supported at the top and continuous round the other edges. The restraining moments, at the edges where the slabs are continuous, can be assumed in mathematical forms of trigonometric series.

BENDING MOMENTS IN RECTANGULAR CONCRETE TANKS

By

Prof. Dr. M. BAKHOUM, Ph.D.
Dr. M.M. TAWFIK, Ph.D.
and
Dr. MOHAMED H. EL-KATEB, Ph.D.

INTRODUCTION

Proper determination of stresses has not been thoroughly investigated in rectangular concrete tanks with constant wall thickness and supported on its bottom edges. During the extensive study of this problem, two general approaches have been used. One of these is to apply the concept of load distribution on the five panels of the tank. The other approach has been to use the plate theory. Some investigators (3, 9, 10)* only considered the wall of the tank as a single plate with various edge conditions and subjected to hydrostatic pressure. Others (4,6,8) treated the walls of the rectangular tank as continuous round their vertical sides and completely fixed to the floor. In most of these studies, interaction between the walls and the floor of the rectangular tank has not been considered, except by Davies (1) in his analysis of square tanks.

A test (5) of a reinforced concrete reservoir was carried out at Lausanne. Measured stresses in its walls were compared with the analytical results according to the regulations used in Germany, France and Switzerland. There was a wide discrepency between the experimental and analytical results. In fact, the beam (or strip) method is an approximate technique. It depends on distributing the load into two orthogonal directions, and considering the strip in each one to be acting as a beam.

Young (10) presented an analysis for tanks, square in plan, with constant wall thickness and a very thick floor. He treated the wall as a plate, free at the top and totally fixed along the other three sides under hydrostatic loading. Poisson's ratio is equal to zero in his analysis.

Flatt and Perks (3) prepared a method to comply with the code of practice of The Institute of Civil Engineers. In their analysis, the wall was considered as a separate plate with either of the two following conditions : 1. The wall is fixed along all its sides ; or 2. the wall is free at the top and fixed along the other three sides. Their solution is a rather approximate and does not take into consideration the effect of continuity between the different panels of the tank.

The Portland Cement Association (8) collected data for the design of rectangular concrete tanks in the form of tabulated coefficients of moments and shears. In the case of tanks, square in plan, the walls become fixed at their vertical sides, while the other edges are considered as follows : 1. The top and bottom edges are hinged ; 2. the top edge is free and the bottom edge is hinged ; and 3. the top edge is free and the bottom edge is fixed. In the general case of rectangular tanks, an adjustment was made to allow for side rotations in a manner similar to the method of moment distribution. The method cannot be applied as simply to the case of continuous tank walls, as it can be applied to framed structures. An approxima-

* Numerals in parentheses refer to corresponding items in Appendix I. — References.

Province. Besides, the banks of Nasser Lake, at Aswan, are the ideal spot for their propagation. Date-palms can be also cultivated on banks of canals and drains and along the sides of rural roads.

21. Due to the fact that no previous precedent had actually been established for the design of load-carrying concrete members reinforced with date-palm mid-ribs, more exploratory research work has to be done in order to obtain :

a) data on the behaviour of concrete members reinforced with date-palm mid-ribs and subjected to sustained loads.

b) data on the use of splices or lapped mid-ribs.

c) more exact data on concrete columns reinforced with mid-ribs.

d) data on the use of mid-ribs taken from other locally grown species of date-palms.

SELECTED REFERENCES*

1. AGBIM, C.C. : "Concrete reinforced with Glass-Fibers". Magazine of Concrete Research, vol. 16 1964.

2. BOND, CAPT. PAUL STANLEY : Book "Some Experiments in the Use of Bamboo for Hasty Bridge Construction". 1913.

3. CAMUS, EDMOND GUSTAVE : Book "Les Bambusees". 1913.

4. CREPPS, R.B. : "Glass Fibers as Tensioning Element in Prestressed Concrete". United States Conference on Prestressed Concrete Proceedings, Cambridge. March 1951.

5. DATTA, K. : "Versuche uber die Verwendurg von Bambus im Betonbau". Bauingenieur, vol. 17 January 24, 1936.

6. "Experimental Studies of New Reinforcing Medium for Concrete". Eng. and Contract Rec., vol. 54 February 19, 1941.

7. FAIRCHILD, DAVID G. : "Japanese Bamboos and their Introduction into America". 1903. U.S. Department of Agriculture, Bulletin No. 43.

8. "Glass Reinforcement for Concrete". Eng.-Journal, vol. 23 No. 12 December 1940.

9. GLENN, H.E. : "Sugar-Cane, Native Cane Reinforcement for Concrete". Civil Eng. (N.Y.), vol. 13 August 1943.

10. HOLME, A.S. : "Substitutes for Steel Reinforcement — Trials of Bamboo and Asbestos-Cement". Concrete and Constructional Engineering, vol. 36 March 1941.

11. KUMPE, G. : "Experimental Bamboo Truss". Military Engineer, vol. 29 July-August 1937.

12. MARSHALL, W..T. : "Glass Strips as Reinforcement for Concrete". Civil Eng. (London), vol. 35 No. 412 October 1940.

13. RUBINSKY, I.A. : "Apply Prestress with Glass". Eng. News-Records, vol. 146 No. 9 March 1951.

14. RUBINSKY, I.A. and RUBINSKY, A. : "Preliminary Investigation of the Use of Fiber-Glass for Prestressed Concrete". Magazine of Concrete Research, vol. 6 No. 17, September 1954.

15. SODEN, A.W. : "Glass Reinforcement for Concrete". Civil Eng. (London), vol. 35 No. 410 August 1940. Concrete and Constructional Eng., vol. 35 September 1940. Engineer, vol. 170 No. 4410 July 19, 1940. Engineering, vol 150 No. 3899 September 1940. Water and Water Eng., vol. 42 No. 527 August 1940.

16. YOUSSEF, M.A. REDA : "Non Metallic Reinforcement for Concrete Structural Elements". M.Sc. Thesis, Cairo University, Jan. 1969.

* Related to other non-metallic reinforcing materials, since no previous research work, except the authors', has been published on date-palm mid-ribs.

treatment for mid-ribs reinforcement. This treating agent has proved to be very successful in completely eliminating the swelling cracks and giving the higher values for bond strength between concrete and mid-ribs, together with preventing the formation of wet rot.

11. In placing the reinforcing mid-ribs in the concrete member, care should be taken to ensure having a clear spacing of not less than 2.5 to 3.0 cm between the individual mid-ribs in each row as well as between the successive rows of reinforcement. Care should be also taken to avoid having the top row of reinforcement being too close to the neutral axis of the concrete section, otherwise there may be insufficient concrete to resist horizontal shear stresses.

12. The basal and distal ends of mid-ribs should be alternated in all rows to ensure a fairly uniform cross section of the reinforcement throughout the whole length of the concrete member. The resulting wedging effect will materially increase the bond between concrete and mid-ribs reinforcement.

13. High quality concrete with high cement content is recommended for concrete members reinforced with mid-ribs, together with using High Early Strength cement in the concrete mixes since it has some merit in preventing swelling cracks of the concrete member.

14. In providing diagonal tension reinforcement for concrete members reinforced with mid-ribs and subjected to flexure, it is recommended to use vertical pieces of mid-ribs acting as stirrups and covering the whole length of the member, with more closer spacings at the parts of high shear stresses. It is to be noted, however, that there is no possibility of bending up the rows of longitudinal mid-ribs reinforcement due to the sudden tensile failure of the mid-ribs at the bents occurring during the bending up procedure.

15. The same procedure, as that used for the design of concrete members reinforced with conventional steel and subjected to flexure, may be used for members reinforced with date-palm mid-ribs, provided using the given value for the modulus of elasticity in tension of mid-ribs together with the above recommended design values of allowable tensile and bond stresses.

16. In order to delay the appearance of cracks in concrete members reinforced with mid-ribs and subject to flexure, it may be recommended to use either some kind of prestressing of the reinforcement or a small percentage of longitudinal steel reinforcement with the main reinforcement of mid-ribs.

17. The factor of safety against bond failure may be increased by using larger number of reinforcing mid-ribs having the same required total cross sectional area.

18. The use of inverted concrete T-section, with the concrete flange being to the tension side, is recommended to provide for better distribution of reinforcement in the tension zone of the beam. This will lower the neutral axis of the concrete section with the result of utilising more concrete in the compression zone.

19. According to the latest census of 1965, there exists about eight million date-palms in Egypt distributed among the different governorates. Knowing that the palm tree produces yearly an average amount of 40 kilograms of mid-ribs, a total amount of 300,000 tons or more of mid-ribs can be possibly obtained from the existing eight million date-palms. This amount is capable of covering most of the needs of the rural housing projects if it is to be used as reinforcement in light concrete structures and one-storey buildings.

20. It is highly recommended to increase the land areas cultivated with date-palms taking an advantage of the reclaimed areas in the New Valley and Al-Tahrir

CONCLUSIONS AND RECOMMENDATIONS

The principal conclusions and recommendations, indicated from the results of tests carried out in this investigation on native date-palm mid-ribs, may be summarized in the following major findings :

1. The use of date-palm mid-ribs as reinforcement does not prevent the cracking of a concrete member at loads materially in excess of those at ultimate failure of a similar concrete beam without any reinforcement. However, using higher percentages of mid-ribs does slightly delay the discovery of the first crack formed under loading. On the other hand, the mid-ribs reinforcement does increase the ultimate load capacity of the concrete beam to about four times that of an unreinforced concrete beam.
2. The ultimate load capacity of a concrete beam increases remarkably with the increase in percentage of longitudinal mid-ribs reinforcement up to a value of 4 to 5 per cent of the cross sectional area of the beam. Moreover, the use of higher percentages of reinforcement increases the ultimate failure load but with comparatively smaller amounts.
3. Although mid-ribs have a fairly high tensile strength (values as high as 1550 kg/cm^2 have been reported), its tensile modulus of elasticity is relatively low (usually less than one-tenth of that of conventional steel reinforcement). This low tensile modulus leads to large deflections and wide cracks for concrete members reinforced with mid-ribs when subjected to excessive loads.
4. Design values not in excess of 250 to 300 kg/cm^2, for the allowable tensile stresses in the mid-ribs reinforcement, must be used if the maximum deflection of the concrete beam is to be kept under 1/360 of the span length. When these low design values are used, a factor of safety of more than 2.0 usually results against ultimate failure of the member.
5. Design values, not in excess of 3 to 5 kg/cm^2, are recommended for the allowable bond stresses between concrete and mid-ribs reinforcement.
6. Concrete columns reinforced with date-palm mid-ribs give ultimate load capacities nearly of the same order as those given by steel reinforced concrete columns, provided that the cross sectional area of mid-ribs reinforcement is from ten to eleven times that of steel. It may be recommended, therefore, to take the safe working loads half the values at elastic limit, although no general conclusions for the design principles of columns could be really drawn out from the attained limited test results.
7. The use of steel hoops for concrete columns reinforced with mid-ribs seems to be inevitable since it is completely impossible to fabricate similar hoops from mid-ribs.
8. Date-palm mid-ribs are much more economical than steel when used as reinforcement for concrete structural members. Mid-ribs from locally grown date-pams can be obtained nearly free, except the cost of transport, from many localities in Egypt. No manufacturing process is required beyond treating the reinforcing material with a suitable water-repellent agent. Besides, mid-ribs reinforcement gives lighter weight to the concrete members in general, (specific gravity of mid-ribs is ranging from 0.69 to 0.78).
9. The use of green unseasoned mid-ribs as reinforcement in concrete members is not recommended. Instead, mid-ribs should be cut and allowed to dry and season for at least four to six weeks before being used.
10. The use of two brush coatings of the blown bitumen paint used in this investigation, followed by dusting with sand, is recommended as a water-repellent

Table (7) — Results of Compression Tests on Concrete Columns (20 × 20 × 200 cm.) Reinforced with Steel and with Date-palm Mid-ribs.

Mark on column	*Control cubes C (kg/cm²)*	*Load at elastic limit P (ton)*	*Strain at elastic limit (mm/mm)*	*Load at failure P (ton)*	*Strain at failure (mm/mm)*
S	385	70.00	3.82×10^{-4}	108.00	6.80×10^{-4}
D	360	60.00	4.30×10^{-4}	100.00	8.80×10^{-4}

* C = Compressive strength of control cubes at age of 14 days.

* Elastic limit was considered to be that point at the end of the straight line part of the load-deformation diagram.

* All strains were measured on G.L. = 25.0 cm.

* No sweiling cracks were recorded for the concrete beam (D) reinforced with date-palm mid-ribs.

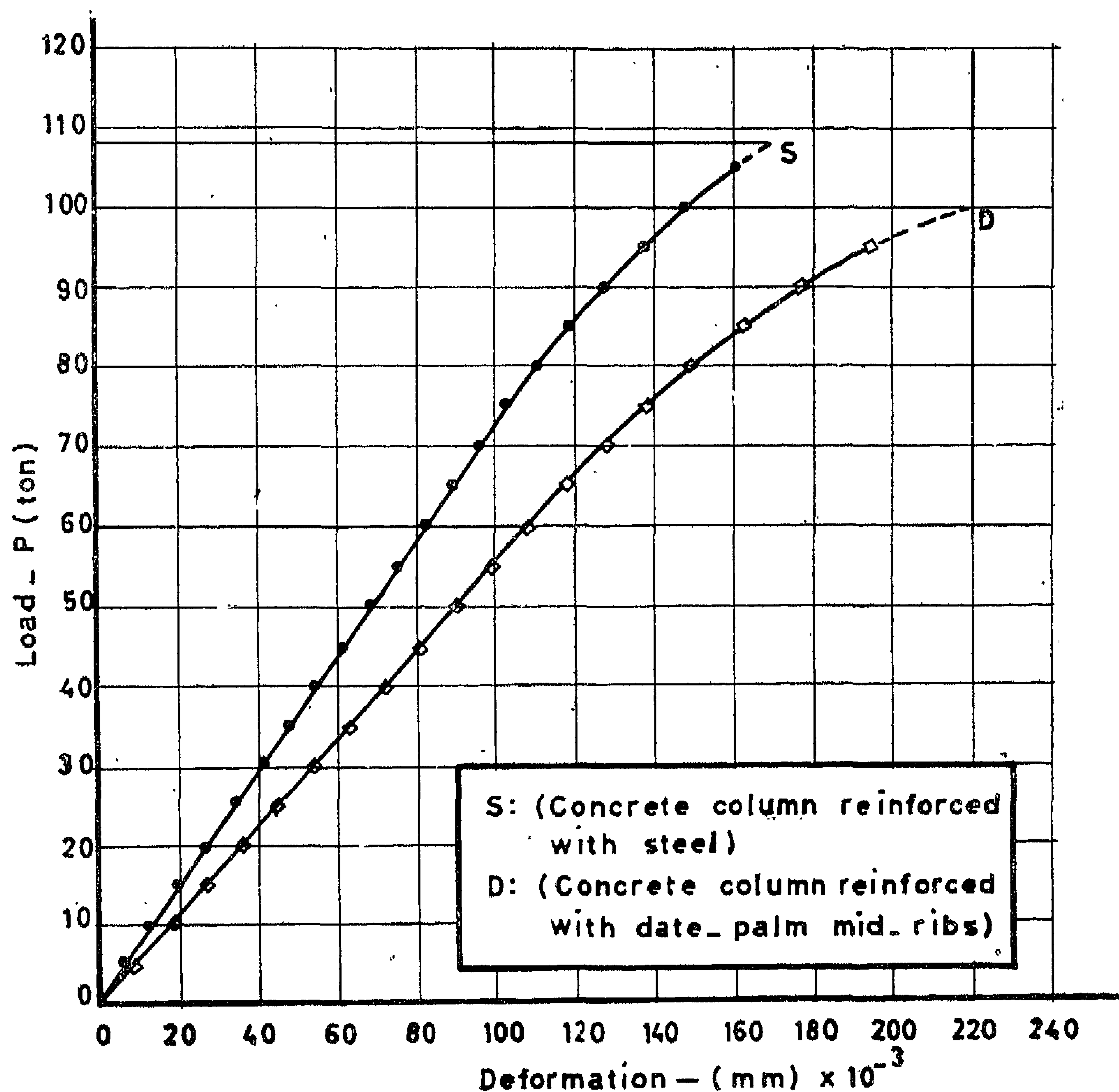


Fig. 14 _ LOAD DEFORMATION DIAGRAMS OF COMPRESSION TESTS ON CONCRETE COLUMNS REINFORCED WITH STEEL AND WITH DATE_PALM MID_RIBS

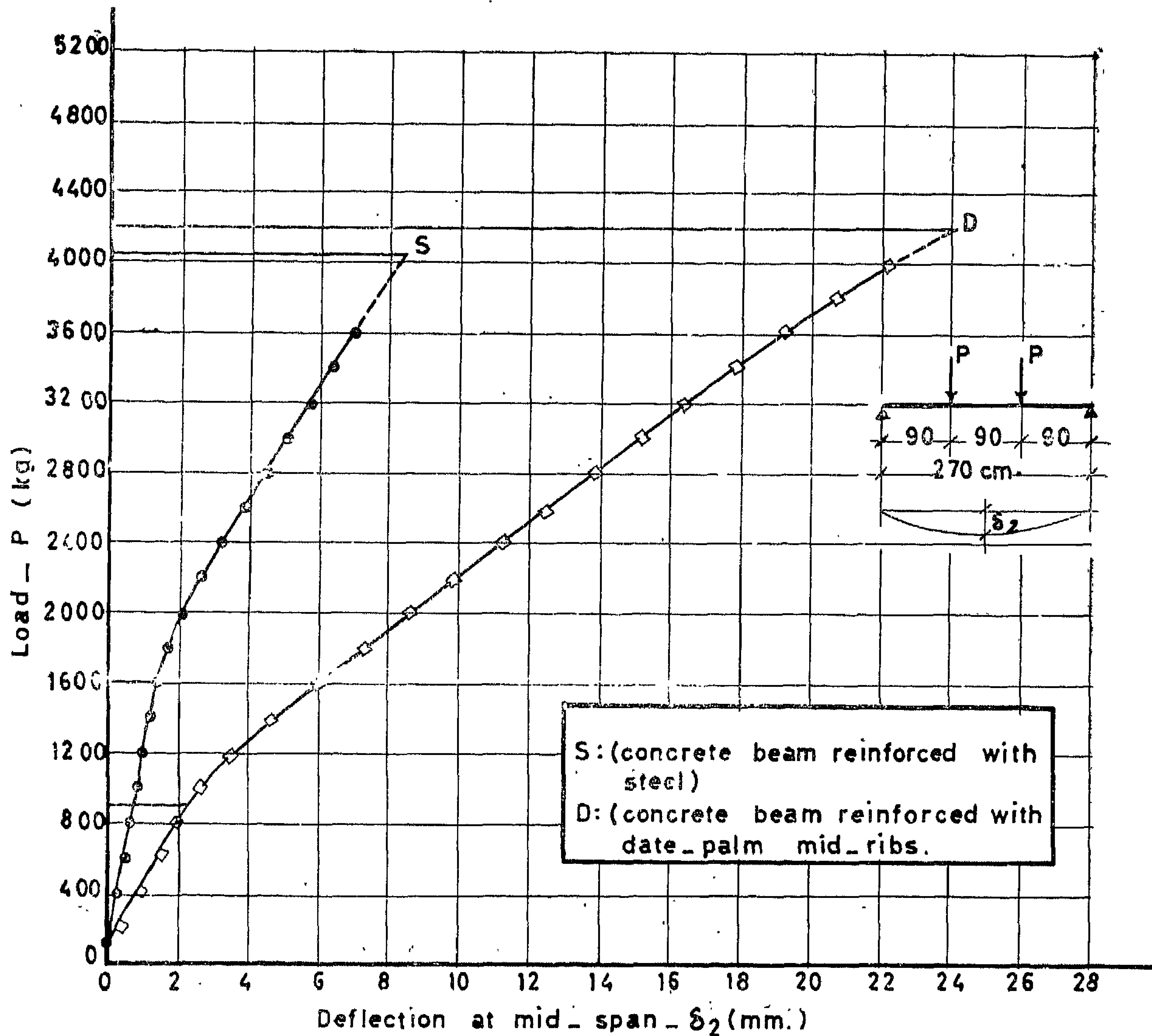


Fig. 13 — LOAD-DEFLECTION CURVES OF FLEXURE TESTS ON CONCRETE BEAMS (22.5 × 30 × 300 cm) REINFORCED WITH STEEL AND WITH DATE-PALM MID-RIBS.

and distal ends of the mid-ribs in order to have a fairly uniform cross sectional area of reinforcement through the whole height of the column. The column was tied by steel hoops in the same way as in the steel reinforced concrete column.

The concrete columns were cast vertically using two external form vibrators together with an internal one. They were cured using wet burlap and sand until tested at age of 14 days.

Deformation readings were measured, at the middle of the column height from the four sides, using four mechanical strain gages each with a 25—cm gage length. The test results of both columns are given in Table (7), and the load-deformation diagrams are shown in Fig. (14).

c) Tests on Columns (20 × 20 × 200 cm) :

Two concrete columns were prepared, one reinforced with mid-ribs and the other with conventional mild steel, and both were of square cross section of 20 × 20 cm and a total height of 200 cm. They were fabricated using a concrete mix with a cement content of 400 kg/m³ of High Early Strength cement and the mix proportions by weight were 1 : 1.65 : 3.06 with (W/C) ratio of 0.44.

The steel reinforced concrete column was provided with four steel bars of 3/8 in. diameter placed in the four corners as main reinforcement, and tied by steel hoops of 3/16 in. diameter placed every 10 cm in the middle part of its height and every 5 cm over a length of 35 cm at both ends.

The other concrete column was reinforced with 16 mid-ribs, having a total cross sectional area of about 30 cm², and treated with two brush coatings of "Shell Pipe Primer" then dusted with sand. The mid-ribs reinforcement was distributed along the column sides such that a clear spacing of 2.0 cm resulted between the individual mid-ribs. Besides, care was taken to alternate the basal

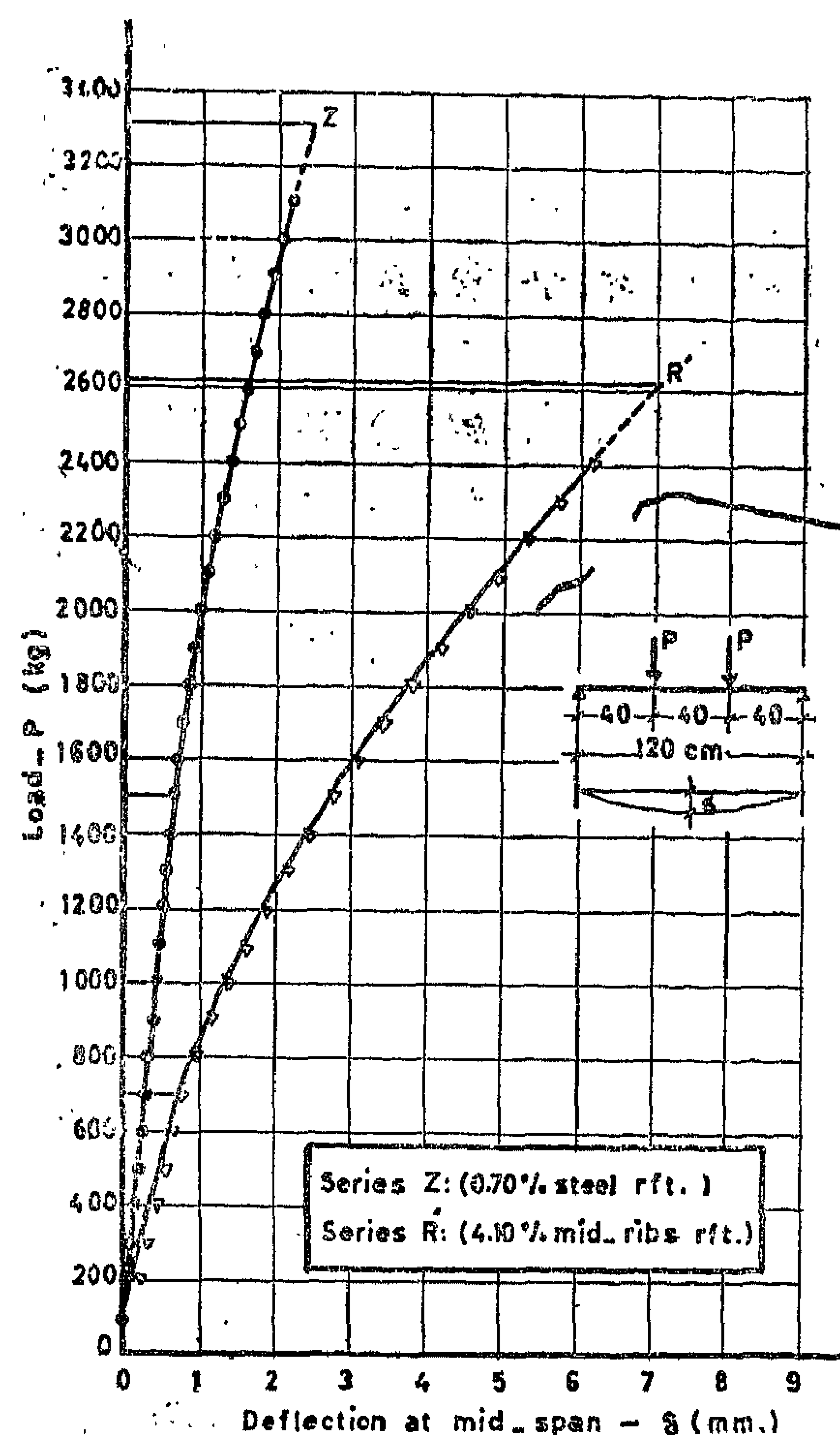


Fig. 12 - LOAD-DEFLECTION CURVES OF CONCRETE BEAMS REINFORCED WITH STEEL & WITH DATE-PALM MID-RIBS.

Table (6) — Maximum Tensile Stresses in Reinforcement for Different Values of Load P applied on Concrete Beam (22.5 × 30 × 300 cm) Reinforced with Date-palm Mid-ribs. (average modulus of elasticity of mid-ribs was taken 190 t/cm²).

Applied load P (kg.)	*Maximum tensile strain in reinforcement (mm/mm)*		*Maximum tensile stress in reinforcement (kg/cm²)*	
	Measured on G.L. = 25.0 cm	*Measured on G.L. = 2.0*	*Calculated from strains measured on G.L. = 25.0 cm*	*Calculated from strains measured on G.L. = 2.0 cm*
800	0.50×10^{-3}	0.78×10^{-3}	95	148
1600	1.50×10^{-3}	2.20×10^{-3}	285	418
2400	2.85×10^{-3}	3.45×10^{-3}	540	655
3200	4.30×10^{-3}	4.80×10^{-3}	815	912
4000	5.70×10^{-3}	6.20×10^{-3}	1080	1180

* P = Load applied at third points of the span ; equals half the total load on beam.

* For G.L. = 25.0 cm, strains were measured at the middle of the span on the concrete cover at the same level as the lower row of reinforcement.

* For G.L. = 2.0 cm, strains were measured directly on the lower row of reinforcement by removing the concrete cover at the middle of the span .

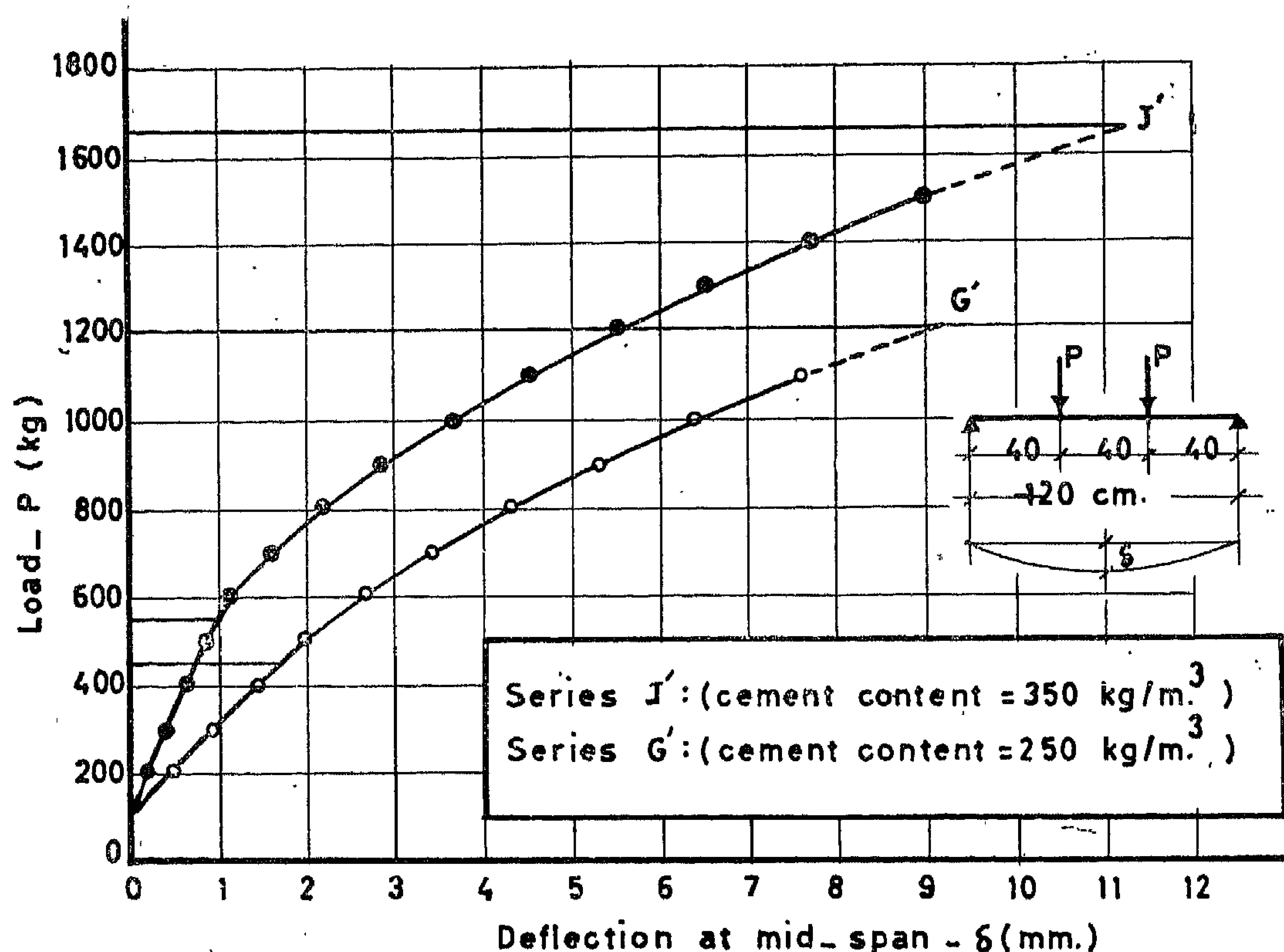


Fig. 11_ EFFECT OF CEMENT CONTENT ON LOAD_DEFLECTION CURVES OF CONCRETE BEAMS REINFORCED WITH DATE_PALM MID_RIBS

diagonal tension reinforcement consisted of vertical pieces of mid-ribs placed 10 cm on centres at both sides of the beam, with two horizontal pieces of mid-ribs connecting each two opposite vertical ones forming a box section. The whole reinforcing mid-ribs were treated with two brush coatings of "Shell Pipe Primer", then dusted with sand and left to dry in air for 24 hours.

The two beams were cured using wet burlap and sand until tested at age of 14 days. Each beam was supported on a 270—cm span and loaded to failure with two concentrated loads applied at third points of the span.

Deflection measurements were made at both the third-points and the middle of the span. For determining the strain distribution across the depth of each beam, mechanical strain gages each with a 25—cm gage length were fixed at mid-span at different levels across the beam depth. For measuring the maximum strains in the mid-ribs reinforcement, a Huggenberger extensometer was fixed directly on the lower row of mid-ribs on a gage length of 2.0 cm. The ultimate load and the type of failure were re-recorded together with the compressive strength of the control concrete cubes.

The steel reinforced concrete beam failed by tension due to yield of steel at an ultimate total load of 8100 kg, while the beam reinforced with mid-ribs showed an ultimate failure caused by diagonal tension followed by compression failure at a total load of 8400 kg. The measured strains and the corresponding stresses for the mid-ribs reinforcement are given in Table (6) for the different stages of loading, while the load-deflection curves of the two concrete beams recorded for the central deflection are shown in Fig. (13).

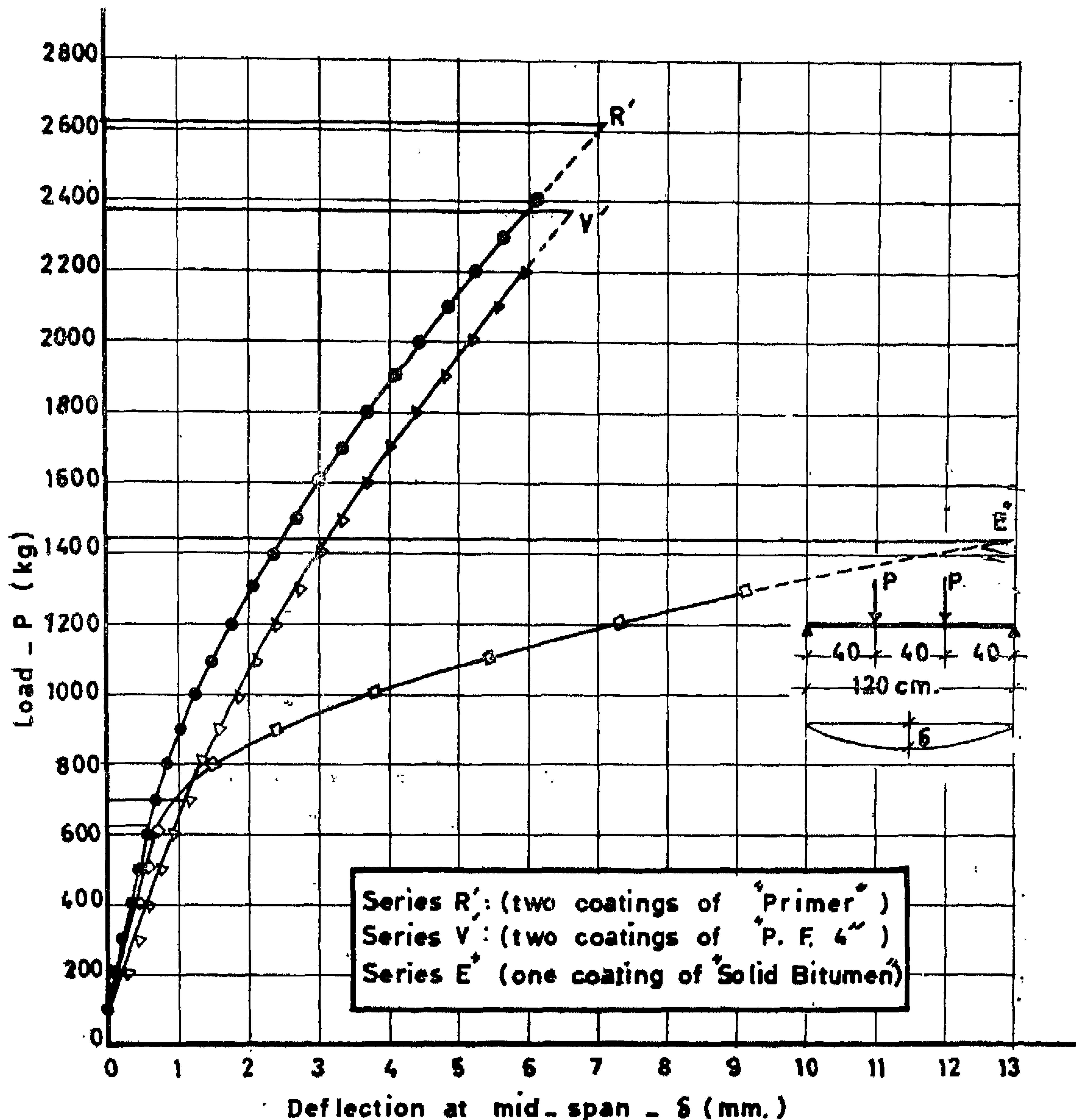


Fig. 10 – EFFECT OF TYPE OF TREATMENT OF REINFORCEMENT ON LOAD-DEFLECTION CURVES OF CONCRETE BEAMS REINFORCED WITH DATE-PALM MID-RIBS.

They were fabricated using the same concrete mix designed before with cement content 350 kg/m³ of High Early Strength cement.

The steel reinforced concrete beam was provided with six steel bars of 3/8 in. diameter placed at bottom in one row as longitudinal reinforcement, together with closed stirrups of 3/16 in. diameter placed vertically 10 cm on centres.

The other concrete beam was reinforced with 18 date-palm mid-ribs as longitudinal reinforcement placed in four rows with a clear spacing, between the individual mid-ribs as well as between the successive rows of mid-ribs, of slightly more than 2.0 cm. Care was taken to alternate the basal and distal ends of mid-ribs in all rows. The total cross sectional area of longitudinal mid-ribs reinforcement was about 34.0 cm². The

Table (4) — Average Results of Flexure Tests on Rectangular Concrete Beams (15 × 20 × 130 cm) Reinforced with Date-palm Mid-ribs.
(for all series, results are the average of two beams.)

Series number	Control cubes C (kg/cm²)	Percentage of rft. μ (%)	Load at first crack P (kg)	Deflection at first crack δ (mm)	Load at failure P (kg)	Deflection at failure δ (mm)
A'	180	2.23	—	—	360	—
C'	180	4.80	—	—	600	—
D'	240	2.14	—	—	560	—
F'	250	4.57	—	—	780	—
G	200	4.00	450	2.10	1215	9.75
J'	248	3.95	550	1.25	1665	11.60
L'	180	4.17	525	2.08	1340	7.78
M'	165	4.27	450	2.15	980	6.38
D''	258	2.35	550	1.35	1200	12.80
E''	255	4.05	625	0.90	1440	13.18
F''	270	5.75	700	0.72	1590	13.08
R'	263	4.10	700	0.85	2620	7.28
V'	253	6.14	700	1.25	2370	6.80

Table (5) — Average Results of Flexure Tests on Plain and Steel Reinforced Concrete Beams (15 × 20 × 130 cm).
(for all series, results are the average of two beams.)

Series number	Control cubes C (kg/cm²)	Percentage of rft. μ (%)	Load at first crack P (kg)	Deflection at first crack δ (mm)	Load at failure P (kg)	Deflection at failure δ (mm)
Q	173	0.70	1100	0.76	2940	3.05
U	195	0.70	1300	0.75	3110	2.88
Z	253	0.70	1500	0.70	3310	2.60
S	165	—	—	—	480	0.50
T	180	—	—	—	550	0.70
W	253	—	—	—	700	0.79

* C = Compressive strength of control cubes at age of 28 days.
* μ = Area of reinforcement divided by total cross sectional area of the concrete beam.
* P = Load applied at third points of the span ; equals half the total load on beam.
* δ = Deflection at mid-span.

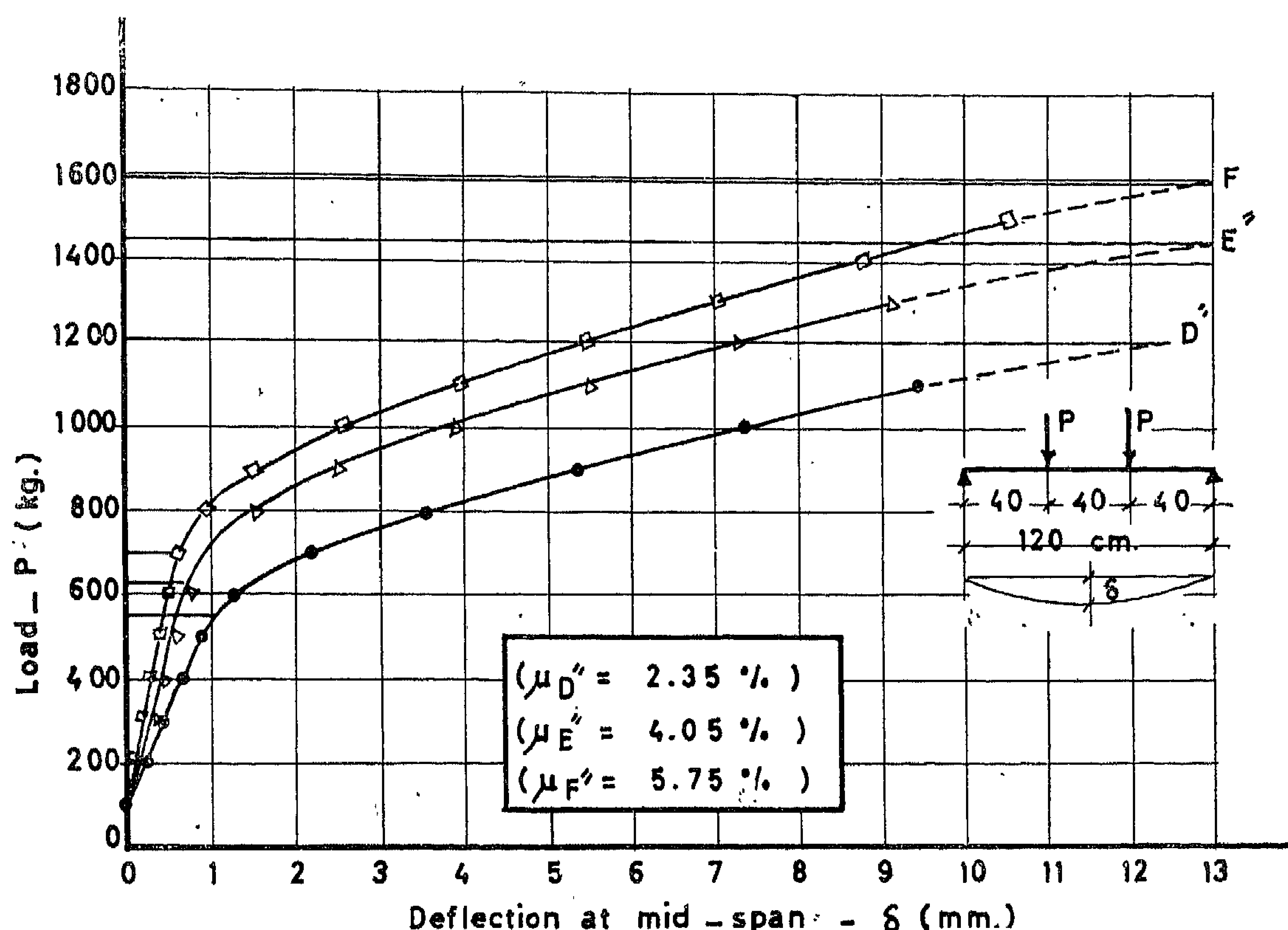


Fig. 8_ EFFECT OF PERCENTAGE OF LONGITUDINAL REINFORCEMENT ON LOAD _ DEFLECTION CURVES OF CONCRETE BEAMS REINFORCED WITH DATE _ PALM MID_ RIBS.

swelling cracks if any, and the compressive strength of control cubes cast from the same concrete mix of the beam.

The average test results of concrete beam series reinforced with date-palm mid-ribs are recorded in Table (4), while those of plain and steel reinforced concrete beams are given in Table (5).

The load-deflection curves for the different beam series were plotted into groups showing the effect of the different factors previously mentioned. Figures (8 to 12) show some selected groups of curves.

b) *Tests on Beams (22.5 × 30 × 300 cm):*

In addition to the tests conducted on the relatively small concrete beams reinforced with mid-ribs, tests were carried out on bigger size concrete beams to secure further information. Two concrete beams were prepared, one reinforced with mid-ribs and the other with conventional mild steel, each having a width of 22.5 cm, a total depth of 30 cm, and a total length of 300 cm.

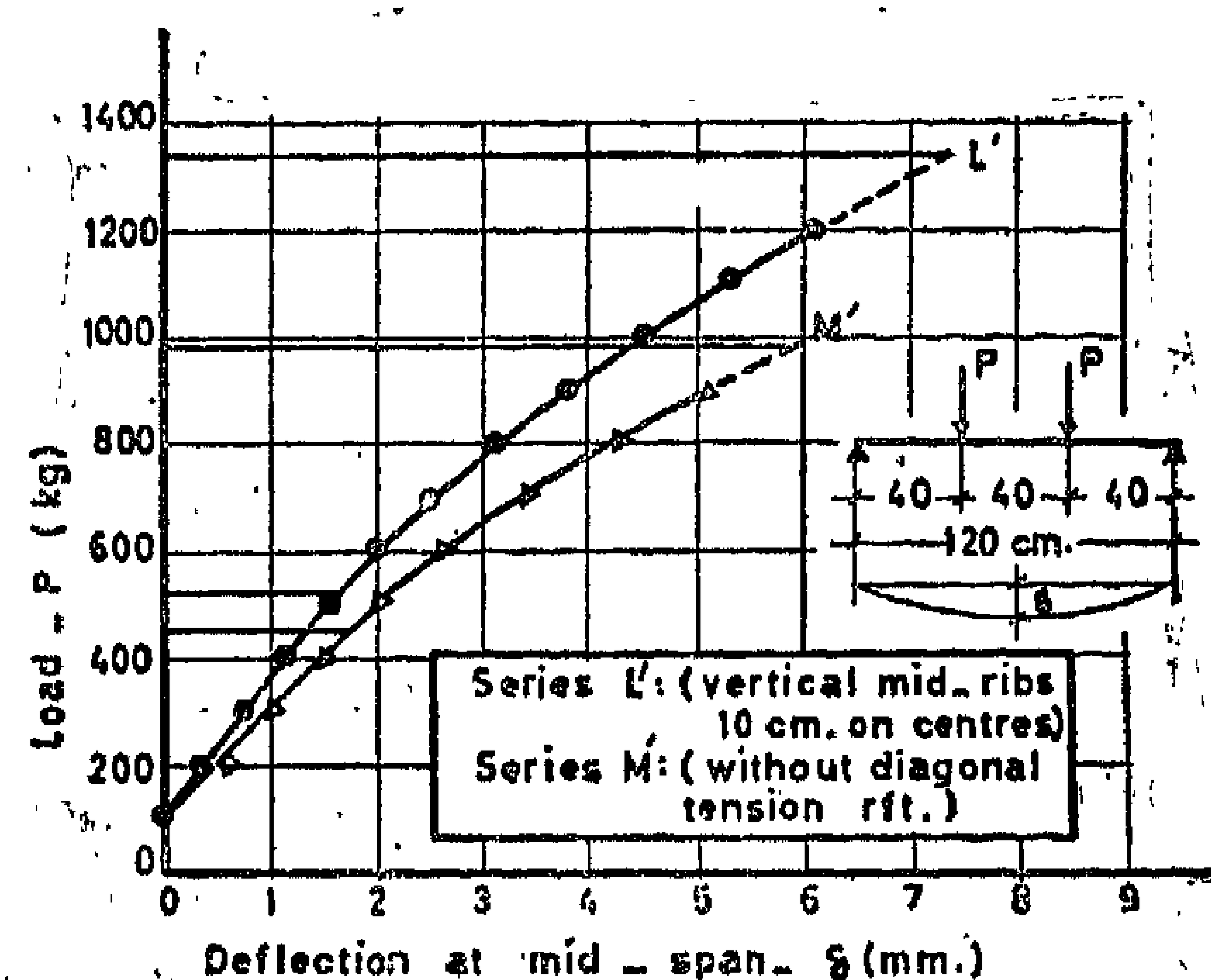


Fig. 9_ EFFECT OF DIAGONAL TENSION REINFORCEMENT ON LOAD-DEFLECTION CURVES OF CONCRETE BEAMS REINFORCED WITH DATE_PALM MID_RIBS.

A full description of the concrete beams reinforced with mid-ribs and used in this research work is recorded in Table (3), and the arrangements of mid-ribs reinforcement for the various beam series are shown in Fig. (7).

To obtain the data required for comparison, control beam series of plain concrete and steel reinforced concrete were prepared using the same mix proportions previously mentioned. The steel reinforced concrete beams of the different series were prepared, each having 3 Φ 3/8 in. mild steel bars as main reinforcement, together with vertical closed stirrups of diameter 3/16 in. placed 10 cm on centres. For a cement content of 250 kg/m^3, Beam Series (Q,S) were fabricated using Ordinary Portland cement while Series (U,T) were made using High Early Strength cement. For a cement content of 350 kg/m^3, Series (Z,W) were made using High Early Strength cement.

All beams were cured using wet burlap and sand until tested at age of 28 days. Each beam was supported on a 120—cm span and loaded to failure with two concentrated loads applied at third points of the span. For each beam, after test, a complete record was made for the ultimate failure load, the type of failure, the load-deflection readings, the cracking loads and crack pattern, the initial

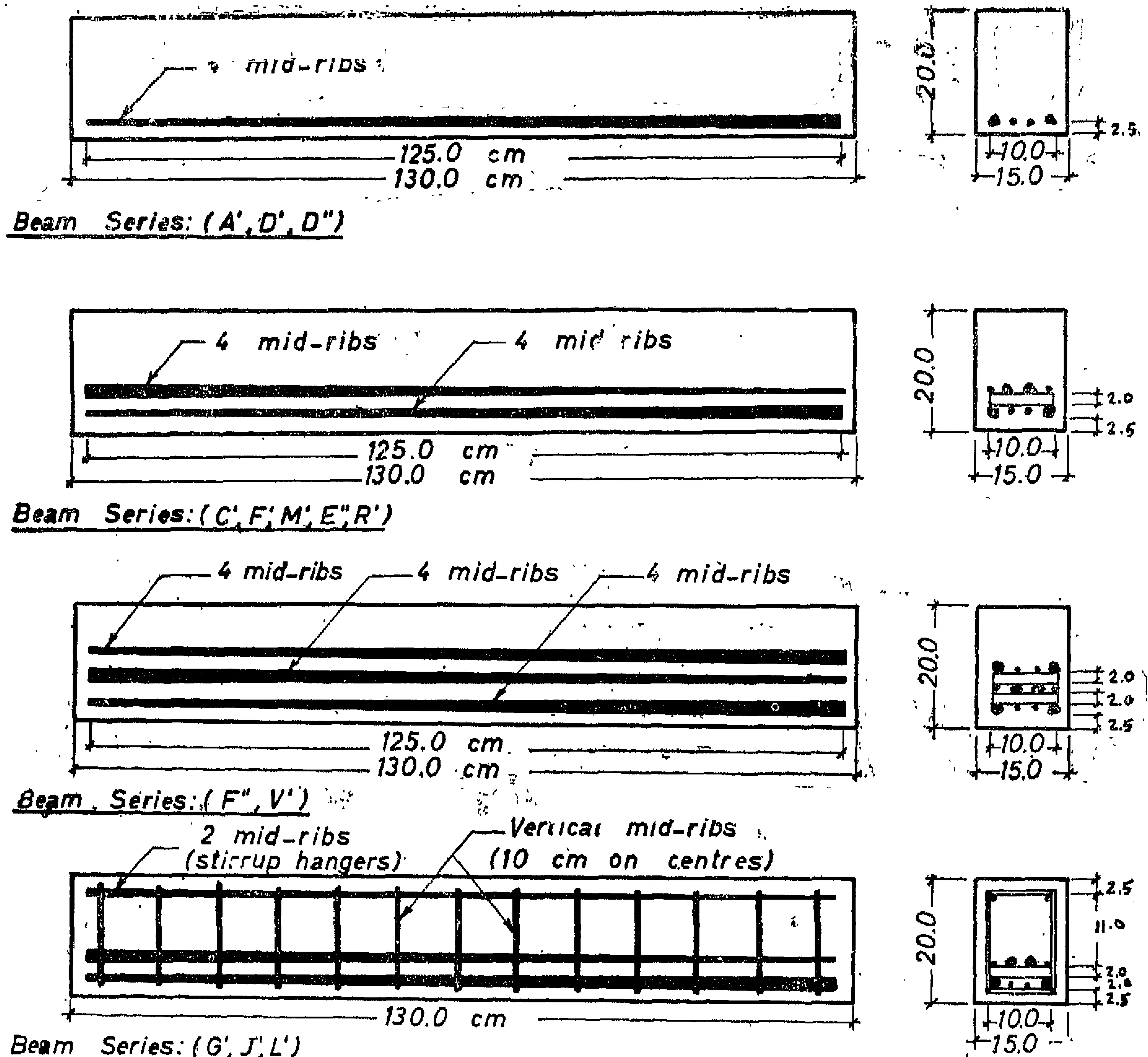


Fig. 7 — RECTANGULAR CONCRETE BEAMS (15 × 20 × 130 cm) REINFORCED WITH DATE-PALM MID-RIBS.

Table (3) — List of Rectangular Concrete Beams Reinforced with Date-palm Mid-ribs.
(all beams were 15 × 20 × 130 cm)

Beam number	*Type of cement*	*Cement content (kg/m³)*	*Type of treatment of rft.*	*Arrangement of date-palm mid-ribs rft.*	*Area of rft. (cm²)*	*Percentage of rft. μ (%)*	*Diagonal tension reinforcement*
A′ — 1	High Early Strength (Supercrete)	250	Untreated	4 mid-ribs, one row	6.5	2.17	None
A′ — 2	»	250	»	» »	6.9	2.30	»
C′ — 1	»	250	»	8 mid-ribs, 2 rows	14.0	4.67	»
C′ — 2	»	250	»	» »	14.8	4.93	»
D′ — 1	»	350	»	4 mid-ribs, one row	6.0	2.00	»
D′ — 2	»	350	»	» »	6.8	2.27	»
F′ — 1	»	350	»	8 mid-ribs, 2 rows	13.4	4.47	»
F′ — 2	»	350	»	» »	14.0	4.67	»
G′ — 1	»	250	»	» »	11.7	3.90	Vertical mid-ribs 10 cm on centres
G′ — 2	»	250	»	» »	12.5	4.17	»
J′ — 1	»	350	»	» »	11.5	3.84	»
J′ — 2	»	350	»	» »	12.2	4.07	»
L′ — 1	Ordinary Portland Cement	250	Two coatings of « Varnish »	» »	12.0	4.00	»
L′ — 2	»	250	»	» »	13.0	4.33	»
M′ — 1	»	250	»	» »	12.8	4.27	None
M′ — 2	»	250	»	» »	12.8	4.27	»
D″ — 1	High Early Strength (Supercrete)	350	One coating of «Solid Bitumen»	4 mid-ribs, one row	6.9	2.30	»
D″ — 2	»	350	»	» »	7.2	2.40	»
E″ — 1	»	350	»	8 mid-ribs, 2 rows	12.0	4.00	»
E″ — 2	»	350	»	» »	12.3	4.10	»
F″ — 1	»	350	»	12 mid-ribs, 3 rows	17.0	5.67	»
F″ — 2	»	350	»	» »	17.5	5.83	»
R′ — 1	»	350	Two coatings of « Primer »	8 mid-ribs, 2 rows	12.0	4.00	»
R′ — 2	»	350	»	» »	12.6	4.20	»
V′ — 1	»	350	Two coatings of « P.F.4 »	12 mid-ribs, 3 rows	18.0	6.00	»
V′ — 2	»	350	»	» »	18.8	6.27	»

* Cement content in kilograms per cubic meter of finished concrete.
* μ = area of reinforcement divided by total cross sectional area of the concrete beam.

An evaluation of test results obtained from both the bond and absorption tests, concerning the choice of the most suitable water-repellent treatment for mid-ribs, gave the following conclusions :

1. Concerning the bond strength, it seems that "Varnish" and "Primer" are the most suitable treating agents, provided that they are to be applied in double coatings.

2. Regarding the ability of water-repellency, treatment with "Varnish" seems to be superior than the others. However, since all the absorption tests were carried out using fresh drinking water, there would be a possibility for a chemical reaction with cement in the concrete mix. This was detected in further tests carried out on concrete beams reinforced with mid-ribs treated with "Varnish".

3. Although the "Primer" treatment gave comparatively higher values for water absorption than "Varnish" after the five-days period, it would be convenient to use "Primer" since it gave values of water absorption over the first day close to those given by "Varnish".

4. Concerning the price and cost, it was found that "Varnish" costs seven times as much as "Primer" treatment. In spite of the coverage area of "Varnish" coating which is 12 m^2/kg, approximately double as much as that of "Primer" treatment, "Varnish" is still much more expensive.

CONCRETE STRUCTURAL MEMBERS REINFORCED WITH MID-RIBS

An experimental investigation was carried out on concrete beams and columns reinforced with date-palm mid-ribs in an effort to obtain an evaluation of the effectiveness of the material as a substitute for steel reinforcement.

The carried out tests were classified into the following three groups :

a) Tests on beams (15 × 20 × 130 cm).

b) Tests on beams (22.5 × 30 × 300 cm).

c) Tests on columns (20 × 20 × 200 cm).

a) Tests on Beams (15 × 20 × 130 cm) :

All beams used in this group of tests were rectangular in section with a width of 15 cm, a total depth of 20 cm, and a total length of 130 cm. They were longitudinally reinforced with different percentages of mid-ribs with and without diagonal tension reinforcement, treated with various types of water-repellent agents, and fabricated using two types of cement with two cement contents.

They were made to be tested in flexure in order to determine :

1. Effect of percentage of longitudinal mid-ribs reinforcement.

2. Effect of diagonal tension mid-ribs reinforcement.

3. Effect of type of water-repellent treatment of reinforcement.

4. Effect of type of cement and cement content used in the concrete mixes.

5. Comparative study between the behaviour of steel and mid-ribs reinforced concrete beams under loads.

In fabricating these concrete beams, two cement contents of 250 and 350 kg/m^3 were used together with two types of cement; namely Ordinary Portland cement and High Early Strength cement. The designed mix proportions by weight were just the same as those used in fabricating the concrete bond cylinders.

sections as much alike as possible. For each water-repellent agent two groups of test pieces were made, the first treated with one brush coating and the other with two brush coatings. One control untreated group of three test pieces was also prepared for comparison.

It was decided not to test the "Solid Bitumen" treatment for water absorption, regarding the obtained bond test results indicating complete failure in bond strength due to the high lubricating effect of the treating agent.

After being weighed, the treated and untreated test pieces were completely immersed in fresh water at room temperature. For five days, the test pieces were removed periodically from water and weighed to determine the amount of absorbed moisture. It was believed that testing the mid-rib test pieces for only five days would be reasonable, since it is only the absorption values over the first few hours during setting and initial drying of concrete that are significant.

Curves of the gain in moisture content with time are shown in Figures (5,6) for the different water-repellent agents applied either in single or double coatings.

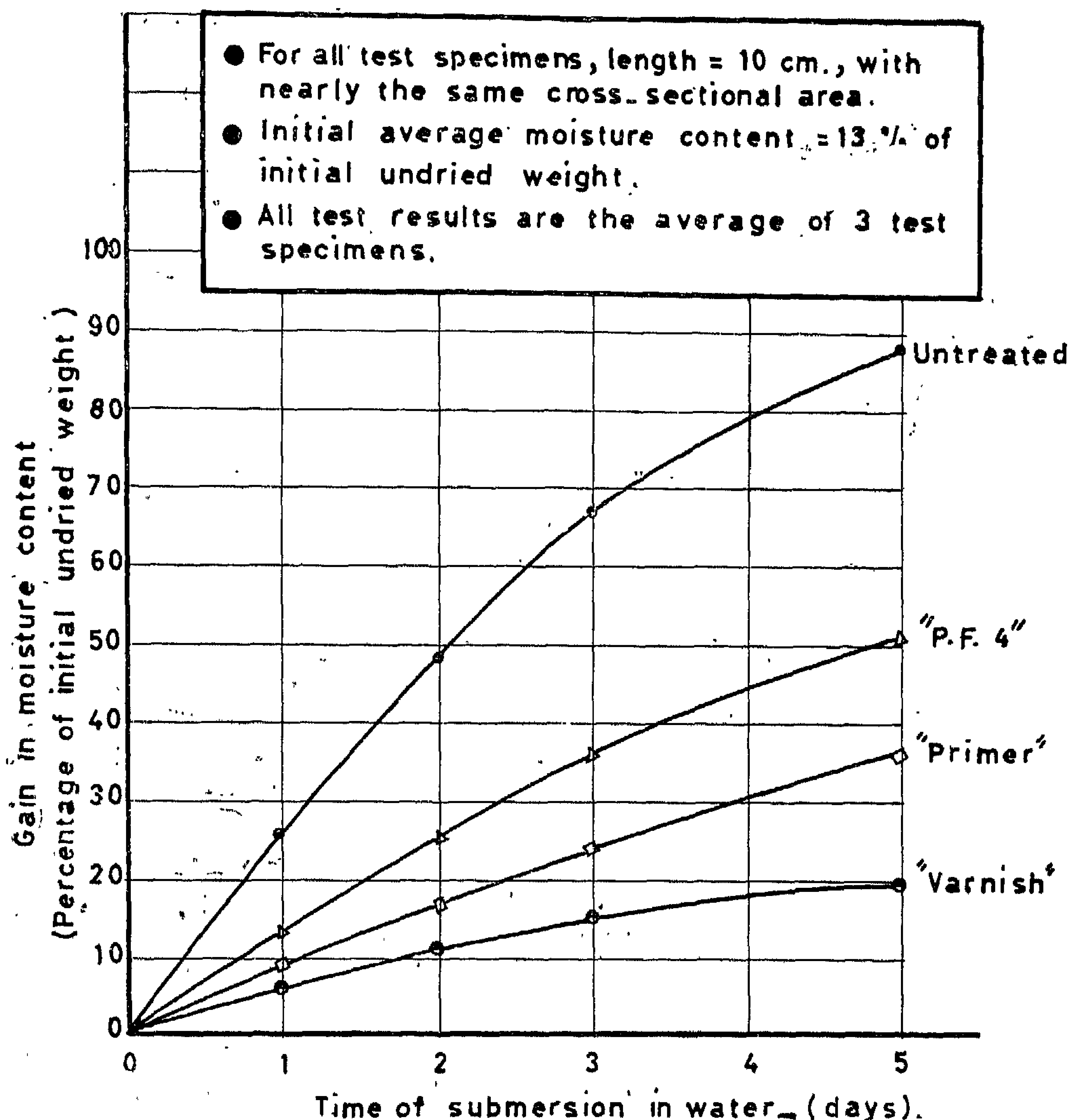


Fig. 6. EFFECT OF TYPE OF TREATMENT ON WATER ABSORPTION OF DATE-PALM MID-RIBS.
(All types of treatment were applied in two coatings)

for two types of cement; namely Ordinary Portland cement and High Early Strength cement commercially named "Supercrete". For concrete mixes of cement content 250 kg/m^3, the cement-sand-gravel mix proportions by weight were 1 : 2.77 : 5.15 with a water-cement ratio (W/C) of 0.60. Those for concrete mixes of cement content 350 kg/m^3 were 1 : 1.88 : 3.50 with (W/C) ratio of 0.44.

In treating the reinforcing mid-ribs, care was taken to add sand to the external layer of treatment in the proper amount and at the proper time so as to make it stick effectively to the treated surface.

The average test results of bond strength between mid-ribs and concrete are recorded in Table (2).

b) Absorption Tests :

Small seasoned test pieces of mid-ribs were prepared, then divided into groups each containing three test pieces having the same length of 10 cm and all with their cross

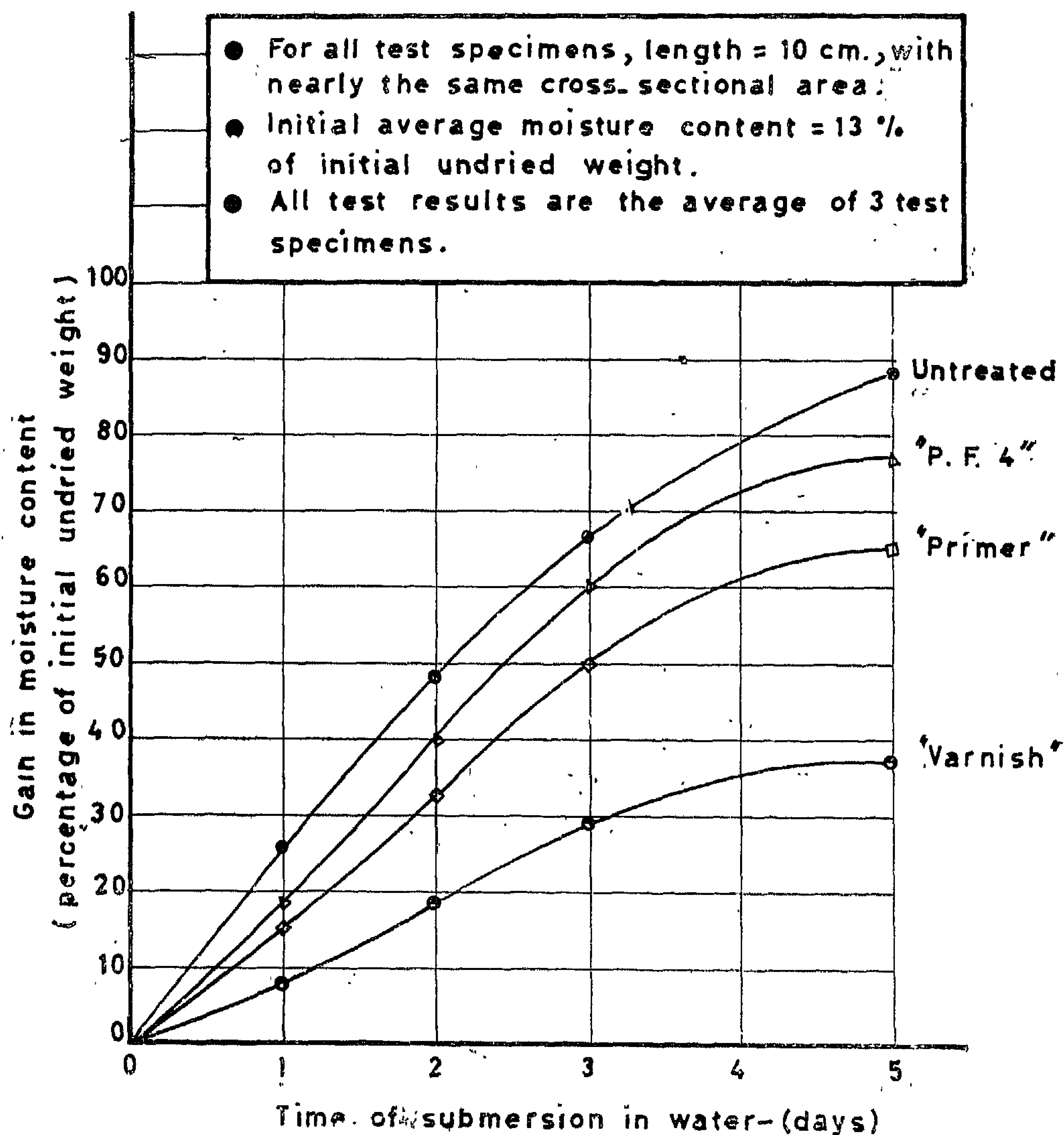


Fig. 5 - EFFECT OF TYPE OF TREATMENT ON WATER ABSORPTION OF DATE - PALM MID-RIBS
(All types of treatment were applied in one coating).

green unseasoned mid-ribs without treatment. The test results showed complete failure in bond due to the drying and shrinkage of mid-ribs while encased in concrete. Considering these test results, the use of green unseasoned mid-ribs was abandoned at an early stage and all the tests were only made on mid-ribs seasoned by air drying in shade for seven weeks.

In fabricating the concrete bond cylinders, four concrete mixes, having the same combined aggregate grading, were made using two cement contents of 250 and 350 kg/m³

Table (2) — Average Results of Tests on Bond between Concrete and Seasoned Date-palm Mid-ribs.

(in all series, concrete cylinders 15 × 15 cm were cured using wet burlap and sand until tested at age of 28 days.)

Series number	*Type of cement*	*Cement content (kg/m³)*	*Type of treatment*	*Control cubes C (kg/cm²)*	*Average bond strength (kg/cm²)*
A′	Ordinary Portland Cement	250	Untreated	160	3.8
B′	»	250	Two coatings of « Varnish »	160	8.2
C′	»	350	Untreated	240	5.1
D′	»	350	Two coatings of « Varnish »	240	8.9
E′	High Early Strength (Supercrete)	250	Untreated	195	5.7
I′	»	250	Two coatings of « Primer »	190	9.2
J′	»	250	Two coatings of « Varnish »	190	9.5
K′	»	350	Untreated	265	6.8
M′	»	350	One coating of « Solid Bitumen »	265	0.6
N′	»	350	Two coatings of « P.F. 4 »	250	8.2
O′	»	350	Two coatings of « Primer »	260	9.9
P′	»	350	Two coatings of « Varnish »	260	10.4

* Cement content in kilograms per cubic meter of finished concrete.

* C = Compressive strength of control cubes at age of 28 days.

* Bond strength = Load at first slip, of free end of test specimen, divided by surface area in contact with concrete.

* All test results are the average of 3 test specimens.

to select the most suitable agent, two groups of tests were devised. The first group was made to ascertain the bond strength developed between concrete and mid-ribs treated wi' the various agents. Tests from this group were also made to compare between the values of bond strength for the treated and untreated mid-ribs. The second was carried out to evaluate the ability of each treating agent to prevent water absorption by the treated mid-ribs.

a) Bond Tests :

Concrete cylinders 15 cm in diameter and 15 cm high were prepared, each provided with a central reinforcing seasoned mid-rib and tested using the pull-out test procedure. Preliminary bond tests were made using

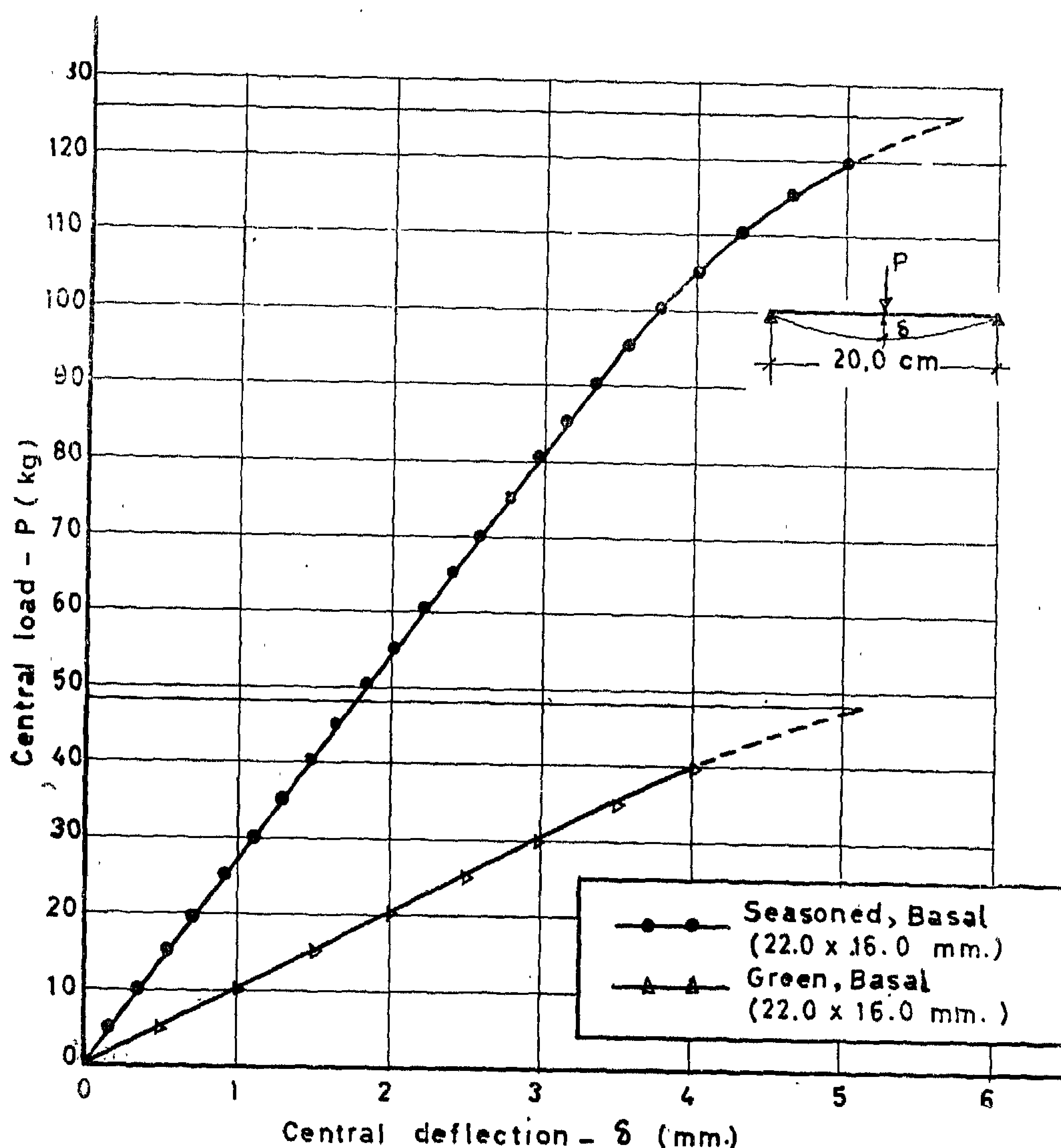


Fig. 4 – TYPICAL LOAD – DEFLECTION DIAGRAMS FOR GREEN & SEASONED DATE – PALM MID – RIBS IN FLEXURE.
(Section of failure was considered as a triangle having the base width W = 22.0 mm. and the depth d = 16.0 mm.)

Table (1) — Summary of the Average Values of Mechanical Characteristics of Date-palm Mid-ribs.

Mechanical Characteristics	*Green Mid-ribs*		*Seasoned Mid-ribs*	
	distal	*basal*	*distal*	*basal*
Ultimate tensile strength (kg/cm^2)	730	636	1230	1450
Modulus of rupture in flexure* (kg/cm^2)	675	485	1063	1258
Modulus of elasticity in tension (kg/cm^2)	127,600	103,800	182,000	204,000
Modulus of elasticity in flexure (kg/cm^2)	89,900	65,300	155,600	167,700

* Calculated at the fiber of maximum tensile stress using the formula ($f = M.y/I$) with $y = d/3$ and $I = W.d^3/36$, where section of failure was considered as a triangle having the base width (w) and the depth (d).

WATER-REPELLENT TREATMENT FOR MID-RIBS REINFORCEMENT

Date-palm mid-ribs, being used as reinforcement in concrete members, would be subjected to high percentages of moisture existing in the concrete mass during the first few hours after casting. It was found, therefore, that using a suitable water-repellent treatment would be essential to ensure volume constancy of the reinforcing material while encased in concrete, hence eliminating the swelling cracks destroying the concrete member.

It was believed that the most suitable water-repellent treatment would be that which gives the higher values of bond strength between concrete and reinforcement and the lower values of water absorption, together with the reasonable economical cost.

The water-repellent agents selected in this investigation for treating the mid-ribs reinforcement were those commercially available and economical in price. The chosen agents are as follows :

- *"Flatting Varnish 601" :*

A commercial name for a locally produced varnish used for painting different types of woody surfaces, including furniture and flooring, to give a hard shiny transparent cover.

- *"Shell Pipe Primer" :*

A commercial name for a blown bitumen paint locally produced by Misr Petrol Company.

Composition: 35% blown bitumen R 115/15
65% solvent (mineral turpentine + toluene).

- *"P.F. 4" :*

A commercial name for a special bitumenous paint locally produced by Misr Petrol Company.

Composition: 46% hard bitumen H 80/90
54% solvent (Naphta)

- *"Solid Bitumen" :*

A hard grade bitumen locally produced and used for road surfacing as a hot molten mix at a temperature of about 200°C.

All of the above water-repellent agents were applied in brush coatings on the surface of the material to be treated. In order

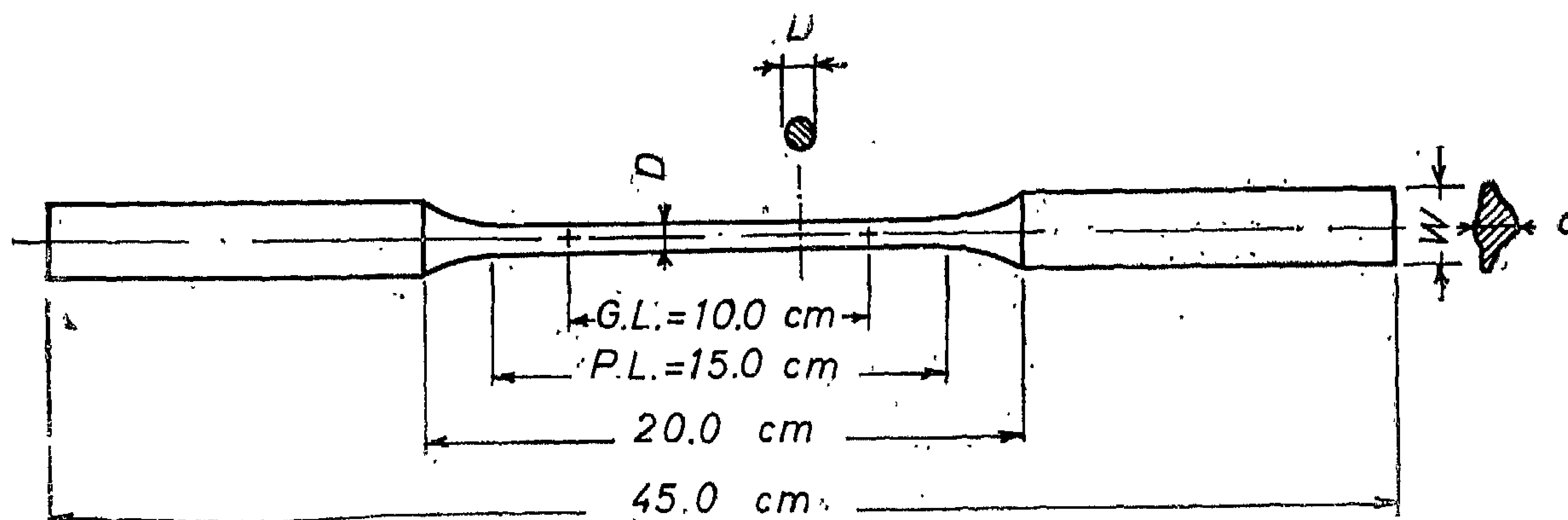


Fig 2– Tensile Test Specimen of Date-palm Mid-ribs

is expected to probably add to strength and stiffness.

For all of the specimens tested in flexure, an initial compression failure was most commonly recorded, followed by an ultimate tensile failure causing fracture of the section.

In calculating the moment of inertia used in obtaining the modulus of rupture as well as the modulus of elasticity in flexure, the cross sectional area of the tested specimen was assumed to be a triangle with its base to the tension side. Accordingly, the modulus of rupture calculated at the fiber of maximum tensile stresses was obtained by substituting into the formula (f = M.y/I) with "y" equals one third of the total depth of the triangle.

The average values of test results for the mechanical characteristics of date-palm mid-ribs in tension and flexure are recorded in Table (1), while typical stress-strain diagrams for green and seasoned mid-ribs in tension and flexure are shown in Figures (3,4). When calculating the average values of strength and stiffness, some values of test results were excluded in order to have the maximum deviation within ± 10% of the average value.

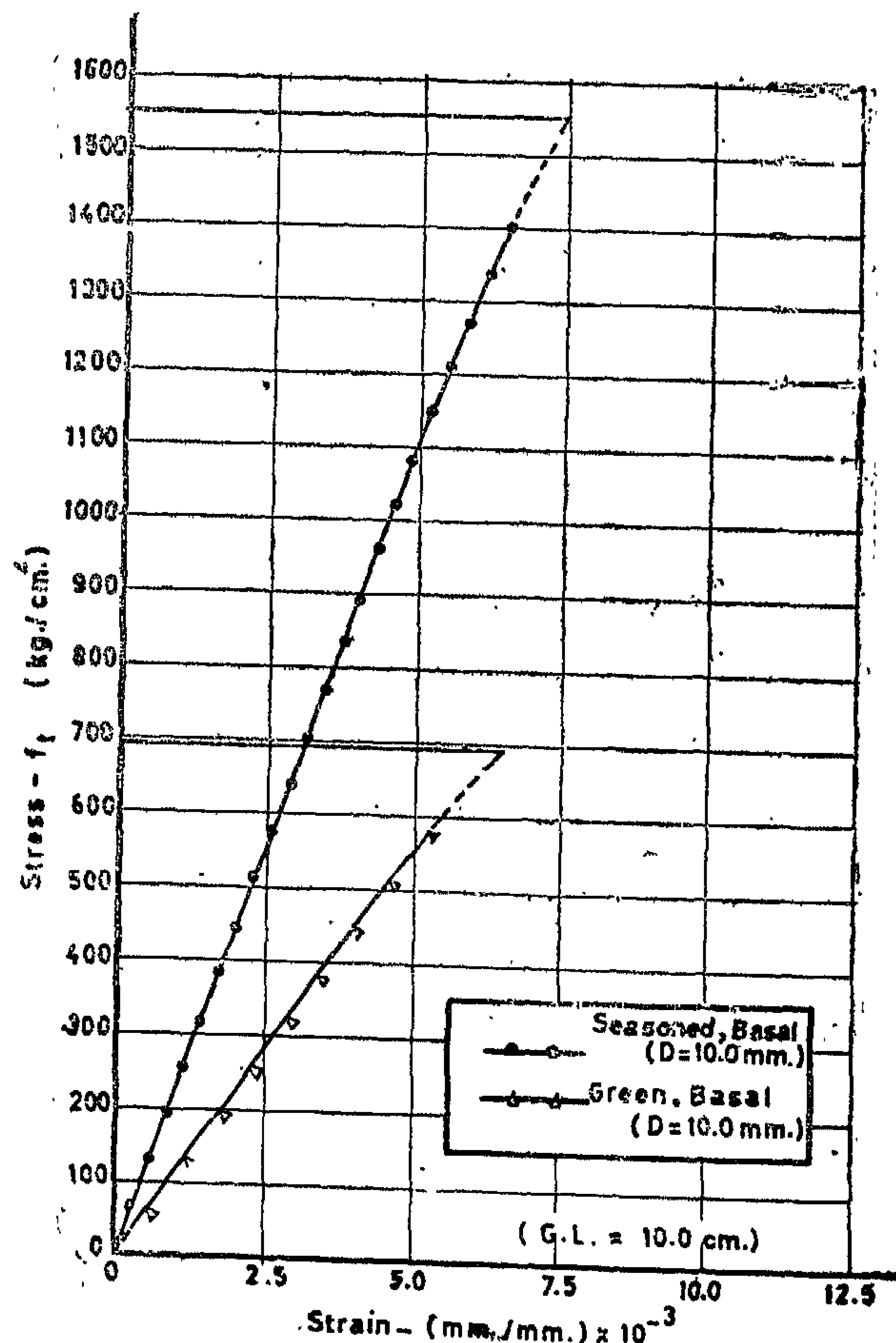


Fig. 3 – TYPICAL STRESS – STRAIN DIAGRAMS FOR GREEN & SEASONED DATE–PALM MID–RIBS IN TENSION

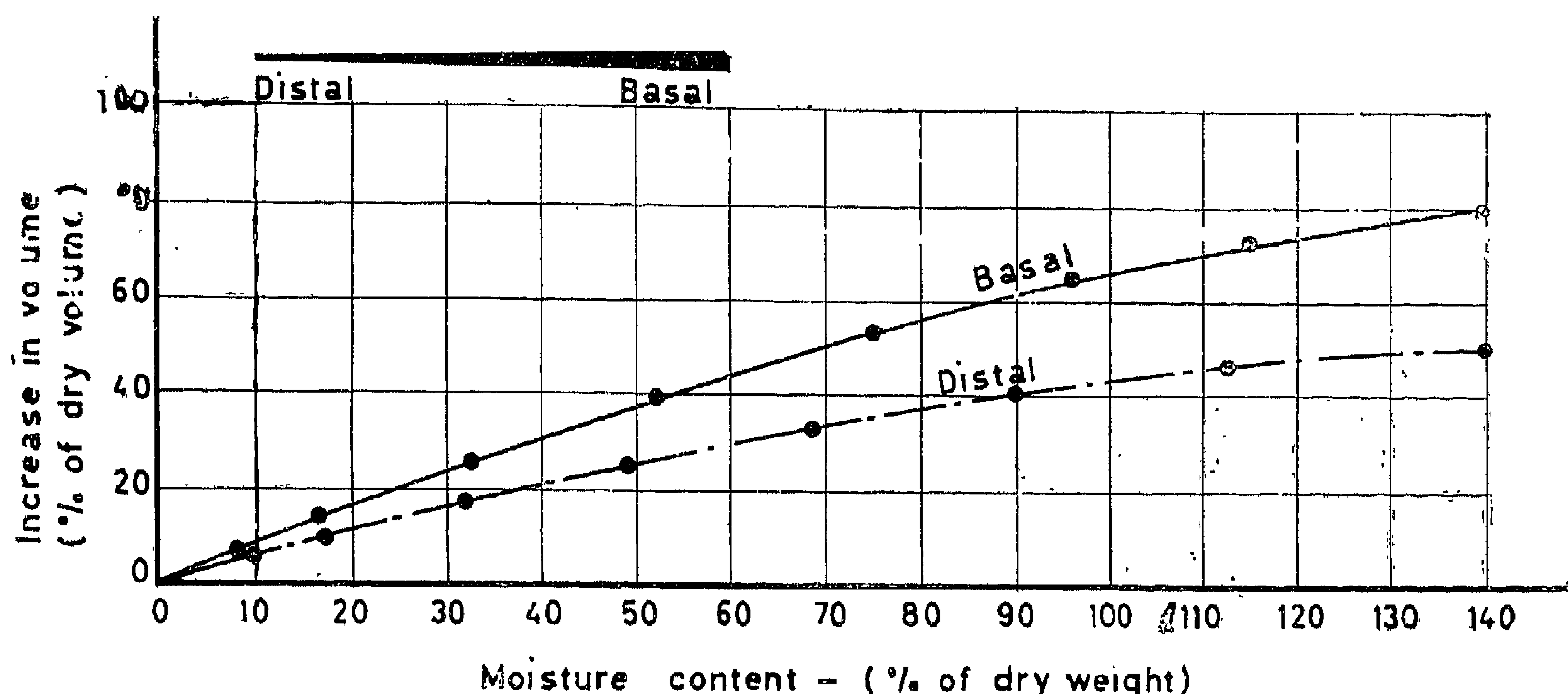


Fig. 1 – EFFECT OF MOISTURE CONTENT OF DATE-PALM MID-RIBS ON THE INCREASE IN VOLUME OF BASAL AND DISTAL PARTS.

(Results are the average of 6 test specimens)

MECHANICAL CHARACTERISTICS OF MID-RIBS

For determining the mechanical characteristics of mid-ribs in tension and flexure, tests were devised to determine the variation in characteristics due to the degree of seasoning and the position from which the test specimen was taken, either from distal or basal parts.

a) *Test Specimens :*

For each of the tension and flexure tests, six individual date-palm mid-ribs in the green unseasoned stage, and another additional six seasoned by air drynig in shade for nearly seven weeks, were used. From each mid-rib to be tested, two specimens from basal end and two additional ones from distal end were cut and prepared.

For preparing tensile test specimens, each specimen was divided into three parts, the end parts for the gripping in the tensile testing machine, and the central part to be prepared for a reduction in size to facilitate tensile breaking. Reducing the size of central part was a free-hand operation done using bastard file, followed by a smooth one, and finishing with sandpaper with the result of having a circular cross section at the central part ending with gradual transitions at its both ends. The shape of the tensile test specimen is shown in Fig. (2). There was no need for a reduction in size operation within the central parts of the specimens required for flexure test.

b) *Test Results :*

A direct tensile failure was recorded for most of the tested tensile specimens, except for a few cases where failure occurred due to a combination of direct tensile failure, at the center of the circular cross section, and splintering of the external fibers.

It is of great importance to know that the preparation of tensile test specimens, done by reducing the cross section along the middle part of the specimen length, necessitated the removal of the external fibrous layer which

From among the locally available and cheap non-metallic materials, date-palm mid-ribs were chosen to be judged as a substitute for steel reinforcement in concrete structural members. This choice was made regarding the unfailing success of the primitively used mid-ribs for roofing native rural houses and making farm-yard fences.

In carrying out this investigation, the following definite objectives were set forth:

1. To establish the main physical and mechanical characteristics of date-palm mid-ribs which would be needed in the design of concrete members reinforced with the material.
2. To find a suitable water-repellent treatment for the mid-ribs reinforcement to ensure its volume constancy and prevent it from being rotten while encased in concrete.
3. To evaluate the effectiveness of mid-ribs as a substitute for steel reinforcement in concrete beams and columns.
4. To establish and recommend practical construction procedures and reliable design principles for load-carrying concrete members reinforced with mid-ribs.

The date-palm mid-ribs used in all the tests carried out in this investigation were obtained from one date-palm species locally named "Amhat Date-palm".

PHYSICAL CHARACTERISTICS OF MID-RIBS

For both distal and basal parts of date-palm mid-ribs, tests were made to determine the natural moisture content, the apparent specific gravity, and the volumetric changes due to variation in moisture.

The percentage moisture content was calculated as the ratio of the loss in weight to the final dry weight of the test specimen, expressed in per cent. The natural moisture content, taken as the average of six test specimens, was found to be 25% for distal parts and 92% for basal parts.

The apparent specific gravity was calculated as the ratio of oven-dry weight of test specimen to its volume obtained by immersing in mercury. Taking the average of six test specimens, the apparent specific gravity was found to be ranging from 0.69 for distal parts, to 0.78 for basal parts.

The determination of volumetric changes due to variation in moisture was found to be essential since the mid-ribs would be subject to high percentages of moisture while encased in the fresh concrete, especially within the first few hours after casting. Accordingly, six test specimens taken from three individual mid-ribs were prepared for each of the distal and basal parts, providing that all have nearly the same dimensions. All the specimens were then oven dried and both the dry weight and volume were determined. Consequently, they were repeatedly allowed to absorb water and in each time the new weight together with the corresponding new volume were obtained.

Calculating the different values of moisture content, given as percentages of dry weight, and the corresponding values of the increase in volume, given as percentages of dry volume, curves shown in Fig. (1) were plotted showing the effect of moisture content on the increase in volume of basal and distal parts.

NON-METALLIC REINFORCEMENT FOR CONCRETE STRUCTURAL ELEMENTS*

By

Prof. Dr. AHMED A. EL-ERIAN
Head of Materials Testing Department
Cairo University

Prof. Dr. MOHAMED M. TEWFIK
Structural Engineering Department
Cairo University

MAHMOUD A. REDA YOUSSEF
B.Sc., M.Sc. (Structural Eng.)
Cairo University

PART 2 — DATE-PALM MID-RIBS

SYNOPSIS

The paper described herein is a part of an investigation studying the possibilities of using cheap and locally available non-metallic materials as reinforcement in concrete members for suitable structural applications. This part reports an experimental investigation carried out on mid-ribs of native date-palms to establish their main physical and mechanical characteristics, to find a suitable water-repellent treatment for the mid-ribs reinforcement, and to evaluate their effectiveness as a substitute for steel reinforcement in concrete beams and columns. An attempt has been also made to establish and recommend practical construction procedures and reliable design principles for concrete structural members reinforced with mid-ribs.

Another part dealing with native bamboo was published earlier.

On the basis of the results obtained through this research, it was concluded that there are certain cases in construction where it would be safe and much more economical to utilise date-palm mid-ribs as a substitute for steel reinforcement. Date-palm mid-ribs are recommended to be used as reinforcement in concrete structural members of small building units as in many of the rural housing projects, especially the one-storey buildings. The material is also highly recommended to be used as reinforcement for various concrete structural precast units.

A special recommendation is given to the authorities to increase the land areas cultivated with date-palms taking an advantage of the reclaimed areas in the New Valley and Al-Tahrir Province as well as Nasser-Lake, at Aswan, whose banks are the ideal spot for the propagation of date-palms.

INTRODUCTION

This investigation was made under the immediate incentive of saving iron ore and steel to cover the demands of the national economic development plan in various sectors, to serve for the national defence requirements, and to meet the increasing local consumption of steel in the field of construction.

* This paper is based on an M. Sc. Thesis by the third author.

INFORMATION

- The editors welcome for publication engineering researches and articles as well as discussions on any material appearing in this periodical.
- This periodical does not hold itself responsible for the opinions expressed in it.
- Any material intended for publication must be sent to the Secretariat at the address of the Engineering Society at Cairo.

SUBSCRIPTIONS

All members of the Engineering Society at Cairo are ipso facto subscribers of this periodical.

Subscription for engineers P.T. 60 per annum.

Subscription for others P.T. 200 per annum.

HEAD OFFICE

Egyptian Society of Engineers,

28, Ramses Avenue, Cairo. Tel. 52106

ADVERTISEMENTS

Sole agents for advertisements appearing in this periodical:

Moassasset Misr for Printing and Publication,

19, Str., Souk El Tawfikieh, Cairo.

Tel. 72192

JOURNAL OF
THE EGYPTIAN SOCIETY OF ENGINEERS
U.A.R.

QUARTERLY SCIENTIFIC PROCEEDINGS

ISSUED BY

THE EGYPTIAN SOCIETY OF ENGINEERS—U.A.R., CAIRO

Vol. X — No. 2, April-May-June 1971

CONTENTS

ENGLISH SECTION

Page

Mon-Metallic reinforcement for Concrete Structural Elements.
Dr. AHMED A. EL-ERIAN, Dr. MOHAMED M. TEWFIK, MAHMOUD A. REDA YOUSSEF 7

Bending moments in rectangular concrete tanks
Dr. M. BAKHOUM, Dr. M.M. TAWFIK, Dr. MOHAMED H. EL-KATEB 29

A study on the design of impervious blankets in earthen dams with particular reference to the High Dam at Aswan.
Dr. A.H. EL-RAMLI, HASSAN ABDOUN 46

IR Sources detecting and Tracking systems.
Dr. A.H. HALLOUDA 55

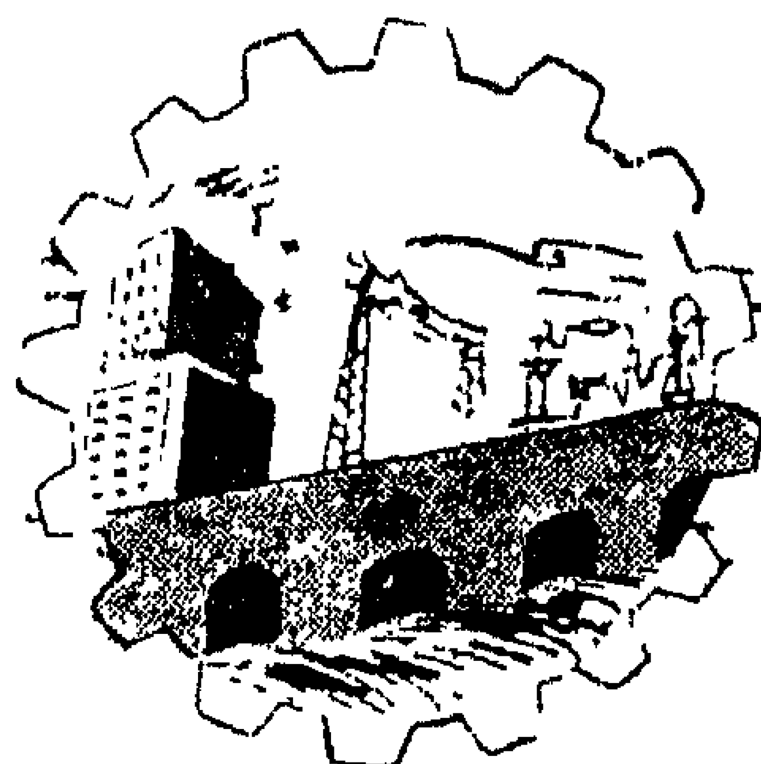
Some hydrogeochemical studies of underground water of Ras-Gharib Oil-field and its potentials for industry.
Dr. NASRY Z. BISHAY 70

Design of Modern Crude Oil Loading Facilities.
Dr. IBRAHIM M. EL-ASSIOUTI 85

ARABIC SECTION

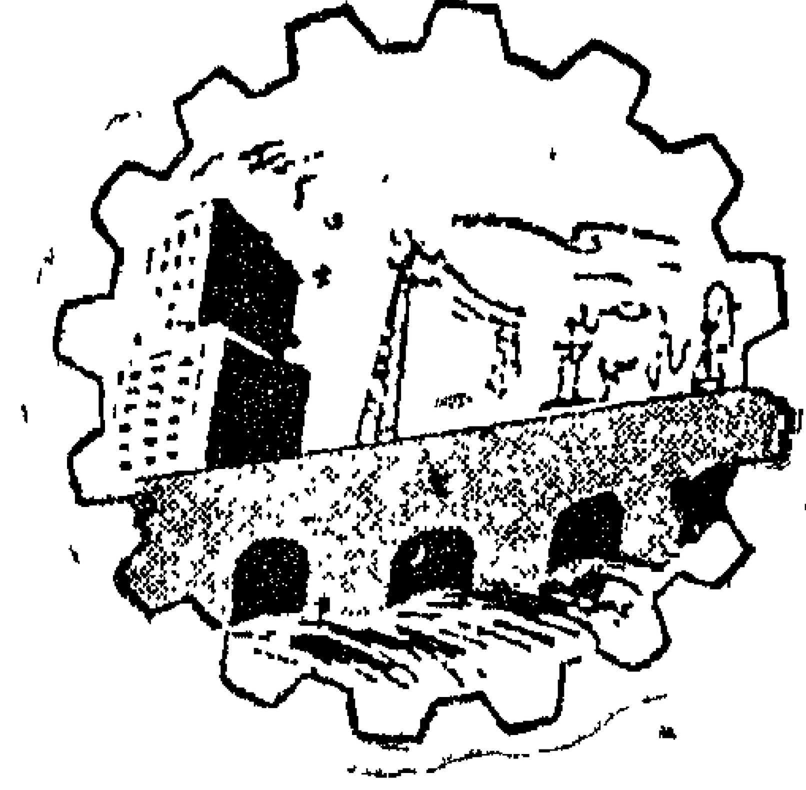
The role of standardization in generation and Distribution of electric energy.
Dr. FOAD TAHER 7

«Mondiale» Press—Cairo



JOURNAL OF THE EGYPTIAN SOCIETY OF ENGINEERS U. A. R.

April-May-June 1971
Vol. X
No. 2



مجلة

جمعية المهندسين المصرية

يوليو - اغسطس - سبتمبر ١٩٧١ | المجلد العاشر | العدد الثالث

رقم الإيداع بدار الكتب المصرية ٢٩٨ / ١٩٦٩

المطبعة العالمية ١٦، ١٧ شارع ضريح سعد بالقاهرة

مجلة

جمعية المهندسين المصرية

مجلة علمية هندسية - تصدرها كل ثلاث شهور

جمعية المهندسين المصرية بالقاهرة

السنة العاشرة | العدد الثالث | يوليو - أغسطس - سبتمبر ١٩٧١

محتويات هذا العدد

القسم العربي

صفحة

- الأقلمة المناخية للمواد والمنتجات الكهربائية ٧
- مشاكل النقل البرى (بالسيارات) للركاب بين المدن وفى الريف فى الدول النامية ... المهندس سمير فهمى ١٥

القسم الأفرنجى

- تأثير السرعات الحرجة «الرفرفة» بزاوية سحب الحافة الأمامية لأسطح التحكم المتحركة كلية ... ... — للدكتور المهندس محمد يوسف محمد عفيفى و د. المهندس صبرى فوزى جرجس ٧
- سريان الغازات خلال الأوساط المسامية ... ... — للدكتور المهندس محمد فكرى شابى ١٩
- المعادلات الهيدروديناميكية للانسياب ... ... — للدكتور المهندس محمد حمدى الكاتب ٢٨
- الضغوط العرضية فى الصوامع ... ... — للدكتور المهندس صبرى سمعان ٣٣
- تأثير القص على التصميم الحدى للخرسانة المسلحة ... ... — للدكتور المهندس محمود نصر ٤١
- نفخ الأفران العالية بحلوان بالبخار والمازوت ... ... — للدكتور المهندس أبو بكر مراد والدكتور المهندس سامى عطيوه والدكتور المهندس سعيد عز والمهندس محمد أبو السعادات ٤٦
- دراسة تجريبية وعملية عن استخدام المفرقعات فى إزالة الصخور من مناطق المشروع ... ... — للدكتور المهندس على اسماعيل الجوهرى والدكتور محمد فتحى العطار ٥٩
- تأثير الاجهادات المتغيرة والثابتة على قدرة المعادن على كبت الاهتزازات — للدكتور المهندس محمد يوسف محمد عفيفى والمهندس كمال عبد الفتاح مصطفى ٦٨

بيانات

مقر المجلة

جمعية المهندسين المصرية

٢٨ شارع رمسيس بالقاهرة

تليفون : ٥٢١٠٦

- جميع أعضاء جمعية المهندسين مشتركون فى المجلة بحكم عضويتهم
- الاشتراك السنوى لغير الأعضاء : ٦٠ للمهندس ، ٥٠٠ للهيئات
- ترسل البحوث والموضوعات والتعليقات إلى أمانة التحرير بمقر جمعية المهندسين المصرية بالقاهرة
- ترحب المجلة بما يرسل إليها من بحوث وموضوعات هندسية وأى تعليقات علمية للمناقشة
- المجلة غير مسئولة عن الآراء التى تنشر بها وتعبر عن رأى كاتبها فقط .

لجنة التحرير

الاقلمة المناخية للمواد والمنتجات الكهربائية

تستخدم المعدات والأجهزة الكهربية فى مختلف بقاع العالم تحت ظروف إقليمية ومناخية متباينة تبعاً لمكان وجودها وعملها . وتتأثر خواص المواد الكهربية وعمل المعدات والأجهزة الكهربية بكثير من العوامل الجوية . لذلك كان من الطبيعى أن تهتم الهندسة الكهربية بدراسة العوامل المناخية وتأثيرها على المواد والمعدات الكهربية ، وتقسيم العالم إلى أقاليم مناخية من وجهة نظرها بطريقة تختلف عن التقسيمات الجغرافية للأقاليم المناخية . إذ يغلب اهتمام التقسيمات الجغرافية للأقاليم المناخية بالنواحى الحيوية والحرارية دون عوامل أخرى مثل عامل رطوبة الهواء الذى يحظى بأهمية بالغة فى التقسيم المناخى الذى تحدده الهندسة الكهربية .

وسنتكلم أولا عن العوامل المناخية وتأثيرها على المواد والمعدات الكهربية ، ثم بعد ذلك عن تقسيم العالم إلى أقاليم مناخية من وجهة نظر الهندسة الكهربية .

أولا — العوامل المناخية وتأثيرها على المواد والمعدات الكهربية :

العوامل المناخية التى تهم الهندسة الكهربية هى درجة حرارة الهواء ونسبة الرطوبة فيه والضغط والمؤثرات البيلوجية وتلوث الجو والإشعاعات والعواصف الرعدية .

(١) درجة حرارة الهواء :

درجة حرارة الهواء تكون إما مرتفعة أو منخفضة أو سريعة التغيير . وارتفاع درجة حرارة الهواء المحيط (أكثر من + ٤٠°م) قد يتسبب فى ليونة العوازل وفى تلف خواصها العازلة ويساعد على سرعة تعميرها وتقصير فترة حياتها . كما أن ارتفاع درجة حرارة الهواء المحيط قد يتسبب فى زيادة حرارة المعدات والأجهزة الكهربية فوق معدلها مما يخل بسلامة أدائها ويعرضها للتلف .

فإذا وضعنا ارتفاع درجة حرارة الهواء المحيط فى الاعتبار يمكن تصميم معدات وأجهزة كهربية واختيار مواد عازلة تلائم ظروف التشغيل هذه ، على أن يتم ذلك على أساس اقتصادى . ودرجة حرارة الهواء المنخفضة (أقل من — ٤٠°م) تكون سبباً فى أن تفقد المواد مرونتها وتزيد لزوجة الشحوم وتتغير الخواص الميكانيكية لبعض المواد .

وتؤدى سرعة التغير فى درجة الحرارة إلى ظهور إجهادات ميكانيكية فى أجزاء المعدات .

٢ — نسبة رطوبة الهواء :

درجة رطوبة الهواء تكون إما مرتفعة أو منخفضة أو متغيرة وارتفاع نسبة رطوبة الهواء المحيط ينتج عنه أن يتشوه العازل بالانتفاخ . كما أن امتصاص العازل للرطوبة يتلف خواصه الكهربية والميكانيكية. ويساعد ارتفاع الرطوبة على سرعة تآكل المعادن .

وينتج عن انخفاض نسبة رطوبة الهواء المحيط أن يتشوه العازل بالانكماش ، كما أن تجفيف العازل يتلف خواصه الميكانيكية . وتغير نسبة الرطوبة يساعد على تكثف الرطوبة على المعدات الكهربية . كما أن تكوين الندى يتلف الخواص الكهربية لأسطح العوازل .

وفى حالة وجود درجة حرارة مرتفعة بالإضافة إلى نسبة رطوبة عالية يحدث ذلك أضراراً بالغة لخواص عزل عديد من المواد إذ يقلل من المقاومة الكهربية ويزيد من زاوية فقد العزل والمجاوزية وينقص من الشدة الكهربية .

٣ — ضغط الهواء :

ضغط الهواء المنخفض يقلل من شدة عزل الهواء ، كما أنه يضر بالتهوية . أما الأعاصير فتحدث أجهدات ميكانيكية للتركيبات الكهربية عند اصطدامها بها .

٤ — تلوث الجو :

يتلوث الجو بأتربة السهول وبرمال الصحارى وبأملاح البحر وبالمواد الكيماوية الناتجة عن الصناعة . والأتربة والرمال التى تثيرها الرياح تساعد على زرجنة الأجزاء المتحركة وتآكل أجزاء المعدات الكهربية .

كما أن الأتربة والرمال فى السهول والصحارى والضباب المملح والأملاح فى الأماكن البحرية والمواد الكيماوية فى المناطق الصناعية تترسب على أسطح المواد العازلة وتكون عليها غشاءاً يتلف خواص السطح ، هذا بالإضافة إلى أنها تساعد على تآكل الأجزاء المعدنية .

ويمكن أن تطلى الأجزاء المعدنية المعرضة لذلك بغشاء يحميها من التآكل . ولحماية المعدات الكهربية أثناء النقل والتخزين تغلف عادة بأحكام بمادة إصطناعية لاتنفذ منها الأتربة والأملاح .

٥ — المؤثرات البيولوجية :

درجة حر الحرارة العالية للهواء وخاصة المصحوبة بنسبة رطوبة مرتفعة وأمطار تساعد على سرعة نمو كائنات ميكروسكوبية ونباتات وحيوانات ضارة . وعندما تصل الفطريات والكائنات الميكروسكوبية إلى مولد يمكن أن تكون غذاءاً لها فإنها تتكاثر بسرعة وتسبب أضراراً بالغة لتلك المواد ، وقد تتلفها كلية فى بعض الأحيان .

ويلاحظ أن لبعض المواد العازلة حساسية شديدة للعفن الذى ينمو عليها بسرعة ويتلفها . ومن هـذه المواد ذات الأساس السليولوزى مثل الورق والخشب وغزل القطن وكذلك طبقات الورنيش التى تستخدم زيوت تجفيف نباتية مثل زيت بذر الكتان .

وكقاعدة لاينمو العفن عملياً على المواد العازلة الغير عضوية كما أن المركبات العضوية التى تحتوى على النتروجين والكلور والزئبق تسمم الفطريات ولا تساعد على نموها ويمكن تغطية العوازل بمواد مسممة للفطريات لحمايتها منها . وتوجد حشرات مختلفة مثل الأرضه ، وقوارض مثل الفئران لها القدرة على إتلاف بعض العوازل والكابلات . كما أنها تسبب فى حدوث قصر بين الوصلات فى التركيبات والمعدات الكهربية .

٦ — الاشعاعات :

التعرض لأشعة الشمس لمدة طويلة يكون له تأثير ملحوظ على عديد من المواد العازلة كالكاوتشوك وزيت المحولات مثلا إذ يعجل بتعميرها وخاصة فى حالة اتصال أوكسوجين الهواء مباشرة بها . وتؤثر الأشعة تحت الحمراء من طيف أشعة الشمس على المواد العازلة تأثيراً حرارياً .

أما الأشعة فوق البنفسجية من طيف أشعة الشمس فلها تأثير ضار بكثير من المواد العضوية ، إذ تقلل من مرونتها ومن متانتها الميكانيكية وتسبب تشققها وسقوط طبقة الورنيش من عليها .

الأشعة الذرية وأشعة إكس المستخدمة فى المعدات الحديثة تغير من الخواص الـكهربية والطبيعيه والـكيماوية المواد . فمثلا تزيد المقاومة الـكهربية للنحاس والمواد موصلة أخرى ، وتتلف عمل النصف موصلات . أما العواصف الرعدية فتعرض المعدات الـكهربية للدمار .

ثانيا : تقسيم العالم إلى أقاليم مناخية من وجهة نظر الهندسة الـكهربية .

توجد فى العالم كثير من الظروف المناخية المختلفة مما يتطلب تقسيمه إلى أقاليم مناخية محدودة لها تقريباً نفس التأثير على المواد والمعدات الـكهربية . وعليه يمكن اختيار المواد وتصميم المعدات لتقاوم تأثير العوامل الجوية للأقليم المناخى التى تعمل به ، دون أن تتعرض لسوء فى الأداء أو قصر فى عمر الخدمة .

ويمكن أن نختار لتقسيم الأقاليم المناخية أحد طريقين . أما طريق أكبر تركيز أو طريق أكبر تمييز .

وطريق أكبر تركيز يؤدى إلى أقل عدد ممكن من الأقاليم المناخية ومن ثم إلى أقل عدد ممكن من الطرازات المناخية التى تصمم لنوع واحد من المعدات ، وهـذا مايلائم طريقة الانتاج بالجملة

أما طريق أكبر تمييز فيؤدى إلى تفصيل كبير للأحوال المناخية فى كل منطقة ، وهذا مايلائم إنتاج قطعة واحدة من المعدات لمكان معين فقط حيث يراعى فى التصميم الأحوال المناخية لمكان التشغيل .

هذا ويمكن أيضاً عمل تقسيم للأقاليم المناخية يوفق بين طريق أكبر تركيز وطريق أكبر تمييز حسب مقتضيات الظروف العملية .

حسب طريق أكبر تركيز يمكن تقسيم العالم إلى الأقاليم المناخية الآتية :

— مناخ استوائى رطب أو جاف — مناخ بارد مناخ عادى .

١ — المناخ الاستوائى الرطب

هو المناخ الذى تكون فيه الرطوبة والحرارة مرتفعة نسبياً ، إذ توجد رطوبة نسبية أعلى من ٨٠ ٪ عند درجة حرارة + ٢٠°م لفترة لاتقل عن شهرين فى ١٢ ساعة يومياً ولمدة لاتقل عن شهرين فى السنة . ويسقط مطر استوائى بغزارة يتجمع إلى ١٠٠ مم فى ١٠دقائق. وتسطع الشمس بقوة . وتنمو النباتات وتعيش الحيوانات الضارة (تنمو بسرعة الفطريات والحشرات والقوارض .. الخ).

ويوجد المناخ الاستوائى الرطب فى مناطق منها غانا وغينيا والـكونغو والهند وباكستان وسيلان وأندونيسيا وجنوب الصين وجنوب اليابان وفلوريدا وبعض ولايات الجنوب الشرقى للولايات المتحدة وكوبا وبعض مناطق الشمال الشرقى لأمريكا الجنوبية .

٢ - المناخ الاستوائى الجاف

هو المناخ الذى فيه يصل المتوسط السنوى لأقصى درجة حرارة على المدى الطويل إلى +٤٠°م أو يزيد . وقدتصل درجة الحرارة فى الظل إلى ٥٥°م وتسطع الشمس بقوة مع رطوبة منخفضة نسبياً وتثير الرياح رمالا وأتربة فى الصحارى والسهول وخاصة عندما يشتد هبوبها . وتنمو كذلك نباتات وتعيش حيوانات ضارة ، ولـكن بدرجة أقل من حالة المناخ الإستوائى الرطب .

ويوجد المناخ الإستوائى الجاف فى مناطق منها الجمهورية العربية المتحدة وتونس ومالى وصحارى شمال أفريقيا وإيران وشبه الجزيرة العربية وشمال الهندوغرب باكستان وصحارى غرب الصين ووسط وجنوب استراليا وكاليفورنيا وجنوب غرب الولايات المتحدة .

٣ — المناخ البارد

هو المناخ الذى يصل فيه المتوسط السنوى لأقل درجة حرارة على المدى الطويل إلى — ٤٠°م أو أقل . ويوجد هذا المناخ فى المناطق الباردة مثل القطب الشمالى وشمال كندا وسيبريا وشمال آسيا .

٤ — المناخ العادى

هو المناخ الذى فيه لايصل المتوسط السنوى لأعلى درجة حرارة إلى أكبر من + ٤٠°م ولا يصل المتوسط درجة حرارة إلى أقل من — ٤٠°م . كما أن عدد الشهور فيها يزيد متوسط ضغط بخار ماء الجو عن ١٥ مم زئبق تكون أقل من ثلاثة شهور .

ويوجد هذا المناخ فى المناطق التى لم يشملها التقسيم السابق للأقاليم المناخية الإستوائية أو الباردة كدول أوربا مثلا .

ثالثا : نموذج تطبيقى

(أ) التقسيم المناخى للجمهورية العربية المتحدة :

تقع ج ع م من حيث التقسيم المناخى فى إقليم إستوائى جاف حسب تقسيم أكبر تركيز . وبتفصيل أكثر يمكن تقسيم ج ع م إلى ثلاث مناطق مناخية كالآتى :

١ — منطقة الساحل الشمالى
٢ — منطقة الدلتا والقاهرة
٣ — منطقة مصر العليا

أخذنا عينات إحصائية لمنطقة الساحل الشمالى هى سيدى برانى والسلوم ومرسى مطروح والاسكندرية ودمياط وبور سعيد .

فصلنا القاهرة عن الدلتا لأهميتها . وأخذنا عينات إحصائية لمنطقة الدلتا هى السرو وبلقاس والمنصورة ودمنهور وطنطا والزقازيق وبنها . ثم أخذنا عينات إحصائية لمنطقة القاهرة هى هليوبوليس والعباسية والأزبكية والجيزة .

أخذنا عينات إحصائية لمنطقة مصر العليا هى الفيوم وبنى سويف والمنيا وأسيوط وقنا ونجع حمادى والأقصر وكوم امبو وأسوان .

اعتمدنا فى معلوماتنا الإحصائية عن الحرارة والرطوبة النسبية وسقوط الأمطار على نشرة مصلحة الأرصاد الجوية عن المعدلات المناخية للعناصر الجوية . وعليه أمكن بالحساب الحصول على الجدول التقريبى التالى :

المنطقة المناخية	المتوسط السنوى			الحرارة		متوسط سنوى رطوبة نسبية ٪	المتوسط السنوى للمطر مم		
	لأقصى حرارة م°	لأقل حرارة م°	للحرارة م°	أقصى	أقل		كلى	عدد أيام	عدد أيام
الساحل الشمالى	٢٤	١٦	١٩,٥	٤٧	—٢	٧٣	١٢٤	٢٨	٢١
الدلتا	٢٨	١٤	٢٠,٥	٤٧	—٢	٧٥	٥٥	١٦	١٢
القاهرة	٢٨	١٤	٢٠,٥	٤٨	—٤	٦٨	٢٤,٥	١٠	٥,٥
مصر العليا	٣٢	١٥	٢٣,٠	٥١	—٧	٢٩,٥	معدم	معدم	معدم

(ب) تحليل مناخي لجمهورية مصر العربيـة :

بالنسبة للحرارة فظاهر من الجدول الموضح بعاليه أن الحرارة تزيد كلما اتجهنا من الساحل الشمالي نحو الجنوب حتى أسوان حيث وصلت أقصى درجة حرارة إلى ٥١°م. هذا بالإضافة إلى أن التغير في درجة الحرارة بين الليل والنهار ومن وقت لآخر يصل في مصر العليا إلى أكثر من ضعف قيمته على الساحل الشمالي ومن المعروف أن سرعـة التغير في درجة الحرارة تؤدى إلى ظهور إجهادات ميكانيكية في أجزاء المعدات .

فيما يختص بالرطوبة النسبية — فظاهر أنها تنخفض كلما اتجهنا من الساحل الشمالي نحو الجنوب. ولـكن الرطوبة تعتمد على ظروف المنطقة الموجودة بها وتتغير بتغير تلك الظروف . فمثلا يحتمل ارتفاع نسبة الرطوبة فى مناطق مصر العليا التى يتحول فيها رى الحياض إلى رى دائم أو التى ستزرع فيها مناطق جديدة نتيجة لمشروع السد العالى .

تساقط المطر على منطقة الساحل الشمالى له متوسط سنوى ١٢٤ مم وعدد الأيام التى يسقط فيها مطر ١,٠ مم أو أكثر حوالى شهر في السنة أما عدد الأيام التى يسقط فيها مطر ١٠,٠ مم أو أكثر فهى ثلاثة أسابيع ثم يقل المطر فى منطقة الدلتا إلى حوالى خمس معدلة على الساحل ويستمر المطر فى النقصان كلما اتجهنا جنوبا إلى أن ينعدم تقريباً فى مصر العليا .

يظهر تأثير المطر بشكل واضح على العزل الخارجى المعرض للعراء مثل عازلات خطوط نقل القوى مما يؤثر فى قدرتها على تحمل الإجهادات الـكهربية عند سقوط مطر طفيف يبلل سطح العازل . فإذا وجد أيضاً تلوث متراكم من قبل على العازل ، فإن ذلك يؤدى إلى التقليل من قـدرة العازل على تحمل الإجهادات الـكهربية . أما إذا هطل المطر بغزارة فى فترات متقاربة على مدار السنة ، فإن ذلك يؤدى إلى تنظيم طبيعى للعازلات من التلوث .

وجدير بالذكر أن تأثير الرطوبة وحدها أو التلوث وحده على عازلات خطوط القوى ليس خطير . أما إذا كان العازل ملوثاً ومعرضاً لرطوبة عالية فى نفس الوقت فإن جهد الوميض على سطحه ينخفض بدرجة كبيرة .

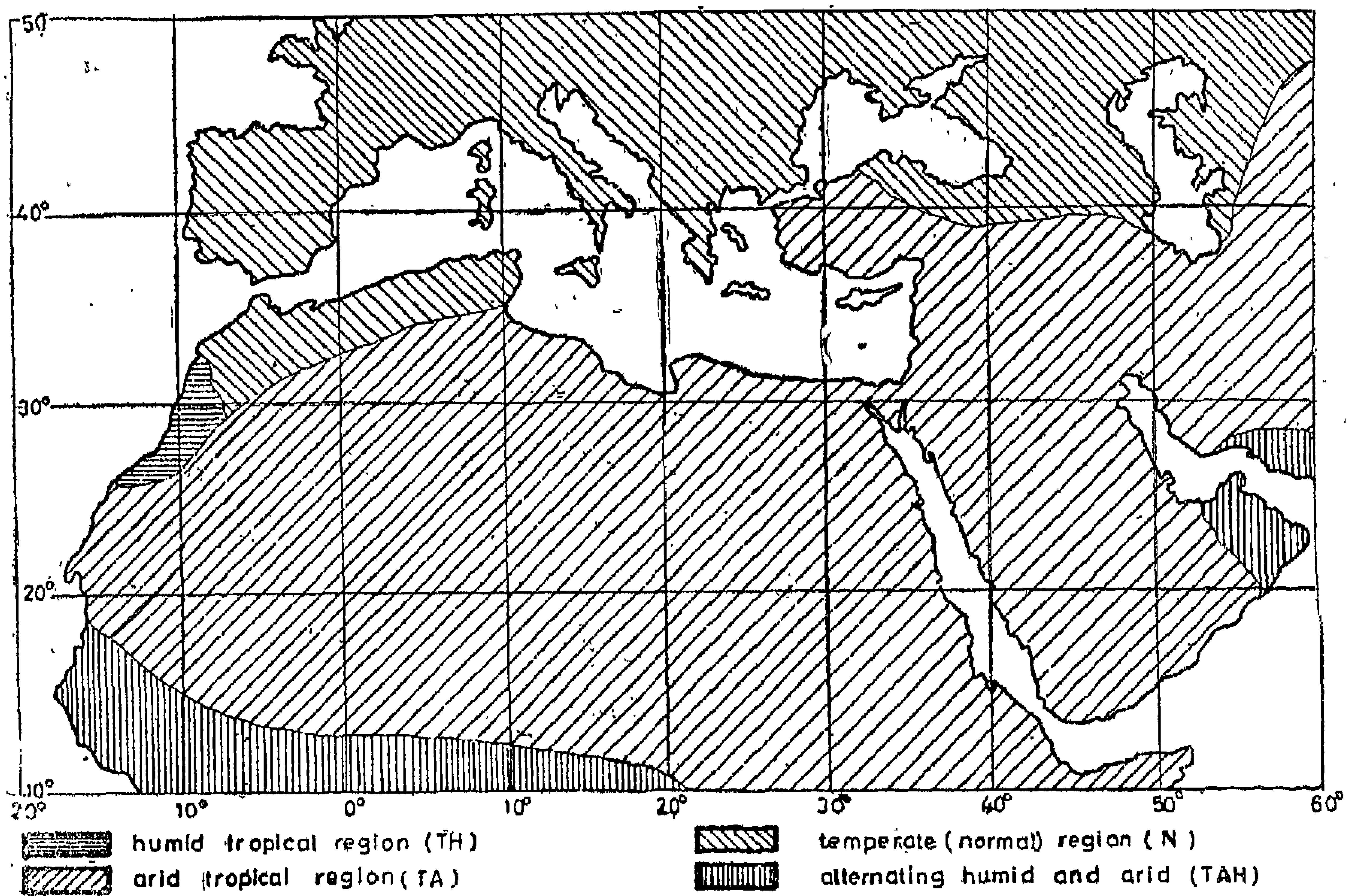
لما كانت الأمطار والرطوبة منخفضة نسبياً بشكل عام ، فإن المؤثرات البيولوجية تـكون أقل وهذا لايمنع طبعاً من أن تنمو نباتات وتعيش حيوانات ضارة بدرجة أقل من حالة المناخ الإستوائى الرطب وتنتشر القوارض كالفئران مثلا ، التى تتسبب فى تلف مختلف الـكوابل والأسلاك المعزولة وتقرض المواد العازلة وتحدث قصراً بين الموصلات .

ذكرنا أن ج م ع تقع فى إقليم استوائى جاف ، وهذا ينطبق أكثر على منطقة مصر العليا . وكلمة جاف هنا تعنى أن الرطوبة النسبية منخفضة فى أغلب أوقات السنة ، ولـكن هذا لايمنع أن ترتفع الرطوبة النسبية إلى درجة كبيرة فى بعض الأحيان خاصة عند انخفاض درجة الحرارة فى الصباح الباكر .

وقد وجد مثلا فى منطقة مصر العليا التى تمثل أكثر المناخ الاستوائى الجاف فى ج ع م أن الرطوبة النسبية ترتفع كثيراً فى الساعات المبـكرة من الصباح ، وخاصة فى فصل الشتاء لانخفاض درجة الحرارة فى تلك الفترة فتصل إلى أكثر من ٩٠ ٪ لمدد متفاوتة . وحسب بيانات مصلحة الأرصاد وصلت هذه المدد إلى ٨٠ ساعة فى شهر ديسمبر ١٩٦٧ بمنطقة المنيا ، وإلى ١٠٠ ساعة فى شهر فبراير ١٩٦٨ بمنطقة غرب القاهرة .

طالما توجد رطوبة نسبية مرتفعة — ولو لفترات قصيرة — تظهر أهمية التلوث ، لأن ترسب الأتربة والأملاح على أسطح العازلات بالإضافة إلى رطوبة عالية يعرض العازلات للوميض إذ أن قـدرة العازلات على تحمل الإجهادات الـكهربية تتأثر بكمية مايترسب عليها من أملاح قابلة للذوبان فى الماء ودرجة الرطوبة فى الجو المحيط .

توزيع الحرارة والرطوبة والمطر على المناطق المختلفة ج ع م



تهب الرياح والرمال التى تلوث الجو ، وخاصة أثناء هبوب رياح الخماسين فى فصل الربيع . كما يحدث تلوث من الضباب المملح على منطقة السواحل . هذا بالإضافة إلى التلوث بالمواد الكيماوية فى المناطق الصناعية . لذلك نجد أن التلوث يختلف من منطقة إلى أخرى حسب طبيعة وضعها .

كما أن اشتداد الريح المحملة بالرمال يعرض الأسطح التى تصدم بها للنمش .

العوامل الفعالة بالنسبة للتلوث هى

١ — مكونات التلوث

٢ — معدلات التراكم

فمكونات التلوث تحدد طبيعة تأثيره على العازلات والمعدات الكهربية (مثلا التآكل والإتلاف الميكانيكى وإتلاف خواص العزل الكهربى للاسطح) . كما أن معدات تراكم التلوث تكون من العوامل التى تحدد مدى التأثير .

أمثلة :

١ — وكمثل عملى عن التلوث — حسب تقرير لجنة العزل — فقد تم تجميع عينات من الأتربة فى نقط مختلفة على مسار الخط الكهربى من أسوان إلى القاهرة ، وتم تحليلها لمعرفة الأملاح المختلفة التى تدخل فى تكوينها مثل الكلوريدات والسلفات والكربونات وأكاسيد الكالسيوم والمغنسيوم وأظهرت النتائج أن نسبة الأتربة القابلة للذوبان فى الماء تتراوح بين ١٢ ٪ ، ٣٨٪ من الوزن الكلى للاتربة المتراكمة على العازلات . كما أن كمية الأتربة المتراكمة على أسطح العازلات فى المسافة بين أسيوط وملوط وصلت فى خلال مدة حوالى ثمانية أشهر إلى مقدار ٢ر٣٩ ملجم / سم٢ .

وفى حالة حدث نسبة رطوبة عالية فى الصباح الباكر بالإضافة إلى التلوث ، تنخفض خواص العزل الكهربى للاسطح ويحدث وميض على أسطح العازلات عندما تكون الخطوط محملة .

٢ — يلاحظ أن المتممات Relays المستخدمة فى ج م ع تعانى من تراكم التلوث والأتربة على أماكن التوصيل . ويقلل من هذا التأثير إذا كان المتمم فى وضع رأسى وليس فى وضع أفقى . ويستحسن حماية المتمم من التلوث بوضع غطاء محكم حوله . كما يمكن استخدام متممات مملوءة بالغاز أو متممات ذات تنظيف ذاتى .

٣ — بالنسبة لارتفاع درجة الحرارة يراعى عند إستخدام معدات كهربية فى جمهورية مصر العربية أن يكون تصميمها واختيار مكوناتها قد تم مع الوضع فى الإعتبار ارتفاع درجة الحرارة المحيطة ، ويلاحظ أن استخدام الشمع فى عزل مكونات ترتفع حرارتها إلى درجة عالية نسبياً كالمحولات مثلا ، يسبب متاعب . لأنه عندما تصل حرارة القطعة المعزولة بالشمع إلى درجة انصهاره ، نجد أن الشمع يتساقط على الأجزاء الأخرى تاركا القطعة الأصلية بدون عزل . كذلك يلاحظ أن الوضع الرأسى للشاسيه فى الأجهزة الالكترونية يساعد على عملية التبريد الطبيعى للمكونات المركبة على الشاسيه كما يساعد على إنقاص كمية الأتربة المتراكمة على الشاسيه ككل . وهنا يتبادر لنا تساؤل هل تراكم الأتربة على القطع مثل المقاومات مثلا يؤثر على مقدار الحرارة المشتتة منها ؟ .. ربما يحتاج ذلك إلى بحث .

٤ — لوحظ أن أنواع المكثفات بعد فترة من استخدامها فى جمهورية مصر العربية تتلف نتيجة لارتفاع الحرارة ، مع وجود جفاف ، لأن ذلك يتسبب فى جفاف طبقة الورق العازل وتشققها وحدوث قصر فى المكثفات الغير محكمة الغلق .

٥ — يلاحظ أن أسطح التوصيل المتحركة المثبتة على مادة عازلة صناعية مثل الفبر أو الورق المضغوط المشبع يحتمل أن تسبب متاعب عندما تستخدم فى جو حار جاف كجو

ج م ع . لأن المادة العازلة قد تتقلص وتختلف شكلها مما قد ينتج عنه أن تبعد أسطح التوصيل عن بعضها وتفقد مهمة القيام بدورها . وقد حدث ذلك فى بعض مجزئات الضغط التى تستخدم فى ج م ع بعد فترة من استخدامها .

هذه بعض الأمثلة التى يمكن أن تعطى فكرة عن تأثير العوامل المختلفة وخاصة إذا اجتمع أكثر من عامل مثل التلوث والرطوبة ، والتلوث والحرارة والجفاف .

رابعاً : ختام

بمجرد ألقاء نظرة سريعة عن هذا يتبين أنه على خريطة الأقلمة المناخية للمواد والمنتجات الكهربية يتضح بجلاء أن معظم الدول العربية تقع فى إقليم المناخ الاستوائى الجاف . وعلى ذلك فإنه يمكن استخدام النموذج التطبيقى الذى تم إعطاءه فيما سبق كمثل لعمل تقسيمات مناخية جزئية داخل أى من الدول العربية .

واستكمالا لذلك تظهر ضرورة إنشاء محطة لدراسة الأقلمة المناخية بأحد الدول العربية ، وذلك لدراسة ملاءمة مختلف المواد والمعدات لأجزاء الدول العربية ، ويمكن أن يتم ذلك بالتنسيق بين مختلف الدول العربية تحت لواء أحد الأجهزة العربية المتخصصة فى النواحى المتعلقة بتلك المجالات .

مشاكل النقل البرى "بالسيارات" للركاب بين المدن وفي الريف في الدول النامية مع تركيز خاص على تجربة الجمهورية العربية المتحدة

دراسة من إعداد السيد / المهندس سمير فهمى
رئيس مجلس إدارة
شركة النيل العامة لأتوبيس شرق الدلتا

فى مواجهة مشاكل حصر احتياجات المستقبل وتحليلها وبحثها ، ومشاكل تطوير شبكات النقل البرى للركاب فى معظم الدول النامية ، عادة ما يصادف خبراء النقل من الاقتصاديين والفنيين سلسلة من المشاكل الفريدة يمكن اعتبار كل واحدة منها مشكلة كبرى قائمة بذاتها وذلك بالقياس بالمشاكل التى تواجه مستويات الدول المتقدمة .

وبينما تختلف الظروف السائدة اختلافاً كبيراً من دول نامية إلى أخرى اعتماداً على خلفيات البيئة فى فترة ما قبل التنمية ، وعلى الأوضاع الثقافية والتعليمية ، وعلى المستوى الاقتصادى ، وعلى طبيعة التركة الصناعية والفنية ، وعلى عادات السكان وتقاليدهم ، فإن المرء يصادف فى كل حالة تقريباً قيوداً كبيرة محددة تتجمع عادة لخلق عقبة ، على الأقل فى المراحل التمهيدية للتنمية ، فى طريق معالجة تصميم شبكة للنقل البرى مناسبة وكذلك تطويرها .

والخبير الاقتصادى يعنى بمشكلة تخصيص الموارد واستخدامها من الناحية الاقتصادية فيما يتعلق بنقل الركاب . ومع ذلك فعليه أن يعترف بأثر التطورات الفنية ومغزى الإجراءات السياسية والقانونية والتنظيمية التى تؤدى بمقتضاها الخدمات .

أما الخبير الفنى فيختص بتأثيرات النقل المتقدم ، والتطورات فى تكنولوجيا النقل ، والاعتبارات الفنية والاقتصادية التى تتحكم فى اختيار العربات التى تناسب الظروف المحلية السائدة ، وذلك عن طريق فهم واضح ودقيق لنطاق سياسة اقتصادية متكاملة للتنمية ، ومعرفة كافية باتجاه الدولة فى مجال تخصيص الموارد .

أولا : مشاكل النمو العامة فى مرحلتى التخلف والتنمية

إن الخصائص المشتركة فى مرحلتى النمو فى الدول الأقل تقدماً يحددها التعريف ذاته : دخل محدود ، وقلة رأس المال المتجمع ، ومستويات فنية وتكنولوجية متأخرة . والخط الفاصل بين هاتين المرحلتين وبين مرحلة التقدم أو مرحلة التنمية الكاملة هو خط مفروض (تعسفى) ، ولا يمكن أن تعلق أهمية تحليلية على هذا الخط .

كما أن هناك اختلافات كبيرة فى معدل النمو لكل من الدخل الحقيقى الإجمالى ودخل الفرد فى مختلف الدول النامية : وعلى هذه الأسس فقد تقدمت بعض الدول النامية بسرعة أكبر من غيرها فى عشرات السنين الأخيرة . وهناك على العموم اختلافات كبيرة فى الثروة ، ومعدل التقدم الفنى ، والظروف السياسية والاجتماعية التى تزيد من النمو أو تؤخره ، بين هذه المجموعة من الدول التى تسهم فى ثلثى سكان العالم .

وتوجد فى كثير من الدول النامية مدن ومناطق تعدينية وصناعية لها خصائص الدول المتقدمة من حيث مستويات المعيشية ، والإنجازات الفنية والتقدم التجارى . إن المجال فى الاختلافات الإقليمية الداخلية قد يكون فى الحقيقة أكبر فى الاقتصاد النامى منه فى الاقتصاد الأكثر تقدماً : فالتخلف فى المواصلات ، وهو من المعالم السائدة فى النظم الاقتصادية المتخلفة والنامية ، يعوق الاتصال الاقتصادى والثقافى حتى بين المدن أو المناطق القريبة جغرافياً والتى تخضع لنفس الحكومة ولنفس النظام النقدى .

أن الدخل المحدود والعمل الفنى المتأخر فى معظم النظم الاقتصادية النامية ما هما إلا اثنتان من المعالم الاقتصادية الكثيرة التى يختص بها الخبير الاقتصادى ، وهذه المعالم هى : الثقافة والحضارة ، (١) عودة القانون والنظام (وهو ألزم شرط للنمو الاقتصادى) ، إنماط الإنتاج وطرقه المستقرة ، الاختلافات السكانية فى معدل النمو السكانى ، الاختلافات فى الإجراءات التنظيمية أو فى الموارد الطبيعية أو فى اتجاهات السكان ، الحواجز السياسية والتنظيمية ، الداخلية ، الضغوط الامبريالية والاستعمارية الخارجية وكذلك التدخل التى تعوق معدل النمو وإمكانية تزايد النمو ، وجذب استثمارات جديدة ، (٢) والجهود والنكوص .

تنشأ فى عدة دول نامية بعض المشاكل الاجتماعية والسياسية والاقتصادية الحالية من معدل التنمية السريع وغير التكافىء أما فى مختلف القطاعات الجغرافية والوظيفية لنفس النظام الاقتصادى ، أو لأن العلاقات الاقتصادية للسكان هى أسرع وأشد من التغييرات فى الجوانب الأخرى للحياة الاجتماعية والسياسية وسنحاول أن نعالج بعض مخاطر البنيان الاقتصادية فى الدول النامية والمتخلفة :

١ — التوزيع الوظيفى والتقييم الاقتصادى :

هناك شواهد على الأهمية الكمية لما يسمى بالإنتاج الثالث فى النظم الاقتصادية النامية . فهذا الإنتاج يتخذ شكل الخدمات المنزلية ونشاط التجارة والنقل . فالدور الهام للتجارة والنقل فى الإسراع فى عملية النمو الاقتصادى وفى توسيع الاقتصاد النقدى هو موضوع معروف فى تاريخ الاقتصاد . وهذا النشاط فى النظم الاقتصادية النامية وبشكل أكبر فى النظم الاقتصادية المتخلفة ، هذا النشاط يميل إلى أن يكون نشاطاً مضنياً بسبب المستوى المنخفض لرأس المال والمواصلات الضعيفة .

٢ — قيمة الموارد الاقتصادية :

أن قيمة المورد لا يتوقف على خصائصه الطبيعية أو كفاءته الفنية وحدها ، فهناك شبكة معقدة من تأثيرات الأسواق فى الحاضر وفى المستقبل تكون جزءاً من البيئة التى تأخذ فيها الموارد قيمتها .

ويستتبع ذلك أن قيمة أى مورد يتوقف على قيمة الموارد الأخرى . ولذا فإن دراسة موارد معينة أو مصنفات من الموارد دراسة منعزلة عن غيرها هى دراسة مضللة بعض الشيء ومفروضة (تعسفية) ما لم يؤخذ فى الاعتبار أن الموارد تعتمد بعضها على البعض الآخر . كما أن القدرة الإنتاجية وقيمة العمل ، ورأس المال ، والموارد المادية تتأثر تأثراً كبيراً بحالة التكنولوجيا ، وطرق التنظيم أو الإنتاج ، وكفاءة الحكومة وسياستها ، وتنظيم المنشآت عامة .

٣ — علاقة الموارد الطبيعية بالتنميه الاقتصادية :

هناك بعض المناطق التى تتأثر فيها التنمية الاقتصادية تأثراً بالغاً بعوقات الظروف الطبيعية غير الملائمة . ولكن فى معظم العالم المتخلف لا يوجد مثل هذا النقص فى الموارد الطبيعية ، كما أن الظروف المناخية ليست بالدرجة التى تشكل بها حواجز ، فى طريق التنمية .

ففى خلال التاريخ المدون ، انتقلت الزعامة الصناعية والتجارية مراراً من دولة أو منطقة إلى أخرى ، حتى وإن لم تختلف هذه الدول أو المناطق اختلافاً كبيراً أو واضحاً فى مواردها الطبيعية .

وحتى فى العصور الأخيرة فهناك دول كانت فى المقدمة ثم فقدت سيادتها الاقتصادية وأصبحت الآن فى صفوف الدول الأقل تقدماً (١) .

ومع ذلك فإن الوصول إلى الموارد يؤثر فى الوضع الاقتصادى لأجزاء كثيرة من العالم المتخلف تأثيراً حيوياً ، وأن التغييرات فى الوصول إلى الموارد كان لها نتائج كبيرة فى فترة قصيرة فى الإنتاج للأسواق فى أعقاب إقامة مواصلات نسبياً . ويمكن ذكر أمثلة عديدة للنمو السريع وظروف سياسية مستقرة . كما ينبغى على النظم الاقتصادية النامية أن تحرص على ألا تسمح للحواجز التنظيمية فى أن تؤثر فى استعمال مواردها الطبيعيه بكفاءة ، وهذه النظم فى حماستها لتحقيق النمو الاقتصادى ينبغى عليها أيضاً ألا تسمح لقوى الاستعمار الاقتصادى والاستغلال الشريرة فى أن تعوق أو تقضى على قدرتها (قدرة النظم) فى المستقبل على اتباع سياسة مرنة فى التحكم فى أنفع عائد فيما يختص بالاستثمارات فى زيادة التنمية واستخدام الموارد الطبيعية لاقتصادها (٣) .

٤ — الموارد البشرية :

إن التقدم الاقتصادى يستلزم تغييرات كبيرة فى النظم الاجتماعية وفى الناس الذين يعيشون فى ظل هذه النظم (كما أن التقدم الاقتصادى) يسبب هذه التغييرات فالبنيان الاجتماعى يتغير فى الشكل ، وتظهر فرص جديدة ، وتتزايد السكان ، وتصبح للصفات الكامنة قيمة أكبر كما أنها تستخدم ، وتقدم حوافز جديدة .

ومن الممكن أن تكون عملية التكيف لمعظم الأفراد للنظام الاجتماعى والاقتصادى الجديد أقصر وأقل صعوبة مما يظن غالباً . وهناك موقف صعب ينتج من احتمال الصراع بين الرغبة فى النمو السريع التى تبديها جماعات لها نفوذ فى النظم الاقتصادية الأقل تقدماً وبين صعوبات التكيف للنمو السريع .

٥ — نظام المقاولات :

إن التجديد فى نظام المقاولات وممارسته يعنى خلق فرص لم يفكر فيها أحد أو الاستفادة منها ، فرص النشاط الاقتصادى المربح ، وغالباً ما يؤثر تأثيراً كبيراً فى التقدم الاقتصادى . فالتقدم المادى لأى مجتمع قد يلقى المساعدة الكبيرة عندما تتوفر صفات هذا النظام (نظام المقاولات) وكذلك الاستعداد لتخطيط التغير والخروج على الطرق التقليدية وقدرة الأفراد على رؤية فرص جديدة للربح والقدرة على استغلال هذه الفرص والرغبة فى ذلك لها أهمية كبيرة فى التنمية الاقتصادية .

ويكون النظام الاقتصادى حسن الحظ عندما تتوفر صفات المقاول فى أفراد يتسمون أيضاً بسمة الحيلة والتدبير والجد ، ولهم المهارات الفنية والإدارية ويرغبون فى النظر البعيد .

ويوجد فى المجتمعات الأقل تقدماً من الناحية الاقتصاديه صعوبات فى طريق تنمية هذه الصفات واستعمالها . فقوة القادة وعدم مرونة الأوضاع ، والريبة فى الأفكار الجديدة وفى ممارسة الاستطلاع الفكرى كلها تتجمع لخلق جو ضار بالتجريب والتجديد .

بينما يشكل الدور الهام الذى يقوم به الخبراء ورجال الأعمال الأجانب فى التنمية الاقتصادية واحدة من المعالم البارزة فى التاريخ الاقتصادى عامة ، فإن هناك حالات من التدخل فى السياسة الداخلية وعدم اتباع سياسة موالية للنظام الاقتصادى الذى طلب منهم مساعدته . وأدى هذا إلى خلق شعور من الريبة والتردد من جانب الحكومات التقدمية الوطنية ومؤسساتها فى الاستفادة الكاملة من هذه المعونة الضرورية التى تستطيع النظم الاقتصادية المتقدمة أن تعطيها استجابة للطلب المتزايد فى النظم الاقتصادية الأقل تقدماً للامكانيات والخبرات التى لدى رجال الأعمال الأجانب ، كما أن — الشعور الشعبى المعادى لهؤلاء قد يتزايد فى عدائه لهم .

٦ — المستوى المنخفض لرأس المال :

يتضمن التعريف الحقيقة القائلة بأن مستوى رأس المال منخفض فى الدول الأقل تقدماً ، وأن النشاط الاقتصادى فيما يتم دون مساعدة كبيرة من مقومات رأس المال (المواصلات ، والآلات ، والمعدات والأدوات) المادية فى الدول الأغنى والأكثر تقدماً من الناحية الفنية .

والمستوى المنخفض لرأس المال يتجه إلى جعل أسعار الفائدة عالية ، وهذا يدفع المقرض والمقترض إلى الاستفادة الكاملة من رأس المال المتاح ومحاولات تثبيت سعر الفائدة بأقل من مستوى التوازن عن طريق التشريع قد تكون محاولات غير مجدية ؟ ولو أثمرت هذه المحاولات فإنها عادة تؤدى إلى تقليل رأس المال المقدم وإلى استعماله استعمالا غير اقتصادى.

أن طريقة الإنتاج القائمة على رأس المال المضغوط قد تكون أكثر الطرق اقتصاداً وأرخصها فى أى نظام اقتصادى تكون فيه الأجور الحقيقية عالية وسعر الفائدة منخفضاً ، ولا يستلزم ذلك أن تكون نفس الطريقة اقتصادية فى نظام اقتصادى آخر يكون العمل ورأس المال فيه بنسبة مختلفة تماماً .

ومع ذلك فمن الضرورى اتباع أنماط معينة فى توزيع رأس المال بين القطاعات والأعمال فى النظم الاقتصادية الأقل تقدماً . ومن الاقتصاد (التوفير) استخدام رأس المال المتاح فى كل منهما (القطاعات والأعمال) إلى الدرجة التى تجعل العائد الحدى لرأس المال فيها مساوياً للعائد فى الاستخدامات الأخرى التى تتنافس على موارد رأس المال المحدودة .

٧ — رأس المال الأجنبى فى مساعدة النظم الاقتصادية الأقل تقدماً :

بينما يسهم المال الأجنبى مساهمة كبيرة فى التنمية الاقتصادية للكثير من الدول بنفس الطريقة التى يسهم بها رجال الأعمال والأفراد الأجانب يدعون على غير أساس بأن معوقات معينة فى طريق استثماراتهم تنتج من عدم استقرار العلاقات الأساسية والاقتصادية والمالية بين الدول .

كما يدعون بأن الإجراءات المتبعة فى دول نامية معينة لاتشجعهم بل تهدف إلى عقابهم وهذه الإجراءات تتضمن المشاركة القومية ، والضرائب الخاصة ، والمعاملة المتحيزة للشركات المحلية فى تخصيص تصاريح الاستيراد والنقد الأجنبى ، وقيود الهجرة إلى داخل البلاد . وهؤلاء المستثمرون يتجاهلون دائماً الشعور الوطنى ، والخوف من السيطرة السياسية والاستغلال ، وحقوق السيادة للدولة ، والخبرة المريرة لتلك النظم الاقتصادية فى مواجهة الاستغلال والضغط المتزايدين من جانب مجموعة النظم الاقتصادية المتقدمة التى تمثل الاستعمار الجديد .

ثانياً : بعض خصائص النقل البرى للركاب بين المدن وفى الريف :

غالباً ما يشير خبراء النقل من الاقتصاديين المدنيين بنقل الركاب إلى صناعتهم على أنها « خدمة عامة » ، وأحياناً يشيرون إليها على أنها «مرفق » والافتراض الذى ينظر إلى النقل العام على أنه مرفق عام هو افتراض جوهرى ، وذلك لأن معظم الدول تعتقد أن المرافق العامة تدار على أحسن وجه تحت السيطرة المباشرة لسلطة القطاع العام .

ومع ذلك فالمعيار الهام هو استعداد الجمهور لدفع ثمن الخدمة إذا ما قدمت بسعر تجارى وبكفاءة فى السوق الحر. وإذا لم يكن لديهم الاستعداد لذلك فإن هذا يؤدى على الأقل إلى الافتراض لأول وهلة بأن هذه الخدمة ليست مطلوبة .

والنقل يمثل حالة خاصة بمعنى أن إنتاجه النهائى هو تقديم خدمة وليس تقديم بضائع مادية . وخدمات النقل تضيع فى لحظة إنتاجها ، فإذا لم يتم بيع نتاج الأتوبيس على هيئة (مقاعد كيلو مترية) فإن هذا النتاج يضيع سدى لأنه لا يمكن تخزينه . فهذا الضياع يجعل المهارات الإدارية ضرورية ، كما أنه يفقد اقتصاديات هذه الصناعة .

الآراء المعارضة للتنافس فى نقل المسافرين :

كثير من الآراء المتخصصة تساند القول بأن الإدارة التجارية لا تناسب صناعة النقل العام ، وبالذات النقل بين المدن والمناطق الريفية . والمفروض أن التنافس فى هذا المجال هو أمر خطير وغير اقتصادى وغير كفء وإن عدم الرغبة فى تغطية شبكة بأكملها وتقديم خدمات متكاملة للمجتمع ما هو إلا نتيجة لاعتبارات اقتصادية وتكنولوجية ترتبط بأحوال شبكة الخطوط واقتصاديات حجم السيارات التى تستخدم فى تقديم الخدمة العامة .

وغالباً ما يستند الرأى القائل بان التنافس فى مجال النقل العام خطير على الافتراض بان الشخص الذى يقدم الخدمة العامة سواء كان الغرض منها التجارة أو التنافس سوف يدفع لأن يزيد من أرباحه على المدى القصير ، وذلك بواسطة تخفيض حجم الأموال التى تصرف للحفاظ على مستوى أمن الركاب ، وعلى التفتيش المنتظم للسيارات والصيانة الوقائية ، وأن هذا الشخص يزمع أيضاً لأن يشجع القيادة الرديئة .

وإذا كان للمسافر أن يختار بين الركوب فى سيارة يتمتع صاحبها بسجل أمن جيد وسمعة طيبة ، أو الركوب فى سيارة يمتلكها شخص سيىء السمعة ، فإن المسافر سيفضل الأول .

وهكذا فإن التنافس سوف يفضل من الناحية المنطقية صاحب العمل الذى يتمتع بسجل طيب وقد يكون هذا صحيحاً على المدى البعيد إلا أن فعالية هذا كعامل إلزامى لصاحب العمل الذى لايتمتع ببعد النظر سوف تكون محدودة وتجىء التجربة وعامل الزمن فى المقام الأول بالنسبة للتمييز بين الغث والثمين ، وأن فقدان الحياة أثناء ذلك سوف يكون ثمناً لا يطاق كى يدفع من أجل إبراز إحدى الحقائق فى الاقتصاديات . وزيادة على ذلك فإن صاحب العمل عديم الضمير الذى يسعى وراء الربح السريع كهدفه الوحيد قد يتجاهل بطريقة متعمدة العامل الإلزامى وينسحب بما جمعه من مكاسب وذلك بمجرد أن يتوقف الطلب على خدمته أو تتعطل سياراته . ومثل هذه الأعمال مالوفة فى الدول المتخلفة التى تفتقر إلى اللوائح المنظمة للنقل العام .

وبالرغم من أنه لا يمكن القول بأن التنافس فى حد ذاته كاف لحماية المستهلك من الاستغلال بهذه الطريقة أو لحماية أمن الطرف الثالث ، فإنه لا يجب الافتراض بأن الاحتكار أو الرقابة العامة هى البديل الوحيد . ومن الضرورى التدخل التشريعى لحماية المستهلكين من الاستغلال الاحتكارى بطريقة مماثلة تقريباً .

إن التدخل القانونى هو أمر ضرورى على أية حال وذلك إذا كان الهدف منه ضمان مستويات كفيلة بمواجهة الحرية التجارية لصاحب العمل ، واستغلال المحتكر ، وحق لمواجهة احتمال التراخى من جانب مؤسسات القطاع الخاص .

وإن القول بأن التنافس فى مجال النقل العام غير اقتصادى يقوم على أساس المعارك التى تنشب بين أصحاب الأعمال وشركات السيارات التى تتنافس على النسب والتعريفة ، ومضاعفة خدمات السيارات على الطرق الرئيسية ، والتنافس مع خطوط السكك الحديدية التى تمتد بمحاذاة طرق السيارات وعادة ما تكون تكاليف السكك الحديدية أقل بكثير . وإن الأمثلة المتطورة التى ترتبط بمشاكل تزايد الطلب كثيراً ما تسمى « باستخلاص الفائدة » وعلى العموم هناك نغمة من التحقير فى كثير من الأمثلة التى يذكر فيها صاحب العمل الذى يكون سعر تكلفة نتاجه منخفض . ومن الناحية الظاهرية يبدو أن هذا النتاج غير اقتصادى .

إن الهدف من وراء الاستثمار هو الحصول على نسبة من الأرباح على رأس المال المستثمر وتكوين احتياطى لمواجهة تكاليف الخسائر وفى كثير من فروع النقل العام قد يتوقع صاحب العمل أن تستمر السيارات صالحة للاستخدام لفترة طويلة . ومن ناحية أخرى ، دائماً مايكون هناك ابتكار فى التحسينات التصميمية والتكنولوجية وقد يصبح نوع ما من أنواع السيارات عتيق الطراز قبل انتهاء حياته الميكانيكية المفيدة بفترة طويلة ، ويرجع ذلك إلى اعتبارات ترتبط بالتنافس وراحة وذوق المسافر ومظهر السيارات إلى آخره وكل هذه الاعتبارات تؤدى إلى تغيير فى درجة التفضيل بين المسافرين ومن الطبيعى أن هذا الأسلوب لا يناسب النظم الاقتصادية المتخلفة والنامية حيث أن استثمارات رأس المال عادة ما تكون ضئيلة . وفى حالة ما إذا وجدت هذه الاستثمارات فإنه يفضل أن تستخدم فى التنمية الصناعية والإنتاج أحسن من أن تضيع فى سد احتياجات أذواق المسافرين المتغيرة ، ولكن يجب الحرص على ألا يحرم المسافر تماماً من المكاسب التى حققها التقدم التكنولوجى فى حالة ما إذا كانت هناك مؤسسة تجارية عامة تقوم باستغلال أو بادارة الخدمات العامة .

وهنا نسوق مثل آخر للاستثمار أحياناً يوصف بأنه غير اقتصادي . ويحدث هذا عندما يقوم مشروع باستثمار المال في خدمة عامة جديدة وعندئذ يكتشف أن نجاح هذه الخدمة العامة يجذب منافسين جدد .

وأخيراً يقال أن التنافس غير كفء وأن مثل هذا القول يوحي بأن التنافس في مجال النقل العام يؤدي إلى قيام كثير من الخدمات في مكان ، وافتقار مكان آخر لهذه الخدمات ، بدون أي اعتبار لاحتياجات كل من السكانين . وهناك أيضاً الرأي القائل بأنه كلما زاد الطلب زاد النتاج ، ومن المسلم به أن النقل العام من طبيعته أن يزيد الإنتاج . أن ضياع الإنتاج وتركيز الطلب في طريق واحد أمر لا يمكن للادارة الحكيمة أن تحد من أثر هذا إلى أدنى درجة ممكنة . وقد يكون المشروع الذي يتمكن من بيع ٥٠٪ من المقاعد الكيلو مترية على درجة عالية من الكفاءة . ويستند القول بأن التنافس غير كفء إلى الرأي الذي يقول إن كل أصحاب الأعمال سيحاولون التركيز على الخطوط الأكثر ربحاً ويهملون الخطوط الفقيرة . ومن الناحية النظرية فإن صاحب العمل الذي تتكلف سياراته تكاليف قليلة سوف يدفع لأن يعمل على الخطوط الكثيفة والأكثر ربحاً ويترك الخطوط الفقيرة

وليس من المؤكد على الاطلاق أن هناك دافع واحد قوي يجعله يقوم بهذا ، فمن المفروض أنه سوف يستمر في العمل على الخطوط الفقيرة طالما كانت هذه الخطوط تدر عليه أرباح

ومن المحتمل أيضاً أن يجد أن العمل على الخطوط الغنية أغلى من ناحية التكاليف ، حيث أنها تتطلب عدد كبير من العربات ، وتتطلب منه عملية تشغيل هذه الخطوط أن يدفع أموالا أكثر .

وإذا نجح فان تكاليفه سوف ترتفع ، وعندئذ يجد أن تشغيل الخطوط الفقيرة عملية لم تعد مربحة ، وهكذا تصبح الخدمة على إحدى الشبكات المتكاملة في حالة عدم استقرار وانتظام ويصبح المسافر تحت رحمة التحول في أرباح صاحب العمل .

ثالثا : النقل البري في المناطق الريفية وبين المدن في الدول النامية :

وبناء على الجزء الأول والجزء الثاني من هذا البحث فإن المشاكل الاقتصادية والتكنولوجية البارزة التي تواجه النظم الاقتصادية المتخلفة والمشاكل المرتبطة بالنقل البري في المناطق الريفية وبين المدن عامة ، فاننا الآن نبدأ في استخلاص الجوانب الرئيسية التي تؤثر على الحاجة المتزايدة لتطوير هذه الخدمة العامة الجوهرية في الدول النامية وقصر نموها السريع على نسبة توازن الطلب المتزايد على هذه الخدمة العامة . ولا يمكن وضع أي قواعد صارمة وسريعة بخصوص الدرجة أو النسبة التي يمكن عندها أن يؤثر كل من هذه العوامل على النمو المطلوب في هذه النظم الاقتصادية كشرط سابق للتنمية البيئية ، وكشرط يختص برأس المال والطبوغرافيا ، حيث أن المؤسسات تختلف بدرجة كبيرة من نظام اقتصادي إلى آخر ، وبالتأكيد يمكن أن يعزى أي تأخير في عملية التنمية إلى النتيجة المترتبة على كل هذه العوامل مجتمعة .

ويمكن تقسيم المشاكل الكبرى التي تواجهها معظم الدول النامية إلى الثلاثة أقسام التالية :

١ — القيود الاقتصادية .
٢ — المستويات التكنولوجية .
٣ — الأساليب التنظيمية .

القيود الاقتصادية تؤثر على تطوير النقل البري :

وكما سبق أن شرحنا في هذا البحث ، أن النظم الاقتصادية النامية تتميز أساساً بالدخل المحدود وتفتقر إلى المخزون من رأس المال ، وبالرغم من الاختلاف الكبير في نسبة النمو في مجموع الدخل الحقيقي ودخل الفرد في مختلف الدول النامية فان هذا الدخل ليس شيئاً إذا ما قورن بالدول المتقدمة تماماً .

إن تخصيص الموارد في معظم البلاد النامية يتبع أسلوب محدد وهو التركيز على الاستثمار في الصناعة والانتاج ، على الأقل في المراحل الأولية من عملية التنمية . وأن الناتج الثانوي للنمو الصناعي هو زيادة دخل الفرد ، والنتيجة المترتبة على ذلك هو زيادة الطلب على هذه الخدمة العامة . والناتج الثانوي الآخر هو خلق اختلافات إقليمية داخلية

تؤدى بدورها إلى زيادة الطلب على وسائل مواصلات أفضل وكنتيجة لهذه الظاهرة فان أى استثمارات محدودة فى تنمية النقل البرى لا تفشل فى الإيفاء بهذه المطالب فحسب ، ولكنها لا تكاد تكون كافية لتطوير وتغيير طاقة النقل العام المتدهورة وكانتاج من الدرجة الثالثة فان النشاط فى مجال النقل العام لا يعود بدخول مجزية على الاستثمار ، ولذا فانه لا يوضع ضمن أولويات التخطيط . ولقد بينت التجربة أن المخططين فى النظم الاقتصادية النامية يميلون إلى تجاهل أهمية تنمية شبكات طرق النقل البرى ، إلى أن يجىء الوقت التى تسوء فيه المشكلة بسبب عدم التوازن القريب بين العرض والطلب ، وتزداد المشكلة حدة ويصبح من المطلوب إيجاد استثمارات لخلق توازن معقول ، بيد أن هذه الاستثمارات يكون من الصعب تحقيقها على الأقل فى فترة قصيرة .

وثمة مشكلة أخرى هامة تنشأ بسبب قيود الاستثمارات فى المواصلات وهى مشكلة التنمية الفرعية لشبكات النقل البرى ، ويرى أن مثل هذه التنمية أمر ضرورى . وفى حالة عدم وجود خطة تنمية شاملة لتطوير وتوسيع شبكات المواصلات فان مشاكل إعادة النظر وإعادة تخطيط وتوسيع المشروعات التى سبق لها أن نفذت هى مشاكل باهظة التكاليف من وجهة نظرنا ولقد استطاعت بعض الدول النامية أن تستفيد من التجارب الأخرى وذلك عن طريق عمل خطة طويلة الأجل لتطوير الطرق والنقل البرى على أن تتفق فى التنسيق مع الخطة الشاملة لتنمية الاقتصاد القومى .

إن رأس المال الأجنبى كعامل مساعد للتنمية الاقتصادية عامة والنقل البرى خاصة قد لعب دور هام فى مشروعات التنمية التى سبق أن حققت فى كثير من النظم الاقتصادية ولكن السؤال التقليدى ما هو الثمن ؟ ولا يكاد يكون هناك اختلاف فى أن تجارب معظم الأنظمة الاقتصادية النامية تميل بطريقة غير خاطئة إلى استغلال الانجازات الاقتصادية التى حققتها النظم الاقتصادية فى الدول الاستعمارية والدول المتقدمة . إن هذا الاتجاه الجديد قد ظهر كبديل للسيطرة العسكرية أو الاستعمار والدليل الواضح على هذه النظرية هو عدم رغبة النظم الاقتصادية المتقدمة على الاشتراك أو التعاون فى خطط التنمية الاقتصادية الخاصة بأحلاف الدول الاشتراكية والحرة الجديدة[1] . وأن المعاملة التى تقوم على أساس التفرقة والتفضيل والتى تستند إلى درجة القبول للانضمام لأحلاف معينة أو التعاون داخل كتل معينة كانت أيضاً واضحة كل الوضوح ومن هنا فان الرد على ادعاء المستثمرون الأجانب الذى لا يقوم على أى أساس بأن الإجراءات التى تتبعها دول نامية معينة لا تشجعهم .

* أن البنك الدولى للانشاء والتعمير ومنظمة التنمية الصناعية التابعة للأمم المتحدة قد يكونا المنظمتان الدوليتان اللتان تساعدان بحق فى تقديم رأس المال للاستثمار بغرض تنمية الدول وتقدم أيضاً الاستشارة التكنولوجية والتنظيمية لهذه الدول وذلك بعد أن تدرس وتقيم بعناية المشروعات التى تقدمها لها هذه الدول بغرض طلب الحصول على مساعدة اقتصادية .

* لقد وجد أن تخطيط القوى العاملة الذى يعتبر من الضروريات بالنسبة لزيادة سرعة التنمية ، يتغير بسبب تخطيط استثمار رأس المال عامة فى النظم الاقتصادية النامية ، وأن هذا ينطبق على القوى العاملة على كل المستويات ومجالات التخصص والمهارات وهنا نرى أن التخلف واضح كل الوضوح فى مشروعات تنمية المواصلات وبالذات فى مجال النقل البرى .

* ويبدو أن النقص وعدم الدقة فى المعلومات والسجلات الإحصائية هى أكثر الملامح المميزة لتنظيم النقل فى الدول النامية ، وفى حالة عدم توافر المعلومات الإحصائية الدقيقة والتاريخية والحديثة عندئذ يكون أمام المرء فرصة بسيطة كى يتنبأ ويحلل بدقة المطالب فى المستقبل ، ويقيم الأرصدة المطلوبة فى المستقبل والتخصصات والمهارات المتنوعة من القوى العاملة المطلوبة للعمل فى مجال النقل العام .

* إن سياسات الأسعار الخاصة بالخدمات تعتبر من المشاكل الفريدة التى تواجه البلاد النامية فى مجال النقل

(١) قيام الولايات المتحدة وبريطانيا بسحب أموال بناء السد العالى فى عام ١٩٥٦ .

البرى للركاب . إن زيادة دخل الفرد لايعكس بالضرورة استعداد الأفراد لأن يدفعوا مبالغ أكبر من أجل الخدمات الأحسن التى تقدمها خطط التنمية . وإن أى تحسن فى دخل الأفراد يوجه دائماً إلى سد احتياجاتهم الأخرى من السلع الاستهلاكية ونتيجة لذلك فإن أى تعديل فى النسب والتعريفة يتناسب مع مستوى تحسين الخدمات العامة من الصعب جداً إدخاله ، والنتيجة المترتبة على ذلك هو النقص فى حجم العائد.

المستويات التكنولوجية

معظم النظم الاقتصادية النامية تعتبر أن التخلف التكنولوجى يعتبر من المشاكل الضخمة وأن الاستثمار فى المشروعات والمصانع والمعدات تؤدى إلى عائد سريع ولكن الاستثمار فى تطوير المستويات التكنولوجية والخبرات والمهارات الفنية عادة ما تبين أن عائدها بطىء نسبياً .

أن المستويات التكنولوجية المرتبطة بنقل الركاب تنقسم إلى قسمين : المستويات المرتبطة بصناعة وتجميع السيارات المناسبة لتقديم الخدمات العامة ، والمستويات التكنولوجية الخاصة بتخطيط وتطوير وتشغيل وصيانة شبكات نقل الركاب . وأن صناعة السيارات فى الدول النامية عامة تتبع واحد من أسلوبين : الانتاج بمقتضى تصاريح من كبرى شركات صناعة السيارات أو تجميع السيارات التى سبق أن صنعت ، والانتاج المحلى لبعض الأجزاء والأنواع البسيطة وعادة مايقوم هذا على الصناعات التى تغذى ذلك .

ولكن فى كلتا الحالتين يواجه المرء صعوبة أساسية ، وهى النقص فى الخلفية التكنولوجية وشعور بالعرقلة فى الانتاج وذلك على مستوى التخطيط والتصميم والتصنيع ومراحل الرقابة فى هذه الصناعة ، وأن هذا يعتبر من السمات المميزة للنظم الاقتصادية الأقل تقدما . ومن الطبيعى أن هذا يعزى إلى النسبة المئوية المنخفضة فى التعليم على كل المستويات والثروة المحدودة الخاصة بالتجربة وخلفية المعلومات الصناعية والتكنولوجية ، وكل منهما يؤدى إلى عدم وجود شعور بالابتكار أو التخطيط ، وعدم وجود القدرات أو الصفات الخيالية على مستوى التنظيم .

وأن مثل هذه الحالة تؤدى إلى النقص الملموس فى الانتاجية ، ورداءة نوع الإنتاج وزيادة نسبية فى تكاليف الانتاج وأن العامل الآخر الذى يساهم فى رفع تكاليف الانتاج هو حجم الانتاج نفسه الذى لايصل أبداً إلى الحجم الاقتصادى فى المراحل الأولية من النمو . إن الطلب الداخلى على المنتجات النهائية محدود وأن التصدير فى هذه المرحلة أمر لايمكن التفكير فيه وذلك بسبب الخاصية واعتبارات التكاليف التى تجعل التنافس فى السوق الحرة يعانى من النقص .

إن قدرة الاقتصاد على تغيير وتطوير هذه المستويات التكنولوجية الغير مرضية بنسبة سريعة سوف تؤدى إلى نتائج مدهشة وذلك بالنسبة لتحقيق مستويات إنتاج مقبولة .

وتنطبق نفس النظرية بالنسبة للمستويات التكنولوجية فى تخطيط وتصميم وتشغيل وصيانة شبكة النقل البرى للركاب فى مواجهة منافسة المشروعات القوية المستقرة مثل النقل بالقطارات ووسائل النقل المملوكة لأفراد والتى تكون الأجرة فيها زهيدة أو مخفضة .

وتعتبر دراسة الإمكانيات المتصلة بنطاق العمليات ، وتقييم مدى الطلب على الخدمة وتناسبها مع شبكات النقل البرى القائمة واختيار المركبة المناسبة للخدمة والتخطيط وتحديد مواقع معدات التشغيل والتجديد الشامل والاصلاح والصيانة وتحديد مواعيد الخدمة وتعيين المركبات على الخطوط المختلفة للشبكة المقترحة بالتنسيق مع الطلب الذى تم تقييمه كل هذه تعتبر متطلبات هامة لأى نظام تشغيل كفء .

كما أن تحديد مواعيد التفتيش والصيانة الوقائية ووضع البرامج للتجديد الشامل كلها تعمل على إطالة عمر الأصول المستخدمة فى التشغيل .

كل هذه العوامل بالإضافة إلى نظام دقيق للرقابة وتحليل نتائج التشغيل والمرونة والاستعداد لتغيير أنماط التشغيل بهدف رفع كفاءة الشبكة إلى أقصى حد ممكن وتحقيق الطلب تحتاج بالتأكيد لدرجة عالية من القدرة التكنولوجية التى قلما توجد فى المراحل الأولى لنمو المشروع .

الأنماط التنظيمية :

وقد سبق مناقشة مزايا المشروعات الاحتكارية والمشروعات التى يحتكرها أفراد قليلون والمشروعات العامة والتى لها أنماط تنظيمية على طرفى النقيض مع الأنماط التى

تفرضها المنافسة الموجودة ، فى تشغيل خدمات نقل الركاب فى الجزء الثانى من هذا البحث .

ولتجنب احتمال استغلال الجمهور نتيجة السعى للحصول على أقصى حد من الربح تميل الدول الاشتراكية النامية والدول ذات الاقتصاد النامى والتى تتبع نظم المشروعات الحرة على نطاق واسع إلى اعتبار نقل الركاب الداخلى كمرفق عام يجب أن تديره هيئة عامة أو أن يكون تحت سيطرة الحكومة على الأقل .

وقد اتبعت بعض الدول ذات الاقتصاد النامى تماماً هذه النظرية هذه الأيام بعد أن شعرت بمزايا التكامل التام لمرفق نقل الركاب الداخلى وذلك بهدف تجنب الازدواج والمنافسة غير الضرورية والاستثمارات الضائعة .

غير أن الصعوبة فى معظم الدول النامية تنشأ من قدرة المهارات الادارية القادرة على تنظيم وتشغيل مشروع بهذا الحجم على مختلف مستويات الادارة .

والمشاكل المعقدة المتصلة بإدارة أى مؤسسة كبيرة واضحة تماماً . فمشاكل التخطيط والتنظيم وحشد القوة العاملة وتشغيل وفرض الرقابة على مؤسسة كبيرة وعلى المستويات الحديثة وعلى مستوى مقبول من الإنتاجية قد أصبح يدخل فى نطاق أساليب العمل المعقدة .

كما أن عمليات التنمية والتأميم قد زادت صعوبة الموقف ووسعت الهوة بين الطلب على إدارة تتميز بالكفاءة والمهارات الإدارية المحدودة المتاحة المؤهلة مسئوليات من هذا النوع .

وقد ظهرت خطط تنمية الادارة التى تتضمن الادارة العليا والوسطى . والادارة التنفيذية وإدارة الصف الأول من المشرفين والادارة الاستشارية كظاهرة بارزة لخطط التنمية الاقتصادية فى معظم الدول النامية .

وتجارب الهند ويوغوسلافيا وجمهورية مصر العربية فى هذا المجال ملحوظة تماماً . كما ساعدت المعونات الأجنبية لتنمية الادارة إلى حد كبير على الإسراع على هذا المتطلب الأساسى للدول ذات الاقتصاد النامى . وجدير بالذكر أن نشير إلى مساهمة جامعة هارفارد م. س. ت M.S.T. ومؤسسة فورد، ى.م.أ.د.أ. I.M.E.D.E. والأمم المتحدة.

والتدريب على جميع مستويات السلم التنظيمى ، وتنمية المهارات وأساليب العمل والتخطيط والتنويع الوظيفى كلها تعتبر مشاكل تواجه المؤسسات الكبيرة فى الدول ذات الإقتصاد النامى والإسراع أو التأخر فى التنمية فى هذه البلاد يتم بناء على معدل نجاح هذه البلاد فى التغلب على هذه المشاكل .

رابعاً : نقل الركاب فى الأقاليم وبين المدن فى جمهورية مصر العربية . خلفية تاريخية :

يمكن تقسيم النقل البرى فى مصر و ج. م.ع إلى ثلاث فترات مميزة :

١ — تبدأ الفترة الأولى فى الثلاثينيات وتنتهى مباشرة قبل الحرب العالمية الثانية .

٢ — تبدأ الفترة الثانية مع بداية الحرب العالمية الثانية وتمتد حتى قيام الثورة الإشتراكية فى مصر فى عام ١٩٥٢ .

٣ — الفترة الثالثة وتبدأ من عام ١٩٥٢ حتى الآن .

وتتميز المرحلة الأولى بقيام شركات مساهمة صغيرة خاصة دخلت مجال التجريب فى حقل تشغيل النقل البرى وذلك فى إطار نمط اقتصاد رأسمالى كان سائداً فى ذلك الوقت . وكان استغلال الجمهور واضحاً تماماً . فقد كانت المركبات دون الحد الأدنى من الراحة والأمن . وقد كانت التعريفات وأجرة النقل مرتفعة نسبياً وكانت الخدمة غير منتظمة إلى حد ما .

ومع انعدام كل من المنافسة تدخل الحكومة والتشريع سادت هذه الحالة اللاخلاقية والمحفوفة بالمخاطر ميدان النقل بين المدن والنقل فى الريف للركاب . فقد كان أصحاب المشروعات يعتبرون هدفهم الوحيد هو الحصول على أكبر ربح ممكن على حساب المصلحة العامة والأمن . وبالرغم من عدم وجود أية حالات احتكارية فى هذه المرحلة إلا أن العرض كان أقل بكثير من الطلب مما سمح بخلق جو مناسب ساعد أصحاب المشروعات القائمون على التشغيل على رفع الأجره كلما شعروا بحاجة لزيادة أرباحهم . كما كانت أوضاع التوظف دون المستوى المقبول قياساً على المستويات فى البلدان المتحضرة .

أما المرحلة الثانية فتتميز بالأنماط الاحتكارية بواسطة أفراد قليلين حيث اندمجت معظم الشركات المملوكة بواسطة أفراد والشركات الصغيرة فى مجموعات أو هيئات نقل كبيرة نسبياً . ونتجت تبعاً لذلك الحاجة للتخطيط والتنظيم كما كان لابد من إعادة النظر فى ظروف العمالة بعد إنشاء نقابات عمالية للنقل البرى . غير أن الجمهور ظل يعانى من الاستغلال وكان أى تحسين لمستوى الخدمة أو ظروف العمالة يعكس ارتفاعاً فى أجور نقل الركاب . كما كانت مركبات الجيش المعدلة تستخدم على نطاق واسع فى هذه الفترة .

وقد جاء تدخل الحكومة فى النقل البرى للركاب لأول مرة فى عام ١٩٤٧ عندما صدر أول تشريع ينظم عقود امتياز المرافق العامة . وكانت الإشارة إلى النقل البرى محدودة جداً فى هذا القانون باستثناء فقرة واحدة حددت أقصى عائد للاستثمار فى المرافق العامة بـ ١٠٪ مع توجيه أية أرباح إضافية لتحسين وتنمية الخدمة العامة ولتخفيض الأسعار والأجرة التى تدفع مقابل هذه الخدمة .

غير أن ضغوطاً معينة من الجماعات الإحتكارية التى تساندها الدوائر ذات النفوذ فى الحكومة والمجموعات الرأسمالية نجحت فى المحافظة على الإتجاهات السابقة من استغلال الجمهور وتقديم تفسيرات عدة للقانون مما أدى إلى عدم اعتبار نقل الركاب كمرفق عام وأدى هذا إلى عدم سريان تشريع ١٩٤٧ فيما يختص بالنقل .

واستمر عدم امان وعدم انتظام الخدمة إلى أن صدر أول قانون يحكم النقل البرى للركاب فى ١٩٥٠ . وكان من أهم الفقرات التى تنظم هذه الخدمة فى هذا التشريع مايلى :

(أ) النقل البرى للركاب مرفق عام .

(ب) تقسيم شبكة الطرق فى مصر إلى مناطق محددة .

(جـ) لا يمكن الحصول على عقود امتياز النقل البرى للركاب سوى عن طريق عطاءات عامة ولايمكن إصدار أى تصريح للتشغيل عن طريق وزير المواصلات .

(د) يسمح للشركات المساهمة التى لها عقود امتياز صدرت فى وقت سابق بفترة انتقال لمدة ثلاث سنوات يظل فيها الإمتياز قائماً وذلك لكى تستهلك أصولها الحالية وبعد هذه الفترة تصبح هذه الإمتيازات لاغية من نفسها .

وقد حدث التدخل المجدى للحكومة فى النقل البرى للركاب بعد ثورة ٢٣ يوليو مباشرة .

النقل البرى للركاب وتدخل الثورة الإشتراكية :

وضع تشريع عام ١٩٥٠ والقانون الذى تلاه فى عام ١٩٥١ بخصوص تقسيم شبكة نقل الركاب بين المدن وفى الريف إلى مناطق وخطوط سير معدلة موضع التنفيذ بعد الثورة مباشرة كما تم إدخال نظام جديد لعقود الامتياز فى عام ١٩٥٣ متضمنة شروط معينة اجبارية للتشغيل مثل تحديد مستوى المركبات المستعملة ومستوى الأمن والصيانة ومنشآت نهايات الخطوط ، وخط سير وعدد المشاوير على كل خط يومياً والحد الأعلى للاجرة بالنسبة لكل خط . كما كانت هناك شروطاً أخرى معينة بالنسبة لاستخدام الأيدى العاملة بما فى ذلك الأجور وساعات العمل والنص على بعض الحوافز والعلاج والرعاية الطبية .

وقد مارست الحكومة رقابة شديدة على النقل البرى للركاب وصدرت فى هذا الصدد عدة تشريعات وكانت الحكومة تمارس سيطرتها وتدخلها بالنسبة لقطاع النقل فى الريف وبين المدن عن طريق هيئة عامة أنشئت فى عام ١٩٦٠ وقد تبع ذلك ظهور تحسن ملموس فى هذه الخدمة العامة . كما فرضت الحراسة على أصحاب المشروعات وأصحاب الامتياز الذين لم يتمكنوا من العمل حسب نصوص عقد الامتياز وتم ذلك فى عام ١٩٦٠ ، ١٩٦١

واستمر أصحاب الامتياز فى التشغيل فى ظل الاتجاهات التنافسية التى نوقشت فى الجزء الثانى من هذا البحث كما استمروا فى استغلال الجمهور بقدر استطاعتهم فى إطار سياسة مخططة تخطيطاً جيداً وهذا من خصائص المشروعات الخاصة وذلك عن طريق التفسير الخاطىء لفقرات عقد الامتياز والدخول فى منازعات قانونية .

وقد طبقت قوانين التأميم الصادرة فى يوليه ١٩٦١ على جميع شركات نقل الركاب فى الريف وبين المدن وكان هذا إيذاناً ببدء عهد جديد فى مجال نقل الركاب .

وفى عام ١٩٦٤ أنشئت مؤسسة عامة لنقل الركاب فى الريف وبين المدن . ويتبع هذه المؤسسة أربع شركات

رئيسية هى شركات أتوبيس شرق الدلتا، وسط الدلتا، غرب الدلتا والصعيد .

وقد تكونت هذه الشركات بإدماج أجهزة نقل الركاب الصغيرة المؤممة . وبدأت هذه الشركات الأربعة فى التنمية المخططة لهذه الخدمة العامة الأساسية وفى ظروف تشغيل قاسية وجو غير ملائم نشأ عن حالة التخلف الموروثة فى أسطول النقل وإمكانيات صيانته .

وإن الإنجازات التى تحققت حتى الآن بواسطة هذه الشركات التابعة للقطاع العام بعد خمس سنوات منذ إنشائها ليعتبر شيئاً مرموقاً حقاً .

والجدول التالى الذى يبرز نمو مرفق النقل الركاب البرى فى الريف وبين المدن بين سنوات ١٩٦٢ – ١٩٦٧ ليعكس التقدم الذى حدث منذ التأميم .

خامساً – بعض المشاكل التى واجهت عملية التقدم السريع لمرفق النقل البرى للركاب :

واجهت إدارة شركات القطاع العام المنشأة حديثاً لتشغيل وتنمية شبكة النقل البرى للركاب فى الريف وبين المدن فى ج. م. ع مشاكل متنوعة وضغوط وقيود تعتبر عادية بالنسبة لمعظم الدول ذات الإقتصاد النامى . كما كان هناك قيوداً أخرى ظهرت نتيجة المشاكل الموروثة المتعلقة بالاستغلال غير الأخلاقى للجمهور فى فترة ماقبل التأميم بواسطة المسئولين عن التشغيل فى أساطيل النقل الخاصة والمتعلقة بالتنافس والمشاكل المتعلقة باتجاهات تحقيق أكبر ربح ممكن واستغلال القوى العاملة المستخدمة .

وفيما يلى بعض الصعاب التى واجهت الإدارة فى هذا القطاع وبعض الجهود التى بذلت للاسراع بتنمية هذا القطاع .

١ – نقص المعلومات والبيانات الاحصائية :

تعتبر هذه المشكلة مشكلة عامة بالنسبة للدول ذات الاقتصاد النامى وتجعل هذه المشكلة التخطيط صعباً للغاية . فقد كان أصحاب هيئات النقل الخاصة بما لهم من تفكير محدد مهتمون بتحقيق الربح فى المدى القريب متجاهلين تمام التجاهل إعتبارات المدى البعيد. ومن هنا كانت ضرورة التخطيط للشركات الجديدة . وفى عدم وجود أى بيانات إحصائية ، كانت أى عملية تقدير للطلب فى المستقبل أو

	شرق الدلتا		وسط الدلتا		غرب الدلتا		الصعيد	
	١٩٦٢	١٩٦٧	١٩٦٢	١٩٦٧	١٩٦٢	١٩٦٧	١٩٦٢	١٩٦٧
عدد العربات التى تملكها الشركة	٥٩٦	٨٥٩	٢٨٠	٤١١	١٨٠	٢٨٥	٤٦٤	٧١٢
طول الشبكة بالكيلو مترات	٨٠٧٧	٩٥٩٨	٥٣٤١	٥٤٧٠	٣١٠٧	٤٤٩٨	٩٣٢٢	١١٢٥٨
عدد خطوط السير	١٣١	١٧٥	٧٠	٩٧	٣٧	٧٦	١٤٥	٢١٢
المسافة المقطوعة يومياً بآلاف الكيلو	١١٩	١٣٥	٥١	٧٣	٤٤	٤٩	١٠٣	١٢٩
عدد المشاوير يوميا	١٠٤٧	١٦٤٤	٤٩٨	٧٢٢	٢٦٦	٤٩٣	١٠٢٤	١٤٠٦
عدد الركاب بالمليون	٥٠	٨٨	٣١	٤٠	١٩	٢٦	٣٧	٦٦
عدد القوة البشرية المستخدمة	٥١٥٩	٦٢١٥	٢٠٢٢	٢٥٠١	١١٨٧	١٨٠٣	٢٣١٩	٣٩٠١
الأجور سنوياً بآلاف الجنيهات	١٠٧٨	١٧٦٩	٣٦٦	٧٠٣	٢٤٣	٥٧٠	٤٣٤	٩٨٦
الدخل السنوى بآلاف الجنيهات	٣٤٣٧	٤٦٧٠	١١٦٧	٢١٧٩	٥٤٩	١٣٣٣	١٧٤٧	٣٥١٨

دراسة تأثير المنافسة وموسمية الطلب ودراسة الخصائص البارزة يعتبر عملا من الصعب القيام به .

وقد أدخل نظام الكشوف الارتجالية والبيانات الاحصائية على الفور وأمكن بذلك تقدير الطلب في المستقبل بسهولة . ونتيجة لتحسن الموقف قامت بعض الدراسات المفيدة مستخدمة الأساليب الحديثة كما قامت بحوث عن التشغيل بهدف إدخال التحسينات على كفاءة التشغيل في أساطيل هذه الشركات ومقابلة الطلب المتذبذب والموسمي لهذه الخدمة بقدر الامكان . وقد قامت شركة أتوبيس شرق الدلتا بدراسة في هذا الصدد بالتعاون مع مركز الرياضيات التابع لمعهد التخطيط القومي كما هو موضح في الملحق «أ» من هذا البحث .

٢ — الاستثمار المحدد لرأس المال :

وهذه أيضاً إحدى المشاكل الرئيسية في الدول النامية وجمهورية مصر العربية كدولة ذات اقتصاد نام وكدولة تطبق التخطيط المركزي في عملية التنمية الاقتصادية وضعت أولويات خلال المرحلة الأولى للتنمية التي بدأت ١٩٥٩ مؤكدة أهمية أصناف الانتاج من الدرجة الأولى والثانية أي التنمية الزراعية والصناعية .

وحيث أنه اعتبر كانتاج من الدرجة الثالثة فقد أعطى أهمية أقل في الخطة الخمسية الأولى للتنمية . وببداية خطة السنوات الخمس الثانية للتنمية الاقتصادية خصصت استثمارات أكبر للخدمات العامة بما في ذلك المواصلات وبذلك بدأ الموقف يتحسن . وبرغم الضغط الاقتصادي من الدول الاستعمارية في مناسبات مختلفة (ما بين عام ١٩٥٦ وعام ١٩٦٧) والاعتداءات المتكررة على جمهورية مصر العربية بواسطة إسرائيل والدول الاستعمارية استمر النمو الاقتصادي لمعدل يعتبر مذهلا ومرضياً للغاية بالنسبة لشعب جمهورية مصر العربية .

ولا يجب أن نتجاهل الموارد الاقتصادية والمصروفات الرأسمالية التي استنفدت في الحفاظ على الإنجازات الثورية التي حققها النظام الاقتصادي لجمهورية مصر العربية تحت الظروف التي سبق ذكرها والتي كان يمكن أن تستخدم استخداماً مفيداً في الإسراع بعملية التنمية . كما يجب ألا نغفل المرارة التي يشعر بها الشعب الحر في هذا الجزء من العالم والتي لها ما يبررها تجاه قوى الشعب الاستعمارية .

٣ — المساعدة الأجنبية :

وقلما استفاد مرفق النقل في جمهورية مصر العربية كقطاع عام من المعرفة الأجنبية . فقد قامت الجهود الوطنية بتمويل وإدارة جميع مشروعات التنمية في هذا القطاع بالذات وربما كانت هذه حالة فريدة بين تجارب الدول النامية الأخرى .

٤ — مقاييس تكنولوجية :

تتولى شركة النصر للسيارات إنتاج الأوتوبيسات في جمهورية مصر العربية كما تتولى إنتاج أنواع أخرى من العربات والجرارات الزراعية .

ويتم ذلك عن طريق إنتاج تجميعي متكامل بناء على تصريح واتفاقية معقودة مع شركة دويتس الألمانية . يتم إنتاج معظم الأجزاء الخاصة بالعربات محلياً بينما تستورد الشركة نسبة مئوية قليلة من بعض الوحدات والأجزاء الأخرى لتجميعها محلياً . ومعظم الأجزاء التي تقوم بامدادها الشركات الصناعية يتم إنتاجها محلياً في شركات تأسست أخيراً في إطار خطة التصنيع في جمهورية مصر العربية .

وبالنظر إلى تطور المقاييس التكنولوجية في جمهورية مصر العربية نسبياً ، فان نوع العربات المنتجة يعتبر مرضى تماما ، كما وأن التشغيل يعتبر مقبولا في أي مستوى .

غير أن عامل النقد يلعب دوراً خاصاً بالنسبة لتأثيره على مستويات الأسعار وذلك بخلاف اعتبارات أخرى بسيطة لا يعتد بها خاصة بالشركة نفسها والتي يجري التغلب عليها تدريجياً عن طريق زيادة التمرين للعمال وكذلك عن طريق

مجلة

جمعية المهندسين المصرية

مجلة علمية هندسية — تصدرها كل ثلاثة شهور

جمعية المهندسين المصرية بالقاهرة

الاشتراك السنوى لغير الأعضاء :

للمهندس	٦٠ قرش
للهيئات	٢٠٠ قرش

CANAL HARBOUR WORKS Co.

SUEZ CANAL AUTHORITY
Al Zouhour District,
Nasr City — Cairo

Telephones { 833304 / 832861

COMPANY'S ACTIVITIES :

The Canal Harbour Works Company which is affiliated to the Suez Canal Authority, was founded in 1965 with a capital of two million Egyptian pounds, to fill in a long existing gap in the field of erection of harbours, protection of shores and salvage and towage of ships.

This field was monopolised in the past by foreign foundations. The Canal Harbour Works Co., has since replaced these foundations. When, as a result of the Israelian aggression in the Suez Canal, the navigation in the waterway was interrupted, the Canal Harbour Works Co. transferred a part of its activities to other countries with the intention of opening new international fields of action and naturally increasing the national income in foreign currency.

In spite of the competition of other world specialized companies, the Canal Harbour Works Co. succeeded in signing contracts for the execution of important works in Syria for the amount of thirty two million Syrian Liras. Meanwhile, the company is now studying projects which are of vital importance for the Lybian Arab Republic and Kuwait.

For the execution of these works, the Company has provided Syria with the necessary most modern equipment and adequate machinery, the cost of which amounting to practically three million pounds. That besides the necessary experienced staff.

CONCLUTIONS

From the above investigation, the following conclutions are obtained :

1 — The relation between the damping decrement $\triangle$ p for metals and the alternating stress f_o is as follows :

$$\triangle_p = (C_1/f_o) \cdot e^{-} C_2/f_o$$

where C_1 and C_2 are constants.

Theoretically the damping increases with the increase of the alternating stress up to 1350 kg/cm² for copper, but experimentally it is found that the relation is correct *only* up to a total stress of about (480 — 580) kg/cm², and outside this range the relation is not valid.

2 — The relation between the increase in the damping decrement δ ($\triangle$ p) and the mean stress f_m is as follows :

$$\delta (\triangle p) / (\triangle p_o) = C_1' \cdot e^{-} C_2/f_m$$

where $\triangle p_o$ is the damping decrement at zero mean stress.

C_1' and C_2 are constants.

Theoretically the damping decrement increases as the mean stress increases, but experimentally it is found that this relation is *only* correct (for copper) up to a mean stress of about 160 kg/cm².

REFERENCES

1 — Koehler J.S. ; Imperfection in nearly perfect crystal (1952), P. 197.

2 — Nowick A.S. ; J. Appl. Ph., 25-1124, and 80-349, 1954.

3 — J. Weertman and E. I. Salkovitz ; J. Appl. Ph. 26-202, 1955.

4 — Mott and Nabarro ; Proc. Ph. Soc. (LOND.), 58-669, 1946.

5 — Granto and K. Lucke ; J. Appl. Ph., 27-538, 1956.

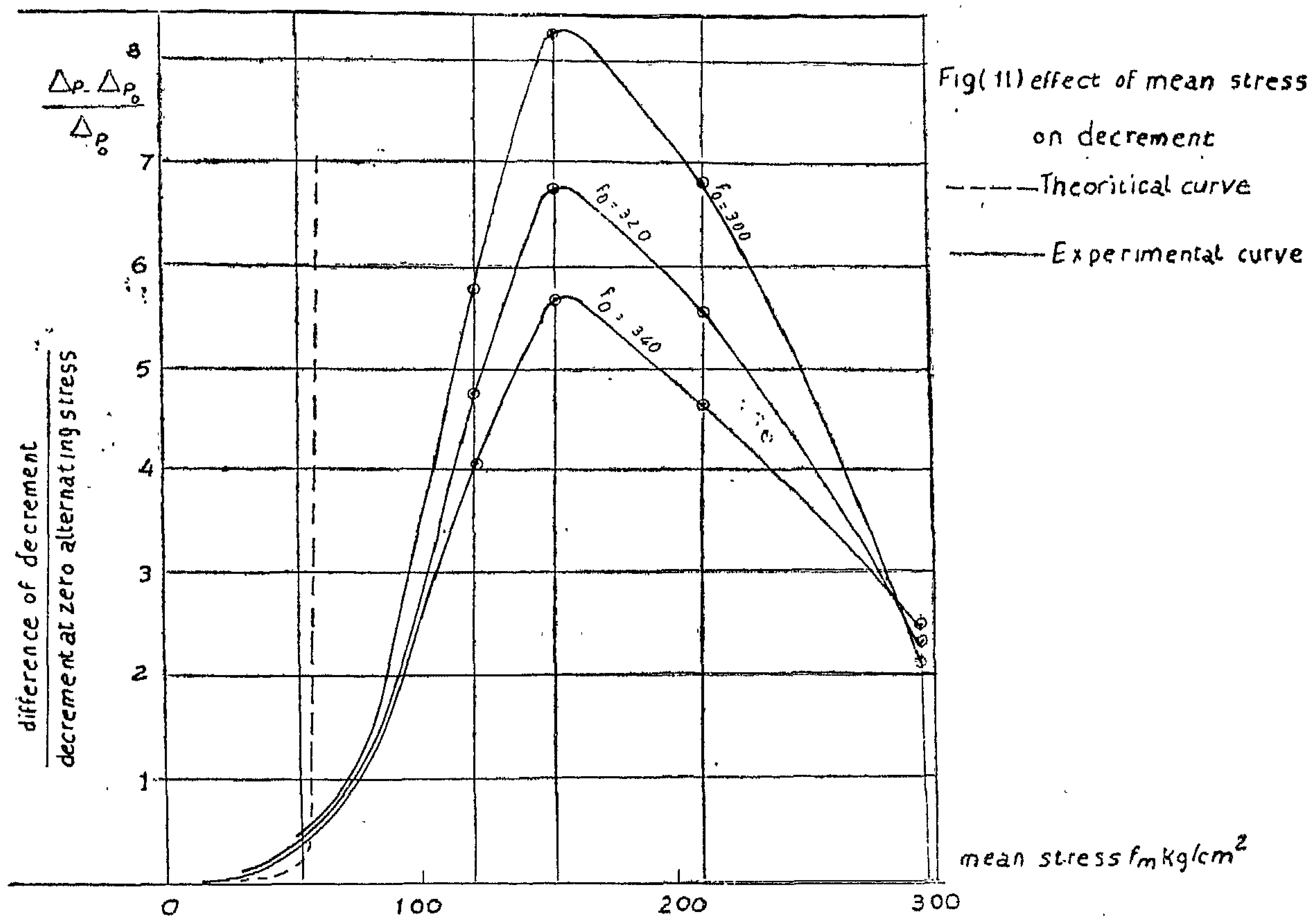
6 — Ruel V. Churchill ; Modern operational mathematics in Engineering, 1944.

7 — K.A. Mostafa ; M.Sc. Thesis "An investigation into the effect of alternating and mean stress on the damping properties of materials." Ain Shams University, F. of Eng. Library.

8 — George E. Dieter ; J. Mech. Mettalurgy, 1961.

9 — F.R.N. Nobarro ; Theory of crystal dislocation, 1967.





aggregation of vacancies, and these sources would act as a Frank-Read source for dislocation multiplication. This type of dislocation sources is mathematically too complicated.

b) There are other dislocation multiplication systems in the crystal but the Frank-Read source is the major one.

c) The viscous damping effect.

d) The grains are considered perfect spheres of equal sizes, but actually the grains have random shapes and sizes.

ii) At high stress region :

In this region the theoretical curve increases to ∞, but the experimental shows a peak at a mean stress of about 160 kg/cm² This is most probably due to the following :

a) The dislocations interact with each other in the same glide plane, also the dislocations of one system interact with the dislocations in other systems. As a result of these dislocation interactions, their motion is somewhat impeded, and thus the rate of increase of decrement decreases.

b) In spite of the increase of the dislocation density, the major loop length L_n decreases because of the formation of more nodes and the possibility of vacancy interaction, which leads to a decrease in the decrement.

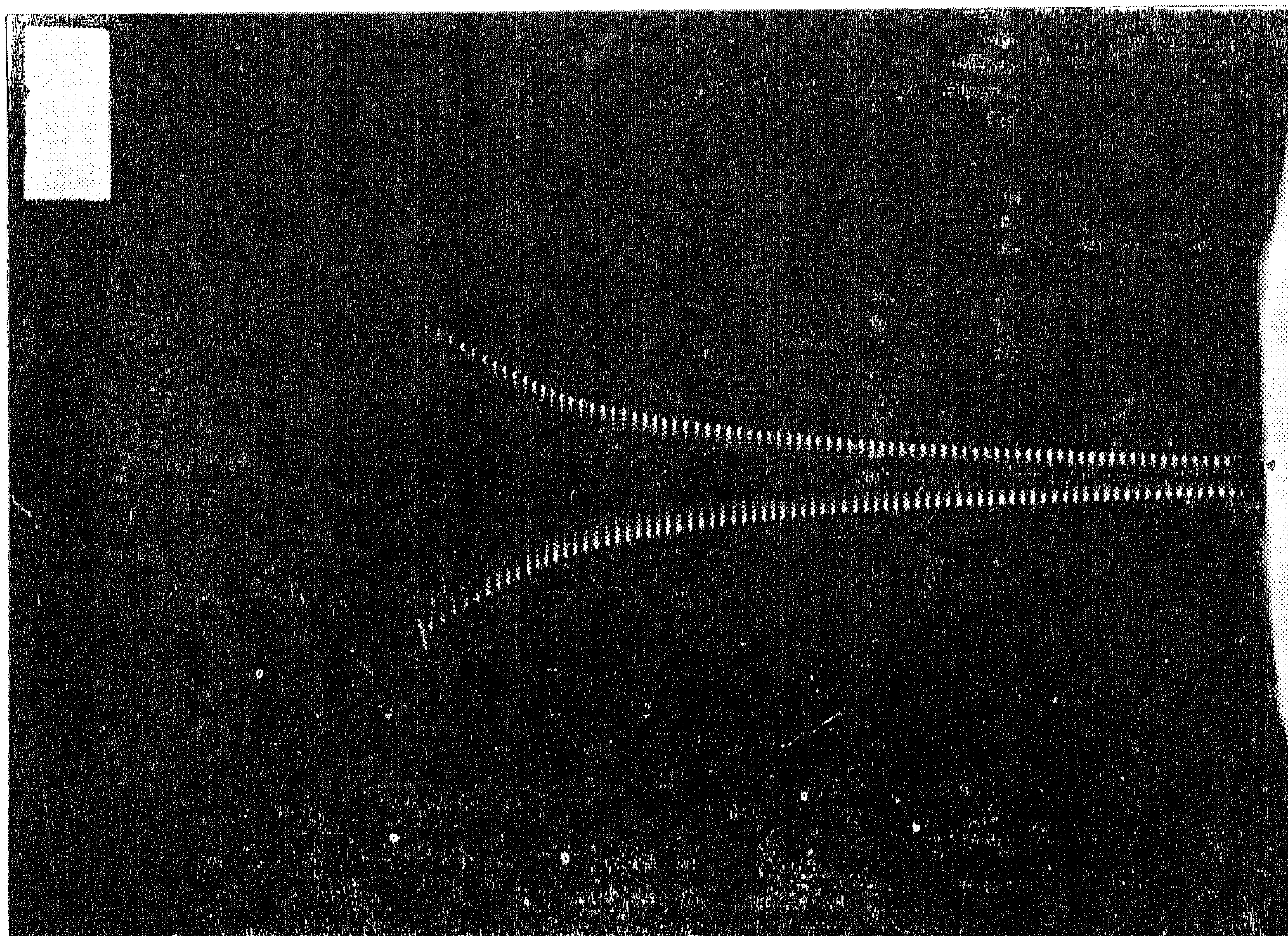


Photo (2) : Run out diagram of the compensation test piece for mean load of 0 Kg./cm².

From Fig. (10), values of $\partial (\Delta_p) / \Delta_{p\infty}$ at different mean stresses for the alternating stress as a criterion are calculated and plotted in Fig. (11), together with the theoretical curve from relation (27).

Analysis of Results :

The following points can be deduced from the rsults and curves :

1 — Refering to Fig 10.

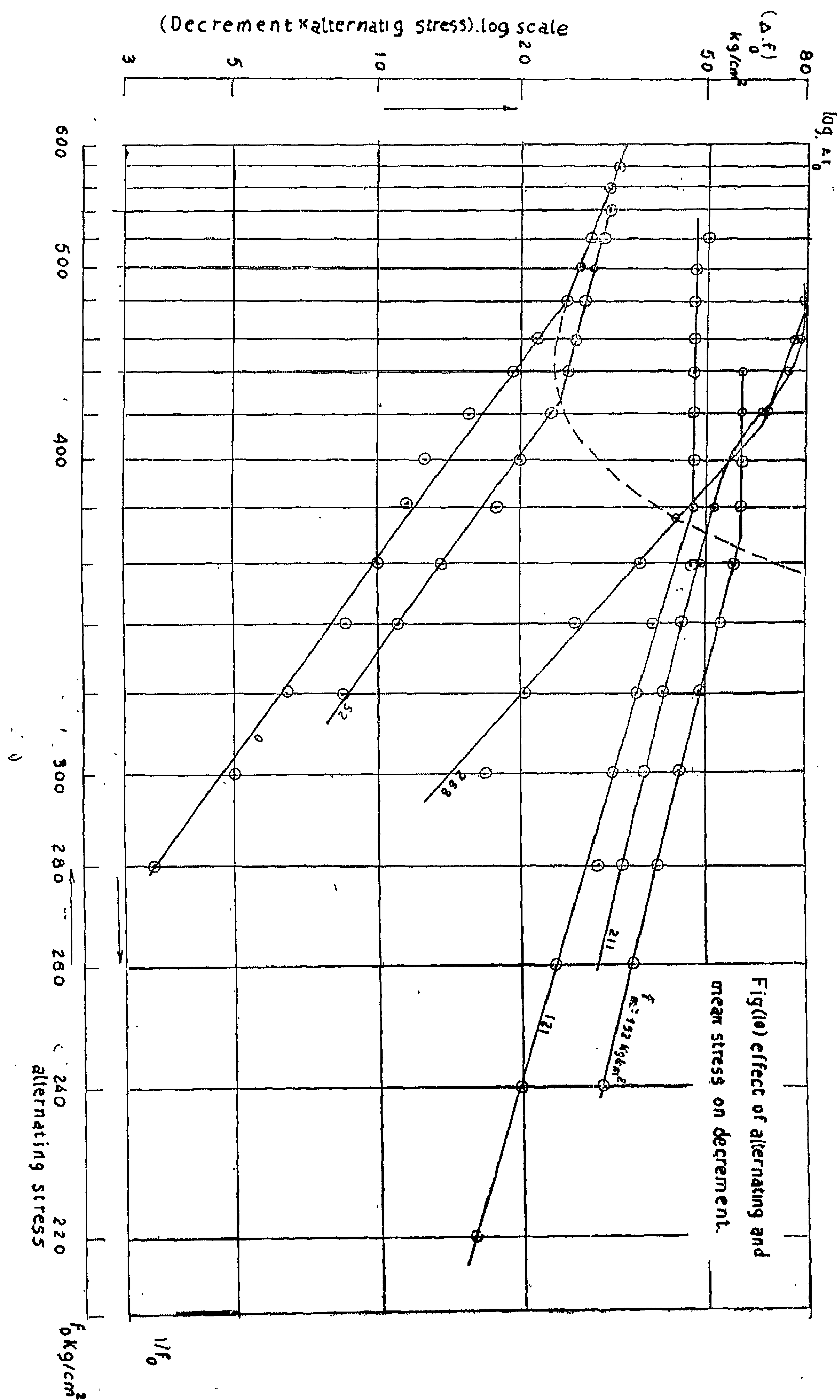
a) The plot is linear up to a mean stress of about (480 — 580) kg/cm² which verifies the theoretical relation (28), but beyond that limit the slope is suddenly decreases, which is most probably is due to sudden break-away of dislocation lines from their pinning points.

b) The slope of the straight line part, decreases slightly as the mean stress increases, this is due to increase in the minor loop length and also as a result of break-away of some loops.

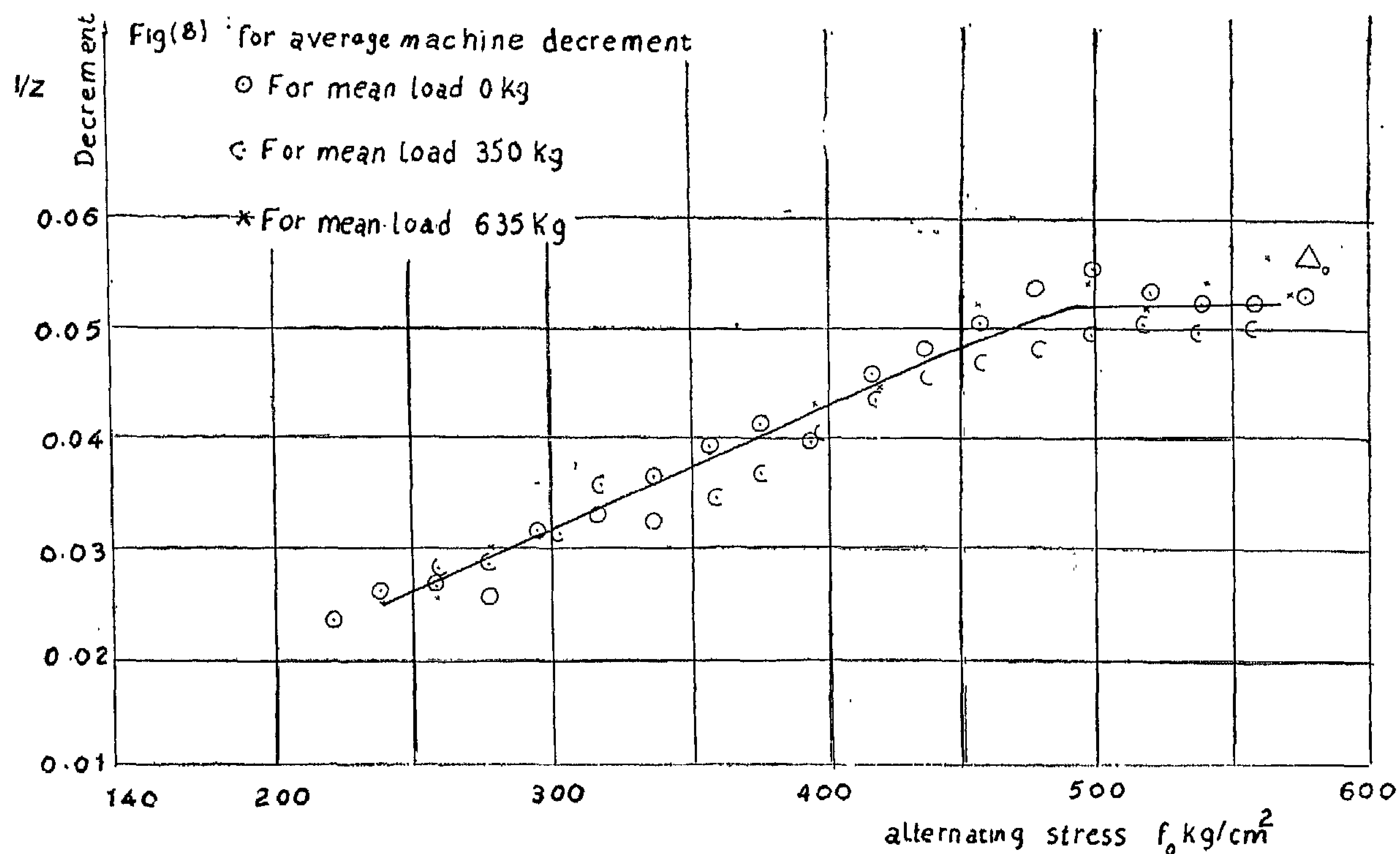
2 — Refering to Fig. 11, the theoretical results are less than the experimental up to a mean stress of about 60 kg/cm², then it increases rapidly than the experimental. These deviations are most probably due to the follow-

i) At low stress region.

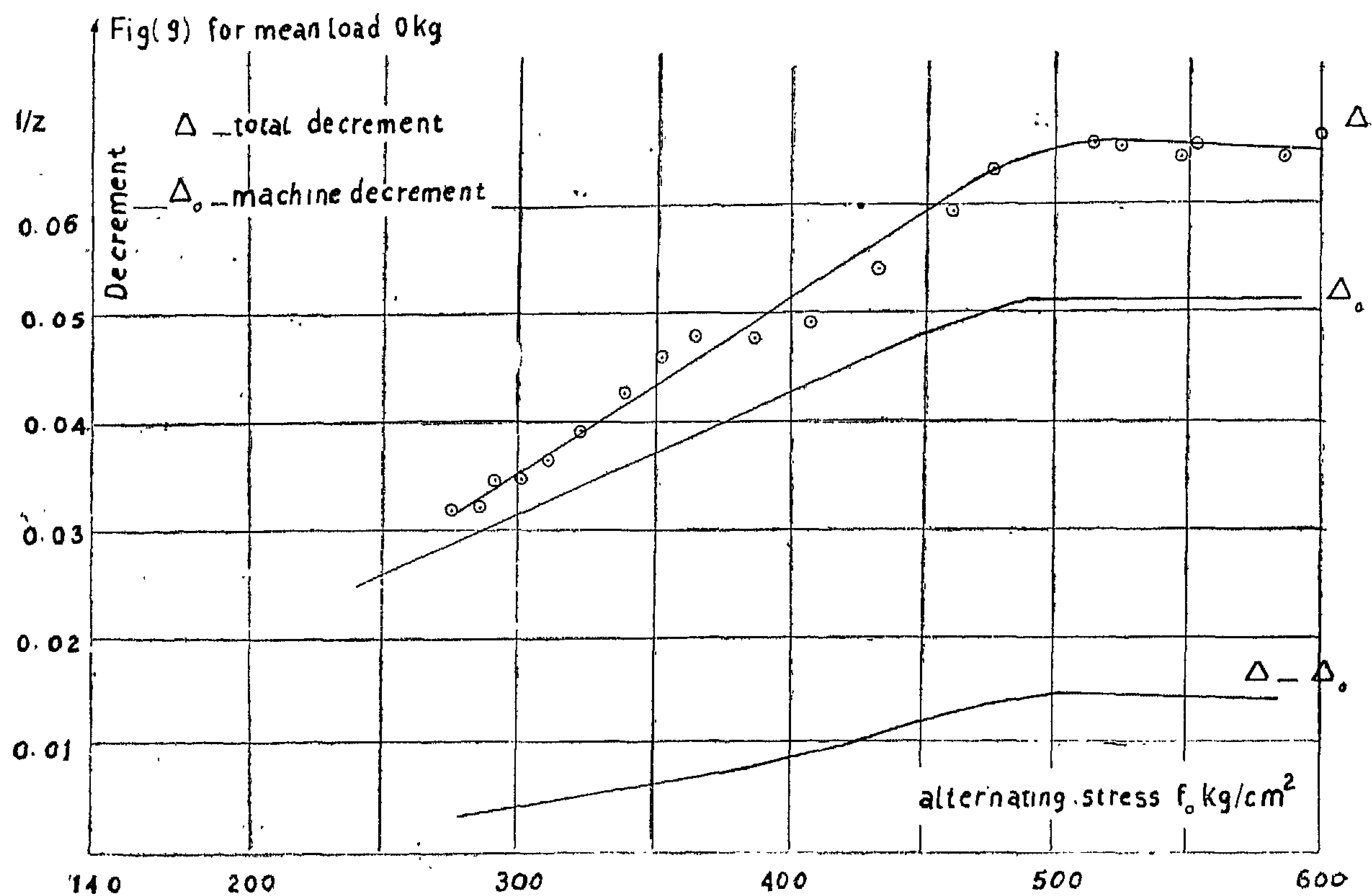
a) The original dislocation density does not remain constant during the stress cycles. There are new dislocation sources created e.g. the prismatic dislocation which is formed by



Fig(10) effect of alternating and mean stress on decrement.



Fig(8) for average machine decrement
⊙ For mean load 0 Kg
C For mean load 350 Kg
* For mean load 635 Kg
1/z
Decrement
0.06
0.05
0.04
0.03
0.02
0.01
140
200
300
400
500
600
alternating stress f_o kg/cm^2
Δ_o



Fig(9) for mean load 0 kg
1/z
Decrement
Δ _total decrement
Δ_o _machine decrement
0.06
0.05
0.04
0.03
0.02
0.01
140
200
300
400
500
600
Δ
Δ_o
$\Delta - \Delta_o$
alternating stress f_o kg/cm^2

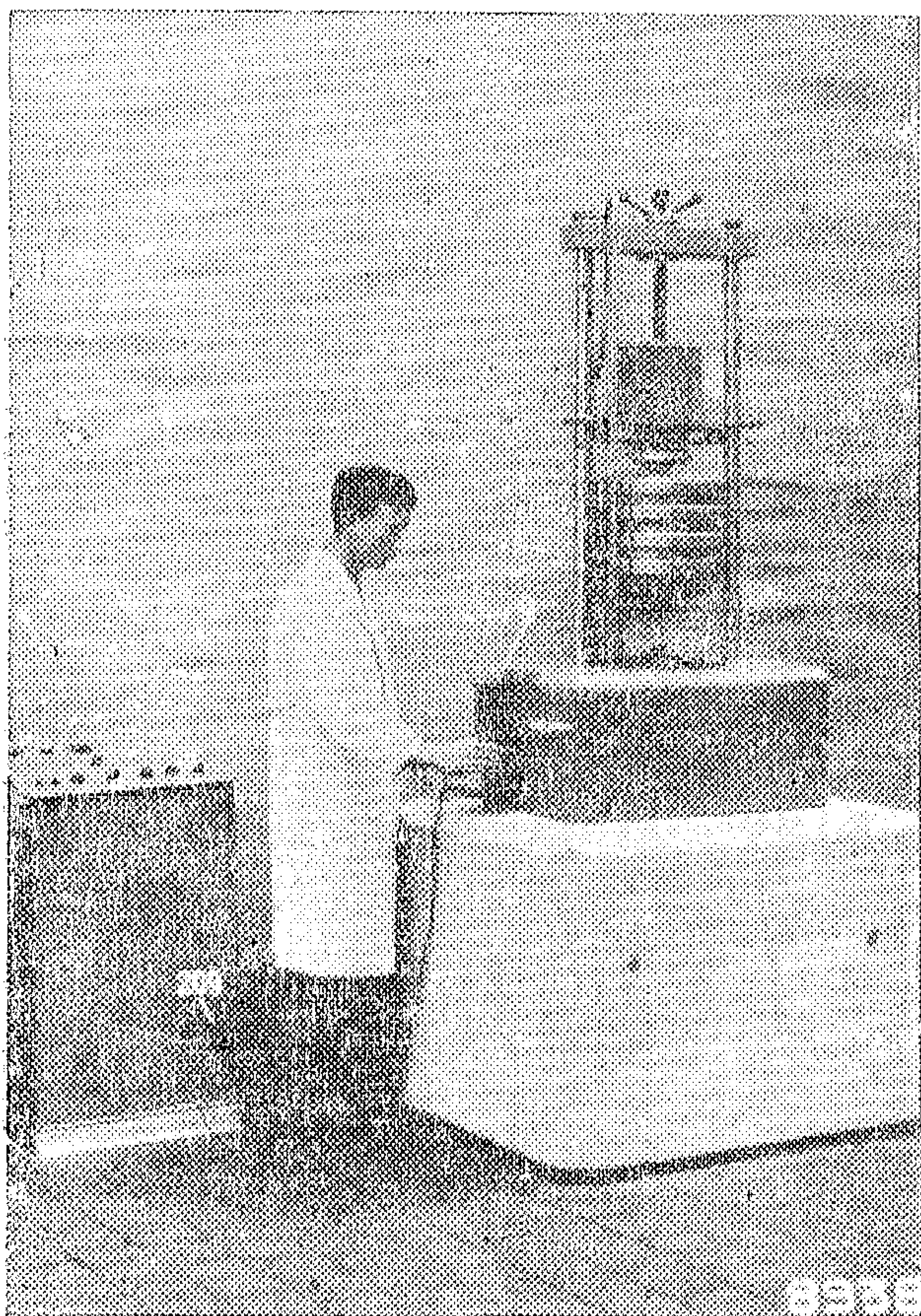


Photo (1) : Testing machine (vibrophore).

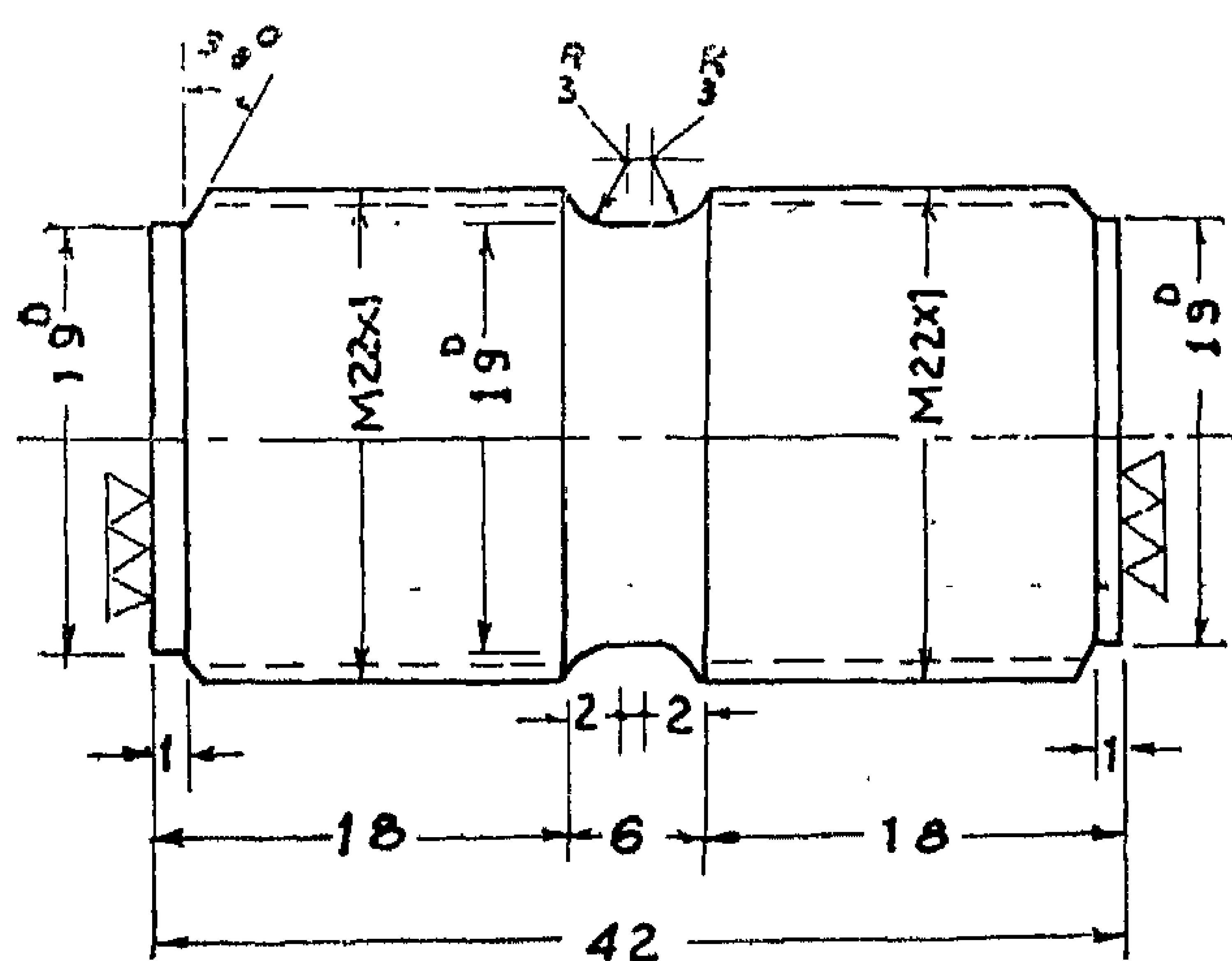


Fig. (7) Compensation test piece.

C — Procedure :

After fixing the specimen into the machine, it is switched on, the loaded camera is fixed. After the specimen is subjected to about 600000 cycles, the machine is switched off, and the camera motor on. As soon as the edge of the film just passes the slit, the shutter is opened, and the film is exposed for one revolution of the drum. After fixing and developing the film, it is enlarged, by means, of a projector, to about three times its original size before recording the required parameters.

D — Determination of the damping capacity : from the decay diagrams.

The rate of dying out of the amplitude from the decay diagram of the main specimen represents the total damping of the whole vibrating system, and that of the compensation specimen represents the damping capacity of the machine and the end fixation. The difference between these two values is the damping capacity of the tested metal.

E — Results :

Photos are taken for six main specimens and six compensation specimens, and as the diagrams for the later specimens are similar, calculations for the machine decrement ($\triangle_o$) are carried out for three mean loads 0, 350, 635 kgs. Photo 2 represents the decay diagram of the machine. Fig. 8, represents the average machine decrement.

For the main specimens, calculations are carried out for the six specimens at 0, 150, 350, 455, 635, 840 kg. mean load. For each mean load, a curve is drawn for the decrements as a function of the variable stress, from a stress of about 200 kg/cm^2 to 600 kg/cm^2 ; Fig. (9) shows the curve for the mean load 0 kgs.

From the above results and curves, a series of curves are drawn Fig. 10, for the relation (26) in a logarithmic form i.e.

$$\log (\triangle_p . f_o) = \log C_1 - (C_2 . \log e) . (1/f_o) \quad (28)$$

Adjustment of the above relations in terms of measured quantities :

As the break-away length for a stress ζ_m is,

$$L' = F'/a\,\zeta_m \qquad (20)$$

where[8] $F' = 4\,G\,\varepsilon'\,a^4 / z^2$ (21)

$\therefore\ \Gamma = L'\,\zeta_m/L_c$, from (20) and (21)

$$\Gamma = 4\,G\,\varepsilon'\,a^3 / L_c\,z^2 \qquad (22)$$

Substituting in (19), and replacing $\zeta_m = R\,f_m$, R is a constant.

$$\therefore\ \Delta\Lambda/\Lambda_i = C_1'\,.\,e^{-C_2/f_m} \qquad (23)$$

where $C_1' = 8\,(a/z)^2\,.\,(D/L_c)^2.\,\varepsilon'$

$C_2 = k\,a\,E\,\varepsilon'/L_c$,

$k = 4\,G\,a^2 / R\,E\,z^2$

k is a parameter depends upon the orientation and anistropy.

The total dislocation density at any mean stress will be :

$$\Lambda_t = \Lambda_i + \Delta\Lambda$$

$$= \Lambda_i\,(1 + C_1'\,.\,e^{-C_2/f_m}) \qquad (24)$$

Substituting Λ_t instead of Λ in (15) :

$$\therefore\ \Delta_p = \frac{\Delta_o'\,\Lambda_t\,L_n^2}{\pi}\,.\,\frac{L_n}{L_c}\,.\,\frac{\Gamma}{\zeta_m}\,.\,e^{-\Gamma/\zeta_o} \qquad (25)$$

Multiplying (25) by the orientation factor T[5,9] and taking[7] $\zeta_o = R\,f_o$,

From (22) and (25), $\Delta_p = (C_1/f_o)\,.\,e^{-C_2/f_o}$ (26)

where $C_1 = T\,\Lambda_t\,L_n^3\,\Delta_o'\,\varepsilon'\,a\,E\,.\,k/\pi\,L_c^2$

$\because\ \delta(\Delta_p) / \Delta p_o = \Delta\Lambda/\Lambda_i$

where $\delta(\Delta p)$ is the increase in the damping decrement

Δp_o is the damping at zero mean stress.

From (23)

$$\delta(\Delta p) / \Delta p_o = C_1'\,.\,e^{-C_2/f_m} \qquad (27)$$

Experimental Analysis :

A — Apparatus :

The tests are carried out on the high frequency machine "The Vibrophore" shown in Fig. 5, and photo 1.

B — Test Specimens :

Are made of an electrolytic copper of purity 99.66%, from the same barstock, to ensure homogenity, and they are annealed to remove cold working effects and to ascertain the same initial dislocation denity. The dimensions of the main specimens, Fig. 6, and that of the compensation specimens, Fig. 7, are taken from the manufacturer catalog.

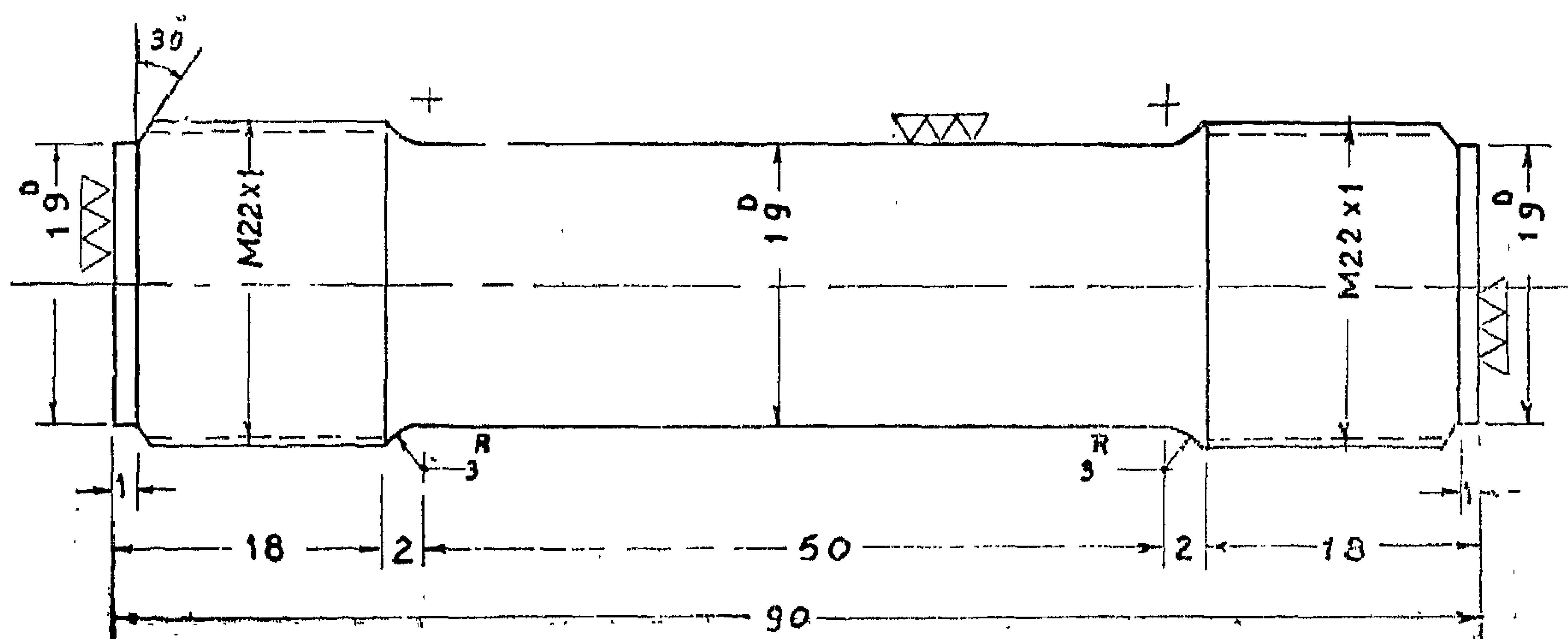


Fig (6). test piece. Scale 2:1 Dim. in m/m.

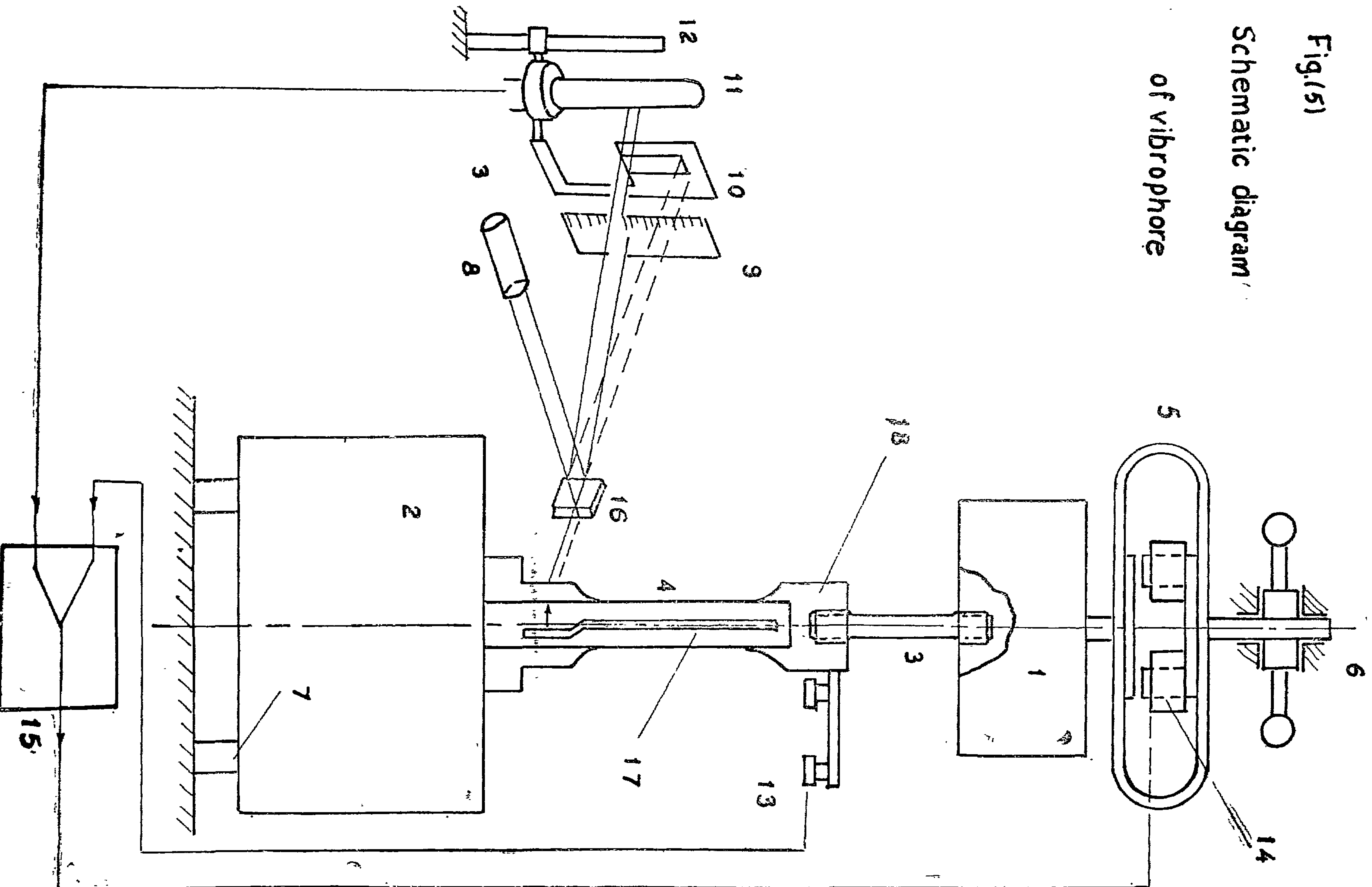


FIG. 5. THE VIBROPHORE:

1 — Main moving mass.
2 — Opposing mass.
3 — Specimen.
4 — Dynamometer.
5 — Preload spring.
6 — Adjusting spindle.
7 — Vibration isolation.
8 — Optical projector.
9 — Dynamometer scale.
10 — Diaphragm.
11 — Photo-electric cell.
12 — Slide of photo-electric cell.
13 — Impulse generator.
14 — Driving magnet.
15 — Amplifier.
16 — Oscillating mirror.
17 — Comparison strip (bar).
18 — Specimen holder.

Since no break-away occurs when $L' \geqslant L_n$, q is from $0 \leqslant q \leqslant \nu$, thus the wve term can be neglected. Also as $\nu >> 1$, then $\nu - 1 \simeq 1$, and substituting for Ψ from (8), relation (11) will be reduced to :

$$\varepsilon_1 \simeq Q \left[1 + \frac{\nu^3}{3!} \left(\frac{\Gamma}{\zeta} + 1 \right) e^{-\Gamma/\zeta} \right] . \zeta \qquad (12)$$

where $Q = 8 a^2 \Lambda L_c^2 3 ! / \pi^4 C$

Similarly the dislocation strain for the function N_2 (L) d (L) for the decreasing stress part will be :

$$\varepsilon_2 = Q \left[1 + \frac{\nu^3}{3} \left(\frac{\Gamma}{\zeta_0} + 1 \right) e^{-\Gamma/\zeta_0} \right] . \zeta \qquad (13)$$

The energy loss per cycle, Fig. 4 :

$$\triangle W = 2 \int_0^{\zeta_0} (\varepsilon_2 - \varepsilon_1) \, d\zeta$$

$$= (Q \nu^3 \zeta_0 \Gamma e^{-\Gamma/\zeta_0}) / 3 ! \qquad (14)$$

The potential energy at the beginning of any vibration cycle $W = \zeta_0^2 / 2G$. Defining the damping decrement $\triangle p = \triangle W / 2W$, and substituting the value of Q ;

$$\therefore \triangle_p = \frac{\triangle_0' \Lambda L_n^2}{\pi} . \frac{L_n}{L_c} . \frac{\Gamma}{\zeta_0} . e^{-\Gamma/\zeta_0} \qquad (15)$$

where $\triangle_0' = 8 G a^2 / \pi^3 C$

Effect of the mean stress on the decrement.

If the shear stress ζ_m is applied to the dislocation loops. Fig. (1, A). The lengths L_n may be broken away or act as a "Frank-Read" source. For metals, generally break-away occurs before the actuation of Frank-Read source. Since the break-away process is a catastrophic one, the loop after break-away will be the major net work length L_n, which is assumed constant for all the loops.

Consider the source to be at the center of a grain of diameter D, the maximum number of dislocations that can be generated by a single source in the center of a spherical grain of diameter D is[8] :

$$n = \pi \zeta_m D / 4 G a$$

And as the dislocation density can be defined by one of the following definitions :

1 — N_s the number of dislocations crossing unit area.

2 — N_v the total length of dislocation lines in unit volume of the solid.

and $N_v \simeq 2 N_s$

$\therefore$ for one source

$$N_s = 2n / (\pi D^2/4) \ cm^{-2}$$

Substitute for n,

$$\therefore N_v = 4 \zeta_m / G a D \ cm^{-2}$$

The total length of dislocation lines per source, in a sphere of diameter D will be :

$$N_v' = 4 \pi (D/2)^3 . N_v / 3 = 2 \pi \zeta_m D^2/3 G a \ \text{cm/source} \qquad (16)$$

Also, the number of loops which will actuate Frank-Read source is a function of the mean stress, and equals the total number of loops that are already broken away from their minor pinning points and still pinned at the nodes. From (9),

$$N'(L)d(L) = (\Lambda_i/L_n) . \delta (L - L_n). M. d (L) \qquad L' \leqslant L \leqslant \infty \qquad (17)$$

$$M = (\nu - 1) (q_m + 1). e^{-q_m}, \text{ and } q_m = \Gamma / \zeta_m$$

From the definition of the delta function, and denoting N′ (L) d (L) by Φ, the number of loops that have the constant length L_n per unit volume, at any mean stress is , $\Phi = \Lambda_i M/L_n$ source/cm^3 (18)

The increase in dislocation density due to Frank-Read sources generated by the mean stress ζ_m is, $\triangle \Lambda = \Phi N_v'$

From (16) and (18), and substituting for $\nu - 1 \simeq \nu$ and for $q_m + 1 \simeq q_m$

$$\therefore \triangle \Lambda/\Lambda_i = (2 \Gamma D^2 \nu . e^{-\Gamma/\zeta_m})/L_n G a \qquad (19)$$

i.e. the displacement y is composed of two periodic motions :

1 — The one with the natural frequency w_n, which can be neglected as it will damp down due to the viscous drag.

2 — The forced vibration term with frequency w, which will represent the vibration in its steady state.

Considering the first mode of vibration, i.e. for $n = 0$, $w_o = \pi b/L$.

Substituting in (4) :

$$y = \left(\frac{4\,aL^2\,\zeta_o}{\pi^3\,C} \,.\, \sin\frac{\pi\,x}{L}\right) \cos wt \qquad (5)$$

The average value of the amplitude Y is :

$$Y' = \frac{1}{L}\int_0^L \frac{4\,aL^2\,\zeta_o}{\pi^3\,C} \,.\, \sin\frac{\pi\,x}{L}\,dx$$

$$= \frac{8\,aL^2\,\zeta_o}{\pi^4\,C} \qquad (6)$$

As the dislocation strain is defined,[5]

$$\varepsilon = \Lambda.a.Y \qquad (7)$$

$$\therefore \quad \varepsilon = \Lambda.a.\frac{8\,aL^2\,\zeta_o}{\pi^4\,C} \,.\, \cos wt$$

For a single dislocation loop, i.e. $\Lambda = L$

$$\varepsilon = \frac{8a^2L^3\,\zeta_o}{\pi^4\,C} \cos wt = \Psi\,L^3 \qquad (8)$$

From (8), it is clear that, for the same disturbing stress, the dislocation strain depends on the loop length. The loop lengths are not constant because of the impurity atoms which are randomly arranged along the dislocation line. At the beginning of the increasing stress part of the vibration cycle, the minor length L_c can be considered as an average loop length.

From the distribution function derived by Koehler[1], the number of loops N(L)d(L), which have lengths between L and (L + dL) with L_c as an average loop length is :

$$N(L)\,d(L) = \frac{\Lambda}{L_c^2} \,.\, e^{-1/L_c} \,.\, d(L)$$

As the stress increases, successive breakaway from the pinning points occurs, until the stress reaches certain limit at which all the loops will have the major length L_n. (This length is assumed to be constant). This type of distribution is called delta distribution and is given by :

$$N(L)\,d(L) = \frac{\Lambda}{L_n}\,\delta\,(L - L_n)\,d(L)$$

(i.e. $= \Lambda/L_n$)

At any intermediate variable stress, the distribution function is assumed to consist of two parts as follows :

$$N'(L)\,d(L) = \begin{cases} \dfrac{\Lambda}{L_c^2} \,.\, e^{-1/L_c} \,.\, J \,.\, d(L) & 0 \leqslant L \leqslant L' \\ \dfrac{\Lambda}{L_n} \,.\, \delta\,(L - L_n) \,.\, M.d(L) & L' \leqslant L \leqslant \infty \end{cases} \qquad (9)$$

where[5] $J + M = 1$

$$J = 1 - (\nu - 1)\,(q + 1)\,.\,e^{-q}$$
$$M = (\nu - 1)\,(q + 1).\,e^{-q}$$
$$q = L'/L_c = \Gamma/\zeta\,, \;\&\; \nu = L_n/L_c \qquad (10)$$

Substituting the values of J and M from (10) into (9), will give the distribution function N_1 (L) d (L) for the quarter cycle when the stress is increasing. And as the constant loop length L_n collapse elastically the distribution N_2 (L) d (L) for the quarter cycle when the stress is decreasing can be obtained by replacing q by $q_o = \Gamma/\zeta_o$ in **(10)** before substituting in (9).

From (8), the dislocation strain for the distribution function N_1 (L) d **(L)** will be :

$$\varepsilon_1 = \int_0^\infty (\Psi\,L^3)\,N_1\,(L)\,d\,(L)$$

Integration will give :

$$\varepsilon_1 = \Psi\,\Lambda\,L_c^2\,3\,!\,\Big(1 + e^{-q}\Big\{\frac{\nu^2\,(\nu - 1)\,(q + 1)}{3\,!} - \left[\frac{q^3}{3} + \frac{q^2}{2} + (q+1) + (\nu - 1)\,(q+1)\right]\Big\}\Big) \qquad \textbf{(11)}$$

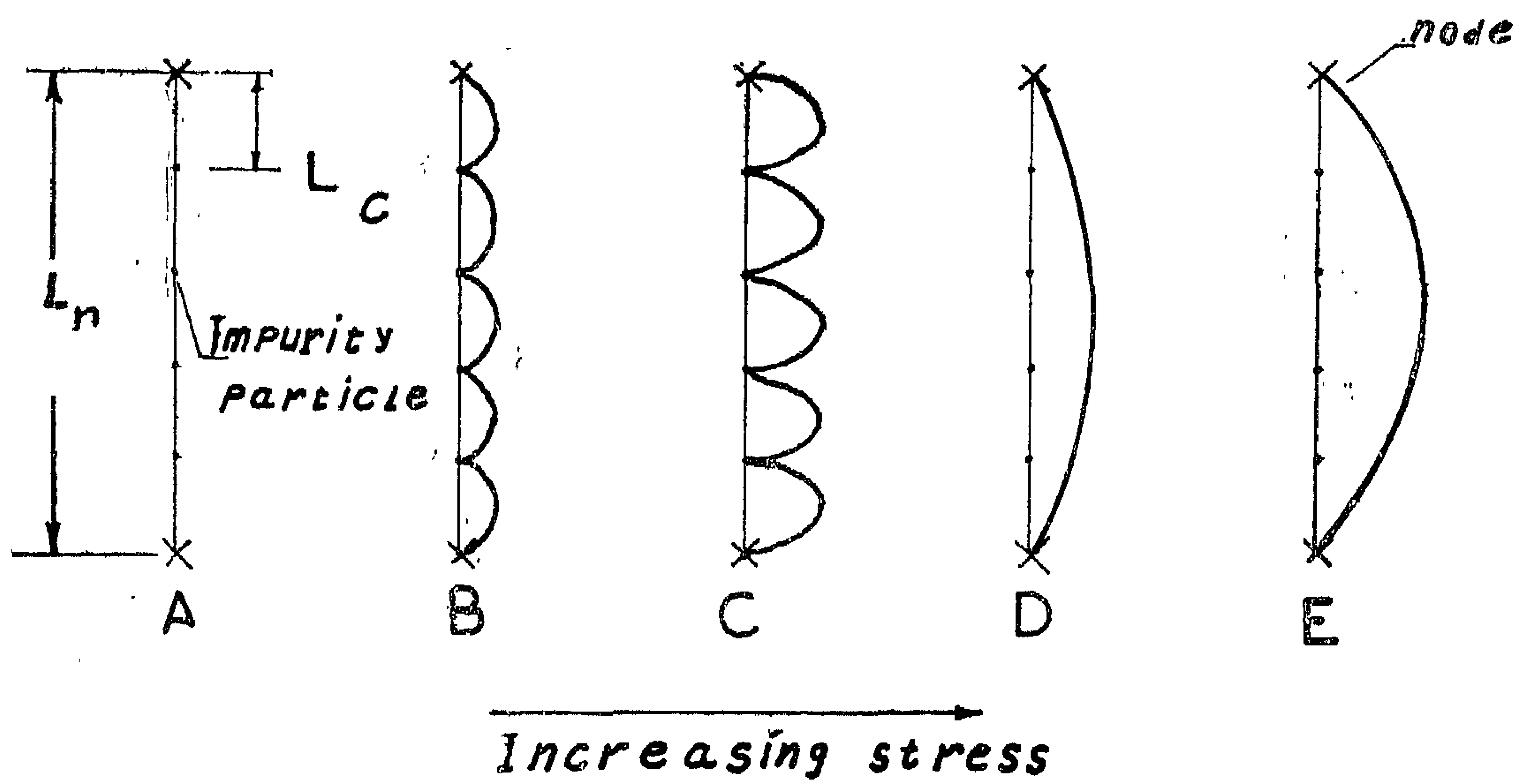


FIG 1

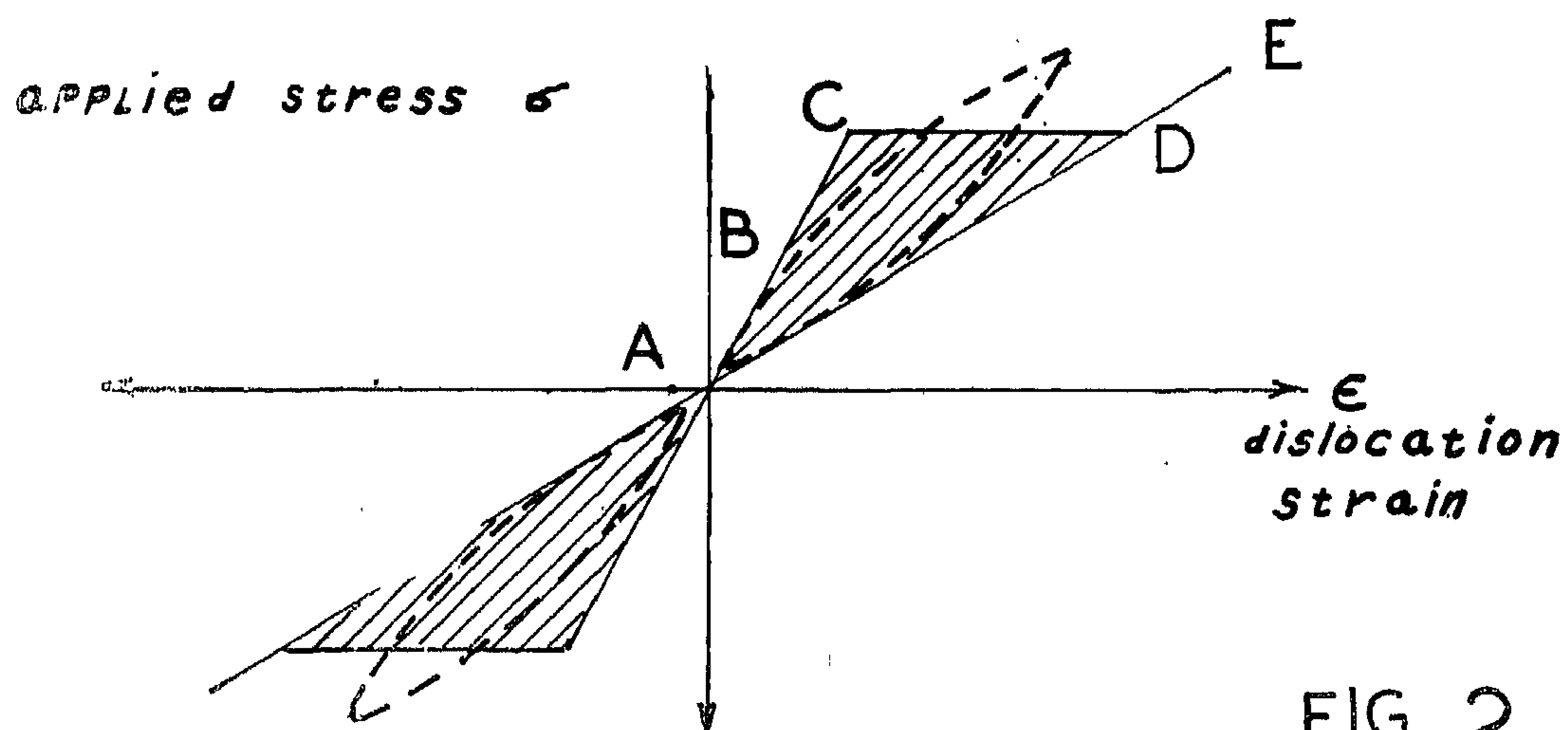


FIG 2

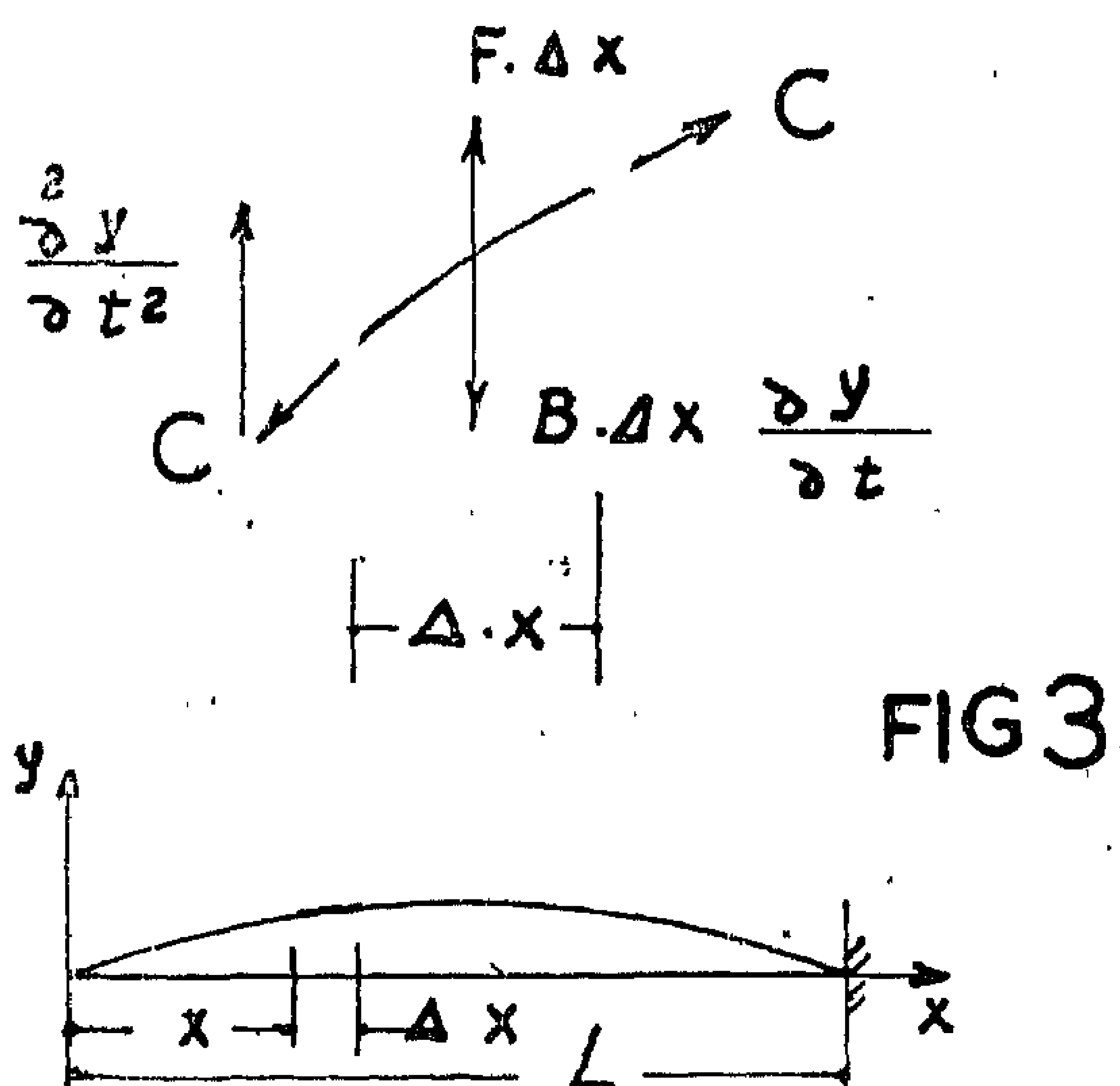


FIG 3

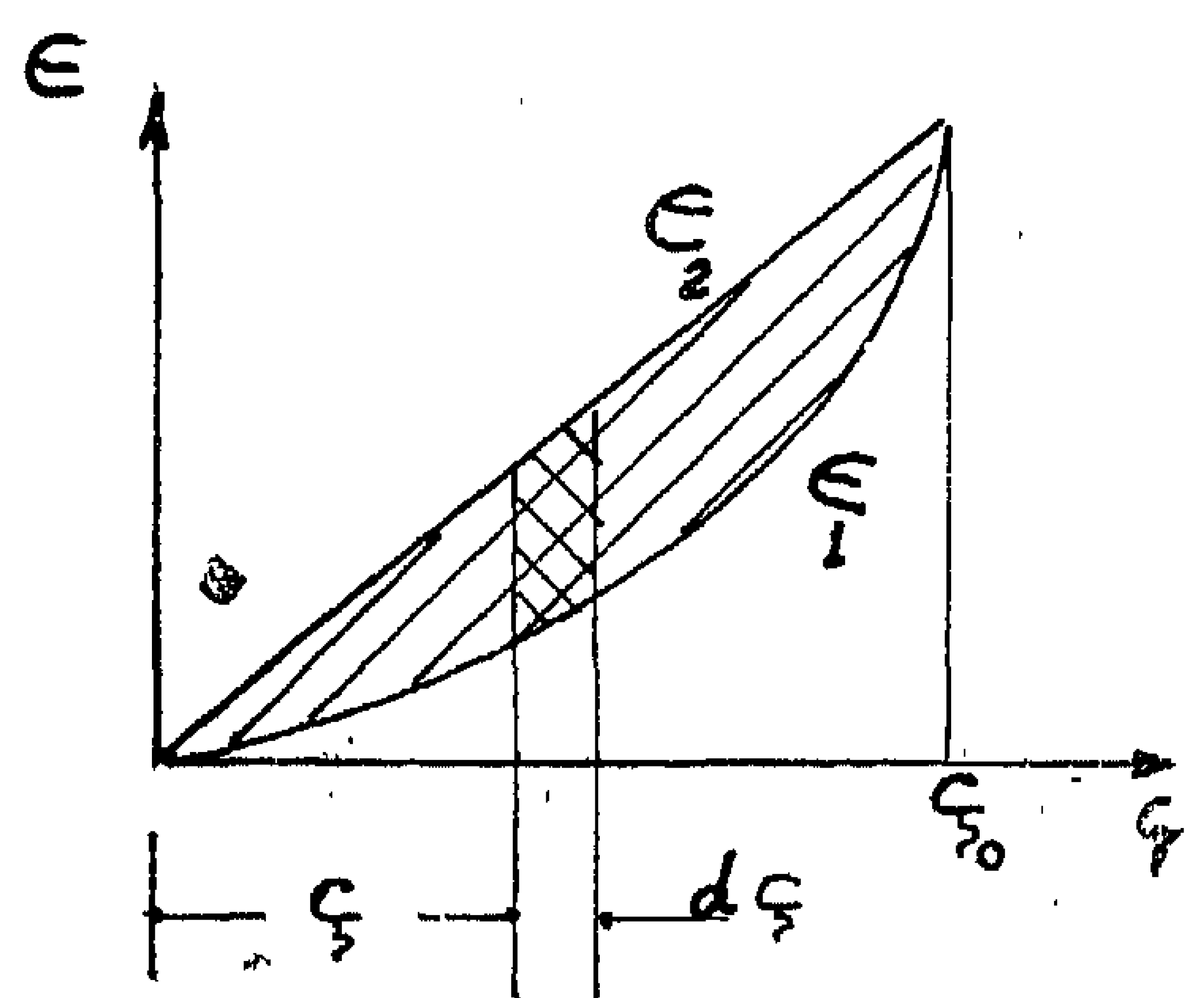


FIG 4

L dislocation length.

Y' average displacement of dislocation line.

ε dislocation strain.

Λ dislocation length per unit volume (dislocation density).

Γ break-away stress corresponding to L_c.

γ ratio between major and minor loop lengths L_n/L_c.

L' break-away length of the dislocation segment.

$\triangle W$ damping energy dissipated during one stress cycle.

W potential energy at the beginning of the stress cycle.

$\triangle_p$ damping decrement of the test specimen.

$\triangle_o$ damping decrement for the machine (vibrophore) and the compensation test specimen.

$\triangle$ damping decrement for the machine and the main test specimen.

n number of dislocations.

G modulus of rigidity.

E modulus of elasticity.

Λ_i initial dislocation density.

Λ_t total dislocation density.

F' maximum binding force which a pinning point can hold a dislocation line.

ε' miss fit parameter.

z distance from the impurity to dislocation center line.

f axial alternating stress.

f_o amplitude of the axial alternating stress.

f_m axial mean stress.

THEORETICAL ANALYSIS

Granto and Lucke assumed that a pure single crystal contains before deformation, a net-work of dislocations. The length L_n of a loop defined by the intersections of the net-work loops is further pinned down by impurity particles to minor lengths L_c.

Fig. 1, illustrate the bowing out of a pinned dislocation line due to increase in stress. Fig. 2, illustrate the hystresis loop of a dislocation line under the effect of alternating stress.

Refering to Fig. 3, the partial differential equation of the forced damped vibration of a string is :

$$C \frac{\partial^2 y}{\partial x^2} - B \frac{\partial y}{\partial t} + F = A \frac{\partial^2 y}{\partial t^2} \qquad (1)$$

Assuming the disturbing force F, acting on the string length is of the form.

$$F = a \zeta_o \cos wt \qquad (2)$$

Neglecting the viscous damping i.e. $B = 0$, and substituting for F,

$$\frac{\partial^2 y}{dt^2} - \frac{C}{A} \frac{\partial^2 y}{dx^2} = \frac{a \zeta_o}{A} \cos wt \qquad (3)$$

The boundary conditions are ,

$$y_{(o,t)} = 0 \text{ and } y_{(L,t)} = 0$$

And for initial conditions ,

$$y_{(x,o)} = 0 \text{ and } \frac{\partial y}{\partial t}_{(x,o)} = 0$$

Using Laplace transformation and the theory of complex variables,[6] the solution of equation (3) will be[7]:

$$y_{(x,t)} = \frac{4 a \zeta_o}{\pi A} \sum_{n=0}^{\infty} \frac{1}{w_n^2} \frac{1}{2_n + 1} \sin (2n + 1) \frac{\pi X}{L} . (\cos wt - \cos w_n t) \qquad (4)$$

where $w_n = (2n + 1) \pi b/L$,
and $b^2 = C/A$

EFFECT OF ALTERNATING AND MEAN STRESSES ON THE DAMPING CAPACITY OF METALS

By

Dr. M.Y.M. AFIFI — Eng. K.A. MOSTAFA
Faculty of Eng., Ain Shams University.

SUMMARY

An investigation on the effect of both alternating and mean stresses on the damping capacity of metals. The theoretical analysis is based on the theory of dislocation. Theoretical relations for the damping capacity of metals as a function of alternating stress and as a function of mean stress are deduced. The limits for applying these relations for copper are determined experimentally.

INTRODUCTION

Recently considerable attention has been given to the problem of constructing a dislocation theory capable of quantitatively explain the damping capacity of metals. Koehler[1]* (1952) develops the analogy between the vibration under alternating stress of a dislocation line segment pinned down by impurity particles and the problem of the forced damped vibration of a string. According to his theory the energy loss in internal damping of metals depends on the frequency, but according to experimental work carried out by A.S. Nowick[2] it is independant of frequency up to about 1 Mega cycle/sec. Weertman and Salkovitz [3] (1955) construct specific hysterisis model using the theories of Mott and Nabarro[4] from which they are able to make semi-quantitative calculations of the damping decrements. Granto and Lucke[5] found a solution for the damping differential equation for all frequencies, as a function of physical quantities depending on the length of dislocation loops which can be analyzed and applied.

In this work, the differential equation for a dislocation line, which is considered as a string, is sloved using Laplace transformation and the theory of complex variables[6]. The mean stress is introduced as a parameter and its effect on the damping capacity of metals is investigated.

NOMENCLATURE

L_c	length of segment as determined by impurities (minor length).
L_n	net work length (major length).
C	line tension of dislocation line.
B	viscous damping force per unit length and velocity.
F	applied shearing force per unit length.
A	mass per unit length.
y	displacement of dislocation line.
a	Burger's vector, (atomic spacing).
ζ_o	amplitude of the applied alternating shear stress.
ζ	applied alternating shear stress.
ζ_m	mean shear stress.
w	angular frequency of applied force F.
t	time.
w_n	natural angular frequency for transverse vitration of dislocation line.

* Numbers in brackets designate reierences at end of paper.

CONCLUSION

Field experiments at the side of the High Aswan Dam were undertaken to determine the most effective amount of charge required to give practical sizes of muck output. Also a set of controlled laboratory tests were made to determine this particular value of charge. It was found that an explosive consumption coefficient K of 0.67 kg/m^3 resulted in field conditions and of 1.0 kg/m^3 in laberatory conditions. The discrepency is partly due to the presence of cracks, fissures and faults in the rock in the field whereas the rock used in the laboratory was free from these defects, and partly due to having the charge in field more distributed over a number of spots whereas in the laboratory tests it was concentrated in one borehole.

If the quantity of charge was overestimated, the result would be blocks of rocks with very large sizes. On the other hand if the quantity of charge was underestimated, the blasting will result only in cracks happening to the volume of rock. Between these two limits the optimum explosive consumption coefficient will give the smallest possible sizes of rock output and this value should be adopted in field for engineering purposes.

REFERENCES

1. Boring and explosion works, Moscow 1960, by : Assonove, Dokoutchaev and Koukounov.
2. Boring and Explosion Works. by : Nedin and Ibraev, Moscow 1960.
3. Albomes of Saad El-Aali project. Hydroproject design effice, Moscow 1960 — 1961 — 1962.
4. Mining Engineering Handbook, third edition, volume 1 and 2 by Robert Peel, Columbia University.
5. Mining Explosives. by Moadan, R. and Westwork, R., London 1958.
6. Blasting of rock in mines, quarries, etc. by Daw, A.W., London.

6. Blasting of rock in mines, quarries, etc. by Daw, A.W., London.

7. Specific explosive coefficient as a function of strength of rock. by Skopatov, A.E., Moscow 1961.
8. Wave Spread due to blasting rock. by Khanykaev. Moscow 1962.
9. Calculation of boreholes diameter for blasting purposes, by Bronnekov, Moscow.
10. Quantity of explosives in boreholes. by Marchanko, L.N. and Kydreachov, B.S. Moscow 1960.
11. Blasters handbook. by Technical service section of the explosive department- Wilmington, U.S.A.

LABERATORY EXPERIMENTS

To check the results obtained from field experiments and to climinate any uncontrolled factors that might have interfered with the experiments in the field. This is done by controlling the experiments conditions in the laberatory a task which normally is very difficult in field.

The rock choosen for making the test cubes was very hard sandy line stone from the Mokkatum quarry chosen from a spot where no cracks or fissures existed and where no change in stratum was apparent. Seven cubes with the dimensions of 18 × 18 × 18 cms) each were made out of the large block of stone. The sides of the cubes were throughly polished. a borehole of 1.7 cms diameter and 10 cms length was carefully drilled in the centre of one of the sides in each cube. The object of this hole was to house the charge, the stemming material and the detenator.

The explosions took place inside a specially made steel container 80 × 80 × 80 cms. The explosive used for charging the seven test cubes was dynamite and the detenators were No 8 standard detenators.

Seven different charges of dynamite of 2.91, 3.49, 4.66, 5.83, 6.99, 9.91, and 12.24 grams were used corresponding to specific explosive consumption coefficient of 0.50, 0.60, 0.8, 1.0, 1.2, 1.7, 2.1 kg/m^3 respectively thus giving a wide range of K, in fact four fold range. Special care was directed to having the seven tests done under exactly the same conditions of charging, compaction and detonation.

After each blasting took place. The resulting muck was collected from the steel container for sieve analysis. The sieves used for analysis were standard sieves no 38, 19, 9.5 and 4.75 mms; The results are shown in Figure 12 where the explosive consumption coefficient is plotted against the sizes of muck output as expressed in the form of percentage by weight passed by a certain sieve and retained on the next.

It is clear from (Figure 12) that the sizes of muck decreases with increasing the explosive consumption coefficient till it reaches a certain limit after which, increasing the charge will result in a corresponding increase in the sizes of muck output. This means that there is a specific value for the explosive consumption coefficient which will give the smallest possible sizes of muck output. This particular value of K is called the optimum explosive consumption coefficient. It is advisable to use this specific value when designing blasts in field. This particular value of K is in the range of 1.0 kg/m^3 which is about 40% higher than that obtained from field experiments. This is partly due to the fact that the rock in field contains a large number of fissures, cracks and faults whereas the test cubes were free from these defects and partly due to the fact that in field, the distribution of charge chambers is so scattered thus helping each other in the blast.

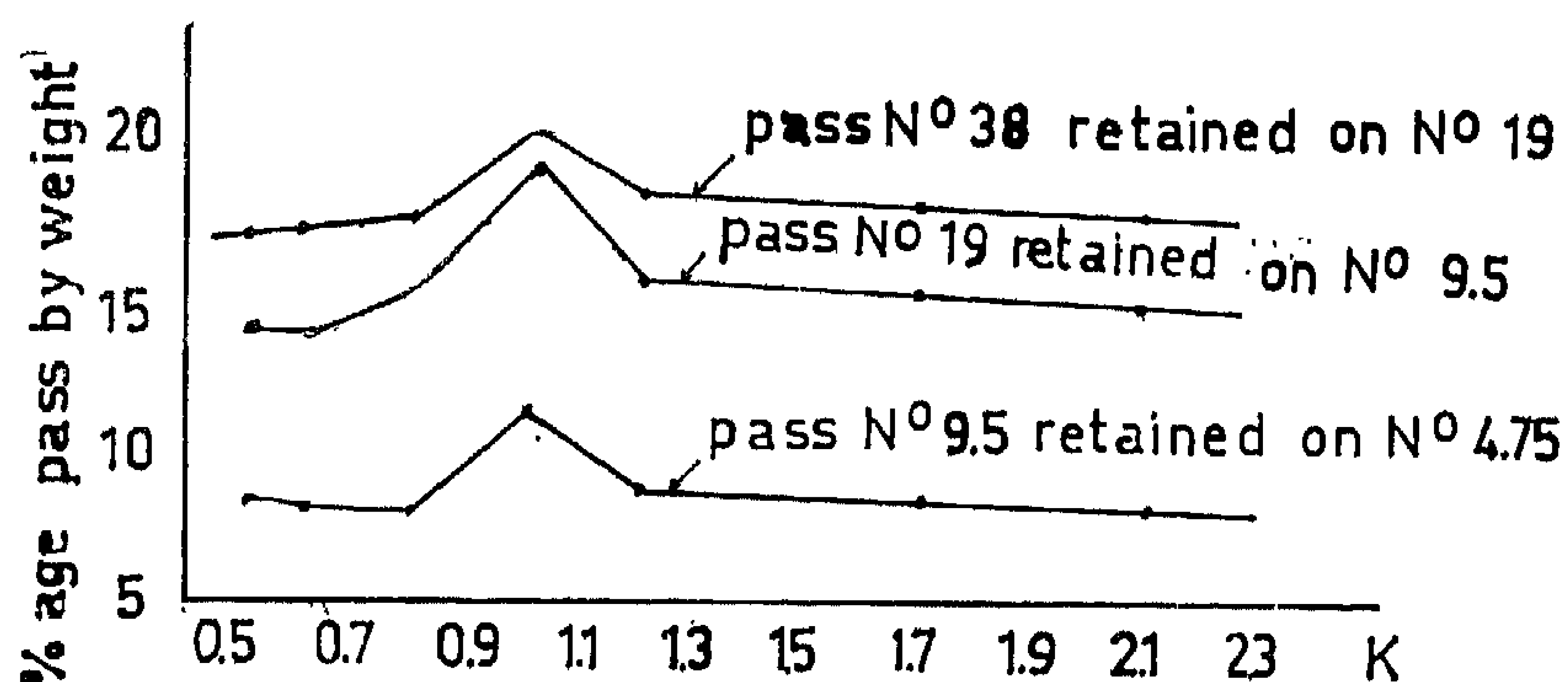


Fig. 12: Laboratory Experiments at Military Factory 18

Table 1 — Experimental Results.

Addit. No. K	kg/m3	Distance covered by muck ms	Percentage pass 80	Pars pass 20	By weight pass 5
26	0.57	25	24.5	15	9.2
24	0.68	35	46.7	23.1	15.0
25	1 19	100	22.5	12.5	9.3

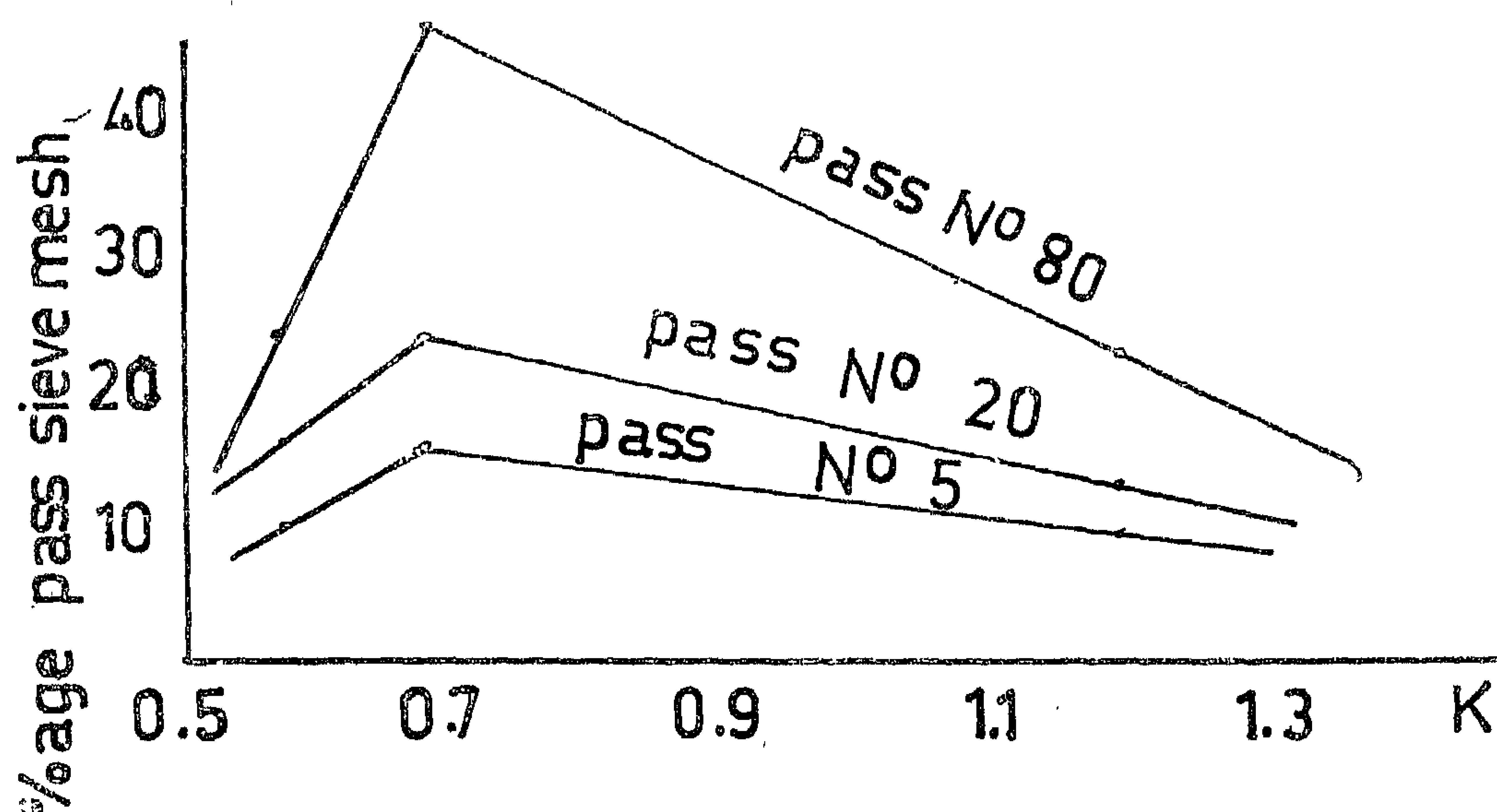


Fig. 10 : Field results at High Aswan Dam.

The results are plotted in (Figure 10) and it is clear from the Figure that the percentage pass of a certain size of rocks increases with the increase of the explosives consumption coefficient K to a certain point, the docreases systematically as K increases.

It is also clear that the value of K at which the percentage pass is maximum is the same for the three sizes and is nearly 0.68 kg/m³. This means that there is a particular value of K at which the rocks of small sizes are predominant and these of large sizes are on the diminishing side. Using a smaller value of K will increase the percentage of the grains of large sizes whereas if K had a greater value will again result in the same effect. Thus the most effective value of K for minimum sizes of muck output (Optimum explosives consumption coefficient) is in the region of 0.68 kg/m³.

Also from the table, it is seen that as K increase the distance covered by the flying debris (the dangerous zone) increases propotionally in a more or less linear manner (Figure 11).

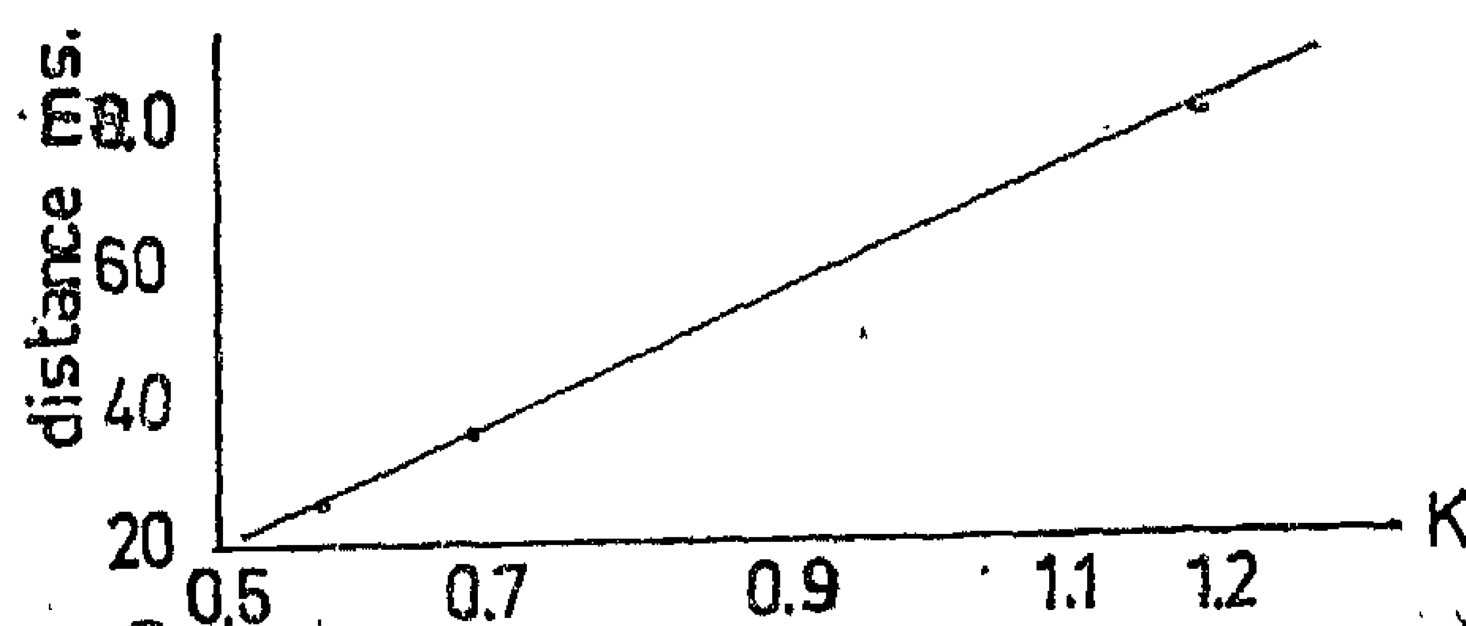


Fig. 11 : Distance covered by flying debris

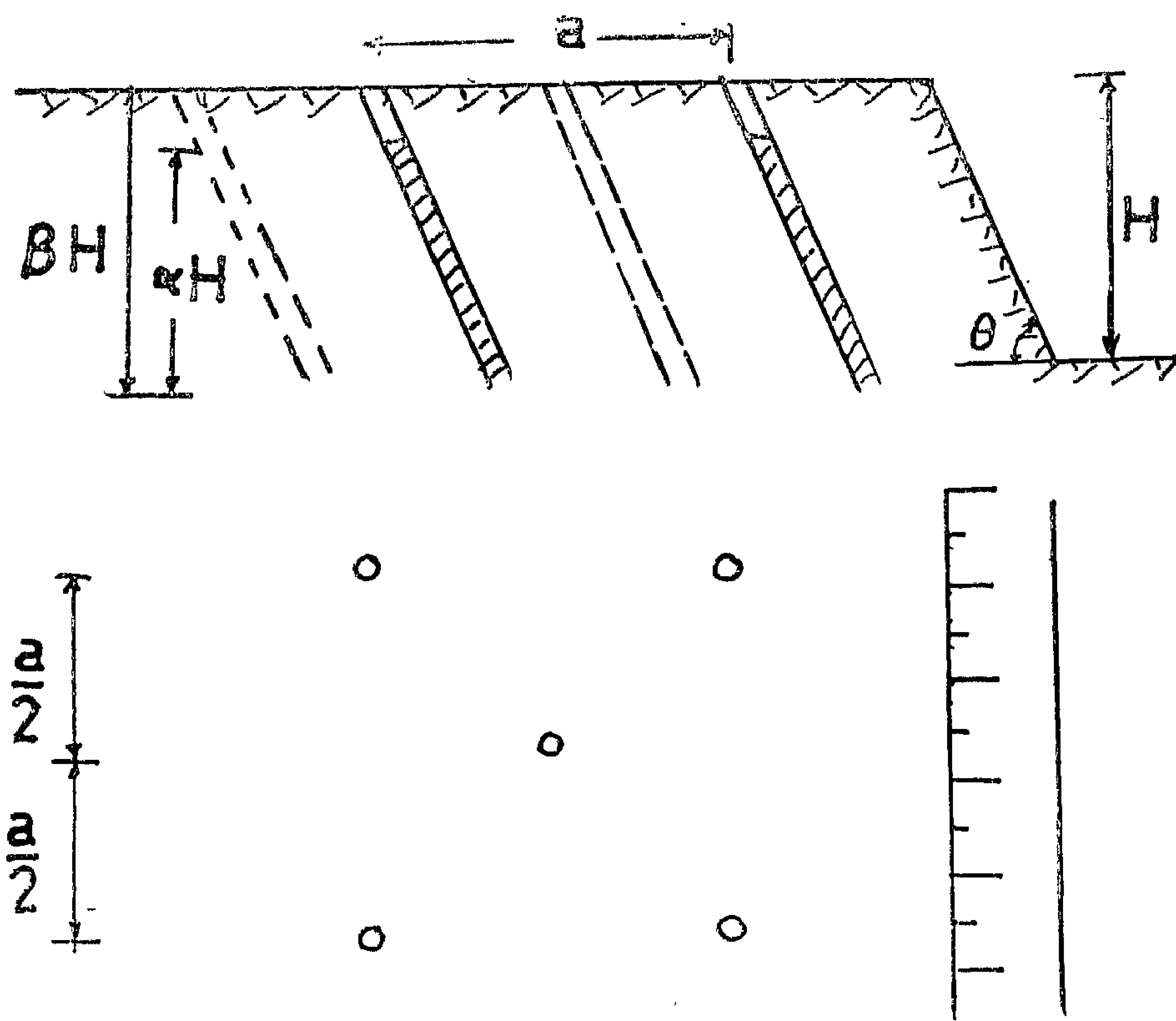


Fig. 9 : Spacing of boreholes (inclined).

III — FIELD OBSERVATIONS AND EXPERIMENTS

In the project of the Aswan High Dam, excavating the diversion canal in the rock necissated the use of blasting by explosives and also building the body of the dam from rockfill of various sizes required blasting additional volumes of rock from site. A total of 60 addits were made for this purpose.

Due to some unforseen factors, the muck output in some addits had sizes falling outside the desired values, and in some other cases the charge was overestimated with the result of giving very large sizes of muck output. In some of the addits the charge was underestimated with the result of having only cracks in the rocks that should have been blasted out.

From these observations it was evident that there is a distinct relation between the explosives consumption coefficient and the resulting sizes of muck output. To study this relation, three fieled experiments were undertaken in addits No. 24, 25 and 26 downstream the diversion canal, of the Aswan High Dam. These three addits had nearly the same height of bench and in locations of similar geological formations. Also the same conditions of clogging and detonation were the same for the three adits. The explosive consumption coefficient for three adits was respectively 0.68, 1.19 and 0.57 kg/m^3. In each experiment, several representative samples of muck output were taken at various levels of the cross section and sieve analysis was made for them. The sieve sizes available for that purpose were 80, 20 and 5 mms where the 80 mm sieve was made specially for this purpose. The results of the three experiments are given in the Table 1.

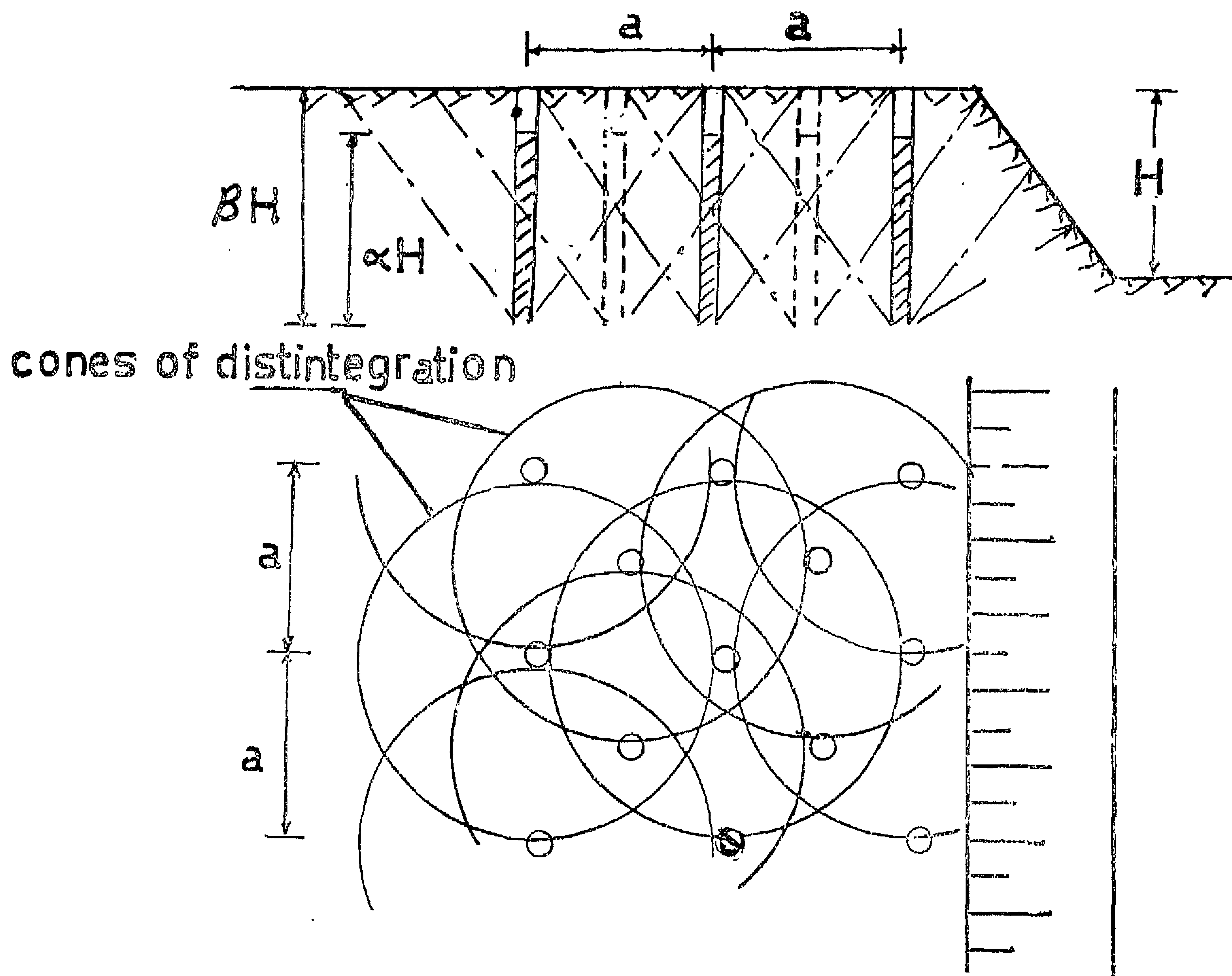


Fig. 8 : Spacing of vertical boreholes.

a factor allowing for overlapping and B is the ratio between the length of borehole and the height of bench.

In the case of inclined boreholes (Figure 9) the above equation will take the form :

$$a = 0.396 \sqrt{\frac{\Delta \rho \alpha B}{K}} \sec \Theta \quad \rightarrow \quad (6)$$

Where Θ is the angle of inclination of the borehole. Horizontal drilling is adopted when the height of bench H does not exceed 5.0 m. The volume of rock blasted by one borehole (Figure 9) is

V = a w L where w is the length of the line of least resistance and L is the length of borehole.

The weight of charge necessary for blasting the borehole is thus

$$Q = K \cdot a w L \quad \rightarrow \quad (7)$$

but from equation (1) we have :

$$Q = 0.0785 \, d^2 \cdot \Delta \cdot \rho \cdot L \quad \rightarrow \quad (8)$$

equating (7) and (8) thus :

$$a = 0.0785 \, d^2 \frac{\Delta \rho \alpha}{K w}$$

When using the system of charged chambers the distance between each two chambers is chosen to equal the average length of the line of least resistance for the two chambers.

If V is the volume of rock to be blasted by a single chamber, then the weight of charge necessary to do the blasting normally is KV where K is the explosive consumption coefficient i.e. the weight of explosives necessary for blasting a unit volume of rock.

In the case of blasting by borehole system, to find the weight of explosives required for blasting one meter length, the following emperical formual provides a reasonab^l estimate :

$$P = 0.0785\ d^2.\ \triangle.\ \rho \qquad (1)$$

where d = diameter of borehole in cms

$\triangle$ = specific weight of explosives in tons/m³

and ρ is a coefficient depending on tthe method of charging and P is in kgms.

The volume of the cone of rock blasted by the borehole will equal.

$$V = \frac{1}{3}\,\frac{\pi}{4}\,D^2 \times H \qquad (2)$$

Where D is the diameter of the base of cone of disintegation and H is the height of this cone (Figure 7).

The weight of explosives Q necessary for blasting is thus :

$$Q = K.\,\frac{1}{3}\,\frac{\pi}{4}\,D^2.\ H \qquad (3)$$

This weight is distributed along the borehole and can be put in the form :

$$Q = \frac{\pi\ d^2}{4}\ H.\ \triangle.\ \rho.\ \alpha. \qquad (4)$$

where α is the ratio between the charged length and the total length of the borehole = 0.6 → 0.80, α is a coefficient depending on the method of charging and $\triangle$ is the specific weight of explosives.

From equations (3) and (4)

$$\therefore\ D = d\ \sqrt{\frac{3}{K}\ \triangle\,\alpha\,\rho} \qquad \rightarrow \quad (5)$$

The boreholes are usually spaced in a staggered rows so as to have the circles of convex buckling overlaping in such a manner as to have the smallest possible volume of rocks which are not affected directly by explosion (Figure 8).

The spacing a between two successive boreholes is determined from equation (5) in such a way that a is smaller than D to allow for overlaping, thus :

$$a = 0.396\ d\ \sqrt{\frac{\triangle\,\rho\,\alpha\ B}{K}}$$ where 0.396 is

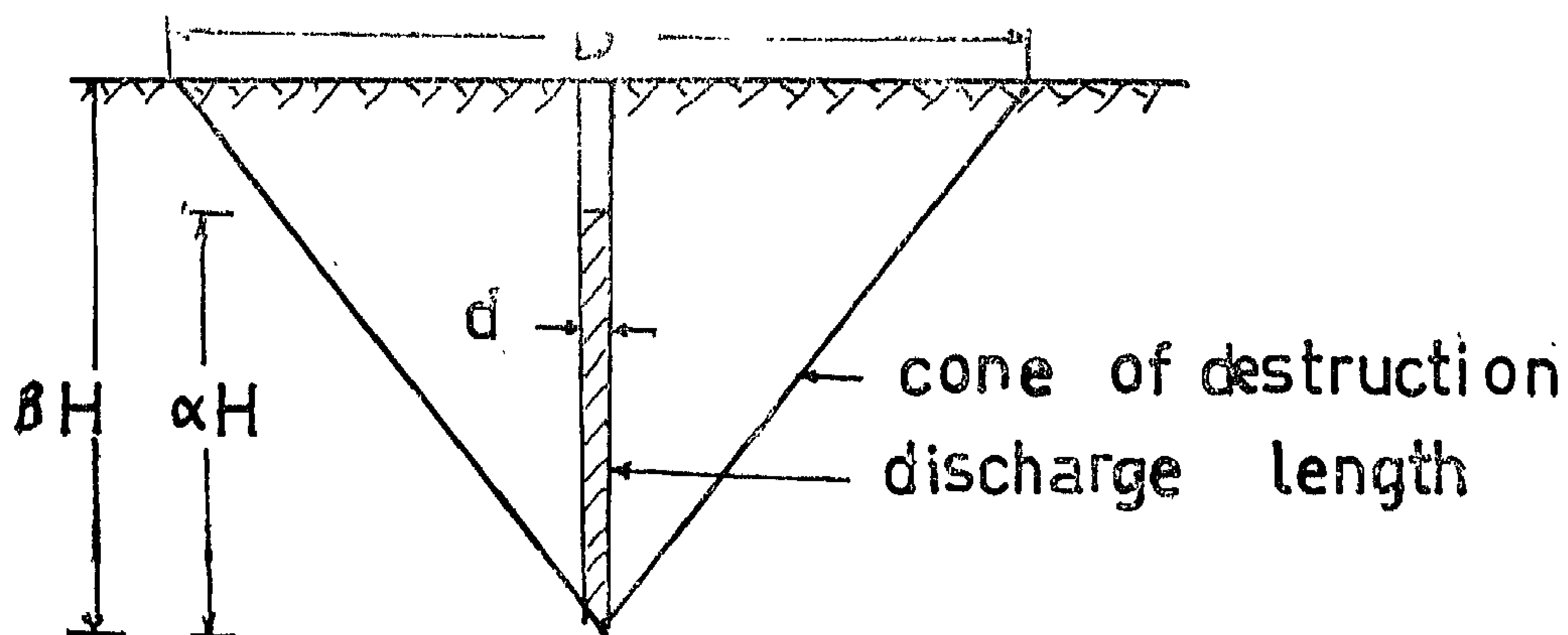


Fig. 7 : Blasting by a single borehole.

In the method of charge chambers, the charge is distributed in a number of chambers located in such manner as to have the total volume of bench disintegrated by the blast. The chambers are connected with each other by a system of horizontal tunnels or addits and a portal for access to these tunnels (Figure 4).

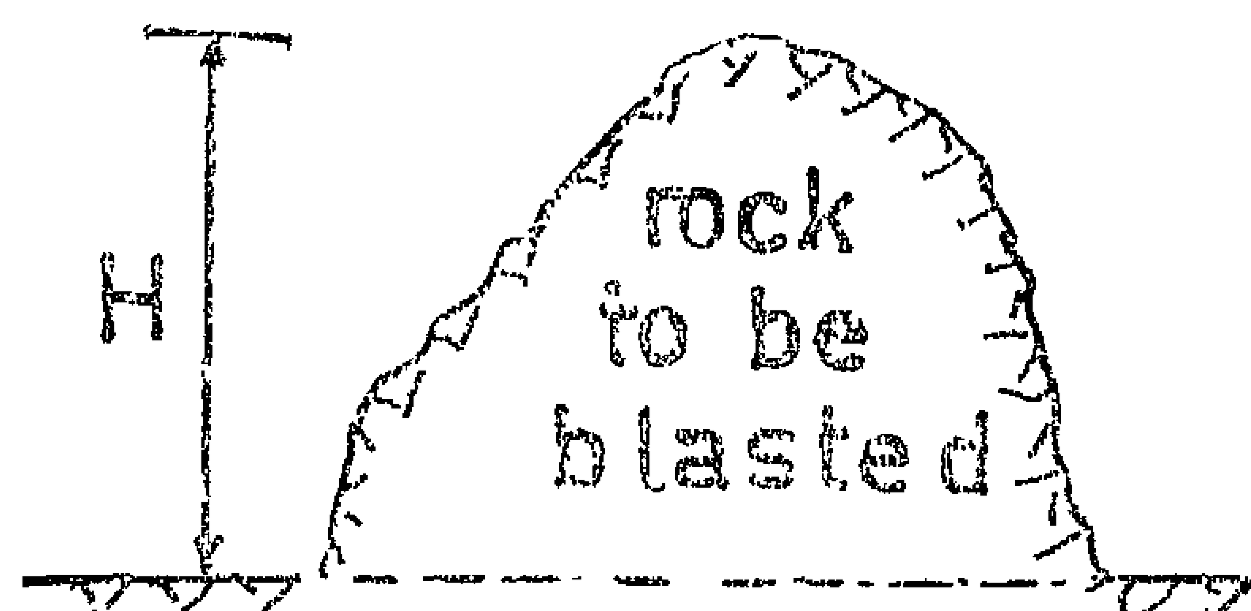


Fig. 3 : Heights of bench.

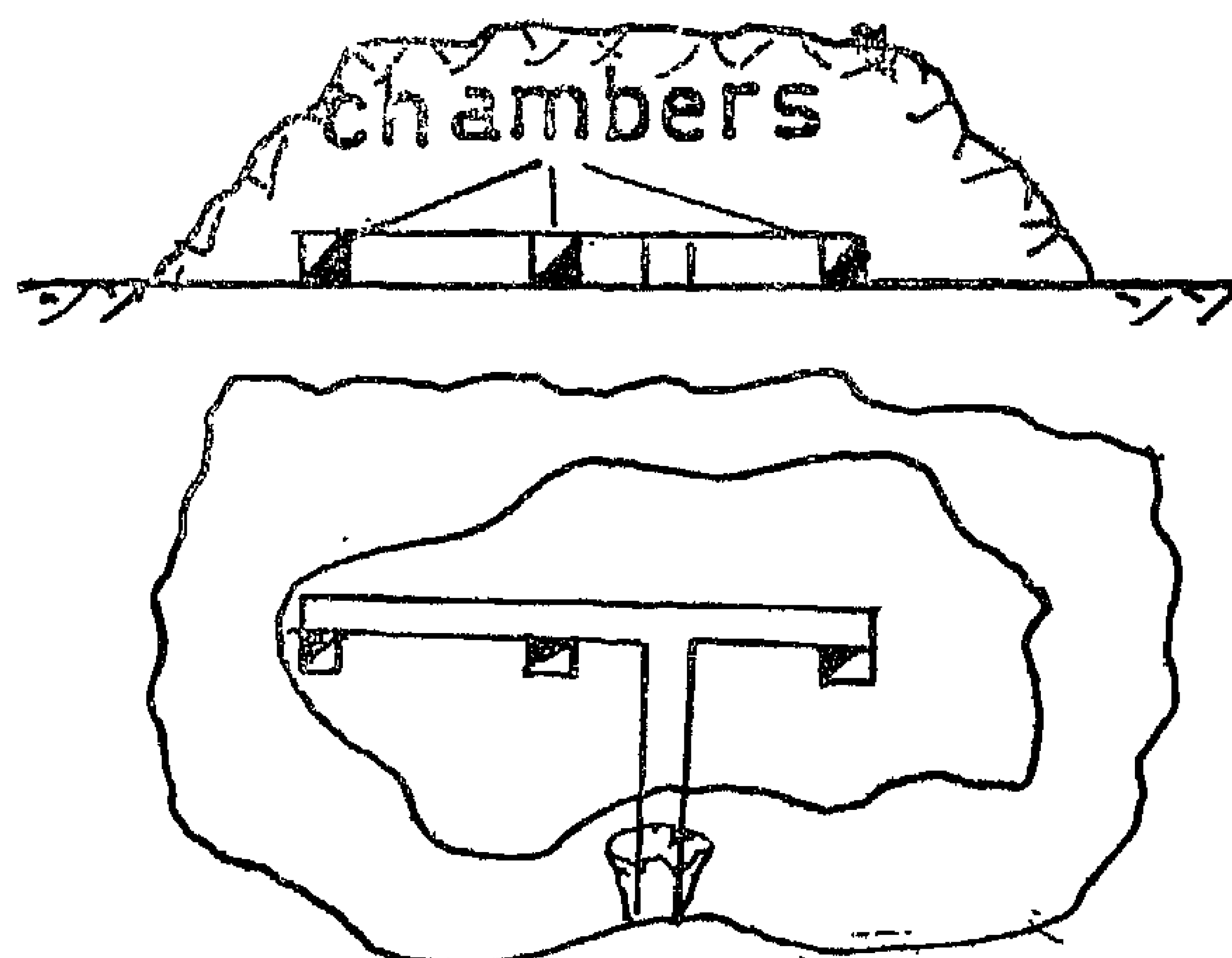


Fig. 4 : Blasting by chambers.

In the second method a number of boreholes are drilled either vertical, horizontal or inclined (Fig. 5) and the boreholes are arranged at such locations to have the total volume of bench climinated after blasting.

In general, the two methods of blasting are used in combination like in excavating a deep channel in a rocky zone. The system of charged chambers are used first to eliminate the bulk of rock volume (zone A in Fig. 6). A system of boreholes is then used to blast zone B and then another system of boreholes is used to blast zon C if the depth of canal is too large.

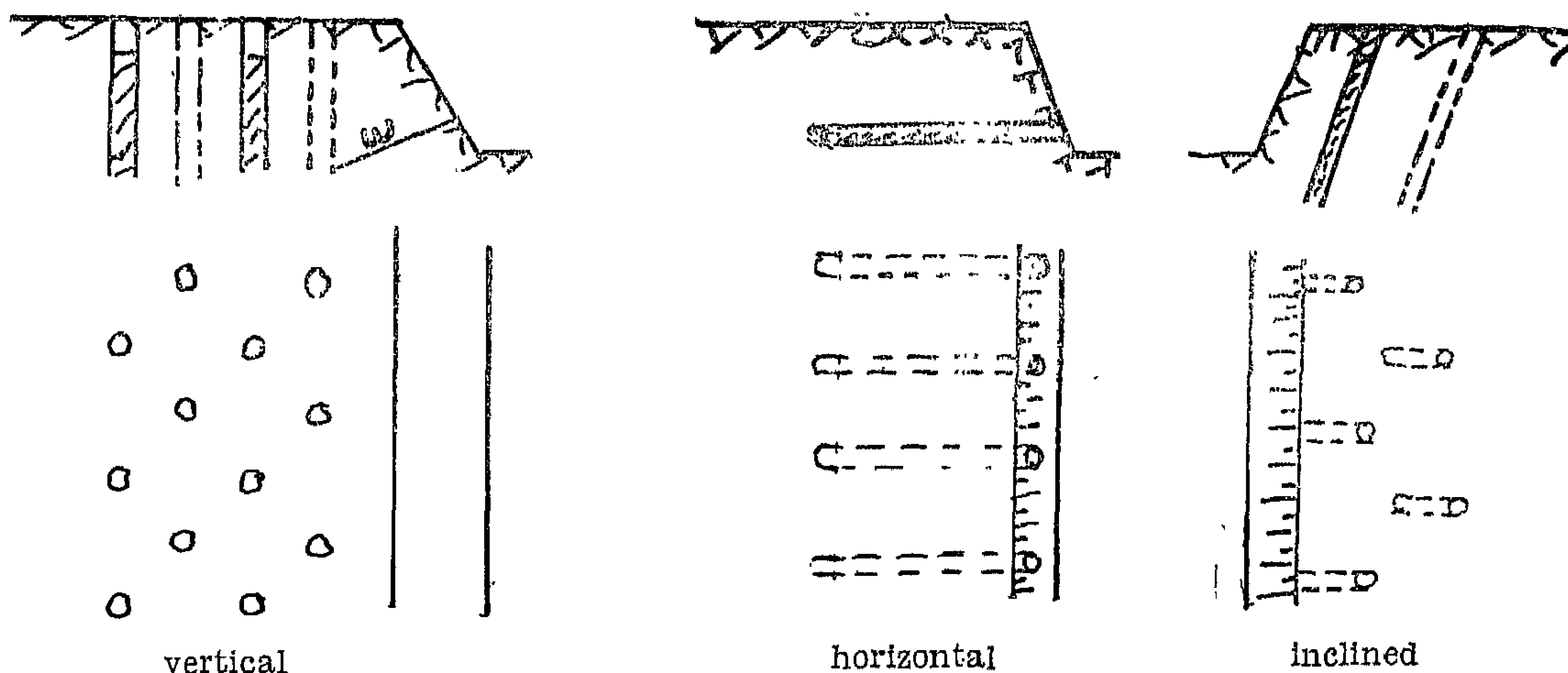


Fig. 5 : Blasting by borehole system.

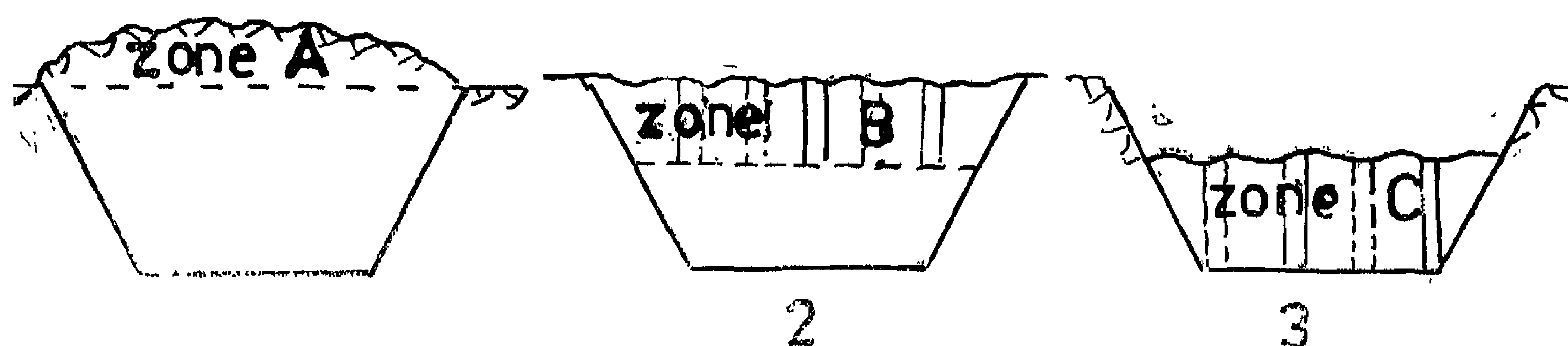


Fig. 6 : Excavation of a large channel by blasting.

The charge of explosives is housed in a space called the charge chamber drilled in the rock to a certain volume V in m^3 given by the formula suggested by Assanove (1960) :

$$V = \frac{Q}{\triangle} . K_v$$ where Q is weight of charge in tons, $\triangle$ is the density of explosives in ton/m^3 and k_v is a factor ranging between 1.1 and 1.8 depending on the charging conditions and method of timbering.

When the charge is detonated, the walls of the charge chamber are subjected to dynamic chock resulting from the rapid conversion of explosives into gasses. An impact wave is created and spreads in all directions causing the blasting action at a spread velocity

$$= \sqrt{\frac{g E}{\gamma}}$$ where g is the gravational acceleration, E is the modulus of elasticity of the rock material and γ is the specific weight of rock.

The resulting stresses will be maximum in the immediate neighbourhood of the charge and gradually diminishing as we proceed farther from the centre of detonation. The zone where disintegration of rock takes place is called the sphere of disintegration with radius Rs. This zone is surrounded by another zone of radius R_d called the zone of destruction in which the stresses are not enough to cause disintegration but enough to cause destruction. The zone of destruction is surrounded by a third zone called the zone of vibrations of radius R_v in which the blasting stresses only cause vibration in the rock and probably few cracks (Figure 1).

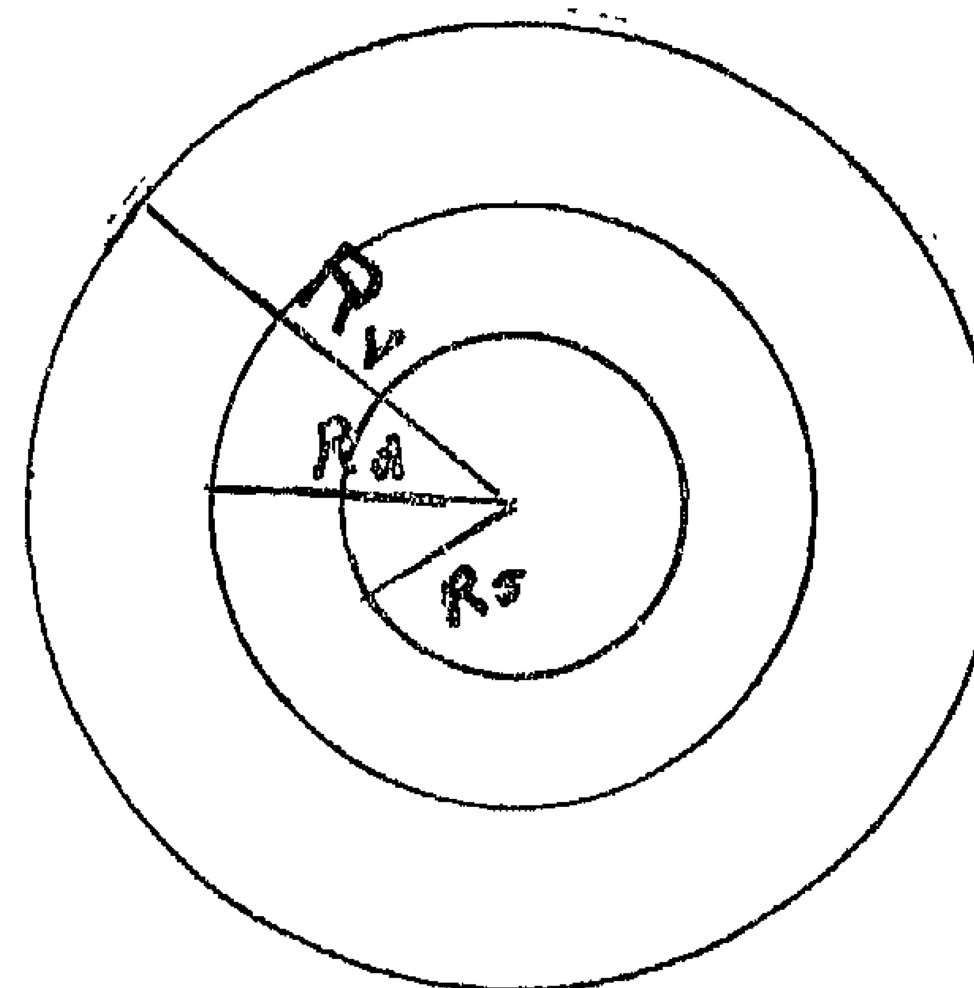


Fig. 1 : Unlimited blasting.

When the distance between the centre of charge and the ground surface is less than R_d, i.e. if the environment is limited, the stresses will follow the line of least resistance of length w and the zone of destruction will take the shape of an inverted cone with the centre of charge as its vertex (Figure 2).

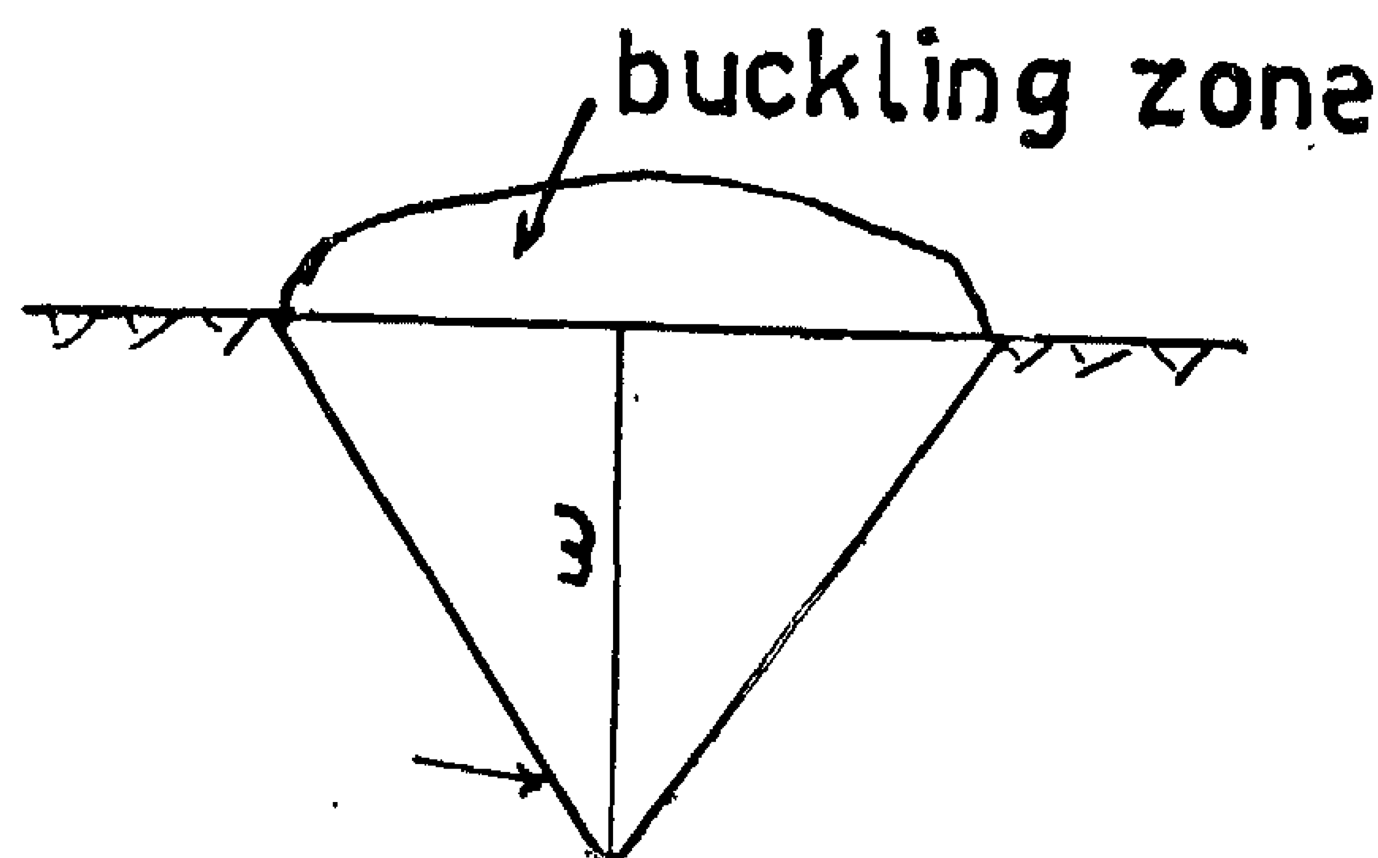


Fig. 2 : Blasting environment (Limited)

II — METHODS OF BLASTING

There are two major methods of blasting, blasting by charged chambers or addits and blasting by boreholes. The choise of a specific method depends on the height of bench H which has to be blasted and on the availability of moderate slopes on any face of the bench to give an access for drilling equipment to be transported up the slope. For small values of H up to 15 ms and if there exists a moderate slope for transportation of equipment, blasting by boreholes will be more economical. For heights of bench between 15 and 30 ms. blasting by charge chambers will be more economical. For H = 30 ms, the blasting is done at a number of stages using charge chambers or the borehole system or both.

EXPERIMENTAL AND PRACTICAL STUDY OF THE USE OF EXPLOSIVES IN REMOVING ROCK FROM PROJECT AREAS

By

Dr. ALY ISMAIL ELGAWHARY
B.Sc., D.I.C., Ph.D.

and

MOH. FATHY ELATTAR
B.Sc., M.Sc.

INTRODUCTION

In many large engineering schemes like building dams, water tunnels or excavating large canals, great masses of rock have to be removed from certain spots and transported to some other spot where it can be used or dumped. In most cases, the usual mechanical ways of excavating these masses of rock become impractical and engineers have to resort to blasting methods using explosives.

The object of the present work is to study the most effecient amount of explosives which is used in blasting a given volume of rock will yield good results of muck output. The experimental results used in the study are both field experiments carried out in the site of the Aswan High Dam and laboratory experiments done on idealized forms of rocks in the Ballistic laboratory of the Military factory No. 18.

The effect of the amount of explosives on the size of the muck output has been studied. This lead to the study of the Optimum explosive consumption coefficient and the various parameters affecting its value. We advice that this value should be used in the design of blasts to get economical and favourable results.

Also a formula for the best design of adit system based on the use of the optimum explosive consumption coefficient has been introduced.

I — EXPLOSIVES AND EXPLOSION

High explosives used in blasting in engineering projects can be classified to the following main kinds :

1. Straight dynamite of which the essential ingradients are Nitroglycerin, sodium nitrate and combustable material like wood bulb.
2. Amonia dynamite in which the essential ingradients are similar to straight dynamite with the addition of sodium Nitrate.
3. Straight gelatine in which the essential ingradients are Nitroglycerin and nitro cotton sodium with a suitable combustable material.
4. Amonia gelatine which is the same as the straight gelatine with the addition of amonia nitrate.
5. Blasting gelatine with nitroglycerin and nitrocotton as essential ingradients.
6. Granual dynamite with sodium nitrate, sulpher and coal sensazied by nitroglycerin as essential ingradients.
7. Liqued Oxygin explosives : The essential ingradients are liqued oxygin and finely devided carbon.

Table (11) : Operational results of oil injection at Helwan blast furnaces for one year.

A period of month	Coke rate Kg./ton metal		Oil rate Kg./ton metal		Replacement ratio		% increase in production	
	BF. 1	BF. 2	BF. 1	BF. 2	BF. 1	BF. 2	BF. 1	BF. 2
1	1154	1066	74	75	1.4	1.39	9.0	11.2
2	1165	1081	68	61	1.4	1.45	8.2	9.0
3	1156	1084	67	58	1.5	1.48	8.4	8.5
4	1152	1086	75	57	1.46	1.47	10.3	10.1
5	1145	1077	82	63	1.4	1.48	11.0	8.0
6	1179	1091	61	50	1.52	1.58	8.4	12.8
7	1164	1086	64	53	1.5	1.59	8.9	10.5
8	1153	1097	66	45	1.6	1.62	11.9	9.5
9	1148	1081	71	60	1.57	1.48	9.9	8.2
10	1147	1077	75	65	1.52	1.43	8.7	9.7
11	1139	1082	77	63	1.56	1.4	9.1	8.6
12	1172	1083	56	59	1.58	1.47	8.8	7.5

REFERENCES

1. J. Fulton ; Meeting of the Engineering Society of Western Pennsylvania, Dec. (1941).
2. J. Gayley; A.I.S.I. Year book, (1905).
3. C. Agnew; Iron age, Nov. (1958).
4. N. Gol'dshtein and N. Khromchenko ; Stal, March (1965).
5. A. Decker ; J. metals, Jan. (1961).
6. J. Raick and J. Brassert; Iron and Steel Engineer, Dec. (1952).
7. A. Decker; C.N.R.M. Report, Liege, (1960).
8. Oil and steel "Special report", After Esso, (1962).
9. M. Hazard; Iron and steel coal trades Rev., June (1961).
10. W. Rombough ; AIME Blast Furnace and Coke Oven Raw Mat Comm., Phildaelphia, April (1961).
11. Yu. Borisov and A. Fofanov; Stal, June (1961).
12. Norwood, B. Melcher and J. Morris ; Bureau of Mnies report of investigation No. 5621.
13. W. Dowhaniuk; Blast furnace and steel plant, March (1963).
14. Z. Nekrasov and F. Moskalina ; Stal, Sep. (1962).
15. K. McCutcheon; Blast furnace and steel plant, Oct. (1965).
16. J. Hohn and O. Pavlik ; Steel times, March (1966).
17. V. Loginov and A. Chechuro; Stal, July (1963).
18. J. Cordier; proc. A.I.M.E., *19* (1960).

Effect of Fuel Oil Injection on Blast Furnace Economy :

The economy of fuel oil injection in the blast furnace depends mainly on the relative prices of oil and coke. In Egypt the price of one ton oil is 7 pounds while the price of one ton coke is 16.5 pounds; so even at the lowest replacement ratios attained in the present study saving is certain. If the optimum value of oil rate for maximum increase in production (70 Kg. oil/ton metal) is used a coke saving of about 100 Kg./ton metal can be achieved which results in about 6.9% decrease in total production cost.

Continuous Blast Furnace Operation With Fuel Oil Injection :

Table (11) shows the results of operation of the two blast furnaces at Helwan with fuel oil injection for 12 months.

As blast furnace No. 2 was operated with a charge having 85% sinter on the average and 15% Aswan iron ore, the coke rate was lower than for blast furnace No. 1 which operated with 85% ore and 15% sinter.

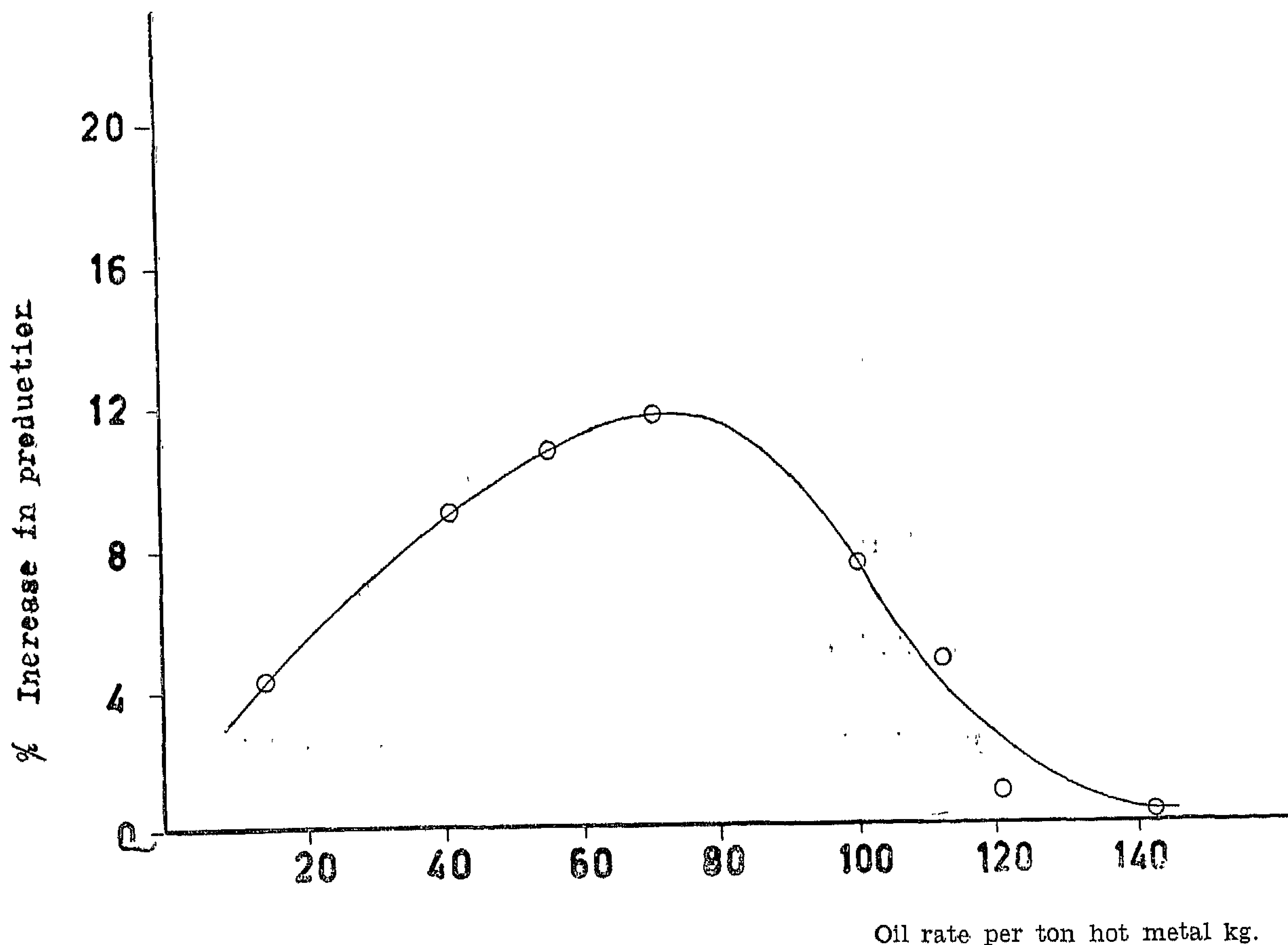


FIG. 6 : Effect of oil injection on production.

Relation Between Oil Rate and Replacement Ratio: Table (7) gives the replacement ratios for different oil rates; the replacement ratio is the ratio between coke saved and oil injected. The relation is represented in figure, (5), from which it is clear that the replacement ratio decreases with the increase in the oil rate till it approaches one at the higher oil rates used.

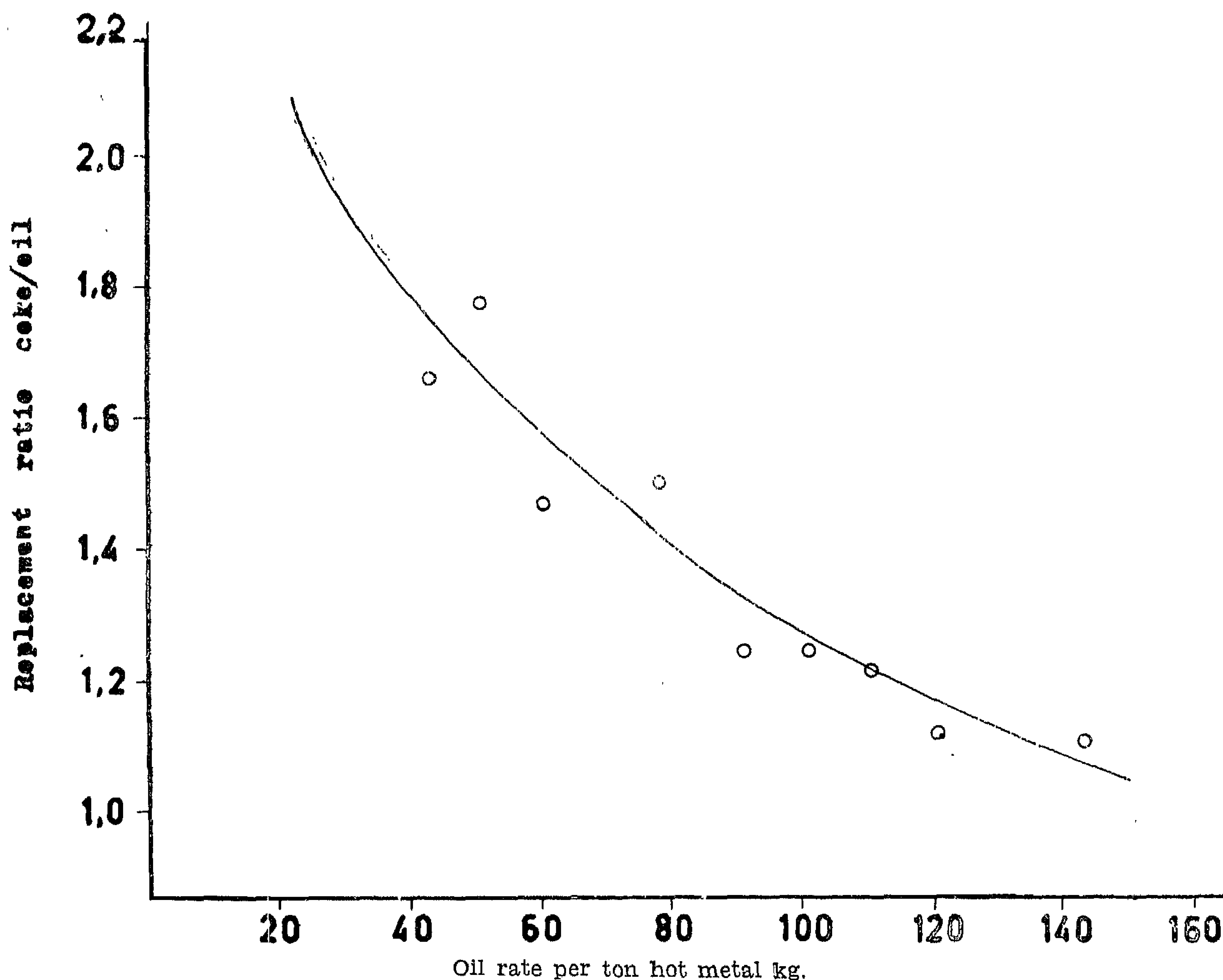


FIG. 5 : Relation between oil rate and replacement ratio.

Effect of Oil Injection on Blast Furnace Productivity; Table (7) gives the average daily production during oil injection through the ten-weeks test period. The increase in production was caluclated and a relation between oil rate and increase in productivity is graphically represented in Fig. (6).

At an oil rate of about 70 Kg./ton hot metal the percent increase in production was maximum. When the oil rate was increased over this value the increase in production declined till an oil rate of 145 Kg./ton metal when there was no increase in production. This means that at an oil rate of 70 Kg./ton metal the oxygen available after the combustion of injected fuel oil, is just enough to burn the coke and in this case the smelting power of the furnace will be at its maximum. For oil rates over 70 Kg./ton metal, the excess oil will pick up the oxygen and thus there will be no sufficient oxygen for the coke. The coke will thus burn more slowly and the furnace will be driven at a lower rate. This result complies with Cordier's view[18].

Table (10) : Effect of Oil temperature on oil injection.

Oil temp. °C.	Oil rate Kg./ton metal	Observation
80	70	Carbon black in settler
	95	Carbon black in settler
95	70	No carbon black
	95	No carbon black

Effect of Oil Injection on Coke Saving : Table (7) shows the amount of coke consumed per ton pig iron for the different oil rates used. The amount of coke saved was computed for each case and the relation between oil rate and coke saved is given graphically in figure (4), from which it is clear that coke consumption decreases by the increase in oil rate.

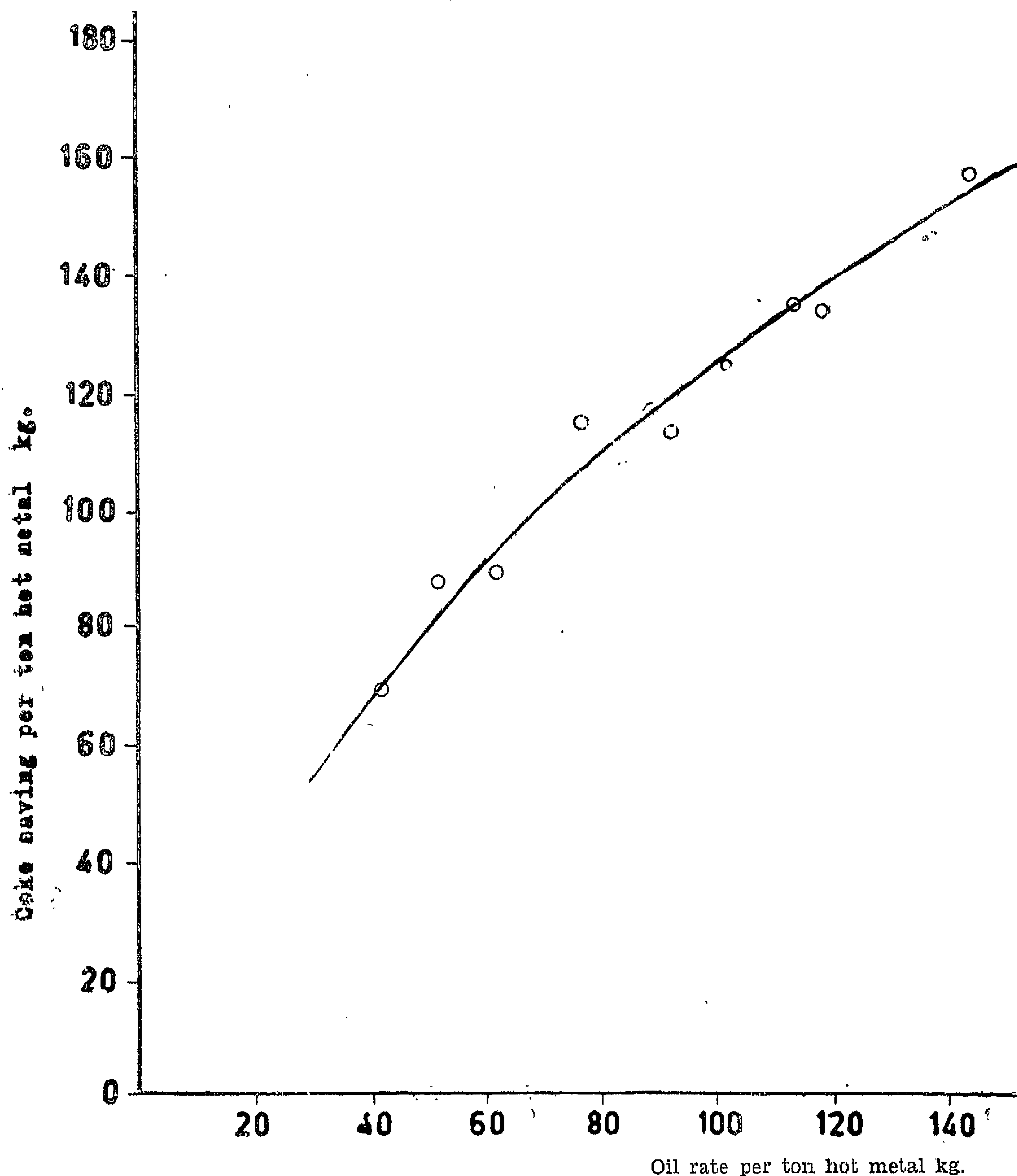


FIG 4 : Effect of oil injection on coke saving.

Effect of Oil Injection on Top Gas Composition: There was no appreciable change in the CO/CO_2 ratio wether without oil injection or with different rates of injection.

Effect of Oil injection on Pig Iron Analysis : Pig iron analysis before and with injection was practically the same with the exception of the sulphur content which increased gradually but slightly by the increase in oil rate; being about 0.04% before injection and increasing to about 0.06% at the maximum oil rate used. This increase is presumably due to the relatively high sulphur content of the fuel oil used.

Effect of Blast Temperature on Oil Injection: At two oil rates, 70 and 95 Kg./ton hot metal, four blast temperatures were used. The results are given in table (8) from which it is clear that the blast temperature must be over 700°C to avoid the formation of carbon black.

Table (8) : Effect of blast temperature on oil injection performance.

Av. Blast temp., °C	Oil rate Kg./ton metal	Observation	Av. Blast temp., °C	Oil rate Kg./ton metal	Observation
630	70	Carbon black in settler	630	95	Carbon black in settler
680	70	Less carbon black in settler	680	95	Less carbon black in settler
740	70	No carbon black	740	95	No carbon black
780	70	No carbon black	780	95	No carbon black

Effect of Oil Pressure on Oil Injection : For two oil rates, 70 and 95 Kg./ton hot metal, three oil pressures were used. As shown in table (9) it is clear that the oil pressure must not be less than 6 atmosphere to avoid the formation of carbon black in the settler.

Table (9) : Effect of oil pressure on oil injection performance.

Oil pressure	Oil rate Kg./ton metal	Observation
4 atm.	70	Carbon black in the settler
	95	Carbon black in the settler
5 atm.	70	Less carbon black in the settler
	95	Less carbon but slightly more than for 70 Kg./ton
6 atm.	70	No carbon black
	95	Traces of carbon black

Effect of Oil Temperature on Oil Injection : At the two oil rates 70 and 95 Kg./ton hot metal, two oil temperatures were used and the results as shown in table (10), indicate that the oil temperature must not be less than 95°C to keep the oil fluid in the pipeline, facilitating the atomization process.

A summary of spray observations obtained during the test is given in table (6).

Table (6) : Effect of injector retraction on spray performance.

Injector retraction at 90 lit./hr.	Performance	Injector retraction at 360 lit./hr.	Performance
2.5 D	Unsatisfactory	2.5 D	Unsatisfactory
3.0 D	Satisfactory	3.0 D	Satisfactory
3.5 D	Satisfactory	3.5 D	Satisfactory
4.0 D	Satisfactory	4.0 D	Satisfactory
4.5 D	Slight unsteadiness of spray	4.5 D	Slight unsteadiness of spray
5.0 D	Spray unsteady and sides of tuyere glowing	5.0 D	Spray unsteady and sides of tuyere glowing

The appearance of the oil spray was noted by looking through the tuyere eye-glass.

Glowing of the sides of tuyere at high retractions is attributed to the impingement of oil droplets and their combustion on the tuyere sides.

It was decided to use a retraction ratio of 4.0 D in the main work.

Full Scale Fuel Oil Injection :

Table (7) gathers the operational data during the first ten weeks of full scale oil injection. (The operational data during the seven days of each week are averaged in this table).

The coke rate without oil injection was 1260 Kg./ton metal which, by comparison with the coke rate figures in the table, indicates a considerable saving in coke consumption. Also, the average production increased as compared with that without oil injection which is 296 ton hot metal per day.

Table 7 : Operational data of oil injection

Week No	Average coke rate Kg./t. metal	Average oil rate Kg./t. metal	Replacement ratio (Coke : Oil)	Average production ton/day
1	1257	8.4	—	297
2	1190	42	1.67	326
3	1173	49	1.77	338
4	1170	61	1.47	359
5	1144	76	1.52	355
6	1145	91	1.26	331
7	1132	101	1.27	317
8	1122	111	1.24	308
9	1123	120	1.14	299
10	1099	142	1.14	296

four tuyeres 2, 4, 6 and 8, then covered the eight tuyeres. The increase in oil rate was accompanied by an increase in blast temperature till the maximum rate was attained when the temperature was fixed at an average temp. of 740°C.

A slight increase or decrease in oil rate was made to control the temperature of the furnace taking into consideration that an increase of one gram of oil per cubic meter of blast is equivalent to a decrease of 5.8°C in the blast temperature. This enables the furnace operator to attain a quick adjustment of the hearth temperature. Another measure could be taken for the same reason by decreasing the amount of coke in blast furnace charge. However, the effect of this last measure will appear after a period of about 8 hours. The operational conditions and results were recorded daily.

RESULTS AND DISCUSSION

Steam Injection :

The effect of steam injection on the coke rate, blast furnace productivity and pig iron analysis were investigated. Due to the industrial nature of the experiments conducted and the difficulty of fixing sharply the conditions of the experiments the investigation had to be run for a long period (two months) so that definite conclusions could be arrived at. The blast temperature was kept constant at about 810°C during the test period. This necessitated changing the quantity of steam injected between 15 and 28 gm./cu.m. of blast due to variations in burden analysis during the test period which resulted in changes in the thermal load of the furnace.

From every cast a pig iron sample was taken and analysed. The figures obtained show that the pig iron analysis was not affected by the amount of steam injected. This indicated that the effect of steam injection was completely compensated by an adequate increase in the blast temperature.

Single Tuyere Oil Injection :

The effect of the retraction ratio on the tuyere cooling water temperature, oil discharge pressure and shape of the oil spray was investigated. Table (5) shows the oil pressure and tuyere cooling water temperature at different retractions using the two oil rates 90 and 360 liters per hour. It is clear that the discharge pressure remained constant indicating no oil coking; also the tuyere cooling water temperature remained fairly constant indicating no tuyere over heating.

Table (5) : Oil pressure and cooling water temperature during the single tuyere test.

Injector retraction at oil flow rate 90 lit./hr.	Oil pressure atm. gauge	Tuyere cooling water temp. °C	Injection retraction at oil flow rate 360 lit./hr.	Oil pressure atm. gauge	Tuyere cooling water temp. °C
2.5 D	1.09	37	2.5 D	1.86	38
3.0 D	1.02	37	3.0 D	1.88	38
3.5 D	0.98	36	3.5 D	1.88	37
4.0 D	0.98	35	4.0 D	1.90	35
4.5 D	1.02	33	4.5 D	1.90	34
5.0 D	1.02	33	5.0 D	1.90	33

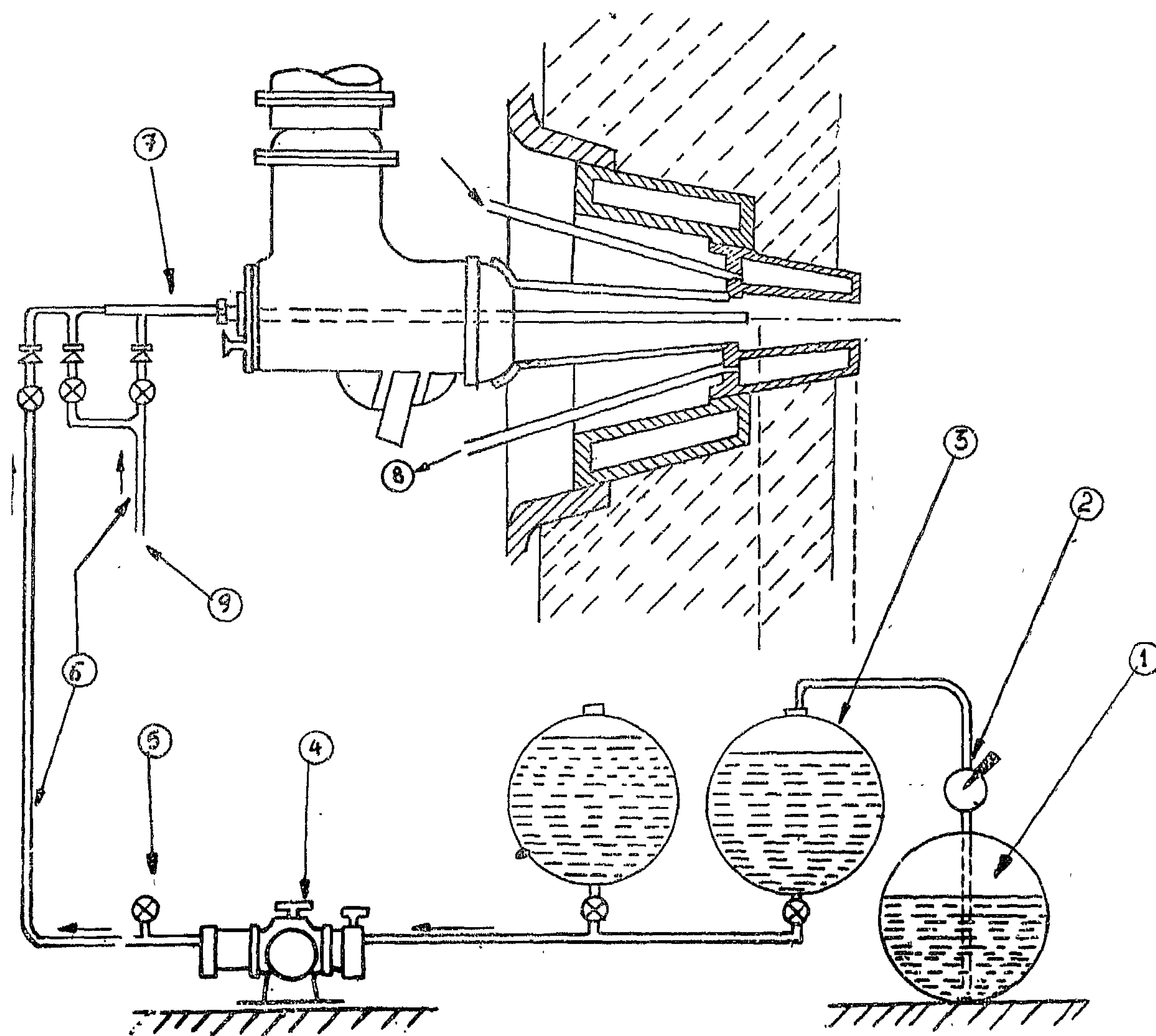


FIG. 3 : Arrangement of rig for single tuyere oil injection tests.
(1) Oil reservoir. (2) Oil transfer pump. (3) Oil drums. (4) Oil metering pump. (5) Pressure gauge. (6) Flexible hoses. (7) Injection lance. (8) Cooling water outlet. (9) Air supply.

Oil comes to the furnace through a pipe line, beside which a steam line is installed to reserve the oil temperature and the two are insulated together with glass wool. A set of valves is provided to control the quantity of oil injected through each tuyere. A tracing air line is connected to the system of injection so that when the oil is stopped the tracing air is automatically passed through the nozzle to prevent the coking of oil in it.

A pipe through which the injecting nozzle is fixed and to which compressed air is connected is screwed to the tuyere blow pipe. The stainless steel nozzles are connected to the main line of oil surrounding the furnace by means of flexible steel hoses.

All measuring and control instruments are connected to recorders and alarms gathered for each furnace with the operating switches on one instrumental pannel.

At the start of the operation oil was injected from two opposite tuyeres (No. 4 and 8) with a rate of 100 lit./hr./tuyere for one day. Oil injection was then carried out from

The blast temperature was raised gradually from 600°C., being the average temperature before the start of the test campaign, to 810°C. and kept at this level. To obtain this comparatively high blast temperature, the heating cycle of the stoves had to be changed from the normal which was based on heating the stove with 12000 cu.m./hr. of blast furnace gas to heating it with 25000 cu.m./hr. ; changing of stoves was done every half an hour.

The injection of steam in the cold blast pipe started at a rate of 5 grams per cubic meter of blast and increased gradually till an average of 20 gm./cu.m. was attained. When the furnace became comparatively hotter than normal, that is when the silicon content of the pig iron was higher than that specified for Thomas steel, the quantity of steam injected was raised. An increase of 2 gms./-cu.m. corresponds to a decrease of 6.25°C in blast temperature. On the other hand, when the pig iron produced appeared to be cold, the quantity of steam was proportionately lowered to increase the temperature of the furnace.

Single Tuyere Oil Injection :

The aim of this test is to find out the best position of the lance to ensure satisfactory oil atomization. Twelve experiments were carried out beginning with a lance retraction of 2.5 times the diameter of the tuyere and ending with a retraction of 5.0 times the diameter of the tuyere. At every retraction two oil rates were used 90 and 360 lit./hr.

Gas oil was used for these tests since it has the correct atomizing viscosity without preheating. The specifications of this oil are shown in table (3).

Table (3) : Gas oil specifications

Specific gravity at 15°C.	0.453
Flash point (closed)	137°C.
Water %, volumetric	0.1%
Kinetic viscosity at 37° C.	24 sec.
Carbon residue	3%
Sulphur conteent	0.09%
Hydrogen content	16%

A portable fuel injection rig was used for lance positioning (Fig. 3). The injcetion lance was inserted through a sealing gland in the modified face plate of the tuyere.

The injection procedure was as follows ;

1) The two barrels (3) were filled with oil by the hand transfer pump (2).
2) The lance (7) was set at the required retraction.
3) The metering pump (4) was put into operation and controlled to give the required oil rate.
4) The oil pressure was measured by the pressure gauge (5) as a check that no fuel coking occurs in the lance.
5) The tuyere cooling water outlet temperature was continually recorded.
6) The appearance and effective diameter of the oil spray were noted.

Full Scale Fuel Oil Injection :

The raw materials listed in tables (1) and (2) were also used in this series of experiments, while the fuel oil specifications are given in table (4).

Table (4) : Fuel oil specifications

Specific gravity at 15°C.	0.951
Flash point (closed)	210°C
Pour point	8-13°C.
Water %, volumetric	0.8 maximum
Kinetic viscosity at 37°C.	500 sec.
Viscosity red wood No. 1 at 37°C.	1500
Carbon residue	12%
Sulfur content	2.8%
Hydrogen content	12%

A 180 ton capacity storage tank is provided with a steam heater to raise the oil temperature to about 80°C. Three electrically diven rotary displacement pumps each rated at 3600 liters per hour, feed the oil to three electric oil heaters to raise its temperature to 105-110°C.

Table (1) : Raw materials average analysis (percent)

Constituent	Aswan ore	Sinter used during steam test	Sinter used during fuel oil test	Lime stone	Dolomite
Fe	42	39.5	42	—	—
FeO	—	19.8	13.8	—	—
SiO_2	21	19.65	21	2.8	0.26
Al_2O_3	5	5.12	2	0.56	0.063
CaO	4	6.19	14	53.0	31.19
MgO	1.3	1.62	0.8	0.97	20.1
Mn	0.8	0.29	0.5		
P	1.0	0.67	0.6		
S	0.15	0.25	0.02		

Table (2) : Proximate analysis of coke

Constituent	Content %
Fixed carbon	87.5
Ash	10.7
Volatile matter	1.74
Sulphur content	1.2
Moisture content	4.6

Calorific value 7022 Cal/kg.

Steam Injection :

The system for steam injection is illustrated in Fig. (2). Steam was superheated to 250°C while its pressure was about 10 atm. The test was performed on blast furnace no. 2.

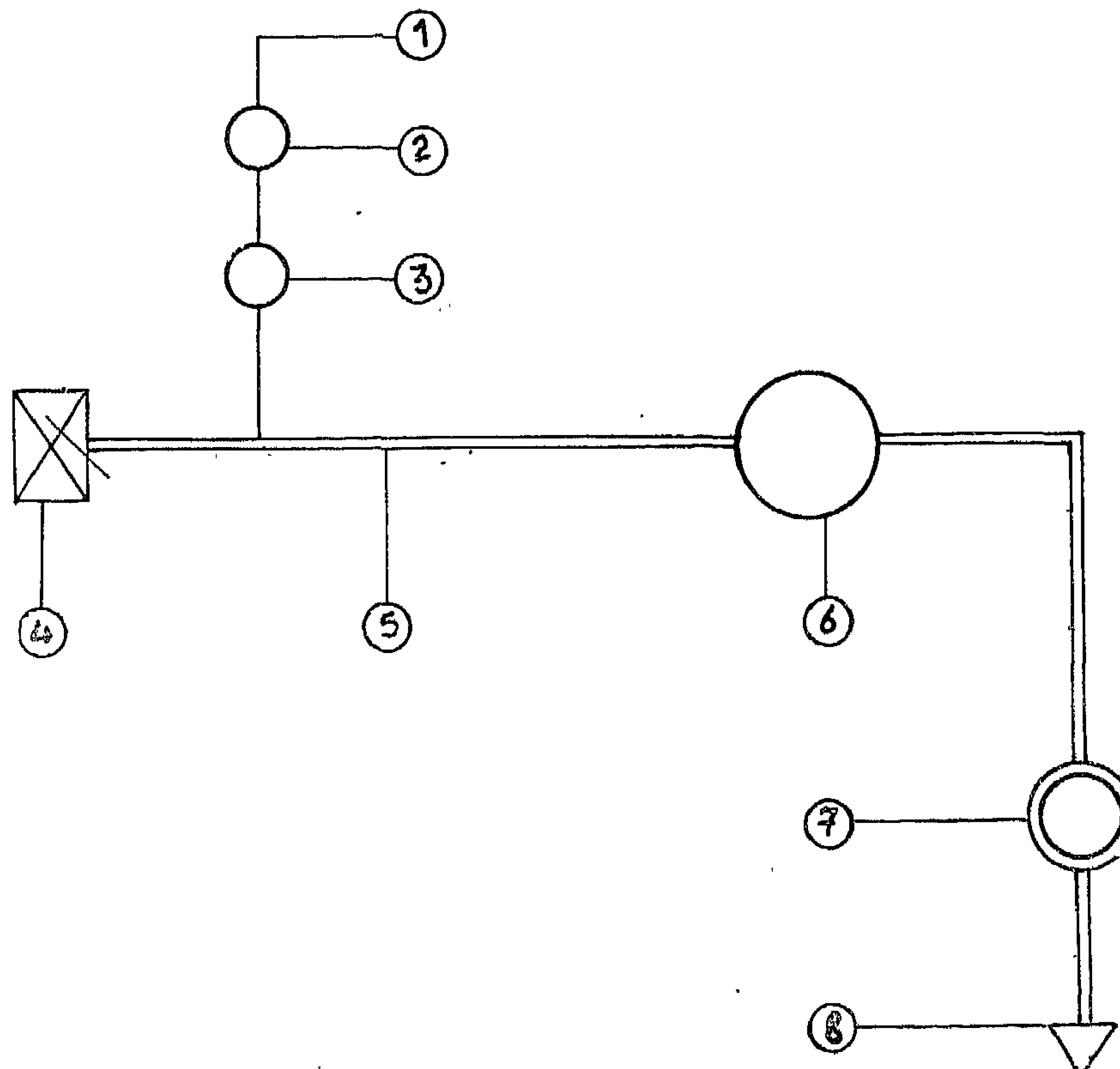
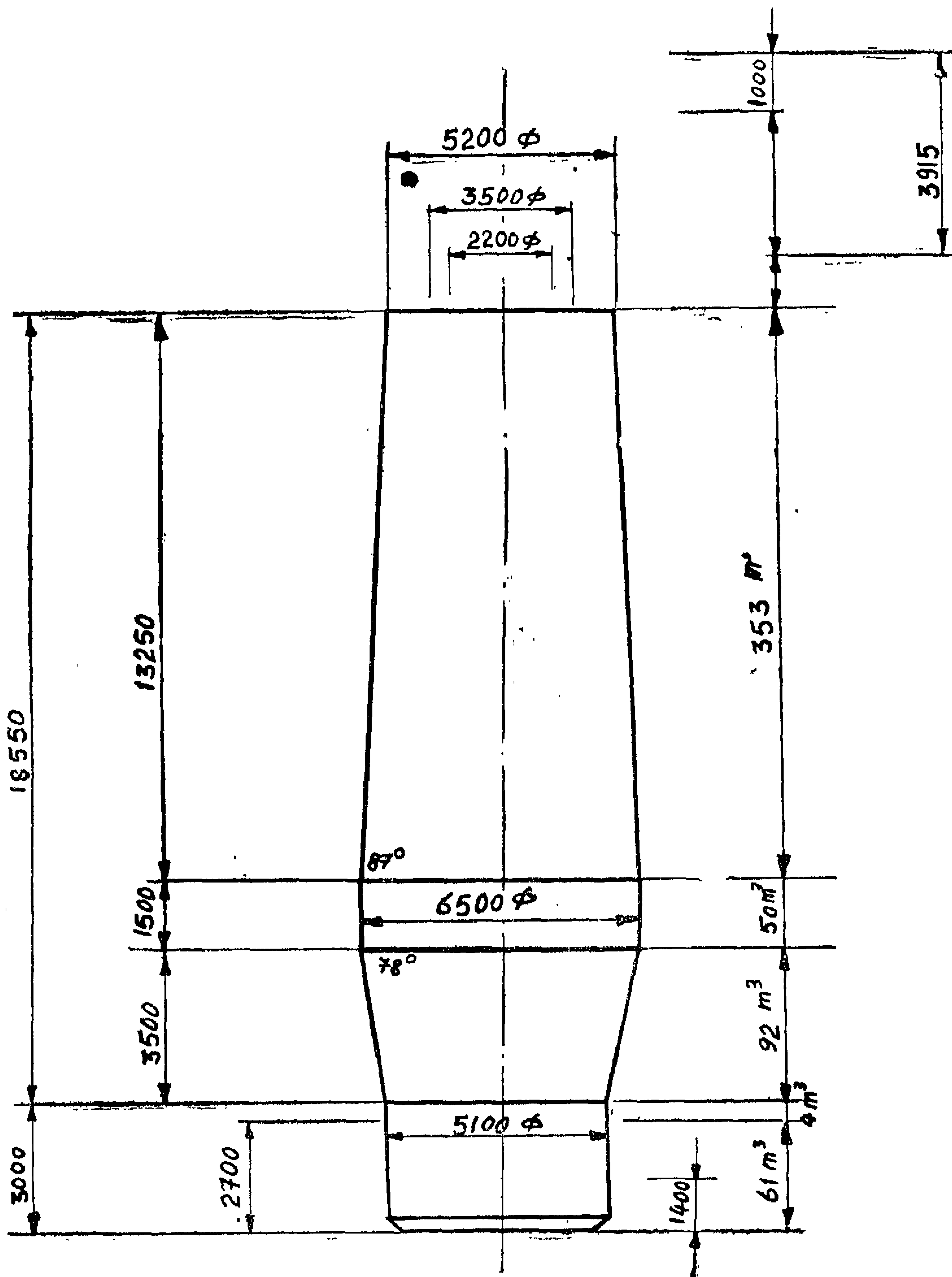


FIG. 2 : Arrangement of steam injection.
(1) Steam line. (2) Manometer. (3) Flow-meter. (4) Blower house. (5) Cold blast pipe. (6) Hot blast stove. (7) Hot blast main. (8) Tuyeres.

ore with a CaO/SiO_2 ratio which varies between 0.8 and 1.0. The fluxes were limestone and a small percentage of dolomite to obtain a fluid slag.

The average analysis of the raw materials are shown in table (1) while table (2) gives the proximate analysis of coke.



Useful volume : 499 m³
Total volume : 556 m³

FIG. 1 : Blast furnaces main dimensions.

The blowing of steam in the tuyere's zones creates the water gas reaction between steam, carbon and carbon monoxide with the formation of hydrogen. According to the experiments carried out by N. Goldstun and N. Khromchenko[4] the degree of conversion of steam increases, under all conditions, with the decrease of its concentration in blast. As for the hydrogen formed Norwood and Decker[5] reported that throughout the tests they performed, hydrogen utilization was found to be about 40-45% and the sum of the moles of hydrogen and carbon engaged in direct reduction was practically cotnstant. The endothermic reduction operation occurring to the lower oxides with hydrogen at the high temperature zone of the furnace proceeds at a high velocity.

Hydrocarbons Injection :

Trials on blast furnace injection for the partial substitution of coke started in 1949[6]. The first serious test was done on the international low-shaft blast furnace at Liege, Belgium in 1958[7]. In the mean time Esso Research was busy in developing a proper injector for the fuel oil[8]. In 1960 light fuel was used in Pompey, France[9], while heavy fuel oil was used in Hamilton, Ontario, Canada[10].

Tests done on the 4 ft experimental blast furnace at the U.S.B.M. station at Pittsburgh proved the possibility of increasing oil injection by increasing blast temperature. 90 Kilograms of oil per ton of iron decreased coke consumption by 174 Kilograms and increased the production by 8.8%[11]. Using natural gas, they could achieve about 30% saving in coke consumption with an increase of same percent in productivity[12]. When coke oven gas was injected into the blast furnace at a rate of 4% of the blast volume, coke consumption was decreased by 12.6% while productivity increased by 9.5[13].

Nekrasov and Moskalina[14] reported that the reaction between hydrocarbons and oxygen takes place in the race way in a stepwise manner and as a result different intermediate products appear as alcohols, aldehydes etc., before the formation of the ultimate products of cracking and reforming (i.e.) hydrogen and carbon monoxide.

Kenneth et al[15] found that the size and temperature of the tuyere race way are affected by the analysis and temperature of the gases entering from the tuyeres. To keep the race way temperature constant, the blast temperature should increase with the increase in the amount of fuel injected, to subtitute for the heat losses due to the endothermic nature of the reactions taking place.

Investigations throughout the height of the blast furnace showed that injection is accompanied by a considerable activity in the whole furnace resulting in lower CO/CO_2[16]. Nekrasov et al[14] working with natural gas, and Borisov and Fofanov[11] working with fuel oil reported that a considerable portion of the hydrogen formed is consumed in reduction at the lower parts of the stack.

The decrease in coke consumption due to hydrocarbons injection results in decreasing the charge permeability particularly at the lower parts of the furnace where slag formation and semi fusion start to take place. This, in turn, leads to a rise in the over all pressure drop through the furnace[17].

EXPERIMENTAL

The work in the present study was performed on the two 400 t/day blast furnaces of the Helwan Iron and Steel works. Fig. (1) gives the blast furnaces main dimensions.

Raw Materials :

During the test period the charge used was a mixture of non fluxed sinter of Aswan

TRIALS ON STEAM AND FUEL OIL INJECTION IN A 400 TON/DAY BLAST FURNACE

By

M. ABO EL-SAADAT, A.B. MOURAD, M.S. ETEWA and S.Y. EZZ

ABSTRACT

Steam injection has no effect on pig iron analysis as long as the hearth temperature is kept constant. Coke consumption increases if the blast temperature is kept constant without any compensation for the endothermic steam reaction associated with steam injection. Under such condition the productivity of the furnace will decrease.

As to fuel oil injection, a single tuyere test determined the best retraction distance of the lance and it was found to be four times the tuyere's diameter.

From the full scale oil injection tests it was found that the hydrogen content of the blast furnace gas increases by the increase in oil rate and so does the CO/CO_2 ratio. The sulphur content of the pig iron increased slightly due to the high sulphur content of the fuel oil used.

Coke consumption decreased by the increase in oil rate and so did the replacement ratio. The optimum value of oil rate for maximum productivity was found to be about 70 Kg./ton hot metal at which coke saving was 100 Kg. and the total decrease in production cost was about 6.9%.

INTRODUCTION

An iron and steel plant was erected in Egypt and started operation in 1958. It constitutes two 400 tons/day blast furnaces. The ore used is a low grade ore with more than 20% silica. This results in high coke consumption (up to 1260 Kg./ton iron). Coke rate is recalculated on the basis of 100% Aswan ore burden excluding all other metallic components. Coke is imported with hard currency and iron production is expensive. Due to the fact that excess fuel oil is available at low cost from local petroleum refineries, it has been decided to inject it in the blast furnace.

This study follows the construction of the equipment and instruments used, describes the trials, and gives the results as to the effect of different conditions and factors on operation and coke consumption.

THEORETICAL CONSIDERATIONS AND LITERATURE SURVEY

Steam Injection :

Two contradicting ideas were put forward for the effect of steam injection on blast furnace operation[1],[2]. Trials were made since 1930 to dehumidify the air blast on the assumption that moisture consumes heat and consequently coke consumption will increase[2]. However, it was found that dry blast actually decreased driving rates, so these trials were stopped. In 1950 it was recognized that although moisture consumes coke, it produces hydrogen instead and the driving rate of the furnace increases[1]. Mathematically, Agnew[3] found that steam can benefit or harm blast furnace operation according to the operation conditions and to its content in the blast.

CONCLUSION

The present work submits a comprehensive analysis of the shear effect on reinforced concrete structures, when designed by LIMIT DEFORMATION METHOD. It has clearly verified that the negligence of shear effect leads to a diminution of the safety of the structure. The concrete can reach its compressive strength although the calculations are based on limit value of concrete stress, producing a state of collapse, which spoils all advantages of LIMIT DESIGN THEORY. A practical procedure has been achieved to determine the appropriate valaue of the concrete compressive stress, which can be utilised correctly in the LIMIT DESIGN.

REFERENCES

1) Flaechentragweks by Prof. Dr. Ing. Karl Girkmann.

2) Code et manuel d'application pour le calcul et l'execution du beton arme (UNESCO).

3) Recommendations for an international code of practice for reinforced concrete, issued by Cement and Concrete Association.

4) Die Statik im Stahlbetonbau by Prof. Dr. Ing. Kurt Beyer.

5) Formulas for stress and strains by Prof. Raymond Roak McGraw-Hill Book Company, Inc.

6) Analysis of Designing Reinforced Concrete Structures by Dr. Ing. Mahmoud Nasr Proceedings of Engineering Societies Vol. IX — No. 1, 1970.



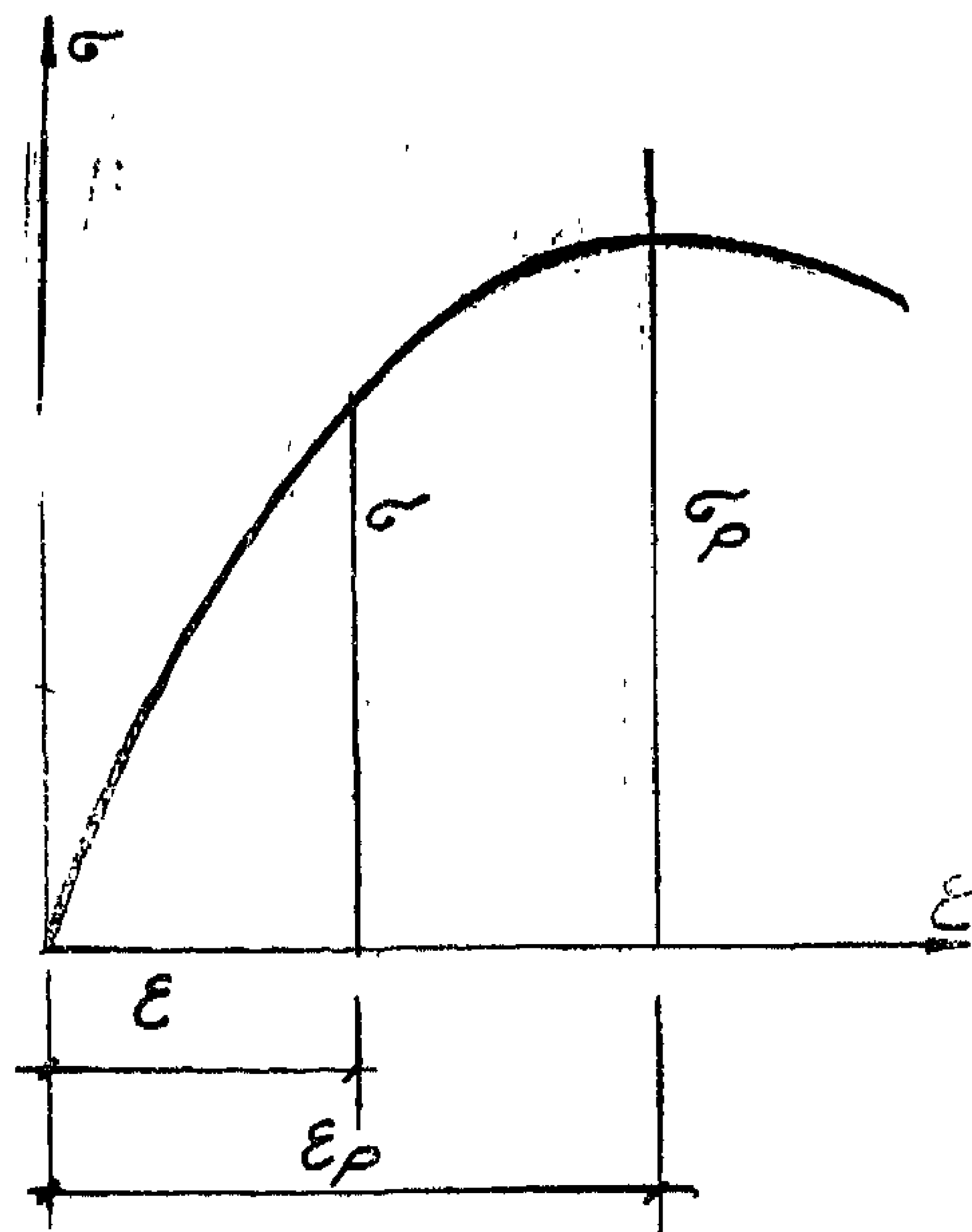


Fig. 3.

When reducing the field of concrete strength by determining the LIMIT curve "L", which is analogeous to curve "C", but reduced with the value Φ, Fig. 4, then we have the FIELD OF LIMIT STRENGTH, which is the area inside the curve "L". Therefore when fixing the circle, which curve "L" is its envelope, its intersection with the τ axis represents the LIMIT SHEAR STRENGTH and hence the value σ_c is the LIMIT CONCRETE COMPRESSIVE STRESS. Concequently in the LIMIT DESIGN the calculations must be assessed upon the value σ_c, and not the value σ.

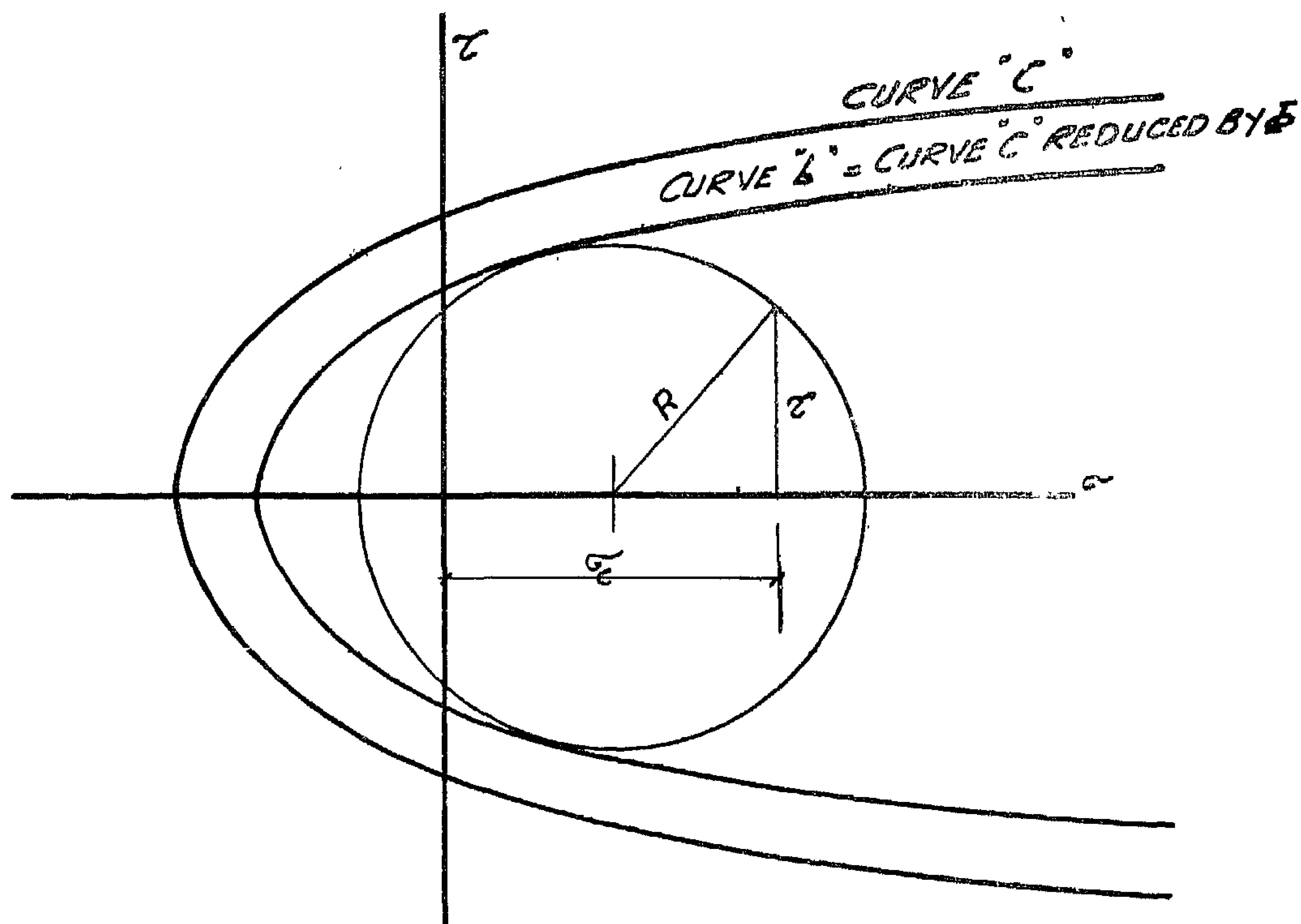


FIG. 4

LIMIT FIELD CONCRETE STRENGT

The coeffecients a, b and c can be found from following boundary conditions :

$\sigma = C_t$	$\tau = 0$	for pure simple tension
$\sigma = C_c$	$\tau = 0$	for pure simple compression
$\sigma = 0$	$\tau = C_t$	for pure simple shear

The equation (8) can be written in the form:

$$\tau^2 = \frac{C_t}{C_c} (C_c - \sigma) (C_t + \sigma) \tag{9}$$

For any concrete type equation (9) of fers a direct method for determining the curve "C" Fig. 2.

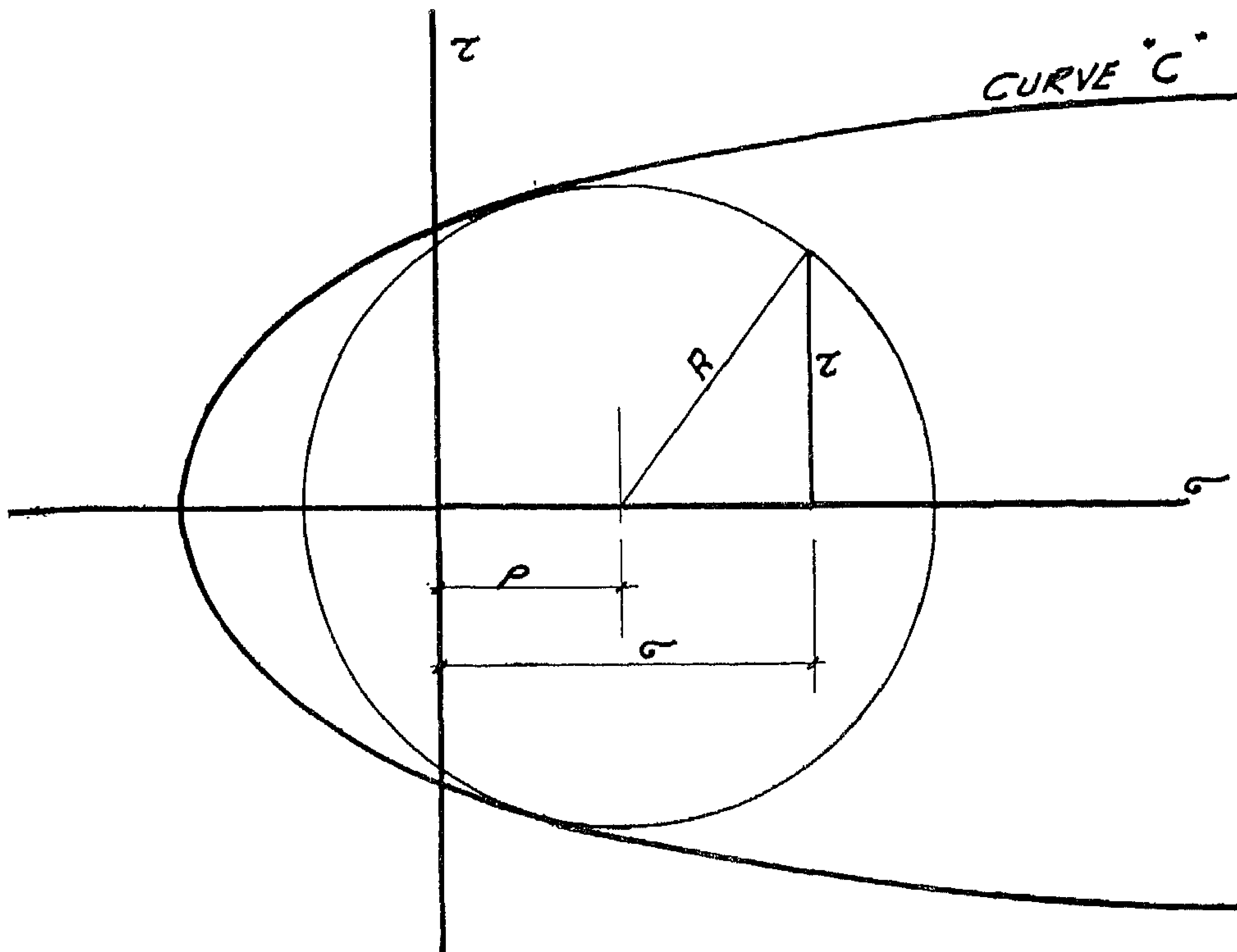


FIG. 2

FIELD OF CONCRETE STRENGTH.

DETERMINATION OF CONCRETE COMPRESSIVE STRESS IN LIMIT DESIGN

The LIMIT DESIGN is assessed upon fixing the strain ε and its corresponding stress σ, Fig. 3 and then both are given in terms of ε_p and σ_p as follows :

$$\varepsilon = \Psi \, \varepsilon_p$$

$$\sigma = \Phi \, \sigma_p$$

$$\Phi = \frac{\sigma}{\sigma_p}$$

$$\Phi = \frac{\text{limit allowed concrete strength}}{\text{final specified concrete strength}}$$

$$\Phi < 1$$

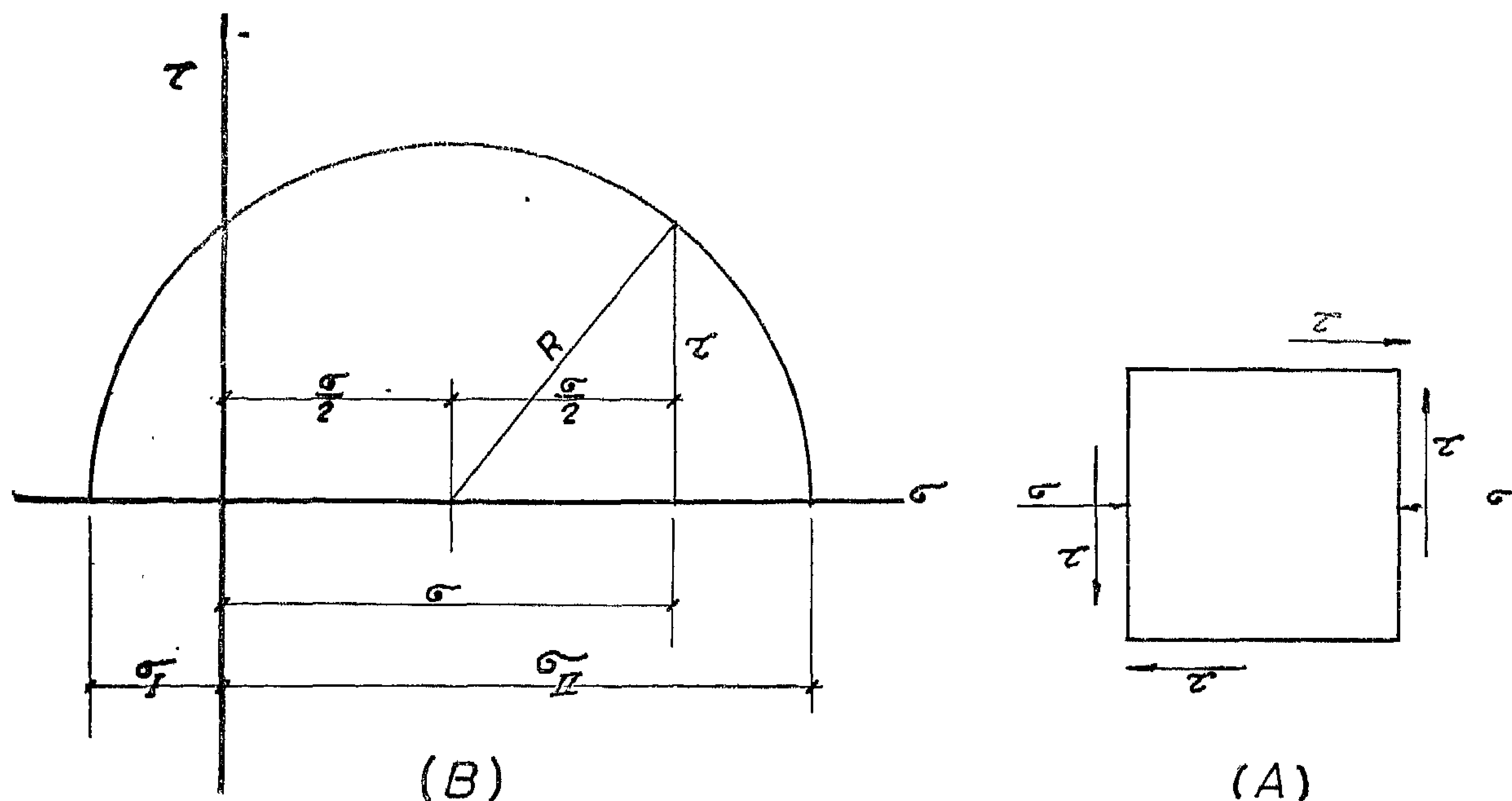


FIG. 1

MOHR'S CIRCLE FOR DETERMINING THE PRINCIPAL STRESSES

According to Mr. Caquot, the curve "C" is the envelope of the circle :

$$(\sigma - p)^2 + \tau^2 = r^2 \qquad (2)$$

The magnitude of p and r can be found from the following relations :

$$(p + C_t)^2 = r^2 - \frac{r^3}{R} \qquad (3)$$

where :

C_t = concrete tensile strength

C_c = concrete compressive strength

$$R = \frac{C_c^3}{8\ C_t\ (C_t + C_c)} \qquad (4)$$

$$= 1.5\ C_c\ \left(\text{Generally } \frac{C_c}{C_t} = 13\right) \qquad (5)$$

According to the envelope theory, the contact point of both the circle and its corresponding envelope is given by :

$$\sigma = \frac{3\ pr - 2\ C_t\ R}{2\ R + 3\ r} \qquad (6)$$

and $\sigma = 0$

if $\quad 3\ p\ r - 2\ C_t\ R = 0 \qquad (7)$

From equations (3), (4) and (7) the values of p and r can be obtained for any concrete type and hence the curve "C" is determined, Fig. 2.

Mr. Chalos proposed another method for determining the curve "C" stating that it is an ellipse having the relation :

$$\sigma^2 + a\ \tau^2 + b\ \sigma + c = 0 \qquad (8)$$

SHEAR EFFECT ON REINFORCED CONCRETE LIMIT DESIGN

By

Dr. Ing. MAHMOUD NASR
Assistant Professor
Faculty of Engineering, Cairo University.

INTRODUCTION

Many investigators have criticised the modular ratio theory for designing reinforced concrete structures, since no homogeneous factor of safety is involved and the relevant required steel is almost weak in tension and wasteful in compression. The recent trend of designing reinforced concrete elements is based on the plastic behaviour of concrete. Consequently ULTIMATE CAPACITY (ULTIMATE LOAD DESIGN) or LIMIT DEFORMATION (LIMIT DESIGN) have been thoroughly investigated and applied as an alternative methods for designing reinforced concrete structures.

ULTIMATE LOAD DESIGN is assessed upon taking a factor of safety against collapse, which is not an appropriate solution for reinforced concrete due to the formation of excessive deflection and very wide cracks. On the contrary LIMIT DESIGN is based on fixing —to a certain limit— the strains in both concrete and steel and then the corresponding stresses in both materials are introduced in the calculations.

The present work aims to clarify the necessity of taking into consideration the effect of shear when utilising the LIMIT DESIGN, because its negligence leads to a diminution of the safety of the reinforced concrete structures.

FIELD OF CONCRETE STRENGTH

For any normal stress σ combined with shear stress τ as shown in Fig. 1 (A), the resultant principal stresses are fundamentally given by :

$$\sigma_{I,II} = -\frac{\sigma}{2} \pm \sqrt{\left(\frac{\sigma}{2}\right)^2 + \tau^2} \qquad (1)$$

The values of both σ_I and σ_{II} can be also determined by Mohr's circle as illustrated in Fig. 1 (B).

When applyig the same principal to concrete, it is obvious that the safety is not secured, if in the LIMIT DESIGN the shear stress is neglected and the calculations are uniquely based on the stress σ, which is mainly determined as a function of the limit strain ε. The designer should not feel satisfied under the hypothesis that the stress σ is not always accompanied with the shear stress τ. Due to the existance of shear stress τ, the concrete can reach its compressive strenght—if σ_{II} = concrete prismatical strenght — under the action of the normal stress σ and consequently the structure will be subjected to a state of collpase; spoiling in this case all advantages of the LIMIT DESIGN THEORY. Neverthless the assumption that the fibres, where maximum normal stress σ takes place, are not subject to any shear stress τ, is only valid in simple cases.

To establish a sound procedure for the right evaluation of the normal stress σ, that can be applied in the LIMIT DESIGN, one has to determine for every concrete type its FIELD STRENGTH, which is specified as the area inside the curve "C" that envelopes Mohr's Circle.

8. *CONCLUSION*

It is shown that the classical method of estimating the pressures in silos, and which has been the basis of the design of silos for more than 70 years, is only a rough approximation which may not always be on the safe side. The modern methods still depend mainly on empirical values. Extensive experimental investigations and also measurments on full size silos are therefore still necessary.

It may also be recommended here, for a better utilisation of the construction materials, to introduce different factors of safety for the different cases of loading. For instance, the maximum pressures during emptying the silo when it is totally full occur only for a comparatively short period of time ; and therefore a smaller factor of safety might be allowed for this case of loading than that for permanent pressures. On the other hand if the material is stored for a long period of time without motion, it will consolidate under its own weight, and arching effect will be developed giving rise to high pressures. The estimation of these high pressures is still uncertain.

REFERENCES

1. H.A. Janssen : Versuche uber Getreidedruck in Silozellen. Zeitschrift des Vereins deutscher Ingenieure, Aug. 1895, p. 1045-49.
2. W. Airy: Theory of Silos : Inst. Civil Engineers, Vol. 13, 1897, p. 347-58.
3. J. Jacky: Pressure in Silos : Proc. of the 2nd Intern. Conf. on Soil Mechanics and Founds Eng., 1948, Vol. I, p. 103-107.
4. E. Friedich, Vertikale und horizontale Spannungen in Silowanden, Osterr. Ing. Zeitschrift, 15 July 1962, p. 221-233.
5. D. Lenzner : An investigation into the behaviour of sand in model silos. The Struct. Eng., Dec. 1963, p. 389.
6. Leonhardt, Boll and Speidel : Zur Frage der sicheren Bemessung von Zement-Silos. Beton — und Stahlbetonbau v. 55, March 1960, p. 49-58.
7. Lastannahmen fur Bauten. Lasten in Silozellen. Deutsche Normen DIN 1055 Blatt 6, Nov. 1964.



7. NUMERICAL EXAMPLE

A deep silo of height 20.0 m and of internal dimensions of 4.0 × 4.0 m is considered. It is filled with wheat of volume weight 0,75 t/m³. The angle of internal friction is 30°. The horizontal pressures are computed according to

1. the classical method, by Janssens formula with $K = K_a = (1 - \sin \Phi) / (1 + \sin \Phi)$,
2. Janssen, with $K = K_o = 1 - \sin \Phi$ (This same curve represents approximately the pressures given by Jaky),
3. Janssen, with K = 0,70 (as given by Janssen's tests),
4. DIN 1055, case during filling,
5. DIN 1055, case during emptying and
6. Airy

The results are plotted in Fig. 6. The theory of Airy gives the lowest pressures. Below a depth of about 6.0 m below the top surface the pressures according to Airy remain, for this special case, nearly constant. The maximum lateral pressures are given by the German Specifications for the case of emptying.

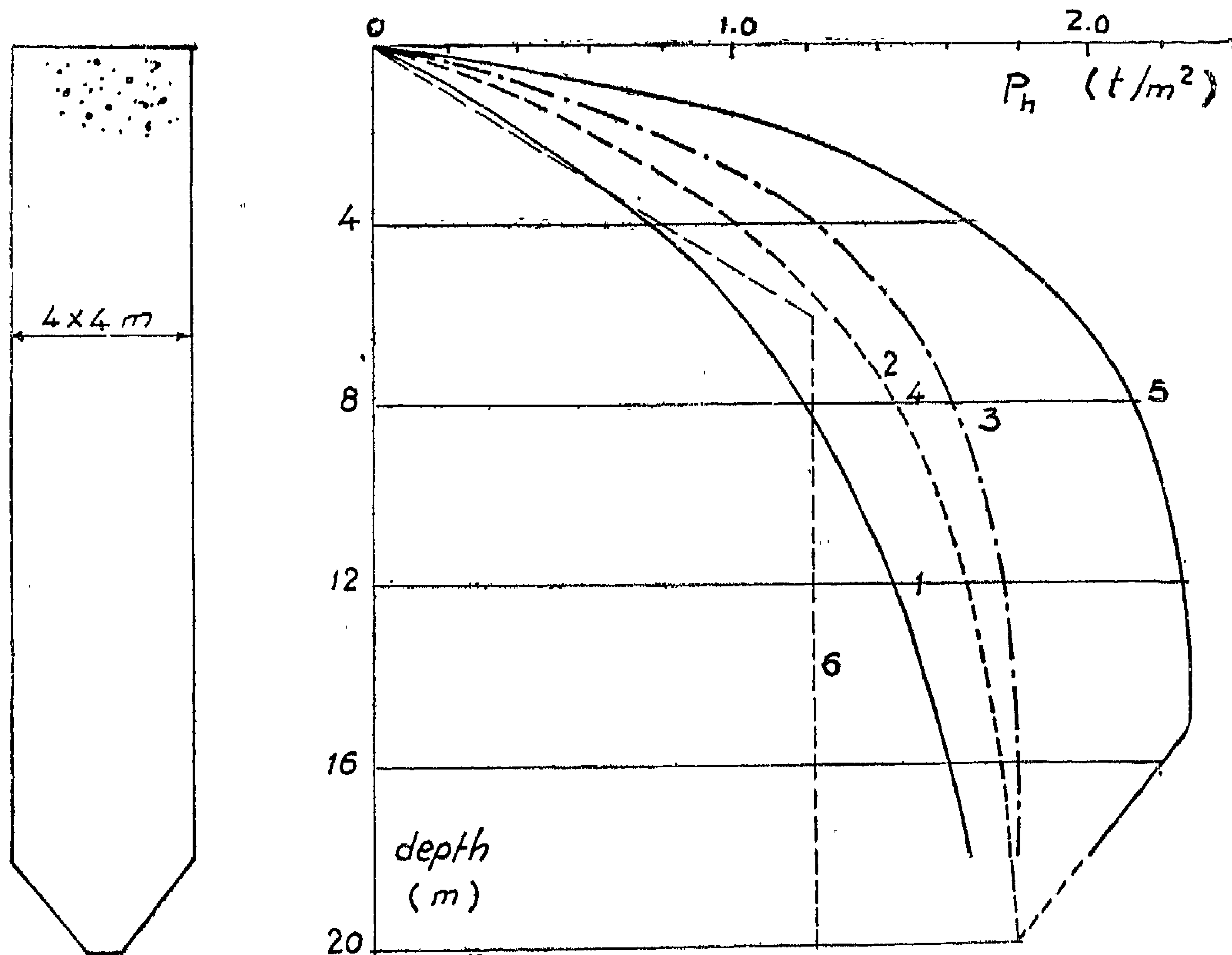


Fig. 6

4. The theory of Friedrich contributes in fact to the comprehension of the increase of pressures created by the arching effect. It may not however be applied yet to the computation of pressures until the included assumptions and the deliberately assumed factors have been experimentally verified.

5. Nevertheless, the derivation of a more accurate formula for P_v with variable k is a very good contribution and can be very useful if a more accurate distribution of K may be obtained.

6. GERMAN SPECIFICATIONS (1964)[7]

The load assumptions for pressures in silos given in the recent German specifications (DIN 1055 Blatt 6) are the results of the up to date experimental and theoretical investigations on the subject. It is however stated in the introduction to this specification that further extensive investigations are still necessary.

According to DIN 1055 the pressures in silos may be calculated by Janssen's formula (see 2. above) but with certain specified values for Φ' and K. Two cases are considered :

a) pressures during filling the silo and

b) pressures during emptying the silo.

In the first case the vertical load carried by the base of the silo reaches the maximum, whereas in the second case the lateral pressures and frictional forces on the walls are maximum.

The angle of friction Φ' between the filling material and the walls of the silo is to be assumed as follows. It is independent of the roughness of the wall surface.

	during filling	*during emptying*
Granular material with mean diameter > 0.20 mm	$\Phi_f' = 1.75\ \Phi$	$\Phi_e' = 0.60\ \Phi$
Fine material (e.g.. cement) with mean diameter < 0.02 mm	$\Phi_f' = \Phi$	$\Phi_e' = \Phi$

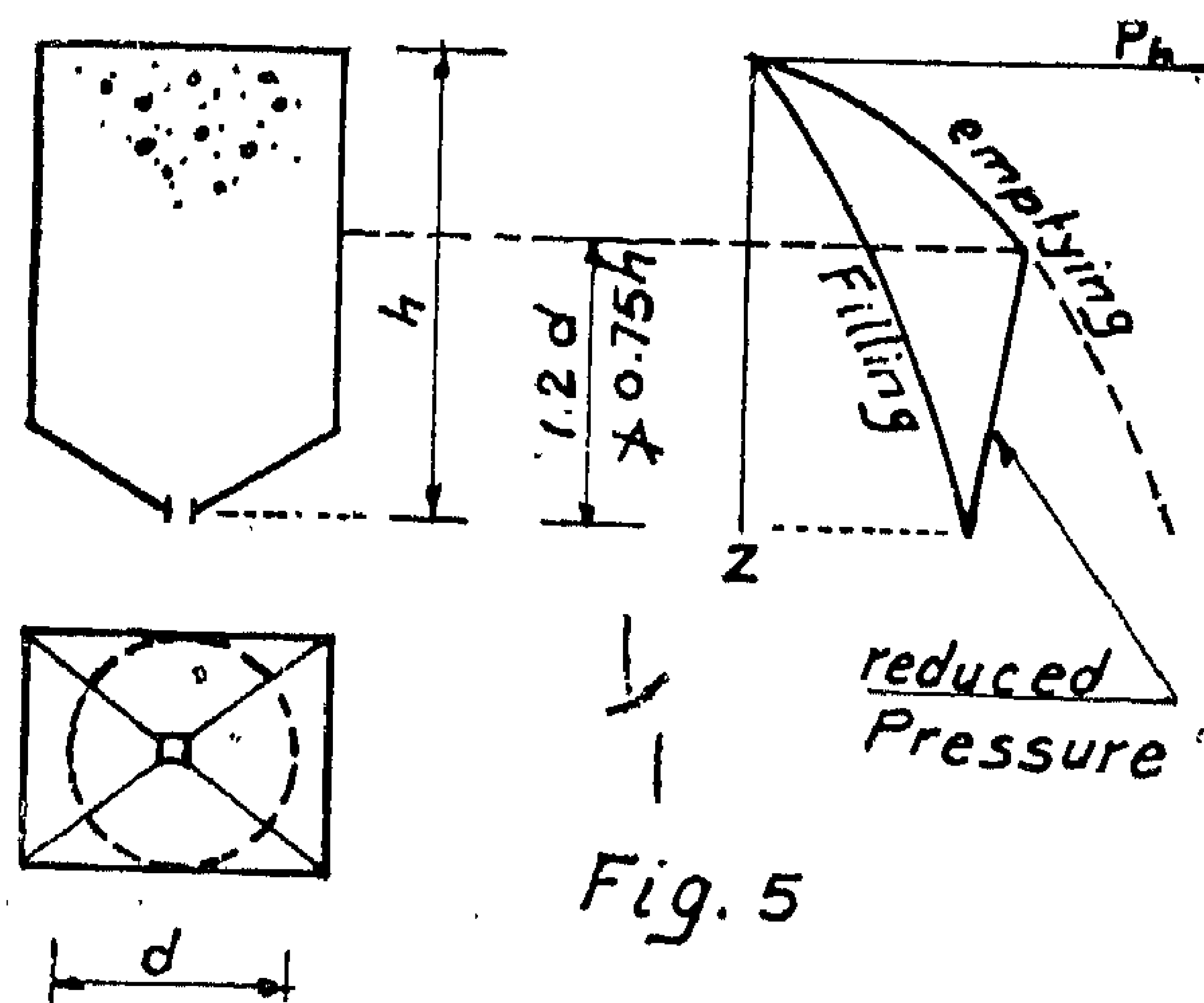


Fig. 5

The ratio K of the horizontal pressure to the vertical pressure is given, independent of the size of the filling material as follows :

during filling	*during emptying*
$K_f = 0.50$	$K_e = 1.00$

The pressures during emptying may be reduced near the bottom of the silo as shown in Fig. 5.

$$+ p\, e^{-\frac{K \tan \Phi'}{m} y}$$

The solution was based on considering K to vary between zero and ∞. The actual values of k had to be found out of experiments; but as an approximation the following assumptions were made :

It was assumed that the lateral pressure might be confined in a zone with a deliberately chosen height of 10 times m, (zone II in Fig. 4), where $m = \frac{\text{Area}}{\text{Perimeter}}$.

In the upper zone I it was assumed that the fill might stand vertically as an integrated block totally separated from the walls. This was equivalent to assuming $k = 0$.

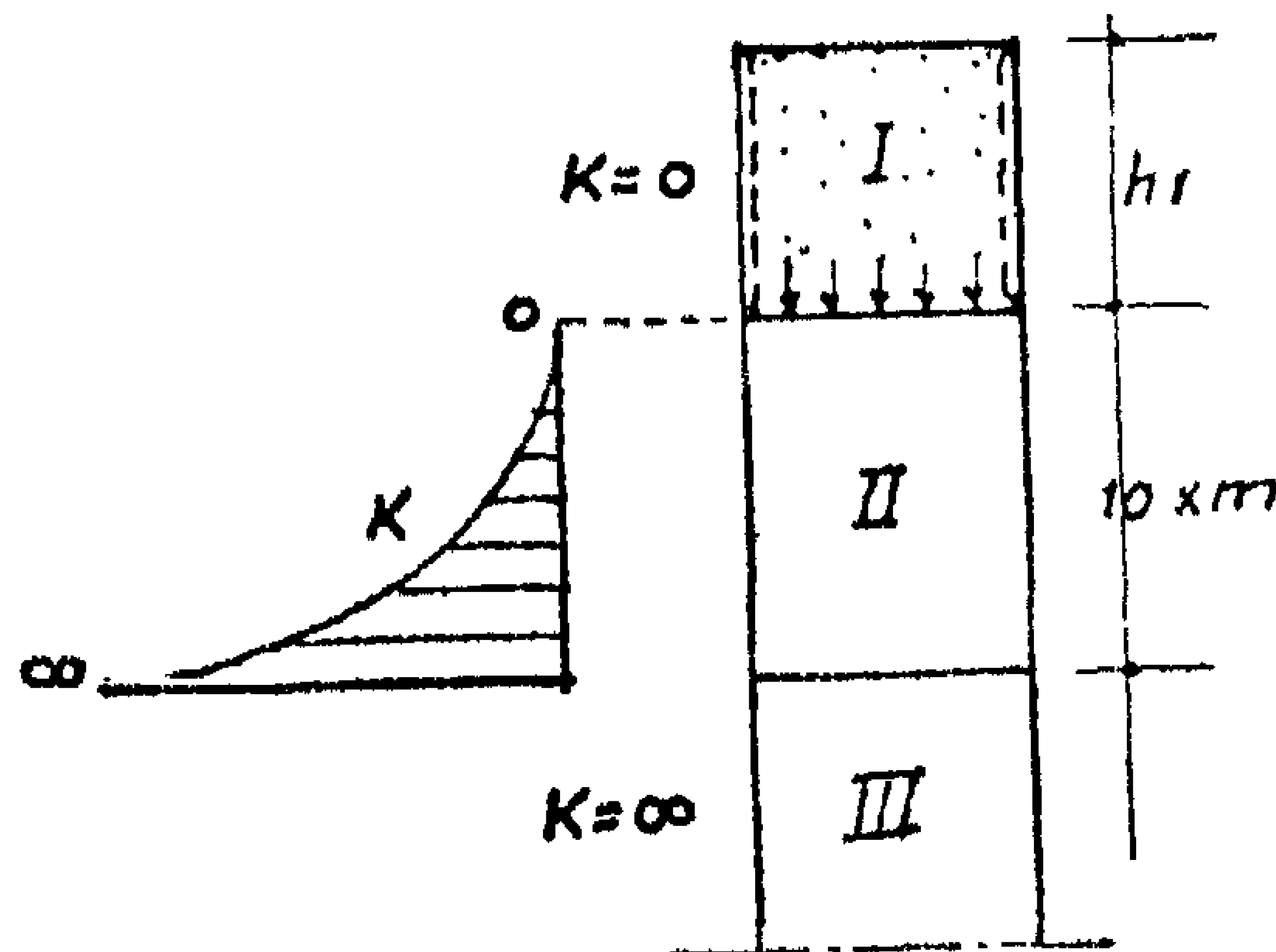


Fig. 4

In the lowest zone III it was assumed that the weight of all the fill was carried by the walls through arching effect. This was equivalent to assuming.

$$K = \frac{P_h}{P_v} = \frac{P_h}{0} = \infty$$

In the zone II, the zone under consideration, the value of K varied from zero at the top to ∞ at the bottom. The variation was deliberately assumed according to the function:

$$K = \frac{10 \,.\, n}{100 - n^2}\ ;\ n = 0 \rightarrow 10.$$

P_v was to be calculated from the formula given above, which in this case would only be an approximation, as it was originally based on the assumption of constant K. τ was then computed numerically from equilibrium considerations and

$$P_h = \frac{\tau}{\tan \Phi'}$$

could be calculated.

It was suggested that this procedure should be carried on for three different positions of zone II, i.e. at the top, in the middle and at the bottom of the silo and to trace the distribution of P_h in each case. The enveloping line gave the design values of P_h.

For a worked numerical example, the results agreed fairly well with a suggestion made by Leonhardt(6).

A more accurate formula for P_v was derived with variable K. Keeping the same assumptions given above, the new formula gave slightly smaller values of P_h than those given by the approximate formula.

5.2 Remarks on the Theory of Friedrich.

1. It seems impossible that the granular material may stand vertically totally separated from the walls of the silos, as assumed in zone I.

2. The assumption of the variation of K according to the function $K = \frac{10\, n}{100 - n^2}$, which is in fact the basic formula in the solutaion, is not adequately justified.

3. The formula for P_v is based on considering the equilibrium of a horizontal slice of fill. This might not be in agreement with the arching phenomena.

The Final Formulae :

$$y_o = \frac{b}{\sqrt{K_o}} \text{ where } K_o = 1 - \sin \Phi . \; y \leqslant y_o : P_v = \gamma y - \frac{a}{2} y^2,$$

$$P_h = K_o \gamma y - \frac{a K_o}{2} y^2 - \frac{a}{2} x^2, \qquad \tau = a x y , \quad a = \frac{\lambda_o K_o \gamma}{b (1 + \sqrt{k_o \lambda_o})}$$

$$y \geqslant y_o : P_v = \frac{C_1}{K_o} e^{-\frac{\mu_1}{b} y} + \frac{C_2}{K_o} e^{-\frac{\mu_2}{b} y} + \frac{b \gamma}{\lambda_o K_o},$$

$$P_h = C_1 \left(1 + \frac{\mu_1^2 x^2}{2 K_o b^2}\right) e^{-\frac{\mu_1}{b} y} + C_2 \left(1 + \frac{\mu_2^2 x^2}{2 K_o b^2}\right) e^{-\frac{\mu_2}{b} y} + \frac{b \gamma}{\lambda_o},$$

$$\tau = \left(\gamma + \frac{C_1 \mu_1}{K_o b} e^{-\frac{\mu_1}{b} y} + \frac{C_2 \mu_2}{K_o b} e^{-\frac{\mu_2}{b} y}\right) x ;$$

where $\mu_1 = \frac{1}{\lambda_o} (1 + \sqrt{1 - 2 K_o \lambda_o^2})$, $\mu_2 = \frac{1}{\lambda_o} (1 - \sqrt{1 - 2 K_o \lambda_o^2})$,

$$C_1 = K_o \frac{b (a y_o - \gamma) - \mu_2 \left(\gamma y_o - \frac{a}{2} y_o^2 - \frac{b \gamma}{\lambda_o K_o}\right)}{\mu_1 - \mu^2} e^{-\frac{y_o \mu_1}{b}}$$

$$C_2 = K_o \frac{\mu_1 \left(\gamma y_o - \frac{a}{2} y_o^2 - \frac{b \gamma}{\lambda_o K_o}\right) - b (a y_o - \gamma)}{\mu_1 - \mu_2} e^{\frac{y_o \mu_2}{b}}$$

To pass from plane to spacial state of stresses the value of b is substituted by m, as mentioned at the beginning. The results show fairly good agreement with the results of earlier experiments carried on a timber silo filled with wheat.

4.2 Remarks on Jaky's Theory :

1. Substituting m in place of b does not completely justify the validity of the application to silos with any shape of cross section.
2. The assumptions made for the part with $y \geqslant y_o$ are very close to the assumptions in Janssen's formula. In fact Lenczner (5) found that Jaky gave results very close to Janssen if we substituted in Janssen's formula the value of $K = K_o = 1 - \sin \Phi$.

5. THEORY OF FRIEDRICH

5.1 Theory of FRIEDRICH (1962)[4] :

Friedrich suggested an approximate method of calculating the lateral pressure in deep silos taking into consideration the arching effect.

The classical formula of Janssen was first extended to allow for a surcharge pressure P, then :

$$P_v = \frac{m . \gamma}{K \tan \Phi'} \left(1 - e^{-\frac{K \tan \Phi'}{m} y}\right)$$

3.2 Remarks on AIRY's Theory :

1. The wedge considered is of unit theckness; therefore the conditions at the sides S_3 and S_4 (Fig. 2 c) are not fulfilled.
2. In considering the equilibrium of the wedge ABCD (Fig. 2 b) the pressures exerted by the side CD are assumed zero, which is not correct.

4. THEORY OF JAKY

4.1 Theory of JAKY (1948)[3] :

Jaky investigated the pressures in a deep container with two parallel walls at distance 2b (Fig. 3) filled with granular material. After deriving the formulae for the pressures, b was replaced by

$$m = \frac{\text{Area of cross section}}{\text{perimeter}}$$, to make the formulae valid for any arbitrary silo having an axis of symmetry.

The variation of pressures during storing time is not dealt with, nor are pressure problems of emptying and filling.

The conditions of equilibrium of an infinitismal prism dx dy, of unit length, deliver two equations for the three values P_v, P_h and τ. A third equation is assumed empirically, out of the interpretation of some experimental results.

The upper part with depth y_o below the top free surface, (Fig. 3) is treated separately. In this part the surfaces of sliding cut the upper free surface of the fill.

A Basic Assumption :

At the line of symmetry ($x = 0$) and for all values of y it is assumed that $P_h = K_o P_v$, where $K_o = 1 - \sin \Phi$ = coeff. of earth pressure at rest.

For $y \leqslant y_o$ (where y_o is an unknown length, derived later). An empirical formula for τ is assumed, namely $\tau = a\ x\ y$, where a is an unknown constant.

The edge condition $P_v = 0$ at $y = 0$ yields the result that P_v is uniformly distributed over the horizontal section. The unknowns a and y_o are obtained from the empirically assumed distribution of λ, where $\lambda = \tau/P_h$ at $x = b$; namely at $y = y_o$:

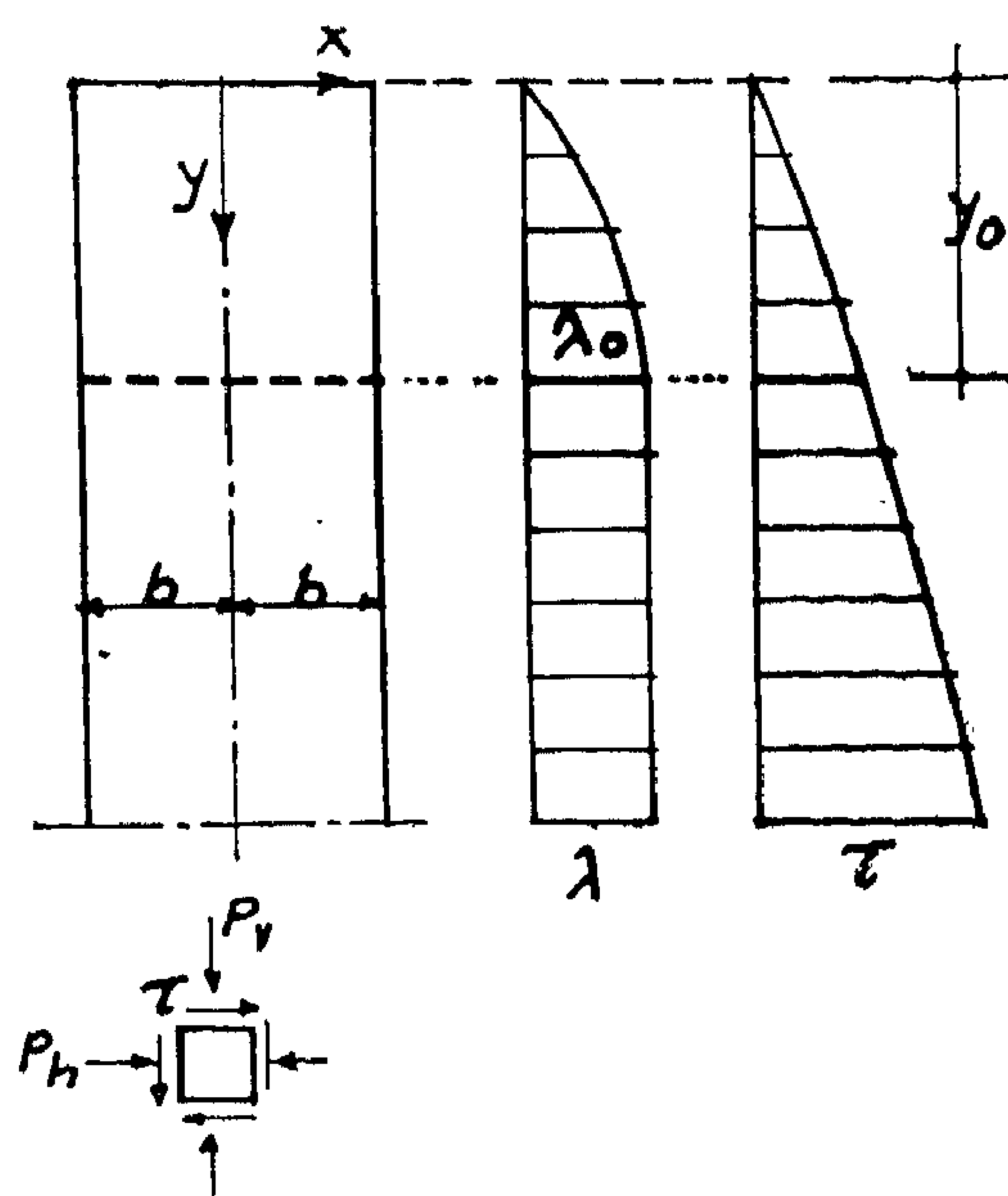


Fig. 3

$$\lambda = \lambda_o = \text{constant and } \frac{d\lambda}{dy} = 0.$$

For $y \geqslant y_o$

The missing equation is assumed empirically as $\lambda = \lambda_o$ = const., i.e. constant coeff. of friction. This assumption leads to a differential eqn. of the 2nd order in P_v. To maintain the continuity with the above part, P_v is assumed uniformly distributed over the horizontal section as obtained above. The two constants of integration are obtained from the two conditions of continuity of the P_v curve at $y = y_o$, i.e. [P_v and $\frac{dP_v}{dy}$] in the part $y \geqslant y_o$ = [P_v and $\frac{dP_v}{dy}$] in the part $y \leqslant y_o$.

In verifying the formula experimentally Janssen could check only the vertical load carried by the bottom of timber silos filled with wheat. The bottom was for this purpose separated from the walls of the silo and mounted on a weighing-balance.

2.2 Remarks on Janssen's Theory

1. The theory doesn't take into consideration the arching effect which may come into action especially in long time storing.
2. The value of K still remains unknown. In applying Janssens formula to the design, it has been usually assumed that $K = K_a = (1 - \sin \Phi) / (1 + \sin \Phi)$, where Φ is the angle of internal friction of the fill.
3. The rather high value of K = 0,70 is due to the nature of the experiment. Namely, the weight on the bottom of the silo could only be measured after that the bottom began to sink down.
4. The conditions arising during filling and emptying of the silo are not explicitly considered. A fairly good estimate for the pressures during filling and emptying may however be reached simply by changing the values of Φ' and K (see German Specifications below).
5. The formula doesn't give the distribution of P_v and P_h in the horizontal direction. Both values remain only average values.
6. It is to be noted that D. Lenczner in his paper (5) stated that the uniform distribution of P_v on the horizontal section was one of the two fundamental assumptions of Janssen's theory. This is shown here to be not correct.

3. THEORY OF AIRY

3.1 Theory of AIRY (1895)[2)] :

Airy investigated the following two cases :

1. The top part of the silo, where the plane of sliding causing the maximum horizontal pressure cut the upper surface of the fill :

   Equilibrium of the wedge ABC of unit width was considered. For the determination of the three unknowns P_h, R and Θ, (Fig. 2a) there were two equations of equilibrium of planar forces and a third condition for maximum P_h, i.e.

$$\frac{d\ P_h}{d\ \Theta} = 0.$$

Hence the resultant horizontal pressure P_h (see Fig. 2) was given by :

$$P_h = \frac{\gamma\ h^2}{2\tan\Theta} \frac{\tan\Theta - \mu}{1 - \mu\mu' + (\mu + \mu')\tan\Theta}$$

$$\tan\Theta = \mu + \sqrt{\mu \cdot \frac{1 + \mu^2}{\mu + \mu'}}$$

where $\mu = \tan\Phi$, $\mu' = \tan\Phi'$

Max height of the top part $h_o = b. \tan\Theta$.

2. The lower part, $h > h_o$:

The equilibrium of the wedge ABCD of unit width (Fig. 2b) was considered in the same way as for the upper part. Then :

$$P_h = \frac{\gamma\ b}{2} \frac{(2h - b.\tan\Theta)(\tan\Theta - \mu)}{1 - \mu\mu' + (\mu + \mu')\tan\Theta}$$

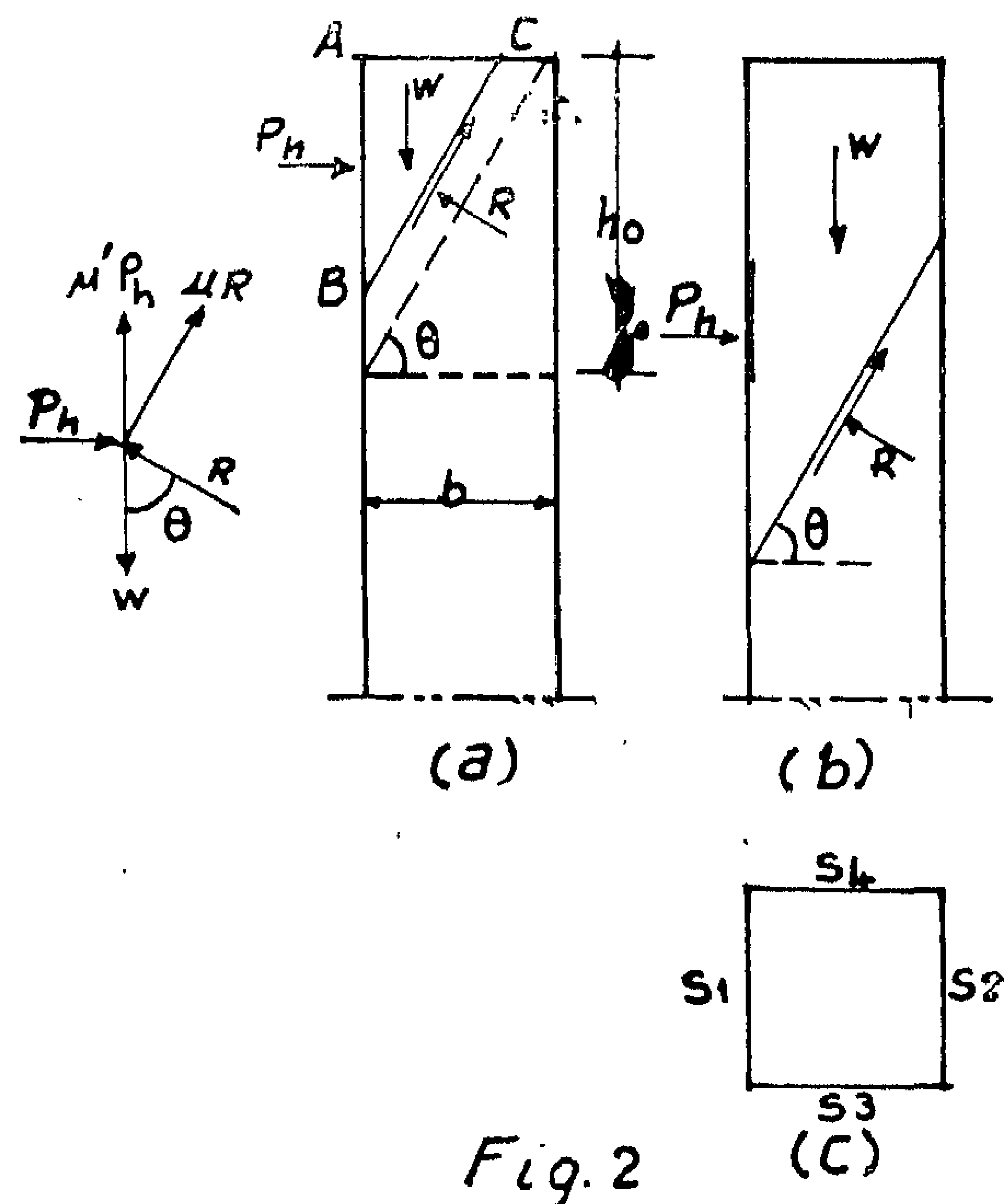


Fig. 2

LATERAL PRESSURES IN SILOS

By

Dr.-Ing. SABRI SAMAAN

1. INTRODUCTION

The analysis of structures has been greatly advanced in the recent years. Many complicated structures, which — because of mathematical difficulties or tedious computations — were previously analysed by introducing different more or less rough approximations, can nowadays be analysed fairly exact without much more trouble. Yet the estimation of loads, which is a basic factor in the design of structures is still far behind this progress. This is e.g., the case in the design of silos. The theories for the estimation of pressures in silos are still based on empirical factors. The purpose of this paper is to discuss a number of these theories which are of different approaches.

2. THEORY OF JANSSEN

2.1 Theory of JANSSEN (1895)[1] :

Due to its simplicity Janssen's formula is still the most widely applied formula for the design of silos. The formula is derived from the equilibrium condition of a horizontal slice of the filling material (Fig. 1a). Thus it is enough to know one unknown only which is chosen to be P_v = the average vertical pressure on a horizontal section. The other two unknown values P_h and τ are related to P_v through the following assumptions :

1. The ratio $P_h/P_v = K$ is a constant, which was suggested by Janssen to be obtained from test results.
2. The ratio $\tau/P_h = \lambda$ = constant = $\tan \Phi'$, where Φ' is the angle of skin friction between the fill and the walls of the silo.

The formula is :

$$P_h = KP_v = \frac{\gamma \cdot m}{\tan \Phi'} \left(1 - e^{-\frac{k \tan \Phi'}{m} y}\right)$$

where γ = volume weight of fill,

$$m = \frac{\text{Area of cross section of silo}}{\text{perimeter}}$$

There are no restrictions on the shape of the cross section. In spite of that Janssen suggested that P_h was uniform only in a circular section. In a square section he assumed the radial pressure to be constant, and therefore the distribution of P_h was a consine curve (Fig. 1b). Nevertheless, the value of P_h obtained from the formula was the average value.

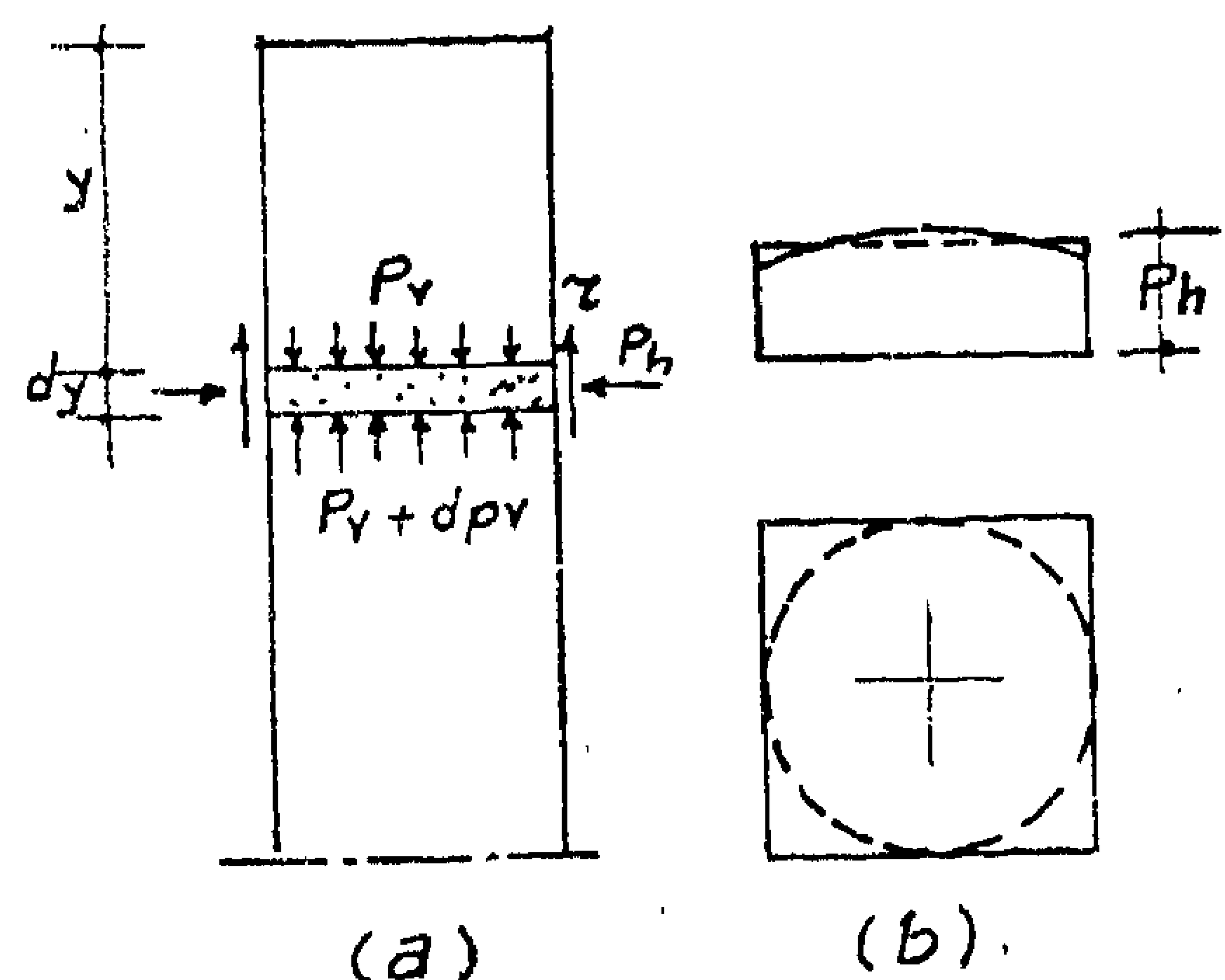


Fig. 1

APPENDIX I, — REFERENCES

1 — Chow, V.T., "Open Channel Hydraulics, "McGraw-Hill Book. Co., Inc., New York, 1959.

2 — Jaeger, C., "Engineering Fluid Mechanics, "Translated from Germany by P.O. Wolf, Blackie and Son Ltd., London and Glasgow, 1956.

3 — Rouse, H., "Advanced Mechanics of Fluids," John Wiley and Sons, Inc., 1959.

APPENDIX II. — NOTATION

h_1, h_2 = Scale factors,

i = $\sqrt{-1}$;

K_n = Curvature of the potential line ;

K_s = Curvature of the streamline ;

$\log_e$ = Natural logarithm ;

P = Pressure ;

(s,n) = Curvilinear coordinate system along the steamline and normal to it ;

V = Local velocity ;

V_s, V_n = Velocity components of the local velocity parallel to s, n directions ;

(x,y) = Rectangular coordinate system

Z = x + iy, complex variable ;

Θ = Angle of velocity vector with respect to the positive X-axis,

ρ = Density of fluid ;

Φ = Velocity potential, and

Ψ = Stream function ;

Ω = Gravitational force.



the total derivative of the term $(\frac{P}{\rho} + \frac{1}{2} V^2 + \Omega)$ in Eqs. 17 and 18, one can readily obtain.

$$\frac{1}{h_2} \frac{\partial V}{\partial \Psi} + K_s V = 0 \qquad (20)$$

Using the result shown by Eq. 11 and substituting Eq. 12 into Eq. 20 and Eq. 13 into Eq. 19 yields.

$$\frac{\partial V}{\partial \Psi} - V \frac{\partial \Theta}{\partial \Phi} = 0 \qquad (21)$$

$$\frac{\partial V}{\partial \Psi} + V \frac{\partial \Theta}{\delta \Phi} = 0 \qquad (22)$$

Alternatively, Eqs. 21 and 22 can be witten as :

$$\frac{\partial V}{\partial n} - V \frac{\partial \Theta}{\partial s} = 0 \qquad (23)$$

and

$$\frac{\partial V}{\delta s} + V \frac{\partial \Theta}{\partial n} = 0 \qquad (24)$$

Considering the Cauchy-Riemann relations given by Eqs. 10, Eqs. 21 and 22 can be transformed into

$$\frac{\partial V}{\partial y} - V \frac{\partial \Theta}{\partial x} = 0 \qquad (25)$$

$$\frac{\partial V}{\partial x} + V \frac{\partial \Theta}{\partial y} = 0 \qquad (26)$$

which are represented in the Cartesian coordinate system. Eqs. 25 and 26 are considered the basic relation ships in this study for the determination of V and Θ.

Rearranging Eqs. 25 and 26 gives

$$\frac{1}{V} \frac{\partial V}{\partial y} = \frac{\partial \Theta}{\partial x} \qquad (27)$$

$$\frac{1}{V} \frac{\partial V}{\partial x} = - \frac{\partial \Theta}{\partial y} \qquad (28)$$

Differentiatin of Eqs. 27 and 28 with respect to x and y, respectively, and then adding yields

$$\frac{\partial^2 \Theta}{\partial x^2} + \frac{\partial^2 \Theta}{\partial y^2} = 0 \qquad (29)$$

Also multiplying Eq. 27 by dy and Eq. 28 by dx and then adding produces :

$$\frac{dV}{V} = (\frac{\partial \Theta}{\partial x} dy - \frac{\partial \Theta}{\partial y} dx)$$

or

$$\log_e (\frac{V}{V_o}) = \int (\frac{\partial \Theta}{\partial x} dy - \frac{\delta \Theta}{\partial y} dx) \qquad (30)$$

Eqs. 29 and 30 represent the two basic equations required for the solution of Θ (x,y) and V (x,y) at any point in an irrotational flow field.

CONCLUSIONS

Eqs. 29 and 30 represent two basic relations which have been derived for potential flow in rapidly varied flow with pronounced curvature of the streamlines. The treatment is based on the assumptions that the fluid is ideal and the flow is irrotational. These are fair assumptions in rapidly varied flow especially for the type of flow where the streamlines are converging. It seems from Eq. 29 that Θ satisfies Laplace equation. Its solution yields the function Θ. If Θ is obtained, the magnitude of the local velocity V can be found from Eq. 30. It follows that further study is needed to obtain solutions of Eqs. 29 and 30. This may be done graphically or analytically.

From the condition of orthogonality, it can be shown that

$$\frac{\partial x}{\partial \Psi}\frac{\partial x}{\partial \Phi} + \frac{\partial y}{\partial \Phi}\frac{\partial y}{\partial \Psi} = 0 \qquad (6)$$

Substitution of Eqs. 4, 5 and 6 into Eq. 3 yields

$$h_1 = [(\frac{\partial x}{\partial \Phi})^2 + (\frac{\partial y}{\partial \Phi})^2]^{1/2} \qquad (7)$$

$$h_2 = [(\frac{\partial x}{\partial \Psi})^2 + (\frac{\partial y}{\partial \Psi})^2]^{1/2} \qquad (8)$$

As the flow is irrotational, the scale factors at any point must be the same in all directions, nameley $h_1 = h_2$. The verification of this result can be easily made by the application of complex variables. The complex variable $W = \Phi + i\Psi$ is called the compex potential in which Φ and Ψ satisfy the Cauchy-Riemann equations. It is well known that W is an analytic function of $Z = x + iy$. Thus,

$$Z = f(W) = f(\Phi + i\Psi) = x(\Phi, \Psi) + iy(\Phi, \Psi) \qquad (9)$$

From this inverse relation $x(\Phi, \Psi)$ and $y(\Phi. \Psi)$ also satisfy the Cauchy-Riemann conditions as follows :

$$\frac{\partial x}{\partial \Phi} = \frac{\partial y}{\partial \Psi}, \quad \frac{\partial x}{\partial \Psi} = -\frac{\partial y}{\partial \Phi} \qquad (10)$$

Substitution of Eqs. 10 into Eqs. 7 and 8 leads to

$$h_1 = h_2 \qquad (11)$$

It is further assumed that Θ represents the inclination to the x-axis of the tangent at any point M of the streamline as shown in Fig. 1. The curvatures of the streamline and the equipotential line are defined as K_s and K_n, respectively at any point in the flow field.

Since $\Theta = \Theta(x,y)$, then

$$-K_s = \frac{\partial \Theta}{\partial s} = \frac{1}{h_1}\frac{\partial \Theta}{\partial \Phi} \qquad (12)$$

and

$$K_n = \frac{\partial \Theta}{\partial n} = \frac{1}{h_n}\frac{\partial \Theta}{\partial \Psi} \qquad (13)$$

Furthermore, Fig. 1 is considered to derive relations between h_1, h_2 and the curvatures K_s and K_n. Therefore

$$\frac{(h_1 - \frac{\partial h_1}{d\Psi} d\Psi) \cdot d\Phi}{h_1 \, d\Phi} = \frac{\frac{1}{K_s}}{\frac{1}{K_s} - h_2 \, d\Psi}$$

and

$$\frac{(h_2 + \frac{\partial h_2}{\partial \Phi} d\Phi) \, d\Psi}{h_2 \, d\Psi} = \frac{\frac{1}{K_n} + h_1 \, d\Phi}{\frac{1}{K_n}}$$

which finally reduce to :

$$K_s = \frac{-1}{h_1 h_2}\frac{\partial h_1}{\partial \Psi} \qquad (14)$$

$$K_n = \frac{1}{h_1 h_2}\frac{\partial h_2}{\partial \Phi} \qquad (15)$$

Also, it is easily seen that :

$$\frac{\partial h_1}{\partial \Phi} = 0 \text{ and } \frac{\partial h_2}{\partial \Psi} = 0 \qquad (16)$$

Using Eqs. 14, 15 and 16, the Navier-Stokes equations for irrototional flow of an idea fluid can be obtained as (3)

$$\frac{1}{h_1}\frac{\partial}{\partial \Phi}(\frac{P}{\rho} + \frac{1}{2}V^2 + \Omega) = 0 \qquad (17)$$

$$\frac{1}{h_2}\frac{\partial}{\partial \Psi}(\frac{P}{\rho} + \frac{1}{2}V^2 + \Omega) = \frac{V}{h_2}\frac{\partial V}{\partial \Psi} + K_s V^2 \qquad (18)$$

and the equation of continuity becomes

$$\frac{1}{h_1}\frac{\partial V}{\partial \Phi} + V K_n = 0 \qquad (19$$

in which P is the pressure, ρ is the density of the fluid, V is the local velocity and Ω is the gravitational force.

Along the streamline, the Bernoulli equation should be satisfied. Therefore, from

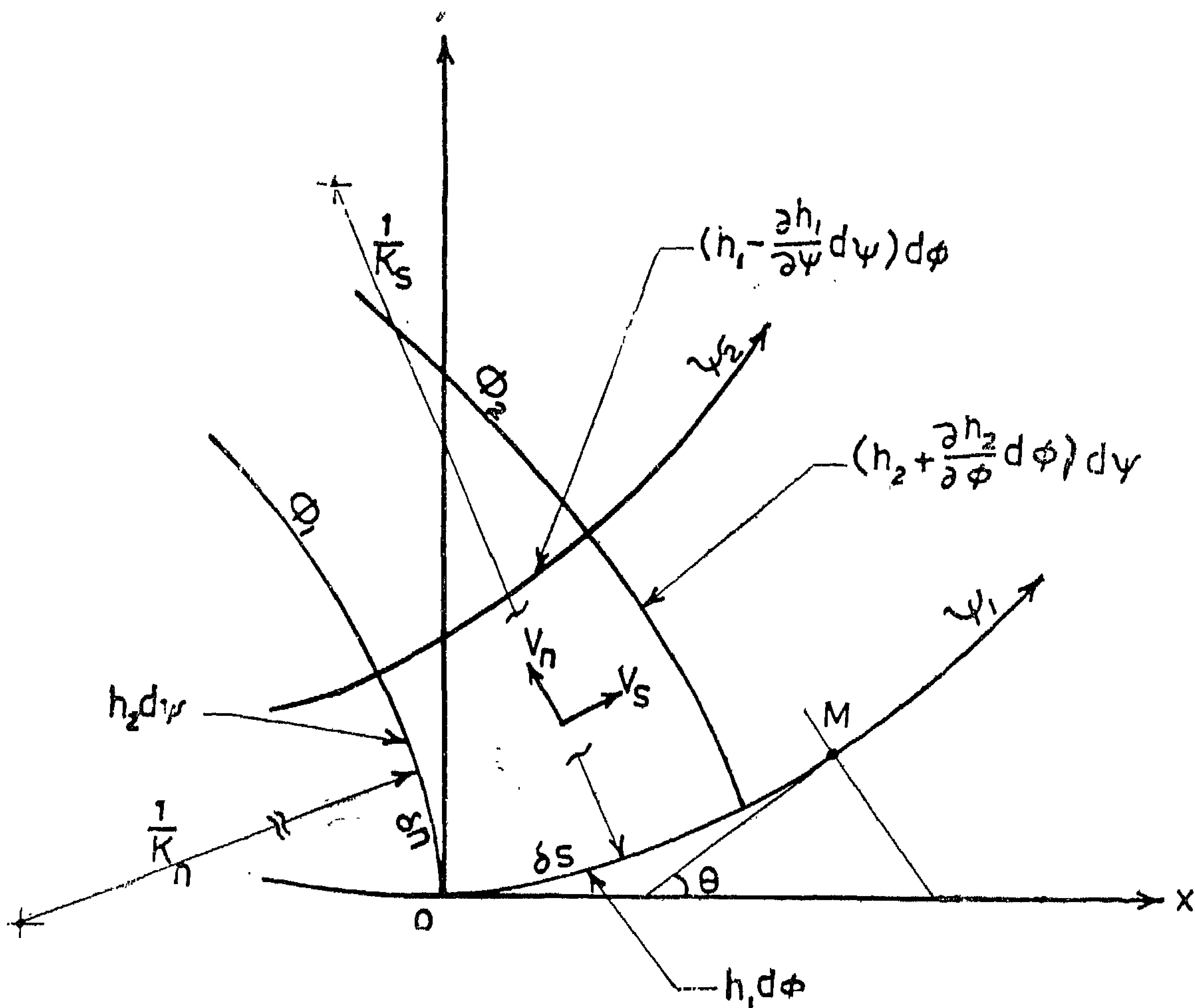


FIG. 1.- DEFINITION SKETCH OF CURVILINEAR ORTHOGONAL COORDINATE SYSTEM

Let Θ be taken as the inclination to x-axis of the tangent at any point M of the streamline as shown in Fig. 1.

The curvatures of the streamline and equipotential line are defined as K_s and K_n, respectively.

The lengths of the elements of curve in the direction of the streamline and the equipotential line can be denoted, respectively by

$$ds = h_1 \, d\,\Phi \qquad (1)$$

and

$$dn = h_2 \, d\,\Psi \qquad (2)$$

in which h_1 and h_2 are termed metrie coefficients (scale factors) of the curvilinear orthogonal coordinate system along s and n, respectively.

Furthermore, the distance d L between the points (Φ, Ψ) and $(\Phi + d\,\Phi, \Psi + d\,\psi)$ is given by

$$(d\,L)^2 = h_1^2 \, (d\,\Phi)^2 + h_2^2 \, (d\,\Psi)^2 = (dx)^2 + (dy)^2 \qquad (3)$$

Since $x = x\,(\Phi, \Psi)$ and $y = y\,(\Phi, \Psi)$, it follows that :

$$dx = \frac{\partial x}{\partial \Phi} d\,\Phi + \frac{\partial x}{d\Psi} d\,\Psi \qquad (4)$$

and

$$dy = \frac{\partial y}{\partial \Phi} d\,\Phi + \frac{\partial y}{\partial \Psi} d\,\Psi \qquad (5)$$

HYDRODYNAMIC EQUATIONS FOR CURVILINEAR FLOW

By

Dr. MOHAMED HAMDY EL-KATEB[1]

INTRODUCTION

Potential theory is based on the assumption that the flow considered is assumed to be inviscid, irrotational, two-dimensional, incompressible and steady. An ideal fluid is assumed to have no component of velocity normal to the boundary. In addition, it experiences no shearing stresses and slips tangentially with solid boundaries. It follows that the stream function and velocity potential exist in the flow field. It is well known that this approach plays an important role in the solution of rapidly varied flow with pronounced curvature of the streamlines. There are many practical problems which can be solved with fair precision by the potential theory, as stated by Jaeger (2) and Chow (1). Flow over spillways or sharp-crested weirs and flow in converging passages are cases well suited to analysis by such technique since they are understood to be approximately irrotational in nature. The data necessary for analysis must include sufficient information concerning all of the boundaries. The possible conditions specified for a boundary of any flow field may include its nature whether solid or free surface, its geometrical form, the pressure and velocity distribution on it.

The study reported herein is conducted for the purpose of developing the fundamental equations of potential flow in rapidly varied flow with pronounced curvature of the streamlines.

Notation :— The symbols adopted for use in this paper are defined where they first appear and are arranged alphabetically in the Appendix.

GOVERNING EQUATIONS

The equations of motion for a two-dimensional flow of an ideal fluid can be formulated. Consider the intrinsic or natural coordinate system which can be moved to any particular point of interest in the flow field as shown in Fig. 1.

It has mutually perpendicular axes s. n with s directed along the streamline Ψ_1 and n along the equipotential line Φ, perpendicular to s. Let V_s and V_n be the velocity components at any point M in the flow field in the direction of increasing potential function Φ and the stream function Ψ, respectively. Since there is no flow across the streamline $V_n = O$, the subscripts s of V_s is dropped out, hereafter for no confusion.

The following assumptions are made in this study :

1 — The fluid is incompressible,
2 — The fluid is frictionless, and
3 — The flow is irrotational, i.e., a velocity potential exists.

---

(1) Lecturer of Civ. Engrg., Cairo Univ., Giza, Egypt, U.A.R.

(2) Numerals in parentheses refer to corresponding items in Appen dix 1. — References.

ρ = Fluid density.

μ = Fluid viscosity.

α = Viscous resistance coefficient.

∂_p = Mean particle diameter. (The arithmatic average dimension of the two screens defining the particle fraction).

∂ = Average pore diameter.

Δp = Pressure drop through the porous media.

ε = Porosity of porous media.

λ = Particle shape factor = $\frac{\text{Area of Particle}}{\text{Volume of Particle}} \times \frac{\partial_p}{6}$

Ψ, Ψ' = Friction factors.

REFERENCES

1) Blick, E.F., Ind. and Engineering Chemistry, January 1966. Vol. 5 No. 1 page 90.

2) Blick, E.F. High Speed Flow through Porous Media, Ph.D. dissertation, pp. 15, 43, University of Oklahoma, 1963.

3) Burdine, N.T., et al, Trans. A.I.M.E 189, 195 (1950).

4) Brownell, L.E., Katz, D.L., Chem. Eng. Progr. 43, 537 (1941).

5) Calhoun, J.C. "Fundamentals of Reservior Engineering", University of Oklahoma 1953.

6) Carman, P.C. Trans. Inst. Chem. Engrs. 15, 150 (1937).

7) Chalabi M.F. et al. "Factors Affecting the Permeability of Filter Cakes" — Assuit University Tech. Bulletin, U.A.R. 1969. and Journal of the Egyptian Society of Engineers, Vol. IX, No. 4, 1970.

8) Foust, A.S., et al., "Rrinciples of Unit Operations", p. 475, Wiley, New York, 1960. Credit to Ergun, Chem. Eng. Prog., 48, 89, (1952).

9) Henderson, J.H., Producers Monthly 14, 32 (1949).

10) Kawakami, M., J. Chem. Soc. Japan 53, 1085, (1932).

11) Mach, E., Dechema Monographien 6, 38, (1939).

12) Norman, W.S. "Absorption, Distillation and Cooling Towers", Longmans, 1961.

13) Purcell, W.R., Trans. A.I.M.E. 186, 39 (1949).

14) Rainard, L.W., Textile Res. J. 17, 167 (1947).

15) Scheidegger, A.E., Producers Monthly 17, 17., (1953).

16) Smith, W.O., Physics 3, 139 (1932).

17) Uchida. S., Fujita, S., J. Soc. Chem. Ind. Japan, (Suppl. Binding) 37, 724, B, 791 B (1934).

18) Weger, E., Greenberg, D.B. "Investigation of Viscous and Inertial Coefficients for the Flow of Gases through Porous Sintered Metals with High Pressure Coefficients". Tech. Rept. No. 1 Contract No. DA — 36-034 — ORD — 2353 — U.S. Army Research Office, Durham, N.C. (March 1959).

19) Weger, E., Greenberg, D. B., "Transient Gas Flow in Porous Media. "The Pressure Decay Process". Final Tech. Rept., Contract No. DA-36-034-ORD-2353 U.S. Army Research Office, Durham, N. C. (May 1960).

particles. Also it is observed that all experimental data points do not fall on a single line or curve which establishes the effect of the particle shape. It was then decided to introduce the shape factor as parameter in the friction factor.

It has been found by mathematical analysis that experimental points fall on a single curve if the friction factor is represented by the equation.

$$\Psi' = \frac{\Psi}{\lambda^2} = \frac{-(P_2^2 - P_1^2)\, M\, \delta\, \varepsilon^2\, g_o}{2\, L\, G^2\, Z\, R\, T\, \lambda^2} \quad \ldots\ldots \quad (25)$$

Fig. (4) shows the experimental data points expressed as Ψ' against Re from which it is well seen that all points lie on or very close to a single curve represented by equation (26).

$$\Psi' = \frac{74}{Re} + \frac{0.74}{Re^{0.1}} \quad \ldots\ldots \quad (26)$$

On the same figure is also illustrated Foust's equation for spherical particles ($\lambda = 1$). Combining the two figures (3) and (4) it can be seen that Foust's correlation as represented by equation (17) does not hold *for porous media consisting of nonsperical* particles; also even if the particle shape is accounted for it does not hold at high values of Reynolds No.

CONCLUSION

The permeability equation (5) can be used to determine the viscous resistance coefficient and equation (7) may be used to predict pressure drop through porous media at low gas rates where $\frac{V\, \rho}{\mu\, a}$ is less than 2.

Internal porosity of particles has no effect on the permeability of a porous bed consisting of particles of definite size and shape.

The pressure drop through porous media varies with the particle shape due to its direct effect on the shape of the pores forming the intertices between the particles. Equation (26) gives good agreement with experimentally measured pressure drops over a wide range of gas rates and its advantage over Foust's equation is that it accounts for the effect of the shape of the particles constituting the porous media.

NOMENCLATURE

a = Surface area of particles per unit bed volume.

C_f Skin friction coefficient.

C_D = Drag coefficient for the orifice plate.

C_o = Orifice coefficient.

d = Internal diameter of pipe.

d_e = Equivalent diameter of the bed passages.

g_o = Newton's law conversion factor = Gravitational Constant.

G = Mass flow rate per unit area.

h = Orifice diameter.

K = Permeability.

k & k' = Constants.

l = Length of pipe.

L = Depth of porous bed.

M = Molecular weight of gas.

P = Fluid pressure.

R = Universal gas constant.

Re = Reynolds Number.

S = Specific surface of particle.

T = Absolute gas temperature.

u = Fluid velocity through the pores or pipe.

V_m = Molecular voume of gas.

V = Superficial fluid velocity.

Z = Compressibility factor of gas.

Also we have

$$a \propto \frac{\delta}{\delta^2} \propto \frac{1}{\delta} \left(= \frac{\text{constant}}{\delta}\right) \quad \ldots\ldots \quad (22)$$

Substituting equations (21) and (22) in equation (20) we get :

$$\frac{P_1 - P_2}{L\ G^2} \cdot g_c \cdot \frac{P_1 + P_2}{2} \cdot \frac{M}{RT} \cdot \frac{\varepsilon^2 . \delta}{Z} = k'/Re \quad (23)$$

Equation (23) is reduced to the form

$$\Psi' = \frac{-(P_2^2 - P_1^2)\ M\ \delta\ \varepsilon^2 .\ g_c}{2\ L\ G^2\ Z\ R\ T} = k'/Re \quad (24)$$

The experimental data was then expressed in terms of Ψ' as expressed by equation (24) and Reynolds NO. as expressed by equation (12). The pore diameter was calculated from Foust's equation (15) by substituting the mean particle diameter δ_p and the porosity ε. Experimental results expressed as Ψ' and Re are shown in Fig. (3). One the same figure is also illustrated Foust's semi-empirical equation (17). It is seen that agreement between experimental results and equation (17) is satisfactory for rounded particles whereas disagreement is clear for irregular nonspherical

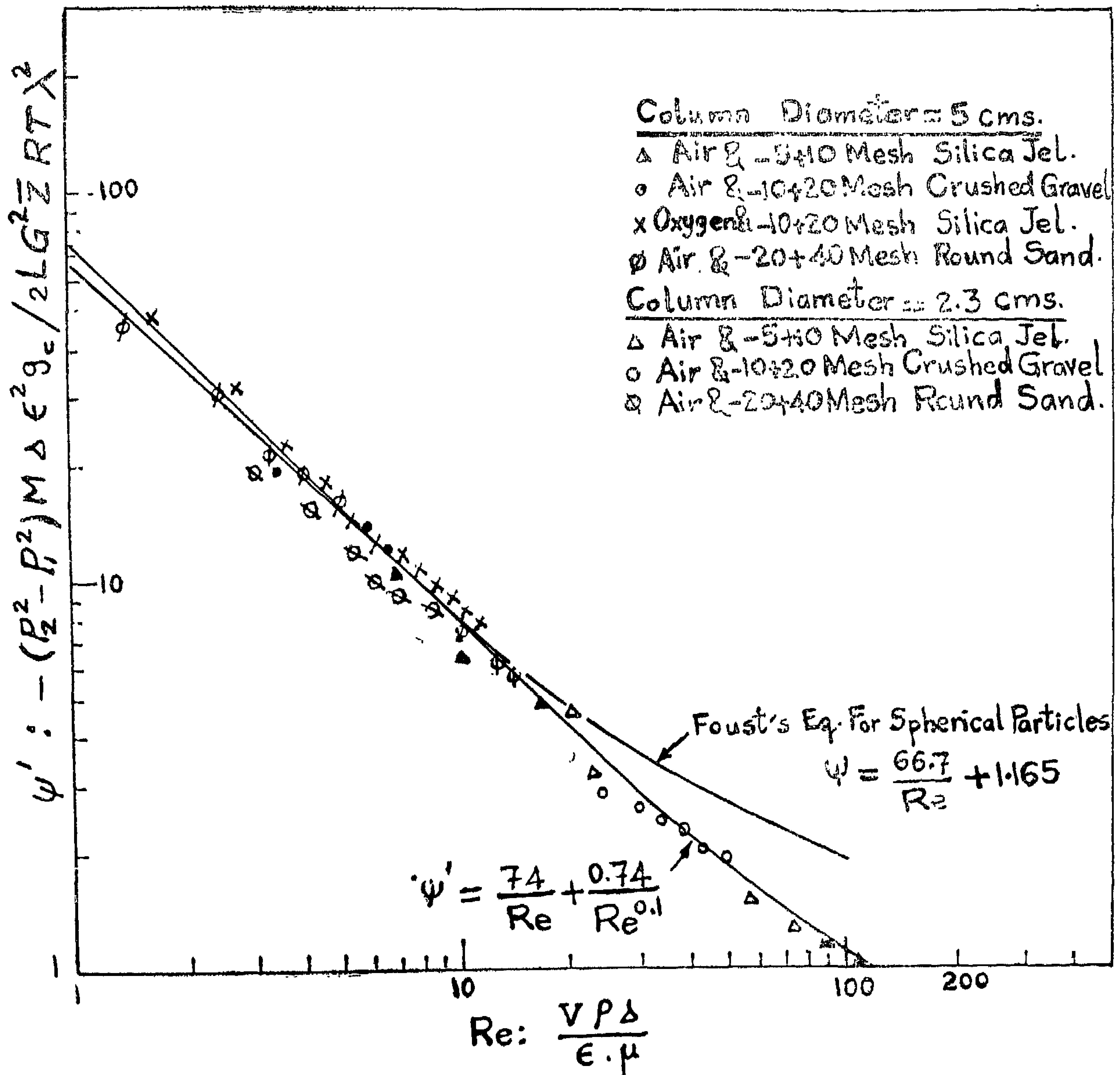


FIG. 4 : Friction Factor VS. Reynolds No. Considering Particle Shape.

The last equation is based on the assumption that the expansion of the gas is isothermal and that the molecular volume V_m is measured at mean gas pressure which represents a large number of cases for gas flow through porous media (2).

Replacing $V_m = M/\rho$ in the last equation we get :

$$\left(\frac{P_1 + P_2}{2}\right) \frac{M}{\rho} = \bar{Z} R T$$

$$\text{(i.e.)} \quad \rho = \left(\frac{P_1 + P_2}{2}\right) \cdot \frac{M}{ZRT} \quad \ldots\ldots \quad (21)$$

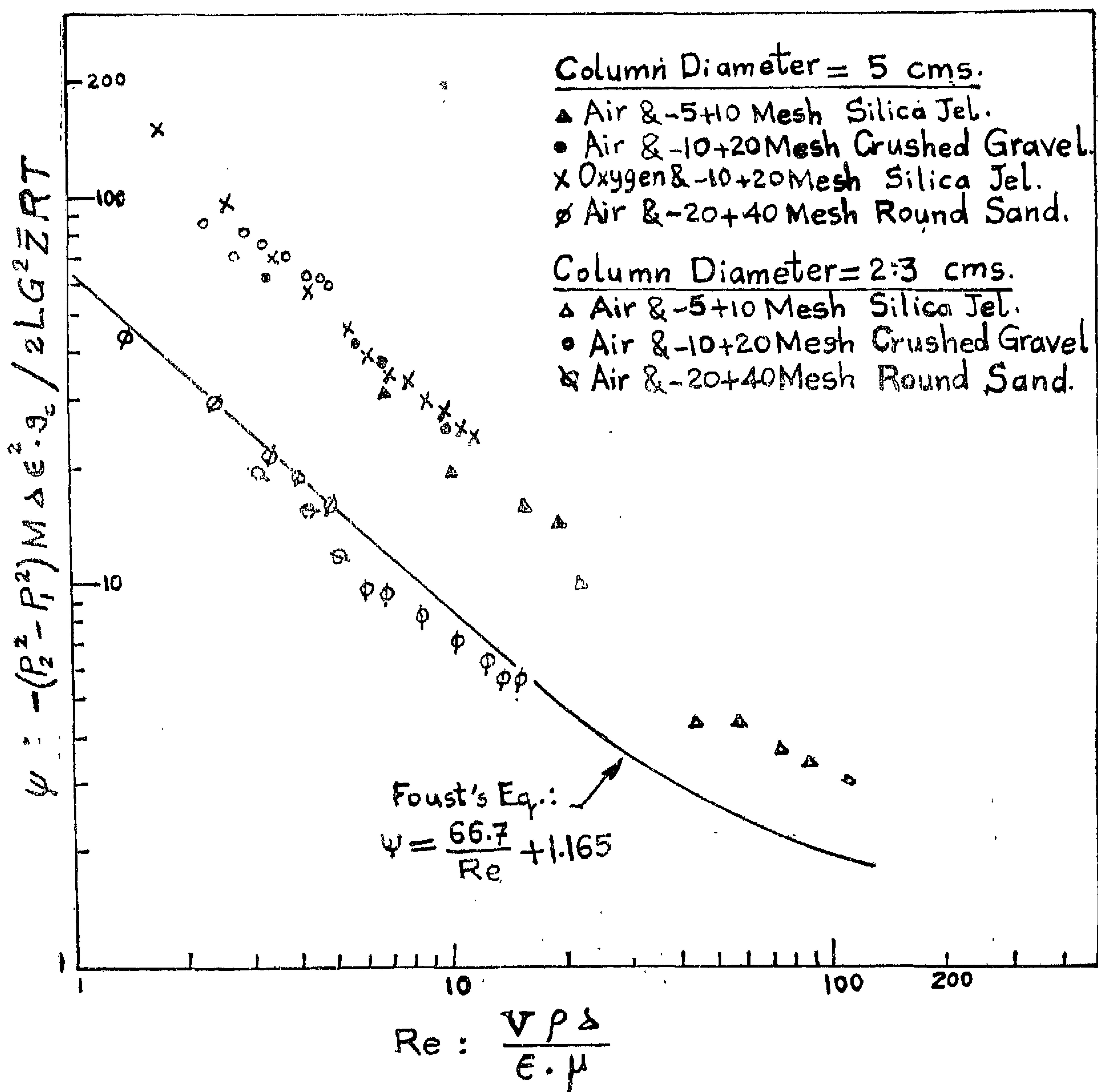


FIG. 3 : Friction Factor VS. Reynolds No. (Neglecting Particle Shape).

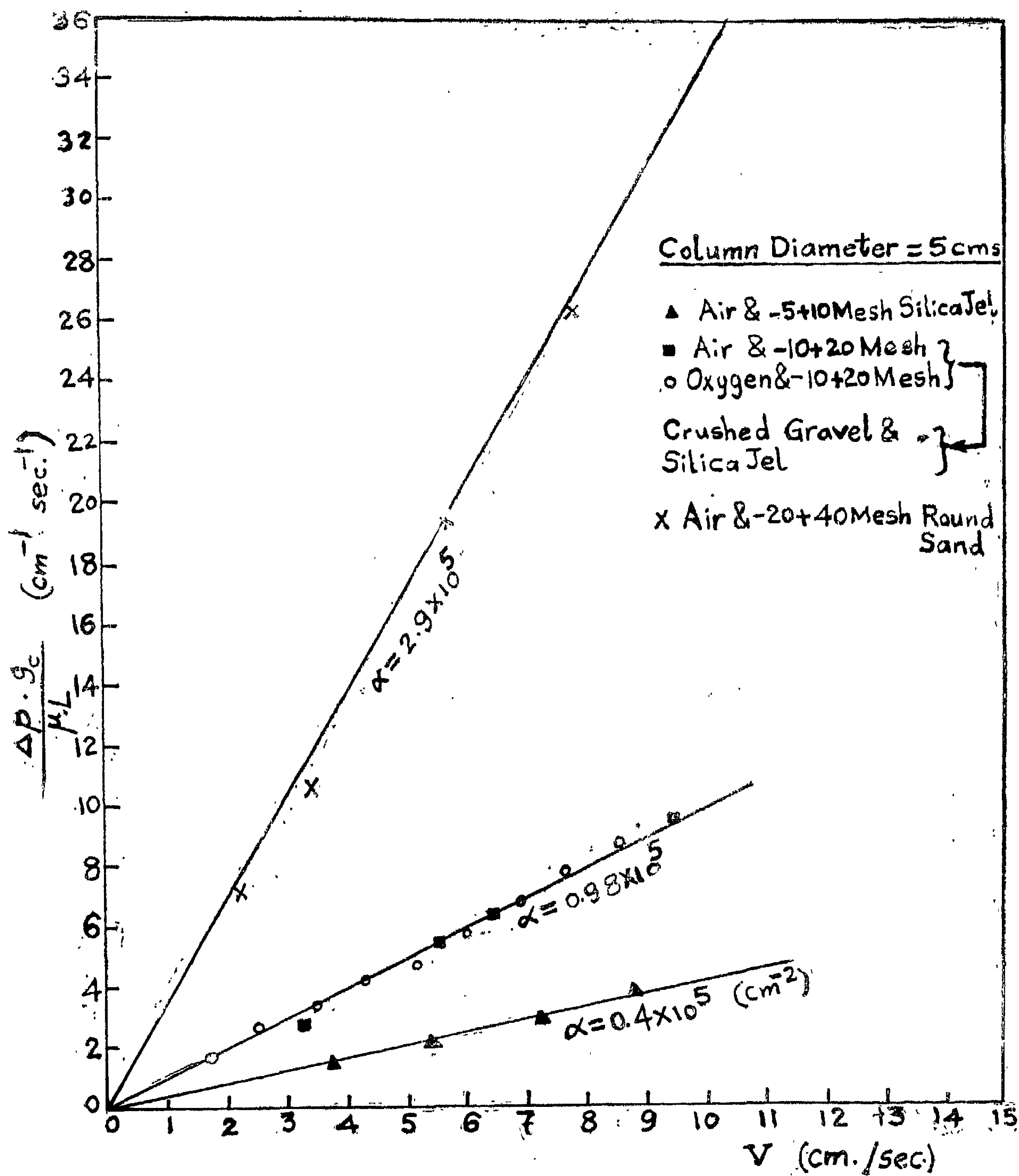


FIG. 2 : Viscous Resistance Coefficient at Different Porous Media.

Two different sizes of columns were used, one measuring 2.3 cm and the second 5 cm in diameter. The smaller diameter column was used to achieve higher super ficial gas velocities than in the case of the larger diameter column. In each run a known amount of solid particles of a certain fraction was placed in the column between two retaining wire screens, one on the supporting perforated plate and the second in close contact with the bed surface to prevent fluidization of the bed in case of high speed flow of the gas. The gas flow rate through each bed of particles was gradually increased and the pressure drop through the porous media was determined at each measured gas rate. The porosity of the bed was determined from the actual volume of the bed and the true volume of the solid particles constituting the bed.

The permeability of each fraction was determined by applying equation (5) where

$$S = \frac{6\,\lambda}{\delta_p} \qquad \ldots\ldots \quad (18)$$

The viscous resistance coefficient (reciprocal of permeability) was then determined and compared with that obtained from the experimental data applying equation (6). Figure (2) illustrates experimental results and the corresponding viscous resistance coefficient.

Table (2) gives the comparison between experimental and calculated coefficients applying equation (5).

Table (2)

Fraction (Mesh)	Gas	Experimental Coeff. (cm-2)	Calculated Coeff. (cm-2)
-- 5 + 10 Silica Jel	Air	0.4×10^5	0.402×10^5
— 10 + 20 Crushed Gravel	Air		
-- 10 + 20 Silica Jel	Air	0.98×10^5	0.915×10^5
-- 10 + 20 Silica Jel	Oxygen		
— 20 + 40 Sand	Air	2.9×10^5	2.9×10^5

It is observed from table (2) that good agreement exists between experimental and calculated values so that the validity of equation (5) is extended for gas flow through porous media. Also it is observed that the experimentally measured permeability at crushed gravel and silica jel is the same for the fraction — 10 + 20 mesh which indicates that the internal porosity of the particles has no effect on bed permeability.

In order to study the variation of pressure drop over a wide range of gas flow rates the experimental results were expressed as a friction factor Ψ against Reynolds number based on the pore (i.e.) $Re = \frac{u\,\delta\,\rho}{\mu}$. An expression for the friction factor Ψ in case of gas flow was derived by modifying equation (7) as follows :

$$\frac{\Delta\,\rho .\ g_c .\ \varepsilon^2}{L.\ \rho .\ V^2 .\ a^2\ \delta} = k\ \frac{\mu}{\rho . V . \delta} \qquad \ldots\ldots \quad (19)$$

By substituting $G = V.\rho$ equation (19) becomes.

$$\frac{(P_1 - P_2)\ g_c\ \rho\ \varepsilon^2}{L\ G^2\ a^2} = \frac{k}{Re} \qquad \ldots\ldots \quad (20)$$

We have per one mole of a gas.

$$p\ V_m = \bar{Z}\ R\ T$$

or $$\frac{(P_1 + P_2)}{2} . V_m = \bar{Z}\ R\ T$$

EXPERIMENTAL WORK, RESULTS, AND DISCUSSION

A diagramatic sketch of the apparatus used in this investigation is shown in figure (1) and the properties of the materials are given in table (1). The shape of the different particles was determined by microscopic examination.

Table (1)

A. Properties of solid particles constituting the porous beds

Material	Size	δp (mm.)	Shape	Shape factor	Particle density (gm/cm^3)
Crushed Gravel	— 5+10 Mesh	2.32	Irregular, nonporous	1.75	2.5
	—10+20 »	1.242	» »	1.75	2.5
Silica Jel	— 5+10 »	2.32	Irregular, porous	1.75	1.5
	—10+20 »	1.242	» »	1.75	1.5
Round Sand	—20+40 »	0.591	Rounded, nonporous	1	2.5

B. Properties of gases at 1 atm. and 20°c

Air : Density = 1.2×10^{-3} gm/cm^3 and Viscosity = 18×10^{-5} poise

Oxygen : Density = 1.3×10^{-3} gm/cm^3 and Viscosity = 20×10^{-5} poise

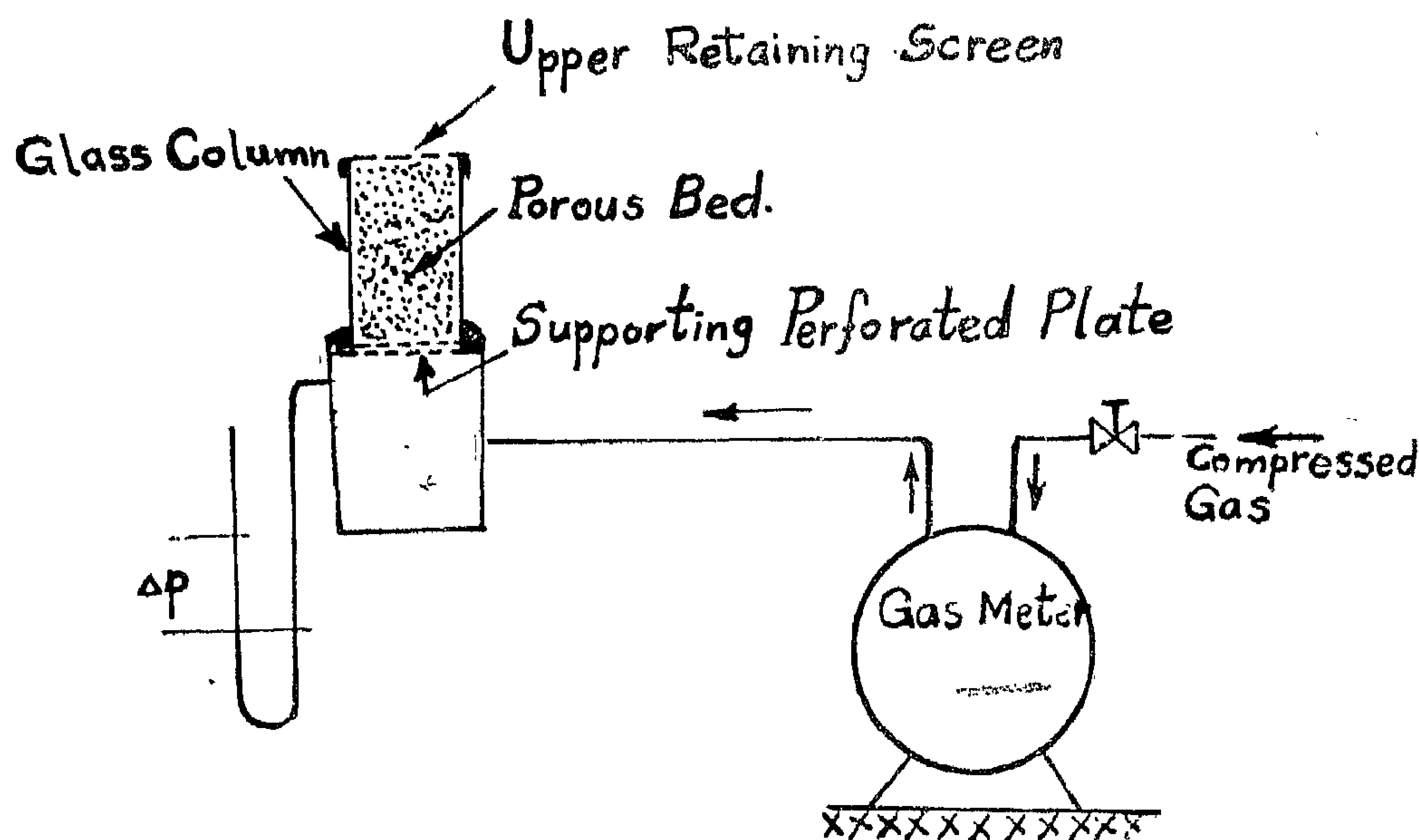


FIG. 1 : Diagramatic Sketch of the Apparatus.

Chalabi et al (3) predicted the following equation for permeability :

$$K = 0.1 \frac{\varepsilon^2}{S^2 \ (1-\varepsilon)^2} \qquad \ldots\ldots \quad (5)$$

Combining the above equation with that representing the experimentally measured permeability. (i.e.).

$$K = \frac{V \ \mu \ L}{\triangle \ p. \ g_c} \qquad \ldots\ldots \quad (6)$$

we get the following equation for the pressure drop in the stream line segime.

$$\triangle p = 10 \frac{\mu \ L \ V \ a^2}{g_c \ . \ \varepsilon^2} \qquad \ldots\ldots \quad (7)$$

Equations (5) and (7) were predicted from experimental data using water flow through different porous media and it is one of the objects of this work to test its applicability to gas flow.

Scheideggar (15), Kawakami (10), Smith (16), Rainard (14), Henderson (9), Purcell (13), Burdine (3), and Calhoun (5) assumed the porous media to consist of a system of capillaries in order to derive a mathematical model for predicting flow behaviour in porous media. They investigated the correlation of permeability with average pore size or with the pore size distribution curve. The reported mathematical models do not adequately predict high speed flow through media.

Blick (1) proposed the capillary — orifice model to predict the flow behaviour in porous media. This model assumes porous media to be made up of bundles of capillary tubes with orifice plates spaced throughout the tubes at a distance equal to the tube diameter. He obtained the following equation for determining the pressure drop by applying the laws of conservation of mass and momentum and assuming is othermal gas flow through the porous media.

$$\Psi = 2 \ C_F + \frac{C_D}{2} \qquad \ldots\ldots \quad (8)$$

where

$$\Psi = (P_1^2 - P_2^2) \ M \ \delta \ \varepsilon^2 \ (2 \ L \ G^2 \ Z \ R \ T)^{-1} \qquad \ldots\ldots \quad (9)$$

$$c_F = \frac{16}{Re} \text{ in laminar flow} \qquad \ldots\ldots \quad (10)$$

and

$$1/C_F = 4 \log_{10} Re \sqrt{C_F} - 0.4$$

in turbulent flow ...... (11)

$$Re = \frac{u \ \delta \ \rho}{\mu} = \frac{V.\delta.\rho.}{\varepsilon \ \mu} \qquad \ldots\ldots \quad (12)$$

$$C_D = (1 - \frac{h^2}{\delta^2}) \ (\frac{\delta^4}{h^4} - 1) \ / \ C_o^2 \qquad (13)$$

Blick (1) reported deviations between the theoretical pressure drop as calculated by equation (8) and that determined experimentally. Deviations reached 40% of the experimental values reported by Blick (2) ; Weger and Greenberg (18), (19), Mack (11), Brownell (4), Uchida and Eujita (17).

Foust et al (8) reported the following semi-empirical equation for the pressure gradient in packed beds.

$$\frac{-dp}{dx} = 150 \ \frac{(1-\varepsilon)^2}{\varepsilon^3} \ \frac{\mu.V}{\delta_p^2} + 1.75 \ \frac{(1-\varepsilon)}{\varepsilon^2} \ . \ \frac{\rho. \ V^2}{\delta_p} \qquad \ldots\ldots \quad (14)$$

This can be combined with Foust's equation relating mean pore diameter to mean particle diameter,

$$\delta_p = \frac{1.5 \ \delta \ (1-\varepsilon)}{\varepsilon} \qquad \ldots\ldots \quad (15)$$

to give $\frac{-dp}{dx}$

$$= \frac{66.7}{\varepsilon \ \delta^2} \ . \ \mu.V + \frac{1.165}{\varepsilon^2 . \ \delta} \ \rho. \ V^2 \ \ldots. \quad (16)$$

On integrating the last equation assuming isothermal expansion we get

$$\Psi = \frac{66.7}{Re} + 1.165 \qquad \ldots\ldots \quad (17)$$

GAS FLOW THROUGH POROUS MEDIA

By

Dr. CHALABI, M.F. (Assistant Professor)
Dept. of Chem. Eng., Cairo University, U.A.R.

ABSTRACT

The pressure drop through beds of porous media was measured at different gas flow rates. Screened fractions of particles having different shapes were used as the porous media. The viscous resistance coefficient determined experimentally was found to agree with that predicated from the permeability equation reported by Chalabi et al. The semi-empirical equation of Foust et al was compared with the experimental results over a wide range of gas rates. It is shown that at low values of Reynolds number agreement is satisfactory in case the porous media consisted of rounded particles. A more general correlation has been derived which may be used to predict the pressure drop at higher values of Reynolds number in beds consisting of non-spherical particles.

INTRODUCTION

A fluid passing through a bed of solid particles follows a series of irregular channles forming the intertices between the particles. At low fluid velocities less than a certain limit, the pressure drop per unit length is propertional to the superficial velocity as given by D' Arcy's equation for water flowing in beds of sand.

$$V = k. \frac{\triangle P}{L} \quad \ldots\ldots \quad (1)$$

The constant k in the previous equation equals the permeability coefficient divided by the fluid viscosity.

Norman (12) reported anology between streamline flow in a pipe and fluid flow in a bed of solid particles. He used Poiseuille's equation for stream line flow in a pipe.

$$\triangle P = 32 \frac{\mu_1 u}{g_c d^2} \quad \ldots\ldots \quad (2)$$

as basis to derive an expression for the pressure drop in a bed of solid particles. He assumed that the velocity U in the intertices is proportional to the superficial velocity divided by the bed porosity, and that the distance traversed by the fluid is proportional to the depth of bed. The equivalent diameter of the passages in the bed is taken as the diameter of a circular pipe having the same ratio of volume to wallarea. On substitution in equation (2) Kozeny equation results as :

$$\triangle P = \frac{k' L u}{g_c d_e^2} = \frac{k \mu L V a^2}{g_c \varepsilon^3} \ldots\ldots \quad (3)$$

The constant k must be determined experimentally and it equals 5 for smooth regular solid particles.

Carman (6) showed that the Kozeny equation for stream line flow agrees with the experimental data for values of Reynolds number $(\frac{V \rho}{\mu a})$ less than 2. The experimental data for Re ranging 0.01 to 10,000 were represented by a single equation :

$$\frac{\triangle \rho g_c \varepsilon^3}{L \rho V^2 a} = 5 \left(\frac{V \rho}{\mu a}\right)^{-1} + 0.4 \left(\frac{V \rho}{\mu a}\right)^{-0.1} \ldots\ldots \quad (4)$$

From Fig. 6, it is clear that for the same f_t, increasing f_b gives a slight increase in M_c, but incresing of f_t shows a considerable increase in M_c. Also it is clear that for each f_t, an increase in f_b at the high swept-back angles has a better effect on the flutter characteristic than at low swept back angles.

CONCLUSIONS

From the above results and curves, it can be concluded that :

1 — All-moving one-piece stabiliser, wit L.E. swept-back angle 60°, are flutter free up to 1.8 Mach.

2 — An additional improvement in the flutter characteristics of the 60° L.E. swept-back angle stabiliser can be achieved by increasing both the bending and rotational rigidities.

REFERENCES

1 — Dr. M.Y.M. AFIFI, Eng. S.F. GIRGIS : "The elasto-mechanical properties of swept-back, all-moving stabilisers." Bul. Ain Shams Un., No. 5, 1970.

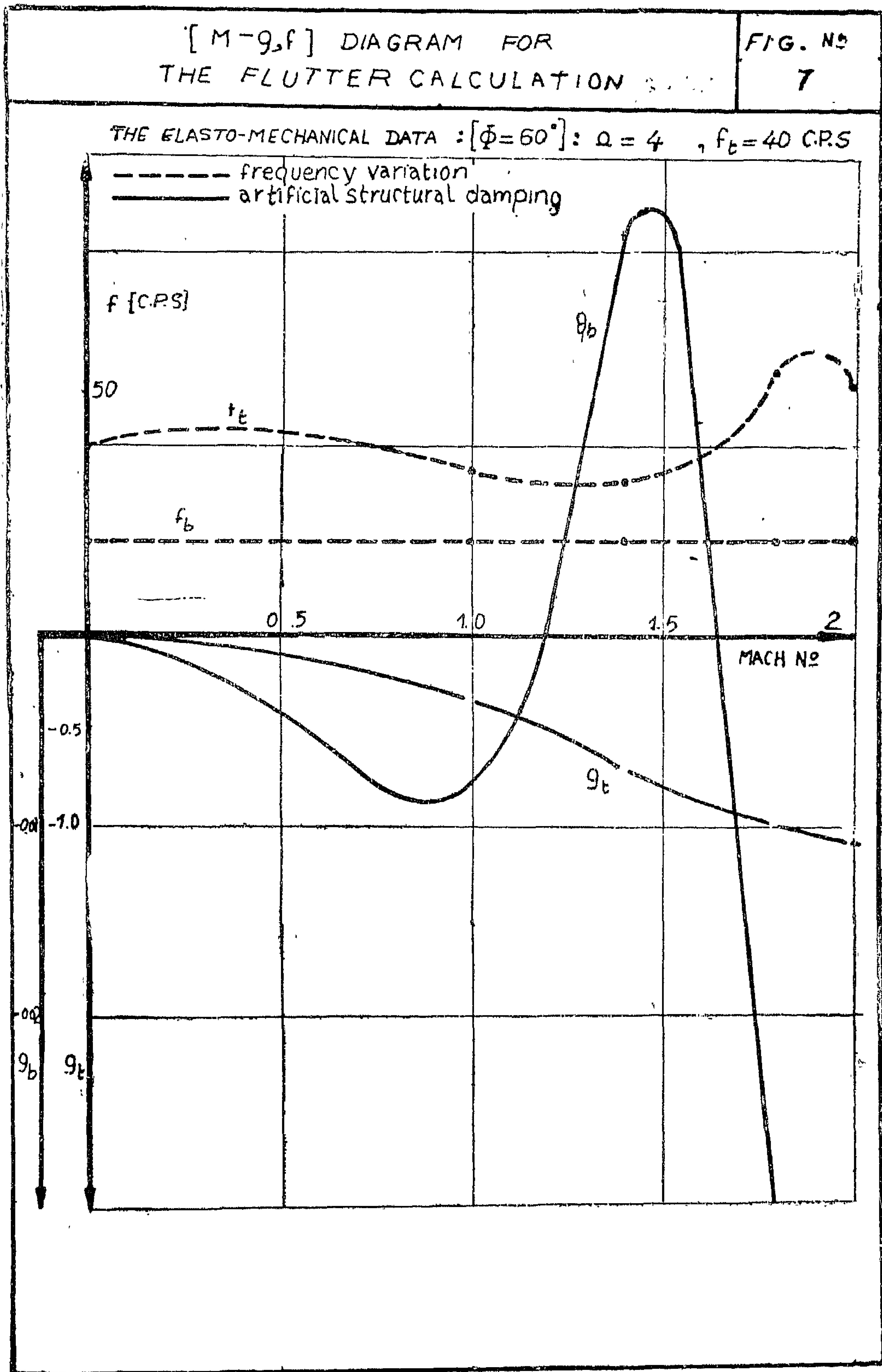
2 — Scanlan H.R., and Rosenbaum : "Introduction of the study of the Aircraft vibration and flutter" The Mach. Co. N.Y. 1951.

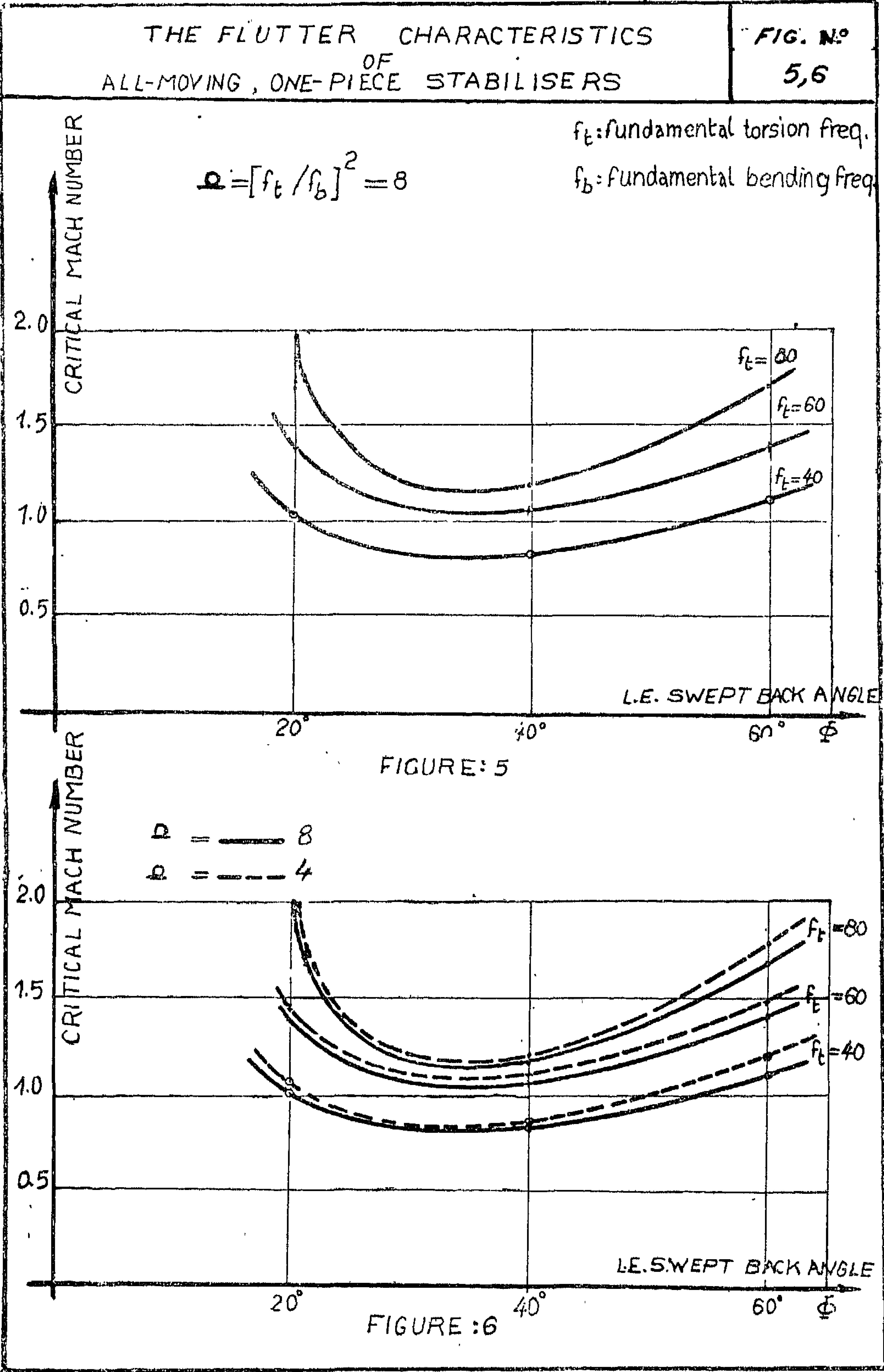
3 — Jordan P.F. : "Aerodynamic flutter coefficients for subsonic and supersonic flow (Linear two dimensional theory". R. and M. No. 2932, 1957.

4 — S.F. Girgis : "The flutter characteristics of all-moving, one-piece control surfaces with different angles of sweep." M.Sc. Thesis, 1967 ; Fac. of Eng. Lib. Ain Shams University.

5 — Bisplinghoff L.R., Ashley and Robert L. Hakfman, 1955, "Aeroelasticity" Addison-Wesley Publishing Co. Inc.




[M-g,f] DIAGRAM FOR
THE FLUTTER CALCULATION
FIG. No
7
THE ELASTO-MECHANICAL DATA : [Φ=60°] : Ω = 4 , f_t=40 C.P.S
frequency variation
artificial structural damping
f [C.P.S]
50
f_t
f_b
g_b
g_t
0.5
1.0
1.5
2
MACH No
-0.5
-1.0
g_b
g_t


THE FLUTTER CHARACTERISTICS
OF
ALL-MOVING, ONE-PIECE STABILISERS
FIG. No
5,6
$\Omega = [f_t / f_b]^2 = 8$
f_t: fundamental torsion freq.
f_b: fundamental bending freq.
CRITICAL MACH NUMBER
2.0
1.5
1.0
0.5
$f_t = 80$
$f_t = 60$
$f_t = 40$
L.E. SWEPT BACK ANGLE
20°
40°
60°
Φ
FIGURE: 5
Ω = 8
Ω = 4
CRITICAL MACH NUMBER
2.0
1.5
1.0
0.5
$f_t = 80$
$f_t = 60$
$f_t = 40$
L.E. SWEPT BACK ANGLE
20°
40°
60°
Φ
FIGURE: 6

For a particular value of k_o (reference reduced frequency), the determinant expands into one complex polynomial in z, for this two degrees of freedom system. This polinomial can be factored by the quadratic formula[5] ;

$$z^2 - 2 A z + B = 0$$

where :

$$A = \frac{1}{2} [1 + F_{22}/m_2 + \Omega (1 + F_{11}/m_1)]$$
$$B = \Omega [1 + F_{11}/m_1 + F_{22}/m_2 + F_{11} F_{22}/m_1 m_2 - F_{12} F_{21}/m_1 m_2]$$

The aerodynamic flutter coefficients :

The aerodynamic integrals have integrands L_h, $L\Theta$, M_h, $M\Theta$ which vary along the span for a particular choice of k_o. Thus for each k_o, the aerodynamic flutter coefficients were determined by interpolation from the curves given by Jordan[3]. The integrals are then evaluated by Simpson's rule, for several choices of k_o and M. (M = 0, 0.5, 0.7, 0.9, 1, 1.25, 1.625, 2).

For each k_o, at certain M, the quadratic formula leads to two complex roots. Each of them has its value of speed, frequency and the artificial structural damping g, that corresponds to one of the two normal modes introduced in the flutter calculation.

Solution of the flutter stability equation :

The roots of the quadratic equation are :

$$z_1 = A + \sqrt{A^2 - B}\ , \ \& \ z_2 = A - \sqrt{A^2 - B}$$

where ,

$$z_1 = (w_t/w_{1c})^2 (1 + i g_1) = X_1 + i Y_1$$
$$z_2 = (w_t/w_{2c})^2 (1 + i g_2) = X_2 + Y_2 i$$

then $g_1 = Y_1/X_1$, and $g_2 = Y_2/X_2$ are the artificial structural damping coefficients for the flutter condition at a given k_o and M. Since $k_o = w_c C_o/V$; and from equating the real quantities we get :

$$X_1 = (w_t/w_{1c})^2$$

$$\therefore f_{1c} = f_t / \sqrt{X_1} \quad \text{and } V_1 = 2 \pi f_{1c} . C_o/k_o$$

$$X_2 = (w_t/w_{2c})^2$$

$$\therefore f_{2c} = f_t / \sqrt{X_2} \quad \text{and } V_2 = 2 \pi f_{2c} . C_o/k_o$$

Adopting the V-g method[5] ; for each Mach number to determine the amount of artificial structural damping required to satisfy the flutter condition, at a speed corresponding to the pre-assumed M. Finally, the artificial structural damping versus the real Mach number can be plotted.

When g is negative means that the structure at this mode is stable.[1] And conversely small positive value of g describes the state of instability.

RESULTS AND DISCUSSIONS

The lowest critical Mach numbers at altitude of 2000 meters, for the three surfaces (with L.E. swept-back angles 20°, 40°, 60°) are calculated[4]. The results are shown in Fig. 5.

The effect of the frequency ratio Ω, and of the torsional frequency for constant frequency ratio at different L.E. swept-back are shown in Fig. 6.

From Figs. 5 and 6, the minimum flutter speed occurs at swept back angles $\Phi = 35° - 40°$. And the flutter speed increases as the swept-angle increases.

The final results of the flutter calculations are plotted in a series of curves[4] M — g, f. One of them is shown in Fig. 7, from which it is clear, that there is no interference or coupling between the normal coupled modes, since there is no intersection of frequency at the critical Mach number. The flutter in all these curves are due to the fundamental bending modes, which are shown by the drop in the M — g_b curves.

From Figs. 3 and 4, the rotational part in the fundamental bending mode of the stabiliser with 60° L.E. swept-back angle, is smaller than that for 40° L.E. swept-back, which is one of the reasons for the improvement in the flutter characteristic at this high swept back L.E. surfaces.

THEORETICAL ANALISIS.

The flutter calculation is based on the strip theory, and thus the amplitude at station x,y for a general vibratory motion can be expressed as a superposition of the various coupled modes, as follows :

$$h\ (y,t) = \sum_{r=1}^{\infty} h_r(y)\,q_r(t)$$

$$\simeq [h_1(y)\,q_1(t) + h_2\ (y)\ q_2\ (t)\ ]$$

$$\Theta\ (y,t) = \sum_{r=1}^{\infty} \Theta_r(y)\,q_r(t)$$

$$\simeq [\Theta_1(y)\,q_1(t) + \Theta_2(y)\,q_2(t)\ ]$$

The generalised aerodynamic forces Q_1 and Q_2 to be introduced in the flutter equations[1] are deduced as follows :

The virtual work done $\triangle W_r$ by an air force Q_r in varying q_r to $(q_r + \triangle q_r)$, all other degrees of freedom being held constant during the displacement, is[2]:

$$\triangle W_r = Q_r \,.\, \triangle q_r$$

Each of the four aerodynamic forces acting on the surface with rigid chord, is represented by a single force coefficient. The four coefficients are , L_h , $L\Theta$ and M_h , $M\Theta$.[3] and

$$L' = \zeta\ C\ V^2\ e^{iwt}\ (h\ L_h + \Theta\ L\Theta)\ ;$$

$$M' = \zeta\ C^2\ V^2\ e^{iwt}\ (h\ M_h + \Theta\ M\Theta)$$

$\therefore$ The total work done, $\triangle W_r = \triangle q_r \int_0^{span} (L'\ h_r + M'\ \Theta_r)\ dy$

$\therefore$ The generalised aerodynamic forces for the two modes are :

$$Q_1 = \int_0^{span} (L'\ h_1 + M'\ \Theta_1)\ dy\ ;$$

$$Q_2 = \int_0^{span} (L'\ h_2 + M'\ \Theta_2)\ dy$$

Thus if $Q_1 = w^2\ (F_{11}\ q_1 + F_{12}\ q_2)$; and $Q_2 = w^2\ (F_{21}\ q_1 + F_{22}\ q_2)$.

The aerodynamic integrals F_{rs} can be determined from the expressions used by Scantan[3] and Rosenbaum, after modifying them for the effect of the L.E. swept back angle Φ[4], as shown in table 2.

Lagrang's equations of motion[1] can then be written as follows :

$$m_1\ddot{q}_1 + m_1\ w_b^2\ (1 + i\ g_1)\ q_1 = w^2\ (F_{11}\ q_1 + F_{12}\ q_2)$$

$$m_2\ddot{q}_2 + m_2\ w_t^2\ (1 + i\ g_2)\ q_2 = w^2\ (F_{21}\ q_1 + F_{22}\ q_2)$$

where : m_1 , m_2 are the generalised masses of the first and second modes respectively[1].

As the flutter condition is that, the system will vibrate with simple harmonic motion with constant amplitude at a circular frequency w equals the critical circular frequency w_c.

Substituting $q_r = q_o\ e^{iwt}$ in the above equations, and deviding by $-w^2$, we get :

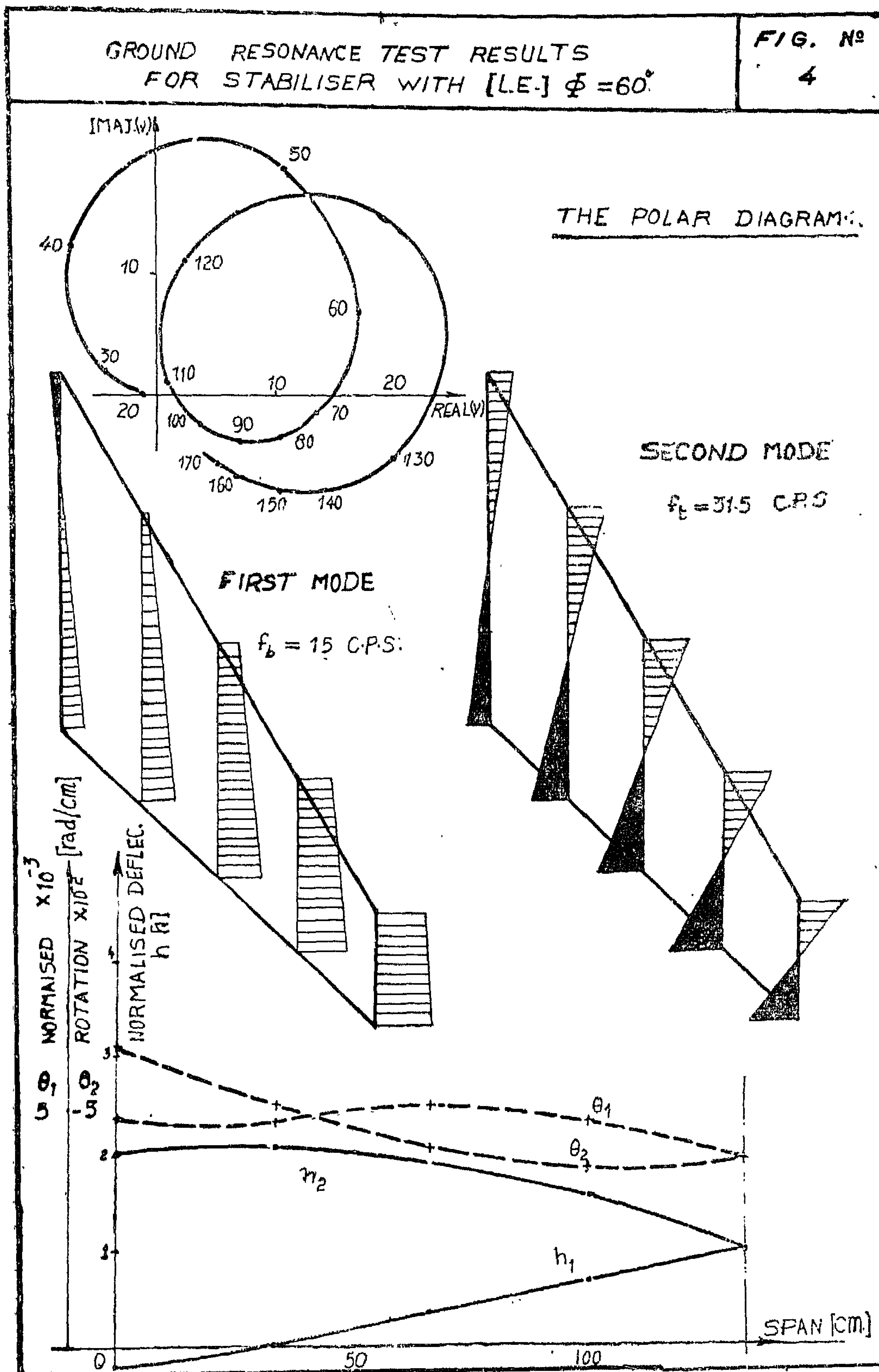
$$[m_1 - m_1\ (1 + i\ g_1)\ (w_b/w)^2 + F_{11}]\ q_1 + F_{12}\ q_2 = 0$$

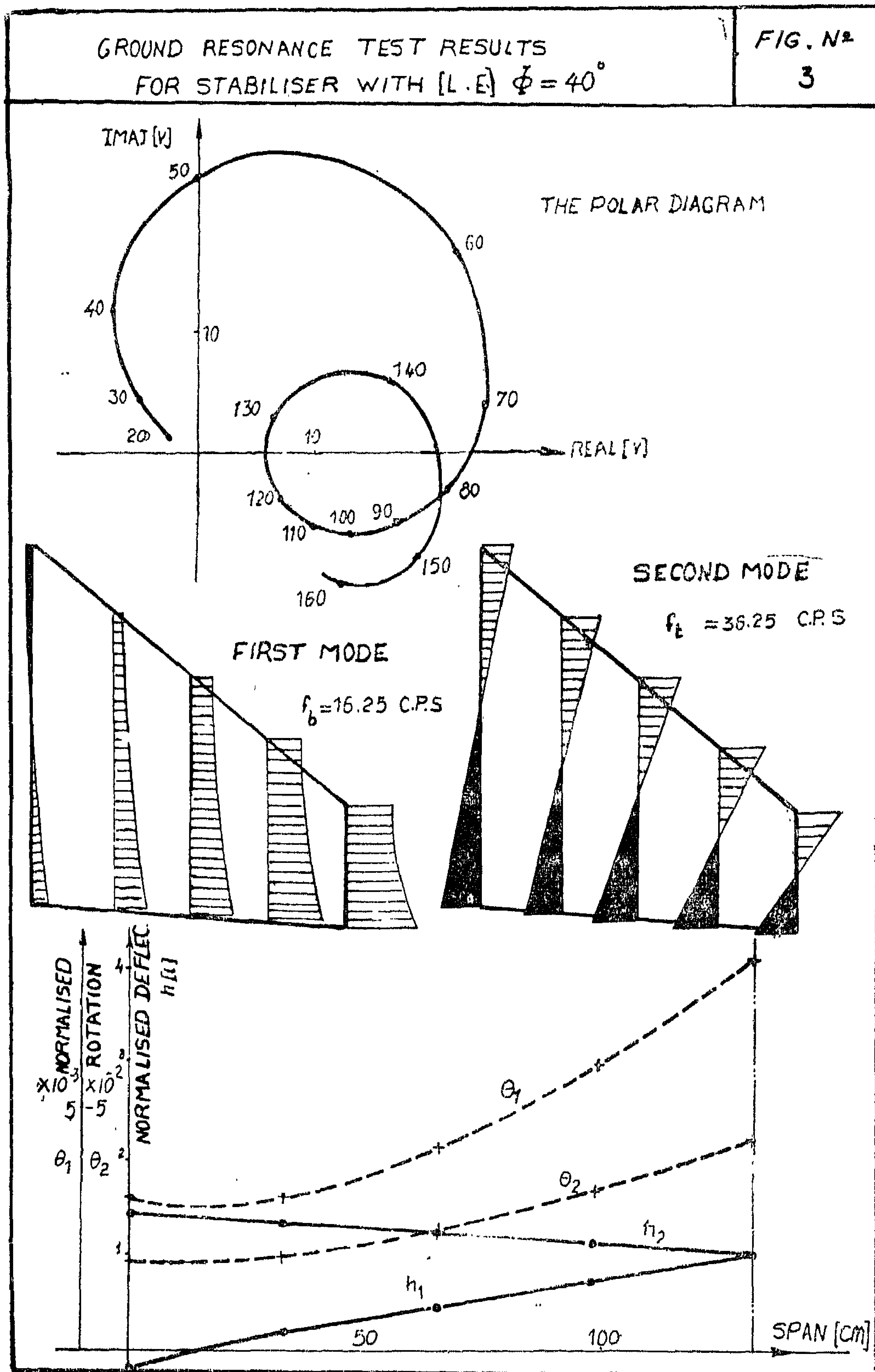
$$F_{21}\ q_1 + [\ m_2 - m_2\ (1 + i\ g_2)\ (w_t/w)^2 + F_{22}]\ q_2 = 0$$

The necessary and sufficient condition that solutions for the above simultaneous equations exist (other than $q_1 = q_2 = 0$), is that the determinant of the coefficients vanishes, i.e.

$$\begin{vmatrix} m_1 - m_1\ (1 + i\ g_1)\ (w_b/w)^2 + F_{11} & F_{12} \\ F_{21} & m_2 - m_2\ (1 + i\ g_2)\ (w_t/w)^2 + F_{22} \end{vmatrix} = 0$$

Assuming $g_1 = g_2 = g$[5]; g is regarded as one of the unknowns, and it is always joins the other unknown $(w_t/w)^2$ in the single complex combination $z = (w_t/w)^2\ (1 + i\ g)$.


GROUND RESONANCE TEST RESULTS
FOR STABILISER WITH [L.E.] Φ =60°
FIG. № 4
THE POLAR DIAGRAM
IMAJ.(v)
REAL(V)
FIRST MODE
f_b = 15 C.P.S.
SECOND MODE
f_t = 31.5 C.P.S
NORMAISED ×10⁻³
ROTATION ×10⁻² [rad/cm]
NORMALISED DEFLEC. h [h]
θ1 θ2
5 -5
θ1
θ2
h2
h1
SPAN [cm]
0
50
100


GROUND RESONANCE TEST RESULTS
FOR STABILISER WITH [L.E] Φ = 40°
FIG. No 3
IMAJ [V]
THE POLAR DIAGRAM
REAL [V]
50
60
40
10
140
30
130
70
20
10
80
120
100
90
110
150
160
FIRST MODE
f_b=16.25 C.P.S
SECOND MODE
f_t =36.25 C.P.S
NORMALISED ROTATION
NORMALISED DEFLEC h [L]
θ1
θ2
h2
h1
50
100
SPAN [cm]

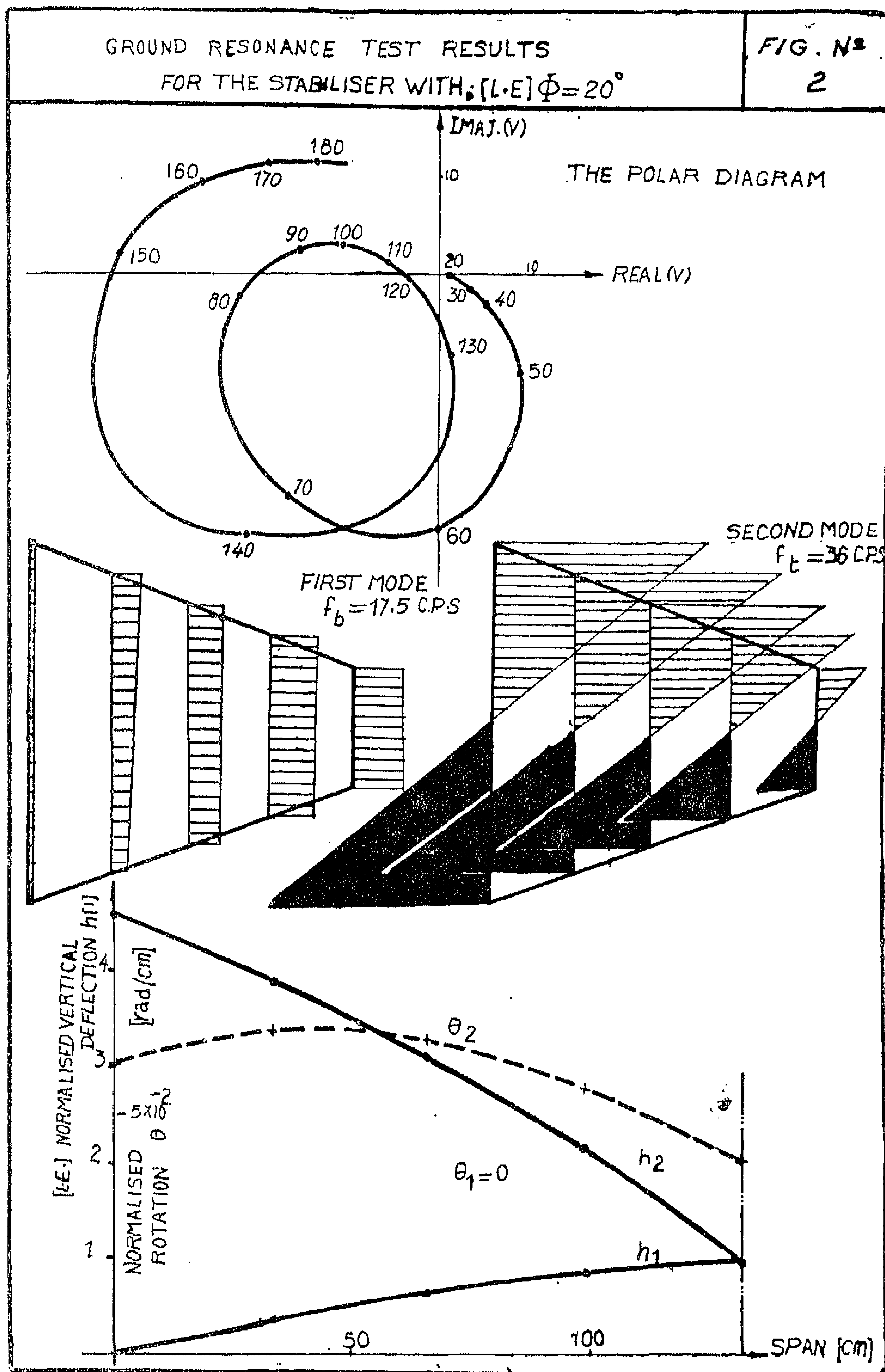

GROUND RESONANCE TEST RESULTS
FOR THE STABILISER WITH; [L.E] Φ=20°
FIG. No 2
IMAJ.(V)
THE POLAR DIAGRAM
REAL (V)
180
160
170
150
90
100
110
20
120
80
30
40
130
50
70
140
60
10
SECOND MODE
f_t = 36 C.P.S
FIRST MODE
f_b = 17.5 C.P.S
[L.E.] NORMALISED VERTICAL DEFLECTION h[1]
[rad/cm]
NORMALISED ROTATION θ
5×10⁻²
θ2
h2
θ1=0
h1
4
3
2
1
50
100
SPAN [cm]

Table 1

The elastomechanical parameters of the stabilisers.

L.E. Swept back angle Φ	Mode	Fig. No.	Resonance Frequency c.p.s.	Generalised mass kg. cm²	Frequency ratio Ω f_t/f_h
20°	First Second	2	17.5 36	9.251 129.577	2.06
40°	First Second	3	16.25 36.25	9.390 12.530	2.23
60°	First Second	4	15 31.5	17.769 35.423	2.1

Table 2

THE AERODYNAMIC INTEGRALS

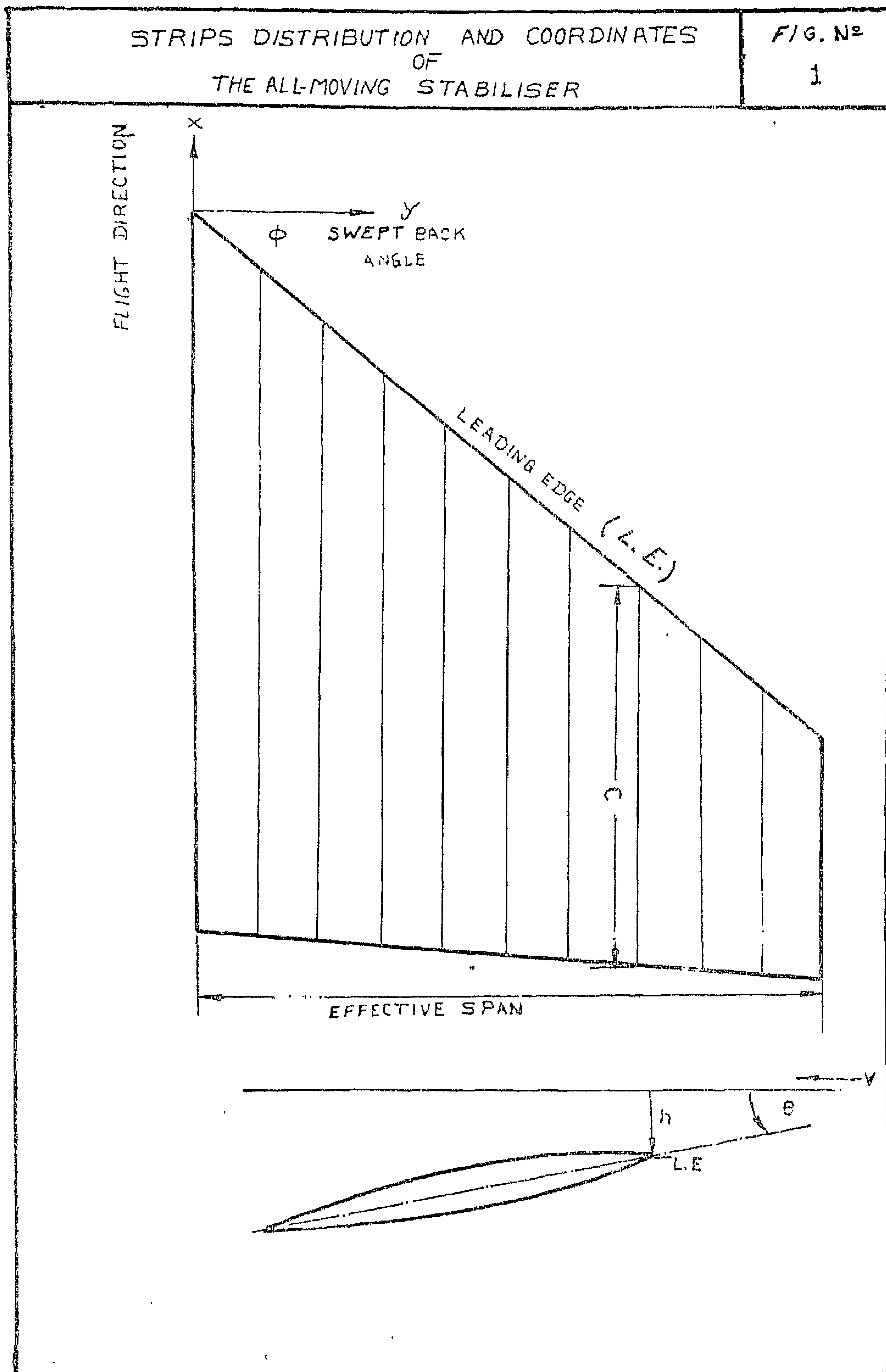
$$F_{rs} = d \cos \Phi \int_0^{SPAN} \left[C_1^2 h_r h_s \left(\frac{L_h}{k^2}\right) + C^3 h_r \theta_s \left(\frac{L_\theta}{k^2}\right) + C^3 \theta_r h_s \left(\frac{M_h}{k^2}\right) + C^4 \theta_r \theta_s \left(\frac{M_\theta}{k^2}\right) \right] q_s \, dy$$

$$F_{11} = d \cos \Phi \int_0^{SPAN} \left[C^2 h_1^2 \left(\frac{L_h}{k^2}\right) q_1 + C^3 h_1 \theta_1 \left(\frac{L_\theta}{k^2}\right) q_1 + C^3 \theta_1 h_1 \left(\frac{M_h}{k^2}\right) q_1 + C^4 \theta_1^2 \left(\frac{M_\theta}{k^2}\right) q_1 \right] dy$$

$$F_{12} = d \cos \Phi \int_0^{SPAN} \left[C^2 h_1 h_2 \left(\frac{L_h}{k^2}\right) q_2 + C^3 h_1 \theta_2 \left(\frac{L_\theta}{k^2}\right) q_2 + C^3 \theta_1 h_2 \left(\frac{M_h}{k^2}\right) q_2 + C^4 \theta_1 \theta_2 \left(\frac{M_\theta}{k^2}\right) q_2 \right] dy$$

$$F_{21} = d \cos \Phi \int_0^{SPAN} \left[C^2 h_2 h_1 \left(\frac{L_h}{k^2}\right) q_1 + C^3 h_2 \theta_1 \left(\frac{L_\theta}{k^2}\right) q_1 + C^3 \theta_2 h_1 \left(\frac{M_h}{k^2}\right) q_1 + C^4 \theta_2 \theta_1 \left(\frac{M_\theta}{k^2}\right) q_1 \right] dy$$

$$F_{22} = d \cos \Phi \int_0^{SPAN} \left[C^2 h_2^2 \left(\frac{L_h}{k^2}\right) q_2 + C^3 h_2 \theta_2 \left(\frac{L_\theta}{k^2}\right) q_2 + C^3 \theta_2 h_2 \left(\frac{M_h}{k^2}\right) q_2 + C^4 \theta_2^2 \left(\frac{M_\theta}{k^2}\right) q_2 \right] dy$$


STRIPS DISTRIBUTION AND COORDINATES
OF
THE ALL-MOVING STABILISER
FIG. №
1
FLIGHT DIRECTION
X
Y
Φ SWEPT BACK ANGLE
LEADING EDGE (L.E.)
C
EFFECTIVE SPAN
V
h
θ
L.E

$q_r(t)$	Generalised coordinate of the r^{th} mode, function of time, the amplitude of which expresses how much of each normal mode is introduced in the general vibrating motion.

Aerodynamical quantities :

a $cm.s^{-1}$	Velocity of sound.
V $cm.s^{-1}$	Velocity of undisturbed flow.
V_c $cm.s^{-1}$	Critical velocity of flow at flutter.
$M = V/a$	Mach number of flight.
$M_t = M \cos \Phi$	Theorticial Mach number.
$K_o = w\ C_o/V$	Reference reduced frequency.
ζ kg. cm^{-3}	Air density.
$k = wC(y)/V$	Reduced frequency $= k_o\ C\ (y)/C_o$.
$Q_r(p)$ kg. $cm^{-1}s^{-2}$	Generalised aerodynamic force due to the ampl. h_r at (p).
L′ kg. $cm.s^{-2}$	Aerodynamic force on the profile strip.
M′ kg. $cm.^2s^{-2}$	Aerodynamic moment on the profile strip. related to L.E.
Q′ kg. $cm.^{-1}s^{-2}$	Generalised aerodynamic force per unit surface due to the amplitude h_r.
L_h, $L\Theta$	Coefficients, of the aerodynamic force, the components are : $L_h = L_h'' + L_h'''\ i$, $L\Theta = L\Theta'' + L\Theta'''\ i$
M_h, $M\Theta$	Coefficients of the aerodynamic moment, components are : $M_h = M_h'' + M_h'''\ i$, $M\Theta = M\Theta'' + M\Theta'''\ i$
F_{rs} cm	Generalised aerodynamic integrals.

Arithmetical quantities :

r , s	Indexing numbers
i	Imaginary unit
I_m	Imaginary part
R_e	Real part

Data of the all-moving, one-piece stabiliser.

i) Geometrical data :

Fig. 1 is a drawing of the surfaces to be investigated.

Aspect ratio : $(span)^2$ / Area	1.32	
Taper ratio : root chord/tip chord	3	
Finess raito: max. thickness/chord	4%	
Effective span :	132	cms.
Effective root chord	150	cms.

Leading edge swept-back angles

$$\Phi = 20°, 40°, 60°.$$

Aerodynamically, the control surface is considered as a thin surface in the x-y plane of the x,y,z coordinate system, and the surface of the control are assumed to move in the positive x direction at a uniform speed V. The undisturbed position of the surface is in the region of the x-y plane, with the x-axis along the root chord and the origin at the nose.

ii) Elastomechanical Data :

From ground vibration tests carried out on dynamically similar models,(1) the fundamental resonance frequencies and the basic mode shapes of the surfaces were determined. Aalso, the generalised masses were calculated. The results for the basic modes of each surface are shown in table 1, and Figures 2,3,4.

THE FLUTTER CHARACTERISTICS OF SWEPT-BACK ALL-MOVING STABILISERS

By

Dr. M.Y.M. AFIFI, and Eng. S.F. GIRGIS*

SUMMARY

The paper presents the effect of varying the leading edge sweptback angle on the flutter characteristics of all-moving one piece stabilisers. Data regarding the normal modes of vibration, which appears in the stability equations, was determined experimentally.[1].

Investigations were carried out on surfaces with swept-back angles of 20°, 40°, and 60°. The results show that the minimum flutter speed occurs at swept back angles of 35°—40°. For highly L.E. swept-back angles, all-moving type stabilisers, the flutter speed is increased. Also, an improvement in the flutter characteristics up to Mach number 1.8 can be achieved by using a swept-back angle of 60° together with high torsional rigidity and bending rigidity.

INTRODUCTION

The flutter behaviour of all-moving, one-piece stabilisers used in guided flying vehicles is some what different from the behaviour of common type of lifting surfaces with fixed root, or lifting surfaces with two parts. In these all-moving surfaces the coupling of the aerodynamic forces and moments arises equally at the root and at the tip, whereas with a root fixed system most of the aerodynamic coupling comes from the part of the surface near the tip.

Although, the all moving type stabilisers are more effective at sonic and supersonic speeds ; and they are used nowadays in high speed aircrafts and rockets, but the available data regarding the flutter characteristics of such surfaces are very little. The object of this paper is to show the effect of the L.E. swept-back angles upon the flutter speeds of such surfaces at different Mach numbers up to 1.8 M.

SYMBOLS

Geometrical Quantities :

t sec;	Time
w rad. s^{-1}	Angular frequency
f cycle. s^{-1}	Frequency
Ω	Torsion freq. / Bending freq. (f_t/f_b)
x,y,z	Cartesian coordinates
C_o cm	Reference chord length at 3/4 of the span.
C(y) cm	Total chord length at y
b cm	Effective span
Φ °	Leading Edge (L.E.) swept-back angle.

Elasto-mechanical quantities.

$h_r(y)$ cm	Normalised amplitude of translation of the surface at the L.E. point in the r^{th} mode.
$\Theta_r(y)$ radi. cm^{-1}	Normalised amplitude of rotation of the surface profile about L.E. in the r^{th} mode.
$h_o=1$ cm	Normalised reference amplitude at the reference point (i.e. Tip chord L.E. point).

* Dr. M.Y.M. AFIFI : Ass. Prof., Fac. of Eng., Ain Shams University. Eng. S.F. GIRGIS : Technical office, Helwan Aircraft Factory.

INFORMATION

- The editors welcome for publication engineering researches and articles as well as discussions on any material appearing in this periodical.
- This periodical does not hold itself responsible for the opinions expressed in it.
- Any material intended for publication must be sent to the Secretariat at the address of the Engineering Society at Cairo.

SUBSCRIPTIONS

All members of the Engineering Society at Cairo are ipso facto subscribers of this periodical.

Subscription for engineers P.T. 60 per annum.

Subscription for others P.T. 200 per annum.

HEAD OFFICE

Egyptian Society of Engineers,

28, Ramses Avenue, Cairo. Tel. 52106

ADVERTISEMENTS

JOURNAL OF
THE EGYPTIAN SOCIETY OF ENGINEERS
A.E.R.

QUARTERLY SCIENTIFIC PROCEEDINGS

ISSUED BY

THE EGYPTIAN SOCIETY OF ENGINEERS—U.A.R., CAIRO

Vol. X — No. 3, July-August-September 1971

CONTENTS

ENGLISH SECTION

Page

The flutter characteristics of swept-back all-moving stabilisers.
Dr. M.Y.M. AFIFI. 7

Gas flow through porous media.
Dr. M.F. CHALABI 19

Hydrodynamic equations for curvilinear flow.
Dr. M.H. EL-KATEB 28

Lateral pressures in silos.
Dr. SABRI SAMAAN 33

Shear effect on reinforced concrete limit design.
Dr. MAHMOUD NASR 41

Trials on steam and fuel oil injection in a 400 ton/day blast furnace.
Dr. ABO EL-SAADAT, A.B. MOURAD, M.S. ETEWA and S.Y. EZZ 46

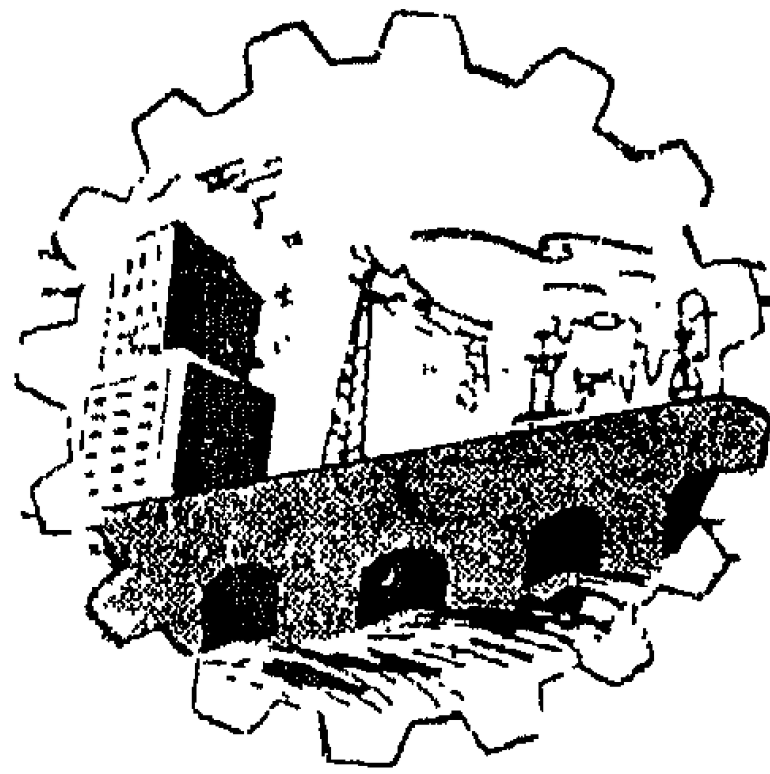
Experimental and practical study of the use of explosives in removing rock from project areas.
Dr. ALY ISMAIL EL-GAWHARY and MOH. FATHY EL-ATTAR 59

Effect of alternating and mean stresses on the damping capacity of metals.
Dr. M.Y.M. AFIFI, K.A. MOSTAFA 68

ARABIC SECTION

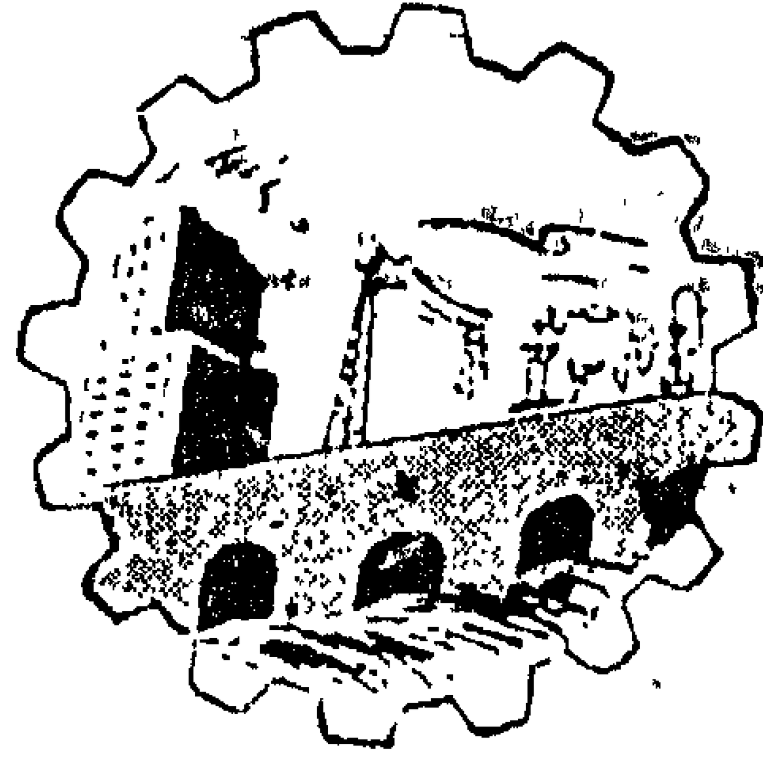
Climatization of Electric Substances and products. 7

"Mondiale" Press—Cairo



JOURNAL OF
THE EGYPTIAN SOCIETY
OF ENGINEERS
A. E. R.

July-August-September 1971
Vol. X
No. 3



مجلة

جمعية المهندسين المصرية

اكتوبر – نوفمبر – ديسمبر ١٩٧١ المجلد العاشر العدد الرابع

رقم الإيداع بدار الكتب المصرية ٢٩٨/١٩٦٩

المطبعة العالمية ١٦، ١٧ ش ضريح سعد بالقاهرة

مجلة

جمعية المهندسين المصرية

مجلة علمية هندسية - تصدرها كل ثلاث شهور

جمعية المهندسين المصرية بالقاهرة

السنة العاشرة — العدد الرابع — أكتوبر — نوفمبر — ديسمبر ١٩٧١

محتويات هذا العدد

القسم العربى

صفحة

— نحو عمارة عربية حديثة ومدى صلتها بالتراث القديم ... ... للدكتور المهندس على رأفت ٥

— مشاكل النقل البرى (بالسيارات) للركاب بين المدن وفى الريف فى الدول النامية — ٢ — للمهندس سمير فهمى ١٧

— تأثير القنابل والصواريخ على المنشآت — ٢ — ... ... المهندس عز الدين فرج ٢٧

القسم الأفرنجى

— تأثير ضغوط المواد الحبيبية على الصوامع وممرات الخام ... ... للدكتور المهندس حسن فهمى امام والمهندس محمد مرسى الوجيه ٥

— الاختزال المباشر بالهيدروجين لخام حديد البحرية فى الحالة المميعة ... ... للدكتور المهندس م. الحلوجى والدكتور المهندس أ. عبد الديم والمهندس س. العفيفى ١٤

— طرق تحسين سلوك عازلات خطوط الكهرباء فى الأمكنة المعرضة للتلوث والرطوبة العالية ... ... للدكتور المهندس السيد عبد الحى ٢٣

— قياسات دينامية على مسخن أنبوبى بالبخار ... ... للدكتور المهندس م. الرفاعى والدكتور المهندس م. صالح والمهندس ه. يوسف ٣٠

— العوامل المؤثرة فى تشغيل رمل المسبك آلياً ... ... للدكتور المهندس صلاح سعيد والدكتور المهندس محمود فرج والمهندس م. محمد طه ٣٤

بيانات

مقر المجلة

جمعية المهندسين المصرية

٢٨ شارع رمسيس بالقاهرة

تليفون : ٥٢١٠٦

- جميع أعضاء جمعية المهندسين مشتركون فى المجلة بحكم عضويتهم
- الإشتراك السنوى لغير الأعضاء : ٦٠ قرشاً للمهندس ، ٢٠٠ قرش للهيئات
- ترسل البحوث والموضوعات والتعليقات إلى أمانة التحرير بمقر جمعية المهندسين
- المصرية بالقاهرة
- ترحب المجلة بما يرسل إليها من بحوث وموضوعات هندسية وأى تعليقات علمية للمناقشة
- المجلة غير مسئولة عن الآراء التى تنشر بها وتعبر عن رأى كاتبها فقط.

بيانات خاصة بالبحوث المطلوب نشرها
بمجلة جمعية المهندسين المصرية

---

١ — تنشر المجلة البحوث المقدمة سواء كانت باللغة العربية أو الإنجليزية .

٢ — في حالة تقديم البحث للنشر باللغة العربية ترجو المجلة أن يقدم الأصل مكتوباً على الآلة الكاتبة .

٣ — في حالة تقديم البحث للنشر باللغة الانجليزية ترجو المجلة أن يقدم الأصل على الآلة الكاتبة أو بخط اليد المفرد .

٤ — تكون الرسومات المرفقة بالبحث على ورق كلك « شفاف » وبالحبر الشيني والكتابة عليها بمعرفة خطاط . . أو تكتب البيانات المطلوبة على الرسم بالرصاص لإمكان كتابتها بمعرفة المجلة وأن تكون مقاسات الرسم تسمح بتصغيره على ربع أو نصف أو على كامل اتساع الصفحة .

٥ — تكون الصور المطلوب نشرها نسخة أصلية واضحة وبدون ألوان .

٦ — يرفق بالبحث ما يلى :

(أ) موجز للبحث باللغة العربية فى حدود صفحتين فولسكاب إذا كان البحث باللغة الإنجليزية .

(ب) موجز للبحث باللغة الإنجليزية فى حدود صفحتين إذا كان البحث باللغة العربية .

(ج) خمسة سطور عن مضمون البحث باللغة الإنجليزية لنشره فى صفحة البطاقات بالمجلة .

(د) أن يكون عنوان البحث باللغتين العربية والإنجليزية .

(هـ) مختصر لعنوان البحث فى حدود لا تتجاوز خمس كلمات باللغتين العربية والإنجليزية .

(و) يرفق بالبحث صورة للباحث مقاس ٤ — ٦ .

(ز) يرفق بالبحث التاريخ العلمى للباحث ويتضمن :
سنة التخرج — الدرجات العلمية وتاريخ الحصول عليها والجامعة — عضوية الجمعيات العلمية — والمؤتمرات التى شهدها الباحث — الوظيفة الحالية للباحث .

برجاء أن يكون البحث متضمناً هذه البنود لتسهيل إجراءات النشر ؟

رئيس التحرير

نحو عمارة عربية حديثة

ومدى صلتها بالتراث القديم

الدكتور المهندس على رأفت

مقدمـــة :

لكى نصل للدور الذى ينبغى أن تلعبه العمارة المصرية الحديثة لتطوير العمارة العربية القومية يجب أن نناقش أولا ونصل إلى قرار فى مدى إمكانية تحقيق ذلك عن طريق بعث التراث القديم والتعبير عنه بأساليب العصر الحديث .

لقد تردد مثل هذا الشعار كثيراً فى المحيط المعمارى وخاصة فى القرن التاسع عشر وهو يخفى وراءه اتجاهات وفلسفات رومانتيكية ظهرت فى الأدب والشعر والفن ثم انتقلت إلى العمارة ، ومن مظاهرها التطلع إلى البعد الزمنى أو البعد المسافى — تطلع إلى الماضى بجماله وعظمته وبطولاته وذكرياته أو إلى الحاضر البعيد بغموضه وصوره المشوقة الغريبة الجديدة على محيطنا .

هذه الاتجاهات الرومانتيكية يبررها دائماً تبريرات منطقية فى ظاهرها تحدد الجمال المضمون الدائم فى الطرز القديمة كلاسيكية كانت أو قوطية أو إسلامية (هذه الطرز جربت لمدة قرون وأجمعت الآراء والأذواق على جمالها) تحت هذا الشعار رجع معماريو عصر النهضة إلى الطرز الكلاسيكية وطوروها وحذا معماريو القرن التاسع عشر حذوهم وطبقوها بدون تصرف أو تطوير بعد أكثر من ألف وخمسمائة عام على نشأتها (وقد تفسر هذه الاتجاهات على أسس محلية أو قومية أو دينية) جميع هذه الأسس استندت إلى أن الحاضر ما هو إلا تتمة الماضى ورفعت شعاراً تقليدياً مهماً وهو بعث القديم والتعبير عنه بأساليب العصر الحديث .

والتطبيق هنا تقابله صعوبات تنوع التراث وتباين أشكاله وصوره ، فالمعمارى المصرى أمامه الطراز الفرعونى والقبطى والعربى والمعمارى الإيطالى أمامه الطراز الكلاسيكى — والقوطى وطرز عصر النهضة فى فلورنسا والبندقية وبولونيا وروما والانجليزى والفرنسى لا تقل مشاكلهما إن لم تزد (والأخير اختار فى أوائل القرن التاسع عشر الطراز الكلاسيكى والانجليزى اختار الطراز القوطى وسماه طراز الملكة فيكتوريا والأمريكى لم يلجأ للعمارة الهندية كتراث ، بل لجأ طوال القرن التاسع عشر إلى الطراز الإغريقى لأسباب سياسية وثقافية إلى أن أوقفت الحرب الأهلية هذا الاتجاه . كما اتجه بعض معمارى القرن التاسع عشر إلى اعتناق مبدأ اللامبالاة وفى هذا تنفذ المبانى على الطراز المناسب لطابع المبنى أو الطراز السائد حوله) والمعمارى يتردد بلا مبالاة بين الكلاسيكية والقوطية (وطراز عصر النهضة والباروك والعربى والفرعونى ويستعمل منها ما يشبع رغبات عصره الرومانتيكية) وهو قد يخصص لكل طراز نوعاً معيناً من المبانى . وهكذا تردد المعمارى المصرى ومن استعان بهم من خبراء فى بداية القرن العشرين بين الطراز الكلاسيكى الذى خصص للمحاكم ودور الشهر العقارى وجامعة القاهرة وبعض المصالح الحكومية ، وبين الطراز العربى الذى خصص للمساجد وللمبانى الدينية عامة وبعض محطات السكك الحديدية شمال خط عرض ٣٠° [خط عرض القاهرة] والطراز الفرعونى الذى خصص المبانى جنوب هذا الخط . وقد كان لهذه القاعدة بعض

شواذ فى جامعة الإسكندرية وبعض مبانى القاهرة التى نفذت بالطراز الفرعونى . وقد يعتنق المعمارى مبدأ ثالثاً هاماً وهو المبدأ الاكلكتيكى الذى انتقل إلى العمارة من الفلاسفه فى منتصف القرن التاسع عشر . وفى العمارة طبق على أساس التصميم بالتجميع أو بالاقتباس من كل بستان زهرة ، حيث أن الحاضر هو مصب لكل تجارب الماضى . وعلى هذا المبدأ ظهرت مبانى تجمع بين طرز مختلفة ظهرت على مدى قرون عدة . وقد يكون ظاهرها كلاسيكى ودواخلها فرعونى أو بيزنطى أو عربى . وقد تتنوع الحجرات والصالات والطرقات فى صورها وأشكالها وديكوراتها .

وقد يحقق المعمارى الرومانتيكى أهواءه عن طريق التطلع إلى البعد المسافى بنقل صور معمارية بعيدة للتمتع بها رومانتيكياً لأنها تذكره أو تذكر مستعملى المبنى بزيارات أو أشعار أو صور وتخيلات . وقد شجع على ذلك ظهور نظريات ترجع الجمال إلى مدى ما يبعثه العمل الفنى من خيال فى نفس المشاهد . كما ساعد على ذلك كثرة الفتوحات الإستعمارية والأسفار السياحية والبعثات الدراسية وتطور وسائل الاعلام وأهمها الصور الفوتوغرافية وانتشارها عن طريق المجلات . وقد ظهرت تطبيقات فرعونية فى فرنسا وأمريكا وخاصة بعد حملة نابليون وصور لعمارة الشرق الأقصى وخاصة الهندية والصينية واليابانية فى إنجلترا . وحديثاً فى مصر مازلنا نرى امتداداً لهذه التطلعات الرومانتيكية فى تطبيقات لعمارات معاصرة بعيدة ظهرت مع ازدياد البعثات إلى الخارج. فلدينا أعمالا تقلد العمارة السويسرية أو الأمريكية أو الإنجليزية أو تنقل اتجاهات مدارس أو أساتذة أو مهندسين معينين كنتيجة لذكريات واحتكاكات شخصية أو منقولة . كما أن لدينا تطلعات رومانتيكية لأعمال مهندسين أمثال فرانك لويد رايت ولوكوربوزييه وميزفان ديروه وادوارد ستون أو المدارس كمدرسة زيورخ ومدرسة الفنون الجميلة العليا بباريس وجامعة ليفربول وغيرها من الجامعات فى أمريكا أو ألمانيا .

وصلت حالة العمارة عالميا تحت سيطرة الرومانتيكية إلى حالة لم تهبط إليها فى تاريخ التطور المعمارى . تردت العمارة فى غيبوبة الفن للفن . أغمضت العيون عن واقع المجتمع وعن المواد الإنشائية الجديدة التى غيرت وجه العالم وهى الحديد والصلب والخرسانة المسلحة وأصرت على استعمال الحجارة على أنها المادة الكلاسيكية الطبيعية النبيلة التى تظهر ما تبطن . وعندما اضطرت تحت ضغط الظروف الواقعية المحيطة لاستعمال الصلب والخرسانة غلفتها بغلاف حجرى خادع . كما أهملت بل حاربت الماكينة وما تنتجه مرتبطة رومانتيكياً بالصناعة اليدوية إلى أن اضطرت أخيراً للإعتراف بها تحت ضغط الظروف الاقتصادية الملحة . وعلى انقاض عمارة القرن التاسع عشر الغريبة من نوعها قامت العمارة المعاصرة لتعترف بالواقع وما يمكن أن يتيحه لنا من حياة أفضل وبالتالى تشكيلات فنية جديدة جميلة فى حد ذاتها . رفعت العمارة الحديثة شعار الوظيفية الذى يضع استيفاء احتياجات مستعملى المبنى المادية والمعنوية بوسائل الإنشاء الحديث كهدف أساسى ومصدر رئيسى للتشكيل المعمارى الجديد . وقد رفعت العمارة

الحديثة فى أولها شعار الدولية على أساس شيوع الوسائل الحديثة للانشاء ومعالجة الظروف الطبيعية . ثم تطور ذلك بعد التجربة العملية لتظهر تطبيقات إقليمية وتعبيرات محلية كرد فعل لشعار الدولية . من هذه التطبيقات ماكان رومانتيكيا فاندثر ومنها ما كان منطقياً أصيلا فازدهر . ومن الاتجاهات الشكلية طرز مفروضة لأسباب سياسية فى ألمانيا الهتلرية وفى إيطاليا أيام موسيليني . ومنها الطراز الكلاسيكي الذى فرض فى أول الأمر على الاتحاد السوفييتى فتأخرت عمارته رغم تقدمه الهائل فى المجالات الأخرى إلى أن تحررت من هذا القيد لتلعب دوراً طليعياً فى مجال تعاون العمارة مع الصناعة المتقدمة .

الآن وفى سعينا نحو وضع أسس لعمارة مصرية إقليمية يجب أن نبتعد على أساس من خبرة بالماضى القريب عن الرومانتيكية بكلا تطلعاتها نحو الماضى أو الحاضر البعيد ، فكلا الاتجاهين لن يصلا بنا إلى خدمة احتياجات مجتمعنا المعمارية والجمالية الجديدة . كلاهما تقليد ومحاكاة لفنون معمارية أصيلة خدمت وما زالت تخدم أهلها بنجاح تحت ظروف خاصة بعيدة فى هيكلها ومضمونها وتفصيلاتها عن ظروف مجتمعنا الحالية . ذلك المجتمع الذى يتطلب مبانى لم يكن أغلبها موجود أو معروف منذ قرن مضى،مبانى المواصلات لمحطات السكك الحديدية والمطارات والمصانع الكبيرة للصناعات الخفيفة والثقيلة ومبانى الخدمات العامة من محطات كهرباء وبريد وبوليس ومكتبات ومتاحف ومستشفيات . أغلب هذه المبانى من نتاج القرنين التاسع عشر والعشرين وهى فى عملها تتطلب مبانى على درجة عالية من الكفاءة فى التوزيع والعمل قبل كونها ذات صلة بالتراث القديم . وهى فى عددها وتوزيعها تتطلب إنشاء على درجة عالية من الكفاءة والاقتصاد مع سرعة فى التنفيذ . لقد خطط مجتمعنا لإنشاء السد العالى فى سبع سنوات فى حين بنيت كتدرائية ميلانو فى حوالى ستمائة عام . نحن الآن فى صراع مع الزمن ولا يمكننا أن ننفق من الوقت والمال على مبنى عام ما أنفق منه على معبد الكرنك أو مسجد السلطان حسن . كما لا يمكننا أن نقلد أى منهما فى أشكاله أو زخارفه . سوف يهوى أى تقليد سريع رخيص لهذه الأعمال العظيمة الخالدة إلى مهاوى الفشل الانتفاعى والإنشائى والجمالى . لتكن عمارتنا نابعة من واقعنا الحاضر الذى يفخر بالتراث الماضى لا ليقلد أشكاله كالقردة بل ليدرس تجاربه ويكتسب منها مبادىء حلول للتطبيق الواعى الخلاق .

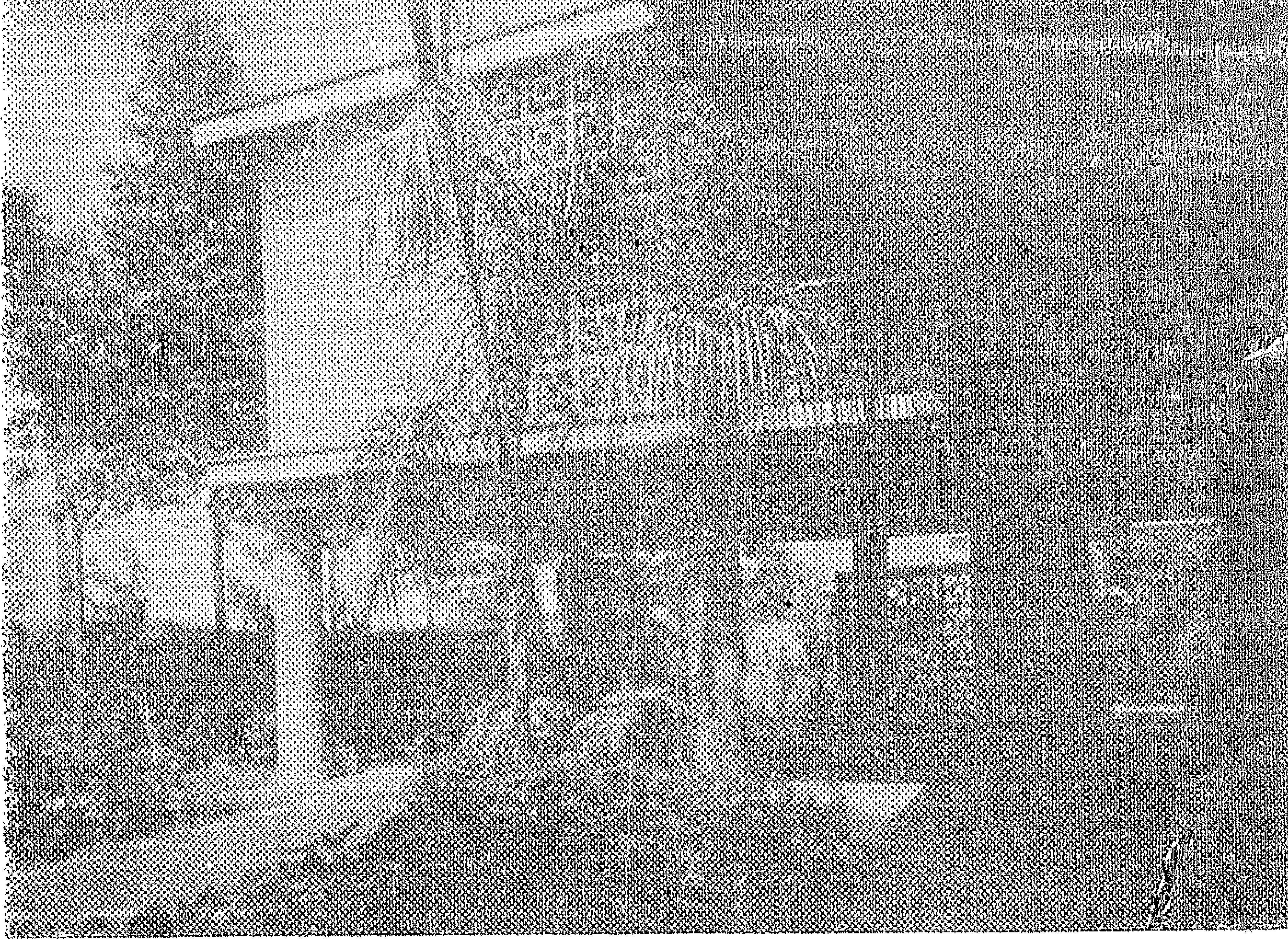
* * *

دور العمارة المصرية فى خلق عمارة حديثة ومدى صلتها بالتراث القديم :

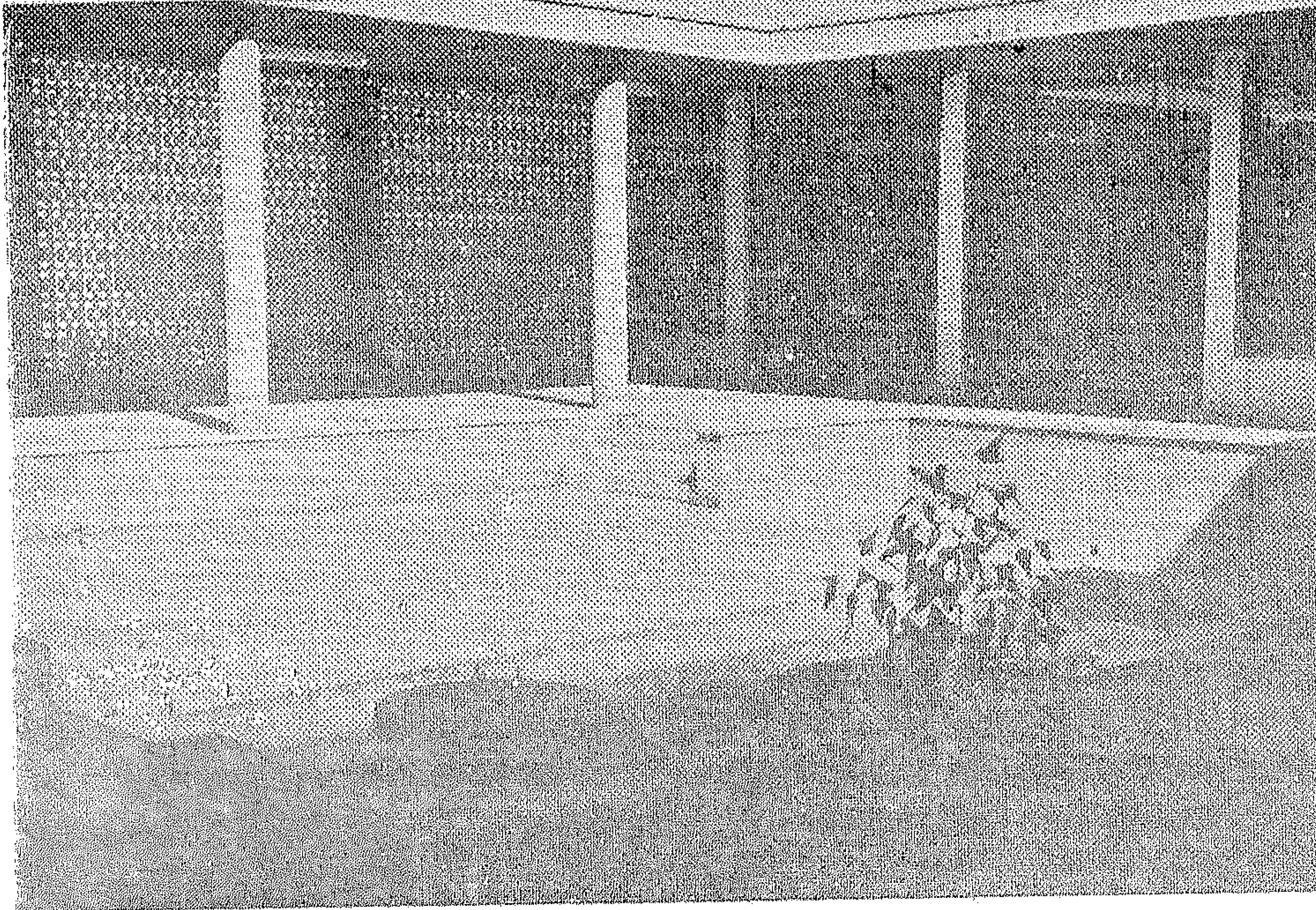
يجدر بنا أن نؤكد أن خلق الطابع المعمارى الإقليمى لا يكون من عمل فرد عبقرى أو جماعة أو لجنة دراسية باحثة أو ندوة معمارية وإنما هو تطوير اجتماعى فنى لأجيال متعاقبة واعية بمسئوليتها واثقة من طريقها حساسة للظروف المحيطة بها . وواجب العمارة المصرية نحو هذا الهدف هو الدراسة الجدية بامكانياتها العلمية والفنية لظروف العالم العربى لمحاولة الوصول إلى حلول تجمعها فيما تشترك فيه ظروف متشابهة مع مرونة كافية لمقابلة التباين المحلى فى القطر الواحد أو بين قطر وآخر .

والآن هل ستكون العمارة الحديثة المبنية على الدراسة المنطقية للحياة العربية واحتياجاتها وإمكانياتها نشاذاً من تراثنا المعمارى القائم بيننا فى مدننا وقرانا ؟ وهل سيفرض علينا تفادى هذا النشاز وعدم التوافق تضحيات لتقريب الهوة بين الجديد والقديم ؟ نحن نؤكد أنه لاحاجة لمثل هذه التضحيات ولا حاجة لتوجيهات شكلية متعمدة حيث أن الصلة الفنية بين القديم والحديث متوفرة طالما أن الاثنين تعبيران سليمان عن حياة متطورة فى مكان واحد ومستمدة من ظروف وإمكانيات طبيعية واحدة . الدراسة المنطقية السليمة للظروف المحلية بكامل صورها والتى سنورد عرضاً سريعاً لمعالمها سوف تؤدى دون أدنى شك إلى عمارة متطورة ولكنها متآلفة مع سوابقها ومع ما تحيط بها من تشكيلات معمارية ناجحة .

الحياة الاجتماعية الجديدة هى أهم هذه المعالم الهادية للمعمارى الحديث -- الحياة الاشتراكية بما تكفله من حق السكن والطعام والتعليم والعمل والعلاج والترفيه بكافة صوره . وهنا نجد أن توفير المسكن الصحى الاقتصادى لكافة الأسر هو الهدف الأساسى للمخطط المعمارى — هذا يتطلب إعادة تقدير لعاداتنا السكنية لمحاولة تطويرها بما يتناسب مع الحياة الجديدة مع المحافظة على طابعنا وحياتنا العربية الشرقية . هذان الشقان لهدف واحد سيطوران أحياءنا السكنية مع الاحتفاظ بالشخصية الشرقية العربية ، لدينا أسر حديثة التكوين تشغل وحدات سكنية ذات عدة حجرات غير مستعملة مراعاة لمظاهر بالية . هذا أمر غير مقبول اقتصادياً يجب أن تتجه دراساتنا إلى الاقتصاد فى المسطحات مع الزيادة فى الانتفاع . كما لم يعد هناك مجال لترك الحلول الإسكانية فى يد ملاك أفراد هدفهم الربح المادى دون تخطيط أو تنسيق فى عدد الوحدات وتصميماتها وعدد حجراتها . يجب أن تتدخل الجمعيات التعاونية والهيئات والشركات بصورة أوضح لإنشاء أحياء سكنية متكاملة مع خدماتها وملحقاتها من مدارس ومحلات تجارية ونوادى وحدائق ومتنزهات وغيرها من الخدمات العامة مع المحافظة على طابع حياتنا الشرقية فى التخطيط العام وفى الوحدات السكنية بتفاصيلها . فمازالت حياتنا ذات طابع مترابط متماسك . الأسر المتجاورة تميل إلى الانتماء إلى بعضها فى مجموعات متحابة متعاونة تشترك فى أفراحها وأحزانها ومشاكلها اليومية . هذه ميزة لمجتمعنا يجب تأكيدها وتشجيعها ، ومع ذلك فما تحقق من المجموعات السكنية لا يشجع مثل هذه الروابط . بلوكات متراصة متوازية كالجنود فى طابور عسكرى تتجه كل منها بواجهتها الخلفية إلى زميلتها . والنتيجة شكوى نفسية اجتماعية عامة بين السكان الجدد لهذه المشروعات . كل منهم يتمنى أن يعود إلى حيه القديم حيث يشعر بالانتماء إلى مجموعة ولو حتى على حساب راحته المادية . يجب الاتجاه بتصميماتنا نحو تشجيع هذه الروح الجماعية بتنسيق البلوكات السكنية فى مجموعات حول حديقة داخلية للعب الأطفال وللاجتماعات بين سكان المجموعة المحيطة هذا مع تأكيد طابع حياتنا الشرقية المحافظة . فما زالت حرمات أسرنا مصونة عن أعين المارة الغرباء ومع ذلك فقد اتجهت تصميماتنا الحديثة المنقولة نحو كشف شرفاتنا على الشوارع مباشرة بسور من الحديد المفتوح . كما كشفت حجراتنا بفتحاتها الكبيرة على الطرق العامة الضيقة بطريقة استعراضية . مثل هذه الشرفات



(شكل ١) فيلا المهندس فؤاد شلبي
المهندسان المعماريان د. على رأفت ، د. عبد الرحمن مخلوف

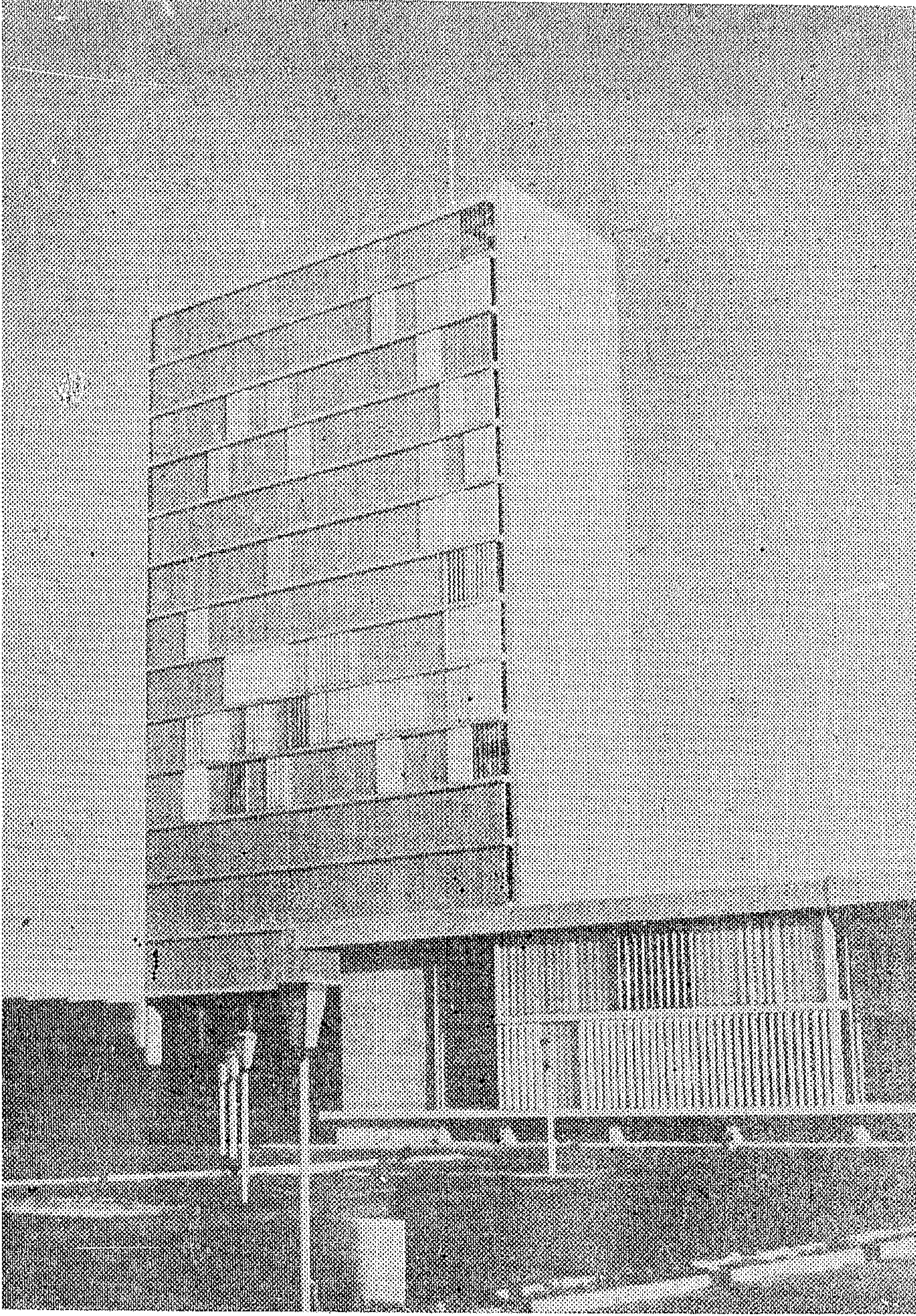


(شكل ٢) المركز القومى للبحوث الاجتماعية والجنائية
المهندس المعمارى الدكتور على رأفت

المكشوفة تظل حالياً بلا استعمال والفتحات الكبيرة تظل مغطاة بالستائر طول الوقت منعاً للحرارة وأنظار الغرباء . هذه الاتجاهات الاستعراضية فيها تعبير يتناقض مع حياتنا وتقاليدنا مع تراثنا المعمارى ذو الفتحات الخارجية الصغيرة أو المعدومة والفتحات الداخلية الواسعة وذو الشرفات المغطاة بساتر يجعلها أوسع استعمالا وألطف جواً .

وتأكيداً لمؤسساتنا وتقاليدنا الروحية والاجتماعية يجب أن يكون للمساجد وأمكنة العبادة منزلتها ومكانتها وبالتالى وضعها المميز فى تخطيط الأحياء القروية والحضرية . كما يجب أن نؤكد ونطور مؤسسات اجتماعية ظهرت فى الريف كنواة للتخطيط الجديد للقرية كالأسواق المكشوفة والمغطاة والساحات الشعبية والدواوير كأمكنة للاجتماع والمناقشة ومسارح خيال الظل والأراجوز فى الهواء الطلق وقهاوى فى الحدائق الداخلية المظللة والحمامات الشعبية . يجب المحافظة على هذه المؤسسات وتطويرها طالما لم تظهر حاجة لتغييرها وفى هذا استمرار وتطور طبيعى لطراز معمارى قائم .

الصلة الفنية الشكلية المطلوبة بين التراث القديم والحاضر ستتواجد تلقائياً إذا ما روعيت ظروف المناخ المحلى . هذه الظروف التى لم تتغير من آلاف السنين . فمناخنا فى الجمهورية العربية المتحدة الحار الجاف صيفاً والمعتدل الممطر شتاء هو المناخ الذى بنى فيه مهندسو رمسيس الثانى معبد الكرنك ومهندسو عمرو بن العاص جامعه المشهور واستمر إلى يومنا هذا . صحيح أن لدينا الآن وسائل ميكانيكية للتحكم فى ظروف المعيشة الداخلية لكنها ما زالت وستظل باهظة التكاليف الأساسية والمستمرة . فما زلنا وما زال العالم معتمداً على الوسائل التى اعتمد عليها أسلافنا فى حل مشاكل الصيف القائظ . يجب أن نعود إلى استعمال وتطوير هذه الوسائل الطبيعية فى التصميم من حدائق داخلية ومفارج يلتف حولها المنزل (شكل ١) أو المبنى العام (شكل ٢) فتمنحه مصدراً مظللا بارداً للهواء ومكاناً للمعيشة الخارجية وفى هذه الحدائق الداخلية تقام البرجولات والتكعيبات وتزرع الأشجار والحشائش المحاطة بالمياه وكل ما من شأنه أن يلطف الجو الداخلى . يجب أن نختفى من واجهاتنا الفتحات الزجاجية الواسعة وخاصة على الواجهات الشرقية والغربية والقبلية والتى استعملناها فى الكويت وبغداد وأسوان وأسيوط والقاهرة فأخرجت فراغات غير مريحة وواجهات غريبة علينا منافية للطابع العام . على العكس من ذلك فإن جونا فى مصر وفى أغلب مناطق الشرق العربى يتطلب فتحات صغيرة مظللة بالبواكى وكاسرات الشمس الرأسية (شكل ٣) أو الأفقية إلا إذا أشرفت الفتحات على حدائق داخلية أو مناظر جميلة تستدعى تكبيرها . كما يتطلب المناخ الحار استعمال السقيفات والبرجولات فوق الأسطح النهائية لتلطيف حرارة الشمس على الأدوار العليا . كما يجب مراعاة استقبال أكبر كمية من الهواء البارد بفتحات متقابلة تسحب هواء مظللا . ورفع المبانى على أعمدة تبعد عنها حرارة الأرض وتهىء مكاناً بارداً للمعيشة الخارجية تحت المبانى (شكل ٤) . هذا وقد أهملنا حديثاً الشراعات فوق



(شكل ٣) مقر الإذاعة السعودية — جدة
المهندسان المعماريان د. على رأفت ، د. عادل القطان

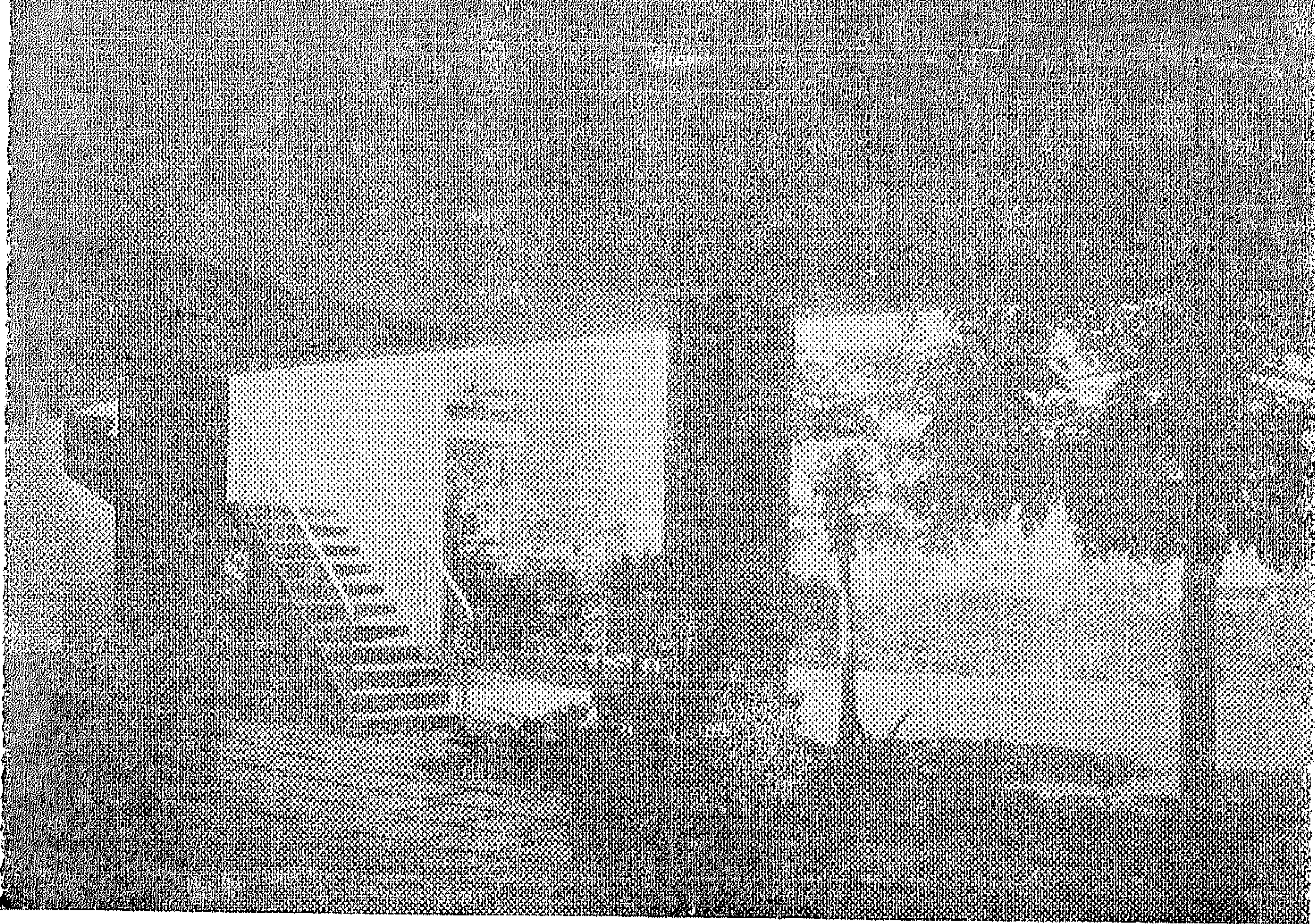
النوافذ والأبواب والفتحات العليا فى الحجرات سعياً وراء التقليد مع كونها على قدر كبير من الأهمية فى سحب الهواء من الحجرات وإليها . جميع هذه الوسائل الطبيعية فى التصميم ذات فائدة فى تخفيف الأحمال الحرارية فى الفراغات المكيفة صناعياً علاوة على تأكيدها لطابع الإقليم ودورها فى وصل الحديث بالقديم .

هذا ولا يكتمل اتجاه معمارى بدون اهتمام بطريقة الإنشاء فهى العامل الأساسى فى التشكيل الحديث . والمجهودات المصرية سواء أكانت فى الجامعات ومعاهد بحوث البناء يجب أن تتجه إلى دراسة جدية نحو تطوير مواد الإنشاء التقليدية المتوفرة محلياً فى العالم العربى وكذلك مواد الإنشاء الحديثة مع دراسة طرق عمالتها وإمكانيات تصنيعها فى ظروف تطورنا الصناعى وأوضاعنا الاقتصادية العربية . هنا سيكون المجال مفتوحاً أمام المجهودات الفنية المصرية الحديثة لتلعب دوراً بناءاً فى تطوير العمارة العربية بوجه عام .

فى القرى المصرية مثلا لا تتوفر المواد وطرق الإنشاء الحديثة وتكون طرق الإنشاء التقليدية المتوفرة الاقتصادية هى الأنسب والأفضل ويكون إهمالها أمراً غير مقبول منطقياً وإنشائياً ، واستعمالاتها بعد تطويرها علمياً ستكون أليفة وذات صلة طبيعية ومنطقية بالواقع ومبانيه القائمة التقليدية . فالبناء بالطوب النى بعد تحسينه وتطويره بإضافة الأسمنت أو الجير ليكتسب قوة والأسفلت ليكتسب مناعة ضد المياه اتجاه طبيعى ومنطقى فى الريف المصرى (شكل ٥) والمعمارى لا يسعه إلا استعماله فى حوائط سميكة ذات فتحات صغيرة وبأسقف معقودة أو مستوية باستعمال البامبو مع خليط الطين والأسمنت . كما يمكنه أن يكون من تجميعات الطوب والفراغات حوائط مفتوحة للأسوار والدراوى دون حاجة لاستيراد مواد غريبة ومكلفة . وما يقال بالنسبة للطوب يقال بالنسبة للمبانى الحجرية ، فالحجارة متوفرة فى أغلب بقاع الجمهورية وفى أغلب مناطق الشرق العربى وقد أهملناها تقليداً لمرحلة زالت من العمارة الدولية الحديثة ، هذه المرحلة اتجهت بها إلى استعمال البياض والزجاج ثم تحررت العمارة من هذا القيد الشكلى البحت . وما زلنا نقوم بإنشاء الحوائط والهياكل من الطوب والخرسانة وتغطى الجميع من الخارج والداخل بقشرة رقيقة ضعيفة من البياض لا تتحمل الشمس ولا الرياح ولا الأتربة ، وسرعان ما تشقق وتتسخ وتضعف ألوانها . أهملنا بهذا النوع من المبانى الإنشاء الحجرى الذى يصلح اقتصادياً بعد إدخال الماكينات فى تقطيعه وصقله — كمادة إنشائية فى المبانى ذات الارتفاعات المحدودة ، ستظهر باستعماله عمارة ذات أسطح مصقولة قوية تتحمل عوامل الجو المختلفة غنية بالألوان الطبيعية ، عمارة ذات صلة طبيعية بعمارة الماضى حين كان الحجر مادة الإنشاء الوحيدة ، عمارة محلية فى طابعها عالية فى أهميتها .

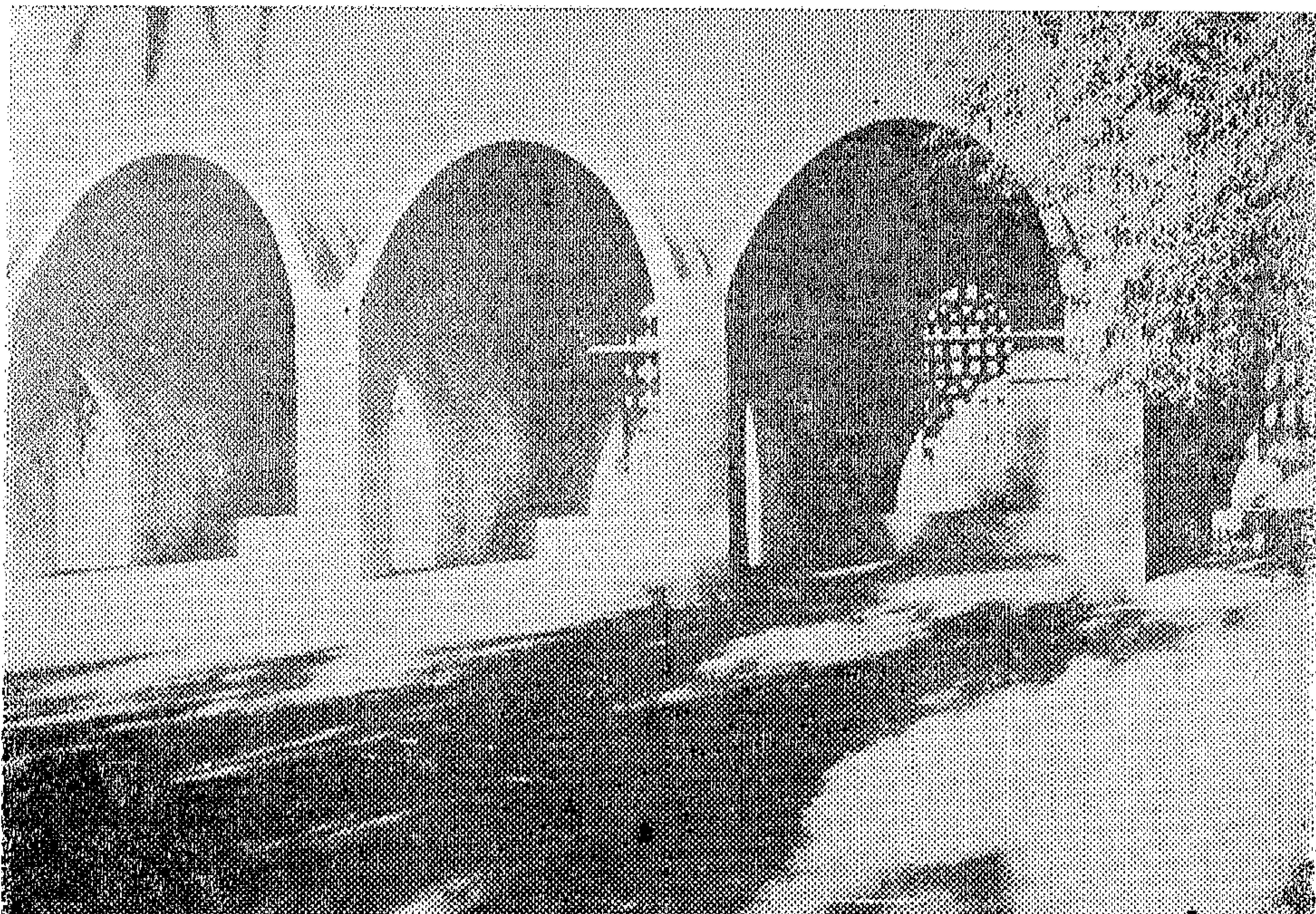
كما أن هناك من المواد المصنعة ما يجدر بنا أن نطوره كمواد قوية جميلة بديلة للبياض الخارجى والداخلى . من هذه المواد طوب الواجهات بألوانه المتعددة والطوب المزجج الملون، والبلاطات الفخارية والسيراميكة بأنواعها المختلفة . جميع هذه المواد على درجة عالية من القوة والتحمل، سهلة الصيانة . غنية بامكانيات اللون والزخرفة .

ومن الواجب أن تتجه مجهوداتنا المصرية المعمارية نحو تطوير الإستعمال المعمارى للخرسانة المسلحة فهى المادة الإنشائية الحديثة المنتشرة فى أغلب بقاع العالم العربى . فموادها الخام متوفرة



(شكل ٤) فيلا اللواء محمود الدباغى — الدقى

المهندس المعمارى د. على رأفت



(شكل ٥) مبنى السوق — قرية الحرية

المهندس المعمارى حسن فتحى

والعمال والمهندسون المصريون منتشرون في أغلب بقاع العالم العربي يعملون في نشرها وفي زيادة الوعي الإنشائي المحلي بها. إلا أن إستعمالها ما زال بدائياً من ناحية المواد والعمالة وعلينا الآن تطوير البحوث الجدية نحو تصنيعها في وحدات جاهزة أو نصف جاهزة لمقابلة إحتياجات متزايدة للفراغات السكنية المتكررة في تصميمات تتناسب مع حياتنا الإجتماعية وظروفنا الإقتصادية ولا زلنا حتى الآن نعاملها كمادة غير جديرة بالكشف مما يشجعنا على إساءة انتاجها إعتماداً على قشرات البياض التي تسوي ما أفسدته العمالة الرديئة والشدات غير المستوية. علينا أن نقوم بمحاولات جدية للاستعمال المكشوف للخرسانة المسلحة كسطح خارجي قوي ذو إمكانيات فنية تعبيرية هائلة من ناحية الملمس واللون والشكل. وهي بهذه الإمكانيات البلاستيكية ستغنينا عن استعمال قشرات البياض وستكون مجالات للتعبير المحلي. ويمكن التصرف في قوالبها لتأخذ أشكالا زخرفية متكررة مستوحاة من الزخارف العربية المصبوبة (الأرابسك) وقد أتاحت الخرسانة المسلحة فرصاً واسعة أمام مهندسي البرازيل والمكسيك واليابان للوصول إلى تشكيلات وأسطح إقتصادية جميلة وما أجدرنا أن نستغلها على النطاق العربي كوسيلة بلا حدود للتعبير المحلي الخلاق.

وأخيراً أمامنا طاقات محلية هائلة للتعبير العربي ما زالت بعيدة عن مجال التطور المعماري. هذه هي إمكانيات الفنون التطبيقية والرفيعة. والعمارة كأم الفنون كانت دائماً ولا تزال ميداناً رحباً للعرض الحي للفنون المختلفة قريباً من الإنسان منذ طفولته إلى كهولته. وهي ميدان هام للتثقيف والمتعة الفنية للشعب. فالمجموعات السكنية ذات المباني المتكررة الجرداء وذات الشوارع والميادين القفراء والمدارس الخالية من التعبيرات الفنية تقتل أي إحساس فني لدى الأطفال والبالغين. وقد اهتمت الدول المتقدمة إهتماماً خاصاً بالمدارس والأحياء السكنية والمباني العامة فاشترطت نسباً معينة من الانفاق على الأعمال الفنية البحتة. وخرجت الأعمال الفنية من المعارض والمتاحف لتعرض في محطات السكك الحديدية والمترو والمطارات. وفي هذا تشجيع لشباب الفنانين وزيادة لمتعة الجمهور بالمبني وبالحياة عامة عن طريق تذوقهم للفن ووسيلة لإعطاء الطابع المحلي للفراغات المعمارية. وهنا يكون المجال مفتوحاً للتعبير الفني المتأثر بالتراث المصري والعربي بطريقة غير معطلة للانتفاع المعماري للفراغ بل مساعدة ومكملة له.. الأعمال المعدنية بالنحاس المطروق والمصدف لصور من الحياة المحلية.. أعمال الخرط والنحت الخشبي.. أعمال السيراميك والفخار والزجاج الملون المعشق بالجبس والقيشاني الملون.. عمال السجاد والأكلمة والنسيج وغيرها من المهارات العربية.. جميعها يجب أن تتعاون مع العمارة في تكوين أسطح داخلية وخارجية وقواطيع وبانوهات على درجة عالية من الظل والنور واللون والتعبير. مثل هذه الصناعات توارثناها أباً عن جد خلال حضارات متعاقبة وتكونت منها مدارس واتجاهات وكفاءات قل أن نجد لها منافساً في العالم أجمع. وما يقال عن الفنون التطبيقية يقال عن الفنون الجميلة من نحت وتصوير بموادها التعبيرية المختلفة.

مثل هذه الفنون يجب أن تتجه جميعها لتأكيد الانتفاع المعمارى فى المداخل والصالات والردهات والطرقات والقاعات العامة وفى المفارج والحدائق والميادين بالإضافة إلى دورها فى التعبير المحلى وإيجاد الصلة بين الحديث والقديم . ويعتبر إهمال هذه الكفاءات المحلية لأسباب اقتصادية خطأ انتفاعياً ومنطقياً وضياعاً لفرصة فنية لا تعوض .

الدور الذى يمكن أن تقوم به العمارة المصرية الحديثة نحو خلق تعبير معمارى عربى عام كبير لن يتحقق بالتطلع الرومانتيكى إلى الماضى لمحاولة بعث التراث العربى القديم أو بالنقل الرومانتيكى لعمارات معاصرة غريبة علينا ، ولكن بدراسة واقعنا الاجتماعى وظروفنا الطبيعية وبتطوير إمكانياتنا الإنشائية التقليدية والمستحدثة وباستغلال الإمكانيات المحلية الغير محدودة فى الفنون التطبيقية والجميلة . ولن يتحقق ذلك فى جيل واحد بل فى أجيال جادة متعاقبة . وبسيرنا الجدى على هذا الطريق السليم نكون قد قمنا بواجبنا نحو خلق عمارة عربية على أسس منطقية وفنية سليمة .

مشاكل النقل البرى "بالسيارات" للركاب بين المدن وفي الريف في الدول النامية مع تركيز خاص على تجربة الجمهورية العربية المتحدة

دراسة من إعداد السيد / المهندس سمير فهمى
رئيس مجلس إدارة
شركة النيل العامة لأوتوبيس شرق الدلتا

(٢)

شركة أتوبيس شرق الدلتا تمثل واحدة من أربع شركات رئيسية تعمل تحت رقابة المؤسسة العامة لنقل الركاب بين المدينة والمناطق الريفية . وهى مؤسسة القطاع العام الوطنى التى أنشئت عقب تأميم قطاع نقل الركاب فى الجمهورية العربية المتحدة عام ١٩٦٢ .

وكما يتضح من اسم هذه الشركة فهى مسئولة عن تيسير أوتوبيسات ركاب فى المنطقة الجغرافية التى تقع فى شرق الدلتا والتى تغطى شبكة الطرق فى ثمانى محافظات هى السويس وبور سعيد والإسماعيلية ودمياط والدقهلية والشرقية والقليوبية وسيناء ، وذلك بخلاف طرق المدينة التى تربط المناطق الريفية فى هذه المحافظات بمدينة القاهرة .

وقد أنشئت الشركة بعد التأميم عن طريق إدماج ثلاث شركات مساهمة رئيسية لنقل الركاب هى شركة المنيا والبحيرة وشركة الشرقية وشركة الدقهلية ، مضافاً إليها ست شركات خاصة صغيرة أخرى كانت تعمل أيضاً فى محيط نقل الركاب ومن ضمن المشاكل الرئيسية التى واجهت إدارة هذه الشركة الجديدة بعد إدماجها ازدواج الطرق والخطوط وتداخلها فى بعضها البعض بطريقة غير اقتصادية تتميز بالإسراف فى المسافات ضمن عدد من المشاكل الفنية والتجارية الأخرى .

وقد أدت المجهودات المتصلة التى بذلتها الإدارة منذ عام ١٩٦٤ إلى التغلب على هذا الوضع غير المرضى بينما كان من غير المعقول القيام بتحليل كامل شامل فى المراحل الأولية لعدم وجود إحصائيات دقيقة بالقدر الكافى .

وقرب نهاية سنة ١٩٦٨ وعقب القيام بعملية موضوعية شاملة لإعادة تنظيم السجلات الإحصائية للشركة ، قامت الشركة بإعداد بحث دراسى شامل لشبكة الطرق ، وقد قاد هذا البحث الدراسى إلى نتائج هامة .

والغرض من هذا البحث هو إيضاح نتائج المرحلتين الأوليتين لذلك البحث الدراسى الذى يجرى حالياً تدعيمه ببحثين يقوم بإعدادها معهد التخطيط القومى .

هذا وتقدم الشركة جزيل شكرها وامتنانها للمساعدة التى قدمها لها مركز التقديرات الحسابية التابع لمعهد التخطيط القومى فقد كان لهذه المساعدة الأثر الكبير فى صياغة نماذج

التحليل وفى عملية تنسيق المعلومات التى قدمتها الشركة .

هذا وقد أخذت الاعتبارات الآتية عند إعداد هذا البحث الدراسى :

أولا : تختلف الخطوط اختلافاً كبيراً من حيث الطول والدرجة (لوكس — اكبريس — عادى) .

ثانيا : كذلك تختلف الخطوط من حيث درجة بنائها وحالتها (فمنها ما بنى بنوع فاخر من الأسفلت ومنها ما بنى بأسفلت عادى ومنها غير المسفلت) .

ثالثا : وتختلف أيضاً الأوتوبيسات التى تسير على هذه الخطوط اختلافاً كبيراً من حيث صناعتها وحمولتها وعمرها .

رابعا : يختلف الطلب على الخطوط من فرع لآخر بل وأيضاً من مسار لآخر فى نفس الفرع . كذلك يختلف الطلب على المسار الواحد من وقت لآخر (الطلب الموسمى) مما يعطى نموذج غريب وغير مفهوم . وقد لوحظت بعض الاعتبارات الهامة فى هذا الصدد .

وبالنظر للأسباب السالفة فقد أوصى المختصون أن يقوم البحث الدراسى على أساس التحليلات المرتبطة بالنقط الآتية :

أولا : طلب الركاب على المسارات فى كل فرع على حدة شهراً بعد شهر على مدار العام .

ومن الطبيعى أن يختلف هذا الطلب من شهر إلى آخر وكان الغرض من ذلك إعادة توزيع الحمولة الإضافية للاتوبيسات التى تسير فى بعض الفروع أثناء الفترة التى يقل فيها الطلب بغرض تشغيلها فى فروع أخرى مما يصل الطلب فيها إلى الذروة فى نفس الفترة .

ثانيا : تعميم البحث بحيث يصبح على مستوى الشركة ككل بدلا من أن يخص كل فرع وذلك لإعادة توزيع بعض الخطوط على فروع أخرى للوصول إلى موازنة بالنسبة للطلب فى مختلف فروع الشركة آخذين فى الاعتبار الأيدى العاملة المتاحة والعمال الذين لا يجوز نقلهم إلى فروع أخرى وكذلك التسهيلات التى لا يمكن تغييرها فى المدى القريب .

ثالثا : جرى ضبط الفترة التى تمر بين وصول الأوتوبيسات التى تعمل على كل خط للاستفادة من هذه النتائج فى محيط التفتيش وخطط الصيانة الوقائية وذلك لتفادى عدم التفتيش المنتظم ولتفادى عدم إجراء الصيانة الدورية المنتظمة ولتفادى توقف التفتيش والصيانة وذلك لضمان الحد الأقصى فى كفاءة التشغيل .

رابعاً : إعادة توزيع الأوتوبيسات التى تسير على مختلف الخطوط بناء على دراسات اقتصادية بنيت على نوع الأتوبيس وعمره وعدد مقاعده .

وبالنسبة للطبيعة المتغيرة لمختلف الخطوط فقد كان من الضرورى اتباع برنامج حسابى مبنى على تفصيلات ومعلومات دقيقة .

دراسة شبكة المناطق القروية :

ولما كانت الشركة — وهى جزء من الشركات التى تقدم خدماتها فى محيط نقل الركاب تعمل على إرضاء الجمهور ومقابلة ما يتطلبه واحتياجاته ، فقد رؤى أن هدف خدمتها « أثناء عملية التخطيط الطولى » هو مقابلة الطلب لخدمة الركاب فى كافة الحالات .

وتختلف الطريقة التى اتبعت فى هذا المجال اختلافاً كبيراً عن الطرق التقليدية التى غالباً ما يتركز غرضها على الحصول على أعلى نسبة من الأرباح . لذلك ظهرت الحاجة إلى اتباع نماذج حسابية جديدة تتمشى مع هذه الطريقة الجديدة .

والملخص الآتى يوضح النماذج التى اتبعت فى إجراء الدراستين الأوليتين .

مقدمة للنموذج الحسابى :

بالنسبة لتعقيد النموذج العام فقد رأينا أنه من الضرورى تقديم الإيضاح الآتى :

يتكون النموذج من ثلاث مراحل هى :

١ — المرحلة الإجرائية الأولى .

٢ — المرحلة الثانية .

٣ — فترة الركود التي يقل فيها إقبال الركاب .

وقد احتجنا إلى الاصطلاحات الآتية لشرح هذه المراحل

P. الرحلة .

K.P. طول الرحلة بالكيلو مترات .

C.P. عدد العربات « الأتوبيسات » المخصصة لكل رحلة .

سعة العربة .

R.P. عدد الأدوار يومياً لكل رحلة

N.P. الطلب الشهرى « عدد الركاب » لكل رحلة

D.P. طلب الركاب اليومى بالكيلومترات

S.P. عرض الركاب اليومى بالكيلومترات

D. مجموع الطلب

S. مجموع العرض

N. المجموع الكلى للعربات «الأوتوبيسات» المتاحة

M. عدد المسارات المأخوذة فى الاعتبار .

K. الحد الأعلى للمسافة التى يسافرها الأوتوبيس يومياً .

هذا ويمكن تطبيق الثلاث مراحل شهرياً كالآتى :

الصف : المرحلة الأولى « المرحلة الإجرائية الأولية »

أولا : احتساب الطلب الكلى على مســـار واحد مستخدمين وحدة ركاب « س » (X) كيلو مترية .

ومن ثم احتساب الطلب على كل المسارات والفروع كما يلى :

$$ND = \frac{\Sigma\ p^N\ p^K}{1}\ \frac{1}{30 \times 2k}\ \Sigma_P\ p^N\ p^K$$

معلومات أساسية

أسطول الشركة	٩٥٦
متوسط المقاعد	تتراوح بين ٣٠ ، ٤٤
مجموع المقاعد	٣٧٤٠٠

عدد خطوط الشبكة ٢٢٩ (بخلاف خدمة الأتوبيسات الريفية بداخل المدن) .

طول شبكة المواصلات بين

المدينة والمناطق الريفية	١٤٨٠٠ كيلو متر
متوسط عمر العربة	٥ سنوات وشهران
عدد الفروع	١٢ فرعاً

الرمز + N يمثل عدد عربات الأوتوبيس المتاحة لكل فرع من الفروع وتوجد هنا ثلاثة احتمالات :

(ا) أن يكون الرمز + N أقل من N

(ب) أن يكون الرمز + N مساو N

(ﺣ) أن يكون الرمز + N أكبر من N

وبذلك تنتهى المرحلة الأولى .

(ب) المرحلة الثانية (<u>المرحلة الثانوية</u>) :

وتأسيساً على الحالات الثلاث (أ، ب ، ﺣ) التى اشتقت فيما تقدم من مرحلة الإمكانية الأولية ، تكون معالجة المرحلة الثانية أو إنتاجها كالآتى :

• إذا ما كان إنتاج المرحلة الأولى يمثل الحالة (ا) فإنه يختلف عنه اختلافاً كبيراً (وتفاصيل مثل هذا النموذج لا تدخل فى نطاق هذا التقرير) .

• وإذا كان انتاج المرحلة يماثل الحالة (ب) فإنه يتعين استخدام نموذج فاصل محدد .

• وإذا كان الإنتاج يماثل (ج) فعلينا أن نستخدم نموذجاً ثالثاً يهدف إلى تلبية مطالب الخطوط المختلفة وفقاً لأولويات تحددتهما لأهمية تلك الخطوط بالنسبة للطلب عليها

وهكذا تنتهى المرحلة الثانية .

٢ — المرحلة الثالثة (<u>مرحلة التراخى</u>)

وجدت هذه المرحلة من الضرورة بمكان من وجهة النظر الحسابية البحتة ولتحديد المبررات المتصلة بالحد الأمثل للكفاية الإنتاجية ؛ وهى إلى ذلك تتيح لنا سعة إضافية تتمثل فى عدد الرحلات على كل خط، ويمكن الإفادة بها وقت بلوغ الحركة ، لذروتها أو كلما اشتد الطلب .

وباستكمال المرحلة الثالثة ينتهى برنامج تخصيص سيارات الأوتوبيس للفروع المختلفة ويتاح الحصول على النتائج النهائية .

خطوات التقرير باستخدام النموذج الحسابى .

(ا) الدراسة الأولى :

• يدرس كل من فروع الشركة الاثنى عشر على حدة

• تعمل التقريرات « باستخدام المراحل الثلاثة المبينة بعاليه » عن كل شهر على حده لمدة اثنى عشر شهراً متصلا تبدأ فى يوليو سنة ١٩٦٧ وتنتهى فى يونيو سنة ١٩٦٨ .

• تفترض ثلاثة افتراضات عن السعة المحددة للعربة أو الأوتوبيس .

(ا) السعة العادية المحددة ٥٠ راكباً

(ب) السعة المتجاوزة المجموع ٧٥ راكباً

(ح) زيادة المجموع زيادة مفرطة أو خطرة ١٠٠ راكباً

كما تؤخذ الافتراضات الآتية فى الحسبان :

(ا) فى الخطوط الفاخرة والسريعة تحدد السعات بـ ٦٠٪ فقط من الأرقام السابقة ويقطع الركاب كامل مسافة الرحلة « ا » بالكيلومترات .

(ب) يتم تحميل عربات الخدمة العادية بالكيفية المبينة فيما تقدم ، ويقطع الركاب ٦٠٪ فى المتوسط من مسافة الرحلة « أ » مما يسمح بالتوقف العادى للركاب داخل العربات وخارجها فى المواقف العديدة التى تتوسط الطريق .

* كافة تقديرات الطلب مستخرجة من دفاتر الشركة الإحصائية ومن بعض الملاحظات الميدانية المادية الخاصة عن بعض الخطوط الرئيسية .

* أعيد عمل التقديرات جميعاً بافتراض زيادة مقدرة فى الطلب قدرها ١٥٪ وهى زيادة يعتقد الآن أنها فقدت نتيجة المنافسة لما يطرأ على الخدمة من توقف ولعدم كفاءة سعة النقل للأسطول الحالى .

المرحلة الثانية :

عملت التقديرات على نفس الأسس السابقة إلى حدما وذلك باستثناء التغيرات الرئيسية الآتية :

* أخذت كافة خطوط الشركة فى الاعتبار على وجه إجمالى .

صورت لكل خط سعة واحدة وأبقيت هذه السعة ثابتة لأغراض الدراسة ، وقد اختيرت هذه السعة المقررة على أساس العوامل المتصلة بالبحث بما فى ذلك طبيعة الطريق والظروف البيئية ومستوى الطريق وطوله بالكيلو مترات .

اختيرت لكل طريق مسافة قصوى معينة بالكيلو مترات تقطعها العربة يومياً .

الحاجة إلى استخدام العقل الالكترونى :

بالنظر إلى تعدد العمليات الحسابية وضخامة شبكة طرق الشركة ورغبة فى الإسراع بتلك العمليات مع توخى الدقة فى إجرائها ، فقد نشأت الحاجة إلى استخدام العقل الألكترونى للقيام بالعمليات الحسابية المطلوبة ، ولا شك أن كل من له إلمام بالوسائل الفنيـة لتشغيل العقول الالكترونية سوف يقدر الصعوبات التى تكتنف إعداد البيانات وذلك لضرورة اتباع الخطوات المتتالية الآتية :

(أ) يتعين إعداد النموذج المقرر لكل مرحلة على حدة .

(ب) وجوب مراجعة كل نموذج على حده كذلك لضمان سلامته وصلاحيته للتطبيق .

(ج) تجميع كافة النماذج أو تلخيصها لتكوين نموذج واحد متكامل .

(د) الاعتبارات المتصلة بكل دراسة قد أخذت فى الحسبان عند إعداد النموذج النهائى .

هذا وقد أعد هذا النموذج النهائى بحيث يتيح الاحتمالات الآتية :

(أ) تغيير الحمولة المقررة للعربة .

(ب) تغيير المسافة القصوى التى تقطعها السيارة فى أى يوم من الأيام والمقررة لكل طريقة .

(ج) تعديل الزيادة المئوية المتوقعة فى الطلب والتى اختيرت أصلا بنسبة ١٥٪ .

نتائج الدراسة الأولى :

١ — عدد الأوتوبيسات اللازمة بكل فرع يختلف من شهر إلى آخر وفقاً لبرنامج مناسب من شأنه أن يجعل تخصيص العربات للفروع على مدار السنة ، أمراً ميسور التنفيذ .

٢ — الافتراض القائل بأن السعة المقررة لكل سيارة يمكن أن تكون ٥٠ راكباً ، قد ثبتت عدم واقعيته، إذ وجد أن كافة السعات المقررة حسب الإحصائيات الحالية للأسطول فى مختلف الفروع تتراوح بين ٧٥ ، ٩٠ راكباً وهو وضع محفوف بالخطر وتخشى عواقبه ، وهو يدل على معدل عال لاستهلاك الوحدات وارتفاع مصروفات الصيانة بالكيلومتر المقطوع مع ما يصحب ذلك من سرعة إهلاك العربات المستخدمة على هذا الوجه .

٣ — الوضع الأخير الذى انتهى إليه البحث يمثل أنسب توزيع للعربات فيما بين الفروع فهو يسمح بسعة إضافية محتملة بالنسبة للرحلات غير المنفذة والتى يمكن ادخارها لمواجهة الظروف غير المنظورة أو لإحلالها محل العربات التى يتم سحبها لفحصها فحصاً دورياً أو لإجراء أعمال الصيانة الوقائية والفحص العام .

٤ — البيانات المتعلقة بعدد العربات التى فى الخدمة بكل فرع فى الوقت الحاضر ، إذا ما أضيفت إلى الرسوم البيانية المرفقة يتضح منها وجود ثمة علاقة بين التغيير فى عدد الركاب المنتفعين بالخدمة وعدد الأوتوبيسات العاملة على مختلف الخطوط . وفضلا عن ذلك ، منذ أوضحت هذه العلاقة عند رسمها رسماً بيانياً ، معالم مماثلة لخط بيان الطلب إلى حد ما ، وهذا يدل على أن جانباً كبيراً من تقلب الطلب يمكن نسبته إلى الخدمة غير المنتظمة أو المتصلة وذلك نتيجة حجز بعض العربات وقتاً أطول من اللازم لأعمال الصيانة ، وما تتعرض له من عطل فى الطريق .

٥ — بالرغم من ضخامة عدد الرحلات اليومية، وجد أن السعة المقررة تتراوح بين ٧٥ ، ٩٠ راكباً للاوتوبيس الواحد ، وهو يدل على وجود طلب كبير على خدمات الشركة رغم المنافسة الخارجية .

الدراسة الثانية :

• نفس البيانات المتصلة بالطلب على مختلف خطوط الشركة موضوع الدراسة الأولى ، طبقت هنا مع إدخال نظام جديد للرموز الرقمية (منها ثلاثة أرقام للطريق ورقمان للفرع) .

• قررت لكل عربة سعة واحدة لكل طريق ، وقدر طول الطريق بالكيلو مترات وعدد الركاب فى كل حالة ، ومجموع الأوتوبيسات اللازمة لأداء الخدمة داخل شبكة الطرق على مدار السنة قدر على أساس شهرى بالنسبة للشركة ككل .

• عملت التقديرات مرة أخرى بافتراض زيادة فى الطلب قدرها ١٥ ٪ إذا ما زيدت وحدات الأسطول بحيث تتسع لنسبة معينة من حركة الركاب غير المستوعبة فى الوقت الحاضر نظراً للمنافسة من جانب سيارات الأجرة والسيارات تحت الطلب ، وما ترتب عليها من خدمة مقيدة .

• يتضح من الجداول الإحصائية والرسوم البيانية المرفقة ، بعض النتائج التى تم التوصل إليها حتى الآن .

نتائج المرحلة الثانية :

١ — عدد الأوتوبيسات المطلوبة للقيام بالخدمة على الطرق المختلفة بشبكة الشركة يختلف من شهر إلى آخر .

٢ — إذا أخذت الطرق جميعها فى الاعتبار بوصفها خدمة شاملة أو متكاملة تكاملا تاماً ، وأعيد تخصيص عربات الأوتوبيس لها ، فإنه يمكن تصور تحقيق الطلب عليها بشرط

أن ترفع الكفاية الإنتاجية إلى حدها الأقصى (١٠٠ ٪) وهو ما لا يمكن تحقيقه فى ظل النظام الحالى لتخفيض السيارات للفروع .

٣ – السعة الحالية للأسطول لا يمكنها تلبية الطلب إذا افترضنا زيادة فيه قدرها ١٥ ٪ .

٤ – الخطة المقترحة للعمليات تتيح نسبة معينة من الرحلات الاحتياطية التى يمكن القيام بها وقت الطوارىء أو فى حالة سحب العربات لعطل غير منظور أو إعطال فى الطريق أو الفحص والصيانة الدورية .

٥ – كافة العربات التى تملكها الشركة يجب أن تعمل لتلبية الطلب ، فإذا كانت سعة الأسطول المستخدمة بصفة مستمرة تمثل ٨٠ ٪ منه فقط ، فلا بد أن يترتب على ذلك عجز كبير فى مواجهة الطلب .

توصيات مقدمة فى صور نتيجة الدراسة الثانية :

(ا) يتعين على الشركة أن تشرع فى بحث إعادة تخصيص الخطوط وبالتالى ، سيارات الأوتوبيس ، لمختلف الفروع وذلك وفقاً لخطة مركزية .

(ب) يجب دراسة مشروع لإعادة تخصيص السيارات على أساس شهرى ، للوصول بكافة التشغيل إلى ذروتها .

(ح) دراسة احتمال رفع سعة التشغيل للأسطول العادى الحالى إلى ١٠٠ ٪ بدلا من ٨٠ ٪ ، ويمكن تحقيق ذلك عن طريق التنسيق الوثيق مع برنامج معدل للصيانة وتجديد الوحدات .

(د) رفع كفاية الأسطول الحالى بما لا يقل عن ٤٠ ٪ لمواجهة الزيادة الإضافية فى الطلب والبالغة ١٥ ٪ التى تفقدها الشركة الآن نتيجة المنافسة ، وكذا تلبية الزيادة السنوية العادية فى خدمات نقل الركاب فى المدى القصير .

شركة سيارات شرق الدلتا
تحليل شبكة الخطوط

أجرى هذه الدراسة
الوليد الشافعى
شعبة أبحاث العمليات
معهد التخطيط القومى

تحليل للفرع رقم ٢

الحالة رقم ٣

سعة الأوتوبيسات ١٠٠
العدد المتاح من السيارات ٤٣
العدد المقدر للسيارات ٤٠

نتيجة التحليل المبدئى – استخدم تعلميات

رقم الطريق	عدد الركاب	طول الطريق	عدد الرحلات للسيارة الواحدة	عدد السيارات	العدد الأمثل للرحلات	عدد الرحلات الإضافية

التقدير المعدل لعدد السيارات : ٤٥

تحليل للفرع رقم ٢

ملخص لتحليل الفرع رقم ٢ – الطلب العادى

الشهر	رقم الحالة	العدد المتاح من السيارات	العدد المقدر للسيارات	التقدير المعدل

تحليل للفرع رقم ٦

تحليل للشهر السابع
فى حالة الطلب العادى

الحالة رقم ١ سعة الأوتوبيسات ٥٠
المدد المتاح من السيارات ١٠٢
العدد المقرر للسيارات ٨٣

نتيجة التحليل المبدىء

رقم الطريق	عدد الركاب	طول الطريق	عدد الرحلات للسيارة الواحدة	عدد السيارات	العدد الأمثل للرحلات	عدد الرحلات الإضافية

التقدير المعدل لعدد السيارات ١٠٩

تحليل للفرع رقم ٧

تحليل للشهر الخامس
فى حالة الطلب العادى

الحالة رقم ١ سعة الأوتوبيسات ٥٠
المدد المتاح من السيارات ٣٦
العدد المقدر للسيارات ٣١

نتيجة التحليل المبدئى

رقم الطريق	عدد الركاب	طول الطريق	عدد الرحلات للسيارة الواحدة	عدد السيارات	العدد الأمثل للرحلات	عدد الرحلات الإضافية

التقدير المعدل لعدد السيارات ٣٩

تحليل للفرع رقم ٧

ملخص لتحليل الفرع رقم ٧ فى حالة الطلب العادى

الشهر	رقم الحالة	السيارات المتاحة	العدد المقدر للسيارات	التقدير المعدل

تحليل للفرع رقم ١٢

تحليل عن الشهر الثانى عشر
فى حالة الطلب العادى

الحالة رقم ١ : سعة الأوتوبيسات ٥

عدد السيارات المتاحة ٧٣

العدد المقدر للسيارات ٨

نتيجة التحليل المبدئى — الحل رقم

رقم الطريق	عدد الركاب	طول الطريق	عدد الرحلات للسيارة الواحدة	عدد السيارات	العدد الأمثل للرحلات	الرحلات الإضافية

التقدير المعدل لعدد السيارات ٨١

تحليل عن الفرع رقم ١٢

ملخص تحليل الفرع رقم ١٢ فى حالة الطلب العادى

الشهر	رقم الحالة	عدد السيارات المتاحة	العدد المقدر للسيارات	التقدير المعدل

فرع الزقازيق

الطلب عند حمولة ٥٠ راكباً

الطلب عند حمولة ٧٥ راكباً

الطلب عند حمولة ١٠٠ راكباً

عدد الرحلات

الشهر

عدد السيارات

التقدير المعدل

السيارات المتاحة

فرع دمياط

الطلب عند حمولة ٥٠ راكباً

الطلب عند حمولة ٧٥ راكباً

الطلب عند حمولة ١٠٠ راكباً

عدد الرحلات

الشهر

عدد السيارات

السيارات المتاحة

التقدير المعدل

فرع القنال

الطلب عند حمولة ٥٠ راكباً

الطلب عند حمولة ٧٥ راكباً

الطلب عند حمولة ١٠٠ راكباً

عدد الرحلات

الشهر

التقدير المعدل

السيارات المتاحة

تحليل عن الشهر الرابع

فى حالة الطلب العادى

عدد السيارات المتاحة ٩٦٤

العدد المقدر للسيارات ٤

نتيجة التحليل المبدئى

رقم الطريق	طول الطريق	سعة السيارة	العدد الاقصى للكيلو مترات	عدد الركاب	عدد الرحلات للسيارة	عدد السيارات	العدد الأمثل للرحلات	الرحلات الإضافية

التقدير المعدل لعدد السيارات ٧٥٣

ملخص تحليل شبكة الخطوط — الطلب العادى

الشهر	السيارات المتاحة	عدد السيارات التقديرى	التقدير المعدل

تحليل عن الشهر السادس

حالة الطلب الافتراضى

عدد السيارات المتاحة ٩٦٤

عدد السيارات التقديرى ٦

نتيجة التحليل المبدئى

رقم الطريق	طول الطريق	سعة السيارة	العدد الأقصى للكيلو مترات	عدد الركاب	عدد الرحلات للسيارة	عدد السيارات	العدد الأمثل للرحلات	الرحلات الإضافية

التقدير المعدل لعدد السيارات : ١١٥٩

ملخص تحليل شبكة الخطوط

الشهر	السيارات المتاحة	عدد السيارات التقديرى	التقدير المعدل

ملخص تحليل شبكة الخطوط

الشهر	السيارات المتاحة	عدد السيارات التقديرى	التقدير المعدل

جملة الطلب المنتظر	جملة الطلب الواقعي
عدد السيارات	عدد السيارات
(١٠٠ ٪) سعة الأسطول بالكامل	(١٠٠ ٪) سعة الأسطول بالكامل
(٨٠ ٪) من سعة الأسطول	(٨٠ ٪) من سعة الأسطول
الشهر	الشهر

وبهذه الكيفية يمكن أن نفترض باطمئنان أن النموذج النهائي يتسم بأنه ذو طبيعة عامة ويمكن تطبيقه على أى طريقة من الطرق . وقد استخدم For tron II في وضع برنامج النماذج .

الخطوات التابعة و المؤدية إلى التقديرات النهائية :

١ — كافة البيانات المتصلة بخصائص الطلب تم تجميعها عن كل طريق شبكة طرق الشركة على حدة ، وعلى أساس شهرى فى المدة من سبتمبر سنة ١٩٦٧ إلى أغسطس سنة ١٩٦٨ وقد رمز للطرق برمز وقسمت إلى مجموعات على أساس الفروع .

٢ — أخذت البيانات السابقة وأطوال كل طريق على حدة بالكيلو مترات كمعلومات أساسية لاتستخدمها فى إعداد النموذج الحسابى الأخير، وقد عملت التقديرات عن كل شهر على حدة .

٣ — تم حساب العربات اللازمة لكل فرع على حدة بالمستويات الثلاث التى تم بحثها فيما تقدم ، وذلك على أساس شهرى (نرجو الرجوع إلى الجداول الإحصائية والبيانية المرفقة) .

تأثير القنابل والصواريخ على المنشآت

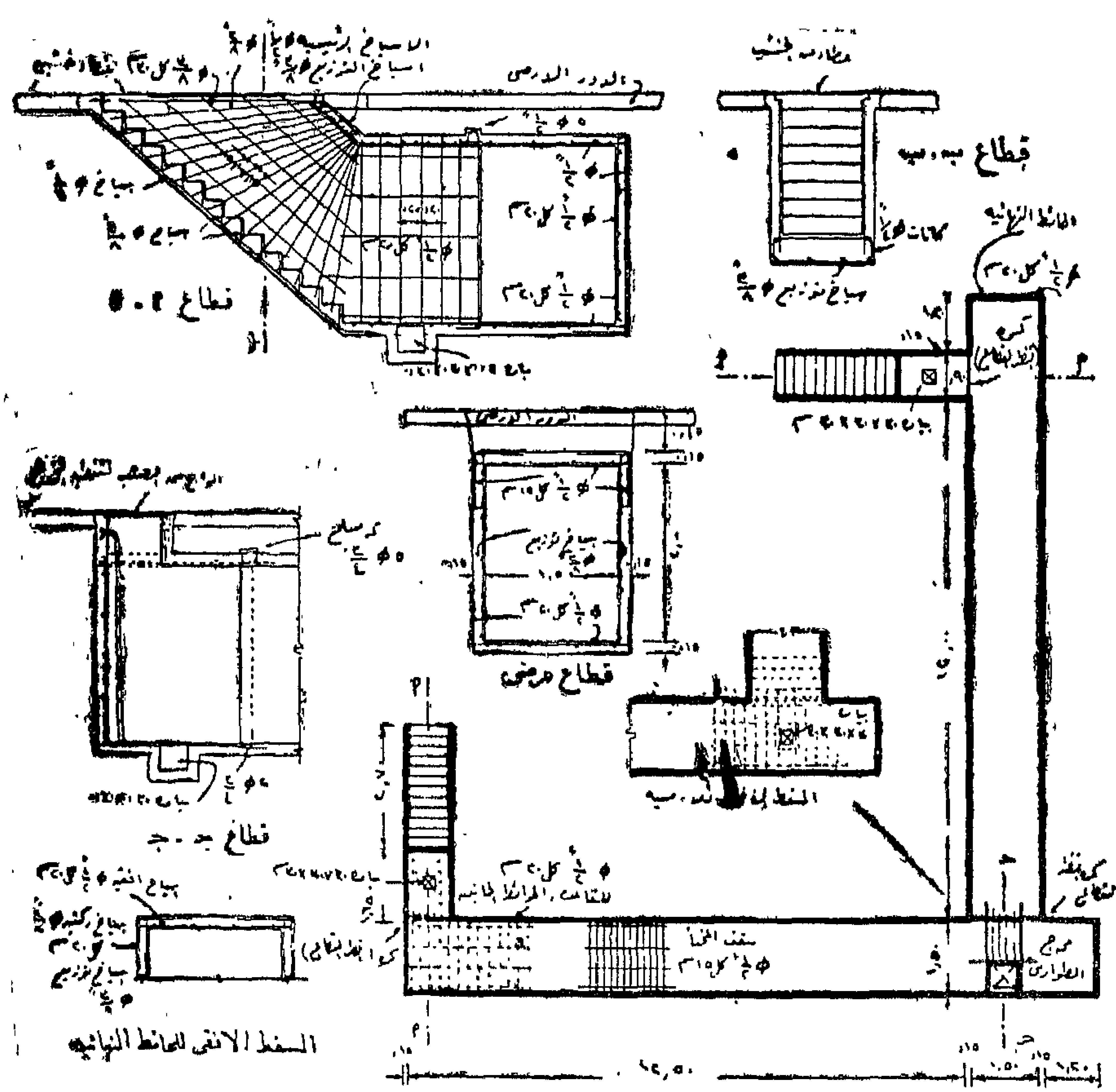
تصميم الأعمال الوقائية

بقلم
للمهندس عز الدين فرج

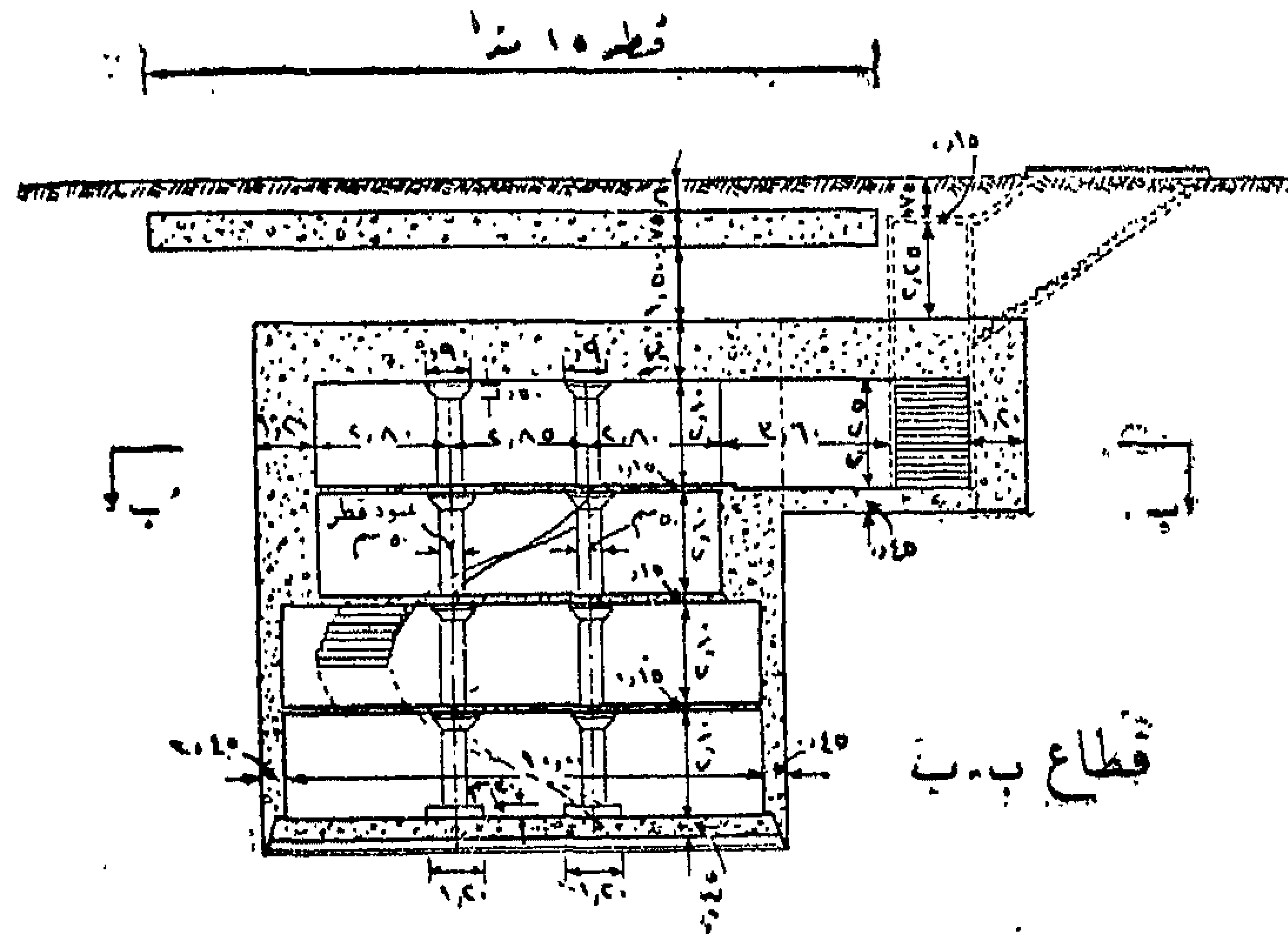
- ٢ -

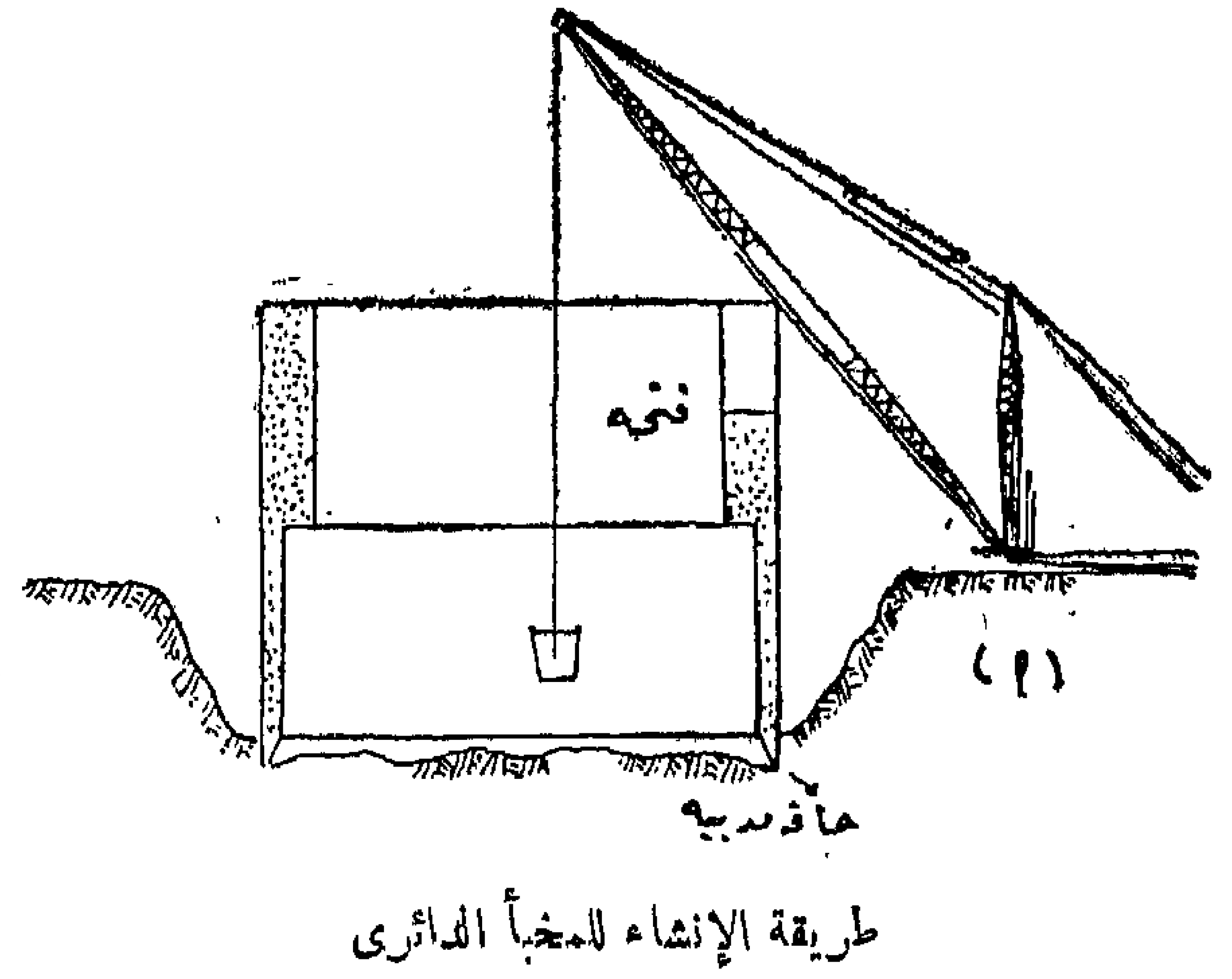
يستكمل فى هذا العدد باقى موضوع تصميم الأعمال الوقاية المنشور فى العدد الرابع للعام ١٩٧٠ وتبدأ بأشكال متعددة لنوعيات من المخابىء التى تم إنشاؤها فى الحرب العالمية الثانية ولاتتقيد بالأسماك الواردة فى الأشكال إنما تصمم طبقاً لما ورد فى المعادلات المجلة والغرض من الأشكال إعطاء الدارس أفكاراً متنوعة عن التصميم المعمارى لها. ومرة أخرى لا تتقيد بالأسماك اردة بالأشكال - وتحسب كالمعادلات.

وننهى البحث بأمثلة محاولة كتطبيق للمعادلات السابقة التى آثرنا تلخيصها فى أول الأمثلة . كما نشير إلى التأثير الذرى فى نهاية البحث .

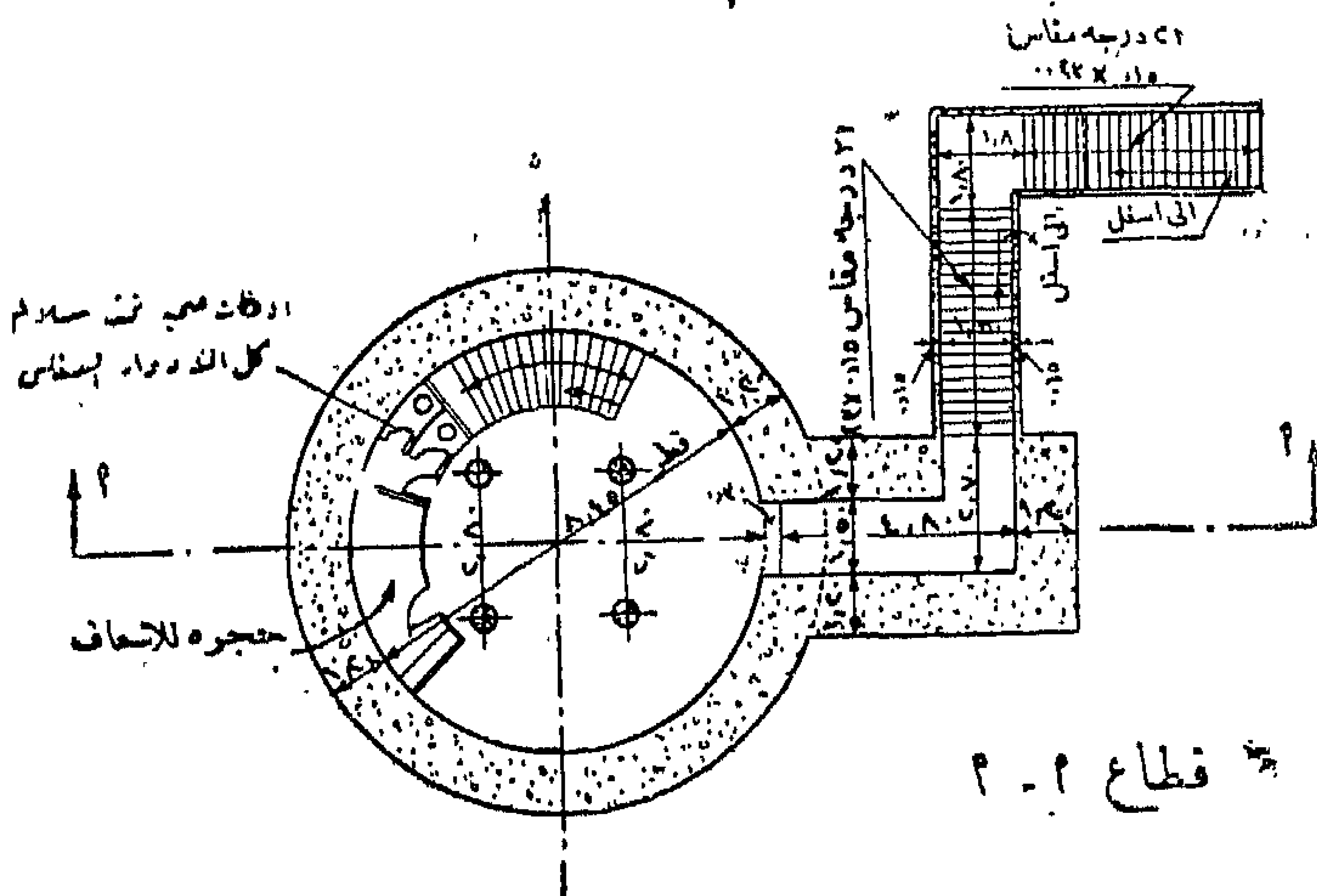


(شكل ٩٥) خندق من الخرسانة المسلحة منشأ تحت الدور الأرضى لمصنع من دور واحد
ويلاحظ أنه فى حالة المبانى ذات الطابق الواحد تفضيل لإنشاء خندق تحت الدور الأرضى
يعمل له مخرج طوارىء

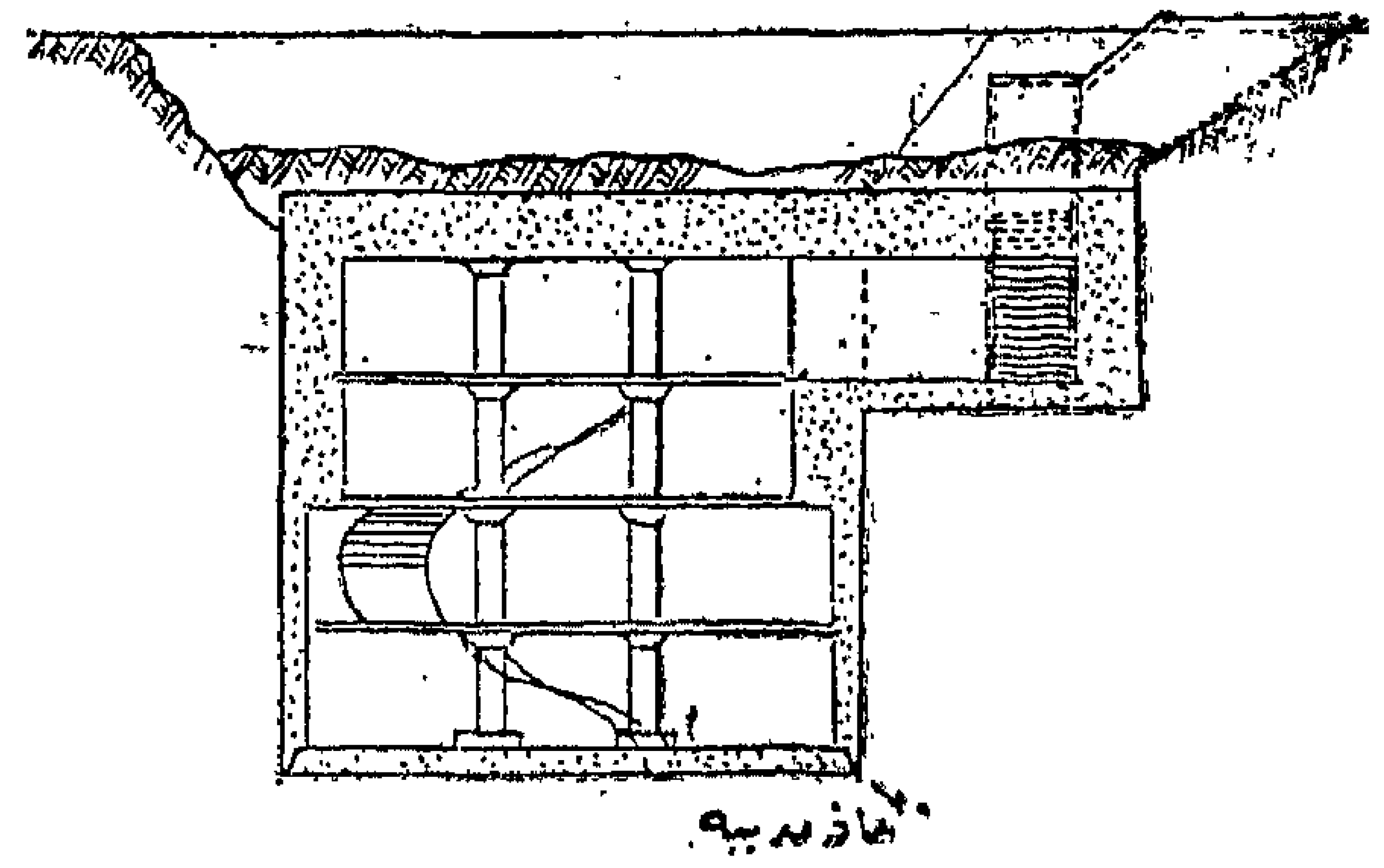




طريقة الإنشاء للمخبأ الدائرى



مخبأ دائرى ضد الاصابات المباشره لقنابل تزن ½ طن

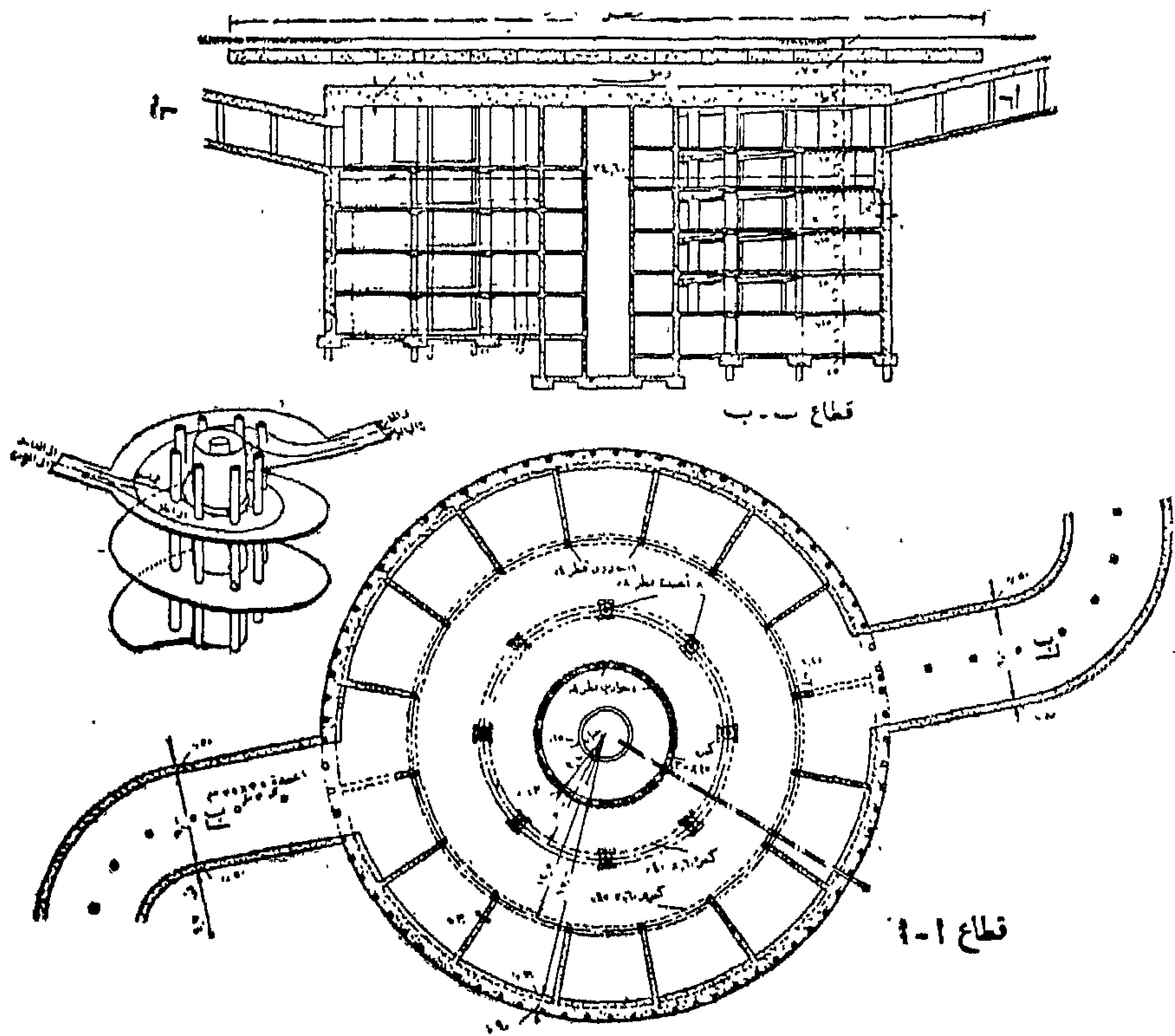


طريقة الانشاء للمخبأ الدائرى الواقى ضد القنابل نصف طن

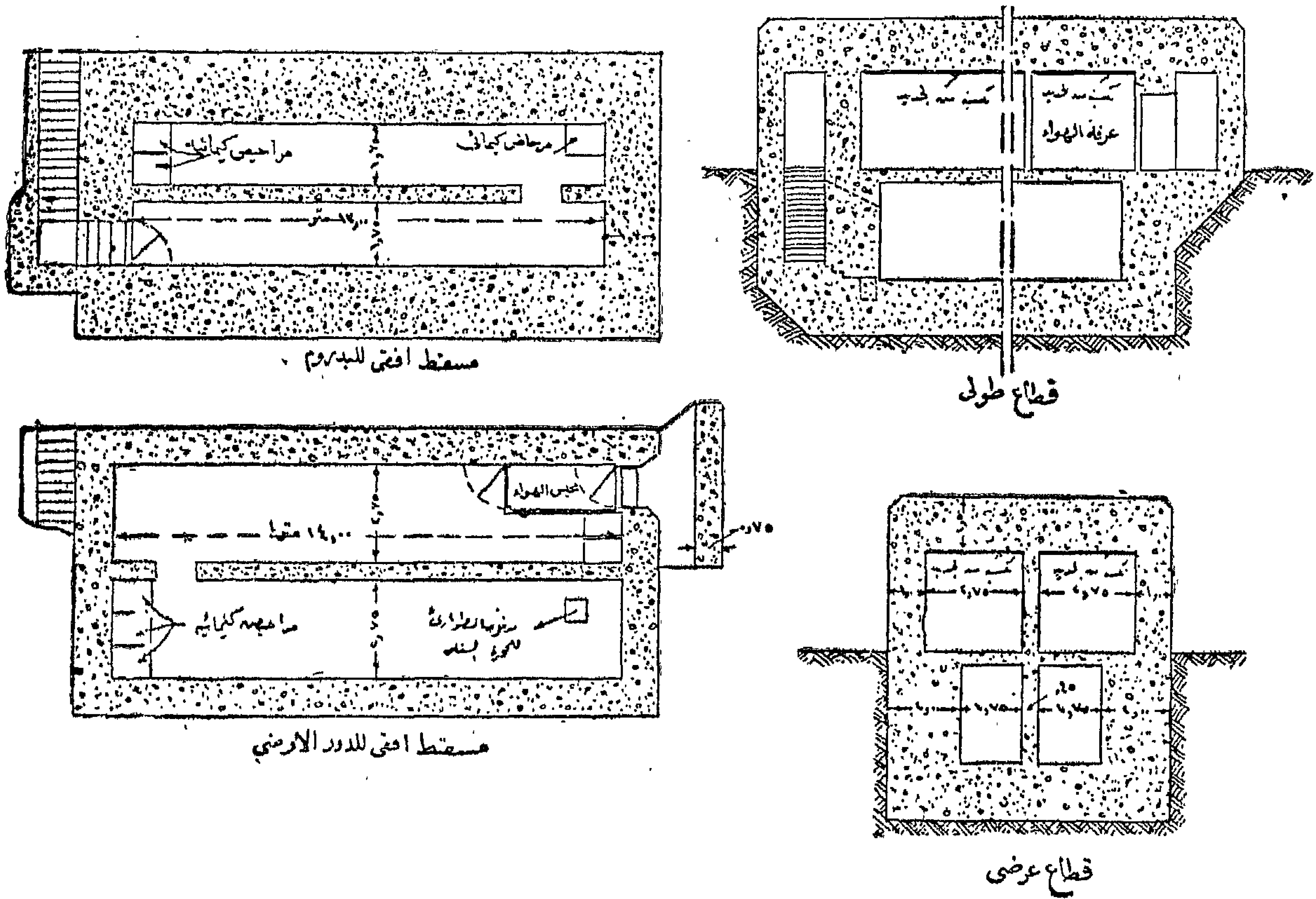
(ا) يبتدأ فى التغطيس بعد الانتهاء من إنشاء الحوائط الخرسانية للاسطوانة بكامل ارتفاعها .

(ب) بعد انتهاء التغطيس تنشأ بلاطات الأرضية والأسقف السلالم الحلزونية ثم توضع الأتربة فوق البلاطة العليا .

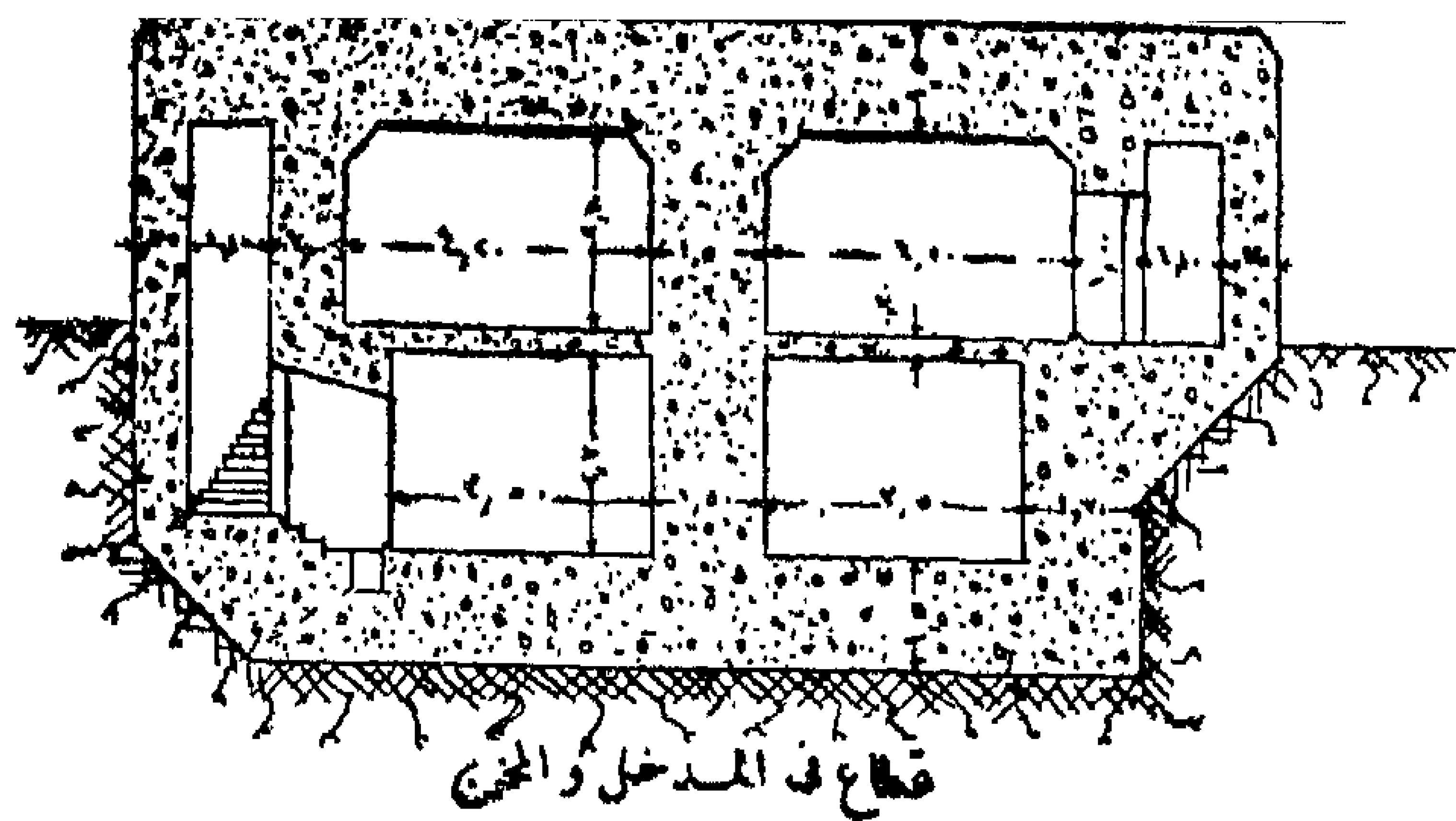
(شكل ٦٦)

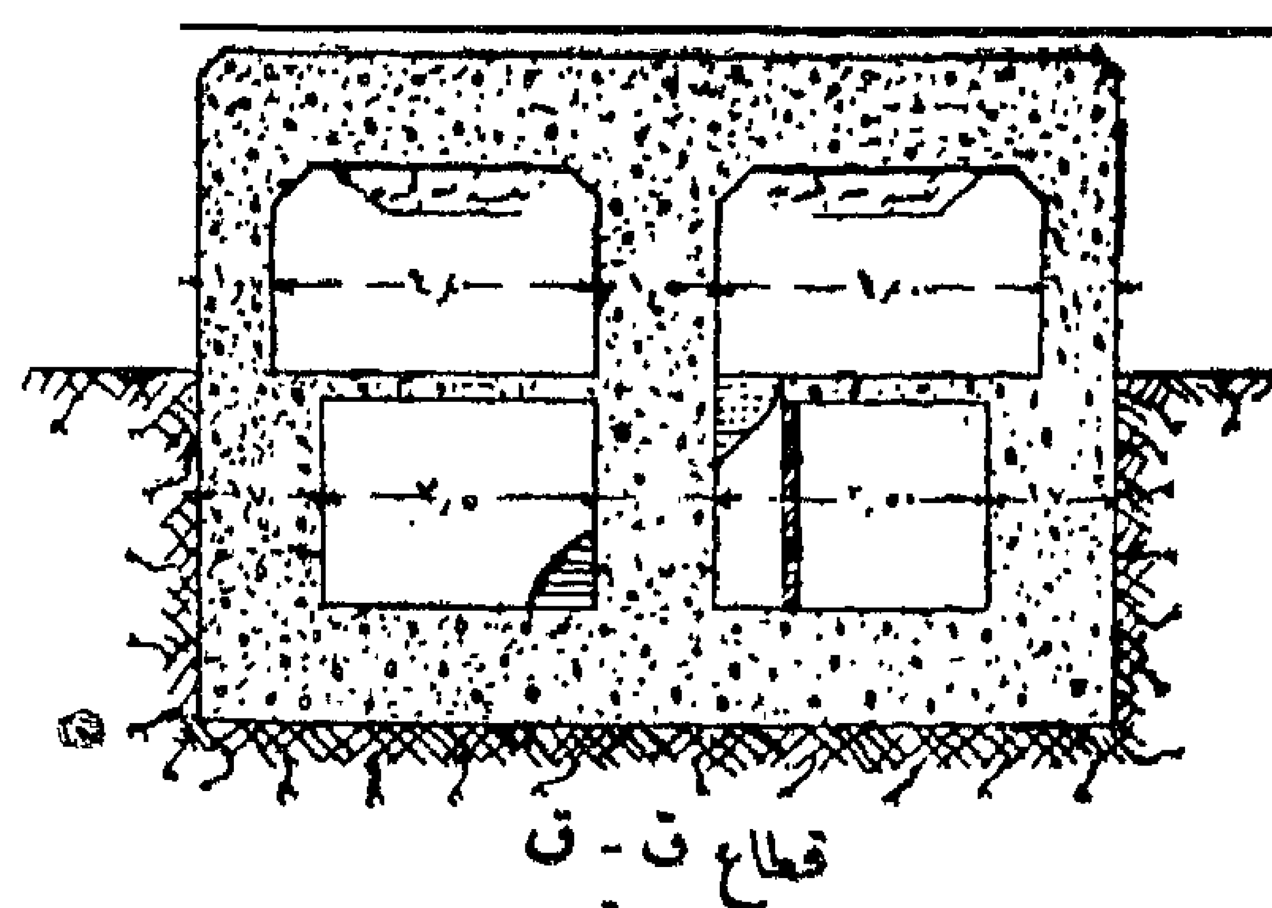


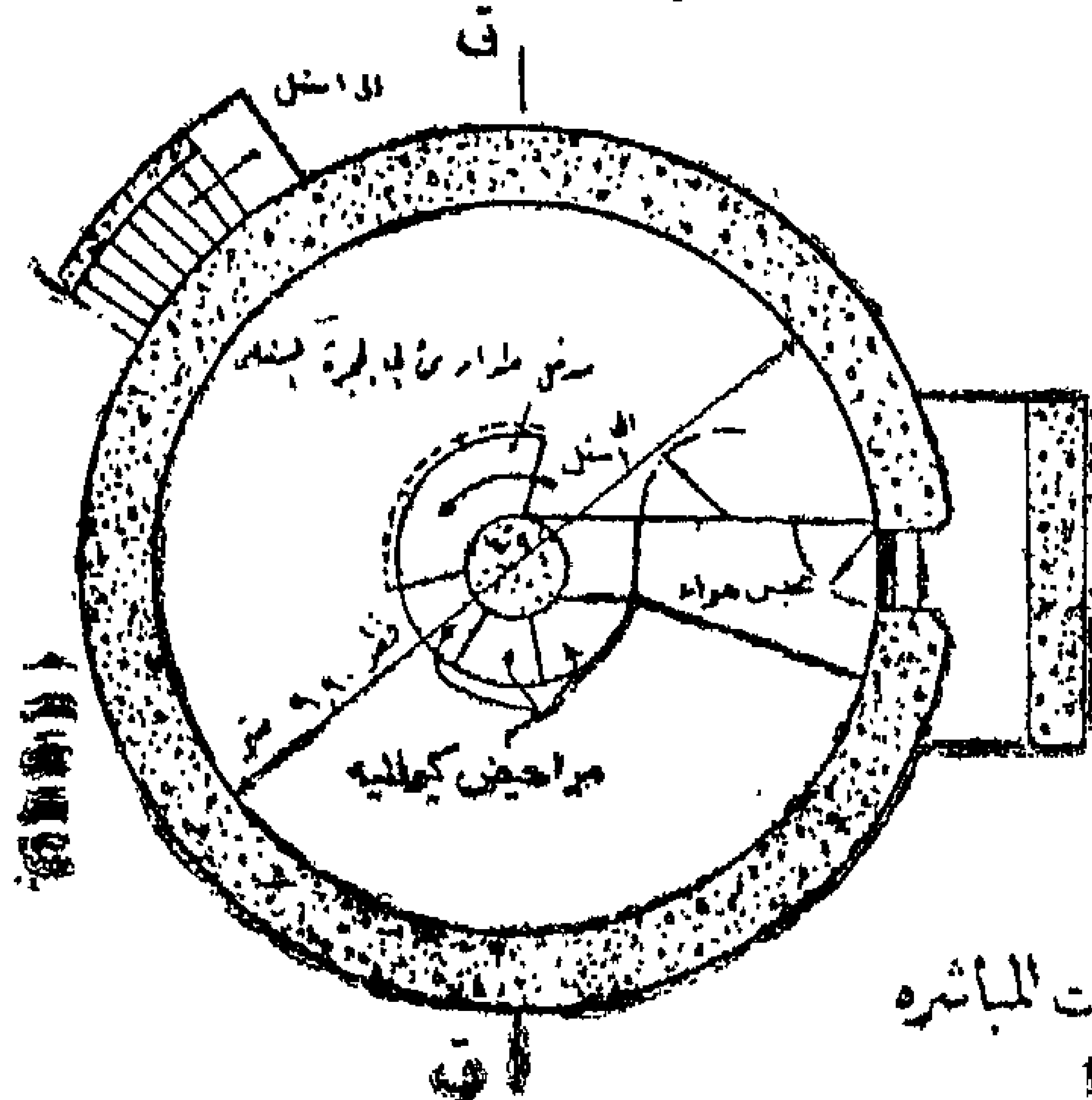
مخبأ نبنسبرى العظيم
ضد الاصابات المباشرة لقنابل تزن ½ طن
يسع ٧٦٠ شخصا
شكل (٦٧)

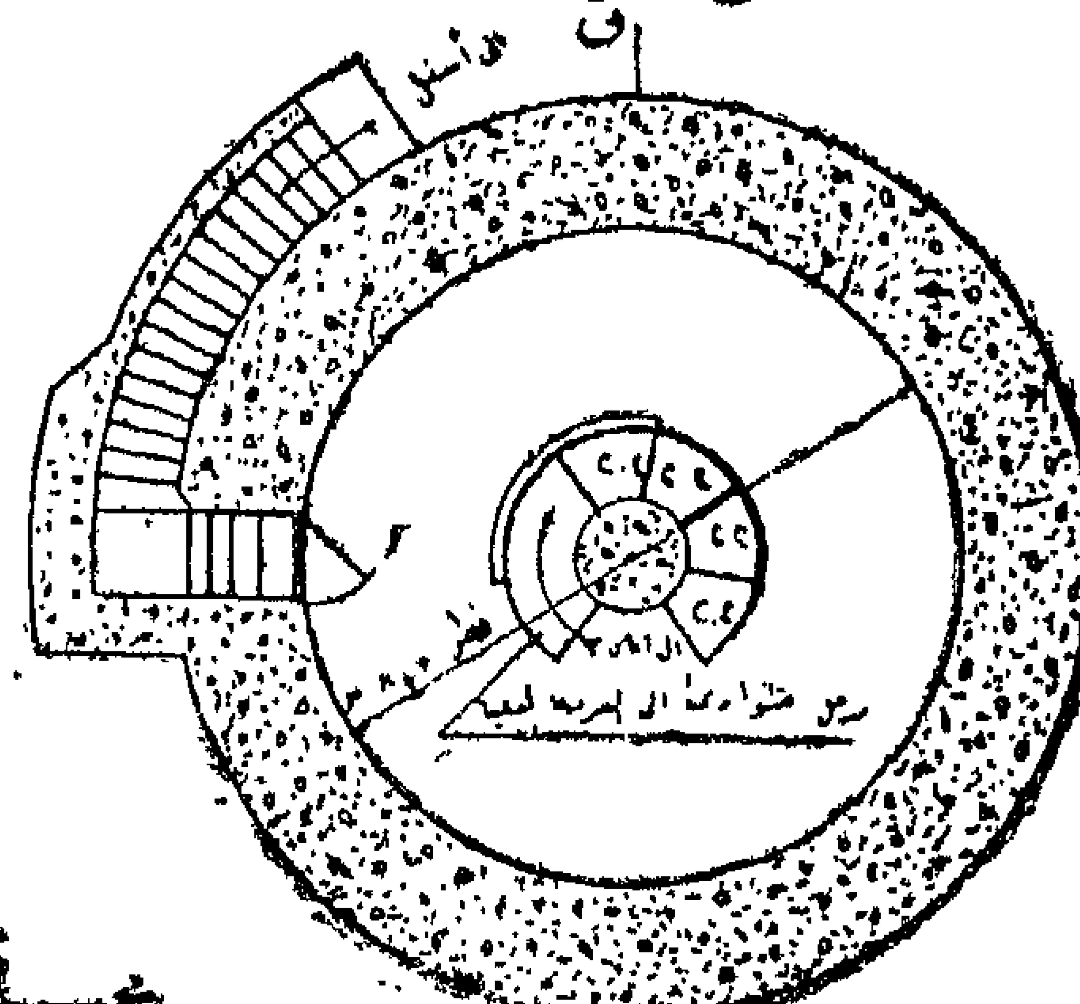


مخبأ مستطيل ضد الاصابات المباشرة
يسع ٢٠٠ شخصا
(شكل ٦٨)



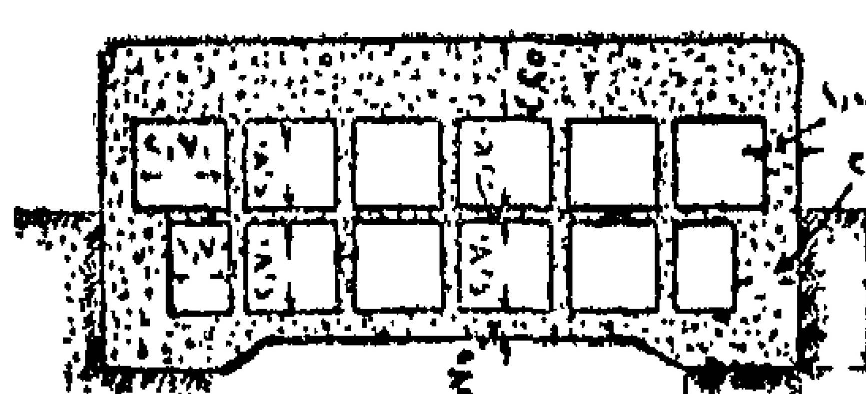


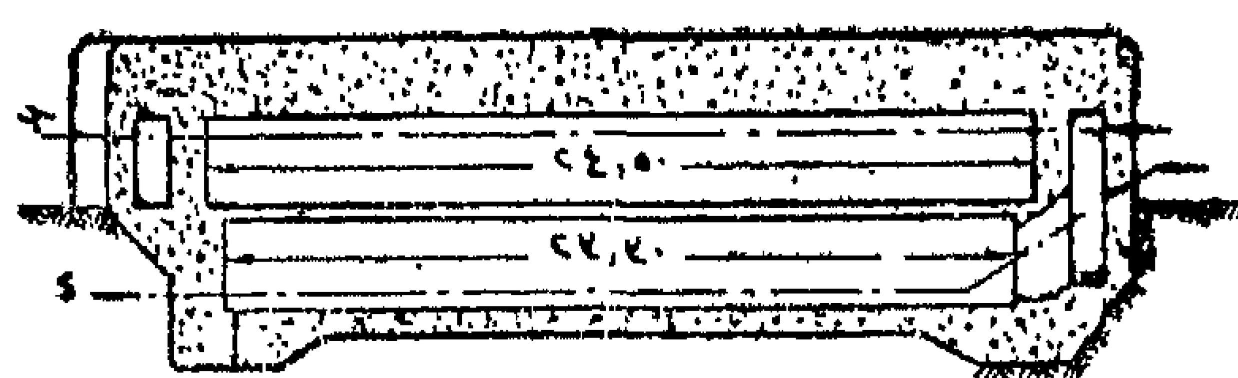


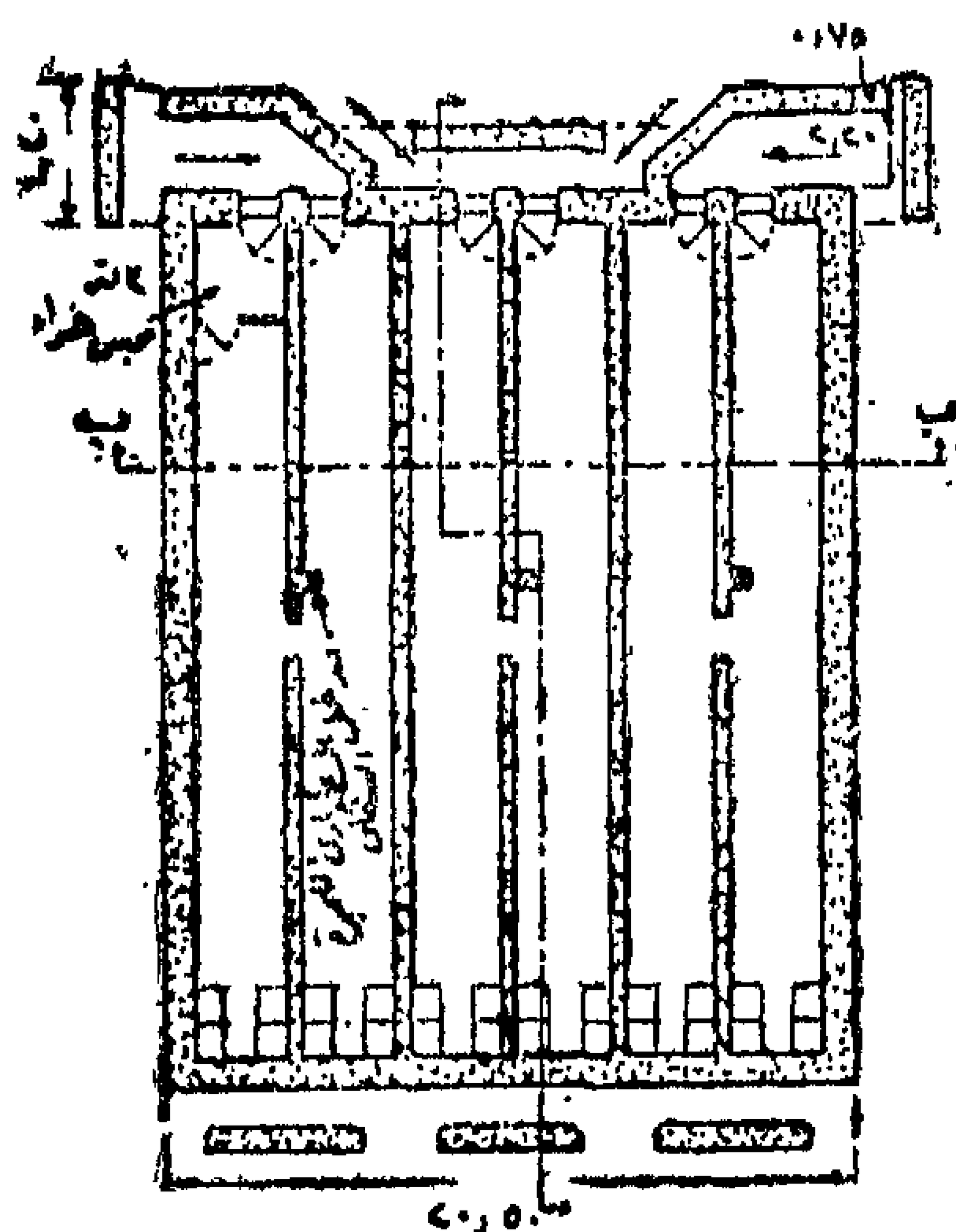


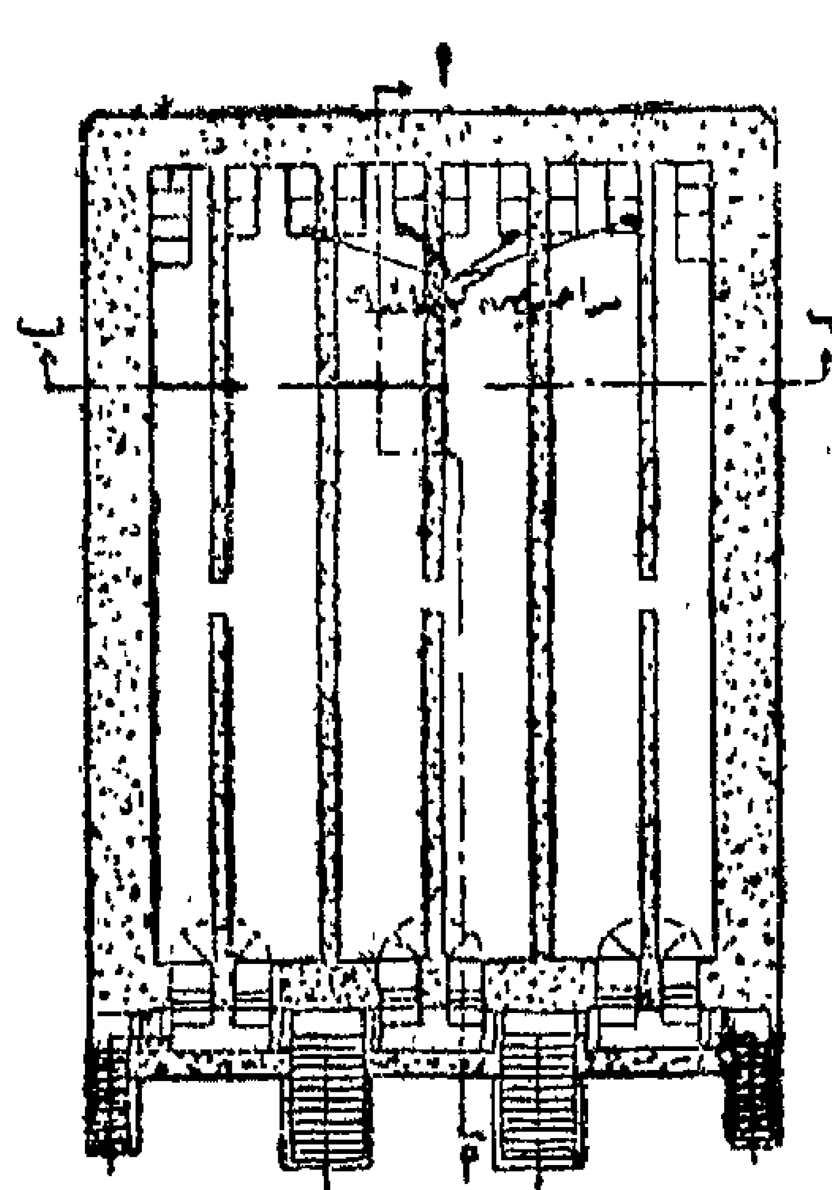
مخبأ دائرى ضد الاصابات المباشرة
يسع ٢٠٠ شخصا

(شكل ٦٩)





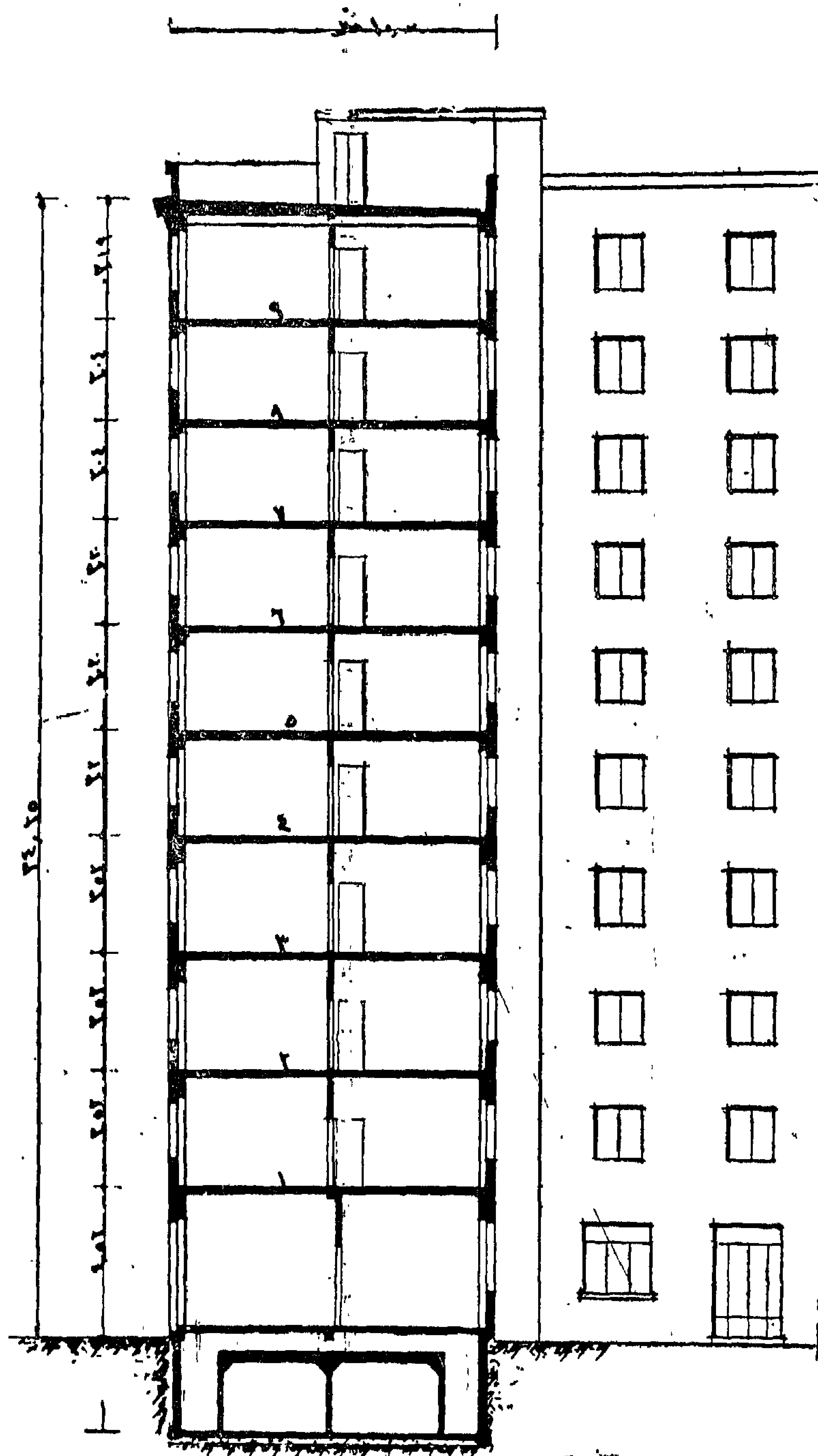




مخبأ مستطيل ضد الاصابات المباشرة
اليسع ١٢٠٠ شخصا

(شكل ٧٠)

طريقة انشاء المخابئ في المباني الموجودة والجديدة



عمارة مكونة من تسعة أدوار يحدث الانفجار قبل وصول القنبلة الى سقف المخبأ ولذلك صمم السقف ليتحمل انهيار أنقاض الادوار العليا وحسب لذلك الحمل الميت ×١٫٥ فقط لجميع الادوار كحمل اضافي على سطح المخبأ

انظر تفاصيل القطاع عن ستلهورف

(شكل ٧١)

قطاع للمخبأ العمومى (الوارد فى الصفحة السابقة) للوقاية من اصابة مباشرة لقنبلة وزنها ٣٠٠ كيلو
السطح السفلى عمل بأكبر سمك تخترقه قنبلة وزنها ٣٠٠ بدون أن تنفجر فاذا حدث الانفجار
فى هذه البلاطة تمزقت وكان السطح كافيا للمقاومة تمرق الهواء وتحمل الانقاض (عن ستلجوهرف)

(تابع شكل ٧٢)

يسع ٥٠ شخصا

يسع ٥٠ شخصا

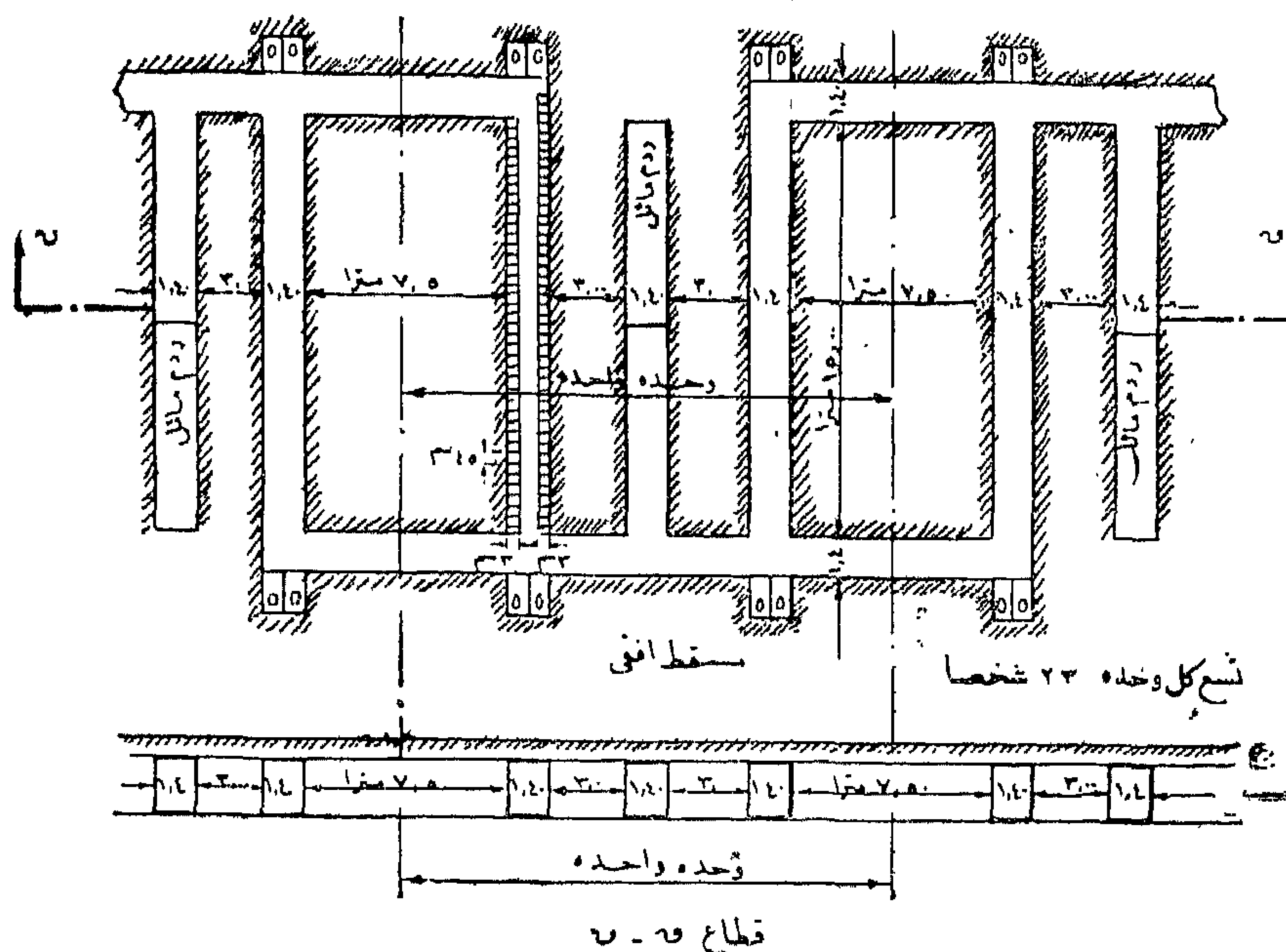
قطاع افقى

(شكل ٧٣) نموذج لمخبأ مصنوعة حوائطه من الطوب يسع ١٠٠ شخصاً



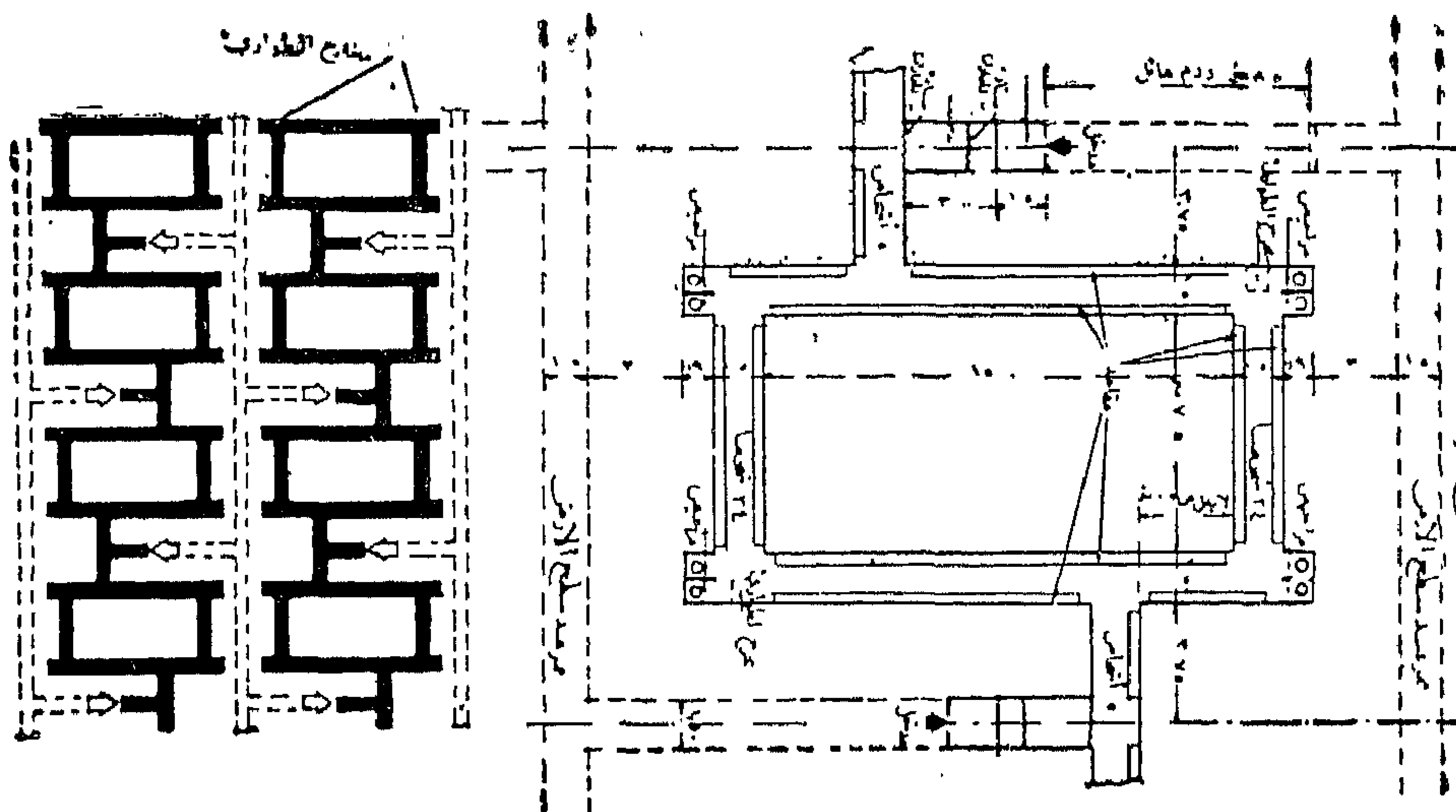
نموذج لمخبأ مصنوعة حوائطه من الطوب يسع ٥٠ شخصا
قطاع أفقي ا-ب
قطاع طولي
قطاع جـ-د
قطاع هـ-و
قطاع ك-م
تفصيل المقاعد
تفصيل مخرج الطوارئ
مخرج الطوارئ
مرحاض

(شكل ٧٤)



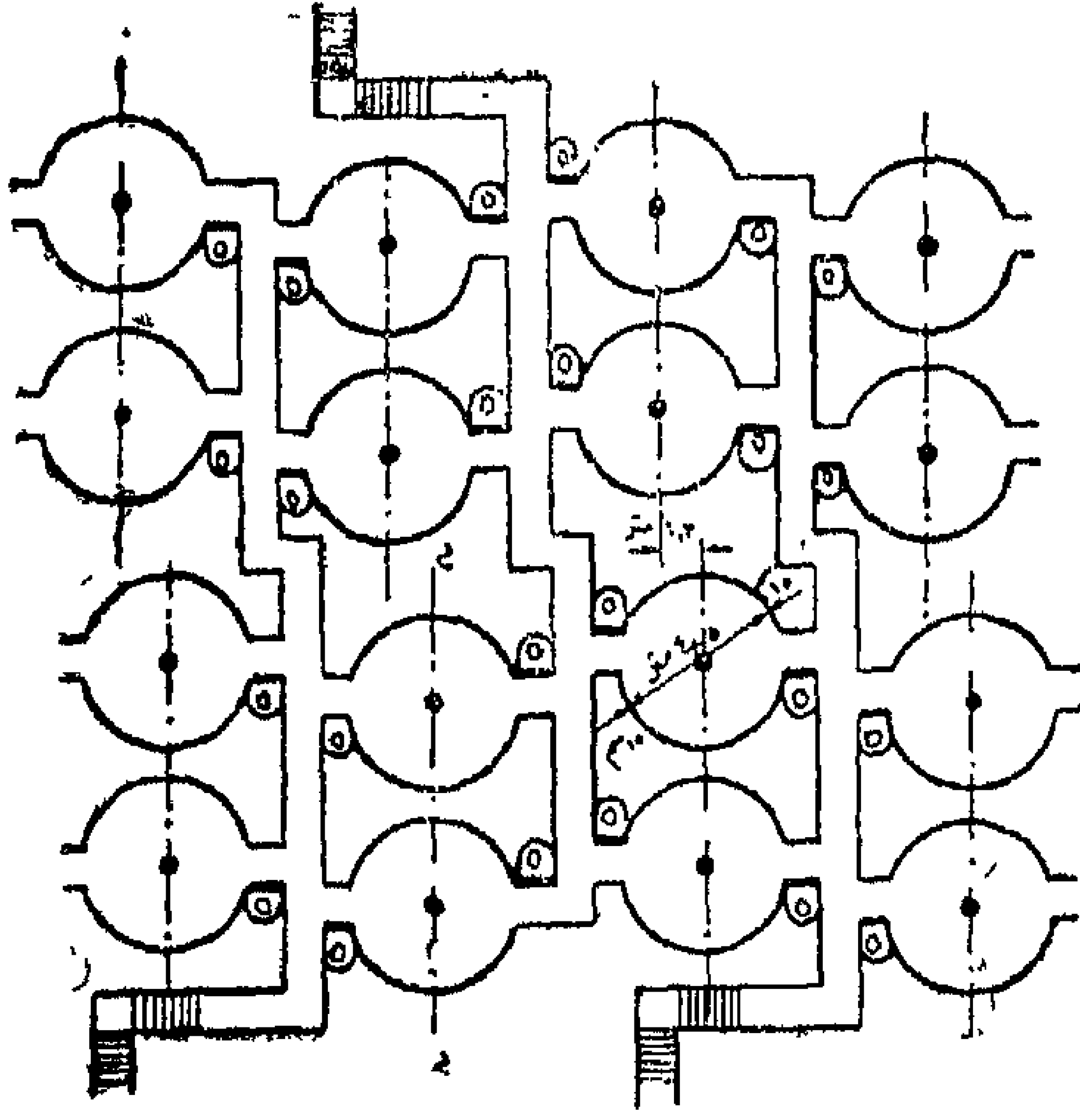
(شكل ٧٥)

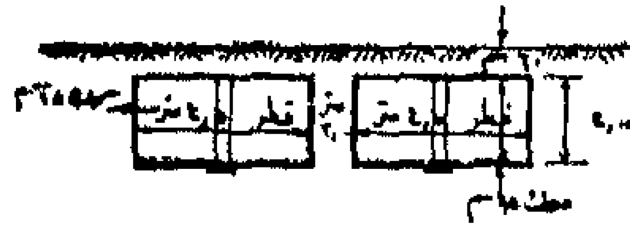
مجموعة من الخنادق طول الخندق ١٥ متر والمسافة من الخندق والآخر ٧,٥ متر وتسع كل وحدة ٣٣٠ شخص (التغلب على صعوبة إنشاء خنادق كافية فى مساحات محدودة) .



(شكل ٧٦)

مجموعة خنادق كبيرة فى مساحة محدودة تسع ١٢٠٠ شخص فى فدان واحد من الفضل الإنشاء بالخرسانة المسلحة ولا تنشأ الحوائط من الطوب إلا بانشاء حوائط عرضية بعدد كاف تعلوها كمرات يرتكز عليها السقف

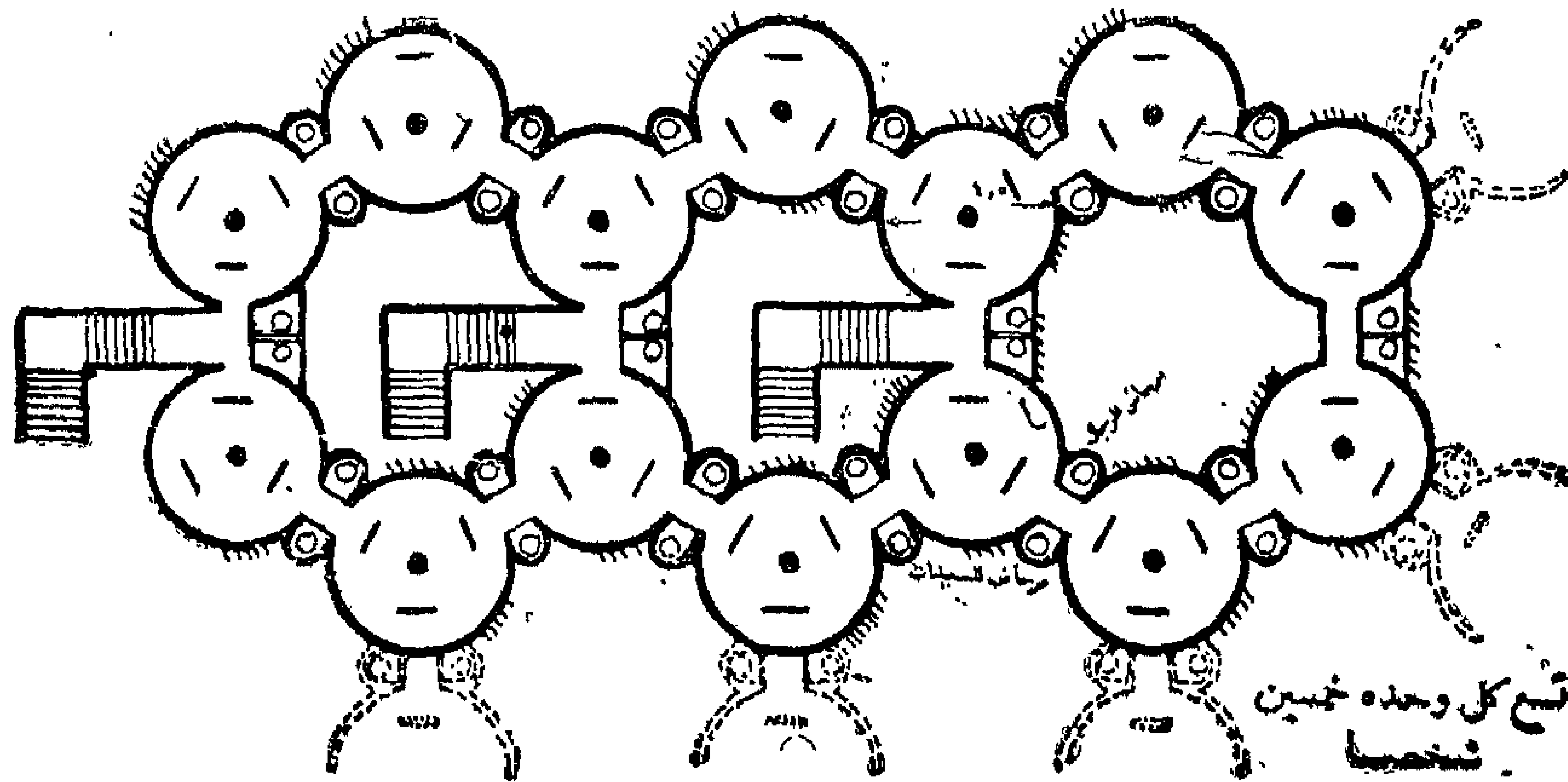




(شكل ٧٧)

مجموعة من الخنادق الدائرية كلها من الخرسانة المسلحة ويمكن إنشاء الحوائط من الطوب مع إنشاء عمود خرسانة مسلحة فى المنتصف متصل تماماً بسقف المخبأ وقاعدته وهى الأخرى من الخرسانة المسلحة.

العمود مصمم لحمل السقف وما يحتمل أن يسقط فوقه من أنقاض فى حالة إنفصال الحوائط عن السقف .



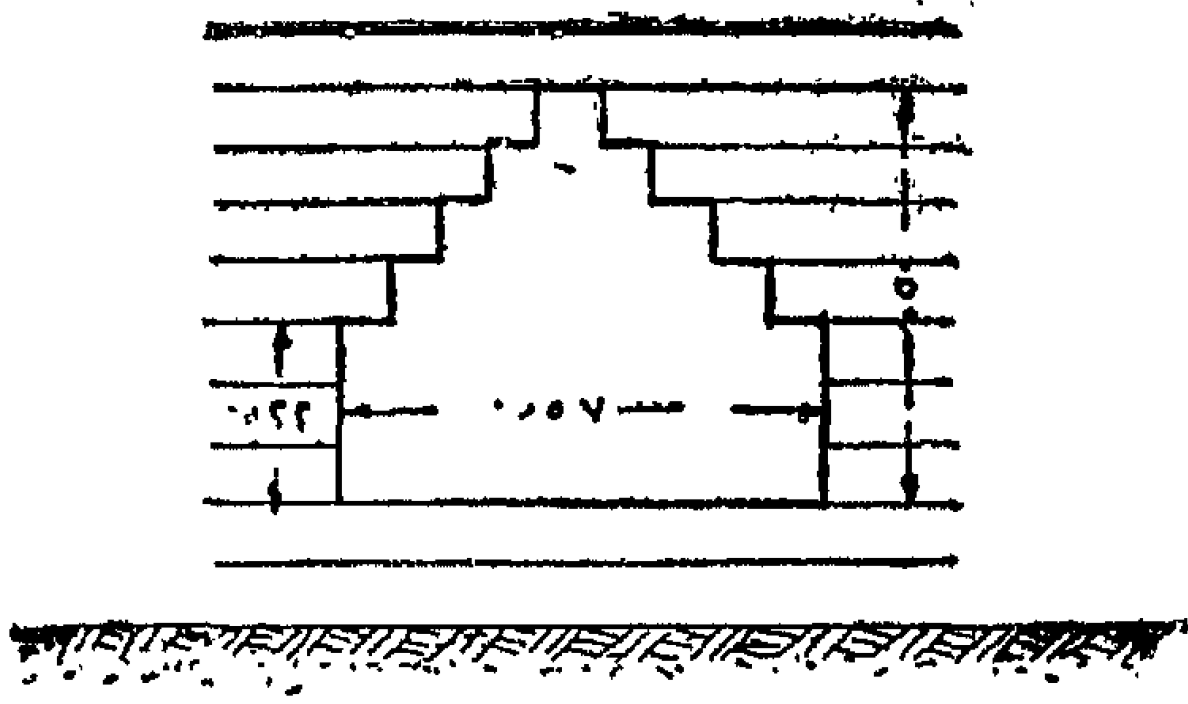
(شكل ٧٨)

طريقة أخرى لترتيب المخابىء الدائرية وهى أحسن أنواع الترتيبات . ويسهل الوصول منها لبعضها . فى هذا النوع يلاحظ إمكان ترك حجوم كافياً من الأرض البكر بين الوحدات . ويصعب تحريك الوحدات بسهولة من الضغط الناشىء عن الانفجار .

الفدان الواحد يمكن أن يسع ٤٠٠٠ شخصاً بهذه الطريقة بينما لو كانت مستطيلة فالفدان لا يسع سوى ٢٠٠٠ — ٣٠٠٠ شخصاً .

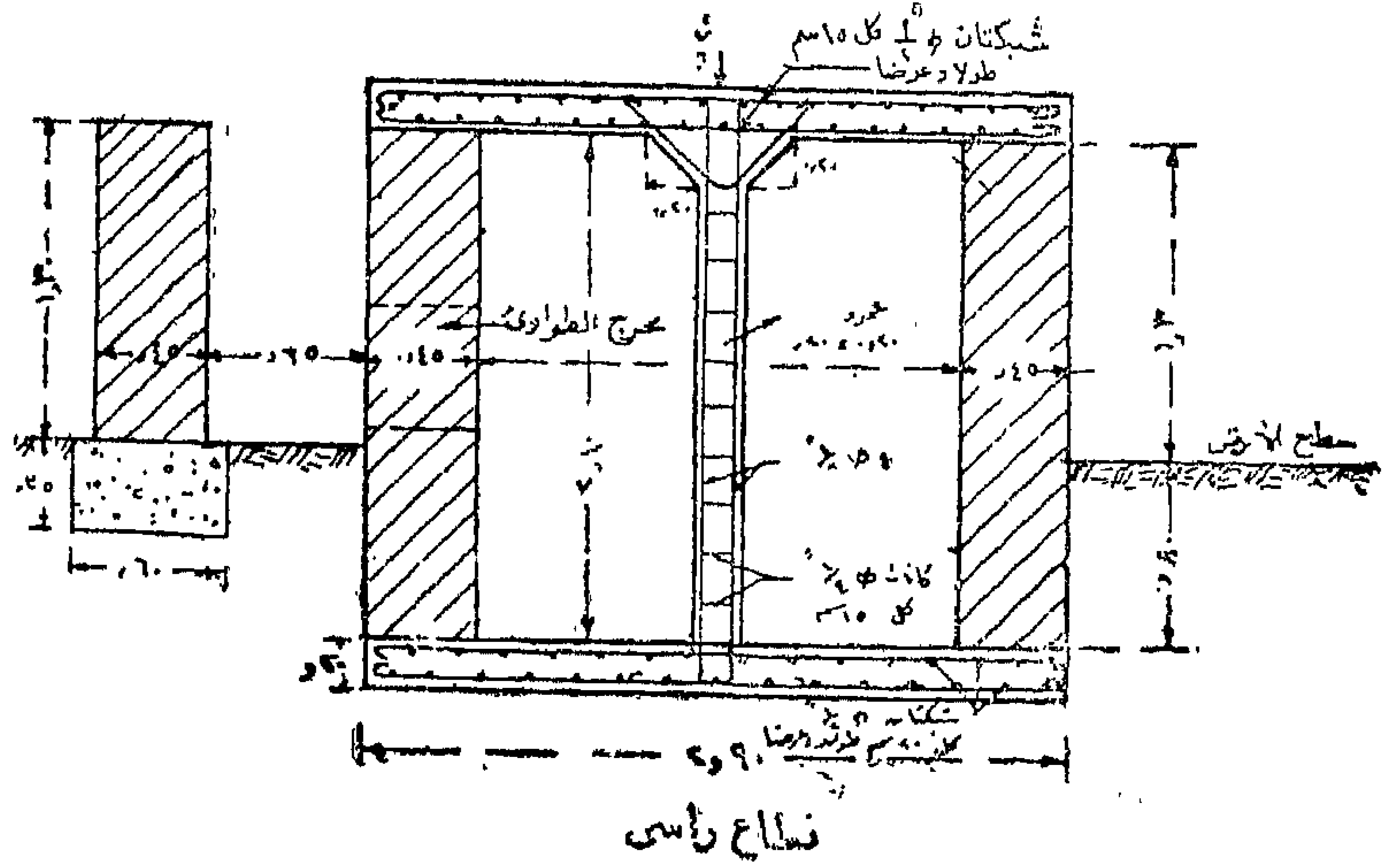
وإذا صعب الانشاء دائرياً يمكن عمل منحن أو مسدس منتظم أو مربع .

المخابىء العائلية

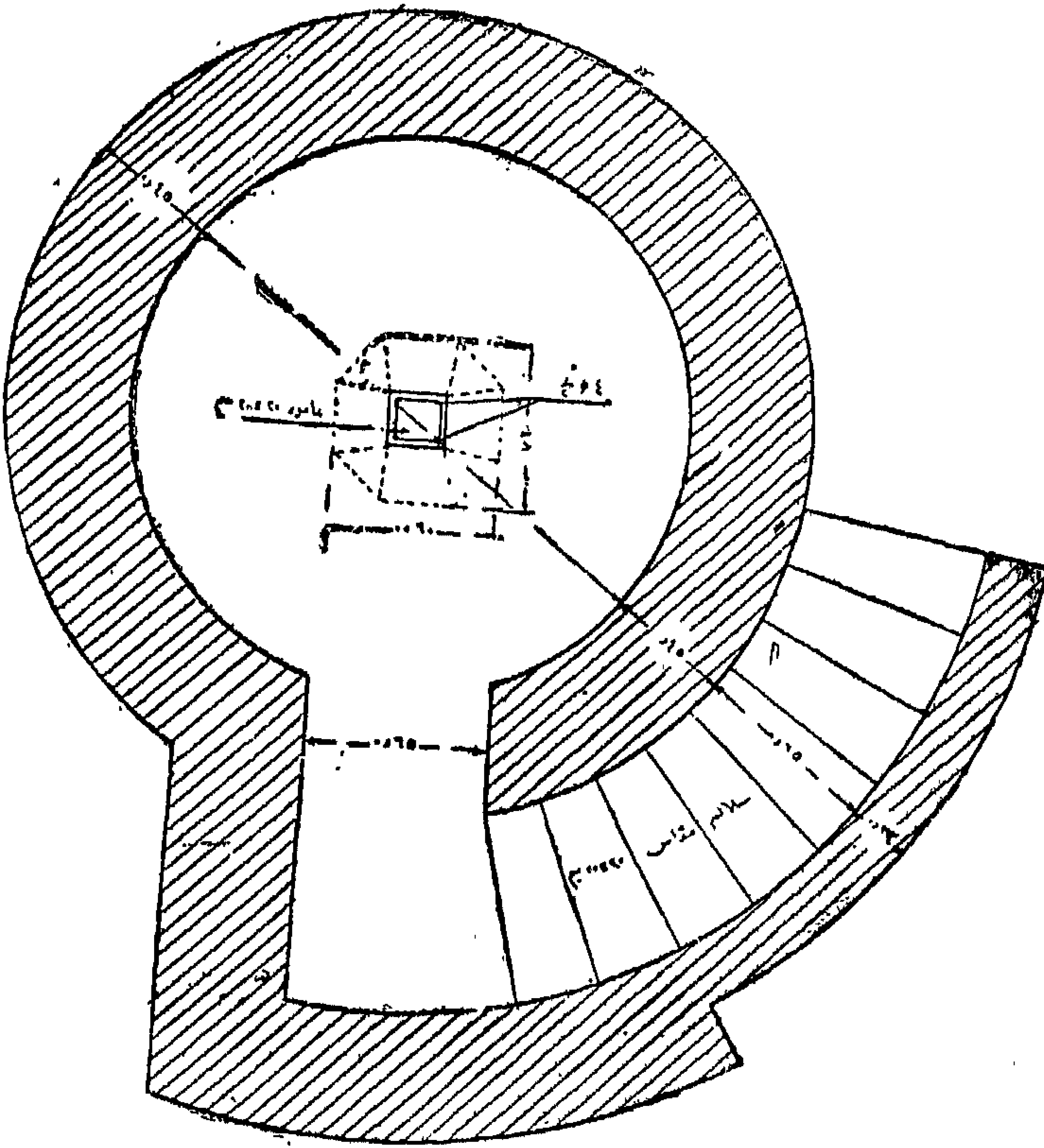


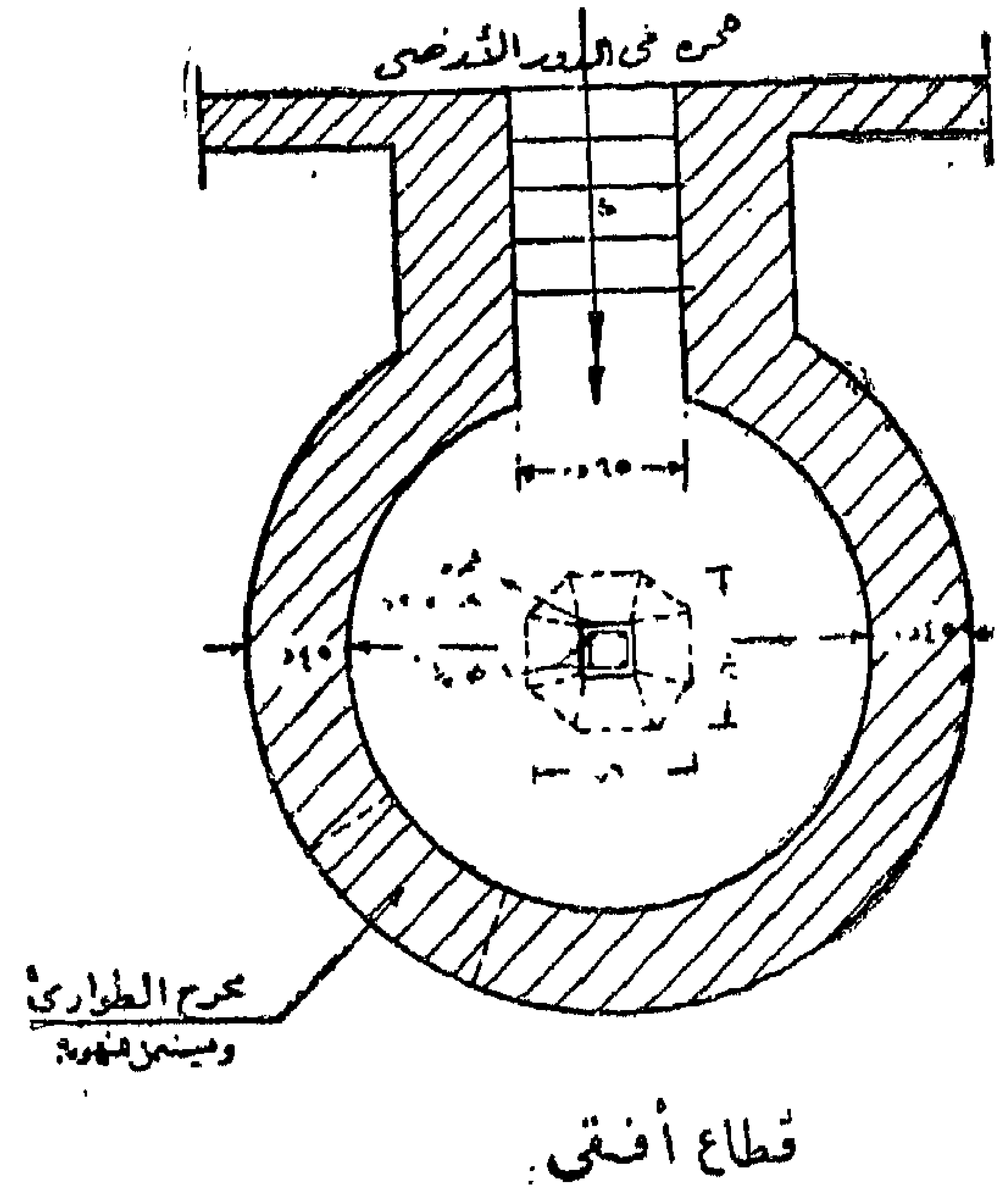
تفصيل مخرج الطوارئ

تفصيل مخرج الطوارىء للمخبأ المتين



قطاع رأسى





قطاع أفقى

مخبأ عائلى يسع ١٠ اشخاص

قطاع أفقى لمخبأ عائلى قوى يسع ١٠ أشخاص

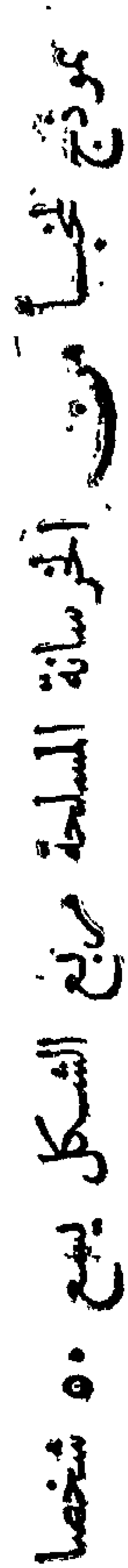
قطاع أفقى لمخبأ عائلى قوى يسع ١٠ أشخاص

(شكل ٧٩)

مخبأ عائلى يمكن إنشاؤه فى حديقة المنزل متصلا بباب حجرة فى الدور الأرضى مثلا — حوائطه من الطوب سمك ٤٥ سم قاعدته من الخرسانة المسلحة سمك ٢٠ سم متصلان معا بواسطة عمود خرسانة مسلحة لاحظ مخرج الطوارىء الذى يستعمل للتهوية فى نفس الوقت وأمامه حائط واق .

أقوى من سابقة — حوائطه طوب سمك ٤٥ سم القاعدة خرسانة مسلحة سمك ٢٠ سم تفاصيل التسليح فى الشكل التالى

ملحوظة : هذا مجرد مثال لاتتمسك بالاسماك الواردة هنا بل يرجع إلى جدول الأسماك الواقية طبقاً لعيار القنبلة .

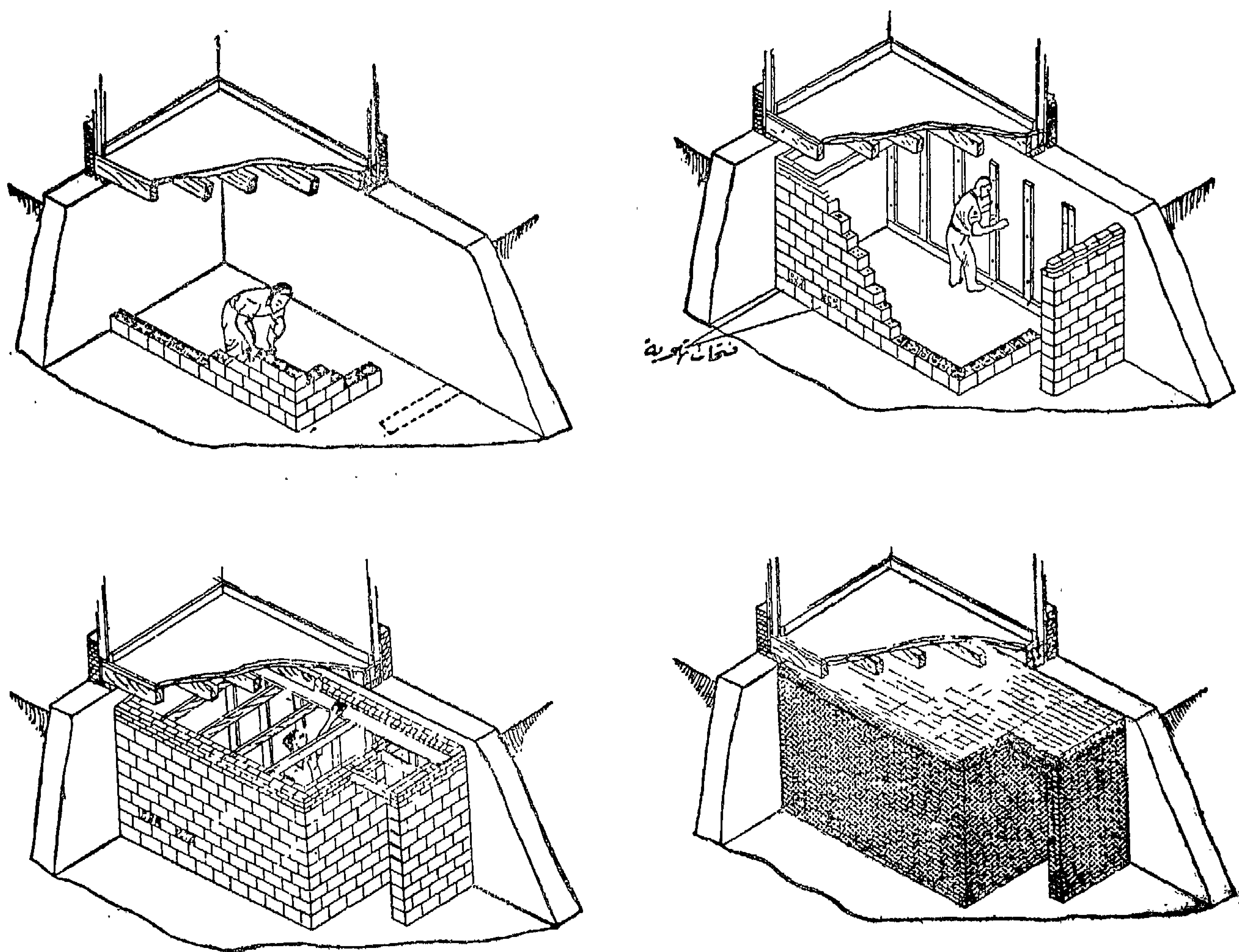


(شكل ٨٠)

— الحوائط والسقف والقاعدة خرسانة مسلحة .

— لا يختلف عن سابقه إلا فى أنه مربع الشكل .

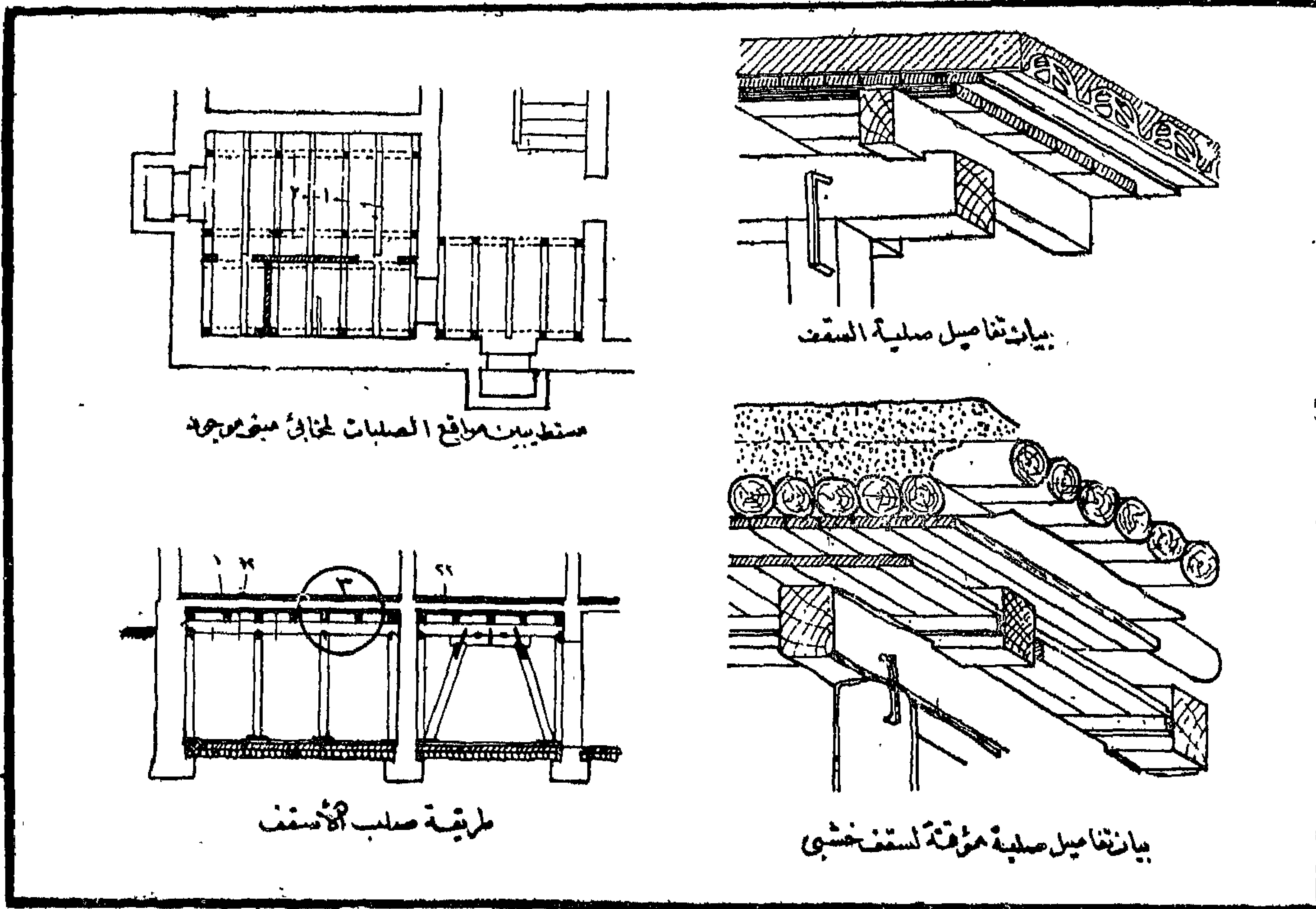
— يوضع فى وسطه عمود خرسانة مسلحة ٣٠ × ٢٠ يرتكز عليه السقف بواسطه كمرة مع زيادة سمك الأساس تحت قاعدة العمود .

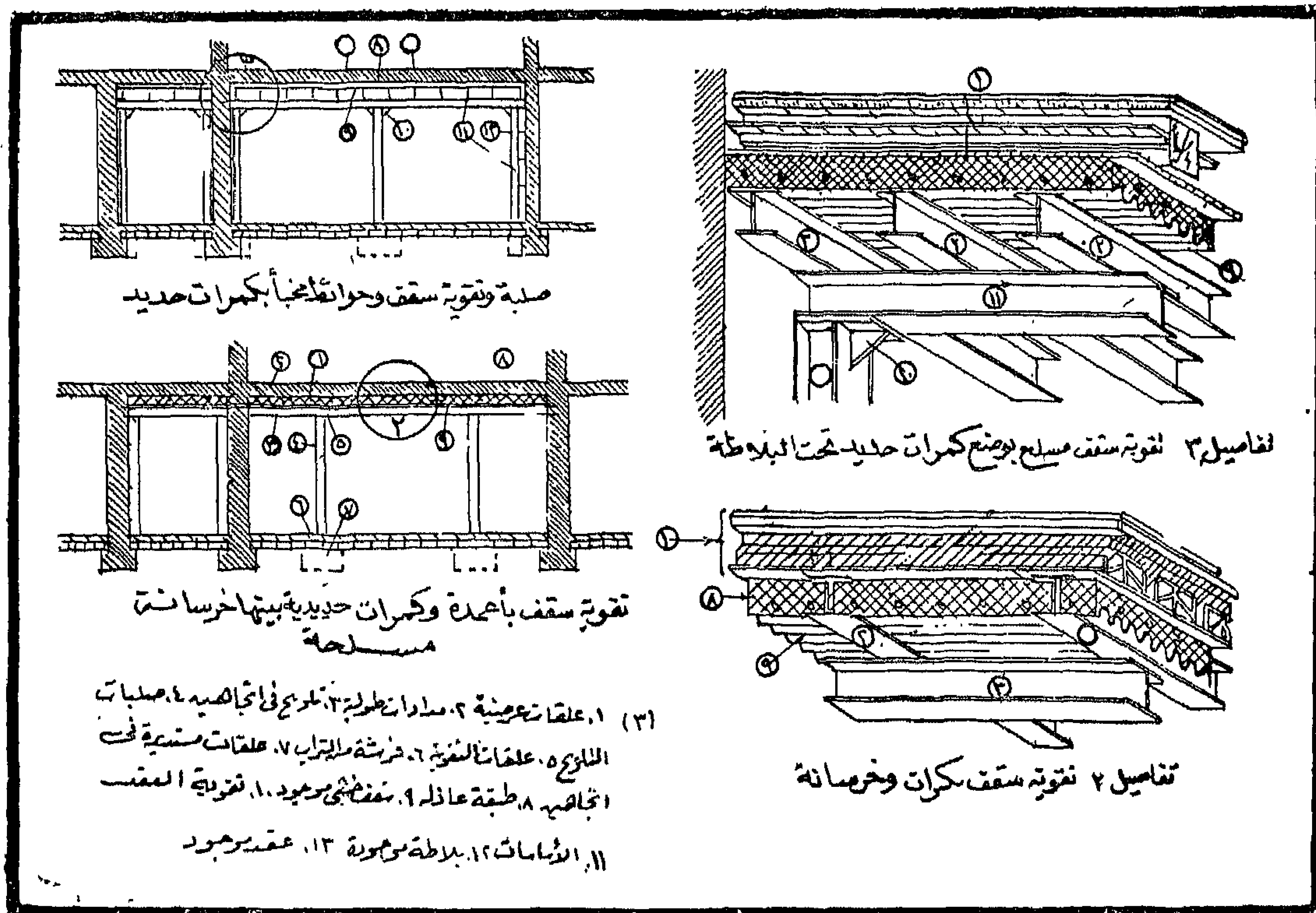


كيفية إقامة مخابئ البدرومات

(شكل ٨١)

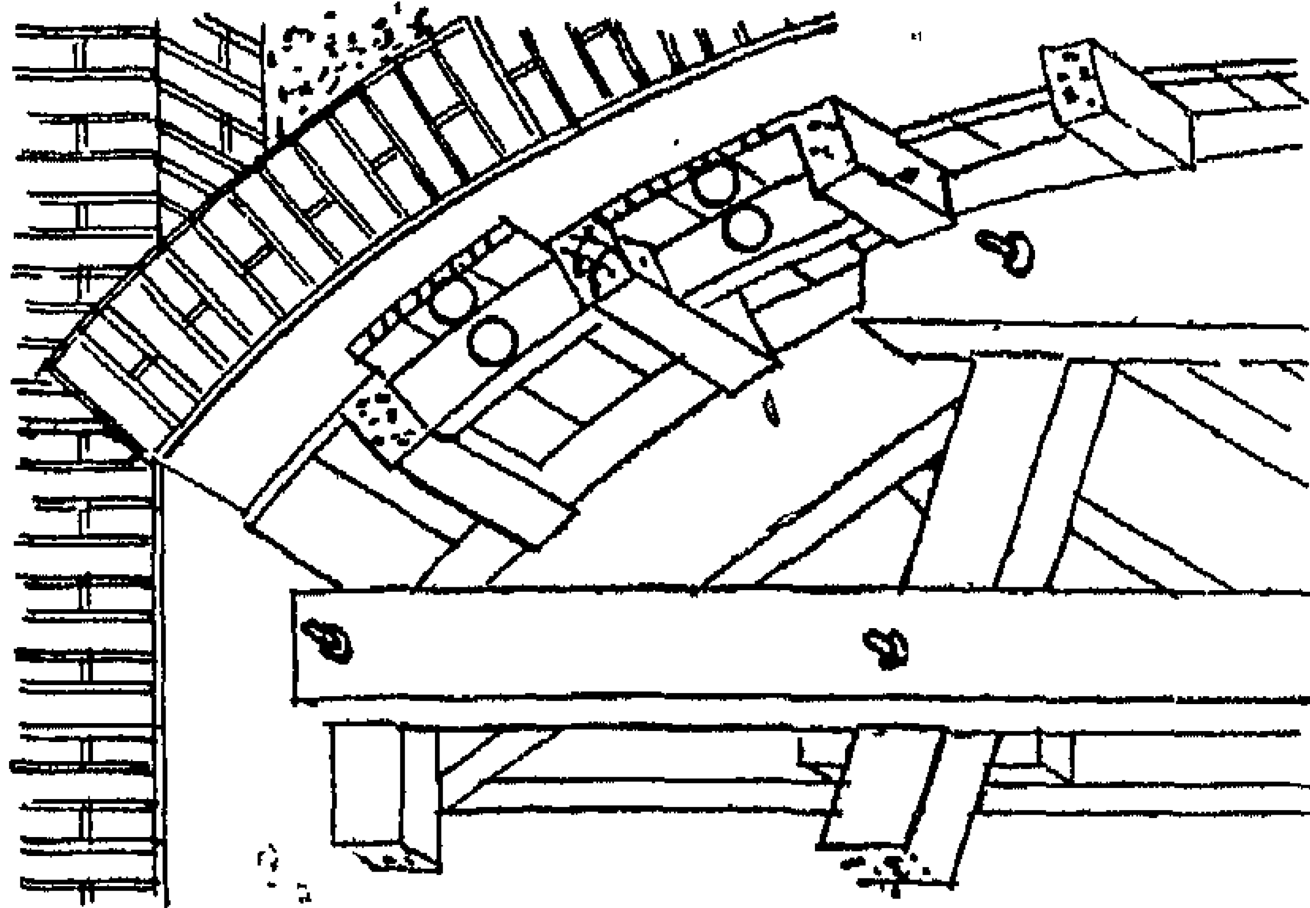
وسائل تدعيم الحوائط والأسقف بأعمال الصلبات المختلفة

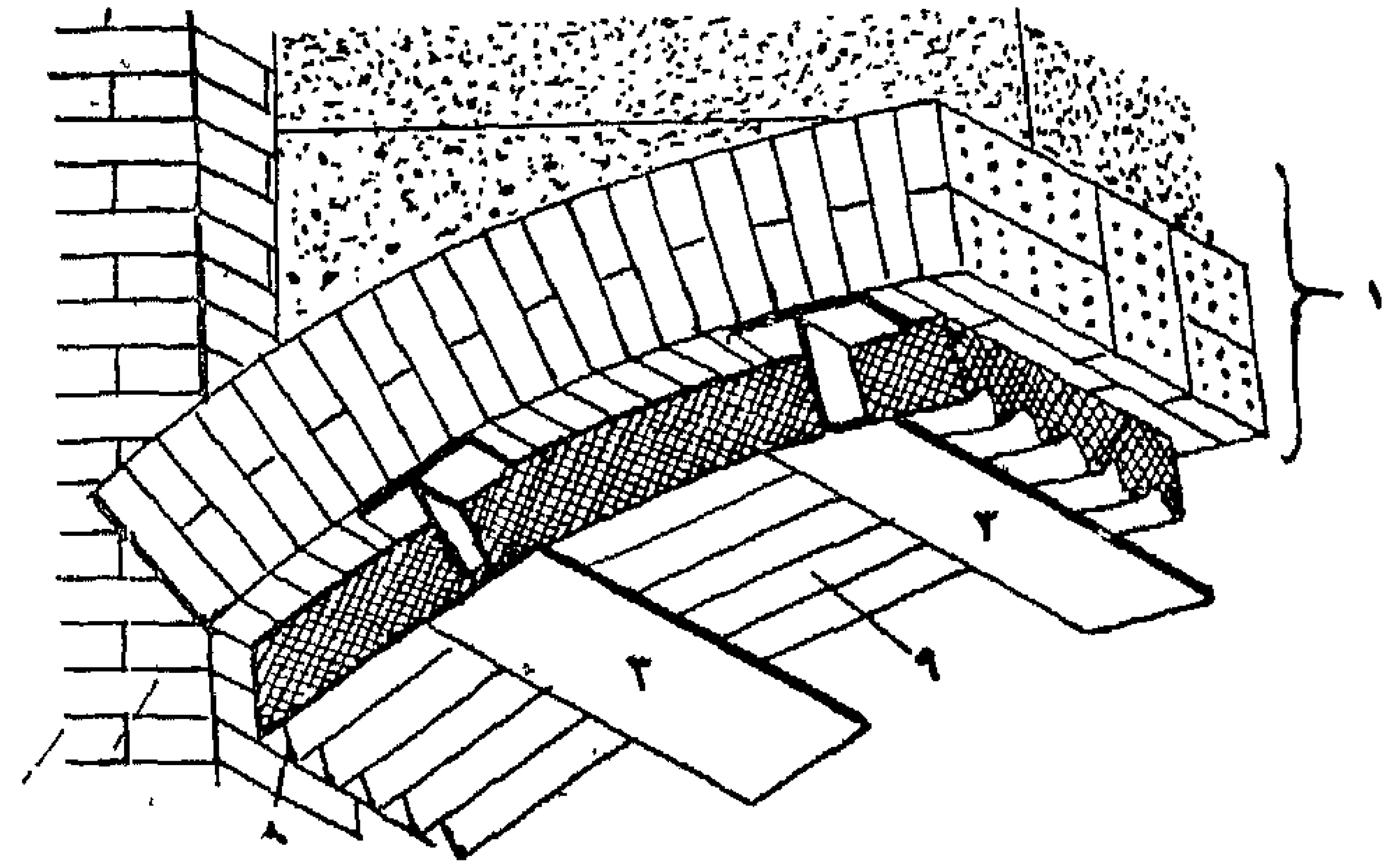




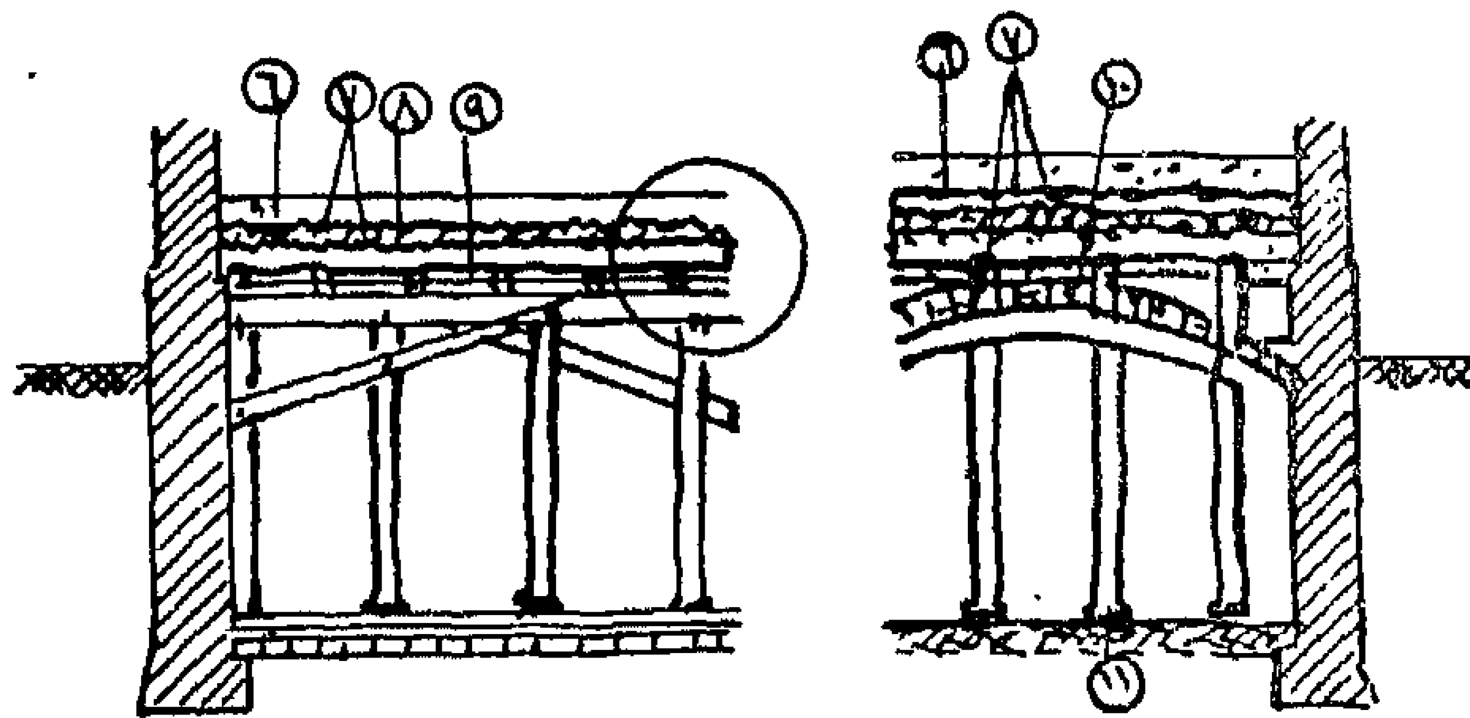
(شكل ٨٢)

إعداد المخابىء فى المبانى القائمة يتطلب إعداد الأسقف زيادة الأسماك والصلبات (القوائم) المختلفة .

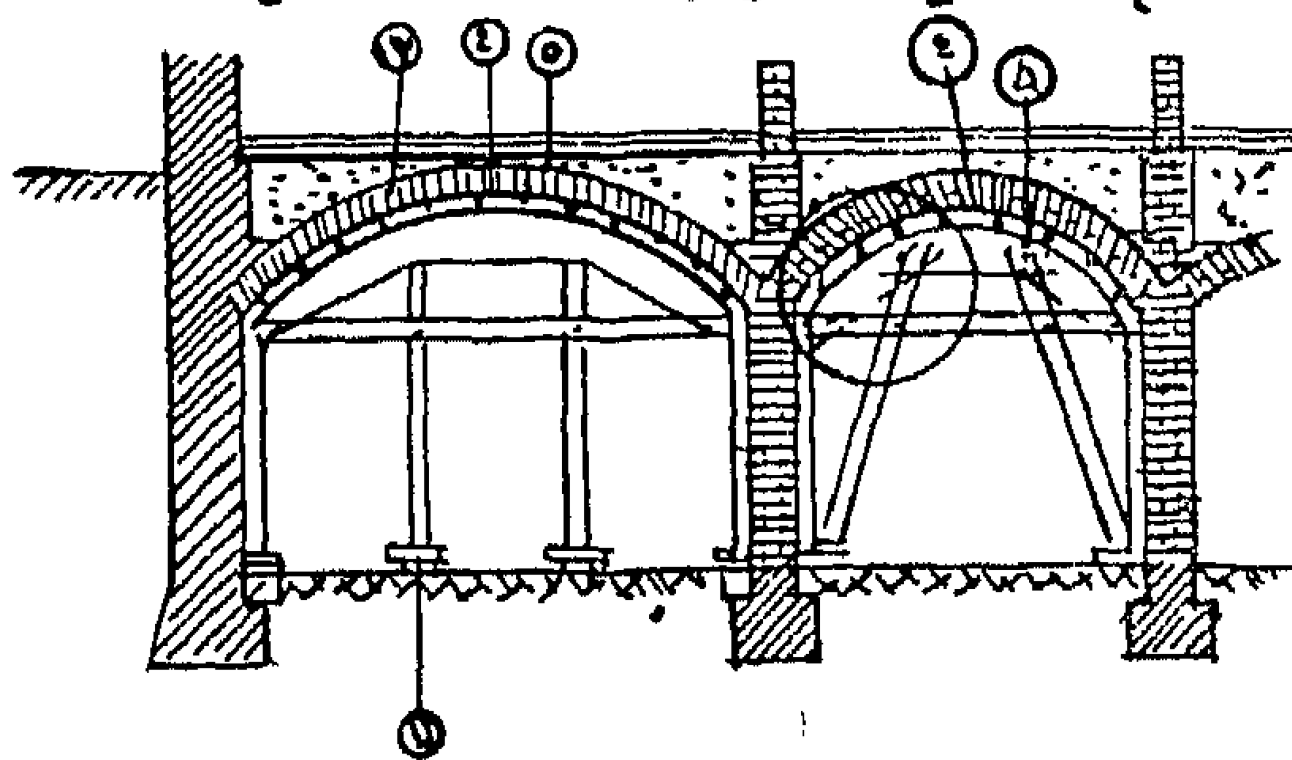


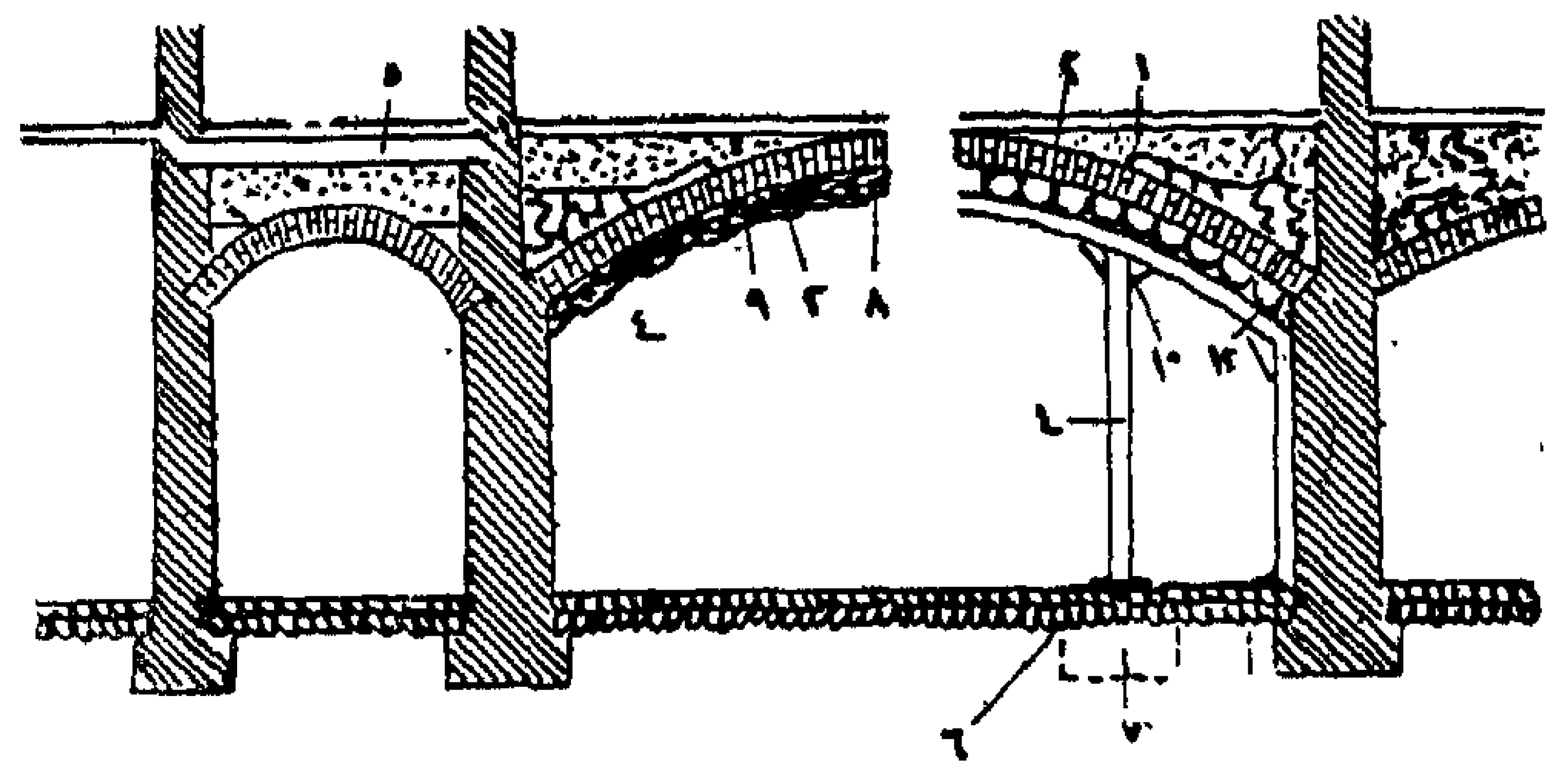


٤ تقوية سقف معقود



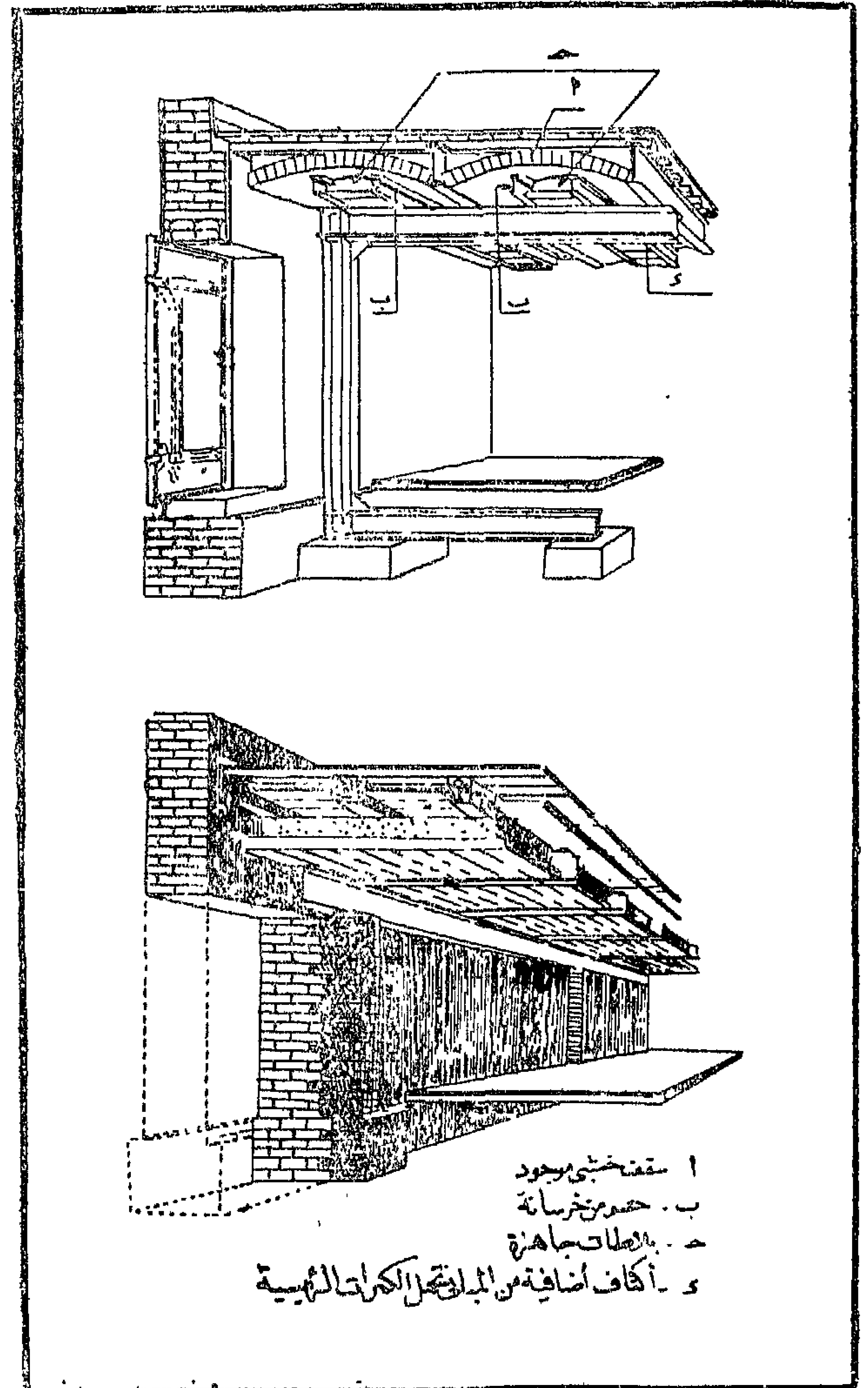
صلبة اضافية لتقوية أسقف خشبية



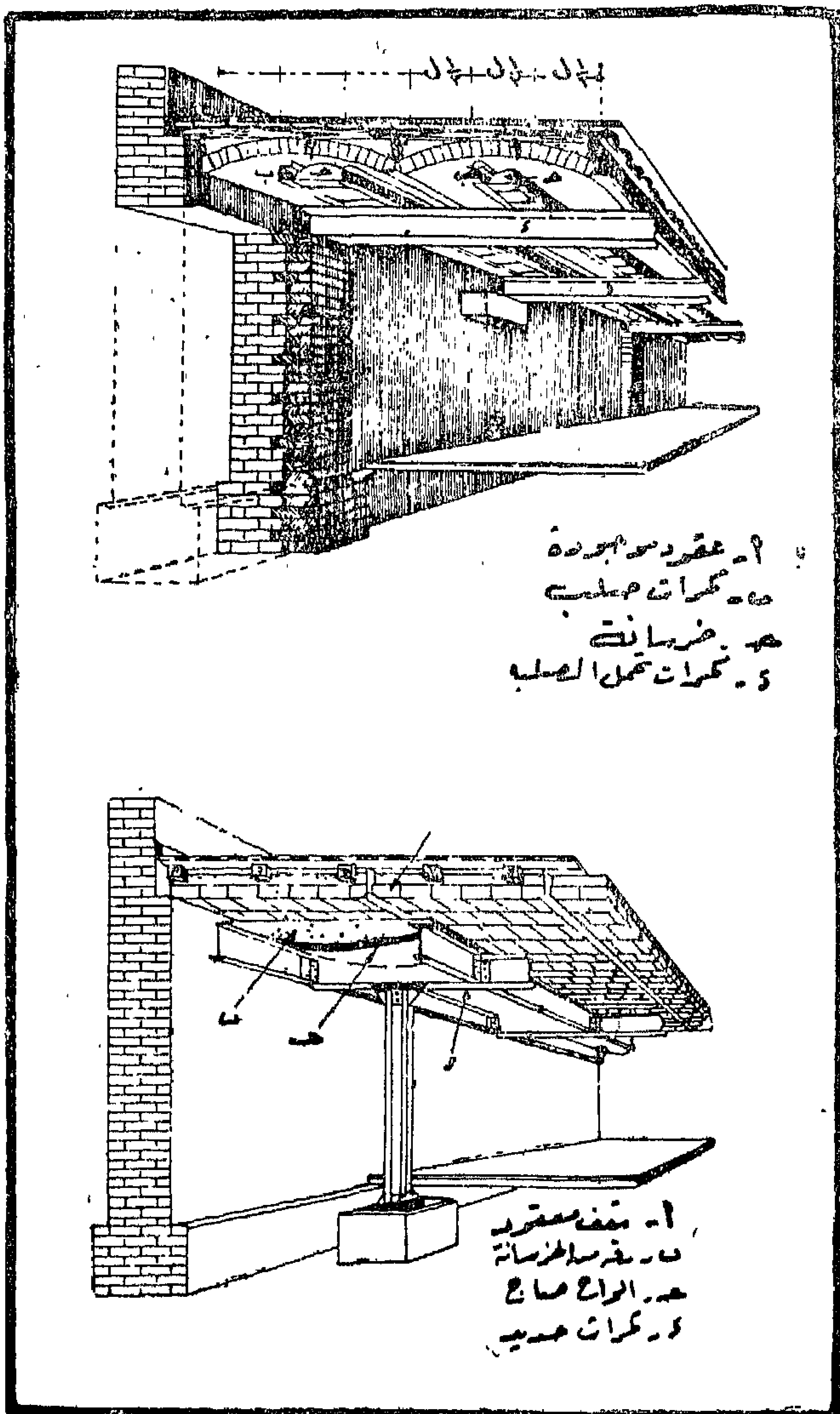


(شكل ٨٣)

(شكل ٨٤)



(شكل ٨٥)
تقوية عقود بكمرات حديدية وأعمدة إضافية



(شكل ٨٦)
تقوية سقف بكمرات وأعمدة حديد

Tests have shown that for blast resistance purposes a structural — grade steel is much better for reinforced than a hard-grade. When a reinforced-concrete structure is subjected to heavy blast forces and damage occurs, the softer steel may elongate or deform without failure where the hard grade steel snaps. More energy is absorbed in the plastic range by the structural-grade steel. Accordingly, the use of a structural grade reinforcing steel is recommended. In the usual case such a selection will have little effect on rigidity.

Fire Protection :

Fires are started by radiant heat and by secondary effects such as overturning of stoves and ruputure of gas pipes. Fire resistant construction and avoidance of fabrics and other light material of inflammable character are essential to reduce fire damage. The possible distruption of water supply and the tremendous demand for fire-fighting services in time of disaster must be kept in mind.

All of the proved methods of design to reduce fire damage are fully applicable in plans to minimize the effect of atomic bomb. Extreme fire protective measures are indicated under certain conditions. The value of protection of steel columns and other steel members from fire is emphasized by the distortion of exposed structural steel frames in Japan. Narrow fire breaks in Japan were of little use. Fire breaks which may be provided for in city planning, or demolition once fires have started, must be adequate for a major conflagration.

The provision of an adequate water supply is probably the most important single element in control of fires. In Nagazaki, it was estimated that almost immediately after the detonation, fires were started in dwellings within a 3000 ft. radius from ground zero. Beyond this distance, fires were caused largely by spread ; nearly all fires were secondary. The water pressure was only 30 pounds per square inch at the time of the explosion and because of breaks in mains and house service lines, soon dropped to 10 pounds and on the following day was zero.

The experience at Nagazaki gives some idea of the area immediately affected and that in which some control may be possible. As indicated earlier, there are certain areas of most big cities that would contain probable targets. The enemy would probably want to damage facilities or plants most important to the war effort. However, there would be no assurance that the explosion might not occur at some other point because of errors by the attacking force a reasonable approach would be to study the may of the installation and make various assumptions as to areas in which large scale fires might be started by an atomic bomb with loss of water supply occuring in the same area. The objective would be to provide for the localization of the loss of pressure and water in order to assure adequate pressure and supply for fire-fighting in fringe areas.

We can see that it is possible to calculate the effects which we do receive from an explosion both above ground and below ground. The general effect of an atomic blast varies with a number of factors, the distances from the explosion, the direction and vertical angle from the explosion, the shape and size of the structure, and the equalization of pressure by local failure such as window breakage. Remember to design your reinforce concrete structures for a horizontal wind component of 90 ft^2. and a vertical of 70 ft^2.

It should be noted that in derving the above relation, the height of burst remains at 2000 ft. and only the size of the weapon is varied. A similar study of neurons is unwarranted in view of their limited range.

Thermal radiation may be calculated in a similar manner by use of the distance calorie graph.

For a nominal 20 KT atomic explosion at 2000 ft. and an equation like that given in the foregoing paragraph. Atmospheric conditions have a strong influence on thermal radiation and may be a greater factor than weapon size. The following figures show the relative thermal radiation distance for various sizes of bombs.

	10 KT	20 KT	40 KT	80 KT
Effective Thermal Radiation Distance (10 cal)	0.59	1	1.39	1.88
Effective Thermal Radiation Area (10 cal)	0.35	1	1.49	3.52

General Considerations :

Rigidity, redundancy, and ductility are important factors affecting resistance of buildings to blast. All of these increase resistance but it is now necessary to suggest design methods for improving resistance in the respects. Stability is also a factor, but in the usual case will be less important. The stresses produced by overturning effect should be considered in all cases, however.

It is believed that the general solution of the problem of designing a building to resist high lateral and downward pressures is to provide addition resisting elements, such transverse shear walls, lateral beams, and deep lateral trusses, and to design concrete floors and roofs to transmit the lateral forces to shear walls. In bending caused by frame action. The conventional use of the column as the resisting elements is unsatisfactory for high lateral forces. The establishment of design requirements for a static wind load is largely arbitrary to include any design feature that will provide greater strength where cost is not materially increased. It will also be found that limiting the height of buildings is desirable in order to avoid high lateral stresses.

Redundancy is the quality of a structure to resist damage when certain members fail, by bringing into play other structural elements. Suppose, for example, that first-story columns were damaged by shearing action but that there were reinforced-concrete walls that would help support the load from above. The walls may be damaged too, but they may continue to support the second floor of the building. In a Manila public building several column in a row in the first story were destroyed by artillory fire. The second floor sagged slightly but the damaged portion was bridged by the undamaged structure above. In general, reinforced-concrete structures have this quality. No absolute guide can be laid down for design, but a study of probable points of failure and possible support that might be provided by adjacent portions of the building should indicate to the designer both possible and practical means of adding to the blast resistant quality of the building.

Ductility in a building material refers to its quality of yielding gradually under stress, or of undergoing deformation before failing. Usually a ductile material would deform to a greater extent within the elastic limit under the same load than one that is less ductile. In that sence a requirement for ductility is not consistent with rigidity. Nevertheless, ductility is an important consideration in resisting collapse. When the elastic limit of a ductile material such as steel is exceeded, considerable yield results before failure occurs. On the other hand a brittle material such as concrete would yield only to a limited extent before failing.

For example, the 20 KT bomb creates a pressure of 5 psi at 2,000 yards (d_1) ; the distance d_2 at which this pressure will be found for a 60 KT bomb is obtained by substituting and solving for d_2.

$$\frac{2000}{x} = \frac{(20)^{1/3}}{(60)} \qquad x = 2880 \text{ yards}$$

Because pressure varies exponentically with distance, no simple formula can be derived express the relationship between pressures at a given distance and a given size of bomb.

Since the area is proportional to the square of the radius, the effective blast damage area A increases as the two-thirds power of the ratio of the bomb sizes. Thus,

$$\frac{A_1}{A_2} = \frac{(W_1)^{2/3}}{(W_2)}$$

For example, if the effective area for a 20 KT bomb is 4 square miles, the effective area for an 80 KT bomb would be $4 \times \frac{(80)^{2/3}}{(20)} = 10$ sq mi.

A reasonable assumption is that the penetrating radiation released is directly proportional to the total energy released by a bomb. Thus the number of neutrons or gamma rays in roentgon units "r" at a particular range varies directly with the bomb size. As the dosage — distance curve varies exponentionally, the lethal radius or area increases slowly with increase in bomb size. Thus

$$\frac{\text{Dosage at distance d for a 20 KT bomb}}{\text{Dosage at distance d for W — KT bomb}} = \frac{20}{W}$$

For example, the gamma ray dosage at 1750 yeards for a 20 KT bomb is 50 roentgens. For a 60 KT bomb, the dosage would be 150 roentgens, derived as follows :

$$50/x = 20/60 \qquad x = 150 \text{ roentgens}$$

The comparison of roentgen dosages for any given size of bomb at various distances merely requires solveng an equation similar to the above. However, if it is desired to consider the relative penetration for various sizes of bombs with regard to the 20 KT bomb, a given level of radiation is selected as a basis of comparison.

For example, to determine the distance to which 400 r extends for bombs of different yields, scale off the distance corresponding to $\frac{400r}{\frac{W}{20}}$ on the dosage — distance curve for the air burst of a nominal 20 KT weapon. The following figures show the relative penetration for various sizes of bomb compared to the 20 KT bomb.

Size of bomb :	10 KT	20 KT	40 KT	80 KT
Effective Penetrating Radiation Distance (400r)	0.89	1	1.13	1.28
Effective Penetrating Radiation Area (400r)	0.79	1	1.28	1.64

ings would be proportionately more resistant as the pecentage of horizontal to vertical design load increases.

The effect on steel frame buildings, such as multiple storied office and hospital structures, should be approximately the same as that on reinforced concrete. Tall buildings having heavy steel frames and a long period of vibration should withstand the effect of blast vertical.

U.S.A. steel industrial buildings would probably fare no better than those in Japan. The saw-tooth roofs designed as rigid frames would be especially vulnerable to blast damage.

Recommendation on Construction :

For multistoried reinforced concrete steel-frame buildings the designer should assume a horizontal wind component of 90 pounds per square foot and a vertical component of 70 pounds per square foot for protection against structural collapse for an atomaic bomb of 20 KT energy equivalent. In addition, buildings and their component parts should be designed employed the methods, allowable stresses, and details employed in wind — or earthquake-resistant design. The building should be limited to a height of 100 feet.

For smaller reinforced-concrete buildings, design for the same pressures as prescribed for the multistoried reinforced-concrete buildings.

In the design of steel mill buildings, again design for a horizontal wind component of 90 pounds per square foot and a vertical component of 70 pounds per square foot for resistance of the frame at a horizontal distance of one-half mile and height of burst of 2,000 ft. This assumes that failure of corrugated metal or asbestos-cement siding and roofing will reduce the load one frame, thus compensating for lighter weight. Use of a material, such as asbestos-cement which will break up more readily than corrugated metal will contribute to reduction in load on the frames and reduce injuries and damage from pieces of siding or roofing that strike occupants and equipment.

The explosion of two atomic bombs over the Japanese cities of Hiroshima and Nagazaki have provided considerable information concerning the effects of a 20 Kiloton TNT equivalent weapon. By direct measurement, laboratory testing, and theoretical analysis, scientists have established distance and time relations for blast, thermal and nuclear radiation effects for the so-called nominal bomb. It is possible given this set of characteristics for an air burst at 2,000 ft., to derive by means of scaling laws, similar quantitative characteristics which apply to atomic explosions in general. The existance of simple scaling laws for blast depend on the hydrodynamical equations which apply to shock waves. From these it is possible to show that two explosions, having the same initial conditions, differ only with respect to a scaling factor applied to both distance and time. It should be noted that in scaling for blast, both the distance from ground zero and the height of burst change, since the pressure is reflected from the ground as well as being influenced by the MACH effect. A different set of scaling laws apply to thermal and initial nuclear radiation where only the slant distance is considered.

The scaling laws have been simplified for practical use by use of the rotation given below :

d	=	distance in yards from ground zero
w	=	TNT equivalent in kilotons
KT	=	Kilotons
A	=	effective blast area in square miles
psi	=	pounds per square inch
r	=	roentgen units of radiation intensity
cal	=	calories per square centimeter

The distance at which a given pressure may be found for two bombs is directly proportional to the cube root of their TNT equivalents. That is,

$$\frac{d_1}{d_2} = \frac{(w_1)^{1/3}}{(w_2)}$$

but most cranes were of low capacity. Construction was generally comparable to that in the United States. The first effect of blast was to strip off the siding and the roof material. Since this did not occur instantaneously, a large impulsive force was applied to the frame. Sever damage occured up to a distance of 6,000 feet.

There were several types of failure of such structures. At close range the buildings were pushed over bodily, while at greater distances they were left leaning away from ground zero in many cases. The columns, being long and slender, offered little resistance to the lateral force. Sometimes columns failed by a combination of lateral force that caused flexure and at the same time, an increased downward loads from the vertical compenent of blast on the roof. This caused buckling and collapse. Roof trusses were buckled by compression resulting from blast on the exposed side of the building. A difference was noticed in the effect on the frame depending upon whether a brittle material like asbestos-cement or a material of high tensile strength such as corrugated sheet iron was used for roof and siding. Asbestos-cement broke up more readily and transferred less force to the steel frame with less structural damage.

Fire produced heavy damage to unprotected steel members so that it was impossible to tell exactly what the blast effect had been. In general, the steel frames were badly disorted and would have been of little use even though siding and roofing material had been available for repairs.

Wood trusses were also used to support the roofs. These were vulnerable to blast because of poor framing and connections and were readily burned out by fire. Concrete columns were usedin some cases with steel roof trusses. The concrete columns were more resistant to buckling than the steel.

Smaller buildings constructed with light load-bearing walls collapsed. large buildings with cross walls and of somewhat heavier construction were more resistant but failed at distances up to 6,200 feet. Even when the building remained standing, cracks were observed at the junction of cross walls and side walls.

While the quality of the workmanship in timber-framed buildings was high, little attention was paid to engineering principles. Mortise and tenon joints were weak points and connections in general were poor ? Timbers were notched excessively or splices were put in improper locations. In general the construction was not well adaped to resist lateral or twisting action. Housing collapsed at Nagazaki up to a distance of 7,500 feet and there was structural damage up to a distance of 8600 feet. Roofs, wall panels, and partitions were damaged out to a distance of 9,000 feet. While the structural effects observed in Japan are comparable in general to what would be expected in this country. Some differences are worthly of consideration in this course.

In Japan, reinforced concrete buildings of earthquake resistant design withstood blast quite well. These buildings were designed for a laterial force equal to 10 percent of the vertical load. When lateral pressure tends to displace the top of the building with respect to the foundation, the resulting action is roughly the same as if earthquake forces moved the foundation against the interial resistance of the structure.

Our mulistory buildings in this country are generally designed to withstand wind only. Therefore, our reinforced concrete buildings would be generally less resistant to collapse than those designed for earthquake resistance in Japan. In the 11 western states of U.S.A. the building codes provide for the design of structures to resist horizontal earthquake forces varying from 2 to 16 percent of the vertical load, which is usually taken as dead weight plus half the vertical design live load. Of the earthquake zones, the Pacific coast area has the highest requirements. The earthquake design requirements as stipulated in the building codes are similar to those for wind loads, but call for a 33 percent increase in the allowable working stresses. These build-

Reinforced concrete buildings are also the most fire resistant, for the concrete protects the steel structural members from the heat. However, if the contents of the building are combustible and continue to burn intensely for some hours, the concrete can crumble and thus expose the reinforcing steel. This may then be weaken by the heat and the building may colapse.

There were many multistory reinforced concrete frame buildings of this type in Hiroshima and smaller number in Nagasaki. The earthquake construction code (1932) limited the height of these buildings to 100 feet with a designed lateral load one-tenth the gravity load.

Close to the explosion, the vertical component of blast was more important than the lateral (side wise), so that there was heavy damage caused by the downward force exerted on the roof.

Depending upon its strength, the roof was either pushed down and left sagging or failed completely. The remainder of these buildings were loss damaged than similar buildings at greater distances because of the lesser horizontal force.

At greater distances the lateral force was proportionately greater and cause a buckling and failure of the roof slab by lateral compression. This was apparently caused by the force applied to the side of the building which in turn was transferred to the roof, tending to push it back. Since roof was restrained by connections to less affected portions of the — building, it failed in compression. A similar failure occurred in the bays between the first row of interior columns and the affected wall. Buckling was usually upward.

Craking of concrete and over-stressing of concrete and steel at haunches and connections was apparent in a large number of buildings and is readily explained by the tremendous lateral force applied.

Columns in the first stories were cracked diagonally. This was probably caused by the higher shearing force in the first story resulting from the lateral pressure on the building. Since these columns would receive a heavier lateral force than these above, it is quite natural that they would fail first.

On the side towards the blast, walls were dished inward. The degree of such action depended upon the distance from ground zero, the strength of the wall, and the number of windows which, by breakage, assisted equalizing pressure rapidly.

Floors were most affected by direct blast in those cases where pressure equalizations was not possible. For example, the floors overenclosed basements were pushed downward when higher floors were undamaged.

In addition to the before-mentioned damage, there was heavy damage to false ceilings, plaster, and partitions. Such damage occured in varying degrees out to a distance of 12,000 feet in Nagazaki. Glass window panes were blown out as far as 12,000 feet from ground zero. This type of damage is extremely important because of the large number of casualities caused by missiles and flying glass.

There was only one multistory steel frame buildings, located in Nagazaki, of which any record has been kept. This building was located at 4,750 feet from ground zero. The roof was dished three feet but the remainder of the frame was largely unaffected. The only part of the structure not classified as being of heavy construction was roof, which was of thin concrete supported by unusally light steel trusses. The downward failure of the roof was the only structural damage in the building. reinforced concrete buildings at the same distance were undamaged. However, it is difficult to draw any conclusion as to relative resistance of the two types.

In Nagazaki there were many steel buildings used for manufacturing ; these were generally of the shed type, with some of the sawtooth design. Roofs and siding were of corrugated sheet metal or asbestos cement. In some cases there were rails for heavy gantry cranes,

the pressure on the outside walls. The strength is determined mainly by the type of construction, but this can be modified by various structural details which are not obvious to the eye. The strongest buildings are heavily- framed steel and reinforced concrete structures, while the weakest are probably certain shed-type industrial buildings (shops) having light frames and long spans of unsupported beams.

The effect of shape is not very marked since most buildings are rectangular in form. A long, narrow structure will be more resistant to blast striking on the narrow end than on the side. However, if struck on the side, such a building would probably suffer more than one having similar dimensions in both directions.

The shape effect is more evident in certain auxiliary parts of structures, such as smoke stacks and chords of bridges. Because of the rapid equalization of pressure around them, smoke stacks are supprisingly resistant to blast. They often remain standing when adjoining structures are leveled to the ground. On the other hand, flat surfaces, such as windows and doors, in a wall, will tend to give way easily.

The rapid failure of window panes, light siding, and other flat, weak portions of a structure of often advantageous. When such failure occurs in a very short space of time, there will be a tendency for equalization of the pressure inside and outside the building. This reduce the destructive effect of the blast on the structure as a whole

These general remarks apply to the effects of air blast from explosion of all types. The atomic bomb introduces an additional factor because of its tremendous energy release and the long duration of the blast wave. This is something like a second, as compared with a few thousandths of a second for an ordinary HE bomb. Thus, while a conventional bomb will affect only part of a building, the blast from an atomic bomb can engulf and damage whole buildings.

The foregoing description of damages has been somewhat general in character. For defensive purposes it is necessary to know something of how individual structures and particular types of equipment are likely to survive an atomic attack. Consequently, the effects of blast, shock and fire on specific kinds of buildings and material will be outlined. Radioactive contamination will not be mentioned unless there is some special characteristic to which attention should be called.

Certain of the Japanese structures at Hiroshima and Nagasaki were designed to be earthquake resistant which probably made them stronger than their counterparts in this country. Other construction was possibly lighter than our own. However, contrary to popular conceptions concerning the flimsy characteristics of Japanese residences, a group of highly qualified architects and engineers who surveyed the damage concluded that the resistance to blast of American residences in general would not be markedly different from that observed in those cities. At Hiroshima and Nagasaki, virtually *complete destruction* occurred out to a radius of approximately one-half mile from ground zero. (This is approximately three-quarters of a square mile). In addition, damage ranging from severe to destructive occured out to a radial distance of about a mile from ground zero (foursquare miles).

Reinforced Concrete and Heavy Steel-Frame Building.

While all types of structures can be damaged by sufficiently high blast pressures, some are less vulnerable than others. Reinforced concrete buildings and those with heavy steel frames are the most resistant types of construction. When partial fail are occurs, for example, buckling or collapse of roof and floors, or fracture of columns, the undamaged members can often still carry the whole of the structure. In these circumstances, complete collapse will not occur, and the damage portions of the buildings are more likely distort than to break.

over an extended period of time in the form of gamma and beta radiation from the fission products remaining after the atomic explosion. Because of natural radioactive decay, the activity of the fission products fall off or decay in the course of time.

Characteristics of an Atomic Explosion :

The air burst of an atomic bomb is accompanied by the formation of an intensely hot, luminous sphere of compressed gas called the ball of fire. As this ascends and cools, an expanding column of smoke forms and rises to a height of from 5 — 8 miles before spreading out to produce the characteristic mushroom-shaped atomic cloud.

The explosion is followed by the formation of a shock wave, moving outward at high speed. The overpressure in the shock wave and the accompanying wind are responsible for the blast damage to structures. At a certain distance from ground Zero, the direct shock wave fuses with the wave — reflected from the surface, causing the Mach effect. The overpressure at the surface is thereby greatly increased.

Thermal radiation is omitted from the ball of fire in two pulses. The first lasts for little more than a one-hundredth part of a second and contains a large proportion of ultraviolet radiation. The second pulse, lasting up to 3 second and carrying most of the thermal energy omitted by the bomb, consists mainly of visible and infrared rays. Except near ground Zero, it is the second radiation pulse which is responsible for skin burns and some incendiary action.

The immediate nuclear radiation which reaches the earth from the ball of fire and the atomic cloud at the time of the explosion consists of gamma rays and neutrons. The lethal range of the noutrons is small in comparison with that of the gamma rays and so they be ignored.

The residual radioactivity, consisting of gamma rays and beta particles from the fission products and alpha particles from the uranium or plutonium that has not undergone fission, is that which remains on the ground after the explosion. In the case of an air burst, it will usually be negligible.

Increasing the energy release of the bomb increases the effective ranges of the shock wave, the thermal radiation, and the immediate nuclear radiation, but the area of damage always increases less rapidly than the energy release. The effect of the immediate nuclear radiation becomes relatively less important, with respect to blast and thermal radiation, as the energy of the bomb is increased.

Structural Damage :

The damage to structures and material that results from an atomic explosion is due to two main causes ; (1) blast and shock, (2) heat and fire. Neither the immediate nuclear radiation nor the residual radioactivity proproduce any mechanical destruction, although radiation from the contamination may make it hazardous for personnel to remain in a building or to operate equipment for some time. In general, structures and material will be rendered useless by the combined action of two or more of the factors. But since they produce damage in different ways they will be considered separately.

The general nature of the effect on a structure of a shock or blast wave in air is that of a giant blow, due to the sudden onset of pressure, followed by a more or less steady force. This continues until the pressure wave reaches the rear of the structure, when it exerts a crushing or squeezing effect. Because of the action of these forces, a properly anchored weak structure may be crushed without being displaced bodily. On the other hand, a strong structure may move without being crushed.

The ability of a building to withstand blast depends primarily on its strength and, to a lesser degree, on its shape and on the number of openings which can serve to relieve

ATOMIC EXPLOSION

Introduction to atomic explosion :

We have discussed the effects of conventional weapons with regard to impact, penetration, and explosion. We have examined the characteristics of pressure and impulse transmitted through the air and the earth.

Now we want to continue our discussion of modern weapons and examine an atomic explosion. While current literature centers about the atomic bomb dropped on Hiroshima and Nagasaki, which was the equivalent of 20 Kilotons of TNT, we may relate their effects to bombs of other size by use of the appropriate scaling laws. The basic principles, however, will apply to atomic weapon of all sizes.

This instruction will consist of a detailed examination of the structural effects of an atomic explosion. In addition, we shall also deel with the radiation effects insofar as they may control protective requirements at certain distances from the explosion. Our purpose is to familiarize you with the various factors which must be considered in planning protective construction to resist atomic weapons.

Classification of Atomic Explosions :

Here me will not go to receive a thorough orientation as to the characteristics and effects of an atomic bomb; however, before we begin discussion the effects of an atomic explosion on protective structures, let's refresh our minds as to the effects asociated with an atomic explosion.

The medium in which a bomb is burst determines in great measure the physical effects. In particular, large difference in the effects result, depending upon whether the detonation occurs in air high above the surface, at the surface, or beneath the surface. It is convenient, in presenting the effects information, to discuss it by these type of burst. During this instruction we shall discuss only the air burst bomb — or that which is burst in air at a height greater than the maximum radius of the fire ball.

The yield of an atomic bomb is expressed as the weight of TNT which would give the same total energy release. A convenient unit is 1000 tons of TNT energy equivalent and is expressed briefly as 1 KT (Kiloton). In our instruction we shall study the "nominal" atomic bomb which has an approximate yield of 20 KT.

Atomic Bomb Compared to High explosive :

The explosion of an atomic bomb resembles that of an ordinary HE bomb in the respect that it is due the rapid release of a large amount of energy in a small space. The energy produced in the HE bomb is due to a chemical reaction, and in the atomic bomb it results from a nuclear process, namely — the fission (splitting) of nuclei of particular forms (isotopes) of the elements urainum or plutonium. However, weight for weight, the energy released in fission is millions of times greater than that produced by a chemical explosive. It is this great concentration of energy, and its rapid liberation, in about a one-millionth part of a second, that accounts for the tremendous power of that atomic bomb.

At least half of the total energy of the bomb contributes to the blast or shock effects. The atomic bomb is thus essentially a blast weapon, like an HE bomb.

The large energy release in a small space in an atomic bomb results in the attainment of a very high temperature, approaching that in the interior of the sun. Consequently, and intense thermal (heat) radiation, carrying about one-third of the total fission energy, emanates from the bomb. It can produce slight skin burns as far away as 2 miles, on a moderately clear day, and the warmth may be felt more than 10 miles aways.

A small amount of the bomb energy is carried off by escaping neutrons and gamma rays at the instant of the explosion. The remaining energy of the atomic bomb appears

SOLUTION

Table 12 :

1) Underground
Note more than 3 hrs.
Ventilation

From table we get the following data :—
Ventilation rate per person
= 180 ft^3/hr.
Total surface area per person
= 25 ft^2
Floor area per person
= 6 ft^2
Volume per person
= 50 ft^3

2) Surface area = $18 \times 18 \times 2 + 18 \times 18 \times 2 + 18 \times 8 \times 2 = 1224$ ft^2
Floor area = $18 \times 18 = 324$ ft^2
Volume = $18 \times 18 \times 8 = 2592$ ft^3

3) *Checks :*
Check surface are

$$\frac{1224}{25} = 48.96 \text{ persons} = 48$$

Check floor area =

$$\frac{324}{6} = 54 \text{ persons}$$

Check Volume =

$$\frac{2592}{50} = 51.84 = 51 \text{ person.}$$

4) Therefore, the structure can accomodate 48 persons.

5) Air required $48 \times 180 = 8640$ ft^3/hr.
We have $150 \times 60 - 1000 = 8000$ ft^3/hr.
8000 is less than 8640
Hence we need one more.

Problem 5 :

If in the previous example the dimensions are 20 × 9 × 7 fect The shelters underground and will not be occupied for more than 3 hours at any one time. No ventilation will be used.

Required :

The number of person to occupy the shelter. Noticing that air must be changed by 25%).

SOLUTION

Total surface are = $2\,(9 \times 20) + 2\,(7 \times 20) + 2\,(7 \times 9) = 766$ ft^2

Floor area = $9 \times 20 = 180$ ft^2

Volume = $20 \times 7 \times 9 = 1860$ ft^3

Checks :

Check Total surface area

$$\frac{766}{75} = 10 \text{ persons}$$

Check floor area =

$$\frac{180}{6} = 30 \text{ persons}$$

Check Volume =

$$\frac{1860}{200} = 6 \text{ persons.}$$

⁂ Max number to occupy is 6 persons.

$$AD = \frac{5}{\cos 22} = 5.39$$

AD is less than AC

∴ Bomb must penetrate the concrete cover as Fig. (1).

C) Here we must notice that the striking velocity V at the ground surface which is 825 ft/sec will be uniformly — decelerated inside earth.

i.e. ∴ A long a path AB the velocity V (825) becomes (0) after 22 feet.

D) So we can know how much it can loose till it reaches the pt D when it strikes the concrete cover and the difference will give us the new striking velocity (V_1)

For a length 22 (AB) we loose 825 ft/sec
For a length 5.39 (AD)″ loose ?

$$? = \frac{5.39 \times 825}{22} = 202$$

∴ $V_1 = 825 - 202 = 623$ ft/sec

After knowing this the problem now will be easy and it will be similar to problem 1. So we can say that we have a problem of the following form.

A bomb strikes a concrete surface with a striking velocity 623 fect ses, Calculate the depth of penetration and explosion.

Step 1 :

$$x = \frac{222 \times p \times d^{.215} \times V^{1.5}}{Y} + .5\ d$$

$$= \frac{222 \times 4.64 \times 1.8 \times .5}{50} + \frac{11.8}{2}$$

$= 23.4''$

Step 2 : Corrected path of penetration

For angle 22 and $V_1 = 623$ (less than 1000)

From fig. 5 using line A, factor of correction = .7

∴ Path = .7 × 23.4 = 16.4″.

$$\frac{P}{d} = \frac{16.4}{11.8} = 1.39 \text{ calibers}$$

Step 3 . Depth due to explosion

$$\frac{P}{d} = 6100 \left(\frac{W}{d^3}\right)^{.4}$$

$$= 6100 \times \left(\frac{150}{11.8^3}\right)^{.4} = .4 \text{ calibers.}$$

Step 4

Total penetration = 1.39 + .4 = 1.79 calibers.

From fig 6 — for caliber 1.79 we get thickness = 4.6 calibers.

∴ Thickness = 4.6 × 11.8 inches

Step 5 :

Total thickness
1.15 × 4.6 × 11.8 = 4 5.2

Result :

But the original design is of concrete thickness 4 feet, hence it is not sufficient as a cover and it must be of thickness not less than 5.2 feet.

Problem 4 :

You have been assigned the task of analysing the collective protection of several reinforced concrete shelters to be used for the protection of persons working in a certain plant. The inside dimensions of these shelters are 18 × 18 × 8 feet. The shelters will be constructed underground and will not be — occupied for more than 3 hours at any one time. Collective protectors available with a capacity of 150 c.f.m (cubic feet per minute) of pure air will be used in the shelters.

The leakage in the structure is 1000 c.f.h. (Cubic feet per hour).

Required :

a) Determine if these shelters are large enough to accomdate 50 persons.

b) Will one collective protector be sufficient? If not, how many should we use ?

Problem 3 :

You have been assigned the task of analying the design of a reinforced concrete structure. You are to check the thickness of the head cover to see if its is adequate. The following design criteria has been used.

The structure is to withstand the penetration of a 500 lb SAP bomb dropped from a plane flying 11000 ft above the structure at a true air speed of 250 m.p.h The overhead cover consists of 5 ft of sandy loam earth and 4 ft of reinforced concrete. The compressive strength of the concrete is 2500 PSI.

Required :

Using a safety factor of 15% for the concrete, will the overhead cover be sufficient to prevent scabbing ?

SOLUTION

Introduction :

A) First we have to prepare all data as followed before.

From table 1 :

P = 4.64
d = 11.8 inches
W = 150 lb

From Fig. 4 :

$d^{.215}$ = 1.8

From table 2 :

for concrete strength 25000 PSI
Y = 50

From Fig. 1 :

(for ht. 11000, air speed 250)
V = 825 ft/sec
angle of fall = 68°
∴ angle of obliquity = 22°

From Fig. 3 :

$V^{1.5}$ = .5

From table 3 :

K = 7.6

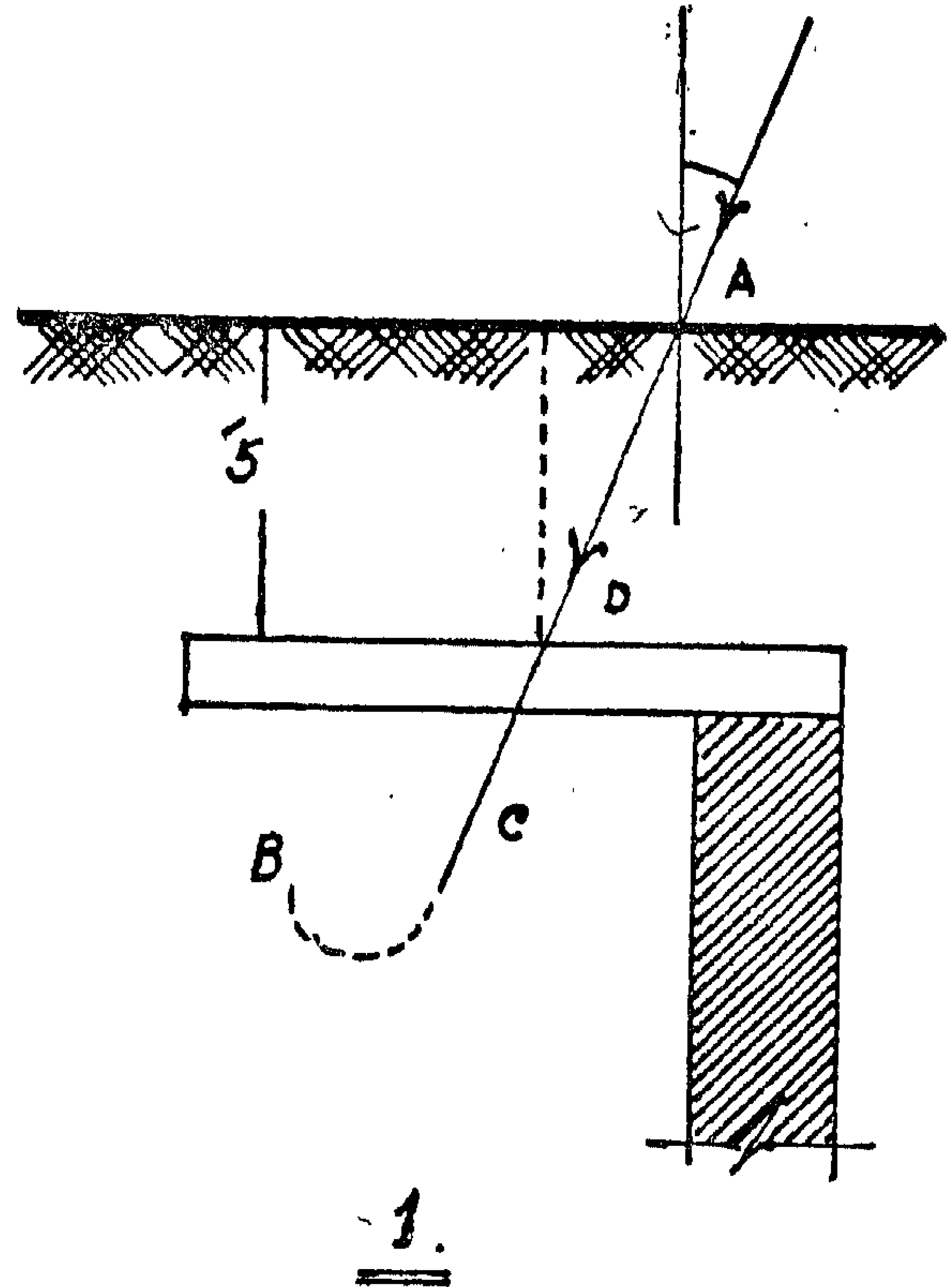
From Fig. 8 :

For V = 825
S = .625

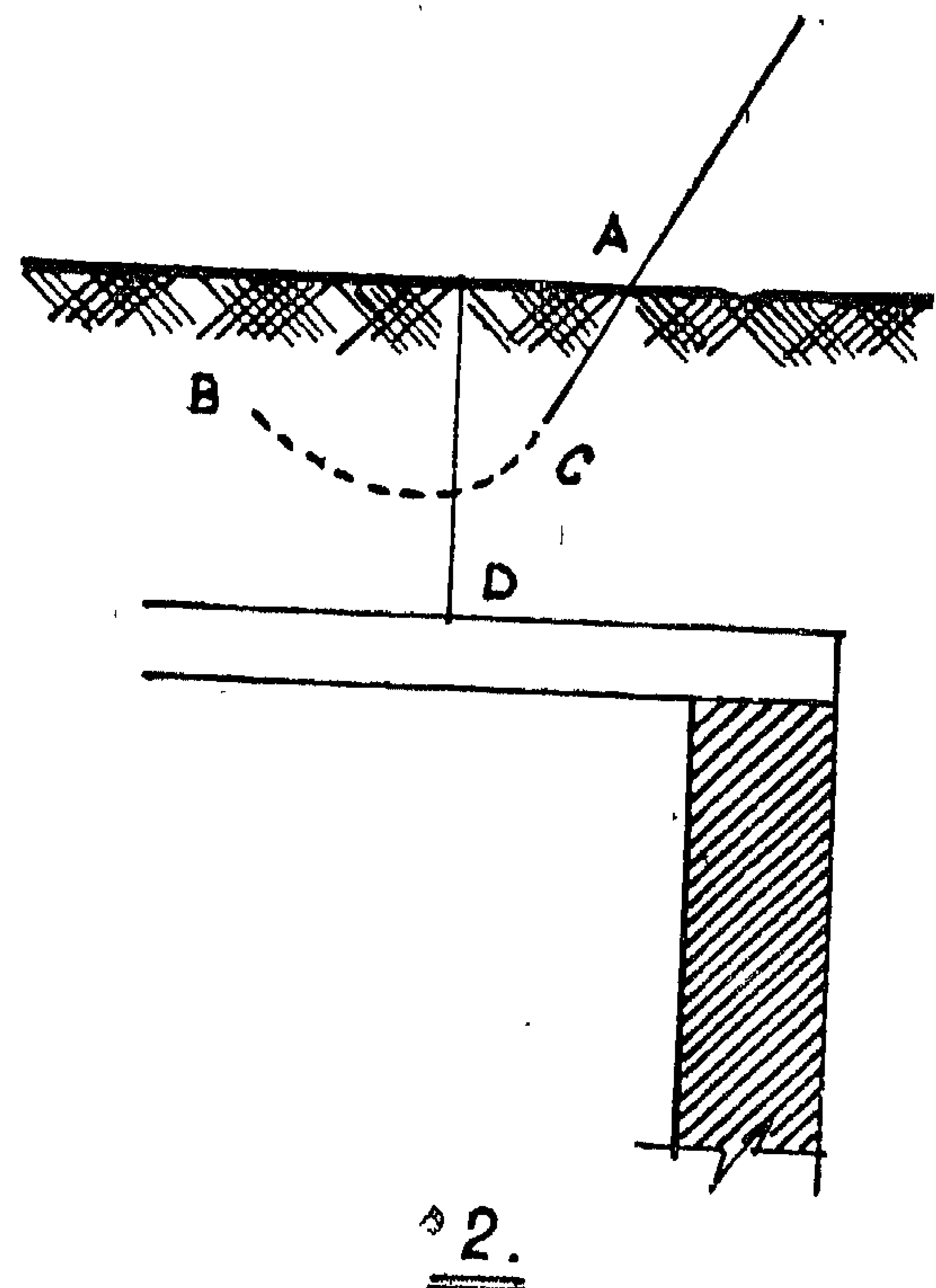
B) We have to see if the bomb after penetration in soil had it reached the concrete cover and penetrated it (Fig. 1) or not (Fig. 2) ? To know this we have to calculate the total path in soil.

$X = K\,P\,S$
$= 7.6 \times 4.64 \times .625 = 22$

$AC = \frac{2}{3} \times = \frac{2}{3} \times 22 = 14.7$



1.



2.

Step 4 :

Total thickness due to scabbing

(Fig. 6 — for caliber 2 we get thicknes — 5 calibers

i.e. = 5 × 14.2 = 71″

Step 5 :

Add 15 % if we are not going to use anti scabbing plates.

∴ Total required depth against scabbing = 71× 1.15 = 81.65″ (Answer).

Problem 2 :

A 500 lb (SAP) bomb is dopped from a plane travelling 350 (m.p.h.) (true air speed) at an altitude of 20,000 feet. Calculate the ap proximate penetration in sandy loam.

SOLUTION

(1) X = KPS feet

From table 3 :

K for sandy loam (7.6)

From table 1 :

p = 4.64

From Fig. 1 :

(For 350 air speed and height 20,000
V = 1000 ft/sec
α of fall 69°)
∴ α of obliquity 21°

From Fig. 8

For V = 1000
S = .75

X = KPS
= 7.6 × 4.64 × .75
= 26.4 feet

(2) Corrected path :

For angle of obliquity 21°, V = 1000 ft/sec.

From Fig. 5 line A

correction factor = .72
∴ Vertical path = .72 × 26.4 = 19 feet

(3) Add imperically factor of 20%

∴ Total vertical path due to penetration in soil
= 19 × 1.2 = 22.8 feet

(4) Effect of explosure :

Explosure will cause a crater of certain depth.

But the most important required depth is that of vibrations.

Vertical radius of rupture

$V_{RR} = .83\ H_{RR} = .83\ (F\ w^{1/3})$ (timber)
$= .83 \times (.7\ F\ w^{1/3})$ (concrete)

From table 4 :

F = 6.67

From table 7

w = 150

V_{RR} (concrete $= .83 \times .7 \times 6.67 \times 150^{(1/3)}$

∴ V_{RR} = 20.4 feet

Total depth = 22.8 + 20.4 = 43.2 feet

That means any concrete structure below this depth will be very safe from the effect of bomb.

Also any concrete structure far from the centre of explosure by the distance H_{RR}.

i.e. $.7\ F\ w^{1/3}$
$= .7 \times 6.67 \times 150^{1/3}$
$= .7 \times 6.67 \times 5.4 = 25.21$ feet

At such a distance the concrete structure will be also safe.

N.B. Any concrete structure in the ellipsoide will be damaged.

Step (2) (correction of path)

Angle of obliquity 21, V = 1000 ft/sec

Use line A Fig. 5) Correction = .72.

⁂ Corrected depth of penetration

$= .72 \times 30.1$

$= 22.3''$

⁂ Corrected depth in Calibers $= \dfrac{x}{d} = \dfrac{22.3}{14.2} = 1.54$ Calibers

Step (3) :

Penetration due to explosive in calibers

$$\frac{\text{Pexplosion.}}{d} = 6100 \left(\frac{w}{d^3}\right)^4$$

$$= 6100 \left(\frac{267}{(14.2)^3}\right)^4$$

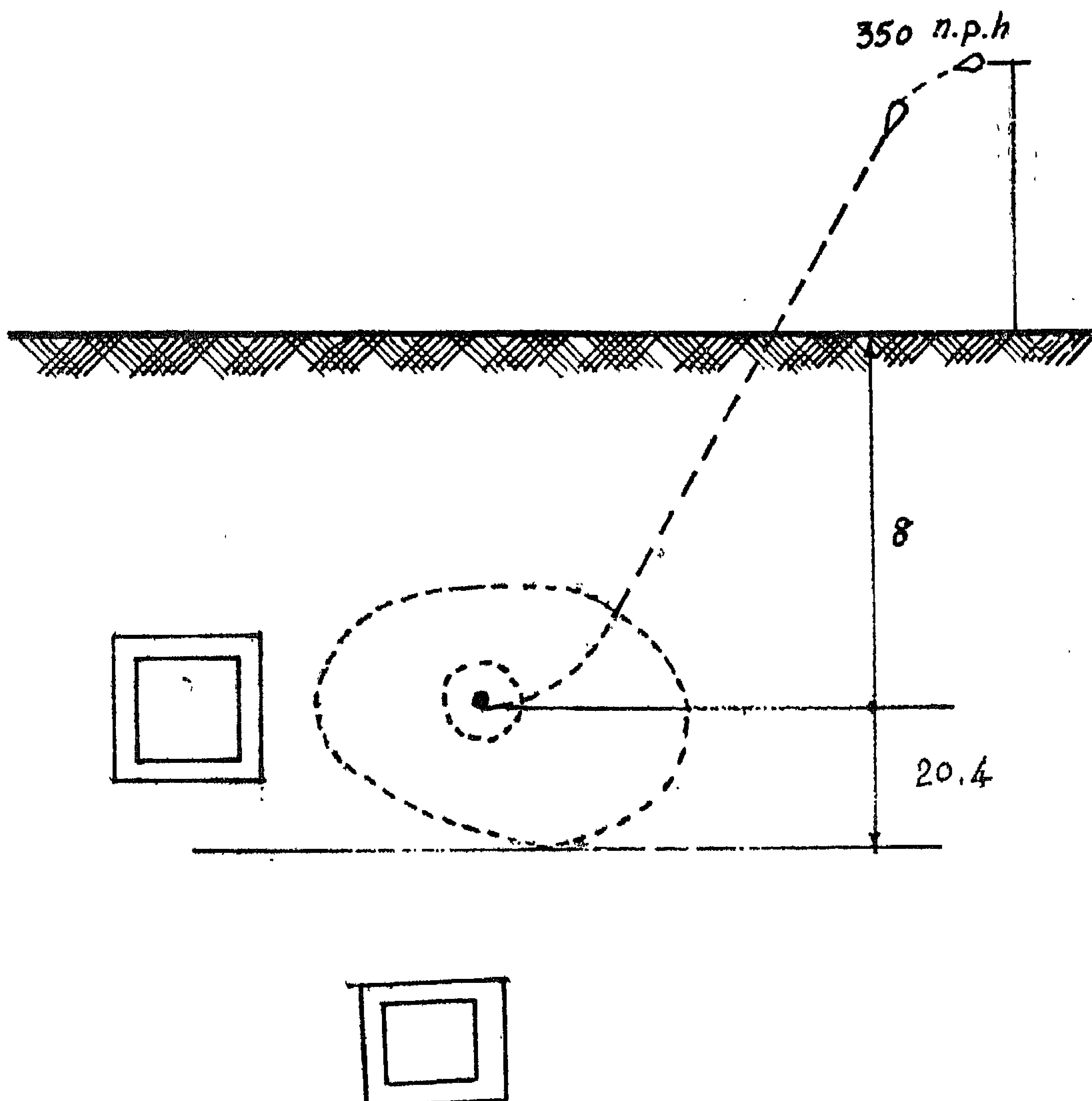
$$= 6100\ (.0934)^4$$

$$= 6100\ (.0000759)$$

$= .46$ Calibers.

⁂ Total depth due penetration and explosion in calibers

$= 1.54 + .40 = 2$ calibers.

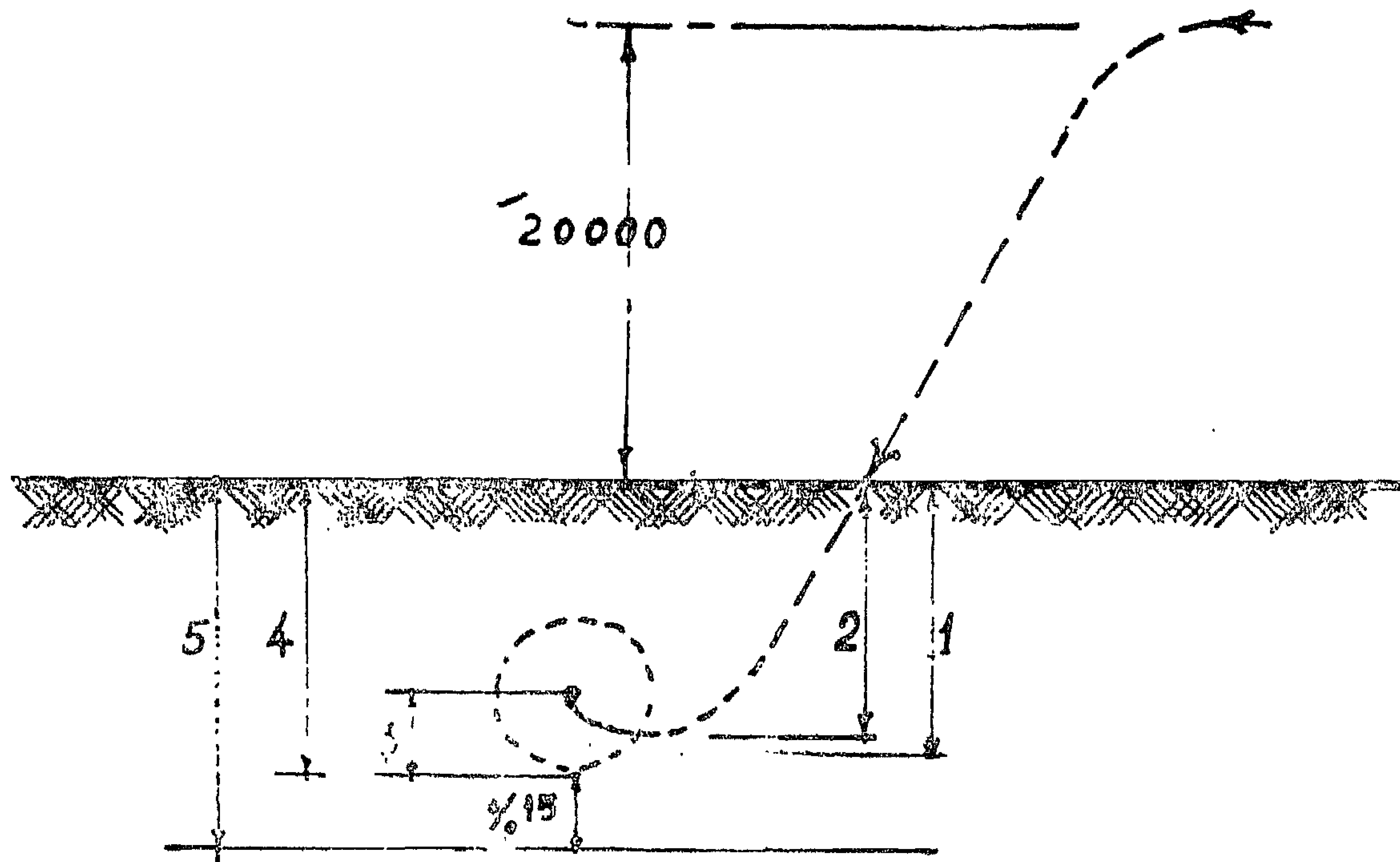


H — *ILLUSTRATIVE Computation*

Problem — 1

A 500 (Lb) GP bomb is dropped from an air plane travelling 350 mph (true aire speed) at an altitude of 20,000 feet. If the bomb lands on the roof of a concrete bunker, what thickness is needed to prevent scabbing ?

(Assume compressive strength of concrete to be 3000 PSI)



SOLUTION

Step 1 :

$$X = \frac{222 \times P \times d^{.215} \times v^{1.5}}{Y} + \frac{d}{2}$$

From table 1 :—

p = 3.28 lb/□
d = 14.2″
v = 267 lb

From Fig 2 :

for height 20,000 and speed 350 we get from curve :—

v = 1000 ft/sec
α of fall 69°
⁂ angle of obliquity 21°

From table 2 :

for concrete strength 3000 lb/□² we get Y — square root of conc. comp. strength

From Fig. 4 :

For d = 14.2 we get
$d^{.215} = 1.752$

From Fig. 3 :

For v = 1000
$v^{1.5} = 1$

(In the curve $V^{1.5}$ is devided on 1000)

$$⁂\ x = \frac{222 \text{ x } 3.28 \text{ x } 1.752 \text{ x } 1}{54.8} + \frac{14.2}{2}$$

$$= 23 + 7.1 = 30.1''$$

3. *THICKNESSES OF GROUND FLOORS FOR A REINFIRCED CONCERTE STRUCTURE.*

a. If the bomb is liable to come to rest under the floor and then explode, use the following formula.

$T = 1.4\ w^{1/3}$.

b. If the bomb will not pass inside the "heel" point before exploding.

$T = 0.7\ w^{1/3}$

T = Required thickness in ft.

w = Weight of charge (Table 1).

---

4. *PENETRATION IN EARTH, ROCK GRAVEL AND OTHER NON-HOMOGENOUS MATERIALS :*

a. *Inert Penetration.* The penetration of bomb in earth will generally follow a "J" shape with the straight portion 2/3 of the total path length, the curved portion 1/3 of the total path length, and the radius of the curved portion 1/5 of the total path Length, we can use this information to calculate the required depth below the surface of the ground we would have to place a protective structure,

(1) Total path length. (Modified petry formula).

$X = KPS$ feet

where :

x = total penetration in feet.

K = a constant depending on the nature of the resisting material. (Table 3)

P = sectional prssure (Table 1).

S = a constant depending on striking velocity. (Fig. 8).

b. *Radius of rupture.* When bombs explode in soil, rocks, or gravel ; the distance at which we will sustain no damage is called the maximum radius of rupture.

(1) Horizontal radius of rupture (—HRR)

(a) Timbered Galleries.

$H_{RR} = F\ w^{1/3}$.

H_{RR} = Horizontal radius of rupture in feet.

F = a constant depending on the resisting material (Table 4).

w = weight of the charge in pounds (Table 1).

(b) Reinforced concrete

$H_{RR} = 0.7\ F\ w^{1/3}$

(2) Vertical radius of rupture (V_{RR})

$V_{RR} = H_{RR} \times 0.83$.

c. *Steps in calculating* the required depth below the surface of the ground for a reinforced concrete structure.

(1) Data for substitution in Formulas

K = (Table 3)

P = (Table 1)

V = (Fig. 1, 2)

S = (Fig. 8)

Angle of fall — (Fig. 1, 2)

(2) Total path length

$x = KPS$

(3) Angle of obliquity (horizontal)

Angle of obliquity = 90° — angle of all

(4) Actual depth of bomb penetration below the surface of the ground.

Depth (y) = correction factor for obliquity multiplied by total path length.

(5) Safety factor

Depth (y) x 1.20

Up to this point we have calculated the depth required below the surface of the gound because of inert penetration. Now we will calculate the additional depth required because of the explosion.

(6) Data for substitution in the radius of rupture formula :

(a) F (table 4)

(b) w (Table 1)

(7) Horizontal radius of rupture (reinforced concrete).

$H_{RR} = .7\ F\ w^{1/3}$

(8) Vertical radius of rupture

$V_{RR} = (H_{RR})\ (0.83)$

(9) Total required depth below the surface of the ground for a reinforced concrete structure.

Inert penetration = V_{RR}

G - FORMULA REFERENCE

G — Consolidated Formula Reference for the Design of Protective Structures (Bomb Resistant)

---

1. *PENETRATION IN REINFORCED CONCRETE*

   a. *Normal inert penetration in reinforced concrete.*

$$X = \frac{222 \times P \times d^{215} \times v^{1.5}}{y} + 0.5d$$

x = penetration — inches

P = secontional pressure — psi — (table 1)

d = diameter of bomb — inches — (table 1)

v = striking velocity — fps (Fig. 1 and 2)

y = square root of compressive strength of reinforced concrete (table 2).

   b. *Penetration in reinforced concrete from explosion.*

$$\frac{P_e}{d} = 6100 \frac{(w)^4}{(d^3)^4}$$

P_e = penetration in iches

d = diameter of bomb (table 1)

w = weight of charge in pounds (table 1)

   c. *Steps in calculating the scabbing limit thickness for the roof of a reinforced concrete structure,*

(1) Characteristics of the bomb (Table 1)

(2) Striking velocity and angle of fall (Fig. 1 and 2)

(4) d^{215} (Fig. 4).

(5) $v^{1.5}$ — (Fig. 3).

(6) Y — (Table 2).

(7) Normal inert penetration

$$x = \frac{222 \times P \times d^{.215} \times v^{1.5}}{Y} + 0.5d$$

(8) Correct for obliquity (Fig. 5) Correction factor times normal penetration.

(9) Calibers of inert penetration
x/d = calibers

(10) Penetration due to explosion

$$\frac{P_e}{d} = 6100\ (w/d^3)^4$$

(11) Total penetration due to the flight of bomb and explosion. (calibers).

(12) Scabbing Limit thickness (calibers) (Fig. 6).

(13) Scabbing limit thickness (SLT) in inches. Calibers x diameter of missile.

(14) Safety factor.
(1.15) (SLT) = Required thickness in inches

---

2. *THICKNESSES OF WALLS FOR CONTACT EXPLOSIONS FOR REINFORCED CONCRETE STRUCTURES.*

   a. *Above ground*

   $T = 0.80\ w^{1/3}$

   T = Thickness in ft.

   w = weight of the charge (Table 1)

   b. *Below ground*

   (1) Scabing limit thickness $SLT = 1.4\ w^{1/3}$.

   (2) Moderate damage thickness.
   $MDT = 1.2\ w^{1/3}$.

   (3) Heavy damage thicknesses
   $HDT = 1.0\ w^{1/3}$

مجلة

جمعية المهندسين المصرية

مجلة علمية هندسية — تصدرها كل ثلاثة شهور
جمعية المهندسين المصرية بالقاهرة

الاشتراك السنوى لغير الأعضاء :

المهندس	٦٠ قرش
للهيئات	٢٠٠ قرش

REFERENCES

1. Mohammed A. Taha. The Effect of Maadi-Sand properties on mould and casting qualities, thesis for M.Sc. Ain Shams University, 1968.

2. M.Z. Mounir. The Relationship of the Properties of Moulding sand, Thesis for Ph.D. Cairo University, March, 1950.

3. M.Z. Mounir, The Property of Mouldability relationship and application to Foundry sands, 1957.

4. A.M. Hamouda, Behaviour of Local Foundery sands in the mechanical ramming, thesis for M.Sc. Alex. University, 1965.

5. B.S. Yearley, Effect of green properties on ramming of sands (Part I) Foundry, October, 1963.

6. B.C. Yearley, Effect of green properties on ramming of sand (Part II) Foundry, November 1963.

7. B.C. Yearley, and R.R. Schaaf, Jolting and Squeezing of Green sand moulds, foundry, December 1963.

8. B.C. Yearley, Relative density new mould quality rating, Foundry September, 1966.

9. B.C. Yearley, How moulding sand reacts to ramming, Foundry, October 1966.

10. R.W. Heine, Mixing and moulding foundry green sand, Foundry October, 1961.

11. C..T Marek, Loss in mould rigidity in the early stages of solidification due to reduction in the green strength of the moisture transport zone, modern casting, v. 48, no. 6, p. 91, december 1965.

12. C.T. Marek, Transformation zones in green sands, modern casting, v. 43, no. 5, p. 185, May 1963.

13. H. Henschel and R.W. Heine. Casting dimensions and mould dilation, Modern casting, v. 50, no. 2, p. 83, August 1966.



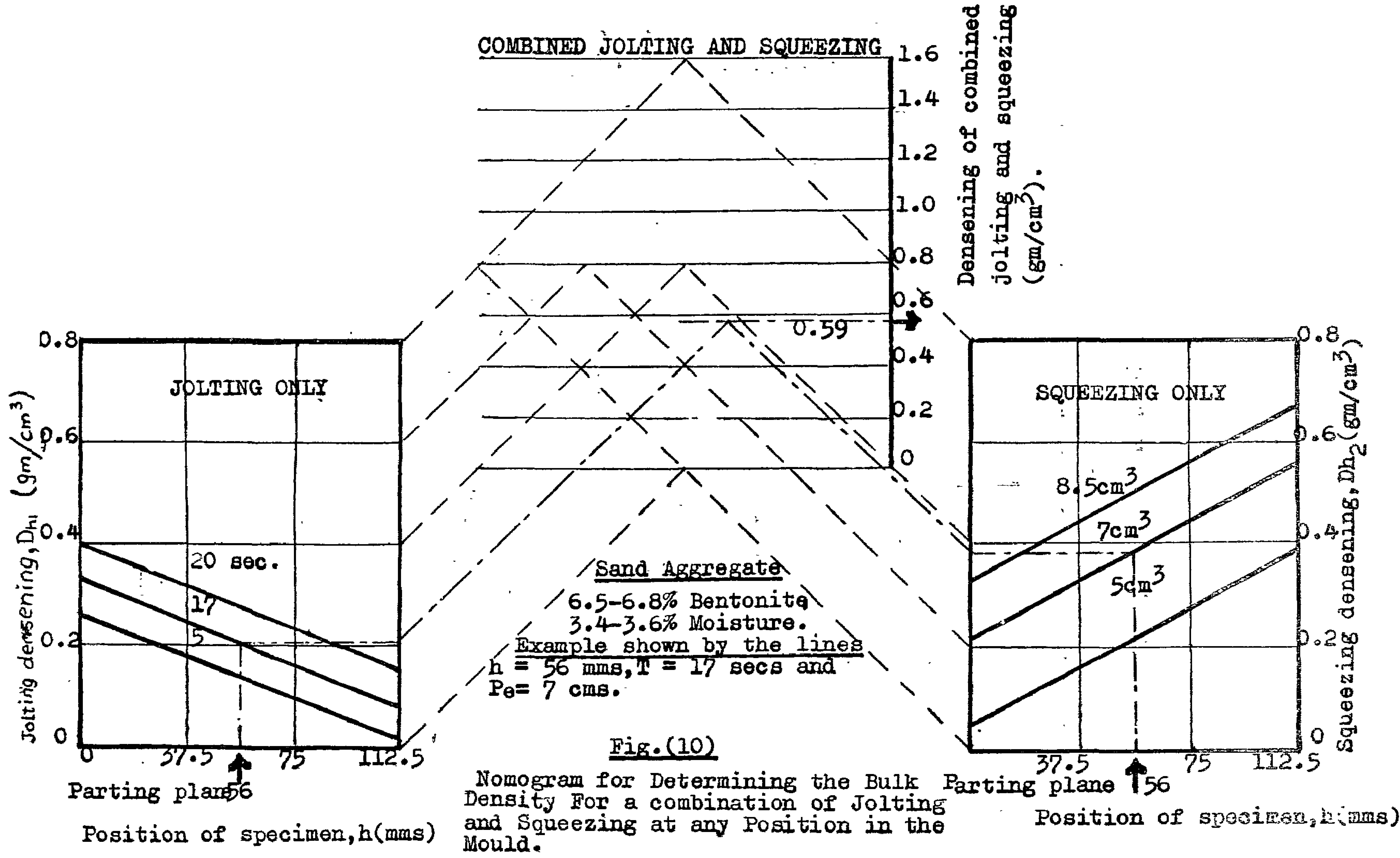


Fig. (10)

Nomogram for Determining the Bulk Density For a combination of Jolting and Squeezing at any Position in the Mould.

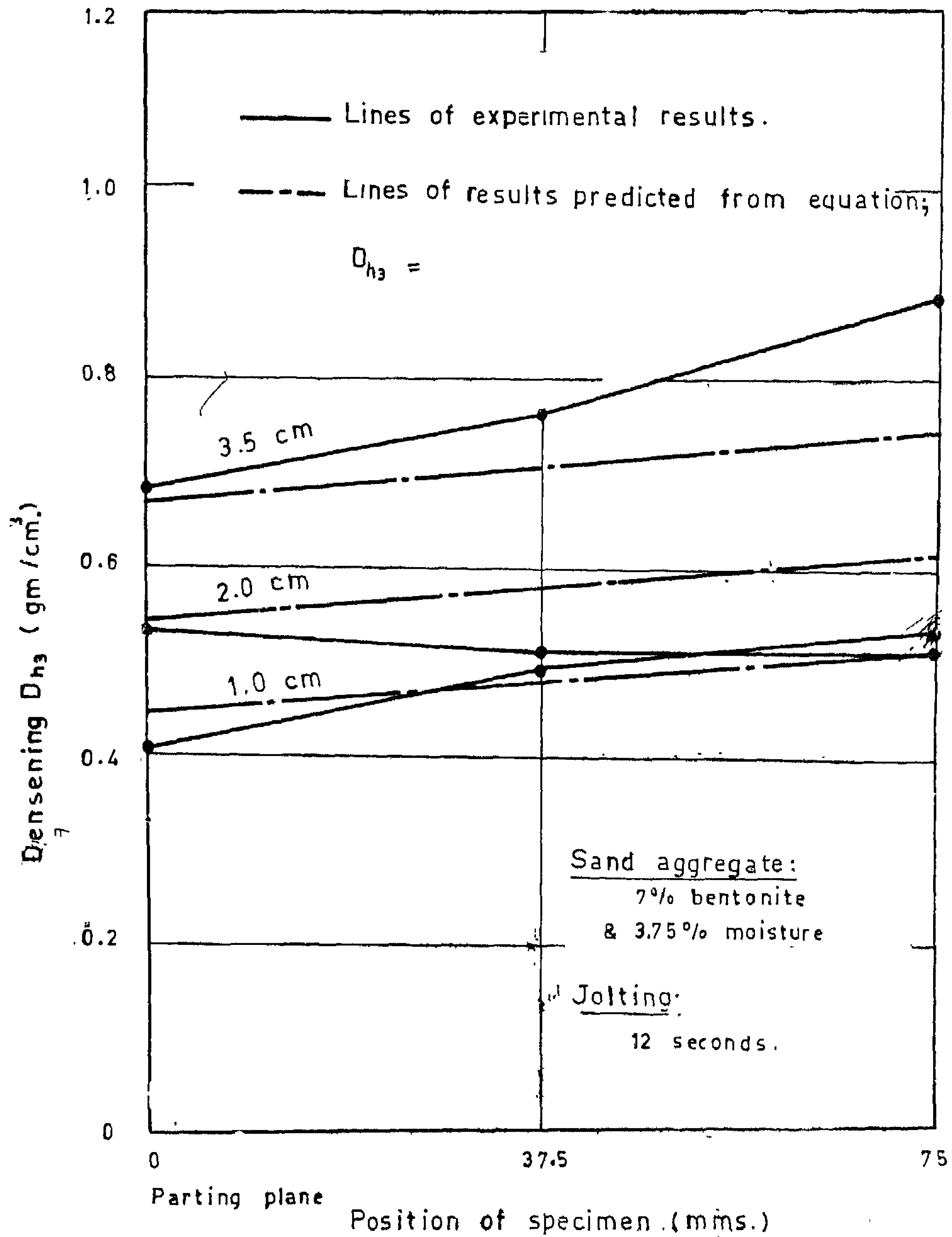


FIG. 9 : Densening gradient along the mould height for combined jolting and squeezing.

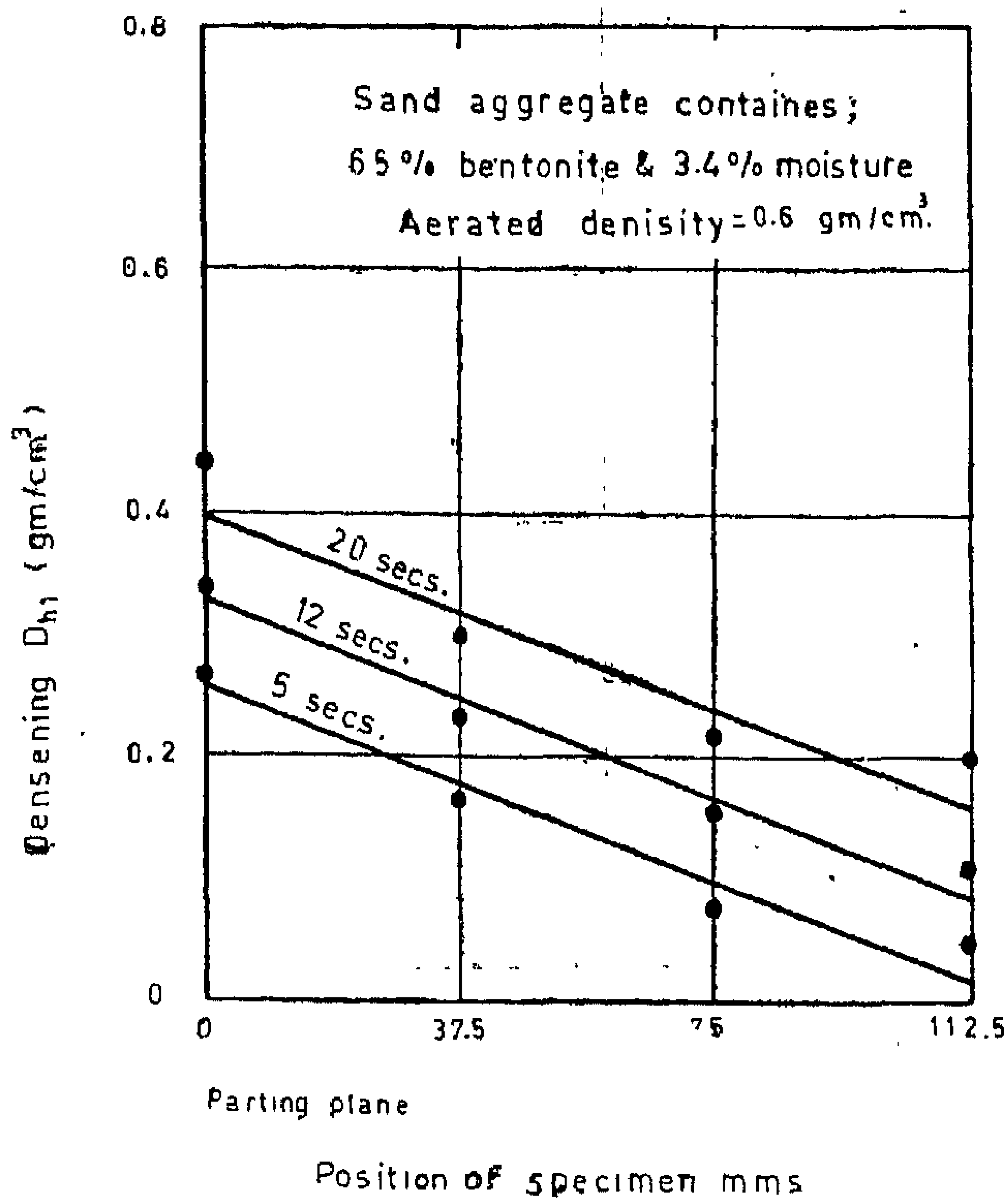


FIG. 7 : Densening gradient along the mould height for different jolting times and no squeezing.

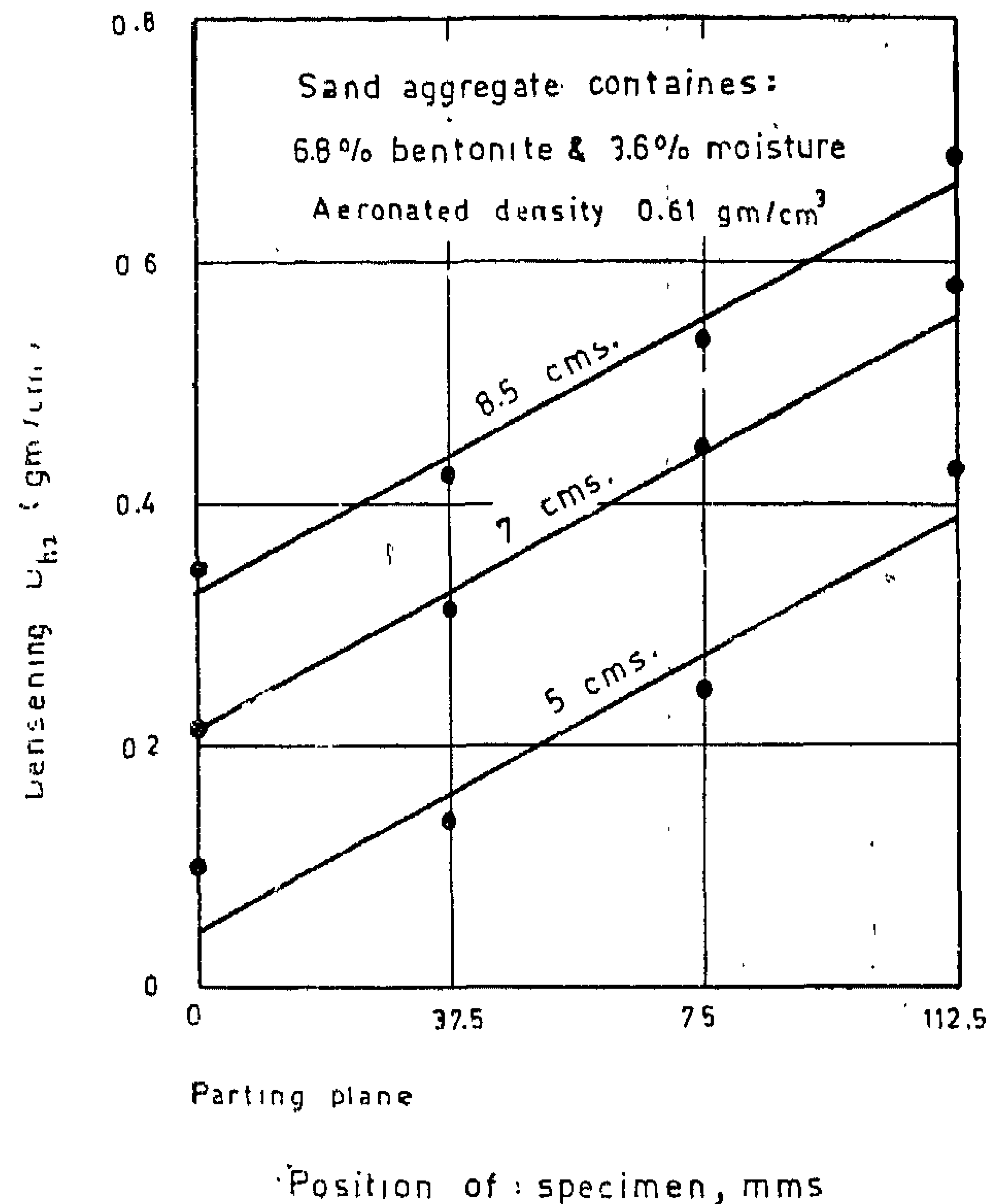


FIG. 8 : Densening gradient along the mould height for different squeeze head penetration and no jolting.

CONCLUSIONS

From the above discussions, it can be concluded that the densening mechanism, in the jolting operations depends mainly on the jolting time, and in squeezing operations, depends mainly on the d squeeze head penetration. The combined effect of jolting and squeezing is additive with negligible interaction between the different densening mechanisms.

The sand mixture characteristics do not affect the densening values, but affect the bulk density values through the variation of their aerated densities.

The uniformity of densening along the mould height does not depend on the jolting time or the squeeze head penetration. It only depends on the sand aggregate variables.

The densening value due to combined jolting and squeezing at any point in the mould can be approximately predicted by the equation.

$D_{h3} = 0.045\,(T)^{0.024} + 0.08\,(P_e)^{0.065} + 0.001\,h.$
and the solution is given in the nomogram of Fig. (10).

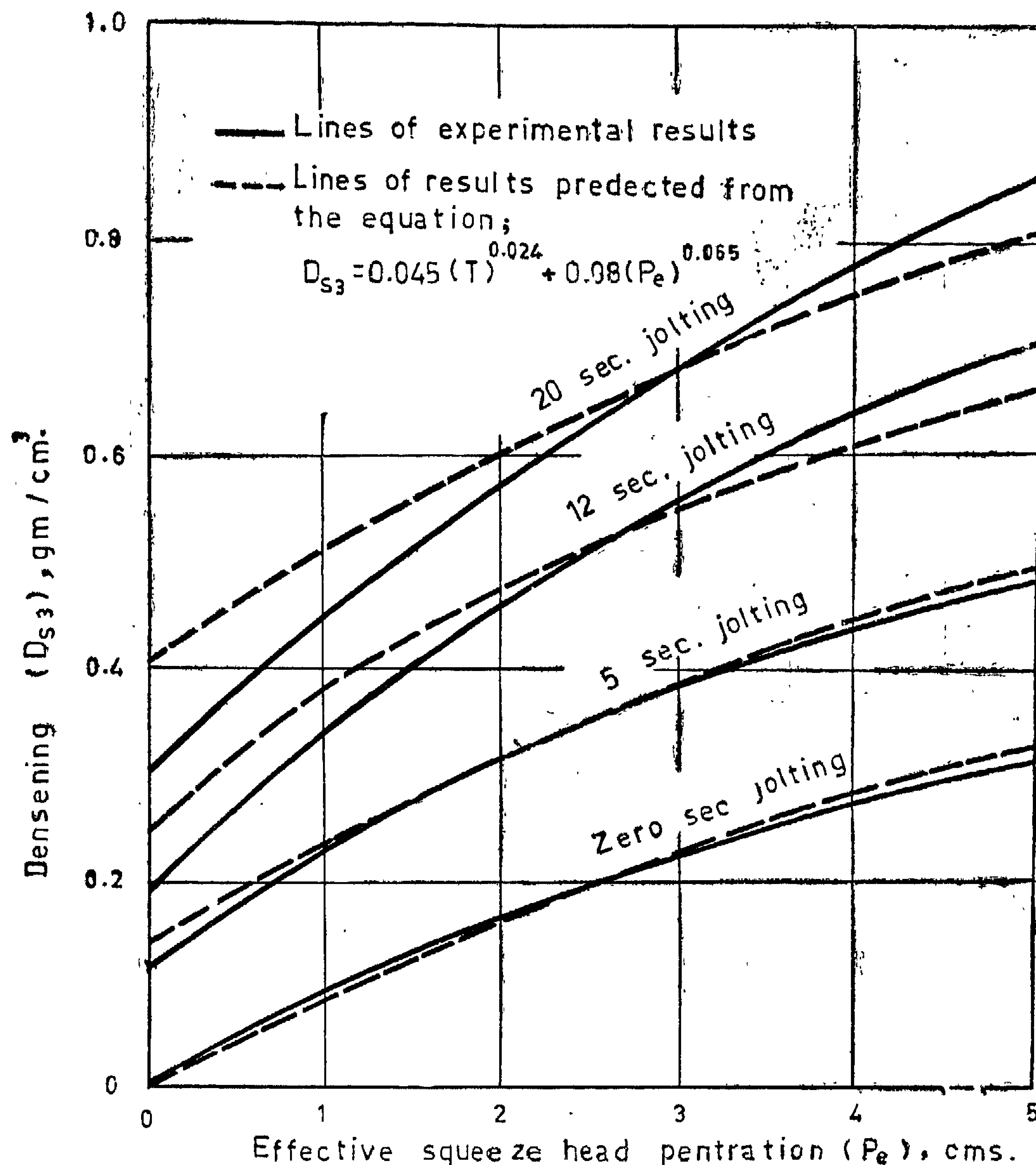


FIG. 6 : Relation between densening due to combined jolting and squeezing and the effective squeeze head penetration at different levels of jolting times.

By substituting the appropriate values for jolting time, effective penetration, and height in equation (10) it is possible to predict the (D_{h3}) values for the tested compaction combinations. The predicted values, together with the experimental ones for some combinations of jolting and squeezing are shown in Fig. (9).

Comparison of the experimental values with those predicted by equation (10) shows reasonable agreement in most of the cases. Better agreement could have been obtained of more complicated functions, other than the straight line were chosen for the variation of the densening values along the mould height. However, the resulting equation, would be too complicated and cumbersome to be used in practice and equation (10) was chosen on basis of simplicity.

The solution of equation (10) is facilitated by the nomogram shown in Fig. (10). This nomogram is designed for the practicing engineer who is interested in getting the best combination of compaction variables for a required job.

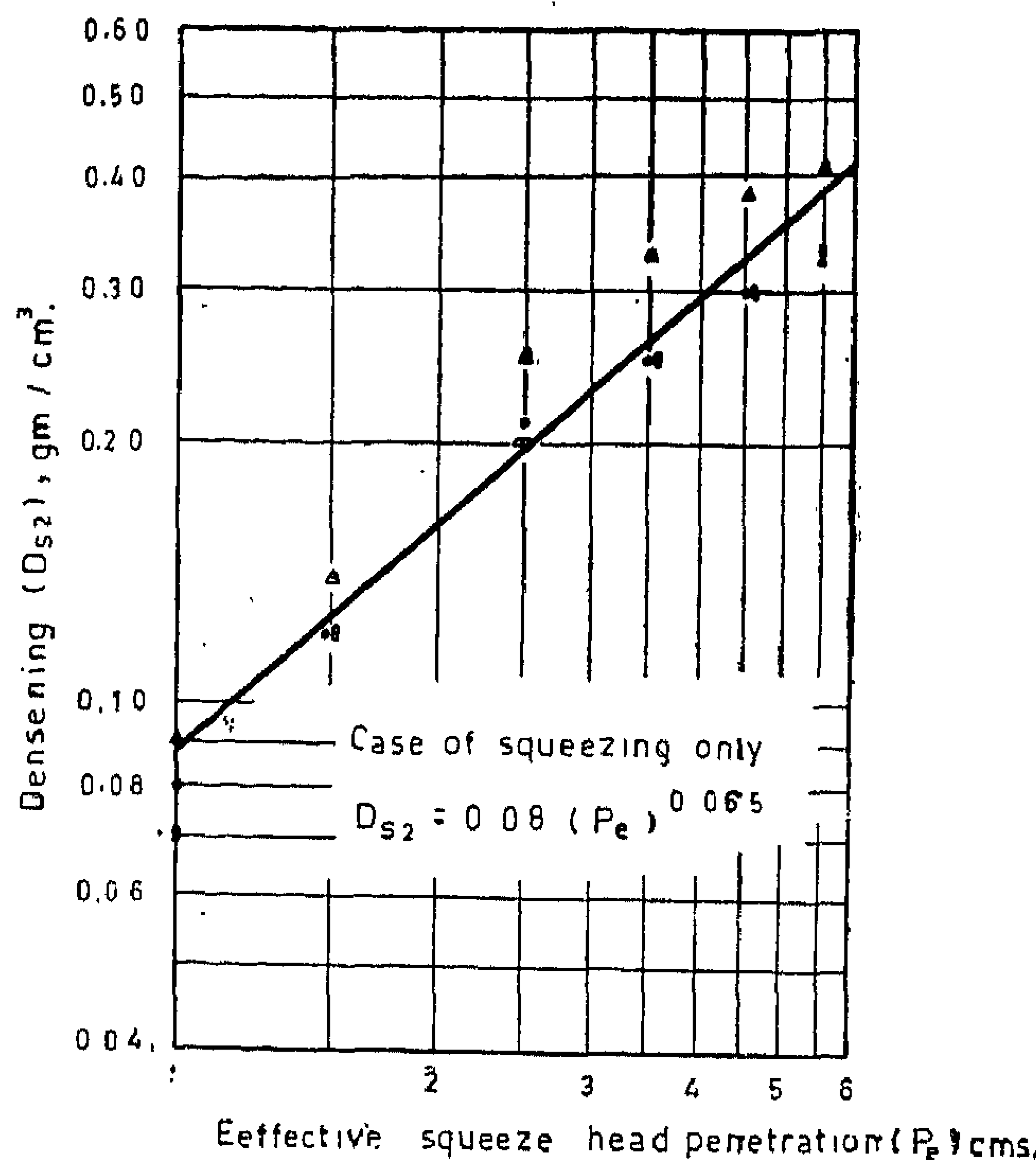


FIG. 5 : Relation between densening due to squeezing only and effective squeeze head penetration for different sand aggregates.

The variation of density along the mould height :

An example of the variations in the densening values along the mould height due to jolting is shown in Fig. (7). As expected, the densening decreases from a maximum at the parting plane to a minimum at the top layers of the mould. The results indicate that, for the range of jolting times tested, the variation of densening values along the mould height can be approximately represented by a straight line of the form :

$$D_{h_1} = K_{h_1} - m_1 h \quad \ldots\ldots \quad (6)$$

where h is the height measured from the parting plane (mm) m_1 is the slope of the straight line relationship and K_{h_1} is the densening value at the parting plane (gm/cm^3).

The present results indicate that (m_1) does not depend on the jolting time, which means that the densening gradient in jolting is a function of the sand aggregate variables only.

Since the variation of K_{h_1} with the jolting time is given by equation (2), equations (2) and (6) can be combined to yield a more general equation giving the densening values at any point in the mould after a given jolting time.

Thus :

$$D_{h_1} = 0.045\ (T)^{0.024} - 0.002 \quad \ldots\ldots \quad (7)$$

The expected variations in densening values due to squeezing are also found along the mould height as shown in Fig. (8). Here again, straight lines can be drawn to approximately represent the variation of densening values due to squeezing.

Thus :

$$D_{h_2} = K_{h_2} + m_2 h \quad \ldots\ldots \quad (8)$$

where h is the height measured from the parting plane (mm), m_2 is the slope of the straight line relationships and K_{h_2} is the densening value at the parting plane.

In this case also (m_2) does not depend on the squeeze head penetration, which means that the densening gradient in squeezing is a function of the sand aggregate variable only.

In a similar fashion to equation (7), a more general equation giving the densening values at any point in the mould after a given effective equeeze head penetration can be obtained by combining equations (4) and (8).

$$D_{h_2} = 0.08\ P_e^{0.065} + 0.003\ h \quad \ldots\ldots \quad (9)$$

In view of the successful combination of equations (2) and (4) to give equation (5), it was suggested that the densening due to the combined jolting and squeezing at any point in the mould can be represented by a general equation obtained by combining equations (7) and (9).

$$D_{h_3} = 0.045\ (T)^{0.024} + 0.08\ (P_e)^{0.065} + 0.001\ h \quad \ldots\ldots \quad (10)$$

where different combinations of compaction with different jolting times and effective penetrations were given to the sand. The results are given by the solid lines of Fig. (6).

With equations (2) and (4), in mind, it was suggested that the densening at the parting plane, due to the combined jolting and squeezing can be represented by the equation :

$$D_{S3} = D_{S1} + D_{S2} = 0.045\ (T)^{0.024} + 0.08\ (P_e)^{0.065} \quad \text{...... (5)}$$

By substituting the appropriate values for the jolting time and effective penetration in equation (5) it is possible to predict the D_{S3} values for the tested compaction combinations.

The predicted values are represented by the broken lines of Fig. (6).

Comparison of the experimental values with these predicted by equation (5) reasonable agreement and the deviations are within the experimental scatter of the results. This indicates that the combined effect of jolting and squeezing is additive with negligible interaction between the different densening mechanisms. This is understandable since equation (2) shows that the densening in jolting is a function of the jolting time only, and the densening in squeezing is a function of the effective penetration only as shown by equation (4).

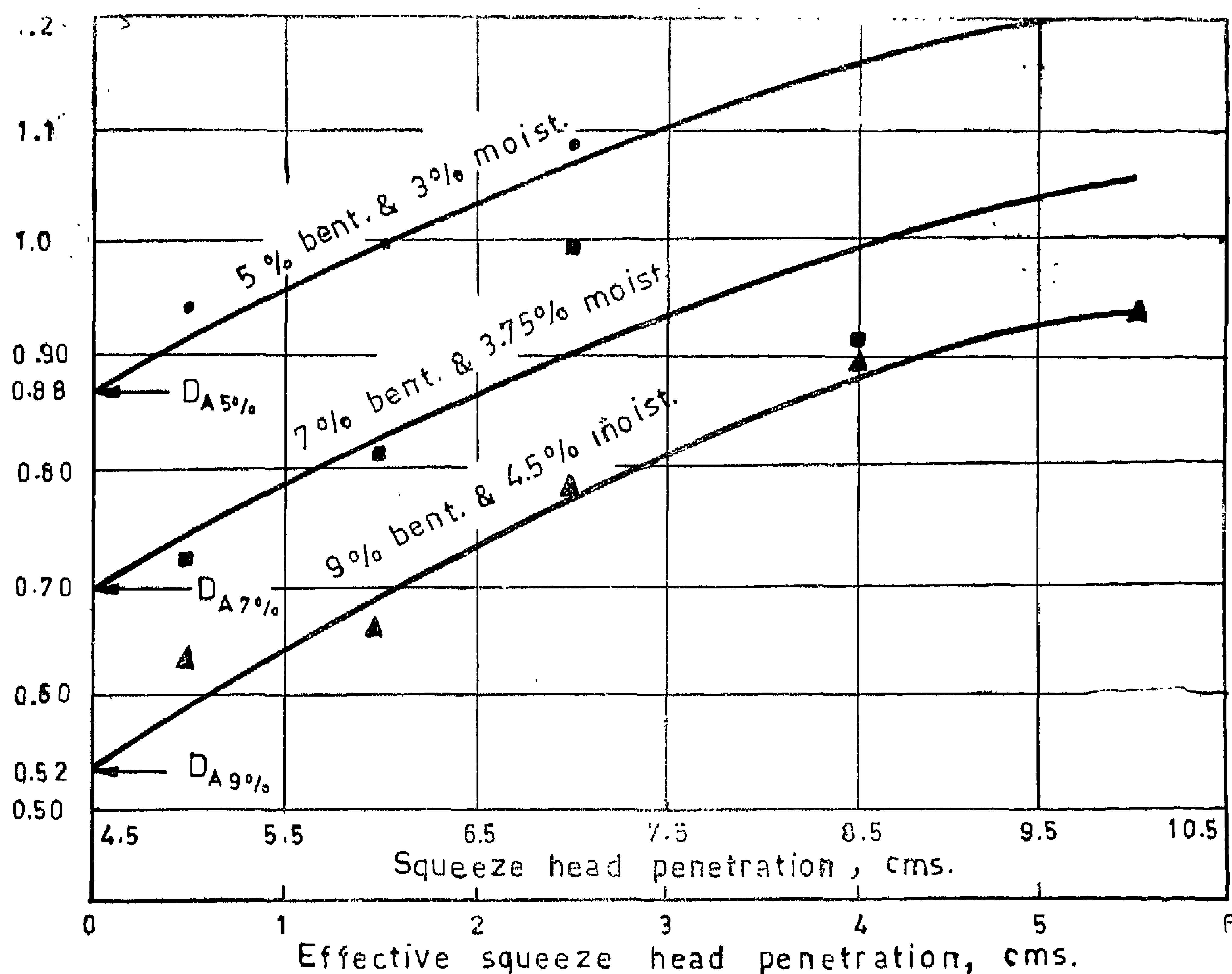


FIG. 4 : Effect of squeeze head penetration on the bulk density (no jolting).

Fig. (5) indicated that all the results for the different sand mixtures fall on a single straight line which can be represented by the equation :

$$D_{S2} = 0.08\ P_e^{0.065} \qquad \ldots\ldots \quad (4)$$

Here again, as in the case of jolting, when the initial differences between mixtures, due to aerated density variations, and when the redundant squeeze head movement are eliminated ; all mixtures behave in the same manner.

This leads to the conclusion that the densening mechanism in the squeezing operations, depends mainly on the effective penetration and is hardly affected by the sand mixture characteristics, in the range or variables tested.

4. *Effect of Combined Jolting and Squeezing on the Bulk density at the parting plane :*

The effect of the combined jolting and squeezing on the bulk density at the parting plane was studied in a series of experiments

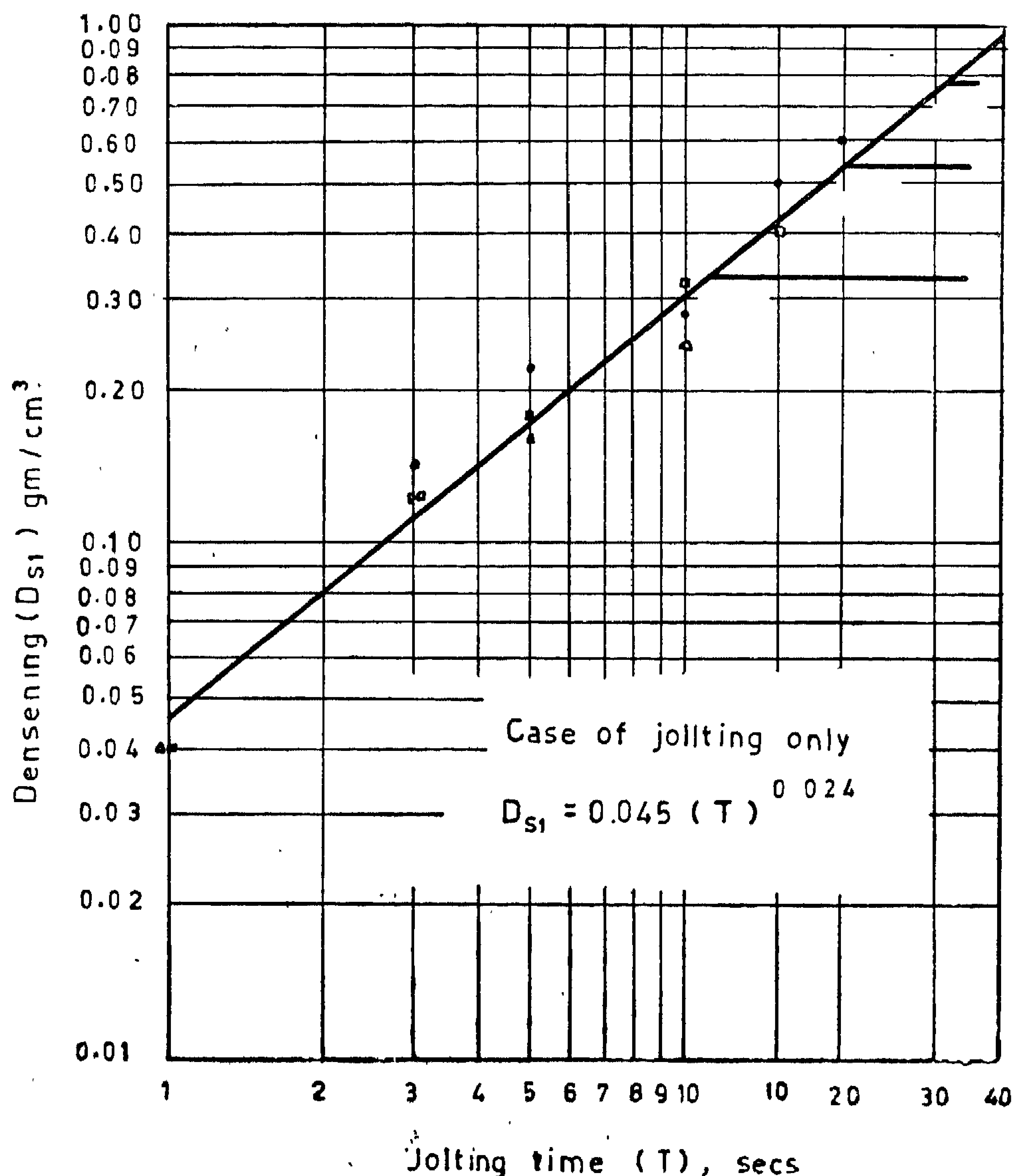


FIG. 3 : Relation between densening due to jolting only and jolting time for different sand aggregates.

From the above discussion, it can be concluded that the densening mechanism, in the jolting operations, depends mainly on the jolting time and the sand aggregate characteristics have little, if any, effect on the compaction mechanism in the range of variables tested.

3. *Effect of squeezing on the bulk density at the parting plane :*

The effect of the squeeze head penetration on the bulk density, at the parting plane, is shown on a logarithmic scale in Fig. (4). The results indicate a straight line relationship which can be represented by the equation :

$$D_{B_2} = K_2 \, P^{0.065} \quad \ldots\ldots\ldots \quad (3)$$

where K_2 is the bulk density after a unit squeeze head penetration, it varies with the variation of the aerated density, of the sand aggregate as shown in Table (1).

In this case also, the effect of variations in aerated density of the different sand aggregates can be eliminated by using the densening instead of the bulk density values. Fig. (5) is constructed from the results of Fig. (4) and represents the relation between the densening (D_3) and the effective penetration (P_e) drawn on logarithmic scales. The use of the effective penetration values instead of the squeeze head penetration eliminates the redundant head movement, which would confuse matters.

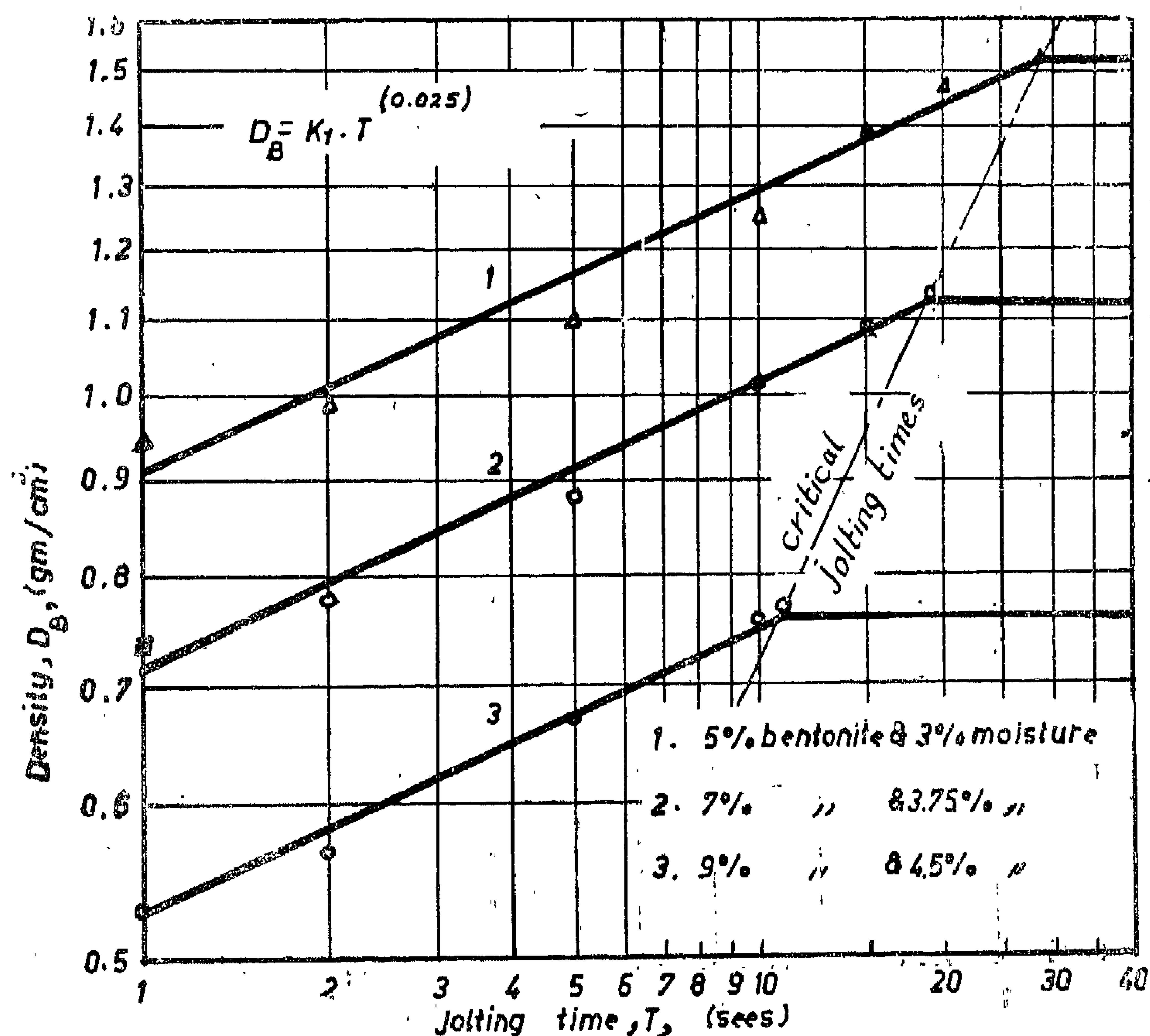


FIG. 2 : Relation of bulk density and jolting time at zero squeeze

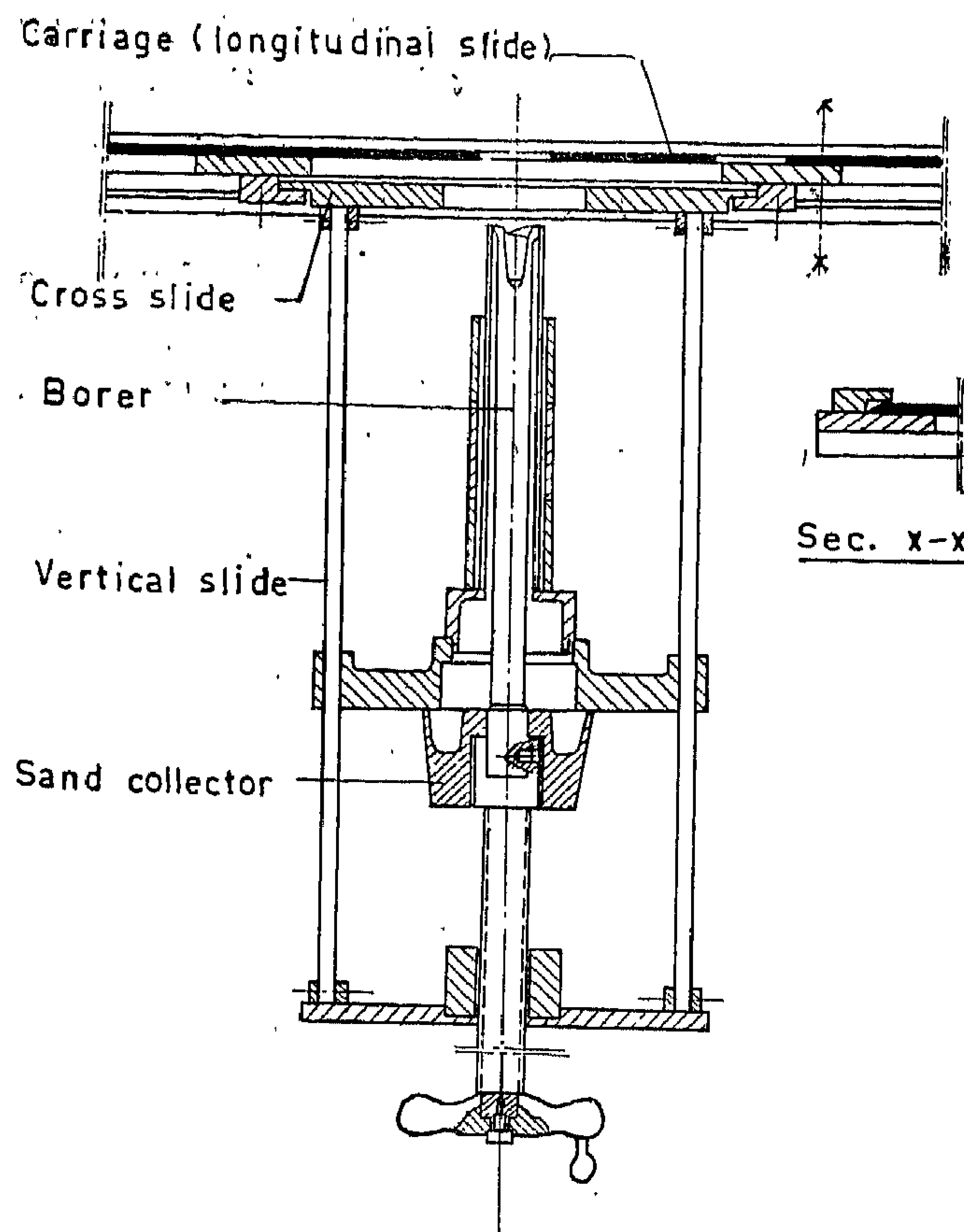


FIG. 1 : The apparatus of bulk density measurement.

The sand was first jolted to the test jolting time and then squeezed to the test squeezing head penetration.

The moulding machine used was a jolt/squeeze type RPA—la. Working pressure of compressed air was 6—7 atms.

To measure the bulk density for a certain condition, 3 moulds were prepared where 3 readings were taken for each mould. The bulk density reading was taken as the average o the nine readings.

The "boring in mould" technique was used for taking specimens for bulk density measurements. This technique was used by other workers[4], and was found to give accurate results.

A specially designed apparatus was built to get constant volume samples at different points in the mould. By weighing these samples the bulk density was calculated. The specimen bored out was 20 mm. diameter × 37.5 mm. height giving a total volume of 11.8 cc. Fig. (1) show the important parts of the apparatus which is described in detail elsewhere[1].

EXPERIMENTAL RESULTS AND DISCUSSION :

1. Effect of sand aggregate on bulk density :

For all the combinations of ramming used, the results presented in Figs. (2,4,7,8) show that sands with lower bentonite and moisture contents produce moulds with higher bulk density values. This is in agreement with the results of other workers[4,6], and can be attributed to the variation in the aerated density values. The effect of sand aggregate on the aerated density is hown in Table (1).

2. The effect of jolting on the bulk density at the parting plane :

The effect of jolting time on the bulk density at the parting plane, is shown on a logarithmic scale in Fig. (2). Up to the critical jolting time (T_c) the results indicate a straight line relationship which can represented by the equation :

$$D_{B1} = K_1 \ (T)^{0.024} \qquad \ldots\ldots \quad (1)$$

where K_1 is the bulk density after a unit jolting time, it varies with the variation of the aerated density of the sand aggregates as shown in table (1).

To eliminate the effects of variations in aerated density (D_A) of the different sand aggregates the densening [$D_S = D_B - D_A$], is used instead of the bulk density Fig. (3) is constructed from the results of Fig. (2) and represents the relation between the densening sening (D_S) and the effective penetration scales. The figure shows that all the results for the different sand aggregates can be fitted to a single straight line represented by the equation.

$$D_{S1} = 0.045 \cdot (T)^{0.024} \qquad \ldots\ldots \quad (2)$$

This shows that once the initial differences between different aggregates are eliminated, by using the densening values instead of the bulk density, they behave in the same manner.

In this way a fairly uniform degree of ramming can be obtained throughout the flask.

In squeezing operations, if the static force is too high, the clay film surrounding sand grains will be squashed out at the points of contact and enters the pores between the grains which reduces the permeability of mould.

The sand compaction mechanisms have been discussed by several worker[4,6,10]. However, no quantitative study of the effect of the various factors involved exists. In the present work an attempt is made to formulate the relations between the jolting time, the squeeze head penetration and the bulk density of various sand mixtures.

LIST OF SYMBOLS :

D_A = aerated density "before any compaction".

D_B = Bulk density "after compaction".

D_S = $D_B - D_A$ = densening, increase in density due to compaction.

D_{S1} = Densening due to jolting alone.

D_{S2} = Densening due to squeezing alone.

D_{S3} = Densening due to combined jolting and squeezing.

T = Jolting time in seconds.

d_{50} = Average grain size = seive opening at 50% of the summation weight.

U_r = Uniformly factor = $\frac{\text{seive opening at 75\% of the summation of weight}}{\text{seive opening at 25\% of the summation of weight.}}$ $= \frac{d_{75}}{d_{25}}$

P_c = critical penetration = squeeze head penetration necessary to produce the first signs of densening on the parting plane.

P_e = Effective penetration = total squeeze head penetration — critical penetration = $P_{total} - P_c$.

T_c = cririrical jolting time.

h = height of any point along the mould.

D_{h1} = densening at any point along the height due to jolting.

D_{h2} = densening at any point along the height due to squeezing.

D_{h3} = densening at any point along the height due to combined jolting and squeezing.

MATERIAL USED :

The raw sand used in the mixtures employed in the present work was mined from Bir-El-Fahm area in Maadi and had the following characteristics :

Average grain size :	d_{50} = 0.29 mm.
Uniformity factor	U_r = 0.68
Grain shape	Semi angular.

The bentonite used in all experiments was of the English type (Volclay) of composition 92 to 95% montmorrilonite 8 to 5% feldsbar. Three bentonite contents used were studied (5%, 7%, and 9% bentonite). The corresponding moisture contents were chosen so as to give optimum permeability. The three mixtures were (5% bentonite, 3% moisture), (7% bentonite, 3.75% moisture) and (8% bentonite 4.4 moisture).

APPARATUS AND EXPERIMENTAL TECHNIQUES :

The sand mixtures were prepared in a mix muller of 500 kg. capacity. Batches of 300 Kgs. were mixed for 4,5 min., which was found to be the optimum mixing time[1].

The flask (400 × 310 × 200 mm.) was put on the moulding machine table and filled with aerated sand, using a hand screen of 1.5 mm. opening size. The excess sand was then removed.

FACTORS INFLUENCING COMPACTION MECHANISMS IN FOUNDRY SAND

By

Dr. SALAH M. SAID*
M. Sc., Ph. D., A.M.I. Prod. E.

Dr. M.M. FARAG**
B.Sc., M. Met., Ph.D.

Eng. M.A. TAHA***
B.Sc. M.Sc.

SUMMARY

The present investigation was initiated to study the behaviour of foundry sand when mechanically rammed. The sand of Bir-El-Fahm in Maadi was chosen for this purpose as it represents the average type of sands used in the Egyptian Foundries.

Experimental work was carried out on three mixtures (5% bentonite and 3% moisture), (7% bentonite and 3.75% moisture) and (9% bentonite and 4.5% moisture). The bulk density was measured at different positions in the moulds by using a boring apparatus specially constructed for this work.

It was found that the densening in jolting depends mainly on the time and in squeezing, it depends mainly on the squeeze head penetration.

The combined effect of jolting and squeezing was found to be additive with little interaction between the different compaction mechanisms. The densening in this case is given by

$$D_{S3} = 0.045\ (T)^{0.024} + 0.08\ (Pe)^{0.065}$$

It was found that uniformity of densening along the mould height does not depend on the jolting time or the squeeze head penetration. It only depends on the sand aggregate variables.

The densening value due to combined jolting and squeezing at any point in the mould can be approximately predicted by the equation :

$$D_{h3} = (T)^{0.024} + 0.08\ (Pe)^{0.065} + 0.001\ h.$$

The solution of this equation is given in a nomogram to make it more practical for the practicing engineer to get the best combination of variables for a required job.

INTRODUCTION

Jolting and squeezing are the two commonly used methods in the foundry for ramming moulds. Jolting compacts the sand through the conversion of its momentum to work at the instant of jolt. Due to the nature of the operation, the bulk density of the sand decreases from a maximum at the parting plane to a minimum at the top layer of the mould. In the case of squeezing, the bulk density decreases from a maximum at the upper layers to a minimum at the parting plane. This is due to the fact that the static force of squeezing continuously decreases at it is transmitted downwards through the sand due to the grains diversion effect[2].

Jolting and squeezing can be combined to give uniform density in the vertical direction. The required ramming on the mould face is obtained by jolting and the tendency to softness in the upper parts of the mould is corrected by squeezing after the jolting is completed.

* Asst. Professor of Production Engineering, Ain Shams University.
** Lecturer in Production Engineering, Ain Shams University.
*** Helwan Company for Military and Civil Castings.

slope — $1/\tau$ and intercept ln T_P (exp $(\bar{t} - D)/\tau - 1$) as shown in Figure (5). The value of the time constant for the run was taken as the average of those obtained for the early and the decaying parts of the response.

Correlation of the time constants :

Figure (6) relates th ecalculated average time constants to the ambient air temperature. It is seen that the time constant increases slightly with the temperature of the ambient air and that the data is fairly well approximated by an empirical straight line. The values of the time constants indicated by this line were then used to recompute the response at selected points in various runs. The deviation between actual and computed data never exceeded 5% which means that the first order plus dead time model adequately represents the data. It was not possible to investigate the effect of ambient air humidity on the time constant because it did not vary over a wide range.

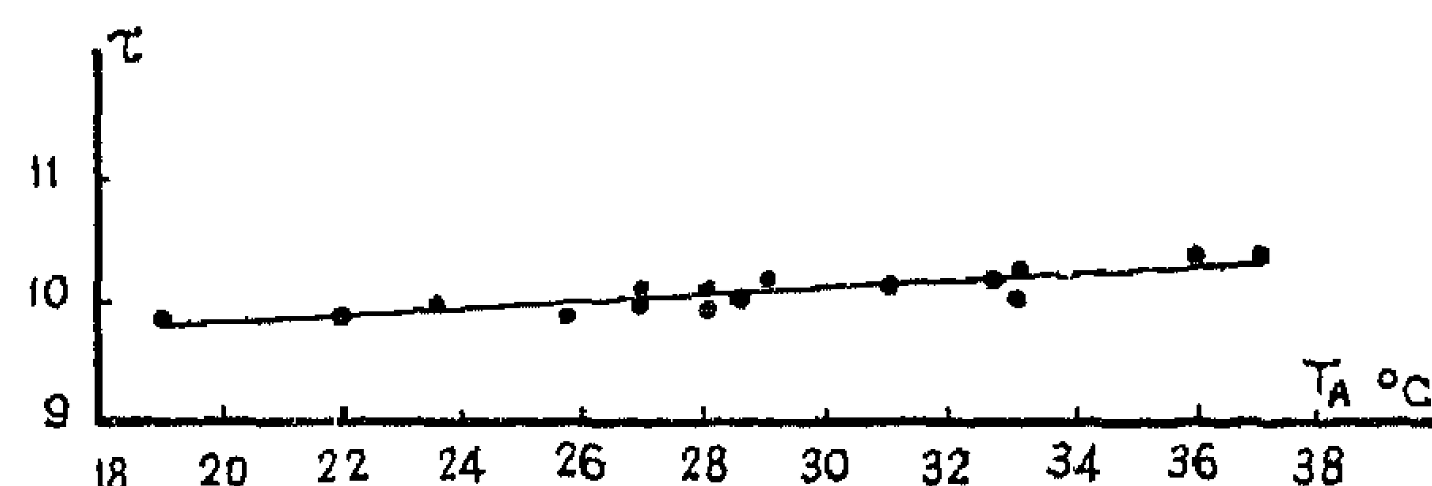


FIG (6) – AVERAGE TIME CONSTANTS VERSUS T_A

CONCLUSION

A dynamic model has been formulated to describe the pulse response of an air-steam heater given the ambient air temperature and the duration of the steam pulse. The results of 16 experimental runs have shown that a transfer function comprising a time constant and a distance-velocity lag provided an approximate convenient representation of the data. Subsequent computations associated with the optimization of the reactivation cycle (10) of the adsorber indicated that this model was reliable in predicting the effluent air wet bulb temperature and enthalpy responses for various ambient air temperatures, humidities and pulse durations.

REFERENCES

1 — Masubuchi, M., Trans. A.S.M.E., Series D., 82, 51-65 (1960).

2 — Iscol, L. and Altpeter, R.J., A.S.M.E. Pap. No. 59-IRD-4 (1960).

3 — Famularo J. in "The use of computers in chemical Engineering Education", Univ. of Mich., p. 784, (1963).

4 — Cohen, W.C. and Jhonson E.F., Chem. Eng. Prog. Symp. Ser. 36, 57-86 (1961).

5 — Morris, H.J., Proc. 1st IFAC Congress, Butterworth, London, p. 354, (1961).

6 — Hougen, J.D. and Walsh R.A., Preprint H., Am. Inst. Chem. Engrs. Annual meeting (1960).

7 — Smith, O.J.M., I.S.A., Journal, 6, 28-33, (1959).

8 — Jhonson, E.F., Automatic Process Control, McGraw-Hill book Co., p. 74-76, (1967).

9 — Zeigler, J.G. and Nichols, N.B., Trans. A.S.M.E., 64, 759 (1942).

10 — Youssef H.A., Msc. Thesis, Cairo, Univ. (1971).

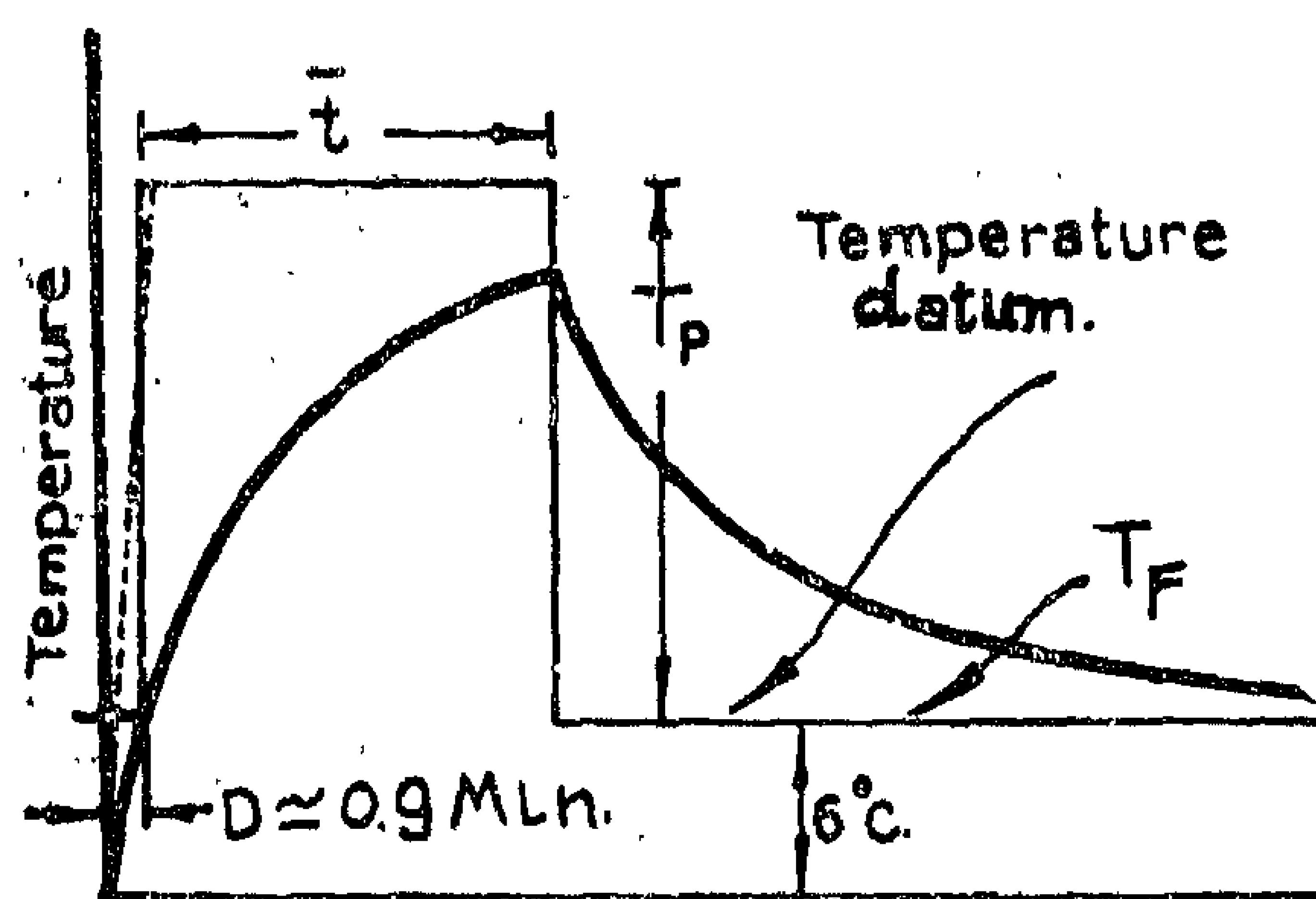


FIG.(3)_ TYPICAL RESPONSE SAW TOOTH

that of the decaying part is given by :

$$T = T_P \left(\exp (\bar{t} - D) / \tau - 1\right) \exp -$$

$$(t - L) / \tau \text{ for } t > \bar{t} . \qquad (2)$$

where D is the dead time, τ the time constant, $\bar{t}$ the pulse duration in Minutes, T is the heater effluent temperature (above the final steady state temperature) and T_P is the potential steady-state temperature that would be reached on prolonged steam addition.

The usual methods of estimating the time constant from the early part of the reaction curve could not be used because the experimental-determination of the value of T_P would have interfered with the normal operation of the plant. The temperature at any time was therefore related to the peak temperature :

$$T/T_{peak} = (1 - \exp - (t - D) / \tau) /$$

$$(1 - \exp - (\bar{t} - D) / \tau) \qquad (3)$$

Equation (3) was plotted for different experimental values of $\bar{t}$ and t as shown in Fig. (4). The experimental values of T/T_{peak} at several points on the response curve were then used in obtaining the corresponding value of τ. The reproduction of approximately the same value for each run indicates that the postulated

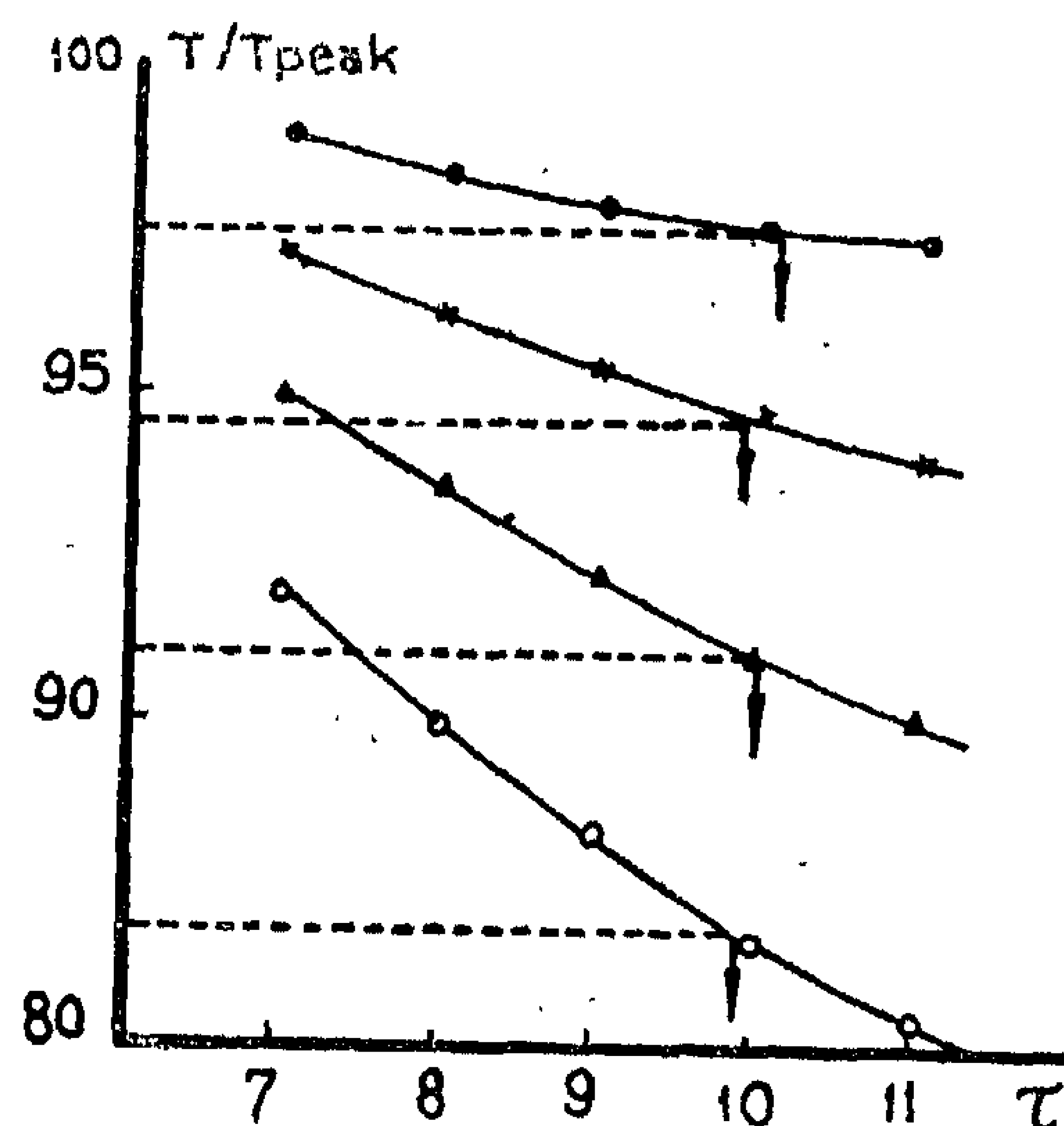


FIG.(4)_ DETERMINATION OF τ FROM T/Tpeak AT VARIOUS TIMES FOR t̄ = 23.2

model is a good representation of the data. The arithmetic average of four values of τ which were closest to each other was taken as the average time constant for the early part.

The average time constant corresponding to the decaying part of the response was obtained by plotting the logarithm of T versus ($\bar{t}$ — D). It is clear from equation (2) that such a plot would result in a straight line of

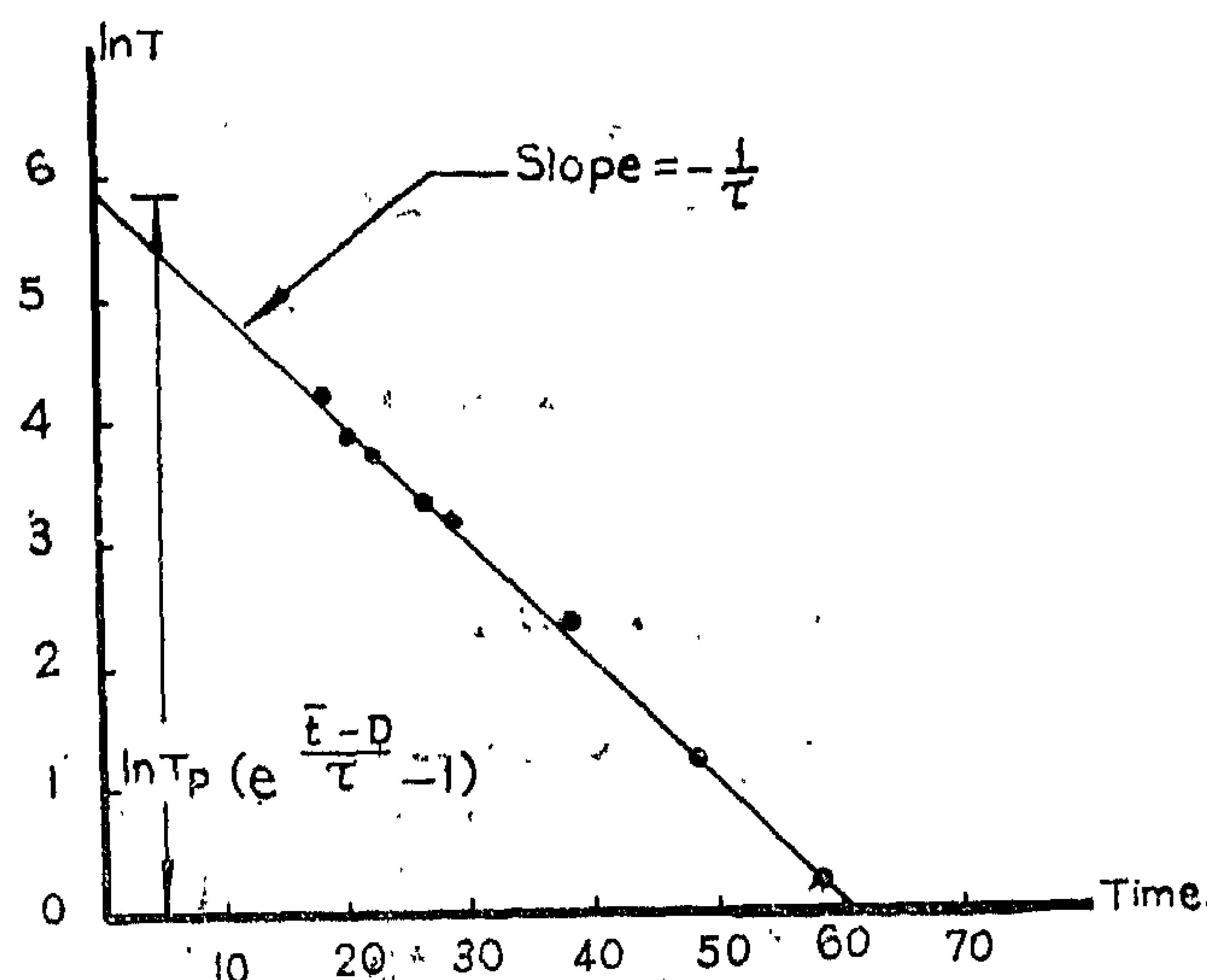


FIG.(5) _DETERMINATION OF τ FOR THE DECAYING PART OF THE RESPONSE.

EXPERIMENTAL RESULTS

Pulse response measurements undertaken for different ambient air temperatures and humidities and pulse durations are presented in Figure (2). Figure (3) typifies the shape of the response curve obtained in the above 16 runs. It is noticed that the temperature of the effluent air after stopping the steam admission levels out to a value slightly above the ambient temperature. This rise in temperature was found to be about 6°C in all cases and was attributed to compression, heat transfer in the fan where the temperature is increased owing to the effect of friction between the moving parts and to stagnation on the measuring thermometer. It is also noticed that the early part of hte response is slightly sigmoid in shape due to the presence of the thermometer lag and the distributed parameter character of the heater.

Attempts to fit the data of Figure (2) to a two-time constant plus dead time model (7, 8) have not been successful because the obtained values of the dead time were not reliable; moreover, although the sum of the two time constants was more or less reproducible, their ratio was scattered. A first order plus dead time model (9) gave the most consistent results. In all cases, the response curve first crossed the final steady-state temperature after about 0.9 Minutes as shown in Figure (3).

Manipulation of the data :

The early part of the response of the first-order plus dead time model is given by :

$$T = T_P \left(1 - \exp - (t - D) / \tau\right) \text{ for } t > (t - D) > 0 \quad (1)$$

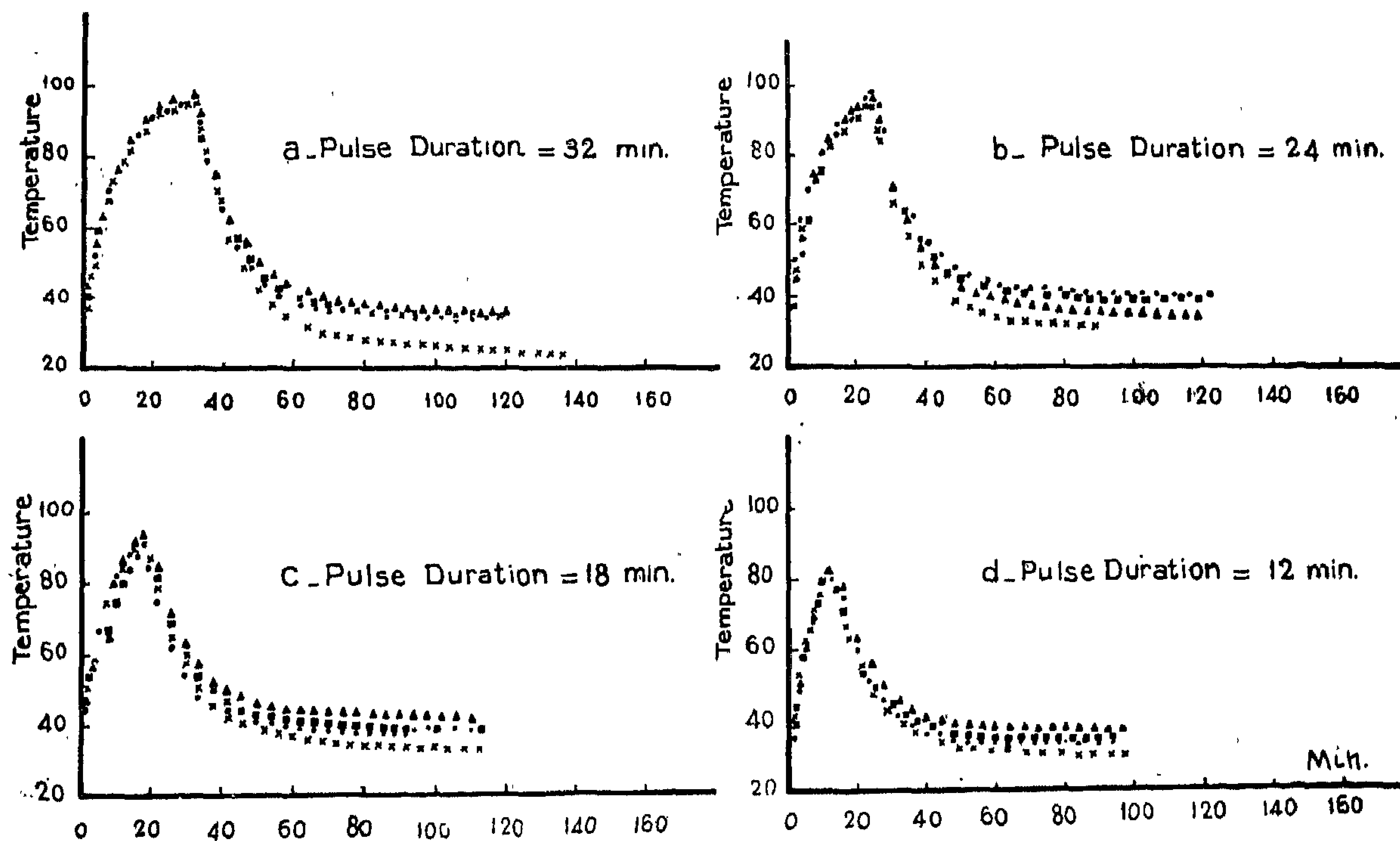


FIG. (2) _ EFFLUENT AIR TEMPERATURE RESPONSE FOR DIFFERENT AIR HUMIDITIES AND DURATIONS OF THE STEAM PULSE.

DYNAMIC MEASUREMENTS ON A SHELL AND TUBE STEAM HEATER

By

M.A. EL-RIFAI, H.A. YOUSSEF
and M.A. SALEH
*Chem. Eng. Dept., Fac. of Eng.,
Cairo University.*

ABSTRACT

Experimental measurements of the pulse response of an air-steam heat exchanger have been undertaken under various ambient air temperatures and humidities for four differferent pluse durations. It is found that the experimental data can be adequately fitted to a lumped model involving a dead time and a transfer lag which increases slightly with the increase of the ambient air temperature.

INTRODUCTION

Although the dynamic behaviour of shell and tube heat exchangers recieved considerable theoretical attention (1, 2, 3), experimental studies on industrial full scale equipment are relatively scanty (4, 5, 6). The present article presents the results of an experimental investigation of the pulse response of a large single pass steam heater in which a heat pulse is introduced into an air stream. As shown in Figure (1), the air leaving the exchanger is used in the through circulation drying and cooling of a hot moist adsorbent bed. In order to optimize the operating cycle of the adsorption battery, a dynamic model relating the heater effluent air temperature saw tooth to various operating conditions had to be formulated. On the basis of this model, the optimum duration of the heat pulse resulting in minimum time of combined drying and cooling of the activated carbon bed, could be determined for various operating conditions.

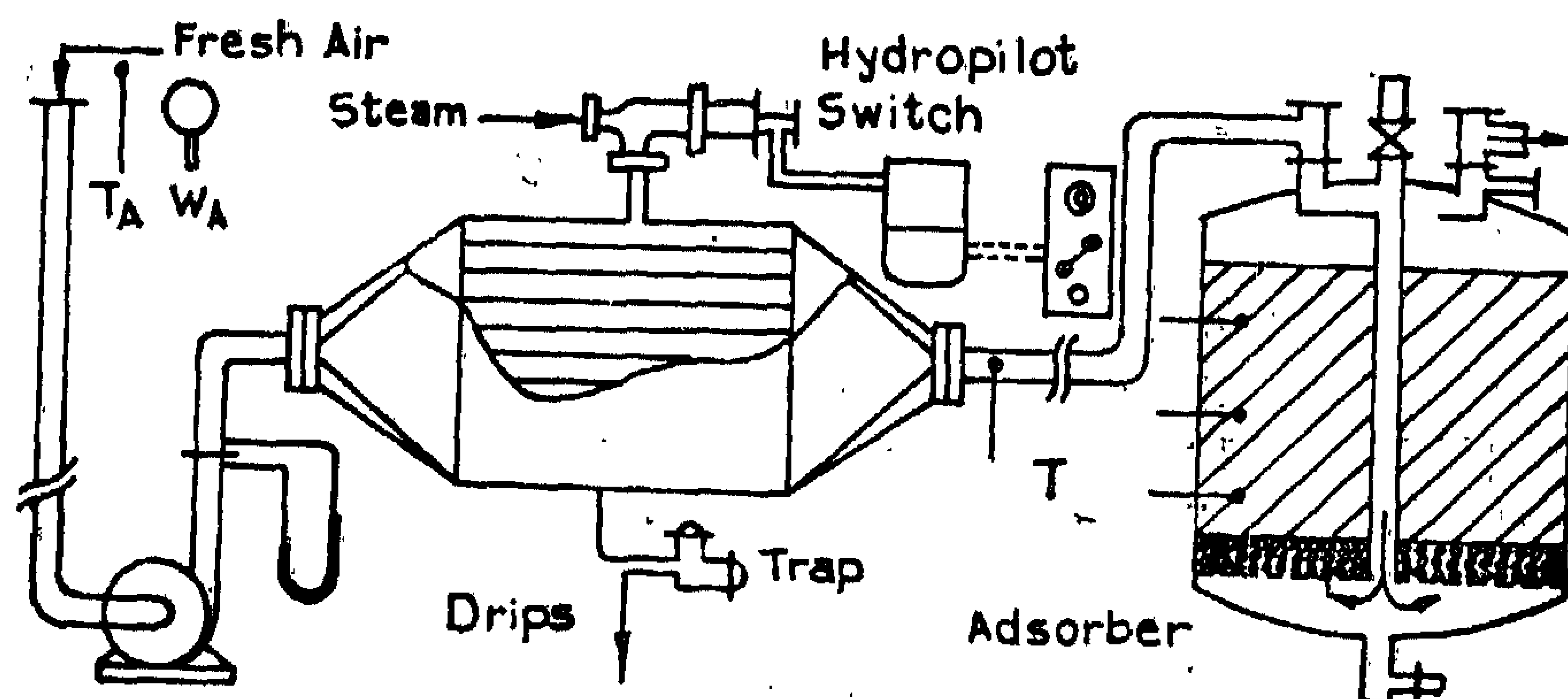


FIG.(1)_ SCHEMATIC OF THE PROCESS.

4 — Test Result :

The results of the tests are illustrated in tables Nos. (1) and (2) for both resistivities of water P = 1550 and 415 Ω cm. respectively.

Table No. (1) P = 1550 Ω — cm.

Water jet length (meters)	Applied voltage (kv)	Notes
14.8	975	Breakdown occurred.
	950	Withstand for one minute.
12.8	945	Breakdown occurred.
	900	» »
	850	» »
	825	Withstand for one minute.
11.0	850	Breakdown occurred.
	800	» »
	750	» » after 40 s.
	700	Withstand for one minute.
9.0	700	Breakdown occurred.
	600	Withstand for one minute.

Table No. (2) P = 425 Ω — cm.

14.8	970	Breakdown occurred.
	950	» » after 50 s.
	940	Withstand for one minute.
12.8	840	Breakdown occurred.
	800	Withstand for one minute.
11.0	650	Breakdown occurred.
	580	Withstand for one minute.

5 — Discussion and Conclusions :

The lengths of the water jet (up to 14.8 meters) against the breakdown and the one — minute withstand voltages for water resistivities of 1500 and 415 Ω — cm. are presented in Figs. Nos. (3) and (4) respectively. These relations are found to be linear. The resistance of the water jet "R" may be expressed as follows :

$$R = R_w + R_a$$

where R_w is the resistance of the cylindrical column of water and R_a is the resistance of air through the particles of water.

It is found that a water jet of 3.3 meters long and has a resistivity of 1550 Ω — cm. withstands an applied voltage of 303 kV (phase to ground voltage of the 500 kV T.L.) for one minute.

The value of the dielectric strength of water stream, intended for washing the 500 kV T.L. insulators are chosen under conditions of overvoltages influence to the stream.

The value of the overvoltage factor in case of the 500 kV T.L. with compensating reactors at three phase antomatic reclosure is about 2.5. In case of single phase automatic reclosure, with which the 500 kV T.L. between Aswan and Cairo is equipped at present time, an overvoltage factor of 2 may be considered.

Therefore, the length of the water jet used for live line washing of the 500 kV T.L., must be not less than 12 meters and the water resistivity must be greater than 400 Ω — cm.

ACKNOWLEDGEMENTS

The author is grateful to the staff of the E.H.V.R.C. and the staff of the Main Network General Inspectorate for their contribution in carrying out the investigations, and for providing the hydraulic system and the telescopic tower.

REFERENCES

1. E.A.H. Aly, F. kilany and M. Mongy, "Studies and Characteristics of Cap and Pin Insulators Under Natural Pollution Condition", M.Sc. Thesis 1960, Submitted to Technical University of Gdansk — Poland.
2. P.J. Lambeth and others, "Surface Coatings For H.V. Insulators In Polluted Areas.", Proc. IEE, Vol. 113, No. 5, May 1966.
3. F.H. Last and others, «Live Washing of H.V. Insulators In Polluted Areas", Proc. IEE, Vol. 133, No. 5, May 1966.
4. A. Stalewski, "Remately Controlled Live line Washing," Electrical Review, 12, May 1967.
5. Private Communication with General Silicones Ltd., Australia.

The basket of the telescopic tower where the nozle was fixed was controlled manually by means of a rope as illustrated in photograph (4).

Before carrying out the investigations, the wind direction was determined by means of a wind meter to maintain the water jet direction as that of the wind.

The resistivity of the water used for the investigations was measured by means of the Ammeter-Voltmeter method. The ratio of the cross sectional area of the copper electrodes to the length of the glass cylinder is 0.032. By knowing the voltage and the current the resistivity was determined from the simple relation $R = P.\frac{1}{A} = \frac{V}{I}$ where P is the resistivity of water in Ω — Cm. and V is the voltage in volts, and I is the current in amperes. To change the resistivity of water, sodium chloride was added to the water taken from the water tap to decrease its resistivity to 415 Ω — cm.

After adjusting the telescopic tower for the first length of water jet (14.8 meters) and filling the water carrier and being sure of the connections, the voltage was increased gradually to a certain value below the breakdown voltage of the water jet (which was gained by experience), then the water jet was applied to the high tension contact and the voltage was increased rapidly until breakdown occured. The breakdown voltages were recorded for the various lengths of water jet by the same method. Also the one minute withstand voltages were recorded.

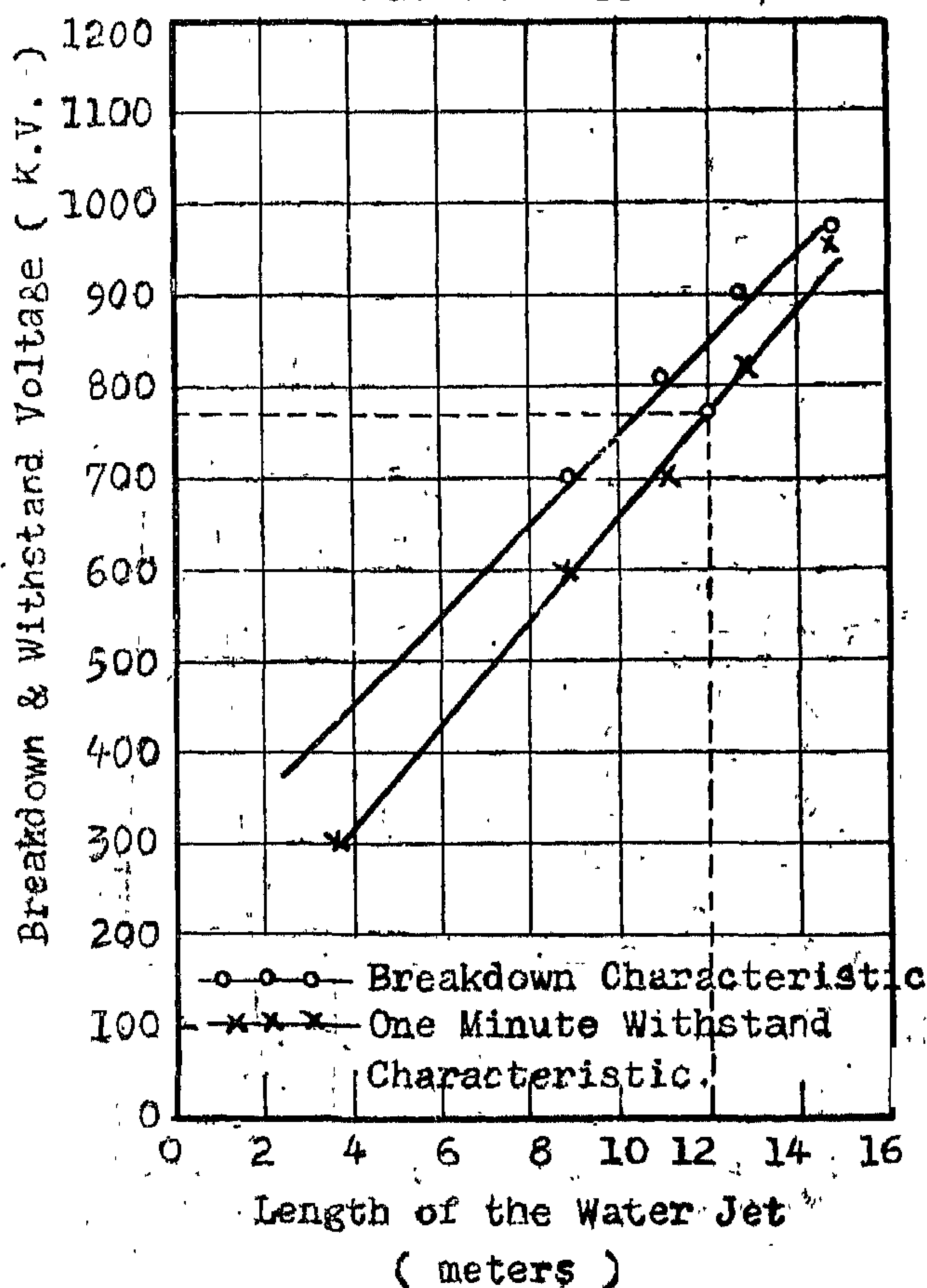


FIG. No. 3 : Breakdown Characteristics of Water Jet.

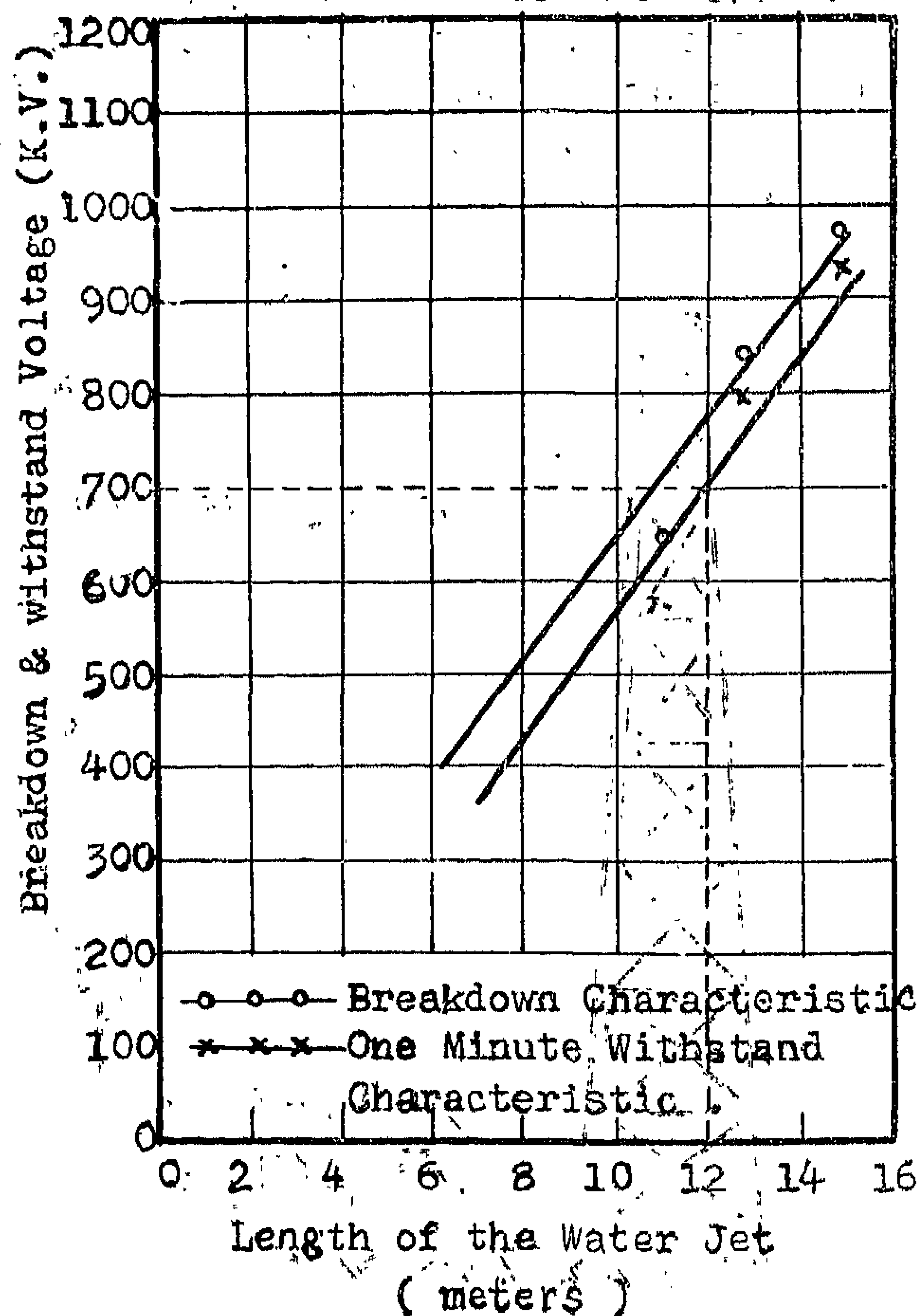
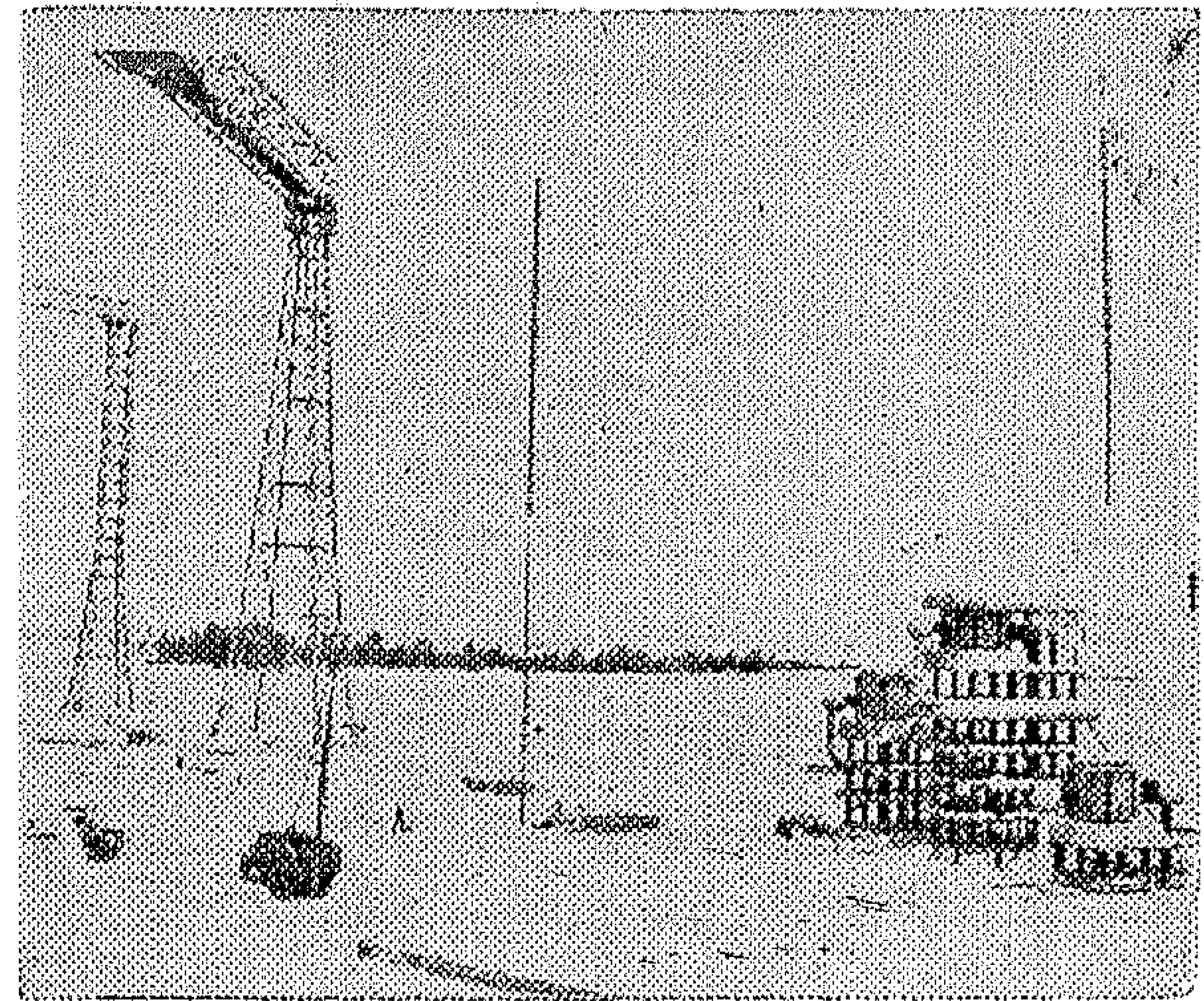


FIG. No. 4 : Breakdown Characteristics of Water Jet.

down. A mixture of distilled and ordinary water was controlled to obtain this specified value of resistance. This water resistance was isolated from earth by means of a chain of 55 disc insulators of the Russian type π Ф E-11. The high tension was then connected to an alluminium wire cage round 5 disc of insulators isolated from earth by 55 disc insulators from both sides as illustrated in Fig. No. (2). The bottom end of the string was fixed to ground to avoid its oscillations or string during carrying out the ingestigations. The hydraulic system consisted of the following :

a) A water carrier of capacity 3 m^3;
b) A fire engine, the pump of which has a pressure of 7 — 8 atmospheres;
c) Nozzle with a hose of diameter of 17 mms, and
d) A telesbscopic tower.

The water jet was directed to the high tension cage, and by moving the telescopic tower it was possible to control the water jet lengths of 14.8, 12.8, 11 and 9 meters respectively. The specific consumption of water



Photograph No. 4 : H.V. Transformer, Telescopic Tower and Hydraulic System.

was 490 litres / minute. Arcing rings were placed near the high tension contacts to improve the voltage distribution on the strings and to prevent the occurence of flashover accross the insulators chains and not through the water jet. The telescopic tower, the fire engine and the nozle were well connected to earth by means of earthing conductors the cross section of the which was not less than 16 mm 2.

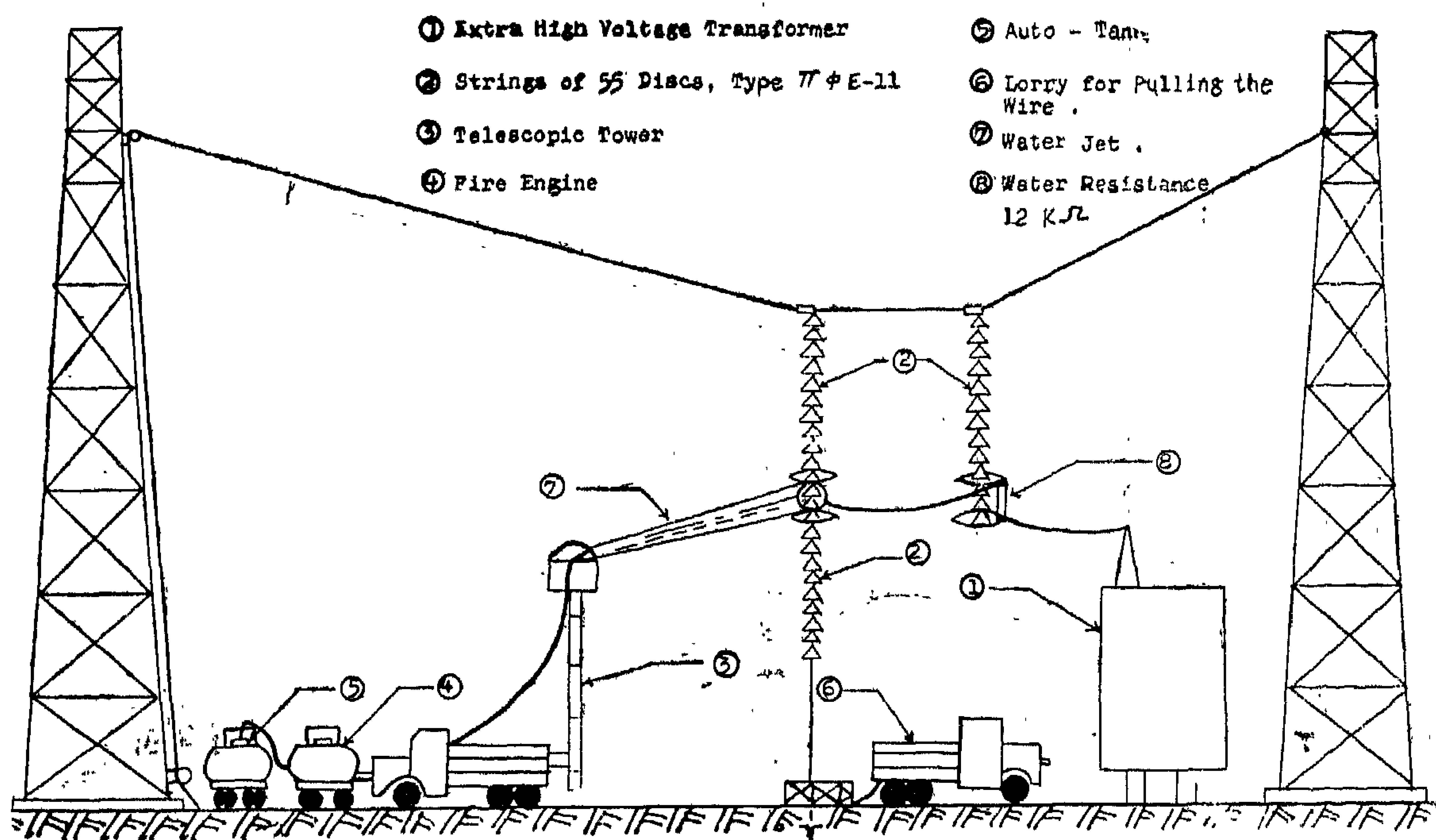


FIG. 2

pollution flash-over prevention by the development of techniques for live line application. They produced a certain type of grease which is specifically for application to insulators under live line conditions, and it was mentioned that spraying the insulators surfaces by a layer of this grease gave excellent results on the 220 kV lines in Australia. Photograph No. (3).

2.3 Using oil — path insulators[3] :

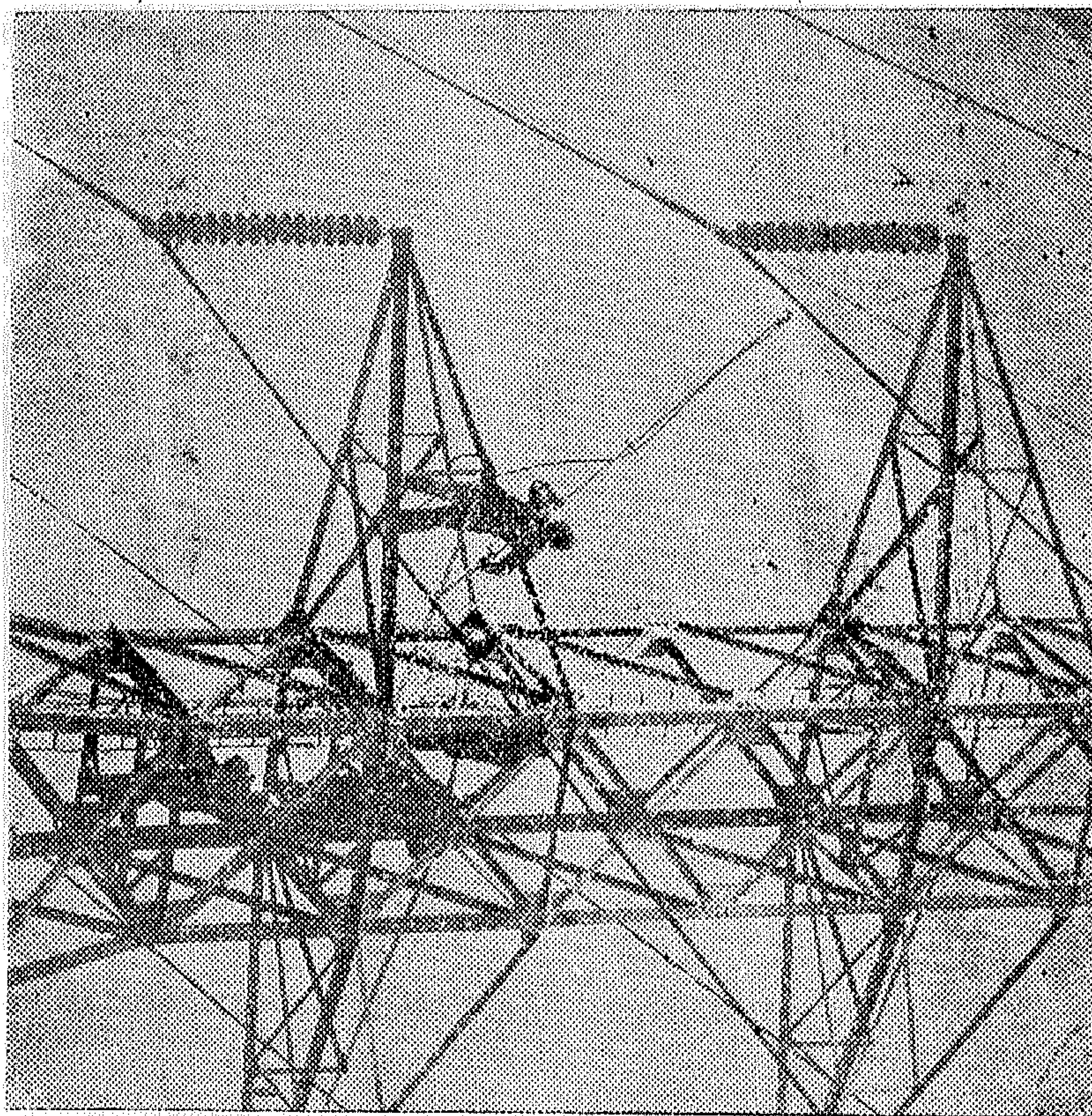
Concerning the oil — path insulators, these undoubtely improve also the insulators performance in polluted and humid atmospheres, but this method is expensive. The oil should be replaced from time to time and consequently it is not frequently used.

2.4 Live line washing[4],[6] :

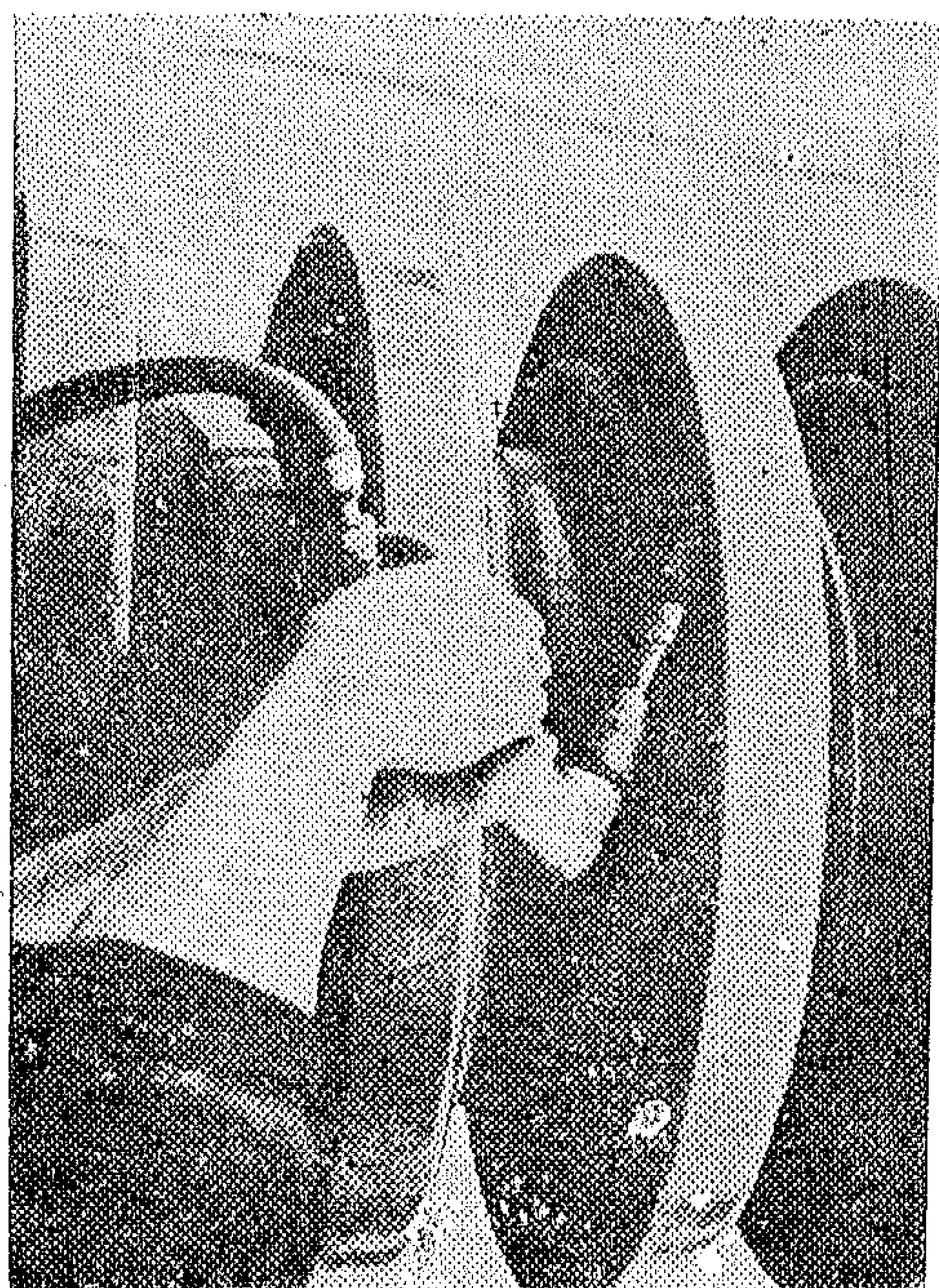
Live line washing is also one of the methods to maintain reliability of transmission systems and thus security of supply. This method has been used with success in different countries. To secure the safty of personnel, the water used must have a certain resistivity and the length of the water jet must be adequate. Live line washing techniques is to be used in the U.A.R. for the 500 kV lines. Consequently, the water jet length, resistivity of water used must be determined before using the live line washing technique which is the purpose of the investigations carried out.

3 — Description of experimental method.

The schematic representation of the hydraulic system and the high voltage testing transformer is shown in Fig. No. (2) and photograph No. (4). The high voltage transformer was connected in cascade to give about 2000 kV. A water resistance of about 12 k Ω was connected in series in its secondary to damp the oscillations and to limit the short circuit current during the water jet break-



Photograph No. 3 : Live Line Spraying of Silicone Grease.



Photograph No. 1 : Removing of Contaminated Layer (275/132 kV. Corby S/S, England).

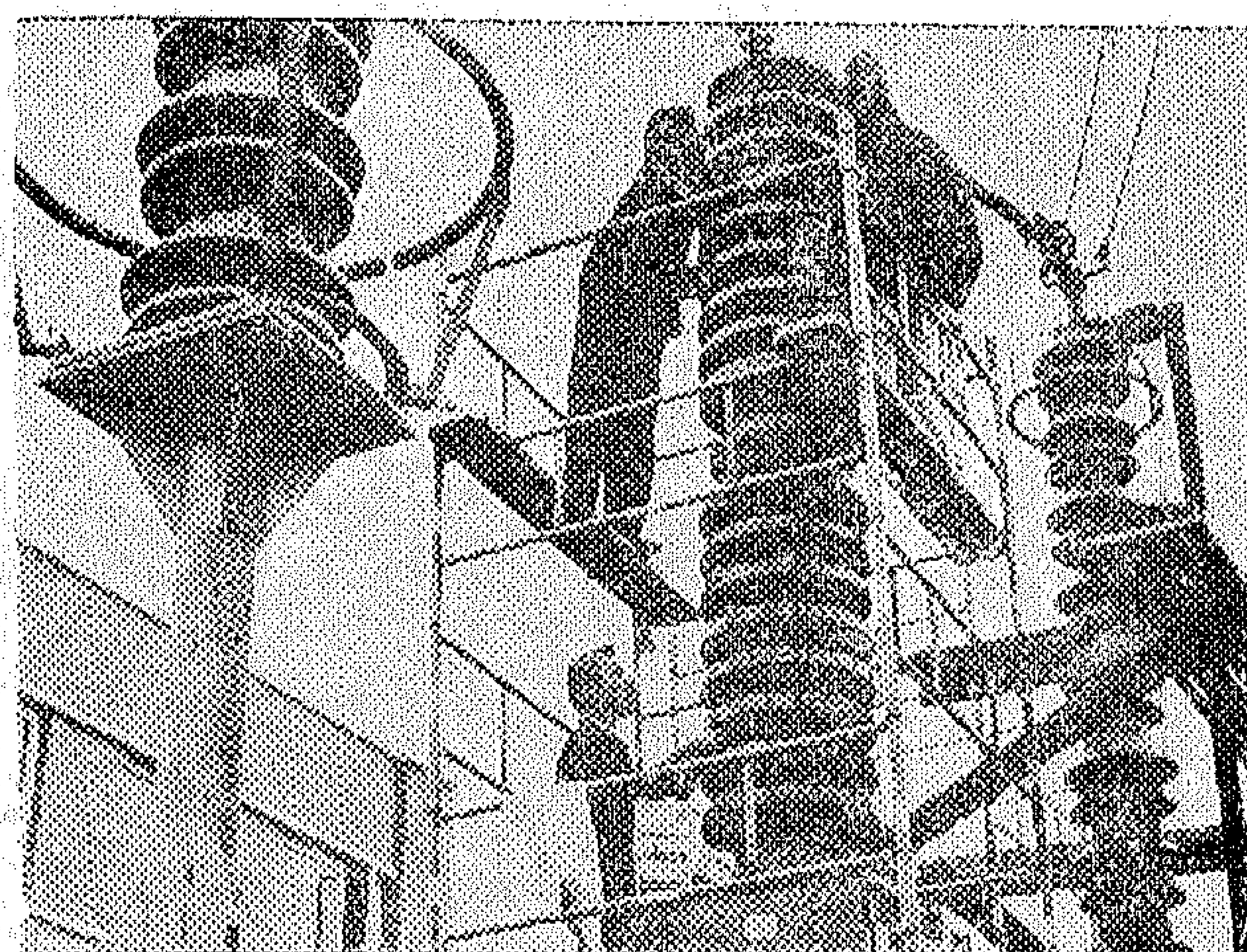
workmen and furthermore, it is comparatively expensive. In fact this method has been used in different countries e.g. it has been used in England for substations of 400 kV and 275 kV*. These substations are located near industrial regions and they are exposed to high humidity. This method has been proved effective where chemical reaction occurs between the pollution particles and it becomes too difficult to clean the insulators by the normal methods. On the other hand covering the insulators surface by a layer of grease makes it easy to clean it, as the pollution particles are absorbed in the grease. The following steps should be observed before greasing:

1) All insulator surface should be thoroughly cleaned. This may be effected by using paraffin rags.
2) If the dirt is particularly persistent, a solution of hot caustic soda may be used.
3) A final rinsing with clean water should be given and the insulators should be allowed to dry off.

The fundamental requirement of the grease is that it shall remain stable on the insulators in the highest ambient temperatures likely to be experienced and that it shall not be washed off by heavy rain. On the other hand, it should not be so hard that it will not readily absorb dust. The action of the grease when dirt is deposited on it is such that the grease enfolds the particles there by absorbing them. Continuation of this process with time causes the grease to become so impregnated with dirt that a conducting path through the grease results. Replacement of the grease has therefore to be carried out before this stage is reached. A second function of the grease is to break up any continuous film of moisture into droplets thereby again preventing a conducting path forming over the insulator.

However, covering the insulator surface with a layer of silicon grease is comparatively expensive as has been already discussed. e.g. It was estimated for covering a long rod string of 220 kV with a 0.75 mm layer of silicon grease, a sum of about L.E. 3 added to the charge necessary for cleaning it well before greasing.

However, in the last few years some companies (General Silicones) contributed to



Photograph No. 2 : Covering Insulators with a Layer of Silicone Grease (275/132 kV. Corby S/S, England).

Photographs Nos. (1) and (2).

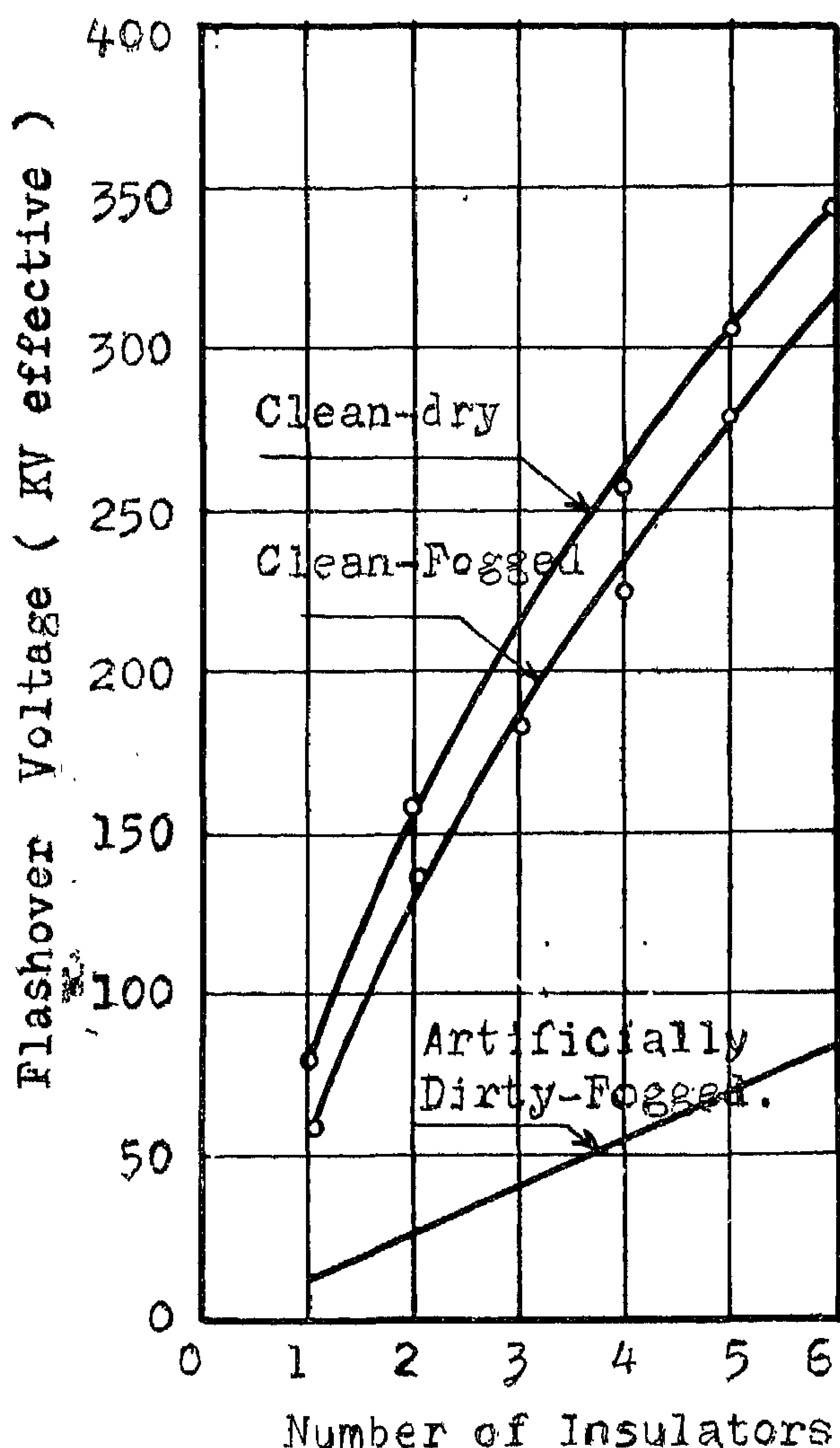


FIG. No. 1 : Flashover Voltage of Suspension Insulators.

clean insulator in humid atmosphere. On the other hand the flash over voltage drops to a great extent if the insulator is contaminated and is exposed to high humid atmospheres.

2 — Methods for improving the performance of insulators in polluted and humid atmospheres.

Various methods for improving the performance of insulators in polluted and humid atmospheres have been adopted.

2.1 Increasing the leakage path using anti-fog insulators or increasing the frequency of insulators cleanings :

These two methods are closely related i.e. By increasing the leakage path, the number of times necessary for cleaning the insulators will be decreased and vice versa. This, of course, depends on the weather conditions where the overhead T.L.s are constructed, and upon the type of contamination in these areas. In some areas insulators cleaning is done by rain or by wind, while in other places, where it does not rain frequently, the cleaning of insulators must be done manually. In some countries like England or Poland, where it does rain frequently and heavily, flash-over has not occured to insulators being in operation for a period of about 3 to 10 years. This is due to the natural cleaning of insulators by heavy rain. In areas where it does not rain, cleaning of the insulators depends upon the surrounding windy atmospheres. In areas were wind is not sufficient for self-cleaning, then it is necessary to clean manually.

The period between two successive cleanings of the insulators depends upon the weather conditions, the length of the leakage path, and upon the rate of salty dust deposits on the surface of insulators. Consequently, the choice of the length of the leakage path or the frequency of cleaning are closely related. The choice is according to economical comparison between the currency necessary for increasing the leakage path and the expenditures necessary for cleaning the insulators several times.

2.2 Covering the insulators surface by a layer of silicon grease(2) :

Experience in operation of electric power systems, has shown that lengthening the leakage path is not very effective in some industrial regions where the pollution is either too severe or it is too difficult to remove. For this reason, it is recommended, by different firms to cover the insulators surface by a layer of silicon grease to prevent the formation of a continuous conductive layer on the insulators surface.

Covering the insulators surface by a layer of silicon grease has been found suitable only in the substations as it requires many

METHODS FOR IMPROVING T.L. INSULATORS PERFORMANCE IN POLLUTED AND HUMID ATMOSPHERES

An Investigation into dielectric strength of Low Pressure Water Jet Used for Live Line Washing

By

EL SAYED A.H. ALY
B.Sc., M.Sc., Ph.D.

SYNOPSIS

The investigations were carried out at the extra high voltage laboratory of the Egyptian Electricity Corporation using the 2250 kV, 2250 KVA cascade transformer. The one minute withstand and the breakdown voltages were found for water jets of different lengths and having resistivities of 1550 and 415 Ω -cm respectively. The purpose of the investigations was to determine the minimum length of water jet with a primary diameter of 17 mm at a pressure of 7-8 atmospheres at which the safety of the live line washing personnel should be guaranteed under the prevailing weather conditions in the U.A.R.

1 — INTRODUCTION

The insulation of high voltage systems is exposed to overvoltages during operation. These overvoltages are due to :

a) lightning surges,

b) internal overvoltages resulting from switching on and off, and from earth faults, and

c) natural frequency working voltages.

The performance of the insulators of the overhead transmission lines are affected by surrounding weather conditions which affect its ability of withstanding overvoltages to which it is exposed during operation. Heavy pollution and high humidity are the most important factors which affect the performance of insulators. Experience in operation of the overhead transmission lines shows that the ability of insulators to withstand overvoltages differ from one place to another according to the areas where the overhad T.L.s are constructed. The performance of insulators differs according to the kind of pollution contaminated on their surfaces whether this contamination is natural dust or ashes resulting from factories.

Since this dust may contain soluble salts, the performance of insulators are undoubtly affected by the quantity of these salts and upon the humidity of the surrounding atmospheres. This will cause a conductive layer on the surface of insulators and local discharges will appear. These local discharges initiate the complete flash-over on the surface of insulator.

It has been verified experimentally[1] that the effect of either contamination or humidity alone is not so severe, but the effect is severe under humid contamination. From Fig. No. (1) it is seen that the value of the flash-over voltage of clean insulators under dry atmospheric conditions increases by a small extent than that of a polluted dry or

Dr. Aly is with the General Egyptian Electricity Corporation, Cairo.

2. The effect of gas velocity at constant ore-to-gas ratio seems to be of little effect in both fixed and fluid beds. Some differences between the two cases are present at low gas velocity. In the fluidised-bed case, and at the lowest gas velocity employed, the reduction rate is higher during the initial reduction stage, and is lower during the final stages than at any other higher velocity.

3. A comparison between reduction rates in fluidised and fixed beds shows that the rate of reduction in the fluidised state is lower than for the fixed state up to about 80% reduction, but becomes higher at higher conversion. The differences are attributed to the combined effect of gas and solid backmixing.

REFERENCES

1. Ezz, S.Y., Trans. AIME, *218*, 709 (1960).
2. Bhat, E.P., and Wood, C.E., U.S. Bureau of Mines R.I. No. 4569 (1949).
3. Feinman, J., and Drexel, T., AICHE J., *7*, 584 (1961).
4. Venkitakrishan, G.R., and Bhat, G.N., J. Appl. Chem., 16, 356 (1966).
5. Ezz, S.Y., Egyptian Patent, No. 1 (January 1954).
6. El-Tobgy, A.H., M.Sc. Thesis, Cairo University (1964).
7. Aly, A.F.A.M., M.Sc. Thesis, Cairo University (1966).
8. Fakhoury, S.S., M.Sc. Thesis, Cairo University (1966).
9. Lewis, W.K., U.S. Patent, No. 2, 638, 414 (May 1953).
10. Shipley, E.H., U.S. Patent, No. 2, 752, 234 (June 1956).
11. Stelling, P.O., Swed. Patent, No. 160, 876 (Oct. 1957).
12. El-Afifi, S.E.Y., M.Sc. Thesis, Cairo University (1969).

ACKNOWLEDGEMENTS

The authors are grateful to the National Research Center for providing the experimental facilities. Thanks are also due to Professor E.M. Khairy, dean of the Faculty of Science, Cairo University, for his kind interest and encouragement.

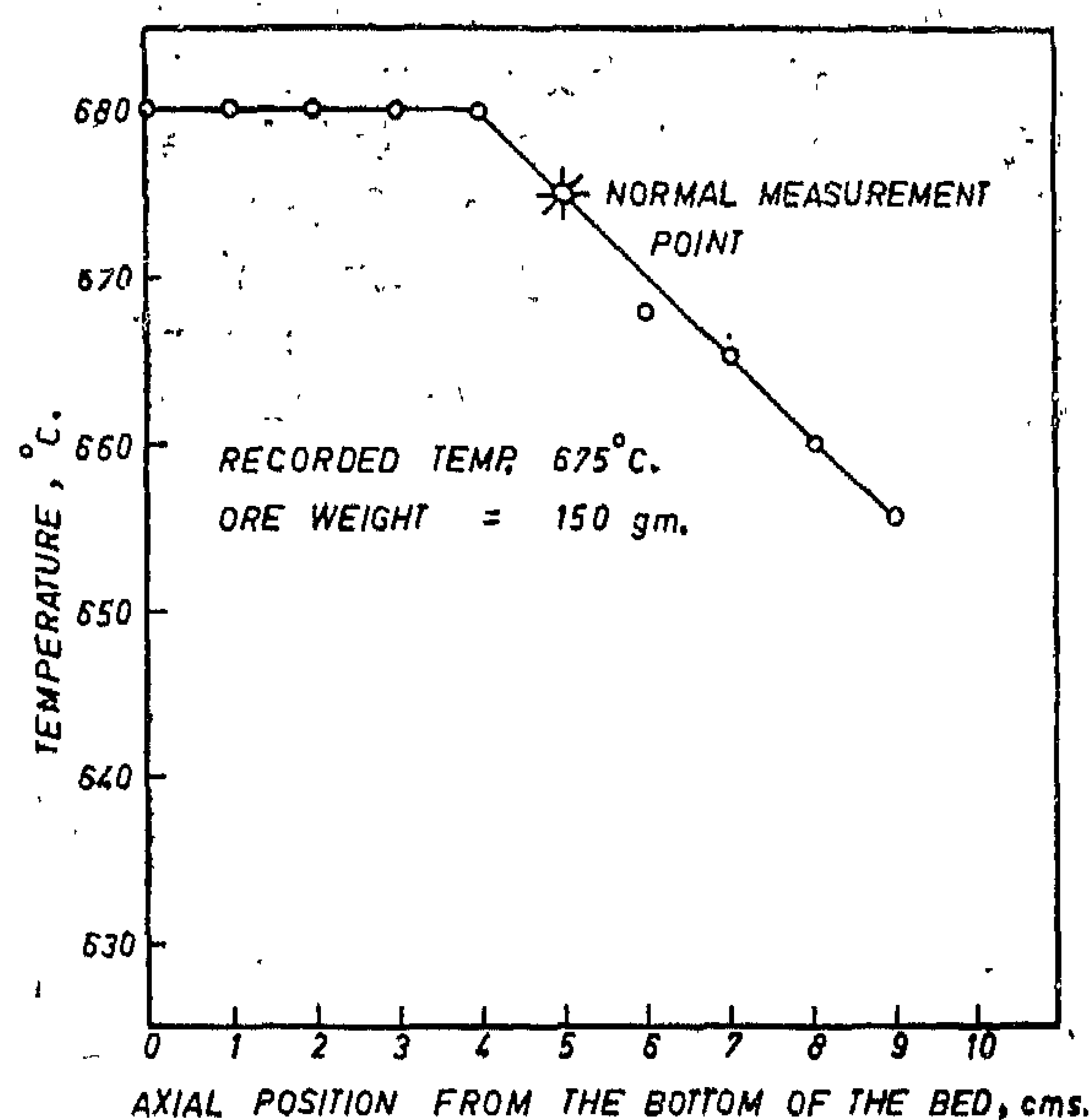


FIG. -9- .LONGITUDINAL TEMPERATERE GRADIENT IN FIXED-BED REACTOR.

plug-flow conditions with no gas backmixing, the fluidised bed is known to be an extremely non-ideal flow reactor in which, among other factors, gas bypassing as well as gas and solids backmixing take place. In accordance with the two-phase concept of fluidised beds, it is commonly accepted that all the gas fed in excess of that required to incipiently fluidise the bed, passes upward at high linear velocities in the form of bubbles. Thus, unless interphase mass transfer between the gas bubbles and the dense-phase gas is very efficient, the overall conversion would be markedly decreased. The dense phase, on the other hand, is characterised by intensive backmixing and a high degree of circulation. Since the reaction is invariabley limited to the dense phase, the extent of conversion becomes much less than that for non-mixed plug-flow systems.

In view of the above-mentioned concepts, the conversion in the fluidised bed should be lower than in the fixed-bed case. This is in good agreement with experimental results up to about 85% conversion. The observed reversal above this reduction needs, however, some recapitulation.

Although most of the facts tend to indicate a lower fluid-bed conversion, two main factors may, under certain circumstances, outweigh the other disadvantageous effects. These are enhanced gas-phase diffusion and vigorous solids movement. In the fluidised bed, the diffusional resistances are much smaller than those in fixed beds and thus the rate of gaseous diffusion from the bulk of the gas phase to the gas-solid interface is much faster. It may be argued, however, that this is contrary to the fact that it has been proven by the fixed-bed results that the effect of gaseous diffusion is negligible. Yet, at low gas velocities and in the later stages of reduction, the fluidised-bed reduction results, as discussed before, tend to indicate some effect.

The effect of solids movement and circulation is believed, however, to be the most important factor. Thus, it may be speculated that during the last stages of reduction where most of the ore has been reduced, the vigorous salids circulation and turnover tends to cause considerable surface renewal, and in effect increases the availability of the unreacted solid to the reducing gas, and consequently the probability of their interaction. This same reasoning may also be utilised to give some explanation to the reversal trend observed for the effect of gas velocity using constant ore-to-gas ratio at the lowest gas velocity.

CONCLUSIONS

The main conclusions evolving from this work are summarised in the following :

1. From the variables investigated, the gas velocity, temperature and the feed-gas water content have paramount influences on reduction in the fluidised state. The general trends of the effect of these variables in both fluidised and fixed beds under similar conditions are qualititatively identical.

COMPARISON OF FLUIDISED AND FIXED BED PERFORMANCE

A general comparison of the shapes of the reduction curves in the fluidised and fixed-bed states indicated qualitative similarities, particularly from the standpoint of the step-wise behaviour of the reduction process. A closer examination, however, reveals differences pertaining in particular to the last reduction stage. Thus whereas this stage starts around 80% reduction in the case of fixed beds, its onset is somewhat delayed in the fluidised-bed case where it starts at about 90% reduction. Moreover, the rate of reduction in the fluidised bed pertaining to this last stage does not fall as sharply as it does in the case of fixed-bed reduction.

In Figure 8, values of the percentage reduction at the same time intervals from the start of reduction and the same velocities (4.9, 8.1, and 13.1 cm/sec) are plotted for fixed and fluidised beds for each gas velocity. Since no apparent trend is observed in the points representing fluid-bed reduction, a single curve was plotted to facilitate comparison of gross differences.

As can be deduced from Figure 8, the fixed bed indicates better performance than

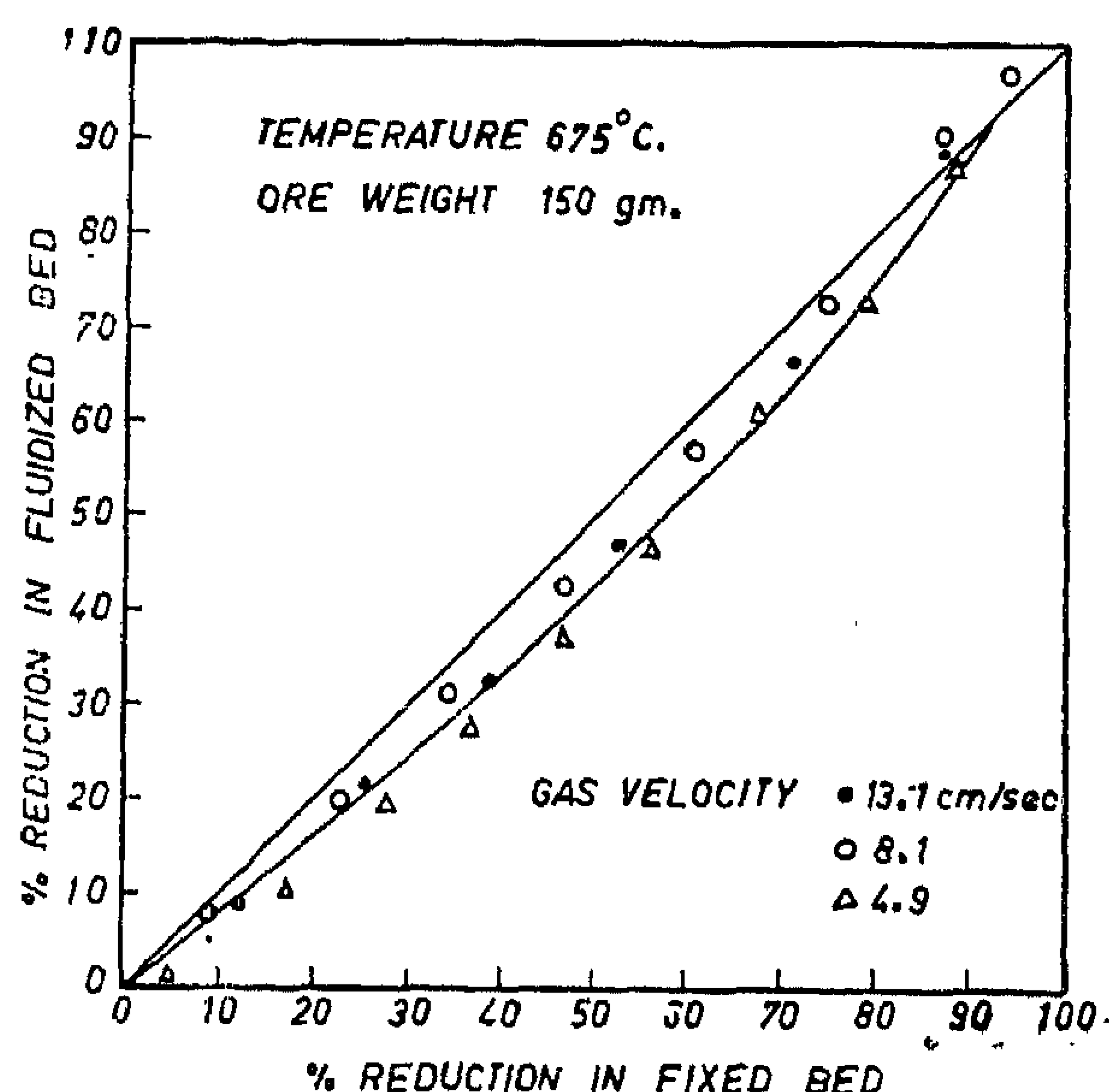


FIG. -8- .COMPARISON BETWEEN REDUCTION IN FIXED AND FLUIDIZED BEDS.

the fluid bed over most of the reduction range, and up to about 85% reduction. Above this conversion, the fluidised-bed performance becomes similar, or even better than that of the fixed bed. Similar observations have been noted by Venkitakrishan and Bhat (4).

These noted differences evolve as a result of differences associaetd with heat transfer and hydrodynamics of the two types of beds. Because of their complex nature, the hydrodynamics of fluidised beds ; particularly those pertaining to such aspects as solid-gas contact, solids circulation patterns, and gas bypassing and backmixing, are not by far well understood. Nevertheless, discussion of the results will be attempted in the light of the available and most accepted evidences.

Starting with the heat-transfer factor, it is realisable at the outset that heat transfer is much more efficient in fluidised than in fixed beds. As a matter of fact, fluid beds can be considered isothermal, with no existent temperature gradients. On the other hand, temperature gradients, both axially and radially, can exist in fixed beds because of their inferior heat-transfer characteristics and the very low heat capacity of gases relative to heats of reaction. Accordingly, the integral conversion over the whole fixed bed may be quite different from that in the fluidised bed. The longitudinal tmeperature gradient in the fixed-bed reactor was thus measured and is shown in Figure 9. It is seen that temperature differences are not appreciable since heat has been supplied externally in order to compensate for the endothermic heat of reaction. It is therefore believed that the role of heat transfer in the present case is not of primary importance in inducing the observed differences.

Turning next to the hydrodynamic aspects related in particular to the internal flow patterns and mixing characteristics, it can be readily conceived that they are exceedingly different in the two kinds of beds. Whereas the fixed bed can be considered very close to ideal-

Effect of Ore-to-Gas Ratio : The effect of ore-to-gas ratio was studied by changing the gas flow rate at a constant bed inventory. The effect of gas velocity at a constant initial ore-to-hydrogen ratio is shown in Figure 5. Careful inspection of this plot reveals that, within the experimental accuracy, conversion is independent of gas velocity in the higher velocity range from 4.9 to 10.6 cm/sec. Contrary to fixed-bed results, an anamolous behaviour was observed at the lowest gas velocity of 2.4 cm/ses. It the initial reduction stage (up to about 50% reduction), the percentage reduction at this lowest velocity is higher than that for the higher velocities. In the final reduction stages, the trend reverses, and the percentage reduction at the lowest gas velocity becomes the lowest. In the previous work conducted with fixed bed, the effect of the initial ore-to-gas ratio was consistent, and the reduction rate increased markedly with decreasing this ratio. Thus, it seems that the anamolous behaviour noted in the fluid-bed reduction experiments, is a direct consequence of the complex interaction of the internal flow patterns and mixing characteristics of the fluidised bed. This will be further discussed when the performances of fluid and fixed beds are compared.

Effect of Water Addition in Feed Gas : The effect of varying steam content of the feed gas is depicted by Figure 6. The results are qualititively similar with those of fixed beds in that both the reduction rate and the percentage completion of the reduction are adversely affected by increasing the water content of the feed gas. The decrease in the rate of reduction with increasing water contents gives further evidence to the conclusion evolving from the previous fixed bed results that water desorption has a dominant role on the overall kinetics of the reaction.

As can be seen from Figure 7, both the rate and the equilibrium values are lower in the fluidised than in the fixed-bed reduction. Such differences are believed to be primarily attributable to gas backmixing characteristics of fluidised beds which effect a considerable decrease of hydrogen concentration level of the inlet gas stream.

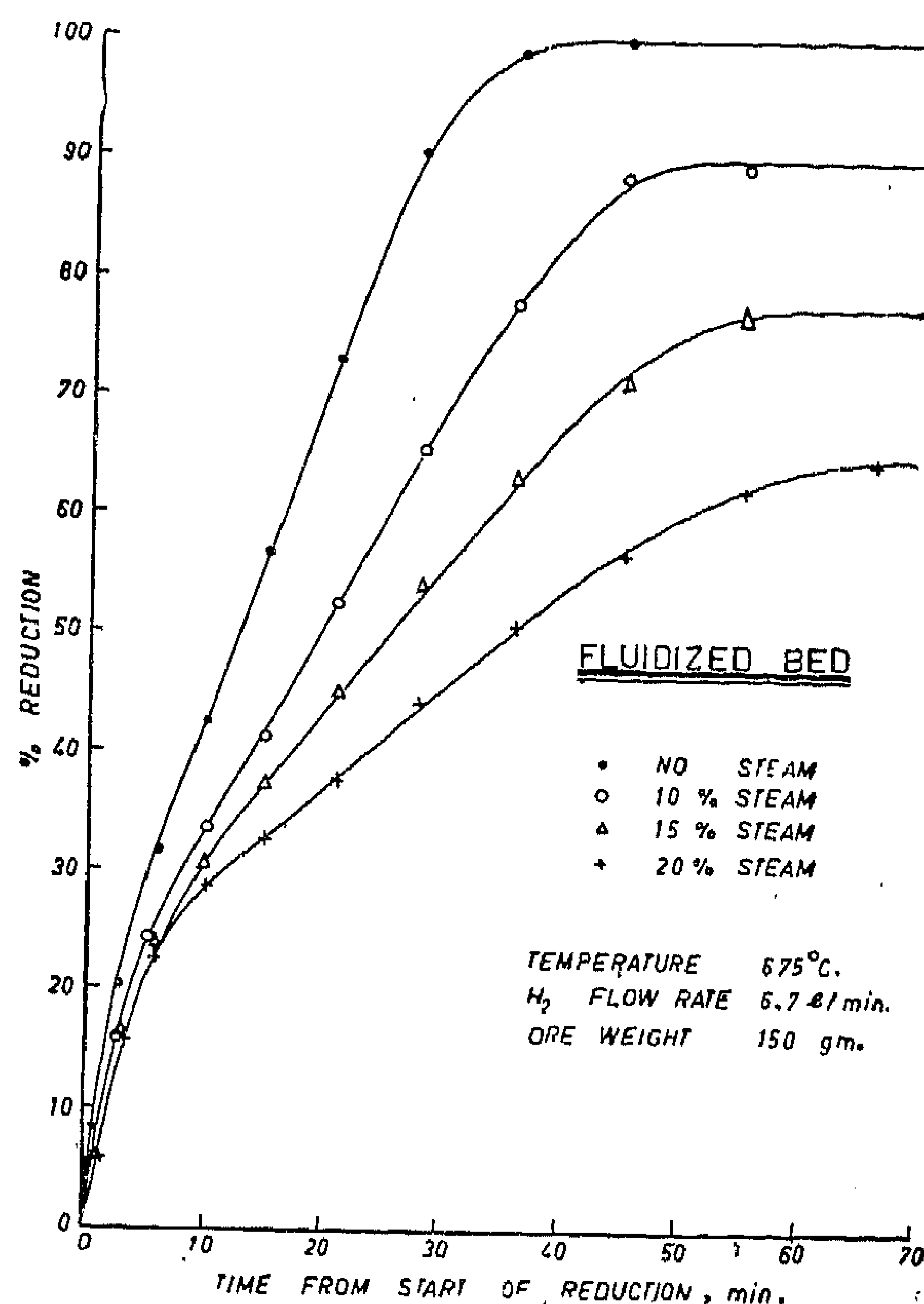


FIG. -6- . EFFECT OF STEAM ADDITION IN FEED GAS FOR REDUCTION IN FLUIDIZED BED.

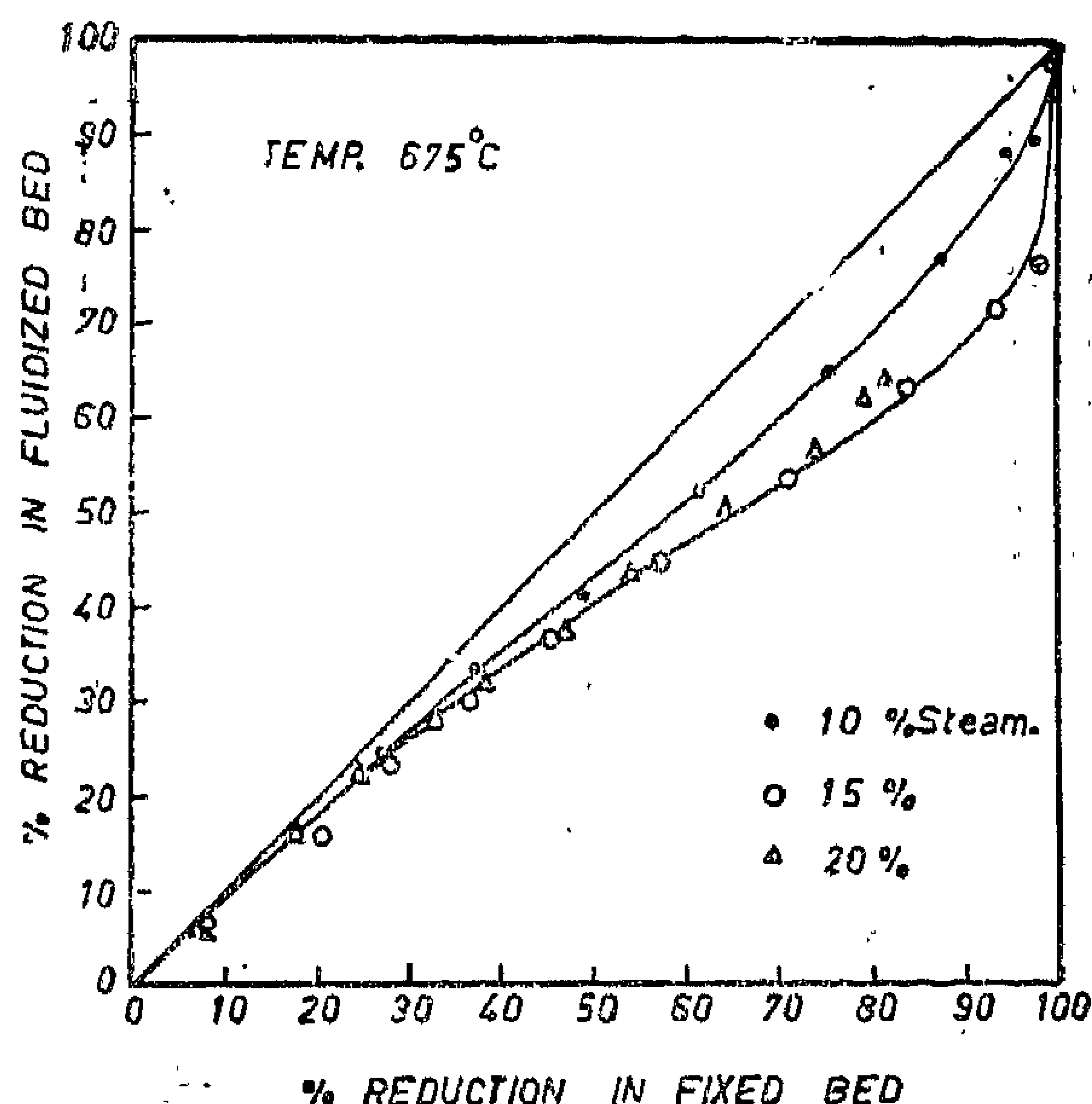


FIG. -7- . COMPARISON BETWEEN FLUIDIZED AND FIXED BEDS ON STEAM ADDITION IN FEED GAS.

particle size, ore-to-gas ratio, gas flow rate, temperature and steam addition to feed gas, on the rate of reduction. Of these variables, the most important are : ore-to-gas ratio, temperature and feed-gas composition. Particle size and gas velocity are of minor effect. The results showed that the reduction proceeds in a stepwise manner, and that the rate-controlling step appears to be the desorption of water vapour from the reaction seat.

In the following subsections, the effect of the various investigated variables will be first described and discussed, and the results will then be compared with fixed-bed results under similar conditions.

Effect of Gas Flow Rate : The effect of gas flow rate at a constant initial bed inventory is shown in Figure 3 It is seen that the gas flow rate has a marked effect on the rate of reduction. The rate increases with increasing the gas flow rate. This may be pr bably due to the decreased water vapour partial pressure in the gas resulting from the higher hydrogen concentrations. This tends to facilitate the desorption of water vapour from the reaction sites; the rate of which is directly proportional to the difference in partial pressures between the seat of the reaction and the bulk of the gas phase.

Effect of Temperature : The results of these experiments are shown in Figure 4. It is quite clear that the temperature has a strong influence on the rate of reduction. As would be normally expected with nearly all operations involving a chemical change, the increase in temperature is accompanied by an increase of the rate.

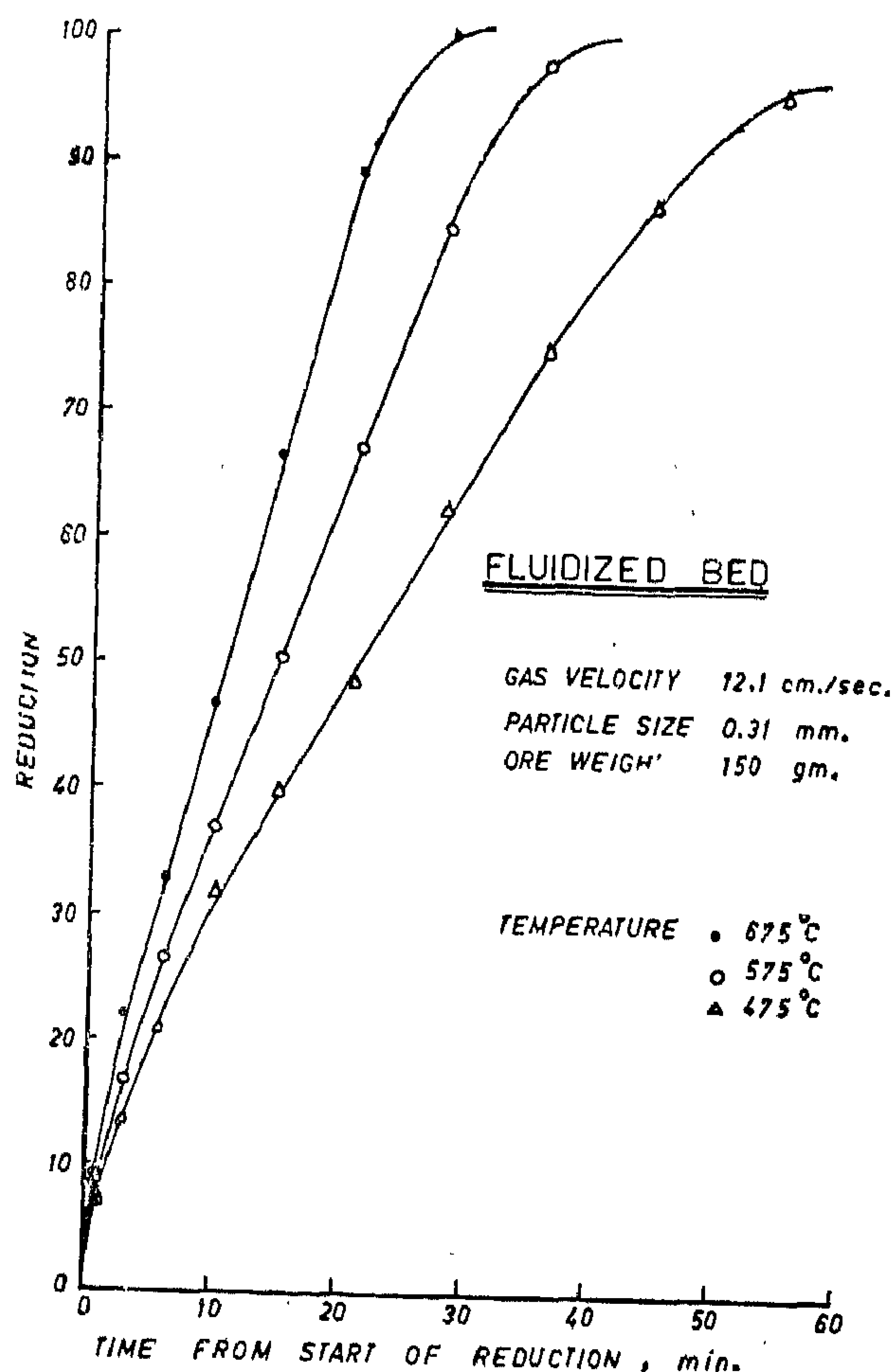


FIG. 4 . EFFECT OF TEMPERATURE ON REDUCTION IN FLUIDIZED BED.

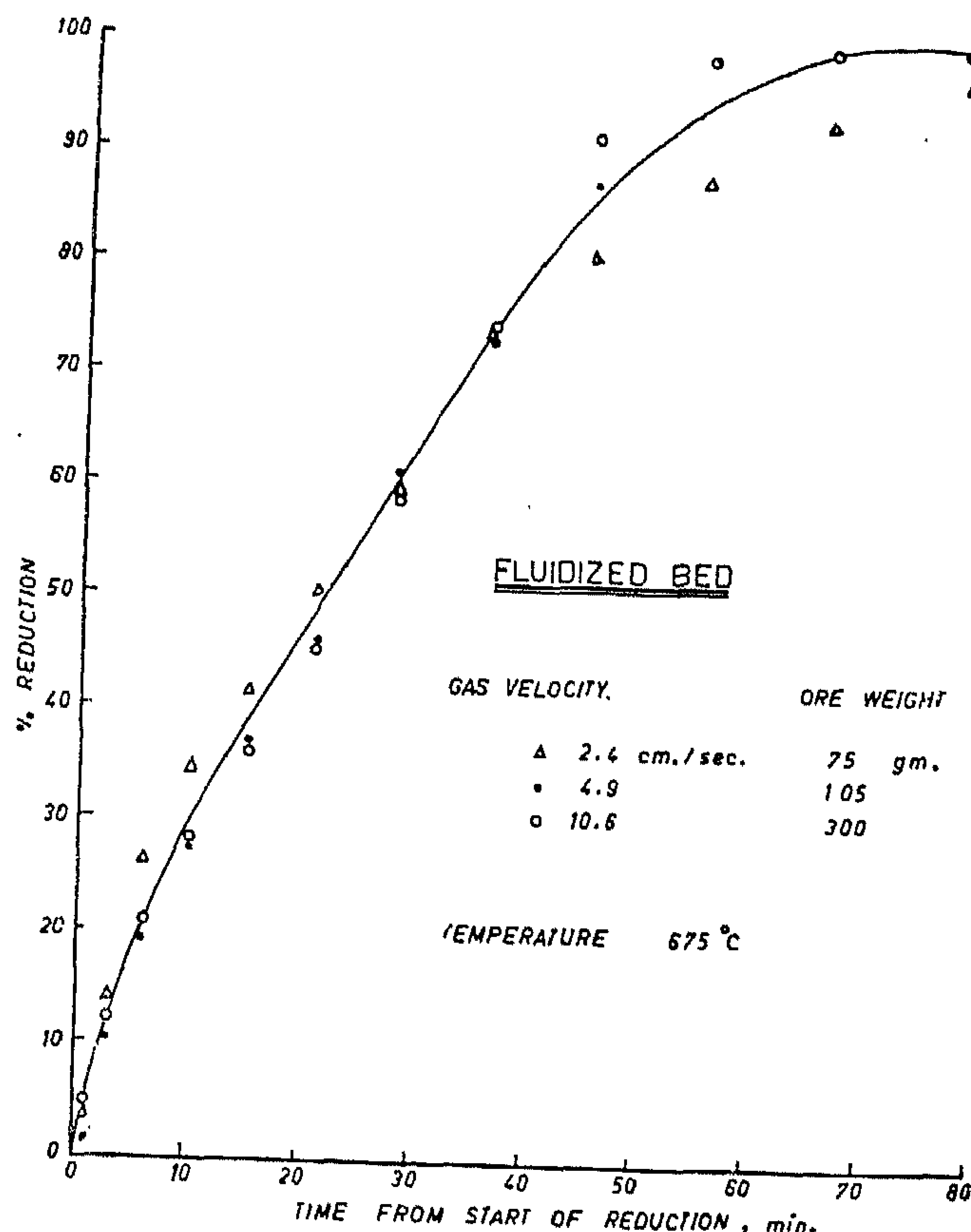


FIG. -5- . EFFECT OF GAS VELOCITY AT CONSTANT ORE TO GAS RATIO ON REDUCTION IN FLUIDIZED BED.

carbons that may be present, by passing it through the purification system. The hydrocarbons are removed by cracking at 900°C over iron turnings. Oxygen is eliminated by reaction with hydrogen over copper turnings heated to about 700°C. Moisture is removed by absorption with calcium chloride. The purified gas is fed then either directly to the reactor, of after passing through the humidifying unit when water addition is desired. Figure 2 shows details of the gas humidification unit. Steam formed by the reaction is first condensed from the reactor effluent gases, and is next completely removed by calcium chloride dryers. The dry gases are then metered in a wet-gas meter and finally vented.

PROCEDURE :

A typical reduction experiment consisted of charging the reactor with the required weight of the ore, and the whole system was checked for any possible leaks. Nitrogen was passed through the system and the reactor is heated to the required operating temperature. Nitrogen was then bypassed and hydrogen fed at the predetermined rate. The run was then started by taking simultaneous wet-gas meter readings with time. These measurements gave the cumulative outlet gas volume with time from the start of reduction. The difference between imput and output cumulative volumes represented the hydrogen consumed in the reaction.

RESULTS AND DISSCUSION

As has been mentioned, the present paper represent a part of an integrated work constituting three basic parts. The first is related to fluidisation dynamics and characteristics; the second with ore reduction in the fixed state; and the third part which is of primary interest here, is the ore reduction in the fluidised state.

Because of their pertinence to the present work, it is worthy to summarise important conclusions evolving from the first two parts. Full results are reported elsewhere (12).

In the study concerning the fluidisation dynamics, the minimum fluidisation velocities as well as bed expansions were measured and correlated with the kind of fluidising gas, particle size, bed height-to-diameter ratio and temperature. The most important factors affecting the minimum fluidisation velocity of the employed ore were found to be : the particle size and gas viscosity. Regarding the bed expansion, the data were best correlated in terms of bed voidage and was found to be uniquely related to the ratio of fluidising gas velocity to that at the incipient fluidisation condition.

Reduction experiments carried out in fixed beds were aimed at investigating the effect of

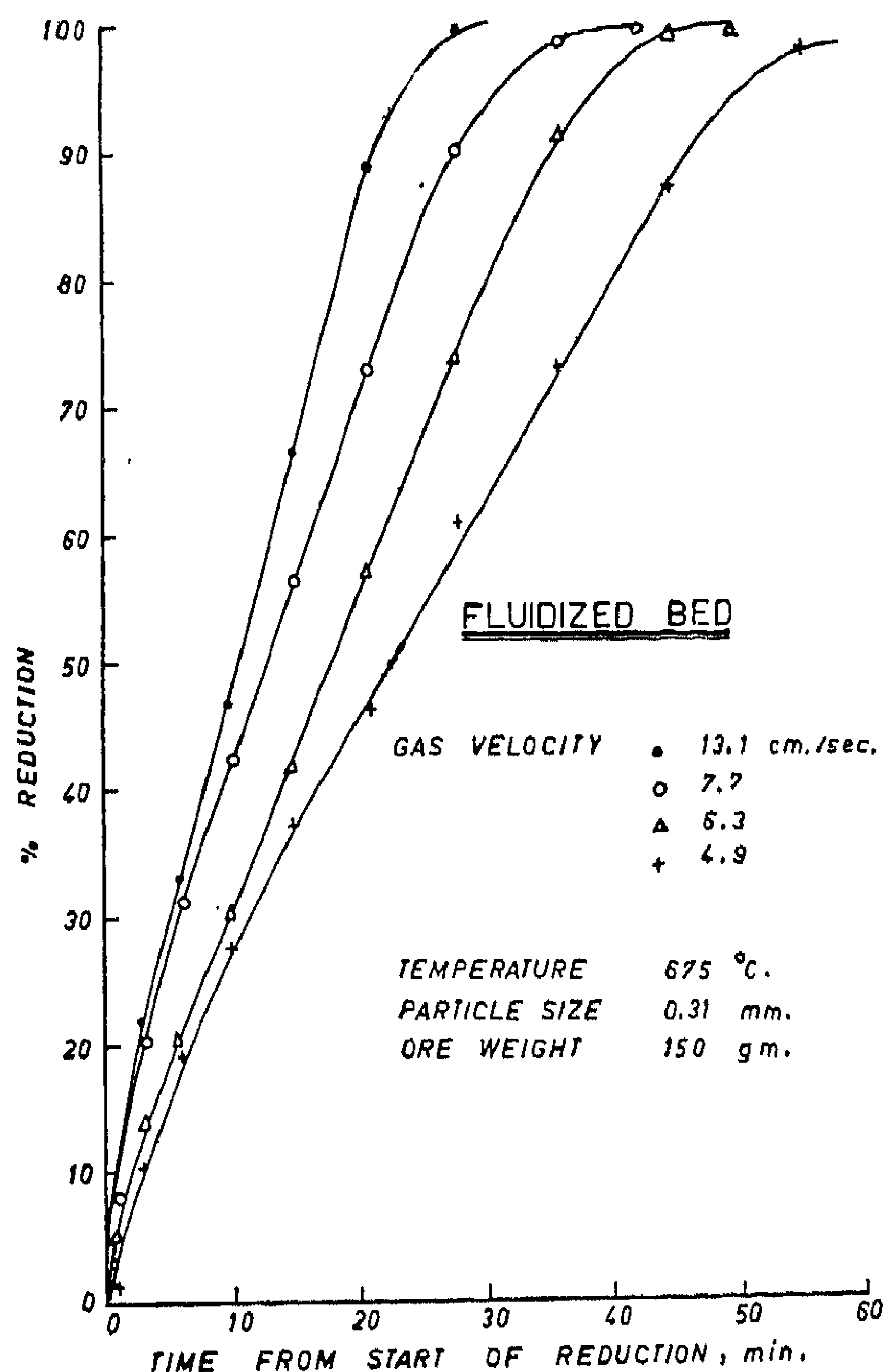


FIG.-3-. EFFECT OF GAS VELOCITY ON REDUCTION IN FLUIDIZED BED.(VARIABLE ORE TO GAS RATIO).

EXPERIMENTAL

The main purpose of this investigation was to study the effect of the most relevant operating conditions, and to examine possible differences in behaviour that may be caused by the additional interaction of fluidisation flow patterns as contrasted with fixed-bed results.

The following variables were investigated: ore-to-gas ratio, gas flow rate, temperature, and steam addition to feed gas. Particle size was found to have no effect, and was not therefor changed. A particle size of 0.31 mm. was used throughout this work. The composition of a representative sample is : 85.8% Fe_2O_3. 2% SiO_2 6.3% loss on ignition, 2.4% Al_2O_3, and 3.5% of other traces.

APPARATUS

The flow chart of the reduction setup is shown in Figure 1. It consists of hydrogen and nitrogen supplies with their purification systems; as stainless-steel reactor; a feed gas humidifying unit for water-vapour addition and adjustment; a condensation and absorption system for steam in the reactor off-gas; as well as the necessary accessories for measurements and control.

The pre-regulated feed gas is first freed from any traces of moisture, oxygen or hydro-

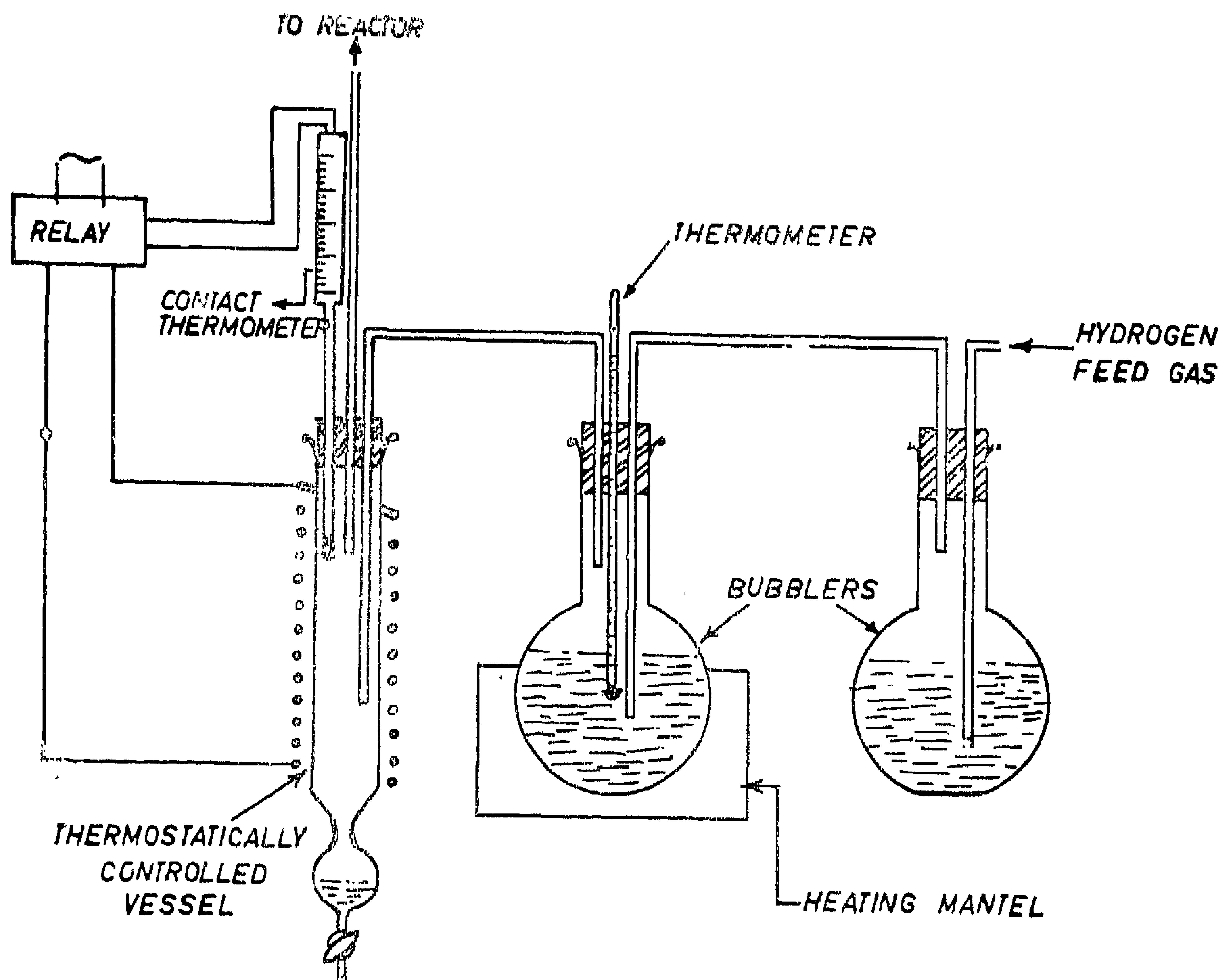


FIG. - 2 - GAS HUMIDIFICATION SYSTEM

PREVIOUS WORK

The fluidised-solids technique, being seemingly well adaptable to iron-ore reduction, has received much attention in this respect. Numerous experimental investigations have been reported, many patents issued, and several processes are under development.

Ezz (1) studied the effect of different factors mostly at 700°C and concluded that the most important factor was the rate of hydrogen supply. Similar findings are reported by Bhat and Whitehead (2). Feiumann and Drexel (3), in their investigation of the kinetics of reduction of ferrous oxide with hydrogen, found that decreasing the gas flow rate and ore-to-gas ratio favoured reduction. Differences in performance of reduction of hematite with hydrogen in fixed and fluidised beds were found to be primarily attributed to the solid movement characteristics of the system and the bubbling phenomenon occuring in fluidised systems (4).

Most of the local investigations in A.R.E. were performed in conjunction with an Egyptian project, "The Electrogen Furnace" proposed by Ezz (5). El-Tobgy (6) investigated the effect of different factors mainly on the reduction of a porous Aswan ore in the fluidised state. Aly (7) studied the different factors affecting the sintering of fine local ores in the fluidised state. Fakhory (8) studied among other factors the effect of oxygen injection during reduction of an Aswan ore in the fluidised state. He found that the rate of reduction increased with temperature and hydrogen flow rate, but was retarded by the addition of steam or oxygen.

Several patents have been issued proposing fluid-bed reduction processes (for example 5, 9-11). Few processes, however, have been developed to the pilot or semi-commercial scale.

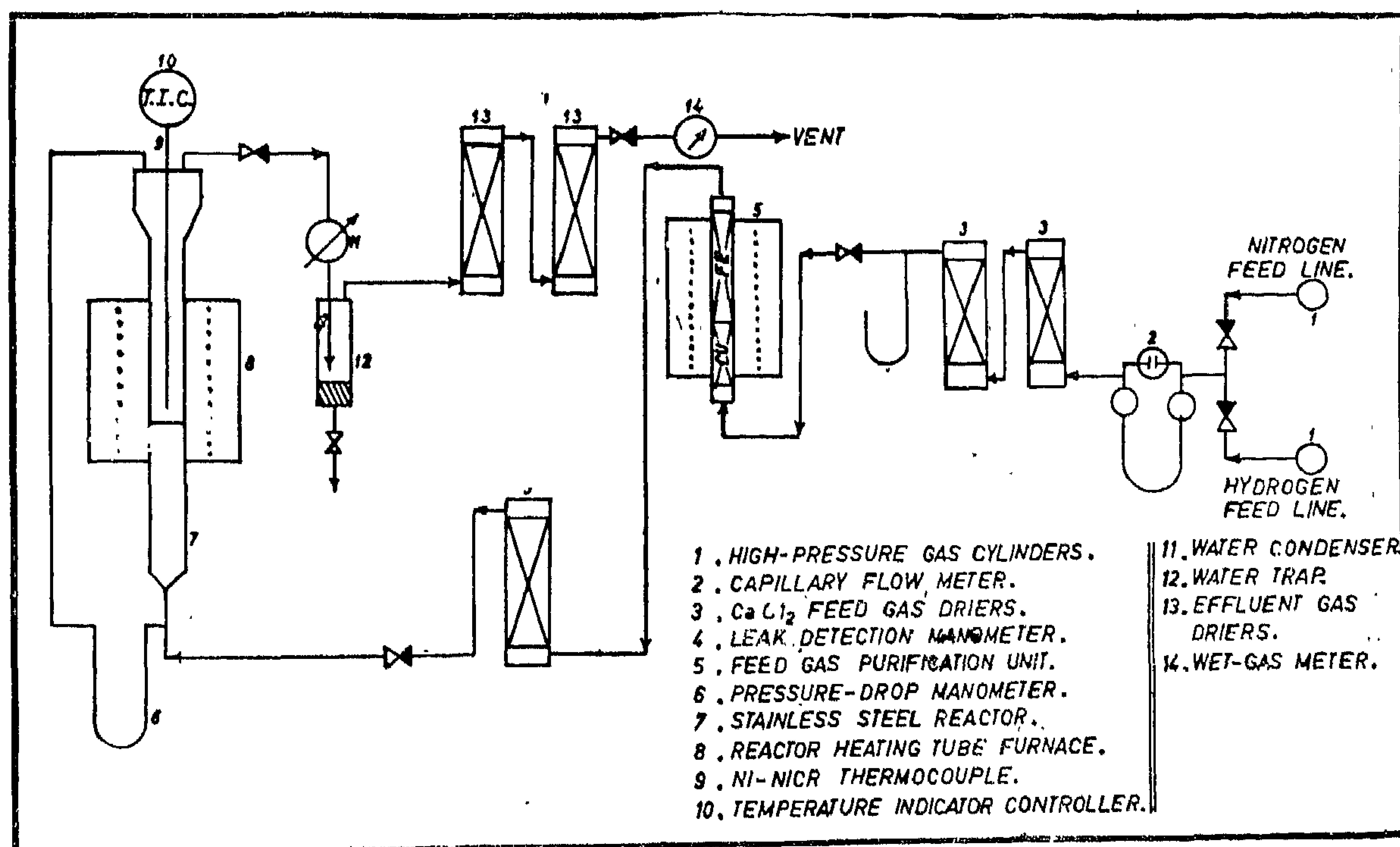


FIG. -1- SCHEMATIC FLOW DIAGRAM OF THE REDUCTION ASSEMBLY.

DIRECT REDUCTION OF ELBAHARYIA IRON ORES IN THE FLUIDISED STATE WITH HYDROGEN

By

M.M. EL-HALWAGI, M.Sc. Ph.D.,
A.M. ABDEL DAYEM, Ph.D.,
and S. EL-AFIFI, M.Sc.
Pilot Plant Laboratory, National Research Center.

SYNOPSIS

Reduction of El-Baharyia iron ores with hydrogen was conducted in a 5-cm. fluidised bed. High-grade ore sampels taken from El-Gedeeda locality were employed, and the pertinent factors affecting the reduction process in the fluidised state were studied.

Results indicated that the most significant variables are : the gas velocity, temperature and feed-gas composition. The general trends manifested by the results of fluid-bed reduction are generally in qualitative agreement with those previously obtained in fixed beds under similar conditions. However, the rate of reduction in the fluidised state is lower than that in the fixed state up to about 80% reduction; but the rate becomes higher at higher conversions. These differences are interpreted basically in terms of gas bacKmixing and solids circulation.

INTRODUCTION

Blast furnaces are widely used for the reduction of iron ores. However, because of some drawbacks associated with their operation, such as their high capital investment and the necessity for high-grade coke, efforts have been made to develop other reduction processes. A number of processes for direct reduction of iron ores by means of reducing gases have been well established.

In the A.R.E. there is a lack for high-grade coking coal; and the main supply of such coke depends chiefly on import. Thus, to establish an independent iron-and-teel industry, the problem of coke shortage has to be solved. One solution is to use gaseous reducing agents as a substitute. This is particularly advantageous in the A.R.E. because of the availability of a large amount of natural and refinery gases that can be used after suitable processing.

The use of the fluidised-bed technique seems to be ideal for the reduction of iron ores with reducing gases. It offers many favourable characteristics. Principal among these are : close temperature control, high heat-transfer rates and continuity of operation. Furthermore, they are able to treat fine ores, which cannot otherwise be used directly in the blast furnace.

The present work is a part of an integrated program aimed at investigating the basic factors influencing the reduction of iron ores with hydrogen. Samples from El-Baharyia ores, one of the main ore sources in the A.R.E., were chosen for this purpose because of their relative abundance and hence future potential use. In this plan the study was divided into three main parts. The first was concerned with the physical fluidisation characteristics of the ore; the second with the kinetics of reduction in fixed beds, and the last with the reduction of the ore in a fluidised-bed reactor.

7) Jenike, A.W., *"Better Design For Bulk Handling"*, Chem. Eng., December 1954, Vol. 61, pp. 175.

8) Jenike, A.W., *"Gravity Flow of Bulk Solids,* Bull 108, University of Utah, Eng. Exp. Station, Vol. 52 No. 29, Salt Lake Vity October 1961.

9) Pariseau, W.G., *"The Gravity Induced Movement of Maerials in Ore Passes Analysed as a problem in Coulomb Plasticity"*, A Thesis Submitted to the graduate faculty of the University of Minnessota, March, 1966.

10) Demin W.E. and Mehring A.L., *"The Gravitational Flow of Fertilizers* and *Other Comminuted Solids,"* Industrial Eng. Chem. 1929, 21 pp. 661.

11) Rudd, *"How Does Material Flow From Bins"* Food Eng., Vol. 26, No. 2, 1954.

12) Franklin and Johanson, *"Flow of Granular Material Through a Circular Orifies"* Chem. Eng. Science, 1955, V. 4, pp. 119.

13) Tatsua Tanaka, *"What Do You Know About Bin Design"*, Rock Product, Feb. 1961.

14) Runo, W.R., *"How Orifice Shape Affects Material Flow"* Modern Material Handling, Feb. 1956, 90.

15) Ketchum, M.S. *"Walls, Bins and Grain Elevators," McGraw* Hill, New York, 1919.

16) Moore, R.L., *"Pressure in Shallow Rectangular Bins"*, ASCE TR. Vol. 117, 1952. pp. 370.

17) Toitz, M., *"Discussion on Grain Pressure In DEEP Bins,"* Can. Soc. C.E. TR. Vol. 17, 1903, pp. 641.

18) Dale, Robinson, *"Pressure in Deep Grain Storage Structures,"* Agriculture Eng. August 1954, Vol. 35, pp. 570.

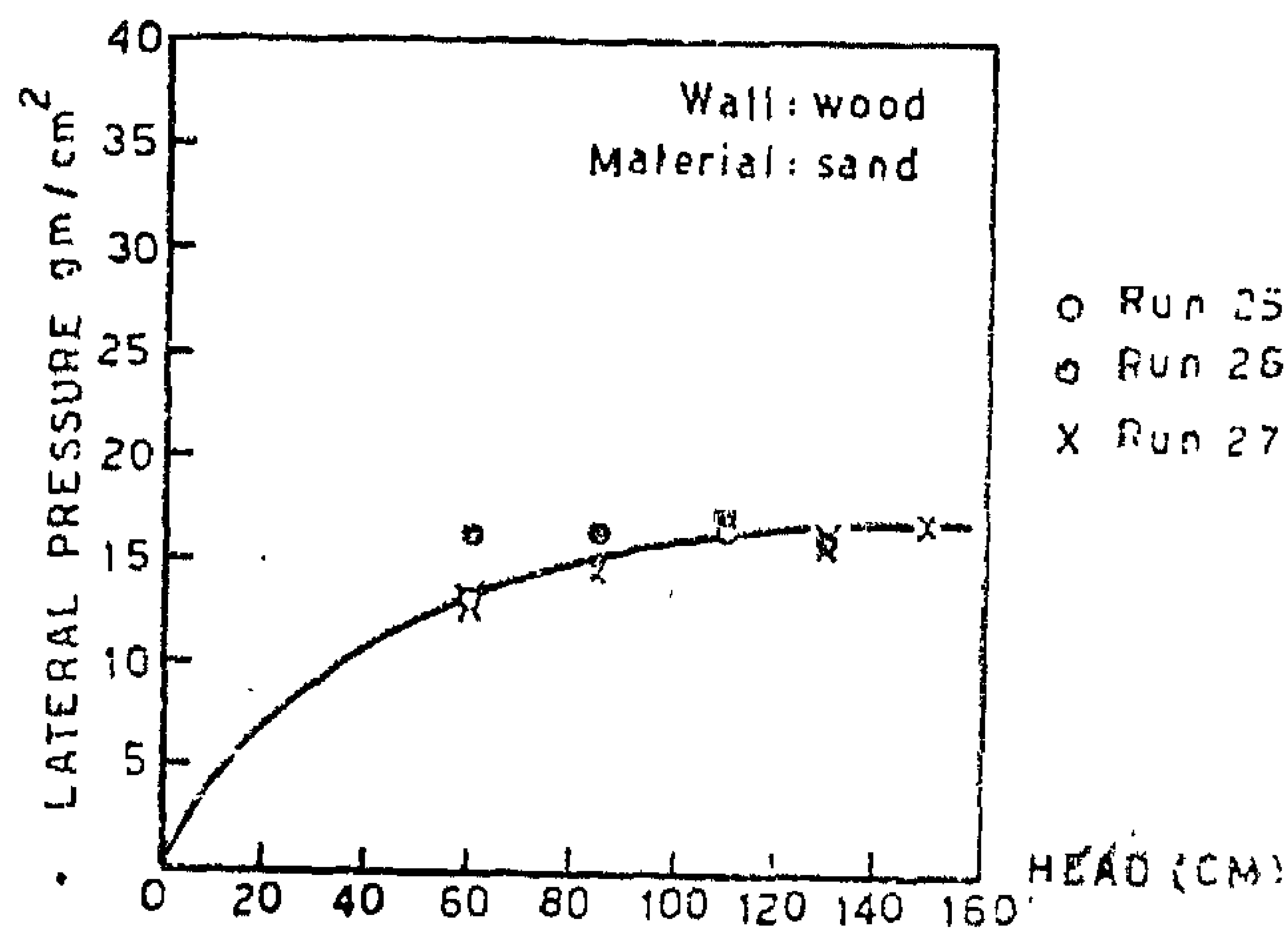
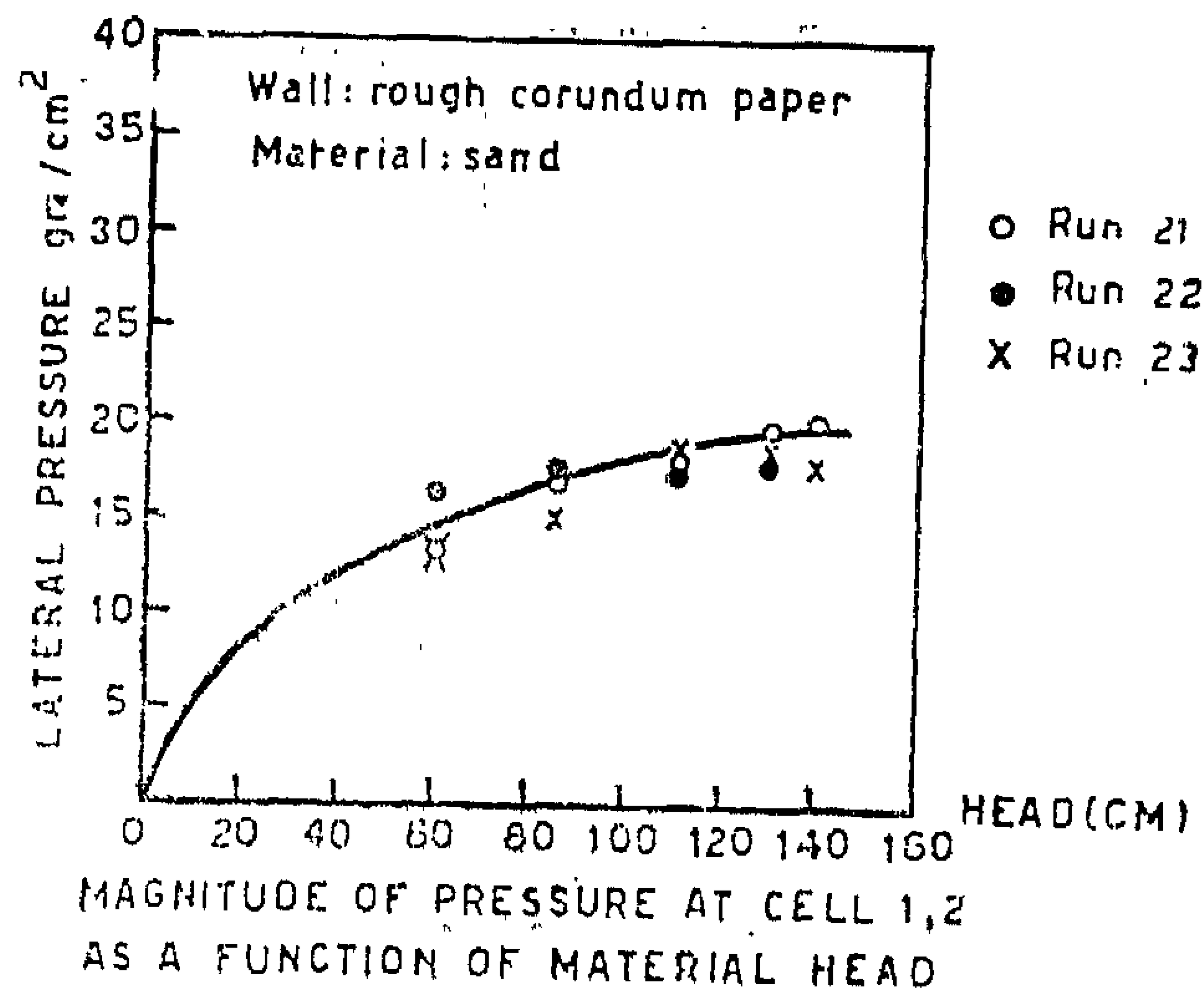


FIG 19



MAGNITUDE OF PRESSURE AT CELL 1,2 AS A FUNCTION OF MATERIAL HEAD

FIG 20

NOTATIONS

All equations in this paper may be used with any consistent set of units:

Φ	= The angle of repose of the material.
Φ'	= The angle of friction on the bin walls.
u	= tan Φ = coefficient of friction of material on material.
u'	= tan Φ' = coefficient of friction of material on bin walls.
w	= unit weight of material.
V	= unit vertical pressure of grains at depth y.
L	= unit lateral pressure of grains at depth y.
$P_{max.}$	= maximum basic lateral static unit pressure.
h	= height of container.
y	= depth, below top of fill, at point for which the pressure are being caculated.
c	= characterstic abscissa, constant which depends on shape of bin and properties of stored materials.
c_d	= correction factor for dynamic effect.
K	= L/V
R	= hydraulic radius.

REFERENCES

1) Janssen, H.A., *"Versuche Uber Getreided in Silozellen"*, VDI Zeitschrift (Dusselorf), V. 49, Aug. 31, 1885, pp. 1045.

2) Airy, W., *"The pressure of grain"*. Minutes of proceedings, Institute of civil Engineers, London, V. 131, 1897, pp. 347.

3) Reimbert, Marcel, and Reimbert, Andrie, *Silos-Traite Theorique et Prtique* Editions Eyrolles, Paris, 1961, pp. 255.

4) Saragis S. Safarian, *"Design Pressure of Granular Materials in Silos"* ACI Journal, No. 8, Proceedings, V. 66. August 1969, pp. 647.

5) Chesman, A. Lee, *"New Ideas About Bins,"* Chem. Eng., April 1952, pp. 153.

6) Chesman, A. Lee, *Hoppers By Calculations*, Chem. Eng., December 1954, pp. 181.

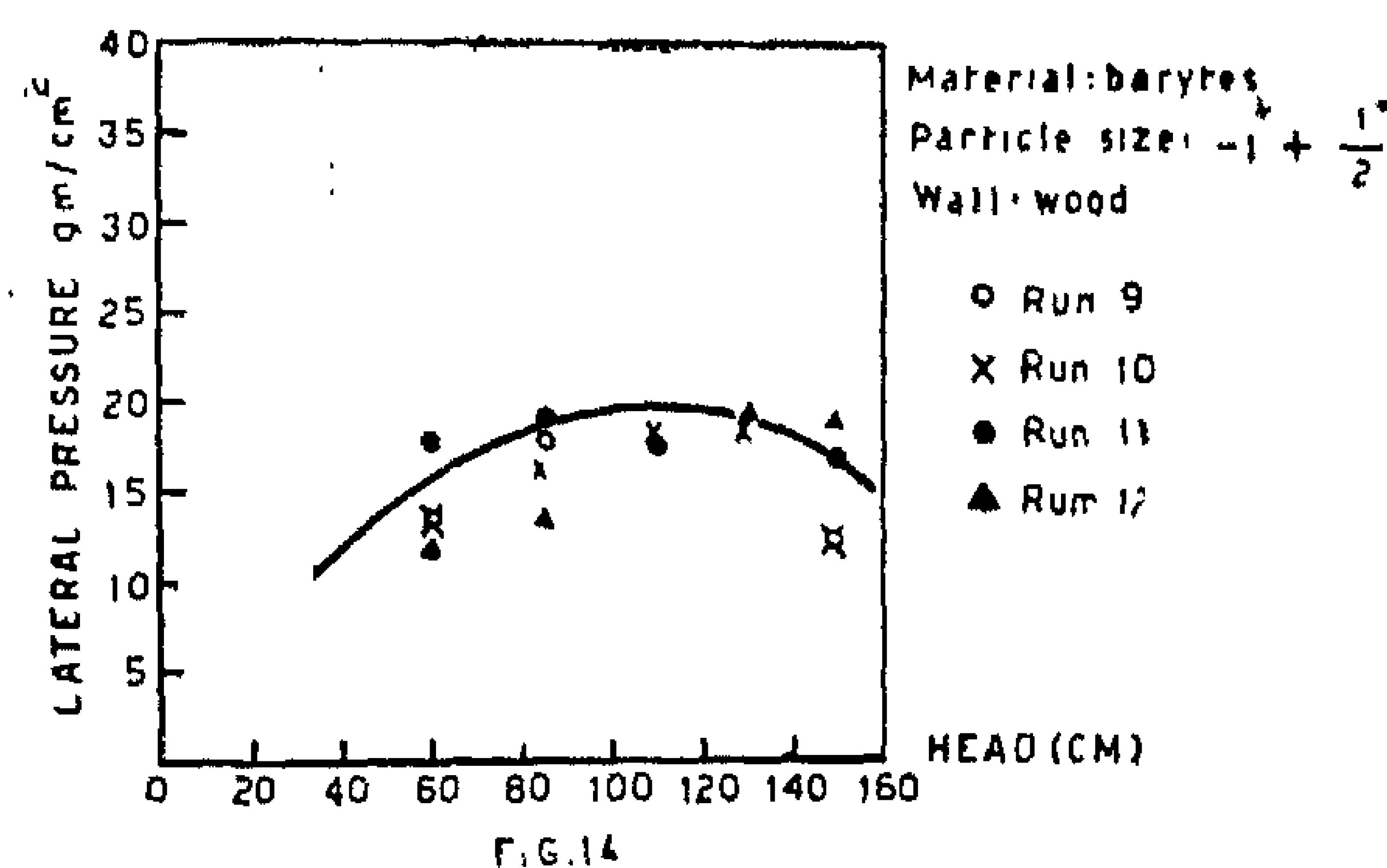
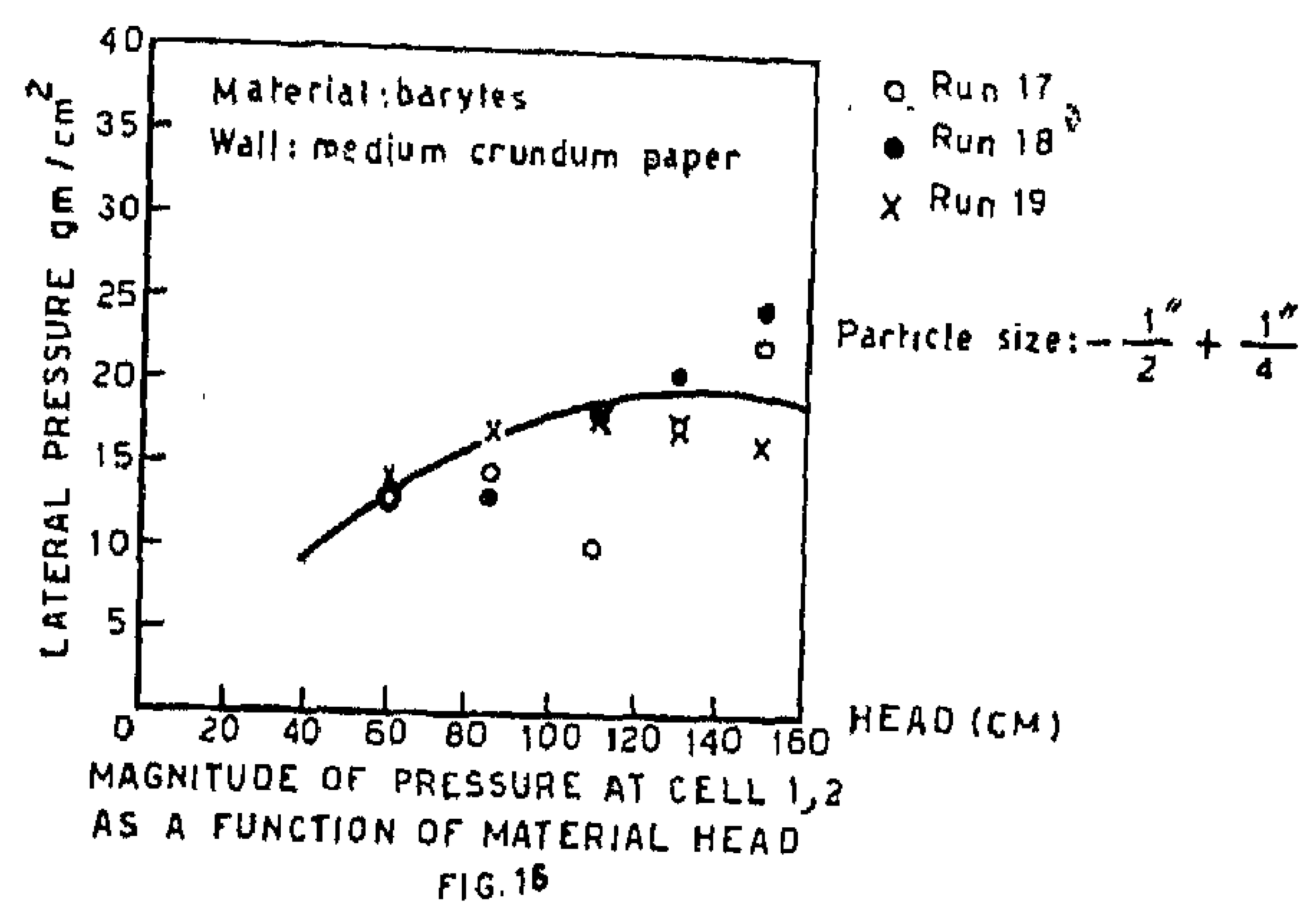


FIG.14



MAGNITUDE OF PRESSURE AT CELL 1,2 AS A FUNCTION OF MATERIAL HEAD
FIG.16

3) *Effect of wall roughness :*

Fig. (15) represents the results of a series of tests carried out on barytes of particle size (— 1/2″ + 1/4″) and the walls of the channel varied. For the same particle size, it is observed that the rougher the wall, the smaller the pressure is. The difference in roughness between the two limiting cases, i.e. wood and the roughest corundum paper, gives differences in pressure of about 8%, this is due to the fact that arching of the flowing materials finds a favourable condition when the roughness of the container walls is great. Figs. (16, 17) illustrates a non-linear behaviour of lateral pressure with respect to the material head.

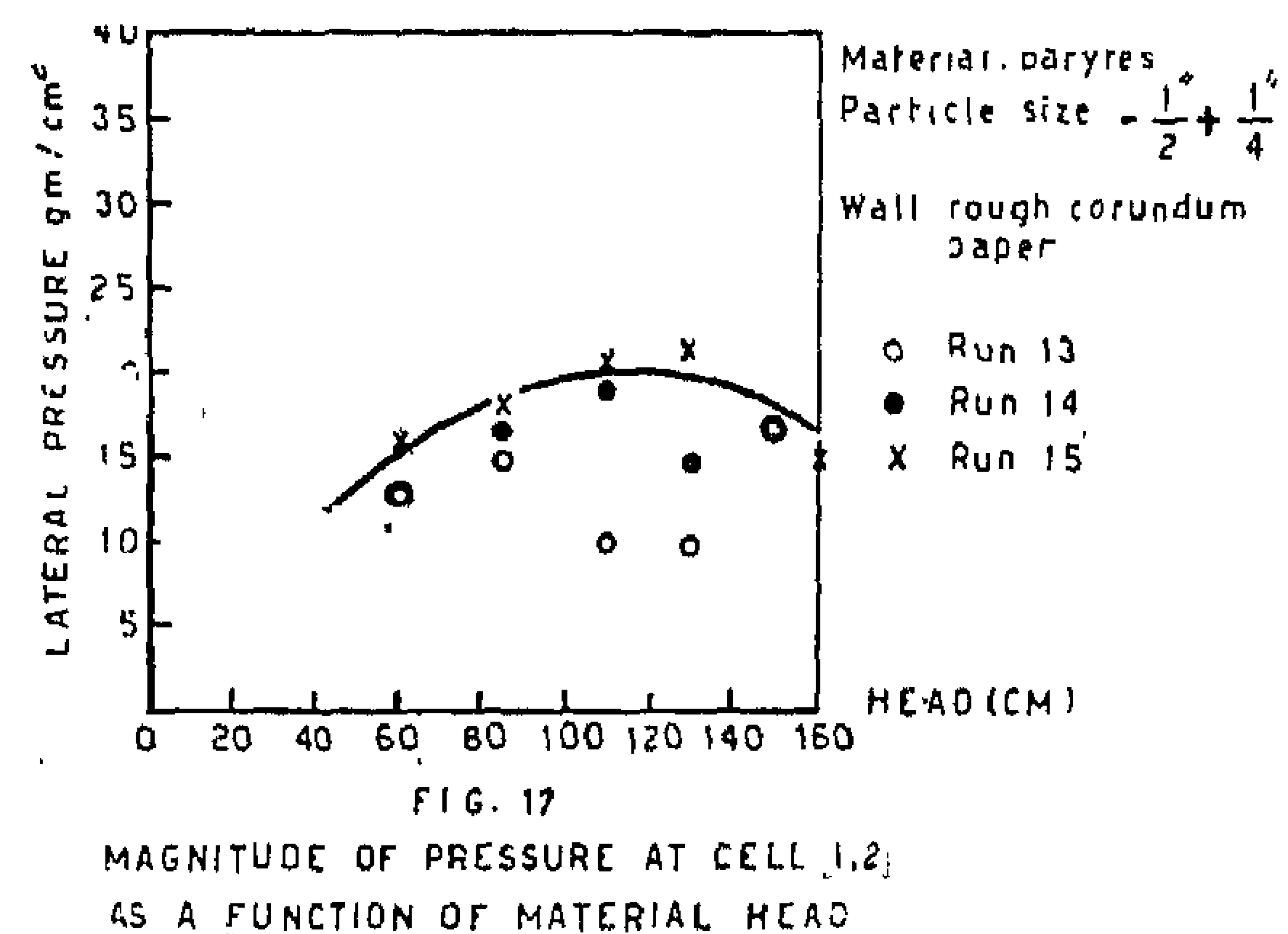
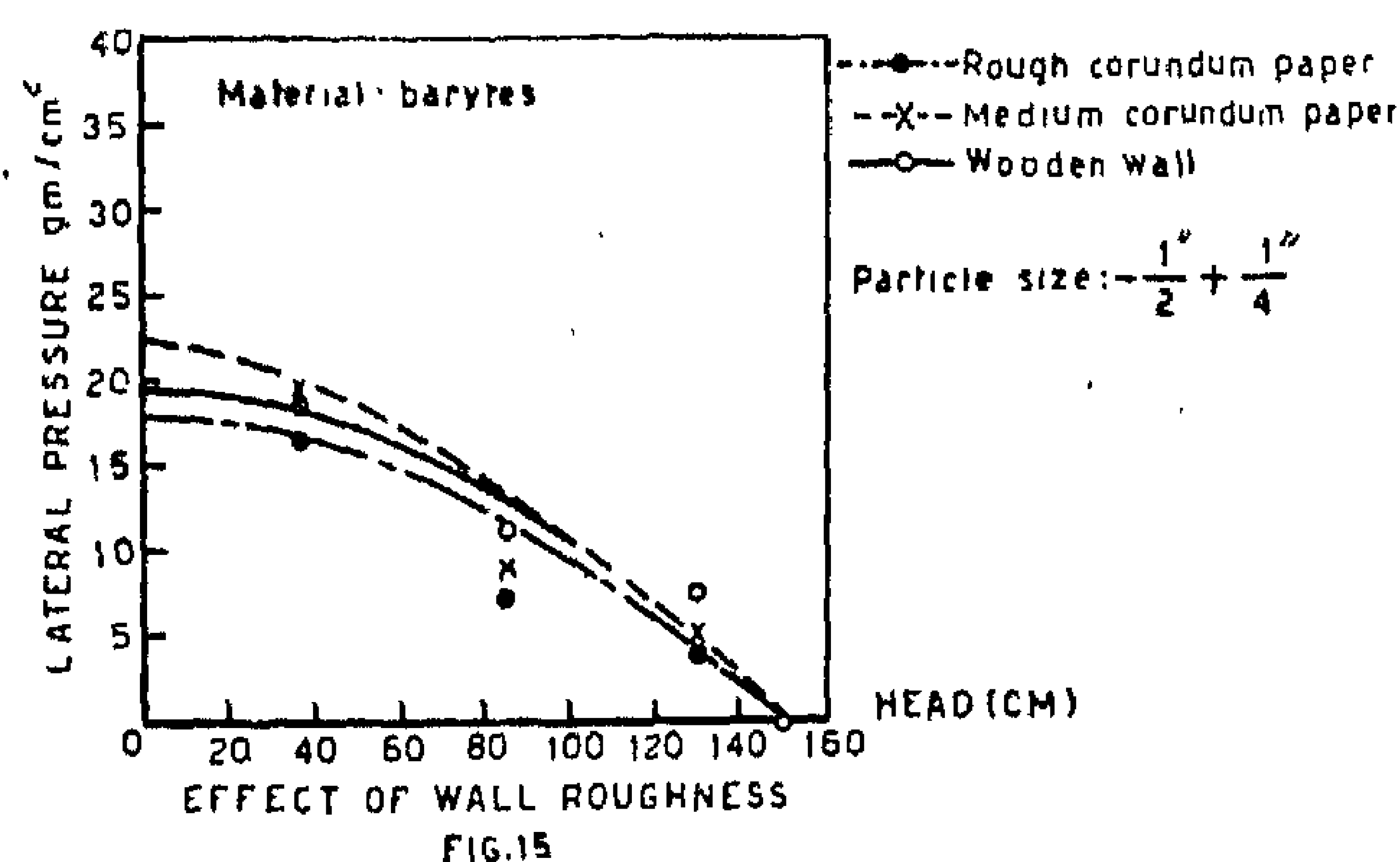
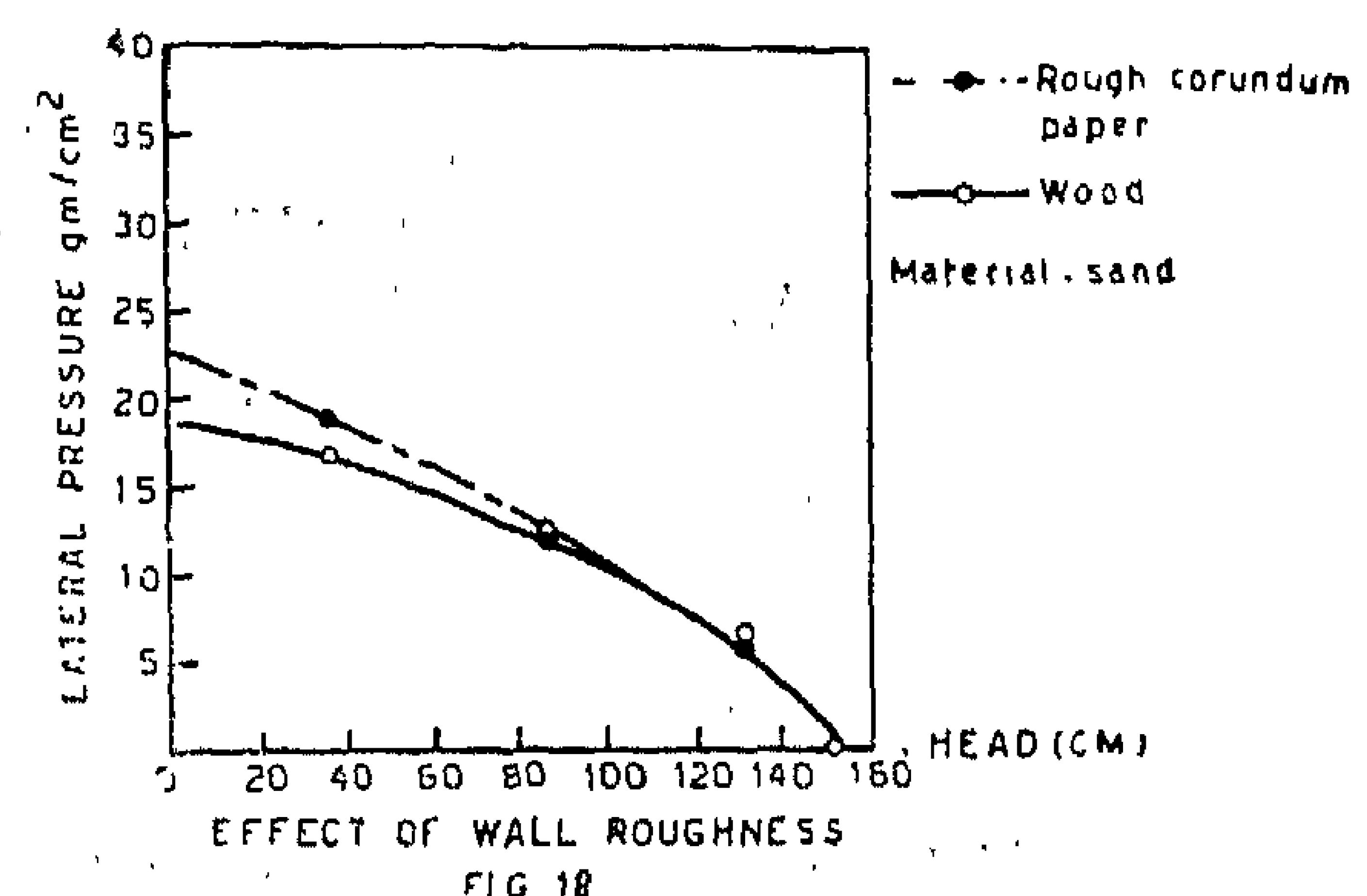


FIG. 17
MAGNITUDE OF PRESSURE AT CELL 1,2 AS A FUNCTION OF MATERIAL HEAD

The same series of tests has been repeated using sand as a flowing material and the measured results are shown in Figs. (18, 19 and 20). Still the rough corundum papers give lower pressures on the sides of the walls specially at higher heads.



EFFECT OF WALL ROUGHNESS
FIG.15



EFFECT OF WALL ROUGHNESS
FIG 18

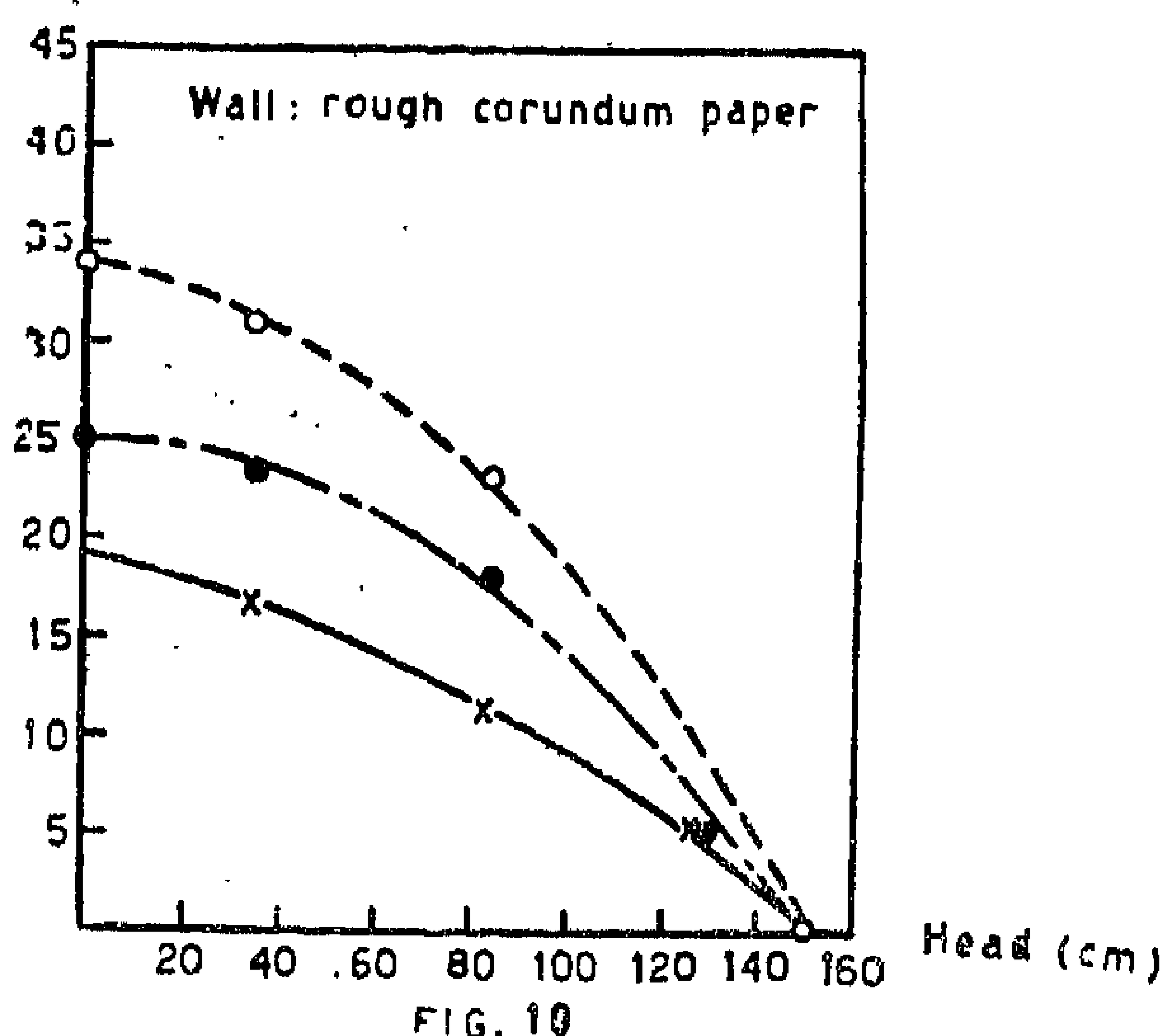


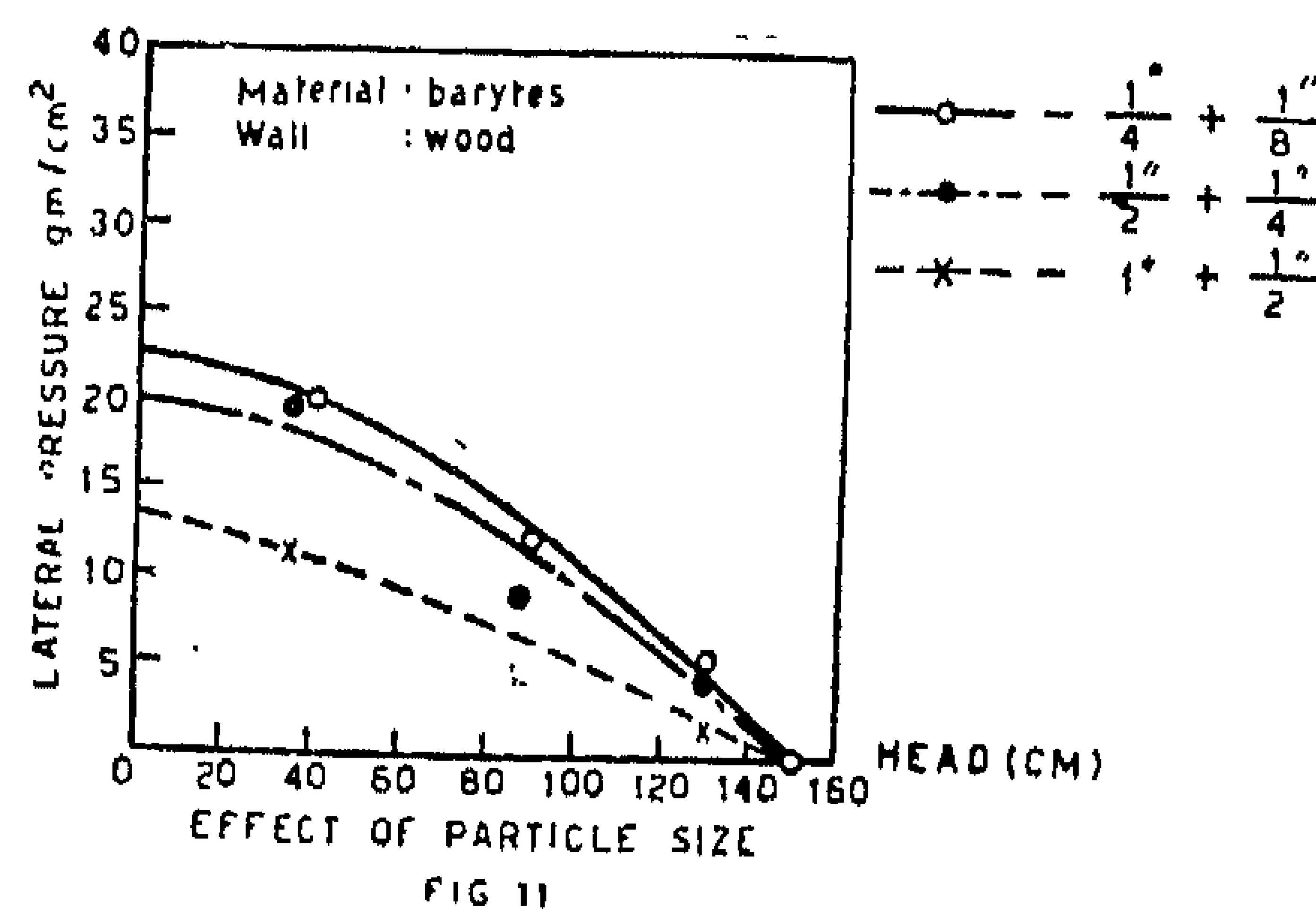
FIG. 10

From the writer's view, higher values of pressure computed from such equations may be due to the fact that these equations neglect the properties of flowing materials and other variables which contribute to the pressure magnitude and distribution. More over, the similarity to retaining wall conditions assumed by these equations does not hold true in case of bins and bin-like containers, since the bulk material will be limited in volume and the static conditions were not maitained.

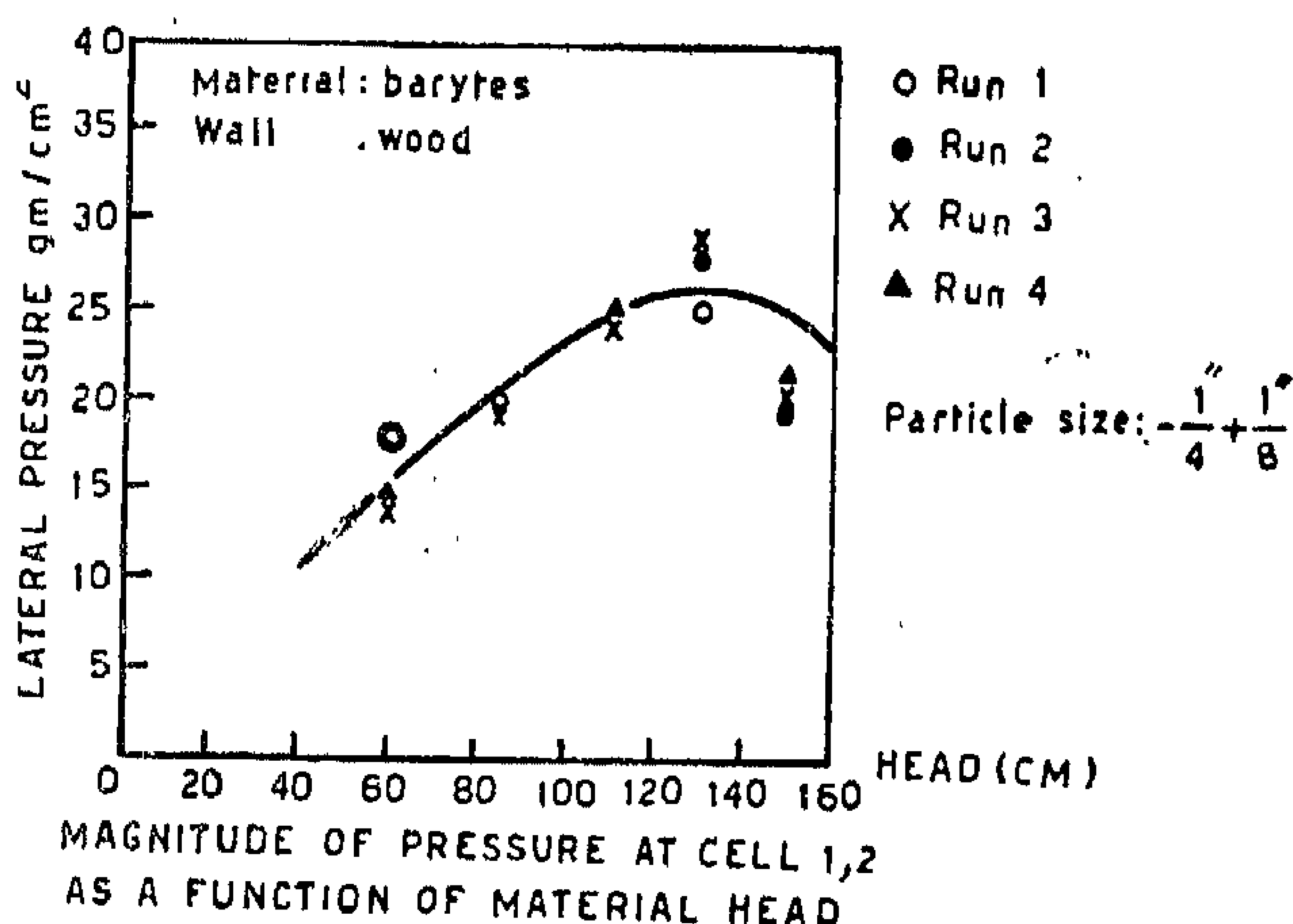
2) Effect of particle size :

Fig. (11) illustrates clearly the effect of particle size on the magnitude of lateral pressure. The magnitude and distribution of pressure on the sides of the channel used were inevrsely proportional to particle size of the bulk material. The magnitude of variation for the same material ranges from 30 to 40%. This result may be due to the fact that the bulk density for small sizes is greater than that of large sizes; moreover, the possibility of formation of microdomes by mechanical interlocking will be greater for large particle sizes. Writers believe that such mechanism will increase the supporting forces inside the bulk, and consequently will lead to the decrease of pressure on the bin sides. Figs. (12, 13, and 14) show the variation of pressure as a function of material head which is not linear, and the pressure on bin sides reaches a maximum value at a certain head then decreases as the head increases.

Such phenomena may be due to the strength built up in the material under the action of the compacting pressure of the superimposed material, leading to arching. Once such strength reaches an effective value the magnitude of pressures on bin sides is decreased.



EFFECT OF PARTICLE SIZE
FIG 11



MAGNITUDE OF PRESSURE AT CELL 1,2
AS A FUNCTION OF MATERIAL HEAD
FIG 12

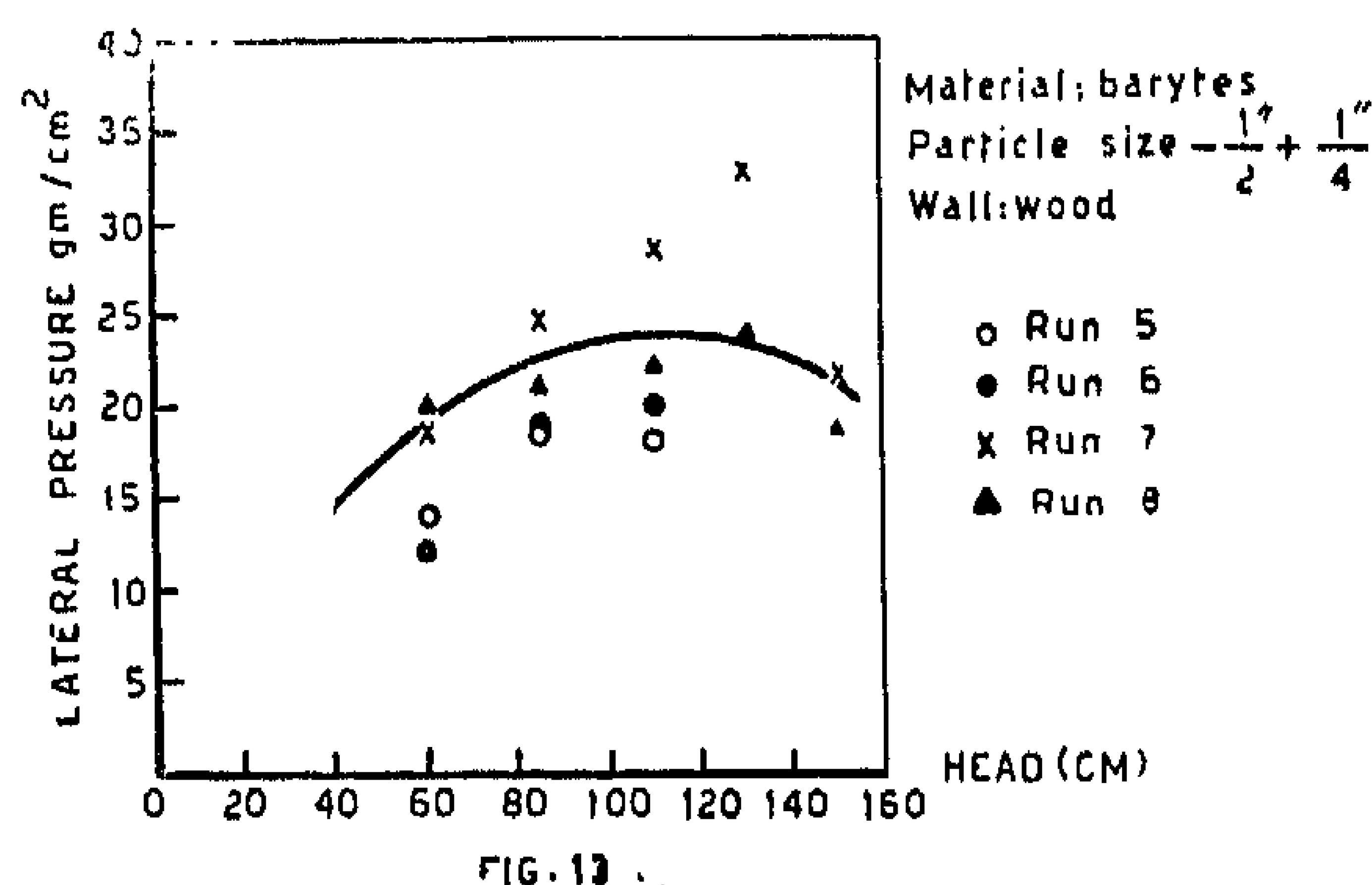


FIG. 13

Variables :

Variables considered during the course of experimentation are :

a) Particle size, shape and bulk density.

b) Coefficient of internal friction between particles. This is achieved by using different sizes, and accordingly the shear properties were varied.

c) Coefficient of friction between materials and walls, and this has been achieved by using corundum paper of different grades of roughness (low, medium, and high) pasted on channel walls.

V) RESULTS AND DISCUSSION

1 — Checking Janssen's and Airy's equations:

Fig. (7) represents the results of a series of tests carried out on baryes of particle size (— 1/2″ + 1/4″) and the channel wall conditions were smooth (wood). Results shown in fig. (7) indicate that the computed values by Janssen's equation give higher values (75%), and those computed from Airy's is almost (100%) higher than the experimentally measured values.

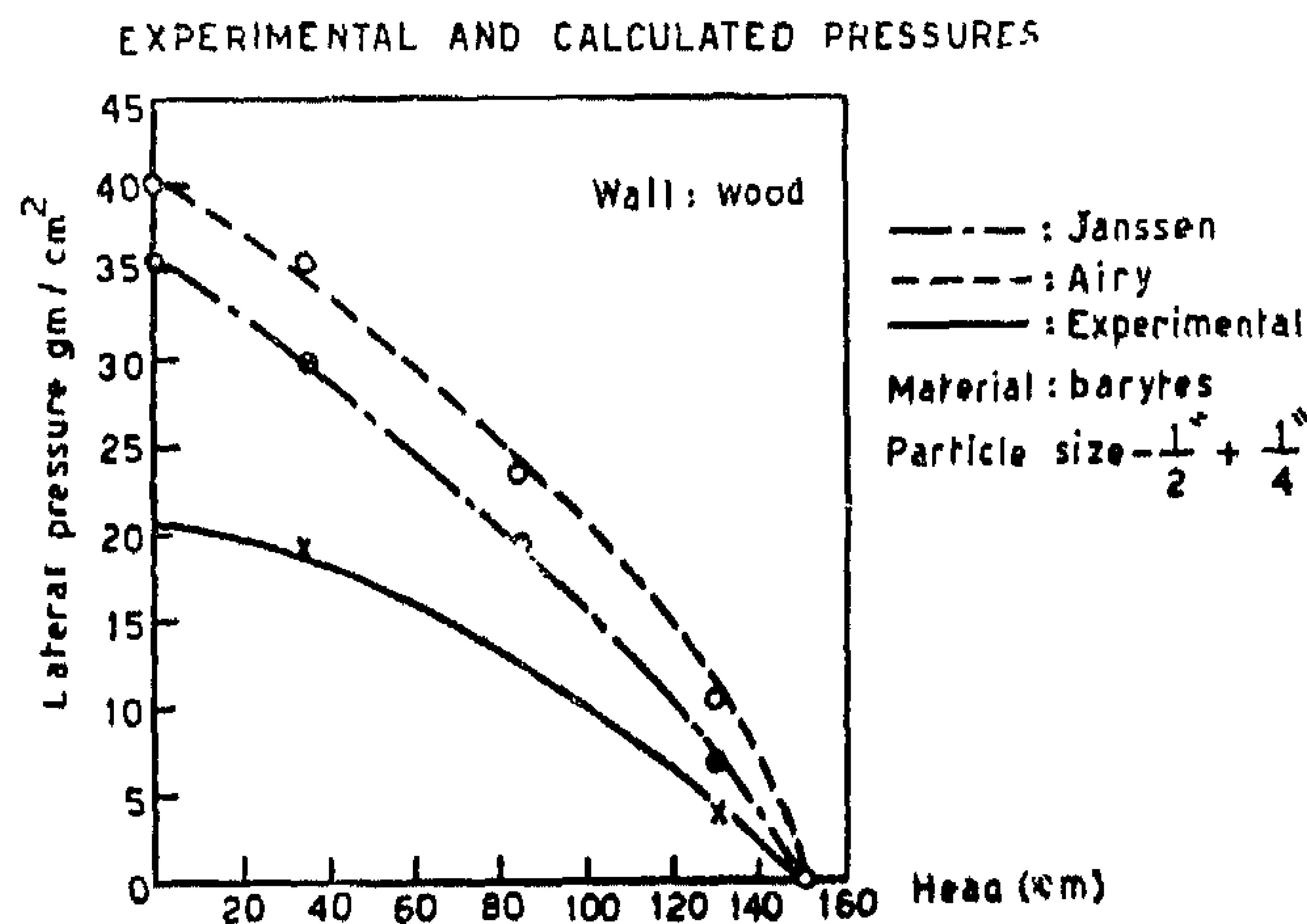


FIG. 7

When changing the wall conditions by using corundum paper the magnitudes, but not the distribution of lateral pressure, were influenced as shown in Fig. (8).

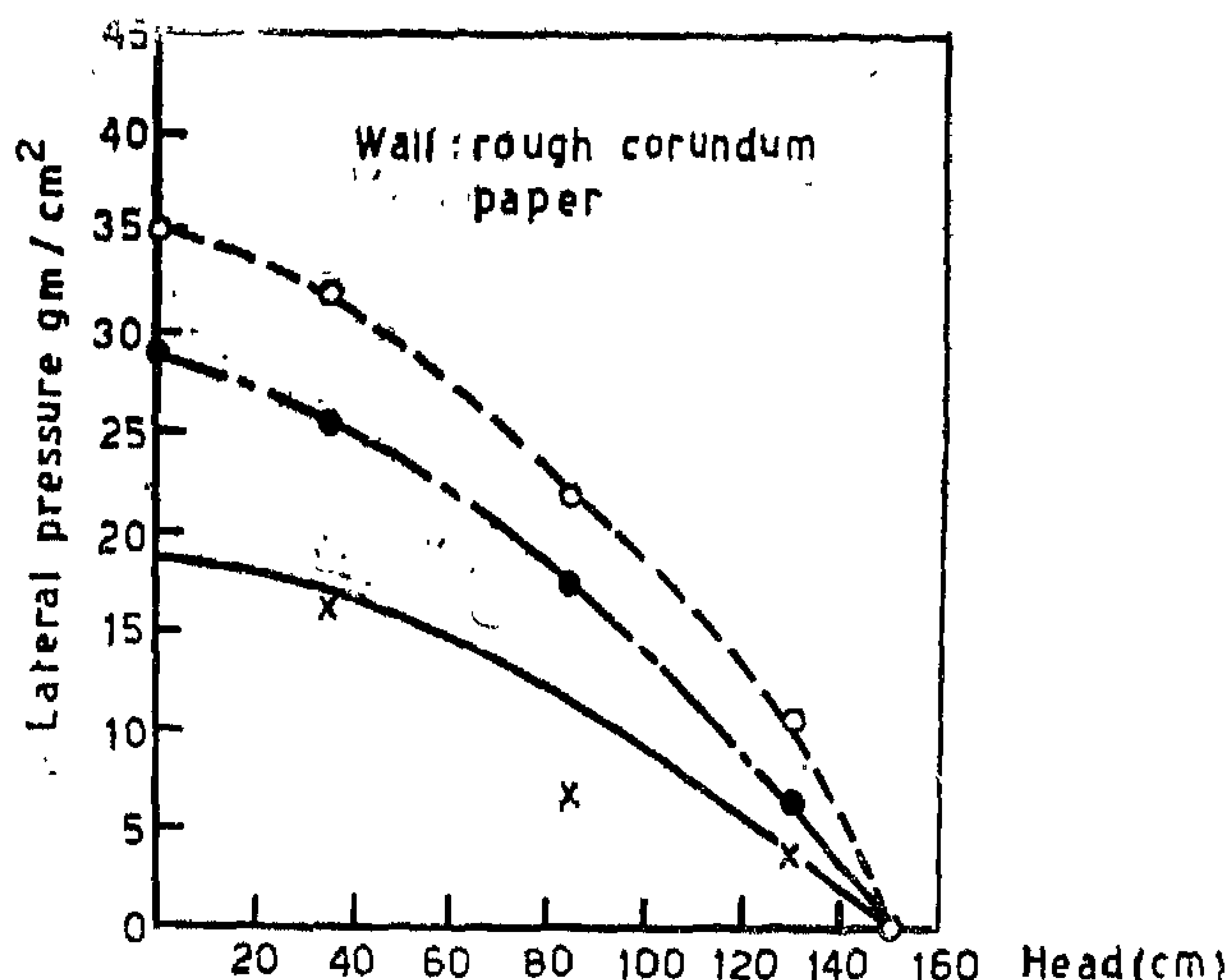


FIG.8

Repeating the above tests using sand as bulk material, the obtained results were shown in Figs. (9,10).

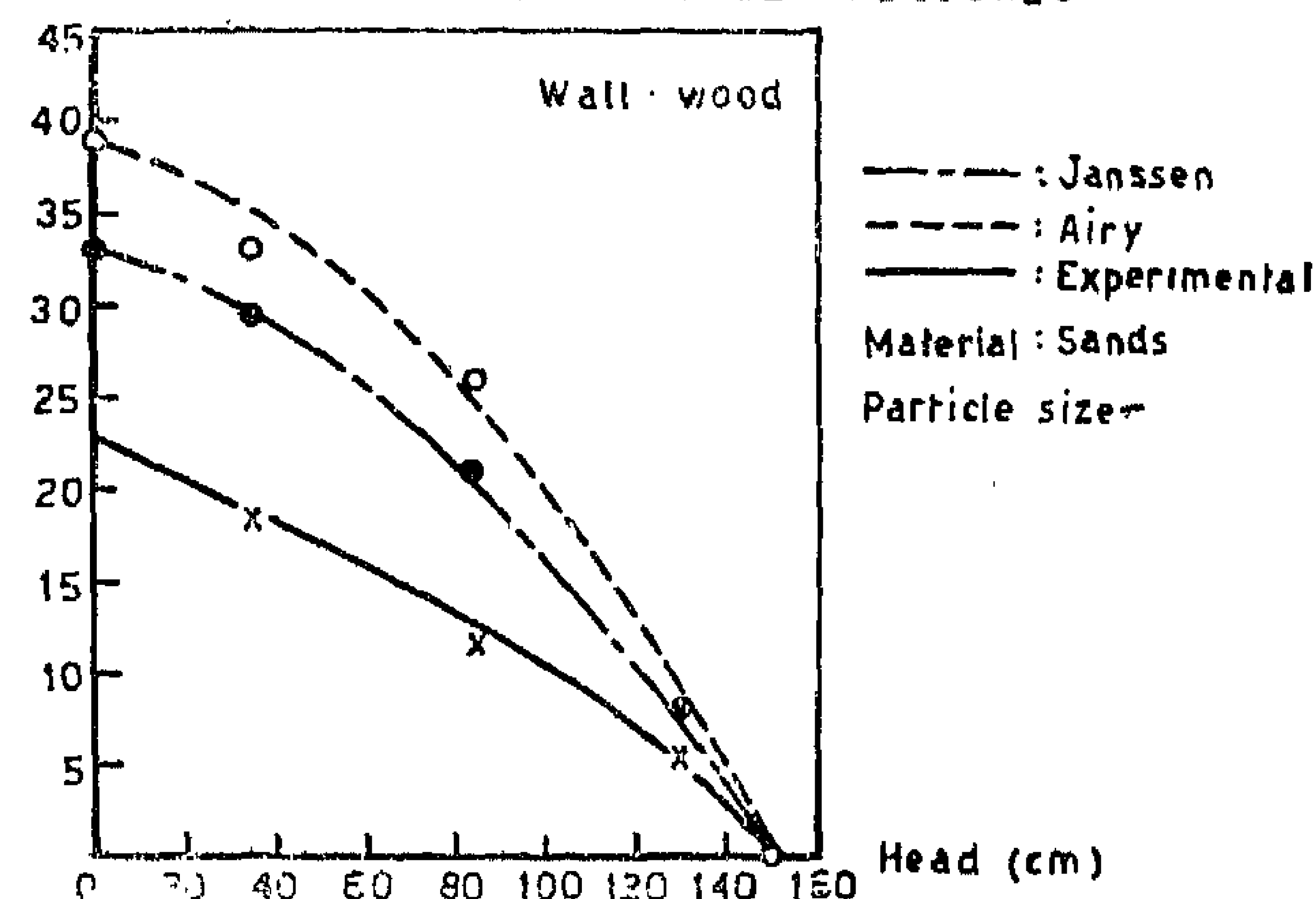
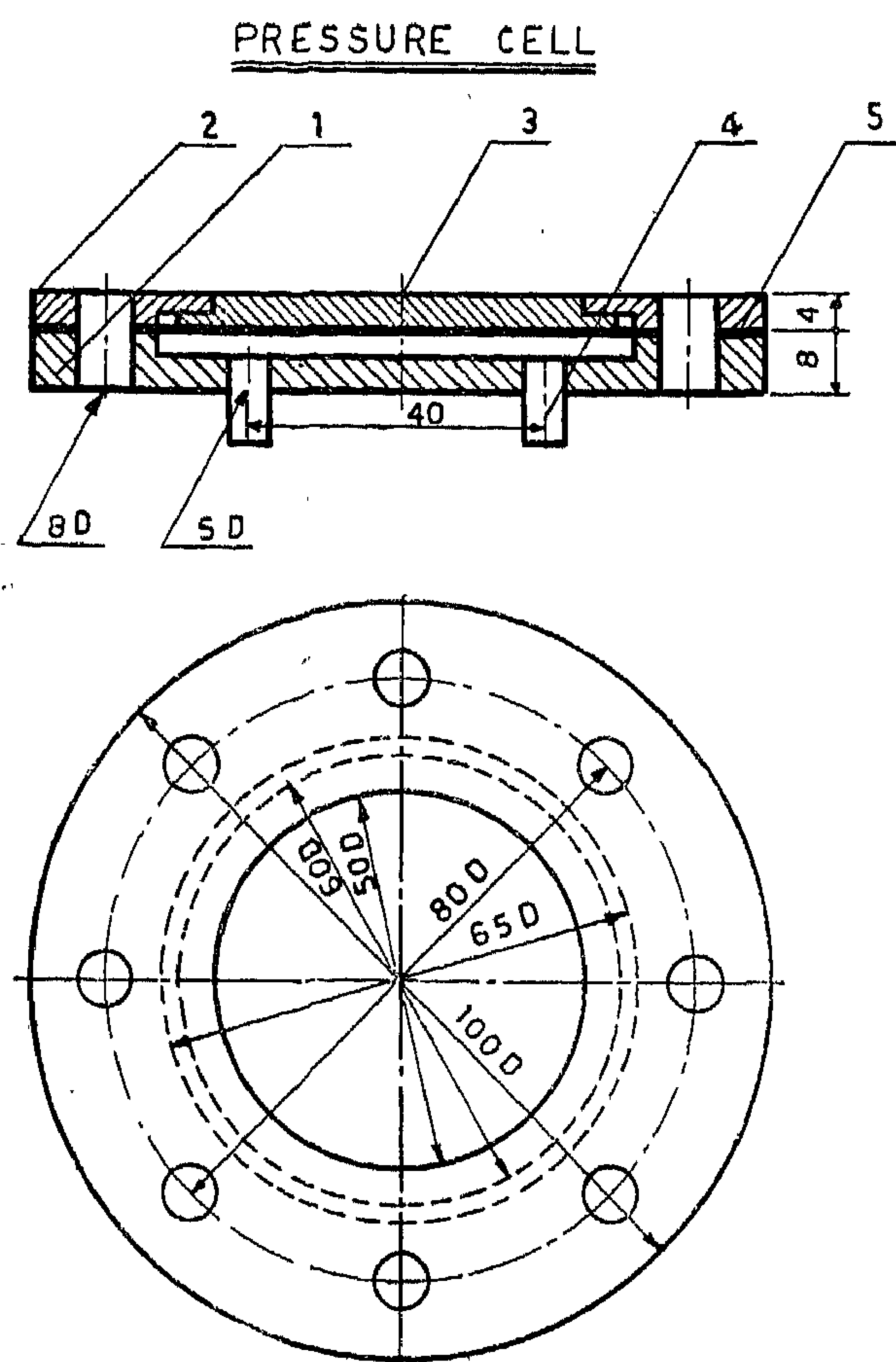


FIG 9

From the above tests it is found that the calculated pressures from theoretical equations have the tendency to be higher than the experimental, values.



1. BRASS CASE
2. COVER
3 PISTON
4. MOUTH PIECE
5 RUBBER MEMBRANE

Dim in mms
Scale 1/1

FIG. 5

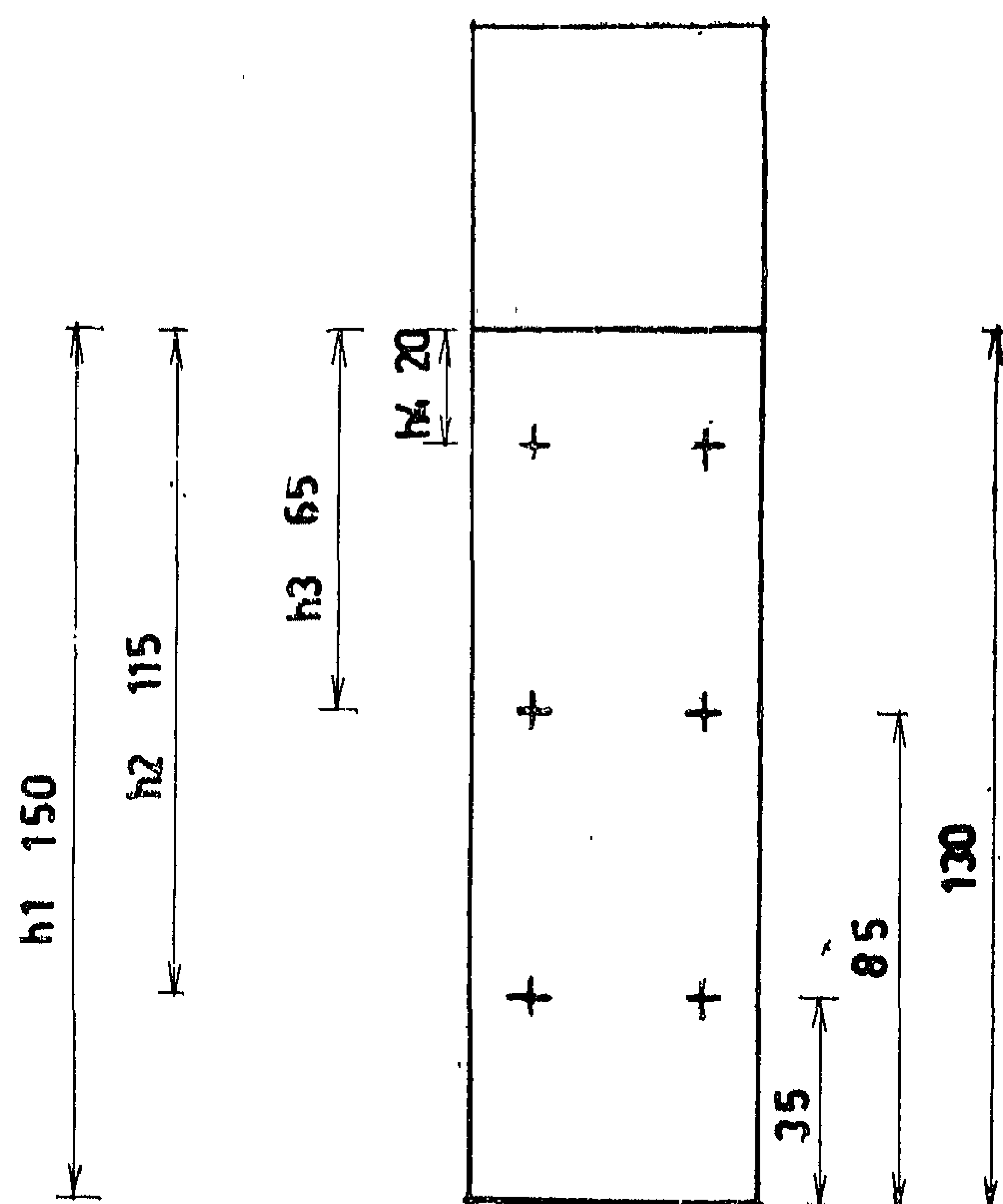


Fig 6

Materials :

Materials of different physical properties were used. Tables (I), (II) and (III) summerize their properties.

TABLE (I)
Bulk Density for Barytes

Size	Bulk Density
— 1/4″ + 1/8″	2.45 gm/cm³
— 1/2″ + 1/4″	2.35
— 1″ + 1/2″	2.23

TABLE (II)
Size distribution for sand
Weight of Specimen = 150 gm

Mesh	Weight retained	%
+ 10	7.3	4.7
— 10 + 20	17.3	11.5
— 20 + 30	30.2	20.2
— 30 + 40	27.5	18.4
— 40 + 60	56.0	37.5
— 60 + 100	9.9	6.6
— 100 + 150	0.1	0.6
— 150 + 200	0.1	0.6

TABLE (III)
Physical Properties of Materials

Properties	Barytes	Sands
Particle size	— 1/4″ + 1/8″	— 3/16″
B. Density lb/ft³	150	92
Φ	48°	32°
Φ' wood	28°	25°
Φ'' C. paper	39°	35°

where :

$P_{max.}$: is dependent on the shape of the bin and is a function of w,d, and u′

c : an expression that depends on the shape of bin and is a function of d,u, and Φ

III) FACTORS INFLUENCING PRESSURE VALUES AND DISTRIBUTION

It may be of some interest to review all factors that are considered to influence quantitatively or qualitatively the pressures on bin sides, and their distribution. Effects of some of these factors have been studied and reported by other investigators,(5-18), and some factors still need to be studied. These factors may be classified from writers' view into two categories :

(1) Factors related to container geometry :

a. Height and inclination of the container.
b. Dimensions and shape of the cross-section.
c. Slope of sides.
d. Dimensions and shape of the opening.
e. Degree of wall roughness.
f. Rate of flow.

(2) Factors related to material characterstics:

a. Particle size and shape.
b. Bulk density of material.
c. Density of loose and fully compacted material, with various moisture contents.
d. Adhesion and cohesion.
e. Material shear strength.
f. Static and dynamic angle of repose.
g. Coefficient of friction between particles.
h. Grain to wall coefficient of friction.

In present work, writers will attempt to evaluate quantitatively the influence of some factors on pressures exerted by bulk materials on sides of bin-like containers.

IV) EXPERIMENTAL INVESTIGATION

In order to investigate the actual pressure distribution on sides and bottom of bin, chutes, ... etc, and check the validity of current design practices, the following experimental program was set up.

Model :

The model used in experimentation is shown in Fig. (4) and consists of :

1 — Wooden channel of dimensions 50 × 50 × 200 Cms., and has an openings of dimensions 20 × 10 cms.

2 — Pressure cell shown in Fig. (5) developed and designed to measure the pressure values on channel sides. Six pressure cells were fixed on the flow channel walls as shown in Fig. (6) and each cell has been attached to two peizometers.

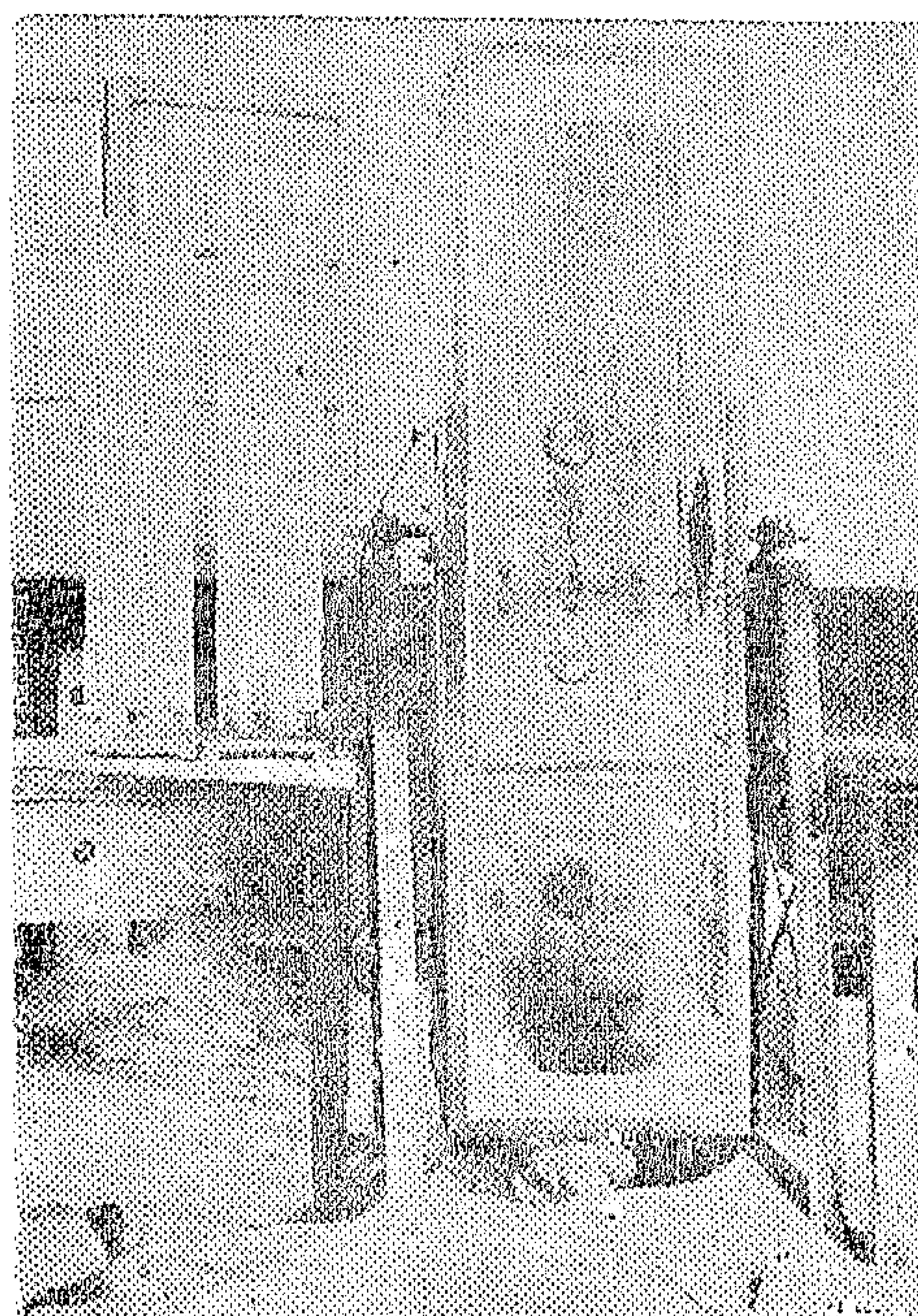


FIG. 4

Thus, according to Janssen analysis, the following expressions for state of pressure on bin sides have been derived :

$$V = \frac{w.R.}{k.u'.} (1 - e^{-ku'y/R})$$

$$L = k.V$$

Where :

V is the vertical unit static pressure at depth "y".

L is the lateral unit static pressure at depth "y".

$$k = \frac{1 - \sin \Phi}{1 + \sin \Phi}$$

R = hydraulic radius = Area/circumference.

2 — Airy's' Approach :

This approach is based essentially on the following assumptions :

1. Similarity between retaining wall conditions and bin loaded by materials.
2. The pressure on the walls of the bin and bin-like containers has been assumed to be due to a wedge of material between the wall and the plane of rupture.

There are two cases depending on the ratio of the width or diameter of the bin to the depth of material.

Case (1) : *shallow bins :*

Defined as the case where the plane of rupture cuts the surface of the material within the bni, Fig. (2). The fundamental formulas which governs the pressure distribution in

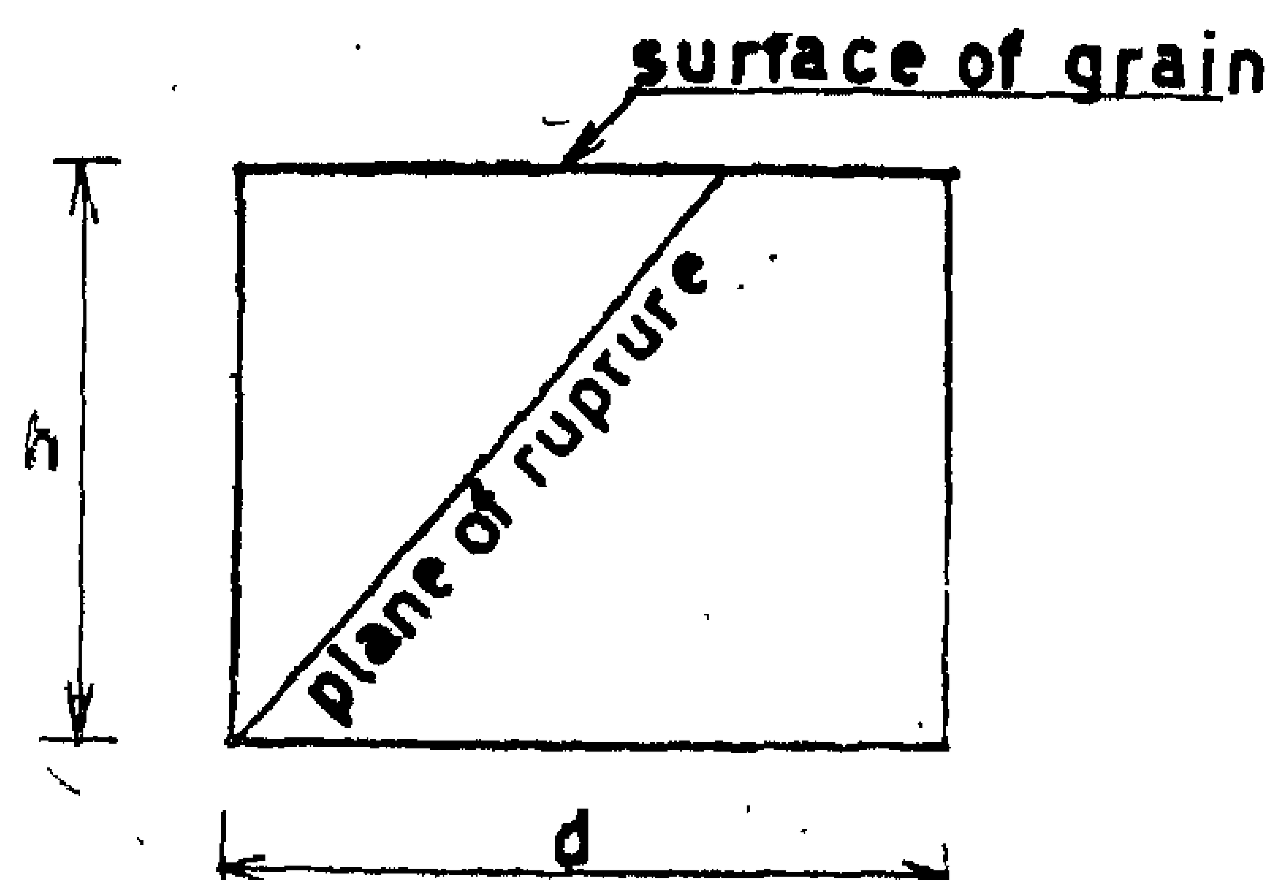


FIG. 2

this case were expressed in the following forms :

$$L = w.y \left[\frac{1}{\sqrt{u\,(u+u')} + \sqrt{1+u^2}} \right]$$

$$V = L/k$$

Case (II) : *Deep bins :*

Defined as the case where the plane of rupture intersects the side of the bin wall Fig. (3). The fundamental formulas which governs the pressure distribution in this case were expressed in the following forms :

$$L = \frac{w.d}{u+u'} \left[1 - \frac{\sqrt{1 + u^2}}{\sqrt{\frac{2h}{d}(u+u') + 1 - u\,u'}} \right]$$

$$V = L/K$$

Where : V,L, and K are as defined before.

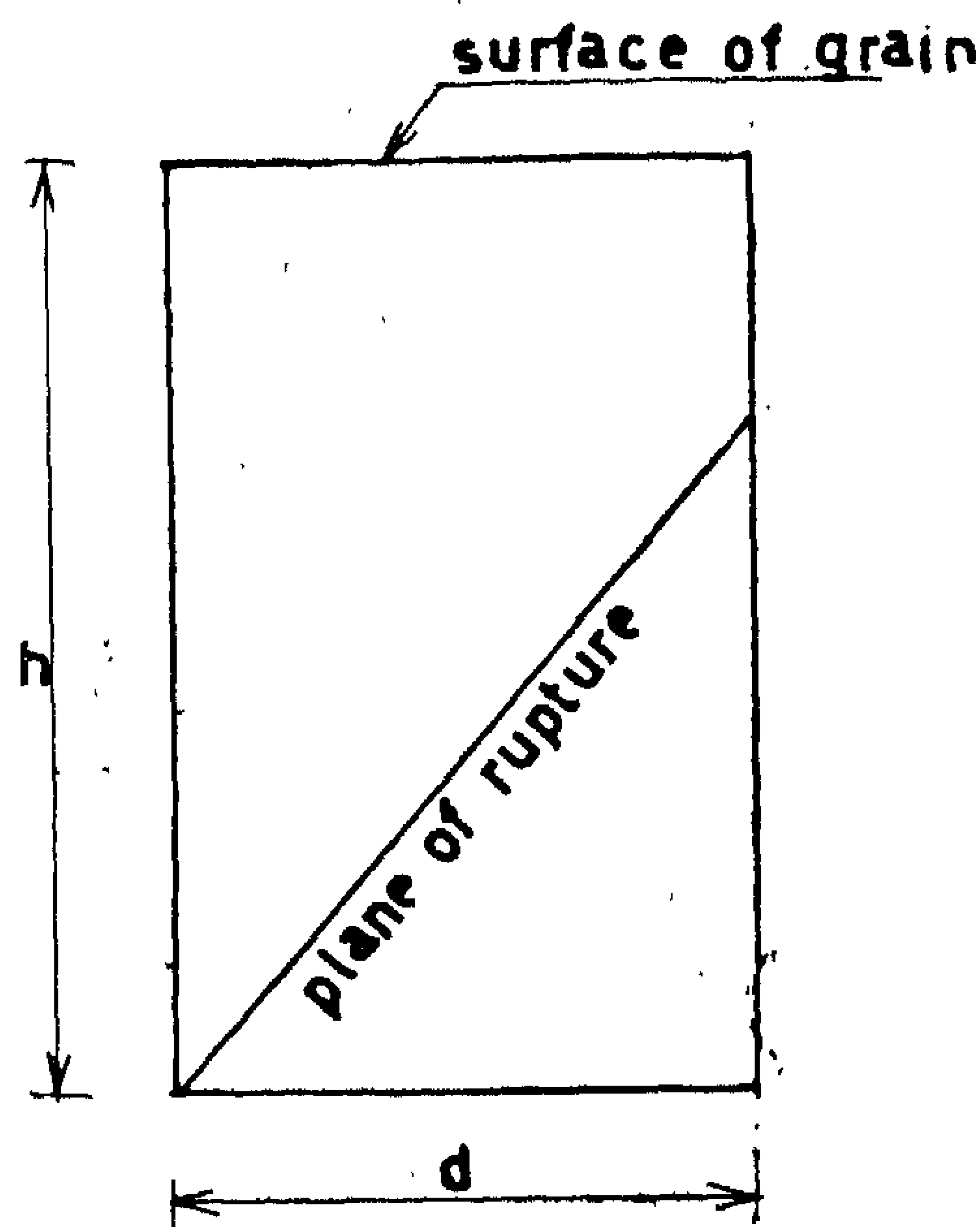


FIG. 3

3 — Reimbert's approach :

According to this analysis the following expressions have been used for design purposes :

$$L = P_{max.} \left[1 - \left(\frac{y}{c} + 1\right)^{-2}\right]$$

$$V = w \left[y \left(\frac{y}{c} + 1\right)^{-1}\right]$$

ON PRESSURES OF GRANULAR MATERIALS ON BINS AND ORE PASSES

By

IMAM, H.F., M.Sc., Ph.D., A.I.M.E. member*
ELWAGEAH, M.A., M.Sc.**

ABSTRACT

A series of experiments on bulk materials has been performed in order to investigate the factors that influence the pressure distribution on bin walls. Special interest was paid to study the influence of particle size, shape, wall roughness, and material head. Pressure cell has been developed. Data obtained have been analysed.

1) INTRODUCTION

The problem of calculating pressures of granular materials on bins, chutes, and ore passes walls constitute one of the main phases of flow of bulks research programs. Evaluation of such pressures will be of vital necessity for design purposes. Designs, as they are practiced now, are based on the classical theories introduced by Janssen(1) and later modified by Airy(2), or on the analysis reported by Reimbert(3). These theories suggest similarity between conditions and principles of design of retaining walls and that of design of bins, and similar containers when loaded by granular material. But from practical point of view, such similarity is not valid, since material is limited in extent, and the condition of static equilibrium is disturbed by drawing the material out from the bottom of the container, and hence it is expected to have the calculated values of pressure on sides deviated from actual situation. The purpose of present investigation is to tackle the pressure distribution problem on chutes and ore passes walls experimentally in order to obtain more realistic quantitative informations about their values and distribution.

II) CRITICAL REVIEW OF DESIGN LOADS CRITERIA

Basic fundamental approaches used in calculating pressure exerted by granular materials when at rest on walls and bottom of the container are ciritically reviewed as follows :

1 — Janssen's Approach :

This approach is based essentially on the following main assumption :

1. Similarity between retaining wall conditions, and that of bin loaded by materials,
2. In order to derive the mathematical expressions, material in bin form arches or domes superimposed on each other, Fig. (1).

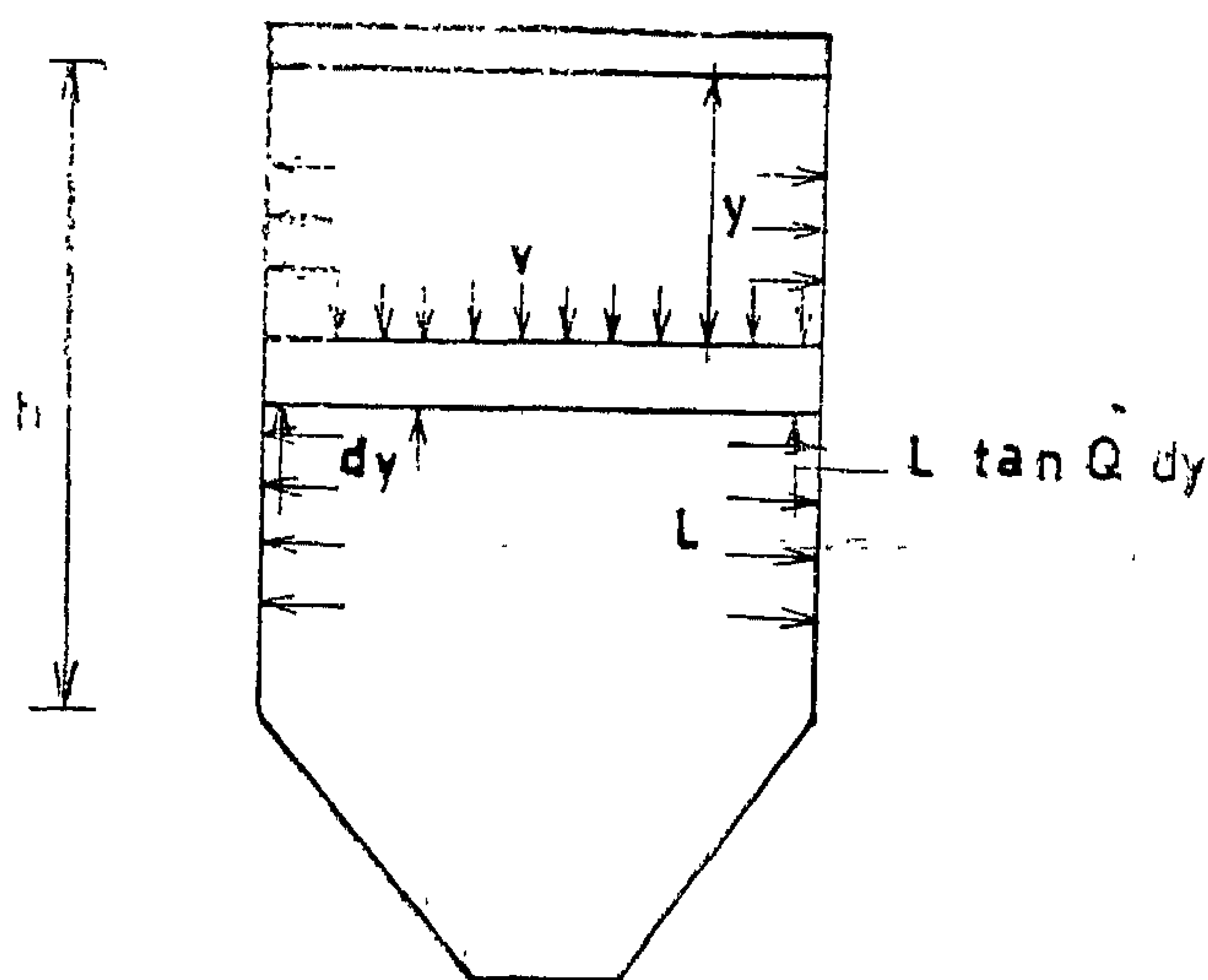


FIG. 1

* Associate Prof., Faculty of Engineering, Cairo University.
** Teaching Assistant, Facu.ty of Engineering, Cairo University.

THE EGYPTIAN
SOCIETIES OF ENGINEERS

- Issued Quarterly (Jan. — Feb. — Mar., — Apr. — May — June, July — Aug. — Sept., Oct. — Nov. and Dec.) and sent to subscribers on or about : March 15, July 1, September 15 and January 1.

- Contributers are invited to submit material for editorial consideration and should be addressed to the Editor Dr. S. Mortada, Egyptian Society of Engineers, 28, Ramses Street, Cairo, A.R.E. The Editor cannot accept responsibility for loss or damage to any material.

- It is requested that contributers exercise care in writing scientific and proper names. References to other publications should be in accordance with the forms used in the pages of this Journal. The manuscript should be typewritten with double space lines and must be preceded by a brief abstract. Galley proof will be sent authers when, in the editor's opinion, the subject matter is such as will require correction by the author.

SUBSCRIPTIONS

All members of the societies receive their copies free.
Engineers' rates are P.T. 60 per annum.
Subscription for others P.T. 200 per annum.
All subscribers are requested to submit their addresses to the Secretariat, at the address of the Engineering Society at Cairo.

HEAD OFFICE

Egyptian Society of Engineers,
28, Ramses Street, Cairo. Tel. 52106

JOURNAL OF
THE EGYPTIAN SOCIETY OF ENGINEERS
A.R.E.

QUARTERLY SCIENTIFIC PROCEEDINGS

ISSUED BY

THE EGYPTIAN SOCIETY OF ENGINEERS—A.R.E. CAIRO

Vol. X — No. 4, October-November-December 1971

CONTENTS

ENGLISH SECTION

Page

On pressures of granular materials on bins and ore passes.
Dr. H.F. IMAM, EL-WAGEAH 5

Direct reduction of el-baharyia iron ores in the fluidised state with hydrogen
Dr. M. EL-HALWAGI, A.M. ABDEL DAYEM, S. EL-AFIFI ... 14

Methods for improving T.L. insulators performance in polluted and humid atmospheres.
Dr. EL-SAYED A.H. ALY 23

Dynamic measurements on a shell and Tude steam heater.
Dr. M.A. EL-RIFAI, H.A. YOUSSEF, M.A. SALEH 30

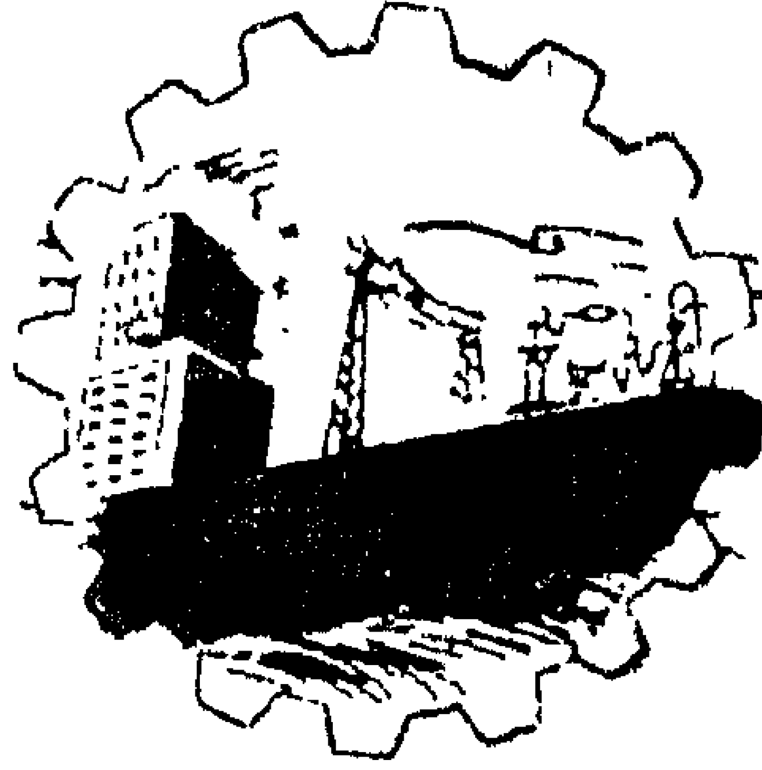
Factors influencing compaction mechanisms in in foundry sand.
Dr. SALAH M. SAID, Dr. M.M. FARAG, Eng. M.A. TAHA 34

ARABIC SECTION

Towards a Contemporary Arabic Architecture and its relation to tradition.
Dr. ALY RAAFAT 5

Problems land transportation by cars in towns and villages in developing countries.
Dr. SAMIR FAHMY 17

Design of protective constructions — 2 —
Eng. EZZ EL-DIN FARAG 42



JOURNAL OF THE EGYPTIAN SOCIETY OF ENGINEERS A. R. E.

October-November-December 1971
Vol. X
No. 4